JOURNAL OF PHYSICS AND CHEMISTRY OF SOLIDS

AN INTERNATIONAL JOURNAL

VOLUME 56 No. 12 ISSN 0022-3697

1995 DECEMBER

EDITORS

Arun Bansil

Boston

Yasuhiko Fujii

Tokyo

George A. Sawatzky

Groningen

Robert N. Shelton

Davis

19960430 121

SPECIAL ISSUE

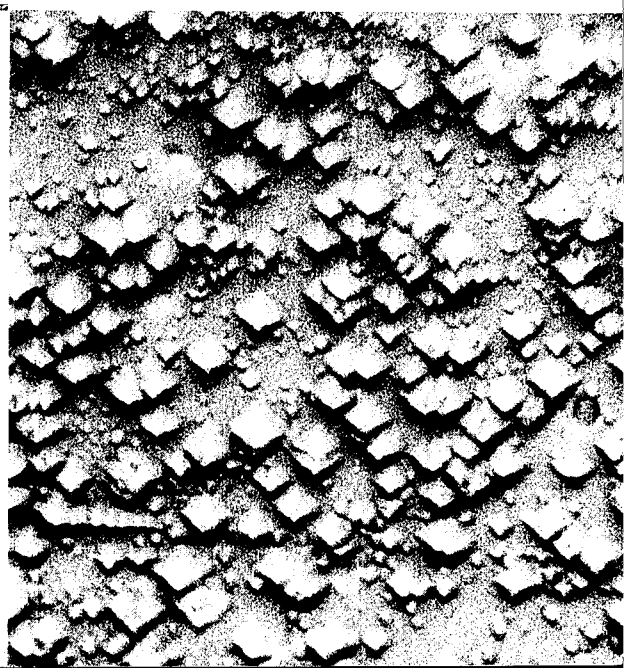
Spectroscopies in Novel Superconductors

GUEST EDITORS

ZHI-XUN SHEN, D. H. LIEBENBERG and A. BANSIL

PERGAMON

DTIC QUALITY INSPECTED 3



DISCLAIMER NOTICE



THIS DOCUMENT IS BEST QUALITY AVAILABLE. THE COPY FURNISHED TO DTIC CONTAINED A SIGNIFICANT NUMBER OF PAGES WHICH DO NOT REPRODUCE LEGIBLY.

JOURNAL OF PHYSICS AND CHEMISTRY OF SOLIDS

(FOUNDER EDITOR: HARVEY BROOKS)

Senior Advisory Editors

DAVID E. COX, ARTHUR C. DAMASK, GEORGE J. DIENES, JACQUES FRIEDEL, JOHANN PEISL, SIR JOHN THOMAS, YASUSADA YAMADA and GUAN WEIYAN

Editors

ARUN BANSIL, *Physics Department, Northeastern University, Boston, MA* 02115, *U.S.A.*

YASUHIKO FUJII, *Institute for Solid State Physics, The University of Tokyo,* 7-22-1 *Roppongi, Minato-ku, Tokyo* 106, *Japan*

GEORGE A. SAWATZKY, *Laboratory of Applied and Solid State Physics, Materials Science Centre, University of Groningen, Nijenborgh* 4, 9747 *AG Groningen, The Netherlands*

ROBERT N. SHELTON, *Department of Physics, University of California, Davis, CA* 95616, *U.S.A.*

Editorial Advisory Board

F. BASSANI, Pisa, Italy
A. S. BOROVIK-ROMANOV, Moscow, Russia
R. C. BOWMAN, JR, Azusa, CA, U.S.A.
E. BURSTEIN, Philadelphia, PA, U.S.A.
C. R. A. CATLOW, London, U.K.
A. K. CHEETHAM, Santa Barbara, CA, U.S.A.
J. R. CHELIKOWSKY, Minneapolis, MN, U.S.A.
M. DATE, Ibaraki, Japan
F. J. DI SALVO, Ithaca, NY, U.S.A.
R. C. DYNES, La Jolla, CA, U.S.A.
J. FINK, Dresden, Germany
QINGQUAN GOU, Chengdu, Sichuan, China
C. HAAS, Groningen, The Netherlands
P. HAGENMULLER, Bordeaux, France
E. E. HALLER, Berkeley, CA, U.S.A.
F. J. HIMPSEL, Yorktown Heights, NY, U.S.A.
C. J. HUMPHREYS, Cambridge, U.K.
T. ISHIGURO, Kyoto, Japan
P. W. M. JACOBS, Ontario, Canada
J. A. KRUMHANSL, Ithaca, NY, U.S.A.
K. KAWASAKI, Fukuoka, Japan
S. C. MOSS, Houston, TX, U.S.A.
B. C. SALES, Oak Ridge, TN, U.S.A.
H. SUEMATSU, Tokyo, Japan
T. TIMUSK, Ontario, Canada

Production Editor

M. LAZENBY, *Elsevier Science Ltd, The Boulevard, Langford Lane, Kidlington, Oxford OX5 1GB, U.K.*
Tel: (01865) 843880; *Fax*: (01865) 843923; *e-mail to*: m.lazenby@elsevier.co.uk

Publishing, Subscription and Advertising Offices: Elsevier Science Ltd, The Boulevard, Langford Lane, Kidlington, Oxford OX5 1GB, U.K.; and Elsevier Science Inc., 660 White Plains Road, Tarrytown, NY 10591-5153, U.S.A.

Published monthly. Annual Institutional Subscription Rates 1996: North, Central and South America, US$2147.00, Rest of World £1350.00. Associated Personal Subscription Rates are available on request for those whose institutions are library subscribers. Sterling prices exclude VAT. Non-VAT registered customers in the European Community will be charged the appropriate VAT in addition to the price listed. Prices include postage and insurance and are subject to change without notice. Subscription enquiries from customers in North America should be sent to: Elsevier Science Inc., 660 White Plains Road, Tarrytown, NY 10591-5153, U.S.A. and from the Rest of the World to: Elsevier Science Ltd, The Boulevard, Langford Lane, Kidlington, Oxford OX5 1GB, U.K. Subscription rates for Japan are available on request.

Back issues of all previously published volumes, in both hard copy and on microform, are available direct from Elsevier Science offices (Oxford and New York). Complete volumes and single issues can be purchased for 1990–1995. Earlier issues are available in high quality photo-duplicated copies as complete volumes only. Back volumes on microfilm are available from UMI, 300 North Zeeb Road, Ann Arbor, MI 48106, U.S.A.

Copyright © 1995 Elsevier Science Ltd

SECOND CLASS POSTAGE PAID AT NEWARK, NEW JERSEY AND ADDITIONAL ENTRY POINTS. The *Journal of Physics and Chemistry of Solids* (ISSN 0022–3697) is published monthly, January to December in one volume by Elsevier Science Ltd, The Boulevard, Langford Lane, Kidlington, Oxford OX5 1GB, U.K. The annual subscription in the U.S.A. is $2147. The *Journal of Physics and Chemistry of Solids* is distributed by Virgin Mailing and Distribution, 10 Camptown Road, Irvington, NJ 07111-1105. POSTMASTER: Please send address corrections to *Journal of Physics and Chemistry of Solids*, c/o Elsevier Science Inc., 660 White Plains Road, Tarrytown, NY 10591-5153, U.S.A.

Whilst every effort is made by the publishers and editorial board to see that no inaccurate or misleading data, opinion or statement appear in this journal, they wish to make it clear that the data and opinions appearing in the articles and advertisements herein are the sole responsibility of the contributor or advertiser concerned. Accordingly, the publishers, the editorial board and editors and their respective employees, officers and agents accept no responsibility or liability whatsoever for the consequences of any such inaccurate or misleading data, opinion or statement.

Scanning Electron Micrographs on cover courtesy of John Simpson, II-VI MBE Group, Heriot–Watt University, Edinburgh, U.K.

REPORT DOCUMENTATION PAGE

Form Approved
OMB No. 0704-0188

Public reporting burden for this collection of information is estimated to average 1 hour per response, including the time for reviewing instructions, searching existing data sources, gathering and maintaining the data needed, and completing and reviewing the collection of information. Send comments regarding this burden estimate or any other aspect of this collection of information, including suggestions for reducing this burden, to Washington Headquarters Services, Directorate for Information Operations and Reports, 1215 Jefferson Davis Highway, Suite 1204, Arlington, VA 22202-4302, and to the Office of Management and Budget, Paperwork Reduction Project (0704-0188), Washington, DC 20503.

1. AGENCY USE ONLY (Leave blank)	2. REPORT DATE	3. REPORT TYPE AND DATES COVERED
	4/16/96	Final Report 11/1/94 - 10/31/95

4. TITLE AND SUBTITLE
Spectroscopies in Novel Superconductors

5. FUNDING NUMBERS
G
N00014-95-1-0290

6. AUTHOR(S)
Prof. Zhi-xun Shen

7. PERFORMING ORGANIZATION NAME(S) AND ADDRESS(ES)
Ruth Kaempf
Stanford University
Sponsored Projects Office
856 Serra
Stanford, CA 94305

8. PERFORMING ORGANIZATION REPORT NUMBER
SPO No: 14668
1DYA401

9. SPONSORING/MONITORING AGENCY NAME(S) AND ADDRESS(ES)
Dr. D.H. Liebenberg, ONR
800 N. Quincy Street, Code 312
Electronic Division
Arlington, VA 22217-5660

10. SPONSORING/MONITORING AGENCY REPORT NUMBER

11. SUPPLEMENTARY NOTES

12a. DISTRIBUTION/AVAILABILITY STATEMENT

DISTRIBUTION STATEMENT A
Approved for public release
Distribution Unlimited

12b. DISTRIBUTION CODE

13. ABSTRACT (Maximum 200 words)

See next page

A copy of the proceedings published in the Journal of Physics and Chemistry of Solids is included as a part of the report.

14. SUBJECT TERMS			15. NUMBER OF PAGES: 4 + proceedings.
			16. PRICE CODE
17. SECURITY CLASSIFICATION OF REPORT	18. SECURITY CLASSIFICATION OF THIS PAGE	19. SECURITY CLASSIFICATION OF ABSTRACT	20. LIMITATION OF ABSTRACT

DTIC QUALITY INSPECTED 1

Final Report for ONR Symposium Grant: Navy# N00014-95-1-0290

Symposium Title: Spectroscopies in Novel Superconductors

Prepared by: Zhi-xun Shen, Department of Applied Physics and Stanford Synchrotron Radiation Laboratory, Stanford University

- Date and location of the symposium:

  March 15-18, 1995
  Stanford Synchrotron Radiation Laboratory
  Stanford University, California

- Report of the conference

In the field of high-Tc superconductivity research, various spectroscopies are playing critical roles to reveal the microscopic origin of this remarkable phenomenon. This conference brought together different spectral aspects of high-temperature superconductors. Through the four days planned program, the conference helped the participants to obtain the latest information about both experimental and theoretical issues. The discussion facilitated by the conference generated new ideas and helped resolved some of the outstanding issues. Attached are copies of the scientific program and the conference proceeding which is published as a special volume in the Journal Physics and Chemistry of Solids.

The Conferences on Spectroscopies in Novel Superconductors started with the Argonne meeting in 1991, where the k-resolved spectroscopies of electronic states at and near the Fermi energy were discussed. The spectroscopies included in the Argonne conference were photoemission, de Haas-van Alphen, positron 2D-ACAR and tunnelling. In the following conferences in Sendai, July, 1992 and in Santa Fe, March, 1993, the scope of the conference expanded to include optical, microwave, transport, NMR and NQR measurements. The Stanford conference further broadened the conference scope by including neutron, quantum interference and thermodynamics experiments. This evolution reflects the growing sophistication of the field and the increasing importance of spectroscopies to understanding the novel superconductors.

It has always been a tradition of this conference series to have a strong theoretical component. Theoretical models ranging from band theory to highly correlated electron systems, and those concentrated as much on the mechanisms of superconductivity as they did on Fermi surface properties were presented. Like the Santa Fe conference, a special evening session was organized at the Stanford conference to discuss issues related to, but not limited to, the superconducting pairing symmetry.

The Stanford conference generated considerable interest in the scientific community. About two hundreds scientists from fourteen countries attended the conference: United States, Japan, Canada, Germany, Switzerland, France, The Netherlands, Sweden, India, Israel, Argentina, China, Finland and Russia. There were about 140 papers presented at the conference with one to two mixtures of theory and experiment.

SPECTROSCOPIES IN NOVEL SUPERCONDUCTORS

GUEST EDITORS

Zhi-xun Shen
Stanford University/SSRL

Donald H. Liebenberg
Office of Naval Research

Arun Bansil
Northeastern University

AIMS AND SCOPE

The *Journal of Physics and Chemistry of Solids* is a well-established international medium for publication of research in condensed matter and materials science. Emphasis is placed on experimental and theoretical work which contributes to a basic understanding of and new insight into the properties and behaviour of condensed matter.

General areas of interest are the electronic, spectroscopic and structural properties of solids, the statistical mechanics and thermodynamics of condensed systems, including perfect and defect lattices, surfaces, interfaces, thin films and multilayers, amorphous materials and nanostructures, and layered and low-dimensional structures. Typical examples include the preparation and structural characterization of novel and advanced materials, especially in relation to the measurement and interpretation of their electrical, magnetic, optical, thermal and mechanical properties, phase transitions, electronic structure and defect properties, and the application of appropriate experimental and theoretical techniques in these studies.

Articles are encouraged in all the above areas, but especially those which emphasize fundamental aspects of materials science. From time to time, Special Issues of the *Journal* containing invited articles devoted to topical or rapidly developing fields are published.

Publishing, Subscription and Advertising Offices: Elsevier Science Ltd, The Boulevard, Langford Lane, Kidlington, Oxford OX5 1GB, U.K. and Elsevier Science Inc., 660 White Plains Road, Tarrytown, NY 10591-5153, U.S.A.

Copyright © 1995 Elsevier Science Ltd

It is a condition of publication that manuscripts submitted to this journal have not been published and will not be simultaneously submitted or published elsewhere. By submitting a manuscript, the authors agree that the copyright for their article is transferred to the Publisher if and when the article is accepted for publication. However, assignment of copyright is not required from authors who work for organizations which do not permit such assignment. The copyright covers the exclusive rights to reproduce and distribute the article, including reprints, photographic reproductions, microform or any other reproductions of similar nature and translations. No part of this publication may be reproduced, stored in a retrieval system or transmitted in any form or by any means, electronic, electrostatic, magnetic tape, mechanical photocopying, recording or otherwise, without permission in writing from the copyright holder.

PHOTOCOPYING INFORMATION FOR USERS IN THE U.S.A.

The Item-Fee Code for this publication indicates that authorization to photocopy items for internal or personal use is granted by the copyright holder for libraries and other users registered with the Copyright Clearance Center (CCC) Transactional Reporting Service provided the stated fee for copying beyond that permitted by Section 107 or 108 of the United States Copyright law is paid. The appropriate remittance of $9.50 per copy per article is paid directly to the Copyright Clearance Center Inc., 222 Rosewood Drive, Danvers, MA 01923, U.S.A.

PERMISSION FOR OTHER USE

The copyright owner's consent does not extend to copying for general distribution, for promotion, for creating new works, or for resale. Specific written permission must be obtained from the Publisher for such copying.

The Item-Fee Code for this publication is: 0022-3697/95 $9.50 + 0.00

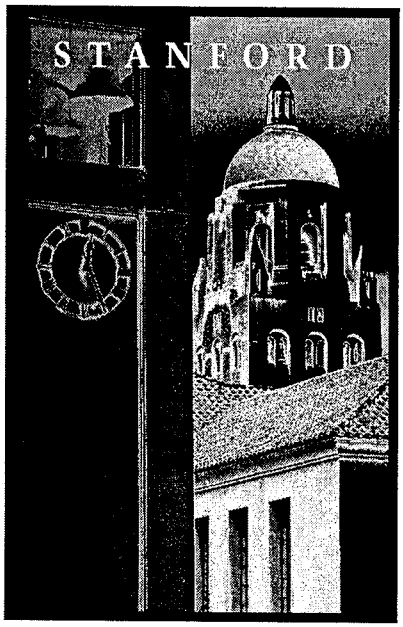
♾™The paper used in this publication meets the minimum requirements of American National Standard for Information Sciences—Permanence of Paper for Printed Library Materials, ANSI Z39.48-1984.

Whilst every effort is made by the publishers and editorial board to see that no inaccurate or misleading data, opinion or statement appear in this journal, they wish to make it clear that the data and opinions appearing in the articles and advertisements herein are the sole responsibility of the contributor or advertiser concerned. Accordingly, the publishers, the editorial board and editors and their respective employees, officers and agents accept no responsibility or liability whatsoever for the consequences of any such inaccurate or misleading data, opinion or statement.

Proceedings of the Conference on

SPECTROSCOPIES IN NOVEL SUPERCONDUCTORS

Stanford Linear Accelerator Center
Stanford, California
March 15-18, 1995



Z.-X. Shen, *Stanford University* (Co-Chairman)
W.E. Spicer, *Stanford University* (Co-Chairman)
A. Bansil, *Northeastern University* (Program Chairman)

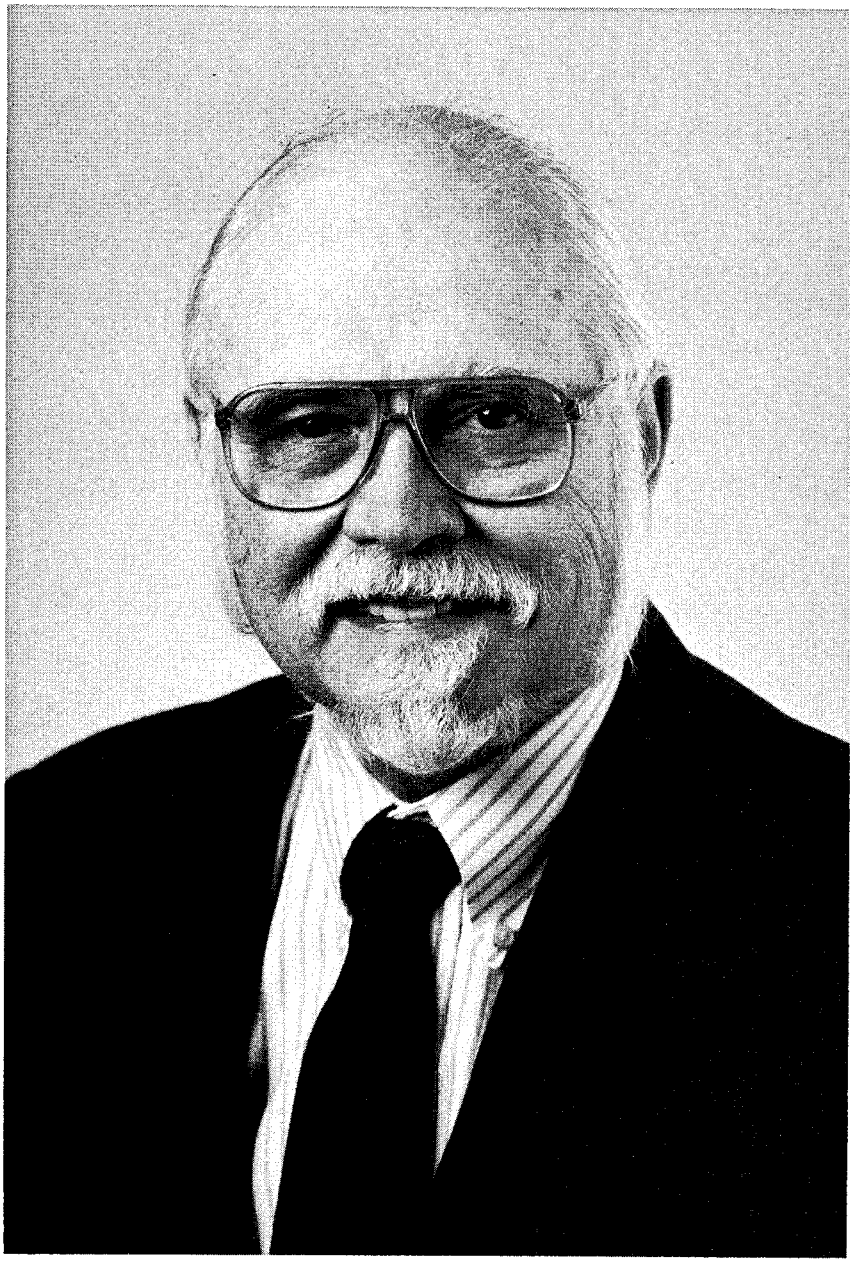
Sponsored by:

ARPA
Argonne National Laboratory
ISTEC-SRL
Lawrence Berkeley Laboratory
Los Alamos National Laboratory
Office of Naval Research
Stanford University, Office of the Dean of Research
Stanford University, School of Humanities and Sciences
Stanford Synchrotron Radiation Laboratory

Dedicated to Professor William E. Spicer

in honor

of his 65th birthday and retirement from Stanford University



CONTENTS

SPECIAL ISSUE

SPECTROSCOPIES IN NOVEL SUPERCONDUCTORS

Z.-X. Shen, D. Liebenberg and A. Bansil	xv	Preface
	xvii	List of Participants
	xxi	Scientific Program of the Conference
Theory		
A.A. Abrikosov	1567	On the nature of the order parameter in HTSC and influence of impurities
O.K. Andersen, A.I. Liechtenstein, O. Jepsen and F. Paulsen	1573	LDA energy bands, low-energy Hamiltonians, t′, t″, $t_\perp(k)$, and $J_\perp$
P.W. Anderson	1593	A battery of smoking guns (for the non-Fermi liquid-interlayer theory of high-T_c cuprates)
N. Bulut and D.J. Scalapino	1597	Evolution of the single-particle spectral weight with doping
S. Doniach	1601	Reflections on the superconductor-insulator transition
P.J. Hirschfeld	1605	Impurity scattering and order parameter symmetry in high-T_c superconductors
L.B. Ioffe and A.J. Millis	1611	Magnetic properties of high temperature superconductors: a spin liquid approach
H. Kajueter and G. Kotliar	1615	Spectral functions of correlated electron systems in the local impurity self consistent approximation
C. Kallin, A.J. Berlinsky, A.L. Fetter, M. Franz and P.I. Soininen	1619	Vortices in *d*-wave superconductors
V.Z. Kresin, S.A. Wolf, S.D. Adrian, M.E. Reeves and Yu. N. Ovchinnikov	1623	Energy spectrum of high-T_c oxides: two-gap structure, gaplessness, and implications
R.B. Laughlin	1627	Evidence for electron decay in photoemission from $Sr_2CuO_2Cl_2$
P.A. Lee and K. Kuboki	1633	Energy gap structure in bilayer oxide superconductors
R.S. Markiewicz	1637	Pseudogaps in the van Hove Jahn-Teller scenario
A.J. Millis, L.B. Ioffe and H. Monien	1641	Spin gaps in high temperature superconductors
A. Moreo, A. Nazarenko, S. Haas, A. Sandvik and E. Dagotto	1645	Study of ARPES data and *d*-wave superconductivity using electronic models in two dimensions
D. Pines and P. Monthoux	1651	$d_{x^2-y^2}$ pairing and spin fluctuations in the cuprate superconductors: a progress report
R. Preuss, R. Putz, W. Hanke and W. von der Linden	1659	Continuous evolution of the 2D Hubbard model from an insulator to a metal
T.M. Rice, M. Troyer and H. Tsunetsugu	1663	The *d*-wave resonance valence bond state

D.J. Scalapino	1669	Distinguishing high-T_c theories
J.R. Schrieffer and A.P. Kampf	1673	ARPES: novel effect in the energy and momentum distributions
A. Sokol	1679	Magnetic behavior of the cuprate superconductors
C.M. Varma	1685	Symmetry of the superconducting state in copper oxides
J. Ashkenazi	1691	Two types of charge carriers in the high-T_c cuprates
B. Barbiellini, M.J. Puska, A. Harju and R.M. Nieminen	1693	Positron annihilation and positron-electron correlation effects in high-T_c oxides
A.J. Berlinsky, A.L. Fetter, M. Franz, C. Kallin and P.I. Soininen	1695	Ginzburg-Landau theory of the Abrikosov lattice in a *d*-wave superconductor
H.A. Blackstead and J.D. Dow	1697	Charge-transfer and the location of superconducting holes in $La_{2-\beta}Sr_{\beta}CuO_4$
B.H. Brandow	1699	A valence-fluctuation mechanism with highly anisotropic *s*-wave pairing
J.M. Byers and M.E. Flatté	1701	Two-protrusion STM on an anisotropic superconductor
C. Chen	1703	Correlation-induced electron-lattice interaction in the Hubbard model: its effects on the spectral distribution
L. Chen and P. Benard	1705	Spin fluctuations in high-T_c superconductors with two Fermi surface sheets
A.V. Chubukov, D.M. Frenkel, G. Blumberg and M.V. Klein	1707	Resonant two-magnon Raman scattering in antiferromagnetic insulators
E. Dagotto, A. Nazarenko, A. Moreo and S. Haas	1709	A simple theory for the cuprates: the antiferromagnetic van Hove scenario
T.P. Devereaux	1711	Raman scattering in disordered unconventional superconductors
M.V. Eremin, S.G. Solovjanov and S.V. Varlamov	1713	Some novel features of the bands in HTSC
M.E. Flatté	1717	Measuring a superconductor's gap anisotropy with EELS
N. Hamada, H. Sawada and K. Terakura	1719	Electronic band structure of $La_{1-x}Ba_xMnO_3$
S. Kashiwaya, Y. Tanaka, M. Koyanagi, H. Takashima and K. Kajimura	1721	Tunneling spectroscopy of *d*-wave superconductors
H. Kim and E.J. Nicol	1725	Effect of impurity scattering on a *d*+*s* wave superconductor: low temperature behavior of penetration depth
V.N. Kostur and B. Mitrovic	1727	Weak electron-phonon interaction and strong phonon features in *a*-*b*-plane optical conductivity of high-T_c superconductors
S. Liang	1729	Correlation energy hierarchy in two dimensional Hubbard model
D.Z. Liu, J. Maly and K. Levin	1733	π junctions in *s*-wave superconductors: bi-layer effects
K. Matho	1735	Photoemission: low-energy and high-energy scales

N. Nagaosa and T.-K. Ng	1737	Nonmagnetic impurities in high-Tc cuprates
B. Normand, H. Kohno and H. Fukuyama	1739	Superconductive phonon anomalies in high-T_c cuprates
Y. Ohta and R. Eder	1741	Hole pockets, shadow bands, and spin bags in the doped *t-J* model
F. Onufrieva	1743	Evidence for $d_{x^2-y^2}$ symmetry of superconducting order parameter in YBCO from neutron scattering data
C.-H. Pao and H.-B. Schüttler	1745	Isotope effect in spin fluctuation models
W.O. Putikka	1747	Magnetic frustration and spin-charge separation in 2D strongly correlated electron systems
Y. Ren, J.H. Xu and C.S. Ting	1749	Spontaneous generation of *s*-wave component in a purely *d*-wave superconductor
C.O. Rodriguez, R. Weht, M. Weissmann and N.E. Christensen	1751	Are surface effects to be included in the study of the electronic structure of high temperature superconductors?
S.K. Sarker	1753	Confinement in the three-dimensional anisotropic *t-J* model: a mean-field study
H. Sawada, N. Hamada and K. Terakura	1755	Phase stability and magnetic property of $LaCo_{1-x}Ni_xO_3$
J. Tanaka, M. Shimizu and K. Kamiya	1759	Interpretation of electronic Raman and angle resolved photoemmision spectra of $Bi_2Sr_2CaCu_2O_8$
Y. Tanaka and S. Kashiwaya	1761	Josephson effect in $d_{x^2-y^2}$–wave superconductors
A.M. Tikofsky and D.B. Bailey	1763	A gapless time-reversal symmetry violating superconductor
Y. Ushijima, Y. Tanaka and H. Tsuchiura	1767	Energy spectrum of quasiparticles for various pairing states in 2-D extended Hubbard model
Y.M. Vilk and A.-M.S. Tremblay	1769	Destruction of the Fermi liquid by spin fluctuations in two dimensions
G. Wendin and V.S. Shumeiko	1773	Giant Josephson current through a single bound state in a superconducting tunnel junction
Z.Y. Weng, D.N. Sheng and C.S. Ting	1775	Spin-charge separation in the *t-J* model
V.M. Yakovenko and I.I. Mazin	1777	On the interpretation of neutron scattering in superconducting $YBa_2Cu_3O_7$
S. Yunoki and S. Maekawa	1779	Effects of long-range interaction in one-dimensional electron systems
Y. Zha, S.L. Cooper and D. Pines	1781	Spin pseudogap and *c*-axis transport
Quantum Interference and Tunneling		
H.R. Ott and D.A. Brawner	1783	Experimental evaluation of the order parameter symmetry of superconductors
C.C. Tsuei, J.R. Kirtley, M. Rupp, J.Z. Sun, L.-S. Yu-Jahnes, C.C. Chi, A. Gupta and M.B. Ketchen	1787	Flux quantization in tricrystal cuprate rings—a new probe of pairing symmetry

D.A. Wollman, D.J. Van Harlingen, J. Giapintzakis and D.M. Ginsberg	1797	Tunneling in Pb-YBCO junctions: determining the symmetry of the pairing state
R. Aoki, H. Murakami, T. Kita, M. Shirai, V.M. Svistunov, A.I. Dyachenko and D.N Afanassyev	1801	Tunneling observation of phonon contribution to the pairing interaction in oxide superconductors
H.L. Edwards, D.J. Derro, A.L. Barr, J.T. Markert and A.L. de Lozanne	1803	A study of the CuO chains in $YBa_2Cu_3O_{7-x}$ by scanning tunneling microscopy and spectroscopy
J.H. Miller, Jr., Q.Y. Ying, Z.G. Zou, J.H. Xu, M.F. Davis and N.Q. Fan	1805	Use of cuprate tricrystal microbridges as probes of superconducting pairing state symmetry
H. Murakami and R. Aoki	1807	LT-STM/STS observation on different atomic layers of BSCCO(2212)
J.M. Valles, Jr., S.-Y. Hsu and J.A. Chervenak	1809	Electron tunneling spectroscopy near the magnetic field tuned superconductor to insulator transition
Optical and Raman Spectroscopies		
H. Eisaki and S. Uchida	1811	Optical study of high-T_c superconductors and related oxides
B. Parks, J. Orenstein, R. Mallozzi, D.T. Nemeth, F. Ludwig, J. Clarke, P. Merchant, D.J. Lew, I. Bozovic and J.N. Eckstein	1815	Re-examining the vortex state of cuprate superconductors with gap anisotropy
T. Timusk, D.N. Basov and C.C. Homes	1821	The strange interplane conductivity of HTSC
D. van der Marel and J.H. Kim	1825	In-plane and out-of-plane charge dynamics of high-T_c cuprates
A. Bock, R. Kürsten and U. Merkt	1829	Oxygen diffusion in laser heated $YBa_2Cu_3O_7$ films
G.S. Kino, I.M. Fishman, X.D. Wu and W.R. Studenmund	1831	Modulation measurements of $YBa_2Cu_3O_{7-\delta}$ optical reflectivity using a thermal wave technique
A.P. Litvinchuk, M. Käll, L. Börjesson, P. Berastegui and L.-G. Johansson	1833	Substitution of Pr for Y in $YBa_2Cu_4O_8$ and $YBa_2Cu_{3.5}O_{7.5-\delta}$ superconductors: phonon modes and charge transfer effects
A. Matic, M. Käll, L. Börjesson and Y. Eltsev	1835	Influence of Zn-doping on the electronic Raman scattering of $YBa_2Cu_3O_{7-\delta}$
K.M. Paget, T.R. Lemberger, S.R. Foltyn and X. Wu	1837	Comparison of chain (Co) and plane (Zn) dopants on charge transport in $YBa_2Cu_3O_{7-\delta}$
J. Schützmann, S. Tajima, S. Miyamoto and S. Tanaka	1839	Doping dependence of the optical c-axis conductivity in $YBa_2Cu_3O_y$
B. Stadlober, G. Krug, R. Nemetschek, M. Opel, R. Hackl, D. Einzel, C. Schuster, T.P. Devereaux L. Forró, J.L. Cobb, J.T. Markert and J.J. Neumeier	1841	Study of k-dependent electronic properties in cuprate superconductors using Raman spectroscopy

W.R. Studenmund, I.M. Fishman, G.S. Kino and J. Giapintzakis	1843	Symmetry of differential optical responses of normal and superconducting phases in single-crystal YBCO
Photoemission Experiments		
P. Aebi, J. Osterwalder, P. Schwaller, H. Berger, C. Beeli and L. Schlapbach	1845	Complete Fermi surface mapping of Bi-cuprates
J.W. Allen, G.-H. Gweon, R. Claessen and K. Matho	1849	Fermi liquids and non-Fermi liquids—the view from photoemission
A. Bansil and M. Lindroos	1855	Angle-resolved photo-intensities in high-T_c's: surface states, CuO_2 plane bands, lineshapes, and related issues
J.C. Campuzano, H. Ding, A. Bellman, M.R. Norman, M. Randeria, G. Jennings, T. Yokoya, T. Takahashi, H. Katayama-Yoshida, T. Mochiku and K. Kadowaki	1863	ARPES studies in the normal and superconducting state of $Bi_2Sr_2CaCu_2O_8$
D. King, D.S. Dessau, A.G. Loeser, Z.-X. Shen and B.O. Wells	1865	Electronic structure evolution from Mott insulator to superconductor—an angle-resolved photoemission investigation
B.O. Wells, Z.-X. Shen, A. Matsuura, D.M. King, M.A. Kastner, M. Greven and R.J. Birgeneau	1871	Band mapping of the model insulator $Sr_2CuO_2Cl_2$—dispersion of a single hole in an antiferromagnetic background
A. Fujimori, K. Kobayashi, T. Mizokawa, K. Mamiya, A. Sekiyama, H. Takagi, H. Eisaki, S. Uchida, R.J. Cava, J.J. Krajewski and W.F. Peck, Jr.	1875	Spectral weight transfer and mass renormalization in $Ln Ni_2B_2C$ (Ln=Y,La)
S. Gonda, M. Kawasaki, S. Ohashi, Y. Kotaka, K. Kishio and H. Koinuma	1877	Superconducting gap observation by high-resolution photoelectron yield spectroscopy
C.G. Olson, J.G. Tobin, G.D. Waddill, D.W. Lynch and J.Z. Liu	1879	The 1 eV peak: a consistent feature of the cuprate superconductors
D.M. Poirier, C.G. Olson, D.W. Lynch, M. Schmidt, B.K. Cho and P.C. Canfield	1881	Observation of band dispersion in YNi_2B_2C
N. Terada, K. Tokiwa, H. Ozawa, A. Iyo, S. Ishibashi and H. Ihara	1883	Photoemission spectroscopy of $Cu_{1-x}Ba_2Ca_{n-1}Cu_nO_{2n+4-\delta}$ ceramics and thin films
T. Yokoya, A. Chainani, T. Takahashi, H. Katayama-Yoshida, M. Kasai and Y. Tokura	1885	Angle-resolved and resonant photoemission study of Sr_2RuO_4

Transport and Thermodynamic Properties

C.W. Chu, Y.Y. Xue, Y. Cao, and Q. Xiong	1887	Doping effect on the penetration depth of $HgBa_2CuO_{4+\delta}$
Z. Fisk and J.L. Sarrao	1891	Materials and high-T_c
K. Krishana, J.M. Harris and N.P. Ong	1895	Quasi-particle mean-free-path and thermal Hall conductivity in $YBa_2Cu_3O_7$
K.A. Moler, A. Kapitulnik, D.J. Baar, R. Liang and W.N. Hardy	1899	Specific heat of $YBa_2Cu_3O_{7-\delta}$ single crystals: implications for the vortex structure
C. Boekema, I.M. Suarez-Barnes, V.A. Gubanov, D.W. Cooke and M. Leon	1905	Anomalies in vortex states of cuprate superconductors
J.A. Clayhold and C.W. Chu	1907	Quasiparticle contribution to the mixed-state thermopower in $Tl_2Ba_2CaCu_2O_{8+\delta}$
Y.Y. Xue, Y. Cao, Q. Xiong, F. Chen and C.W. Chu	1909	Field-independent magnetization and fluctuations in Hg-based cuprates

Neutron and NMR Experiments

G. Aeppli, T.E. Mason, H.A. Mook and S.M. Hayden	1911	Magnetic fluctuations in lamellar copper oxides
R.J. Birgeneau, A. Aharony, N.R. Belk, F.C. Chou, Y. Endoh, M. Greven, S. Hosoya, M.A. Kastner, C.H. Lee, Y.S. Lee, G. Shirane, S. Wakimoto, B.O. Wells and K. Yamada	1913	Magnetism and magnetic fluctuations in $La_{2-x}Sr_xCuO_4$ for x = 0 (2D antiferromagnet), 0.04 (3D spin glass) and x = 0.15 (superconductor)
T. Imai, C.P. Slichter, J.L. Cobb and J.T. Markert	1921	Superconductivity and spin fluctuations in the electron-doped infinitely-layered high T_c superconductor $Sr_{0.9}La_{0.1}CuO_2$ (T_c=42 K)
B. Keimer, H.F. Fong, D. Reznik, F. Dogan and I.A. Aksay	1927	Resonant neutron scattering from $YBa_2Cu_3O_7$
Y. Kitaoka, K. Ishida, G.-Q. Zheng, H. Tou, K. Magishi, S. Matsumoto, K. Yamazoe, H. Yamanaka and K. Asayama	1931	NMR study in novel superconductors: heavy Fermion system and high-T_c cuprate
P. Bourges, Y. Sidis, L.P. Regnault, B. Hennion, R. Villeneuve, G. Collin, C. Vettier, J.Y. Henry and J.F. Marucco	1937	Comparison of antiferromagnetic fluctuations in zinc-free and zinc-doped YBCO in fully oxidized samples. Studies by inelastic neutron scattering
Y.-Q. Song, A.P. Reyes, X.P. Tang, W.P. Halperin and D. Hinks	1939	^{63}Cu NMR in heavily doped La_2CuO_4

Microwave Experiments

D.A. Bonn, S. Kamal, K. Zhang, R. Liang and W.N. Hardy 1941 The microwave surface impedance of $YBa_2Cu_3O_{7-\delta}$

T. Jacobs, S. Sridhar, C.T. Rieck, K. Scharnberg, T. Wolf and J. Halbritter 1945 Microwave surface impedance of $Y_1Ba_2Cu_3O_{7-\delta}$ crystals—experiment and comparison to a *d*-wave model

Positron Spectroscopy and Other Experiments

A.A. Manuel, A. Shukla, L. Hoffmann, T. Jarlborg, B. Barbiellini, S. Massidda, W. Sadowski, E. Walker, A. Erb and M. Peter 1951 Fermi surfaces of high-T_c superconductors by positron 2D-ACAR

S. Ishibashi, A.A. Manuel and L. Hoffmann 1955 Positron 2D-ACAR in TTF-TCNQ

Other Systems

G. Baskaran 1957 Are there similarities between the layered nickel borocarbide and cuprate superconductors?

M.B. Maple, Y. Dalichaouch, M.C. de Andrade, N.R. Dilley, J. Herrmann and R. Movshovich 1963 Recent issues in the physics of heavy Fermion materials

Summary

P.B. Allen 1969 Spectroscopies in novel superconductors—a conference summary

After Dinner Talk

T.H. Geballe 1973 An after dinner talk–a gap that shouldn't be

Preface

This volume is the collection of invited and contributed papers presented at the Conference on Spectroscopies in Novel Superconductors which was held at the Stanford Synchrotron Radiation Laboratory, Stanford University, California, March 15-18, 1995. In order to help the reader locate material of specific interest, the articles are grouped by subject matter with the invited and contributed papers separately alphabetized, and the scientific program of the meeting is reproduced in the front part of the volume.

It is with great pleasure that we dedicate this volume to Professor William E. Spicer to honor the occasion of his 65th birthday and retirement from Stanford University. Following his initial work at the RCA laboratories (1955-62), Professor Spicer started his group at Stanford in 1962 in order to develop photoemission spectroscopy. Since then—stretching over a span of more than three decades—Professor Spicer has been a major driving force in developing and applying photoelectron spectroscopy and related techniques as modern tools for probing electron states in wide classes of materials. Professor Spicer has received numerous honors, awards, and prizes for his pioneering scientific contributions, among these, the Buckley Solid State Award of APS, the Welsh Medal of the American Vacuum Society, and the Industrial Research and Development Magazine Scientist of the Year Award (1981). Interestingly, as long ago as 1966, Professor Spicer had already started investigating the transition metal oxides which have turned out to be a central ingredient in the new superconductors. Following the discovery of the high T_c superconductors, photoelectron spectroscopy has played an important role in elucidating the electronic structure and pairing mechanism in these materials. Bearing all this in mind, we enthusiastically dedicate this volume to honor Professor Spicer's many scholarly accomplishments over a long and distinguished career.

The present conference is the fourth in the series of meetings started at Argonne (March 1991), followed by meetings at Sendai (July 1992), and Santa Fe (March 1993). As a reference to the proceedings of the previous meetings (all published as special issues of the *Journal of Physics and Chemistry of Solids*) will show, the organizers have deliberately expanded the technical breadth of the program of these meetings over the years. This trend has continued at the Stanford meeting where the range of spectroscopies represented was quite extensive indeed. In keeping with the past tradition, the program at Stanford also possessed a strong theoretical component. The full range of theoretical models, from the weak to the strong coupling scenarios, were discussed with focus on how various models stand up to confrontation with experiment. A special, "Critical Issues" evening session provided opportunities for lively debate on wide ranging aspects even though a consensus with regard to the right theoretical model for the cuprates continues to be elusive.

The international character of this series of conferences has grown over the years. At Stanford, some two hundred scientists from fourteen countries participated. A total of about 140 papers, invited and contributed, were presented by attendees from the United States, Japan, Canada, Germany, Switzerland, France, The Netherlands, Sweden, India, Israel, Argentina, China, Finland and Russia. The conference provided a forum for US graduate students, postdocs, and young faculty to enjoy interaction with the international community.

Members of the Organizing Committee—Mac Beasley, Dan Dessau, Fred Mueller, and Joe Orenstein, deserve a special note of thanks for the success of the Stanford meeting. Members of the Program Committee—Elihu Abrahams, Ole Andersen, Al Arko, Mac Beasley, Dan Dessau, Bob Dynes, Miles Klein, Cliff Olson, Doug Scalapino, and Hiroshi Katayama-Yoshida, were instrumental in putting together a most stimulating technical program. The continuing enthusiasm and moral support of Phil Anderson, Bob Schrieffer, and other members of the International Committee have been a source of inspiration for this series of meetings. Bob Schrieffer was especially helpful in organizing and chairing the exciting Critical Issues evening session.

This bi-annual meeting was sponsored primarily by the Stanford Synchrotron Radiation

Laboratory; we are deeply indebted to Arthur Bienenstock for his strong moral support and providing funding through SSRL/DOE. The tradition of supporting this series of conferences was continued by Argonne National Laboratory through George Crabtree, Material Science Division, and the Los Alamos National Laboratory through Don Parkin, Center for Material Science. Additional funding was provided by the Office of Naval Research and the Advanced Research Projects Agency through Donald Liebenberg and Stuart Wolf, ISTEC-SRL through S. Tanaka and S. Uchida, Lawrence Berkeley National Laboratory through Joe Orenstein, and by the Stanford University through the offices of the Dean of Research, and the School of Humanities and Sciences. The generous support of these institutions contributed substantially to the success of this conference.

Katherine Cantwell, the conference coordinator, deserves a great deal of credit for managing countless day-to-day details with exquisite efficiency and remarkable cheer. Her organizational and leadership skills were the engine that drove the conference planning forward; she has also been instrumental in putting together the present volume. The able help of Gloria Barnes contributed greatly to the smooth running of the conference. Lisa Dunn, Michelle Steger, Todd Slater, and Shirley Robinson have been most generous with their time and energy in connection with this meeting.

We are most grateful to the authors for their cooperation in providing manuscripts in a timely fashion, and to the referees for ironing out various technical details, allowing a rapid publication of this volume.

We look forward to the next Spectroscopies in Novel Superconductors meeting (SNS'97) which will be hosted by Northeastern University, to be held on Cape Cod, September 14-18, 1997.

Zhi-xun Shen
Donald Liebenberg
Arun Bansil

List of Participants

Elihu Abrahams
Rutgers University

Alexei A. Abrikosov
Argonne National Laboratory

Philipp Aebi
Université de Fribourg

Gabriel Aeppli
AT&T Bell Laboratories

James W. Allen
University of Michigan

Philip B. Allen
IRRMA, Lausanne

Ole K. Andersen
Max Planck Institut

Philip W. Anderson
Princeton University

Steven M. Anlage
University of Maryland

Ryozo Aoki
Osaka University

Josef Ashkenazi
University of Miami

Arun Bansil
Northeastern University

Bernardo Barbiellini
Helsinki University of Technology

G. Baskaran
The Institute of Mathematical Sciences

Dimitri N. Basov
McMaster University

Bertram Batlogg
AT&T Bell Laboratories

Malcolm R. Beasley
Stanford University

John Berlinsky
McMaster University

Arthur Bienenstock
SSRL

Robert J. Birgeneau
MIT

Girsh E. Blumberg
University of Illinois

Andreas Bock
Universität Hamburg

Carolus Boekema
San Jose State University

Douglas A. Bonn
University of British Columbia

Philippe Bourges
Laboratoire Léon Brillouin

Ivan Bozovic
Varian Research Center

Baird Brandow
Los Alamos National Laboratory

Nejat Bulut
University of California

Jeff M. Byers
Naval Research Laboratory

Juan Carlos Campuzano
University of Illinois

Changfeng Chen
University of Nevada

Liang Chen
Université de Sherbrooke

Paul C.W. Chu
University of Houston

Andrey V. Chubukov
University of Wisconsin

Jeffrey Clayhold
University of Houston

Marvin L. Cohen
University of California

Elbio Dagotto
Florida State University

Alex L. de Lozanne
University of Texas

Daniel S. Dessau
Stanford University

Thomas P. Devereaux
University of California

Hong Ding
University of Illinois

Sebastian Doniach
Stanford University

Rudolph Douglas
Howard University

John D. Dow
Arizona State University

Robert C. Dynes
University of California

James N. Eckstein
Varian Research Center

Hiroshi Eisaki
The University of Tokyo

Mikhail V. Eremin
Kazan State University

Alexander L. Fetter
Stanford University

Øystein Fischer
Université de Genève

Ilya M. Fishman
Stanford University

Zachary Fisk
Florida State University

Michael E. Flatté
Harvard University

Laszlo Forro
Ecole Polytechnique Fédérale

David Frenkel
University of Houston

Stuart Friedman
Stanford University

Atsushi Fujimori
University of Tokyo

H. Fukuyama
University of Tokyo

Marc Gabay
Université Paris-Sud

Theodore H. Geballe
Stanford University

Jan Genossar
Technion - I.I.T.

Satoshi Gonda
Tokyo Institute of Technology

Roy G. Goodrich
Louisana State University

R. L. Greene
University of Maryland

Rudolf Hackl
Walther-Meissner-Institut

Noriaki Hamada
JRCAT

Werner W.A. Hanke
Universität Würzburg

Walter N. Hardy
University of British Columbia

Tetsuya Hasegawa
University of Tokyo

Arthur F. Hebard
AT&T Bell Laboratories

Frank Herman
IBM Almaden Research Center

Peter J. Hirschfeld
University of Florida

Takashi Imai
MIT

Lev B. Ioffe
Rutgers University

Shoji Ishibashi
Electrotechnical Laboratory

Rittaporn Itti
Superconductivity Res. Lab.

Ove Jepsen
Max Planck Institut

Koji Kajimura
Electrotechnical Laboratory

Mikael Kall
Chalmers University of Technology

Catherine Kallin
McMaster University

Saeid Kamal
University of British Columbia

Arno P. Kampf
Universität zu Köln

Moonsoo Kang
University of Illinois

Aharon Kapitulnik
Stanford University

Satoshi Kashiwaya
Electrotechnical Laboratory

Hiroshi Katayama-Yoshida
Tohoku University

Bernhard Keimar
Princeton University

Heesang Kim
University of Guelph

Jae H. Kim
University of Groningen

David King
Stanford University

Gordon S. Kino
Stanford University

Jens Kircher
Max Planck Institut

Yoshio Kitaoka
Osaka University

Miles V. Klein
University of Illinois

Vladimir Kostour
University of Maryland

Gabriel Kotliar
Rutgers University

Vladimir Z. Kresin
LBL

Robert B. Laughlin
Stanford University

Patrick A. Lee
MIT

Thomas R. Lemberger
The Ohio State University

Kathryn Levin
The University of Chicago

Shoudan Liang
Penn State University

Donald Liebenberg
Office of Naval Research

Ingolf Lindau
Lund University

Matti J. Lindroos
Tampere University of Technology

Alexander P. Litvinchuk
Chalmers University of Technology

Dongzi Liu
University of Chicago

Anthony G. Loeser
Stanford University

Steven Louie
University of California

David W. Lynch
Iowa State University

Sadamichi Maekawa
Nagoya University

Alfred A. Manuel
Université de Genève

M. Brian Maple
University of California

Robert Markiewicz
Northeastern University

Daniel Marshall
Stanford University

Konrad Matho
CNRS-CRTBT

Vladimir Matijasevic
Delft University of Technology

Anne Matsuura
Stanford University

Laszlo Mihaly
SUNY at Stony Brook

John H. Miller
University of Houston

Andrew J. Millis
AT&T Bell Laboratories

Kathryn A. Moler
Stanford University

Hartmut Monien
ETH Zürich

Herb Mook
Oak Ridge National Laboratory

Adriana Moreo
Florida State University

Fred Mueller
Los Alamos National Laboratory

Hironaru Murakami
Osaka University

Yoshimasa Murayama
Hitachi Ltd.

Naoto Nagaosa
University of Tokyo

A.D.S. Nagi
University of Waterloo

Michael R. Norman
Argonne National Laboratory

Bruce G.A. Normand
University of Tokyo

Yukinori Ohta
Nagoya University

Clifford G. Olson
Iowa State University

N. Phuan Ong
Princeton University

Flora Onufrieva
Laboratoire Léon Brillouin

Joseph Orenstein
University of California

H. R. Ott
ETH Hönggerberg

Kathleen Paget
The Ohio State University

Chien-Hua Pao
University of Georgia

Chul-hong Park
Stanford University

Beth Parks
University of California

John D. Perkins
National Renewable Energy Lab.

Yves Petroff
E.S.R.F

David Pines
University of Illinois

Derrick M. Poirier
Iowa State University

William O. Putikka
Florida State University

Mohit Randeria
Argonne National Laboratory

Yong Ren
University of Houston

Hai-cang Ren
The Rockefeller University

T. Maurice Rice
AT&T Bell Laboratories

Carlos O. Rodriguez
IFLYSIB

Mark S. Rzchowski
University of Wisconsin-Madison

Sanjoy K. Sarker
University of Alabama

Hideaki Sawada
JRCAT

George Sawatzky
University of Groningen

Douglas Scalapino
University of California

Matthias Schabel
Stanford University

J. Robert Schrieffer
Florida State University

Bernd Schuttler
University of Georgia

Jurgen Schutzmann
Superconductivity Res. Lab., ISTEC

Zhi-Xun Shen
Stanford University/SSRL

Vitaly S. Shumeiko
Chalmers University of Technology

Neville V. Smith
LBL

Alexander Sokol
University of Illinois-Urbana

Yiqiao Song
University of California

William E. Spicer
Stanford University

Srinivas Sridhar
Northeastern University

Barbara Stadlober
Walther-Meissner-Institut

Raivo Stern
Universität Zürich

William R. Studenmund
Stanford University

T. Takahashi
Tohoku University

Jiro Tanaka
Kanagawa University

Yukio Tanaka
Niigata University

Norio Terada
Electrotechnical Laboratory

Andrew M. Tikofsky
University of California

Tom Timusk
McMaster University

Andre M. Tremblay
Université de Sherbrooke

Chang Chyi Tsuei
IBM

Eric R. Ulm
The Ohio State University

James M. Valles, Jr.
Brown University

Dirk van der Marel
University of Groningen

Chandra M. Varma
AT&T Bell Laboratories

Yury Vilk
Université de Sherbrooke

Kenneth J.E. Vos
Queens University

Russell Walstedt
AT&T Bell Laboratories

Barrett O. Wells
MIT

Gene L. Wells
Physical Review Letters

Fredrick C. Wellstood
University of Maryland

Goran P. Wendin
Chalmers University of Technology

Z.Y. Weng
University of Houston

Paul White
Stanford University

Stuart Wolf
ARPA

David Wollman
University of Illinois

Yuyi Xue
University of Houston

Victor M. Yakovenko
University of Maryland

Seiji Yunoki
Nagoya University

Yuyao Zha
University of Illinois

Shoucheng Zhang
Stanford University

Ming Zhang
Stanford University

Fu-Chung Zhang
University of Cincinnati

Zhongxian Zhao
National Lab for Superconductivity

Ping Zhou
Stanford University

Scientific Program

Wednesday, March 15, 1995

Welcome: A. Bienenstock, Director of SSRL

CRITICAL OVERVIEWS
(E. Abrahams, Rutgers University, Chair)

Some Smoking Guns for the Interlayer Theory of High T_c
P.W. Anderson: Princeton University

Materials and High T_c
Z. Fisk: Florida State University

ARPES: Novel Effect in the Energy and Momentum Distributions
J.R. Schrieffer: Florida State University

THEORY I
(M.L. Cohen, Univeristy of California, Chair)

On the Nature of the Order Parameter in HTSC
A. Abrikosov: Argonne National Laboratory

The Puzzle of Photoemission from the Zone Face of $Sr_2CuO_2Cl_2$
R.B. Laughlin: Stanford University

Systematic Solution of a Model for Cu-O Metals: Anomalous Normal State and Symmetry of the Superconducting State
C. Varma: AT&T Bell Laboratories

QUANTUM INTERFERENCE AND TUNNELING EXPERIMENTS
(J. Eckstein, Varian Research Center, Chair)

Vacuum Tunneling Spectroscopy and Asymetric Density of States of $Bi_2Sr_2CaCu_2O_{8+\delta}$
Ø. Fischer: Université de Genève

Flux Quantization in Tricrystal Cuprate Rings – a new probe of pairing symmetry
C.C. Tsuei: BM Research Center

Tunneling in Pb-YBCO Junctions: Determining the Symmetry of the Pairing State
D. Wollman: University of Illinois-Urbana

Scanning SQUID Measurements of Time-Reversal-Invariant $d_{x^2-y^2}$ Pairing in YBCO
F.C. Wellstood: University of Maryland

OPTICAL SPECTROSCOPY
(W.E. Spicer, Stanford University, Chair)

Coherent Terahertz Spectroscopy of the Vortex-State of Cuprate Superconductors
J. Orenstein: University of California

In-Plane and Out-of-Plane Charge Dynamics of High T_c Cuprates
D. Van der Marel: University of Groningen

Optical Study in High-T_c Superconductors and Related Materials
H. Eisaki: University of Tokyo

POSTER SESSION I
(D. Dessau, Stanford University, Chair)

Thursday, March 16, 1995

PHOTOEMISSION I
(N.V. Smith, Lawrence Berkeley Laboratory, Chair)

Complete Fermi Surface Mapping of Bi-Cuprates: New Results
P. Aebi: Université de Fribourg

Momentum Dependence of the Superconducting Gap in $Bi_2Sr_2CaCu_2O_8$
J.C. Campuzano: University of Illinois

Band Mapping of the Insulator $Sr_2CuO_2Cl_2$ – Dispersion of a Single Hole in an Antiferromagnetic Background
B.O. Wells: MIT

PHOTOEMISSION II
(C.G. Olson, Iowa State University, Chair)

Fermi Liquids and non-Fermi Liquids – the view from photoemission
J.W. Allen: University of Michigan

Angle-resolved Photo-Intensities in High T_c's: lineshapes, surface states, and related issues
A. Bansil: Northeastern University

Momentum Dependence of Electronic Structure and Superconducting Gap
Z.X. Shen: Stanford University/SSRL

THEORY II
(K. Levin, The University of Chicago, Chair)

Magnetic Properties of High Temperature Superconductors: a Spin Liquid Approach
L. Ioffe: Rutgers University

LISA: A first principle approach to modelling the one particle spectroscopy in strongly correlated systems
G. Kotliar: Rutgers University

The d-Wave RVB State
T.M. Rice: ETH-Hönggerberg

THEORY III
(H. Fukuyama, University of Tokyo, Chair)

Vortices in D-Wave Superconductors
C. Kallin: McMaster University

Impurity Scattering and Order Parameter Symmetry in High-T_c Superconductors
P.J. Hirschfeld: University of Florida

Spin Gaps in High Temperature Superconductors
A.J. Millis: AT&T Bell Laboratories

POSTER SESSION II
(A. Loeser, Stanford University, Chair)

Friday, March 17, 1995

TRANSPORT AND RAMAN SPECTROSCOPY
(R.L. Greene, University of Maryland, Chair)

Magnetic Field Dependence of the Specific Heat of $YBa_2Cu_3O_{6.95}$: Implications for the Vortex Structure
K.A. Moler: Stanford University

Mean Free Path of Quasi-Particles in YBaCuO
N.P. Ong: Princeton University

What Electronic Excitations are Revealed in the Electronic Raman Spectra from Cuprate Superconductors
M.V. Klein: University of Illinois-Urbana

MICROWAVE
(T. Takahashi, Tohoku University, Chair)

Surface Impedance and Transport Properties of Electron- and Hole-Doped Cuprate Superconductors
S. M. Anlage: University of Maryland

The Microwave Surface Impedance of $YBa_2Cu_3O_{(7-\delta)}$
D.A. Bonn: University of British Columbia

Pairing, Pair-breaking and Anisotropy in Microwave Experiments on Superconductors
S. Sridhar: Northeastern University

NEUTRON SPECTROSCOPY
(Z.X. Zhao, National Lab for Superconductivity, Chair)

Magnetic Neutron Scattering from High-T_c Oxides
G. Aeppli: AT&T Bell Laboratories

Spin Fluctuations in Srontium and Oxygen-doped La_2CuO_4 Superconductors
R.J. Birgeneau: MIT

Neutron Scattering from Phonons, Gap Excitations and Vortices in $YBa_2Cu_3O_7$
B. Keimer: Princeton University

Neutron Scattering Studies of the Magnetic Excitation in $YBa_2Cu_3O_7$
H. Mook: Oak Ridge National Laboratory

NMR AND POSITRON SPECTROSCOPY
(A. Kapitulnik, Stanford University, Chair)

NMR in High T_c and Related Copper Oxides
T. Imai: MIT

NMR Study in Novel Superconductors–Heavy Fermion, High T_c and Towards Spin Liquid Systems
Y. Kitaoka: Osaka University

Fermi Surfaces of High T_c Superconductors by Positron Annihilation
A.A. Manuel: Université de Genève

EVENING SESSION

(J.R. Schrieffer, Florida State University, Chair)

Doping Effect on the Temperature-Dependence of the Penetration Depth of $HgBa_2CnO_{4+\delta}$
C.W.P. Chu: University of Houston

Symmetry of the Order Parameter from Angle Resolved Photoemission
D.S. Dessau: SSRL

Josephson Tunneling and Transport in YBCO
R.C. Dynes: University of California-San Diego

Energy Gap Structure in Bilayer Oxide Superconductors
P.A. Lee: MIT

What can Photoemission and deHaas-vanAlphen Tell Us About the Superconducting Order Parameter?
M.R. Norman: Argonne National Laboratory

Experimental Evaluation of the Order-Parameter Symmetry in Cuprate Superconductors
H.R. Ott: ETH-Hönggerberg

$d_{x^2-y^2}$ Pairing and Spin Fluctuations in the Cuprate Superconductors: A Progress Report
D. Pines: University of Illinois-Urbana

The Two-Chain Hubbard Model
D. Scalapino: University of California-Santa Barbara

Unresolved Questions Regarding Spin Fluctuation Effects in High-T_c Systems
R. Walstedt: AT&T Bell Laboratories

Gap States in High HTSC by Infrared Spectroscopy
T. Timusk: McMaster University

Saturday, March 18, 1995

THEORY IV

(S. Zhang, Stanford University, Chair)

Down-Folding of LDA Band Structures to Low-Energy Hamiltonians and Applications
O.K. Andersen: Max Planck Institut

Energy Spectrum of High T_c Oxides: Two-gap Structure, Gaplessness, and Implications
V. Kresin: Lawrence Berkeley Laboratory

Pseudogaps in the van Hove Jahn-Teller Scenario
R. Markiewicz: Northeastern University

THEORY V

(S. Maekawa, Nagoya University, Chair)

Evolution of the Single-Particle Spectral Weight with Doping
N. Bulut: University of California-Santa Barbara

Flat Quasiparticle Dispersion and Shadow Bands in the Cuprates
A. Moreo: Florida State University

Magnetic Behavior of the Cuprate Oxides
A. Sokol: University of Illinois-Urbana

Quasiparticle Dispersion of the 2D Hubbard Model: From an Insulator to a Metal
W. Hanke: Universität of Würzburg

OVERVIEW OF OTHER SYSTEMS

(S. Louie, University of California, Chair)

Are there Similarities Between the Y-Ni-B-C System and the Cuprate Superconductors?
G. Baskaran: Institute of Mathematical Sciences

Unconventional Aspects of Superconductivity in the Alkali-Metal Doped Fullerenes
A.F. Hebard: AT&T Bell Laboratories

Recent Issues in the Physics of Heavy Fermion Materials
M.B. Maple: University of California-San Diego

REFLECTIONS OF THE CONFERENCE

(Z.X. Shen, Stanford University/SSRL, Chair)

<u>Experiment</u>
B. Batlogg: AT&T Bell Laboratories
M.R. Beasley: Stanford University
G.A. Sawatzky: University of Groningen

<u>Theory</u>
P.B. Allen: IRRMA
Reflections on the Superconductor-Insulator Transition
S. Doniach: Stanford University

THEORY

Pergamon

J. Phys. Chem. Solids Vol. 56, No. 12, pp. 1567–1572, 1995
Copyright © 1995 Elsevier Science Ltd
Printed in Great Britain. All rights reserved
0022–3697/95 $9.50 + 0.00

0022-3697(95)00090-9

ON THE NATURE OF THE ORDER PARAMETER IN HTSC AND INFLUENCE OF IMPURITIES

A. A. ABRIKOSOV

Materials Science Division, Argonne National Laboratory, 9700 South Cass Ave., Argonne, IL 60439, U.S.A.

Abstract—A model of superconductivity in layered high-temperature superconducting cuprates is proposed, based on the extended saddle point singularities in the electron spectrum, weak screening of the Coulomb interaction and phonon-mediated interaction between electrons plus a small short-range repulsion of Hund's or spin-fluctuation origin. This permits to explain the large values of T_c, features of the isotope effect, photoemission results for the gap and the seemingly conflicting results of Josephson experiments in various geometries. The influence of impurity scattering on T_c, the order parameter at $T = 0$ and the density of states, including the energy gap, are studied for the same model. It is shown that the suppression of the gap in the vicinities of the singularities is weak, and the same is true for T_c. Since the order parameter beyond the singularity is still defined by its value in the singular region, it scales with this value and varies only slightly. However, the energy gap in this region, which does not coincide with the order parameter, varies rapidly with impurity concentration, and the gap becomes isotropic in the strong scattering limit. These conclusions agree with preliminary experimental observations.

The origin and the symmetry of the order parameter in the HTSC have become the hottest topic in the physics of high-temperature superconductors. Unfortunately only a few models are discussed, namely the so called *s*-pairing, when the order parameter has no nodes along the Fermi surface, and the so called *d*-pairing, when the order parameter in the *ab*-plane is believed to be proportional to $\cos k_x - \cos k_y$. Actually the symmetry, even if it is assumed tetragonal, and the order parameter is assumed to be real (this follows from time-reversal symmetry), requires only that at a $\pi/2$ rotation in the *ab*-plane it either does not change, or changes its sign. Symmetry by itself does not tell us how many nodes must exist in either case, or whether the formula $\cos k_x - \cos k_y$ is correct. Therefore the only way to find the order parameter is to study the interaction between electrons, which leads to pairing. The high values of T_c and absence of the isotope effect in YBCO(7) led to the conclusion that this interaction cannot be mediated by phonons. However the experiments by the groups of Franck and Morris [1, 2] showed that a partial substitution of Y by Pr, or of Ba by La leads to the increase of the isotope effect simultaneously with the decrease of the critical temperature, so that at $T_c \approx 40$ K, $\alpha \approx 0.4 (T_c \propto M^{\alpha})$ (Fig. 1). An alternative appears: either these substituted compounds have a different mechanism of superconductivity compared to YBCO(7) with $T_c \approx 90$ K, or the mechanism is always phonons, and the absence of the isotope effect in YBCO(7) is due to something else. I favor the last option.

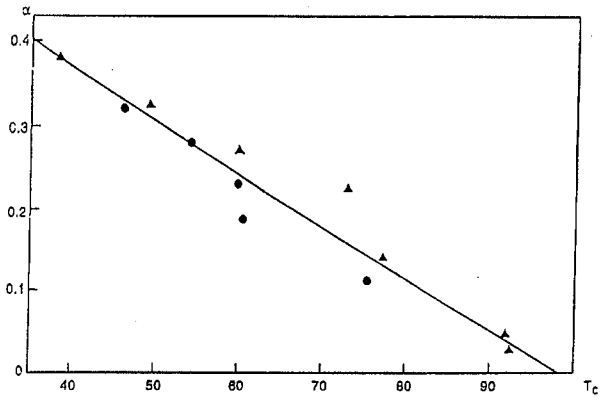


Fig. 1. Experimental results for the isotope shift ($O_{16} \rightarrow O_{18}$) in partially substituted YBCO (Y→ Pr, and Ba → La). The exponent α in $T_c \propto M^{\alpha}$ is presented as function of T_c together with the linear regression.

Not long ago, two experimental groups, Campuzano *et al.* from Argonne [3] and Shen *et al.* from Stanford [4], investigating angle resolved photoemission spectra (ARPES), discovered that the dependence of the energy of quasiparticles on their momentum $\epsilon(k_x, k_y)$ (the dependence on k_z is weak due to quasi-two-dimensionality) has flat regions, where it does not depend on one of the components, so that the spectrum becomes quasi-one-dimensional in these regions (Fig. 2). This was first discovered in YBCO(123), YBCO(124), BiSCCO(2212), and appeared also in band structure calculations by several groups, particularly, Freeman *et al.* [5], for mercury compounds. Such a spectrum was called "extended saddle point singularity". The density of states in the vicinity of such a singularity is proportional to $(\epsilon - \epsilon_0)^{-1/2}$. If the Fermi energy is close to ϵ_0, this enhancement is more than sufficient to explain the high values of T_c assuming the usual strength of the electron–phonon interaction.

The second feature is that the integral entering the BCS equation

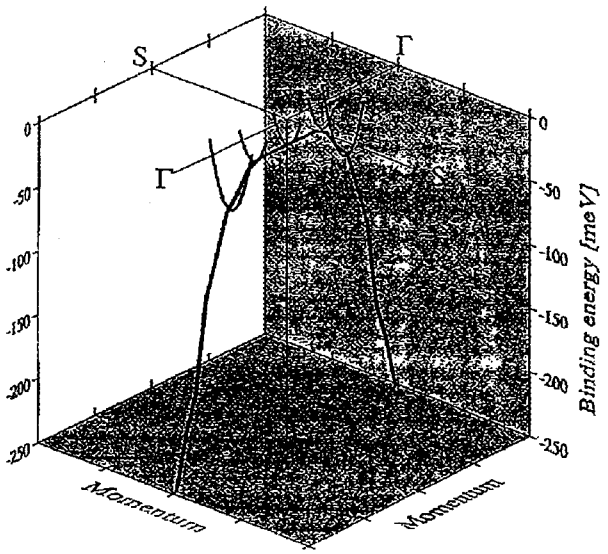


Fig. 2. ARPES result for the dependence of quasiparticle energy on components of quasimomentum in the vicinity of the extended saddle point singularity.

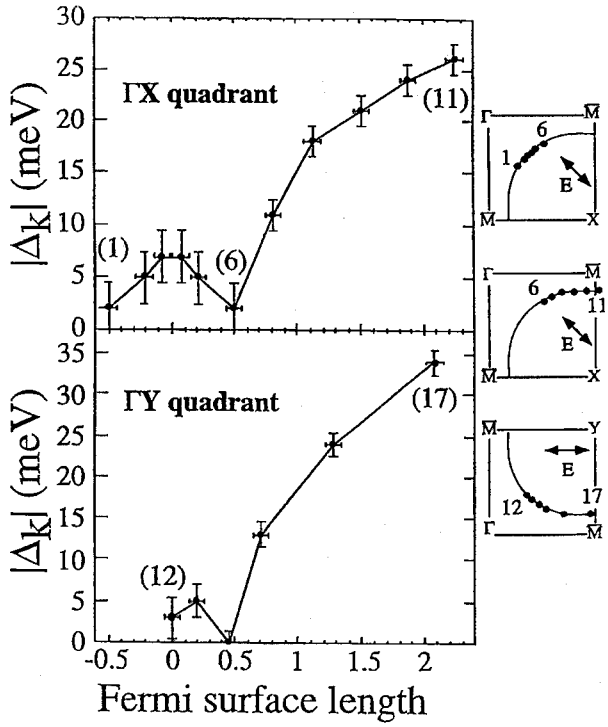


Fig. 3. ARPES result on the dependence of the superconducting energy gap on the momentum at the Fermi surface. The correspondence is established by numbers at the plot and at inserts.

$$\Delta(\mathbf{p}) = \int K(\mathbf{p}, \mathbf{p}') f[\Delta(\mathbf{p}')] \mathrm{d}^3\mathbf{p}' / (2\pi)^3 \qquad (1)$$

which is logarithmically divergent if the density of states is constant, becomes convergent, and in case $\epsilon_F - \epsilon_0 \ll \omega_0$, ω_0 being some characteristic phonon frequency, the

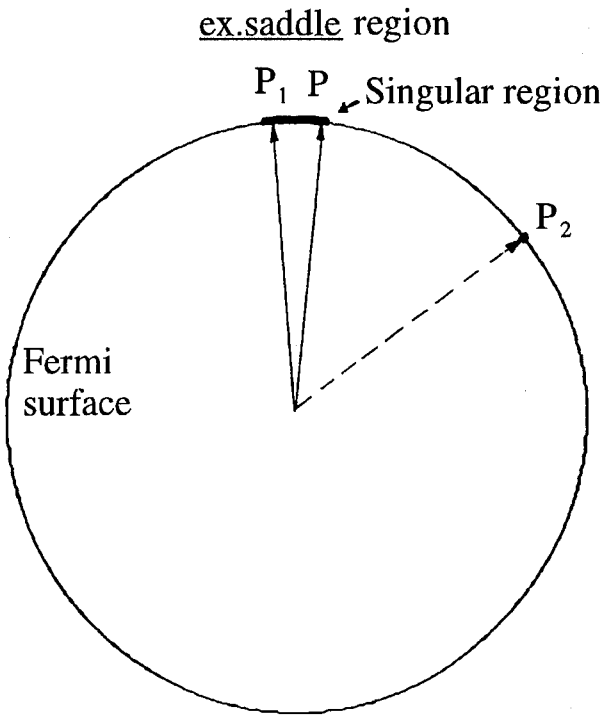


Fig. 4. Fermi surface with a singular region with a high density of states. A short range interaction connects any point with the singular region, whereas a long range interaction connects only points within this region.

critical temperature does not depend on ω_0, and hence there is no isotope effect. The BCS-type formula for T_c for this case has the form:

$$T_c = \frac{8\gamma(\epsilon_F - \epsilon_0)}{\pi} \exp\left[-\frac{4\sqrt{2}\pi^2(n-1)(\epsilon_F - \epsilon_0)^{1/2}}{g m_x^{1/2} \kappa^2}\right] \qquad (2)$$

Most important here is the appearance of $\epsilon_F - \epsilon_0$ in the exponent and in the prefactor (I will not explain the meaning of other notations in this expression). If the distance $\epsilon_F - \epsilon_0$ increases, T_c decreases, and gradually ω_0 replaces $\epsilon_F - \epsilon_0$ in the prefactor, enhancing the isotope effect [6]. This fits the experimental data.

I would like to stress that the usual saddle point singularity, extensively studied by several groups, e.g. Friedel, Labbe, Bok, Newns and Markievicz (see Ref. [7] for quotations) does not lead to such consequences. The enhancement of T_c is weak, and no new energy scale is introduced in the BCS integral, so that the absence of the isotope effect cannot be explained. Therefore, the statement that the flat regions are equivalent to 2D van Hove singularities is wrong.

Under proper assumptions the flat region can dominate in the total density of states; then, however, we encounter another puzzle. The ARPES experiments of the same groups and of Onellion *et al.* group in Wisconsin [8–10] on BiSCCO(2212) established a marked anisotropy of the energy gap (in the BCS theory the gap corresponds to the absolute value of the order parameter). This was first interpreted in favor of *d*-pairing but more precise measurements by Cam-

puzano and his colleagues established a different gap behavior with more nodes (Fig. 3). The usual belief is that with phonon-mediated interaction no anisotropy of the order parameter can be obtained, even if the energy spectrum of the metal is anisotropic. This is due to exchange of phonons with high momenta which effectively connect all points of the Fermi surface in the BCS equation (1) (see Fig. 4).

However, this is true for good metals but the substances under consideration, according to numerous experimental data, are intermediate between metals and ionic crystals. The cross-over between these two limiting cases can be imagined as the change of the Debye screening radius from interatomic distances to infinity, and the HTSC can be viewed as substances where all Coulomb-based interactions are screened at large distances. This refers also to the electron attraction mediated by phonons, since it is due to the electron–ion interaction. Therefore it is reasonable to assume this interaction in the form

$$V(k) = g\left(\frac{\kappa^2}{k^2+\kappa^2}\right)^n \frac{\omega^2(k)}{(\xi-\xi')^2-\omega^2(k)} \qquad (3)$$

where $\kappa \ll K$ is the reciprocal Debye radius, ξ is the electronic energy, and K the reciprocal lattice period. Since different models lead to different powers n, we will simply assume $n > 1$. Under such circumstances the exchange of phonons with small momenta becomes dominant, and we cannot reach the singular region from some distant place (Fig. 4) without decreasing drastically the value of the order parameter. Therefore it becomes very anisotropic, and its maxima are located in the regions with the maximal density of states [11], which in fact is observed in experiment. Moreover the values, distant from the singular regions, will be defined by the maximal value, the connection being established through the BCS equation. Therefore the critical temperature is defined only by this singular region.

In a purely phonon picture there can be no changes of sign of the order parameter, and this is in contradiction to many reliable experimental data. However, apart from phonons, there can exist interactions of some other origin. The isotope effect tells us that the phonons dominate. Therefore these other interactions can become important only if their nature differs substantially from the phonon-mediated attraction. We will assume that this additional interaction is a short-range repulsion coming either from spin fluctuations, or being the renormalized repulsion at the Cu sites. Far from the singular regions, where the influence of the phonon attraction is damped by the large momentum difference, the short-range repulsion can take over. The order parameter in these regions will be defined, as before, by its value in the singular region but the connection will have a different sign. We arrive at the formula [12]

$$\frac{\Delta(\phi)}{\Delta_1} = \frac{2(n-1)P_{0y}}{\kappa^2 d} \times \left\{\left(\frac{\kappa}{2p_0}\right)^{2n}\left[\sin^{-2n}\left(\frac{\phi}{2}\right)+\sin^{-2n}\left(\frac{\phi-\phi_0}{2}\right)\right]-\frac{U}{g}\right\},$$

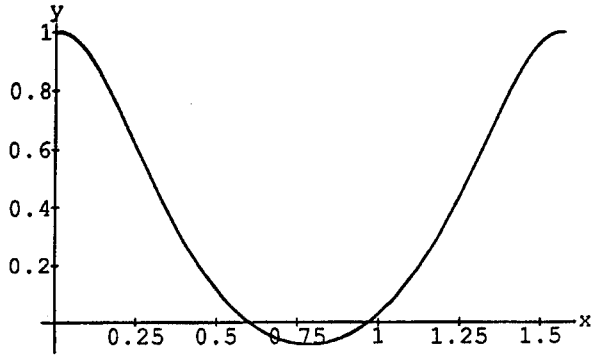


Fig. 5.

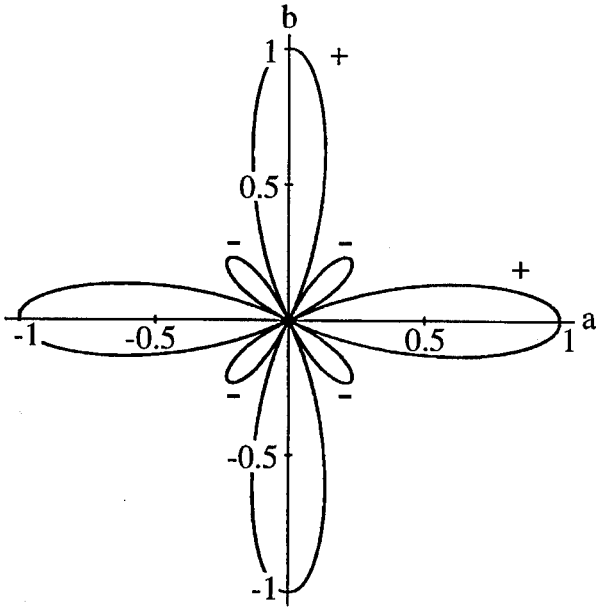


Fig. 6. Polar plot representing the shape of Δ in BiSCCO.

where Δ_1 is the order parameter in the singular region, P_{0y} is the length of the singularity, d is the period in the c-direction, p_0 is the radius of the Fermi surface, which we assume cylindrical, 0 and ϕ_0 are the locations of singularities, and U is the amplitude of the short-range repulsion, which we suppose isotropic. This formula is valid far from the singular region. A simple interpolation permits to describe the whole Fermi surface. Figure 5 presents the plot for some specific choice of constants. The absolute value coincides qualitatively with the results by Campuzano *et al.* [9].

The region with a negative order parameter can appear between two maxima. For BiSCCO, where the deviation from tetragonal symmetry is small, there are four maxima displaced by $\pi/2$, and the negative regions can be in the vicinity of $\pi/4$ (Fig. 6). In YBCO, where the chains destroy the singularities in the b-direction, there are only two maxima displaced by π. Therefore in the latter case the negative

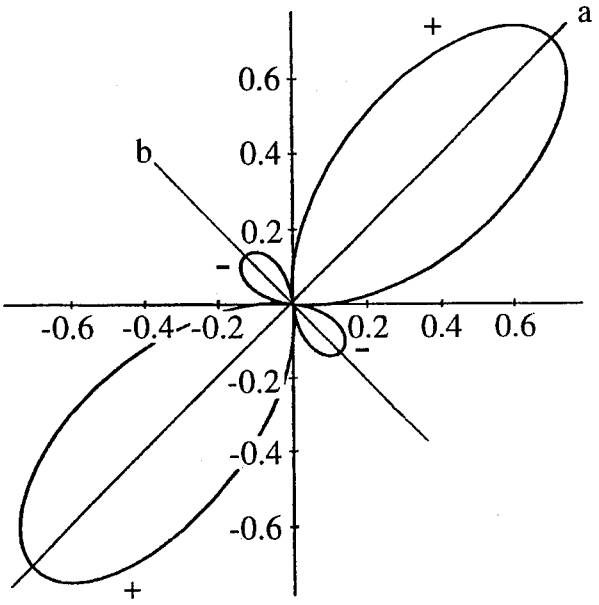


Fig. 7. Polar plot representing the shape of Δ in YBCO.

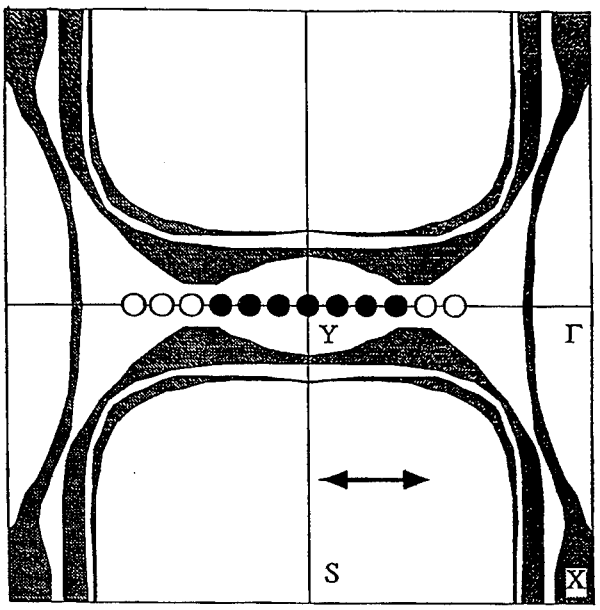


Fig. 9. The Fermi surfaces in $YBa_2Cu_4O_8$.

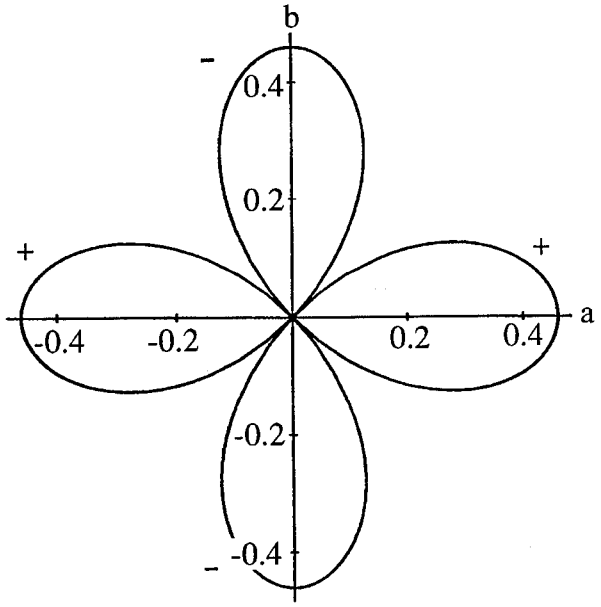


Fig. 8. Polar plot representing the shape of Δ in the d-wave theory.

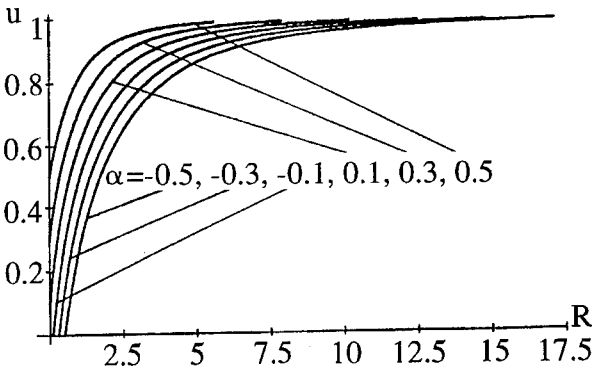


Fig. 10. The minimal gap as function of impurity concentration: $u = E_{g\,min}/\Delta_1$, $R = 1/2\tau_1\Delta_1$, Δ_1 being the maximal gap, and $1/\tau_1$ the scattering probability to the singular region. Here $\alpha = \Delta_{min}/\Delta_1$, where Δ_{min} is the minimal value of the order parameter. In the case, of $\alpha < 0$, the minimal gap is zero up to a certain impurity concentration; then it grows up to the maximal value, and the gap becomes isotropic. In the opposite case the gap starts from a finite value.

values can be expected in the b-direction (Fig. 7), which fits the Josephson-type experiments of the groups of Van Harlingen [13] and Kirtley and Tsuei [14]. On the other hand, since $\int \Delta d\phi \neq 0$ (contrary to the d-paring), there should be a Josephson current in the c-direction, as it follows from experiments by the group of Dynes and Maple [15]. Figure 8 represents, for comparison, the d-pairing case.

According to the present theory, the difference between BiSCCO and YBCO is associated with the orthorombicity of the electron spectrum of the latter (see Fig. 9), which is rather strong, contrary to the difference in lattice periods. The destruction of chains by oxygen depletion makes the system more tetragonal, and the order parameter has to be changed into something closer to BiSCCO, although this change can happen discontinuously with oxygen concentration.

One of the most interesting features is the behavior of the order parameter with increasing impurity concentration. It can be shown (Hirschfeld *et al.* [16]) that in case of d-pairing an arbitrary concentration of impirities makes the substance gapless. This seems to contradict the photoemission data, although these results are preliminary. I will describe what happens in the present model [17]. First of all, the impurities are most likely ionized, and hence their potential acting on

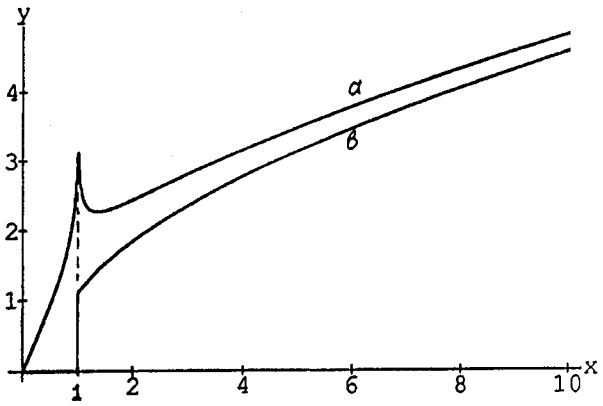


Fig. 11. The density of states as function of energy in the region of energies, small compared to Δ_1. Curve *a* corresponds to a zero minimal gap, and curve *b* to a finite minimal gap. The units are defined by details of the model.

the electrons is a weakly screened Coulomb potential, which leads to small-angle scattering. It is easy to understand that for such a scattering the Anderson theorem is correct, even for an anisotropic metal, i.e. scattering does not affect thermodynamic quantities.

However, even such impurities also give a large angle scattering, although with a much smaller probability; additionally, there can exist neutral defects. For these reasons we will disregard small-angle scatterers and consider a model with a certain concentration of isotropic scatterers. The technique of calculations is a slight modification of the one used by Gor'kov and myself for superconductors with magnetic impurities [18].

Here one has to take into account that the scattering probability is proportional to the density of the final states. In order to produce any changes in the singular region the electrons have to be scattered out of this region, i.e. to come to the regions with much smaller density of states. On the other hand the electrons in the external regions can be scattered into the singular region having a high density of states. Therefore the changes in the singular region are likely to be small, whereas the changes in the regions of the Fermi surface, corresponding to small values of the order parameter, are likely to be much larger.

Since the critical temperature is defined by the vanishing of the maximal order parameter, it is affected rather weakly. The asymptotic values of T_c are

$$T_c \approx \begin{cases} T_{c0} - \pi/(8\tau_0), & \tau_1^{-1} \ll T_{c0} \\ T_{c0}(\pi\tau_1 T_{c0}/\gamma)^{\tau_1/\tau_0}, & \tau_1^{-1} \gg T_{c0} \end{cases} \tag{4}$$

where τ_0^{-1} is the small probability of scattering out of the singular region, τ_1^{-1} is the "large" probability of scattering into the singular region $\gamma = 1.78$; T_{c0} is T_c for a clean metal.

Rather similar formulas describe the variation of the order parameter at the maximum. The asymptotic values are

$$\Delta_1 \approx \begin{cases} \Delta_{1(0)} - 1/(2\tau_0) & \tau_1^{-1} \ll \Delta_{1(0)} \\ \Delta_{1(0)}(e\tau_1\Delta_{1(0)})^{\tau_1/\tau_0}, & \tau_1^{-1} \gg \Delta_{1(0)} \end{cases} \tag{5}$$

Comparing the limiting formulas (5) and (6) we obtain for the ratio $2\Delta_1/T_c$:

$$\frac{2\Delta_1}{T_c} \approx \frac{2\Delta_{1(0)}}{T_{c0}} + \left(\frac{\pi}{8}\frac{2\Delta_{1(0)}}{T_{c0}} - 1\right)(\tau_0 T_{c0})^{-1}$$
$$\approx \frac{2\Delta_{1(0)}}{T_{c0}} + (0.3 \div 0.5)(\tau_0 T_{c0})^{-1}, \quad (\tau_1 T_{c0})^{-1} \ll 1,$$
$$\frac{2\Delta_1}{T_c} \approx \frac{2\Delta_{1(0)}}{T_{c0}}\left(\frac{e\gamma}{\pi}\frac{\Delta_{1(0)}}{T_{c0}}\right)^{\tau_1/\tau_0}$$
$$\approx \frac{2\Delta_{1(0)}}{T_{c0}}(2.7 \div 3)^{\tau_1/\tau_0}, \quad (\tau_1 T_{c0})^{-1} \ll 1.$$

We see that this ratio grows with impurity concentration and then saturates (the ratio τ_1/τ_0 is constant).

It can be shown that the maximal value defines the order parameter at any place of the Fermi surface, and the connection is given by eqn (4) at any temperature and impurity concentration. This means that the order parameter over the whole Fermi surface keeps its shape and scales with the value at the maximum. In particular, the nodes remain at the same locations.

This however is not true for the density of excited states, and, particularly, for the gap in the energy spectrum. The density of states is defined by the formula

$$\nu(\omega) = -\frac{1}{\pi}\mathrm{Im}\int G^R(\mathbf{p}, \omega)\frac{\mathrm{d}^3\mathbf{p}}{(2\pi)^3} \tag{6}$$

where $G^R(\mathbf{p}, \omega)$ is the retarded Green function. Here we obtain

$$\frac{\nu(\omega)}{\nu_{on}} = \mathrm{Im}\int \frac{u[1 + Q(u)]\mathrm{d}\phi/(2\pi)}{\{[\Delta(\phi)/\Delta_1 + Q(u)]^2 - u^2[1 + Q(u)]^2\}^{1/2}} \tag{7}$$

where

$$\nu_{on} = \frac{p_0}{\pi d v_0},$$
$$u = \omega/\Delta_1,$$
$$Q(u) = \left[2\tau_1\Delta_1\sqrt{1 - u^2}\right]^{-1};$$

ν_{on} is the density of states of a normal metal with a cylindrical Fermi surface.

From this formula we can obtain the energy gap for a given ϕ. The limiting formulas for the energy gap E_g far from the maximum are: in the case if $(2\tau_1)^{-1} \ll \Delta_1$

$$E_g = \Delta(\phi) + (2\tau_1)^{-1},$$
$$E_g = -\Delta(\phi) - (2\tau_1)^{-1} \tag{8}$$

The latter formula applies only in the case, if

$$\Delta(\phi)_{\min} < -(2\tau_1)^{-1}$$

and only for those values of ϕ which give positive values of E_g. In the opposite case, $(2\tau_1)^{-1} \gg \Delta_1$, $\Delta(\phi)$ is positive everywhere, and we obtain

$$E_g \approx \Delta_1\left[1 - 16\tau_1^2(\Delta_1 - \Delta(\phi))^2\right]. \tag{9}$$

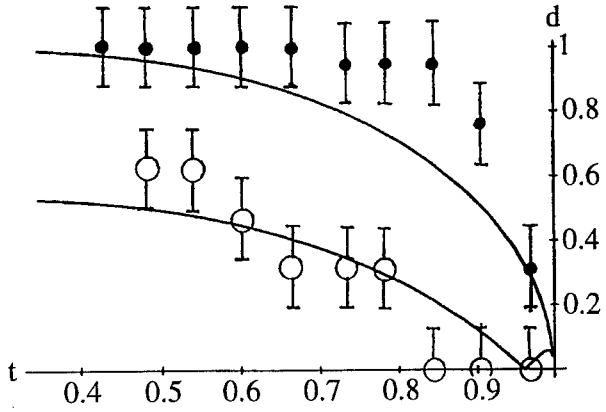


Fig. 12. The temperature dependence of the gap in BiSCCO defined for the maximal gap and for the gap in the median direction between two maxima. The theoretical fit is defined for a small but finite impurity concentration.

The results are plotted in Figs 10 and 11. Figure 10 gives the variation of the minimal gap with impurity concentration. For the case, when the order parameter changes sign, the minimal gap for a clean substance is zero. It starts to deviate from zero at a certain impurity concentration and gradually approaches the absolute value of the maximal order parameter, i.e. the gap becomes isotropic. The same trend exists for the case, when the sign of the order parameter does not change. Then the minimal gap starts from some finite value and grows until it reaches the maximal value. Figure 11 shows the plot of the density of states as function of energy for these two cases. In the case, when the minimal gap is zero, the variation starts linearly, which leads to the linear variation of the penetration depth with temperature observed by the group of Hardy *et al.* .

There are also interesting consequences concerning the variation of the gap at various angles with temperature and impurity concentration. Onellion *et al.* [19] measured the gap in the clean and impure BiSCCO. The measurements were done at the maxima and in the middle between them. A rapid increase of the latter value was observed with impurity concentration and also a peculiar temperature dependence. Figure 12 presents their data together with a theoretical fit.

Note added in proof. Since March 1995, when this talk was given, several new results were obtained. Revised interpretation of the ARPES data led to the disappearance of the maximum in the (π, π) direction at Fig. 3. This created the possibility of an order parameter, having a d-wave symmetry (but not the shape $k_x^2 - k_y^2$ [20]). A criterion was established distinguishing the s-wave and d-wave options. It was shown that the sign change of the order parameter is possible only within the d-wave option. The order parameter, plotted at Fig. 5, does not correspond to the minimal energy. The results with impurities remain correct for the s-wave symmetry where the order parameter never changes its sign.

Acknowledgements—I would like to thank J.-C. Campuzano, J. Franck and M. Onellion for communicating their data prior to publication and for valuable discussions. This work was supported by the Department of Energy under the contracts # W-31-109-ENG-38.

REFERENCES

1. Franck J. P. et al., *Physica B* **169**, 697 (1991); Franck J. P. *et al.* , *Phys. Rev. B* **44**, 5318 (1991).
2. Bornemann H. J. and Morris D. E., *Phys. Rev. B* **44**, 5322 (1991).
3. Abrikosov A. A., Campuzano J. C. and Gofron K., *Physica C* **214**, 73 (1993); Gofron K. *et al.* , *Phys. Rev. Lett.* **73**, 3302 (1994).
4. Dessau D. S. *et al.* , *Phys. Rev. Lett.* **71**, 2781 (1993)
5. Novikov D. L. and Freeman A. J., *Physica C* **212**, 233 (1993); *ibid.* **216**, 273 (1993)
6. Abrikosov A. A., *Physica C* **233**, 102 (1994).
7. Pattniak P. C. *et al.* , *Phys. Rev. B* **45**, 5714 (1992).
8. Shen Z. -X. *et al.* , *Phys. Rev. Lett.* **70**, 1553 (1993)
9. Ding H. *et al.* , *Phys. Rev. Lett.* , in press.
10. Kelley R. J. *et al.*, *Phys. Rev. B* **50**, 590 (1994).
11. Abrikosov A. A., *Physica C* **222**, 191 (1994).
12. Abrikosov A. A., *Phys. Rev.*, in press.
13. Wollmann D. A. *et al.* , *Phys. Rev. Lett.* **71**, 2134 (1993).
14. Tsuei C. C. *et al.*, *Phys. Rev. Lett.* **73**, 593 (1994).
15. Sun A. G. *et al.*, *Phys. Rev. Lett.* **72**, 2267 (1994).
16. Hirschfeld P. J. and Goldenfeld N., *Phys. Rev. B* **48**, 4219 (1993); Borkovski L. S. and Hirschfeld P. J., *Phys. Rev. B* **49**, 15404 (1994).
17. Abrikosov A. A., *Physica C*, in press.
18. Abrikosov A. A. and Gor'kov L. P., *Soviet Phys. JETP* **12**, 1243 (1961).
19. Ma J. *et al.*, preprint.
20. Abrikosov A. A., *Phys. Rev. B*, in press.

Pergamon

J. Phys. Chem. Solids Vol. 56, No. 12, pp. 1573–1591, 1995
Copyright © 1995 Elsevier Science Ltd
Printed in Great Britain. All rights reserved
0022-3697/95 $9.50 + 0.00

0022-3697(95)00269-3

LDA ENERGY BANDS, LOW-ENERGY HAMILTONIANS, t', t'', $t_\perp$ (k), and $J_\perp$.

O. K. ANDERSEN, A. I. LIECHTENSTEIN, O. JEPSEN and F. PAULSEN
Max-Planck Institut für Festkörperforschung, D-70569 Stuttgart, Germany

Abstract—We describe the LDA band structure of $YBa_2Cu_3O_7$ in the $\epsilon_F \pm 2$ eV range using orbital projections and compare with $YBa_2Cu_4O_8$. Then, the high-energy and chain-related degrees of freedom are integrated out and we arrive at two, nearest-neighbor, orthogonal, two-center, 8-band Hamiltonians, H_8^+ and H_8^-, for respectively the even and odd bands of the bi-layer. Of the 8 orbitals, $Cu_{x^2-y^2}$, $O2_x$, $O3_y$, and Cu_s have σ character and Cu_{xz}, Cu_{yz}, $O2_z$, and $O3_z$ have π character. The roles of the Cu_s orbital, which has some Cu_{3z^2-1} character, and the four π orbitals are as follows: Cu_s provides 2nd- and 3rd-nearest-neighbor (t' and t'') intra-plane hopping, as well as hopping between planes ($t_\perp$). The π-orbitals are responsible for bifurcation of the saddle-points for dimpled planes. The 4-σ-band Hamiltonian is generic for flat CuO_2 planes and we use it for analytical studies. The $\mathbf{k}_\parallel$-dependence is expressed as one on $u \equiv \left(\cos bk_y + \cos ak_x\right)/2$ and one on $v \equiv \left(\cos bk_y - \cos ak_x\right)/2$. The latter arises solely through the influence of Cu_s. The reduction of the σ-Hamiltonian to 3- and 1-band Hamiltonians is explicitly discussed and we point out that, in addition to the hoppings commonly included in many-body calculations, the 3-band Hamiltonian should include hopping between *all* 2nd-nearest-neighbor oxygens and that the 1-band Hamiltonian should include 3rd-nearest-neighbor hoppings. We calculate the single-particle hopping between the planes of a bi-layer and show that it is generically: $t_\perp\left(\mathbf{k}_\parallel\right) \approx 0.25\,\text{eV}\cdot v^2\left(1 - 2ut'/t\right)^{-2}$. The hopping through insulating spacers such as (BaO)Hg(BaO) is an order of magnitude smaller, but seems to have the same $\mathbf{k}_\parallel$-dependence. We show that the inclusion of t' is crucial for understanding ARPES for the anti-ferromagnetic insulator $Sr_2CuO_2Cl_2$. Finally, we estimate the value of the inter-plane exchange constant $J_\perp$ for an un-doped bi-layer in mean-field theory using different single-particle Hamiltonians, the LDA for $YBa_2Cu_3O_6$, the eight- and four-band Hamiltonians, as well as an analytical calculation for the latter. We conclude that $J_\perp \sim -20$ meV.

1. INTRODUCTION

For the HTSC materials practitioners of the LDA now basically agree about their results. The major uncertainties come from the compositional and structural data rather than from the computational techniques. For the various materials, the energy bands originating from the CuO_2-planes are fairly similar, merely the position of the Fermi level changes.

For stoichiometric HTSCs such as $YBa_2Cu_3O_7$ the LDA has been successful in reproducing or predicting normal-state structural and phononic properties [1–3], optical excitation spectra at high energies ($\hbar\omega > 1$ eV for metals, $\hbar\omega >$ 3 eV for Mott-Hubbard insulators) [4], and k_z-averaged Fermi surfaces $\epsilon\left(\mathbf{k}_\parallel\right)=0$ for the metals [5,3]. The most surprising LDA prediction for HTSC's with dimpled CuO_2 planes ($YBa_2Cu_3O_7$ [1,3], $YBa_2Cu_3O_{6.5}$ [6]) has been that of bifurcated saddle-points close to the Fermi level. *Extended* saddle-points near ϵ_F were subsequently found in ARPES [7], but whether these are related to the bifurcated LDA saddle-points through "Fermion condensation" [8], or are caused by anti-ferromagnetic spin-fluctuations [9,10], or are due to surface effects [11], remains to be seen. The LDA has finally provided reasonable estimates of the electron-electron (e.g. $U_{\text{Cu }d} \sim 7$ eV) [12–14] and electron-phonon interactions (e.g. $\lambda_{e-ph} \sim 1$ and softening of the Raman-active dimpling modes for $T < T_C$) [1,15,3,16]. $\lambda_{e-ph} \sim 1$ might account for $T_c < 40$ K, but hardly for 100 K.

However, the LDA band structures for HTSCs are complicated, rarely interpreted, not accurate – or even relevant – below 50 meV, and are not delivered in a form useful as the single-particle term of a correlated model Hamiltonian which describes the low-energy excitations. As a result, most theorists neglect the LDA band structure, or at least its non-trivial details, and use the simplest possible Cu-Cu one-band, two-center, orthogonal, tight-binding model with hopping integrals t and t' between only nearest and next-nearest Cu neighbors (see Eq. (16)). A few brave theorists [10,9] use the Emery three-band model.

We have therefore integrated out of the LDA band structure for $YBa_2Cu_3O_7$ the high-energy and chain-related degrees of freedom. In a first step we used the LMTO down-folding technique [17] to derive a two-dimensional, *nearest-neighbor,* two-center, orthogonal, tight-binding Hamiltonian with *eight* orbitals per CuO_2 plane [18]. Of these eight CuO_2 orbitals, four ($Cu_{x^2-y^2}$, $O2_x$, $O3_y$, and Cu_s) have σ character and four (Cu_{xz}, Cu_{yz}, $O2_z$, and $O3_z$) have π character with respect to the plane. Comparisons with full LDA bands calculated for other structurally well-characterized HTSC materials convinced us, that this eight-band Hamiltonian is generic for LDA plane bands.

The present paper starts with a qualitative description of the *full* LDA band structure for $YBa_2Cu_3O_7$ and $YBa_2Cu_4O_8$ in the $\epsilon_F \pm 2$ eV region and emphasizes the

chain-related features. Then we proceed with a quantitative description of the *plane bands* by means of the eight-band Hamiltonian. The roles of the Cu_s orbital, which possesses some Cu_{3z^2-1} character, and the four π-orbitals are specifically explained: Cu_s provides 2nd- and 3rd-nearest-neighbor (t' and t'') intra-plane hopping, as well as hopping between planes ($t_\perp$). The π-orbitals are responsible for bifurcation of the saddle-points. We explicitly show how further high-energy degrees of freedom may be integrated out. The four σ-bands are studied analytically. Their $\mathbf{k}_\parallel$-dependence is most simply expressed as one on $u \equiv (\cos bk_y + \cos ak_x)/2$ and one on $v \equiv (\cos bk_y - \cos ak_x)/2$, where the latter arises solely through the influence of Cu_s. The reduction of the σ-band Hamiltonian to the commonly used 3- and 1-band Hamiltonians is explicitly discussed, and we point out that, to be consistent with the LDA bands, the former should include hopping between *all* 2nd-nearest-neighbor oxygens and the latter should include 3rd-nearest-neighbor hopping. As a first simple application, we calculate the single-particle hopping between the planes of a bilayer and show that it is generically $t_\perp(\mathbf{k}_\parallel) \sim 0.25\ \text{eV} \cdot v^2 (1 - 2ut'/t)^{-2}$. The hopping through insulating spacers such as (BaO)Hg(BaO) is an order of magnitude smaller, but seems to have the same $\mathbf{k}_\parallel$-dependence. These hopping integrals are relevant for c-axis transport and their squares enter the Inter-layer Pair-Tunnelling model [19]. Then we show that the inclusion of t' is crucial for understanding ARPES [20] for the anti-ferromagnetic insulator $Sr_2CuO_2Cl_2$. Finally, we estimate the value of the inter-plane exchange constant $J_\perp$ for a non-doped bi-layer in mean-field theory using different single-particle Hamiltonians, the LDA for $YBa_2Cu_3O_6$, the eight- and four-band Hamiltonians, as well as an analytical evaluation for the latter. We conclude that $J_\perp \sim -20$ meV.

2. LDA BAND STRUCTURES OF $YBa_2Cu_3O_7$ AND $YBa_2Cu_4O_8$.

The full LDA band structure for $YBa_2Cu_3O_7$ [3] between the $\mathbf{k}_\parallel$ points $(0,0)$, $\left(\frac{\pi}{a}, 0\right)$, $\left(\frac{\pi}{a}, \frac{\pi}{b}\right)$, $\left(0, \frac{\pi}{b}\right)$, $(0,0)$, and $\left(\frac{\pi}{a}, \frac{\pi}{b}\right)$ is shown in Fig. 1 for k_z=0 (ΓXSYΓS), and in Fig. 2 for $k_z = \frac{\pi}{c}$ (ZURTZR). Also shown are the cross-sections of the Fermi surface with the k_z=0 and $\frac{\pi}{c}$ planes. Each of the small subfigures gives the projection onto a particular O p or Cu d orbital: The radius of the circle around the $\epsilon_n(\mathbf{k}_\parallel)$-point is proportional to the weight of that orbital in $\psi_n(\mathbf{k}_\parallel)$. Note that Cu and O orbitals have different normalizations in the figures so that weights cannot be compared *between* copper and oxygen. O3 are the plane-oxygens running along b, which is the direction of the chain. O2 are plane-oxygens along a, Cu2 are plane coppers, O4 apical- and O1 chain-oxygens, and Cu1 are chain-coppers.

The FS has four sheets denoted **a, b, c,** and **s**. The essential wave functions for the **a** and **b** sheets are respectively the **a**ntibonding (odd, –) and **b**onding (even, +) linear combinations for the bilayer of the *plane* $pd\sigma$ anti-bonding orbitals ($O2_x$–$Cu2_{x^2-y^2}$–$O3_y$). Essential for the **c** sheet is the *chain* $pd\sigma$ anti-bonding orbital made from $O1_y$ and the $pd\sigma$ anti-bonding dumbbell orbital ($O4_z$–$Cu1_{z^2-y^2}$–$O4_z$). Note that the orbitals denoted z^2 in the figures are d_{3z^2-1} and that $d_{z^2-y^2} = \left(\sqrt{3}d_{3z^2-1} + d_{x^2-y^2}\right)/2$. The orbitals essential for the **s** sheet, the small stick pocket along SR, are two out of the of the three *chain* $pd\pi$ orbitals, which are the two $pd\pi$ anti-bonding dumbbell orbitals ($O4_x$–$Cu1_{xz}$–$O4_x$ and $O4_y$–$Cu1_{yz}$–$O4_y$) plus the anti-bonding linear combination of $O1_z$ with the $pd\pi$ bonding dumbbell orbital $O4_y$–$Cu1_{yz}$–$O4_y$. The anti-bonding linear combination of the two latter orbitals, which both involve $O4_y$, is the essential wave function for the **s**tick.

If the one-electron wave functions stay coherent from chain to chain, as it is assumed in the LDA for a perfect crystal, then for k_z=0 there is neither hybridization between the **a** and **c** sheets, nor between the **b** and **s** sheets. Conversely, for $k_z = \frac{\pi}{c}$ there is neither hybridization between the **b** and **c** sheets nor between the **a** and **s** sheets. For a general k_z, all chain-plane hybridizations are allowed and give rise to a k_z-dispersion of several hundred meV's.

The Fermi level is approximately 20 meV above the odd plane-band saddle-points, which are bifurcated away from X and Y to respectively $X \pm \frac{1}{4}\Gamma X$ and $Y \pm \frac{1}{3}\Gamma Y$. Since $b/a \approx 1.015$ and since the ratio between the $Cu2_{x^2-y^2}$–$O3_y$ and $Cu2_{x^2-y^2}$–$O2_x$ hopping integrals scales roughly as $(b/a)^{-4}$, we expect the saddle-point near X to lie more than 100 meV higher than the one near Y. However, the calculated energy difference is only 10 meV. The reason is that the odd plane band is repelled along ΓY by the below-lying chain $pd\pi$ stick band ($O4_y$ and $O1_z$). Furthermore, the hybridization with the chain $pd\sigma$ band for $k_z \neq 0$ makes the plane-band saddle-points three-dimensional: The saddle-point related to $\left(X \pm \frac{1}{4}\Gamma X,\ -15\ \text{meV}\right)$ is (U, +80 meV) and the one related to $\left(Y \pm \frac{1}{3}\Gamma Y,\ -25\ \text{meV}\right)$ is $\left(T \pm \frac{1}{4}\Gamma T,\ -300\ \text{meV}\right)$. From the figures we see that not only the odd, but also the even plane band has bifurcated saddle-points, but these are about 0.5 eV below ϵ_F.

Whether the above-mentioned k_z-dispersion persists in real $YBa_2Cu_3O_7$ is unclear: In the *double*-chain compound $YBa_2Cu_4O_8$, the LDA dispersion is an order of magnitude smaller than in $YBa_2Cu_3O_7$ because single-electron hopping through a double chain is frustrated by the fact that O1 in one chain plays the role of O4 for the other, and yet, the physical properties of the two compounds are quite similar.

In $YBa_2Cu_4O_8$ the LDA saddle-points of the odd plane band are ($X \pm \frac{1}{5}\Gamma X$, –20 meV), (U, 0 meV), ($Y \pm \frac{1}{4}\Gamma Y$, –160 meV) and (T, –180 meV). The difference between the energies near X and Y is thus as expected when the chain-plane hybridization is small and $b/a \approx 1.013$. The even-odd splitting of the plane bands caused by hopping across the double-layer is ~0.5 eV near X or Y, exactly as in $YBa_2Cu_3O_7$.

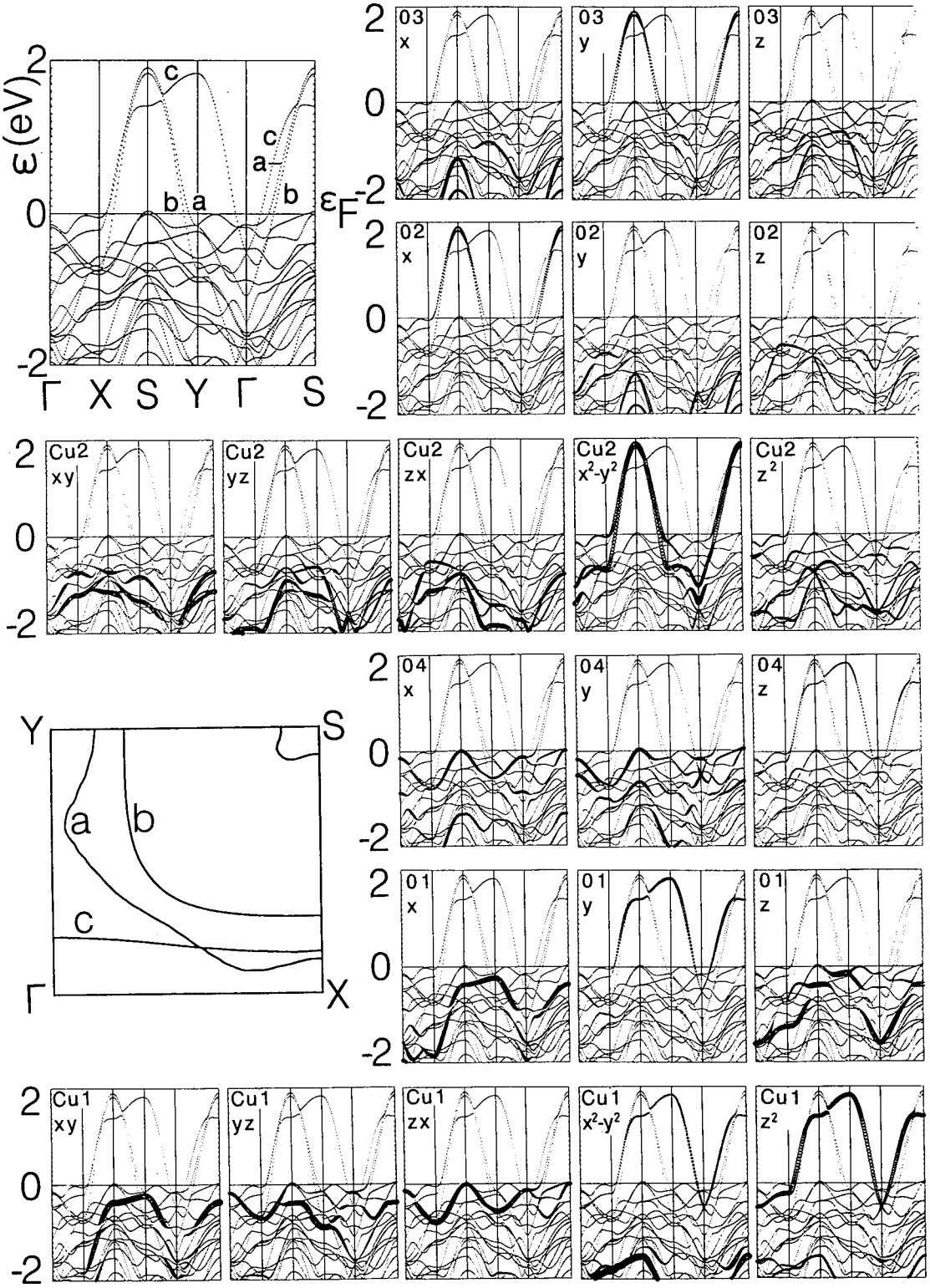


Fig. 1. LDA energy bands, orbital projected bands, and Fermi surface for $YBa_2Cu_3O_7$ and k_z=0.[3]

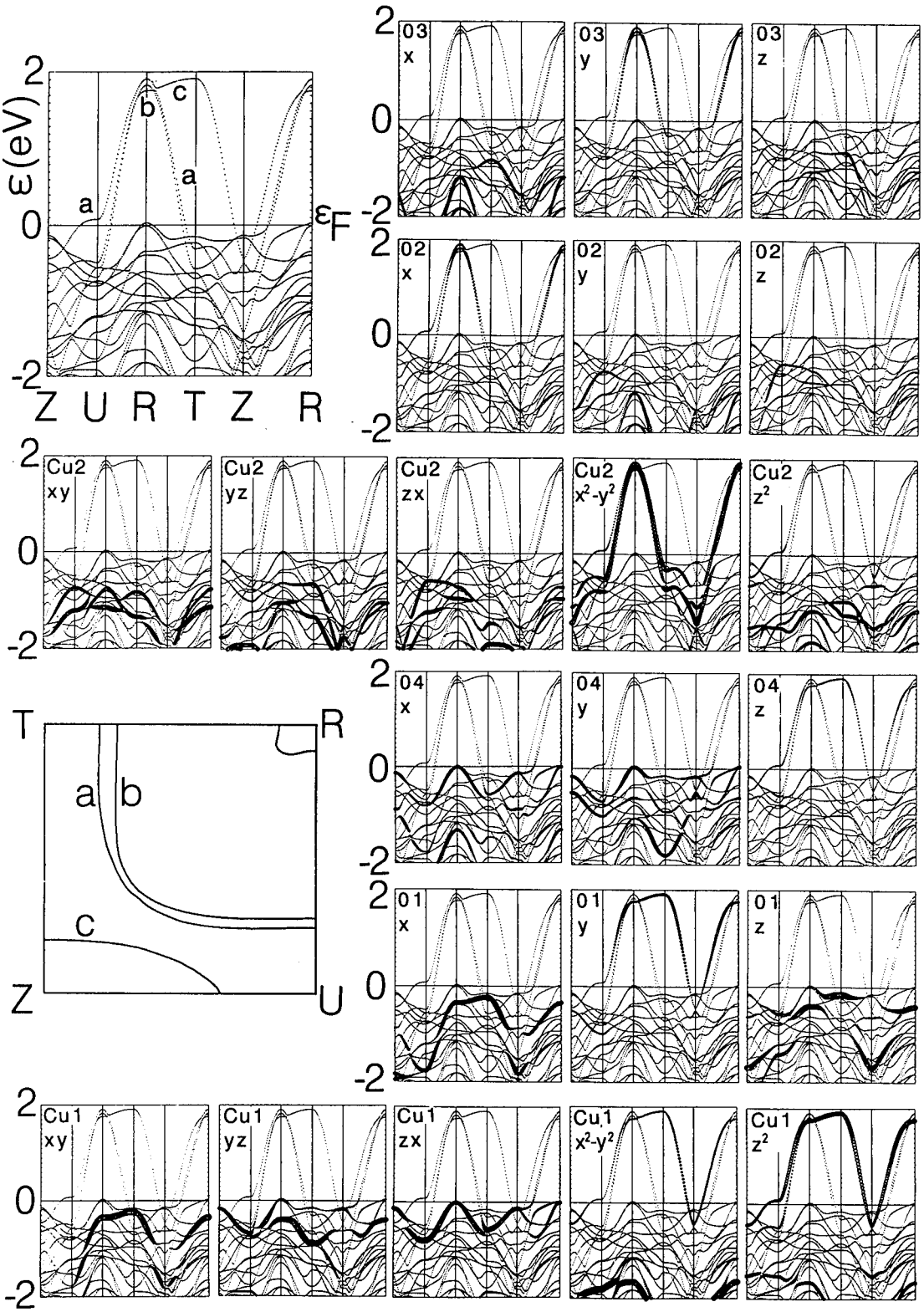


Fig. 2. Same as Fig. 1, but for $k_z = \frac{\pi}{c}$.

3. 8-BAND HAMILTONIAN

The chain degrees of freedom have low energy, but they are not generic because not all HTCS's have chains. In order to derive a generic low-energy few-band Hamiltonian for the *planes*, we have therefore downfolded the LDA multi-band Hamiltonian for $YBa_2Cu_3O_7$ and $k_z=0$ to a two-center, orthogonal, tight-binding Hamiltonian $H_8^-(\mathbf{k}_\parallel)$ with eight *odd* bilayer orbitals interacting through nearest-neighbor hopping. Similarly, we have downfolded the LDA Hamiltonian for $k_z=\frac{\pi}{c}$ to an eight-band Hamiltonian $H_8^+(\mathbf{k}_\parallel)$ for the *even* bilayer orbitals [18]. Over a range of ± 1 eV, H_8^- and H_8^+ accurately describe the odd and even plane bands, respectively, as they are seen in Figs. 1 and 2. The weak hybridization with the chain $pd\pi$ bands has not been removed from, but is folded into these 8-band Hamiltonians.

The downfolding consisted of first integrating out all degrees of freedom with very high energies (e.g. Ba *spdf*, Y *spdf*, Cu *p*, O *sd*). This was done using the LMTO downfolding procedure (see also Sect. 4). Thereafter, all remaining orbitals other than the eight odd (even) *plane* oxygen and copper orbitals specified in the Introduction were deleted from the downfolded LMTO basis, and the odd (even) plane bands were recalculated. These eight-LMTO bands accurately reproduced the corresponding full LDA plane bands over a ± 2 eV range. Finally, the non-orthogonality and long range of the eight odd (even) orbitals were transformed away by fitting the bands in the ± 1 eV range to an orthogonal, two-center, nearest-neighbor, tight-binding Hamiltonian which then, is the one desired.

The reason for keeping in the Hamiltonian particularly those eight orbitals, is that these orbitals are the ones which after orthogonalization describe the LDA plane-bands accurately over a ± 1 eV range with nearest-neighbor hoppings only, that is, with the minimal number of parameters. The 8-band Hamiltonian is thus the one which is "chemically" meaningful and sufficiently simple that further degrees of freedom may be integrated out analytically, as we shall demonstrate in the following section.

By transforming from orbitals even and odd with respect to the yttrium mid-plane of the bilayer to orbitals centered on a specific plane, one obtains a *single-plane* Hamiltonian, $H_8(\mathbf{k}_\parallel)$, plus integrals for hopping *between* the two planes of the bilayer.

Fig. 3 now *synthesizes* the eight plane-bands and gives the most significant parameters of H_8 (tetragonal averages are for instance taken). Ref. [18] provides the accurate values of *all* the matrix elements, as well as the detailed expressions, and the comparison with the full LDA bands. The inter-plane hopping will be discussed separately in Sect. 8.

Shown in the bottom left-hand panel of Fig. 3 are the four σ-orbitals looked upon from above the plane, $|y\rangle \equiv O3_y$, $|d\rangle \equiv Cu2_{x^2-y^2}$, $|x\rangle \equiv O2_x$, and $|s\rangle \equiv Cu2_s$. Below, we see, from the edge of the plane, the $|d\rangle$ orbital and two of the π-orbitals, $|z\rangle \equiv O2_z$ and $|xz\rangle \equiv Cu2_{xz}$. The orbital energies are given at the relevant points of the band structure shown in the left-hand panel, in eV and with respect to the energy of the $Cu2_{x^2-y^2}$ orbital. Hence, $\epsilon_x=\epsilon_y \equiv \epsilon_p$ is 0.9 eV *below* ϵ_d, and ϵ_s is 6.5 eV above. Moreover, $\epsilon_{O2_z}=\epsilon_{O3_z} \equiv \epsilon_z$ is 0.4 eV above ϵ_d, and $\epsilon_{xz}=\epsilon_{yz}$ is 1 eV below. If we now, as shown in the figures at the bottom, include the $pd\sigma$ hopping integrals $t_{xd}=t_{yd} \equiv t_{pd} = 1.6$ eV and the $pd\pi$ hopping integrals $t_{z,xz}=t_{z,yz} = 0.7$ eV, we obtain the band structure shown in the panel above: The σ-orbitals give rise to a bonding, a non-bonding, and an anti-bonding $O2_x$–$Cu_{x^2-y^2}$–$O3_y$ band plus a Cu_s level (full lines), and the π-orbitals give rise to two decoupled pairs of bonding anti-bonding bands which disperse in either the x or y direction (stippled lines). The anti-bonding $pd\sigma$ band, which will develop into the conduction band, has saddle-points at X (and Y) which are well above the top of the π-bands, and which are *isotropic* in the sense, that the absolute values of the band masses in the x and y directions are equal. This means that the FS at half-filling is a square with corners at X and Y.

In the middle panel, the σ and π bands remain decoupled, but we have introduced the Cu_s–$O2_x$ and Cu_s–$O3_y$ hoppings ($t_{sp} = 2.3$ eV), as well as the tiny $O3_z$–$O2_z$ hopping ($t_{zz} = 0.06$ eV). The latter is the only one reaching beyond nearest neighbors and it merely lifts a degeneracy of the anti-bonding π-bands at Γ. The *strong* coupling of the *remote* Cu_s orbital to the $pd\sigma$ orbitals has the pronounced effect of depressing the conduction band near the saddle-points at X and Y, and thereby increasing the mass towards Γ and decreasing it towards S (π, π). The FS passing through X and Y will therefore correspond to finite hole-doping and will bulge towards Γ (see the left-hand panel of Fig. 7). That the Cu_s orbital, which has the azimuthal quantum number $m_z=0$, may mix with the conduction band at X (and Y), but not at $\frac{1}{2}\Gamma S\left(\frac{\pi}{2}, \frac{\pi}{2}\right)$, can be seen from the symmetries of the corresponding two anti-bonding $pd\sigma$ wave functions shown schematically in Fig. 4. That there is, in fact, substantial by-mixing of Cu_s character in the full LDA wave function at X, but none at $\frac{1}{2}\Gamma S$, is proved by the $|\psi(\mathbf{r})|^2$-contours shown in respectively the left and right-hand parts of Fig. 5. The by-mixing of Cu_{3z^2-1} character (which also has $m_z=0$-symmetry) to the so-called Cu_s orbital, is seen to be small. The net downwards shift of the saddle-point energy is the result of down-pushing by pure Cu_s and weak up-pushing by pure Cu_{3z^2-1}, whose energy is below the saddle-point. In Sect. 6 we shall give analytical descriptions of the conduction band in this $dp\sigma$-$sp\sigma$ approximation.

As a result of the hybridization with the Cu_s orbital, the saddle-points of the anti-bonding σ-band straddle off the top of the appropriate π-band, so that even a weak dimple or buckle of the planes will introduce noticeable hybridization between the σ and π bands. This is seen in the right-hand panel where we have turned on the weak $Cu_{x^2-y^2}$–$O2_z$ and $Cu_{x^2-y^2}$–$O3_z$ hoppings ($t_{zd} = 0.24$ eV $\propto \sin\delta$). These couplings become allowed when there is a finite angle δ ($\approx 7^o$

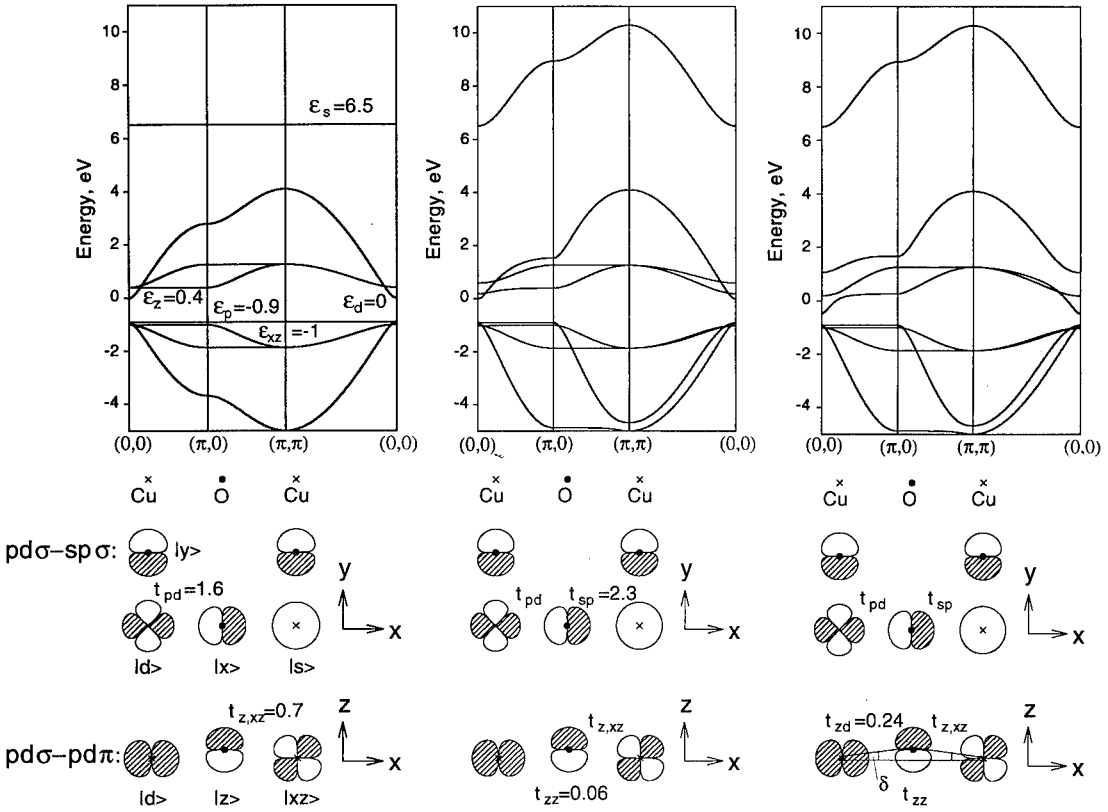


Fig. 3. Specification of the 8-band Hamiltonian and synthesis of its band structure. All energies are in eV. See text.

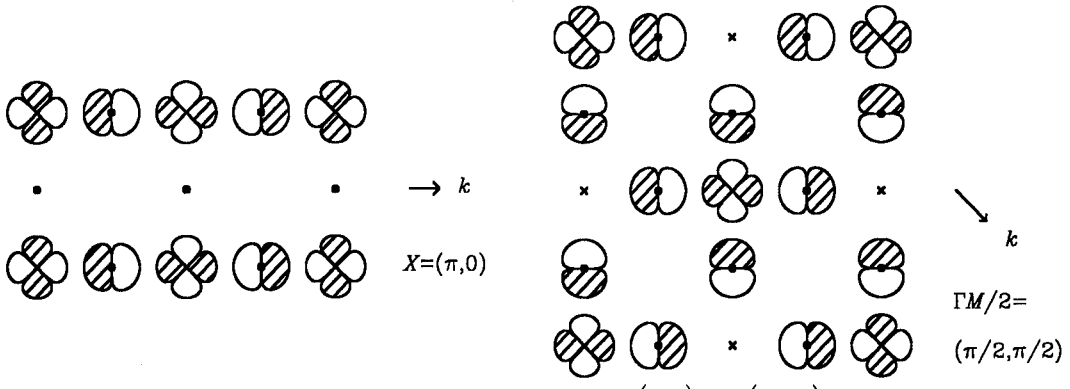


Fig. 4. $O2_x$-$Cu_{x^2-y^2}$-$O3_y$ conduction-band states at $\mathbf{k} = \left(\frac{\pi}{a}, 0\right)$ and $\left(\frac{\pi}{2a}, \frac{\pi}{2a}\right)$, schematic.

in $YBa_2Cu_3O_7$ and $YBa_2Cu_4O_8$) between the Cu-O bond and the plane of the 2D-translations. Since the anti-bonding $pd\sigma$ and Cu_{xz}–$O2_z$ $pd\pi$ orbitals can only hybridize between Γ and X, but not at X, the σ-π hybridization makes the saddle-point bifurcate away from X.

In conclusion, the chemical eight-band Hamiltonian $H_8(\mathbf{k}_\parallel)$, whose eigenvalues give the one-electron bands for a single plane, has the σ-block:

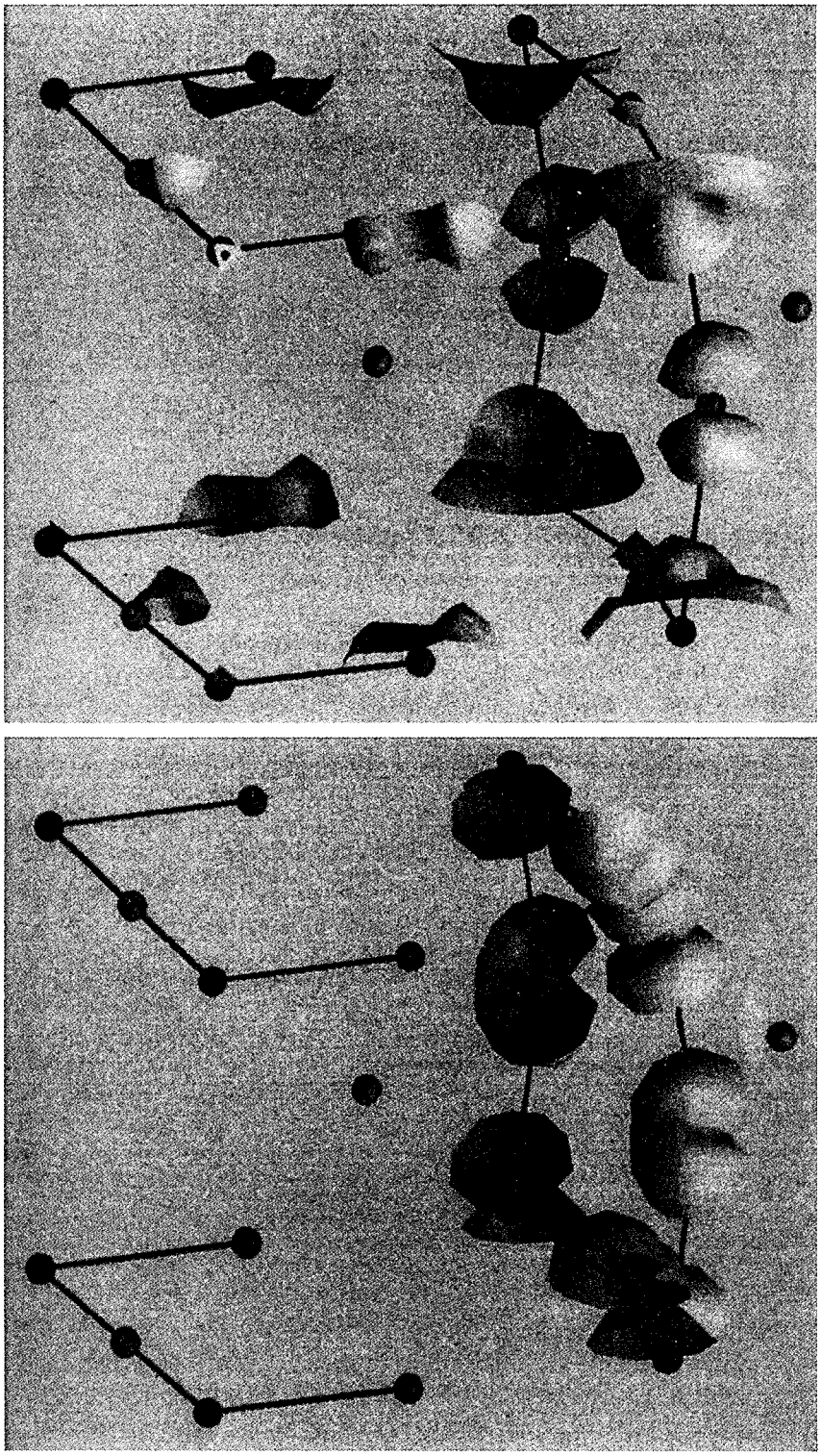


Fig. 5. LDA wave-functions $\left(\text{surfaces of constant } |\psi(\mathbf{k},\mathbf{r})|^2\right)$ for the odd plane conduction band in $YBa_2Cu_3O_7$. *Left:* $\mathbf{k} = \left(\frac{\pi}{a}, 0, 0\right)$ X. *Right:* $\mathbf{k} = \left(\frac{\pi}{2a}, \frac{\pi}{2a}, 0\right)$ $\frac{1}{2}\Gamma S$ [21].

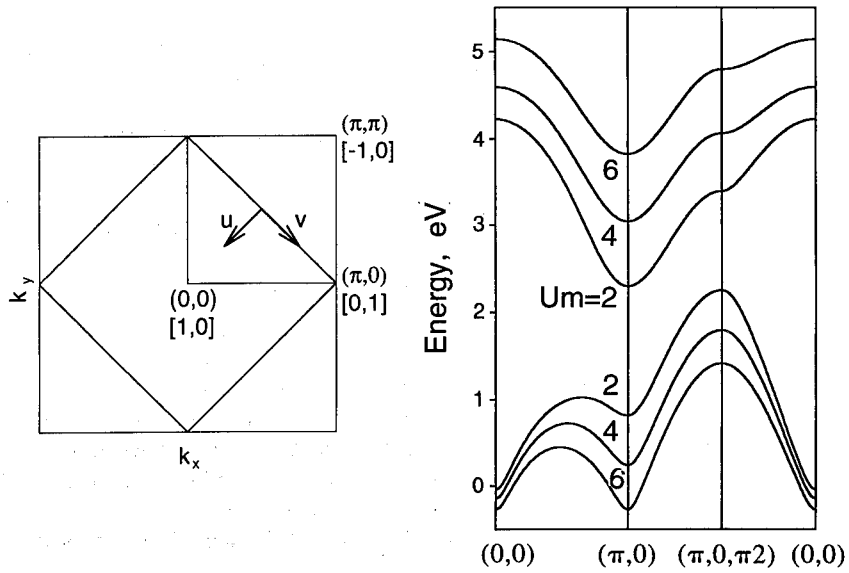


Fig. 6. Non-magnetic and anti-ferromagnetic Brillouin zones and relation between the (k_x, k_y) and $[u, v]$ coordinate systems. *Right:* Energy bands from the 4-band Hamiltonian in the presence of anti-ferromagnetically staggered fields acting on the $Cu_{x^2-y^2}$ orbital and of strengths ±1, ±2, and ±3 eV.

$\langle\sigma\|H\|\sigma\rangle$	$\|\mathrm{Cu}\,d\rangle$	$\|\mathrm{Cu}\,s\rangle$	$\|\mathrm{O2}\,x\rangle$	$\|\mathrm{O3}\,y\rangle$
$\langle\mathrm{Cu}\,d\|$	ϵ_d	0	$2t_{pd}\sin\frac{a}{2}k_x$	$-2t_{pd}\sin\frac{a}{2}k_y$
$\langle\mathrm{Cu}\,s\|$	0	ϵ_s	$2t_{sp}\sin\frac{a}{2}k_x$	$2t_{sp}\sin\frac{a}{2}k_y$
$\langle\mathrm{O2}\,x\|$	$2t_{pd}\sin\frac{a}{2}k_x$	$2t_{sp}\sin\frac{a}{2}k_x$	ϵ_p	0
$\langle\mathrm{O3}\,y\|$	$-2t_{pd}\sin\frac{a}{2}k_y$	$2t_{sp}\sin\frac{a}{2}k_y$	0	ϵ_p

(1)

the π-block:

$\langle\pi\|H\|\pi\rangle$	$\|\mathrm{O2}\,z\rangle$	$\|\mathrm{O3}\,z\rangle$	$\|\mathrm{Cu2}\,xz\rangle$	$\|\mathrm{Cu2}\,yz\rangle$
$\langle\mathrm{O2}\,z\|$	ϵ_z	$-4t_{zz}\cos\frac{a}{2}k_x\cos\frac{a}{2}k_y$	$2t_{z,xz}\sin\frac{a}{2}k_x$	0
$\langle\mathrm{O3}\,z\|$	$-4t_{zz}\cos\frac{a}{2}k_x\cos\frac{a}{2}k_y$	ϵ_z	0	$2t_{z,xz}\sin\frac{a}{2}k_y$
$\langle\mathrm{Cu2}\,xz\|$	$2t_{z,xz}\sin\frac{a}{2}k_x$	0	ϵ_{xz}	0
$\langle\mathrm{Cu2}\,yz\|$	0	$2t_{z,xz}\sin\frac{a}{2}k_y$	0	ϵ_{xz}

and the block mixing the σ and π orbitals for dimpled planes:

$\langle\sigma\|H\|\pi\rangle$	$\|O2\,z\rangle$	$\|O3\,z\rangle$	$\|Cu2\,xz\rangle$	$\|Cu2\,yz\rangle$
$\langle Cu\,d\|$	$2t_{zd}\cos\frac{a}{2}k_x$	$-2t_{zd}\cos\frac{a}{2}k_y$	0	0
$\langle Cu\,s\|$	0	0	0	0
$\langle O2\,x\|$	0	0	0	0
$\langle O3\,y\|$	0	0	0	0

4. INTEGRATING OUT HIGH-ENERGY DEGREES OF FREEDOM

In deriving the 8-band Hamiltonian from the LDA we have numerically integrated out many high-energy degrees of freedom. In the following, we shall integrate out further high-energy degrees of freedom starting from H_8 or $\langle\sigma|H|\sigma\rangle$. We now explain the Löwdin procedure:

Partitioning an orthonormal basis into $|i\rangle$ and $|j\rangle$, and down-folding the H^{jj}-block yields:

$$H_{ii'}(\epsilon) = H_{ii'} - \sum_{jj'} H_{ij}\left[\left(H^{jj}-\epsilon\right)^{-1}\right]_{jj'} H_{j'i'}. \tag{2}$$

This is exact in the sense that $\det[H-\epsilon]$ and $\det[H^{ii}(\epsilon)-\epsilon]$ have identical zeroes, namely the eigenvalues of H. If we now Taylor-expand the down-folded Hamiltonian about ϵ_F: $H^{ii}(\epsilon) = H^{ii}(\epsilon_F) + (\epsilon-\epsilon_F)\dot{H}^{ii}(\epsilon_F) + \ldots$, we see that the energy dependence of the down-folded Hamiltonian to linear order arises from non-orthogonality of the modified i-basis, the overlap matrix being $1-\dot{H}^{ii}(\epsilon_F)$. The higher-order energy dependence of $H^{ii}(\epsilon)$ originates from energy dependence of the basis. The latter, and sometimes even the former energy dependencies can be neglected if the degrees of freedom to be integrated out have high energy, that is, if the energy range of interest lies far away from the eigenvalues of H^{jj}. An *orthonormal* low-energy Hamiltonian $\mathcal{H}$ may be obtained by orthogonalization of the modified i-basis, whose energy dependence has been neglected, e.g.

$$\mathcal{H} = \epsilon_F + [1-\dot{H}^{ii}(\epsilon_F)]^{-\frac{1}{2}}[H^{ii}(\epsilon_F)-\epsilon_F][1-\dot{H}^{ii}(\epsilon_F)]^{-\frac{1}{2}} \tag{3}$$

5. 3-BAND HAMILTONIAN

A popular tight-binding Hamiltonian for flat planes is the 3-band Emery model. This is like $\langle\sigma|H|\sigma\rangle$ in (1), but without the Cu_s orbital, with a renormalized oxygen energy $\left(\epsilon_p \to \epsilon'_p\right)$, and with 2nd-nearest-neighbor $O2_x$–$O3_y$ hopping.

Projecting the Cu_s orbital out of $\langle\sigma|H|\sigma\rangle$ by means of (2) reveals that the values of ϵ_d and t_{pd} are unchanged, but that 2nd-nearest-neighbor $O2_x$–$O3_y$ *as well as* 3rd-nearest-neighbor $O2_x$–$O2_x$ and $O3_y$–$O3_y$ hoppings, all of size $t_{pp} = t_{sp}^2/(\epsilon_s-\epsilon) \sim 1.1$ eV, must be added. Moreover, ϵ_p must be renormalized to $\epsilon'_p = \epsilon_p - 2t_{pp} \sim \epsilon_d - 3.0$ eV which is, in fact, the standard value. All of this comes about, because the Cu_s character (see Fig. 5) is now built into the tails of the neighboring $O2_x$ and $O3_y$ orbitals.

According to the LDA, the Emery model should thus be modified to

H_3	$\|Cu\,d\rangle$	$\|O2\,x\rangle$	$\|O3\,y\rangle$
$\langle Cu\,d\|$	ϵ_d	$2t_{pd}\sin\frac{a}{2}k_x$	$-2t_{pd}\sin\frac{a}{2}k_y$
$\langle O2\,x\|$	$2t_{pd}\sin\frac{a}{2}k_x$	$\epsilon'_p + 2t_{pp}\cos ak_x$	$-4t_{pp}\sin\frac{a}{2}k_x\sin\frac{a}{2}k_y$
$\langle O3\,y\|$	$-2t_{pd}\sin\frac{a}{2}k_y$	$-4t_{pp}\sin\frac{a}{2}k_x\sin\frac{a}{2}k_y$	$\epsilon'_p + 2t_{pp}\cos ak_y$

(4)

Here we have neglected the non-orthogonality and, for the numerical values, we have taken the expansion energy, $\epsilon_F = \epsilon(X) \approx \epsilon_d + 1.53$ eV. As long as $\epsilon - \epsilon_F \ll \epsilon_s - \epsilon_F \sim 5$ eV, this is a good approximation. Orthogonalization by means of (3) would have introduced longer-range hoppings.

6. THE σ-BAND

In order to derive accurate and *transparent* expressions for the flat-plane σ-bands $\epsilon_n(\mathbf{k}_\parallel)$, or their constant-energy surfaces, we return to the 4-band Hamiltonian $\langle\sigma|H|\sigma\rangle$ in (1) and first Löwdin down-fold (2) the oxygen orbitals. The

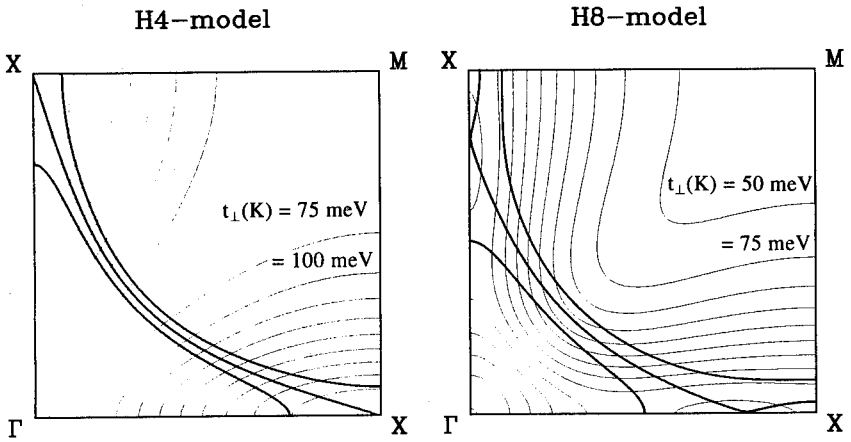


Fig. 7. Contours of constant $t_\perp(\mathbf{k}) \equiv \frac{1}{2}[\epsilon^-(\mathbf{k}) - \epsilon^+(\mathbf{k})]$ calculated for the 4- and 8-band models. The heavy lines give the odd constant energy surfaces passing through the saddle-points, as well as the two neighboring contours corresponding to the energies ±100 meV from the saddle-point.

result is the following energy-dependent $sp\sigma$-$dp\sigma$ Hamiltonian:

$$\begin{array}{lll} H_{sd}(\epsilon) & |\mathrm{Cu}\, d, \epsilon\rangle & |\mathrm{Cu}\, s, \epsilon\rangle \\ \langle \mathrm{Cu}\, d, \epsilon| & \epsilon_d + (1-u)\,(2t_{pd})^2 / (\epsilon - \epsilon_p) & -v\,(2t_{pd})\,(2t_{sp}) / (\epsilon - \epsilon_p) \\ \langle \mathrm{Cu}\, s, \epsilon| & -v\,(2t_{pd})\,(2t_{sp}) / (\epsilon - \epsilon_p) & \epsilon_s + (1-u)\,(2t_{sp})^2 / (\epsilon - \epsilon_p) \end{array} \tag{5}$$

where we have defined the *new* $\mathbf{k}_\parallel$*-coordinates:*

$$u \equiv \frac{1}{2}(\cos ak_y + \cos ak_x) \quad \text{and} \quad v \equiv \frac{1}{2}(\cos ak_y - \cos ak_x), \tag{6}$$

both limited to the range from –1 to +1 and sketched in the left-hand side of Fig. 6. The origin of the uv-system is at $\frac{1}{2}\Gamma\mathrm{S}$ and corresponding values of (k_x, k_y) and $[u, v]$ are: $\frac{1}{2}\Gamma\mathrm{S}\left(\frac{\pi}{2a}, \frac{\pi}{2a}\right)[0, 0]$, $\mathrm{X}\left(\frac{\pi}{a}, 0\right)[0, 1]$, $\Gamma\ (0, 0)\ [1, 0]$, and $\mathrm{S}\left(\frac{\pi}{a}, \frac{\pi}{a}\right)[-1, 0]$. Readers used to think about pairing and gap symmetries, will recognize u as s- and v as d-wave symmetry. The relation to the $\mathbf{k}_\parallel$-coordinates x and y used in Ref. [18] is: $1 - u = x + y$ and $v = x - y$.

The sd-Hamiltonian (5) highlights the $\mathbf{k}_\parallel$-dependence of the LDA σ-bands for a flat CuO_2 plane as follows: Without s-mixing, the bands depend only on u (the saddle-points are isotropic, the FS for half filling is the square: $u = 0$, etc.) and the mixing element is proportional to v.

Further Löwdin down-folding, this time of the $sp\sigma$-block, yields the following energy-dependent 1-band Hamiltonian:

$$H(\epsilon) = \epsilon_d + \frac{(2t_{pd})^2}{\epsilon - \epsilon_p}\left(1 - u - \frac{v^2}{1 + s(\epsilon) - u}\right), \tag{7}$$

which is still equivalent with $\langle\sigma|H|\sigma\rangle$. When there is no mixing with Cu s, that is when $t_{sp}=0$, $s(\epsilon)\to\infty$ so that the term proportional to v^2 vanishes. The quadratic $sp\sigma$-scattering function

$$s(\epsilon)\equiv(\epsilon_s-\epsilon)(\epsilon-\epsilon_p)/(2t_{sp})^2 \tag{8}$$

is fairly constant in the neighborhood of $\epsilon=(\epsilon_s+\epsilon_p)/2\approx 2.8$ eV, where it takes its maximum value $[(\epsilon_s-\epsilon_p)/4t_{sp}]^2\approx 0.65$. For instance is $s(1.5\text{ eV})\approx 0.57$.

The most elegant way of expressing the eigenvalues of $\langle\sigma|H|\sigma\rangle$ is as the roots of the secular equation,

$$[H(\epsilon)-\epsilon]\frac{\epsilon-\epsilon_p}{(2t_{pd})^2}\equiv 1-u-\frac{v^2}{1+s(\epsilon)-u}-d(\epsilon)=0, \tag{9}$$

because from its definition,

$$d(\epsilon)=(\epsilon-\epsilon_d)(\epsilon-\epsilon_p)/(2t_{pd})^2 \tag{10}$$

is a quadratic function of energy which depends only on the $dp\sigma$ scattering. For (9) to vanish, we see that $d(\epsilon)$ must increase from 0 to 2 in the region of the conduction band because $s(\epsilon)$ is positive and because the bottom of the band is at Γ and the top is at S. For a given energy, ϵ, we calculate the values of $s(\epsilon)$ and $d(\epsilon)$ from (8) and (10), whereafter the requirement that (9) be zero gives the exact constant-energy surface. For a given $\mathbf{k}_\parallel$, on the other hand, we can not give an exact, explicit expression for the four eigenvalues, $\epsilon_n(\mathbf{k}_\parallel)$, but near the middle of the conduction band we may exploit the near-constancy of $s(\epsilon)$ and are then led by (10) and (9) to solve the following equation:

$$\epsilon(\mathbf{k})=\frac{\epsilon_p+\epsilon_d}{2}+\sqrt{\left(\frac{\epsilon_p-\epsilon_d}{2}\right)^2+(2t_{pd})^2\left(1-u-\frac{v^2}{1+s(\epsilon)-u}\right)} \tag{11}$$

iteratively [i.e. $\epsilon(\mathbf{k})\to\epsilon$]. For ease of notation, we have dropped the subscript $\parallel$ on $\mathbf{k}_\parallel$, and we shall do so from now on.

With the parameter-values from Fig. 3, we easily obtain: $\epsilon(X)=\epsilon(u{=}0, v{=}1)\approx 1.53$ eV and $\epsilon\left(\frac{1}{2}\Gamma S\right)=\epsilon(u{=}0, v{=}0)\approx 2.78$ eV. The Cu_s level thus pushes the saddle-point down by 1.25 eV. The energy of the bottom of the conduction band, $\epsilon(\Gamma)=\epsilon(u{=}1,v{=}0)=\max(\epsilon_p,\epsilon_d)=0$, and of its top, $\epsilon(S)=\epsilon(u{=}{-}1,v{=}0)\approx 4.10$ eV, are independent of s.

The Cu_d, Cu_s, and O_p (O2+O3) characters of the conduction-band wave function are most easily obtained as the respective derivatives $\partial\epsilon(\mathbf{k})/\partial\epsilon_d$, $\partial\epsilon(\mathbf{k})/\partial\epsilon_p$, and $\partial\epsilon(\mathbf{k})/\partial\epsilon_s$. This follows from 1st-order perturbation theory. By differentiation of (9) and making use of

$$\dot d(\epsilon)=2\frac{\epsilon-(\epsilon_p+\epsilon_d)/2}{(2t_{pd})^2}\quad\text{and}$$
$$\dot s(\epsilon)=2\frac{(\epsilon_p+\epsilon_s)/2-\epsilon}{(2t_{sp})^2} \tag{12}$$

we obtain the simple results:

$$|c_d(\epsilon,\mathbf{k})|^2=\frac{1}{2}\frac{\epsilon-\epsilon_p}{\epsilon-(\epsilon_p+\epsilon_d)/2}\left[1-\frac{\dot s(\epsilon)}{\dot d(\epsilon)}\frac{v^2}{[1+s(\epsilon)-u]^2}\right]^{-1} \tag{13}$$

and

$$\left|\frac{c_s(\epsilon,\mathbf{k})}{c_d(\epsilon,\mathbf{k})}\right|^2=\left(\frac{t_{pd}}{t_{sp}}\right)^2\frac{v^2}{[1+s(\epsilon)-u]^2} \tag{14}$$

and $|c_p(\epsilon,\mathbf{k})|^2=1-|c_s(\epsilon,\mathbf{k})|^2-|c_d(\epsilon,\mathbf{k})|^2$. The Cu_d character is seen to be $\sim\frac{1}{2}[1-..]^{-1}$ when the energy is far away from $\epsilon_p\sim\epsilon_d$. Moreover, the *variation* of Cu d character along a constant-energy surface, e.g. the FS, becomes negligible when

$$1\gg\left|\frac{\dot s(\epsilon)}{\dot d(\epsilon)}\right|=\left(\frac{t_{pd}}{t_{sp}}\right)^2\left|\frac{\epsilon-(\epsilon_p+\epsilon_s)/2}{\epsilon-(\epsilon_p+\epsilon_d)/2}\right|$$
$$\approx 0.48\left|\frac{\epsilon-2.8\text{ eV}}{\epsilon+0.45\text{ eV}}\right|, \tag{15}$$

and vanishes for the energy midway between the O_p and Cu_s energies. With our parameter-values and for ϵ=1.53 eV, $\dot s/\dot d\approx 0.31$, whereas for ϵ=2.78, $\dot s/\dot d=0$. In the following, we shall often neglect $\dot s$, and when this can be done, the Cu_d

character is independent of $\mathbf{k}$ and slightly larger than 0.5. The Cu_s character is proportional to v^2 and, with our values of the hopping integrals and our s-value, $|c_s(\epsilon, \mathbf{k})|^2 \sim 0.12v^2(1-0.6u)^{-2}$, that is, at X there is 61% Cu_d, 12% Cu_s, and 27% $O2_x$ character.

7. 1-BAND HAMILTONIANS

The 1-band Hamiltonian for an orbital which is orthogonal to itself when displaced by a lattice translation, i.e. for a Wannier function, has the $\mathbf{k}$-dependence of a Fourier series:

$$\begin{aligned}\mathcal{H}(\mathbf{k}_\parallel) = \langle\epsilon\rangle &- 2t(\cos ak_x + \cos ak_y) + 4t'\cos ak_x \cos ak_y - 2t''(\cos 2ak_x + \cos 2ak_y) \\ &+4t^{(3)}(\cos ak_x \cos 2ak_y + \cos ak_y \cos 2ak_x) + 4t^{(4)}\cos 2ak_x \cos 2ak_y - 2t^{(5)}(\cos 3ak_x + \cos 3ak_y) \\ &+\ldots - 2t^{(9)}(\cos 4ak_x + \cos 4ak_y) + \ldots \end{aligned} \tag{16}$$

with $t^{(n)}$ being the hopping integral between $(n+1)$st nearest neighbors and $\langle\epsilon\rangle$ being the average energy of the band.

The conduction band shown in the right-hand panel of Fig. 3, which is given by the 8-band Hamiltonian for a plane dimpled by 7°, is well separated from all other bands, and this band is sufficiently smooth that its Fourier series converges at a reasonable pace. The results obtained numerically by diagonalizing H_8^- and H_8^+ (with the parameters given in Ref. [18]) and subsequent Fourier transformation of the odd and even conduction bands are given in the first two rows of the following table:

	$\langle\epsilon\rangle$	t	t'	t''	$t^{(3)}$	$t^{(4)}$	$t^{(5)}$	$t^{(9)}$
$H_8^-(\mathbf{k})$/meV	140	349	96	62	18	1	10	1
$H_8^+(\mathbf{k})$/meV	−140	422	113	110	20	5	32	11
$\varepsilon(\mathbf{k}) \times \dot{d}$		$\frac{1}{4}\left(1+\frac{1}{8}r\right)$	$\frac{1}{4}r(1+\frac{1}{2}r^2)$	$\frac{1}{8}r(1+\frac{1}{4}r^2)$	$\frac{1}{16}r^2$	$\frac{1}{16}r^3$	$\frac{1}{16}r^2$	$\frac{1}{32}r^3$

The corresponding even and odd Wannier orbitals must have fairly long range. The zero of energy in the table is at the average of the even and odd bands. The splitting between these bands will be discussed in Sect. 8.

With decreasing dimpling, the convergence of the Fourier series (16) of the entire conduction band deteriorates even further. Reasons are the near-crossing of the σ and π-bands, and the near-cusp of the σ-band at Γ. The latter can be seen in the middle panel of Fig. 3 and is caused by the near degeneracy of ϵ_d and ϵ_p. For the pure σ-band, a more useful low-energy Hamiltonian is therefore obtained by Fourier transformation, not of the *entire* anti-bonding band, but merely of the part near ϵ_F. We shall now give a simple, analytical derivation of such a low-energy σ-band Hamiltonian. The result is given in the last row of the table with $r \equiv 1/[2(1+s)]$. This Hamiltonian, $\varepsilon(\mathbf{k})$, reproduces the σ conduction band to linear order in $\epsilon - \epsilon_F$ and Eq. (22) below gives the second-order correction.

Let us start with the remark, that Eq. (11) with $s(\epsilon) \equiv s(\epsilon_F)$ is in fact a highly accurate 1-band Hamiltonian for the σ conduction band; it even describes the cusp behavior near Γ where $[u, v] \sim [1, 0]$. However, (11) is not an *orthonormal* 1-band Hamiltonian (16), because such a Hamiltonian must depend *analytically* on u and v. To obtain a 1-band Hamiltonian analytical in u and v, we first expand $d(\epsilon)$ and $s(\epsilon)$ around ϵ_F. If we only go to first order, we can solve Eq. (9) and obtain for the 1st-order estimate:

$$\varepsilon(\mathbf{k}) = \epsilon_F + \left(1 - d - u - \frac{v^2}{1+s-u}\right)\left[\dot{d} - \dot{s}\frac{v^2}{[1+s-u]^2}\right]^{-1} \tag{17}$$

$$\approx \epsilon_F + \dot{d}^{-1}\left[1 - d - u - 2rv^2\left\{1 + 2ru + (2ru)^2 + \ldots\right\}\right]. \tag{18}$$

Note the difference between ε and ϵ. Here, $d \equiv d(\epsilon_F)$, $\dot{d} \equiv \dot{d}(\epsilon_F)$, $s \equiv s(\epsilon_F)$, $r \equiv 1/[2(1+s)]$ and $\dot{s} \equiv \dot{s}(\epsilon_F)$. As an alternative to (12) we may use:

$$\dot{d}^{-1} = \frac{t_{pd}}{\sqrt{d + [(\epsilon_p - \epsilon_d)/4t_{pd}]^2}} \sim \frac{t_{pd}}{\sqrt{d}}. \tag{19}$$

In (18) we have *neglected* $\dot{s} \equiv \dot{s}(\epsilon_F)$ and *expanded* $1/(1+s-u)$ for small u. Substitution of the cosines (6) for u and v and comparing terms with (16) yields the hopping integrals listed in the last row of the table given above. Here the zero of energy is taken at the average band energy

$$\langle\epsilon\rangle = \epsilon_F + \dot{d}^{-1}\left[1 - d - \frac{1}{2}r(1+\frac{1}{2}r^2)\right] \tag{20}$$

and

$$r \equiv \frac{1/2}{1+s} \approx 0.32, \quad \text{so that} \quad \frac{t'}{t} \approx r \quad \text{and} \quad \frac{t''}{t'} \approx \frac{1}{2}. \tag{21}$$

For a flat plane and *without* s-hybridization (r=0), the 1-band 1st-order Hamiltonian $\varepsilon(\mathbf{k})$ only has nearest neighbor interactions. For realistic s-values, hopping to second *and third* neighbors must be included, but farther hoppings can be neglected. In previous many-body calculations, t' was often neglected, but when it was included, $t' \sim 0.3t$ was in fact a standard value. t'' has sofar been neglected.

Had we kept $\dot{s}/\dot{d}$ to lowest order, we should have added to the coefficient of $2rv^2$ in (18) the term $2r(1-d-u)\,\dot{s}/\dot{d}$. Moreover, r in the table and in (20) should be substituted by $r' \equiv r\left[1 - 2r(1-d)\,\dot{s}/\dot{d}\right]$.

As an example, let us take ϵ_F at the saddle-point, $[u, v] = [0, 1]$, then $\epsilon_F \approx 1.53$ eV, as found from (11), $r \approx 0.32$ from (21), $d = 1 - 2r \approx 0.363$ from (9), $\dot{d}^{-1} \approx 2.64$ eV, from (19), $2r(1-d)\,\dot{s}/\dot{d} \approx 0.13$ and $r' = 0.28$. Hence, from the table, $t \approx 0.69$ eV, $t'/t \approx 0.28$, and $t''/t' \approx 0.49$. Using the first-order expression (18) to calculate the energy at $\frac{1}{2}\Gamma S$, which we know from (11) should be 1.25 eV above the saddle-point, we find: $\varepsilon\left(\frac{1}{2}\Gamma S\right) - \epsilon_F = (1-d)/\dot{d} = 2r'\dot{d}^{-1} \approx 1.46$ eV. This discrepancy is due to the lack of higher-order terms in (11).

The second-order corrections to the 1st-order Hamiltonian $\varepsilon(\mathbf{k})$ may be obtained by expanding $d(\epsilon)$ to second order and using (9) and (18) to obtain:

$$\epsilon(\mathbf{k}) + \frac{1}{2}\frac{[\varepsilon(\mathbf{k}) - \epsilon_F]^2}{\epsilon_F - (\epsilon_p + \epsilon_d)/2} = \varepsilon(\mathbf{k}).$$

This is the exact expression for $\epsilon(\mathbf{k})$ (still assuming s constant) because $d(\epsilon)$ is a quadratic function and $\epsilon_F - (\epsilon_p + \epsilon_d)/2 = \dot{d}/\ddot{d}$. For the purpose of deriving an analytical 1-band 2nd-order Hamiltonian, we do not want to solve this equation because the result is the exact Eq. (11), written as:

$$\frac{\epsilon(\mathbf{k}) - \epsilon_F}{\epsilon_F - (\epsilon_p + \epsilon_d)/2} = -1 + \sqrt{1 + 2\frac{\varepsilon(\mathbf{k}) - \epsilon_F}{\epsilon_F - (\epsilon_p + \epsilon_d)/2}}.$$

To obtain an analytical Hamiltonian, we must expand as follows:

$$\epsilon(\mathbf{k}) - \epsilon_F = [\varepsilon(\mathbf{k}) - \epsilon_F]\left[1 - \frac{1}{2}\frac{\varepsilon(\mathbf{k}) - \epsilon_F}{\epsilon_F - (\epsilon_p + \epsilon_d)/2} + \ldots\right] \tag{22}$$

Since $\epsilon_F - (\epsilon_p + \epsilon_d)/2 \sim 2$ eV, this expansion hardly converges for $\varepsilon\left(\frac{1}{2}\Gamma S\right) - \epsilon_F = 1.46$ eV, but only for energies much closer to ϵ_F. This is the cusp-problem, showing up again. Our 1-band 1st-order Hamiltonian including 3rd-nearest-neighbor interactions is therefore appropriate for energies one order of magnitude closer to ϵ_F than $(\epsilon_p + \epsilon_d)/2$, i.e. below 200 meV. To develop an expression more explicit than (22) for a 1-band 2nd-order Hamiltonian which treats higher energies better than $\varepsilon(\mathbf{k})$, seems pointless considering the complication of squaring the Fourier series for $\varepsilon(\mathbf{k}) - \epsilon_F$.

We should also comment on the most obvious way to derive the σ conduction-band Hamiltonian, namely linearization and orthonormalization (3) of $H(\epsilon)$ in (7). Using (9) and (18) it becomes obvious that

$$\mathcal{H}(\mathbf{k}) - \epsilon_F = \frac{H(\epsilon_F) - \epsilon_F}{1 - \dot{H}(\epsilon_F)} = \frac{\varepsilon(\mathbf{k}) - \epsilon_F}{1 + (\varepsilon(\mathbf{k}) - \epsilon_F)/(\epsilon_F - \epsilon_p)}$$
$$\equiv [\varepsilon(\mathbf{k}) - \epsilon_F]\left[1 - \frac{\varepsilon(\mathbf{k}) - \epsilon_F}{\epsilon_F - \epsilon_p} + \ldots\right].$$

Comparison with the correct expansion (22) shows that $\mathcal{H}(\mathbf{k})$ is merely correct to first order, like $\varepsilon(\mathbf{k})$, but it has longer range. In conclusion, $\varepsilon(\mathbf{k})$ seems to be the 1st-order 1-band Hamiltonian with the simplest $\mathbf{k}$-dependence.

Finally we remark that for the 8-band model, too, a 1-band 1st-order Hamiltonian may be derived from Ref. [18] where it is shown that the constant energy contour for an arbitrary energy is a polynomial of second order in $x = \frac{1}{2}(1 - \cos ak_x)$ and in $y = \frac{1}{2}(1 - \cos ak_y)$. By expansion of the coefficients [A(ϵ) through I(ϵ)] to linear order in $\epsilon - \epsilon_F$ and solving, we find $\epsilon - \epsilon_F$ to be given by the *ratio* of two polynomials. Expansion of the denominator gives the orthonormal 1-band Hamiltonian.

8. INTER-PLANE HOPPING, $t_\perp(\mathbf{k}_\parallel)$.

From the parameters of H_8^- and H_8^+ given in [18] for $YBa_2Cu_3O_7$ we derive the values of the integrals

$$t_{ii}^\perp = \frac{1}{2}\left(\epsilon_{ii}^- - \epsilon_{ii}^+\right) \quad \text{and} \quad t_{ij}^\perp = \pm\frac{1}{2}\left(t_{ij}^+ - t_{ij}^-\right)$$

for hopping from orbital i in the lower plane to orbital j in the upper plane of the bilayer. We chose the signs of the hopping integrals in such a way that the integrals are positive if the two orbitals have pure cubic-harmonic character and are strongly localized. In the expression for $t_{ij}^\perp$, the upper sign is therefore chosen for σ-σ and π-π inter-layer hopping integrals, and the lower sign is chosen for σ-π hopping. The (tetragonally averaged and rounded) values of the inter-plane hopping integrals are:

$t_{ss}^\perp$	$t_{sp}^\perp$	$t_{pp}^\perp$	$t_{dd}^\perp$	$t_{zz}^\perp$	$t_{zx,zx}^\perp = t_{zy,zy}^\perp$	$t_{z,zx}^\perp = t_{z,zy}^\perp$	
0.75	0.27	0.12	0.05	0.35	−0.30	−0.15	eV

The negative signs presumably indicate that the corresponding hoppings mostly proceed via yttrium and barium.

For the conduction band, the most important inter-plane hoppings are the vertical $t_{ss}^\perp$ from Cu_s to Cu_s and $t_{sp}^\perp$ from Cu_s in one plane to the nearest $O2_x$ or $O3_y$ in the other plane. This is so, even though the Cu_s character in the conduction band is relatively small. This statement may be verified from the left-hand side of Fig. 7, where we show

$$t_\perp(\mathbf{k}) \equiv \frac{1}{2}\left[\epsilon^-(\mathbf{k}) - \epsilon^+(\mathbf{k})\right], \tag{23}$$

with the odd and even conduction bands calculated by numerical diagonalization of respectively H_4^- and H_4^+ in (1), including all parameters as given in Ref. [18]. The even-odd splitting is seen almost to vanish along ΓM [$M \equiv S = \left(\frac{\pi}{a}, \frac{\pi}{a}\right)$] and to reach its maximum of 0.6 eV at X. This qualitatively follows the $v^2/(1-2ru)^2$ dependence of the Cu_s character (14). Below, we shall work this out in detail. Also shown in the figure (heavy lines) are the constant-energy contour (FS) of the odd band passing through the saddle-point and the two neighboring ones corresponding to energies ±100 meV from the saddle-point.

The right-hand side of Fig. 7 shows the same even-odd splitting and the odd-band constant-energy contours at, and ±100 meV from, the saddle-point, but now calculated from H_8^- and H_8^+. The 8-band Hamiltonian gives a more appropriate description of the even-odd splitting in the dimpled CuO_2 bi-layer (See Figs. 1 and 2 for $YBa_2Cu_3O_7$). The effects of the relatively strong hopping between π-orbitals on different planes are noticeable, but nevertheless, the even-odd splitting still attains its minimum along ΓM and its maximum of 0.6 eV at the saddle-point. That the maximum of $t_\perp(\mathbf{k})$ moves along with the saddle-point as it bifurcates due to dimpling of the plane, is caused by vertical O_z-O_z hopping.

We now give an analytical description of the essentials of $t_\perp(\mathbf{k})$ for a flat plane. Hence, we consider only the σ-band and neglect all inter-plane hoppings other than $t_{ss}^\perp$ and $t_{sp}^\perp$. In this case, the Hamiltonians are $H^P(\epsilon)$ in (7), which depend on the mid-plane parity (P) only through $s^P(\epsilon)$. We therefore immediately realize that the inter-plane hopping is *proportional to* v^2. From (18):

$$\begin{aligned} t_\perp(\mathbf{k}) &= \frac{t_{pd}^2}{\epsilon_F - (\epsilon_p + \epsilon_d)/2}\left(\frac{v^2}{1+s^+-u} - \frac{v^2}{1+s^--u}\right) \\ &\approx t_\perp(X)\left(\frac{v}{1-2ru}\right)^2 \end{aligned} \tag{24}$$

where the maximum is at X [u=0,v=1] and takes the value

$$\begin{aligned} t_\perp(X) &= 4r^2(s^- - s^+)\frac{t_{pd}^2}{\epsilon_F - (\epsilon_p + \epsilon_d)/2} \\ &\approx 8r^2 s\left(\frac{t_{ss}^\perp}{\epsilon_s - \epsilon_F} + 2\frac{t_{sp}^\perp}{t_{sp}}\right)\frac{t_{pd}^2}{\epsilon_F - (\epsilon_p + \epsilon_d)/2} \end{aligned} \tag{25}$$

As usual, $s \equiv s(\epsilon_F)$, $r \equiv [2(1+s)]^{-1} \sim t'/t$, and $\dot{s}$ has been neglected. Taking again ϵ_F at the X-point of the un-split band, we get: $t_\perp(X) \approx 8 \cdot 0.32^2 \cdot 0.57\left(\frac{0.75}{6.5-1.53} + 2\frac{0.27}{2.3}\right)\frac{1.6^2}{1.53+0.45}\text{eV} \approx 0.23$ eV. Inclusion of $\dot{s}$ reduces this value by 13% to 0.20 eV. Had we instead taken $\epsilon_F = \epsilon\left(\frac{\pi}{2a}, \frac{\pi}{2a}\right) = 2.78$ eV, we would have had $\dot{s} = 0$, $s = 0.65$, and $r = 0.30$, so that $t_\perp(X) \approx 0.17$ eV. Both estimates are still the main part of the 0.29 eV obtained when including also those inter-plane

hoppings which do not involve Cu_s. Note that the inter-plane Cu_s-O_p hopping contributes as much to $t_\perp(\mathbf{k})$ as Cu_s-Cu_s. This is because O_p is a major part of the conduction-band wave function. (One might then wonder about the importance of $t_{pp}^\perp$ and $t_{dd}^\perp$, but their effects tend to cancel). The fact that $t_\perp(\mathbf{k})$ in the left-hand side of Fig. 7 is not symmetric around the line XX is mainly due to the factor $(1-2ru)^{-2}$ in Eq. (24).

Inspection of LDA calculations for other multi-layer systems reveals that the $t_\perp(\mathbf{k})$-behavior described above is generic, as we would expect on the grounds that the Cu_s (and Cu_{3z^2-1}) orbital is always present and the inter-layer distance is fairly constant. What might change, are of course ϵ_s and t_{sp} because they depends on the balance between the Cu_s and Cu_{3z^2-1} characters which could be offset if the distance to apical oxygen became unusually short, that is, more than 0.1 Å shorter than the 2.30 Å found in $YBa_2Cu_3O_7$. The bandstructures calculated by Novikov et al. [22] for bi-layer Hg-1212 and tri-layer Hg-1223, which have flat CuO_2 planes separated by Ca, reveal that $t_\perp$ has v^2-dispersion (24) and that $t_\perp(X) \sim 0.25$ eV, like for undimpled $YBa_2Cu_3O_7$. Exactly the same is found from Mattheiss and Hamann's calculation [23] for flat bi-layer $Bi_2Sr_2CaCu_2O_8$ (provided that one looks at the bands where they are purely CuO_2-like). Finally, all calculations for the idealized infinite-layer material $CaCuO_2$ with flat planes and without apical oxygen exhibit k_z-dispersion like $2t_\perp(\mathbf{k}_\parallel)\cos ck_z$, exactly as expected from (24). The maximum bandwidth is 1 eV so that, here again, $t_\perp(X) \sim 0.25$ eV.

A related, but less generic problem is the inter-plane hopping through insulating spacer layers, such as (BaO)Hg(BaO) in the Hg compounds. Here, inspection of both existing calculations [22,24] for the single-layer material reveals that the k_z-dispersion is like $2t_\perp(\mathbf{k}_\parallel)\cos ck_z$, once more, and that $t_\perp(X) \approx 30$ meV in both calculations, that is, *an order of magnitude smaller* than for hopping between multi-layers. Considering the fact, that this "backwards hopping" proceeds mainly through the apical-oxygen z-orbital, v^2-behavior is to be expected, because the $O4_z$-orbital has $m_z=0$ and therefore only couples to Cu_s.

$t_\perp(\mathbf{k})$ is the important quantity in the inter-layer pair tunnelling mechanism of P.W. Anderson et al. [19] for boosting T_c, and v^2-dependence was in fact assumed by Chakravarty inspired by LDA bands. According to the inter-layer pair tunnelling theory, correlation effects block the hopping of single electrons between the planes, but in the superconducting state a Cooper pair may tunnel due to the Josephson coupling:

$$H_J \approx -\sum_{\mathbf{k}} T_J(\mathbf{k}) \left(c_{\mathbf{k}\uparrow}^{(1)\dagger} c_{-\mathbf{k}\downarrow}^{(1)\dagger} c_{-\mathbf{k}\downarrow}^{(2)} c_{\mathbf{k}\uparrow}^{(2)} + h.c. \right)$$

$$\text{where} \quad T_J(\mathbf{k}) \approx t_\perp(\mathbf{k})^2 / t. \tag{26}$$

BCS mean-field theory then yields the following crude estimate of the anisotropy of the superconducting gap and T_c:

$$\Delta(\mathbf{k}_F) \sim \Delta_0(\mathbf{k}_F) + T_J(\mathbf{k}_F)/2 \quad \text{and} \quad T_c \sim \max T_J(\mathbf{k}_F)/4$$

With our parameter values, this means that the gap for a bi-layer should be something like $\Delta_0(\mathbf{k}_F) + 50\text{meV} \cdot v^4/(1-2ru)^4$, traced along the FS (see Fig. 7), and that $T_c \sim 300$ K.

9. BAND DISPERSION IN AN ANTI-FERROMAGNETIC INSULATOR

It has been a challenge to understand how the valence band, or rather, its spectral density, evolves as a function of doping as the material changes from an anti-ferromagnetic insulator (AFI) to a metal, becoming superconducting at low temperature. ARPES [20] for the un-dopable AFI $Sr_2CuO_2Cl_2$ with a single flat CuO_2 plane, gave a valence-band which dispersed little from Γ $(0,0)$ to X $(\pi,0)$ and which rose to a nearly isotropic maximum at $\frac{1}{2}\Gamma S$ $\left(\frac{\pi}{2},\frac{\pi}{2}\right)$ (see Fig. 6). Except for the band-width, this did not agree with many-body calculations for the $t-J$ [9] and $t-U$ [25] Hubbard models, which predicted the rise to be from Γ to X, and the maximum to be flat along the AF zone-boundary $(\pi,0)$-$\left(\frac{\pi}{2},\frac{\pi}{2}\right)$.

In the right-hand side of Fig. 6 we show the calculated band structure of an AFI in the simplest possible approximation where an external staggered field of size $\pm\frac{m}{2}U$ was applied to the $Cu_{x^2-y^2}$ orbital. The results for $Um = 2$, 4, and 6 eV are shown. In order to reproduce the experimental gap of 1.8 eV, one would choose $Um \sim 5$ eV. The single-particle Hamiltonian was taken to be the 4-band Hamiltonian $\langle\sigma|H|\sigma\rangle$. One observes that the calculated dispersion has exactly the *same* characteristics as the experimental one, except that the band-width is 4 times too large, as might have been expected. We made the points [26] that the discrepancy between the experiment and the many-body calculations is caused by the use of an oversimplified single-particle Hamiltonian, namely the 1-band nearest-neighbor Hamiltonian (the t-model), and that inclusion of t' (and t'') should fix the problem. This has turned out to be true [27]. Let us now explain the mean-field results in some detail.

For $Um = 0$ (not shown), the bands are simply the anti-bonding σ-band folded into the AF Brillouin zone. This folding is around the v-axis, so that u and $-u$ become equivalent, and the two bands are degenerate along the v-axis. The dispersion along the v-axis is the 1.25 eV that we calculated in connection with Eq. (11) and which, on the d-scale, is

from 1 to $1-2r$. For the t-model this dispersion does not exist. The relevant feature seen in Fig. 6 is that this dispersion along the AF zone boundary hardly changes when the staggered field is turned on. All that happens is that a gap of about half the size of the field (~ 50% Cu_d character) opens up while the dispersion essentially remains.

The mathematics of this is really simple: The staggered field operates on Cu_d and couples $\epsilon(\mathbf{k})$ to $\epsilon(\mathbf{k}+\mathbf{q})$ with $\mathbf{q} \equiv \left(\frac{\pi}{a}, \frac{\pi}{a}\right)$, that is, $\epsilon(u, v)$ is coupled to $\epsilon(-u, v)$. The energy dependent 1-band σ-Hamiltonian (7) therefore becomes:

$$\begin{array}{lll} H(\epsilon) & |\mathbf{k}\rangle & |\mathbf{k}+\mathbf{q}\rangle \\ \langle\mathbf{k}| & \epsilon_d + \dfrac{(2t_{pd})^2}{\epsilon-\epsilon_p}\left(1-u-\dfrac{v^2}{1-u+s(\epsilon)}\right) & \dfrac{m}{2}U \\ \langle\mathbf{k}+\mathbf{q}| & \dfrac{m}{2}U & \epsilon_d + \dfrac{(2t_{pd})^2}{\epsilon-\epsilon_p}\left(1+u-\dfrac{v^2}{1+u+s(\epsilon)}\right) \end{array} \tag{27}$$

Along the AF zone boundary, $u = 0$, we obtain:

$$\epsilon = \epsilon_d + \frac{(2t_{pd})^2}{\epsilon-\epsilon_p}\left(1-\frac{v^2}{1+s(\epsilon)}\right) \pm \frac{m}{2}U$$

This demonstrates that the dispersion along the v-axis is independent of the staggered field, and that the splitting is independent of v. Hence, the $-2rv^2$ dispersion remains whatever it was for U=0. These statements are of course only true if we neglect the energy-dependences of $\epsilon - \epsilon_p$ and $s(\epsilon)$; in reality the valence band tends to get compressed at energies closer to ϵ_p and to gain O_p character. Solving for ϵ yields (11) with $u = 0$ and ϵ_d substituted by $\epsilon_d \pm \frac{m}{2}U$.

For an energy range which is narrow in comparison with the distances from $\epsilon_p \sim \epsilon_d$ and ϵ_s, we may like in (18) expand the diagonal of the secular matrix $[H(\epsilon) - \epsilon](\epsilon - \epsilon_p) / (2t_{pd})^2$ to linear order around an energy at the center of interest. For consistency, we shall denote this energy ϵ_F, although it will usually not be the Fermi energy. In order that the resulting 2×2 Hamiltonian yields eigenvalues correct to linear order, the off-diagonal matrix element needs only be correct *at* ϵ_F. For simplicity, we shall neglect $\dot{s}$, which is a reasonable approximation for the un-split and for the *upper* Hubbard band because its center is at ~4.1 eV when $Um \sim 5$ eV. The resulting 1st-order Hamiltonian is simply:

$$\begin{array}{lll} \mathcal{H} & |\mathbf{k}\rangle & |\mathbf{k}+\mathbf{q}\rangle \\ \langle\mathbf{k}| & \varepsilon(\mathbf{k}) & \dfrac{m}{2}U|c_d|^2 \\ \langle\mathbf{k}+\mathbf{q}| & \dfrac{m}{2}U|c_d|^2 & \varepsilon(\mathbf{k}+\mathbf{q}) \end{array}, \tag{28}$$

where $\varepsilon(\mathbf{k})$ was given by (18) and $|c_d|^2 = (\epsilon_F - \epsilon_p)(2t_{pd})^{-2}\dot{d}^{-1} = \frac{\epsilon_F-\epsilon_p}{2\epsilon_F-\epsilon_p-\epsilon_d} \sim \frac{1}{2}$ is the Cu_d character (13) at ϵ_F. As previously discussed, $|c_d|^2$ does not depend on $\mathbf{k}$ when $\dot{s} = 0$. Had we gone to higher order in the $\epsilon - \epsilon_F$ expansion, the Hamiltonian would still have been (28), but with $\varepsilon(\mathbf{k})$ and $|c_d|^2$ substituted by respectively $\epsilon(\mathbf{k})$ and $|c_d(\mathbf{k})|^2$. This form holds generally, e.g. also if it were derived from the 8-band model and on-site Coulomb interactions were included on other orbitals, when we define:

$$U|c(\mathbf{k})|^2 \equiv \langle\psi(\mathbf{k})|U|\psi(\mathbf{k}+\mathbf{q})\rangle = \sum c_i^*(\mathbf{k})U_i c_i(\mathbf{k}+\mathbf{q}). \tag{29}$$

From (28), the upper and lower bands are then:

$$E(\mathbf{k}) = \frac{\epsilon(\mathbf{k})+\epsilon(\mathbf{k}+\mathbf{q})}{2} \pm \sqrt{\left(\frac{\epsilon(\mathbf{k})-\epsilon(\mathbf{k}+\mathbf{q})}{2}\right)^2 + \left(\frac{m}{2}U|c(\mathbf{k})|^2\right)^2}. \tag{30}$$

If $\epsilon(\mathbf{k})$ and $|c(\mathbf{k})|^2$ are low-energy expansions, the result of (30) only applies close to ϵ_F. Hence, we must use different ϵ_F's for the upper and lower bands, as is also natural, because their characters are very different when $Um \sim 5$ eV: The valence band is O_p -like and the upper Hubbard band is Cu_d-like. Remember also, that $H(\epsilon)$ in (27) for an anti-ferromagnet describes 8 rather than 2 bands, and that (30) can describe any of them through choice of ϵ_F and the appropriate sign.

10. INTER-PLANE EXCHANGE ACROSS A BI-LAYER, $J_\perp$

For anti-ferromagnetic bi-layer materials, such as $YBa_2Cu_3O_6$, the spin-order across the bi-layer is anti-ferromagnetic and the inter-layer exchange-coupling constant $J_\perp$ is an important parameter in many theories of high-temperature

superconductivity and for understanding the origin of the so-called spin gap [28,29]. From neutron scattering experiments on $YBa_2Cu_3O_{6+x}$ it has been found [30] that, upon hole doping far into the metallic regime, the anti-ferromagnetic spin-correlations between the planes are more persistent that those in the planes. The value of $J_\perp$ is under dispute, but it seems clear that in $YBa_2Cu_3O_6$ the absolute value must exceed 7 meV because the optical spin-wave branch, which should be at energy $2\sqrt{J_\parallel J_\perp}$, could not be detected with neutron scattering up to 60 meV [31], and the intra-plane exchange constant is experimentally known to be –120 meV. From mid-infrared measurements of the spin-wave spectrum in $YBa_2Cu_3O_6$ [32] it was recently concluded that $J_\perp \sim -65$ meV. SEDOR experiments on the $YBa_2Cu_3O_7$-$YBa_2Cu_4O_8$ *metallic* compound [33], on the other hand, indicates that $J_\perp/J_\parallel$ increases strongly with decreasing temperature and reaches a maximum value of 0.3 just above T_c. This presumably puts an upper bound of 50 meV on $J_\perp$. We shall now estimate the value of $J_\perp$ through several implementations of simple mean-field theory. In all cases we assume the value $Um = 5$ eV for the self-consistent field applied to the Cu d orbitals.

We consider the insulating phase, apply the staggered field ±2.5 eV inside each plane, and calculate the tiny difference, $\mathcal{E}(\mathrm{F}) - \mathcal{E}(\mathrm{AF})$, in the sum of the band-structure energies according to whether the orientation of the staggered field is ferro- (F) or anti-ferromagnetic (AF) between the to planes of the bi-layer. This energy difference per Cu spin is $J_\perp/4$. Before we present an analytical calculation based on the results of the two previous sections, we list results of various numerical calculations:

Hamiltonian:	H_8	LDA	H_8	H_4	$H_4\ t_{ss}^\perp, t_{sp}^\perp$	$H_4\ t_{ss}^\perp, t_{sp}^\perp$
Procedure:	$4\langle t_\perp^2/U\rangle$	F,AF	F,AF	$4\langle t_\perp^2/U\rangle$	$4\langle t_\perp^2/U\rangle$	F,AF
U :	$Cu_{x^2-y^2,xz,yz}$	$Cu_{x^2-y^2}$	$Cu_{x^2-y^2}$	$Cu_{x^2-y^2}$	$Cu_{x^2-y^2}$	$Cu_{x^2-y^2}$
$J_\perp$/meV:	–25	–13	–13	–17	–8	–6

These result are seen to scatter between –6 and –25 meV. Our largest calculation (LDA) used the charge-self consistent LDA potential for non-magnetic $YBa_2Cu_3O_6$ and applied the staggered field to the $Cu_{x^2-y^2}$ orbital in a standard multi-orbital band-structure calculation using the orthonormal LMTO representation, diagonalization of the Hamiltonian, and summation over the occupied bands in the AF Brillouin zone to obtain $\mathcal{E}(\mathrm{F})$ and $\mathcal{E}(\mathrm{AF})$. Surprisingly, the same result ($J_\perp = -13$ meV) was obtained with the same brute-force procedure (F,AF), but using H_8^+ and H_8^- for the non-magnetic part of the Hamiltonian. In the latter calculation we took advantage of the fact that the magnetic perturbation for inter-plane F/AF-order is even/odd so that it can not/only mix H^+ and H^-. In this way, the matrices to be diagonalized were only 16×16 for H_8. If we apply the same procedure, but start from the simplified $t_{ss}^\perp, t_{sp}^\perp$-version of H_4 which includes inter-plane hopping via Cu s orbitals only, we find a $J_\perp$ which is only –6 meV. The three remaining numerical calculations listed in the table employed a perturbative procedure labelled $4\langle t_\perp^2/U\rangle$, which we shall now explain.

We use the 1-band expression (30) and calculate the change in the total energy as the *negative* of the change of the total energy of merely the *upper* Hubbard band. This neglects the change of the energy of the highest, Cu_s-like band. Expansion of (30) to lowest order in $[\epsilon(\mathbf{k}) - \epsilon(\mathbf{k}+\mathbf{q})]/Um|c(\mathbf{k})|^2$ (the result (34) will hold beyond this order) yields for the upper band:

$$E(\mathbf{k}) \approx \frac{\epsilon(\mathbf{k}) + \epsilon(\mathbf{k}+\mathbf{q})}{2} + \frac{m}{2}U|c(\mathbf{k})|^2 + \frac{1}{mU|c(\mathbf{k})|^2}\left(\frac{\epsilon(\mathbf{k}) - \epsilon(\mathbf{k}+\mathbf{q})}{2}\right)^2 \tag{31}$$

For a bi-layer, inter-plane F-order couples $\epsilon^\pm(\mathbf{k})$ to $\epsilon^\pm(\mathbf{k}+\mathbf{q})$, while inter-plane AF-order couples $\epsilon^\pm(\mathbf{k})$ to $\epsilon^\mp(\mathbf{k}+\mathbf{q})$. The even and odd upper bands for F-order are therefore:

$$E^\pm(\mathbf{k}) \approx \frac{\epsilon^\pm(\mathbf{k}) + \epsilon^\pm(\mathbf{k}+\mathbf{q})}{2} + \frac{m}{2}U|c(\mathbf{k})|^2 + \frac{1}{mU|c(\mathbf{k})|^2}\left(\frac{\epsilon^\pm(\mathbf{k}) - \epsilon^\pm(\mathbf{k}+\mathbf{q})}{2}\right)^2, \tag{32}$$

while the two upper bands for AF-order are

$$E^{1,2}(\mathbf{k}) \approx \frac{\epsilon^\pm(\mathbf{k}) + \epsilon^\mp(\mathbf{k}+\mathbf{q})}{2} + \frac{m}{2}U|c(\mathbf{k})|^2 + \frac{1}{mU|c(\mathbf{k})|^2}\left(\frac{\epsilon^\pm(\mathbf{k}) - \epsilon^\mp(\mathbf{k}+\mathbf{q})}{2}\right)^2. \tag{33}$$

The difference in total energy per Cu spin thus works out as:

$$\begin{aligned} -\frac{1}{4}J_\perp &\equiv \mathcal{E}(\mathrm{F}) - \mathcal{E}(\mathrm{AF}) \\ &= \frac{1}{2}\left\langle E^1(\mathbf{k}) + E^2(\mathbf{k}) - E^+(\mathbf{k}) - E^-(\mathbf{k})\right\rangle \\ &= \left\langle \frac{t_\perp(\mathbf{k})\, t_\perp(\mathbf{k}+\mathbf{q})}{mU|c(\mathbf{k})|^2}\right\rangle, \end{aligned} \tag{34}$$

where $\langle\rangle$ denotes the average over the Brillouin zone. As usual (23), $t_\perp(\mathbf{k})$ is half the splitting between the odd and even bands for U=0. Expression (34) in real space is, in fact, the familiar one for Anderson super-exchange.

The results labelled $4\langle t_\perp^2/U\rangle$ were now obtained by diagonalizing the appropriate non-magnetic 4×4 or 8×8 Hamiltonians $H^+(\mathbf{k})$ and $H^-(\mathbf{k})$ numerically, extracting the odd-even splitting to form $t_\perp(\mathbf{k})$, the eigenvectors to form $mU|c(\mathbf{k})|^2$, and summing over the Brillouin-zone (34). The result obtained in this way for the simplified 4-band Hamiltonian ($J_\perp$ =–8 meV) is in accord with, but slightly larger than that obtained with the direct procedure for the same Hamiltonian. The result obtained for the full 4-band Hamiltonian ($J_\perp$ =–17 meV) is twice as large. Finally, since the conduction band of the 8-band model has Cu_{xz} and Cu_{yz} components besides $Cu_{x^2-y^2}$, we did a calculation in which $|c(\mathbf{k})|^2$ denoted the sum of the characters for all three Cu d-orbitals, rather than just that of $Cu_{x^2-y^2}$. The corresponding decrease of the denominator in (34) raised $J_\perp$ to –25 meV.

We thus conclude that, for the purpose of calculating $J_\perp$ in the mean-field approximation, H_8 simulates the full LDA Hamiltonian very well, the perturbation-expression (34) for $J_\perp$ is accurate, the assumption of inter-plane hopping via only Cu_s under-estimates $J_\perp$ by a factor 2, by-mixing of Cu $d\pi$ character enhances $J_\perp$, and our *best estimate* of $J_\perp$ is ~–20 meV.

With expression (34) we may evaluate $J_\perp$ *analytically* for H_4, using (13) for the $Cu_{x^2-y^2}$ character and the 1st-order expressions (24) and (25) for $t_\perp(\mathbf{k})$ in the $t_{ss}^\perp, t_{sp}^\perp$-approximation. We obtain:

$$-J_\perp = 4\frac{t_\perp(\mathrm{X})^2}{mU|c_d|^2}\left(\frac{3}{8}\right)^2\left(1+\frac{2}{9}r^2+..\right) \approx 4\frac{(0.17\,\mathrm{eV})^2}{5\,\mathrm{eV}\cdot 0.57}\cdot 0.14 = 6\mathrm{meV} \tag{35}$$

where $t_\perp(\mathrm{X})$ was given in (25) and the last factors come from the Brillouin-zone average:

$$\left\langle\left(\frac{v^2}{1-(2ru)^2}\right)^2\right\rangle = \left\langle v^4\left[1+2(2ru)^2+..\right]\right\rangle = \left(\frac{3}{8}\right)^2\left(1+\frac{2}{9}r^2+..\right) \tag{36}$$

The numerical estimate for $-J_\perp$ was obtained by using the expansion energy $\epsilon_F = \epsilon\left(\frac{\pi}{2a}, \frac{\pi}{2a}\right) = 2.78$ eV, which is at the center of the U=0-band, and for which we can safely neglect s. The –6 meV is in good agreement with the values obtained numerically for the same Hamiltonian. Since the v^4-dependence dominates the ru-dependence in the average over the Brillouin-zone, expression (35) for $J_\perp$ is fairly insensitive to details of the dispersion. If for $t_\perp(\mathrm{X})$ we merely insert the LDA value of 0.25 eV, expression (35) in fact yields: $J_\perp \approx -13$ meV, which is the LDA result.

Barriquand and Sawatzky [34] recently obtained $J_\perp \sim -56$ meV from a real-space evaluation of (34). One reason for the discrepancy with our value is, that these authors only considered the perpendicular hopping integral $t_{pp}^\perp$ and took it to be 2.5 times larger than our value (as given in Sect. 8). It seems to us, that had the perpendicular hopping been dominated by $t_{pp}^\perp$, then $t_\perp(\mathbf{k})$ would have been nearly independent of $\mathbf{k}$, in contradiction with the even-odd splittings found in all LDA calculations.

In a numerical (F,AF)-calculation, we can simulate hole-doping crudely by moving the Fermi level into the valence band. At the same time, the mean field should be reduced in such a way that it vanishes at a hole doping of about 0.2 per plane. Fig. 8 shows the result of such a calculation of $J_\perp$ for many different values of the field. The persistence of the inter-plane anti-ferromagnetic coupling with increasing doping is clearly seen, until a point where $J_\perp$ changes sign and the coupling becomes ferro-magnetic. *Acknowledgements*—We are grateful to T.M. Rice for suggesting that we evaluate $J_\perp$ from our low-energy Hamiltonian. Discussions with Z.-X. Shen, J.C. Campuzano,W. Hanke, D.J. Scalapino, and P.W. Anderson are gratefully acknowledged.

REFERENCES

1. Rodriguez C.O, Liechtenstein A.I.,Mazin I.I., Jepsen O.,Andersen O.K. and Methfessel M. ,*Phys. Rev. B* **42**, 2692 (1990).
2. See review by Cohen R. E., *Computers in Phys.* **8**, 34 (1994).
3. Andersen O.K.,Liechtenstein A.I., Rodriguez C.O., Mazin I.I , Jepsen O., Antropov V.P. , Gunnarsson O., Gopalan S., *Physica* **C185–189**, 147 (1991).
4. Kircher J. , Alouani M. , Garriga M. , Murugaraj P. , Maier J. , Thomsen C. , Cardona M. ,Andersen O.K. and Jepsen O. , *Phys. Rev. B* **40**, 7368 (1989); Kircher J. , Humlicek J., Garriga M. , Cardona M.Cardona , Fuchs D. , Habermeier H.-U., Jepsen O. , Gopalan S. and Andersen O.K ,*Physica C* **192**, 473 (1992); Kircher J. , Cardona M. , Alouani, M., Gopalan S. , Jepsen O. ,Andersen O.K, , Kaldis E. , Kapinski J. and Rusieki, S., *Physica C* **200**, 413 (1992).
5. Pickett W.E.,Cohen R.E. and Krakauer H. ,*Phys. Rev. B* **42**, 8764 (1990).

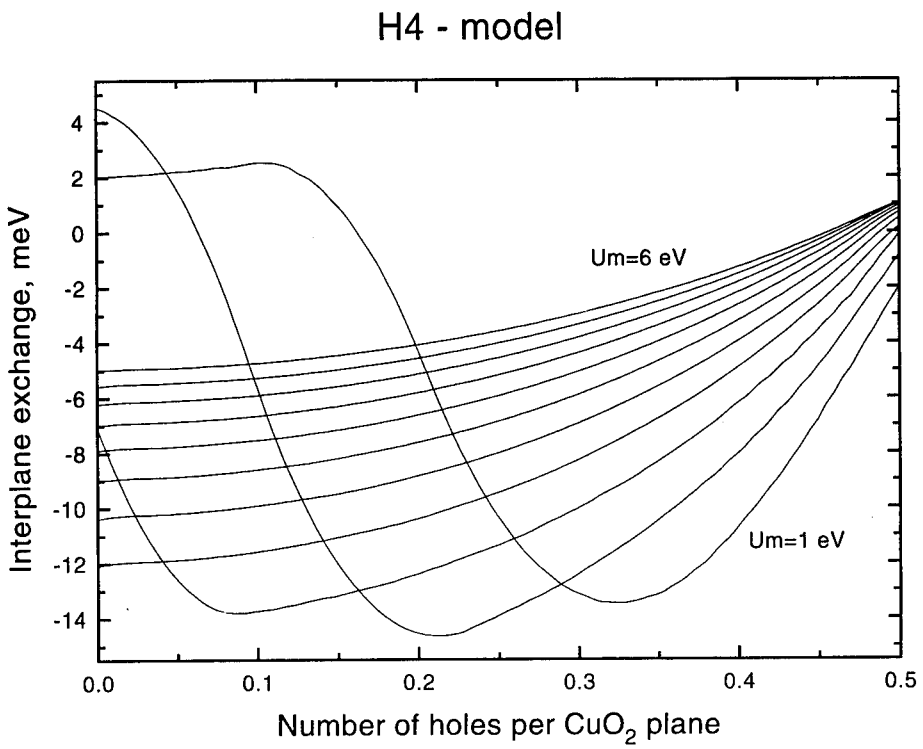


Fig. 8. $J_\perp$ as a function of hole doping calculated for many different values of the staggered field. The single-particle Hamiltonian was H_4 $t_{ss}^{\perp}, t_{sp}^{\perp}$ and the procedure was (F,AF) as explained in the text.

6. Zaanen J., Paxton A.T. , Jepsen O. and Andersen O.K. ,*Phys. Rev. Lett.* **60**, 2685 (1988); Yu J. , Massidda S. , Freeman A.J. and Podloucky R. ,*Physica C* **214** (1993).
7. J.G. Tobin, C.G. Olson, C. Gu, J.Z. Liu, F.R. Solal, M.J. Fluss, R.H. Howell, J.C. O'Brien, H.B. Radousky, and P.A. Sterne, Phys. Rev. B **45**, 5563 (1992); K. Gofron, J.C. Campuzano, H. Ding, C. Gu, R. Liu, B. Dabrowski, B.W. Veal, W. Cramer, and G. Jennings, J. Phys. Chem. Solids, **54**, 1193 (1993); Phys. Rev. Lett. **73**, 3302 (1994); D.S. Dessau, Z.-X Shen, D.M. King, D. Marshall, L.W. Lombardo, P. Dickenson, J. DiCarlo, C.H. Park, A.G. Loeser, A. Kapitulnik, and W.E. Spicer, Phys. Rev. Lett. **71**, 2781 (1993).
8. Khodel V.A. and Shaginyan V.R., JETP Lett. **51**, 553 (1990); Khodel V.A. , Clark J.W. and Shaginyan V.R. , (preprint).
9. Dagotto E. ,*Rev. Mod. Phys.* **66**, 763 (1994).
10. Dopf G., Muramatsu A. and Hanke W. ,*Phys. Rev. Lett.* **68**, 353 (1992).
11. Z.-X. Shen and Dessau D.S. ,*Physics Reports* **253**, 1 (1995).
12. Zaanen J., Jepsen O. , Gunnarsson O. , Paxton A.T. , Andersen O.K. and Svane A.,*Physica C* **153–155**, 1636 (1988); Anisimov V.I., Zaanen J. and Andersen O.K. , *Phys. Rev. B* **44**, 943 (1991).
13. Hybertsen M.S. , Schlüter M. and Christensen N.E. ,*Phys. Rev. B* **39**, 9028 (1989).
14. McMahan A.K., Martin R.M. and Satpathy S. ,*Phys. Rev.* **38**, 6650 (1988).
15. Thomsen C. , Cardona M. , Friedl B. , Rodriguez C.O. , Mazin I.I. and O.K. Andersen ,*Solid State Commun.* **75**, 219 (1990).
16. Krakauer H. , Pickett W.E. and Cohen R.E. , *Phys. Rev. B* **47**, 1002 (1993).
17. Jepsen O. and Andersen O.K. , *Z. f. Physik* **97**, 35 (1995).
18. Andersen O.K. , Jepsen O. , Liechtenstein A.I. and Mazin I.I. ,*Phys. Rev. B* **49**, 4145 (1994).
19. Chakravarty S., SudbøA. , Anderson P.W. and Strong S. , *Science*, **261**, 337 (1993).
20. Wells B.O. , Shen Z.-X., Matsuura A. , King D.M. , Kastner M.A. , Greven M. and Birgenau R.J.,*Phys, Rev. Lett.* **74**, 964 (1995).
21. Rodriguez C.O. , Liechtenstein A.I. , Jepsen O. , Mazin I.I. and Andersen O.K. ,*Computational Materials Science* **2**, 39 (1994).
22. Novikov D.L. and Freeman A.J. , *Physica C* **216**, 273 (1993).
23. Mattheiss L.M. and Hamann D.R. ,*Phys. Rev. B* **38**, 5012 (1988).
24. Rodriguez C.O. , *Phys. Rev. B* **49**, 1200 (1994).
25. Bulut N. , Scalapino D.J. and White S.R. ,*Phys. Rev. Lett.* **73**, 748 (1994).
26. Andersen O.K. , Jepsen O., Liechtenstein A.I. and Mazin I.I., Poster FR-PS 466 at the Conference: *Materials and Mechanisms of Superconductivity High-Temperature Superconductors* (Grenoble, France, 1994).
27. Nazarenko A., Vos K.J.E., Haas S. , Dagotto E. and Gooding R.J., *Phys. Rev. B* **51**, 8676 (1995).
28. Monien H. and Rice T.M. ,*Physica C* **235-240**, 1705 (1994); H. Monien and A.W. Sandvik, (preprint).
29. Menke U. Ubbens and Patrick A. Lee, Phys. Rev. **50**, 438 (1994).
30. Rossat-Mignod J., Regnault L.P., Bourges P., Burlet, C. Vettier, and Henry J.Y. , in *Frontiers in Solid State Sciences*, edited by L. C. Gupta and M. S. Multani (World Scientific, Singapore, 1993), Vol. 1, p.265.
31. Tranquada J.M., Gehring P.M., Shirane G. , Shamoto S. , and Sato M., *Phys. Rev. B* **46**, 5561 (1992).
32. Grüninger M. , Münzel J., Gaymann A. , Zibold A. ,Geserich, H.P. and Kopp T., (preprint).
33. Stern R. , Mali M. , Ross J. and Brinkmann D., (preprint).
34. Barriquand F. and Sawatzky G.A *Phys. Rev. B* **50**, 16 649 (1994).

Pergamon

J. Phys. Chem. Solids Vol. 56, No. 12, pp. 1593–1596, 1995
Copyright © 1995 Elsevier Science Ltd
Printed in Great Britain. All rights reserved
0022-3697/95 $9.50 + 0.00

0022-3697(95)00161-1

A BATTERY OF SMOKING GUNS (FOR THE NFL–INTERLAYER THEORY OF HIGH T_c CUPRATES) ★

P. W. ANDERSON

Joseph Henry Laboratories of Physics, Jadwin Hall, Princeton University Princeton, NJ 08544, U.S.A.

Abstract—After giving an introductory summary of the Luttinger Liquid–Interlayer Tunneling theory of High T_c, I shall describe a sequence of experiments and interpretations which range from conclusive and crucial to strongly indicative for the interlayer tunneling mechanism and its underlying basis, that the normal metal in the cuprates is a 2-dimensional non-Fermi liquid. The introductory summary emphasized the clear separation between the mechanism for superconductivity, which depends on the material between CuO_2 layers, and the properties of the individual layers, which form a strictly 2D electron gas. Figure 1 illustrates the lack of correlation between these two aspects. (Revised by N. P. Ong from a figure of B. Batlogg.)

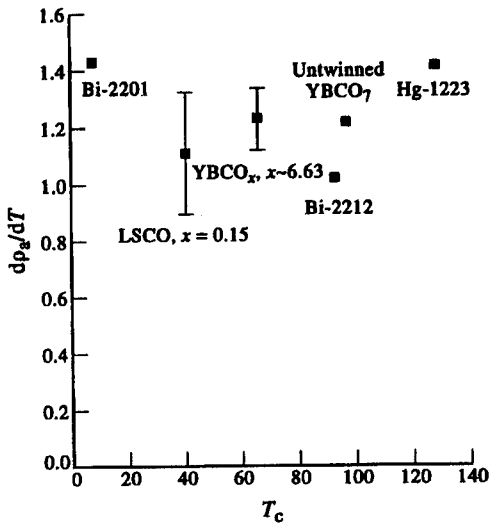


Fig. 1. T_c does not correlate with planar properties for optimally doped materials. Resistivity as here, Hall effect, or susceptibility would all tell the same story.

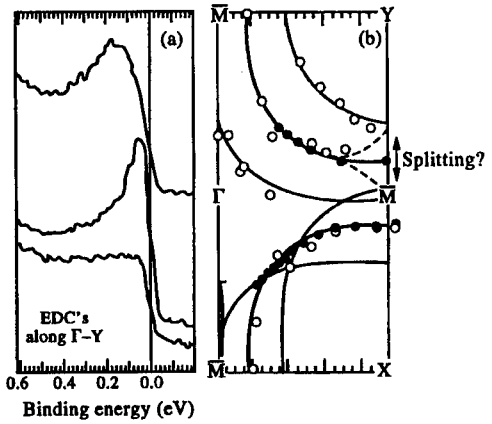


Fig. 2. Black dots: identified points on Fermi surface; other markings are "ghosts" due to superstructure, or other points off the Fermi surface.

The experiments are as follows:

Experiment 1

ARPES experiments on BISCO 2212 by the Campuzano group at Argonne National Laboratory using very high (~ 10 mev) resolution. These exhibit two striking features.

(a) After removing artifacts caused by 5×5 superstructure, they reveal a *single, simple, unsplit* Fermi surface in normal and superconducting states (see Fig. 2). Calculated splittings between "σ" and "π" (even and odd in the two layers of the bilayer) are of order 0.5 ev and should be easily visible. If this observation holds up it verifies a 5 year old prediction of the NFL theory (Central Dogma 4) which is unique to this theory among all contenders: for our theory, this is the crucial experiment. The data of three groups are in essential agreement on this point. (Aebi's "shadowband" is a minor (< 5%) feature, possibly artifactual.)Note that there is no hint of band splitting either in normal or superconducting states; in both, but particularly the latter, transport measurements tell us that quasiparticle widths are less (or much less) than kT_c (0.01 ev).

(b) The detailed structure of the gap as a function of transverse momentum is compatible neither with simple s nor d-wave ideas. The peaks near M are too sharp. See Fig. 3; they fit the interlayer matrix element fairly well, but not a broad BCS-type interaction. Details within the minima are close to resolution and it is premature to interpret them.

★ This work was supported by the NSF, Grant # DMR-9104873.

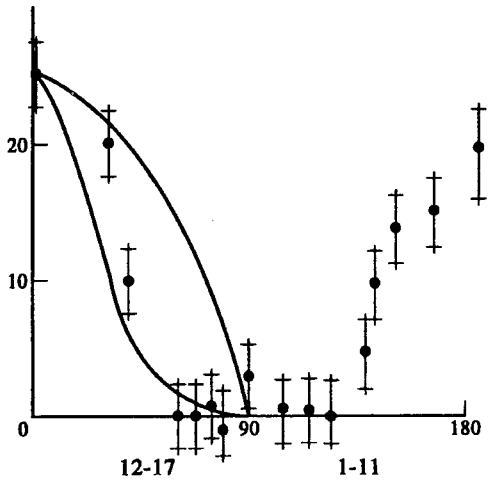


Fig. 3. Variation of gap with angle around Fermi surface. Upper line is d-wave, lower line is tunneling matrix element. gap does *fit* d-wave prediction.

Experiment 2

(a) c-axis infrared studies by Uchida, Timusk and van der Marel on $(La–Sr)_2CuO_4$ all give essentially identical results. There is a small conductivity in the normal state which can only be analyzed as a broad, incoherent continuum (early attempts at a Drude-like interpretation have been abandoned and were not realistic).

In the superconducting state a plasma edge grows in very rapidly as $T < T_c$, at a frequency somewhat below 50 cm^{-1} [see Fig. 4(a) and (b)].

We show that both observations are unique to our theory. The former, that the normal state (and quasiparticle) conductance is absent and is replaced by a broad, weak incoherent background,is analogous to the absence of splitting of the photoemission bands and has been discussed previously.

(b)Novel is the magnitude of the plasma edge, which reflects the magnitude of the conductivity δ-function at $\omega = 0$. This may be described by the dielectric function

$$\epsilon = \epsilon_0 - \frac{\omega_p^2}{\omega^2} + \left(+ i\frac{\sigma_{inc}}{\omega} \right) \tag{1}$$

and the plasma edge is seen at $\omega^2 = \frac{\omega_p^2}{\epsilon_0}$. ω_p^2 is compatible neither with the known c-axis hopping energy $t_\perp \sim 500cm^{-1}$, nor with the Mattis–Bardeen sum rule and the observed σ_{inc}. It can be accurately estimated by describing the interlayer contacts as Josephson junctions and making the Josephson coupling numerically equal to the condensation energy $N(0)\Delta^2$. This fixes ω_p^2, which is c^2/λ^2, where λ is the penetration depth, and the coherence lengthξ which is essentially the interlayer spacing in this one-layer material (smaller in multilayers). These results will soon appear in *Science*.

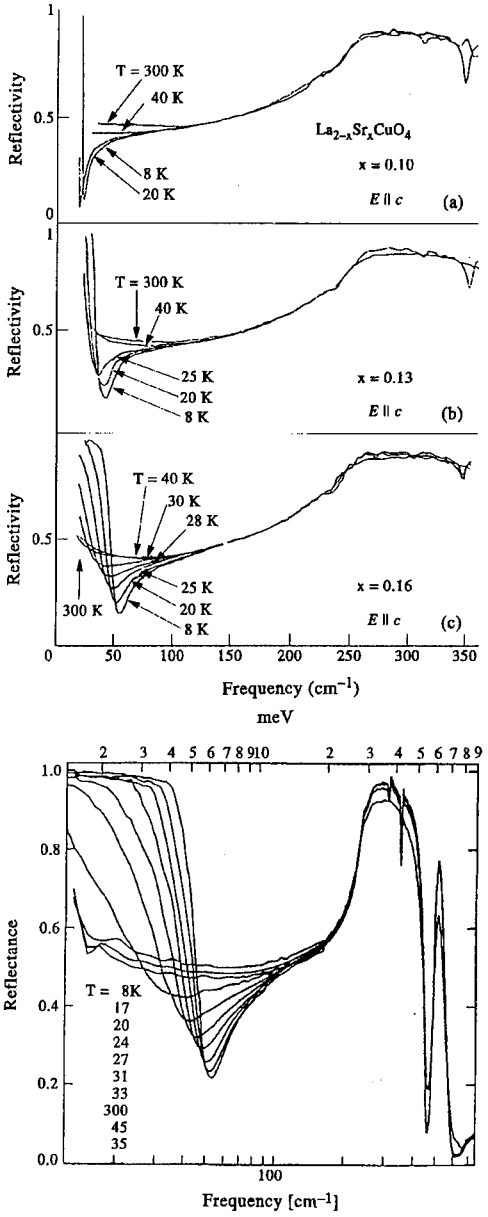


Fig. 4. Data by Uchida group and Timusk group showing rise of c-axis plasma edge below T_c, and "lossy dielectric"behavior above T_c.

Experiment 3

Infrared transmission measurements of *ab* plane conductivity by Bontemps *et al*, on a wide range of cuprate materials from 100–10,000 cm^{-1}, are in essential agreement from substance to substance as to the slope of $\hbar/\tau(\omega)$ vs ω and as to the variation of $m^{\times}(\omega)$ with ω [Fig. 5(a) and (b)] These fit a non-Fermi liquid expression easily derived very generally from the NFL Green's function:

$$\epsilon_{\text{free}} = \left(\frac{\omega_p}{i\omega} \right)^{2(1-\alpha)} \tag{2}$$

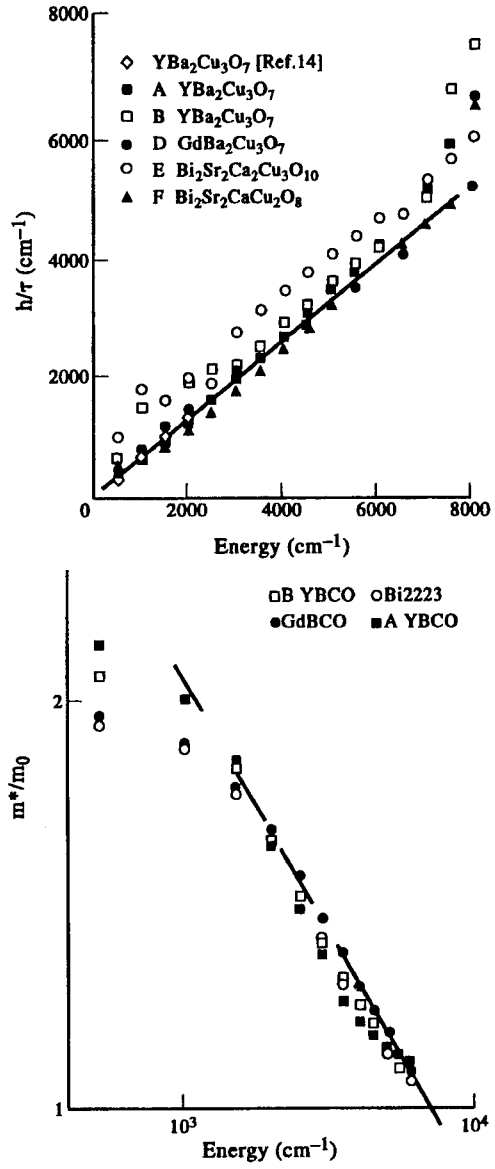


Fig. 5. (a) $\hbar/\tau(\omega)$ for infrared conductivity in *ab* plane defined as $\sigma = \frac{ne^2}{m^{\times}(\omega)} \frac{1}{\omega + i/\tau(\omega)}$ for a number of films measured by transmission. Line is fit from text. (b) $m^{\times}(\omega)$ from same measurement and fit. Line is power law as in text.

with $\alpha \sim .15$–$.2$. This is derived by using the "holon non-drag" approximation where vertex corrections are screened out by phonon and impurity scattering, and the simple two electron bubble is σ. The general homogeneity law for the Green's function

$$G = t^{-1+\alpha} F(r/t) \tag{3}$$

which follows from Luttinger liquid theory, gives (2). (This is also the expression used to derive the *c*-axis conductivity.) Fig. 6 gives a fit of one $\sigma(\omega)$ to this expression.

In the original talk I had intended to present the simple preliminary theory of spin-gap phenomena which follows

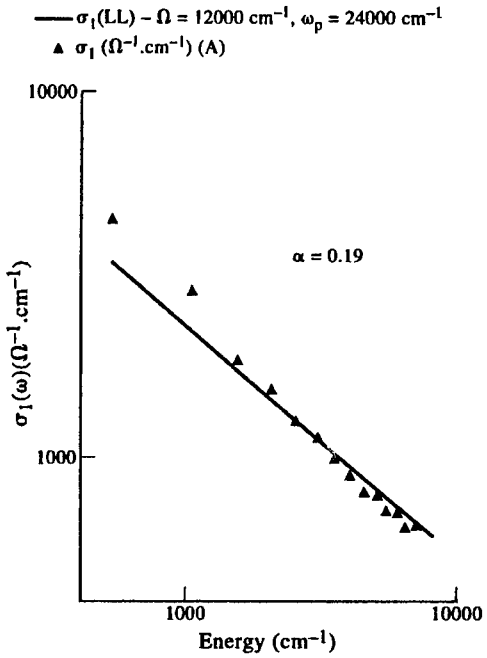


Fig. 6. Overall fit of power law to $\sigma(\omega)$.

Also: spin gap mechanism

Take each *k* separately:

Neglect ═══ inter-bilayer coupling

½ ═══ "BCS coupling"

$$\mathcal{H} = \lambda\delta(c^{+}_{k\uparrow}\, c^{+}_{-k\downarrow})^{1}\,(c_{-k\downarrow} c_{k\uparrow})^{2}$$

E

——— +2λ + H.C.

═══ 0

– – – BCS energy (mean field)

——— −2λ

No transition

$\chi_{\downarrow}$, DOS$_{\downarrow}$ etc

Fig. 7. Schema for spin gap theory.

from decoupling the bilayers from each other, given in the transparency reproduced as Fig. 7. This will appear in a forthcoming publication by Strong and myself. The neutron data of Keimer, and the observation that they seem to show coherence between bilayers, yet identical gap functions for the two layers (or even and odd combinations thereof), and that they peak broadly at the $M - \overline{M}$ wave vector region, are straightforwardly explained in our theory, but not, so far as we can see, uniquely so.

Pergamon

J. Phys. Chem. Solids Vol. 56, No. 12, pp. 1597–1600, 1995
Copyright © 1995 Elsevier Science Ltd
Printed in Great Britain. All rights reserved
0022–3697/95 $9.50 + 0.00

0022-3697(95)00260-X

EVOLUTION OF THE SINGLE-PARTICLE SPECTRAL WEIGHT WITH DOPING

N. BULUT and D. J. SCALAPINO
Department of Physics, University of California, Santa Barbara, CA 93106–9530, U.S.A.

Abstract—We have calculated the single–particle density of states $N(\omega)$ and the spectral weight $A(\mathbf{p}, \omega)$ for the two–dimensional Hubbard model by combining quantum Monte Carlo simulations with the maximum–entropy analytic continuation technique. We present results for various values of the doping, temperature, and Coulomb repulsion U. At half–filling an insulating gap separates incoherent lower and upper Hubbard bands. In addition, narrow quasiparticle bands exist at the top of the lower Hubbard band and at the bottom of the upper Hubbard band. The bandwidth of the quasiparticle bands is of order $2J$, where $J \approx 4t^2/U$. Upon small doping, spectral weight is transferred from states above the insulating gap to the top of the lower Hubbard band, and a narrow quasiparticle band of width $\sim 4J$ forms. We find that the dispersion of this narrow band is similar to the results of the recent angular resolved photoemission measurements of the hole doped cuprates. We argue that the generic nature of the quasiparticle dispersion relation observed in these materials arises from the strong Coulomb interaction and reflects the hole–spin correlations rather than the one–electron interactions which customarily determine the band structure.

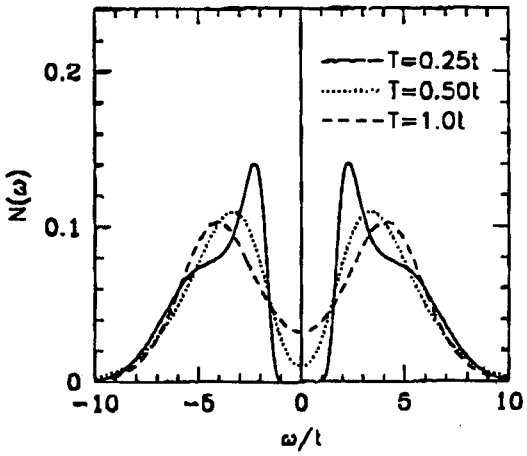


Fig. 1. Density of states $N(\omega)$ at half–filling for $U = 8t$ and different values of T.

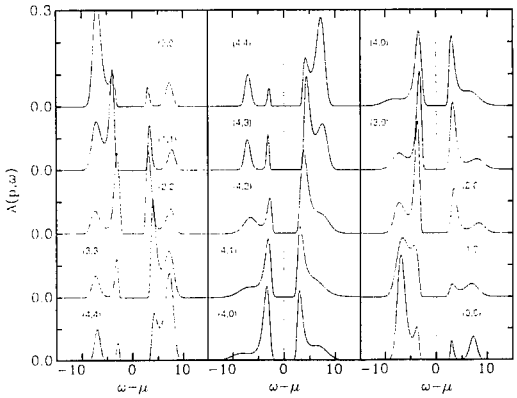


Fig. 2. Single–particle spectral weight $A(\mathbf{p}, \omega)$ at half–filling for $U = 10t$ and $T = 0.25t$ by Moreo *et al.* [7]. The numbers in parentheses denote the momentum $\mathbf{p} = (p_x, p_y)$ in units of $\pi/4$.

Numerical calculations of the single–particle spectral weight of the two dimensional Hubbard model provide insight into the nature of the single–particle excitations in a strongly correlated electron system. Here we review some of the recent results which have been obtained for this model.

The Hubbard Hamiltonian has the well known form

$$H = -t \sum_{\langle i,j\rangle,s} (c_{is}^{\dagger} c_{js} + c_{js}^{\dagger} c_{is}) + U \sum_{i} n_{i\uparrow} n_{i\downarrow}. \qquad (1)$$

Here $c_{is}^{\dagger}$ creates an electron of spin s on site i of a two–dimensional square lattice. The non–interacting $U = 0$ quasiparticle dispersion relation

$$\varepsilon_{\mathbf{p}} = -2t(\cos(p_x) + \cos(p_y)) \qquad (2)$$

has a bandwidth of $8t$. The Coulomb interaction U and the bandwidth $8t$ set the large energy scale. A lower energy scale is set by the exchange interaction $J \approx 4t^2/U$.

At half–filling, the ground state has antiferromagnetic long–range order and antiferromagnetic spin waves characterized by an energy scale J. When the system is doped away from half–filling, it is believed that there is no long–range magnetic order. However, there remain short–range antiferromagnetic correlations. In the following, we will examine the effect of both the onsite Coulomb interaction U and the antiferromagnetic correlations on the single particle properties of the half–filled and the doped system.

Quantum Monte Carlo techniques [1] have been used to provide information on the finite temperature single–particle Green's function

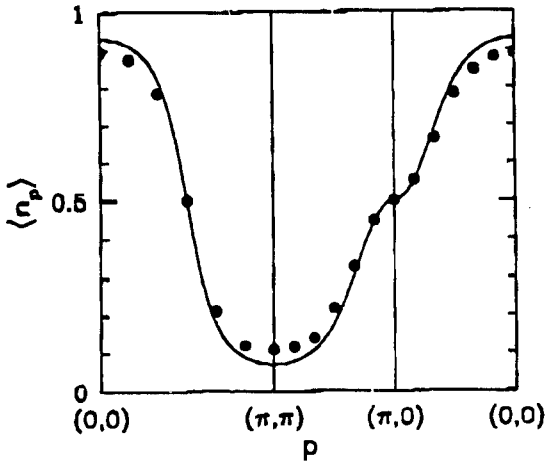


Fig. 3. Momentum occupation number $\langle n_{\mathbf{p}} \rangle$ versus $\mathbf{p}$ at half-filling for $T = 0.125t$. The points are the Monte Carlo data and the solid line is the mean field SDW result.

$$G_{ij}(\tau) = -\langle T_\tau c_i(\tau) c_j^\dagger(0) \rangle. \tag{3}$$

Fourier transforming on $(i-j)$, one obtains $G(\mathbf{p}, \tau)$, which for $\beta > \tau > 0$ is related to the spectral weight $A(\mathbf{p}, \omega)$ by

$$G(\mathbf{p}, \tau) = -\int_{-\infty}^{\infty} d\omega \, \frac{A(\mathbf{p}, \omega) e^{-\tau\omega}}{1 + e^{-\beta\omega}} \tag{4}$$

with $\beta = T^{-1}$. Various maximum entropy methods [2] have been used to estimate $A(\mathbf{p}, \omega)$. The single-particle density of states $N(\omega)$ can be calculated by summing $A(\mathbf{p}, \omega)$ over momenta or analytically continuing $G_{ii}(\tau)$. Finally, setting τ to 0^+ in $G(\mathbf{p}, \tau)$ gives the momentum occupation

$$\langle c_{\mathbf{p}s}^\dagger c_{\mathbf{p}s} \rangle = 1 + G(\mathbf{p}, 0^+). \tag{5}$$

It is also possible to calculate $A(\mathbf{p}, \omega)$, $N(\omega)$ and $\langle c_{\mathbf{p}s}^\dagger c_{\mathbf{p}s} \rangle$ with Lanczos methods on small lattices [4].

In Fig. 1, the single-particle density of states $N(\omega)$ at half-filling is shown at different temperatures for $U/t = 8$ and an 8×8 lattice [5]. At high temperatures, the on-site Coulomb interaction gives rise to incoherent upper and lower Hubbard bands. For $U/t = 8$, the exchange interaction $J \approx 4t^2/U = 0.5t$ so that as T decreases below J, antiferromagnetic correlations develop leading to narrow peaks in $N(\omega)$ and a more clearly defined gap. As first shown by Preuss *et al.* [6] and also reported by Moreo *et al.* [7], the low temperature spectral weight $A(\mathbf{p}, \omega)$, Fig. 2, consists of incoherent upper and lower Hubbard bands along with dispersing quasiparticle bands which can be fit by $\pm E_{\mathbf{p}}$ with

$$E_{\mathbf{p}} = \Delta + \frac{J}{2}(\cos k_x + \cos k_y)^2. \tag{6}$$

The spectral weight shifts [8] in a similar fashion to the mean field SDW result so that at $\mathbf{p} = (\pi/2, \pi/2)$, the weight is equally divided above and below $\omega = 0$ and as $\mathbf{p}$ moves below (above) $\mathbf{p}_F$ the weight shifts below (above) $\omega = 0$. This behavior is seen in the momentum occupation $\langle c_{\mathbf{p}s}^\dagger c_{\mathbf{p}s} \rangle$ plotted in Fig. 3, where the solid line is the mean field SDW result $\langle n_{\mathbf{p}} \rangle = (1 - \varepsilon_{\mathbf{p}}/E_{\mathbf{p}}^{\mathrm{MF}})$ with $E_{\mathbf{p}}^{\mathrm{MF}} = \sqrt{\varepsilon_{\mathbf{p}}^2 + \Delta^2}$ and $\Delta = 2.4t$.

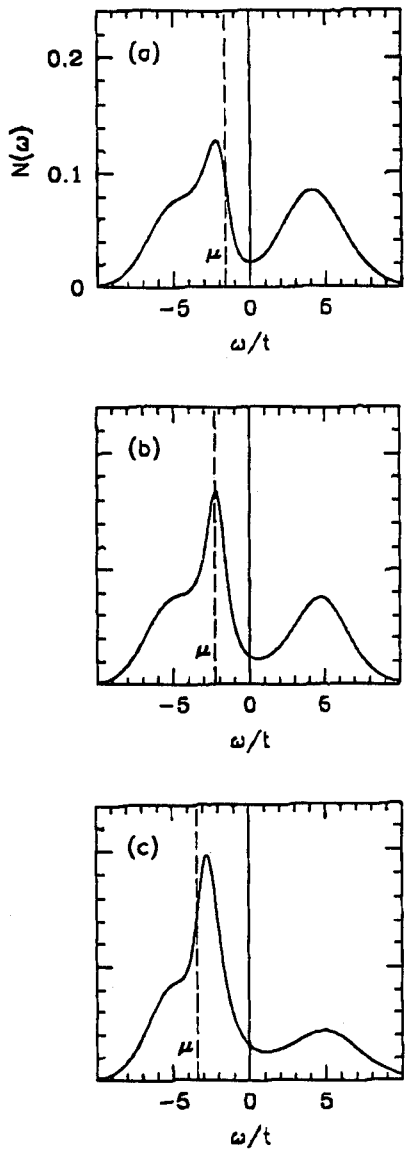


Fig. 4. Density of states $N(\omega)$ at $T = 0.5t$ for (a) $\langle n \rangle = 0.94$, (b) $\langle n \rangle = 0.87$ and (c) $\langle n \rangle = 0.70$.

When the system is doped away from half-filling, the fermion sign problem prevents Monte Carlo calculations from being run at low temperatures. For example with $U = 8t$ and $\langle n \rangle = 0.87$, it is difficult to obtain Monte Carlo data with good statistics at temperatures much below $0.3t$. Since $J \approx 4t^2/U = 0.5t$ for $U = 8t$, one is only just able to resolve energies on the scale of J. While the Lanczos exact diagonalization calculations provide ground state information, the small system size (4×4) again limits what one can conclude.

One feature that appears robust, is the shift of the chemical potential μ upon doping. This is illustrated for several

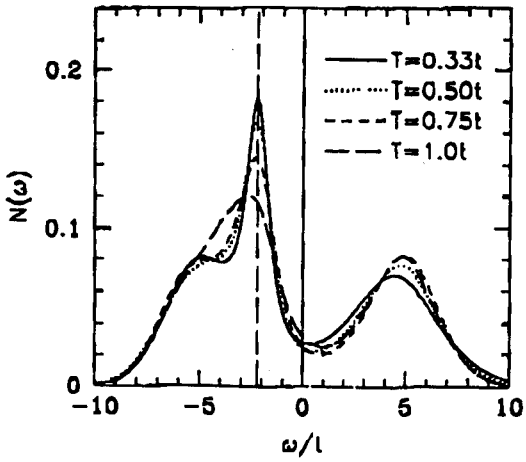


Fig. 5. Temperature variation of the density of states $N(\omega)$ at $\langle n \rangle = 0.87$.

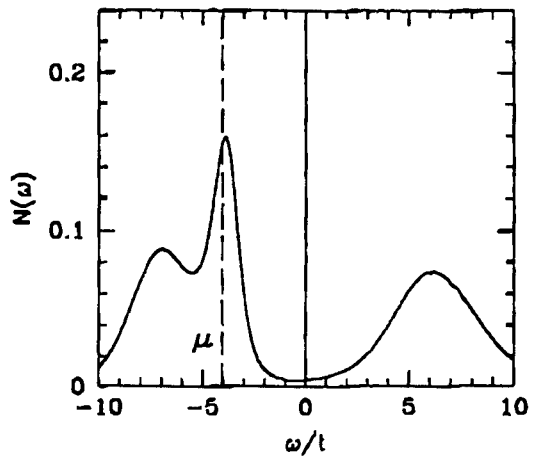


Fig. 6. Density of states $N(\omega)$ for $U = 12t$, $T = 0.5t$ and $\langle n \rangle = 0.87$.

different fillings in Fig. 4. Thus early PES data suggesting that there was only a small shift in μ upon going from the insulating to the metallic state of some cuprates differs from what one would expect if the Hubbard model provides an appropriate starting point for these systems. In addition to the shift of the chemical potential seen in Fig. 4, upon doping ($\langle n \rangle < 1$) spectral weight is shifted from the upper and lower bands of the insulating state forming a pseudogap with a narrow band of states at the upper edge of the lower Hubbard band [4]. Fig. 5 shows the evolution of $N(\omega)$ for the doped case as the temperature is lowered [5]. Just as for the half-filled case, at high temperatures $N(\omega)$ consists of incoherent upper and lower Hubbard bands with μ located near the top of the lower Hubbard band. Then, as the temperature decreases and short range antiferromagnetic correlations develop, a relatively narrow band of states forms at the upper edge of the lower Hubbard band. In Fig. 6, a similar peak is seen for $U = 12t$.

The spectral weight $A(\mathbf{p}, \omega)$ for $U = 8t$ and $\langle n \rangle = 0.87$ on a 12×12 lattice at $T = 0.5t$ is shown in Fig. 7 [9]. The insets show the direction of progression of the momenta for each segment of the figure. Clearly, one would like to have better temperature resolution than $T = J$. However,

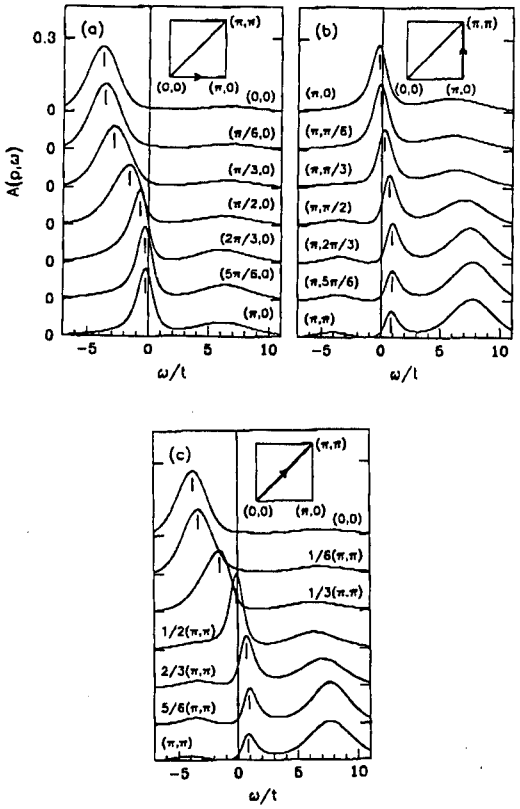


Fig. 7. Single-particle spectral weight $A(\mathbf{p}, \omega)$ versus ω for $U = 8t$, $T = 0.5t$ and $\langle n \rangle = 0.87$.

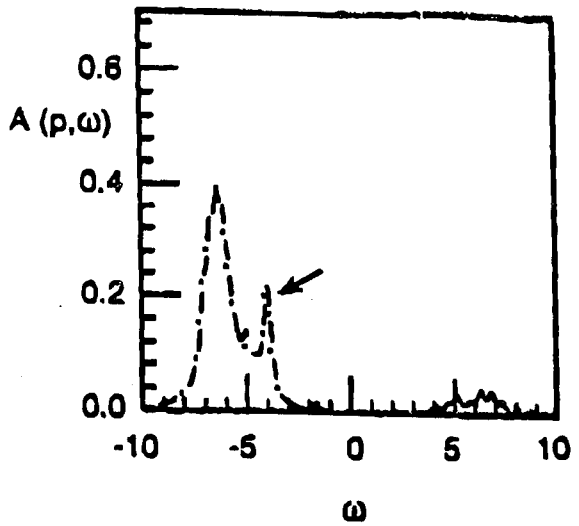


Fig. 8. Single-particle spectral weight $A(\mathbf{p}, \omega)$ versus ω for $\mathbf{p} = (0, 0)$ and $U = 8t$. This result has been obtained by Dagotto *et al.* [4] using the Lanczos exact diagonalization technique for a 4×4 lattice with two holes corresponding to $\langle n \rangle = 0.875$.

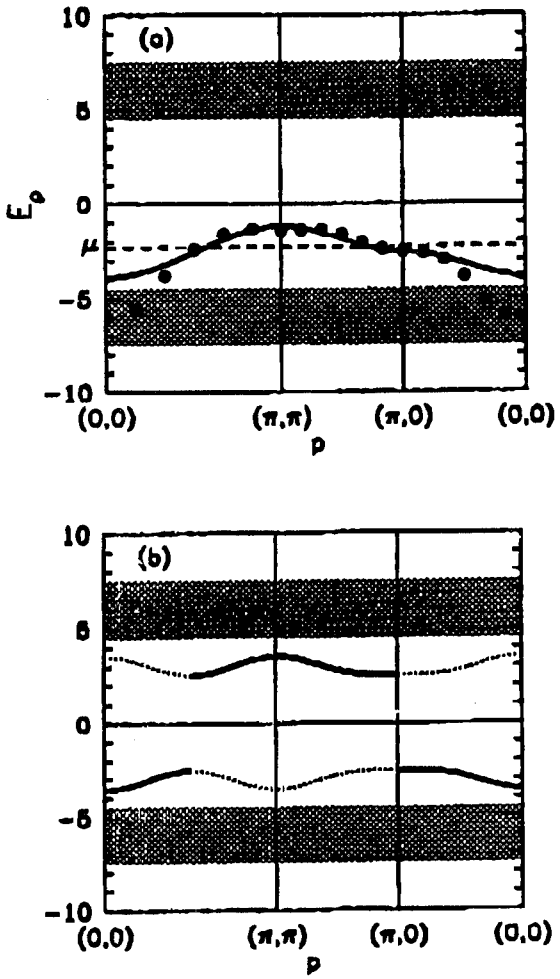


Fig. 9. (a) Quasiparticle dispersion $E_{\mathbf{p}}$ versus $\mathbf{p}$ for $\langle n \rangle = 0.87$. Here, the solid curve illustrates the quasiparticle dispersion obtained by the Lanczos exact diagonalization calculations of Dagotto *et al.* [4] for the 4×4 lattice with two holes. The dashed horizontal line denotes the chemical potential μ for $\langle n \rangle = 0.87$ and $T = 0.5t$. (b) Quasiparticle dispersion of the insulating state obtained by Preuss *et al.* [6] for $T = 0.1t$. The curves that are at the top of the lower Hubbard band and at the bottom of the upper Hubbard band illustrate the SDW–like quasiparticle dispersion. The segments of the dispersion indicated by the dotted curves have smaller weight than those indicated by the solid curves.

within the present Monte Carlo limitations we interpret the results of Fig. 7 as showing upper and lower Hubbard bands and a single narrow dispersing quasiparticle band. In particular, for $\mathbf{p} = (\pi, \pi)$, we can clearly resolve both the upper and lower Hubbard bands, and a low energy quasiparticle peak which has dispersed relative to its position at $\mathbf{p} = (\pi/2, \pi/2)$. Furthermore, the quasiparticle dispersion is significantly less at the $(\pi, 0)$ corner than along the diagonal at $(\pi/2, \pi/2)$. As $\mathbf{p}$ goes towards the Γ point $(0, 0)$, we believe that the quasiparticle peak is obscured by the lower Hubbard band because of the resolution of the maximum entropy technique. Fig. 8 shows $A(\mathbf{p}, \omega)$ for $\mathbf{p} = (0, 0)$ calculated using the Lanczos exact diagonalization technique [4] on a 4×4 lattice. The peak denoted by the arrow is interpreted as the quasiparticle.

In Fig. 9(a) we have plotted as the solid circles the quasiparticle peaks in the spectral weight versus $\mathbf{p}$ obtained from Fig. 7. Here the shading indicates the lower and the upper Hubbard bands. The solid curve at the top of the lower Hubbard band illustrates the quasiparticle dispersion obtained from the exact diagonalization calculations. In Fig. 9(b), on the same scale as Fig. 9(a) we have plotted the quasiparticle dispersion for the half–filled case obtained by Preuss *et al.* [6] on an 8×8 lattice at $T = 0.1t$. The bands at the top of the lower Hubbard band and at the bottom of the upper Hubbard band follow SDW–like dispersion with a bandwidth of order $2J$ [10].

We conclude that the density of states peak for the doped system, which appears as the temperature is lowered below J (see Fig. 5), arises from short range antiferromagnetic correlations, coupled with a strong onsite Coulomb interaction U, just as the quasiparticle dispersion in the half–filled case. However, as shown in Fig. 9(a), for $\langle n \rangle = 0.87$ and $T = 0.5t$, we find a single quasiparticle band which disperses through the fermi surface rather than the SDW–like dispersion seen in the insulator.

Acknowledgements—We thank S.R. White for many helpful suggestions and discussions. We also gratefully acknowledge support from the National Science Foundation under Grant No. DMR92–25027. The numerical calculations reported in this paper were performed at the San Diego Supercomputer Center.

REFERENCES

1. White S. R., Scalapino D. J., Sugar R. L., Loh E. Y., Gubernatis J. E. and Scalettar R. T., *Phys. Rev. B* **40**, 506 (1989).
2. Silver R. N., Sivia D. S. and Gubernatis J. E., *Phys. Rev. B* **41**, 2380 (1990).
3. White S. R., *Phys. Rev. B* **44**, 4670 (1991); **46**, 5678 (1992); Vekic M. and White S. R., *ibid.* **47**, 1160 (1993).
4. Dagotto E., Ortolani F. and Scalapino D. J., *Phys. Rev. B* **46**, 3183 (1992).
5. Bulut N., Scalapino D. J. and White S. R., *Phys. Rev. Lett.* **72**, 705 (1994).
6. Preuss R., Hanke W. and von der Linden W., preprint.
7. Moreo A., Haas S., Sandvik A. and Dagotto E., preprint.
8. Bulut N., Scalapino D. J. and White S. R., *Phys. Rev. Lett.* **73**, 748 (1994).
9. Bulut N., Scalapino D. J. and White S. R., *Phys. Rev. B* **50**, 7215 (1994).
10. It is also known that in the half–filled t–J model the quasiparticle bandwidth is approximately $2J$ [Liu Z. and Manousakis E., *Phys. Rev. B* **44**, 2414 (1992)]. In addition, the exact diagonalization calculations on small t–J clusters find that a metallic band of width $\sim 4J$ forms upon small doping [Stephan W. and Horsch P., *Phys. Rev. Lett.* **66**, 2258 (1991)]. Hence, the main features of the quasiparticle dispersion obtained by numerical calculations for the t–J and the large U Hubbard models are in agreement.

Pergamon

J. Phys. Chem. Solids Vol. 56, No. 12, pp. 1601–1603, 1995
Copyright c 1995 Elsevier Science Ltd
Printed in Great Britain. All rights reserved
0022–3697/95 $9.50 0.00

0022–3697(95)00174-3

REFLECTIONS ON THE SUPERCONDUCTOR–INSULATOR TRANSITION

S. DONIACH
Depts. of Applied Physics and Physics Stanford University, Stanford, CA 94305, U.S.A.

Abstract—The anomalously long superconducting coherence lengths observed in YBCO/PBCO multilayers are interpreted in terms of a boson localization picture for the superconductor–insulator transition in YBCO as Pr is substituted for Y. It is suggested that the combination of finite vortex mass and reduced superfluid density for the proximity-induced order parameter in PBCO should lead to enhanced quantum creep in these multilayer samples.

1. INTRODUCTION

Some years ago Doniach and Inui [1] suggested that the superconductor–insulator transition observed in the cuprates as doping is lowered from that needed for optimal superconductivity is a "boson localization" or "Cooper crystal" transition.

The purpose of this note is to suggest that the insulating state induced in YBCO by Pr substitution for Y is also in this class of localized boson states. This hypothesis is motivated by the extraordinarily long superconductivity proximity tunneling lengths observed in *b*-axis YBCO/PBCO multilayers by Suzuki *et al.* [2] which extends to some 480 Å. If the PBCO contains bound Cooper pairs which are weakly localized, then proximity tunneling from the adjacent YBCO interface will have a proximity coherence length $\xi_p^2 \;/\; 1/\varepsilon_{\text{pair localization}}$ and hence can become very long as the superconductor–insulator boundary is approached in the PBCO. This weak localization could also account for variable range hopping conductivity observed in pure PBCO by Suzuki *et al.* [2].

2. PSEUDO-SPIN MODEL

Because the $T \quad 0$ Ginzburg Landau coherence length ξ_0 is so short (20 Å) in the cuprates, a convenient coarse grained phenomenological model for the superconductor–insulator transition is that of Robasczkiewicz *et al.* [3] generalized to include long range Coulomb interactions. Here, pseudospins τ defined on a lattice with unit cell of order ξ_0 have *x, y* components representing the superconducting order parameter and *z*- components representing the number operator of the Cooper pairs.

In the simplest such model τ will be a spin 1 object for which the $m \quad 0$ eigenstate represents the average Cooper pair density, while $m \quad 1$ eigenstates represent charging fluctuations of $2e$. The Hamiltonian becomes

$$H \quad \sum_i \varepsilon_c^0 (\tau_i^z)^2 \quad J \sum_{<ij>} (\tau_i \; \tau_j \quad hc)$$

$$\frac{4e^2}{\epsilon_1} \sum_{i,j} \frac{(\tau_i^z \tau_j^z)}{\jmath R_i \quad R_j \jmath} \tag{1}$$

where ε_c^0 is the on-site charging energy, J is the Cooper pair tunneling matrix element and ϵ_1 is a phenomenological dielectric constant. In the classical limit $J >> 4e^2/\epsilon_1 \, a$, one has $< \tau_x > \quad 1$ and the superconducting condensate energy becomes

$$E_S \quad a^2 d \frac{H_c^2}{8\pi} \quad 4J \tag{2}$$

where we consider superconductivity in two-dimensional planes of thickness d and square lattice spacing a but treat the long range Coulomb interactions in three dimensions.

A Ginzburg–Landau expansion about the superconductor–insulator transition was given by Doniach [4]. A generalized form which includes the effects of long range Coulomb interactions was proposed by by Doniach and Inui [1]. This phenomenological Ginzburg Landau free energy functional of the complex order parameter $\psi(x) \quad \jmath\psi(x)\jmath e^{i\phi(x)}$ is given by

$$\mathrm{F}\{\psi\} \quad \jmath E_S \jmath \int d^2x \int_0^\beta \left\{ \xi_0^2 \jmath \nabla \psi \jmath^2 \quad (1 \quad \alpha/\alpha_c) \jmath\psi\jmath^2 \right.$$
$$\left. (\xi_0^2/4\varepsilon_c J) \jmath (\nabla \quad \partial_\tau \phi)^2 \jmath \quad (\beta/2) \jmath\psi\jmath^4 \right\} \tag{3}$$

where $\varepsilon_c \quad 4e^2/\epsilon_1 \, a$, $\alpha \quad \varepsilon_c/4J$, $\alpha_c \quad 2$, $\xi_0 \quad a$ and the on–site charging term has (somewhat arbitrarily) been neglected. A similar expression was given by Eckern and Schmid [5] for the Josephson junction array model.

3. PROXIMITY TUNNELING IN PBCO

If we assume that α is greater than, but close to, the critical value in PBCO, then the $\jmath\psi\jmath^2$ term becomes positive and PBCO is an insulator when not coupled to YBCO. However, assuming a boundary condition for the superconducting order parameter of $\psi \quad 1$ at the PBCO–YBCO interface, then ψ will decay exponentially into the PBCO as

$$\psi_{\mathrm{PBCO}}(x) \quad \psi_{\mathrm{YBCO}}\, e^{\,x/\xi_p} \tag{4}$$

where $\xi_p^2 \quad \xi^2\alpha_c/(\alpha \quad \alpha_c)$.

For $\xi_p/\xi \quad (480/20) \quad 24$, the Cooper pair localization energy will be given approximately by the $q \quad 0$ plasmon energy of eqn (3): $\Omega_P \quad \left[4\varepsilon_c J(\alpha/\alpha_c \quad 1)\right]^{1/2}$. Using $\sqrt{4J\varepsilon_c} \quad o\,(KT_c)$, where T_c is the BCS transition temerature one then finds

$$\varepsilon_{\mathrm{loc}} \quad KT_c/24. \tag{5}$$

Hopping of the Cooper pairs with this weak pair-localization energy might account for the variable range hopping in the CuO_2 planes of films of pure PBCO observed by Suzuki *et al.* [2].

4. VORTEX ACTIVATION ENERGIES IN THE YBCO/PBCO COMPOSITE LAYERS

Suzuki *et al.* [2] measure a vortex activation energy $\bar{\varepsilon}_d$ as a function of PBCO spacer thickness in their *a*-axis films. They fit it to the theory of Feigel'man *et al.* [6] for the activated resistivity of a pinned vortex lattice

$$\bar{\varepsilon}_d \quad \varepsilon_d \ln(H_0/H) \tag{6}$$

where $\varepsilon_d \quad \phi_0^2 d/64\pi^3\lambda^2$. For the composite films, $\lambda^{\ 2} \ / \ \lambda_a^{\ 1}\lambda_b^{\ 1}$ where we take b to be the direction of the YBCO/PBCO multilayers. Then

$$\lambda_b^{\ 2} \ / \ \bar{\rho}_S \quad \rho_S\{\frac{L_{\mathrm{YBCO}} \quad \xi_p(1 \quad e^{\,L_{\mathrm{PBCO}}/\xi_p})}{L_{\mathrm{YBCO}} \quad L_{\mathrm{PBCO}}}\} \tag{7}$$

provided $L_{\mathrm{PBCO}} \ < \ \xi_p$, leading to

$$\bar{\varepsilon}_d \quad \varepsilon_d^0\left[\frac{1}{1 \quad \frac{1}{2}\frac{(L_{\mathrm{PBCO}})^2}{\xi_p(L_{\mathrm{YBCO}} \quad L_{\mathrm{PBCO}})}}\right]^{\frac{1}{2}} \tag{8}$$

for intermediate values of L_{PBCO}/ξ_p.

5. FIELD-INDUCED QUANTUM MELTING OF THE VORTEX LATTICE

Use of the phenomenological functional (3) allows an estimate of the vortex mass at the mean field level.

Following Eckern and Schmid [5] we can write the vorttex contribution to the phase $\phi(x,\tau)$ of the order parameter as $\psi(x) \quad |\psi|e^{i\phi(x)}$ with

$$\phi(x) \quad \sum_v q_v \arctan\left[\frac{y \quad y_v(\tau)}{x \quad x_v(\tau)}\right] \tag{9}$$

where $q_v \quad 1$ are the vortex charges and (x_v, y_v) are the vortex positions. Substituting in eqn (3) this leads to a vortex mass

$$M_v \quad 2\pi^2\hbar^2/\varepsilon_c a^2. \tag{10}$$

At sufficiently large applied magnetic field, the vortex lattice will then be driven through a quantum melting transition, at $T \quad 0$, at a value of H which may be estimated using the Lindemann criterion as

$$\sqrt{\frac{\hbar}{M_v\Omega_v}} \ > \ c_L\sqrt{\frac{\phi_0}{H}} \tag{11}$$

where Ω_v is the frequency of the zone boundary phonon modes of the vortex lattice [8].

When the uniform system is close to the insulator/superconductor phase boundary (but on the superconducting side), the effective mass M_v of the vortices starts to become very small due to renormalization by the charging fluctuations of the order parameter as shown by van Otterloo, Fazio & Schön [7]. So as the system approaches the superconductor–insulator phase boundary, the melting field H_M will be driven to smaller values both due to the softening of the vortex lattice as $\rho_s \ ! \ 0$ and due to the renormaliztion of the vortex mass. Thus H_M will tend to zero at the superconductor–insulator phase boundary (see Fisher [9]).

This field-induced quantum melting provides a nice explanation for the field-induced superconductor–insulator transition seen in oxygen-depleted YBCO by Seidler *et al.* [10]. In fact, their measurements provide experimental evidence for the boson-localization mechanism for the superconductor–insulator phase boundary in underdoped cuprate samples. If the application of the field had lead to pair breaking then a transition to a metallic state would be expected, which was not found in these experiments.

The YBCO/PBCO multilayers provide an interesting case where the proximity-induced superconducting order parameter remains finite even though the PBCO segments have crossed into the insulating regime. So in the multilayer case we may expect that the mass reduction to zero caused by the charge fluctuations is inhibited by the proximity effect and M_v will remain finite.

The effect of the charge fluctuations on the mean field estimate of M_v in the presence of the proximity-induced order parameter is hard to estimate. However, there will be a reduction of the melting field H_M due to softening of the vortex lattice as ρ_s is reduced. Thus using eqn (11) we may estimate

$$\frac{H_M^{\mathrm{proximity}}}{H_M^{\mathrm{YBCO}}} \quad \frac{|\psi_{\mathrm{PBCO}}|}{|\psi_{\mathrm{YBCO}}|} \quad e^{\,L_{\mathrm{PBCO}}/\xi_p}. \tag{12}$$

where we have set $\Omega_v \ / \ \rho_s^{1/2}$.

At fields of order $H \ > \ H_M^{\mathrm{proximity}}$, any vortices induced in the PBCO regions will then be driven through the quantum melting transition, thus leading to a field-induced decoupling of the YBCO regions at a critical field whose value will depend on the magnitude of the proximity-induced order parameter.

It would also be interesting to observe if the reduced H_M in the PBCO regions leads to enhanced quantum creep at very low temperatures as the PBCO layer thickness is

increased towards ξ_p.

Acknowledgements—The author wishes to thank Ted Geballe and Yuri Suzuki for many interesting discussions and the NSF for support through grant number DMR-9302882.

REFERENCES

1. Doniach S. and Inui M., *Phys. Rev. B* **41**, 6668–78 (1990).
2. Suzuki Y., Triscone J.-M., Eom C. B., Beasley M. R. and Geballe T. H., *Phys. Rev. Letts* **73**, 328–31 (1994).
3. Robaszckiewicz S., Micnas R. and Chao K. A., *Phys. Rev. B* **23**, 1447 (1981); **26**, 3915 (1982)
4. Doniach S., *Phys. Rev. B* **24**, 5063 (1981)
5. Eckern U. and Schmid A., *Phys. Rev. B* **39**, 6441 (1989).
6. Feigel'man M. V., Geshkenbein V. B. and Larkin A. I., *Physica C* **167**, 177 (1990)
7. van Otterloo A., Fazio R. and Schön G.,*Physica B* **194–196**, 1153–4 (1994).
8. Onogi T. and Doniach S., submitted for publication.
9. Fisher M. P. A., *Phys. Rev. Lett.* **65**, 923 (1990).
10. Seidler G. T., Rosenbaum T. F. and Veal B. W., *Phys. Rev. B* **45**, 10162-4 (1992).

Pergamon

J. Phys. Chem. Solids Vol. 56, No. 12, pp. 1605–1610, 1995
1995 Elsevier Science Ltd
Printed in Great Britain
0022-3697/95 $9.50 + 0.00

0022-3697(95)00207-3

IMPURITY SCATTERING AND ORDER PARAMETER SYMMETRY IN HIGH-T_c SUPERCONDUCTORS

P. J. HIRSCHFELD[1]
Dept. of Physics, Univ. of Florida, Gainesville, FL 32611, U.S.A.

Abstract—I review the theory of impurities in a d-wave superconductor, with a view towards devising tests which can identify the order parameter symmetry in the cuprates, particularly those involving electromagnetic response. Existing microwave data can be semiquantitatively fit by "dirty d-wave" theory, extended to include inelastic scattering by antiferromagnetic spin fluctuations, although some discrepancies remain. The model also yields alternative explanations for some well-known features of the optical conductivity in single crystals. The theory is compared with the predictions for various anisotropic s-wave states which have been proposed recently.

INTRODUCTION

Experimental evidence supporting the identification of d-wave superconductivity in the cuprates falls into two categories. The first is a set of measurements indicating the existence of low-lying excitations below what should be the BCS gap energy scale: these include, but are not limited to, penetration depth, angle-resolved photoemission, thermal conductivity, and nuclear magnetic relaxation experiments [1]. The second category includes probes sensitive to the change of the sign of the order parameter over the Fermi surface, such as Josephson tunneling [2]. While considerably more evidence has accumulated of the former type, it is sometimes accorded less weight than pair tunneling, since experiments of this kind are normally assumed to measure properties sensitive to the order parameter Δ_k only through the Bogoliubov quasiparticle spectrum, $E_k = \sqrt{\xi_k^2 + |\Delta_k|^2}$. Since E_k does not depend on the sign of the order parameter, it appears at first sight that any state with order parameter vanishing linearly near line nodes (as does, e.g. the $d_{x^2-y^2}$ state in tetragonal symmetry) will support low-lying quasiparticle excitations and give rise to similar thermodynamic and transport properties. For example, the three states shown in Fig. 1 all have nodes near the (1,1) directions on the model Fermi surfaces shown; the low-energy density of single-particle states $N(\omega)$ will be the same (linear) in all cases, as will all properties deriving directly therefrom.

When coupled with a reliable model of impurity scattering in the unconventional superconducting state, measurements of quasiparticle *transport* properties can definitively help to identify the order parameter symmetry, however. This conclusion follows from recognizing that the off-diagonal impurity self-energy Σ_1 is nonzero in s-wave states 1a and 1b, but vanishes in the d-wave state 1c. A large Σ_1 prevents the formation of a scattering resonance at the Fermi surface, leading to clean limit low-frequency transport coefficients which for $T \ll T_c$ generically vary weakly in temperature in s-wave gapless states. By contrast, in the d-wave (or other unconventional state where $\Sigma_1 = 0$), resonant scattering leads to transport properties which vary strongly in temperature for $T \ll T_c$ [3]. The resonance characteristic of the dirty d-wave state also gives rise to characteristic features in the microwave and optical conductivities which can be used to determine the order parameter symmetry [4–7]. The full temperature and frequency range can be described if one includes a source of inelastic scattering in the theory. Here a simple model of scattering from 2D Hubbard spin fluctuations, together with the dirty d-wave picture, is shown to account for many qualitative features of the frequency dependent response, including the "residual" Drude peak in the superconducting state and aspects of the "mid-infrared band".

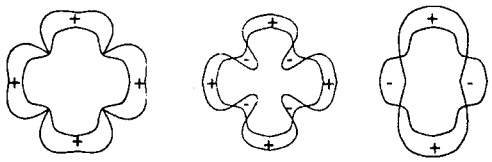


Fig. 1. Order parameters plotted over tetragonal Fermi surface: (a) s-wave state with gap minima at Fermi surface; (b) extended s-wave state; (c) $d_{x^2-y^2}$ state

Impurity scattering

The disorder-averaged matrix propagator describing any of the states (a)–(c) above is written

$$\underline{g}(\mathbf{k}, \omega_n) = -\frac{i\tilde{\omega}_n \underline{\tau}^0 + \tilde{\xi}_k \underline{\tau}^3 + \tilde{\Delta}_k \underline{\tau}^1}{\tilde{\omega}_n^2 + \tilde{\xi}_k^2 + |\tilde{\Delta}_k|^2} \quad (1)$$

[1] Work done in collaboration with L.S. Borkowski, W.O. Putikka, S. Quinlan and D.J. Scalapino

where the $\underline{\tau}^i$ are the Pauli matrices and $\tilde{\Delta}_k$ is a renormalized unitary order parameter. The renormalized quantities are given by $\tilde{\omega}_n = \omega_n - \Sigma_0(\omega_n)$, $\tilde{\xi}_k = \xi_k + \Sigma_3(\omega_n)$, and $\tilde{\Delta}_k = \Delta_k + \Sigma_1(\omega_n)$, where the self-energy due to s-wave impurity scattering has been expanded $\underline{\Sigma} = \Sigma_i \underline{\tau}^i$. The relevant self-energies are given in a t-matrix approximation [8,9] by

$$\Sigma_0 = \frac{\Gamma G_0}{c^2 + G_1^2 - G_0^2}; \quad \Sigma_1 = \frac{-\Gamma G_1}{c^2 + G_1^2 - G_0^2}, \tag{2}$$

where $\Gamma \equiv n_i n/(\pi N_0)$ is a scattering rate depending only on the concentration of defects n_i, the electron density n, and the density of states at the Fermi level, N_0, and we have defined $G_\alpha \equiv (i/\pi N_0)\Sigma_k Tr[\underline{\tau}^\alpha \underline{g}]$. The strength of an individual scattering event is characterized by the cotangent of the scattering phase shift, c. The Born limit corresponds to $c \gg 1$, so that $\Gamma/c^2 \simeq \Gamma_N$, while the unitarity limit corresponds to $c = 0$.

Distinguishing s- and d-wave like states

The distinction between s-wave states (a) and (b) and the d-wave order parameter (c) may now be seen by considering the diagonal and off-diagonal self-energies Σ_0 and Σ_1. The latter vanishes identically for the d-wave case because Δ_k has a reflection symmetry, and therefore the Fermi surface integral G_1 vanishes. This leads to the well-known breakdown of Anderson's theorem for potential scatterers in a d-wave superconductor and the insensitivity of the nodal structure of the gap to pairbreaking. In s-wave states of type (a), however, the off-diagonal integrated Green's function G_1 is nonzero and has the same order of magnitude as its isotropic counterpart. Following the standard theory of pairbreaking in anisotropic s-wave superconductors, it is then easy to see that smearing of the energy gap due to randomization of electronic momenta leads to a lifting of the gap minima and the opening of an impurity-induced energy gap in the quasiparticle spectrum, as pointed out by Borkowski and Hirschfeld and Fehrenbacher and Norman [10,11]. Thermodynamic and transport properties will therefore always exhibit activated behavior at sufficiently low temperatures.

From the symmetry point of view, there is of course no reason the order parameter cannot change sign on the Fermi surface, as in the "extended s-wave" state (b). Interest in such states was heightened when Ding *et al.* presented ARPES measurements on BSSCO suggesting the existence of *pairs* of nodes symmetrically placed near the (1,1) directions as one might expect from Fig. 1(b) [12]. It was difficult to see how these data could be explained simply by a d-wave state, although some suggestions were put forward [13] Very recently, these claims [12] were modified, but there is still great interest in extended-s wave pairing.

Note one can model an extended s-wave state by taking a function over the Fermi circle of type (a), like $\Delta_k = \Delta_0|\cos 2\phi|$, and subtracting a constant, $\Delta_k = \Delta_0(|\cos 2\phi| - \eta_0)$; a fit to the data of Ref. [12] using such a

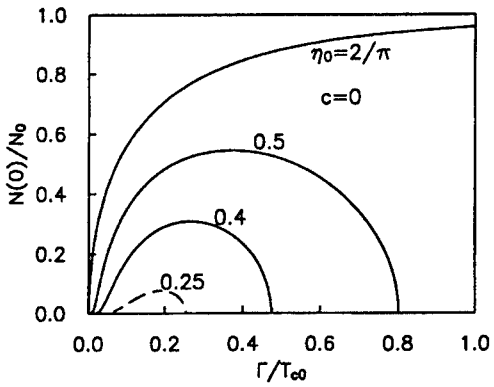


Fig. 2. ARPES determination of BSSCO energy gap as function of angle ϕ around Fermi surface. From Ref. [12], error bars not shown. Solid line: $\Delta_k = \Delta_0(|\cos 2\phi| - \eta_0)$, with $\eta_0 = .25$

form is shown in Fig. 2. For a range of impurity scattering rates $\Gamma_i \lesssim \eta_0$, one even expects low-temperature "gapless" behavior characterized by a residual density of quasiparticle states $N(0) > 0$, as in the d-wave case [11]. Thus, at first sight, many of the same experiments which seem to fit the "dirty d-wave" scenario (see below), could potentially also be explained by such states. Transport properties of extended s-wave states will be considerably different, however, as suggested by the following heuristic argument. Any DC transport coefficient $L(T)$ in a system characterized by well-defined single-particle excitations will vary with temperature roughly as $L(T) \sim N(\omega \simeq T)\tau(\omega \simeq T)$, where $N(\omega)$ is the density of states and $\tau(\omega)$ the relaxation time. In the clean d-wave case, resonant scattering gives $\tau^{-1}(\omega) = 2\Sigma_0''(\omega) \sim N(\omega)^{-1}$ up to logarithmic corrections, yielding $L(T) \sim T^2$. In the Born limit $c \gg 1$, similar arguments yield $L \sim$ const. for d-wave transport coefficients. Impurity-limited transport in the extended s-wave state will be qualitatively similar to the d-wave case if the scattering is weak, $c \gg 1$.

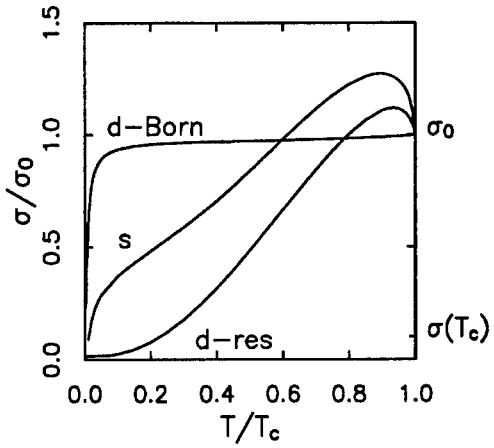


Fig. 3. Comparison of conductivity of clean extended s-wave state ("s"), $\eta_0 = 0.25$, $\Delta_0/T_c = 2.9$, $\Gamma/T_c = 0.1$, $c = 0$ with $d_{x^2-y^2}$ state, $\Delta/T_c = 2.14$. "d−res": $\Gamma/T_c = 0.1$, $c = 0$, "d−Born": $\Gamma/T_c = 10$, $c = 10$. No inelastic scattering included.

For large phase shifts in such a state, resonant scattering does not occur, however, since the denominator of the t-matrix, $c^2 - G_0^2 + G_1^2 \gtrsim (1-\eta_0)^2$ even for $c \to 0$ [10,11]. The frequency dependence of the t-matrix is nevertheless important, giving rise to a crossover scale ω_c set by $1 - \eta_0 = \omega \log(b(\eta_0)/\omega)$, with $b(\eta_0) \simeq 4\eta_0(1-\eta_0)$. The resultant behavior is intermediate between the strong and weak scattering limits of the d-wave transport, as shown by a numerical calculation of the $\Omega \to 0$ limiting quasiparticle conductivity $\sigma(T)$ displayed in Fig. 3. From an experimental point of view (for $\eta_0 = 0.25$, $T > \omega_c \simeq 0.1$), the conductivity may appear quite close to a form $\sigma \simeq \sigma_{res} + AT$, with $\sigma_{res}, A \sim 1/n_i$. It is intriguing to note that this is the form found by Bonn *et al.* [14] in microwave measurements on Zn-doped YBCO crystals, although the same group found in later work that the residual conductivity σ_{res} disappears with removal of twin boundaries [15]. A more detailed analysis, including inelastic scattering, of the frequency and impurity concentration dependence of transport coefficients is necessary before defnitive conclusions can be drawn [16].

Microwave response of d-wave superconductor

For the remainder of this talk I will discuss the microwave and optical response to be expected of a d-wave superconductor. The $q = 0$ electromagnetic response of the system to an applied vector potential $\mathbf{A}(\Omega)$ is given by

$$\mathbf{j}(\Omega) = -\overleftrightarrow{K}(\Omega)\mathbf{A}(\Omega) = -\left[\overleftrightarrow{K}_p(\Omega) - \frac{ne^2}{mc}\right]\mathbf{A}(\Omega), \quad (3)$$

where

$$\overleftrightarrow{K}_p(\Omega) = <[\mathbf{j},\mathbf{j}]^R>(\Omega) \simeq (\frac{-2ne^2}{mc})\times \quad (4)$$

$$\langle \hat{k}\hat{k} \int d\xi_k T \sum_n tr\, \underline{g}(\mathbf{k},\omega_n)\underline{g}(\mathbf{k},\omega_n - \Omega_m)\rangle_{\hat{k}} \,|_{i\Omega_m \to \Omega + i0^+}\,.$$

The Green's functions in eqn (4) are those given in eqn (1) with self-energies given by eqn (2) plus additional lifetimes associated with electron–electron scattering within a one-paramagnon exchange approximation. The Hubbard interaction U is fixed to give a good account of normal state properties, particularly nuclear magnetic relaxation rate and DC resistivity, i.e. $1/\tau_{e-e}(\omega = 0, T_c) \simeq 2T_c$ [17]. In the d-wave state for $T \ll T_c$, the inelastic scattering rate is found to vary as $\sim max(T,\omega)^3$ [17]–the same as for an ordinary Fermi liquid below its degeneracy temperature, plus one additional factor of T or ω to account for the linearly varying number of charge carriers. Thus at the lowest temperatures and frequencies the quasiparticle lifetime is dominated by impurities alone.

Penetration depth

The London penetration depth is given by $\lambda_i(T) = [(4\pi/c)K_{ii}(\Omega = 0; T)]^{-1/2}$. For applied magnetic field in the basal plane, the low temperature penetration depth

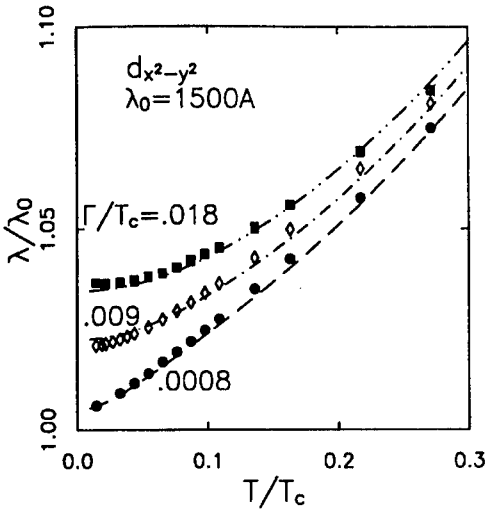


Fig. 4. Comparison of Zn-doped YBCO penetration depth data from Ref. [14] with dirty d-wave theory.

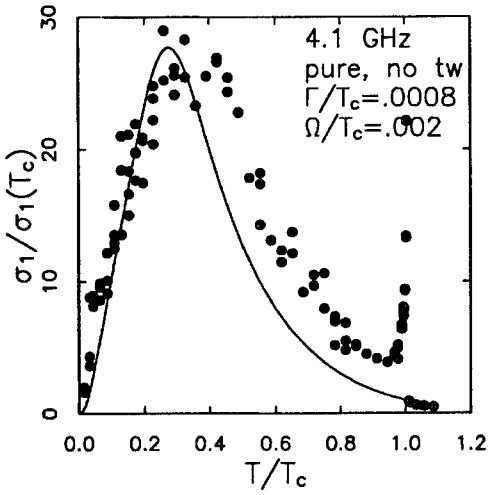


Fig. 5. Comparison of YBCO microwave conductivity data (Ref. [14]) with theory.

reflects the low frequency density of states $N(\omega) \sim \omega$ for all three states (a)–(c) of Fig. 1 in the absence of disorder. Both (b) and (c) will display a disorder-induced crossover in $\lambda(T) = \lambda_0 + \delta\lambda(T)$, $\delta\lambda(T) \sim T \to T^2$ below an energy scale $T^* \propto n_i^{-1/2}$ due to the formation of the "impurity band" (resonance) at low energies [4–6]. In Fig. 4, I show a fit of the dirty d-wave model based on a full numerical evaluation [18] of eqns (3) and (4) in the strong scattering limit $c = 0$ to data of the UBC group on Zn-doped YBCO single crystals [19]. The $T \to T^2$ crossover is clearly visible at the lowest temperatures, while at least in the cleanest samples there is an intermediate temperature range $T^* < T \ll T_c$ which can still be identified with a linear-T behavior. This is one of the clearest signatures of resonant scattering, which only broadens the low-lying quasiparticle states. Similar concentrations of Ni appear to produce little

effect on $\delta\lambda(T)$.

It should be noted that the fits shown in Fig. 4 are performed by adding an arbitrary constant to the penetration depth data, since the experiments are unable to measure the absolute value of λ itself. A check of the resonant scattering model one would like to make on these data, namely the predicted scaling of λ_0 with impurity concentration, is therefore impossible from these experiments. However Kiefl *et al.* [20] have determined the absolute scale of λ in μSR experiments on the same samples as those shown in Fig. 4. They report a λ_0 of $1490A$, and believe the difference in λ_0 between the nominally pure and the 0.31% Zn sample to be roughly 50 A, surprisingly close to the fit result of $\sim 0.04\lambda_0$.

Microwave conductivity

Any model of impurity scattering in a superconductor which leads to a residual densty of states $N(0)$, e.g. s-wave potential scattering in d-wave or extended s-wave states, will qualitatively account for the increase of the zero-temperature penetration depth with disorder and the concomitant creation of a T^2 term in the penetration depth. The real part of the conductivity is a more sensitive test of any such model, however, since it probes the quasiparticle relaxation time directly. The conductivity in the "pure regime" of the d-wave superconductor $T^* < T \ll T_c$ may be cast [18] in the familiar form,

$$\sigma_{xx}(\Omega) \simeq \left(\frac{ne^2}{m}\right) \int_{-\infty}^{\infty} d\omega \left(\frac{-\partial f}{\partial \omega}\right) N(\omega) \mathrm{Im}\left[\frac{1}{\Omega - i/\tau(\omega)}\right], \quad (5)$$

i.e. a "Drude-like" transport expression for free fermions with density of states $N(\omega)$ and one-body relaxation time $1/\tau(\omega)$, as anticipated by Bonn *et al.* on phenomenological grounds. One should be able therefore to reproduce the peak in the conductivity observed, because in the hydrodynamic limit one has $\sigma \sim n_{qp}\tau$, which varies as $\sim 1/T^3$ at temperatures not too far below T_c, when inelastic scattering dominates and $n_{qp} \simeq n$, and as T^2 at low T, where impurities are important. The famous conductivity peak [21] observed in clean samples around $T \simeq 0.3T_c$ is a simple consequence of this crossover. The prediction of a low-T T^2 variation is apparently at odds with experiments in the clean limit [15], however. Because the inelastic scattering rate starts at T_c so much larger than the impurity scattering rate, in the cleanest cases this discrepancy is confined to an unobservably small temperature range, as shown in Fig. 5 [18]. Note that the choice of parameters in this case is not an independent fit, but is fixed by the previous fit to penetration depth data on the same sample. However the variation with increased frequency and Zn doping is *not* correctly described by the theory, and the discrepancy between T and T^2 at low temperatures becomes more apparent [18].

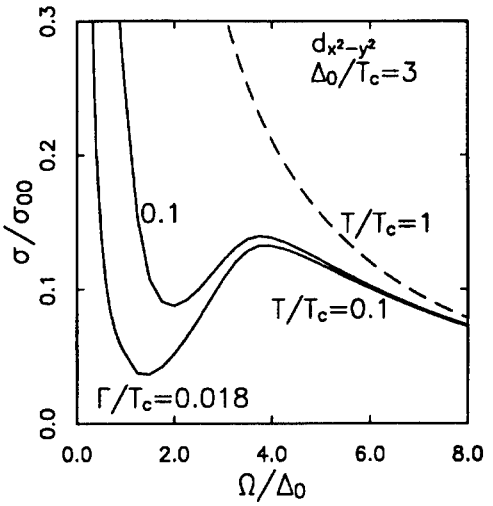


Fig. 6. Optical conductivity for $d_{x^2-y^2}$ state in resonant impurity scattering limit, inelastic $1/\tau$.

Optical conductivity

It is of course possible within the same model to calculate the optical conductivity [22–25]. The inelastic scattering rate within the weak-coupling Hubbard picture is then found to be linear above and varying as $max(\omega, T)^3$ as $\omega \to 0$ below a crossover scale of roughly $3\Delta_0$ [17]. This scale may be understood as the energy needed to create a single quasiparticle excitation scattering off a quasiparticle–quasihole pair, and leads to a threshold in $1/\tau$ in the isotropic s-wave case at 3Δ, as pointed out by Orenstein *et al.* [26], Varma *et al.* [27] and more recently by Coffey and Coffey [28]. To create light absorption in such a state by inelastic processes requires an energy $4\Delta_0$, $2\Delta_0$ to create the quasiparticle–quasihole pair, and a second $2\Delta_0$ to scatter off a spin fluctuation. This leads to a feature in the optical conductivity centered at $4\Delta_0$, and of course considerably broadened in the d-wave state (Fig. 6) due to the gap nodes. It is intriguing to note that this feature occurs at roughly the energy of the mid-infrared band at 1000 cm^{-1} in, e.g. $YBCO_7$, which has been most recently associated with interband processes unaffected by superconductivity. In $YBCO_7$, this feature appears only below T_c, a fact which would find a natural explanation within the context of this model. However at present the measured conductivity at 1000 cm^{-1} is a factor of 2 higher than the prediction. This discrepancy is actually well known from comparisons of marginal Fermi liquid theory, which produces a self-energy in the normal state very similar to that of our model, with optical data [29].

At low frequencies Fig. 6 shows the appearance of a narrow "residual Drude" feature in the superconducting state due to scattering off excited nodal quasiparticles at finite temperature [25]. In the resonant impurity scattering case, however, there should be spectral weight at $\Omega = 0$ even at zero temperature. The values of the impurity scattering parameters required to match the width of the residual Drude

features in experiment are significantly larger than those deduced for clean samples from microwave measurements.

CONCLUSIONS: ASSESSMENT OF "DIRTY d-WAVE" THEORY

Measurements on YBCO crystals below T_c which depend directly on the quasiparticle density of states, such as microwave penetration depth and NMR relaxation, appear to be well-described by the "dirty d-wave model". Systematic Zn and Ni doping studies of both λ and T_1 can be quantitatively fit to the predictions of the theory if the discrepancies between Zn and Ni pairbreaking rates are assumed to originate from the different strengths of scattering of the two impurities in the superconducting state. Recent electron irradiation experiments appear to create planar oxygen defects leading to similar behavior [32]. An important exception to this trend is the specific heat, where a linear-T term in the superconducting state corresponding to a residual density of states $N(0)$ an order of magnitude larger than those extracted from microwave measurements on similar crystals has been observed. This value appears to be very sensitive to twinning and interplane defects which do not influence the penetration depth, however, and it therefore appears possible that accounting for extrinsic effects of this type will allow one to describe the specific heat work within the same general picture [33].

Recent BSSCO ARPES measurements [12], while subsequently retracted, raise the question of the extent to which these experimental results can be equally well understood in the framework of an extended s-wave state. Although such a state does not allow for resonant scattering [10,11], and will therefore not lead, e.g. to a separation of energy scales over which "clean" and "dirty" behavior is observed, e.g. the $T \rightarrow T^2$ crossover in the penetration depth in clean samples, it is not currently clear whether such distinctions can really be observed in experiment. Increasing disorder will lead to an increasing residual density of states much as in the dirty d-wave picture. However, eventually disorder should induce the opening of a true energy gap in the spectrum at a critical concentration n_{ic}, in contrast to the d-wave case [10,11]. This would be a clear signature of s-pairing.

Comparisons of "dirty d-wave theory" with transport properties are less clear. Interpretations of microwave conductivity measurements are typically complicated by the presence of a residual conductivity $\sigma(\Omega, T \rightarrow 0)$ much larger than the "universal" residual conductivity $\sigma_{00} \simeq ne^2/\pi\Delta_0$ predicted for a $d-$wave state. Despite some evidence that this term becomes much smaller with detwinning [15], large values continue to be reported even for untwinned samples [34]. Furthermore, the prediction of the d-wave model for the temperature dependence, $\sigma(T) \simeq \sigma_{00} + aT^2$, is not observed in experiment; instead, a linear-T behavior is usually reported. This suggests that the frequency dependence of the t-matrix may not be treated correctly in the current, certainly oversimplified version of the theory.

A potential problem with the theory which deserves further attention is the predicted T_c supression, which in the d-wave case is identical to the standard Abrikosov–Gorkov (AG) result with pairbreaking parameter $\Gamma_N \equiv \Gamma/(1 + c^2)$. Some comparisons of T_c vs. $\rho(T_c)$ in damaged YBCO samples suggest that T_c is considerably more robust [35]. The experimental situation is not yet clear, however: recent measurements on electron-damaged samples show T_c supressions only a factor of two different from the AG prediction [32]. From a theoretical standpoint, Eliashberg calculations suggest that a slightly renormalized AG expression is correct even in the presence of strong inelastic scattering [36], but this conclusion appears to follow only if the bosons causing pairing are the same as those causing scattering, which need not be the case. My view is that attempts to correlate predictions of the dirty d-wave model in the low-T state (where off-diagonal order is well developed) to a poorly understood instability criterion (for the rather peculiar normal state) are dangerous at this time.

One final difficulty with the theory may be giving us important hints about how impurities are perturbing the superconductor. The impurity scattering rates deduced from fits to penetration dept measurements appear to be a factor of 3–5 smaller than those one would deduce from comparison to *normal state* transport data on Zn-doped YBCO [37], or from the width of the residual Drude feature in the optical conductivity at low temperatures [38]. This suggests that a somewhat better fit can be obtained by considering scattering phase shifts somewhat away from $\pi/2$. The fact that Zn and Ni lead to very similar changes in DC resistivity but affect the superconducting state in dramatically different ways, however, indicates that this deviation from the unitarity limit is a dynamical one, which depends on how the impurity ion influences the superconductivity around the impurity site.

Acknowledgements—I am grateful for many stimulating discussions with S. Anlage, D. A. Bonn, W. N. Hardy, T. Lemberger, M. Norman, Z. X. Shen and D. Tanner, and particularly to N. Goldenfeld and D. J. Scalapino for reinvigorating my interest in this subject.

REFERENCES

1. See, e.g. talks by Anlage S. M., Bonn D. A., Campuzano J. C., Kitaoka Y., Klein M. V., Shen Z. X. and Sridhar S., this conference.
2. See, e.g. talks by Tsuei C. C., Wollman D. and Wellstood F. C., this conference.
3. Pethick C. J. and Pines D., *Phys. Rev. Lett.* **50**, 270 (1986).
4. Gross F. *et al.*, *Z. Phys.* **64**, 175 (1986).
5. Prohammer M. and Carbotte J., *Phys. Rev. B* **43**, 5370 (1991); Arberg P., Mansor M. and Carbotte J. P., *Solid State Commun.* **86**, 671 (1993).
6. Hirschfeld P. J. and Goldenfeld N., *Phys. Rev. B* **48** (1993).
7. Hirschfeld P. J., Putikka W. O. and Scalapino D. J., *Phys. Rev. Lett.* **71**, 3705 (1993).

8. Hirschfeld P. J., Vollhardt D. and Wölfle P., *Solid State Commun.* **59**, 111 (1986).
9. Schmitt-Rink S., Miyake K. and Varma C. M., *Phys. Rev. Lett.* **57**, 2575 (1986).
10. Borkowski L. S. and Hirschfeld P. J., *Phys. Rev. B* **49**, 15404 (1994).
11. Fehrenbacher R. and Norman M., *Phys. Rev. B* **50**, 3495 (1994); *Proc. Grenoble Conf. High Temperature Superconductivity* (1994).
12. Ding H. *et al.*, *Phys. Rev. Lett.* **74**, 2784 (1995).
13. Lee P. A. and Kuboki K., preprint (1995).
14. Bonn D. A. *et al.*, *Phys. Rev. B* **50**, 4051 (1994).
15. Zhang K. *et al.*, *Phys. Rev. Lett.* **73**, 2484 (1994).
16. Borkowski L. S., Hirschfeld P. J. and Putikka W. O., to be published.
17. see Quinlan S., Scalapino D. J. and Bulut N., *Phys. Rev. B* **49**, 1470 (1993) and references therein.
18. Hirschfeld P. J., Putikka W. O. and Scalapino D. J., *Phys. Rev. B* **50**, 10250 (1994).
19. Hardy W. N. *et al.*, *Phys. Rev. Lett.* **70**, 399 (1993).
20. Sonier J. E. *et al.*, *Phys. Rev. Lett.* **72**, 744 (1994).
21. Bonn D. A. *et al.*, *Phys. Rev. B* **47**, 11314 (1993).
22. Klemm R. A. *et al.*, *Z. Phys.* **72**, 139 (1988).
23. Hirschfeld P. J. *et al.*, *Phys. Rev.* **40**, 6695 (1993).
24. Graf M. J., Palumbo M., Rainer D. and Sauls J. A., preprint (1994).
25. Carbotte J. P., Jiang C., Basov D. N. and Timusk T., preprint (1995).
26. Orenstein J. *et al.*, in *Electronic Properties of High-T_c Superconductors* (Edited by H. Kuzmany). Springer-Verlag, Berlin (1990).
27. Varma C. M. *et al.*, *Phys. Rev. Lett.* **63**, 1996 (1989); *ibid.* **64**, 497 (1990); Littlewood P. B. and Varma C. M., *J. Appl. Phys.* **69**, 4979 (1991).
28. Coffey L. and Coffey D., *Phys. Rev. Lett.* **70**, 1529 (1994).
29. Nicol E. *et al.*, *Phys. Rev. B* **43**, 473 (1991).
30. Dagotto E., *Rev. Mod. Phys.* **66**, 763 (1994).
31. Jarrell M. *et al.*, preprint (1995).
32. Giapintzakis J. *et al.*, unpublished (1995).
33. Moler K. *et al.*, this conference.
34. Sridhar S., this conference.
35. Valles J. M. *et al.*, *Phys. Rev. B* **39**, 11599 (1989).
36. Radtke R. J. *et al.*, *Phys. Rev. B* **48**, 653 (1993).
37. Chien T. R. *et al.*, *Phys. Rev. Lett.* **67**, 2088 (1991).
38. Basov D. *et al.*, to be published in *Phys. Rev. Lett.*

Pergamon

J. Phys. Chem. Solids Vol. 56, No. 12, pp. 1611–1613, 1995
1995 Elsevier Science Ltd
Printed in Great Britain
0022-3697/95 $9.50 + 0.00

0022-3697(95)00134-4

MAGNETIC PROPERTIES OF HIGH TEMPERATURE SUPERCONDUCTORS: A SPIN LIQUID APPROACH.

L. B. IOFFE * A. J. MILLIS †

* Physics Department, Rutgers University, Piscataway, NJ 08855, U.S.A.
† AT&T Bell Laboratories, 600 Mountain Ave, Murray Hill NJ 07974, U.S.A.

Abstract—We argue that strongly correlated two dimensional electrons form a spin liquid in some regimes of density and temperature and give the theory of the magnetic properties of this spin liquid using a representation in terms of fermions interacting with a gauge field. We show that this state is characterized by anomalous power law spin correlations and discuss the implications of these correlations for the temperature dependence of NMR relaxation rates $1/T_1$ and $1/T_2$ and for the uniform susceptibility. We also discuss the transition from the spin liquid to antiferromagnet and the critical behavior of these properties at the transition. We compare these theoretical results with data on high T_c superconductors. Finally, we discuss the formation of a spin gap due to the spin exhange interaction between adjacent layers in bilayer materials.

Keywords: spin liquid, gauge field, NMR, spin gap.

In this paper we discuss the properties of an intermediate magnetic phase which may be sandwiched between the Fermi liquid and antiferromagnet in strongly correlated two dimensional electron systems. If the concentration of electrons is low and the interaction between them is weak, the electrons form a Fermi liquid. If the band is half-filled and the interaction between electrons is strong the system is an insulating antiferromagnet. As the interaction between electrons, W, and their density is varied the system evolves from a Fermi liquid to an antiferromagnet. There are at least two scenarios for this evolution [1]:

- There is just one transition leading directly from the Fermi liquid to the antiferromagnet. In the Fermi liquid near the transition line the antiferromagnetic spin fluctuations have a small but non-zero gap. At the energy scales larger than the gap the critical spin fluctuations lead to non-Fermi liquid exponents in the Green function and spin response of the electrons. The low energy properties (at energies smaller than the antiferromagnetic spin fluctuation gap) of the fermion quasiparticles are not qualitatively different from those of the free electrons.
- The evolution from the Fermi liquid to the antiferromagnet goes through the intermediate state as shown in Fig. 1. In this intermediate state Fermi liquid theory is not a correct description of the low energy properties even far from criticality. One theoretical realization of such an intermediate state is known as a "spin liquid" [2]. A spin liquid possesses a Fermi surface, spin 1/2 fermionic excitations with constant density of states at low energies and a particle–hole continuum but the fermions interact via a singular interaction mediated by the gauge field. As discussed below the singular interaction causes anomalous temperature dependence of the susceptibilities and NMR relaxation rates for a range of values of density or interaction.

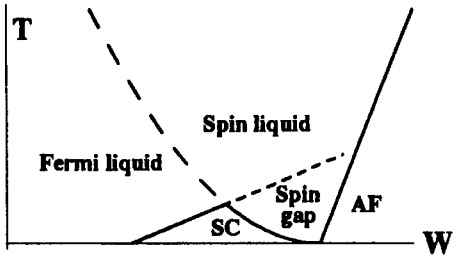


Fig. 1. Phase diagram of a strongly correlated electron system in which transition to the antiferromagnet happens through the intermediate spin liquid phase. T is temperature and W is interaction constant.

The evolution from the Fermi liquid to the antiferromagnet is realized experimentally when the doping is varied in high T_c materials. As discussed elsewhere [3], the available experimental data on the magnetic properties of these materials in the "underdoped" regime are incompatible with the theoretical predictions for the critical behavior in the Fermi liquid scenario. In this paper we focus on the theoretical predictions [4] for the "spin-liquid" scenario. We begin with the sketch of the theoretical reasoning [5] leading to these predictions.

Our starting point for the description of the spin liquid is a Hamiltonian, $H = H_{FL} + H_{gauge}$, where H_{FL} describes fermions moving in a lattice and interacting with each other via a short range four fermion interaction W:

$$H_{FL} = \sum_{p\alpha} \epsilon(p) c^{\dagger}_{p,\alpha} c_{p,\alpha} + W \sum_{p,p',q,\alpha,\beta} c^{\dagger}_{p,\alpha} c_{p+q,\alpha} c^{\dagger}_{p',\beta} c_{p'-q,\beta} \quad (1)$$

and H_{gauge} describes the gauge field and its coupling to the fermions:

$$H_{gauge} = \sum_{p,k,\alpha} \mathbf{a}_k \mathbf{v}(p) c^{\dagger}_{p-k/2,\alpha} c_{p+k/2,\alpha} + \frac{1}{2g_0^2} \sum_k (\mathbf{k} \times \mathbf{a})^2 \quad (2)$$

Here g_0 is the bare fermion–gauge field interaction constant, $\alpha = 1, \ldots N$ is a spin index. In the physical spin liquid $N = 2$; however, to obtain analytical results we consider the limits $N \to 0$ and $N \to \infty$ and interpolate between them [5].

Perturbation theory in g_0 leads immediately to two effects. (i) The gauge field propagator becomes

$$D(\omega, k) = \frac{1}{\frac{N p_0 |\omega|}{2\pi |k|} + \frac{1}{N^{1/2} g^2} k^2} \quad (3)$$

Here the first term in the denominator is due to Landau damping of the gauge field, p_0 is the curvature of the Fermi surface at the point where the normal to the Fermi line is perpendicular to $\mathbf{k}$ and $g^2 = N^{-1/2} g_0^2$. (ii) Using the gauge-field propagator to calculate the self energy one finds [6]

$$\Sigma^{(1)}(\epsilon) = -i \left| \frac{\omega_0}{\epsilon} \right|^{1/3} \epsilon, \qquad \omega_0 = \left(\frac{1}{2\sqrt{3}} \right)^3 \frac{2 v_F g_0^4}{\pi^2 p_0} \quad (4)$$

which dominates fermion Green function at energies less than ω_0.

From the gauge field propagator (3) it is clear that typical scattering involves typical momentum transfer $k \propto N^{1/2} \omega^{2/3}$. Such processes change only slightly the direction $\mathbf{v}_F$ in which the fermion propagates. In the cartesian coordinates associated with $\mathbf{v}_F$ the Green function of the fermion becomes

$$G^{(1)}(\epsilon, p) = \frac{1}{\Sigma^{(1)}(\epsilon) - v_F [p_{\parallel} + p_{\perp}^2 / (2p_0)]} \quad (5)$$

Due to the large momentum transfer in the limit $N \to \infty$ the curvature of the Fermi line becomes important and higher order terms of the perturbation theory are small in $1/N$ [5]. This is reminiscent of the Migdal theorem in conventional electron–phonon problem. In an alternative limit of $N \to 0$ the curvature of the Fermi line is unimportant and the dependence of the fermion Green function on the momentum $p_{\perp}$ can be neglected. In this limit higher order diagrams become the same as in a one-dimensional theory which can be solved by bosonization [7]. The results obtained by this method are qualitatively different from the results of the $1/N$ expansion: the power laws predicted in the $1/N$ expansion (see below) are converted into more rapid exponential dependences. However, the bosonization is only valid in the strict $N \to 0$ limit, at any fixed non-zero $N \ll 1$ the curvature terms become eventually important. We have obtained the leading behavior of the physical quantities at fixed $N \ll 1$ using Ward identities. It turns out that this behavior is qualitatively more similar to the behavior at $N \gg 1$ than to exponentially rapid dependencies of $N \to 0$ limit. Since the properties in the limits $N \gg 1$ and $N \ll 1$ are similar, but the latter case is more technically difficult we will mainly focus on the $N \gg 1$ limit in this paper.

In this limit direct calculations show that at general wavelength $|\mathbf{q}| \neq 2p_F$ response functions of the spin liquid are very similar to properties of the Fermi liquid [5] because of the small phase volume available for virtual processes which leave both fermions with momentum transfer $\mathbf{p} + \mathbf{q} + \mathbf{k}$ and $\mathbf{p} + \mathbf{k}$ close to the Fermi surface. The effects of the gauge field on the fermion vertices with large momentum transfer are more interesting. The situation changes drastically for $|q|$ close $2p_F$. In this case a virtual process with momentum transfer $\mathbf{q}$ along the Fermi surface leaves both fermions with momenta $\mathbf{p} + \mathbf{q} + \mathbf{k}$ and $\mathbf{p} + \mathbf{k}$ near the Fermi surface. The leading contribution in $1/N$ to the fermion spin fluctuation vertex Γ_Q is logarithmically divergent at $Q = 2p_F$; we find that higher powers of N contain higher powers of logarithms; we were able to sum these logarithms using a renormalization group method obtaining [5] power law singularities in Γ_{2p_F}:

$$\Gamma_{2p_F} \simeq \frac{1}{\left(\frac{\omega}{\omega_0} \right)^{\sigma} + \left(\frac{v_F k_{\parallel}}{\omega_0} \right)^{3\sigma/2}} \quad (6)$$

The exponent σ can be calculated in the limits $N \to \infty$ and $N \to 0$. Extrapolation of the results obtained in these limits to the physical case $N = 2$ gives the estimates $1/4 < \sigma < 3/4$.

The singularity of the vertex means that the calculation of the partcle–hole susceptibility must be reconsidered. The change in the fermion Green function and the singularity of the $2p_F$ vertex have profound effects on the fermion polarization operator $\Pi(\omega, q)$. This effect is especially interesting if $\sigma > 1/3$. In this case, the polarization operator becomes singular at $|\mathbf{q}| = 2p_F$ ring in the momentum space [5]:

$$\Pi(\omega, \mathbf{q}) = \sqrt{\frac{\omega_0 p_0}{v_F^3}} \frac{1}{\left[c_{\omega} \left(\frac{|\omega|}{\omega_0} \right)^{2\sigma - 2/3} + c_k \left(\frac{||q| - 2p_F| v_F}{\omega_0} \right)^{3\sigma - 1} \right]} \quad (7)$$

The full susceptibility χ is obtained by combining the irreducible bubble Π with the short-range four fermion vertex W. We have shown [5] that the gauge–field interaction renormalizes a sufficiently weak initial W to zero, so $\chi(\omega, k) = \Pi(\omega, k)$ Thus, in this case, the susceptibility is singular in momentum space for a wide range of W and density.

The divergence of the susceptibility at $\omega = 0$, $Q = 2p_F$ results in a strong temperature dependence of the NMR relaxation rates which are given by summing the appropriate combinations of susceptibilities over momenta [4]:

$$\frac{1}{T_1 T} \sim A^2 \frac{p_F p_0^{1/2} \omega_0^{1/2}}{v_F^{5/2}} \left(\frac{T}{\omega_0} \right)^{\frac{1}{3} - 2\sigma} \quad (8)$$

If $\sigma < 1/2$, the rate T_2^{-1} is non divergent and if $\sigma > 1/2$,

$$\frac{1}{T_2} \sim A^2 \frac{\sqrt{p_F p_0} \omega_0}{v_F^2 a} \left(\frac{T}{\omega_0} \right)^{1 - 2\sigma} \quad (9)$$

Here a is the lattice constant. For the uniform susceptibility we found

$$\chi_U = const + D_0'' (T/\omega_0)^{1+\beta} \quad (10)$$

where D_0'' is a constant of order $\left(\frac{pFg_c}{v_F}\right)^2 W$, whose sign is positive for repulsive W and negative for attractive W. The exponent $\beta(N) = \frac{4}{3} - \frac{1}{N}$.

NMR experiments on $La_{2-x}Sr_xCuO_4$ have shown that the copper T_1 rates has the temperature dependence ${}^{Cu}(T_1T)^{-1} \sim T^{-1}$ for $100K < T < 500K$ [8]. The uniform susceptibility is given by $\chi \sim const + AT$ at least for $150K < T < 400K$ [9]. The strongly coupled spin liquid results with $\sigma \approx 2/3$ are in agreement with these data. However, the recent data show [10] that $1/T_2$ in this material scales as $1/(T_1T)$ in the temperature range 100–300 K, which is not consistent with the weaker dependence (9).

Note that there is a fundamental difficulty in comparing quantitatively the theoretical predictions with data. All such predictions for the spin liquid or alternative scenarios imply that an asymptotic low temperature behavior is reached. At high temperatures non-universal properties such as details of the band structure becomes important. In fact, the existing data cover only a limited range of temperatures and can be fitted in different ways. Therefore, it is very important that the measurements be extended to as low temperatures as possible, especially on materials which do not display spin gaps or superconductivity down to low temperatures.

Underdoped bilayered cuprates are known to exhibit a "spin gap" phenomena in a broad temperature range $T_c < T < T_{sg}$ with $T_{sg} \approx 150\ K$. The theory of this phenomena in the spin-liquid scenario is given by the Cooper pairing of spinons on different planes [11]. This pairing results from the antiferromagnetic interaction between the planes $H = J_\perp \sum_i S_i^{(1)} S_i^{(2)}$ enhanced by long ranged spin correlations in each plane [12,13]. Formally, in the regime of strong interaction with the gauge field the effective interaction between spinons becomes dressed by large corrections given in eqn (6) [14]. Due to the singular momentum dependence of the vertex (6) the gap equation is almost one dimensional, i.e. Cooper pairing occurs almost independently on different parts of the Fermi line. Therefore, the gap opens first only at a small patch of the Fermi line and spreads to the rest of the Fermi line only at lower temperatures. The pairing energy is only weakly sensitive to the symmetry of the gap function. In the absence of local repulsion between spinons the s-state has somewhat lower energy, but such repulsion, induced, e.g. by incoherent tunneling of spinons from one plane to another, would favor the d-state symmetry.

Another direct application of the gauge theory discussed in this paper is to the $\nu = 1/2$ Quantum Hall state in the 2D electron gas if the Coulomb interaction were screened, e.g. by a metallic gate, in this case the charge response at $2p_F$ would be very singular.

REFERENCES

1. Other alternatives have also been discussed, e.g. of propagating spin waves decoupled from fermions, see Chubukov A. V. and Sachdev S., *Phys. Rev. Lett.* **71**, 3615 (1993).
2. Baskaran G., Zou Z. and Anderson P. W., *Solid State Commun.* **63**, 973 (1987); Ioffe L. B. and Larkin A. I., *Phys. Rev. B* **39**, 8988 (1989).
3. Millis A. J., Ioffe L. B. and Monien H., this volume.
4. Altshuler B. L., Ioffe L. B., Larkin A. I. and Millis A. J., submitted to *Phys. Rev. B*; preprint database cond-mat/9501133.
5. Altshuler B. L., Ioffe L. B. and Millis A. J., *Phys. Rev. B* **50**, 14048 (1994).
6. Lee P. A., *Phys. Rev. Lett.* **63**, 680 (1989).
7. Ioffe L. B., Lidsky D. and Altshuler B. L., *Phys. Rev. Lett.* **73**, 472 (1994).
8. Ohsugi S., Kitaoka Y., Ishida K. and Asayama K., *J. Phys. Soc. Jpn* **60**, 2351 (1991).
9. A summary of the data is given in Millis A. J. and Monien H., *Phys. Rev. Lett.* **70**, 2810 (1993).
10. Walstedt R. E., unpublished.
11. Altshuler B. L., Ioffe L. B., *Solid State Commun.* **82**, 253 (1992).
12. Altshuler B. L., Ioffe L. B., Larkin A. I. and Millis A. J., *JETP Lett.* , **59**, 65 (1994).
13. Ubbens M. U., Lee P. A., *Phys. Rev. B* **50**, (1994).
14. Altshuler B. L., Ioffe L. B. and Millis A. J., unpublished.

Pergamon

J. Phys. Chem. Solids Vol. 56, No. 12, pp. 1615–1617, 1995
Copyright © 1995 Elsevier Science Ltd
Printed in Great Britain. All rights reserved
0022–3697/95 $9.50 + 0.00

0022-3697(95)00209-X

SPECTRAL FUNCTIONS OF CORRELATED ELECTRON SYSTEMS IN THE LOCAL IMPURITY SELF CONSISTENT APPROXIMATION

HENRIK KAJUETER and GABRIEL KOTLIAR
Serin Physics Laboratory, Rutgers University, Piscataway, NJ 08855-0849, U.S.A.

Abstract—We describe the evolution of the spectral density as we dope a Mott insulator within a dynamical mean field method. After giving an intuitive description of this Local Impurity Self-Consistent Approximation (LISA) for a model with several orbitals per unit cell, we illustrate its implementation in the context of the Hubbard model in infinite dimensions. For this purpose a new iterative perturbation theory (IPT) scheme is introduced and compared with results from exact diagonalization.

1. INTRODUCTION

The evolution of spectral functions near a Mott transition is a long standing problem in the physics of strongly interacting fermions. Recently some progress has been made using a dynamical mean field method. This approach dates back to the mid seventies under names such as dynamical coherent potential approximation (CPA) or local approximation. It received substantial attention following the pioneering paper of Metzner and Vollhardt [1] pointing out the correct scaling of the hopping integrals necessary to obtain a well defined limit of large lattice coordination.

A very useful formulation of the mean field approach is based on viewing a lattice model impurity embedded in a medium obeying a self-consistency condition. For the Hubbard model, the corresponding impurity model is the Anderson model [2]. Other models of strongly correlated electrons are associated with other impurity models subject to different self-consistency conditions [3].

This method is very powerful because several numerical and analytical techniques which have been developed to analyze impurity models over the years can be implemented to solve the mean field equations. Several approaches have been used successfully for this purpose: qualitative analysis of the mean field equations [2], quantum Monte-Carlo methods [4–6], iterative perturbation theory [2,7], exact diagonalization methods [8], and the projective self-consistent method, a renormalization technique [9].

In this note we present a pedagogical discussion of the main ideas behind the mapping from lattice onto impurity models stressing the generality of the approach and its intuitive character. Then, we will review some aspects of the evolution of the spectral function of the Mott insulator at low temperatures. In this context a new scheme which allows to perform iterative perturbation theory away from half filling will be introduced and compared with results from exact diagonalization.

2. FROM LATTICE MODELS TO IMPURITY MODELS

The starting point of this section is a lattice model of strongly correlated electrons containing various orbitals per unit cell. We use a compact notation where the index $\alpha = (m, \sigma)$ combines the orbital m and the spin σ. The starting Hamiltonian, which could in principle be obtained from an *ab initio* constrained LDA calculation after a suitable folding to low energies as in Ref. [10] or from physical considerations is assumed to be of the form:

$$H_{\text{lattice}} = -\sum_{\langle ij\rangle} c^+_{i\alpha} t_{i\alpha,j\beta} c_{j\beta} + \sum_i (E_{\alpha\beta} - \mu\delta_{\alpha\beta}) c^+_{i\alpha} c_{i\beta} + \sum_i \Gamma_{\alpha\beta\gamma\delta} c^+_{i\alpha} c_{i\beta} c^+_{i\gamma} c_{i\delta} \quad (1)$$

Now we focus on a single unit cell and integrate out all degrees of freedom except for those which reside in the selected unit cell. These are described by operators c_α and no longer carry a site index. The dynamics of the resulting problem are described by an impurity model which describes an impurity c_α coupled to a bath of fermions ($a_{b\mu}$) (see Fig. 1):

$$H_{\text{imp}} = \sum_{\alpha\beta} (E_{\alpha\beta} - \mu\delta_{\alpha\beta}) c^+_\alpha c_\beta + \sum_i \Gamma_{\alpha\beta\gamma\delta} c^+_\alpha c_\beta c^+_\gamma c_\delta + \sum_{b\mu} \epsilon_{b\mu} a^+_{b\mu} a_{b\mu} + \sum_k (V_{b\mu,\alpha} a^+_{b\mu} c_\alpha + h.c.) \quad (2)$$

From the impurity model we can obtain all the local correlation functions, since by construction the local lattice Green's functions are identical to the impurity Green's function $\hat{G} = (G_{\alpha,\beta})$. We use a matrix notation so that the local Green's function is given by

$$G_{\alpha,\beta}(\tau - \tau') = -\langle T_\tau c_\alpha(\tau) c^+_\beta(\tau')\rangle \quad (3)$$

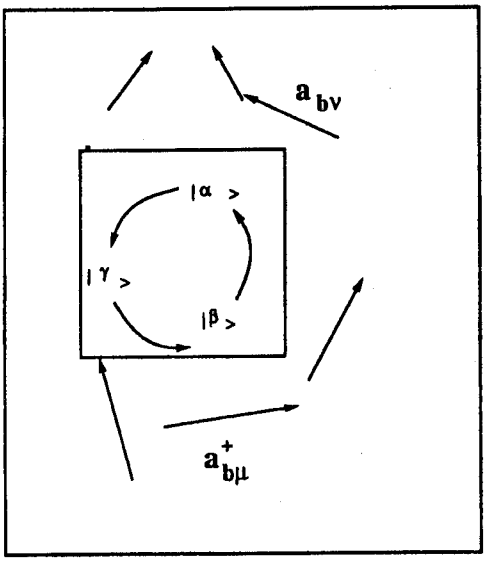


Fig. 1. Illustration of the unit cell containing the local degrees of freedom and the rest of the crystal treated as a bath. In the selected unit cell, different *correlated* configurations are fluctuating. Non interacting electrons describe the effective medium.

This should be viewed as a functional of the parameters $\epsilon_{b\mu}$ and $V_{b\mu,\alpha}$. To determine these parameters we construct the "Weiss field" which describes the effect of the rest of the electrons on the selected cell, $\hat{G}_0^{-1}(i\omega_n) = (i\omega_n + \mu)\hat{I} - \hat{E} - (\sum_{b\mu} \frac{V_{b\mu,\alpha} V_{b\mu,\beta}}{i\omega_m - \epsilon_{b\mu}})$, and the self energy of the impurity, $\hat{\sum}(i\omega_n) = \hat{G}_0^{-1}(i\omega_n) - \hat{G}^{-1}(i\omega_n)$, viewed as a functional of $\epsilon_{b\mu}$ and $V_{b\mu}$. These parameters are determined by requiring that the bath and the local degrees of freedom describe the electrons in the original lattice problem. Namely we can construct the local Green's function from the lattice Green's function obtained by adding a k independent self energy to the non interacting lattice Green's function (obtained from eqn (1) by setting the interaction terms to zero) or from the impurity model.

$$\hat{G}(i\omega_n) = \sum_k \left((i\omega_n + \mu)\hat{I} - \hat{t}(k) - \hat{\sum}(i\omega_n) - \hat{E} \right)^{-1} \quad (4)$$

Notice that the mean field equations for all the models in [3] are particular cases of eqns (2) and (4).

3. IPT AWAY FROM HALF FILLING

To make progress one needs a practical and accurate technique for solving the system of eqn (4). The computational requirements of the exact diagonalization and the quantum Monte-Carlo methods are such that they can only be implemented for very simple Hamiltonians. To carry out realistic calculations it is necessary to have an accurate but fast algorithm for solving the Anderson impurity model. Here we introduce a new perturbative method and illustrate it by applying it to the Hubbard model (one band per unit cell) away from half filling.

The approach is in the spirit of the iterative perturbation theory approach introduced in [7,12]. The key idea is to search for a self energy as a functional of the "Weiss field" such that the self energy expression becomes exact both in the weak and in the strong coupling limit. Moreover, it should have the correct behavior both at small and at large frequencies. The naive extension of the method originally proposed for half filling fails to give reasonable results for finite doping. However, we propose a generalization to arbitrary filling by constructing a self energy expression which has the correct behavior in the limits discussed above:

$$\overset{(2)}{\sum}(\omega) = \frac{\frac{n(1-n)}{n_0(1-n_0)} \sum_0^{(2)}(\omega)}{1 - \frac{(1-n)U - \mu + \tilde{\mu}_0}{n_0(1-n_0)U^2} \sum_0^{(2)}(\omega)} \quad (5)$$

Here $\sum_0^{(2)}(\omega)$ is the normal second order contribution to the self energy evaluated by the bare Green's function $G_0(\omega) = \frac{1}{\omega - \tilde{\mu}_0 - t^2 G(\omega)}$ (Bethe lattice). The parameter $\tilde{\mu}_0$ is determined such that the Luttinger theorem is fulfilled ($\mu_0 = \mu - Un - \sum^{(2)}[\tilde{\mu}_0](\omega = 0)$, $\mu_0 = \mu|_{U=0}$). The particle number is given by $n = \frac{1}{\pi}\int_{-\infty}^{0} \mathrm{Im}G(\omega)\mathrm{d}\omega$. In analogy, n_0 is a fictitious particle number computed from G_0. The self-consistency condition becomes

$$G^{-1}(\omega) = G_0^{-1}(\omega) - \tilde{\mu}_0 + \mu - Un - \overset{(2)}{\sum}(\omega). \quad (6)$$

For the numerical implementation, it is more convenient to fix $\tilde{\mu}_0$ (rather than μ). Then, starting with a guess for G and μ, one can compute G_0, n_0 and n. Afterwards eqn (5) yields $\sum^{(2)}(\omega)$, and we obtain a new μ from the Luttinger theorem. The loop is closed by eqn (6).

It is easy to check that in the case of half filling the procedure reduces to ordinary IPT. In the weak coupling limit eqn (5) is exact to order U^2. Moreover, it can be verified that the expression becomes also exact for $U \to \infty$. The correct low frequency behavior is realized by satisfying the Luttinger theorem. This is the main difference with an earlier scheme which uses related ideas [11] and is essential to obtain good agreement with the exact diagonalization results at low temperatures.

We establish the accuracy of our method by comparing it with results obtained using the exact diagonalization algorithm to solve the impurity model, as described by Caffarel and Krauth [8]. Both methods are in close agreement when used on the imaginary axis. The real advantage of combining our perturbation scheme with the exact diagonalization is shown when we display the spectral functions obtained by these two methods on the real axis (Fig. 2).

It is clear that the exact diagonalization is doing its best in producing the correct spectral distribution. But it is unable to give a smooth density of states. Instead several sharp structures occur as a consequence of treating only a finite number of orbitals in the Anderson model.

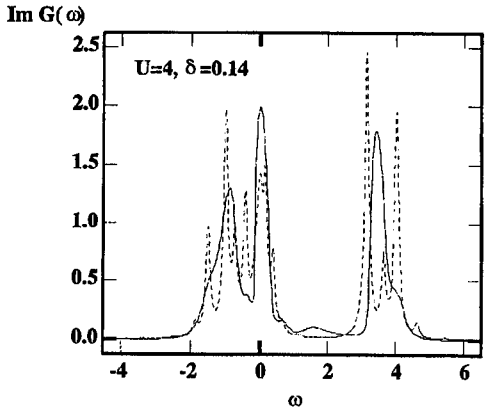


Fig. 2. Im$G(\omega)$ at $T = 0$ for $U = 4D$ and hole doping $\delta = 0.14$: iterative perturbation theory (full line) vs exact diagonalization (dashed line).

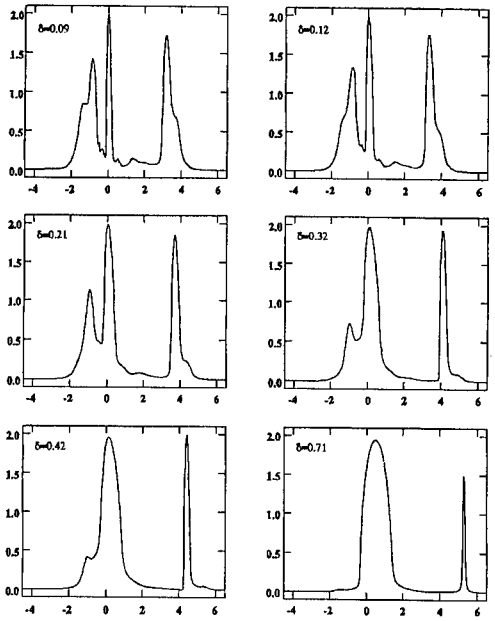


Fig. 3. Evolution of the spectral function for $U = 4$ and $T = 0$ with increasing hole doping δ.

As an example, Fig. 3 shows the evolution of the spectral density of the doped Mott insulator with increasing hole doping δ. The qualitative features are those expected from the spectra of the single impurity [2] and are in agreement with the quantum Monte-Carlo calculations [13]. For small doping, there is a clear resonance peak at the fermi level. As δ is increased, the peak broadens and is shifted through the lower Hubbard band. At the same time the weight of the upper band decreases.

The most striking feature of the evolution of the spectral function as a function of doping is the finite shift of the Kondo resonance from the insulating band edge as the doping goes to zero. It was demonstrated analytically that this is a genuine property of the exact solution of the Hubbard model in infinite dimensions using the projective self-consistent method [14] and is one of the most striking properties of the Hubbard model in large dimensions. This feature did not appear in the earlier studies of Hubbard model in large dimensions using Monte-Carlo techniques [13] at high temperatures, and is also not easily seen in exact diagonalization algorithms [15].

4. CONCLUSIONS

The dynamical mean field approach is widely applicable to the one particle spectroscopy of correlated electrons. The mean field equations are tractable and contain rather rich information. A very important lesson is that it is necessary to use a combination of analytical and numerical techniques to obtain reliable results on the physical content of the mean field theory. This was illustrated in a discussion of the spectral function of the doped Mott insulator. In this context, we reported briefly a new pertubation scheme which allows to perform IPT away from half filling. This approach is very economical and promising and has already been extended to systems with more complex units cells, as will be reported elsewhere.

Acknowledgements—This research was supported by the NSF under contract DMR 92-24000.

REFERENCES

1. Metzner W. and Vollhardt D., *Phys. Rev. Lett.* **62**, 324 (1989).
2. Georges A., Kotliar G., *Phys. Rev. B* **45**, 6479 (1992).
3. Georges A., Kotliar G. and Si Q., *Int. J. Modern Phys.* **6**, 705 (1992).
4. Jarrell M., it Phys. Rev. Lett. **69**, 168 (1992).
5. Rozenberg M., Zhang X. Y. and Kotliar G., *Phys. Rev. Lett.* **69**, 1236 (1992).
6. Georges A. and Krauth W., *Phys. Rev. Lett.* **69**, 1240 (1992).
7. Zhang X. Y., Rozenberg M. J. and Kotliar G., *Phys. Rev. Lett.* **70**, 1666 (1993).
8. Caffarel M. and Krauth W., *Phys. Rev. Lett.* **72**, 1545 (1994); Si Q., Rozenberg M., Kotliar G. and Ruckenstein A., *Phys. Rev. Lett.* **72**, 2761 (1994).
9. Moeller G., Si Q., Kotliar G., Rozenberg M. and Fisher D. S., *Phys. Rev. Lett.* **74**, 2082 (1995).
10. Andersen O. K., Jepsen O., Liechtenstein A. I. and Mazin I. I., *Phys. Rev. B* **49**, 4145 (1994).
11. Ferrer J., Martin Rodero A. and Flores F., *Phys. Rev. B* **36**, 6149 (1987).
12. for an early review see Kotliar G. in: *Strongly Correlated Electronic Materials* (Edited by K. S. Bedell, Z. Wang, D. Meltzer, A. Balatsky and E. Abrahams). Addison Wesley (1994)
13. Jarrell M. and Pruschke T., *Z. Phys. B* **90**, 187 (1993).
14. Moeller G., Ph.D. Thesis (1994); Fisher D., Kotliar G. and Moeller G., preprint.
15. Kajueter H., Kotliar G. and Moeller G., preprint.

Pergamon

J. Phys. Chem. Solids Vol. 56, No. 12, pp. 1619–1622, 1995
Copyright © 1995 Elsevier Science Ltd
Printed in Great Britain. All rights reserved
0022-3697/95 $9.50 + 0.00

0022-3697(95)00178-6

VORTICES IN *d*-WAVE SUPERCONDUCTORS

C. KALLIN*, A. J. BERLINSKY*, A. L. FETTER†, M. FRANZ* and P. I. SOININEN*

* Institute for Materials Research and Department of Physics and Astronomy, McMaster University, Hamilton, Ontario, L8S 4M1 Canada

† Department of Physics, Stanford University, Stanford, CA 94305, U.S.A.

Abstract—Vortex state solutions are studied in mean field theory for the simplest microscopic model of unconventional superconductivity, the nearest neighbor tight-binding model on a square lattice with on-site and nearest neighbor interactions, which has *d*- and extended *s*-wave mean field ground states for suitable values of the parameters. Vortex states of this model are studied by solving the Bogoliubov-de Gennes equations self-consistently in position space for finite lattices with various boundary conditions. The results of such calculations are interpreted in terms of the appropriate Ginzburg-Landau (GL) free energy, and the GL equations themselves are integrated to test our understanding of the microscopic calculations. The order parameter fields for this problem may be described either as complex functions on horizontal and vertical nearest neighbor bonds or as local linear combinations of these with *s*- and *d*-wave symmetry. The *d*-wave component of a single vortex resembles the vortex order parameter field of a conventional superconductor. However the *s*-wave component, which is nonzero in a ring around the vortex core and which dies off at long distances like $1/r^2$, has a nontrivial internal structure involving domains and extra point nodes. The effects of a small orthorhombic distortion are discussed as are the implications of our results for scanning tunneling experiments.

In a typical phonon-mediated conventional superconductor, the size of a Cooper pair is large, and the short-range part of the Coulomb interaction does not modify the form of the pair wave-function significantly. By contrast, in the high T_c oxide superconductors the electronically driven attractive interactions which give rise to the superconductivity are short range and effectively have a hard core (the on-site Coulomb repulsion). In this situation, Cooper pair wave functions with nodes at the origin are expected, and these give rise to non-trivial nodal structures for the gap on the Fermi surface. The situation is analogous to that in superfluid ^{3}He where the hard core repulsion and short-range attraction of the He–He potential favors *p*-wave (and, in that case, spin triplet) superfluidity.

For the mean field theory which is used to model conventional superconductivity, the local order parameter, the gap function, is the average of the probability of destroying a singlet pair at some point in space times the attractive coupling constant [1]. The analogous quantity, in the presence of short range repulsion, is the probability of destroying a singlet pair on a nearest-neighbor *pair* of sites times the attractive nearest neighbor coupling constant. This means that, for a square lattice, the gap function is defined on x and y nearest neighbor bonds, rather than on sites. This order parameter set can be extended to include second- and further-neighbor pairing.

For tetragonal symmetry, x and y bonds are equivalent, and the stable, uniform superconducting state is one with relative phase zero, for (extended) *s*-wave, or π, for *d*-wave, for the gap functions on x and y bonds. The relative stability of these two solutions is sensitive to the parameters of the Hamiltonian. The term "extended *s*-wave" refers to the fact that the *s*-wave order parameter is a linear combination of order parameters defined on bonds. For nearest neighbor pairing, the *s*-wave gap function has the form $\cos k_x + \cos k_y$ in momentum space, which may give rise to point nodes, depending on the size and shape of the Fermi surface. Similarly, the *d*-wave gap function has the form $\cos k_x - \cos k_y$.

For inhomogeneous superconducting states, such as the vortex state which results from a magnetic field, a useful formulation of mean field theory is that of de Gennes [1]. Here we present a slight generalization of that theory due to Soininen *et al.* [2] which applies to a Hamiltonian with nearest neighbor hopping, a repulsive on-site potential and an attractive nearest neighbor interaction. For this case the Bogoliuov–de Gennes equations are

$$\begin{pmatrix} \hat{\xi} & \hat{\Delta} \\ \hat{\Delta}^* & -\hat{\xi}^* \end{pmatrix} \begin{pmatrix} u_n(\boldsymbol{r}) \\ v_n(\boldsymbol{r}) \end{pmatrix} = E_n \begin{pmatrix} u_n(\boldsymbol{r}) \\ v_n(\boldsymbol{r}) \end{pmatrix}, \tag{1}$$

$$\hat{\xi} u_n(\boldsymbol{r}) = -t \sum_{\delta} e^{\frac{2\pi i}{\phi_0} \int_{\boldsymbol{r}}^{\boldsymbol{r}+\delta} \boldsymbol{A}\cdot d\boldsymbol{\ell}} u_n(\boldsymbol{r}+\delta) - \mu u_n(\boldsymbol{r}), \tag{2}$$

$$\hat{\Delta} v_n(\boldsymbol{r}) = \sum_{\delta} \Delta_{\delta}(\boldsymbol{r}) v_n(\boldsymbol{r}+\delta) + \Delta_0(\boldsymbol{r}) v_n(\boldsymbol{r}). \tag{3}$$

Here δ denotes a nearest-neighbor vector; the normal state bandwidth is $8t$; μ is the chemical potential; ϕ_0 is the quantum of flux; and $\boldsymbol{A}$ is the vector potential on the bond connecting site $\boldsymbol{r}$ to site $\boldsymbol{r}+\delta$.

The gap equations for nearest neighbor and onsite pairing are

$$\Delta_{\delta}(\boldsymbol{r}) = \frac{g}{2} \sum_n \left[u_n(\boldsymbol{r}+\delta) v_n^*(\boldsymbol{r}) \right.$$

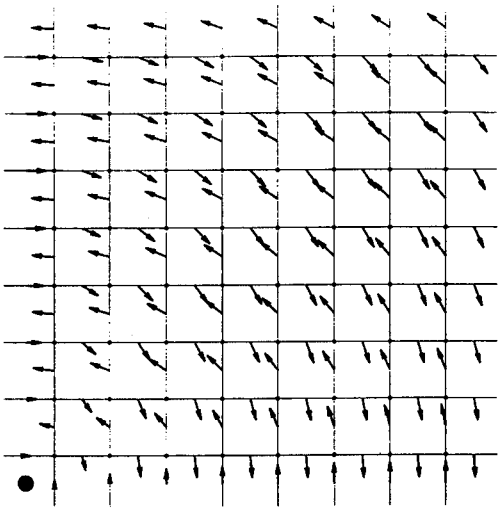


Fig. 1. The first quadrant of the core of a d-wave vortex. The arrows on the nearest neighbor bonds indicate the magnitude and the phase of the order parameter. The black dot denotes the center of the vortex. Far away from the vortex core the x and y bonds have π phase difference indicating a pure d-wave state. The parameters used in the numerical solution of Eqns (1)–(5) were $T = 0.05t$, $\mu = -2t$, $g = 3.195t$, $g_0 = -3t$. Only the central 8×8 region of the full 16×16 quadrant which was studied is shown.

$$+ u_n(r)v_n^*(r+\delta)]\tanh\left(\frac{E_n}{2T}\right), \tag{4}$$

$$\Delta_0(r) = g_0 \sum_n u_n(r)v_n^*(r)\tanh\left(\frac{E_n}{2T}\right). \tag{5}$$

Positive values for the coupling constants g and g_0 correspond to attraction, and negative values to repulsion. The components of the gap function have the symmetry

$$\Delta_\delta(r) = \Delta_{-\delta}(r+\delta). \tag{6}$$

The Bogoliubov–de Gennes equations may be solved self-consistently by computer on a finite lattice with suitable boundary conditions. The output of such a calculation is a set of single-particle energies E_n and eigenfunctions $\left(u_n(r), v_n(r)\right)$, along with self-consistent gap functions, $\Delta_\delta(r)$, defined on bonds. In terms of these gap functions, the s- and d-wave order parameters are given by

$$s(r) = (\Delta_{\hat{x}}(r) + \Delta_{-\hat{x}}(r) + \Delta_{\hat{y}}(r) + \Delta_{-\hat{y}}(r))/4,$$

$$d(r) = (\Delta_{\hat{x}}(r) + \Delta_{-\hat{x}}(r) - \Delta_{\hat{y}}(r) - \Delta_{-\hat{y}}(r))/4. \tag{7}$$

Figure 1 shows the result of such a calculation, where a winding of 2π far from the origin has been imposed as a boundary condition, and the vector potential has been set equal to zero. Each arrow in Fig. 1 represents the magnitude and phase of the order parameter on a bond. Using the definitions of $d(r)$ and $s(r)$ from Eqns (7), one obtains the results for $|d(r)|$ and $|s(r)|$ shown in Fig. 2. The qualitative behavior of both the amplitudes and phases of the s- and d-wave order parameters is shown in Fig. 3. The d-wave

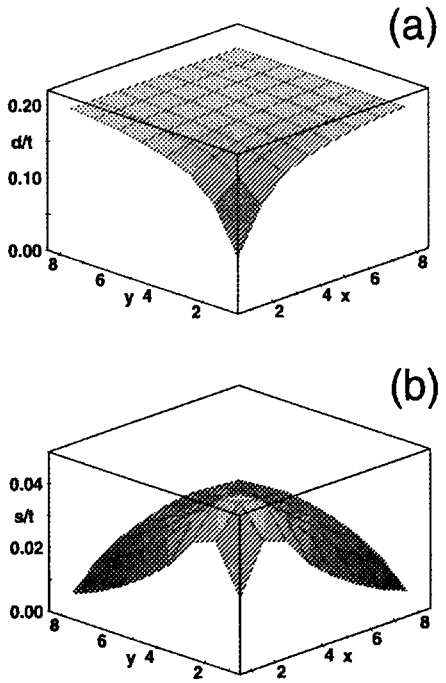


Fig. 2. Same as Fig. 1 but presented in terms of the amplitudes of s- and d-wave pairing denoted with s and d respectively. The center of vortex is situated at the point (0.5, 0.5).

order parameter around a vortex is seen to resemble closely the behavior of the order parameter around a conventional s-wave vortex, growing up from zero in a coherence length and going to a constant value for large r. The s-wave order parameter also grows up in a coherence length and then falls off slowly for large r. The relative phase of the two order parameters shows considerable structure. The results of the microscopic calculation can be interpreted in terms of the relevant Ginzburg-Landau Hamiltonian which was first written down by Joynt [3].

$$\begin{aligned} f = {} & \alpha_s|s|^2 + \alpha_d|d|^2 + \beta_1|s|^4 + \beta_2|d|^4 + \beta_3|s|^2|d|^2 \\ & + \beta_4(s^{*2}d^2 + d^{*2}s^2) \\ & + \gamma_s|\Pi s|^2 + \gamma_d|\Pi d|^2 + \gamma_v\Big[(\Pi_y s)^*(\Pi_y d) \\ & - (\Pi_x s)^*(\Pi_x d) + \text{c.c.}\Big]. \end{aligned} \tag{8}$$

Here $= -i\hbar\nabla - e^*\mathbf{A}/c$, and d is assumed to be the critical order parameter, i.e., $\alpha_s = T - T_s$, $\alpha_d = T - T_d$ with $T_s < T_d$. It is also assumed that β_1, β_2, β_3, γ_s, γ_d and γ_v are all positive [2]. The parameters γ_i are related to the effective masses in the usual way. We use $\gamma_i = \hbar^2/2m_i^*$, for $i = s, d, v$.

Kotliar [4] noted that, if the fourth order coefficient β_4 is positive, then the relative phase of s and d will be $\pi/2$ where the two order parameters coexist. Figure (3) shows that this phase relation holds nearly everywhere in a ring around the core, except in four narrow domain walls where the relative phase changes sign. In order to gain further insight into the behavior of the induced s-wave component, it is necessary to study the Ginzburg–Landau equations in more detail.

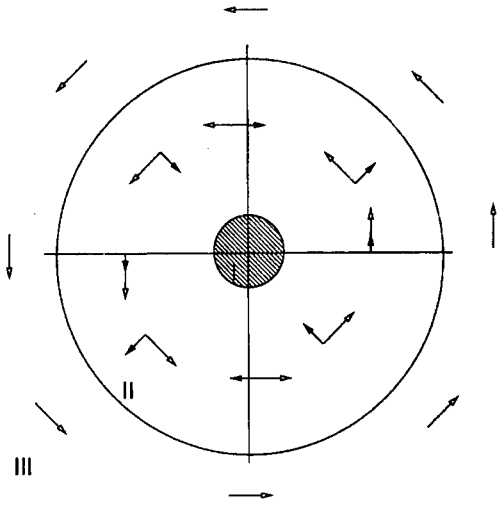


Fig. 3. Three regions of the vortex. The complex s- wave order parameter is represented with a black arrow and the d- wave one with a white arrow. Both the s-wave and d-wave pairing are suppressed in the inner core (labelled I). Localized core excitations are found in this region. This is surrounded by an outer core (labelled II) where d-wave and s-wave pairing coexist. In this region low energy fermionic excitations are absent (except possibly along those directions for which the relative phase between the s- and d-wave components vanishes). Outside the core (region III) the superconductor is in a pure d-wave state. As the opposite winding of the s- and d-wave components is incompatible with the relative phase $\pm\pi/2$, four domains are formed. The regions of relative phase $\pi/2$ and $-\pi/2$ are separated by domain walls (indicated by vertical and horizontal lines) where the relative the phase varies rapidly.

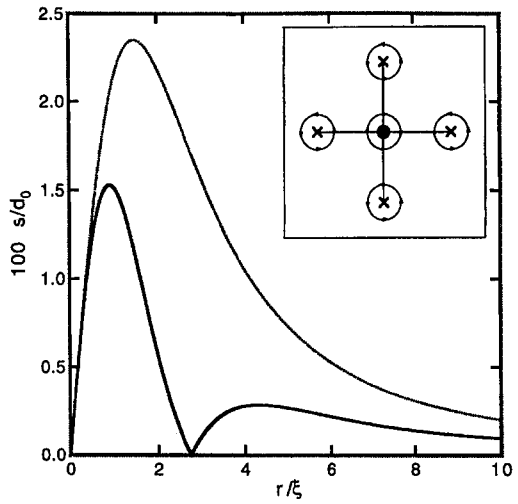


Fig. 4. Amplitude of the s-wave component along the x-axis (solid line) and along the diagonal $x = y$ (dotted line) normalized to the bulk value d_0. The parameters used are: $\gamma_s = \gamma_d = \gamma_v$, $\alpha_s = 10|\alpha_d|$, $\beta_1 = \beta_3 = 0$, and $\beta_4 = 0.5\beta_2$. The inset shows schematically the positions of the s-wave vortices and their relative windings.

The field equations for the order parameters are obtained by varying the free energy (8) with respect to conjugate fields d^* and s^*, giving,

$$\left(\frac{\hbar^2}{2m_d^*}\Pi^2 + \alpha_d\right)d + \frac{\hbar^2}{2m_v^*}(\Pi_y^2 - \Pi_x^2)s + 2\beta_2|d|^2 d + \beta_3|s|^2 d + 2\beta_4 s^2 d^* = 0, \tag{9}$$

$$\left(\frac{\hbar^2}{2m_s^*}\Pi^2 + \alpha_s\right)s + \frac{\hbar^2}{2m_v^*}(\Pi_y^2 - \Pi_x^2)d + 2\beta_1|s^2|s + \beta_3|d|^2 s + 2\beta_4 d^2 s^* = 0. \tag{10}$$

Equations (9) and (10) can be integrated numerically for boundary conditions which generate a single vortex at the origin. In doing this, we assume an extreme type-II limit, where the coupling to the vector potential can be ignored while considering the core structure of the isolated vortex line.

Ren *et al.* [5] have previously shown that for a d-wave order parameter with the asymptotic form,

$$d(r, \theta) = d_0 e^{i\theta}, \tag{11}$$

where $d_0 = \sqrt{-\alpha_d/2\beta_2}$, the asymptotic form of the s-wave order parameter is:

$$s(r, \theta) = g_1(r)e^{-i\theta} + g_2(r)e^{i3\theta}, \tag{12}$$

where $g_1(r)$ and $g_2(r)$ fall off like $1/r^2$ for large r. Furthermore, close to T_d, $g_2(r) \approx -3g_1(r)$ and therefore the winding number far from the core is $+3$. This result combined with the result that close to the core the winding number is -1 [6] implies that four additional positive vortices must exist outside the core [7]. This is a topological result and thus not sensitive to small modifications of the parameters. As is shown below, these vortices lie on the $\pm x$ and $\pm y$ axes. At lower temperatures a topological transition to a state with s-wave winding number -1 could occur. At length scales large compared to the coherence length, but less than the penetration depth, the superconductor is not in a pure d-wave state, but rather in a state characterized by power law decay of the s-wave component. Only at the length scale given by the penetration depth is the pure d-wave state regained.

We have studied the dependence of the maximum of the s-wave component on the GL parameters [7]. Noting that both the d-wave and s-wave components rise over the same length scale given by ξ_d, where $\xi_d^2 = \gamma_d/|\alpha_d|$, gives an order of magnitude estimate for the magnitude of the s-wave order parameter at the maximum,

$$\frac{\max(s)}{d_0} \sim \frac{\gamma_v}{\alpha_s \xi_d^2}. \tag{13}$$

Our numerical results confirm that the constant of proportionality is of the order unity. Note that the temperature dependence of $\max(s)$ is $(1 - T/T_d)^{3/2}$.

Figure 4 shows the behavior of the s-wave amplitude along the x-axis and along the diagonal, obtained by numerical integration of Eqns (9,10). Moving outward from the center of the vortex both the s- and d-wave amplitudes increase over the same length scale ξ_d. Further away from the origin, the relative phase tends to lock to a value $\pm\pi/2$.

The change in the relative phase occurs in narrow "domain walls". To this point, the results are in perfect agreement with the ones obtained within Bogoliubov-de Gennes theory [2]. However, further out the situation changes. The domains of rapid variation of the relative phase vanish. Furthermore, the relative phase then winds in the opposite direction. In Fig. 4 this change manifests itself as a zero in the amplitude of the *s*-wave component. This zero corresponds to the core of one of four "extra" vortices in the *s*-wave order parameter. Identical vortices are found at all four "wall ends". This, combined with the vortex with an opposite charge at the center, gives the total required winding of +3.

The coexistence of *s*- and *d*-wave order parameters in a wide region around the core is significant because of its effect on the local density of states for excitations. Volovik [6] has considered the effect, on the density of states, of the velocity field of a pure *d*-wave vortex. His result will be modified by the presence of an s admixture. An order parameter of the form $s + id$ will, in general, not have nodes on the Fermi surface since this would require two complex functions to vanish at the same point in k-space. The interplay of these two quantities, $s + id$-mixing and the superfluid velocity field, on the quasiparticle density of states around a vortex is not yet well understood.

The effects of orthorhombic distortions are easily understood in terms of a straightforward generalization of Eqn (8). In the bond-picture, the orthorhombic distortion breaks the symmetry of $x-$ and $y-$bonds. The effect is to mix the *s*- and *d*-wave order parameters in the quadratic and higher order terms of f. An additional effect is that the masses in the x and y directions become different. Typically this is incorporated as a change in the x and y length scales. Of course many more fourth order terms are generated by the distortion. However the main effect is the mixing of *s* and *d* in second order. One consequence is to allow tunneling from a conventional *s*-wave superconductor into an orthorhombically distorted $d_{x^2-y^2}$ superconductor, as has been noted by O'Donovan *et al.* [8].

Acknowledgements—This work has been supported by the Natural Sciences and Engineering Research Council of Canada, the Ontario Centre for Materials Reasearch, and by the National Science Foundation under Grant No. DMR-91-20361. We would also like to thank the Aspen Center for Physics, where this collaboration was initiated.

REFERENCES

1. de Gennes P. G., *Superconductivity of Metals and Alloys*. W.A. Benjamin, New York (1966).
2. Soininen P. I., Kallin C. and Berlinsky A. J., *Phys. Rev. B* **50**, 13883 (1994).
3. Joynt R., *Phys. Rev. B* **41**, 4271 (1990).
4. Kotliar G., *Phys. Rev. B* **37**, 3664 (1988).
5. Ren Y., Xu J. H. and Ting C. S.,*Phys. Rev. Lett.***74**, 3680 (1995).
6. Volovik G. E. *Pis'ma Zh. Eksp. Teor. Fiz.* **58**, 457 (1993); *JETP Lett.* **58**, 469 (1993).
7. Berlinsky A. J. *et al. Phys. Rev. Lett.* **75**, 2200 (1995).
8. O'Donovan C., Branch D., Carbotte J. P. and Preston J. S., *Phys. Rev. B, Phys. Rev. B* **51**, 6588 (1995).

Pergamon

J. Phys. Chem. Solids Vol. 56, No. 12, pp. 1623–1626, 1995
1995 Elsevier Science Ltd
Printed in Great Britain
0022-3697/95 $9.50 + 0.00

0022-3697(95)00138-7

ENERGY SPECTRUM OF HIGH-T_c OXIDES: TWO-GAP STRUCTURE, GAPLESSNESS, AND IMPLICATIONS

VLADIMIR Z. KRESIN,* STUART A. WOLF,† STEVEN D. ADRIAN,‡ MARK E. REEVES‡ and Yu. N. OVCHINNIKOV§

* Lawrence Berkeley Laboratory, Berkeley,CA 94720, U.S.A.
† Naval Research Laboratory, Washington, DC 20375, U.S.A.
‡ George Washington University, Washington DC 20052, U.S.A.
§ Landau Institute for Theoretical Physics, Moscow, Russia

Abstract—The energy spectrum of the cuprates depends on the level of doping. Deviations from stoichiometry may introduce magnetic impurities, which, in turn, lead to a gapless scenario with peculiar optical, transport, magnetic, and thermodynamic properties.

1. INTRODUCTION

This paper is concerned with the spectrum of superconducting excitations of the cuprates. The structure of this spectrum depends drastically on the oxygen content, i.e. level of the doping. A closing of the gap appears to be a very important feature which determines many properties of the materials. Many other unique features of the cuprates including their multigap structure, intrinsic proximity effect, and the appearance of gaplessness without a noticeable depression in T_c, have been discussed previously by us [1,2]. Here we describe briefly the key points of our approach, which is based on a conventional Eliashberg formalism, and, in addition, present several new results.

2. TWO-GAP SPECTRUM. STOICHIOMETRIC YBCO COMPOUND

We consider YBaCuO as being composed of two subsystems: CuO planes and quasi-one dimensional CuO chains. For nearly fully oxygenated samples of $YBa_2Cu_3O_{7-x}$, the chain structure is particularly well developed when $x \lesssim 0.04$. The chains provide doping for the CuO planes but also form an independent conducting subsystem. This latter fact is of particular significance to our model, because below T_c each of the subsystems is characterized by its own energy gap. In addition, each of the gaps can be anisotropic. Let us denote by α and β, respectively, the plane and chain subsystems, so that ϵ_α and ϵ_β are the corresponding energy gaps. The opportunity to observe a two-gap spectrum in the high T_c oxides has been considered theoretically by us [1]. The small size of the coherence length in the high T_c oxides allows one the opportunity to observe the two-gap picture, unlike in conventional superconductors where a short mean-free path relative to the coherence length leads to isotropization of the gap and averaging to a single gap. An explicit definition of the two-gap spectrum corresponds to the presence of a two-peak structure in the superconducting density of states (there are two order parameters). The observation of such structure by tunnelling spectroscopy [3] provides strong support for the picture. In the following, we will use a two-gap picture to describe to the two peaks in the density of states.

The plane and chain subsystems are coupled by charge transfer, which leads to a single value of T_c. For the planes, $2\epsilon_\alpha(0)$ is approximately equal to $5T_c$. The value of the chain gap is smaller and very sensitive to the oxygen content: for x=0.04, ϵ_β is approximately equal to T_c. This value of the chain gap is smaller than the BCS value.

The superconducting state in the Cu–O plane, the basic unit for all cuprates, is caused by some intrinsic pairing mechanism (for our present treatment the nature of this mechanism is not essential). As for the chains, the pairing is mainly induced by charge transfer via two channels: (a) an intrinsic proximity effect (here the word intrinsic stresses the fact that, unlike the usual proximity effect observed in a thin-film sandwich structure, we are dealing with a phenomenon occuring on the scale of unit cell. Nevertheless, the physics of the phenomenon is similar to the McMillan picture [4] and represents the tunnelling of a pair from α to β) and (b) mediated charge transfer. The latter channel proceeds when a carrier makes a transition from the α to the β subsystem and emits a phonon (or other excitation). Another carrier absorbs the phonon and also makes a transition to β; as a result of this phonon exchange, the two carriers form a pair in the β subsystem. The equations for the order parameters Δ_α and Δ_β are:

$$\Delta_i(i\omega_n)Z_i(i\omega_n) = \lambda_i \pi T \sum_{n'=-\infty}^{\infty} D_{nn'} \frac{\Delta_i(i\omega_{n'})}{K^i_{n'}} + \lambda_{ik} \pi T \sum_{n'=-\infty}^{\infty} D_{nn'} \frac{\Delta_k(i\omega_{n'})}{K^k_{n'}} + \Gamma_{ik} \frac{\Delta_k(i\omega_n)}{K^k_n} \quad (1)$$

$$Z_i(i\omega_n) = \left[1 + \frac{\lambda_i \pi T}{\omega_n} \sum_{n'=-\infty}^{\infty} D_{nn'} \frac{\omega_{n'}}{K_{n'}^i} + \frac{\lambda_{ik} \pi T}{\omega_n} \sum_{n'=-\infty}^{\infty} D_{nn'} + \frac{\omega_{n'}}{K_{n'}^k} \Gamma_{ik} \frac{1}{K_{n'}^k} \right]$$

Here $K_n^i = [\omega_n^2 + \Delta_i^2(i\omega_n)]^{\frac{1}{2}}$ $(i = \alpha, \beta)$, $\omega_n = (2n+1)\pi T$, $D_{nn'} = \tilde{\Omega}^2/[\tilde{\Omega}^2 + (\omega_n - \omega_{n'})^2]$ is the phonon propogator (the approach can be easily generalized for different mechanisms), $\Gamma_{\alpha\beta} = |T|^2 \nu_\beta$, T is the tunnelling matrix element, ν_β is the density of states.

3. GAPLESS STATE

Consider the case when the chain subsystem contains magnetic impurities. In the absence of impurities the system displays a two-gap spectrum with the YBCO chains in the induced superconducting state. If the β-subsystem (chains) contains magnetic impurities, then we can have an unusual case of gapless superconductivity, namely at some value of the impurity concentration the energy gap disappears, but the shift in T_c is relatively small. This occurs with oxygen depletion in YBCO. Indeed, the removal of oxygen greatly affects the chain states. Instead of a well-developed chain structure, we have a set of broken chains with Cu atoms at the ends. These Cu atoms form local magnetic states Cu^{++}, similar to surface states, which, in turn, act as strong pair-breakers. As a result, a gapless state rapidly develops on the chain. One should note that despite the absence of an energy gap, the system is still superconducting [5]: the material exhibits the Meissner effect and zero resistance. The absence of the gap leads to a power law, rather than an exponential dependences of many properties: the electronic specific heat, surface impedance, penetration depth, etc.

Qualitatively, gapless superconductivity can be viewed as a two-fluid mixture of normal carriers (broken pairs) and superconducting pairs. In this context, the two-fluid model provides a good description of many properties of the cuprates. Scattering by the impurities can be described by additional terms in the renormalization functions Z_β (see e.g. [6]). One can calculate a critical concentration of impurities which leads to the appearance of the gapless state [2]. This corresponds to $YBa_2Cu_3O_{6.9}$ or $x \approx 0.1$. It is essential that, although the magnetic moments are introduced in the chain sites only, the energy gaps close to zero in both the plane and chain subsystems. Note also, that even though the gaps are equal to zero, the density of states displays peaks at $\omega \approx \epsilon_\alpha, \epsilon_\beta$, and these peaks can be observed experimentally by tunnelling measurements.

4. OVERDOPED CUPRATES

Experimental studies, carried out on the Tl and Bi-based cuprates [7–12], have shown that overdoping leads to a drastic decrease in T_c. We conclude that the strong depression of T_c is due to the presence of magnetic impurities at the apical oxygen sites. This is different from YBCO, since the pair-breaking effect occurs directly for the in-plane states, whereas for YBCO the magnetic moments (Cu^{++} ions) are located on the chains. As a result, gaplessness in the overdoped samples leads also to a depression in T_c. (If we assume that the magnetic impurities are associated with the apical oxygen, then the "conventional" behavior of Nd_2CeCuO_4 is explained by the absence of such an oxygen site.) Indeed, it has been reported (see Ref. 12 and also the review, Ref. 10), that the overdoped cuprates are characterized by gapless behavior. We attribute this gaplessness to scattering from localized magnetic moments: the presence of which has been observed in specific heat measurements [11]. We conclude that magnetic impurities are also present in the overdoped Hg-based compounds, hence these materials also display gapless behavior, and consequently, both a depression in T_c and a power law dependence for the penetration depth [9].

5. PENETRATION DEPTH [$\lambda(T)$]

This problem has attracted a lot of attention. While $\lambda(T)$ for the Nd-based compound shows a conventional exponential dependence, the results for YBCO samples are less clear as they vary from sample to sample. Some measurements display a linear temperature dependence, whereas other groups observe the dependence, $\lambda \propto T^2$. In addition, the data for fully oxygenated films are described by an exponential law (see review in [13]). Based on our model, one can prove [13] that the nature of the dependence $\lambda(T)$ is directly related to the oxygen content: the functional form of $\lambda(T)$ is sample dependent and correlates with the oxygen content. The stochiometric compound is gapped and is characterized by an exponential dependence for the penetration depth. Oxygen depletion leads initially to a decrease in the energy gap and then to transition to a gapless state (at $x \approx 0.1$). With further oxygen loss, $\lambda(T)$ follows a power law, initially linear, and then quadratic (for $x \gtrsim 0.15$).

For overdoped materials, such as the Hg-based compound, one would also expect a power law for $\lambda(T)$, since the sample is in the gapless state. In this case, the screening is provided by the planes which are directly affected by magnetic impurities. Such dependence has been observed in [9]. A detailed theoretical calculation of $\lambda(T)$ for the overdoped cuprates will be described elsewhere.

6. PENETRATION DEPTH AND JOSEPHSON JUNCTIONS

We give particular attention to an experiment in which the I–V characteristics of YBCO–Pb Josephson junctions were used in order to determine $\lambda(T)$ and measure its anisotropy

[14]. As might be expected, untwinned samples are characterized by an in-plane anisotropy of λ (see [14]). Indeed, both subsystems contribute to λ_a, whereas λ_b arises from the screening currents in the planes only. It is essential, however, that the charge transfer leads to a change in the value of λ_b upon depletion of oxygen, despite the fact that oxygen is depleted mainly from the chains. This effect has been observed experimentally [14] and follows directly from eqn (1).

It is worth noting that the authors [14] also observed Josephson tunnelling in the c-direction for the Pb–I–YBCO sandwich. We conclude that the tunnelling occurs mainly between Pb and the chain subsystem, based both on the large density of states on the chain layer [15], and on the observation by STM [16] that the chains usually form the surface layer. Since the chain energy gap is small ($\epsilon_\beta \lesssim 0.8T_c$, see above), I_cR smaller than predicted by the Ambegaokar–Baratoff theory [17]. Such a small value has been experimentally observed [14].

7. CRITICAL FIELD

The presence of magnetic impurities drastically affects the dependence of $H_{c2}(T)$ in layered superconductors. One can develop a specific physical model [18] which is based on spin-flip scattering and ordering of the impurities at low temperatures . The model allows us to explain the unusual temperature dependence for the upper critical field observed in the Tl- and Bi-based overdoped cuprates [7,8]. As was noted above, the overdoped cuprates are characterized by the presence of localized magnetic moments. The value of H_{c2} can be determined from the following equation [19]:

$$\ln(T_c/T) = 2\pi T \sum[\omega_n^{-1} - 2D_1(\omega_n, H)] \qquad (2)$$

$$D_1(\omega_n, H) = (\mathrm{sign}\,\omega_n)J(\omega_n, H)[1 - (\tau^{-1} - \tau_s^{-1})J(\omega_n, H)]^{-1}$$

$$J(\omega_n, H) = \left(\frac{2}{\pi e H v^2}\right)^{\frac{1}{2}} \int_0^\infty dy\, \exp(-y)\arctan[v(2eHy)^{\frac{1}{2}}/\alpha)]$$

where $\alpha = 2\omega_n + \tau^{-1} + \tau_s^{-1}$; τ_s is the spin-flip scattering time, τ is the elastic scattering time, and v is the Fermi velocity. We focus on the case H||c. The presence of a layered structure allows us to combine the condition $\Gamma = \tau_s^{-1} \gg \pi T_c$ with the condition $\tau^{-1} \ll \pi T_c$ (clean case for the usual elastic scattering). This arises from the out-of-plane location of the magnetic moments; as a result, the in-plane momentum transfer is small, despite the large value of the amplitude for the spin-flip process. Thus the pair-breaking effect is strong even in spite of the weaker effect of nonmagnetic scattering (which is related to momentum change and is manifested in the transport properties). This is the case for the overdoped cuprates . We speculate that the magnetic moments are localized on the apical oxygen site. The spin-flip-scattering frequency, Γ, can be treated as temperature independent except for a small region near T=0: $\Gamma = \Gamma_\alpha$ =const for $T \gg \theta$, $\theta \approx 1\mathrm{K} \ll T_c$. In the low temperature region the impurities tend to become ordered, which leads to a weakening of the pair-breaking effect. As a result, the superconducting properties are less depressed, and H_{c2} increases. Furthermore, the usual spin-flip process is forbidden for $T < \theta$, and is governed instead by the dipole–dipole interaction $V = -3\mu_e\mu_i(\sigma_e \cdot r)(\sigma_i \cdot r)/r^5$ (r is the distance between the electron and the impurity). This interaction does not conserve total spin: it translates to the electronic orbital momentum. Hence, the amplitude Γ becomes temperature dependent when $T < \theta$.

Based on this physical picture, one can describe the dependence $H_{c2}(T)$ in the entire temperature range $T < T_c$. The theory [18] has only two parameters: $\beta = \Gamma(T_c)/\Gamma(0)$ and θ and model provides excellent agreement with the experimental data [7,8].

8. INTRINSIC T_c, PRESSURE DEPENDENCE OF T_c

One can estimate the value $T_{c0} = 2\gamma\Gamma_{cr}/\pi$ in the absence of magnetic impurities. Here, T_{c0} = 130K exceeds the experimental value obtained at optimal doping, T_c = 90K [7]. This implies that the materials contain magnetic impurities prior to the overdoping, hence T_c is already depressed. Thus it is possible that T_c can be raised above the observed value by applying high pressure [20,21]. The external pressure increases the carrier concentration without a noticeable change in the concentration of the magnetic impurities. As a result, we can obtain a value T_c', such that $T_c < T_c' < T_{c0}$. This contrasts to the case of chemical substitution where the doping is accompanied by the addition of the magnetic impurities, which depress T_c relative to T_{c0}.

9. SUMMARY

The main results can be summarized as follows:

1. The presence of low-dimensional units, such as planes and chains in YBCO, along with the short coherence length leads to an observable two-gap spectrum, that is, to a two-peak structure in the superconducting density of states. Josephson currents in c-direction for the YBCO–Pb junctions involve the chain states (smaller energy gap); as a result, the value of I_cR is smaller than the conventional value.
2. Oxygen depletion in YBCO and overdoping in the other cuprates lead to the formation of a gapless state caused by localized pair-breaking magnetic moments. The region of gaplessness is extended relative to conventional superconductors. The penetration depth in the gapless state is described by a power law, initially linear, and then quadratic.
3. The magnetic moments are located on the apical oxygen site for the overdoped materials and on the chains for YBCO.
4. The depression of T_c in the overdoped cuprates is

caused by spin-flip scattering. However, even samples with $T_c = T_{cmax}$ contain magnetic moments; as a result, the intrinsic value of T_c is higher than the observed value. The application of high pressure leads to an increase in the observed value of T_{cmax} without introducing additional magnetic impurities.

5. The presence of magnetic impurities and their ordering at low temperatures leads to a large increase in the value of H_{c2} and to positive curvature. This is in complete contrast with the conventional picture.

Acknowledgements—The authors are grateful to R. Dynes, J. Geerk, L. Gor'kov and R. Schrieffer for fruitful discussions. The research of VZK is supported by US Office of Naval Research contract No. N00014-95-F0006, and the research of MER and SDA is supported by US Office of Naval Research contract No. N00014-94-1-G027.

REFERENCES

1. Kresin V. and Wolf S., *Phys. Rev. B* **46**, 6458 (1992); *Physica C*, **198**, 328 (1992).
2. Kresin V. and Wolf S., *Phys. Rev. B* **51**, 1229 (1995).
3. Geerk, X. Xi, J. and Linker G., *Z. Phys. B* **73**, 329 (1988).
4. McMillan W., *Phys. Rev.* **175**, 537 (1968).
5. Abrikosov A. and Gor'kov L., *Sov. Phys.- JETP* **12**,1243 (1961); De Gennes P., *Phys. Cond. Matter* **3**, 79 (1964); Maki K., in *Superconductivity* (Edited by R. Parks), p. 1035. Marcel Dekker, New York (1969).
6. Kaizer A. and Zuckermann M., *Phys. Rev. B* **1**, 229 (1970).
7. Mackenzie A. P., Julian S., Lonzarich G., Carrington A., Hughes S., Liu R. and Sinclair D., *Phys. Rev. Lett.* **71**, 1938 (1993).
8. Osofsky M., Soulen R., Wolf S., Broto J., Rakoto H., Ousset J., Coffe G., Askenazy S., Pari P., Bozovic I., Eckstein J., Virshup G., *Phys. Rev. Lett.* **71**, 2315 (1993).
9. Xiong Q., Cao Y., Xue Y., Chu C. W., *Bull. APS* **40**, 71 (1995), preprint.
10. Phillips N., Fisher R. and Gordon J., in *Progress in Low-Temperature Physics* (Edited by D. Brewer), Vol. 13, p. 267. North-Holland, The Netherlands (1992).
11. Wade J., Loram J., Mirza K., Cooper J. and Tallon J., *J. Supercond.* **7**, 261 (1994).
12. Niedermayer C., Bernhard C., Bunninger U., Gluckler H., Tallon J., Ansaldo E. and Budnick J., *Phys. Rev. Lett.* **71**, 1764 (1993); *J. Supercond.* **7**, 165 (1994).
13. Adrian S., Reeves M., Wolf S. and Kresin V., *Phys. Rev. B* **51**, 6800 (1995).
14. Sun A., Gajewskii D., Maple M. and Dynes R., *Phys. Rev. Lett.* **72**, 2267 (1994); Dynes R., *Bull. APS* **40**, 1 (1995).
15. Reeves M. E., Ditmars D. A., Wolf S. A., Vanderah T. A. and Kresin V. Z., *Phys. Rev. B* **47**, 6065 (1993).
16. de Losanne A., private communication.
17. Ambegaokar V. and Baratoff A., *Phys. Rev. Lett.* **10**, 486 (1963).
18. Ovchinnikov Yu. and Kresin V., *Phys. Rev. B*,**52**, 3075(1995).
19. Fischer O., *Helv. Phys. Acta* **45**, 332 (1972); Ovchinnikov Yu., *Sov. Phys. JETP* **39**, 538 (1974).
20. Moulton N., Wolf S., Skelton E., Liebenberg D., Vanderah T., Hermann A. and Duan H., *Phys. Rev. B* **44**, 12632 (1991); Berkeley D., Skelton E., Moulton N., Osofsky M., Lechter W., Browning V. and Liebenberg D., *Phys. Rev. B* **47**, 5524 (1993); Kim C., Skelton E., Qadri S., Browning V., Osofsky M., Reeves M. and Liebenberg D., *Phys. Rev. B* **49**,13075 (1994).
21. Schilling J. and Klotz S., in *Physical Properties of High Temperature Superconductors* (Edited by D. Ginsberg), Vol. 3, p. 59. World, Singapore (1992).

Pergamon

J. Phys. Chem. Solids Vol. 56, No. 12, pp. 1627–1632, 1995
Copyright © 1995 Elsevier Science Ltd
Printed in Great Britain. All rights reserved
0022-3697/95 $9.50 + 0.00

0022-3697(95)00210-3

EVIDENCE FOR ELECTRON DECAY IN PHOTOEMISSION FROM $Sr_2CuO_2Cl_2$

R. B. LAUGHLIN

Department of Physics, Stanford University, Stanford, California 94305, U.S.A.

Abstract—I propose that the strange quasiparticle dispersion relation recently observed photoemission from the antiferromagnetic insulator $Sr_2CuO_2Cl_2$ is actually the dispersion relation of a spinon. The calculations that anticipated this result are reviewed and shown to account for the magnetic properties of the cold, undoped antiferromagnet and the mysterious strong scattering phenomenology of the cuprates.

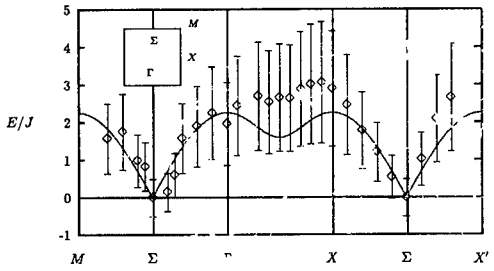


Fig. 1. Dispersion relation of the quasiparticle in $Sr_2CuO_2Cl_2$ reported by Wells *et al* [1] expressed as a multiple of $J = 125$ meV. The broad error bars represent the width of the quasiparticle peak and not the accuracy of the measurement. The solid line is the dispersion relation of the spinon as defined by eqn (1).

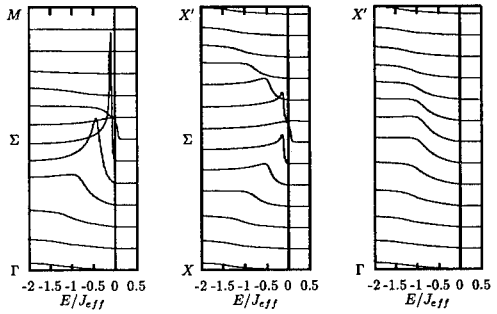


Fig. 2. Theoretical photoemission spectrum calculated using eqn (26).

1. INTRODUCTION

One of the most interesting developments in the the study of high-T_c superconductivity is the recent observation in photoemission by Wells *et al.* [1] of quasiparticle band structure in the insulating cuprate $Sr_2CuO_2Cl_2$ remarkably similar to the "spinon" dispersion relation proposed by me over a year ago in the context of the t–J model. This and the corresponding dispersion relation of the "holon", given by

$$E_k^{spinon} = 1.6J\sqrt{\cos^2(k_x) + \cos^2(k_y)} \quad (1)$$

$$E_k^{holon} = \pm 2t\sqrt{\cos^2(k_x) + \cos^2(k_y)} \quad (2)$$

are scaled version of the "flux" band structure extensively discussed in the early days of high-T_c theory [2]. Equation (1) is plotted against the quasiparticle dispersion reported by Wells *et al.* [1] in Fig. 1. The value of $J = 125$ meV inferred from 2-magnon raman scattering [3] has been assumed. While there are many possible explanations for this good agreement, including its being an accident unique to this undopable cuprate, I wish to promote the view that the literal interpretation is the correct one: the dispersion relation measured in this experiment is actually that of the spinon into which the injected hole decays.

Spinons and holons with the above properties are quite compatible with known properties of the t–J model, and indeed were argued by me to manifest themselves in numerical work in this model as sum rules and decoupling of t and J in certain spectra [4,5]. However it is known that proper photoemission calculations performed with the t–J model agree more poorly with Fig. 1 than do the approximate calculations I shall discuss here [6]. An example of the latter is shown in Fig. 2. The reason for this disparity is not presently known and is the subject of ongoing research. I favor the explanation that either the Hamiltonian or the photoemission matrix element has missing terms that enhance the effects of electron decay in the spectral function, but it is conceivable that the calculations have some subtle technical problem.

It may be seen from Fig. 1 that eqn (1) agrees with the data in three ways:

- The overall bandwidth is 2.2 J, a result also found in numerical studies of the t–J model. The latter find no dependence of this width on t.
- The band minimum is at the Σ-point $(\pi/2,\pi/2)$. This is also found in numerical studies of the t–J model.
- The band minimum is deep and isotropic. The isotropy is *not* found in numerical studies of the t–J model.

The data also disagree with the t–J model in the important respect that quasiparticle width, shown in Fig. 1 as an error bar, is enormous. This width estimate is actually unrealistically conservative. The quasiparticle is so broad at Γ and M that it is effectively nonexistent. An anomalous

width of this kind is common to all the cuprates and, as such, has been incorporated into the marginal fermi liquid phenomenology of these materials through a quasiparticle self-energy satisfying $\hbar/\tau = \max(k_B T, E)$ [7]. However the experiment of Wells *et al.* [1] demonstrates rather clearly that this behavior occurs in the insulator as well and has nothing to do with fermi liquidness, per se.

2. FLUX HAMILTONIAN

Equations (1) and (2) come from a perturbative treatment of the Hamiltonian

$$\mathcal{H} = \sum_{<j,k>} \left\{ \frac{J}{4} \sum_{\sigma\sigma'} f^\dagger_{j\sigma} f^\dagger_{k\sigma'} f_{k\sigma} f_{j\sigma'} + t \sum_\sigma f^\dagger_{j\sigma} f_{k\sigma} b^\dagger_k b_j \right\}$$

$$+ \sum_j U \left\{ \sum_\sigma f^\dagger_j f_j + b^\dagger_j b_j - 1 \right\}^2 \qquad (3)$$

where $< j,k >$ denotes the sum over near-neighbor pairs of a square planar lattice, with each bond counted twice to maintain hermiticity, f and b satisfy

$$\{f_{j\sigma}, f_{k\sigma'}\} = 0 \quad \{f_{j\sigma}, f^\dagger_{k\sigma'}\} = \delta_{jk}\,\delta_{\sigma\sigma'}$$
$$[b_j, b_k] = 0 \quad [b_j, b^\dagger_k] = \delta_{jk} \qquad (4)$$

and the electron is understood to be the composite

$$c_{j\sigma} = f_{j\sigma}\, b^\dagger_j \qquad (5)$$

This is equivalent to the t–J Hamiltonian in the limit of large U. The functional forms of eqns (1) and (2), but not their correct prefactors, are obtained from the Hartree–Fock solution of this problem in the limit of no bosons and small U. We have

$$\mathcal{H}_{HF} = \sum_{<j,k>} \chi_{jk} \left\{ \frac{J}{2} \sum_\sigma f^\dagger_{j\sigma} f_{k\sigma} + b^\dagger_j b_k \right\}$$

$$+ \sum_j U \left\{ \sum_\sigma f^\dagger_j f_j + t\, b^\dagger_j b_j - 1 \right\}^2 \qquad (6)$$

where

$$\chi_{jk} = \sum_\sigma < f^\dagger_k f_j >$$

$$= \pm \frac{1}{2\pi^2} \int_0^\pi dk_x \int_0^\pi dk_y \sqrt{\cos^2(k_x) + \cos^2(k_y)} = \pm 0.48 \qquad (7)$$

The usual sign convention is for all bonds to be "+" except for the x-bonds on even rows, which are "−". Ambiguity in the sign choice is the so-called gauge degree of freedom of this problem. The Hartree–Fock Hamiltonian describes free spinons and holons moving in a fictitious uniform magnetic field of flux π per plaquette.

To get the prefactors correct it is necessary to *double* the factor 0.48 in eqn (7) and sum the Feynman graphs shown in Fig. 3. The doubling, a modification of the Hartree–Fock ground state caused by U seen most clearly in Gutzwiller projection studies [8], increases the prefactors in eqns (1) and (2) to 0.96 J and 1.92 t, respectively. The symbols in Fig. 3 have the following meaning:

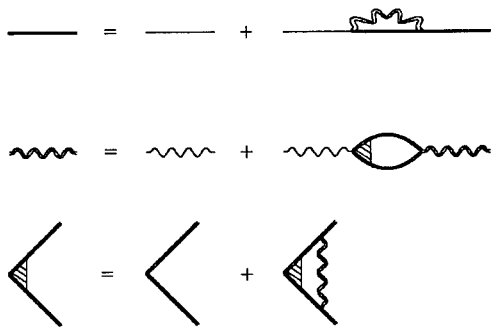


Fig. 3. Feynman graphs discussed in this paper.

- Single straight lines denote the bare Hartree–Fock spinon propagator with energy prefactor set to $0.96J$.
- Single wiggly lines denote the potential U.

The screened potential has a high-frequency plasma pole at a frequency near U that remains important in the U $\to \infty$ limit, the case of interest to us. Integration over this pole renormalizes the spinon spectral weight to zero while exactly compensating this reduction in the vertex correction. The effect is similar to charge renormalization in quantum electrodynamics and has the same meaning: the spinon has no significant amplitude to be an electron. Because of this problem the $U \to \infty$ limit may be taken only after the graphs are reorganized as a power series in the renormalized spinon propagator and vertex. This is accomplished as a practical matter by removing the offending pole from the screened potential by hand and then taking U to infinity. The remaining modification of the spinon prefactor is then obtained as a conventional exchange effect.

3. SPIN DENSITY WAVE GROUND STATE

Let us now evaluate these equations for the cold, undoped insulator. We shall make two major approximations:

- Retardation effects in the effective potential are ignored.
- The "coulomb" potential is assumed to be constant beyond three bond lengths.

I have tested the first approximation by evaluating the equations with retardation included and finding little difference. The exact calculation is too complicated to discuss here. The second approximation is justified by Fig. 4, where the self-consistent potential between spinons is plotted as a function of position. It may be seen that the potential has the logarithmic tail expected of a coulomb potential in two dimensions and a hard repulsive core near the origin. The tail has no effect other than to open a large energy gap between the occupied and empty bands of the spinon propagator, a

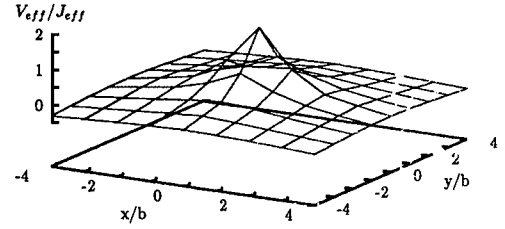


Fig. 4. Zero-frequency screened coulomb interaction defined by eqn (14).

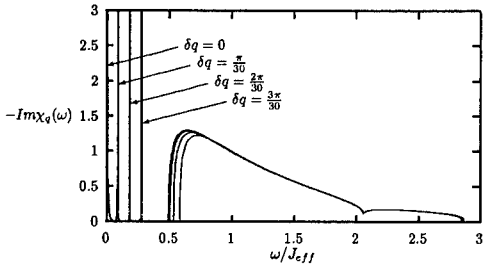


Fig. 5. Spin susceptibility given by eqn (15) for various values of δq, the distance from the magnetic Bragg peak at M.

gap that is invisible in any response functions due to a compensating effect in the vertex correction. It may therefore be set safely to zero when the temperature is zero. The core, on the other hand, has huge effects. It causes, among other things, a spin density wave instability, which is the way this Hamiltonian achieves antiferromagnetic order. We characterize the self-consistent solution with an effective Hubbard interaction $U_{\rm eff}$, an exchange-enhanced spinon bandwidth $J_{\rm eff}$, and a spin density wave mass gap parameter m. The self-consistency equations are

$$\varepsilon_k = \sqrt{\cos^2(k_x) + \cos^2(k_y) + m^2} \tag{8}$$

$$\Pi_q = -\frac{1}{2\pi^2}\int_0^\pi dk_x \int_0^\pi dk_y \frac{1}{\varepsilon_k + \varepsilon_{k+q}} \times\left\{1 - \frac{\cos(k_x)\cos(k_x+q_x) + \cos(k_y)\cos(k_y+q_y) + m^2}{\varepsilon_k \varepsilon_{k+q}}\right\} \tag{9}$$

$$\frac{U_{\rm eff}}{J_{\rm eff}} = -\frac{2}{3\pi^2}\int_0^\pi dq_x \int_0^\pi dq_y \frac{1}{\Pi_q}\left[1 - \cos(3q_x)\cos(3q_y)\right] \tag{10}$$

$$\frac{J_{\rm eff}}{U_{\rm eff}} = \frac{1}{2\pi^2}\int_0^\pi dk_x \int_0^\pi dk_y \frac{1}{\varepsilon_k} \tag{11}$$

$$\frac{J}{J_{\rm eff}} = 1 + \left\{\frac{1}{2\pi^2}\int_0^\pi dk_x \int_0^\pi dk_y \frac{\cos^2(k_x) + \cos^2(k_y)}{\varepsilon_k}\right\} \times\frac{1}{2\pi^2}\int_0^\pi dq_x \int_0^\pi dq_y \frac{1}{\Pi_q}\left[\cos(q_x)\cos(q_y) - \cos(3q_x)\cos(3q_y)\right] \tag{12}$$

Their solution is

$$m = 0.25 \quad \frac{U_{\rm eff}}{J_{\rm eff}} = 1.78 \quad \frac{J_{\rm eff}}{J} = 1.53 \quad \left(\frac{k_B T_N}{J_{\rm eff}} = 0.175\right) \tag{13}$$

The Neèl temperature indicated in parentheses is, of course, unphysical in two dimensions, but may have meaning for weakly-coupled planes. The potential plotted in Fig. 4 is given by

$$\frac{V_{\rm eff}(x,y)}{J_{\rm eff}} = -\frac{1}{2\pi^2}\int_0^\pi dq_x \int_0^\pi dq_y \times\left\{\frac{1}{\Pi_q} + \frac{U_{\rm eff}}{J_{\rm eff}}\right\}\left[\cos(q_x x)\cos(q_y y) - \cos(3q_x x)\cos(3q_y y)\right] \tag{14}$$

The Hartree–Fock ground state found by this procedure is the same as that found by Hsu [9] in his variational study of the Heisenberg antiferromagnet using a Gutzwiller-projected flux ground state, which obtained excellent agreement with the ground state energy and staggered magnetic moment found in numerical studies. The graphical procedure described here produces similar results. In Fig. 5 I plot the transverse magnetic susceptibility of the spin density wave ground state, given (with ω measured in units of $J_{\rm eff}$) by

$$\chi_q(\omega) = \chi_q^0(\omega)\left[1 + \frac{U_{\rm eff}}{J_{\rm eff}}\chi_q^0(\omega)\right]^{-1} \tag{15}$$

where

$$\chi_q^0(\omega) = \frac{1}{4\pi^2}\int_0^\pi dk_x \int_0^\pi dk_y \times\left\{1 - \frac{\cos(k_x)\cos(k_x+q_x) + \cos(k_y)\cos(k_y+q_y) - m^2}{\varepsilon_k \varepsilon_{k+q}}\right\} \times\left\{\frac{1}{\omega - (\varepsilon_k + \varepsilon_{k+q}) + i\eta} + \frac{1}{-\omega - (\varepsilon_k + \varepsilon_{k+q}) - i\eta}\right\} \tag{16}$$

A clear spin wave peak may be seen dispersing with a velocity of $1.6J$, which is, not coincidentally, the same as the velocity of the spinon near Σ obtained from eqn (1). It compares favorably with the spin wave dispersion relation

$$\omega_q^{magnon} = J\sqrt{4 - [\cos(q_x) + \cos(q_y)]^2} \tag{17}$$

obtained by Bogoliubov transformation [10] and with the factor 1.18 with which the spin wave velocity is renormalized by quantum corrections [11]. The transverse near-neighbor static correlation is given in terms of this susceptibility by

$$< S_1^x S_2^x > = < S_1^y S_2^y >$$

$$= -\frac{1}{2\pi^3}\int_0^\pi dq_x \int_0^\pi dq_y \int_0^\infty d\omega\, Im\chi_q(\omega)\left\{\cos(q_x) + \cos(q_y)\right\} = -0.098 \tag{18}$$

The z-axis spin correlation is likewise obtained from eqn (15) but with the sign of m in eqn (16) reversed.

$$< S_1^z S_2^z >= - < S^z >^2 - .059 \qquad (19)$$

If we now assume that the staggered magnetization acquires the value

$$< S^z >= \frac{2mJ_{\rm eff}}{U_{\rm eff}}\left[1 + (\frac{2mJ_{\rm eff}}{U_{\rm eff}})^2\right]^{-1} = 0.260 \qquad (20)$$

we obtain $< S_1 \cdot S_2 >= -0.323$. The correct value for the Heisenberg magnet is -.334. Note that the value of $< S^z >$ obtained from the Gutzwiller projected state is larger than my estimate. The value obtained by Hsu [9] was slightly less than 0.3.

4. SPINON SCATTERING

Having demonstrated that the equations make sense at zero temperature let us consider the high-temperature case for which the formalism was actually designed. We will, for simplicity, confine our attention to the region $k_B T_N < k_B T < J_{\rm eff}$, where T_N is defined as in eqn (13). In this temperature range the spin density wave has collapsed, making the mass parameter m zero, but the particle and hole excitations of the spinon spectrum have only enough energy to populate its linear "Dirac" part. In addition, these particles interact with the strong, short-range force shown in Fig. 4 and are thus expected to scatter each other violently in the s-wave channel. More precisely, the scattering cross-section should saturate at the unitary value $\sigma_{unitary} = 2\pi/k$, thus causing a zero-energy particle to scatter at a rate

$$\frac{1}{\tau} = (\frac{L}{2\pi})^2 \int_0^\infty 2\pi k\, {\rm d}k\, \frac{2\pi c}{kL^2}\frac{1}{\exp(\beta ck)+1} = k_B T\, \log(2) \qquad (21)$$

where c denotes the spinon velocity $1.6J$. A scattering rate equal to the temperature is one of the key phenomenological features of the cuprates. It follows in this calculation from the absence of a scale at the Dirac point in the spinon spectrum. We may similarly ask about the scattering rate of a high-energy spinon due to pair production. As is the case in quantum electrodynamics, such scattering is forbidden by momentum conservation for on-shell particles. However, particles off shell by energy E can decay by pair production, and their rate for doing so is essentially the above expression with E substituted for $k_B T$. The reason is that the matrix elements for scattering and pair production are identical. Thus the scattering rates of the marginal fermi liquid phenomenology fall out of such calculations in a natural way.

An indication of this behavior may be seen even at low orders in perturbation theory. In Fig. 6 I show the real and imaginary parts of the finite-temperature polarizability

$$\Pi_q^0(\omega) = \frac{1}{4\pi^2}\int_0^\pi {\rm d}k_x \int_0^\pi {\rm d}k_y \frac{\exp(\beta\varepsilon_k)\exp(\beta\varepsilon_{k+q})-1}{[\exp(\beta\varepsilon_k)+1][\exp(\beta\varepsilon_{k+q})+1]}$$

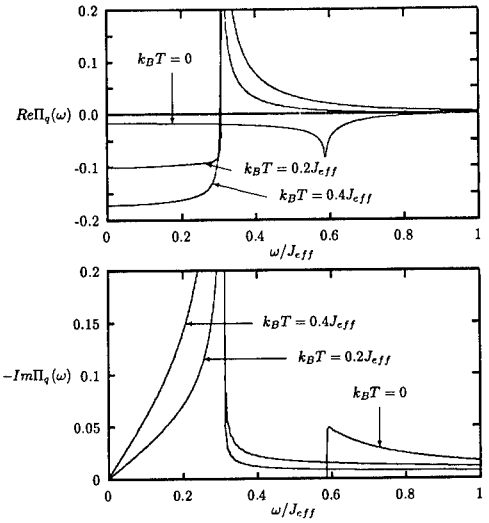


Fig. 6. Frequency-dependent polarizability defined by eqn (22) for $q = (0.1\pi, 0)$.

$$\times\left\{1 - \frac{\cos(k_x)\cos(k_x+q_x)+\cos(k_y)\cos(k_y+q_y)+m^2}{\varepsilon_k\varepsilon_{k+q}}\right\}$$

$$\times\left\{\frac{1}{\omega-(\varepsilon_k+\varepsilon_{k+q})+i\eta} + \frac{1}{-\omega-(\varepsilon_k+\varepsilon_{k+q})-i\eta}\right\}$$

$$+\frac{1}{4\pi^2}\int_0^\pi dk_x \int_0^\pi dk_y \left\{\frac{\exp(\beta\varepsilon_k)-\exp(\beta\varepsilon_{k+q})}{[\exp(\beta\varepsilon_k)+1]\,[\exp(\beta\varepsilon_{k+q})+1]}\right\}$$

$$\times\left\{1 + \frac{\cos(k_x)\cos(k_x+q_x)+\cos(k_y)\cos(k_y+q_y)+m^2}{\varepsilon_k\varepsilon_{k+q}}\right\}$$

$$\times\left\{\frac{1}{\omega-(\varepsilon_k-\varepsilon_{k+q})+i\eta} + \frac{1}{-\omega-(\varepsilon_k-\varepsilon_{k+q})-i\eta}\right\} \qquad (22)$$

for $q = (0.1\pi, 0)$. It may be seen to be dominated by the thermally excited plasma of spinons at the Dirac points, the zero-frequency susceptibility of which is given by

$$\lim_{\omega,q\to 0}\Pi_q(\omega) = -\frac{2\log(2)}{\pi}k_B T\left\{1 + \frac{i}{\pi}\frac{\omega}{q}\right\} \qquad (23)$$

This plasma screens out the long-range part of the "coulomb" potential and supplies low-frequency thermal fluctuations required for scattering but has no effect on the short-range part responsible for for eqn (21). In Fig. 7 I plot the trace of the imaginary part of the approximate spinon self-energy

$$Im\Sigma_k(\varepsilon) = -\frac{1}{32\pi^2}\int_{-\pi}^{\pi} {\rm d}q_x \int_{-\pi}^{\pi} {\rm d}q_y \frac{\cosh(\beta\varepsilon/2)}{\cosh(\beta\varepsilon_{k+q}/2)}$$

$$\times\frac{1}{\sinh[\beta(\varepsilon+\varepsilon_{k+q})]}Im\left\{\frac{1}{\Pi_q^0(\varepsilon+\varepsilon_{k+q})}\right\}\left\{1 - \frac{\mathcal{H}_{k+q}}{\varepsilon_{k+q}}\right\}$$

$$-\frac{1}{8\pi^2}\int_0^\pi {\rm d}q_x \int_0^\pi {\rm d}q_y \frac{\cosh(\beta\varepsilon/2)}{\cosh(\beta\varepsilon_{k+q}/2)}$$

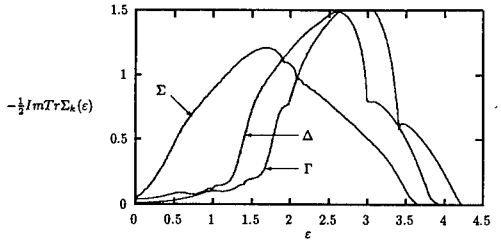


Fig. 7. Imaginary part of spinon self-energy $\Sigma_k(\varepsilon)$ as given by eqn (24) for the case of $k_BT = 0.2$. (All energies are measured in units of J_{eff}.) The symbol Δ denotes the momentum $k = (\pi/2, 0)$.

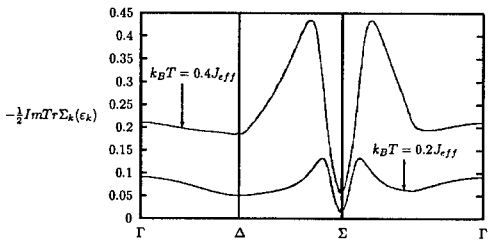


Fig. 8. Imaginary part of on-shell spinon self-energy $\Sigma_k(\varepsilon_k)$.

$$\times \frac{1}{\sinh[\beta(\varepsilon - \varepsilon_{k+q})]} Im\left\{\frac{1}{\Pi_q^0(\varepsilon - \varepsilon_{k+q})}\right\}\left\{1 + \frac{\mathcal{H}_{k+q}}{\varepsilon_{k+q}}\right\} \quad (24)$$

where

$$\mathcal{H}_k = \cos(k_x)\begin{bmatrix} 1 & 0 \\ 0 & -1 \end{bmatrix} + \cos(k_y)\begin{bmatrix} 0 & 1 \\ 1 & 0 \end{bmatrix} \quad (25)$$

for the case of $k_BT = 0.2J_{\text{eff}}$. It may be seen to be quite linear near the Dirac point Σ with *slope approximately one* but suppressed elsewhere in the zone. At higher order in perturbation theory one expects the multi-body collisions to relax the kinematic constraint responsible for this suppression and cause the scattering at Σ to appear at all values of k. In Fig. 8 I plot this same quantity evaluated on-shell, i.e. at the unperturbed spinon energy, as a function of momentum. It may be seen that the low-energy scattering at Σ is artificially suppressed by the same kinematic effect, but rises to about k_BT within a spinon thermal momentum. The graphs responsible for eqn (7) are not included in this calculation, so the appearance of a scattering rate proportional to k_BT is somewhat fortuitous.

5. ELECTRON SPECTRAL FUNCTION

Let us turn finally to the electron spectral function plotted in Fig. 2. Note that there are *six* phenomenological fitting parameters I have optimized to fit the data. The plotted curves are the imaginary part of the propagator

$$G_q(\varepsilon) = G_q^0(\varepsilon)\left\{\alpha + \left[(1-\alpha)(\varepsilon - \varepsilon_1) + \varepsilon_3 - \Sigma(\varepsilon)\right]G_q^0\right\}^{-1}$$

where

$$G_q^0(\varepsilon) = \frac{1}{4\pi^2}\int_0^\pi dk_x \int_0^\pi dk_y \frac{1}{\varepsilon - [\varepsilon_k - 2(t/J_{\text{eff}})(\sqrt{2} - \varepsilon_{k+q})] - \frac{1}{4}\Sigma(\varepsilon)}$$

$$\times\left\{1 + \frac{\cos(k_x)\cos(k_x + q_x) + \cos(k_y)\cos(k_y + q_y)}{\varepsilon_k \varepsilon_{k+q}}\right\} \quad (26)$$

$$\Sigma(\varepsilon) = \varepsilon\left(\frac{\varepsilon}{\varepsilon_2} - 1\right)\log\left(1 - \frac{\varepsilon_2}{\varepsilon}\right) + \varepsilon - \frac{\varepsilon_2}{2} \quad (27)$$

$$\alpha = 1 - \frac{1}{4}\left[\cos^2(q_x) + \cos^2(q_y)\right] \quad (28)$$

The four explicit parameters are

$$\varepsilon_1 = 17.3 \quad \varepsilon_2 = 3.2 \quad \varepsilon_3 = 4 \quad t/J_{\text{eff}} = 3.1 \quad (29)$$

The other two are dimensionless factors in eqns (26) and (29). The fundamental basis of the calculation is eqn (27), which represents the "unperturbed" propagator as a convolution of free-particle Green's functions for the spinon and holon decay products. Because the holon is extremely light, the minimum-energy decay puts all of the center-of-mass momentum into the spinon and none into the holon. The bare spectral function thus consists of a flat continuum with an edge, the position of which maps out the dispersion relation of the spinon. The quasiparticle in this theory is not a proper particle at all but a scattering resonance caused by an attractive potential between the spinon and holon. This is fit by the parameter ε_3 above. In addition to this basic physics there are two other important effects. One is the energy-dependent spinon lifetime discussed in the previous section. This is modeled by the phenomenological self-energy $\Sigma(\varepsilon)$, which also appears as a crude vertex correction in eqn (26). The parameter relevant to this self-energy is ε_2. The other effect is the "transverse" interaction between the spinon and the holon, which causes the spectral function of the t–J model at Γ and M to peak sharply at a mid-band resonance of energy roughly $2t$ [12]. This effect, which makes the spinon and holon bind less readily away from Σ, is simulated by eqn (29). It is characterized by the parameter ε_1.

While many of the consistencies of Fig. 2 with experiment are compromised by the fitting procedure, a few important ones are not:

- Along the line $\Gamma \rightarrow M$ the "quasiparticle" disperses up from below, crosses the "fermi surface" , and vanishes.
- There is a "shadow band".
- Along the line $\Gamma \rightarrow X$ the spectral function forms a shelf but never a peak.
- There is no "fermi surface" at X.
- The "quasiparticle" is sharpest at Σ.

This manuscript and all codes and data relevant to the generation of its figures are available by anonymous ftp in the directory p01mar95 at large.stanford.edu

Acknowledgements—Supported primarily by the National Science Foundation under contract No. DMR-91-20361. Additional support was provided by the NSF MERSEC Program through the Center for Materials Research at Stanford University.

REFERENCES

1. Wells B. O. *et al.*, *Phys. Rev. Lett.* **74**, 964 (1995).
2. Affleck I. and Marston J. B., *Phys. Rev. B* **37**, 3774 (1988).
3. Tokura Y. *et al.*, *Phys. Rev. B***41**, 11657 (1990).
4. Laughlin R. B., Numerical evidence for electron decay in the two-dimensional *t–J* model, in: *Proc. Int. Euroconference Magnetic Correlations, Metal-Insulator Transitions, and Superconductivity in Novel Materials* Würzburg, Germany, 1994.
5. Laughlin R. B., New elementary particles in quantum antiferromagnets and their potential relevance to high-temperature superconductivity, in *Modern Perspectives in Many-Body Physics, Proc. VI Physics Summer School, Canberra, Australia* (Edited by M. P. Das and J. Mahanty), p. 249. World Scientific, Singapore (1994).
6. Dagotto E., Nazarenko A. and Moreo A., *Phys. Rev. Lett.* **74**, 310 (1995).
7. Siré C., Varma C. M., Ruckenstein A. E. and Giamarchi T., *Phys. Rev. Lett.* **72**, 2478 (1994).
8. Zhang F. C., Gros C., Rice T. M. and Shiba H., *Supercond. Sci. Technol.* **1**, 36 (1988); see also Tikofsky A. M., Laughlin R. B. and Zou Z., *Phys. Rev. Lett.* **69**, 3670 (1992).
9. Hsu T. C., *Phys. Rev. B* **41**, 11379 (1990).
10. Kittel C., *Quantum Theory of Solids*, P. 60. Wiley, New York (1963).
11. Trivedi N. and Ceperley D. M., *Phys. Rev. B* **40**, 2737 (1989).
12. Laughlin R. B., *Phys. Rev. B* **45** (1992) 400.

Pergamon

J. Phys. Chem. Solids Vol. 56, No. 12, pp. 1633–1636, 1995
1995 Elsevier Science Ltd
Printed in Great Britain
0022-3697/95 $9.50 + 0.00

0022-3697(95)00211-1

ENERGY GAP STRUCTURE IN BILAYER OXIDE SUPERCONDUCTORS

PATRICK A. LEE and KAZUHIRO KUBOKI[1]
Department of Physics, Massachusetts Institute of Technology, Cambridge, MA 02139, U.S.A.

Abstract—We consider a model for bilayer superconductors where an interlayer pairing amplitude $\Delta_\perp$ coexists with intralayer pairing $\Delta_\parallel$ of $d_{x^2-y^2}$ symmetry. This model is motivated by a recent photoemission experiment reporting the splitting of the nodes of the energy gap. In addition to offering a natural explanation of this observation, the model has a number of new experimental consequences. We find that the new state is accompanied by a spontaneous breaking of the tetragonal symmetry. We also find that the out-of-phase oscillation of $\Delta_\perp$ and $\Delta_\parallel$ gives rise to a new Raman active mode. The phase of $\Delta_\perp$ may also become imaginary, leading to a state which breaks time reversal symmetry, which may have important implications for tunnelling experiments.

In the past two years, a new class of experiments which are phase sensitive have provided strong evidence for a sign change of the order parameter as a function of angle [1,2], consistent with d symmetry. At the same time, there are several experiments which appear to be inconsistent with the simple $d_{x^2-y^2}$ state. For example, Sun *et al.* [3], have made tunnel junctions between $YBa_2Cu_3O_{7-\delta}$ (YBCO) and Pb and obtained Josephson current along the $c-$axis. Secondly, a recent report of fractional vortices tied to grain boundary interfaces [4] has been interpreted as requiring a time reversal symmetry breaking state near the interface [5]. Finally, Ding *et al.* [6] measured the energy gap as a function of angle usng angular resolved photoemission in $Bi_2Sr_2CaCu_2O_8$ (Bi-2212) and claim that the energy gap does not vanish along (π, π) as expected for the $d_{x^2-y^2}$ state. Instead, the node is split into two, lying approximately 10° from the 45° line. Another group [7] also reported a finite energy gap in the (π, π) direction and studied its temperature dependence. Taken together, these experiments suggest that the energy gap structure may be more complicated than $d_{x^2-y^2}$. In this paper we take the point of view that all the experiments mentioned above have been carried out correctly and ask the question: can a modification of the $d_{x^2-y^2}$ state provide a scenario whereby the experiments can be explained? It turns out that by assuming the existence of an interlayer pairing order parameter, an explanation of the experiments naturally emerges. We also show that the assumption leads to a number of predictions which can be tested experimentally.

Band structure calculations have yielded a surprisingly large interlayer hopping term between the bilayers, given by $t_\perp(\boldsymbol{k})c^\dagger_{1\sigma}(\boldsymbol{k})c_{2\sigma}(\boldsymbol{k})$ where 1 and 2 refer to the layers. Chakravarty *et al.* [8] have proposed the parametrization $t_\perp(\boldsymbol{k}) = \frac{1}{4}t^\circ_\perp(\cos k_x a - \cos k_y a)^2$ with $t^\circ_\perp \approx 0.24$ eV. Andersen *et al.* [9] recently showed that the unusual $\boldsymbol{k}$ dependence originates from hopping via the Cu $4s$ orbitals, and that it leads to an interlayer exchange energy of order $J_\perp \approx 20$ meV, consistent with the lower bound of 8 meV given by neutron scattering [10]. It has been proposed [11,12] that the relatively large exchange term, when enhanced by intralayer antiferromagnetic correlations, is responsible for the spin gap phase found in bilayer systems [13]. Furthermore, Ubbens and Lee [11] have argued that in the superconducting phase, a pairing amplitude $\Delta_{12} = \langle c_{i\uparrow}(\boldsymbol{r})c_{2\downarrow}(\boldsymbol{r})\rangle$ appears in addition to the intraplane order parameter $\Delta_{ii}(\boldsymbol{\eta}) = \langle c_{i\uparrow}(\boldsymbol{r})c_{i\downarrow}(\boldsymbol{r}+\boldsymbol{\eta})\rangle$, $i = 1, 2$ which is of d symmetry. This leads to a quasi-particle dispersion relation $\tilde{E}_\pm(\boldsymbol{k}) = (\xi_k^2 + |\Delta_\parallel \pm \Delta_\perp|^2)^{\frac{1}{2}}$ where $\xi_k = \epsilon_k - \mu$, $\Delta_\parallel(\hat{k})$ and $\Delta_\perp$ are proportional to $\Delta_{11} = \Delta_{22}$ and Δ_{12} respectively. Since the nodes of this state are given by the zeros of $|\Delta_\parallel \pm \Delta_\perp|$, if $\Delta_\parallel$ has $d_{x^2-y^2}$ symmetry, the nodes are shifted from the 45° direction and split into two nodes [11]. This provides a natural explanation of the observation by Ding *et al.* [6].

Encouraged by the experiment, we decided to re-examine the interlayer pairing model. Ubbens and Lee [11] included $J_\perp$ but not the $t_\perp$ term in their consideration. In this paper we add both the $t_\perp$ and $J_\perp$ terms to the standard $t-J$ model. Wheras Ubbens and Lee attempted to justify the appearance of Δ_{12} microscopically, in this paper we take a more phenomenological approach and assume the coexistence of $\Delta_\perp$ and $\Delta_\parallel$. This is motivated by experiment: as far as we know, the present scenario is the only one which is consistent with both the node splitting [6] and the sign change of the order parameter as $\hat{k}$ varies from 0 to $\pi/2$, as required by the corner SQUID experiment [1]. The purpose of this work is to explore the consequences of the assumed interlayer pairing amplitude, so that further experiments can confirm or falsify this picture.

We begin by treating the bilayer $t-J$ model (including $t_\perp$ and $J_\perp$) using the slave boson mean field method, which is equivalent to the Gutzwiller approximation. The tight binding band $\epsilon(k) = -2\tilde{t}(\cos k_x a + \cos k_y a)$ is split into bonding and anti-bonding bands $g_\pm = (c_1 \pm c_2)/\sqrt{2}$ with

[1] Permanent address: Department of Physics, Kobe University, Kobe 657, Japan.

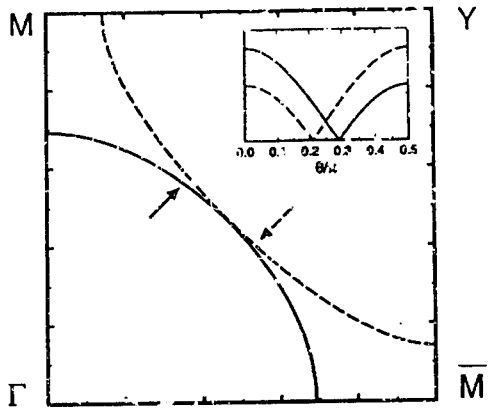


Fig. 1. Mean field calculation of the Fermi surface including hopping between bilayers for hole doping $x = 0.15$. The parameters $t/J = 3, t_\perp^{(0)}/J = 2.4$ and $J_\perp/J = 0.2$ are used. The solid and dashed lines are the Fermi surfaces for the bonding (g_+) and antibonding (g_-) bands. Solid and dashed arrows indicate the approximate location of the nodes associated with Δ_+ and Δ_- in the $d+s$ state. The insert shows a schematic picture of the angular dependence ($\theta = 0$ is along the $\Gamma - \overline{M}$ axis) of the gap functions $|\Delta_+|$ (solid) and $|\Delta_-|$ (dashed) for the $d+s$ state ($\Delta_\perp$ real and positive). Note that $\Delta_\pm$ are associated with the solid and dashed Fermi surfaces respectively. For the $d-s$ state, $|\Delta_+|$ is given by the dashed line.

dispersion $\epsilon_\pm(\boldsymbol{k}) = \epsilon(\boldsymbol{k}) \pm \tilde{t}_\perp(\boldsymbol{k})$, where $\tilde{t}$ is of order J and $\tilde{t}_\perp(\boldsymbol{k}) \simeq X_0 t_\perp(\boldsymbol{k})$ where X_0 is of order x, the doping concentration. Thus, in the mean field theory the effective interlayer hopping is reduced by x, simply because in the strongly correlated metals, the electron, on average, must find a vacancy to hop.

The resulting Fermi surface is shown in Fig. 1 for $x = 0.15$. As emphasized by Anderson [14], in the normal state, coherent hopping is really not possible between the layers. We expect the bonding-antibonding splitting to be smeared out, but a region of low lying excitations may exist in the $\boldsymbol{k}$ space between the two Fermi surfaces. Figure 1 bears a striking resemblance to the photoemission data of Dessau *et al.* [15].

In the superconducting state, coherent hopping between the planes indeed occurs, and we should take the band splitting seriously. With the basis sets $(c_{1,k\uparrow}, c^\dagger_{1,-k\downarrow}, c_{2,k\uparrow}, c^\dagger_{2,-k\downarrow})$, the mean field Hamiltonian takes the form

$$\begin{bmatrix} \epsilon(\boldsymbol{k}) - \mu & \Delta_\parallel(\hat{k}) & \tilde{t}_\perp(\boldsymbol{k}) & \Delta_\perp \\ \Delta^*_\parallel(\hat{k}) & -\epsilon(\boldsymbol{k}) + \mu & \Delta^*_\perp & -\tilde{t}_\perp(\boldsymbol{k}) \\ \tilde{t}_\perp(\boldsymbol{k}) & \Delta_\perp & \epsilon(\boldsymbol{k}) - \mu & \Delta_\parallel(\hat{k}) \\ \Delta^*_\perp & -\tilde{t}_\perp(\boldsymbol{k}) & \Delta^*_\parallel(\hat{k}) & -\epsilon(\boldsymbol{k}) + \mu \end{bmatrix} \tag{1}$$

It is easily seen that the bonding anti-bonding bands $g_\pm$ block diagonalize this matrix, so that the $g_\pm$ bands are separately paired by $\Delta_\pm(\hat{k}) = \Delta_\parallel(\hat{k}) \pm \Delta_\perp$, resulting in the quasi-particle spectrum

$$E_\pm(\boldsymbol{k}) = (\xi^2_\pm(\boldsymbol{k}) + |\Delta_\parallel(\hat{k}) \pm \Delta_\perp|)^{\frac{1}{2}} \tag{2}$$

where $\xi_\pm(\boldsymbol{k}) = \epsilon_\pm(\boldsymbol{k}) - \mu$. We can choose $\Delta_\parallel$ to be real and positive. If $\Delta_\perp$ is also real and positive, the nodes are split as before, but the split nodes are associated with the $\pm$ bands separately, as indicated in Fig. 1. It is clear from Fig. 1 that for real $\Delta_\perp$, the onset of interlayer pairing implies a spontaneous breaking of the tetragonal symmetry of the model. This is a consequence of the inclusion of $t_\perp$. The two degenerate states of the broken symmetry correspond to $\Delta_\perp$ being positive or negative. We shall refer to these degenerate states as $d \pm s$. Due to the vanishing of $t_\perp(\boldsymbol{k})$ along (π, π), this assymmetry is difficult to resolve near the nodes. However, in a given domain, the g_+ band has a different gap along MY than $\overline{M}Y$ and the resulting asymmetry in the electronic state is expected to couple linearly to the orthorhomic strain $\epsilon = (a-b)/(a+b)$.

There is one additional complication to this discussion, in that we should consider the possibility that $\Delta_\perp$ is purely imaginary. We shall refer to this state as $d + is$, which has a minimum gap of $|\Delta_\perp|$. Indeed, a mean field calculation shows that this state is lower in energy than $d+s$. The Ginzburg-Landau free energy is given by $F = F_0 + F_\epsilon$, where for simplicity we have fixed $\Delta_{11} = \Delta_{22} = \Delta_\parallel$,

$$F_0 = a_\parallel|\Delta_\parallel|^2 + b_\parallel|\Delta_\parallel|^4 + a_\perp|\Delta_\perp|^2 + b_\perp|\Delta_\perp|^4 + d_1|\Delta_\parallel|^2|\Delta_\perp|^2 + d_2(\Delta^2_\parallel\Delta^{2*}_\perp + c.c.) \tag{3}$$

$$F_\epsilon = \alpha\epsilon(\Delta_\parallel\Delta^*_\perp + c.c.) \tag{4}$$

where F_ϵ describes the linear coupling to the strain discussed earlier. [17] In mean field theory, we found that $d_1 = 4d_2 > 0$. If we write $\Delta_\perp = |\Delta_\perp|e^{i\phi}$, the d_2 term is proportional to $\cos 2\phi$ with a positive coefficient, and is minimized by $\phi = \frac{\pi}{2}$. The F_ϵ term, on the other hand, is proportional to $\cos\phi$, so that $\phi = 0$ or π (the $d \pm s$ state) is stabilized in systems with pre-existing orthorhomic distortions such as YBCO. In tetragonal systems, we add an elastic energy term $F_E = \frac{1}{2}\kappa\epsilon^2$ to F and minimize with respect to ϵ. This produces a term $-2(\alpha^2/\kappa)|\Delta_\perp|^2|\Delta_\parallel|^2\cos^2\phi$ which opposes the d_2 term. The $d+s$ state is stabilized provided $\frac{\alpha^2}{\kappa} > 2d_2$. The observation of split nodes in the nominally tetragonal Bi-2122 presumably means that this condition is satisfied and $d+s$ is stabilized. Thus we predict that, for bilayer systems with tetragonal symmetry, a superconducting state with split nodes is accompanied by a spontaneous breaking of the tetragonal symmetry. The Bi-2122 compound is not truly tetragonal due to the superlattice modulation in the (π, π) direction, but the a and b lattice constants are predicted to become unequal at low temperature. The best test of the prediction is probably in tetragonal materials such as the bilayer mercury compounds. Even in YBCO, we expect an additional distortion below T_c. There is evidence for this in the literature [16]. The coupling to lattice distortions also lead us to expect anomalies in the transverse ultra sound velocity below T_c [17].

As mentioned earlier, the $d+s$ state explains the photoemission data of ref. 6. Indeed, the lower branch min (Δ_+, Δ_-) shown in the insert of Fig. 1 can be fitted to the experimental data with $\Delta_\parallel(\hat{k} = 0) \approx 30$ meV and $\Delta_\perp \approx$

5 to 9 meV [18]. In ref. 6, only data associated with the g_- band (dashed line in Fig. 1) was shown. The question arises as to what happened to the upper branch of the insert in Fig. 1. Two possibilities need to be examined: the photoemission may be from a single domain of $d+s$ state or from multiple domains of $d+s$ and $d-s$. In the first case we expect a single peak with different gaps ($\Delta_\parallel(\hat{k}=0) \pm \Delta_\perp$) at the $M-Y$ and $\overline{M}-Y$ crossings. In the second case the peak should be a superposition of two peaks with a splitting of $2\Delta_\perp$. The data is consistent with a splitting of 10 meV or less [18] which may require a slight angular dependence of $\Delta_\perp(\hat{k})$ so that it is smaller along $\Gamma-M$ than along $\Gamma-Y$. At present, data is not available which covers both $\Gamma-M$ and $\Gamma-\overline{M}$ quadrants in the same sample, so that these two possibilities cannot be distinguished.

The existence of several order parameters should lead to new collective modes, which are amplitude and phase modes associated with $\Delta_{ij} = |\Delta_{ij}|e^{i\phi_{ij}}, i, j = 1, 2$. The amplitude modes are expected to be high in frequency and damped and we shall focus on the phase modes only. There are three modes corresponding to the three phase degrees of freedom.

(1) The in-phase oscillation of $\Delta_{11}, \Delta_{22}, \Delta_{12}$ is the Bogoliubov-Anderson mode which is coupled to total charge density and pushed up to the plasma frequency.

(2) The out-of-phase mode $\phi_{11} - \phi_{22}$. This is nothing but the Josephson plasma mode. We estimate its frequency to be $\omega_J \approx xt_\perp(\Delta_\parallel/J)^{\frac{1}{2}}$ which is quite high, so that this mode is probably strongly damped.

(3) Finally, the mode which is of greatest interest to us is the out-of-phase oscillation between ϕ_{12} and $\phi_{11} = \phi_{22}$. Since the free energy given by eqn (3) depends weakly on this phase difference, we expect this mode to be low-lying in frequency. Furthermore, this phase mode leads to a rearrangement of the quasi-particle spectrum in the plane, since a change in ϕ_{12} from 0 to $\frac{\pi}{2}$ interpolates between the $d+s$ and $d+is$ states. This should couple to charge oscillation within each plane, but with the total charge conserved within each layer. Thus, we expect this mode to be Raman active.

We briefly discuss the experiment of ref. 5, where a Josephson current is observed along the c axis between YBCO and a conventional superconductor. The $d+s$ state by itself cannot explain why the critical current is relatively insensitive to whether the YBCO is untwinned or highly twinned. This is because the coupling to the lattice strain ϵ [shown in eqn (4)] will lock the $d+s$ state to one set of twins and the $d-s$ states to the other. Since the d order parameter is insensitive to twinning (otherwise the phase sensitive experiment of references 1 and 2 will not work in twinned samples), the Josephson current will have opposite signs on the two sets of twins and tend to cancel. One possible way out of this dilemma is to postulate the existence of regions where the $d+is$ becomes stabilized. This is plausible due to the small energy differences expected and can happen near the twin boundaries. Recently we analyzed how the $d+s$ state is connected to the $d-s$ state across a twin boundary using Landau theory [20]. Naively one might expect that the s component changes sign and vanishes at the twin boundary. However, we find that the system can take advantage of the complex nature of the order parameter and continuously winds the phase of the s order parameter from 0 to π, so that it goes through $\frac{\pi}{2}$ near the twin boundary, i.e., a region of $d+is$ is produced. It is then possible to have coherent Josephson tunnelling into the $d+is$ regions from the conventional superconductors. We believe this scenario offers an explanation of the experiment of Sun, *et al.* [3].

The trapped fluxes on grain boundaries between YBCO films with different orientations are measured and interpreted as being due to the appearance of fractional charged vortices [4]. Such vortices require the existence of a time-reversal symmetry breaking state near the interface [5]. Recently, Kuboki and Sigrist [21] offered an explanation of this state as being due to an admixture with a proximity induced s component of the order parameter. In our picture, the possible existence of the complex $d+is$ state near an interface suggests an alternative origin of the time-reversal symmetry breaking state. The two alternatives can be distinguished by searching for similar effects in single layer materials.

Acknowledgements—We thank Manfred Sigrist, Andy Millis and Mike Norman for many helpful discussions. This work was supported primarily by the Center for Materials Science and Engineering under NSF grant DMR 94-00334. K.K. acknowledges support by the Ministry of Education, Science and Culture of Japan.

REFERENCES

1. Wollman D. A. *et al.*, *Phys. Rev. Lett.* **71**, 2134 (1993); Brawner D. and Ott H., *Phys. Rev. B* **50**, 6530 (1994); Iguchi I. and Wen Z., *Phys. Rev. B* **49**, 12388 (1994).
2. Tsuei C. C. *et al.*, *Phys. Rev. Lett.* **73**, 593 (1994).
3. Sun A. G., Gajewski D. A., Maple M. B. and Dynes R. C., *Phys. Rev. Lett.* **72**, 2267 (1994).
4. Kirtley J. R. *et al.*, IBM Yorktown Hts. preprint.
5. Sigrist M., Bailey D. and Laughlin R. B., *Phys. Rev. Lett.* , to be published.
6. Ding H. *et al.*, *Phys. Rev. Lett.* **74**, 2784 (1995).
7. Jian Ma *et al.*, *Science* **267**, 862 (1995).
8. Chakravarty S., Sudbo A., Anderson P. and Strong S., *Science* **261**, 337 (1993).
9. Andersen O. K. *et al.*, *Phys. Rev. B* **49**, 4145 (1994) and unpublished.
10. Shamoto S., *et al.*, *Phys. Rev. B* **48**, 13817 (1993).
11. Ubbens M. and Lee P. A., *Phys. Rev. B* **50**, 438 (1994).
12. Ioffe L., Larkin A., Millis A. and Altshuler B., *JETP Lett.* **59**, 65 (1994).
13. Millis A. J. and Monien H., *Phys. Rev. Lett.* **70**, 2810 (1993); **71**, 210(E) (1993). For a review, see the article by Millis A. J., this conference proceeding.
14. Anderson P. W., *Phys. Rev. Lett.* **67**, 660 (C) (1991).
15. Dessau D. S. *et al.*, *Phys. Rev. Lett.* **71**, 2781 (1993).
16. You H. *et al.*, *Phys. Rev. B* **43**, 3660 (1991).
17. For a discussion of coupling to lattice distortion see Sigrist M. and Ueda K., *Rev. Mod. Phys.* **63**, 239 (1991).
18. Norman M. R., Randeria M., Ding H. and Campuzano J., Argonne preprint.

19. Sigrist M. and Rice T. M., *Phys. Soc. Jpn* **61**, 4283 (1992); Geshkenbein V. B., Larkin A. and Barone A., *Phys. Rev. B* **36**, 235 (1987).
20. Sigrist M., Kuboki K., Lee P. A. and Millis A. J., preprint.
21. Kuboki K. and Sigrist M., preprint.

Pergamon

J. Phys. Chem. Solids Vol. 56, No. 12, pp. 1637–1639, 1995
Copyright © 1995 Elsevier Science Ltd
Printed in Great Britain. All rights reserved
0022-3697/95 $9.50 + 0.00

0022-3697(95)00181-6

PSEUDOGAPS IN THE VAN HOVE JAHN–TELLER SCENARIO

R. S. MARKIEWICZ
Physics Department and Barnett Institute, Northeastern University, Boston MA 02115, U.S.A.

Abstract—
The van Hove scenario can provide a unified framework for understanding many of the anomalous superconducting and normal-state properties of the high-T_c cuprates. The present paper will review evidence for a novel form of electron–phonon coupling associated with splitting the degeneracy of two van Hove singularities (vHs): a van Hove Jahn–Teller (JT) effect. The JT distortions can give rise to *dynamical* local tilting and breathing modes, and the onset of the instability will appear as a pseudogap phase. The local breathing mode excitations give rise to large polaronic effects. In particular, there can be large polaronic band renormalizations, but *only in the vicinity of a vHs*—even when the vHs is away from the Fermi level. This can provide an explanation for the "extended vHs" observed in the cuprates.

1. INTRODUCTION

Angle-resolved photoemission has posed an interesting conundrum for the van Hove scenario in the high-T_c cuprates: while the Fermi level is pinned close to a van Hove singularity (vHs) in optimally doped $YBa_2Cu_3O_7$ (YBCO) [1] and $Bi_2Sr_2CaCu_2O_8$ (Bi-2212) [2], there are other cuprates (e.g., Bi-2201) for which proximity to a vHs does not lead to high T_c values [3]. This can be caused by competing instabilities, such as charge or spin density waves, but there is no evidence for a long-range ordering transition. Within the vHs model, there is a strong electron–phonon coupling, associated with a novel Jahn–Teller (JT) effect, in which a structural distortion splits the degeneracy of two vHs. These distortions take the form of *dynamic* octahedral tilts in the La cuprates (pyramidal tilts in YBCO). I propose that the competing phase is associated with this short-range structural disorder, and furthermore that the onset of the tilting instability can be identified with the experimentally observed pseudogap phase.

In $La_{2-x}Ba_xCuO_4$ (LBCO) and $La_{2-x}Sr_xCuO_4$ (LSCO), the macroscopic symmetry is such that the vHs degeneracy is split only in the low-temperature tetragonal (LTT) phase. This phase behaves like a static JT phase: when the tilting of the CuO_6 octahedra is large enough, superconductivity is destroyed. However, the vHs can also play a role in the high-temperature tetragonal (HTT) and low-temperature orthorhombic (LTO) phases, via a *dynamic* JT effect, in which locally the octahedra have a predominantly LTT-like distortion, and the macroscopic symmetry is restored by dynamic tunneling between adjacent minima. Quite recently, a number of features of this model appear to have been confirmed experimentally.

In particular, there should be a critical temperature, T^* *within the HTT phase*, marking the onset of this tilt instability. Such a local structural instability can lead to "ghost" Fermi surfaces, peaks in the density of states, and anomalous, T-dependent Hall effects, as a density wave gap starts to open. Such "pseudogap" phases are found in both the HTT phase of LSCO and in YBCO, and moreover the gap onsets are associated with a number of phonon anomalies. The VHS model can reproduce the doping dependence of this pseudogap.

A number of recent experiments which probe local order are providing very suggestive evidence of the dynamic JT state. There appears to be an extremely broad distribution of octahedral tilt angles in the LTO phase, from essentially zero tilt up to some maximum value. Furthermore, the local tilt of an individual CuO_6 octahedron in LBCO was found to have LTT symmetry, even in the LTO phase. The LTO order is built up over an extended domain, of dimensions ~ 10 Å. These observations are in good agreement with the present dynamic JT model.

Recently, I have shown that, in addition to the quadratic tilt mode coupling to electrons, there is a linear coupling with O–O breathing modes. This in turn leads to a polaronic model of the strong electron–phonon coupling.

2. THE VAN HOVE SCENARIO

The 'van Hove scenario' of high-T_c superconductivity may be stated as follows. There is one (or more) van Hove singularity (vHs) in the immediate vicinity of the Fermi level in the cuprates, and this controls the anomalous normal state and superconducting properties. The doping of optimum T_c occurs when the Fermi energy coincides with the vHs, at which point the normal state resistivity is linear in T and ω. Correlation effects tend to keep the Fermi level pinned close to the vHs over an extended doping range. The pairing mechanism may have an anomalous electronic contribution [4], and the gap may have d-wave symmetry [5].

The large density of states associated with the vHs acts to enhance T_c, but it can also enhance other forms of instability, particularly structural (Peierls-like) or magnetic (spin-Peierls). It is the latter, particularly structural, instabilities that this paper is concerned with.

3. THE VAN HOVE JAHN–TELLER EFFECT

The cuprates can have an anomalous electron–phonon coupling, which is a form of band Jahn–Teller (JT) effect, with symmetry-related vHs providing the electronic degeneracy [6,7]. There can be a static JT phase—this seems to be realized in the low-temperature tetragonal (LTT) phase of $La_{2-x}Ba_xCuO_4$ (LBCO) and Nd-substituted $La_{2-x}Sr_xCuO_4$ (LSCO). Here, the structural distortion is associated with an octahedral tilt, which splits the vHs degeneracy and destroys superconductivity.

A more interesting possibility is that the vHs can induce short-range order, via a *dynamic* JT phase [8]. Thus, the low-temperature orthorhombic (LTO) phase of LSCO is also associated with an octahedral tilt, differing from the LTT phase only in the tilt axis. However, the vHs degeneracy is only split in the LTT phase, not the LTO. I have proposed that the LTO phase is a dynamic JT phase, in which the microscopic symmetry is LTT, and splits the vHs degeneracy, but tunneling between adjacent free energy minima restores LTO symmetry on a macroscopic length scale. Similarly, the high-temperature tetragonal phase actually involves a dynamic JT phase, with tunneling between all four minima. The vHs degeneracy is first split at the onset of this tilting instability, which therefore corresponds to the opening of a pseudogap.

4. POLARONS

While the actual soft mode is associated with a tilt instability, there is evidence that other, higher-frequency breathing modes are also softening and contributing to the short-range order. Quite recently, I have analyzed the doping dependence of the LTO transition in LSCO. The dominant ionic effect contributing to this transition is the variation of the in-plane Cu–O bond length with doping. Such large bond-length changes are suggestive of strong valence fluctuation effects, which will lead to strong coupling of electrons with in-plane breathing modes. Short-range fluctuations of these modes can also contribute to the dynamic JT effect, with the important distinction that they can couple linearly to the electrons. This linear coupling can lead to strong *polaronic* effects.

I have been analyzing these effects, both in the Peierls regime in the doped materials, and in the spin-Peierls regime near half filling. Among the results of these studies are: (1) there can be strong electron-phonon coupling even in the insulating phase near half filling. (2) In the doped material, the strongest coupling is with the O–O breathing modes; the Cu–Cu breathing modes do not split the vHs degeneracy. (3) There can be strong polaronic band renormalizations, but *only near the vHs*, even when these are not at the Fermi level [9]! This can provide a plausible explanation for the experimental observations of "extended vHs". For example, Fig. 1 shows the photoemission-derived energy dispersion in $Bi_2Sr_2CaCu_2O_8$. While the overall linewidth is consistent with theory (dashed line), if correlation effects are included, the dispersion is considerably narrower near the vHs. Polaronic coupling narrows the dispersion by a factor of $1/(1+\lambda)$ within a phonon frequency $\hbar\omega$ of the vHs. The solid line in Fig. 1 shows the resultant narrowing, assuming $\lambda = 3$, $\hbar\omega = 40$ meV. Since the narrowing is tied to the vHs, and not the Fermi level, the same theory can also explain the extended vHs observed in $YBa_2Cu_4O_8$, which is $\sim$ 19meV below the Fermi level [1].

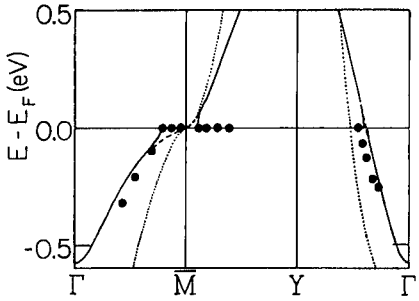


Fig. 1. Polaronic band narrowing near a vHs. Symbols—photoemission data of Ref. [2] for $Bi_2Sr_2CaCu_2O_8$; dashed line—correlation corrected theory; solid line—theory with additional polaronic band narrowing.

The reason that the strong renormalization is localized near the vHs is interesting. At a vHs, the Fermi velocity v_F vanishes, so the system is in an anti-Born–Oppenheimer limit: phononic rearrangements are fast compared to electronic motions. Thus, when a hole hops from one O to another, the ions have time to locally rearrange, giving rise to states of well-defined valence. Equivalently, the system is in an ionic limit near a vHs, and a covalent limit away from the vHs.

5. EXPERIMENTAL EVIDENCE: PSEUDOGAPS

The dynamical JT phase in LSCO can most easily be detected from the onset of the tilting instability in the HTT phase, when the vHs degeneracy first starts to split. This will appear as the opening of a pseudogap, and should be associated with a number of anomalies. The decrease in the dos should be reflected in the susceptibility and heat capacity. Since only the regions of Fermi surface near the vHs are gapped, the Fermi surface topology can change, leading to an anomalous Hall effect and "ghost" Fermi surfaces. Since the gap opens gradually, the Hall effect can have a strong T-dependence [10]. A pseudogap phase with

just these properties was recently observed in LSCO [11].

In YBCO, a neutron diffraction study found evidence for a local instability of pyramidal tilts [12]. Correspondingly, there is considerable evidence for a "pseudogap" in YBCO, including peaks in the magnetic susceptibility [13] heat capacity [14], and dynamic structure factor [15]. The doping dependence of the pseudogap is well described in the vHs model [16]: the pseudogap is actually largest near half filling, and decreases with doping, until it coincides with T_c near optimum doping.

Indeed, most of the phonon anomalies which had been associated with T_c actually track the pseudogap as doping is varied. This includes the softening of the Raman active 335 cm^{-1} phonon [17] and the peak of the B_{1g}-symmetry electronic Raman continuum [18]. Moreover, near the pseudogap onset, there is an anomaly of c-axis phonons, in which the sharp reflectivity peaks of three phonon modes smear out into a broad continuum as T is lowered [19]. More work is needed to confirm that all of these phenomena occur at precisely the same pseudogap temperature, but they all clearly commence at temperatures considerably above the superconducting transition in underdoped materials. Similar extreme ("glassy") phonon disorder is found in $Bi_2Sr_2ACu_2O_8$ (A=Ca,Y) [20], but the onset temperature was not determined.

6. EXPERIMENTAL EVIDENCE: SHORT-RANGE ORDER

There is also some more direct evidence for short-range order consistent with the vHs—JT scenario below the pseudogap transition. Thus, in $La_2CuO_{4+\delta}$, the octahedral tilt angle shows considerable disorder, ranging from nearly zero up to some maximum value [21]. In LBCO, a neutron diffraction study of pair correlation functions [22] finds that the local tilt in the LTO phase has LTT symmetry in domains of ~ 10 Å diameter, with LTO symmetry built up on larger length scales. These observations provide a striking confirmation of the dynamic JT model, since such local order is not expected in most other models. Moreover, such short-range, dynamical fluctuations can themselves provide a significant pairing mechanism. Indeed, similar dynamic JT effects have now been predicted in the C_{60}-based superconductors, and the anomalous properties of "Berryonic matter" are just beginning to be explored [23].

REFERENCES

1. Abrikosov A. A. *et al.*, *Physica C* **214**, 73 (1993); Gofron K. *et al.*, *Phys. Rev. Lett.* **73**, 3302 (1994).
2. D.S. Dessau, *et al.*, *Phys. Rev. Lett.* **71**, 2781 (1993).
3. King D. M., *et al.*, *Phys. Rev. Lett.* **73**, 3298 (1994).
4. Newns D. M. *et al.*, *Phys. Rev. Lett.* **69**, 1264 (1992).
5. Dzyaloshinskii I. E., *JETP* **66**, 848 (1987); Schulz H., *Europhys. Lett.* **4**, 609 (1987).
6. Markiewicz R. S., *Physica C* **193**, 323 (1992).
7. Markiewicz R. S., *Physica C* **200**, 65 (1992).
8. Markiewicz R. S., *Physica C* **210**, 235 (1993).
9. Markiewicz R. S., unpublished.
10. Markiewicz R. S., *J. Phys. Cond. Matt.* **1**, 8911 (1989), *Physica C* **177**, 445 (1991).
11. Hwang H. Y. *et al.*, *Phys. Rev. Lett.* **72**, 2636 (1994).
12. Schweiss P., *et al.*, *Phys. Rev. B* **49**, 1387 (1994).
13. Monien H. *et al.*, *Phys. Rev. B* **43**, 258, 275 (1991).
14. Loram J. W. *et al.*, *Phys. Rev. Lett.* **71**, 1740 (1993).
15. Rossat-Mignod J. *et al.*, *Physica B* **192**, 109 (1993).
16. Markiewicz R. S., *Phys. Rev. Lett.* **73**, 1310 (1994).
17. Litvinchuk A. P. *et al.*, *Solid State Commun.* **83**, 343 (1992).
18. Chen X. K. *et al.*, *Phys. Rev. B* **48**, 10530 (1993).
19. Basov D. N. *et al.*, *Phys. Rev. B* **50**, 3511 (1994).
20. Allen P. B. *et al.*, *Phys. Rev. B* **49**, 9073 (1994).
21. Hammel P. C. *et al.*, *Phys. Rev. Lett.* **71**, 440 (1993).
22. Billinge S. J. L. *et al.*, *Phys. Rev. Lett.* **72**, 2282 (1994).
23. Auerbach A. *et al.*, *Phys. Rev. B* **49**, 12998 (1994); Manini N., Tosatti E. and Doniach S., unpublished.

Pergamon

J. Phys. Chem. Solids Vol. 56, No. 12, pp. 1641–1643, 1995
1995 Elsevier Science Ltd
Printed in Great Britain
0022-3697/95 $9.50 + 0.00

0022-3697(95)00140-9

SPIN GAPS IN HIGH TEMPERATURE SUPERCONDUCTORS

A. J. MILLIS,* L. B. IOFFE †and HARTMUT MONIEN ‡

* AT&T Bell Laboratories, 600 Mountain Ave, Murray Hill, NJ 07974, U.S.A.
† Physics Department, Rutgers University, Piscataway, NJ 08855, U.S.A.
‡ Theoretische Physik, ETH Zurich, CH-8093 Zurich, Switzerland

Abstract—The phenomenology and theory of spin gap effects in high temperature superconductors is summarized. It is argued that the spin gap behavior can only be explained by a model of charge 0 spin 1/2 fermions which become paired into singlets and that there are both theoretical and experimental reasons for believing that the pairing is greatly enhanced in the bilayer structure of the $Y_1Ba_2Cu_3O_{6+x}$ system.

Keywords: NMR, antiferromagnetic correlations, spin-charge separation.

The spin dynamics of the high T_c superconductors are anomalous in several ways. The aspect of interest here is shown in Fig. 1, in which the uniform spin susceptibility $\chi_0(T) \equiv lim_{q\to 0}\chi(q, \omega = 0)$ is plotted for several high T_c materials. Focus first on the data for $YBa_2Cu_4O_8$. This is typical of the "underdoped" members of the yttrium-barium family of high temperature superconductors. Now the optimally doped member of this family, $YBa_2Cu_3O_7$, displays the $\chi(T)$ expected for a fermi liquid: it is large, about 3 states/eV-Cu [1], and temperature independent. $YBa_2Cu_4O_8$ displays two regimes. For $T > T^* \approx 200$ K, $\chi_0(T)/\mu_B^2 \approx A + BT$ with $A = 1.5$states/eV-Cu and $B = 1.6 \times 10^{-3}$states/eV-Cu-K; for $T < T^*$, $\chi_0(T)$ drops more rapidly. Neither temperature regime is compatible with fermi liquid theory; the low temperature regime is particularly difficult to explain. The oxygen relaxation rate $1/^{17}T_1$, shown in Fig. 2 for several high T_c materials, displays similar anomalies. This is related to the low ω limit of the imaginary part of the spin susceptibility as discussed in [1]. The data shown in Fig. 2 therefore imply that the anomalous behavior found in $YBa_2Cu_4O_8$ at $\omega = 0$ and $q \to 0$ persists for a range of q, at small ω.

In a fermi liquid the spin response is determined by a continuum of particle–hole pair excitations. The non-fermi liquid temperature dependences observed in $YBa_2Cu_4O_8$ imply that in this material the particle–hole continuum has been modified in some essential way. We argue that (i) the data for $T > T^*$ imply that in $YBa_2Cu_4O_8$ a particle-hole continuum of spin excitations still exists, (ii) the behavior at $T < T^*$ can only be explained if the fermions making up the particle–hole continuum are pairing into singlets, (iii) because this singlet pairing is not associated with the onset of superconductivity or superconducting fluctuations, spin–charge separation must occur and (iv) there are both theoretical and experimental reasons for believing that the pairing is greatly enhanced in the bilayer structure of the Y–Ba system. These points are not new; here we aim to clarify the issues and summarize the present theoretical understanding.

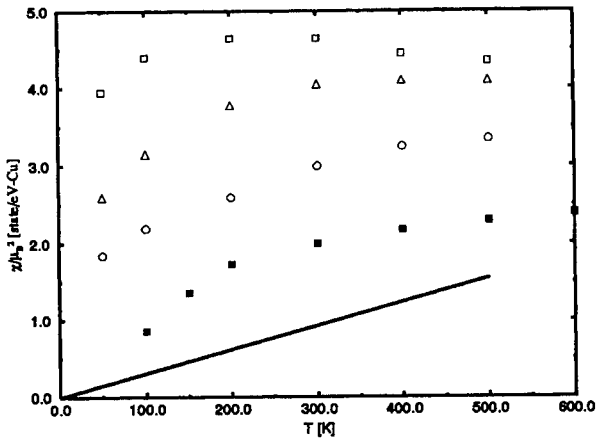


Fig. 1. Spin susceptibilities for $YBa_2Cu_4O_8$ (filled squares) and $La_{2-x}Sr_xCuO_4$ ($x = 0.08$, open circles, $x = 0.14$ open triangles, $x = 0.18$, open squares). The solid line is the slope predicted by the quantum critical regime ofthe $z = 1$ theory with the spin wave velocity appropriate to La_2CuO_4.

We consider $T > T^*$ first. In this regime the copper NMR relaxation rates $^{63}T_1^{-1}$ and $^{63}T_2^{-1}$, both increase by almost a factor of two as T is lowered from 400 K to 200 K [2]. T_1 measures $\lim_{\omega\to 0}\sum_q \chi''(q, \omega)/\omega$ while T_2 measures $(\sum_q \chi'(q, \omega = 0)^2)^{1/2}$ [3]. The simultaneous increase can to our knowledge only be explained by models which assume proximity to a $T = 0$ magnetic critical point or phase. NMR and neutron scattering are not consistent (see e.g. [4]); our view is that there are spin fluctuations not seen by neutron scattering, but the issue is not resolved.

Three classes of models have been proposed: "fermi liquid" models with overdamped spin excitations, "$z = 1$" models with undamped or weakly damped spin waves, and

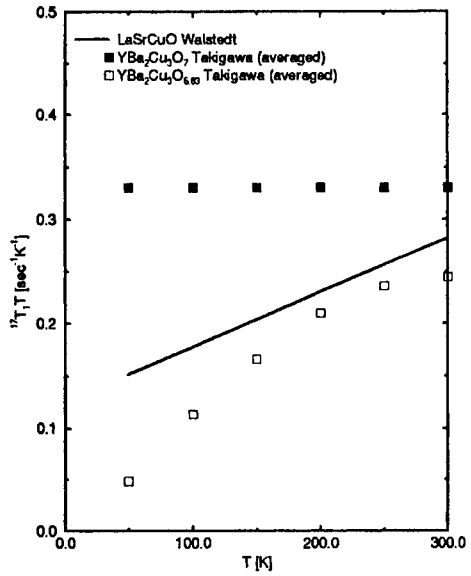


Fig. 2. Oxygen relaxation rates from Refs [1] (Y–Ba) and [4] (La–Sr).

spin excitations. The spin excitations are overdamped because decay of a spin excitation into a particle–hole pair is allowed. There are two sub-cases—either the magnetic wavevector is inside the particle–hole continuum, or it is a "$2p_F$" wavevector of the fermi surface. The critical phenomena of these cases have been worked out [5,6], and the comparison to data is not favorable, as first pointed out in Ref. [8]. The principle difficulty concerns the Cu T_2 rate, which is predicted to vary with temperature as $(T_1T)^{-1/2}$, if the ordering wavevector is inside the continuum, or more weakly, if $Q = 2p_F$, whereas the data suggest $T_2^{-1} \propto 1/T_1T$ [8,4].

The $z = 1$ models take as their starting point the magnetic insulating parent compounds, which are antiferromagnets with spin waves of dispersion $\omega = c[|k| - |Q|]$ ($Q = (\pi, \pi)$ is the ordering vector and, in La_2CuO_4, $\hbar c \sim 0.75$ eV-Å). It is assumed that the doping which converts these materials to superconductors also changes the dispersion to $\omega^2 = c^2[|k| - Q]^2 + \Delta^2$. The critical properties associated with opening the gap have been extensively studied [7]. For $T > \Delta > 0$, the copper NMR T_1 and T_2 rates are predicted to obey $T_2/T_1T \sim$ constant $\sim c$ in agreement with data [2,8]. However, the very restrictive kinematics of spin waves implies that e.g. the oxygen relaxation rate in the spin-wave-only model is given by $1/^{17}T_1T \sim T^2$ [9]. It is therefore argued [8] that the model must be supplemented by a particle hole continuum of fermions which couple only weakly to the spin waves but contribute to the small q response, so that $\chi_0(T) = \chi_{fermion} + \chi_{spinwave}$. However, a quantitative comparison of the theory to $YBa_2Cu_4O_8$ [9] found that the observed T_2/T_1T ratio implied $c \cong 0.35$ eVÅ, implying $d\chi_{spinwave}/dT = 1 \times 10^{-2}$ states/eV-Cu-K, *six* times greater than the observed $d\chi/dT$.

A third alternative is the "spin liquid" picture. This is based on a gauge theory formalism which is one implementation of Anderson's spin–change separation hypothesis [10]. The spin response is given by a particle–hole continuum of spin 1/2 charge 0 fermionic "spinons" which interact via a gauge field. It has been shown that that the gauge field interaction may lead to divergences in the "$2p_F$" susceptibilities of the spinons even if the interaction is not tuned to a critical value, and parameters exist for which the physical consequences are roughly consistent with available data [11].

We now turn to point (ii). For $T < T^* \approx 200$ K, $\chi_0(T)$ drops below the $\chi_s = A + BT$ characterizing the higher T behavior. For 100 K $< T <$ 200 K, $\chi_0(T)$ is roughly linear in T and extrapolates to a slightly negative value at $T = 0$. In other words, in this regime *one should think of the $\chi_0(T)$ as being due to thermal excitations above aground state with a vanishing spin susceptibility*. In order to have $\chi_0(T) = 0$ at $T = 0$ in a spin rotation invariant system one must have a ground state which is a singlet with a gap to spin excitations. We have already argued that there is a particle–hole continuum of spin excitations in $YBa_2Cu_4O_8$. The only known method of opening a gap in a particle–hole continuum is to pair the fermions into singlets, as occurs in a conventional superconductor. Note in particular that the effect of actual or incipient antiferromagnet order on the spin susceptibility is known [6] not to produce a gap; instead it leads in two spatial dimensions to $\chi_0(T) = \chi_0 + DT$, with $\chi_0 > 0$.

The pairing is unlikely to be due to conventional superconductivity for two reasons: the scale, $T^* \approx 200$ K, is much larger than the largest superconducting T_c, observed in any member of the Y–Ba family, and the observed resistivity is very different from the "paraconductivity" observed in materials with strong superconducting fluctuations. In particular, $YBa_2Cu_3O_{6.7}$ exhibits spin gap effects very similar to those found in $YBa_2Cu_4O_8$ but its resistivity has upward curvature for 80 K $< T <$ 150 K and is rather flat between 100 K and $T_c = 60$ K [12]. If strong superconducting fluctuations were present, the resistivity would drop rapidly in this regime. Thus we believe that theories based on formation of conventional Cooper pairs via an attractive interaction [13] are unlikely to be relevant. Rather, the correct theory must involve spin–charge separation in some form.

Next, we argue that although anomalous temperature dependences are present, there is no strong evidence for singlet pairing in $La_{2-x}Sr_xCuO_4$, where interplane coupling is believed to be weak. Spin susceptibility data obtained as in [14] but using more reliable data of [15] are shown in Fig. 1; although there is a pronounced downturn in the susceptibility for $x = 0.08$ and $x = 0.14$ it is also clear that $\lim_{T\to 0}\chi_s(T) > 0$ in these materials. Similarly, $^{17}T_1T^{-1}$, plotted in Fig. 2 at $x = 0.14$, shows no sign of a downturn. Finally, the Cu relaxation rates $1/T_1T$ in $La_{2-x}Sr_xCuO_4$ are monotonic in T [4], in contrast to the Cu relaxation rate in $YBa_2Cu_4O_8$ which exhibits a pronounced downturn beginning almost a factor of two above T_c [2]. We conclude

that the bilayer structure of $YBa_2Cu_4O_8$ is important. This conclusion is not universally accepted; for an alternative point of view see [8].

There is in fact evidence that the two planes in a bilayer are magnetically coupled. Neutron scattering experiments have only detected fluctuations in which the spins on one plane are perfectly anticorrelated with spins on the other [16]. An NMR T_2 "cross-relaxation" experiment in which Cu spins on one plane are pumped and spins on the adjacent plane are probed has been proposed by Monien and Rice [17] and performed by Stern *et al.* [18]. The rate is found to be large (of the order of the in-plane T_2) and rapidly temperature dependent.

Theories of the spin gap have been discussed by many authors [19–22]. Because one must deal with "spinons", the effects of gauge interactions must be included. These lead to a large inelastic lifetime and thus strong pairbreaking which in general suppresses [22] the spinon-pairing instabilities found [19] in one-plane models (for an exception, see [21], where in one model a very weak instability is found). However, in two-plane models the enhanced in-plane magentic susceptibility leads [21,22] to a large enhancement of the between-planes pairing originally proposed in Ref. [20]. In fact, the pairing kernel has essentially the same singularity as the theoretical expression for the "cross-relaxation" T_2 discussed above, so the experiment may be regarded as evidence for that the singular interaction required by the interplane pairing theories exists and has the correct order of magnitude.

To conclude: a magnetic susceptibility which decreases as the temperature is decreased is observed in underdoped high temperature superconductors and is difficult to explain within fermi liquid theory. We have argued that one should distinguish two regimes—a $\chi_0(T) \approx A + BT$ regime which occurs in many materials and must be understood in terms of antiferromagnetism and a particle–hole continuum, and a "spin-gap" regime in which χ drops rapidly to zero, which occurs only in the yttrium–barium family and must be understood in terms of pairing of chargeless fermionic "spinons".

Acknowlegements—We thank Bertram Batlogg for very helpful discussions of susceptibility measurements.

REFERENCES

1. For a review see, e.g. Millis A. J., in *High Temperature Superconductivity: Proceedings* (Edited by K. S. Bedell, D. Coffey, D. E. Meltzer, D. Pines and J. R. Schreiffer), p. 198. Addison Wesley, Redwood City (1990). For oxygen relaxation rates for Y–Ba see Takigawa M. *et al.*, *Phys. Rev. B* **42**, 243 (1991).
2. Itoh Y., Yasuoka H., Fujiwara Y., Ueda Y., Machi T., Tomeneo I., Tai K., Koshizuka N. and Tanaka S., *J. Phys. Soc. Jpn* **61**, 1287 (1992) and Itoh Y., Ph.D. thesis, University of Tokyo, 1993.
3. Pennington C. H. and Slichter C. P., *Phys. Rev. Lett.* **66**, 381(1991).
4. Walstedt R. E., Shastry B. S. and Cheong S. -W., *Phys. Rev. Lett.* **72**, 3610 (1994) and Walstedt R. E., unpublished.
5. Millis A. J., *Phys. Rev. B* **48**, 7183 (1993) and Altshuler B. L., Ioffe L. B., Larkin A. I. and Millis A. J., *Phys. Rev. B*,**52**, 5563 (1995).
6. Ioffe L. B. and Millis A. J., *Phys. Rev. B*, *Phys. Rev. B*,**51**, 16151 (1995).
7. Chakravarty S., Halperin B. T. and Nelson D., *Phys. Rev. Lett.* **60**, 1052 (1988) and *Phys. Rev. B* **39**, 7443 (1988), Chubukov A. V. and Sachdev S., *Phys. Rev. Lett.* **71**, 169 (1993); Chubukov A. V., Sachdev S. and Ye J., *Phys. Rev. B* **49**, 11919 (1994).
8. Sokol A. V. and Pines D., *Phys. Rev. Lett.* **71**, 2813 (1993); Barzykin V., Pines D., Sokol A. V. and Thelen D., *Phys. Rev. B* **49**, 1544 (1994) Barzykin V. and Pines D., unpublished.
9. Millis A. J. and Monien H., *Phys. Rev. B* **50**, 16606 (1994).
10. Anderson P. W., *Science* **235**, 1196 (1987); Baskaran G., Zou Z. and Anderson P. W., *Solid State Commun.* **63**, 973 (1987); Ioffe L. B. and Larkin A. I., *Phys. Rev. B* **39**, 8988 (1989).
11. Altshuler B. L., Ioffe L. B. and Millis A. J., *Phys. Rev. B* **50**, 14048 (1994); Altshuler B. L., Ioffe L. B., Larkin A. I. and Millis A. J., *Phys. Rev. B*,**52**, 4607 (1995).
12. See, e.g. Fig. 3 of Batlog B., p. 37 in Ref. [1]. This figure presents data for $YBa_2Cu_3O_{6.7}$ which has spin gap behavior similar to $YBa_2Cu_4O_8$. The resistivity flattening is present in only the former material, which has more impurity scattering. The sensitivity of ρ to impurities shows that there is no paraconductivity.
13. Randeria M., Trivedi N., Moreo A. and Scalettar R. T., *Phys. Rev. Lett.* **69**, 2001 (1992).
14. Millis A. J. and Monien H., *Phys. Rev. Lett.* **70**, 2810. (1993).
15. Nakano T., Oda M., Manako C., Momono N., Miura Y. and Ido M., *Phys. Rev. B* **45**, 1600 (1994).
16. Tranquada J. M., Shirane G., Keimer B., Shamoto S. and Sato M., *Phys. Rev. B* **40**, 4503 (1989).
17. Monien H. and Rice T. M., *Proc.* 1994 *Grenoble conf.*,to appear in *Physica C.*
18. Stern R. *et al. Phys. Rev. B*, in press.
19. Tanamoto T. Kohno K. and Fukuyama H., *J. Phys. Soc. Jpn* **61**, 1886 (1992).
20. Altshuler B. L. and Ioffe L. B., *Solid State Commun.* **82**, 253 (1992).
21. Altshuler B. L., Ioffe L. B., Larkin A. I. and Millis A. J., *JETP Lett.* **59**, 65 (1994);*Phys. Rev. B*, in press.
22. Ubbens M. and Lee P. A., *Phys. Rev. B* **50**, 438 (1994) and Kubokind K. and Lee P. A., unpublished.

Pergamon

J. Phys. Chem. Solids Vol. 56, No. 12, pp. 1645–1649, 1995
Copyright © 1995 Elsevier Science Ltd
Printed in Great Britain. All rights reserved
0022-3697/95 $9.50 + 0.00

0022-3697(95)00106-9

STUDY OF ARPES DATA AND *d*-WAVE SUPERCONDUCTIVITY USING ELECTRONIC MODELS IN TWO DIMENSIONS

A. MOREO, A. NAZARENKO, S. HAAS, A. SANDVIK and E. DAGOTTO
Department of Physics and National High Magnetic Field Lab,Florida State University, Tallahassee, FL 32306, U.S.A.

Abstract—We review the results of an extensive investigation of photoemission spectral weight using electronic models for the high-T_c superconductors. Here we show that some recently reported unusual features of the cuprates namely the presence of (i) flat bands, (ii) antiferromagnetically induced weight, and (iii) small quasiparticle bandwidths all have a natural explanation within the context of holes moving in the presence of robust antiferromagnetic correlations. Introducing interactions among the hole carriers, a model is constructed which has $d_{x^2-y^2}$ superconductivity, an optimal doping of $\sim$ 15% (caused by the presence of a large density of states at the top of the valence band), and a critical temperature $\sim$ 100 K.

In the last couple of years, angle-resolved photoemission (ARPES) data introduced important constraints on possible theories of high-T_c. These experiments have motivated a considerable body of work by the authors and several collaborators that is here briefly reviewed. We have focused on three recent experiments on the cuprates, discussed elsewhere in this volume, that reported the following information: (i) hole-doped cuprates Bi2212, Bi2201, Y123 and Y124 near optimal doping present a universal flat band dispersion near $(\pi, 0)$ [1] that cannot be explained using band structure calculations. (ii) Data gathered with a novel ARPES technique have produced indications of antiferromagnetically induced photoemission bands in Bi2212 [2]. (iii) The quasiparticle bandwidth of several cuprates at finite doping [1], as well as for the insulator $Sr_2CuO_2Cl_2$ [3], is of order of the Heisenberg exchange J. Before the theoretical analysis, let us remind the reader that just a few years ago the early papers on ARPES applied to high-T_c had the tendency to claim in their conclusions that a good agreement between experiments and band structure calculations was obtained. However, the new ARPES results show that such a conclusion was premature and the influence of strong correlations is *crucial* to explain the data. These are certainly very exciting times for "aficionados" of electronic models for the cuprates!

In recent months, we have documented in the literature the results of an extensive investigation showing that the three experimental features mentioned above can have a natural explanation within the context of simple electronic models for the CuO_2 planes, like the 2D t–J model [4–7]. In addition, we have shown that under mild assumptions, even a d-wave superconducting phase with a critical temperature of about 100 K at an optimal doping of 15% can also be naturally obtained using these ideas [8]. We urge the reader to consult the original literature for details since in the present short review only a sketch of the main results will be presented. Note that we can only provide some of the relevant references. The rest are given in the papers quoted in this short article.

To start the analysis, let us consider the properties of hole carriers in an antiferromagnet. In Fig. 1 we show the dispersion of a hole in a fluctuating Néel background calculated numerically using the two dimensional t–J model on large clusters [4]. We observed that the data can be fitted very well by a dispersion where holes effectively move within their own sublattice to minimize disturbing the antiferromagnetic background. The dispersion has interesting features: (i) the bandwidth (W) is small, proportional to the exchange $J = 0.125$ eV, a fact observed since the early studies of strongly coupled electrons using numerical techniques [9]. A vast literature supports the result that $W \sim 2J$. Recently, Quantum Monte Carlo (QMC) simulations of the one band Hubbard model in strong coupling arrived to similar conclusions although their reported bandwidth scales like $W \sim 4J$ [10]; (ii) the region around $(\pi, 0)$ is anomalously flat. (Actually, plotting the quasiparticle energy together with the experimental results of Ref. [1] a good experiment–theory agreement is obtained [4,11].) QMC simulations show a similar result [11]; (iii) the density of states (DOS) has a large peak at the bottom of the hole band (top of the valence band in the electron language) that will be used below to boost the critical temperature of a gas of quasiparticles once interactions are included.

The numerical value for the quasiparticle bandwidth of this model agrees well with ARPES results both for optimaly doped Bi2212 and also the novel insulator compound $Sr_2CuO_2Cl_2$. This provides strong support to models of correlated electrons of the t–J model family. Even some details of the dispersion match the experiments, as exemplified by the line from $(0, 0)$ to (π, π). On the other hand, theory and experiment disagree for the insulator $Sr_2CuO_2Cl_2$ along the line $(\pi, 0)$–$(0, \pi)$ since the t–J model predicts an anomalously small dispersion in this particular direction. However, some of us in collaboration with K. Vos and R.

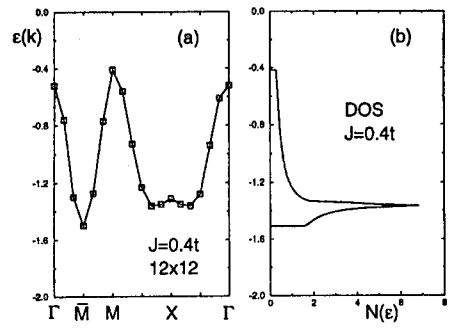


Fig. 1. (a) Energy of a hole in the t–J model, $\epsilon(\mathbf{k})$, vs momentum obtained with a Monte Carlo method on a 12×12 lattice and $J/t = 0.4$ (in units of t). (b) Density of states obtained from our fit of the numerical data Fig. 1(a) showing the van Hove singularity between $\bar{M}$ and X. The unit of energy is t (from Ref. 4).

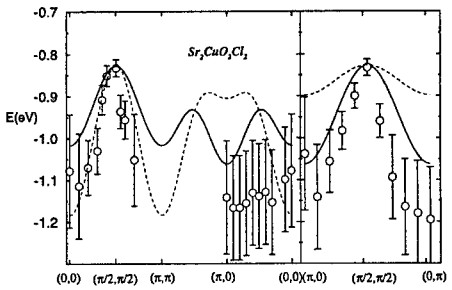


Fig. 2. Quasiparticle dispersion of the t–t'–J model (Ref. [5]) calculated in the Born approximation for an infinite lattice using $t' = -0.35t$ (solid line), $J/t = 0.3$ and $J = 0.125$ eV, compared against the experimental ARPES data (open circles) for $Sr_2CuO_2Cl_2$ of Ref. [3]. The dashed line is the t–J model result of Ref. [12].

J. Gooding have shown in a recent paper [5] that the addition of a small hopping amplitude along the diagonals of the plaquettes on the 2D square lattice greatly improves the theory–experiment agreement for all momenta including the $(\pi, 0)$–$(0, \pi)$ line. The addition of this new parameter in the Hamiltonian, while not quite satisfactory since its microscopic origin is unknown, is not forbidden by symmetry, and thus there is no reason to believe that it cannot be present in the cuprates. The dispersion is shown in Fig. 2. It is also important to remark that an even better agreement between theory and experiment was reported in Ref. [5] once a more sophisticated calculation was carried out using the more general three band Hubbard model. Thus, the partial conclusion of this analysis is that the bandwidth of the quasiparticles in the cuprates is likely described by models of strongly correlated electrons.

It is interesting to note that results similar to those obtained for the 2D t–J model at half-filling can also be obtained using the 2D one band Hubbard model. In Fig. 3 we show results of a Monte Carlo simulation of this model on clusters of 64 sites. The ARPES intensity is obtained with the maximum entropy technique. While this last technique is crude, it seems to provide results in agreement with the

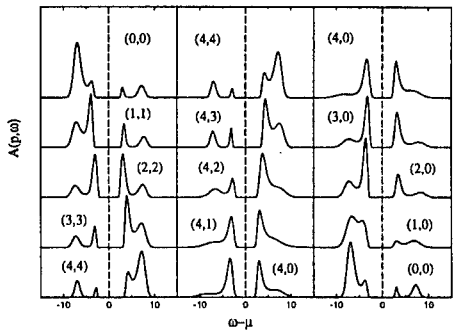


Fig. 3. Spectral weight $A(\mathbf{p}, \omega)$ of the 2D Hubbard model at half-filling obtained with the QMC method supplemented by Maximum-Entropy, on an 8×8 cluster, $U/t = 10$, and $T = t/4$ (from Ref. [6]).

more reliable Exact Diagonalization (ED) analysis of the t–J model. The Hubbard model results of Fig. 3 show that working at large U/t and concentrating near the chemical potential, a band disperses with a bandwidth of order $2J$, in excellent agreement with old predictions for the t–J model [9]. The rest of the weight is incoherent and appears at large energies of the order of the hopping t. We noticed that small variations of the maximum entropy method may induce a mixing of both bands into a single feature, which produces an incorrect larger bandwidth. Temperature effects are also crucial to obtain the proper results in these studies. Thus, we highly advise caution in the use of maximum entropy techniques for correlated electrons. To test their accuracy, the results must necessarily be contrasted against other techniques that provide dynamical information for the t–J model.

Before discussing the influence of doping on our results, we want to remark to the reader an interesting prediction of the t–J model, namely the presence of "string states" in the ARPES photoemission data. These states have the following origin: suppose a hole is injected in an antiferromagnet, as it occurs in the sudden approximation description of a photoemission experiment. When the hole attempts to move, which occurs by moving a spin from a nearest neighbor site j to the original position of the hole i, energy is lost since now the spin at site i is aligned *ferromagnetically* with its neighbors (assuming for simplicity a perfect Néel background). As the hole continues its excursion, say along one axis, more and more spins have ferromagnetic links with some of its neighbors. Actually, the penalization in energy grows proportional to the length of the path followed by the hole. Then, to a good approximation holes are confined into a linear potential caused by the spin background. The solution of the Schrödinger equation for a hole in an effective linear potential has several bound states [13]. The lowest energy state corresponds to the dominant peak in the dispersion (that acquires mobility thanks to the antiferromagnetic fluctuations that sometimes break the linear "string" caused by the hole in its movement), while the excited states are precisely the so-called "string states". These

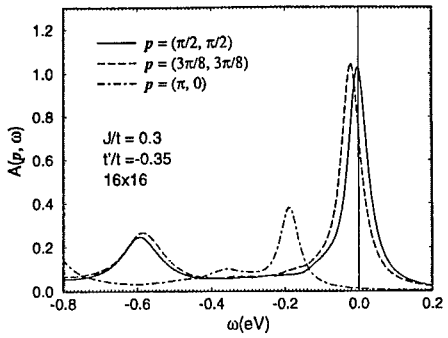


Fig. 4. Spectral weight $A(\mathbf{p}, \omega)$ for one hole in an antiferromagnet calculated using the rainbow approximation. The parameters are shown in the figure. The first excited state in the "string picture" is located at $\omega \sim -0.6$ eV.

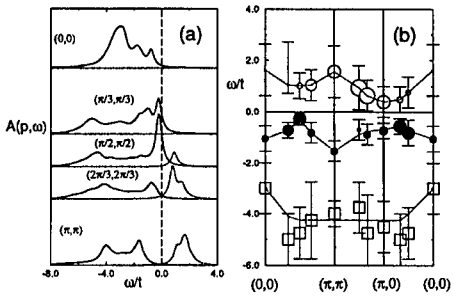


Fig. 5. $A(\mathbf{p}, \omega)$ for density $\langle n \rangle \approx 0.88$ (i.e. two holes on the 16 and 18 sites clusters) using the t–J model. In (a) the PES intensity ($\omega < 0$) is shown with a solid line, while the IPES intensity ($\omega > 0$) is given by a dotted line. The chemical potential is located at $\omega = 0$. In (b) the full and open circles represent the PES and IPES intensities, respectively, of the peaks the closest to the Fermi energy. Their area is proportional to the intensity. The error bars denote the width of the peak as observed in Fig. 5(a) (sometimes to a given broad peak several poles contribute appreciably). The full squares at $\omega \sim -4t$ represent the center of the broad valence band weight, and the area of the squares is *not* proportional to their intensity.

ideas have been discussed since the early studies for correlated electrons using the t–J model and developed by several groups. For details and references see Ref. [9]. Numerical results already in 1990 clearly showed their existence in spite of the strong quantum fluctuations in the ground state [14]. In Fig. 4 we show the main quasiparticle peak, as well asone excited state, for the case of the t–t'–J model in two dimensions using the rainbow approximation [15] (results for the t–J model are very similar). The first string state beyond the quasiparticle peak is clearly observed at a binding energy of 0.6 eV. However, the reader should notice that the calculation of excited states is somewhat less accurate than the evaluation of the properties of the dominant quasiparticle peak, and thus, the 0.6 eV prediction may have large error bars. The expected intensity is of about 20% of the main peak. These states *should* be present in $Sr_2CuO_2Cl_2$ if our analysis based on the t–J and t–t'–J models is correct. This is a clear prediction of these models. We also expect that the main candidate momentum for such an investigation should be $(\pi/2, \pi/2)$, i.e. at the top of the valence band. The only problem for the observation of the string states are effects not taken into account in the theoretical analysis, specially the existence of a robust spurious background in photoemission experiments. We nevertheless encourage our experimental colleagues to search for string states in ARPES data.

The results summarized before have shown that simple electronic models for the cuprates may properly explain several features of the real cuprate materials observed in ARPES data. The theoretical results reported above have been carried out at half-filling, i.e. in the proper density regime for $Sr_2CuO_2Cl_2$. However, the comparison between theoretical predictions and data for hole-doped compounds at *optimal* doping successfully carried out in Ref. [4] required the additional assumption that the dispersion does not change drastically with doping between half-filling and the optimal concentration of about ($\sim$ 15%) [16]. Such an assumption is reasonable since results for both Bi2212 and $Sr_2CuO_2Cl_2$ have similar small bandwidths of the order of J. On the other hand, they differ in some of their fine details specifically about momentum $(\pi, 0)$, and thus a strict rigid band approximation is likely to be non valid. Thus, the main issue is to what extent the assumption of rigid band behavior is a good approximation to describe the low hole density region of the cuprates. A more accurate first-principles calculation is required to check the quality of this approximation. This issue has been recently addressed using numerical techniques, mainly of the ED family since temperature and sign effects in Monte Carlo determinantal methods prevent us from analyzing the low temperature behavior of the Hubbard model away from half-filling. In Fig. 5, results of an ED analysis using clusters of 16 and 18 sites at a density of $\langle n \rangle = 0.88$ using the t–J model are reproduced from Ref. [6]. It is clear that the two-features structure observed in Fig. 3 is still present. The bandwidth and shape of the quasiparticle feature at energies smaller than the chemical potential remain similar to those observed before at half-filling. Of course, and as we reported in Ref. [6], as the hole density increases, eventually the quasiparticle structure with bandwidth of order J disappears. Its existence seems correlated with the presence of robust antiferromagnetic correlations in the ground state.

This is a good place to address another consequence of antiferromagnetic correlations in the ground state of models of correlated electrons, namely the creation of a new structure in the ARPES signal. We have already seen that it produces a small bandwidth of order J and flat regions near $(\pi, 0)$. However, in the introduction we mentioned a third very interesting recent experiment that reported the presence of antiferromagnetically induced bands in Bi2212 [2]. The physics of this effect is as follows. First, consider the half-filled case where the antiferromagnetic long-range order effectively doubles the size of the unit cell, thus reducing the Brillouin zone by half. This dynamically generated reduction causes the appearance of an extra symme-

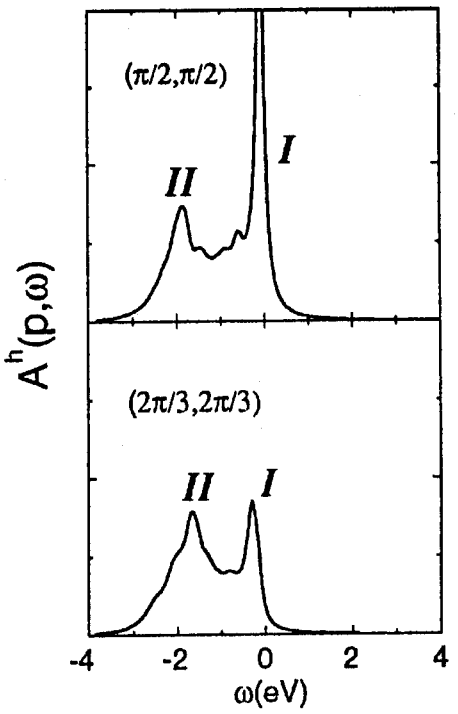


Fig. 6. PES $A(\mathbf{p}, \omega)$ (here denoted as $A^h(\mathbf{p}, \omega)$)for the t–J model at $\langle n \rangle \sim 0.88$, $J/t = 0.4$, and clusters of 16 and 18 sites. We use $\delta = 0.25t$ and $t = 0.4eV$. I is the quasiparticle-like part and II is the incoherent background.

try in the ARPES results. For example, and as shown in Fig. 1, the dispersion along the line from $(0, 0)$ to (π, π) is symmetric with respect to the $(\pi/2, \pi/2)$ point. This means that in the presence of Néel order momenta *above* the Fermi momentum $\mathbf{p}_F$, corresponding to non-interacting electrons for the same density, will show a nonzero signal in an ARPES experiment. The existence of this weight is a direct consequence of strong correlations, and it was discussed some time ago by Kampf and Schrieffer [17] using weak coupling diagrammatic techniques. Motivated by the novel experiments by Aebi *et al.* [2], we decided to carry out a numerical study of the strength of these bands vs the antiferromagnetic correlation length ξ_{AF} in the strong coupling regime. One of our results in shown in Fig. 6. We show there the spectral function studied on small clusters away from half-filling. It is clearly observed that there is a large peak near the chemical potential even for momenta above $(\pi/2, \pi/2)$ where the Fermi surface for a weakly interacting gas of fermions is. This is the effect predicted by Kampf and Schrieffer, i.e. the presence of an antiferromagnetically induced quasiparticle band in models for the cuprates. Note that the momentum dependence of the results is crucial to distinguish this effect from a simple "lower Hubbard band" formation which would occur even in the atomic limit. For details see Ref. [7].

We have observed that the strength of this effect rapidly dies out away from half-filling, but it can still be "observed" at 15% doping where ξ_{AF} is about a couple of lattice spacings (for the definition of what we label as observable in this context, see Ref. [7]). Then, although we cannot prove that indeed Aebi *et al.*'s results are evidence of the bands caused by antiferromagnetic correlations, at least our theoretical results and their data are *compatible*, namely of the same order of magnitude.

After this rapid description of our main results for the normal state ARPES signal, we should address the superconducting state. Interesting progress has been recently made in this context [8]. Let us first assume that the normal state of the cuprates can be roughly approximated by a gas of weakly interacting quasiparticles with the dispersion calculated, for example, in Fig. 1. This approximation is correct even if there is no long range order, as long as ξ_{AF} is robust enough (i.e. such that a hole feels that it is immersed in a *local* Néel environment). The interaction between holes can also be deduced from the behavior of two holes in an antiferromagnet which has been studied using numerical techniques [9]. The effective interaction amounts to an attraction of strength J which is basically operative over a short distance of roughly one lattice spacing. The study of this model is described elsewhere in this volume by Elbio Dagotto *et al.* and will not be repeated here. Let us just say that when the chemical potential reaches the large peak in the DOS of Fig. 1 at the bottom of the hole band, the critical temperature of the effective model reaches its maximum value. The symmetry of the superconducting order parameter is $d_{x^2-y^2}$ and the T_c is about 100 K at a hole doping of 15% [18]. This model, called the "Antiferromagnetic van Hove" (AFVH) model due to its features combining pairing through a magnetic mechanism with the presence of a large DOS causing a large T_c, is very promising, and currently we are actively investigating its properties. It has already been shown that the Hall coefficient [4] and $2\Delta/kT_c \sim 5$ [8] are in good agreement with experiments.

Finally, note that our results are based on the assumption that the quasiparticle dispersion does not change much with doping near half-filling. Figure 5 provides some evidence supporting it. The key point we need for the AFVH scenario is that the large peak in the DOS observed at half-filling survives as carriers are introduced. In Fig. 7 we show the density of states, $N(\omega)$, vs $\omega - \mu$ using exact diagonalization techniques on clusters of 16 and 18 sites and two and four holes. These results show that a large peak is still present in the DOS, and this peak moves across the chemical potential as the electronic density is changed, giving more support to the AFVH ideas.

Summarizing, recently considerable progress has been made in the understanding of ARPES experimental data using models of correlated electrons. Several unusual features have a natural explanation once strong correlations are properly included in the calculations. Flat bands, antiferromagnetically induced bands, and small bandwidths can be accounted for in this way. These results are difficult to explain with band structure calculations. Even superconduc-

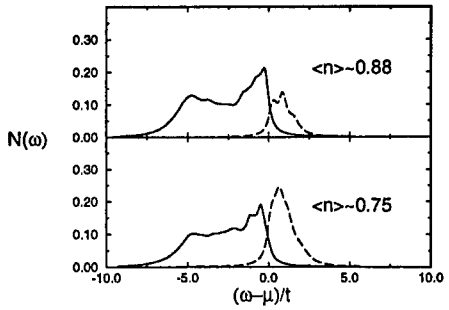


Fig. 7. Density of states of the t–J model obtained with clusters of 16 and 18 sites, at $J/t = 0.4$, and at the electronic densities shown.

tivity in the d-channel is obtained with a T_c of about 100 K.

Acknowledgements—We have benefited from conversations with many colleagues, the list being too large to reproduce here. We warmly thank all of them. The authors are supported by the Office of Naval Research undergrant ONR N00014-93-0495, the donors of the Petroleum Research Fund administered by the ACS, the National High Magnetic Field Lab, and the Supercomputer Computations Research Institute.

REFERENCES

1. Dessau D. S. *et al.*, *Phys. Rev. Lett.* **71**, 2781 (1993); Gofron K. J. *et al.*, *J. Phys. Chem. Solids* **54**, 1193 (1993); Shen Z. -X. and Dessau D. S., preprint (1994); Abrikosov A. A., Campuzano J. C. and Gofron K., *Physica C* **214**, 73 (1993); Ma J. *et al.*, *Phys. Rev. B* **51**, 3832 (1995).
2. Aebi P. *et al.*, *Phys. Rev. Lett.* **72**, 2757 (1994); Osterwalder J. *et al.*, preprint.
3. Wells B. O. *et al.*, *Phys. Rev. Lett.* **74**, 964 (1995).
4. Dagotto E., Nazarenko A. and Boninsegni M., *Phys. Rev. Lett.* **73**, 728 (1994).
5. Nazarenko A., Vos K., Haas S., Dagotto E. and Gooding R., *Phys. Rev. B* **51**, 8676 (1995).
6. Moreo A., Haas S., Sandvik A. and Dagotto E.,*Phys. Rev. B* **51**, 12045 (1995).
7. Haas S., Moreo A. and Dagotto E.,*Phys. Rev. Lett.* **74**, 4281 (1995).
8. Dagotto E., Nazarenko A. and Moreo A., *Phys. Rev. Lett.* **74**, 310 (1995).
9. For a comprehensive review of this issue, see Dagotto E., *Rev. Mod. Phys.* **66**, 763 (1994).
10. Bulut N., Scalapino D. J. and White S. R., *Phys. Rev. Lett.* **73**, 748 (1994).
11. Other papers reporting flat bands are Bulut N., Scalapino D. J. and White S. R., *Phys. Rev. B* **50**, 7215 (1994); Putz R., Preuss R., Muramatsu A. and Hanke W., preprint.
12. Liu Z. and Manousakis E. *Phys. Rev. B* **45**, 2425 (1992).
13. Bulaevskii L. N., Nagaev E. L. and Khomskii D. I., *Zh. eksper. teor. Fiz.* **54**, 1562 (1968); Shraiman B. and Siggia E., *Phys. Rev. Lett.* **61**, 467 (1988). See also Trugman S., *Phys. Rev. Lett.* **65**, 500 (1990) and references therein.
14. Dagotto E. *et al.*, *Phys. Rev. B* **41**, 9049 (1990).
15. Nazarenko A. *et al.*, to be published.
16. Eder R. and Ohta Y., *Phys. Rev. B* **50**, 10043 (1994) and references therein.
17. Kampf A. and Schrieffer J. R., *Phys. Rev. B* **41**,6399 (1990).
18. Note that studies of the one band Hubbard model using a conserving approximation find critical temperatures smaller than 60 K [Monthoux and Scalapino D. J., *Phys. Rev. Lett.* **72**, 1874 (1994)]. The T_cs of the AFVH model are higher. This may reflect on the accuracy of the techniques used, or in some more profound difference between the Hubbard and t–J models.

Pergamon

J. Phys. Chem. Solids Vol. 56, No. 12, pp. 1651–1658, 1995
Copyright © 1995 Elsevier Science Ltd
Printed in Great Britain. All rights reserved
0022-3697/95 $9.50 + 0.00

0022-3697(95)00107-7

$d_{x^2-y^2}$ PAIRING AND SPIN FLUCTUATIONS IN THE CUPRATE SUPERCONDUCTORS: A PROGRESS REPORT

DAVID PINES

Department of Physics, University of Illinois at Urbana-Champaign, 1110 West Green Street, Urbana, IL 61801-3080, U.S.A.

PHILIPPE MONTHOUX

NHMFL & Department of Physics,Florida State University, Tallahassee, FL 32306-4005, U.S.A.

Abstract—We present a simple model calculation of the superconducting pairing potential which makes evident the causal relationship between an effective magnetic interaction between planar quasiparticles which is peaked in momentum space at $Q = \pi/a, \pi/a$, and their transition to a superconducting state with $d_{x^2-y^2}$ pairing. We review recent experimental and theoretical developments which establish the common physical origin of scaling behavior and the spin pseudogap in underdoped systems and consider non-linear feedback effects which could give rise to this behavior in a nearly antiferromagnetic Fermi liquid. We discuss the shortcomings of the present generation of Hubbard model calculations in providing a quantitative account of the normal state magnetic and transport properties, as well as of T_c, and suggest that apart from the SQUID experiments which probe directly the symmetry of the pairing state, measurements of the spin-lattice relaxation times, $^{63}T_1$ and $^{17}T_1$ and the spin-echo decay time, $^{63}T_{2G}$, provide the strongest constraints to date on candidate pairing states. We conclude with a qualitative discussion of the predictions of the magnetic mechanism for the doping dependence of T_c.

1. INTRODUCTION

Some three years ago, in a paper written with Alexander Balatsky, we reported on detailed calculations which supported the proposal that in the cuprate superconductors it is the magnetic interaction between planar quasiparticles which is responsible for their anomalous normal state behavior and high superconducting transition temperature [1]. Our approach differed from the Hubbard Hamiltonian approaches which had been developed earlier [2], and from a contemporaneous approach based on Moriya's self-consistent renormalization theory [3], in that we did not attempt to derive the magnetic quasiparticle interaction and pairing potential from a particular model (a daunting task, both then and now), but chose instead to go directly to what we felt was the heart of the matter: could a spin-fluctuation-induced interaction whose wave vector and frequency dependence was determined by fits to NMR experiments, acting between quasiparticles whose spectrum was determined by fits to ARPES experiments, give rise to the measured normal state resistivity and a high T_c? We found, in a weak coupling calculation, that it could, and that the resulting pairing state had to possess $d_{x^2-y^2}$ symmetry.

However, both this work, and that of Moriya *et al.* [3], left open the question of whether the spin fluctuation mechanism was really viable for high temperature superconductors, since the measured quasiparticle lifetime is quite short ($\hbar/\tau \sim kT$), and the lifetime effects neglected in a weak coupling calculation were expected to reduce T_c dramatically. Indeed, while earlier conserving strong coupling calculations based on the Hubbard model [4] had led to a maximum T_c of order 60 K, such a high T_c was found only for a physically unrealistic hole doping level quite close to half-filling; markedly lower transition temperatures occur if the hole doping is increased, a trend opposite to that found experimentally. The Hubbard-based approach thus seemed capable, at best, of explaining superconductivity in the 2-1-4 system, and could not be expected to provide a quantitative account of the 1-2-3 system, or the Bi and Tl based cuprate superconductors.

We therefore took the necessary next step, carrying out a strong coupling (Eliashberg) calculation of the normal state properties and T_c for $YBa_2Cu_3O_7$ using the model experiment-based planar quasiparticle interaction

$$V_{\rm mag}^{\rm eff}(q, \omega) = g^2\chi(q, \omega)\sigma_1 \cdot \sigma_2. \tag{1}$$

where $\chi(q, \omega)$ takes the form, first proposed by Millis, Monien and Pines [5] (hereafter MMP)

$$\chi_{\rm MMP}(q, \omega) = \frac{\chi_Q}{1 + (Q - q)^2\xi^2 - i\omega/\omega_{\rm SF}}, \tag{2}$$

which provides a quantitative fit to the existing NMR data.

NMR experiments require that $\chi(q, \omega)$ be peaked at the commensurate AF ordering wave vector, ($Q = \pi/a, \pi/a$) and that its behavior be dominated by wave vectors in the vicinity of Q. Indeed, for systems for which measurements have been made of the anisotropic spin-lattice relaxation time, $^{63}T_1$, and the spin-echo decay time, $^{63}T_{2G}$, the three parameters which characterize $\chi_{\rm MMP}(q, \omega)$ can all be determined from experiment [χ_Q, the static staggered magnetic susceptibility, ξ, the antiferromagnetic correlation length

(assumed $\lesssim$ the lattice spacing, a), which measures the fall-off of the static susceptibility as one moves away from $\boldsymbol{Q}$, and ω_{SF}, the frequency of the relaxational mode at or near $\boldsymbol{Q}$, which is quite generally very small compared to the quasiparticle Fermi energy or bandwidth ($\sim$ eV)].

We found that when the full structure of the quasiparticle interaction specified by eqns (1) and (2) is taken into account, although lifetime effects do lead to a dramatic reduction in T_c, for parameters appropriate to $YBa_2Cu_3O_7$ a superconducting transition into a $d_{x^2-y^2}$ pairing state occurs at $T_c \sim 90$ K for comparatively modest values of the coupling constant g [6]. For this same range of coupling constants our calculated resistivity and optical properties were in quantitative agreement with experiment, so that a bridge was built between the measured anomalous normal state charge response, the anomalous normal state spin response, and $d_{x^2-y^2}$ superconductivity at high temperatures [7]. Our calculations thus provided, for fully doped systems such as $YBa_2Cu_3O_7$, a proof of concept of the proposal [8] that the measured anomalous spin and charge properties of the normal state are those of *nearly antiferromagnetic Fermi liquids*, which find their physical origin in the novel magnetic low energy scale, ω_{SF}, brought about by the strong commensurate antiferromagnetic correlations between the quasiparticles.

As we have frequently emphasized, despite this theoretical support for the magnetic mechanism, since our nearly antiferromagnetic Fermi liquid approach predicts unambiguously that the superconducting state of $YBa_2Cu_3O_7$ must possess $d_{x^2-y^2}$ symmetry, experimental detection of that pairing state is a *necessary* condition for the magnetic mechanism to explain high T_c. Following a discussion of some relevant recent theoretical and experimental developments concerning the normal state, we discuss the current experimental evidence for $d_{x^2-y^2}$ pairing and conclude with a qualitative explanation of the doping dependence of T_c.

2. THE EFFECTIVE PAIRING POTENTIAL

We consider the effective pairing potential, eqn (1), and focus on $V_{\rm eff}(\boldsymbol{q}, 0)$, since it determines the dimensionless coupling constant, λ, in the Eliashberg approximation. We further assume a simple model for $\chi(\boldsymbol{q}, 0)$, in which it possesses either four sharp incommensurate peaks,

$$\chi(\boldsymbol{q}, 0) = \sum_{i=1}^{4} \frac{\chi_{\boldsymbol{q}_i}}{4} \delta_{\boldsymbol{q},\boldsymbol{q}_i} \tag{3}$$

where

$$\begin{aligned} \boldsymbol{q}_1 &= \pi(1-\delta, 1); \\ \boldsymbol{q}_2 &= \pi(1+\delta, 1); \\ \boldsymbol{q}_3 &= \pi(1, 1-\delta); \\ \boldsymbol{q}_4 &= \pi(1, 1+\delta) \end{aligned} \tag{4}$$

or, when $\delta = 0$, one sharp commensurate peak. An expression of the form, eqn (3), with four incommensurate peaks at $\chi_{q_1} = \chi_{q_2} = \chi_{q_3} = \chi_{q_4} = \chi_{q_{max}}$, is what one obtains with the Hubbard model, in the limit of strong AF correlations. For eqn (3), it is trivial to calculate the pairing potential in configuration space, $V_{eff}(\boldsymbol{x}, 0)$. If $\boldsymbol{x} \equiv (n_x, n_y)$ describes a point on the lattice, where n_x and n_y are integers, then,

$$V_{\rm eff}(\boldsymbol{x}, 0) = \frac{g^2 \chi_{q_{max}}}{2} (-1)^{n_x+n_y} [cos(\pi\delta n_x) + cos(\pi\delta n_y)] \tag{5}$$

The interaction is thus maximum and repulsive at the origin, while at the nearest-neighbor sites $(\pm 1, 0)$ and $(0, \pm 1)$

$$V_{\rm eff} = -\frac{g^2 \chi_{q_{max}}}{2} [1 + cos(\pi\delta)]. \tag{6}$$

Evidently, the interaction is most attractive when $cos(\pi\delta) = 1$, i.e. when $\delta = 0$ and one has a commensurate spin-fluctuation spectrum. At longer distances, $V_{\rm eff}$ is cut off by the finite correlation length that this simple model ignores, so the main contribution to λ really comes from the nearest-neighbor term (especially for $YBCO_7$ with $\xi \simeq 2$).

It is this on-site repulsion, plus the effective attraction between the nearest neighbors, which is responsible for d-wave pairing; in this pairing state quasiparticles, by virtue of their $l = 2$ relative angular momentum, avoid sampling the on-site repulsion while taking advantage of the attraction between nearest neighbors to achieve superconductivity. That the pairing state must be $d_{x^2-y^2}$ follows from the fact that along the diagonals in configuration space (where $n_x = \pm n_y$), the effective pairing potential, eqn (5), is always repulsive for $n_x \lesssim \xi$, and not too large a discommensuration, δ; hence it is energetically favorable to place the nodes of the gap parameter,

$$\Delta = \Delta_0(\cos k_x a - \cos k_y a) \tag{7}$$

along these same diagonals, since for that pairing state the effective repulsion, which would otherwise be deleterious for superconductivity, is rendered harmless. The same argument shows that if $\delta \sim \pi$, it is the pairing potential along the (1,0) and (0,1) directions that is always repulsive; the pairing state is then d_{xy}, the peaks in χ_q being rotated by 90°.

The above simple model calculation explains why as long as the $\boldsymbol{q}_i$'s in eqns (3) and (4) span the Fermi surface, which appears to be the case for all cuprate superconductors, an effective magnetic interaction which possesses incommensurate peaks will be less effective than one which is peaked at $\boldsymbol{Q}$ in bringing about superconductivity. It also explains why Hubbard calculations of T_c show a T_c which is maximum near half-filling, falling off as the doping increases, since an elementary calculation for the Hubbard model shows that $\delta = 0$ at half-filling, and increases with increased doping.

To see this in more detail, note that in Hubbard calculations [9] the effective magnetic interaction between quasiparticles can be written as $(3/2)U^2\chi_H(\boldsymbol{q}, \omega)$, with

$$\chi_H(\boldsymbol{q}, \omega) = \frac{\tilde{\chi}_0(\boldsymbol{q}, \omega)}{1 - \tilde{U}\tilde{\chi}_0(\boldsymbol{q}, \omega)} \tag{8}$$

where $\tilde{\chi}_0(\boldsymbol{q}, \omega)$ is the non-interacting spin–spin correlation function specified by $\varepsilon_p = -2t[\cos p_x + \cos p_y] - 4t' \cos p_x \cos p_y$ and $\bar{U}$ is the screened Hubbard repulsive on-site potential. Since $\bar{U}$ has no structure, the peaks of χ_H are simply those of $\tilde{\chi}_0(\boldsymbol{q}, \omega)$. Consider then the low frequency behavior of χ_H. At half-filling $\tilde{\chi}(\boldsymbol{q}, 0)$ is peaked at $\boldsymbol{Q}$; as one moves away from half-filling, the peaks of $\tilde{\chi}_0(\boldsymbol{q}, 0)$ become increasingly discommensurate, so that $\tilde{\chi}_0(\boldsymbol{Q}, 0)$ becomes a local mimimum. Indeed, with $t' = 0$ (an assumption often made for simplicity in early Hubbard calculations), at realistic hole concentrations $\tilde{\chi}_0''(\boldsymbol{Q}, \omega) = 0$, for $\omega \leq 2\mu$, since $\boldsymbol{Q}$ cannot span the Fermi surface. This has strong consequences for attempts to use over simplified Hubbard models to fit NMR experiments.

Until recently it was generally believed, on the basis of neutron scattering experiments [10], that while $\chi''(\boldsymbol{q}, \omega)$ was peaked at $\boldsymbol{Q}$ for the 1-2-3 system, for the 2-1-4 system the peaks were incommensurate, being specified by eqn (4),with $\delta = 0.56x$, an effect which was attributed in Hubbard calculations to the somewhat different band structure of this system ($t' = -.15$t rather than $t' = -.45$t). However, as discussed by Barzykin *et al.* [11], the recent NMR experiments of Walstedt *et al.* [12] on the ^{17}O spin-lattice relaxation rate in $La_{1.85}Sr_{0.15}CuO_4$ [which confirmed the earlier measurements of Reven *et al.* [13], show that the peaks for this system must also be commensurate, in which case the incommensuration picked up in neutron scattering, a global probe, represents domain superstructure rather than an intrinsic incommensuration. Further indications of the underlying similarities between the 1-2-3 and 2-1-4 systems come from the NMR and transport experiments we now consider.

3. SPIN AND CHARGE RESPONSE: SOME RECENT DEVELOPMENTS

Experiment now demonstrates that, contrary to the early belief by many theorists that charge and spin are separated in the Cu–O planes, there is an intimate relationship between the anomalous transport properties and the anomalous low frequency magnetic properties of the underdoped cuprate superconductors. Transport experiments on untwinned crystals of $YBa_2Cu_3O_{6.6}$ [14] and single crystals of $YBa_2Cu_4O_8$ [15] show that within experimental uncertainties the planar resistivity in the a crystallographic direction (which has no "chain" contribution) changes its character at the same temperature, T_*, as the spin-lattice relaxation rate, $^{63}T_1$, changes its character. These results which, as discussed below, have been extended to the 2-1-4 system [16][17], establish the inseparability of the spin and charge behavior of the planar excitations and provide direct experimental confirmation of the thesis that the anomalous charge behavior in the underdoped system arises from the magnetic interaction between the quasiparticles.

Much has also been learned recently about the spin pseudo-gap and the low frequency magnetic behavior of the superconducting cuprates. The present generation of NMR experiments includes measurements of the spin-echo decay time, T_{2G}, at three doping levels; $YBa_2Cu_3O_7$ [18], $YBa_2Cu_3O_{6.63}$ [19], and $YBa_2Cu_4O_8$ [20] in the 1-2-3 system as well as for the insulator, La_2CuO_4 [21]. These results have been used to demonstrate that quantum critical $z = 1$ scaling behavior, in which $\omega_{SF} = (\hat{c}/\xi)$, is found above a characteristic temperature T_*, in the underdoped cuprates [22], while Barzykin and Pines [23] have established that the maximum in the uniform susceptibility is found at a temperature close to the upper limit, T_{cr}, of scaling behavior, and discussed the link between scaling and spin pseudo-gap behavior. The magnetic phase diagrams which they obtain for the 1-2-3 and 2-1-4 systems make it evident that the spin pseudo-gap and magnetic scaling are not brought about by interplanar coupling, while the recent analysis of resistivity and Hall effect experiments on the 2-1-4 system by Hwang *et al.* [16] and Nakano *et al.* [17] show that for the 2-1-4 system changes in spin behavior are likewise accompanied by changes in charge behavior. A further indication that the anomalous spin and charge behavior are linked and that both originate in quasiparticle behavior comes from the work of Zha *et al.* [24] who show that by using a temperature dependent quasiparticle density of states taken from Knight shift measurements, one can arrive at a quantitative understanding of the way in which *c*-axis resistivity and optical measurements on both the 2-1-4 and 1-2-3 systems reflect the behavior of planar quasiparticles.

4. NON-LINEAR FEEDBACK EFFECTS

From a Fermi liquid perspective, the only way magnetic scaling and spin pseudo-gap behavior can come about is through a non-linear feedback of the magnetic interaction on the quasiparticles which are in turn the source of that interaction. We first review the non-linear feedback effects at work above T_{cr} and when the system goes superconducting [25], and then consider how similar effects in the normal state could lead to magnetic scaling and spin-pseudo gap behavior below T_*.

As one begins to approach the antiferromagnetic instability, strong coupling effects play a crucial role in stabilizing the normal, nearly antiferromagnetic Fermi liquid state. For instance, in the context of the fluctuation exchange approximation to the 2D Hubbard model [25], if the particle–hole "bubble" χ_0 were calculated using free particle propagators, the expression $1 - U\chi_0(\mathbf{q}, 0)$ in the denominator of the spin-fluctuation mediated interaction would vanish at a rather high temperature for a wave vector near (π, π). However, when this quantity is evaluated using self-consistently dressed Green's functions it is reduced; the Eliashberg renormalization factor Z is > 1, and the resulting negative feedback stabilizes the interaction in the normal state very close to the antiferromagnetic instability.

For instance, assume one were to reduce Z slightly below its self-consistent value. χ_0 would then increase, resulting in a denominator $1 - U\chi_0(q_{max}, 0)$ closer to zero and thus an enhanced spin-fluctuation mediated interaction, which would in turn lead to an increase in the strong coupling renormalization factor Z, restoring it to its self-consistent value. If one the other hand, one were to increase Z slightly above its self-consistent value, χ_0 would be reduced, leading to a decrease of the spin-fluctuation mediated interaction. This decrease would in turn cause a reduction of the renormalization factor Z back to its self-consistent value. Since a comparatively small change in $\chi_0(\mathbf{q}, 0)$ leads to a large enhancement or reduction of the spin-fluctuation mediated interaction through the denominator $1 - U\chi_0(\mathbf{q}, 0)$ when one is close to the antiferromagnetic instability, this negative feedback effect is very strong.

As the system becomes superconducting, since the pairing interaction is mediated by the same electrons which are pairing, there is another feedback effect due to the interplay between the pairing interaction and the formation of a gap in the quasiparticle spectrum. As the gap opens, there is a shift in the spin-fluctuation spectral weight, and thus a suppression of the low frequency spin-fluctuations which, in the normal state give rise to the comparatively short quasiparticle lifetime and make a significant contribution to the Eliashberg renormalization factor Z. However, because one is close to the antiferromagnetic instability, the negative feedback effects present in the normal state now insure that the strength of the pairing interaction remains essentially constant.

A second feedback effect is related to the influence of the low frequency spin-fluctuation excitations on the energy gap. At T_c, these low lying spin-fluctuations also suppress the gap via inelastic scattering. As the gap opens and the low-frequency spin fluctuation spectral weight is reduced, the inelastic scattering processes are suppressed, resulting in an increase in the gap parameter. The increase in the gap in turn leads to a further suppression of the low frequency spin-fluctuation spectral weight. This *positive* feedback, along with the fact that the strength of the pairing interaction remains constant, is responsible for the rapid increase of the gap just below T_c and the large gap ratio $2\Delta/T_c$. Moreover, since the contribution of small momentum transfers to the quasiparticle self-energy is negligible, the negative feedback effects which operate near (π, π) are not operative at long wavelengths. Hence, at $q = 0$, there is nothing to oppose a rapid opening up of the superconducting gap and the long wavelength, static susceptibility is strongly suppressed.

The above considerations suggest the following scenario for feedback effects in a NAFL as the temperature decreases from above T_{cr} to T_c. Above T_{cr},the strong coupling negative feedback gives rise to the measured mean field non-universal behavior, with ξ^{-2} displaying Curie–Weiss behavior. Below T_{cr}, one has weak spin pseudogap behavior, manifested in the linear in T *decrease* of the quasiparticle density of states per unit energy and $\chi_0(T)$. The opening of the spin pseudogap produces $z = 1$ magnetic scaling and alters the temperature dependence of ξ, so that it is now ξ^{-1} which displays Curie–Weiss, linear in T, behavior. At T_*,we conjecture that the spin pseudogap exceeds some threshold value: one gets a crossover from weak spin pseudogap to strong pseudogap behavior so that below T_* the system behaves much as it does below T_c. The negative feedback operative at wave vectors in the vicinity of $(\pi/a, \pi/a)$ acts to freeze the antiferromagnetic correlations, while at long wavelengths there is nothing to oppose the rapid opening up of the spin pseudogap, so that both the quasiparticle density of states and $\chi_0(T)$ fall at a rapid rate between T_* and T_c, while ω_{SF}, in general, reaches a minimum, and then increases as the temperature is further decreased, producing the measured peak in $(^{63}T_1T)^{-1}$.

5. THE EXPERIMENTAL EVIDENCE FOR $d_{x^2-y^2}$ PAIRING

At a time (mid-1989) when it was generally believed that μsr and other measurements of the penetration depth demonstrated that the pairing state must be that of a conventional BCS superconductor, with a finite gap everywhere on the Fermi surface [26], there was already a glitch in the conventional superconductivity scenario: the NMR experiments on the ^{63}Cu spin-lattice relaxation rate [27] and Knight shift [28] measurements were far more easily understood if the gap contained a line of nodes. Thus Monien and Pines [29] showed that the results for the Knight shift and $^{63}T_1$ in the superconducting state could be fit quantitatively using a d-wave gap function which incorporates strong coupling corrections, with $\Delta(T = 0) \sim 5kT_c$. A similar conclusion for T_1 measurements was reached by Bulut and Scalapino on the basis of Hubbard calculations [30]. During the next few years, a second glitch appeared; Annett, Goldenfeld and Renn examined the symmetries allowed by the crystal structure of the cuprate superconductors and called attention to the fact that a T^2 power law provided a better fit to the penetration depth experiments than could be obtained with an exponential fit at low temperatures; they suggested that $d_{x^2-y^2}$ pairing plus impurity scattering might provide a consistent account of experiment [31]. Some two years later Shen *et al.* found an anisotropic gap in angle resolved photoemission studies on Bi2212 samples which was qualitatively consistent with $d_{x^2-y^2}$ pairing [32]. Still, many continued (and some still continue) to believe in the s-wave pairing state which was the natural consequence of a phonon-induced quasiparticle interaction.

Indeed, it was not until two years ago, at the previous meeting of this group in Santa Fe, that one had a special session on the nature of the pairing state, beginning with the report by Charlie Slichter [33] on the measurements by his group on very pure samples of $YBa_2Cu_3O_7$ which showed an anomalous temperature dependence of both the anisotropy of the ^{63}Cu spin-lattice relaxation rate and the

ratio, ($^{63}T_1/^{17}T_1$), and the report by Walter Hardy on measurements by his group [on $YBa_2Cu_3O_7$ samples of comparable purity] of a linear temperature dependence of the penetration depth [34]. At this session, one of us [35] reported on the calculations which showed that one could obtain a quantitative fit to *both* of these experimental results with $d_{x^2-y^2}$ pairing, by using a realistic Fermi surface and a realistic magnetic interaction between planar quasiparticles [36][37]. Doug Scalapino reported on the extent to which Hubbard calculations were likewise consistent with experiment [38], while Phil Anderson continued to express in strong terms his scepticism concerning the magnetic mechanism and the relevance of numerical experiments to an understanding of high T_c [39].

In some sense, the Santa Fe Conference marked the onset of a phase transition in the field; during the past two years the number of experiments which support $d_{x^2-y^2}$ pairing has increased some ten-fold, while those which do not support it can still be counted on the fingers of one hand. Thus at the recent Grenoble meeting, one of us listed some fifteen experiments on clean samples and nine experiments on "dirty" samples which provided strong evidence for $d_{x^2-y^2}$ pairing [40]. We comment on some of these briefly.

First, the pioneering SQUID measurements of a change in phase of the order parameter as one goes from the *a* direction to the *b* direction of an $YBa_2Cu_3O_7$ crystal by Wollman and Van Harlingen [41] (discussed by Wollman [42] at this meeting), provide direct confirmation that the pairing states possesses primarily $d_{x^2-y^2}$ symmetry. These have been repeated and extended by many other groups; the current upper limit for the non $d_{x^2-y^2}$ component of the pairing state is some 3% (Kirtley *et al.* [41]. Second, the Hardy group measurements of the penetration depth, which have been extended to untwinned single crystals of $YBa_2Cu_3O_7$ and $YBa_2Cu_4O_8$, and to $YBa_2Cu_3O_{6.63}$, demonstrate for some samples a linear temperature dependence down to temperatures as low as 2 K; these place a strong upper limit on the size of any energy gap, but do not rule out an anisotropic *s*-wave state which otherwise resembles the $d_{x^2-y^2}$ gap function. Third, the NMR experiments of the Slichter group provide a more stringent test, since Thelen [37] finds that with an anisotropic *s*-wave state which differs from the $d_{x^2-y^2}$ state only in the changed coherence factors, the quantitative fit to experiment obtained by Thelen *et al.* [36] for the $d_{x^2-y^2}$ pairing state goes away; the calculated results differ significantly from experiment. To account for the quantities measured in NMR experiments, the three spin-lattice relaxation rates, [$(^{63}T_1)_\parallel$), $(^{63}T_1)_\perp$,$^{17}T_1$], the spin echo decay rate, T_{2G} (which has now been measured for $YBa_2Cu_4O_8$ [20]), and the ^{63}Cu Knight shift in the superconducting state, one has to get *everything* right: the Shastry–Mila–Rice form factors, the quasiparticle Fermi surface, the strong coupling corrections to the gap function, *and* the coherence factors which depend on the pairing state. Remove any of these, and agreement with experiment disappears. For example, Bulut and Scalapino [43], find with a $d_{x^2-y^2}$ pairing state, and a gap function consistent with the Knight shift results and correct form factors, that the calculated anomalous temperature dependence of the anisotropy of $^{63}T_1$ agrees with experiment, but obtain the wrong temperature dependence for $^{17}T_1/^{63}T_1(T)$ in the superconducting state because they used a Fermi surface which did not incorporate the influence of next nearest neighbor hopping on the Fermi surface. To our knowledge, apart from the calculations of Thelen *et al.* [36], no other group has succeeded in obtaining agreement with experiment for these spin lattice relaxation rates; thus it would seem that these NMR experiments provide an unusually strong set of constraints on candidate pairing theories and Fermi surfaces.

The issue of "dirty *d*-wave" superconductivity was also first discussed two years ago at Santa Fe. A frequently expressed concern about the magnetic mechanism had been that, in contrast to what was seen experimentally, T_c would be quite sensitive to the presence of impurities. One of us reported at Santa Fe on strong coupling calculations which showed that insofar as lifetime effects were concerned, this was not the case. The influence of elastic impurity multiple scattering on normal state quasiparticle properties and T_c was small, essentially because the influence of inelastic scattering against spin fluctuations is so much larger [44].

Of particular interest is the remarkably different influence of Zn and Ni impurities (which enter substitutionally at planar Cu sites) on both T_c and the low temperature superconducting properties of the 1-2-3 system. The NMR experiments of Ishida *et al.* on ^{63}Cu spin-lattice relaxation times in doped $YBa_2Cu_3O_7$ [45] tell us that substituting Zn for Cu has a significant impact on the neighboring Cu^{2+} spins, while Ni substitution leads to no perceptible change in ^{63}Cu spin-lattice relaxation times. Zn has a closed shell, so when it substitutes for a Cu^{2+} spin, it goes in as a "vegetable": the local magnetic order is destroyed, since nearby Cu^{2+} spins will see a different local environment over distances comparable to the correlation length. Substituting Ni on the other hand leads to no measurable change in the local magnetic environment. These two impurities will then present quite different scattering potentials for planar quasiparticles. Because Zn substitution affects a large number of Cu^{2+} spins, the corresponding effective scattering potential will be strong, requiring that multiple scattering effects be included in calculating its influence on quasiparticles (a "t" matrix description of the scattering act rather than the Born approximation); moreover the potential possesses a finite range, comparable to ξ. Taken together, these effects led us to conclude that Zn will always act as an unitary scatterer. By contrast, the corresponding Ni impurity potential will be local (only in its immediate vicinity does a quasiparticle recognize a changed environment); the influence of Ni may be treated in the Born (weak potential scattering) approximation.

Consider now their relative impact on the superconducting transition temperature, T_c, of $YBa_2Cu_3O_7$. Our strong coupling calculations [46], which incorporate multiple scat-

tering, enable us to classify scatterers in terms of their impact on T_c. We find, in the unitary limit,

$$(\Delta T_c/T_c) \sim 9n_U \tag{9}$$

where n_U is the concentration (in %) of "unitary limit" scatterers. Since experimentally

$$(\Delta T_c/T_c) \sim 3.9n_{Ni} \tag{10}$$

we conclude Ni is a sub-unitary scatterer. For Zn, on the other hand, experiment tells us that

$$(\Delta T_c/T_c) \cong 12.6n_{Zn} \tag{11}$$

Zn is therefore a "superunitary" scatterer, which means that it does more than bring about the maximum modification in T_c associated with a "$1/\tau$" change in quasiparticle energy (á la Abrikosov and Gor'kov). Thus, on the basis of its influence on T_c alone, one could argue, in accord with the above physical picture, Zn must change the pairing potential responsible for superconductivity.

The results on the quite different influence of Zn and Ni planar impurities provide the "smoking gun" for the magnetic mechanism, analogous to the isotope effect which served as a smoking gun for a phonon-induced interaction leading to superconductivity in conventional superconductors. What the isotope effect showed was that changing the phonon spectrum, without otherwise altering system properties, led to a significant change in T_c. We have seen that Zn changes the local magnetic order while Ni does not, hence the fact that for comparable concentrations Zn reduces T_c some four times more effectively than Ni *can only be attributed to its influence on the local magnetic order*, and hence on the magnetic pairing potential. Put another way, were the pairing potential of nonmagnetic origin, the effect of the two different impurities on T_c would be comparable. It is not. Therefore the pairing potential possesses a magnetic origin: QED.

We turn now to the low temperature superconducting properties. It was remarked early on, in the study of heavy electron superconductors, that for a gap function with nodes, the properties of the quasiparticles which congregate there at low temperatures will be quite sensitive to the presence of impurities [47]. For the present case of $d_{x^2-y^2}$ pairing in the cuprate superconductors, Lee [48], Hirschfield and Goldenfeld [48], and Hotta [48], have shown that in the unitary limit of strong multiple scattering at low temperatures and low frequencies the quasiparticle density of states per unit energy shifts from an $N(\omega)$ which is linear in ω to a constant value, $N_i(0)$, producing quadratic behavior in $N_0(T)$. The cross-over from quadratic behavior at low temperatures to linear behavior occurs at a temperature $T^* \sim \gamma$, the impurity-induced quasiparticle scattering rate. For zero range impurity scattering, $N_i(0) \sim n_i^{1/2}$; for the finite range ($\sim \xi$) impurity potentials produced by imperfections which destroy local magnetic order, one enters a quasi-one-dimensional region of quasiparticle scattering, with $N_i(0) \sim n_i$, at comparatively low impurity concentrations [49]. Taken together with our calculations which show that Zn is a unitary scatterer, Ni a sub-unitary scatterer, these calculations explain the results reported by Kitaoka on the vastly different influence of Ni and Zn impurities on the low temperature Knight shift and spin-lattice relaxation rates [50], as well as those of Bonn *et al.* [51] on the influence of these impurities on the low-temperature behavior of the penetration depth. Both experiments show that a quite modest concentration of Zn impurities ($\sim 0.3\%$) act to alter the low temperature behavior of $\lambda(T)$ and $\chi_0(T)$ from the linear dependence on T predicted by $d_{x^2-y^2}$ pairing for a clean superconductor to a quadratic dependence, while comparable concentrations of Ni impurities produce no effect.

Our argument about Zn impurities can easily be generalized; we predict that *any* imperfection (extrinsic *or* intrinsic) which destroys local magnetic order will act as a unitary scatterer in its influence on $\lambda(T)$, $\chi_0(T)$, etc. The superstructure found in even the "best" samples of $Bi_2Sr_2CaCu_2O_8$, gives rise to just such a class of intrinsic imperfections, whose effect is clearly visible in low temperature Knight shift and $^{63}T_1$ measurements on $Bi_2Sr_2CaCu_2O_8$ [52]. A second example is provided by thin film experiments which show that even in the best thin films $\lambda(T)$ displays T^2 behavior at low temperatures. The 2-1-4 system may provide a third such example. If, as the theoretical calculations of Martin [53] and the experiments of Hammel [54] suggest, a certain fraction of the holes introduced by Sr doping are localized on nearly planar Cu^{2+} sites, these holes will destroy local magnetic order. As a result, even in the "best" samples of $La_{1.85}Sr_{0.15}CuO_4$, the concentration of such localized holes may be sufficient to destroy any obvious signatures of the nodal structure of a "clean" $d_{x^2-y^2}$ superconductor, an effect we have proposed, with Balatsky [55], as an explanation of the neutron scattering results of Mason *et al.* [10] on this system.

6. DOPING DEPENDENCE OF T_c

In what follows, we give mostly qualitative arguments on how one can begin to understand the doping dependence of T_c on the basis of the magnetic mechanism we have proposed. We begin by making use of the simple arguments given in Section 2 and the results of Monthoux and Scalapino [56] who studied the change in T_c produced by small changes in the spin-fluctuation spectral weight at various frequency and momentum transfers. We have seen that T_c is increased when spectral weight is shifted to large momentum transfers, preferably $\boldsymbol{Q} = (\pi, \pi)$ if this wave vector spans the Fermi surface. Monthoux and Scalapino have shown that since Anderson's theorem does not apply for a d-wave order parameter, low frequency, quasi-static spin-fluctuations ($\omega < T_c$), basically act as impurities and are pair breaking, even at $\boldsymbol{Q} = (\pi, \pi)$. Thus T_c increases if

spectral weight is removed from the low frequency, $\omega < T_c$, region. On the other hand, if spectral weight is removed from the frequency region above T_c for wave vectors near $\boldsymbol{Q} = (\pi, \pi)$, T_c is strongly suppressed.

Consider now the influence of the spin pseudogap on T_c. NMR and neutron scattering experiments show that for wavevectors near (π, π), the pseudogap suppression of the spin fluctuation spectral weight occurs for $(\omega, T) \lesssim T_{cr}$, the temperature which marks the onset of pseudogap behavior. T_{cr}, which is $\gtrsim T_c$ at doping levels appropriate to $YBa_2Cu_3O_7$, and increases rapidly as the doping level decreases, with $(T_{cr}/T_c) \sim 10$ for $La_{1.85}Sr_{0.15}CuO_4$ [23]. Hence as the doping level decreases, the pseudogap removes more and more of the "good" spin fluctuation spectral weight $(T_c \lesssim \omega \lesssim T_{cr})$, while the removal of spectral weight for $\omega \lesssim T_c$, which enhances T_c, plays an increasingly less important role.

What happens when one reaches the fully doped or overdoped regime of hole concentrations $\gtrsim$ those found in $YBa_2Cu_3O_7$, for which there are no longer any spin pseudogap effects? Here the numerical experiments we carried out for fully doped systems [6][7] provide a guide to the change in T_c as one goes from the Y based systems to the Tl and Bi-based systems. These showed that increasing the hole concentration and decreasing ξ act to increase T_c, a scenario which is consistent with NMR results for the Tl and Bi-based superconductors, and which may apply to the Hg-based system as well, although information on magnetic correlations in the latter materials is not yet available. This process continues until one reaches values of $\xi \lesssim a$, after which T_c drops quite suddenly. The simple argument we gave in Section 2 explains this last result. As ξ becomes smaller and smaller, the pairing interaction becomes more and more local, up to the point where only the on-site potential is appreciably different from zero. But since the $d_{x^2-y^2}$ order parameter vanishes at the origin, there is no more pairing in the $d_{x^2-y^2}$ channel and T_c drops to zero.

7. CONCLUDING REMARKS

The well-documented close approach of the cuprate superconductors to antiferromagnetism, the evidence from NMR experiments that the effective magnetic interaction betwen planar quasiparticles is both strong and peaked at $\boldsymbol{Q}$, the demonstration that such an interaction leads naturally to $d_{x^2-y^2}$ pairing, our"proof of concept" that it can yield a $T_c \sim 90$ K in $YBa_2Cu_3O_7$, and our qualitative arguments on the doping dependence of T_c, provide both back-of-the-envelope and detailed theoretical support for the view that the magnetic mechanism provides not only the simplest, but also the most natural, explanation for the appearance of $d_{x^2-y^2}$ superconductivity in the cuprates, and that the measured variation in both normal state and superconducting properties arises primarily from changes in hole doping in the Cu–O planes. There is also a "smoking gun" for the magnetic mechanism: changing the local magnetic order (by substituting Zn for Cu atoms in the plane) produces a change in T_c significantly greater then that found by substituting an impurity (such as Ni) which does not influence the local magnetic order. Taken together with the recent outpouring of experiments on both very clean and dirty samples which support $d_{x^2-y^2}$ pairing, the case for a magnetic quasiparticle interaction leading to a $d_{x^2-y^2}$ pairing becomes a remarkably strong one.

Acknowledgements—It gives us pleasure to thank Bob Corey, Takashi Imai, and Charlie Slichter for communicating their results to us in advance of publication and our collaborators and colleagues in Tallahassee, Urbana, Santa Barbara, and Los Alamos for stimulating discussions on these and related topics. This work has been supported by the Science and Technology Center for Superconductivity under NSF Grant DMR91-20000. The support for P.M. is provided by the State of Florida's E and G funding.

REFERENCES

1. Monthoux P., Balatsky A. and Pines D.,*Phys. Rev. Lett.* **67**, 3448 (1991); *Phys. Rev. B* **46**, 14803 (1992).
2. Bickers N. E., Scalapino D. J. and Scalettar R. T., *Inter. J. Mod. Phys. B* **1**, 687 (1987). For further references and a detailed recent review of Hubbard calculations, see Dagotto E., *Rev. Mod. Phys.* **66**, 763 (1994).
3. Moriya T., Takahashi Y. and Ueda K., *J. Phys. Soc. Jpn.* **59**, 2905 (1990).
4. Bickers N. E., Scalapino D. J. and White S. R., *Phys. Rev. Lett.* **62**, 961 (1989).
5. Millis A. J., Monien H. and Pines D., *Phys. Rev. B* **42**, 167 (1990).
6. Monthoux P. and Pines D., *Phys. Rev. B* **47**, 6069 (1993).
7. Monthoux P. and Pines D., *Phys. Rev. B* **49**, 4261 (1994).
8. Pines D., in *High Temperature Superconductivity* (Edited by K. S. Bedell *et al.*), p. 392. Addison-Wesley, New York (1990).
9. Bulut N. and Scalapino D. J., *J. Chem. Phys. Solids* **54**, 1109 (1993).
10. Mason T. E. *et al.*, *Phys. Rev. Lett.* **71**, 919 (1993).
11. Barzykin V., Pines D. and Thelen D., *Phys. Rev. B* bf 50, 16052 (1994).
12. Walstedt R. *et al.*, *Phys. Rev. Lett.* **72**, 3610 (1994).
13. Reven L. *et al.*, *Phys. Rev. B* **43**, 10466 (1991).
14. Ito T., Takenako K. and Uchida S., *Phys. Rev. Lett.* **70**, 3993 (1993).
15. Bucher B. *et al.*, *Phys. Rev. Lett.* **70**, 2012 (1993).
16. Hwang H. Y. *et al.*, *Phys. Rev. Lett.* **72**, 2636 (1994).
17. Nakano T. *et al.*, *Phys. Rev. B* **49**, 16000 (1994).
18. Imai T. *et al.*, *Phys. Rev. B* **47**, 9158 (1993).
19. Takigawa M., *Phys. Rev. B* **49**, 4158 (1994).
20. Corey R. *et al.*, preprint.
21. Imai T. *et al.*, *Phys. Rev. Lett.* **70**, 1002 (1993).
22. Sokol A. and Pines D., *Phys. Rev. Lett.* **71**, 2813 (1993); Barzykin V. *et al.*, *Phys. Rev. B* **49**, 1554 (1994).
23. Barzykin V. and Pines D., preprint.
24. Zha Y., Cooper L. and Pines D., preprint.
25. Pao C. -H. and Bickers N. E., *Phys. Rev. Lett.* **72**, 1870 (1994);Monthoux P. and Scalapino D. J., *Phys. Rev. Lett.* **72**, 1874 (1994).
26. Batlogg B. in *High Temperature Superconductivity* (Edited by K. S. Bedell *et al.*). Addison-Wesley, New York (1990).
27. Yasuoka H. *et al.*, *J. Phys. Soc. Jpn.* **57**, 2659(1988).
28. Barrett S. E. *et al.*, *Phys. Rev. Lett.* **66**, 108 (1991); *Phys. Rev. B* **41**, 6283 (1990).
29. Monien H. and Pines D., *Phys. Rev. B* **41**, 6297 (1990).

30. Bulut N. *et al.*, *Phys. Rev.* **41**, 1797 (1990).
31. Annett J., Goldenfeld N. and Renn S. R., *Phys. Rev. B* **43**, 2778 (1991).
32. Shen Z. X. *et al.*, *Phys. Rev. Lett.* **70**, 1553 (1993). See also Yokoya Y. *et al.*, preprint.
33. Slichter C. P. *et al.*, *J. Phys. Chem. Solids* **70**, 1439 (1993); Martindale J. *et al.*, *Phys. Rev. B* **47**, 9155 (1993).
34. Hardy W. *et al.*, *Phys. Rev. Lett.* **70**, 399 (1993).
35. Pines D., *J. Phys. Chem. Solids* **54**, 1147 (1993).
36. Thelen D., Pines D. and Lu J. P.,*Phys. Rev. B* **47**, 9151(1993).
37. Thelen D., Ph.D. Thesis, University of Illinois, 1994, unpublished.
38. Scalapino D. J., *J. Phys. Chem. Solids* **54**, 1433 (1993).
39. Anderson P. W., *J. Phys. Chem. Solids* **54**, 1457 (1993).
40. Pines D., *Physica* **C235-240**, 113 (1994).
41. Wollman D. *et al.*, *Phys. Rev. Lett.* **71**, 2134 (1993). See also Van Harlingen D., *Rev. Mod. Phys.*, in press (1995); Kirtley J. *et al.*, preprint.
42. Wollman D., these proceedings.
43. Bulut N. and Scalapino D. J., *Phys. Rev. Lett.* **68**, 706 (1992).
44. Monthoux P., *J. Phys. Chem. Solids* **54**, 1093 (1993).
45. Ishida K. *et al.*, *Physica C* **179**, 29 (1991); *J. Phys. Soc. Jpn.* **62**, 2805 (1993); Zheng G. *et al.*, *[J. Phys. Soc. Jpn.* **62**, 2591 (1993).
46. Monthoux P. and Pines D., *Phys. Rev. B* **49**, 4261 (1994)
47. Gor'kov L. P.,*Sov. Phys. JETP* **40**, 1155 (1985); Pethick C. J. and Pines D., *Phys. Rev. Lett.* **40**, 270 (1986).
48. Lee P. A., *Phys. Rev. Lett.* **71**, 1887 (1993); Hirschfeld P. and Goldenfeld N., *Phys. Rev. B* **48**, 4219 (1993); Hotta T., *J. Phys. Soc. Jpn.* **62**, 274 (1993).
49. Balatsky A., Altschuler B. and Rosengren A., *Phys. Rev. Lett.* **73**, 720 (1994).
50. Kitaoka Y., *J. Phys. Chem. Solids* **54**, 1385 (1993).
51. Bonn D. *et al.*, *Phys. Rev. B* **48**, 13184 (1993); preprint.
52. Ishida K. *et al.*, preprint; Takigawa M. and Mitzi D., *Phys. Rev. Lett.* **73**, 1287 (1994).
53. Martin R., *Phys. Rev. Lett.*, in press (1995).
54. Hammel P. C. *et al.*, in *Phase Separation in Cuprate Superconductors* (Edited by E. Sigmund and K. A. Mller). Springer, Berlin (1994); Hammel P. C. *et al.*, in *Anharmonic Properties of High T_c Cuprates*, preprint.
55. Balatsky A., Monthoux P. and Pines D., *Phys. Rev. B* **50**, 582 (1994).
56. Monthoux P. and Scalapino D. J., *Phys. Rev. B* **50**, 10339 (1994).

Pergamon

J. Phys. Chem. Solids Vol. 56, No. 12, pp. 1659–1661, 1995
Copyright © 1995 Elsevier Science Ltd
Printed in Great Britain. All rights reserved
0022–3697/95 $9.50 + 0.00

0022-3697(95)00101-8

CONTINUOUS EVOLUTION OF THE 2D HUBBARD MODEL FROM AN INSULATOR TO A METAL

R. PREUSS,* R. PUTZ,* W. HANKE* and W. VON DER LINDEN†

* Institut für Theoretische Physik, Universität Würzburg, Am Hubland, D-97074 Würzburg, Germany
† Max-Planck-Institut für Plasmaphysik, EURATOM Association, D-85740 Garching b. München, Germany

Abstract—We present Quantum-Monte-Carlo results for the momentum and frequency dependent spectral weight $A(\boldsymbol{k}, \omega)$ showing the evolution from insulating to metallic behavior in the two-dimensional Hubbard model. As observed in recent photoemission experiments for cuprates, in both undoped and doped cases the electronic excitations display two rather similar general features, i.e. a quasiparticle (QP)-like dispersive band of small width of the order of the exchange interaction J and a broad valence- and conduction-band background. Arguments for one and the same many-body physics namely the continuous reduction of the spin-spin correlation length and related changes in the QP-spin correlations behind the continuous evolution to the metallic QP dispersion are given.

1. INTRODUCTION

Recent results of angle resolved photoemission spectroscopy ("ARPES") [1] revealed strong similarities in the low-energy excitations of a proto-type insulating copper oxide, i.e. $Sr_2CuO_2Cl_2$ [2], and metallic cuprates like *Bi* 2212, *Bi* 2201, etc.: in both cases the quasiparticle (QP) band has rather small dispersion of typically 1 eV width, it is separated from a broad main valence-band "background" (of about 6 eV width) in much the same way, the $\boldsymbol{k}$-dispersion is similar and also the intensity modulation as function of energy is comparable. Thus, it appears that the dispersive metallic band evolves continuously from the insulating limit and has a similar physical origin as the undoped valence band in the cuprates. This has important consequences for the copper oxides: the excitation spectrum in the insulating case is decisively determined by many-body effects, documented by the known difficulties of one-electron bandstructure calculations for the insulating limit [1], which then strongly emphasizes a many-body origin of the QP dispersion also in the metallic case.

We present in this work Quantum-Monte-Carlo (QMC) results for the two-dimensional (2-D) Hubbard model which demonstrate for this "generic" model the above strong similarities between undoped insulating and doped metallic situations.

In order to obtain from the QMC data for the single-particle finite-temperature propagator $G(\boldsymbol{k}, \tau)$ the corresponding spectral weight $A(\boldsymbol{k}, \omega)$ for real frequencies ω, the maximum-entropy method [3] has been used, which provides a controlled way to infer the most reliable $A(\boldsymbol{k}, \omega)$ in the light of the QMC data. To achieve the desired resolution, we used a likelihood function which takes the error-covariance matrix of the QMC data and its statistical inaccuracy consistently into account [4]. Correlations of the data in imaginary time were considered by making use of the covariance matrix in the MaxEnt-procedure [5]. As suggested in previous work by White [6], various moments of the spectral weight were also incorporated in extracting $A(\boldsymbol{k}, \omega)$.

The results presented here are for lattices 8×8 in size, an Coulomb interaction $U = 8t$ and for temperatures ranging from $\beta t = 3$ ($T = 0.33t$) to $\beta t = 10$ ($T = 0.1t$). Covering this temperature range allows us in effect to study (at half-filling) a situation where the spin-spin correlation length ξ is larger (for $\beta t = 10$) than the lattice size. In this case the system behaves as if it were at $T = 0$ and develops an AF gap. For $\beta t = 3$, on the other hand, the spin-spin correlation length is shorter than our finite lattice and, consequently, the gap is diminished and metallic fluctuations exist [7].

2. QUASIPARTICLE DISPERSION OF 2D HUBBARD MODELS

Inspecting Fig. 1 we observe two general features: One is that $A(\boldsymbol{k}, \omega)$ contains a rather dispersion-less "incoherent background", extending both for electronically occupied ($\omega < \mu$) states and unoccupied ($\omega > \mu$) states over $\sim 6t$ ($\sim 6\ eV$) in the $U = 8t$ case. The new structure, which was not previously resolved in QMC work is a dispersing structure at low energies with small width of the order of J, which defines the gap Δ and which is well separated from the higher energy background.

The splitting in the low-energy "band" and the higher-energy "background" is especially pronounced near Γ-(for $\omega < \mu$) and M-(for $\omega > \mu$) points due to a relative weight shift from negative to positive energies as $\boldsymbol{k}$ moves through X or equally through $(\pi/2, \pi/2)$, the midpoint between Γ and M. The overall weight distribution in $A(\boldsymbol{k}, \omega)$ follows roughly the SDW prediction as found in the QMC calcu-

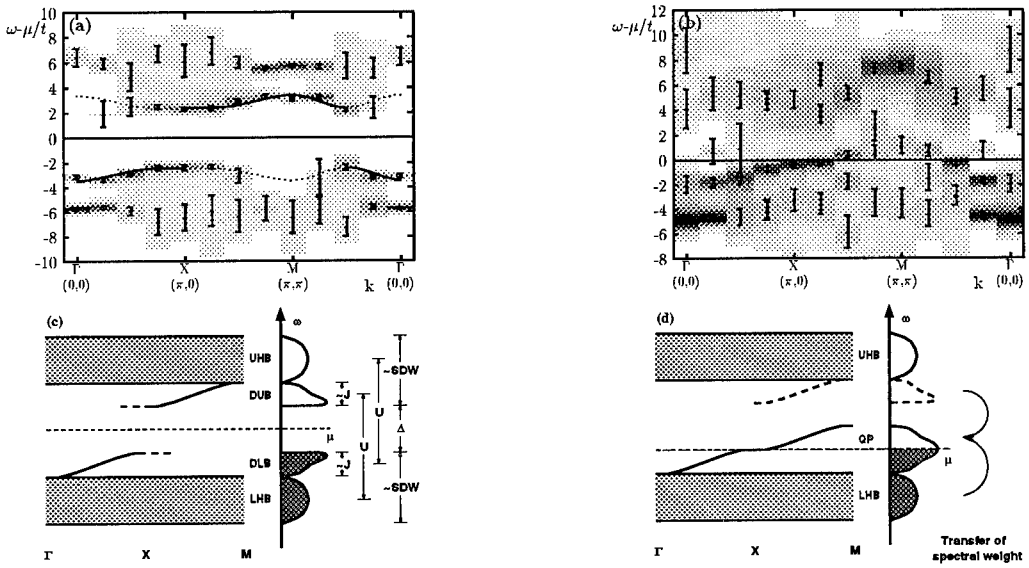


Fig. 1. Single-particle excitation of the 8 × 8 Hubbard model for $U = 8t$: half-filling (left column) and doping $< n >=0.95$ (right column); (a,b) ω versus $\boldsymbol{k}$ "bandstructure", where dark (white) areas correspond to a large (small) spectral weight and peaks in $A(\boldsymbol{k}, \omega)$ are represented by points with error bars; (c,d) schematic plot of the bandstructure.

lation by Bulut et al. [8]: the total integrated weight in the SDW approximation $< n_{\boldsymbol{k}}^{SDW} >= \int_{-\infty}^{0} A^{SDW}(\boldsymbol{k}, \omega) d\omega$, is in good accord with the QMC momentum distribution [8].

However, the dispersion of the structure near the gap does not follow the SDW prediction: its dispersion has a significant (about a factor of 2 for $U = 8t$) smaller width set by the value of J. This result is in good accord with the dispersion and width found for the low energy "foot" in recent angle-resolved photoemission (ARPES) data [2] and t-J model results (there $t \approx 0.4\ eV$) [9]. This is illustrated in Fig. 1(a), where the low-energy peaks in $A(\boldsymbol{k}, \omega)$ are fitted by (full and dotted lines) $E_{\boldsymbol{k}} = \Delta + J/2(\cos k_x + \cos k_y)^2$, with $\Delta = 2.4t$, rather than by the SDW (strong-coupling) result, i.e. $E_{\boldsymbol{k}} = \sqrt{\epsilon_{\boldsymbol{k}}^2 + \Delta^2} \cong \Delta + J(\cos k_x + \cos k_y)^2$.

The overall agreement between the ARPES width and the Hubbard model data (for $t \approx 1eV$) is significant because it shows in fact that the energy scale of the low-lying insulating band is controlled by many-body effects beyond the mean-field SDW result.

If we increase the temperature to $\beta t = 3$ (not shown) a maximum develops in the valence-band at the M-point and not at the X- or $(\pi/2, \pi/2)$-points in contrast to the $\beta t = 10$ results. This at first puzzling "high-temperature" result reflects the fact that at $\beta t = 3$ the spin-spin correlation length ξ is about a factor of 2.5 smaller than the QMC lattice extension. The system then shows precursor effects of a metal, which move the spectral weight (valence-band) maximum – in agreement with the metallic situation in Fig. 1(b) – to the M-point. Otherwise, the low-energy band is found to be essentially unaffected by changing temperature from $T = 0.1t$ to $T = 0.33t$.

Keeping this in mind, we consider in the right column of Fig. 1 the low-energy electronic structure in the metallic regime for doping $< n >=0.95$. Fig. 1(b) shows the dispersion relation with the degree of shading representing the intensity of $A(\boldsymbol{k}, \omega)$, as in Fig. 1(a). Like in the half-filled case, we observe two general features, which are both seen in recent photoemission experiments [1]: a broad "background" of $\approx 4t-6t$ spanning the lower and upper Hubbard band and a pronounced low-energy "foot" of significantly smaller width, which is clearly resolved between $\Gamma \rightarrow X$ and $\Gamma \rightarrow (\pi/2, \pi/2)$. The situation is depicted schematically in Fig. 1(d).

The results for the doped case have several important implications: First, they reveal that the lowest energy "band" in the insulator and the "band" that crosses the chemical potential, $\omega = \mu$, in the hole-doped metal are rather similar: the low-energy band is separated from the broad valence-band background ("LHB" (lower Hubbard band) in the schematic drawings of Fig. 1) in the same way; it has

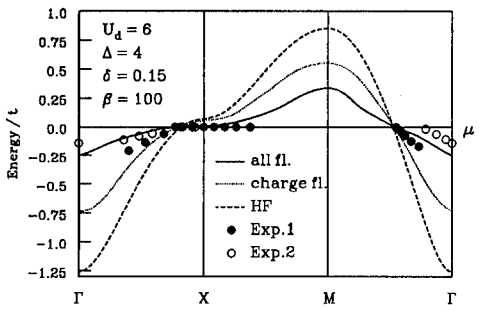


Fig. 2. Quasiparticle dispersion of the three-band Hubbard model: Hartree-Fock (HF) results (dashed line) and FLEX calculations which include only the charge scattering channel (dotted line) and all symmetrically chosen particle-hole and particle-particle channels (full line) are compared to ARPES experiments (open circle: Ref. [1], full circles: Ref. [15]).

similar dispersion and it has a similar intensity modulation as a function of energy. Thus, the lowest-energy metallic band appears to be effected by similar many-body physics as in the insulating regime, namely magnetic correlations connected with the (now) short-range AF order. This is not in contradiction but instead substantiated by the fact that the metallic band develops its maximum at the M-point: as pointed out above, this happens as soon as the spin-spin correlation length ξ is smaller than the length (L=8), a situation obtained for the filling $< n >$=0.95.

Another noteworthy feature of the doped, metallic situation is that the intensity change (but not the width) as a function of $\boldsymbol{k}$ for the higher-energy background in $A(\boldsymbol{k}, \omega)$ still follows essentially the AF SDW picture with, in particular "shadow bands" resulting from the AF short-range order being clearly visible at Γ-($\omega - \mu \sim -5t$) and M-($\omega - \mu \sim +7t$) points. Even remnants can be detected of folded back "shadow bands" near the M-point for $\omega < \mu$, which in the SDW-picture have much less oscillator strength and spectral intensity than the original band (between $\Gamma \rightarrow$X) (see also [10]). The findings confirm to a certain extent a phenomenological work by Kampf and Schrieffer [11].

Finally, we would like to mention that an important detail of the QMC data, the rather extended flatness of the energy band near the X(π, 0)-point, which is in good agreement with ARPES experiments of Dessau et al. [1] for *Bi* 2212, has previously been resolved in QMC work both for the one-band [12] and the three-band [13,14] Hubbard models. This rather extended flatness, extending like the ARPES data not only into X$\rightarrow\Gamma$, but also into the X$\rightarrow$M regions (as displayed in Fig. 3) is already inherent in the undoped low-energy structure near X, a fact which has recently also been found in 2-D t-J model studies by Dagotto et al. [9]. Its extension, in particular into X$\rightarrow$M direction, is not consistent with available one-electron band calculations [1]. It can be explained by a conventional self-energy diagramatic analysis summing over the leading spin-fluctuation diagrams [14]. It is thus a many-body effect related to magnetic correlations consistent with the arguments given in this work.

3. CONCLUSIONS

In summary, we have studied the evolution of the 2-D Hubbard model from insulator to metal in terms of the electronic spectral weight, obtained from the maximum-entropy analytic continuation of QMC data. These results, combined with recent ARPES data, can be taken as strong indication that the QP dispersion of the high-T_c compounds, not only in the insulating limit but – particularly – in the metallic situation, has a many-body origin: the coupling of the quasiparticles to antiferromagnetic correlations. *Acknowledgements*— We would like to thank R. Laughlin, S. Maekawa, A. Muramatsu, D. Poilblanc, H. Schulz, Z.-X. Shen and, particularly, D.J. Scalapino for instructive discussions. The calculations were performed at the HLRZ Jülich and at the LRZ München.

REFERENCES

1. Shen Z.-X. and Dessau D.S., *Phys. Rep.* (to be published); Dessau D.S. *et al.*, *Phys. Rev. Lett.* **71**, 2781 (1993). Care has to be taken for the nomination of the high-symmetry points: The X-point of our two-dimensional cubic lattice corresponds to the M- point for the Bi 2212 compound and the M-point of our calculations corresponds to the X-point in Bi 2212.
2. Wells B.O. and Shen Z. -X. *et al.*, (to be published).
3. Gull S.F., *Maximum Entropy and Bayesian Methods*, ed. J. Skilling (Kluwer, Academic Publishers, 1989); Skilling J., in *Maximum Entropy and Bayesian Methods* ed. P.F. Fougère (Kluwer, Academic Publishers, 1990).
4. von der Linden W., Preuss R. and Hanke W., to be published.
5. Gubernatis J.E., Jarrell M., Silver R.N. and Sivia D.S., *Phys. Rev. B* **44**, 6011 (1991); M. Jarrell, unpublished.
6. White S.R., *Phys. Rev. B* **44**, 4670 (1991);
7. White S.R., *Phys. Rev. B* **46**, 5678 (1992).
8. Bulut N., Scalapino D.J. and White S.R., *Phys. Rev. Lett.* **73**, 748 (1994).
9. Dagotto E. Nazarenko A. and Boninsegni M., *Phys. Rev. Lett.* **73**, 728 (1994).
10. Haas S., Moreo A. and Dagotto E., submitted to *Phys. Rev.* (1994).
11. Kampf A.P. and Schrieffer J.R., *Phys. Rev. B* **42**, 7967 (1990).
12. Bulut N., Scalapino D.J. and White S.R., *Phys. Rev. B* **50**, 7215 (1994).
13. Dopf G., Wagner J., Dieterich P., Muramatsu A. and Hanke W. *Phys. Rev. Lett.* **68**, 2082 (1992).
14. Putz R., Preuss R., Muramatsu A. and Hanke W., submitted to *Phys. Rev. Lett.* (1994).
15. Mante G. *et al.*, *Z. Phys. B* **80**, 181 (1990).

Pergamon

J. Phys. Chem. Solids Vol. 56, No. 12, pp. 1663–1667, 1995
Copyright © 1995 Elsevier Science Ltd
Printed in Great Britain. All rights reserved
0022–3697/95 $9.50 + 0.00

0022–3697(95)00143-3

THE d-WAVE RESONANCE VALENCE BOND STATE

T. M. RICE ‡, M. TROYER † H. TSUNETSUGU *
* Theoretische Physik, ETH-Hönggerberg, 8093 Zürich, Switzerland
† Interdis. Proj. fur Supercomputing, ETH, 8092 Zürich, Switzerland
‡ AT&T Bell Laboratories, Murray Hill, NJ 07974, U.S.A.

Abstract—The properties of strongly correlated electron models in the form of ladders are reviewed. The groundstate of undoped and lightly doped two chain ladders described by the t–J model is a realization of a d-wave resonance valence bond state. Although many properties are those of lightly doped insulators, the strong magnetic polarizability modifies the dispersion relation for quasiparticles to resemble a metal with a large Fermi surface. Some discussion is given of possible relationships of the ladder systems to a two dimensional planar t–J model and of a possible origin of the spin-gap in underdoped cuprates.

1. INTRODUCTION

Recent experiments which use quantum interference in various geometries to test the order parameter symmetry of the cuprates have all favored a $d_{x^2-y^2}$-symmetry [1]. They add further motivation to study strong correlation models which have pairing in the d-wave channel. Two chain ladders described by either the Hubbard Hamiltonian or the strong coupling t–J Hamiltonian, provide us with simple model system which can be analyzed reliably by a number of techniques [2–12]. They are a form of one dimensional model but have behavior on the low energy scale which is distinct from single chain models. At half-filling, for example, the ladder has a spin liquid groundstate [2–5, 9]. Early mean field calculations [6] predicted an evolution of the spin gap of the spin liquid with hole doping leading to pairing of the holes essentially in a d-wave state—although the ladder does not have tetragonal symmetry the crucial sign change of the pairing amplitude between perpendicular directions remains. These mean field results have been confirmed and refined by recent numerical calculations using Lanczos diagonalization [7] and density matrix renormalization group (DMRG) methods [10]. Further several examples of cuprates have been found which have weakly coupled ladders and exhibit the spin liquid groundstate [13–16]. As such they are examples of the resonance valence band (RVB) state of $S = 1/2$ antiferromagnets postulated by Anderson in 1987 in the first theoretical paper on the cuprate superconductors [17].

In the next section a brief review will be given of the properties of the undoped systems on Heisenberg ladders for which there is experimental confirmation of the key ideas. Then the effect of hole doping will be discussed but for the present there are no experimental realizations of the doped systems. The third section will be more speculative in character and discuss the lessons that can be drawn from the analysis of the ladder models for the 2D-planar limit.

2. TWO CHAIN t–J AND HUBBARD LADDERS

2.1. *Undoped systems*

In the absence of carriers all electrons are localized and the strong coupling limit of the Hubbard model reduces to a n.n. Heisenberg $S = 1/2$ model with antiferromagnetic exchange constants $J(J_\perp)$ along the legs (rungs) of the ladder.

$$H_J = J\sum_{j,\alpha}(\boldsymbol{S}_{j,\alpha}\cdot\boldsymbol{S}_{j+1\alpha} - \frac{1}{4}n_{j\alpha}n_{j\alpha+1}) + J_\perp\sum_j(\boldsymbol{S}_{j,\ell}\cdot\boldsymbol{S}_{j,r} - \frac{1}{4}n_{j\ell}n_{jr}) \quad (1)$$

and j runs over L rungs and $\alpha(=\ell, r)$ is an index for the legs.

The limit $J_\perp \gg J$ is simple since then the groundstate is a product of singlets on each rung. The lowest excited state is an $S = 1$ magnon localized on a single rung. A finite coupling J along the legs of the ladder broadens the localized triplet into a band of magnons. The isotropic limit $J_\perp = J$ describes the cuprate ladder compounds. The numerical calculations of Dagotto *et al.* [3] and Barnes *et al.* [5] showed that the minimum of the magnon band at the zone boundary ($k_x = \pi$) is at an energy $\omega(\pi) = J/2$ leading to a finite spin gap and a spin liquid groundstate with exponential decay of the spin correlations. A collapse of the spin gap to zero would signal the onset of longer range correlations. The spins in the triplet at isotropy are spread over several rungs so that n.n.n. and longer range processes enter the magnon dispersion and the finite value of $\omega(\pi)$ is due to the higher order terms [18].

Troyer *et al.* [8] found that a simple expression for the uniform spin susceptibility $\chi_s(T)$ assuming non-interacting magnons but including a hard core repulsion

$$\chi_s(T) = z(T)/T(1 + 3z(T));\ z(T)$$

$$= (2\pi)^{-1} \int_{-\pi}^{\pi} dk_x exp(-\omega(k_x)/T) \qquad (2)$$

fit well to detailed numerical calculations using a Quantum Transfer Matrix method. A similar approach gives an exponential fall off of the NMR relaxation time $1/T_1T$ at low temperatures. Rice *et al.* [15] proposed that the compound family $Sr_{n-1}Cu_{n+1}O_{2n}$, first synthesized by Takano and coworkers [13], would be realizations of ladder structures. The CuO_2-planes in the high-T_c cuprates have all corner sharing CuO_4 squares so that all super-exchange bonds are 180° Cu–O–Cu bonds. However in the $Cu_{n+1}O_{2n}$-planes there are parallel line defects with edge sharing CuO_4 squares leading to 90° Cu–O–Cu bonds. Such bonds are expected to be weak and ferromagnetic and thus frustrated by the strong 180°-bonds. Mean field calculations [19] show the square lattice of Cu^{2+}-spins broken up into weakly interacting ladders whose width depends on the parameter, n. Two chain ladders occur for $n = 3$ and recent susceptibility and $1/T_1T$ measurements by Azuma *et al.* [15] and Kitaoka *et al.* [16] confirm this expectation of a large spin gap. Curiously a substantial discrepancy exists between the spin gap values found in $\chi_s(T)$ ($\omega(\pi) \simeq 400$ K) and $1/T_1T$ ($\omega(\pi) \simeq 700$ K) which is unexplained [16]. The latter value is closer to the single ladder value of $J/2$ but substantial coupling between the Cu_2O_3-planes along the c-axis should reduce the value of the spin gap.

A key prediction of the analysis of the ladder structures is that ladders with even and odd numbers of legs behave differently. This is seen most clearly in the limit $J_\perp \gg J$ where odd numbers reduce at low energies to single $S = 1/2$ chains with an effective exchange, J_{eff}. The DMRG calculations of Noack *et al.* [9] on large systems showed the clear difference between 1- and 3-chain ladders which are gapless and 2- and 4-chain ladders which have finite spingaps. Azuma *et al.* [15] also measured $\chi_s(T)$ in the $n = 5$ compound $Sr_2Cu_3O_5$ and found a finite value as $T \to 0$. Recent μSR measurements found an AF ordering transition at $T_N \simeq 50$ K [16].

A number of other cuprates have ladder structure. The $(La_2CuO_4)_nLa_2Cu_4O_7$ family of compounds [20] contains ladder structures but also other Cu^{2+} sites which are only weakly coupled magnetically and so dominate $\chi_s(T)$. Recently Batlogg *et al.* [21] used a subtraction technique to isolate the ladder contributions and to identify a spin gap $\approx J/4$ in the 4-chain ladders and gapless behavior in the 5-chain ladders.

2.2. *Hole doped systems*

The addition of hole carriers forming mobile low spin Cu^{3+}-ions is described by the t–J model ($H = H_t + H_J$) which is equivalent to the strong coupling limit of the Hubbard model. The kinetic energy for holes gives the term

$$H_t = -t \sum_{j,\alpha,\sigma} (Pc^+_{j,\alpha,\sigma} c_{j+1,\alpha,\sigma} P + h.c.) - t \sum_{j\sigma} (Pc^+_{j\ell\sigma} c_{jr\sigma} P + h.c.) \qquad (3)$$

with a projection operator P which prohibits double occupancy.

In the large $J_\perp$ limit, the addition of a hole breaks one of the singlet bonds. In effect a single electron with an unpaired spin enters the bonding state of a rung and gains an energy, $-t$. The bonding (antibonding) states are created by operators

$$c^+_{j,b(a),\sigma} = 2^{-1/2}(c^+_{j,\ell,\sigma} \pm c^+_{j,r,\sigma}) \qquad (4)$$

and a singlet electron pair on the jth rung is created by

$$2^{-1/2}(c^+_{jb\uparrow} c^+_{jb\downarrow} - c^+_{ja\uparrow} c^+_{ja\downarrow}) \qquad (5)$$

The hole propagates along the ladder a matrix element $(t/2)$ leading to a simple dispersion law. In this limit the properties of the hole are similar to those of a hole in any nonmagnetic insulator with spin 1/2 and charge $|e|$ and an energy minimum at the zone boundary $k_x = \pm\pi$, [7]. In the isotropic limit $J_\perp = J$ and $J < t$, the unpaired spin and charge are no longer confined to the same rung and simultaneously the dispersion relation is modified by n.n.n. and longer range hops. The result is that the minimum energy of a hole moves away from the zone boundary and at the same time the bonding and antibonding bands start to overlap [7]. These developments are consequences of the high magnetic polarizability of the insulator in this case. For example, the hole dispersion relations in the channels which are even (odd) under reflection about the center line of the ladder (i.e. the bonding (antibonding) hole states) can be fit with the forms [22] ($\tau = b, a$)

$$\epsilon_\tau(k_x) = +\epsilon^0_\tau + \alpha_\tau \cos(k_x) + \beta_\tau \cos(2k_x) + \gamma_\tau \cos(3k_x)\ldots \qquad (6)$$

For $J = t/2$ the coefficients determined by diagonalizing a (2×10) ladder are (in units of t)

$$\epsilon^0_b = -0.865;\ \alpha_b = .26;\quad \beta_b = 0.19;\ \gamma_b = -7 \times 10^{-3}$$
$$\epsilon_a = -0.79;\ \alpha_a = -0.31;\ \beta_a = 0.225;\ \gamma_a = -11 \times 10^{-3} \qquad (7)$$

It is instructive to compare this dispersion relation to the band structure for non-interacting electrons, which has overlapping bonding and antibonding bands

$$\epsilon_\tau(k_x) = -2t\ \cos k_x \mp t \qquad (8)$$

At half-filling the chemical potential is exactly at zero energy and the bonding (antibonding) bands intersect the Fermi energy at wavevectors, $k_{Fb} = \pm 2\pi/3$ and $k_{Fa} = \pm\pi/3$ respectively. The occupied regions of the bands closely resemble the central portion of hole bands described by eqn (6). In other words the k-space dispersion of a single hole in the t–J ladder looks more like a metal with a large Fermi

surface than a semiconductor. Note the bandwidth scales with J not the band structure value, t. ARPES measures in principle the dispersion relation upon removing an electron (or injecting a hole) and it would measure in this case an apparent large Fermi surface although the starting material is an insulator with no broken symmetries which would change the size of the Brillouin zone. The insulating nature of the parent state would show up clearly if we tried to inject an electron (i.e. do a BIS experiment). This is of course impossible at low energies. This contrast is an example of the interesting duality between metallic and semiconducting properties.

The one particle spectral function $A_{\tau,\sigma}(k_x, \omega)$ $(= \pi^{-1}\mathrm{Im}G_{\tau,\sigma}(k_x, \omega))$ can also be calculated in the presence of two holes in a 2×10 ladder which mimics a finite hole density [22]. In this case there is a finite weight for adding electrons, but a clear asymmetry shows up if we integrate over k_x. The equivalent of the angle integrated one particle density of states $N(\omega)$ $(= (2\pi)^{-1}\int_{-\pi}^{\pi} dk_x \sum_{\tau,\sigma} A_{\tau,\sigma}(k_x, \omega))$ has a width $\sim 4t$ mostly due to incoherent states for $\omega < \mu$ but only a width of $1t$ for $\omega > \mu$. The magnitude of $N(\omega)$ is approximately equal so that the sum rules, $\int_{-\infty}^{\mu} N(\omega)d\omega = n_e$ and $\int_{\mu}^{\infty} N(\omega)d\omega = 2n_h$ (the electron and hole number respectively), are satisfied by the large asymmetry in the effective width. Thus although the ARPES Fermi surface appears large, the strong correlation condition restricts the width in energy to add electrons and so reduces the weight of the quasiparticle-quasihole excitations by a factor of n_h at small hole doping.

The ground state of the two-hole t–J ladder is a singlet [7, 22]. An examination of the hole–hole correlation function shows binding at large $J_\perp$ which extends down to isotropy and values $J_\perp = J = t/3$. The excitation spectrum in the charge ($S = 0$) and spin ($S = 1$) channels are quite different. In the charge channel there is a collective mode with zero excitation energy in the long wavelength limit, $k_x \to 0$. This mode is simply the sound mode of the system. At short wavelengths the weight in the density–density correlation function is concentrated at high energies of the order of several times t and is due to local excitations of the hole in the polarizable medium.

An energy gap however is maintained in the spin channel, but there are now new kinds of spin excitations. In addition to the magnon mode which evolves continuously with doping, the presence of bound hole pairs gives rise to new quasiparticle excitations in which the holes are placed on widely separated rungs and the accompanying spins are in a triplet configuration. At large $J_\perp$ the energies of these two excitations are quite distinct with values $J_\perp - J$ and $J_\perp - 2t$ respectively. The spin gap i.e. the lowest $S = 1$ excitation, is now determined by the 2 quasiparticle excitation and so is discontinuous upon doping. Similar behavior occurs at isotropy and $J \sim t/3$ although now the two types of excitation interact. There is an important difference in weight between the two types of excitations since the number of quasiparticle excitations is strictly limited by the hole number whereas the magnons evolve continuously as $n_h \to 0$. This shows that the magnon excitations are not collective excitations of the quasiparticles. The RVB insulator differs from a standard insulator in its magnetic polarizability due to the magnon modes and these are responsible for the change in the k-space dispersion of the quasiparticles.

The presence of a spin gap and collective sound modes as the only low lying excitations are typical of a Luther–Emery liquid rather than the Tomanaga–Luttinger liquid that usually occurs in 1D models with repulsive interactions [11]. The low energy properties of Luther–Emery liquids are determined by a strong coupling fixed point, which Efetov and Larkin [23] described of a liquid of bosons. In the present case the Efetov–Larkin bosons are hole pairs. The exponent K_ρ governing the density and superfluid correlations has been calculated by Tsunetsugu *et al.* [11] and in the parameter region of interest for cuprates ($J_\perp = J \approx t/3$), $K_\rho \approx 0.5$. The density correlations of the E–L bosons are longer range than the superfluid correlations. This result agrees with DMRG calculations by White *et al.* who reported explicit calculations of these correlation functions for a Hubbard model [10].

One point of interest is that the holes are paired essentially in the d-wave channel, with pairing amplitude having opposite signs along the legs and rungs of the ladder. This form was predicted by the mean field calculations of Sigrist *et al.* [6] and confirmed in the DMRG calculations of White *et al.* [10]. Explicit calculation of the Gorkov pairing order parameter for two holes in a 10×2 ladder also confirm the essential d-wave character of the hole pairs [22].

Lightly doped ladders are explicit examples of a d-wave RVB state. They behave as dilute fermion systems with a strong attraction in the d-wave channel but simultaneously the high magnetic polarizibility modifies the k-space dispersion which has a form resembling the overlapping and partially filled bands one obtains in a bandstructure. The result is an intriguing combination of features associated with a dilute attractive fermion gas and a metallic liquid with a large Fermi surface.

3. LESSONS FOR TWO DIMENSIONS

Isolated ladders can be analyzed reliably and accurately and a clear picture of the properties of the undoped and lightly doped systems follows. However it is also of interest to relate these results to 2D, i.e. an infinite plane described by the t–J model. In the undoped case the situation is clear. The short range RVB groundstate of the two-chain ladder is fundamentally different than the groundstate of the planar Heisenberg model which has long range AF order. Thus if we consider the crossover between a set of coupled ladders and the isotropic plane, there will be a critical interladder coupling J_c' at which the minimum magnon energy drops to zero. $J' = J_c'$ is a quantum critical point, separating the spin liquid and AF ordered phases [11].

The doped systems however may be different since there is considerable evidence a d-wave RVB state is the stable ground state in 2D for a range of J/t and hole concentration, n_h. As a result one expects a smooth crossover from coupled ladders to the isotropic 2D limit. There are grounds to postulate such a smooth crossover. For example, Tohyama, Horsch and Maekawa [24] recently contrasted the behavior of the density-density, $N(q, \omega)$ and spin–spin $S(q, \omega)$ correlation functions as calculated for a finite 1D chain and a finite 2D cluster. They concluded that the key features that characterize a Luttinger liquid could be clearly seen in the chain results but were not present in the 2D cluster. Recently Troyer *et al.* [22] compared the 2-chain ladder results for $N(q, \omega)$ and $S(q, \omega)$ and also found a marked difference to Luttinger liquid behavior but a strong similarity to the 2D cluster results. This supports the idea of a smooth crossover at finite hole doping. There is a proviso however, namely the cluster results may result from the boundary conditions which strongly favor total singlet states and thus may not be representative of the infinite plane. Nonetheless the qualitative comparison found by Troyer *et al.* [22] is support for the existence of a d-wave RVB groundstate for the infinite plane.

Turning to experiment, there is an intriguing similarity between the spin gap found at low hole doping of the two-chain ladder and spin gap found experimentally in underdoped cuprates. Elsewhere in this volume, Millis *et al.* [25] argue that the spin gap has a strong empirical correlation with the occurrence of bilayers in the structure and they propose a magnetic origin for the spin gap based on interlayer pairing due to the magnetic coupling between the bilayer planes. Examining this proposal from the present point of view, then the key question is whether interplane coupling will stablize the magnon and so drive the system through the quantum critical point required for the transition between AF order and a spin liquid with finite spin gap. From the present viewpoint it is hard to see how the interlayer magnetic interaction can be the driving force. Interlayer coupling at least in the undoped system enhances the bandwidth of the magnon and therefore should drive the minimum magnon energy down in energy and so act to destabilize rather than stabilize the spin liquid phase. This leads us to look for a different mechanism to stabilize the spin liquid phase.

As we remarked earlier, the spin gap phase of the two-chain ladder has powerlaw order in both the CDW and singlet superconductivity (SS) correlation functions corresponding to the tendencies to crystalline and superfluid order of the E–L bosons, i.e. the hole pairs. This supersolid behavior that occurs in the one dimensional ladders could be extended also to the 2D-planes. Tsunetsugu *et al.* [11] discussed the crossover from ladders to planes for the t–J model in terms of the competition between CDW and SS as the interladder coupling is increased. A key point is whether the E–L-bosons (hole pairs) attract or repel between ladders and concluded that in the interesting parameter regime ($J \sim t/3$) they repel so that the CDW form would be a crystal of hole pairs. Quantum fluctuations however will tend to destabilize a hole pair crystal but interlayer Coulomb interactions in a bilayer should enhance the tendency to form CDW. This in turn suggests an interpretation of the appearance of a spin gap as a sign of enhanced CDW fluctuations. Certainly if the CDW were to effectively break up the plane into weakly coupled magnetic clusters, then spin gap would reflect the great stability of a singlet or $S = 0$ groundstate. This idea is speculative but would be worth pursuing.

4. CONCLUSIONS

The flexibility of cuprate chemistry gives rise to many possible structures intermediate between single CuO_4-chains and 2D-CuO_2-planes. It opens up new avenues to explore and can give us new insights into strongly correlated electron systems. In particular ladders with an even number of legs or chains are well defined model systems which on the one hand give us new theoretical insights into the d-wave RVB state and on the other hand may possibly be realized experimentally.

Acknowledgements—The authors wish to thank M. Sigrist, F. C. Zhang, S. Gopalan, D. V. Khveshchenko, D. J. Scalapino, R. Noack, D. Poilblanc, S. R. White, M. Takano, Z. Hiroi, M. Azuma, Y. Kitaoka and B. Batlogg for many conversations and scientific exchanges during the course of this work. The financial support of the Swiss National Science Foundation is gratefully acknowledged.

REFERENCES

1. See articles by Ott H. R., Tsuei C. C., Wellstood F. C. and Wollman D. A. in these proceedings.
2. Hirsch R., Diplomarbeit University Köln, unpublished (1988).
3. Dagotto E., Riera J. and Scalapino D. J., *Phys. Rev. B* **45**, 5744 (1992).
4. Strong S. P. and Millis A. J., *Phys. Rev. Lett.* **69**, 2419 (1992).
5. Barnes T., Dagotto E., Riera J. and Swanson E. S., *Phys. Rev. B* **47**, 3196 (1993).
6. Sigrist M., Rice T. M. and Zhang F. C., *Phys. Rev. B* **49**, 12058 (1994).
7. Tsunetsugu H., Troyer M. and Rice T. M., *Phys. Rev.* **49**, 16078 (1994).
8. Troyer M., Tsunetsugu H. and Würtz D., *Phys. Rev. B* **50**, 13757 (1994).
9. Noack R. M., White S. R. and Scalapino D. J., *Phys. Rev. Lett.* **73**, 882 (1994).
10. White S. R., Noack R. M. and Scalapino D. J., *Phys. Rev. Lett.* **73**, 886 (1994).
11. Tsunetsugu H., Troyer M. and Rice T. M., , *Phys. Rev. B* **51**, 16456 (1995).
12. Khveshchenko D. V., *Phys. Rev. B* **50**, 380 (1994).
13. Takano M. *et al.*, *Jpn J. Appl. Phys.* **7**, 3 (1992).
14. Rice T. M., Gopalan S. and Sigrist M., *Europhys. Lett.* **23**, 445 (1993).
15. Azuma M., Hiroi Z., Takano M., Ishida K. and Kitaoka Y., *Phys. Rev. Lett.* **73**, 3463 (1994).
16. Kojima K. *et al.*,*Phys. Rev. Lett.*,**74**,2812 (1995); Kitaoka Y. (this proceedings).

17. Anderson P. W., *Science* **235**, 1196 (1987).
18. Reigrotzki M., Tsunetsugu H. and Rice T. M., *J. Phys. Cond. Matt.* **6**, 9235 (1994).
19. Gopalan S., Rice T. M. and Sigrist M., *Phys. Rev. B* **49**, 8901 (1994).
20. Cava R. J. *et al. J. Solid State Chem.* **94**, 170 (1991).
21. Batlogg B. *et al.*, *Bull. Am. Phys. Soc.* **40**, 327 (1995).
22. Troyer M., Tsunetsugu H. and Rice T. M., *Phys. Rev. B* (in press).
23. Efetov K. B. and Larkin A. I., *Sov. Phys. JETP* **42**, 390 (1975).
24. Tohyama T., Horsch P. and Maekawa S., *Phys. Rev. Lett.* **74**, 980 (1995).
25. Millis A. J., Monien H. and Ioffe L. these proceedings.

Pergamon

J. Phys. Chem. Solids Vol. 56, No. 12, pp. 1669–1672, 1995
Copyright © 1995 Elsevier Science Ltd
Printed in Great Britain. All rights reserved
0022-3697/95 $9.50 + 0.00

0022-3697(95)00166-2

DISTINGUISHING HIGH-T_c THEORIES

D. J. SCALAPINO
Department of Physics, University of California, Santa Barbara, CA 93106-9530, U.S.A.

Abstract—A number of experiments suggest that the gap in the high-temperature superconducting cuprates has dominantly $d_{x^2-y^2}$ symmetry. Assuming that this is the case, we discuss what this tells us about the basic pairing mechanism and examine how one might distinguish between different theories which predict a $d_{x^2-y^2}$ gap.

Many different experiments on the high-temperature cuprate superconductors can be understood if the dominant momentum dependence of the gap on the Fermi surface has $d_{x^2-y^2}$ symmetry [1–3]. Suppose then, for this discussion, we assume that the gap has $d_{x^2-y^2}$ symmetry. What does this tell us about the basic pairing mechanism? Why are there still so many different possible theories? How might the different theories be distinguished?

From the BCS equation [4]

$$\Delta_p = \sum_{p'} V_{pp'} \frac{\Delta_{p'}}{2E_{p'}}, \tag{1}$$

it is clear that the momentum dependence of the gap reflects the momentum dependence of the pairing interaction $V_{pp'}$. For example, within this framework, the electron–phonon interaction (with $\omega_n = (2n+1)\pi T$ and $\omega_{n'}$ the usual Matsubara frequencies)

$$V_{pp'}(\omega_n - \omega_{n'}) = -\frac{2|g_{pp'}|^2 \omega_{p-p'}}{(\omega_n - \omega_{n'})^2 + \omega_{p-p'}^2} \tag{2}$$

is approximated by its zero frequency strength

$$V_{pp'} \approx \begin{cases} -\dfrac{2|g_{pp'}|^2}{\omega_{p-p'}}, & |\varepsilon_p - \varepsilon_{p'}| < \omega_0 \\ 0, & |\varepsilon_p - \varepsilon_{p'}| > \omega_0 \end{cases} \tag{3}$$

for energy transfers $|\varepsilon_p - \varepsilon_{p'}|$ less than a typical phonon frequency ω_0. The dominant phase space contributions come from large momentum transfers where both $|g_{pp'}|$ and $\omega_{p-p'}$ are slowly varying. In this case the solution of the BCS gap equation for a nearly spherical Fermi surface has the simple s-wave form

$$\Delta_p = \begin{cases} \Delta_0, & |\varepsilon_p - \varepsilon_{p'}| < \omega_0 \\ 0, & |\varepsilon_p - \varepsilon_{p'}| > \omega_0. \end{cases} \tag{4}$$

Alternatively, if the pairing interaction for a two-dimensional Hubbard model doped near half-filling is approximated by the Berk–Schrieffer [5] RPA form

$$V_{SF} \approx \frac{3}{2} U^2 \chi(p - p', \omega_n - \omega_{n'}), \tag{5}$$

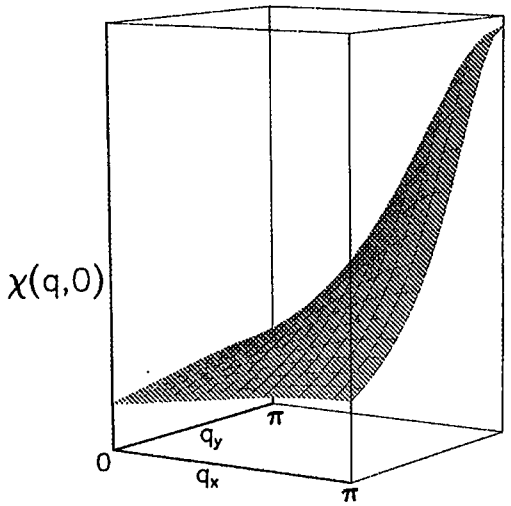


Fig. 1. Momentum dependence of $\chi(q, 0)$ for a nearly antiferromagnetic system.

and $\chi(p-p', 0)$ peaks at large momentum transfer as shown in Fig. 1, one finds that the gap is well approximated by the $d_{x^2-y^2}$ form

$$\Delta_p = \frac{\Delta_0}{2}(\cos p_x - \cos p_y). \tag{6}$$

The basic difference from the electron-phonon case is that the spin-fluctuation interaction, Eqn (5), is *positive* and strongly *momentum dependent, increasing* in strength at large momentum transfers for $\mathbf{p} - \mathbf{p}'$ near (π, π). Thus while the real-space Fourier transform of the phonon-mediated interaction, Eqn (2), corresponds to a short-range interaction which is attractive due to retardation, the real-space Fourier transform of V_{SF} leads to an interaction which has the spatial structure shown in Fig. 2. This interaction is repulsive on site but attractive on near-neighbor sites and has an extended spatial structure [6] arising from the momentum dependence of V_{SF}. A similar picture of the interaction is seen in Monte Carlo calculations [7]; however, these are typically carried out at temperatures of order J, and it is not known

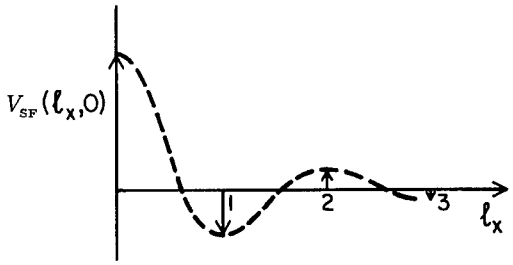


Fig. 2. The spatial Fourier transform of Eqn (5), $V_{SF}(\ell_x, \ell_y)$ versus the lattice spacing ℓ_x for $\ell_y = 0$. This shows the repulsive on-site and attractive near-neighbor structure of the effective pairing interaction which arises from the exchange of antiferromagnetic spin fluctuations.

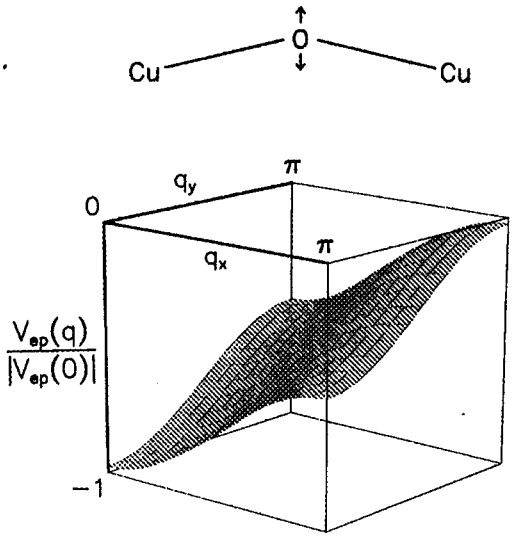


Fig. 3. The momentum dependence of $V_{ep}(q)$, Eqn (8), for the c-axis O phonon mode illustrated in the inset.

numerically what happens at low temperature.

The scenario just described shows why the observation of a $d_{x^2-y^2}$ gap forms an important finding for theories [8–10] in which antiferromagnetic spin-fluctuation exchange provides the pairing mechanism. However, things are in fact not clear-cut. Consider the electron–phonon interaction arising from the c-axis vibration of an O ion on a bent Cu–O–Cu bond illustrated in the inset of Fig. 3. In this case, the square of the electron–phonon matrix element for momentum transfer $p - p' = q$ is

$$|g(q)|^2 = \frac{|g|^2}{M\omega_0}\left(\cos^2\frac{q_x}{2} + \cos^2\frac{q_y}{2}\right) \tag{7}$$

and

$$V_{ep}(q) = -\frac{2|g(q)|^2}{\omega_0} = -\frac{2|g|^2}{M\omega_0^2}\left(\cos^2\frac{q_x}{2} + \cos^2\frac{q_y}{2}\right) \tag{8}$$

has the momentum dependence shown in Fig. 3. Thus $V_{ep}(q)$ becomes less negative at large momentum transfers. If an on-site repulsive U term were added so that

$$V_{ep}(q) = -\frac{2|g(q)|^2}{\omega_0} + U \tag{9}$$

were positive, the momentum dependence of $V_{ep}(q)$ would look a lot like V_{SF}. In fact, a calculation [11] using Eqn (8) shows that this type of electron–phonon interaction favors $d_{x^2-y^2}$ pairing. Recently Litvinchuk and Kulic [12] have argued that Coulomb correlation vertex corrections to the electron–phonon interaction reduce the strength of the phonon mediated interaction at large momentum transfers, and within a conserving approximation, they find that this enhances $d_{x^2-y^2}$ pairing.

Now one could argue that there are other reasons to believe that it is the Coulomb interaction between electrons that is responsible for the pairing mechanism in the high-T_c cuprates. So again, suppose we assume this to be the case. There still remain many choices for mechanisms which are compatible with a $d_{x^2-y^2}$ gap. Anderson [13] has proposed an interlayer pair transfer mechanism which can support whatever symmetry is generated by the in-plane interactions. The spin-bag mechanism of Schrieffer *et al.* [14] is consistent with a $d_{x^2-y^2}$ gap on a large Fermi surface. Various gauge RVB theories [15–17] lead to a gap with $d_{x^2-y^2}$ symmetry. Thus while antiferromagnetic spin-fluctuation theories predict a $d_{x^2-y^2}$ gap, there are a number of alternative theories which give rise to $d_{x^2-y^2}$ gaps.

Clearly one needs further constraints, and certainly the normal state as well as superconducting state transport properties provide such constraints. However, it appears possible to fit various transport properties to different theories, so that it is important to look for specific tests. One class of measurements that could provide a way of distinguishing different theories involves studying the frequency dependence of the gap. For the traditional low-temperature superconductors, the frequency dependence of the gap reflected in tunneling I–V characteristics as well as the conductivity $\sigma_1(\omega)$, when combined with neutron scattering data on the phonon density of states, provided detailed evidence that the pairing in these materials was mediated by the exchange of phonons [18,19]. For the cuprates, tunneling measurements [20] along with the single-particle spectral weight $A(p, \omega)$ obtained from ARPES [21] should provide information on the frequency dependence of the gap. Then with both the momentum and frequency dependence of $\Delta(p, \omega)$, one would hope to have a clearer picture of the momentum and energy structure of the pairing interaction.

For example, if the basic mechanism involves the single exchange of a spin-fluctuation, Eqn (5), one would expect to see the frequency structure in $\mathrm{Im}\chi(q, \omega)$ reflected in $\Delta(p, \omega)$. Within a conserving approximation, χ in the effective interaction, Eqn (5), has the form

$$\chi = \frac{\chi_0(q, \omega_m)}{1 - \bar{U}\chi_0(q, \omega_m)}, \tag{10}$$

with

$$\chi_0(q, \omega_m) = -\frac{T}{N}\sum\left(G(p+q, \omega_n + \omega_m)\, G(p, \omega_n)\right.$$

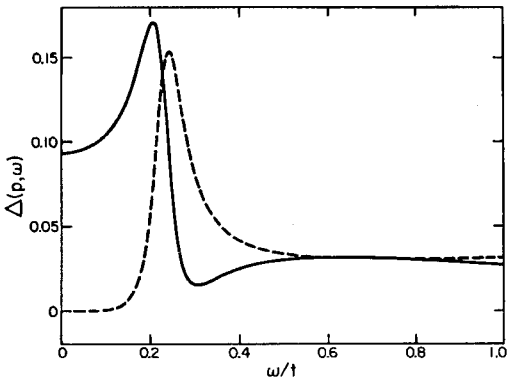


Fig. 4. The real (solid) and imaginary (dashed) parts of $\Delta(p, \omega)$ versus ω calculated within a conserving fluctuation exchange approximation for the two-dimensional Hubbard model.

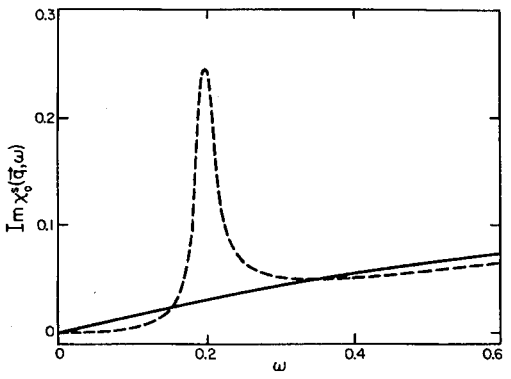


Fig. 5. The imaginary part of the irreducible magnetic susceptibility vs ω for $q = (\pi, \pi)$ at $T = T_c$ (solid curve) and $T = 0.38\,T_c$ (dashed curve) (from Ref. [22]).

$$+ F(p + q, \omega_n + \omega_m)\,F(p, \omega_n)\Big). \quad (11)$$

Thus χ_0 depends self-consistently upon $\Delta(p, \omega)$ through the G and F propagators. Figures 4 and 5 show results [22] for $\Delta(p, \omega)$ and $\mathrm{Im}\chi_0(q, \omega)$ with $q = (\pi, \pi)$, respectively, in which one sees this interplay. When the $d_{x^2-y^2}$ gap opens, the low-frequency spectral weight in $\mathrm{Im}\chi_0(q, \omega)$ decreases and a peak appears. This can occur for a $d_{x^2-y^2}$ gap since $\Delta_{p+(\pi,\pi)} = -\Delta_p$, and the coherence factor $\frac{1}{2}(1 - \Delta_{p+q}\Delta_p/E_{p+q}E_p)$ associated with quasi-particle pair production goes to unity. This peak in $\mathrm{Im}\chi(q, \omega)$, Fig. 5, is in turn reflected in the structure of $\Delta(p, \omega)$ shown in Fig. 4. In this framework, the peak in the neutron spin-flip scattering [23–25] from YBCO observed at 41 Mev for $q = (\pi, \pi, \pi)$ should produce structure in $\mathrm{d}I/\mathrm{d}V$ and $A(p, \omega)$ for $\omega \sim$ 41 Mev + Δ_0, where Δ_0 is the antinode $d_{x^2-y^2}$ gap value. However, if the basic interaction involves the cross-exchange of two or more spin-fluctuations as in the spin-bag model or is associated with an RVB or magnetic bipolaron mechanism, one would expect that structure in $\mathrm{Im}\chi(q, \omega)$ would be washed out in $\Delta(p, \omega)$ because multiple spin-fluctuations would be involved.

In addition to the frequency structure in $\Delta(p, \omega)$, the

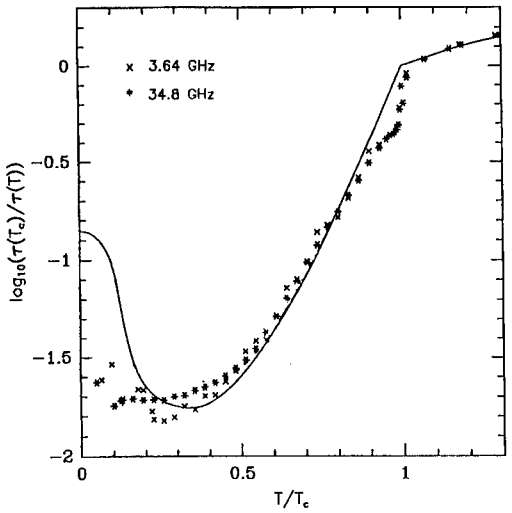


Fig. 6. Quasi-particle decay rate due to spin-fluctuation and unitary impurity scattering. The symbols are results for τ^{-1} determined from the microwave conductivity experiments by Bonn *et al.* ([26]).

frequency and temperature dependence of the quasi-particle lifetime provides information on the dynamic properties of the basic interaction. Microwave conductivity [26] as well as Hall thermal conductivity measurements [27] show that the quasi-particle scattering rate τ^{-1} decreases with temperature below T_c in much the same manner as the decrease in the nuclear spin-lattice relaxation time T_1. Calculations of this lifetime provide a dynamic test for different theories. Figure 6 shows results for τ^{-1} calculated [28] using the spin-fluctuation interaction V_{SF}, Eqn (5), with χ calculated for a $d_{x^2-y^2}$ gap using Eqns (10) and (11). For a $d_{x^2-y^2}$ gap, this leads to an inelastic spin-fluctuation scattering rate that varies as T^3 at low temperatures, similar to the behavior of the nuclear relaxation rate T_1^{-1}. The results shown in Fig. 5 for τ^{-1} contain both an inelastic spin-fluctuation piece as well as an elastic unitary impurity contribution. The latter becomes dominant for $T/T_c \lesssim 0.25$. In this problem, contrary to the usual Eliashberg electron–phonon case, there are strong feedback effects which arise from the fact that the same electrons that form pairs are also responsible for the spin fluctuations in χ. Calculations of the quasi-particle lifetime or more generally the single-particle spectral weight remain to be carried out for some of the other models. It will be interesting to see the differences in the dynamic predictions for theories that predict a $d_{x^2-y^2}$ momentum dependence of the gap. The frequency dependence of $\Delta(p, \omega)$ as well as the regular part of the single-particle self-energy should help distinguish between various high T_c theories.

Acknowledgements—I would like to acknowledge the Program on Correlated Electrons at the Center for Material Science at Los Alamos National Laboratory, where this work was written and discussed. I would like to thank N. Bulut, A. Balatsky, K. Bedell and J. Engelbrecht for useful discussions. This work was partially supported by the Department of Energy under grant

DE–FG03–85ER45197. The computations were carried out at the National Energy Research Supercomputing Center and the San Diego Supercomputing Center.

REFERENCES

1. *J. Phys. Chem. Solids* **54**(10) (1993).
2. Schrieffer J. R., *Solid State Commun.*,**92**, 129 (1995) ;Scalapino D. J., *Phys. Reports* **250**, 329 (1995); Van Harlingen D.,*Per. Mod. Phys.*,**67**, 515 (1995).
3. *Proc. Stanford Conference Spectroscopies in Novel Superconductors, J. Phys. Chem. Solids*, this issue (1995).
4. Bardeen J., Cooper L. N. and Schrieffer J. R., *Phys. Rev.* **108**, 1175 (1957).
5. Berk N. F. and Schrieffer J. R., *Phys. Rev. Lett.* **17**, 433 (1966).
6. Scalapino D. J.,*Random Magnetism, High-Temperature Superconductivity* (Edited by W. P. Beyermann, N. L. Huang-Liu and D. E. MacLaughlin), pp. 155–164. World Scientific, Singapore (1994).
7. Bulut N., Scalapino D. J. and White S. R., *Phys. Rev. B* **50**, 9623–9626 (1994).
8. Bickers N. E., Scalapino D. J. and Scalettar R. T., *Int. J. Mod. Phys. B* **1**, 687 (1987); Bickers N. E., Scalapino D. J. and White S. R., *Phys. Rev. Lett.* **62**, 961 (1989).
9. Moriya T., Takahashi Y. and Ueda K., *J. Phys. Soc. Jpn* **59**, 2905 (1990); *Physica C* **185** 114 (1991).
10. Monthoux P., Balatsky A. and Pines D., *Phys. Rev. Lett.* **67**, 3348 (1991); Monthoux P. and Pines D., *Phys. Rev. Lett.* **69**, 961 (1992).
11. Bulut N. and Scalapino D. J., UCSB preprint.
12. Litvinchuk A. P. and Kulic I., preprint.
13. Anderson P. W., *Superconductivity, Proceedings ICTP Spring College* (Edited by P. Butcher and Y. Lu). World Scientific, Singapore (1992); Chakravarty S., Sudbo A., Anderson P. W. and Strong S., *Science* **251**, 337 (1993).
14. Schrieffer J. R., Wen X. -G. and Zhang S. -C., *Phys. Rev. Lett.* **60**, 944 (1988); *Phys. Rev. B* **39**, 11663 (1989).
15. Gros C., Joynt R. and Rice T. M., *Z. Phys. B* **68**, 425 (1987).
16. Inui M., Doniach S., Hirschfeld P. J. and Ruckenstein A. E., *Phys. Rev. B* **37**, 2320 (1988).
17. Kotliar G. and Liu J., *Phys. Rev. B* **38**, 5142 (1988).
18. Schrieffer J. R., Scalapino D. J. and Wilkins J. W., *Phys. Rev. Lett.* **10**, 336 (1963).
19. McMillan W. L. and Rowell J. M., *Superconductivity* (Edited by R. D. Parks). Dekker, New York (1969).
20. Renner Ch. and Fischer O., *Phys. Rev. B* (1995), to be published.
21. Dessau D. S. *et al.*, *Phys. Rev. Lett.* **67**, 2573 (1991).
22. Monthoux P. and Scalapino D. J., *Phys. Rev. Lett.* **72**, 1874–1877 (1994).
23. Rossat-Mignod J. Regnault L. P., Vettier C., Burlet P., Henry J. Y. and Lapertot G., *Physica B* **169**, 58 (1991).
24. Mook H. A., Yethiraj M., Aeppli G., Mason T. E. and Armstrong T., *Phys. Rev. Lett.* **70**, 3490 (1993).
25. Fong H. F., Keiner B., Anderson P. W., Reznik D., Dogan F. and Aksay I. A., preprint.
26. Bonn D. A. *et al.*, *Phys. Rev. B* **47**, 11314 (1993).
27. Ong N. P., these proceedings.
28. Quinlan S. M., Scalapino D. J. and Bulut N., *Phys. Rev. B* **49**, 1470 (1994).

Pergamon

J. Phys. Chem. Solids Vol. 56, No. 12, pp. 1673–1677, 1995
1995 Elsevier Science Ltd
Printed in Great Britain
0022-3697/95 $9.50 + 0.00

0022-3697(95)00227-8

ARPES: NOVEL EFFECT IN THE ENERGY AND MOMENTUM DISTRIBUTIONS

J.R. SCHRIEFFER
National High Magnetic Field Laboratory and Department of Physics Florida State University, Tallahassee, Florida 32306, U.S.A.

A.P. KAMPF
Institut für Theoretische Physik, Universität zu Köln 50937 Köln, Germany

Abstract—The physical origin of two effects, i.e. shadow bands and three peaked energy spectra in the ARPES and inverse photoemission spectra of strongly correlated electron systems, such as the cuprates, are discussed. Shadow bands arise from quasi elastic exchange Bragg scattering from residual antiferromagnetic spin correlations in the paramagnetic phase. Three peaked energy spectra arise as a superposition of the central Landau quasi particle peak of the weakly correlated system and the upper and lower band peaks split by the SDW and/or Mott Hubbard pseudo gap 2Δ of the strongly correlated system. The coexistence of these three resonances is explained in terms of quasi particles propating in a medium with $\Sigma(k, \omega)$ exhibiting strong anomalous dispersion, i.e. multiple fermionic modes for fixed k.

The spectral function $A(\mathbf{k}, \omega)$ governing photo– and inverse photoemission in antiferromagnets, like superconductors, is qualitatively different from that in weakly correlated metals in that two peaks at quasi particle energies $\pm E_{\mathbf{k}} = \pm\sqrt{\epsilon_{\mathbf{k}}^2 + \Delta_{\mathbf{k}}^2}$ occur in the energy distribution for fixed $\mathbf{k}$ in the former while a single Landau quasi particle peak occurs at $\epsilon_{\mathbf{k}}$ in the latter. Furthermore, because of Bragg exchange scattering, the antiferromagnet (AF) exhibits quasi particle states

$$\gamma^c_{\mathbf{k}s} = u_{\mathbf{k}} c_{\mathbf{k}s} + 2s v_{\mathbf{k}} c_{\mathbf{k}+\mathbf{Q}s} \qquad \text{(particle-like)}$$
$$\gamma^v_{\mathbf{k}s} = v_{\mathbf{k}} c_{\mathbf{k}s} - 2s u_{\mathbf{k}} c_{\mathbf{k}+\mathbf{Q}s} \qquad \text{(hole-like)} \qquad (1)$$

which are linear combinations of the Landau–like states, where $\mathbf{k}$ is inthe first magnetic Brillouin zone, $\mathbf{Q}$ is the AF wavevector and $s = \pm\frac{1}{2}$ the spin quantum number along the AF sublattice direction. Thus, for fixed binding energy $E_{\mathbf{k}}$, one has electron emission with momenta $\mathbf{k}$ and $\mathbf{k} + \mathbf{Q}$ ("magnetic umklapp") with relative intensities $v_{\mathbf{k}}^2$ and $u_{\mathbf{k}}^2$. In contrast, in fermi liquids electron emission occurs only at $\mathbf{k}$ (except for crystal lattice umklapp at $\mathbf{k} + \mathbf{G}$, where $\mathbf{G}$ is a reciprocal crystal lattice vector).

AF spin fluctuation systems, with spin correlation length L_s and characteristic frequency ω_0, were shown by the present authors to exhibit novel spectral features $A(\mathbf{k}, \omega)$ in both the momentum and energy distributions,[1] namely:

(1) **for fixed energy** ω, broadening magnetic umklapp beams occur in photoemission andare centered around $\mathbf{k} + \mathbf{Q}$, with integrated intensity, $u_{\mathbf{k}}^2$,where $\mathbf{Q}$ is magnetic reciprocal lattice vector of the ordered AF, and

(2) **for fixed k**, *three* peaks occur in the energy distribution corresponding to the coexistence of the split peaks $\pm E_{\mathbf{k}}$ of the ordered AF phase *plus* the Landau peak of the fermi liquid phase.

The magnetic umklapp effect, i.e. presence of spectral weight for $\mathbf{k}$ *not only* in the first magnetic Brillouin zone (MBZ) is termed the shadow band effect. With an impressive experimental setup this shadow band effect (i) has recently been reported in room temperature ARPES experiments on the cuprate superconductor *Bi*2212.[2,3] While shadow band effects are clear from the physical point of view, less clear is how a Landau quasi particle peak (admittedly of small spectral strength) survives well into the spin fluctuation (SF) regime, where the SF frequency ω_0 is small compared to 2Δ and band tails into the pseudo gap are small. The explanation of this phenomenon is given below in terms of anomalous dispersion. This situation is analogous for the acoustic modes of an organ pipe containing a driven sound mode.

Beginning with the ordered AF, the mean field energy bands are plotted in Fig. 1a in the *reduced* zone scheme, Fig. 1b in the *extended* zone scheme, and in Fig. 1c the *periodic* zone scheme. It is the latter representation which smoothly connects with the SF regime. To illustrate this point, we plot the AF bands as a function of Bloch momentum $\mathbf{k}$ (labelling the $c_{\mathbf{k}s}$ of the non–magnetic crystal schematically as opposed to the magnet eigenstate "Neel momentum") labelling γ_k in the ordered AF. The shading of the lines represents the spectral weight at each $\mathbf{k}$ and ω, namely

$$u_{\mathbf{k}}^2 = \tfrac{1}{2}\left(1 + \frac{\epsilon_{\mathbf{k}}}{E_{\mathbf{k}}}\right) \qquad \text{(upper band)}$$
$$v_{\mathbf{k}}^2 = \tfrac{1}{2}\left(1 - \frac{\epsilon_{\mathbf{k}}}{E_{\mathbf{k}}}\right) \qquad \text{(lower band)} \qquad (2)$$

with $u_{\mathbf{k}}^2$ and $v_{\mathbf{k}}^2$ plotted in Fig. 1d.

Working with a periodic Kondo or spin fermion model

$$H = \sum_{\mathbf{k}s} \epsilon_{\mathbf{k}} n_{\mathbf{k}s} + J \sum_i \psi_i^\dagger \underline{\sigma} \psi_i \cdot \mathbf{S}_i + H_{ss} \qquad (3)$$

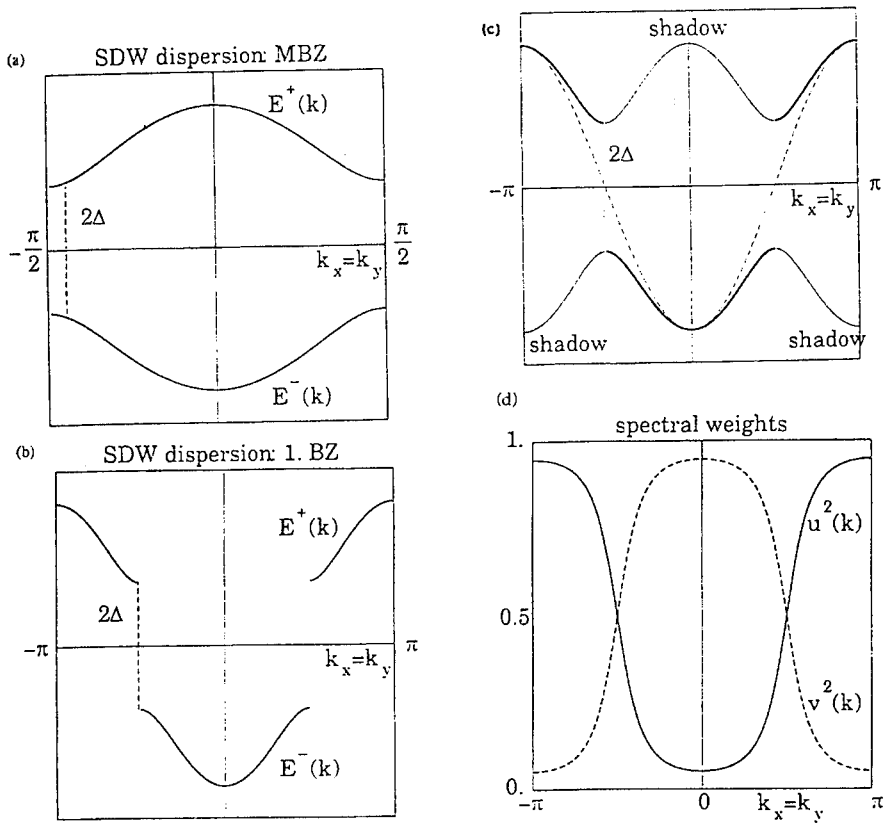


Fig. 1. Energy bands in the SDW state along the zone diagonal $k_x = k_y$in (a) the reduced magnetic Brillouin zone, (b) the extended first Brillouin zone, and (c) the repeated zone scheme. In (c) the shading of the lines represents their relative spectral weight. The dashed line indicates the expected dispersion in the spin fluctuation phase without long range magnetic order. (d) Spectral weight functions $u^2()$ and $v^2(\mathbf{k})$ along the zone diagonal.

or alternatively with a one–band Hubbard model, and assuming a simple model form of the spin propagator

$$\chi(\mathbf{q}, \omega) = -\lambda^2 a^2(\Gamma) \sum_{\mathbf{Q}=(\pm\pi,\pm\pi)} \frac{\Gamma}{(q_x - Q_x)^2 + \Gamma^2} \times \times \frac{\Gamma}{(q_y - Q_y)^2 + \Gamma^2} \int g(\nu) \frac{2\nu}{\omega^2 - \nu^2 + i\delta} d\nu \quad (4)$$

the authors found the electron self–energy

$$\Sigma(\mathbf{k}, \omega) = -iU^2 \frac{1}{N} \sum_{\mathbf{q}} \int \frac{d\nu}{2\pi} \chi(\mathbf{q}, \nu) G_0(\mathbf{k} - \mathbf{q}, \omega - \nu) \quad (5)$$

shows anomalous behavior compared to that of a conventional fermi liquid;[1] examples are shown in Fig. 2. In Eq. (4) Γ is the inverse of the spin–spin correlation length and the frequency distribution function $g(\omega)$ is chosen linear up to a characteristic SF cutoff frequency ω_0. The prefactor $a(\Gamma)$ normalizes the area of the Lorentzians around the AF wavevectors to unity. The authors showed why these results are very insensitive to the form of $\chi(q, \omega)$, so long as χ is strongly peaked about $\mathbf{q} \simeq \mathbf{Q}$ and ω_0 is small compared to the fermionic pseudo gap 2Δ, as for the MMP[4] forms of χ.

In the AF phase, the mean field self–energy is

$$\Sigma^{AF}(\mathbf{k}, \omega) = \frac{\Delta^2}{\omega + \epsilon_{\mathbf{k}}} \quad (6)$$

as shown in Fig. 3a. $\epsilon_{\mathbf{k}}$ is the tight binding dispersion for the noninteracting electrons, e.g. $\epsilon_{\mathbf{k}} = -2t\,(\cos k_x + \cos k_y)$ for the square lattice. The divergence of Σ at $\epsilon_{\mathbf{k}}$ pushes *up* energy states above $\epsilon_{\mathbf{k}}$ and pushes *down* states below $\epsilon_{\mathbf{k}}$. This is the cause of the gap 2Δ, as in a superconductor. In contrast, in a fermi liquid, Σ typically depends weakly on $\mathbf{k}$ and Σ has a *negative* slope near the chemical potential $\mu \equiv 0$ as shown in Fig. 3b, pushing *down* high energy states and *up* low energy states near $\omega = 0$; i.e. a mass enhancement m^*/m 1. The remarkable result that *both* features are simultaneously present in this antiferromagnetical metal spin fluctuation phase, as shown in Fig. 3c, although the negative slope near $\omega = 0$ extends only tothe characteristic spin fluctuation energies $\simeq \pm\omega_0$ significant strength (spectral weight) exists only for $\mathbf{k}$ near $\mathbf{k}_F$, i.e. $|k - k_F| < \omega_0/v_F$, where $v_F = |\nabla\epsilon_{\mathbf{k}}|_{k_F}$.

Since the poles of $G(\mathbf{k}, \omega)$ give the quasi particle energies,

$$G^{-1}(\mathbf{k}, \omega) = \omega - \epsilon_{\mathbf{k}} - \Sigma(\mathbf{k}, \omega) = 0 \quad (7)$$

it appears from Fig. 3c that five peaks would appear in $A(\mathbf{k}, \omega)$ for fixed $\mathbf{k}$. It is readily seen that poles labelled 2 and

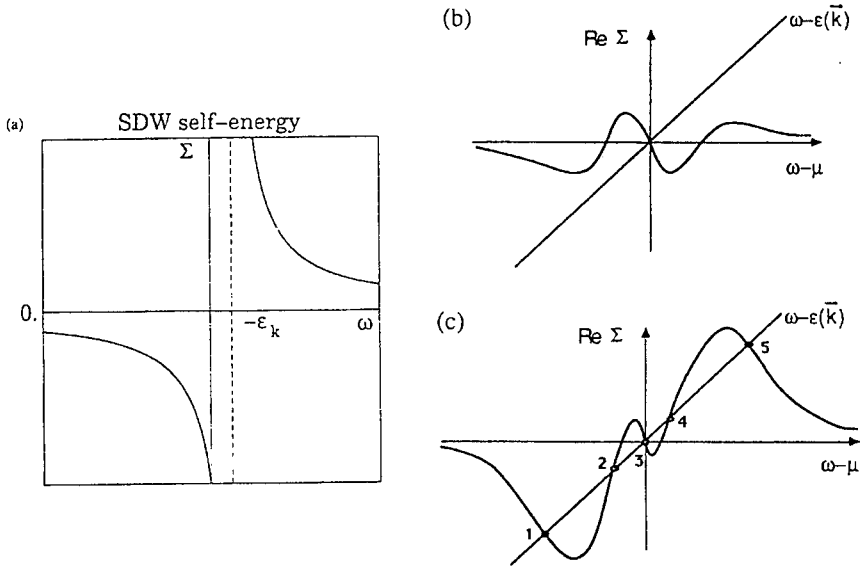


Fig. 3. (a) Real part of the mean-field self-energy in the SDW state.(b) Typical shape for the frequency dependence of $\Re\Sigma$ in a Landau fermi liquid. (c) Modified shape of $\Re\Sigma$ in the spin fluctuation regime. Indicated in the figure are the intersections of$\Re\Sigma$ with $\omega - \epsilon_{\mathbf{k}}$ for $k = k_F$ determining the peak energies of the spectral function.

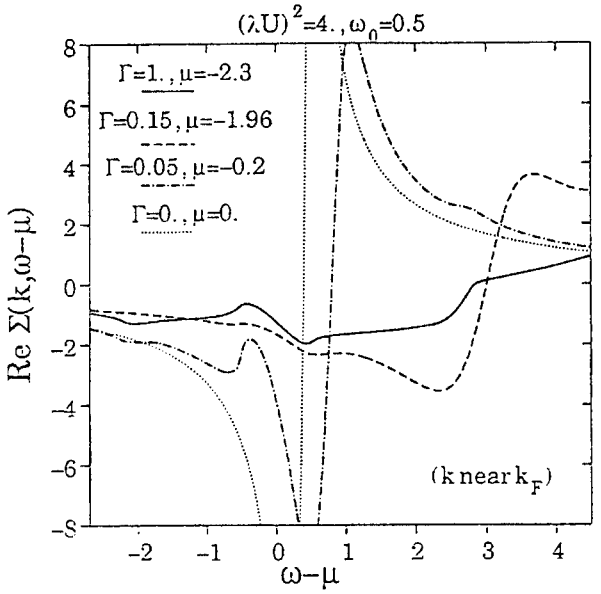


Fig. 2. The real part of the one-loop self-energy calculated with the model susceptibility Eq. (4) for the parameter sets as indicated in the figure. Energies are measured in units of the hopping amplitude t for the tight binding dispersion on a square lattice. $\Sigma(\mathbf{k}, \omega)$ has been calculated on a 108×108 lattice for a momentum $\mathbf{k}$ along the diagonal of the Brillouin zone (i.e. $k_x = k_y$); $\mathbf{k}$ has been chosen as the momentum closest below $\mathbf{k_F}$ along the zone diagonal.

4 are heavily damped and contribute only to the incoherent background, while poles 1 and 5 are the AF lower and upper bands and pole 3 is the Landau peak, whose weight z_3 is extremely small for $L_s \gg a \equiv 1$ (the crystal lattice spacing).

Therefore, in addition to the shadow contours in $A(\mathbf{k}, \omega)$ for fixedω there is also a novel structure in the binding energy distribution at fixed momentum $\mathbf{k}$. In essence, the single peak Landau–like spectrum for very short L_s crosses over to the two–peak spectrum of the ordered SDW in a smooth manner. Namely, rather than the Landau peak at $\epsilon_{\mathbf{k}}$ splitting into two peaks at the energies $E_{\mathbf{k}}^{\pm} = \pm\sqrt{\epsilon_{\mathbf{k}}^2 + \Delta^2}$ of the energies of the SDW phase we found that the $E_{\mathbf{k}}^{\pm}$ peaks grow out of the incoherent background of the Landau spectrum, while the Landau peak continues to exist but with strongly reduced weight.[1]

The corresponding evolution of the spectral function $A(\mathbf{k}, \omega - \mu)$ as calculated from the model susceptibility Eq. (4) for a specific parameter set is demonstrated in Fig. 4. The density of states (DOS) which follows from the momentum integration of the spectral functions is shown in Fig. 5. Remarkably, once the chemical potential has moved into the energy range near the top of the valence band for intermediate and small $\Gamma = 1/L_s$ a peak in the DOS appears close to μ, quite similar to what is found in the numerical studies of the 2D Hubbard model.[5,6]

Of course, in a complete analysis of a microscopic SF model the dynamical spin susceptibility $\chi(\mathbf{q}, \omega)$ would have to be determined self consistently from the model. L_s would diverge for the AF parent compound for$\mu = 0$ and μ would be negative for finite L_s and $\omega_0 > 0$ in the hole doped material. Both L_s and μ would have a model specific dependence on the doping. Nevertheless, it has proven to be instructive to varyL_s, ω_0 and μ independently as a test for the sensitivity of $A(\mathbf{k}, \omega)$ to each of these parameters.

In numerical simulations for the 2D Hubbard model the chemical potential has been found to move very rapidly with hole doping from $\mu = 0$ in the AF insulator at half–filling into the energy range of the former SDW valence band.[5] We therefore have analyzed the electronic spectrum which

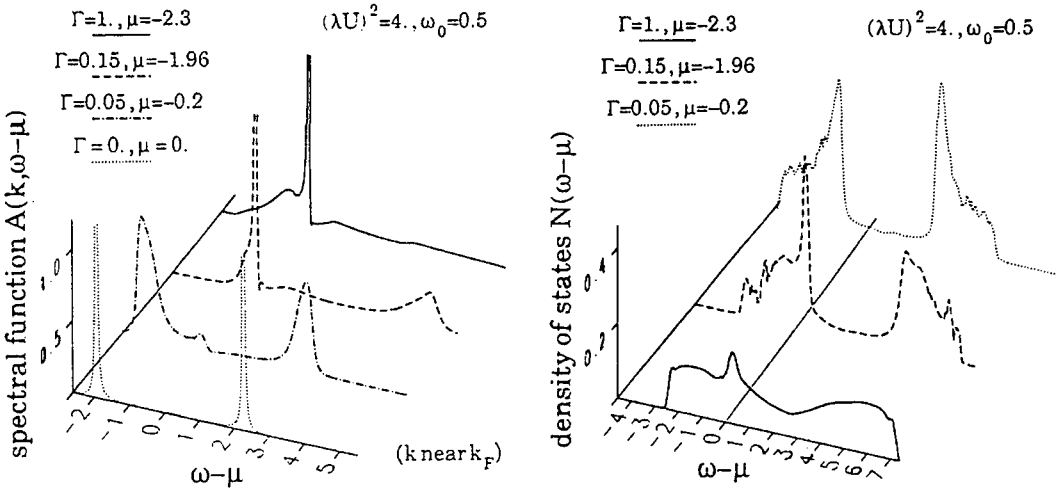


Fig. 4. Frequency dependence of the spectral functions $A(\mathbf{k}, \omega - \mu)$for the same parameter set as in Fig. 2. The figure shows the evolutionwith decreasing spin-spin correlation length $L_s = 1/\Gamma$ from the two-peak structure of the SDW state (dotted line) and to the three-peak structure at $L_S = 20$ (dashed dotted line), and to the Landau like single peak spectrum at $L_S = 1$ (solid line). In the intermediate case(dashed line) the chemical potential is located in the energy range ofthe remnant structure of the valence SDW band.

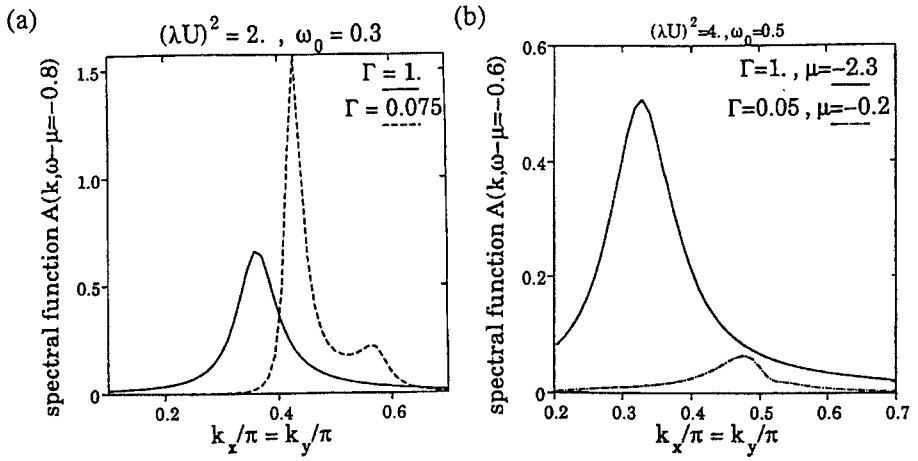


Fig. 5. Densities of states for the same parameter sets as in Figs. 1,2, and 3 showing the evolution with increasing spin-spin correlation length to the pseudogap structure at large L_S. For the three different parameter sets the electron densities are 0.59 (solid line),0.71 (dashed dotted line), and 0.98 (dotted line), respectively.

followsfrom the self–energy Eq. (5) for the situation of a rapidly moving μ at low hole doping under the assumption that fairly long range AF correlations [i.e. a small Γ in the model susceptibility Eq. (4)] still persist. This motivates the specific choice of parameters used in the calculations for Figs. 2,4, and 5.

Clearly, the correlation of Γ with μ determines the doping window in which the three–peak spectrum is realized. Specifically, for the 2D Hubbard model the doping window around half–filling for the three–peak structure must be tiny. For the small lattice sizes explored so far in numerical simulation studies the three–peak spectrum may be not observable, since on the small lattices already a single hole represents a doping concentration of afew percent and the three–peak spectrum may be inaccessible. Our phenomenological model analysis is therefore not in conflict with the numerical simulation studies forthe 2D Hubbard model.

The situation is different for the observability of the shadow band effect (i)when ARPES spectra are scanned in momentum. Figure 6 shows the $\mathbf{k}$ dependence along the Brillouin zone diagonal at a fixed frequency (binding energy) below the chemical potential for the same parameter set as used above. Only a single Landau like quasiparticle peak is visible when the magnetic correlation length is comparable to the lattice spacing, i.e. for $\Gamma = 1$. The additional shadow peak rises with increasing L_s at a large momentum above k_F due to the magnetic umklapp effect described above mixing momentum states $|\mathbf{k}\rangle$ and $|\mathbf{k} + \mathbf{Q}\rangle$. Note, however, that in the case of the three–peak spectrum the central small weight quasiparticle peak does not have a shadow structure in the

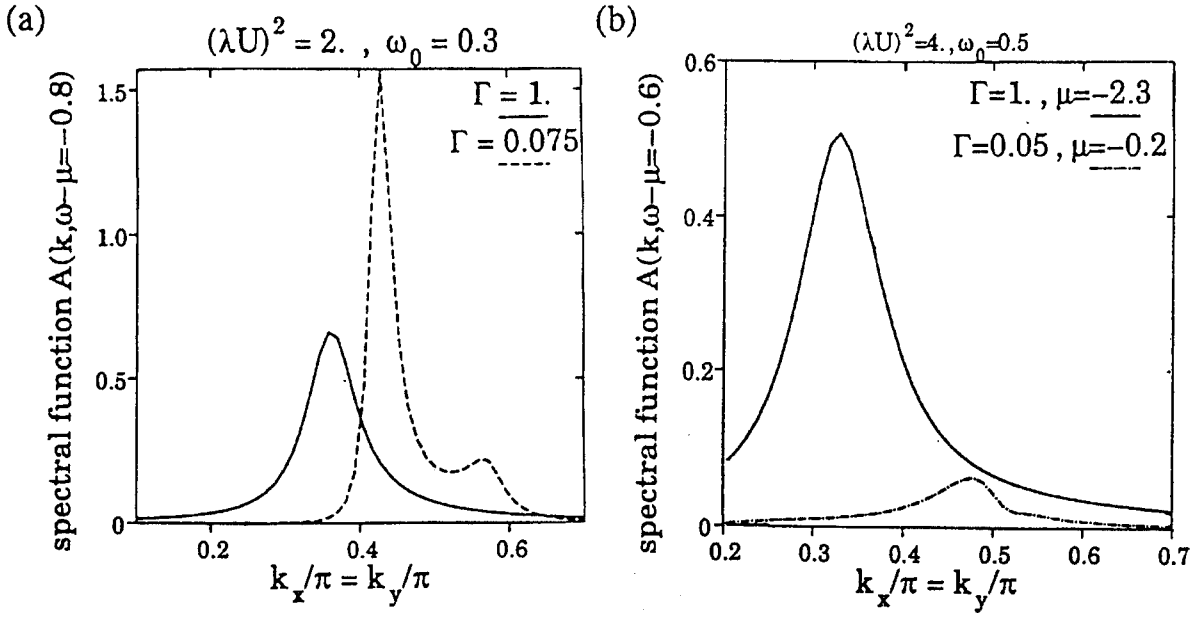


Fig. 6. Spectral functions $A(\mathbf{k}, \omega - \mu)$ for a fixed frequency below the chemical potential plotted as a function of momentum $\mathbf{k}$ along the diagonal of the Brillouin zone. For the Landau like spectrum [solid line in Figs. (a) and (b)] only a single peak appears in the ARPES spectrum. However, for sufficiently long range spin correlations [dashed line in (a)] a shadow peak with smaller weight appears at larger momentum above k_F besides the dominant quasiparticle peak. Note that no shadow structure of the Landau peak appears in the three-peak spectrum (dash–dotted line in Fig. (b), compared also with Fig. 4 for the same parameter set).

momentum dependence of the spectral function.

Thus, one sees that the persistence of Landau peak well into the spin fluctuation phase, $L_s \gg 1$, and its coexistence with the Mott-Hubbard-Slater upper and lowerbands is simply understood in terms of quasi particles propagating in a highly dispersive medium, in that $\Sigma(\mathbf{k}, \omega)$ has a pole at $\omega \cong \epsilon_k$. This property leads to multiple zeros of $G^{-1}(\mathbf{k}, \omega)$ with nonzero residues of G (fermion quasi particlemodes) just as several (boson) modes of sound occur for given $\mathbf{q}$in superfluid ^{4}He. Details will be provided in a forthcoming paper.

Acknowledgements—This work was supported in part by NSF grants 92-22-682 and 5024-501-22 (JRS).A.P.K. gratefully acknowledges support through a Heisenberg fellowship of the Deutsche Forschungsgemeinschaft (DFG). A.P.K.'s research has been performed within the program of the Sonderforschungsbereich 341 of the DFG.

REFERENCES

1. Kampf A.P. and Schrieffer J.R., *Phys. Rev. B* **41**, 6399(1990).
2. Aebi P., Osterwalder J., Schwaller P., Schlapbach L., Shimoda M., Mochiku T. and Kadowaki K., *Phys. Rev. Lett.* **72**, 2757 (1994).
3. Aebi P. et al., this volume.
4. Millis A.J., Monien H. and Pines D., *Phys. Rev. B***32**, 167 (1990).
5. Dagotto E., Moreo A., Ortolani F., Poilblanc D. and Riera J.,*Phys. Rev. B***45**, 10741, (1992); Dagotto E., Ortolani F. and Scalapino D.J., *Phys. Rev. B* **46**, 3183 (1992).
6. Scalapino D.J., *Physica* **C185–188**, 104 (1991).

Pergamon

J. Phys. Chem. Solids Vol. 56, No. 12, pp. 1679–1684, 1995
Copyright © 1995 Elsevier Science Ltd
Printed in Great Britain. All rights reserved
0022–3697/95 $9.50 + 0.00

0022–3697(95)00228-6

MAGNETIC BEHAVIOR OF THE CUPRATE SUPERCONDUCTORS

ALEXANDER SOKOL

Department of Physics, University of Illinois at Urbana-Champaign, Urbana IL 61801, U.S.A. and L.D. Landau Institute for Theoretical Physics, Moscow, Russia

Abstract—I review recent work on magnetic dynamics of the high temperature superconductors using a model that combines two weakly interacting species of low-energy excitations: the antiferromagnetic spin waves which carry spin-1 and no charge, and Fermi-liquid-like quasiparticles which carry spin-1/2 and charge e. The model allows conversion of spin waves into electron-hole pairs; however, the low-energy spin waves are not collective modes of the quasiparticles near the Fermi surface, but rather are a separate branch of the low-energy spectrum. With certain experimentally justified assumptions, this theory is remarkably universal: the dependence on the detailed microscopic Hamiltonian and on doping can be absorbed into several experimentally measurable parameters. The $z = 1$ theory of the insulators and $z = 2$ theory of the overdoped materials, are both reproduced as limiting cases of the theory described here, which predicts that the underdoped materials remain in $z = 1$ universality class at sufficiently high temperature. This theory provides a framework for understanding both the experimental results and microscopic calculations, and in particular yields a possible explanation of the spin gap phenomenon. I also discuss some of the important unresolved issues.

1. INTRODUCTION

The evolution of the normal state properties of the high temperature superconductors with doping is schematically described by the phase diagram in Fig.1. The stoichiometric insulators La_2CuO_4 and $YBa_2Cu_3O_6$ undergo an antiferromagnetic transition at T_N, and exhibit short-range antiferromagnetic correlations well above T_N. Upon doping by more than several per cent strontium or oxygen, these systems become metallic and no longer have a long-range antiferromagneticorder, but short-range magnetic correlations remain. It is universally agreed that the normal state properties of this metallic state are far from the conventional metallic behavior, and the term "strange metal" has been coined to describe them. Some of the key properties of the "strange metal" are: (i) short-range antiferromagnetic correlations,seen by NMR and neutron scattering; (ii) both the resistivity and the uniform magnetic susceptibility increase as the temperature increases; (iii) some, but not all, of the materials exhibit a suppression of the low-frequency spectral weight for magnetic excitations for $T < T^* \sim 150K$ (spin gap). At higher doping, the normal state properties become increasingly similar to the Fermi liquid (FL) behavior with short-range antiferromagnetic correlations. While Landau Fermi liquid theory in the orthodox sense requires temperature-independent spin correlations, the temperature dependence is weak in $YBa_2Cu_3O_7$ and other fully doped materials, where close proximity of the FL state is evident.

High-temperature superconductivity occurs in the intermediate strange metal phase in Fig.1. Currently, there is no consensus regarding the precise microscopic Hamiltonian of this phase. In what follows, I describe a theoretical approach to this problem which bypasses the missing information about the microscopic Hamiltonian by assuming continuous evolution of the low-energy magnetic and charge excitation spectrum between the antiferromagnetic insulator and the Fermi liquid phases, through the intermediate strange metal phase (see, e.g. [1–6], and references therein, and relevant earlier work [7–10]).

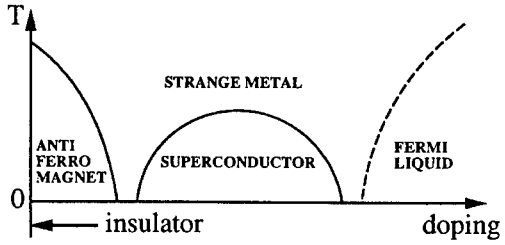


Fig. 1. A phase diagram of the high-temperature superconductors as a function of doping and temperature. In the limit of zero doping, the insulating parent materials develop a long-range Néel order and their low-energy excitation spectrum has only one species of excitations — the spin waves. The overdoped materials at low temperatures exhibit Fermi-liquid-like properties;there, the quasiparticles are the only species of low-energy excitations. We attempt to understand the properties of the intermediate "strange metal" phase, where superconductivity occurs, by combining the excitations found in the extreme doping limits, namely the spin waves and the quasiparticles, and allowing spin waves to convert into electron-hole pairs.

2. NEARLY ANTIFERROMAGNETIC FERMI LIQUID

The approach of Refs.[1–6] is based on combining the low-energy excitations encountered in the two extreme doping limits in Fig.1: the undoped antiferromagnetic insulators where the low-energy excitations are spin waves, and

the overdoped limit where the low-energy excitations are the usual Fermi liquid quasiparticles. I emphasize that such an approach makes no explicit assumptions about the microscopic Hamiltonian, and also it makes no assumptions regarding the mechanism through which the two types of low energy excitations are formed. Instead, the theory is based on the premise that at low energies, the spectral weight of the system is *shared* between the spin waves and the quasiparticles, and that the primary interaction mechanism is spin wave to electron-hole pair conversion. A microscopic basis for this theory is provided by the mean-field spin density wave (SDW) calculations, described in [5].

The presence of the first species of low-energy excitations, the quasiparticles, is evident from photoemission experiments. Such quasiparticles at low energies must be similar to the quasiparticles of the Landau Fermi liquid theory, and carry both charge e and spin $S = 1/2$, in order to account for the sharp quasiparticle peak near the Fermi energy, observed in photoemission. The quasiparticles are gapless and form a Fermi surface, the shape of which is very important for the interaction between the quasiparticles and spin waves.

The other species of low energy excitations, the spin waves, are the only low-energy modes in the antiferromagnetic insulators La_2CuO_4 and $YBa_2Cu_3O_6$. Below T_N, the spin waves are gapless, and in small-q limit have a linear spectrum $\omega_q \simeq cq$ and a mean-free path that is longer than the wavelength. When elevated temperature or doping destroy the long-range order, and only short-range antiferromagnetic correlations remain (the correlation length ξ is finite), the spin waves are no longer gapless and also are overdamped for $q < \xi^{-1}$. Nevertheless, for larger wavevectors $q > \xi^{-1}$, the spin waves remain nearly the same as in the presence of long-range order, because they sample only the local order for distances of order wavelength $\lambda = 2\pi/q \ll \xi$, and a therefore are nearly insensitive to the absence of antiferromagnetic correlations at distances larger than ξ. The evidence for their existence in the strange metal phase is based primarily on NMR and neutron scattering measurements, and is discussed in what follows. The spin waves carry spin $S = 1$ and no charge.

Whereas on the microscopic level an antiferromagnetic spin wave can be regarded as a coherent electron-hole pair, the contribution from the quasiparticle states near the Fermi surface accounts for only a fraction of the total spectral weight of the spin wave, if there is no nesting. The spin waves are therefore a separate branch of excitations, rather than a collective mode of low-energy quasiparticles. In that sense, the theory described here is somewhat similar to the spin-charge separation theory, where low-energy spin excitations cannot be represented as collective modes of low-energy charge excitations, even though on the microscopic level both originate from electrons. The difference between our model [1–6], and the spin-charge separation picture applied to the high temperature superconductors [11], is that in our model one species of excitations (spin waves) carries only spin, while the other (quasiparticles) carries both spin and charge, therefore there is charge separation, but not spin separation. Recently, Sachdev [3] and Laughlin [12] have pointed out that in a system with spin-charge separation, some of the spinon and holon excitations may form bound states which carry both spin and charge, and in many respects are similar to conventional quasiparticles.

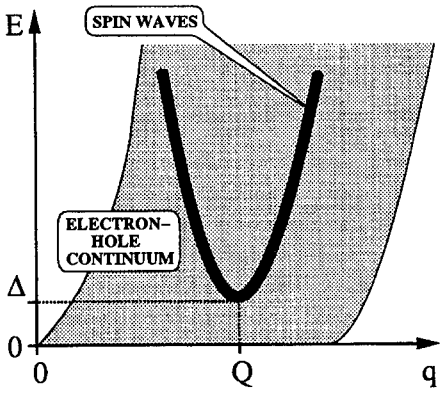


Fig. 2. Magnetic excitation spectrum of type (B) model (classification due to Millis [10]), where $\mathbf{Q} = (\pi/a, \pi/a)$ can connect two points on the Fermi surface. The minimum of the spin wave dispersion $\omega_q = (c^2|\mathbf{q} - \mathbf{Q}|^2 + \Delta^2)^{1/2}$ is located inside the electron-hole continuum.

One of the key factors that affect the magnetic and charge properties is the position of the minimum of the spin wave spectrum, $\mathbf{Q} = (\pi/a, \pi/a)$ for the commensurate short range order discussed here, with respect to the electron-hole continuum. If the spin wave spectrum is located inside the electron-hole continuum, as it is illustrated in Fig.2, the spin waves can convert into electron-hole pairs. This conversion process becomes the dominant contribution to spin wave damping at low energies, and has a profound effect on the magnetic properties. In the classification introduced by Millis, this situation is called model B. For a discussion of the opposite case, when $\mathbf{Q}$ cannot connect two points on the Fermi surface (model A), see Refs.[10,3,5].

The results of recent photoemission measurements [13] indicate that model B is relevant to the Y- and Bi-based high-temperature superconductors. In what follows, I concentrate exclusively on model B.

3. SPIN GAP

The spin gap behavior is the suppression of the low frequency spectral weight for magnetic excitations, which can be observed by NMR and neutron scattering. In the model at hand, this suppression is expected already in a very crude approximation which treats spin wave and quasiparticle excitations as noninteracting, free modes. Below, I describe a qualitative picture of the spin gap behavior suggested by Sokol and Pines [2,4], and derived starting from model B by Sachdev, Chubukov, and Sokol.[5]

In the non-interacting approximation, the density of

states for magnetic excitations is a sum of spin wave and quasiparticle contributions. For frequencies below the gap for spin wave excitations, $\omega < \Delta = c/\xi$, only the quasiparticles contribute to the magnetic density of states. For frequencies $\omega > \Delta$, both the spin waves and the quasiparticles contribute. In a measurement of the total magnetic density of states, for example in a NMR relaxation or neutron scattering measurement at low temperatures, one expects to see a gap-like suppression of the density of states for magnetic excitations for $\omega < \Delta$.

Beyond the non-interacting approximation, the lifetime of spin waves primarily is due to their conversion into electron-hole pairs. Upon increasing doping, the spin gap is washed out by a combination of two separate effects: first, the spin waves become overdamped because the rate of conversion increases; second, the gap for spin-wave excitations $\Delta = c/\xi$ increases as ξ decreases. The remaining spin waves, which are pushed to much larger energies, can in principle be seen by neutron scattering. At least two recent experiments seem to allow such an interpretation: the evidence for the magnetic character of the 41 meV peak in $YBa_2Cu_3O_7$ by Keimer *et al.* [14] and the observation of the zone-boundary magnon in $La_{2-x}Sr_xCuO_4$ by Aeppli *et al.* [15]. Keimer [14] and Barzykin and Pines [6] have suggested that the 41meV feature is a coherent, triplet, electron-hole pair – in other words, a spin wave (several alternative interpretations have been suggested as well). The zone boundary high-energy spin wave (a magnon), which continuously evolved from the identical mode in the insulator, seems to be the only viable interpretation of Aeppli's measurements; however, this data is very preliminary [15].

4. UNIVERSAL THEORY OF MAGNETIC DYNAMICS

In this section, I describe recent work by Sachdev, Chubukov, and Sokol [5], where the universal behavior of the magnetic correlations near $\mathbf{Q}$, and of the bulk susceptibility, was calculated using the rate of the Landau damping of spin waves as an input parameter. Several important assumptions about the microscopic model are built into this theory. First, we limit our study to systems with short-range order at $T = 0$. The region at low doping where the long range Néel order exists at $T = 0$ requires separate consideration. Second, we require that there is no nesting, i.e. the areas of the Fermi surface that are adjacent to the points connected by $\mathbf{Q}$, are not parallel to each other. The photoemission measurements [13] show that this is the case in Y- and Bi-based superconductors. Third, we assume that there is no substantial q-, ω-, and T-dependence of the Landau damping for $|\mathbf{q} - \mathbf{Q}| \sim 1/\xi$ and $\omega \sim \Delta$, respectively. This assumption is more difficult to verify experimentally; it holds in mean field theory on the disordered side if the correlation length is large enough.

Under these assumptions, the additional damping due to the spin wave to electron-hole pair conversion can be included into the theory by inserting its rate Γ into the noninteracting spin wave dynamical response function (a similar expression was introduced by Barzykin, Pines, Sokol, and Thelen [16] on phenomenological grounds):

$$\chi(\mathbf{q}, \omega) \sim \frac{\text{const}}{\omega_q^2 - \omega^2} \rightarrow \frac{\text{const}}{\omega_q^2 - \omega^2 - i\omega\Gamma}, \qquad (1)$$

where the spin wave spectrum for finite ξ (short-range correlations) has the following form:

$$\omega_q = \sqrt{c^2|\mathbf{q} - \mathbf{Q}|^2 + \Delta^2}, \quad \Delta = c/\xi. \qquad (2)$$

The exact dynamical susceptibility of the model is obtained by calculating the effects of mutual scattering of spin waves, primarily the additional damping, on $\chi(\mathbf{q}, \omega)$ given by Eq.(1). When the Landau damping processes dominate dissipation, the result of such a calculation differs only slightly from Eq.(1).

With these assumptions, the dynamical magnetic susceptibility near the staggered wavevector, $|\mathbf{q} - \mathbf{Q}| \ll a^{-1}$, is given by:

$$\chi(\mathbf{q}, \omega) = \frac{\mathcal{Z}}{T^{-\eta}} \left(\frac{c}{T}\right)^2 \Phi_s \left(\frac{c|\mathbf{q} - \mathbf{Q}|}{T}, \frac{\omega}{T}, \frac{\Delta}{T}, \frac{\Gamma}{T}\right), \qquad (3)$$

and the temperature-dependent part of the uniform magnetic susceptibility, χ_u, by:

$$\chi_u(T) - \chi_u(T = 0) = (1 + \alpha')\frac{T}{c^2}\Phi_u \left(\frac{\Delta}{T}, \frac{\Gamma}{T}\right). \qquad (4)$$

Here, α' is a non-universal constant, both Φ_s and Φ_u are universal and computable functions of their arguments, and η is a universal critical exponent which is very small and for all practical purposes can be replaced by zero.

Eqs.(3,4) apply when all dimensionful parameters and variables are smaller than the respective lattice cutoffs, which roughly translates into the following:

$$\omega, T, \Delta, \Gamma \ll \min(J, E_F), \quad \xi^{-1}, |\mathbf{q} - \mathbf{Q}| \ll a^{-1}, \qquad (5)$$

where J is the exchange constant, E_F the Fermi energy, and a the lattice spacing. If the conditions (5) apply, the magnetic dynamics near $\mathbf{Q}$ depends on four dimensionful parameters, two of which describe the spin wave spectrum (c and Δ), one is set by the size of spin ($\mathcal{Z}$), and one is determined by the rate of the Landau damping (Γ). The temperature-dependent part of the bulk susceptibility, which adds to the Pauli term, is also universal up to the overall prefactor $1 + \alpha'$.

For a low-energy theory this number of parameters is not excessive because they include *all* the information about the material that is reflected in its magnetic behavior. Three of them are the overall scales of magnetic moment, distance, and energy, and are therefore unavoidable in any low-energy theory; determination of these three parameters from the experimental data is straightforward and is a matter of simple normalization. The fourth parameter serves as the single crossover variable which describes the evolution from the

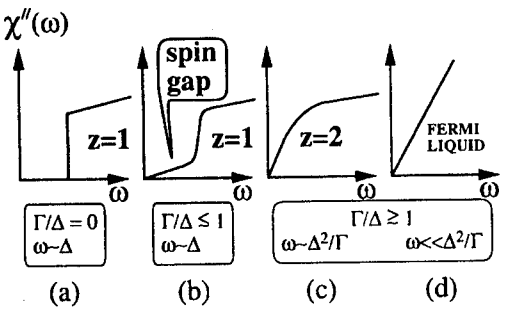


Fig. 3. Evolution of $\chi_L''(\mathbf{q},\omega) = \int d\mathbf{q}\,\chi''(\mathbf{q},\omega)$ at $T = 0$ as a function of the dimensionless crossover parameter Γ/Δ. The underdoped materials $YBa_2Cu_3O_{6.63}$ and $YBa_2Cu_4O_8$ are in regime (b), and have $z = 1$. The same applies to $La_{1.85}Sr_{0.15}CuO_4$ at high temperatures; at low temperatures, some modifications of the theory due to the incommensurability of short-range order are necessary. The fully doped material $YBa_2Cu_3O_7$ is in regime (c), and has $z = 2$.

scaling behavior of the insulators (the dynamical exponent $z = 1$) to that of the overdoped materials ($z = 2$). One of the key results of [5] is that there is only *one* such crossover parameter. Here the dynamical exponent z relates temperature dependences of the characteristic frequency scale for magnetic correlations, $\bar{\omega}$, and the characteristic length scale (the correlation length, ξ):

$$\omega \sim \xi^{-z}. \tag{6}$$

Fig.3 illustrates the evolution of zero temperature magnetic properties with doping on the example of the local dynamical magnetic susceptibility:

$$\chi_L''(\omega) = \int d\mathbf{q}\,\chi''(\mathbf{q},\omega), \tag{7}$$

which shows a gradual crossover, observed as a function of Γ/Δ, from $z = 1$ regime ($\Gamma/\Delta \lesssim 1$ [1,2,5]) to $z = 2$ regime ($\Gamma/\Delta \gtrsim 1$ [9,10]). The crossover between $z = 1$ and $z = 2$ regimes at low temperature is expected, and observed experimentally, as doping increases; in the universal theory, a similar crossover is also expected at a fixed doping as the temperature increases; it is however not observed experimentally because scaling fails altogether when at high temperatures the correlation length becomes very short, $\xi/a \lesssim 2$ (Barzykin and Pines [6]). The $z = 2$ phase shows a further crossover to the Landau Fermi liquid when Δ^2/Γ becomes larger than ω or T.Fig.3 describes the sequence of crossovers observed as Γ/Δ increases.

4.1. z=1 *limit* ($\Gamma/\Delta \lesssim 1$)

The limit $\Gamma/\Delta = 0$ and $\Delta > 0$ corresponds to an insulator with short-range antiferromagnetic correlations at $T = 0$ (Fig.3a). Such an insulator has a true energy gap Δ because creating any combination of excitations (spin waves which have a gap) above the ground state requires a finite energy, hence $\chi_L''(\omega < \Delta) = 0$. While this limit has no direct relevance to the cuprate oxide insulators (which develop Néel long-range order at $T = 0$ and have gapless spin waves), it helps to understand the behavior of the underdoped materials where $\Gamma/\Delta \lesssim 1$. The effect of small doping is shown in Fig.3b: $\chi_L''(\omega)$ becomes finite for all ω, but it remains much smaller for $\omega < \Delta$ compared to $\omega > \Delta$. The gap which existed for $\Gamma/\Delta = 0$ transforms into a knee-like feature at $\omega \sim \Delta$ for $\Gamma/\Delta \lesssim 1$. This behavior reproduces the essential features of the spin gap observed in some of the underdoped high-temperature superconductors.

At high temperatures $T \gg \Delta$, the behavior of $\Gamma/\Delta \lesssim 1$ underdoped system is similar to that of the $\Gamma/\Delta = 0$ insulator, because for energies $\omega \gtrsim \Delta$ the spectral weight of the two systems is nearly the same, and in both cases is dominated by the spin wave contribution (compare Figs.3a,b). As a result, the magnetic dynamics in this temperature range is in the $z = 1$ universality class, and exhibits quantum critical behavior $\bar{\omega} \sim \Delta \sim T$ [1,7].

The NMR measurements in the underdoped materials $YBa_2Cu_3O_{6.63}$ (Takigawa [17]) and $YBa_2Cu_4O_8$ (Imai *et al.* [18], Stern *et al.* [19], and Corey *et al.* [20]) are consistent with $z = 1$ predictions by Sokol and Pines [2]: both materials have a spin gap at low temperatures, and $T_1T/T_{2G} \approx$ const at high temperatures. In $La_{1.85}Sr_{0.15}CuO_4$, $1/T_{2G}$ has not yet been measured, but $1/T_1$ at high temperatures ($T = 500 - 1000K$) is nearly the same as in the insulator (Imai *et al.*[21]), and therefore has to be dominated by the spin wave contribution, which obeys the $z = 1$ theory. At low temperatures, the application of this theory to $La_{1.85}Sr_{0.15}CuO_4$ requires modifications due to the incommensurability of short range order. According to the theory described here, $La_{1.85}Sr_{0.15}CuO_4$ should have a smaller spin gap than the underdoped YBCO materials, which appears to be almost obscured by the superconducting phase (see Ref.[6] for a discussion).

4.2. z=2 *limit* ($\Gamma/\Delta \gtrsim 1$)

Figs.3c,d describe different regions of the same frequency dependence of $\chi_L''(\omega)$ at $T = 0$ in the overdoped case, where $\Gamma/\Delta \gtrsim 1$: (c) corresponds to $\omega \sim \Delta^2/\Gamma$, and (d) to $\omega \ll \Delta^2/\Gamma$. Regime (c) is $z = 2$ quantum critical; regime (d) is $z = 2$ quantum disordered, which is equivalent to the Landau Fermi liquid. The theory of magnetic behavior in the $z = 2$ regime has been developed by Millis, Monien, and Pines [9] and Millis [10].

For temperatures $T \gg \Delta^2/\Gamma$, the characteristic frequency scale for magnetic correlations $\bar{\omega} \sim T$ modulo $\log(\Delta/T)$ corrections, and the correlation length is given by Eq.(6) with $z = 2$. In the opposite limit $T \ll \Delta^2/\Gamma$, the correlation length is nearly T-independent, as is expected for the Landau Fermi liquid.

The fully doped material $YBa_2Cu_3O_7$ is in the $z = 2$ universality class, and its behavior between T_c and room temperature is intermediate between the $z = 2$ quantum critical regime (Fig.3c) and $z = 2$ quantum disordered regime (Fig.3d). The NMR experiments find $T_1T/T_{2G}^2 \approx$ const in

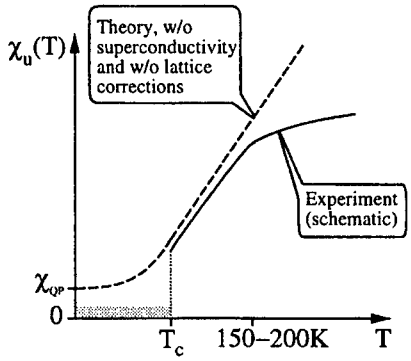


Fig. 4. A sketch of the uniform spin susceptibility $\chi_u(T)$ in the underdoped YBCO (solid line), and the theoretical prediction of Eq.(4)(dashed line). Since Eq.(4) is only valid in the normal state, comparisons below T_c are not meaningful. Above T_c, the experimentally observed $\chi_u(T)$ increases rapidly, and its slope is qualitatively consistent with that predicted by Eq.(4). At higher temperatures, the theory predicts continuing linear increase, whereas the experimental data shows saturation at $T \sim 150 - 200K$. Following the analogy with similar behavior of $\chi_u(T)$ for the insulating antiferromagnets at $T \sim 0.7 - 0.9J$,one may speculate that the discrepancy is due to lattice corrections.

agreement with the $z = 2$ quantum critical prediction (Imai *et al.* [22]); however, both of the rates do not vary strongly with temperature, which is an indication of the proximity of the Fermi liquid phase, where they saturate. This material does not have a spin gap, in agreement with its assignment as being in the $z = 2$ regime.

5. UNIFORM SUSCEPTIBILITY

The approach of Ref.[5] allows one to calculate the temperature-dependent part of the uniform spin susceptibility,$\chi_u(T) - \chi_u(T = 0)$, and correctly predicts that it monotonically increases as a function of T above T_c, that its slope becomes smaller as doping increases, and that temperature-independent Pauli $\chi_u(T)$ is recovered in the overdoped case.

However, the experimentally observed slope of $\chi_u(T)$ sharply decreases above $T \sim 150 - 200K$ compared to the slope below this temperature but above T_c [23,17,19], whereas the universal theory predicts that the increase of $\chi_u(T)$ continues with the same slope (Fig.4). One may speculate that this deviation is due to lattice corrections; detailed calculations must be performed to determine whether or not this speculation is correct.

Millis, Ioffe, and Monien [24] recently presented a scenario of spin gap formation based on spin-charge separation, accompanied by singlet pairing of spin-carrying excitations (spinons). Since holons do not have spin and therefore do not contribute to the magnetic density of states, the bulk susceptibility must vanish upon singlet pairing of spinons at low temperatures. They went on to argue that the observed decrease of the bulk susceptibility at low temperatures in underdoped YBCO can only be explained with this scenario.

However, their conclusion relies on the assumption that both $\chi_L''(\omega \to 0, T)$ and $\chi_0(T)$ would extrapolate to zero at low temperatures even without the superconducting transition, a statement that cannot be verified experimentally. In our view [5], no conclusion can be drawn from the experimental data on $\chi_u(T)$above T_c as to whether at $T \to 0$ the magnetic density of states without superconductivity would decrease all the way down to zero, as it is required by their model, or would become much smaller than at high temperatures, but remain finite, as it is expected in our model.

6. UNRESOLVED ISSUES AND CHALLENGES

The universal scaling theory yields a qualitative scenario for the evolution of magnetic behavior with doping which is consistent with the experiment. It also has been very successful in quantitatively explaining as well as predicting the results of some of the experimental measurements, notably the NMR relaxation rates in the insulators and doped materials. However, it fails to explain the detailed temperature dependence of $\chi_u(T)$ at high temperatures. This failure is likely to be caused by the lattice corrections in the broad sense: the influence of the Brillouin zone boundary on q-integrations, the non-linearity of the spin-wave spectrum at large wavevectors, bilayer coupling in YBCO, or energy dependence of the Landau damping rate Γ.

Different quantities are differently affected by the lattice corrections, and some are more robust than others. For instance, over a range of temperatures, χ_u in the Heisenberg model is affected by the lattice corrections, while the characteristic frequency $\bar{\omega}$ is not. Furthermore, some of the lattice corrections that do appear, can be absorbed into the dimensionful parameters of the model, while the universal scaling functions remain nearly unaffected[25,26]. A detailed study of these lattice effects may allow their inclusion into a phenomenological extension of the scaling theory to expand its range of applicability.

Another important challenge is to determine the precise role of bilayer coupling, which is central to the scenario of spin gap formation by Millis and Monien[27]. In the theory described here, the bilayer coupling affects the dimensionful parameters of the model, but does not affect any observables expressed as a function of these parameters, unless the size of bilayer coupling is comparable to other low-energy scales. Note that in our model, the spin gap may form with or without bilayer coupling, but it is enhanced if bilayer coupling is present.

Finally, it is very important to understand on the microscopic level how the spin waves and the quasiparticles share the spectral weight for intermediate doping, and in particular the mechanism of the experimentally observed reduction of the Pauli contribution to the uniform spin susceptibility in the underdoped case. The experimental data indicate that the spin wave to electron-hole pair conversion rate is also

suppressed in the underdoped materials, which in the theory described here results in spin gap formation. The cause of such a reduction is not fully understood, and may be a consequence of either a reduced density of states for the quasiparticles, which is also seen in the doping dependence of $\chi_u(T = 0)$, or a reduction of the interaction between the two species which results from vertex corrections at large ξ, as suggested by Bonesteel and Schrieffer [28].

Studies of microscopic models for the high-Tc cuprates should help to clarify whether the experimentally observed evolution of the key parameters of the model discussed here is similar to that obtained in microscopic calculations, thereby allowing one to check the validity of the proposed theory.

Acknowledgements— I would like to thank my collaborators Andrey V. Chubukov and Subir Sachdev for many comments and suggestions; Victor Barzykin and David Pines for informing me of their work [6] before publication;and S. Chakravarty, R.B. Laughlin, A.J. Millis, D. Pines, and S. Sondhi for helpful discussions. The author was supported by an Alfred P. Sloan Research Fellowship during the preparation of this manuscript.

REFERENCES

1. Chubukov A.V., Sachdev S. and Ye J., *Phys. Rev. B* **49**,11919 (1994); Chubukov A.V. and Sachdev S., *Phys. Rev. Lett.* **71**,169 (1993).
2. Sokol A. and Pines D., *Phys. Rev. Lett.* **71**, 2813(1993).
3. Sachdev S., *Phys. Rev. B* **49**, 6770 (1994).
4. Sokol A., Proceedings of the 1993 Los Alamos Symposium (in press).
5. Sachdev S., Chubukov A.V. and Sokol A., *Phys. Rev. B*, in press (May 1995).
6. Barzykin V. and Pines D., preprint (1995).
7. Chakravarty S., Halperin B.I. and Nelson D.R., *Phys. Rev. B* **39**, 2344 (1989).
8. Shraiman B.I. and Siggia E.D., *Phys. Rev. B* **42**,2485 (1990).
9. Millis A.J., Monien H. and Pines D. *Phys. Rev. B* **42**, 197(1990).
10. Millis A.J., *Phys. Rev. B* **48**, 7183 (1993).
11. Anderson P.W., *Science* **235**, 1196, (1987);Baskaran G., Zou Z. and Anderson P.W., *Solid State Comm.* **63**, 973,(1987); Ioffe L.B. and Larkin A.I., *Phys. Rev.* **B39**, 8988, (1989).
12. Laughlin R.B., Proceedings of the Stanford Conference on Spectroscopies in Novel Superconductors (1995).
13. Liu R. *et al.*, *Phys. Rev. B* **45**, 5614 (1992);**46**, 11056 (1992) for YBCO; Shen Z.-X. *et al.*, *Physica B* **197**, 632 (1994), and Ma J. *et al.*, preprint (1994) for Bi 2212.
14. Keimer B., Proceedings of the Stanford Conference on Spectroscopies in Novel Superconductors, and preprint (1995).
15. Aeppli G., Proceedings of the Stanford Conference on Spectroscopies in Novel Superconductors (1995).
16. Barzykin V., Pines D., Sokol A. and Thelen D., *Phys. Rev. B***49**, 1544 (1994).
17. Takigawa M. *et al.*, *Phys. Rev. B* **43**, 247 (1991);Takigawa M., *Phys. Rev. B* **49**, 4158 (1994).
18. Imai T., O'Hara K., Slichter C.P., Yoshimura K., Katoh M., Kosuge K.,Cobb J.L. and Markert J.T., Grenoble M2-HTSC Conference Proceedings (1994), and private communication.
19. Stern R., Mali M., Roos J. and Brinkmann D., preprint (1994);see also Zimmermann H., Mali M., Brinkmann D., Karpinski J., Kaldis E. and Rusiecki S., *Physica C* **159**, 681 (1989).
20. Corey R.L., preprint (1995).
21. Imai T. *et al.*, *Phys. Rev. Lett.* **70**, 1002 (1993).
22. Imai T. *et al.*, *Phys. Rev. B* **47**, 9158 (1993).
23. For a review, see Johnston D.C. *Journal of Magnetism and Magnetic Materials* ,**100**, 218 (1991), and references therein.
24. Millis A., Ioffe L.B. and Monien H., Proceedings of the Stanford Conference on Spectroscopies in Novel Superconductors, and preprint (1995).
25. Elstner N., Glenister R.L., Singh P.R.R. and Sokol A., *Phys. Rev. B* **51**, 8984 (1995).
26. Sandvik A.W. and Scalapino D.J., preprint (1994).
27. Millis A.J. and Monien H. *Phys. Rev. Lett.* **70**, 2810 (1993).
28. Schrieffer J.R, Proceedings of the Stanford Conference on Spectroscopies in Novel Superconductors (1995).

Pergamon

J. Phys. Chem. Solids Vol. 56, No. 12, pp. 1685–1689, 1995
Copyright © 1995 Elsevier Science Ltd
Printed in Great Britain. All rights reserved
0022-3697/95 $9.50 + 0.00

0022-3697(95)00215-4

SYMMETRY OF THE SUPERCONDUCTING STATE IN COPPER OXIDES

C. M. VARMA
AT&T Bell Laboratories, 600 Mountain Ave., Murray Hill, NJ 07974, U.S.A.

Abstract—I briefly summarize the important experimental results concerning the symmetry of the superconducting state in copper oxide metals and discuss superconducting states in which all of them may be mutually reconciled.

INTRODUCTION

A variety of experiments touching on the important issue of the symmetry of the superconducting state in copper oxides have been performed. I believe the following experiments are probably all correct and wish to find the pairing mechanism which leads to states in which they can all be reconciled.

(1) Various transport experiments, most notably the temperature dependence of the London Penetration depth in $YBa_2Cu_3O_7$ [1] (123), the magnetic field dependence of the low temperature specific heat [2], all of which are consistent with a density of states at low energies $n(\omega) \sim \omega$ in very pure samples.
(2) The infrared and Raman scattering experiments as well as the London penetration depth measurements [3] in the electron-doped metal $Nd_{2-x}Ce_xCuO_4$ (NCCO) which do appear consistent with a simple BCS exponential density of states at low energies.
(3) The Josephson experiments [4], which beyond a reasonable doubt give a π phase shift between the a and b faces of 123. In the same category, is the ingenious experiment with tri-crystal 123 films [5].
(4) The c-axis Josephson tunneling experiment between twinned and untwinned samples of 123 and Pb which finds a Josephson current, albeit of about an order of magnitude less than that expected between two s-wave superconductors [6].
(5) The Josephson experiments using grain-boundary junctions between various faces of a hexagonal shaped island of 123 cut in a larger film of 123 which finds nearly the same Josephson current density from all faces of the hexagon [7]. Experiments (iii)–(v) are reviewed in Ref. [8].
(6) The very slow reduction of T_c with residual resistivity in 123 samples where resistivity is changed by radiation damage [9]. T_c approaches 0 only for $E_f\tau$ approaching 1 rather than $\Delta\tau$ approaching 1. In fact the behavior of T_c is similar to quasi-two dimensional films of Pb where with damage a superconductor to insulator transition is found.
(7) The angle resolved photoemission experiments in $Bi_2Sr_2Ca_1Cu_2O_8$ (2212), which see an s-wave symmetry gap function with nodes [10].
(8) Inelastic neutron scattering experiments in $La_{1.85}Sr_{.15}CuO_4$ (124), which within the range of q that they can measure do not see, within their resolution a q-dependent diminution of the particle–hole spectrum below the superconducting transition [11] at low energies.

In trying to find the superconducting state in which all the above seemingly irreconcilable experiments may be true, I am also guided by the belief that the fundamental physics of all the copper oxide metals is very similar, be they tetragonal or orthorhombic and hole-doped or electron-doped.

PRELIMINARIES

(1) A very important consideration for the nature of the gap function in CuO metals is that the inter-electronic repulsion on CuO is on the same scale as the bandwidth. Therefore the pair wavefunction amplitude on Cu-ions should be 0. Taking the Cu ion in each cell as the origin of coordinates

$$\psi(r = 0) = \sum_{\sigma} \langle c_\sigma(0) c_{-\sigma}(0) \rangle = 0 \qquad (1)$$

This implies, by Fourier transforming that

$$\sum_{\mathbf{k}} \psi(\mathbf{k}) = \sum_{\sigma} \langle c_\sigma(\mathbf{k}) c_{-\sigma}(-\mathbf{k}) \rangle = 0 \qquad (2)$$

The pair wave-function should then be positive in parts of the Brillouin zone and negative in other parts and therefore has lines or points at which it is zero. $\psi(k)$ can therefore not be of the BCS variety, which has the same sign throughout the zone. This is basically the reason why liquid ^3He and heavy-fermion superconductors are not simple S-wave superconductors.

Note that the gap function

$$\Delta(\mathbf{k}) = E(\mathbf{k})\psi(\mathbf{k}), \qquad (3)$$

has nodes where the pair wave-function does. But eqn (2) does not imply that $\sum_k \Delta(k) = 0$, unless there are symmetry reasons that this must be so.

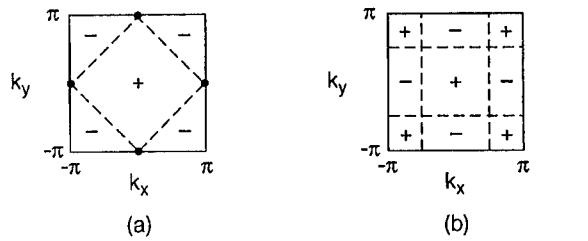


Fig. 1. (a) Zeros of the generalized s-wave gap function $\sim \cos k_x + \cos k_y$, and (b) $\sim \cos k_x \cos k_y$. Note that whether or not there is a gapless excitation spectrum depends on the size and shape of the Fermi-surface.

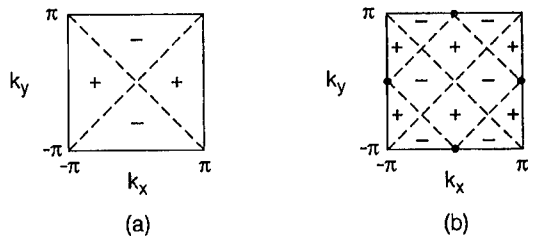


Fig. 2. (a) Zeros of the d-wave gap function $\sim \cos k_x - \cos k_y$, (b) $\cos 2k_x - \cos 2k_y$. The excitation spectrum is always gapless.

has nodes where the pair wave-function does. But eqn (2) does not imply that $\sum_k \Delta(k) = 0$, unless there are symmetry reasons that this must be so.

(2) If, as is almost certainly the case, pairing is caused by electronic excitations which lead also to the anomalous normal state properties, the effective electron–electron interaction is essentially non-retarded. Then the gap function over the complete Brillouin zone must then be specified, unlike traditional metals where it is non-zero only over a tiny strip near the Fermi-surface.

(3) A point of nomenclature only but rather important for a sane discussion of superconductivity in solids: When one speaks of the symmetry of the superconducting state, one specifies how the order parameter transforms under the full point group and space group symmetry operations of the lattice. If it transforms as identity, we may call it an s-wave. If we have a tetragonal crystal (four-fold rotation axis) and if it change sign under a $\pi/2$ rotation, we may call it a d-wave. In an orthorhombic symmetry, such as in 123 there is no 4-fold axis and no sensible classification as s or d-waves. They will in general always be linearly coupled and one cannot in general be present without the other. It does however make sense to ask, whether it is possible to have a sign change under rotation by $\pi/2$ in orthorhombic crystals, if their physical mechanism for superconductivity is the same as in tetragonal crystal, and the latter exhibit s-wave superconductivity.

It does not make sense, under any circumstances, given the points 2 and 3 above to classify superconducting states as s,p,d,f,g, etc., depending on how many times the gap function changes sign on the Fermi surface. A correctly classified gap function may change sign any number of times depending on the vagaries of the Fermi surface.

CANDIDATE STATES

In tetragonal crystals the two leading singlet superconducting states that meet the requirement eqn (1), are:

Generalized s-*wave states*

Where the gap function is a linear combination of 1, $\cos k_x + \cos k_y$, $\cos k_x \cos k_y$, etc.

$$\Delta_s(\mathbf{k}) = \Delta_{os} + \Delta_{1s}(\cos k_x + \cos k_y) + \Delta_{2s} \cos k_x \cos k_y \quad (4)$$

Note that the first of these is allowed because $\sum_k \Delta(k)$ is not required to be zero. On a square Brillouin zone $\cos k_x + \cos k_y$ has zeros shown by the dashed lines in Fig. 1(a) and ($\cos k_x \cos k_y$) has zeros shown by the dashed lines in Fig. 1(b). If the Fermi surface is small enough, the gap on the Fermi surface never changes sign; if it is large enough, it changes sign an even number of times in each quadrant of the Fermi surface for any of these states or their linear combination. The points of zeroes, needless to repeat, are determined not by symmetry but by details.

d-*wave states*

Here the gap function is a linear combination of states which change sign under a $\pi/2$ rotation, for instance $\cos k_x - \cos k_y$, $\cos 2k_x - \cos 2k_y$, etc. The zeroes of these are shown in Fig. 2(a) and (b). Unlike the generalized s-wave states the gap function must always have nodes on the Fermi surface. Depending on the details of the Fermi surface, Δ may change sign any odd number of times on each quadrant.

In orthorhombic crystals, one may only talk of the relative admixture of the two sorts of states above.

SIMPLE PHYSICS OF d-WAVE STATES

d-wave states were first thought of in connection with heavy-Fermions in order to understand their transport properties [12]. A phenomenological analysis suggested that strong anti-ferromagnetic fluctuations favor such states [13]. The same conclusion is arrived at from derivation of the effective electron-electron interaction from the Hubbard model in the random phase approximation [14]. They have been extensively discussed in connection with copper oxide metals [15]. The physics, in the limit of very strong AFM correlations and very strong pairing interactions (real space pairs) is very simply described:

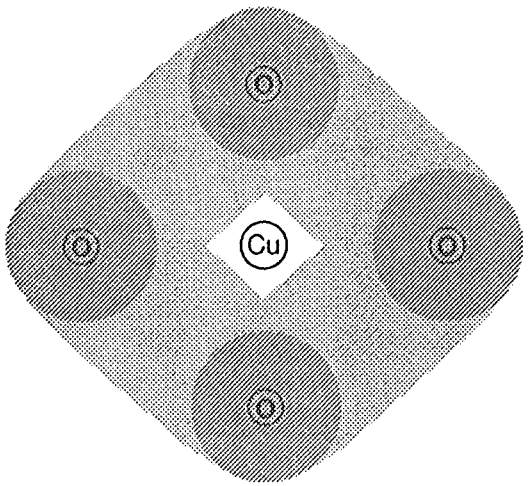


Fig. 3. Shape of the generalized s-wave function (in the strong-coupling limit) in the Cu–O lattice. There is a zero of the pair wave function on Cu and pairing on oxygen and on neighboring oxygens with the full symmetry of the lattice.

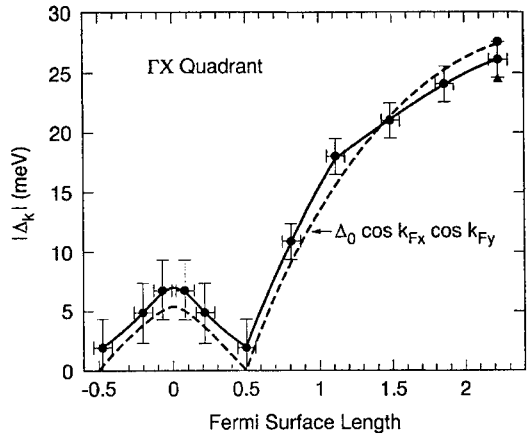


Fig. 4. The measured gap function in 2212 Ref. [10] compared to the generalized s-wave gap $\Delta_o \cos k_x \cos k_y$ (after Norman *et al.*, private communication). Note that this fit is not unique. Other combinations in eqn (4) can also fit the data.

On a square lattice let there be strong AFM correlations at the π, π point;

$$\chi(q, 0) \sim \delta(q_x - \pi)\, \delta(q_y - \pi) \tag{5}$$

Delete this text

Transforming to real space gives an effective electron–electron interaction $\sim \cos x \cos y$. This is attractive for $x = 0$, $y = \pm\pi$, and for $x = \pm\pi$, $y = 0$ and repulsive for $x = 0$, $y = 0$ and $x = y$. A real space pair function which is favored by such a potential is $x^2 - y^2$, i.e. a d-wave function.

PHYSICS OF GENERALIZED s-WAVE STATES

Extended s-wave states first arose in calculations [16] which derived the pairing interaction in copper oxide models with electron–electron interactions between copper and oxygen ions besides the local interactions on copper ions [17]. It was shown that such interactions induce charge transfer resonances between copper and oxygen ions which are strongest in the A_{1g} channel. These resonances lead to effective electron–electron attractions on oxygen ions and between nearby Oxygen ions, as speculated earlier. With repulsion on copper the symmetry of the superconducting pair wave function is of the extended s-wave type, as illustrated in Fig. 3.

The conclusions from such approximate calculations is supported by numerical diagonalization of such models in one dimension to calculate the asymptotic decay of correlation functions [18]. Recently a phenomenological model for superconductive pairing, with specified local and nearest neighbor interactions has been considered [19]. The interactions are projected to the band of states crossing the Fermi-level and the BCS equation for the gap function has been solved. The conclusion is that the on-site oxygen-attractions favor a s-wave pairing of the form, $\cos k_x + \cos k_y$ while the nearest neighbor attraction favors pairing of the $\cos k_x \cos k_y$ form. For reasons already mentioned, in general the pairing will be a linear combination, as in eqn (4).

EXPERIMENTS AND THE d-WAVE LIKE STATE

Consider an orthorhombic single layer per unit cell crystal. The gap function may be written in general in the form

$$\Delta_{ortho}(\mathbf{k}) = \Delta_s f_s(\mathbf{k}) + \Delta_d f_d(\mathbf{k}), \tag{6}$$

where $f_s(k)$ is preserved in a $\pi/2$ rotation and $f_d(k)$ changes sign under a $\pi/2$ rotation. We will call a state a d-wave like state if $\Delta_d \gg \Delta_s$, and an s-wave like state if $\Delta_s \gg \Delta_d$, with the fs normalized so that their maximum value is unity. For a tetragonal crystal, Δ_s or $\Delta_d = 0$.

The d-wave like state is consistent with experiment (i) of the Introduction. It is also consistent with experiments of (iii) in (123).

It is inconsistent with the experiments (ii) in NCCO. For an untwinned single crystal, it is consistent with experiment (iv) only due to a finite Δ_s. But these experiments have also been done in a twinned samples of 123 with about 10^4 twins in the tunneling area. One would then expect a Josephson current of order 10^{-2} times Δ_s/Δ_d of the usual value. A Josephson current smaller than the theoretical value for simple s-wave superconductors by less than an order of magnitude is found. Although suggestive that this is inconsistent with an almost d-wave, one can draw definitive conclusions only if experiments of the c-axis Josephson currents in tetragonal crystals are performed.

The almost d-wave state is also inconsistent with the Josephson experiments in the geometry of (v).

In relation to experiments (vi), the usual theory predicts that with $\Delta_s = 0$, $T_c \to 0$ as the scattering time τ due to non-magnetic impurities approaches $\tau\Delta(pure) \approx 1$. So

experiments (vi) in 123 present a very serious difficulty for d-waves. Again similar controlled damage experiments in tetragonal samples will be useful.

The latest angle resolved photoemission experiments (vii) in the very nearly tetragonal crystal 2212 are not consistent with d-wave symmetry. They are in conflict, however with conclusions drawn from earlier experiments also on (2212) [20].

Some of the disagreements with the experiments noted above, especially (ii), (iv), (v) and (vi) do not disappear if refinements such as the bi-layer geometry are included in the analysis.

EXPERIMENTS AND THE s-WAVE STATES

The simple isotropic s-wave state or its nodeless anisotropic variations is in conflict with experiments (i), (iii) and (vii) [21]. It is consistent with experiments (ii) on NCCO, and (iv)-(vi) and (viii) in hole-doped materials. The inconsistencies are of a nature such that this state does not appear to me to be a viable candidate.

The generalized s-wave states with nodes is consistent with experiments under (i), (vi), (v) and (viii). It is consistent with (vi) provided the relative areas of the positive and negative phases on the Fermi-surface are very different. It is remarkably well consistent with (vii), the photoemission experiment in (2212). Figure 4 shows the experimentally determined variation of the gap in one quadrant of the Fermi surface together with the gap function $\Delta(k) = \Delta(\cos k_x \cos k_y)$ calculated on the measured Fermi surface. Only the coefficient Δ is adjusted. As mentioned earlier such a gap function arises for models with on-site repulsion on copper together with nearest neighbor attraction on the oxygen ions.

Given a mechanism of superconductivity that produces generalized s-wave states, one can get nodeless s-wave state or a noded s-wave state at the Fermi surface depending on details such as the size and shape of the Fermi-surface. So, the generalized s-wave states may be considered consistent with experiments (ii).

s-wave states of eqn (4) are apparently in complete conflict with the remarkable and undoubtedly correct series of experiments (iii). These experiments are all done on (123) samples, which are orthorhombic and have two layers in the c-direction per unit cell. Therefore it is worth asking whether under these circumstances, the physics that leads to a gap function which in a single layer tetragonal crystal is of the generalized s-wave type would give the observed results. These require a π phase shift under $\pi/2$ rotation. Note that we are not discussing a point of symmetry here, but a point of the plausibility of a physical scheme.

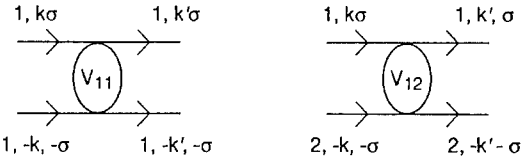


Fig. 5. The intra-layer and inter-layer interactions V_{11} and V_{12}.

BI-LAYERS AND ORTHORHOMBICITY

Josephson experiments to elucidate the symmetry of the superconducting state have so far only been done on $YBa_2Cu_3O_7$, which is both orthorhombic and has a bi-layer in the c-direction in each cell. To discuss the gap function in such a crystal structure, I rely on a recent preprint by Liu, Levin and Maly [22], who solved the gap equation for various assumed interactions. Below, I give a reformulation relying on a Ginzburg–Landau expansion.

In a bi-layer structure there are, in general two sheets of the Fermi surface which are even and odd in reflection. Denote the two layers by 1 and 2 and the gap on the two Fermi surfaces, Δ_o and Δ_e. The leading terms in the Landau–Ginzburg Free energy are

$$\sum_{\mathbf{k}} a_e|\Delta_e(\mathbf{k})|^2 + a_o|\Delta_o(\mathbf{k})|^2 + a_m Re\Delta_e^*(\mathbf{k})\Delta_o(\mathbf{k}) \qquad (7)$$

Because of the last term, Δ_e and Δ_o will always be non-zero simultaneously. Further if a_m is positive, it follows that Δ_e and Δ_o are π out of phase at each angle on the Fermi surface. If a_m is negative Δ_e and Δ_o are in phase

To determine the sign of a_m, first note that time-reversed pairs can be constructed, in general, only from both particles on the even Fermi surface or on the odd Fermi surface. Construct general interactions V_{ee}, V_{oo} and V_{eo}, which can be expressed in terms of the inter-layer interactions V_{11}, V_{22} and V_{12}, (see Fig. 5) as

$$V_{ee} = V_{oo} = V_{11} + V_{22} + 2V_{12}$$
$$V_{eo} = V_{11} + V_{22} - 2V_{12}. \qquad (8)$$

The relation between $\Delta_{e,o}$ and the pair wave-functions $\psi_{e,o}$ is (schematically)

$$\Delta_e = V_{ee}\psi_e + V_{eo}\psi_0$$
$$\Delta_o = V_{oo}\psi_0 + V_{oe}\psi_e. \qquad (9)$$

The coefficients of the leading order terms, eqn (7) in the free-energy can now be calculated from the one-loop diagrams. The conclusion is that given an attractive intra-layer interaction $V_{11} = V_{22}$ giving rise to a generalized s-wave pairing in a single layer system, $a_m > 0$ in a bi-layer system if the inter-layer V_{12} interaction is repulsive and $|V_{12}| > |V_{11}|$. In that case, a linear combination $|\Delta_e| - |\Delta_o|$ (for the special case $a_e = a_0$) is chosen over the other, $|\Delta_e| + |\Delta_o|$.

Consider now the fourth order terms: given eqn (8) they are of the following form only

$$\sum_{\mathbf{k}} b_e\ |\Delta_e(\mathbf{k})|^4 + b_0|\Delta_o(\mathbf{k})|^4 + b_m\ \mathrm{Re}\Delta_e^*(\mathbf{k})\Delta_o(\mathbf{k})(|\Delta_e(\mathbf{k})|^2 + |\Delta_o(\mathbf{k})|^2). \quad (10)$$

Suppose the combination $(\Delta_e(\mathbf{k}) - \Delta_o(\mathbf{k}))$ has the lower energy from the quadratic terms. We can write the fourth order terms in terms of this state and the orthogonal combination and drop the latter. Then the Free energy contains, besides others, terms of the form

$$b' \int dk \int d\Omega_k |\Delta_e^2(\mathbf{k})||\Delta_o^2(\mathbf{k})|,\ b' > 0. \quad (11)$$

In an orthorhombic system Δ_e and Δ_o have in general different magnitudes along the principal axes. The relative orientation of Δ_e and Δ_o are determined by eqn (11) and the last term in eqn (7).

Ref. [22] has found conditions in which the major axis of Δ_e and Δ_o are rotated by $\pi/2$. Under the above conditions $(\Delta_e - \Delta_o)(\mathbf{k})$ changes sign under a $\pi/2$ rotation. This is enough to give the π phase-shift observed in experiments (iii). With Δ_e and Δ_o of different magnitudes, it is also consistent with experiments (iv) and (v).

FURTHER EXPERIMENTS

In crystals with tetragonal symmetry, single layer or multilayers, a phase shift of π under $\pi/2$ rotation is impossible if the physics leads to an *s*-wave state in a single layer. Therefore, it is very important to do Josephson experiments of the type (iii) for such crystals. Here the experiments in corner junctions [4] should be distinguished from those in the tricrystal junctions [5]. In the former observation of π phase shifts would be an unambiguous sign of *d*-wave pairing; its absence would be an unambiguous sign of *s*-wave pairing. The situation in tri-crystal junctions is a little more complicated. For *d*-waves in a tetragonal crystals the nodal plane of the gap function is unambiguously given by symmetry. So one knows precisely the geometries in which a π phase shift is to be expected. If none is found, *d*-wave pairing is ruled out. But if a π phase shift is found, it is not a proof of *d*-waves since nodal planes are present in generalized *s*-wave states as well and their position is not given by symmetry. More than one geometry has then to be examined in the tri-crystal experiments to rule out *s*-waves. For this reason and because of the fact that the present tri-crystal experiments are done with twinned crystals of (123), the only definitive conclusion that can be drawn is that pairing functions have nodal planes crossing the Fermi surface.

For reasons discussed earlier *c*-axis Josephson experiments in tetragonal crystals should be quite enlightening. The photoemission experiments can be used to test whether nodes in the gap function disappear on degrading the sample. This should happen for generalized *s*-waves, but not for *d*-waves. In interpreting the data, an imaginary part of the gap function must however be included.

If pairing is indeed of the *d*-wave type, satisfactory explanations must be found for some experiments, especially [4] and [5]. Also, mechanisms of pairing other than antiferromagnetic fluctuations must be sought. Unlike heavy-fermion metals, such fluctuations are invisible in neutron scattering experiments in $YBa_2Cu_3O_{6.9}$.

Acknowledgements—I wish to thank E. Abrahams, P. B. Littlewood and A. Sudbo for many useful discussions and for our collaborations.

REFERENCES

1. Hardy W. N. *et al., Phys. Rev. Lett.* **70**, 399 (1993).
2. Moler K. A. *et al, Phys. Rev.z Lett.* **73**, 2744 (1994).
3. Wu D. H. *et al., Phys. Rev. Lett.* **70**, 85 (1993); Stadlober B'*et al.*, preprint.
4. Wollman D. A. *et al., Phys. Rev. Lett.* **71**, 2134 (1993); Branner D. A. and Ott H. R. , *Phys. Rev. B* **50**, 6530 (1994), Mathai A. *et al.*, preprint.
5. Tsuei C. C. *et al., Phys. Rev. Lett.* **73**, 593 (1994).
6. Sun A. G. *et al., Phys. Rev. Lett.* **72**, 2267 (1994).
7. Chaudhari P. and Lin S.-Y., *Phys. Rev. Lett.* **72**, 1084 (1994).
8. Barone A., to be published in Il Nuovo Cimento, Suppl. (1995).
9. Sun A. G. *et al., Phys. Rev. B* **50**, 3266 (1994).
10. Ding H. *et al., Phys. Rev. Lett.* **74**, 2784 (1995).
11. Mason T. E. *et al., Phys. Rev. Lett.* **71**, 919 (1993).
12. Schmitt-Rink S., Miyake K. and Varma C. M., *Phys. Rev. Lett.* **57**, 2575 (1986).
13. Miyake K., Schmitt-Rink S. and Varma C. M., *Phys. Rev. B* **34**, 6554 (1986).
14. D. Scalapino, E. Loh and J. Hirsch, Phys. Rev. **B34**, 8190 (1986).
15. For a recent review, see Scalapino D., *Phys. Reports* (to be published).
16. Littlewood P. B., Varma C. M. and Abrahams E., *Phys. Rev. Lett.* **63**, 2602 (1989); Littlewood P. B., *Phys. Rev. B* **42**, 10 075 (1990).
17. Varma C. M., Schmitt-Rink S. and Abrahams E., *Solid State Commun.* **62**, 681 (1987).
18. Sudbo S. *et al., Phys. Rev. Lett.* **70**, 978 (1993); Stechel E. *et al., Phys. Rev. B* **51**, 553 (1995).
19. Sudbo A. and Varma C. M. (unpublished).
20. Shen Z. X. *et al., Phys. Rev. Lett.* **70**, 1553 (1993).
21. These include the states arising from the so called "Interlayer tunneling mechanism of superconductivity", Chakravarty S., Sudbo A., Anderson P. W. and Strong S. P., *Science* **261**, 337 (1993).
22. Liu D. Z., Levin K. and Maly J. preprint.

Pergamon

J. Phys. Chem. Solids Vol. 56, No. 12, pp. 1691–1692, 1995
Copyright © 1995 Elsevier Science Ltd
Printed in Great Britain. All rights reserved
0022–3697/95 $9.50 + 0.00

0022-3697(95)00102-6

TWO TYPES OF CHARGE CARRIERS IN THE HIGH-T_c CUPRATES

J. ASHKENAZI
Physics Department, University of Miami, P. O. Box 248046, Coral Gables, FL 33124, U.S.A.

Abstract—It is shown that the charge carriers in the high-T_c cuprates are either spinless polarons or anomalous carriers of charge and spin. The physical properties of the cuprates are thus understood, and transitions between pair states of the two types of carriers provide the pairing mechanism.

A microscopic theory has been worked out [1], explaining the anomalous normal state properties of the cuprates, and the occurrence of high-T_c superconductivity. Within this approach, the orbitals around E_F are decomposed into "large-U" orbitals, and "small-U" orbitals created by fermion operators $c^\dagger_{\nu\sigma}(\mathbf{k})$, where ν, σ and $\mathbf{k}$ are band, spin, and wave vector indices, respectively. The large-U states are treated by the "slave fermion" method, within which a site i in a CuO_2 plane is occupied either by a chargeless spin boson, created by $s^\dagger_{i\sigma}$, or by a spinless charged fermion, created by $e^\dagger_i$ ("n-type"), or $p^\dagger_i$ ("p-type").

Within a mean-field approach (MFA), the boson "spinon" excitation energies $\bar{\epsilon}^\zeta(\mathbf{k})$, of the s spins system, have a minimum at $\mathbf{k}=\mathbf{k}_0$, which is close to one of the four points obtained from $(\frac{1}{2}\frac{\pi}{a}, \frac{1}{2}\frac{\pi}{a})$ by the tetragonal group operations. If $\bar{\epsilon}^\zeta(\mathbf{k}_0)=0$ one gets an antiferromagnetic (AF) state, and if $\bar{\epsilon}^\zeta(\mathbf{k}_0)>0$ one gets a "spin-fluctuation" (SF) state, characterized by AF fluctuations, and stabilized for sufficient "doping".

Bonding effects result in binding between the e (p) and the s fields. One type of fermion quasiparticles obtained, referred to here as "semi-MFA carriers", carry both charge and spin, and hybridize with the c electrons. Their excitation energies $\bar{\epsilon}^g_i(\mathbf{k})$ form quasi-continuous ranges of bands. In a SF state a range of $\bar{\epsilon}^g_i(\mathbf{k})$ bands, of varying degrees of bonding, crosses E_F. If the center of this range is below E_F at a given $\mathbf{k}$ then free-energy minimization will introduce to it such a width that the energies of minimal bonding may be pushed above E_F. This explains the linewidths $\sim|E-E_F|$ observed in ARPES results [2], and marginal-Fermi-liquid like behavior of generalized susceptibilities [1].

Another type of fermion quasiparticles is of "spinless polarons", resulting from the trapping of e (p) carriers by neighboring s spins and a local lattice deformation. In a SF state these polarons form a coherent liquid of bandwidth $\gtrsim$ 10 meV. Transitions between semi-MFA and polaron states require spinon $\bar{\epsilon}^\zeta(\mathbf{k})$ excitations, and though both semi-MFA and polaron energies are found very close to E_F, the existence of $\bar{\epsilon}^\zeta(\mathbf{k}_0)>0$ provides a gap for transitions between them. Since a spin-wave excitation consists of two spinons, the 41 meV excitation peak observed [3] at $\mathbf{k}\cong(\frac{\pi}{a}, \frac{\pi}{a})$ by neutron scattering in $YBa_2Cu_3O_7$ is interpreted as $2\bar{\epsilon}^\zeta(\mathbf{k}_0)$. This peak is strongly damped above T_c since the spinon and semi-MFA operators do not commute [1].

Processes of electron emission/absorption from/into polaron states include the effect of spinon excitation, and lead to excited phonon and spinon states; thus they do not detect the narrow polaron band, but a wider ($\gtrsim$0.1 eV) spectral background [2]. Similarly, optical transitions between polaron states, or between them and semi-MFA states, result in the "mid-infrared peak". The "extended van Hove singularities" observed near E_F [2] are interpreted as LDA saddle-point singularities renormalized due to a dynamic Jahn-Teller effect where semi-MFA states are coupled to the polarons. This amplifies the compatible effect of AF fluctuations [4], and results in "shadow bands" [2].

The semi-MFA structure explains the systematic behavior of the resistivity and the Hall constant in the cuprates [1]. The polarons contribute significantly to the thermopower S. Since polarons and semi-MFA carriers do not mix, their contributions, S^a and S^g, add: $S=S^a+S^g$. The polaron contribution S^a is identified with the narrow-band result [5] which applies to a major contribution to S. One finds [5] $S^a=0$ close to the optimal stoichiometry of the cuprates, corresponding to an occupation of ~50% of a CuO_2 plane by the polarons [a polaron site extends over a number of (eight [6]) lattice sites] as has been observed [6].

Unlike single particles, pairs of opposite-spin semi-MFA carriers and of spinless polarons can mix without exciting spinons. Virtual transitions of a pair at E_F to an empty band close to it lowers its energy, and thus can lead to pairing [7]. In $Bi_2Sr_2CaCu_2O_{8+y}$, "polaron stripes" were found [6] in the CuO_2 planes below $T^*\sim$120K. These stripes are the result of an expected charge density wave transition at T^*, where the narrow polaron band splits, and at least one sub-band lies ~ 10 meV away from E_F, serving as the empty band for virtual pair transitions from the semi-MFA states at E_F. Thus the conditions for such a mechanism are optimally fulfilled. Since the pairing interaction is enhanced below T^*, one expects $T_c\lesssim T^*$, resulting in a T_c equation which is consistent with the "Uemura plots", and with their "boomerang-type" behavior in overdoped cuprates [8].

The charge carriers in the high-T_c cuprates are shown to be either spinless polarons or anomalous carriers of both charge and spin. Their behavior is consistent with the anomalous physical properties, and hybridization between their pair states results in high-T_c superconductivity.

REFERENCES

1. Ashkenazi J., *J. Supercond.* 7, 719 (1994); *ibid.* **8** (1995).
2. Dessau D. S., *et al.*, *Phys. Rev. Lett.* **71**, 2781 (1993); Aebi P., *et al.*, *ibid.* **72**, 2757 (1994).
3. Mook H. A., *et al.*, *Phys. Rev. Lett.* **70**, 3490 (1993); Fong H.-F., *et al.*, *preprint* (1995).
4. Dagotto E., *et al.*, *Phys. Rev. Lett.* **74**, 310 (1995).
5. Fisher B., *et al.*, *J. Supercond.* **1**, 53 (1988); Obertelli S. D., *et al.*, *Phys. Rev. B* **46**, 14928 (1992).
6. Bianconi A, *et al.*, *J. Phys. I (France)* **4**, 361 (1994).
7. Kondo J., *Prog. Theor. Phys.* **29**, 1 (1963); Entin-Wohlman O. and Imry Y., *Phys. Rev. B* **49**, 4455 (1994).
8. Niedermayer Ch., *et al.*, *Phys. Rev. Lett.* **71**, 1764 (1993).

Pergamon

J. Phys. Chem. Solids Vol. 56, No. 12, pp. 1693–1694, 1995
Copyright © 1995 Elsevier Science Ltd
Printed in Great Britain. All rights reserved
0022–3697/95 $9.50 + 0.00

0022–3697(95)00091-7

POSITRON ANNIHILATION AND POSITRON–ELECTRON CORRELATION EFFECTS IN HIGH-T_c OXIDES

B. BARBIELLINI, M. J. PUSKA, A. HARJU and R. M. NIEMINEN
Laboratory of Physics, Helsinki University of Technology, Fin-02150 Espoo, Finland

Abstract—We have calculated electron and positron states in the $Nd_{2-x}Ce_xCuO_4$ compound, for the perfect bulk lattice as well as when vacancy defects are included. We study the sensitivity of the results to different approximations in the positron potential. We also compute the annihilation rate and the electron-positron momentum density using the local density approximation and the newly developed gradient correction for the electron-positron contact term. Our main goal is to give predictions for the Fermi surface signals.

Keywords: A. oxides, C. *ab initio* calcualtions, C. positron annihilation spectroscopy, D. electronic structure, D. superconductivity.

Positron annihilation can be used to determine the Fermi surface and to monitor electronic structure changes produced by impurities and defects in high temperature superconductors [1]. The local positron annihilation rate $\Lambda(r)$ is treated as a function of the electron density $n(r)$ in the local density approximation (LDA) [1]. However, quite generally, the LDA underestimates the positron lifetime, especially when d electrons are involved. This problem can be cured by the generalized gradient approximation (GGA) for the annihilation rate [2]. In the GGA, $\Lambda(r)$ depends also on the density gradient $\nabla n(r)$ and the gradient correction reduces the annihilation enhancement due to the electron-positron correlation. Our results for several metals and semiconductors show that the GGA corrects the LDA and systematically improves the agreement with the experimental lifetimes. We believe that the GGA scheme is a powerful tool for extracting detailed electronic structure information from positron annihilation spectroscopy in the high-T_c oxides. Among these compounds, a good candidate for probing the Cu-O planes is $Nd_{2-x}Ce_xCuO_{4-\delta}$ because several calculations [1,3,4] indicate a substantial overlap of the delocalized positron wave function with the Cu-O planes. In the case of this compound, the effect of including the positron-electron correlation in the positron potential is small on the positron density distribution, and the positron charge is closer to the Cu-O planes. According to the superimposed atom method with the LDA positron-electron correlation potential, the metal ion vacancies bind the positron strongly, with a binding energy of 1.3 eV for Cu and 3.1 eV for Nd. The binding at the oxygen vacancies is weak especially in the Cu-O plane. These trends are also reflected in the localization of the positron at the different vacancies. Using the electron and positron densities, we have calculated the positron lifetimes according the formula given in ref. [2].

The bulk lifetimes are 131 ps in the LDA and 165 ps in the GGA. For the ideal Cu, Nd, O1 and O2 vacancies, we obtain the lifetimes of 172, 199, 134, 137 ps, in the LDA, respectively, and in the GGA, 220, 268, 170, 172 ps, respectively.

The measured lifetimes (204-207 ps) [3] are closer to that of copper vacancies (in the GGA), indicating the presence of these defects in the real samples. Their formation is thought to happen through the rearrangement and migration of metallic ions during the long reduction of the $Nd_{2-x}Ce_xCuO_{4-\delta}$ crystals [3]. Substitutional metal ions (Ce) do not bind positrons and they do not change the lifetime significantly. If the positron is delocalized, the FLAPW and LMTO calculations indicate that the Fermi surface signal should be experimentally visible [3]. The Lock-Crisp-West (LCW) folding of the momentum density in the first Brillouin zone gives information about partial annihilation rates for different wave-vectors. The amplitudes of the Fermi surface signals (for both LDA and GGA) are about one percent of the constant background, if valence and core annihilation are included (the partial rate with the 5p Nd core orbital is particularly important).

However, the GGA is more sensitive to the electronic structure than the LDA [2], therefore the partial annihilation rates vary more and the LCW spectrum is more modulated (Fig. 1). In particular, the c projection of the LCW spectrum calculated with the GGA shows a strong local minimum at the Γ point superimposed on a cross-like structure due to the Cu-O plane Fermi surface.

It is very encouraging that the Geneva experimental group has recently observed a Fermi surface signal in the $Nd_{2-x}Ce_xCuO_{4-\delta}$ [5], which agrees qualitatively with the present calculations.

Acknowledgement—We wish to thank A.A. Manuel, L. Hoffmann, A. Shukla, T. Torsti and P. Hautojärvi for discussions. One of the authors (B.B.) was supported by the Swiss National Science

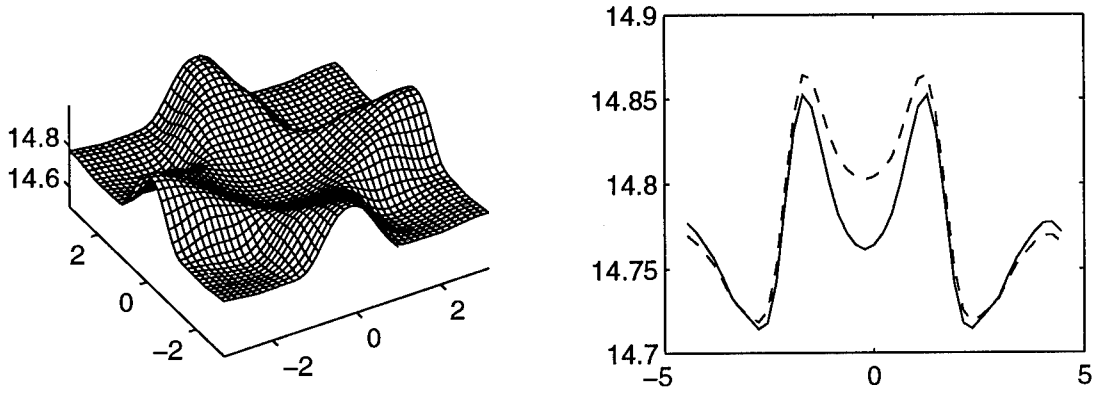


Fig. 1. The $Nd_{2-x}Ce_xCuO_4$ LCW spectrum calculated using the GGA (left) and its diagonal cut (right) shown by a solid line; the dashed line is the result of the LDA calculation. The Γ point is in the middle of the cross-like structure. The units for the wave-vectors are mrad.

Foundation grant number 8220-037167

REFERENCES

1. Nieminen R. M. *J. Phys. Chem. Solids* **52**, 1577 (1991); Puska M. J. and Nieminen R.M., *Rev. Mod. Phys.* **66**, 841 (1994).
2. Barbiellini B., Puska M. J., Torsti T. and Nieminen R. M., *Phys. Rev. B* **51**, 7341 (1995).
3. Blandin P. *et al.*, *Phys. Rev. B* **46**, 390 (1992).
4. Sundar C. S. *et al.*, *Phys. Rev. B* **42**, 426 (1990).
5. Manuel A. A. *et al.*, (this conference).

Pergamon

J. Phys. Chem. Solids Vol. 56, No. 12, pp. 1695–1696, 1995
Copyright © 1995 Elsevier Science Ltd
Printed in Great Britain. All rights reserved
0022-3697/95 $9.50 + 0.00

0022-3697(95)00171-9

GINZBURG–LANDAU THEORY OF THE ABRIKOSOV LATTICE IN A d-WAVE SUPERCONDUCTOR

A. J. BERLINSKY,* A. L. FETTER,† M. FRANZ,* C. KALLIN* and P. I. SOININEN*

* Institute for Materials Research and Department of Physics and Astronomy, McMaster University, Hamilton, Ontario, L8S 4M1 Canada

† Department of Physics, Stanford University, Stanford, CA 94305, U.S.A.

Abstract—We consider the Ginzburg–Landau free energy for the case of coexisting s- and d−wave order parameters, coupled to a gauge field, for a system in which the minimum energy state in the absence of magnetic fields is uniform d−wave. The eigenvalue equation arising from the coupled Ginzburg–Landau equations, in the presence of a uniform magnetic field, is implicitly non-linear and has no obvious closed-form solution. We employ a simple variational two-component wave function to minimize the quadratic free energy, and use linear combinations of these wave functions to construct variational Abrikosov lattice solutions which minimize the total free energy. The resulting lattice has an oblique structure, similar to that observed by small angle neutron scattering.

The free energy of a $d_{x^2-y^2}$ superconductor may be expressed in terms of two order parameters, $s(\mathbf{r})$ and $d(\mathbf{r})$, with appropriate symmetries, as follows [1]

$$\begin{aligned} f = {} & \alpha_s \mid s\mid^2 + \alpha_d|d|^2 + \beta_1|s|^4 + \beta_2|d|^4 \\ & + \beta_3|s|^2|d|^2 + \beta_4(s^{*2}d^2 + d^{*2}s^2) \\ & + \gamma_s|\Pi s|^2 + \gamma_d|\Pi d|^2 + \gamma_v\big[(\Pi_y s)^*(\Pi_y d) \\ & - (\Pi_x s)^*(\Pi_x d) + \text{c.c.}\big]. \end{aligned} \tag{1}$$

Here $\Pi = -i\hbar\nabla - e^*\mathbf{A}/c$, $\alpha_s = T - T_s$, $\alpha_d = T - T_d$ with $T_s < T_d$. It is assumed that β_1, β_2, β_3, γ_s, γ_d and γ_v are all positive [2]. The parameters γ_i are related to the effective masses in the usual way, $\gamma_i = \hbar^2/2m_i^*$, for $i = s, d, v$. The field equations for the order parameters are obtained by varying the free energy (1) with respect to conjugate fields d^* and s^*. We consider the problem of the structure of the vortex lattice in the vicinity of the upper critical field H_{c2} and study the linearized field equations. In the Landau gauge ($\mathbf{A} = \hat{y}Bx$) these linearized field equations are satisfied by taking $d(\mathbf{r}) = e^{iky}d(x)$, $s(\mathbf{r}) = e^{iky}s(x)$. Then we are left with the one dimensional problem:

$$(\mathcal{H}_0 + \alpha_d)d + Vs = Ed\,,\; Vd + (\mathcal{H}_0 + \alpha_s)s = Es, \tag{2}$$

where $\mathcal{H}_0 = \hbar\omega_c(a^\dagger a + 1/2)$ and $V = \epsilon_v(\hbar\omega_c/2)(a^\dagger a^\dagger + aa)$ are expressed in terms of raising and lowering operators, $a = [(x - x_k)/l + l(\partial/\partial x)]/\sqrt{2}$, $l = \sqrt{\hbar c/e^*B}$ is the magnetic length, $x_k = kl^2$, and $\omega_c = (e^*B/mc)$. We have assumed, for simplicity, that $m_d^* = m_s^* \equiv m$, and have set $\epsilon_v = \gamma_v/\gamma_s = m_s^*/m_v^*$. $E = 0$ corresponds to the physical solution for $B = H_{c2}(T)$, and solutions for $E < 0$ will be used when we consider the stability of various vortex lattice structures. Taking $\varphi^\pm = d \pm s$, we consider a variational solution in terms of normalized ground state harmonic oscillator wave-functions, $\varphi_k^\pm(x) = \mathcal{N}e^{-\sigma_\pm^2(x-x_k)^2/2}$. σ_+ and σ_- will be determined by minimization of the expectation value $\langle E\rangle$.

We next construct a vortex lattice. Consider a periodic solution of the form

$$\chi_{d/s}(\mathbf{r}) = \sum_n c_n e^{inqy}[\varphi_n^+(x) \pm \varphi_n^-(x)], \tag{3}$$

where $\varphi_k^\pm(x)$ are defined above and $k = qn$, (n integer), which gives periodicity in y with period $L_y = 2\pi/q$. Solution (3) will also be periodic in x provided that the constants c_n satisfy the condition $c_{n+N} = c_n$. We consider only the case of $N = 2$ so that $c_{2n} = c_0$ and $c_{2n+1} = c_1$. The period in the x direction is $L_x = 2l^2q$, and $BL_xL_y = 2(hc/e^*) = 2\Phi_0$, i.e. there are two flux quanta per unit cell. The resulting lattice may be thought of as centered rectangular with two quanta per unit cell or, equivalently, as an oblique lattice with lattice vectors of equal length and one flux quantum per unit cell. We describe this shape by the ratio, $R = L_x/L_y = (l^2/\pi)q^2$. $R = 1$ corresponds to the square, while $R = \sqrt{3}$ corresponds to the triangular vortex lattice.

At $B \approx H_{c2}(T)$ all solutions (3) are degenerate. It is the fourth order terms in the free energy that lift this degeneracy below H_{c2} and determine the vortex lattice configuration. The minimum free energy is $F_{\min} = -\frac{1}{4}\langle f_2\rangle^2/\langle f_4\rangle \equiv -\langle E\rangle^2\beta_A^{-1}$, where β_A is the generalization of the usual Abrikosov parameter [3]. For values of ϵ_v close to 0, $\beta_A(R)$ is minimized by $R_{\min} = \sqrt{3}$, i.e. the triangular lattice is stabilized. As ϵ_v is increased, the minimum of β_A moves toward smaller values of $R_{\min} < \sqrt{3}$ and an oblique vortex lattice is preferred. Finally, at some value of ϵ_v (which depends on other parameters) the minimum of β_A reaches $R_{\min} = 1$, corresponding to a square vortex lattice. Further increase of ϵ_v has no effect on the lattice structure which remains square. The typical dependence of β_A on R is displayed in Fig. 1 [4].

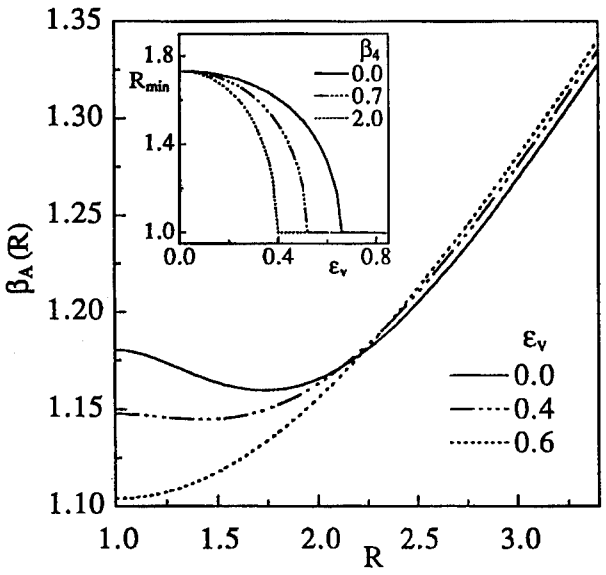


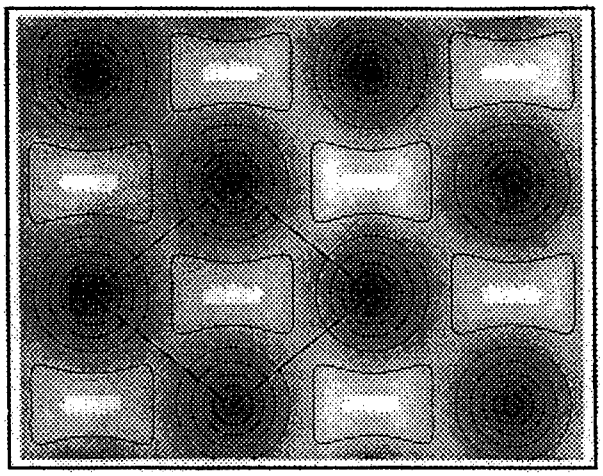
Fig. 1. Abrikosov ratio β_A as a function of the lattice geometry factor $R = L_x/L_y$ for different values of ϵ_v and $T_s = 0.5T_d$, $T = 0.75T_d$, $\beta_1 = \beta_2 = \beta_3 = \beta_4 = 1$, and $B = 0.8H_{c2}$. The inset shows the dependence of the minimum R_{min} on the parameter ϵ_v for different values of β_4.

This continuous dependence means that in a *d*-wave superconductor one should observe a general oblique vortex lattice, unless ϵ_v is very small or very large. Such an oblique structure, with nearly equal lattice constants and an angle of $\phi = 73°$ between primitive vectors, has in fact been observed in $YBa_2Cu_3O_7$ by Keimer *et al.*[5]. Our result, obtained from Eqs. (3), is shown in Fig. 2 [4]. Keimer *et al.* further report that one principal axis of the oblique unit cell coincides with the (110) or (1$\bar{1}$0) direction of the crystal. This is at variance with our result that one lattice vector of the larger rectangular cell is oriented along (100) or (010). However, we note that the energy cost of rotating the vortex lattice is small compared to the energy needed to deform the lattice. It is thus possible that (110) twin boundaries bind lines of vortices and hence orient one of the oblique lattice vectors along (110).

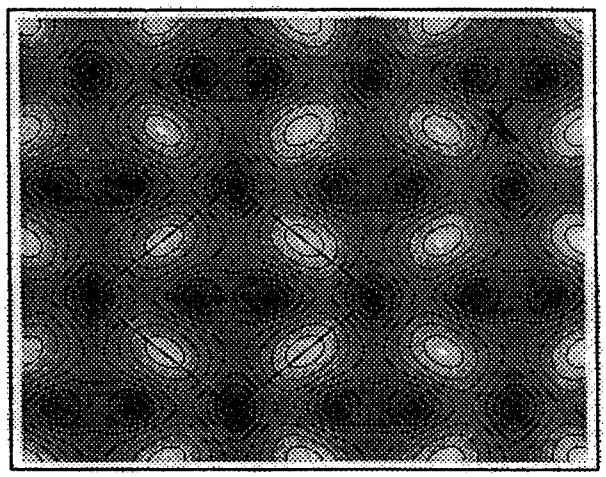
Acknowledgements—This work has been supported by the Natural Sciences and Engineering Research Council of Canada, the Ontario Centre for Materials Reasearch, and by the National Science Foundation under Grant No. DMR-91-20361. We would also like to thank the Aspen Center for Physics, where this collaboration was initiated.

REFERENCES

1. Joynt R., *Phys. Rev. B* **41**, 4271 (1990).
2. Soininen P. I., Kallin C. and Berlinsky A. J., *Phys. Rev. B* **50**, 13883 (1994).
3. Abrikosov A. A., *Zh. Eksp. Teor. Fiz.* **32**, 1442 (1957); *Sov. Phys. JETP* **5**, 1174 (1957).



(a) d-wave



(b) s-wave

Fig. 2. Contour plot of the amplitudes of (a) *d* component and (b) *s* component of the order parameter. GL parameters are the same as in Fig. 1 with $\epsilon_v = 0.45$, resulting in an oblique vortex lattice with $R_{min} = 1.29$ and the angle between primitive vectors $\phi = 76°$. The lightest regions correspond to the largest amplitudes.

4. Berlinsky A. J. *et al. Phys. Rev. Lett.***75**, 2200 (1995).
5. Keimer B. *et al., J. Appl. Phys.* **76**, 1 (1994).

Pergamon

J. Phys. Chem. Solids Vol. 56, No. 12, pp. 1697–1698, 1995
Copyright © 1995 Elsevier Science Ltd
Printed in Great Britain. All rights reserved
0022-3697/95 $9.50 + 0.00

0022-3697(95)00132-8

CHARGE-TRANSFER AND THE LOCATION OF SUPERCONDUCTING HOLES IN $La_{2-\beta}Sr_\beta CuO_4$

HOWARD A. BLACKSTEAD
Department of Physics, University of Notre Dame, Notre Dame, IN 46556, U.S.A.

JOHN D. DOW
Department of Physics and Astronomy, Arizona State University, Tempe, AZ 85287-1504, U.S.A.

Abstract—As β increases in $La_{2-\beta}Sr_\beta CuO_4$, holes transfer from the cuprate-planes to the La–O layers—the opposite of what the charge-transfer hypothesis predicts. We interpret this analyzed charge-transfer as indicating that the superconductivity originates in the vicinity of La–O layers, not in the cuprate-planes—contrary to previous interpretations of measurements which place the origin of superconductivity in the cuprate-planes.

Keywords: A. superconductors, C. neutron scattering, D. superconductivity, D. $La_{2-\beta}Sr_\beta CuO_4$, D. charge-transfer.

Of the high-temperature superconductors, $La_{2-\beta}Sr_\beta CuO_4$was one of the first discovered, and is now one of the most studied. As a function of Sr content β, this material has its highest critical temperature, $T_c \approx 40$ K, for $\beta \approx 0.15$ [1]. By consensus, the superconductivity is associated with oxygen 2p holes [2], and so it would be interesting to verify that those holes are located where most researchers suppose them to be: on the oxygen ions in the cuprate planes.

The crystal structure of $La_{2-\beta}Sr_\beta CuO_4$is layered and features a sequence of one cuprate plane followed by two La–O layers (or, more correctly, (La,Sr)–O layers). A widely accepted picture of superconductivity in $La_{2-\beta}Sr_\beta CuO_4$is that holes from the La–O layers migrate to the cuprate-planes, where they dope the cuprate-planes p-type, induce p-type superconductivity (once the hole concentration is sufficiently large), and increase the critical temperature for superconductivity as the hole-concentration in the cuprate-planes increases. (This picture is called the "charge-transfer hypothesis" [3].) Of course, one expects that this picture can be verified by simply extracting the charges on each of the ions from bond-length data, using the bond-valence-sum method [4].

We have applied the method to $La_{2-\beta}Sr_\beta CuO_4$[5], and extracted from the neutron scattering data of Radaelli *et al.*, the effective charges of Fig. 1 vs Sr content β. For increasing β, the charges for all of the ions except cuprate-plane-O(1) become more positive, and only the charge on O(1) becomes more negative. For small Sr contents β, this means that holes migrate to all ions except O(1) as T_c increases. However, O(1) is an oxygen ion in a cuprate-plane, and is the one ion that actually becomes more negative and gains electrons as the Sr content increases. The total charge of the cuprate-planes [Cu plus two O(1) ions] also becomes more negative with increasing β. Thus the charge-transfer to the cuprate-planes has the opposite sign to that expected on the basis of the charge-transfer hypothesis!

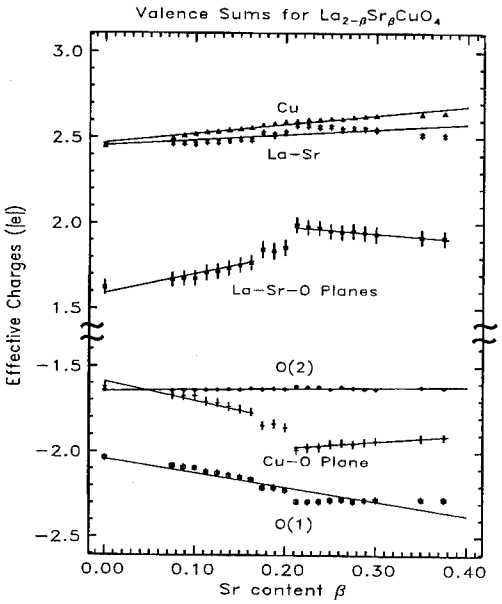


Fig. 1. Bond-valence-sum charges on individual ions, the cuprate-planes (Cu–O Plane), and the (two) La–O planes (La–Sr–O Plane) in $La_{2-\beta}Sr_\beta CuO_4$(in units of |e|) extracted from the neutron scattering data of Ref. 1 vs Sr content β. O(1) and O(2) refer to oxygen in the cuprate-planes and in the La–O layers, respectively. The La and Sr ions are treated in a virtual-crystal approximation, and averaged. The cuprate-planes are under compression, and the La–O planes are under tension, and hence their effective charges are large and small in magnitude, respectively. With increasing β, positive charge transfers from the cuprate-planes to the La–O layers.

The neutron data produced an average bond-length and

our analysis assumes a corresponding average or virtual-crystal cation $La_{1-(\beta/2)}Sr_{(\beta/2)}$. Although one might argue that physics beyond the virtual-crystal approximation could be important in $La_{2-\beta}Sr_{\beta}CuO_4$, the kernel of the charge-transfer analysis is a simple chemical fact that transcends such issues: if one transfers an electron to an oxygen ion from its neighboring cations, its bonds shorten due to the Coulomb force. Thus O(1) bond-shortening implies the acquisition of electrons in the cuprate planes.

If the hypothesis of hole-transfer to the cuprate-planes is invalid despite earlier work apparently confirming it [6], and if the superconducting holes are not in the cuprate-planes, then all the theories of cuprate-plane superconductivity must be invalid, and searches for explanations of high-temperature superconductivity should concentrate on non-cuprate-plane models based on oxygen [7] or on defects [8].

Acknowledgements—We thank the Office of Naval Research, the Air Force Office of Scientific Research, and the Department of Energy for their generous support (N00014-9410147, AFOSR-F49620-94-10163 and DE-FG02-90ER45427).

REFERENCES

1. Radaelli P. G., Hinks D. G., Mitchell A. W., Hunter B. A., Wagner J. L., Dabrowski B., Vandervoort K. G., Viswanathan H. K. and Jorgensen J. D., *Phys. Rev. B* **49**, 4163 (1994), and references therein.
2. Nücker N., Fink J., Fuggle J. C., Durham P. J. and Temmerman W. M., *Phys. Rev. B* **37**, 5158 (1988).
3. Cava R. J., Hewat A. W., Hewat E. A., Batlogg B., Marezio M., Rabe K. M., Krajewski J. J., Peck Jr W. F. and Rupp Jr L. W., *Physica C* **165**, 419 (1990).
4. Brown I. D., *J. Solid State Chem.* **82**, 122 (1989).
5. A first-order orthorhombic-to-tetragonal phase-transition at $\beta \approx 0.2$ manifests itself as a jump in charge (or bond-length), while second-order transitions such as the onset of superconductivity are accompanied by a continuous charge, whose derivative with respect to β changes discontinuously (not discernible with statistical significance in Fig. 1).
6. For a review, see Ginsberg D. M., in *Physical Properties of High-Temperature Superconductors* Edited by D. M. Ginsberg, p. 1. World Scientific, Singapore (1989).
7. Blackstead H. A. and Dow J. D., *Pis'ma Zh. Eksperim. Teor. Fiz.* **59**, 262 (1994) [*JETP Lett.* **59**, 283–289 (1994)] and reference therein; and to be published.
8. Phillips J. C., *Phys. Rev. B* **46**, 8542 (1992).

Pergamon

J. Phys. Chem. Solids Vol. 56, No. 12, pp. 1699–1700, 1995
Copyright © 1995 Elsevier Science Ltd
Printed in Great Britain. All rights reserved
0022–3697/95 $9.50 + 0.00

0022–3697(95)00093-3

A VALENCE-FLUCTUATION MECHANISM WITH HIGHLY ANISOTROPIC s-WAVE PAIRING

B. H. BRANDOW
Center for Nonlinear Studies, Los Alamos National Laboratory, Los Alamos, NM 87545, U.S.A.

Abstract—We report on a fairly *ab initio* theory of cuprate superconductivity, based on the concept that the above-T_c state is a normal Fermi liquid with strong correlations of the type found in valence-fluctuation and heavy-fermion materials. These correlations (within an assumed normal ground state) are found to provide a satisfactory source or mechanism in the pairing. Many electronic features of the cuprates are quantitatively reproduced by this theory, and for some there is even semi-quantitative agreement. This report focuses especially on the gap form, on major aspects of the cuprate T_c systematics, and on evidence suggesting that this mechanism is also operating (together with phonons) in a number of other superconductors.

Keywords: Valence-fluctuation mechanism, anisotropic-s gap, T_c systematics, exotic superconductors.

We have developed a fairly *ab initio* theory of cuprate superconductivity [1], based on the concept that the above-T_c state is a normal Fermi liquid with strong electronic correlations of the type found in valence-fluctuation (VF) and heavy-fermion materials. The ground-state-correlation aspect is found to provide a satisfactory source or mechanism for the pairing. In addition to the high T_cs, this explains many of the unusual features of cuprate super conductivity, as outlined below.

The many-body calculation proceeds by a variational approach, which is well suited for the strong-coupling aspect of this problem. Starting with the fiction of a normal ground state, our variational ground-state energy (fully optimized) is differentiated with respect to quasiparticle occupation numbers to generate the Landau quasiparticle energy spectrum $\epsilon_{k\sigma}$ and interaction $f(k_\uparrow, k'_\downarrow)$, for all k and k' in the Brillouin zone. The pair interaction $V_{kk'}$ is then obtained from this f by an analytic continuation. An Anderson-lattice form of model Hamiltonian is used (the usual three-band model, with a single $U = U_{dd}$), with input parameters taken from a careful reanalysis of the photoemission and inverse-photoemission data for CuO [2]. The claim of *ab initio* character for this theory is based on the use of a realistic model Hamiltonian, realistic input parameters, and a highly refined calculational technique. Our consistent $(1/N)^1$ level of approximation goes considerably beyond previous Anderson lattice treatments; this incorporates a new and previously unsuspected feature which arises specifically from the lattice aspect.

The various semi-quantitative results are quite encouraging: (a) we adjust one Hamiltonian parameter (the charge-transfer energy Δ_{CT}) to obtain a typical $T_c(\sim 100\ K)$. The resulting Δ_{CT} is found to be reasonably close to the value deduced from photoemission data. (b) The quasiparticle (pdσ antibonding) bandwidth ($\sim$ 1.6 eV) is close to a value ($\sim$ 1.4 eV) deduced from angle-resolved photoemission [3]. (c) The coherence length ξ is found to be extremely short, just a few lattice spacings, consistent with experiment. (d) The large $2\Delta/k_BT_c$ ratio ($\sim$ 6) emerges mainly as a consequence of strong gap anisotropy. [In a simpler in-plane-isotropic model, the large effect of a pair-breaking reduction of T_c is compensated by a very small value (1.75) for the "bare" gap ratio obtained from the simple gap equation.] (e) At the Fermi surface, the angle-averaged quasiparticle interaction $\langle f_{\uparrow\downarrow}\rangle$ is found to be *large* and *repulsive*, $\approx$ +0.5 eV. This *magnitude* is about the value required to account for the strong quasiparticle damping, and thus presumably also for the large normal-state resistivity, according to calculations of quasiparticle scattering [4]. (These calculations show that the linear behavior is due to the unusual band geometry, for ϵ_F close to the van Hove saddle point.) The *repulsive sign* leads to an expected Stoner enhancement factor of $\sim$ 2–3, which is also consistent with available evidence.

Also significant are a number of results which are more qualitative in nature: (a) a clear proximity to a magnetic instability, at reduced hole-doping. (b) Evidence for a strong pair-breaking reduction of T_c, apparently due to quasiparticle damping from the above-mentioned quasiparticle scattering. (c) A highly anisotropic (although s-like) gap, which may or may not have nodes, perhaps depending on the material. (d) A simple argument for expecting a highly anomalous form of $H_{c2}(T)$, consistent with what has been observed [5]. (e) Qualitative explanations for major features of the T_c systematics (see below).

The net pair attraction is due to a very strong k dependence in the pair interaction V'_{kk}. For small k, k' (near the zone center Γ) this V is very attractive ($\sim$ several eV), while for large k, k' [near the zone corner (1,1)] this becomes very

function, with the full point-group symmetry of the CuO_2 plane. The resulting gap function Δ_k is quite large (positive) at small ks and also large (negative) at large ks, with a single node line in between. (There is thus substantial pairing throughout the entire Brillouin zone.) The node line lies close to and mainly outside of the Fermi surface. Study of the gap anisotropy for a realistic band structure showed that the gap Δ (essentially, Δ_k on the Fermi surface) is largest in the direction of the Cu–O bonds, in agreement with experiment. Midway between the bond directions Δ is far smaller, and it may be either positive or negative. The negative case corresponds to intersection of the node line with the Fermi surface, leading here to an 8-node gap form. The gap nodes in this case are expected to be closer to the (1,1) or 45° directions than to the (1,0) or bond directions.

There are several lines of evidence favoring this type of anisotropic-s gap (with or without nodes), as contrasted to the d-wave $x^2 - y^2$ form: (a) although gap nodes are confirmed in YBCO, there is evidence against such nodes in $(Nd,Ce)_2CuO_4$ [6]. This difference is reconciled most simply in the anisotropic-s scenario, which requires only a modest deformation of the node line. (b) Inner-gap features have been observed in tunnelling in at least five different cuprates. Some of the data even shows a non-monotonic or reentrant form [7], consistent with the 8-node gap form [8]. (c) Recently, more direct evidence for the 8-node form has been obtained from angle-resolved photoemission for Bi-2212 [9], and from thin-film tunnelling for YBCO [10].

Major aspects of the T_c systematics are rationalized, such as the strong dependence on the hole-doping "x". T_c is driven down on the low-doping side by the x dependence found in the numerical results [1], and on the high-doping side by local Madelung-potential changes induced by the doping. It is particularly noteworthy that this theory provides a qualitative explanation for the empirical dependence of T_c on the Madelung potential of the apical oxygens—a correlation which which is very strong [11] and which was quite unexpected. [The apical oxygen $2p_z$ orbitals interact strongly with the copper 4s orbitals, which in turn interact strongly with the planar oxygen Bloch orbitals near the (1,0) point, so that a Madelung effect on the $2p_z$ energy level is reflected in a shift of the charge-transfer energy difference, $\Delta_{CT} = \epsilon(3d) - \langle\epsilon_k(2p\sigma)\rangle$.] A corollary of this is that T_c also depends strongly on the number of apical oxygens per planar Cu ion; a reduction or elimination of apicals is generally quite beneficial, as can be seen in the data. We also argue that the apparent evidence for strong dependence of T_c on inter-plane coupling is an illusion, and is mainly a reflection of the effects just mentioned.

There is a considerable variety of evidence suggesting that the present mechanism is operating also in a number of other families of superconductors, especially the "exotic" superconductors of Uemura [12] and the "bad actors" of Anderson and Yu [13]. (The borocarbides also fit this general pattern, e.g. [14].) This evidence includes anomalously short coherence length, anomalously high resistivity, a highly anomalous form of $H_{c2}(T)$, and a number of features which we argue should help to justify an Anderson-lattice form of model Hamiltonian. These latter features include large Us, "conduction" (non-d-like) bands, reduced dimensionality and/or clustering, ligand ions with electronegativity considerably different from the "localized" (d-like) ions or clusters, and large penetration depths (small carrier density and large effective mass).

Acknowledgement—This work was partially supported by the U. S. Department of Energy.

REFERENCES

1. Brandow B. H., *J. Phys. Chem. Solids* **54**, 1137 (1993); *Int. J. Mod. Phys. B* **8**, 2667 & 3859 (1994).
2. Brandow B. H., *J. Solid State Chem.* **88**, 28 (1990); in *High-Temperature Superconductivity* (Edited by J. Askenazi *et al.*), p. 583. World Scientific, Singapore (1992).
3. Dessau D. S. *et al.*, *Phys. Rev. Lett.* **71**, 2781 (1993).
4. Pattnaik P. C. *et al.*, *Phys. Rev. B* **45**, 5714 (1992); Gopalan S. *et al.*, *ibid.* **46**, 11798 (1992).
5. Mackenzie A. P. *et al.* , *Phys. Rev. Lett.* **71**, 1238 (1993); Osofsky M. S. *et al.*, *ibid.* **71**, 2315 (1993).
6. Anlage S. M. *et al.*, *Phys. Rev. B* **50**, 523 (1994).
7. Valles J. M. *et al.*, *Phys. Rev. B* **44**, 11986 (1991), see especially Fig. 10.
8. Mahan G. D., *Phys. Rev. B* **40**, 11317 (1989); Fedro A. J. and Koelling D. D., *ibid.* **47**, 14342 (1993).
9. Ding H. *et al.s*, *Phys. Rev. Lett.* **74**, 2784 (1995).
10. Lin S. -Y. *et al.* (1995), preprint.
11. Ohta Y. *et al.*, *Phys. Rev. B* **43**, 2968 (1991).
12. Uemura Y. J. *et al.*, *Phys. Rev. Lett.* **66**, 2265 (1991); *Physica B* **186–188**, 223 (1993).
13. Anderson P. W. and Yu C. C., in *Highlights of Condensed-Matter Theory, Proceedings of the International School of Physics "Enrico Fermi", Course* 89 (Edited by F. Bassani *et al.*), p. 767. North Holland Italia (1985).
14. Cywinski R. *et al.*, *Physica C* **233**, 273 (1994); Godart C. *et al.*, *Phys. Rev. B* **51**, 489 (1995).

Pergamon

J. Phys. Chem. Solids Vol. 56, No. 12, pp. 1701–1702, 1995
1995 Elsevier Science Ltd
Printed in Great Britain
0022–3697/95 $9.50 + 0.00

0022-3697(95)00205-7

TWO-PROTRUSION STM ON AN ANISOTROPIC SUPERCONDUCTOR

JEFF M. BYERS * and MICHAEL E. FLATTÉ †

* Naval Research Laboratory, Washington, D.C. 20375, U.S.A.
† Division of Applied Sciences, Harvard University, Cambridge, MA 02138, U.S.A.

Abstract—The differential conductance of an STM with two atomically sharp protrusions separated by at least several atomic spacings depends on the electronic transport in the sample between those protrusions. This allows direct probing of any gap anisotropy experienced by propagating quasiparticles.

Keywords: scanning tunneling spectroscopy, high-temperature superconductivity.

We propose an experiment which should provide detailed angular information about local transport on a superconducting sample. The apparatus consists of a spatially extended STM tip, manufactured with two protrusions each ending in a single atom. Here we point out that new information is obtainable when these protrusions are separated by more than 10 Å. Such two-protrusion tips are often found by chance. Atomic-scale tunneling from more than one site has been proposed as a probe of local transport [1,2], but these proposals require two separate contacts. It should be noted that probing electronic properties by scattering electrons off an impurity has already had some success [3,4].

On a homogeneous sample the transport quantities of interest would determine the desired separation of protrusions on the STM contact. Measurements of quantities with long length scales (100–1000 Å) such as mean free paths, transitions from ballistic to diffusive propagation, low-T_c coherence lengths, charge-density-wave correlation lengths, and angularly anisotropic density-of-states effects [4] would most benefit from the increased signal of the two-protrusion configuration relative to the two-contact configuration. The two-protrusion configuration has a higher signal than the two-contact configuration because the interference term between the two tips is of lower order in the tunneling matrix elements. However, to make such an experiment feasible the sample would have to be rotated or several domains which differ by their crystallographic orientation would have to be examined. Normalizing the signal for comparison among the different orientations could be done by comparing currents across the voltage range.

For the two-protrusion STM the differential conductivity is

$$\begin{aligned}\frac{dI}{dV} \propto\ & [\mathrm{Im}\tilde{g}(x_1,x_1;0)\mathrm{Im}\tilde{G}(r_1,r_1;V)\\ & +\mathrm{Im}\tilde{g}(x_2,x_2;0)\mathrm{Im}\tilde{G}(r_2,r_2;V)\\ & +\mathrm{Im}\tilde{g}(x_1,x_2;0)\mathrm{Im}\tilde{G}(r_1,r_2;V)\\ & +\mathrm{Im}\tilde{g}(x_2,x_1;0)\mathrm{Im}\tilde{G}(r_2,r_1;V)] \qquad (1)\end{aligned}$$

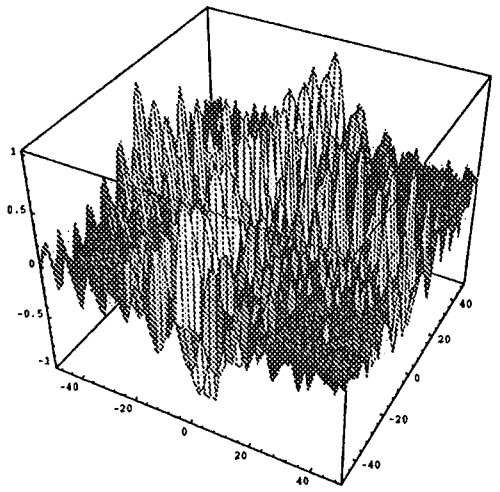


Fig. 1. Differential conductance as function of relative protrusion separation in position space (units of $k_F^{-1} \sim 1$ Å). The gap is $\Delta_{\mathbf{k}} = \Delta_0 \cos(2\phi_{\mathbf{k}})$ and $eV = 1.1\Delta_0$.

where $\tilde{G}$ and $\tilde{g}$ are the Green functions in the sample and tip respectively, convoluted with the tip shape. The first two terms describe direct tunneling through the two protrusions, but the last two terms are interference terms between the two protrusions.

We apply eqn (1) to transport on $Bi_2Sr_2CaCu_2O_8$. In a heuristic sense, gap anisotropy produces an angularly-dependent density of states, which can be qualitatively different at different energies. For a $d_{x^2-y^2}$ gap, which has four nodes, at voltages much less than the gap quasiparticles can only travel in the real-space directions roughly parallel to node momenta, yielding "channels" of conductance [1]. At voltages slightly higher than the gap maximum there are more states for momenta near the gap maximum, so the channels would appear rotated by 45°. By examining transport at different energies a two-protrusion STM has the capability of measuring gap anisotropy via short-length scale transport measurements.

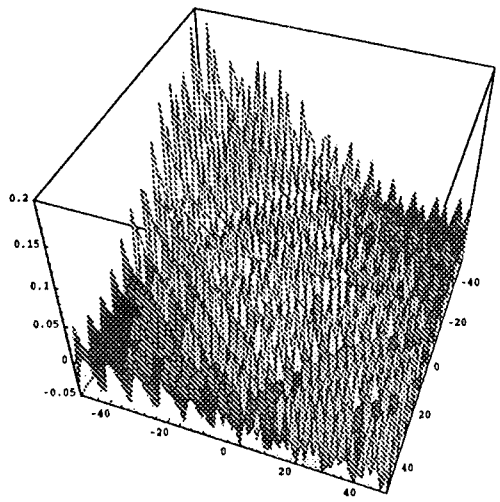


Fig. 2. Similar to Fig. 1, but only one quadrant and $eV = 0.1\Delta_0$.

REFERENCES

1. Byers J. M., Flatté M. E., *Phys. Rev. Lett.* **74**, 306 (1995).
2. Niu Q., Chang M. C. and Shih C. K., Phys. Rev. B.
3. Crommie M. F., Lutz C. P. and Eigler D. M., *Nature* **363**, 524 (1993).
4. Byers J. M., Flatté M. E. and Scalapino D. J., *Phys. Rev. Lett.* **71**, 3363 (1993).

Pergamon

J. Phys. Chem. Solids Vol. 56, No. 12, pp. 1703–1704, 1995
Copyright © 1995 Elsevier Science Ltd
Printed in Great Britain. All rights reserved
0022–3697/95 $9.50 + 0.00

0022-3697(95)00173-5

CORRELATION-INDUCED ELECTRON–LATTICE INTERACTION IN THE HUBBARD MODEL: ITS EFFECTS ON THE SPECTRAL DISTRIBUTION

CHANGFENG CHEN
Department of Physics, University of Nevada, Las Vegas,
Las Vegas, Nevada 89154-4002, USA

Abstract—The photoemission spectrum of the Hubbard model with a correlation-induced electron–lattice interaction is examined using exact diagonalization techniques. By adjusting the strength of the electron–lattice interaction, its effects on the spectral distribution are systematically investigated. This interaction, which was found in an earlier work to enhance the superconducting pairing in the system, causes non-trivial transfer of spectral weight accompanied by a change in the energy range of the spectral distribution. The calculated results are analyzed in a many-body picture to gain physical insights into the role of the electron–lattice interaction in determining the spectroscopic behavior of the system. It is found that both the single-particle and many-body effects manifest themselves in the spectrum and both must be considered to understand the observed phenomena.

The electron–lattice interaction plays a key role in BCS superconductivity [1]. Its role in novel superconductors such as high-T_c cuprates has been the subject of intensive investigation and debate. It has been proposed [2] that a charge-density dependent, static electron–lattice interaction constitutes an effective attractive electron–electron interaction under certain conditions. This is based on the study of a Hubbard model, which, in various limits or under specific conditions, has been suggested to represent the high-T_c systems [3]. The model which incorporates the electron–lattice interaction is defined by the following Hamiltonian

$$\begin{aligned} H = & -t \sum_{<i,j>;\sigma} c^{\dagger}_{i\sigma} c_{j\sigma} (1 - n_{i\bar{\sigma}})(1 - n_{j\bar{\sigma}}) \\ & - (t + \delta) \sum_{<i,j>;\sigma} c^{\dagger}_{i\sigma} c_{j\sigma} [n_{j\bar{\sigma}}(1 - n_{i\bar{\sigma}}) + n_{i\bar{\sigma}}(1 - n_{j\bar{\sigma}})] \\ & - (t + \gamma) \sum_{<i,j>;\sigma} c^{\dagger}_{i\sigma} c_{j\sigma} n_{i\bar{\sigma}} n_{j\bar{\sigma}} + U \sum_{i} n_{i\uparrow} n_{i\downarrow} \end{aligned} \quad (1)$$

All notations are standard. The hopping parameters depend on the number of electrons in the $\langle i, j \rangle$ bond. In the limit $\delta = \gamma = 0$ the Hamiltonian reduces to the standard Hubbard model. In the limit $U = 0$ the electron–lattice interaction in the model still makes it a many-body problem. It has been found [2] that as long as the bonds with higher occupation have a larger absolute value of the hopping parameters there will be an effective attractive electron–electron interaction in favor of a superconducting ground state.

In this paper we study the effect of the electron–lattice interaction introduced in Hamiltonian (1) on the spectral distribution. The photoemission spectrum (PES) is calculated in a periodic small cluster approach. We use an eight-site cluster with periodic boundary conditions on a 3D fcc lattice [4] which shares the same structural environment as the tetrahedral cluster used in Ref. [2]. We study the case of seven electrons in the cluster, i.e. an almost half-filled band. A symmetry-projected exact diagonalization technique [5] is applied to the Hamiltonian to obtain all the eigenvalues and eigenstates. The PES is defined as

$$P(\omega) = \sum_{i,\sigma,k} |\langle \phi^{N-1}_k | c_{i\sigma} | \phi^{N}_0 \rangle|^2 \, \delta[\omega - E^{N-1}_k + E^{N}_0 + \mu] \quad (2)$$

where ϕ^N_0 and ϕ^{N-1}_k are the N-electron ground state and the kth $(N-1)$-electron final state, with energies E^N_0 and E^{N-1}_k respectively. The operator $c_{i\sigma}$ destroys an electron with spin σ and orbital index i. The chemical potential $\mu = (1/2)[E^{N+1}_0 - E^{N-1}_0]$ [6].

The calculated PES is shown in Fig. 1. The "bare" hopping parameter t is chosen to be the energy unit. The on-site Coulomb interaction is set to $U/t = 15.0$. The single-particle bandwidth in the limit $\delta = \gamma = 0.0$ is $W = 16t$. The parameters used in the calculations correspond to $U/W \approx 1$, i.e. strongly correlated case. Negative values of δ and γ increase the effective bandwidth (W_{eff}) thus reduce the correlation effect while positive values of these parameters do the opposite. A detailed analysis of the calculated results yields the following conclusions.

(i)There is an obvious reduction in the overall spectral distribution range accompanied by non-trivial spectral weight transfer in Fig. 1 (a)–(e), indicating a reduced effective quasiparticle bandwidth, thus stronger correlation effects with larger U/W_{eff} ratios.

(ii)Satellite peaks driven by the on-site Coulomb interaction U are identified by comparing to the results with $U = 0$. The highest binding energy is indicated by the tip of the letter "V" in each panel in Fig. 1. It is seen that U-driven features grow with increasing δ and γ, consistent with the results in (i).

(iii)A significant reduction of the quasiparticle spectral weight near μ is observed. The lost spectral weight is re-

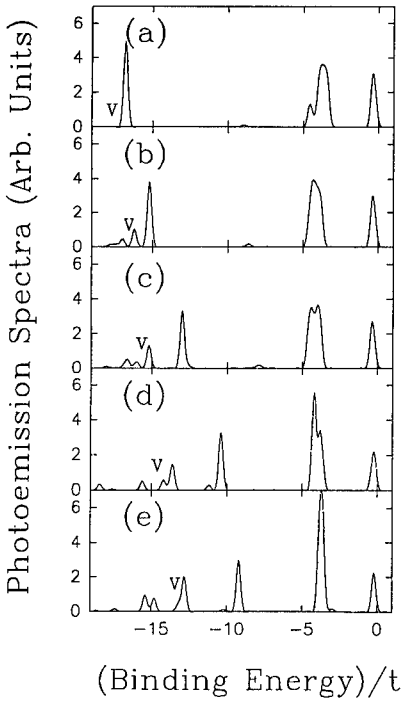


Fig. 1. The calculated PES. The U/t is set to 15.0. Other parameters are $(\delta/t, \gamma/t)$ = (a) $(-0.5, -1.0)$, (b) $(-0.3, -0.6)$, (c) $(0.0, 0.0)$, (d) $(0.3, 0.6)$, (e) $(0.5, 1.0)$. The tip of letter "V" indicates the highest binding energy position for $U = 0$.

distributed at higher binding energies. This phenomenon, within the present model, is solely due to the electron–lattice interaction. This kind of behavior has been recently observed in boride–carbide systems by Fujimori *et al.* [7]. Similar results in other correlated systems are expected.

(iv)The major low-energy peak (second from μ) is drastically narrowed as U/W_{eff} increases [Fig. 1(a)–(e)]. This can be understood as due to an effective *intersite* Coulomb interaction introduced by δ and γ, interactions on the $\langle i, j \rangle$ *bond*. Recently we have found [8] that intersite interactions in the Hubbard model *generally* causes spectral narrowing at low binding energies.

(v)The high-energy quasiparticle peak splits as it shifts towards lower energies. This probably is not a generic feature due to the electron–lattice interaction, but rather a model (energy spectrum) dependent phenomenon.

In summary, we have studied the photoemission spectral behavior of a Hubbard model with an electron–lattice interaction in an exact diagonalization approach. Some interesting interaction-driven spectral features have been observed and discussed in a many-body picture. These results should have implications for a wide variety of strongly correlated materials.

Acknowledgements—This work was supported in part by the National Science Foundation under Cooperative Agreement OSR-9353227 and the U. S. Department of Energy under the EPSCoR program.

REFERENCES

1. Bardeen J., Cooper L. N. and Schrieffer J. R., *Phys. Rev.* **106**, 162 (1957); **108**, 1175 (1957).
2. Proetto C. R. and Falicov L. M., *Phys. Rev. B* **38**, 1754 (1988).
3. Dagotto E., *Rev. Mod. Phys.* **66**, 763 (1994) and references cited therein.
4. For the cluster structure, see Changfeng Chen, *Phys. Rev. B* **47**, 2861 (1993).
5. Changfeng Chen, *Int. J. Mod. Phys. B* **5**, 1147 (1991); *Phys. Rev. B* **50**, 14539 (1994).
6. Callaway J., Tan L. and Zheng H., *Phys. Rev. B* **50**, 1369 (1994).
7. Fujimori A. *et al.*, *Phys. Rev. B* **50**, 9660 (1994).
8. Jianzhong Zheng and Changfeng Chen, *Phys. Rev. B* (to be published).

Pergamon

J. Phys. Chem. Solids Vol. 56, No. 12, pp. 1705–1706, 1995
Copyright © 1995 Elsevier Science Ltd
Printed in Great Britain. All rights reserved
0022–3697/95 $9.50 + 0.00

0022-3697(95)00231-6

SPIN FLUCTUATIONS IN HIGH-T_c SUPERCONDUCTORS WITH TWO FERMI SURFACE SHEETS

LIANG CHEN* PIERRE BÉNARD†

* Département de physique and Centre de recherche en physique du solide, Université de Sherbrooke, Sherbrooke, Québec, Canada J1K 2R1

† Institut de recherche sur l'hydrogène, Université du Québec à Trois-Rivières, Trois-Rivières, Québec, Canada G9A 5H7

Abstract—We present a spin fluctuation study of the two-dimensional t–t' model in the regime of $|t'| > |t|/2$.As a function of band filling, the Fermi surface exhibits rich geometrical and topological properties, which can be used as a model for the Fermi surface structure of $Tl_2Ba_2CuO_6$ as calculated by Singh and Pickett.

Keywords: t–t' model, spin fluctuations, Fermi surface nesting.

1. INTRODUCTION

It is now widely believed that two-dimensional CuO_2 planes are mainly responsible for the electronic properties. Many experiments, as well as theoretical band structure calculations, all seem to be consistent with an effective one-band Hubbard model [1] which in the electron picture takes the form

$$H = -t \sum_{<ij>\sigma} c^{\dagger}_{i\sigma} c_{j\sigma} + t' \sum_{<<ij>>\sigma} c^{\dagger}_{i\sigma} c_{j\sigma} + h.c. + U \sum_i n_{i\uparrow} n_{i\downarrow} , \quad (1)$$

where $c^{\dagger}_{i\sigma}$ is the electron creation operator with spin σ at lattice site i, $c_{i\sigma}$ is the corresponding annihilation operator, $< ij >$ stands for a sum over nearest-neighbor and $<< ij >>$ represents the next-nearest-neighbors. For the most commonly studied systems, it is generally agreed that $t' \approx 0.16t$ for $La_{2-x}Sr_xCuO_4$, and $t' \approx 0.45t$ for $YBa_2Cu_3O_{7-\delta}$. It is perhaps less known that the band structure calculations of Singh and Pickett [2] for the $Tl_2Ba_2CuO_6$ show two Fermi surfaces in the $k_z = 0$ plane: one electron like surface around the Γ point and another hole like surface around the M point. Despite its complexity, it turns out we can model this with $|t'| > |t|/2$.

2. FERMI SURFACE STRUCTURES AND SPIN FLUCTUATIONS

One can easily obtain the following dispersion from eqn (1)

$$\varepsilon(\mathbf{k}) = -2t[\cos(k_x) + \cos(k_y)] + 4t' \cos k_x \cos k_y . \quad (2)$$

In units where $t = 1$ and when $t' > 1/2$, the band minimums are located at $(\pm\pi, 0)$ and $(0, \pm\pi)$, while the band maximums are at $(\pm\pi, \pm\pi)$. In contrast to the well studied case of $t' < 1/2$, it is surprising that in the case of $t' > 1/2$ new nesting wave vectors appear, equal to $(2\arccos(t/2t'), 0)$ and $(0, 2\arccos(t/2t'))$. These nesting vectors connect the flat sections of the Fermi surface that appear when the chemical potential reaches $\mu = -t^2/t'$. Figure 1 shows the typical Fermi surface structure. The saddle points which leads to the van-Hove singularity of the density of states are now located well inside the Brillouin zone. There is an extra jump in the density of states, which corresponds to the closing of the electron-like Fermi surface at the zone center. Thus there are three doping regimes at zero temperature. The first regime corresponds to the range of chemical potentials $-4t' < \mu < -t^2/t'$, the second regime is defined by the range $-t^2/t' < \mu < 4t' - 4t$, and the last regime, by the range $4t' - 4t < \mu < 4t' + 4t$. The jump in the density of states occurs at $\mu = 4t' - 4t$, and the van-Hove singularity is at $\mu = -t^2/t'$. In the first regime, the Fermi surface consists of four distinct pockets centered at$(\pm\pi, 0)$ and $(0, \pm\pi)$. In the second regime, there are two disconnected Fermi surfaces: one electron-like surface centered around Γ point, another hole-like surface centered around M point. This structure of the Fermi surface is thus similar to the calculated band structure of $Tl_2Ba_2CuO_6$ at the $k_z = 0$ plane. In the last doping regimes, the Fermi surface is composed of only hole-like sections.

For two-dimensional systems, the momentum dependence of the spin fluctuations is mainly determined by the Fermi surface nesting properties [3]. In fact for weakly interacting two-dimensional electrons, the magnetic neutron scattering experiments should provide a detailed spectroscopy of the Fermi surface. The structures of the spin susceptibility in **k**-space can be related to the $2k_F$ Kohn

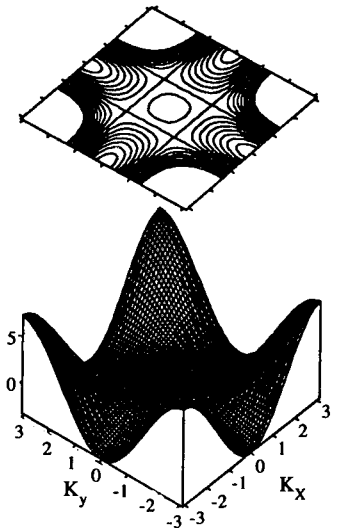


Fig. 1. Fermi surface structure for $t' = 0.8t$.

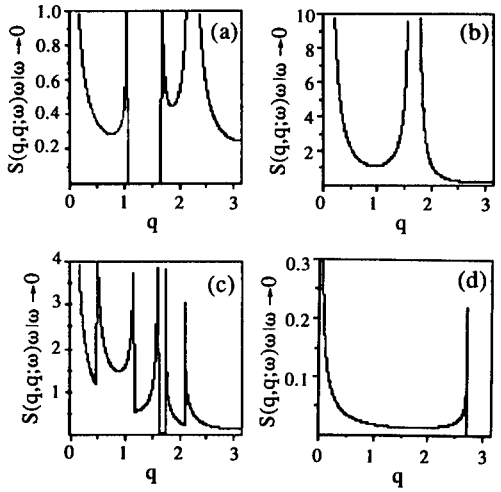


Fig. 2. The zero-temperature, zero-frequency limit of the spin structurefactor devided by frequency as a function of the wavevector $\mathbf{q}$ alongthe (q, q) direction, for $t' = 0.75t$ and for (a) $\mu = -2.25t$, (b)$\mu = -4t/3$, (c) $\mu = -1.25t$ and (d) $\mu = 1.0t$.

anomalies of the imaginary part, which occur whenever a wave-vector $\mathbf{q}$ can join two points of the Fermi surface where the Fermi velocities are parallel or antiparallel. At zero temperature, and as the frequency goes to zero, the structures become singularities. The nature of the singularities can be traced back to the sign of the curvature of the Fermi surface at those points. The bare spin susceptibility can be written as (in units such that $S = 1/2$, $\hbar = 1$ and $k_B = 1$):

$$\chi_0(\mathbf{q}, \omega) = \frac{1}{2N} \sum_{\mathbf{k}} \frac{n(\mathbf{k}+\mathbf{q}) - n(\mathbf{k})}{\varepsilon(\mathbf{k}) - \varepsilon(\mathbf{k}+\mathbf{q}) + \omega + i0^+} . \quad (3)$$

The dynamical spin structure factor can be expressed as

$$S(\mathbf{q}, \omega) = 2\frac{\chi_0''(\mathbf{q}, \omega)}{1 - \exp(-\beta\omega)} . \quad (4)$$

In Fig. 2 we illustrate the results for the magnetic structure factor divided by frequency along the diagonal direction, which is globally the most sensitive to the geometrical features of the Fermi surface. Figure 2(a) shows the situtation in the first doping regime. Asides from the trivial $q = 0$ structure, three peaks and a gap can be seen. At van-Hove singularity [Fig. 2(b)], the Fermi surface is composed of four straight lines. Only two peaks can be seen: the trivial $q = 0$ peak and the strong peak at wavevector $(q_N, q_N)(q_N = 2\arccos(t/2t'))$, which links together the points of the Fermi surface associated to the van-Hove singularities. In the second doping regime [Fig. 2(c)] there are two Fermi surfaces, we can see five peaks which signal the rich topological features of the Fermi surface. Figure 2(d) corresponds the last doping regime where only one peak can be seen.

3. CONCLUSIONS

The t–t' model exhibits a rich Fermi surface topology when $|t'/t| > 1/2$.Of particular interest is the appearence of a new perfect nesting condition when the chemical potential reaches $\mu = -t^2/t'$, and of a doping regime where a hole-like section of the Fermi surface coexists with an electron-like.This doping regime leads to several structures which can be related to specific geometrical features of the Fermi surface. The structures of the magnetic spin susceptibility are especially distinctive in the diagonal direction.

REFERENCES

1. Hybertsen M. S. *et al.*, *Phys. Rev. B* **45**, 10032 (1992); Pickett W. E., *Rev. Mod. Phys.* **61**, 433 (1989).
2. Singh D. J. and Pickett W. E., *Physica C* **203**, 193 (1992).
3. Bénard P. *et al.*, *Phys. Rev. B* **47**, 15217 (1993); Si Q. *et al.*, *Phys. Rev. B* **47**, 9055 (1993)

Pergamon

J. Phys. Chem. Solids Vol. 56, No. 12, pp. 1707–1708, 1995
1995 Elsevier Science Ltd
Printed in Great Britain
0022–3697/95 $9.50 + 0.00

0022–3697(95)00160-3

RESONANT TWO-MAGNON RAMAN SCATTERING IN ANTIFERROMAGNETIC INSULATORS

ANDREY V. CHUBUKOV
Department of Physics, University of Wisconsin-Madison, Madison, WI 53706, U.S.A.

DAVID M. FRENKEL
Texas Center for Superconductivity, University of Houston, Houston TX 77204-5932, U.S.A.

G. BLUMBERG and M. V. KLEIN
Department of Physics, Science and Technology Center for Superconductivity, University of Illinois at Urbana-Champaign, Urbana IL 61801, U.S.A.

Abstract—We report the experimental results and propose a theory of resonant two-magnon Raman scattering from antiferromagnetic insulators. On the experimental side, we present the first measurements on $YBa_2Cu_3O_{6.1}$ at $T = 4$ K, and find the resonant frequency at higher photon energies than previously believed. On the theoretical side, we argue that the conventional Loudon–Fleury theory does not work in the resonant regime, in which the energy of the incident photon is close to the gap between the conduction and valence bands, and identify the most relevant contribution to Raman intensity. We find good agreement between the theoretical prediction for the power-law behavior of the strength of the two-magnon scattering and the data. We argue that this agreement is evidence for the existence of *coherent* quasiparticle states in these materials.

There is a widespread belief that strong electron–electron correlations in the high-T_c compounds may hold a clue to the phenomenon of high-temperature superconductivity. One of the manifestations of these correlations is the fact that the insulating parent compounds are antiferromagnets. An important probe of antiferromagnetism is magnetic Raman scattering [1]. Its prominent signature in the underdoped high-T_c materials is a strong peak observed at about 3000 cm^{-1}. To first approximation, this peak can be attributed to inelastic scattering from the two-magnon excitations [1,2].

The traditional framework for understanding the two-magnon Raman scattering in antiferromagnets has been an effective Hamiltonian for the interaction of light with spin degrees of freedom known as the Loudon–Fleury Hamiltonian [3,4]. This theory works well when the frequencies of the incoming and outgoing photons are considerably smaller than the gap between the conduction and valence bands, which is roughly 2 eV. At higher photon energies we are in the resonant regime. In this regime, the cross-sections sensitively depend not just on magnetic, but on the electronic properties as well, and this makes understanding the data particularly important.

The profile of the Raman cross-section as a function of the *transferred* photon frequency and the behavior of the two-magnon peak height as a function of the *incident* photon frequency in undoped YBCO and related compounds have been studied experimentaly at room temperatures [5]. The key experimental feature was the existence of a single

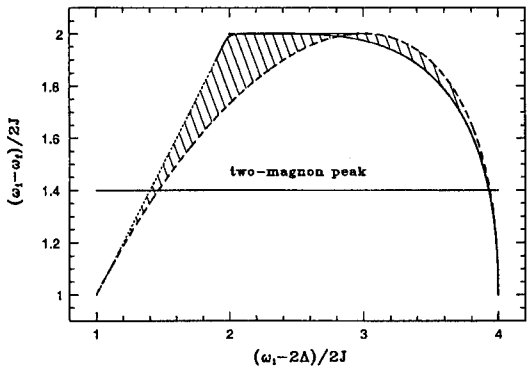


Fig. 1. The triple resonance region (shaded) in the (ω_i, ω) plane, where $\omega = \omega_i - \omega_f$. The horizontal line corresponds to the position of the two-magnon peak which for definiteness we chose to be at $\omega = 2.8J$ which is the value one obtains in the $1/S$ expansion neglecting the renormalization of J.

maximum in the two-magnon peak strength measured as a function of the incident photon frequency (ordinarily, one could expect two maxima, the so-called ingoing and outgoing resonances [6,7]). A comparison with the dielectric constant measurements have shown that this maximum is at least 1 eV away from the band edge, in fact right at the upper end of the features in the optical data that can be interpreted as the particle–hole excitations between the lower and upper Hubbard bands.

We performed the measurements of Raman intensity at low temperatures ($T \sim 4$ K) and found that the resonance

occurs at slightly higher frequencies than been reported previously [5]: the resonance frequency is greater than 3.1 eV.

To understand the experimental results, we develop a diagrammatic approach to Raman scattering valid in both nonresonant and resonant regimes. We consider the one-band Hubbard model and use the large U spin density wave (SDW) formalism [8] to describe the electronic state at half-filling, the excitations around it, and the interaction between fermions and spin waves which in the SDW formalism are the collective modes of fermions. The resonant part of the scattering matrix element M_R is obtained from the term linear in the vector potential in the 2nd order of perturbation theory [6]. In this process, a photon with energy ω_i and momentum which can be safely set equal to zero, creates a virtual particle–hole state of the fermionic system which can emit or absorb two spin-waves with momenta $\mathbf{k}$ and $-\mathbf{k}$ before collapsing into an outgoing photon with the energy ω_f. In the situation when the photon frequencies are much smaller than the Mott–Hubbard gap $2\Delta \sim U$, we recovered diagramatically the Loudon–Fleury theory. However in the resonant region, when the incoming photon frequency is close to the gap value, we found that the most singular contribution to the Raman vertex comes from the diagram which does not contribute to the Loudon–Fleury theory, but for which there exists a region of ω_i and ω_f where all three of the energy denominators vanish simultaneously. This phenomenon is known as a triple resonance [6,7]. Via a combination of analytical and numerical techniques, we found that for relevant ω_i the triple resonance in the Raman vertex occurs only in a narrow range of the final photon energies ω_f. The region of triple resonances is shaded in Fig. 1. In this region, the Raman vertex, M_R, *diverges* in the absence of quasiparticle damping.

It is easy to check that the triple resonance condition is rigorously satisfied only for the diagram which does not contain final-state magnon–magnon interactions. On the other hand, for $S = 1/2$, the dominant contribution to the conventional two-magnon peak at $\sim 3J$ comes from the diagrams with multiple magnon-magnon interactions [2]. In this situation the Raman spectrum $R(\omega)$ can be considered as containing two *independent* peaks: one is due to the triple resonance in the Raman vertex in the shaded region in Fig. 1, and the other, at transferred frequency of about $3J$, is due to the magnon–magnon scattering. Suppose we now fix ω at the two-magnon peak frequency $\sim 3J$, and consider the variation of the peak amplitude as a function of the incident photon frequency ω_i. Obviously, this amplitude will by itself have a maximum when the two peaks in $R(\omega)$ merge, *i.e.*, when the $\omega = const$ line intersects the region of triple resonances. From Fig. 1 we see that the intersection occurs at $\omega_i^{res} \approx 2\Delta + 7.9J$ which is very close to $\omega_i^{max} = 2\Delta + 8J$, where the particle and hole are excited near the *tops* of their respective bands. We calculated the Raman vertex in the vicinity of the intersection and found that it diverges (in the absence of damping) as

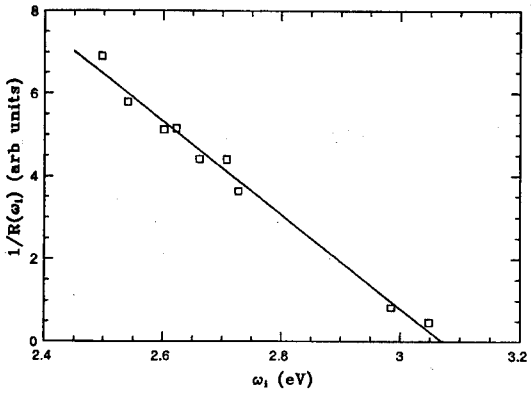


Fig. 2. A fit to the experimental dependence of the inverse two-magnon peak intensity in $YBa_2Cu_3O_{6.1}$ to theoretical $1/(\omega_i^{res}-\omega_i)$ dependence.

$$M_R \sim \frac{\omega_i^{max} - \omega_i}{(\omega_i - \omega_i^{res})^{3/2}}. \qquad (1)$$

The 3/2 power of the denominator in (1) is due to triple resonance, while the small factor in the numerator comes from the vanishing of the numerator in Raman intensity (and optical absorption) right at the top of the band (i.e. at $\mathbf{k} = 0$). In practice, the difference between ω_i^{res} and ω_i^{max} can be neglected, and eqn (1) yields inverse square-root singularity in M_R, which implies a linear singularity in the Raman intensity, $R \sim |M_R|^2 \sim |\omega_i - \omega_i^{res}|^{-1}$.

In Fig 2 we fit the low-temperature data on the peak intensity in $YBa_2Cu_3O_{6.1}$ at $T = 4$ K by eqn (1). We see that the fit to the theoretical dependence is quite good. The inverse linear dependence starts from $\omega_i \sim 2.5$ eV and extends nearly up to the resonance frequency $\omega_i^{res} \approx 3.1$ eV. The effects of fermionic damping are probably relevant only in the immediate vicinity of the resonance. We consider this agreement as a partial verification of the large U SDW picture for the carriers, which, despite much theoretical work, has not been well-established experimentally in these materials.

Acknowledgements—It is our pleasure to thank everyone with whom we discussed this paper. D.F. was supported by the TCS at the University of Houston. G.B. and M.K. were supported by the NSF under DMR 91-20000 through the STCS at the University of Illinois.

REFERENCES

1. Singh R. R. P., *Comments Cond. Mat. Phys.* **15**, 241 (1991).
2. Canali C. M. and Girvin S. M., *Phys. Rev. B* **45**, 7127 (1992).
3. Fleury P. A. and Loudon R., *Phys. Rev.* **166**, 514 (1968).
4. Shastry B. S. and Shraiman B. I., *Phys. Rev. Lett.* **65**, 1068 (1990); *Int. J. Mod. Phys. B* **5**, 365 (1991).
5. Liu R., *et. al.*, *J. Phys. Chem. Solids* **54** 1347 (1993).
6. Cardona M., in *Light Scattering in Solids II*, M. Cardona and G. Güntherodt, eds. Springer-Verlag, New York (1982).
7. Martin R. M. and Falicov L. M., in *Light Scattering in Solids*, M. Cardona, ed. Springer-Verlag, New York (1975).
8. Schrieffer J. R., Wen X. G. and Zhang S. C., *Phys. Rev. B* **39**, 11663 (1989); Chubukov A. V. and Frenkel D. M., *Phys. Rev. B* **46**, 11884 (1992).

Pergamon

J. Phys. Chem. Solids Vol. 56, No. 12, pp. 1709–1710, 1995
Copyright © 1995 Elsevier Science Ltd
Printed in Great Britain. All rights reserved
0022–3697/95 $9.50 + 0.00

0022-3697(95)00133-6

A SIMPLE THEORY FOR THE CUPRATES: THE ANTIFERROMAGNETIC VAN HOVE SCENARIO

E. DAGOTTO, A. NAZARENKO, A. MOREO and S. HAAS
Department of Physics and National High Magnetic Field Lab, Florida State University, Tallahassee, FL 32306, U.S.A.

Abstract—A model of weakly interacting hole quasiparticles is proposed to describe the normal state of the high temperature superconductors. The effect of strong correlations is contained in the dispersion relation of the holes, which is obtained using numerical techniques applied to the t–J model. Many-body effects induce anomalous quasiparticle *flat* bands similar to those observed in recent angle-resolved photoemission experiments. The density of states contains a large peak at the top of the valence band that induces a large critical temperature after interactions are introduced. The model predicts superconductivity in the $d_{x^2-y^2}$ channel, with a typical T_c of about 100K. The concept of "optimal doping" appears naturally in this model, as well as a large ratio $2\Delta/kT_c \sim 5$.

In this paper, a novel theory of hole carriers in an antiferromagnetic background is briefly reviewed. The idea has been recently introduced by the authors and their collaborators under the name of "Antiferromagnetic van Hove" (AFVH) scenario [1,2]. The model explains in a natural way many anomalous properties of the cuprates, and it predicts the presence of d-wave superconductivity, as well as the existence of an optimal doping where the critical temperature is maximized. The main assumption is that the normal state of the cuprates can be described by a weakly-interacting dilute gas of hole-quasiparticles. The influence of antiferromagnetism is contained in the special dispersion relation, $\epsilon(\mathbf{k})$, which is obtained using a numerical method applied to a one band model description of the CuO_2 planes, and also in the interaction between the quasiparticles which is inspired by the two hole problem in the t–J model. The hole density of states (DOS) contains a large peak at the top of the valence band that enhances the superconducting critical temperature. The main unique feature of this novel scenario is that it combines the ideas of antiferromagnetism inducing superconductivity [3], with the van Hove (vH) scenario ideas to enhance superconductivity [4].

Our analysis of the dispersion $\epsilon(\mathbf{k})$ was carried out using the well-known two dimensional t–J model on large clusters [2]. The main *effective* contribution to $\epsilon(\mathbf{k})$ arises from hole hopping between sites belonging to the same sublattice. The total bandwidth, W, is severely reduced from that of a gas of non-interacting electrons due to the antiferromagnetic correlations, as was extensively discussed in previous literature [5]. The excellent agreement between our calculations and experiments regarding the presence of flat bands in hole-doped cuprates [6], the existence of a small bandwidth in the insulator $Sr_2CuO_2Cl_2$, and antiferromagnetically induced bands in Bi2212 have been reviewed by Adriana Moreo *et al.* elsewhere in this volume, and we refer the reader to that contribution, as well as published literature [7], for more details.

Let us now introduce interactions among the quasiparticles. We have followed ideas based on antiferromagnetism to produce the pairing attraction needed for superconductivity. However, there is an important distinction with respect to previous "AF-oriented" literature [3]: the DOS of the quasiparticles has a large peak that induces in a natural way the existence of an optimal doping i.e. a density at which the critical temperature is maximized. Previous AF scenarios in the literature do not explain easily the presence of an optimal doping in the cuprates.

Consider the rigid band approximation for the hole dispersion i.e. we assume that the DOS does not change much with doping near half-filling (numerical results supporting this scenario will be published soon). To build up a model for the cuprates we construct the interaction between the quasiparticles based on the two dimensional t–J model [5]. As shown numerically in many studies, the dominant effective attraction is between nearest-neighbors sites. Thus, the model we will use in our analysis is

$$H = -\sum_{\mathbf{p},\alpha} \epsilon_{\mathbf{p}} c^{\dagger}_{\mathbf{p}\alpha} c_{\mathbf{p}\alpha} - |V| \sum_{\langle \mathbf{ij} \rangle} n_{\mathbf{i}} n_{\mathbf{j}}, \tag{1}$$

where $c_{\mathbf{p}\alpha}$ is an operator that destroys a quasiparticle with momentum $\mathbf{p}$ in sublattice α = A, B; $n_{\mathbf{i}}$ is the number operator at site $\mathbf{i}$; $|V| = 0.6J$ (which can be deduced from the t–J model as discussed in Ref. [1]), and $\epsilon_{\mathbf{p}}$ the dispersion evaluated in Ref. [2]. This Hamiltonian has been constructed based on strong AF correlations, and it has a vH singularity in the noninteracting DOS, thus we will refer to it as the "antiferromagnetic-van Hove" (AFVH) model.

We studied the AFVH model with the standard BCS formalism. Since $|V|/W \sim 0.3$, where W is the bandwidth of the quasiparticles, the gap equation should produce a reliable estimation of T_c since we are effectively exploring the "weak" coupling regime of the AFVH model. Solving the

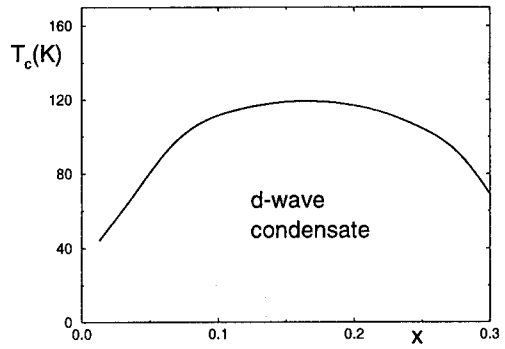


Fig. 1. Critical temperature T_c of the AFVH model as a function of hole density $x = 1 - \langle n \rangle$ (using the BCS gap equation). The superconducting state is d-wave.

gap equation, we observed that the free energy is minimized using a $d_{x^2-y^2}$ order parameter. In Fig.1, T_c against the hole density is shown. Two features need to be remarked: (i) an optimal doping exists at which T_c is maximized which is a direct consequence of the large peak in the DOS of the quasiparticles. Such a peak would have an important effect even in theories where the hole interaction is phonon mediated rather than spin-wave mediated. In other words, one of the main concepts introduced in Refs. [2] and [1], i.e. a vH singularity generated by antiferromagnetism, is not restricted to models where superconductivity is produced by an electronic mechanism; ii) the optimal doping (15%) and optimal $T_c \sim 100$K are in good agreement with the cuprates phenomenology. Although in the AFVH model the natural scale of the problem is $J \sim 1000$K, since the ratio between coupling and bandwidth is small, T_c is further reduced in the BCS formalism to about 100K. Note that this quantitative agreement with experiments is obtained without the need of ad-hoc fitting parameters. The ratio $R(T) = 2\Delta_{max}(T)/kT_c$ can be calculated from the gap equation, (for a d-wave condensate, $\Delta_{max}(T)$ is defined as the maximum value of the gap). At $T = 0$, the AFVH model predicts $R(0) = 5.2$ while recent experiments report results between 6.2 and 4.6 [8].

Several other calculations are in preparation or already published. In particular, the Hall coefficient at finite temperature, specific heat, thermopower coefficient, the possibility of a nonzero isotope effect in the AFVH scenario, influence of disorder on the vH singularity, modifications by the presence of a bilayer CuO_2 structure, the phenomenology of the d-wave superconducting model eqn (1), and many other consequences of the AFVH ideas have already been analyzed by our group.

Acknowledgements—We have benefit from conversations with many colleagues, the list being too large to reproduce here. The authors are mainly supported by the Office of Naval Research under grant ONR N00014-93-0495.

REFERENCES

1. Dagotto E., Nazarenko A. and Moreo A., *Phys. Rev. Lett.* **74**, 310 (1995).
2. Dagotto E., Nazarenko A. and Boninsegni M., *Phys. Rev. Lett.* **73**, 728 (1994).
3. Bickers N. E., Scalapino D. J. and White S. R., *Phys. Rev. Lett.* **62**, 961 (1989); Dagotto E., Riera J. and Young A. P., *Phys. Rev. B* **42**, 2347 (1990); *Phys. Rev. Lett.* **70**, 682 (1993); Ohta Y. *et al.*, *Phys. Rev. Lett.* **73**, 324 (1994).
4. Tsuei C. C. *et al.*, *Phys. Rev. Lett.* **65**, 2724 (1990); Markiewicz R. S., *J. Phys. Condens. Matt.* **2**, 6223 (1990).
5. Dagotto E., *Rev. Mod. Phys.* **66**, 763 (1994).
6. Dessau D. S. *et al.*, *Phys. Rev. Lett.* **71**, 2781 (1993); Shen Z.-X. and Dessau D. S., preprint (1994).; Abrikosov A. A., Campuzano J. C. and Gofron K., *Physica C* **214**, 73 (1993); Ma J. *et al.*, *Phys. Rev. B* **51**, 3832 (1995).
7. Nazarenko A., Vos K., Haas S., Dagotto E. and Gooding R., to appear in *Phys. Rev. B* (1995); Moreo A., Haas S., Sandvik A. and Dagotto E., to appear in *Phys. Rev. B* (1995); Haas S., Moreo A. and Dagotto E., to appear in *Phys. Rev. Lett.* (1995).
8. Vedeneev S. I. *et al.*, *Phys. Rev. B* **49**, 9823 (1994); Ma J. *et al.*, *Phys. Rev. B* **51**, 3832 (1995).

Pergamon

J. Phys. Chem. Solids Vol. 56, No. 12, pp. 1711–1712, 1995
1995 Elsevier Science Ltd
Printed in Great Britain
0022-3697/95 $9.50 + 0.00

0022-3697(95)00235-9

RAMAN SCATTERING IN DISORDERED UNCONVENTIONAL SUPERCONDUCTORS

T. P. DEVEREAUX
Dept. of Physics, University of California, Davis, CA 95616, U.S.A.

Abstract—A theory for the effect of impurity scattering on electronic Raman scattering in unconventional superconductors is presented. The impurity dependence of the the spectra present a clear qualitative way to distinguish between conventional (anisotropic s–wave) or unconventional (d-wave) energy gaps.

Keywords: $d_{x^2-y^2}$-pairing, disorder, unconventional superconductivity.

It was shown in Ref. [1] that the symmetry- (polarization-) dependence of the Raman spectra can be a powerful tool to examine the energy gap symmetry in anisotropic superconductors. The predictions of the theory for clean superconductors with $d_{x^2-y^2}$ pairing symmetry concerning the peak positions and power-law rise of the spectra, provided good agreement with the data on three cuprate materials, $YBa_2Cu_3O_7$, $Bi_2Sr_2CaCu_2O_8$, and $Tl_2Ba_2CuO_6$. However, like other correlation functions, only $|\Delta(\mathbf{k})|$ could be determined from the fit, and thus it could not be ascertained whether the gap changed sign around the Fermi surface. While certain gaps with different anisotropy and behavior near the line nodes lead to different Raman lineshapes, in principle an anisotropic extended s–wave gap which possesses the same anisotropy as a gap with $d_{x^2-y^2}$ symmetry (or at least with a minimum gap around the Fermi surface which was smaller than the level of smearing effects) would give the same lineshape as that calculated for $d_{x^2-y^2}$ pairing[1]. The theory also failed to predict *any* Raman intensity in the normal state due to phase space restrictions (consequence of the limit $\mathbf{q} \to 0$).

These deficiencies can be readdressed by considering impurity scattering[2,3]. The Raman response can be written as

$$\chi''(\mathbf{q} \to 0, i\Omega) = -T \sum_{i\omega} \sum_{\mathbf{k}} Tr\gamma(\mathbf{k})\hat{\tau}_3 \hat{G}(k, i\omega)\hat{\tau}_3 \gamma(\mathbf{k})\hat{G}(\mathbf{k}, i\omega - i\Omega), \quad (1)$$

where Tr denotes the trace, $\hat{\tau}$ are Pauli matrices, and γ is the bare Raman vertex, $\gamma(\mathbf{k}) = \frac{m}{\hbar^2} \sum_{\mu,\nu} e^I_\mu \frac{\partial^2 \epsilon(\mathbf{k})}{\partial k_\mu \partial k_\nu} e^S_\nu$, for a given band structure $\epsilon(\mathbf{k})$ and incident $\mathbf{e}^I$ and scattered $\mathbf{e}^S$ polarization light vectors. We use the standard weak coupling BCS Green's function dressed by the T–matrix impurity self energy,

$$\hat{G}(\mathbf{k}, i\omega) = \frac{i\tilde{\omega} + \tilde{\epsilon}(\mathbf{k})\hat{\tau}_3 + \tilde{\Delta}(\mathbf{k})\hat{\tau}_1}{(i\tilde{\omega})^2 - \tilde{\epsilon}(\mathbf{k})^2 - \tilde{\Delta}(\mathbf{k})^2}, \quad (2)$$

where the tilde indicates the renormalized frequency, gap, and band energy: $i\tilde{\omega} = i\omega - \Sigma_0(i\tilde{\omega})$, $\tilde{\Delta}(\mathbf{k}) = \Delta(\mathbf{k}) + \Sigma_1(i\tilde{\omega})$, $\tilde{\epsilon}(\mathbf{k}) = \epsilon(\mathbf{k}) - \Sigma_3(i\tilde{\omega})$. For particle-hole symmetric systems, the matrix self energy is given in terms of the integrated Green's function $g_i(i\omega) = \frac{1}{\pi N_F} \sum_{\mathbf{k}} Tr\hat{\tau}_i \hat{G}(\mathbf{k}, i\omega)$ as

$$\hat{\Sigma}(i\omega) = \Gamma \frac{g_0(i\omega)\hat{\tau}_0 + g_1(i\omega)\hat{\tau}_1}{c^2 - g_0^2(i\omega) + g_1^2(i\omega)} = \Sigma_0\hat{\tau}_0 + \Sigma_1\hat{\tau}_1. \quad (3)$$

As discussed in Ref. [4], the off-diagonal self energy Σ_1 is zero only for odd-parity states or states which possess reflection symmetry such as $d_{x^2-y^2}$ or d_{xy}.

The results of the theory with the inclusion of impurity scattering in the unitary ($c = 0$) limit are shown in Fig. 1 for polarization orientations which select $B_{1g}[\gamma(\phi) = \cos(2\phi)]$ and $B_{2g}[\gamma(\phi) = \sin(2\phi)]$ channels. The top panels in Fig. 1 were obtained for an energy gap $\Delta(\phi) = \Delta_0\cos(2\phi)$ of $d_{x^2-y^2}$ symmetry, while the bottom panels are for $\Delta(\phi) = \Delta_0 |\cos(2\phi)|$, which possesses anisotropic s–wave symmetry. The main difference for $d_{x^2-y^2}$ and anisotropic s–pairing can be seen in (1) the relative anisotropy of the peak positions, and (2) the low frequency behavior of the spectra in each channel. As a consequence of the gap renormalization for anisotropic s– superconductors, the gap becomes averaged out by the disorder and a threshold develops at $\omega_g = 2\Delta_{min}$[4]. This leads to a reduction of the relative peak positions for the B_{1g} and B_{2g} channels compared to $d_{x^2-y^2}$. As the disorder is increased, the peak positions will coalesce and the spectra recovers a channel independent, isotropic s–wave form [3].

The low frequency behavior of the channel dependent spectra is shown in the insets of Fig. 1. For $d_{x^2-y^2}$ pairing, while the low frequency behavior remains linear in frequency for the B_{2g} channel, below a characteristic frequency $\omega^* \sim \sqrt{\Gamma\Delta}$ the behavior changes from ω^3 to linear in ω for the B_{1g} channel. This is due to a nonzero density of states at the Fermi level, which allows for normal-state-like

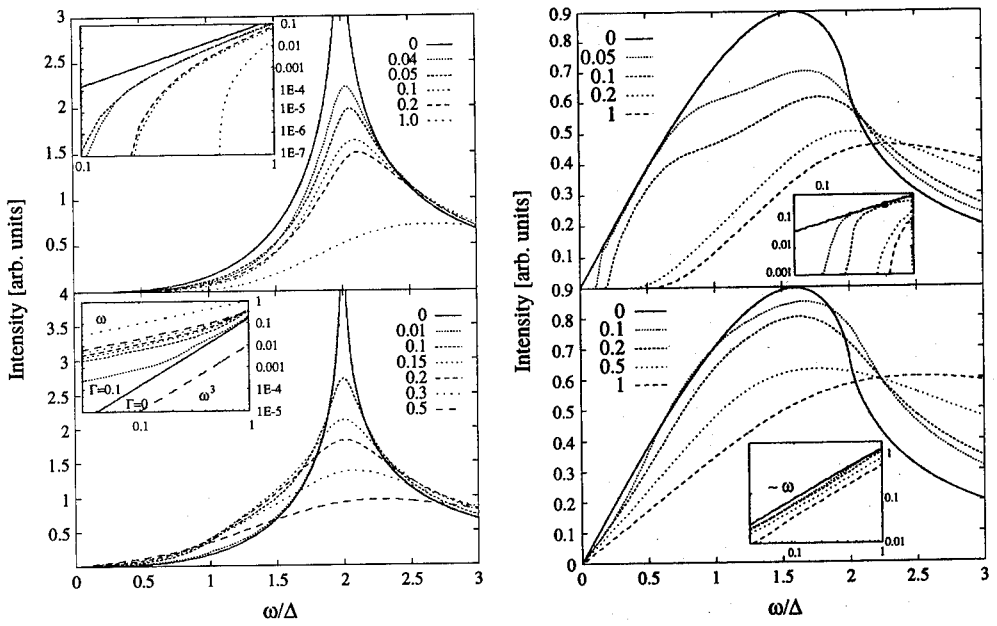


Fig. 1. Raman response for B_{1g} channel (left panel) and B_{2g} channel (right panel) for various values of Γ/Δ_0 given in the Figure. The top panels are for anisotropic $s-$wave superconductors while the bottom panels are for $d_{x^2-y^2}$ pairing.

behavior to be recovered [5]. As in the case of the penetration depth[6], the scale ω^* grows with increasing impurity concentrations. However, *the exponent is symmetry dependent* (remains 1 for B_{2g} and A_{1g} channels, while *decreases* from 3 to 1 for the B_{1g} channel) and is thus unlike the penetration depth. This is in marked contrast to the impurity dependence of the spectra for anisotropic s gap. The low frequency behavior is dominated by the threshold in this case for *all channels*. Moreover, the impurity dependence of the B_{1g} channel is opposite to what one would expect if the gap was anisotropic s-wave. Thus impurity scattering may provide a clear qualitative way of distinguishing energy gaps of different symmetry.

REFERENCES

1. Devereaux T. P. *et al.*, *Phys. Rev. Lett.* **72**, 396 (1994); *ibid.*, preprint.
2. Zawadowski A. and Cardona M., *Phys. Rev. B* **42**, 8798 (1990).
3. Devereaux T. P., *Phys. Rev. B* **45**, 12965 (1992).
4. Borkowski L. S. and Hirschfeld P. J., *Phys. Rev. B* **49**, 15404 (1994).
5. Ueda K. and Rice T. M., in *Theory of Heavy Fermions and Valence Fluctuations* (Edited by T. Kasuya and T. Saso). Springer, Berlin (1985); Gorkov L. P., *Pis'ma Zh. Eksp. Teor. Fiz.* **40**, 351 (1994) [*Sov. Phys. JETP* **40**, 1155 (1985)].
6. Hirschfeld P. and Goldenfeld N., *Phys. Rev. B* **48**, 4219 (1993); Gross F. *et al.*, *Z. Phys. B* **64**, 175 (1986).

Pergamon

J. Phys. Chem. Solids Vol. 56, No. 12, pp. 1713–1715, 1995
Copyright © 1995 Elsevier Science Ltd
Printed in Great Britain. All rights reserved
0022–3697/95 $9.50 + 0.00

0022-3697(95)00175-1

SOME NOVEL FEATURES OF THE BANDS IN HTSC

M. V. EREMIN, S. G. SOLOVJANOV and S. V. VARLAMOV
Kazan State University, 420008 Kazan, Russia

Abstract—We have calculated the energy dispersions, spectral weights and density of states for two relevant bands near the Fermi level in layered cuprates. Calculated energy dispersion and density of states seem to be consistent with the photoemission data.

Keywords: Layered cuprates, strong correlations, energy dispersion.

The photoemission data give the evidence for an unusual narrow band near the Fermi level in doped cuprates. We refer this band to an oxygen hole motion on a background of copper sites, the oxygen hole spin having a strong singlet coupling to the copper spin. The calculations of energy dispersion showed [1,2] that this band is indeed narrow and well consistent with the photoemission data [3] within the experimental accuracy. Here we report new variant calculations of the energy dispersion, when the singlet copper–oxygen state is assumed to be a combination of Zhang–Rice singlet, Cu^{3+} ($S = 0$) and neutral oxygen.

We start from the ordinary Hamiltonian, including Coulomb repulsion and hopping terms. The basis of wave functions is as follows:

$$|\sigma_d> = d_\sigma^+|0>,\ |\sigma_p> = p_\sigma^+|0>\ |dd> = d_\uparrow^+ d_\downarrow^+|0>,$$
$$|pp> = p_\uparrow^+ p_\downarrow^+|0>,\ |pd> = \frac{1}{\sqrt{2}}(p_\uparrow^+ d_\downarrow^+ - p_\downarrow^+ d_\uparrow^+)|0>,$$

where $|0>$ is vacuum, which corresponds to $Cu^+(d^{10})$ state, d^+ is a creation operator for copper hole in $|x^2 - y^2>$ state and p_σ is a Wannier-like operator for oxygen hole [4].

In order to calculate the quasiparticle spectrum we perform three successive transformations. After the first Hubbard-like transformation, we do the second canonical transformation of the type

$$\psi^{\sigma_d,0} = c_d X^{\sigma_d,0} + c_p X^{\sigma_p,0},$$
$$\psi^{pd,0} = c_{dd} X^{dd,0} + c_{pd} X^{pd,0} + c_{pp} X^{pp,0}.$$

As a result of such two trannsformations, the one-site Hamiltonian is diagonalized and can be written as:

$$H_0 = E_d \sum \psi^{\sigma_d,\sigma_d} + E_p \sum \psi^{\sigma_p,\sigma_p} + E_{dd}\psi^{dd,dd} + E_{pd}\psi^{pd,pd} + E_{pp}\psi^{pp,pp}.$$

Here

$$E_{d,p} = \frac{\epsilon_d + \epsilon_p}{2} \pm \frac{1}{2}[(\epsilon_p - \epsilon_d)^2 + 4t_0^2]^{\frac{1}{2}},$$

and E_{dd} , E_{pp} and E_{pd} are determined by equation

$$\begin{vmatrix} I_{dd} + 2\epsilon_d - E & 0 & \sqrt{2}t_0 \\ 0 & I_{pp} + 2\epsilon_p - E & \sqrt{2}t_0 \\ \sqrt{2}t_0 & \sqrt{2}t_0 & I_{pd} + \epsilon_p + \epsilon_d - E \end{vmatrix} = 0.$$

ϵ_d and ϵ_p are the energies of copper and oxygen holes, I_{dd}, I_{pp}, I_{pd} are Coulomb repulsion parameters, $t_0 = -2\lambda_0 t_{pd}$ is hybridization parameter.

It is clear that the low quasiparticle excitation energies are $E_{pd} - E_p$, E_d and $E_{pd} - E_d$. For an isolator, the band E_d is fully occupied,so it is natural to call it as the lower "copper Hubbard" band. The band $E_{pd} - E_d$ corresponds to the singlet correlated oxygen band [1,2]. Both bands have unusual features. Let us write down the equation for the chemical potential. The completeness condition is fulfilled in following form:

$$\psi^{0,0} + \psi^{\uparrow,\uparrow} + \psi^{\downarrow,\downarrow} + \psi^{pd,pd} = 1,$$

and anticommutator relations are:

$$[\psi^{pd,\bar{\sigma}_p}, \psi^{\bar{\sigma}_p,pd}]_+ = <\psi^{pd,pd}>,$$
$$[\psi^{pd,\bar{\sigma}_d}, \psi^{\bar{\sigma}_d,pd}]_+ = \frac{1}{2} + \frac{\delta}{2} = P_{pd},$$
$$[\psi^{\sigma_d,0}, \psi^{0,\sigma_d}]_+ = \frac{1}{2} - \frac{\delta}{2} = P_d.$$

First of all we see that at the number of extra hole per site $\delta = 0$ we get exactly Hubbard-like isolator. So the problem disappears which took place in early of charge transfer isolator theory. On the basis of relations one can find the spectral weight (number of occupied states over number of allowed states) of singlet correlated band as $f_p = 2\delta/(1 + \delta)$. For so called electron-doped layered cuprates the carriers reside at E_d band only. Using then $\delta = -\delta_e$ one has $f_d = (1 - \delta_e)/(1 + \delta_e)$.

The energy dispersion of the bands $\epsilon_d^* = E_d$ and $\epsilon_p^* = E_{pd} - E_d$ are described by the hopping Hamiltonian:

$$H_{hop} = \sum t_{ij}^{(1)} \psi^{pd,\bar{\sigma}_d} \psi^{\bar{\sigma}_d,pd} + \sum t_{ij}^{(2)} \psi_i^{\sigma_d,0} \psi_j^{0,\sigma_d} +$$

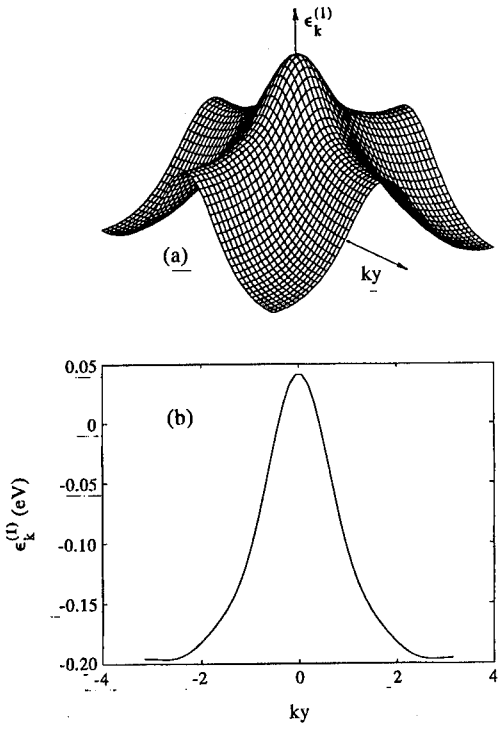


Fig. 1. The energy dispersions singlet correlated oxygen band $\epsilon_k^{(1)}$ (a) in Brilllouin zone, (b) along the line $-\pi < k_y < \pi$.

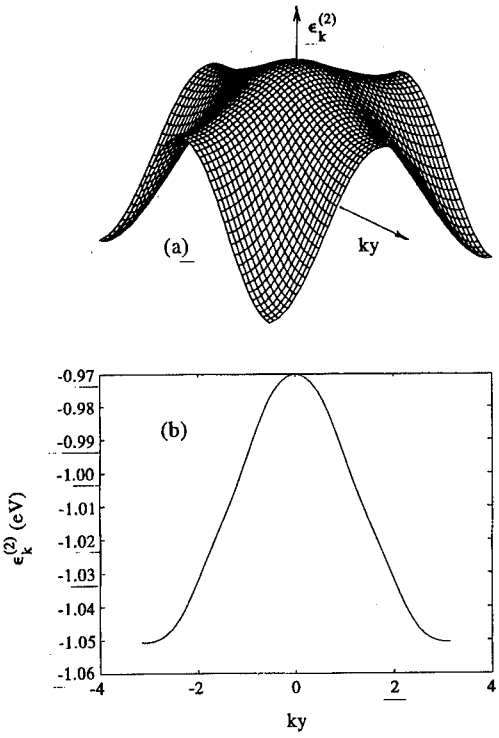


Fig. 2. Calculated energy dispersion for copper-character band $\epsilon_k^{(2)}$ (a) in Brillouin zone, (b) along the line $-\pi < k_y < \pi$.

$$\sum t_{ij}^{(12)}(-1)^{1/2-\sigma_d}(\psi_i^{pd,\bar{\sigma}_d}\psi_j^{0,\sigma_d} + \psi_j^{\sigma_d,0}\psi_i^{\bar{\sigma}_d,pd}).$$

The values of transfer integrals are given in Table. They are calculated by using the following parameters in eV: $t_{pd} = 1$, $t^{(xy)} = 0.6$, $t^{(xx)} = 0.25$. and polaronic reduction factor equals 0.32. The coefficients $c_p, c_d, c_{dd}, c_{pp}, c_{pd}$ were calculated at $\epsilon_p - \epsilon_d = 2.5, I_{dd} = 6, I_{pp} = 3$ and $I_{pd} = -2$. After Fourier transformation, the Hamiltonians yield the following quasiparticle energies

$$\epsilon_k^{(1,2)} = \frac{\epsilon_{dk} \pm \epsilon_{pk}}{2} \pm \frac{1}{2}[(\epsilon_{pk} - \epsilon_{dk})^2 + (t_k^{(12)})^2\gamma]^{\frac{1}{2}},$$

where γ is the doping dependent factor,

$$\epsilon_{pk} = \epsilon_p^* + P_{pd}t_k^{(1)}, \epsilon_{dk} = \epsilon_d^* + P_d t_k^{(2)},$$

The dispersion pictures of these bands are shown in Figs 1 and 2. The density of states is given in Fig. 3. We see in these Figures that the singlet correlated band $\epsilon_k^{(1)}$ has two peaks in a density of states. One of those peaks corresponds to an extended saddle point singularity, whereas another one is connected with the wings [see Fig. 1(a)]. The saddle-peak singularity is well known from the photoemission data [5,6], and the wings-peak is a prediction of our calculations. This singularity is indebted to the hybridization of ϵ_{dk} and ϵ_{pk} bands. The shape of the peak is very sensitive to the values of $t_k^{(12)}$. Another important thing we see in Figs 1 and 2 is that the Fermi surfaces of the p-type and n-type bands can be similar to each other. Indeed, for $(\epsilon_F^{(1)} < -0.2eV)$ and $(\epsilon_F^{(2)} < -1.2eV)$ in the Figs 1 and 2 one has almost

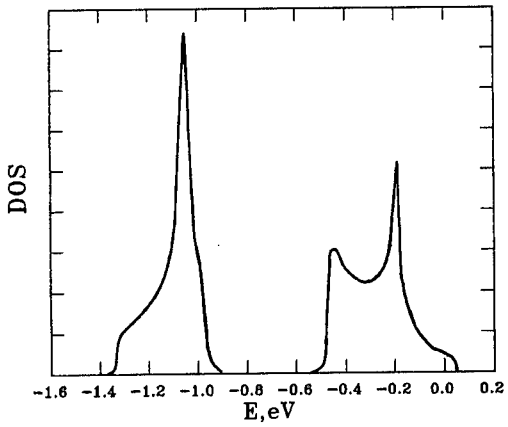


Fig. 3. Calculated density of states (DOS) for both bands $\epsilon_k^{(1)}$ and $\epsilon_k^{(2)}$.

identical similar open Fermi surfaces, which seem to be consistent with those observed by photoemision [7].

Acknowledgements—We are grateful to Dr R. Markendorf for useful remarks. M. V. Eremin thanks to Organizing Committee of Stanford Conference on Spectroscopies in Novel Superconductors for financial support.

Table 1. The transfer integrals in meV

n_x/n_y	1	2	1	2	1	2
		$t^{(1)}_{n_x,n_y}$		$t^{(2)}_{n_x,n_y}$		$t^{(12)}_{n_x,n_y}$
0	106.6	19.5	91.6	13.2	128.4	20.3
1	-26.4	0.6	-6.4	2.2	-17.3	2.2

REFERENCES

1. Eremin M. V. *et al.*, *Solid State Commun.* **88**, 15 (1993).
2. Eremin M. V. *et al.*, *JETP Lett.* **60**, 127 (1994).
3. Gofron K. *et al.*, *J. Phys. Chem. Solids* **54**, 10, 1193 (1993).
4. Zhang F. C. and Rice T. M., *Phys. Rev. B* **37**, 3759 (1988).
5. Dessau D. S. *et al.*, *Phys. Rev. Lett.* **71**, 2781 (1993).
6. Gofron K. *et al.*, *Phys. Rev. Lett.* **73**, 3302 (1994).
7. King D. M. *et al.*, *Phys. Rev. Lett.* **73**, 3298 (1994).

Pergamon

J. Phys. Chem. Solids Vol. 56, No. 12, pp. 1717–1718, 1995
Copyright © 1995 Elsevier Science Ltd
Printed in Great Britain. All rights reserved
0022–3697/95 $9.50 + 0.00

0022-3697(95)00225-1

MEASURING A SUPERCONDUCTOR'S GAP ANISOTROPY WITH EELS

MICHAEL E. FLATTÉ
Division of Applied Sciences, Harvard University, Cambridge, Massachusetts 02138, USA

Abstract—A method of measuring the angle-resolved magnitude and relative phase of the energy gap in a high-temperature superconductor is suggested for electron energy loss spectroscopy (EELS).

Keywords: EELS, High-Temperature Superconductors

Off-specular electron energy loss spectra should show a quasiparticle pair production threshold feature similar to the specular feature associated with the gap. Unlike the specular feature[1–3], which reflects an average of the gap over the (normal) Fermi surface, the energy loss of the off-specular feature depends on the superconducting energy gap at only two locations on the Fermi surface[4]. The onset of the feature reflects the relative phase between these two points. This result is independent of surface characteristics. Such characteristics affect the *magnitude* of the off-specular feature, not its location or onset.

Angle-resolved off-specular electron-energy-loss spectra are sensitive to quasiparticle-pair-creation scattering processes through the imaginary part of the polarizability $\mathrm{Im}P^{ret}_{bulk}(\mathbf{Q}, \omega)$.The differential probability of scattering an electron into final angle Ω with energy transfer ω ($d^2S/d\Omega d\omega$) is proportional to $\mathrm{Im}P^{ret}_{bulk}(\mathbf{Q}, \omega)$.The sensitivity of the polarizability to the angle-resolved gap magnitude and phase was first identified in an analysis of phonon self-energies[5,6] in high-temperature superconductors. The two quasiparticles created in the lowest-energy pair-production scattering process must be created at (or very near) the Fermi surface. In a material with a quasi-two-dimensional Fermi surface, there is usually only one way to create two quasiparticles such that the momentum transfer is $\mathbf{Q}$ and the quasiparticles are on the Fermi surface. The pair-production threshold energy, $\tilde{\Delta}(\mathbf{Q})$, is determined by the sum of the gap magnitudes at the two places on the Fermi surface where quasiparticles are created. If there is more than one way to produce a pair of quasiparticles at the Fermi surface, then there is more than one quasiparticle pair production threshold. Excluding accidental degeneracies, each threshold will produce a distinct onset feature in the EELS spectrum.

On-specular EELS has been successfully performed on$Bi_2Sr_2CaCu_2O_8$[1–3], but these near-zero-momentum scattering processes yield features which depend on an average of the gap. Sharp features should appear in the loss spectra at the (momentum-dependent) minimum energy

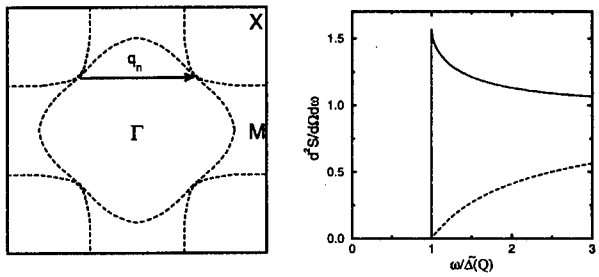


Fig. 1. (a)Fermi surface of $Bi_2Sr_2CaCu_2O_8$[5] with a momentum transfer shown ($\mathbf{q_n}$) which would connect nodes in a $d_{x^2-y^2}$ gap.(b)Feature in the loss spectrum (normalized to metallic value)which would indicate relative phase of 0 (solid) and π (dashed) between the gaps at the two places quasiparticles are created.

$\tilde{\Delta}(\mathbf{Q})$ to create an electron-hole pair.The minimum loss $\tilde{\Delta}(\mathbf{Q})$ for an electronic scattering event with momentum transfer $\mathbf{Q}$ would depend on the sum of the gap magnitudes at the two points on the quasi-two-dimensional Fermi surfacewhere quasiparticles are created.

A momentum transfer of interest, $\mathbf{q_n} = 0.9\pi$, is shown on the Fermi surface of $Bi_2Sr_2CaCu_2O_8$ in Figure 1. This momentum transfer would connect nodes in a $d_{x^2-y^2}$ gap.

The polarizability $P^{ret}_{bulk}(\mathbf{Q}, \omega)$in the superconducting state can be considered to arise from two contributions. There is a "normal" polarization, where the vertex creates an electron and hole, which recombine at the other vertex. There is also an "anomalous" polarization, where the vertex creates an electron and hole, the electron (hole) turns into a hole (electron) through interaction with the gap, and then they recombine at the other vertex. The phase of the gap affects only the anomalous process, which depends on the relative phase $\Delta\phi$ of the gap at the two points where quasiparticles are created. The sum of thes e two processes, at the threshold for electronic scattering processes, determines the size of the discontinuous onset in the differential scattering probability. The ratio of the discontinuity, $\Delta(d^2S/d\Omega d\omega)$,to the normal-state differential probability at T_c,$d^2S_N/d\Omega d\omega$, is

$$\frac{\Delta(d^2S/d\Omega d\omega)}{d^2S_N/d\Omega d\omega} = \frac{\pi}{2}\cos^2\left(\frac{\Delta\phi}{2}\right). \quad (1)$$

The differential scattering probability per unit energy and angle at $T = 0$is plotted in Figure 2 for relative phases of 0 (solid line) and π(dashed line). The full energy dependence for arbitrary relative phase at $T = 0$ is

$$\frac{d^2S(\omega)/d\Omega d\omega}{d^2S_N(\omega)/d\Omega d\omega} = \theta(\omega - \tilde{\Delta}(\mathbf{Q}))\Bigg\{\cos^2\left(\frac{\Delta\phi}{2}\right)E\times$$

$$\left(\left[1-\left(\frac{\tilde{\Delta}(\mathbf{Q})}{\omega}\right)^2\right]^{1/2}\right) + \sin^2\left(\frac{\Delta\phi}{2}\right)\left[\left(\frac{\omega+\tilde{\Delta}(\mathbf{Q})}{\omega}\right)E\times\right.$$

$$\left.\left(\frac{\omega-\tilde{\Delta}(\mathbf{Q})}{\omega+\tilde{\Delta}(\mathbf{Q})}\right) - \frac{2\tilde{\Delta}(\mathbf{Q})}{\omega}K\left(\frac{\omega-\tilde{\Delta}(\mathbf{Q})}{\omega+\tilde{\Delta}(\mathbf{Q})}\right)\right]\Bigg\} \quad (2)$$

where E and K are complete elliptic functions andθ is the Heavyside step function.

A check for $d_{x^2-y^2}$ symmetry is that the onset of a gap feature for all scattering momenta parallel to the $\Gamma - M$ direction should be sharp ($\Delta\phi = 0$). The onset for scattering momenta parallel to $\Gamma - X$ should be smooth and weak ($\Delta\phi = \pi$).

By measuring the shape and energy of the onset of quasi particle pair production using EELS, the magnitude and phase of the energy gap should be mappable around the Fermi surface.

REFERENCES

1. Demuth J.E., Persson B.N.J., Holtzberg F., Chandrasekhar C.V., *Phys. Rev.Lett.* **64**, (1990) 603.
2. Li Y., Huang J.L., Lieber C.M.,*Phys. Rev. Lett.* **68**, (1992) 3240.
3. Li Y., Liu J., Lieber C.M., *Phys. Rev. Lett.* **70**, (1993) 3494.
4. Flatté M.E., *Surface Science* **315**, (1994) L1011.
5. Flatté M.E., *Phys. Rev. Lett.* **70**, (1993)658.
6. Flatté M.E., Quinlan S. and Scalapino D.J.,*Phys.Rev. B* **48**, (1993) 10626.
7. Dessau D.S.,*et al., Phys. Rev. Lett.* **71**, (1993) 2781.

Pergamon

J. Phys. Chem. Solids Vol. 56, No. 12, pp. 1719–1720, 1995
Copyright © 1995 Elsevier Science Ltd
Printed in Great Britain. All rights reserved
0022-3697/95 $9.50 + 0.00

0022-3697(95)00177-8

ELECTRONIC BAND STRUCTURE OF $La_{1-x}Ba_xMnO_3$

N. HAMADA, H. SAWADA and K. TERAKURA
Joint Research Center for Atom Technology (JRCAT),
c/o NAIR, 1-1-4 Higashi, Tsukuba, Ibaraki 305, Japan

Abstract—The electronic structures of $La_{1-x}Ba_xMnO_3$ are calculated by using the all-electron full-potential LAPW method in the local spin-density approximation. The Jahn–Teller distortion is very important to give rise to the A-type antiferromagnetic ground state and the energy band gap for $LaMnO_3$. The ferromagnetic state is stabilized for $La_{1-x}Ba_xMnO_3$ without the Jahn–Teller distortion.

Keywords: Band structure calculation, Jahn–Teller distortion, $La_{1-x}Ba_xMnO_3$.

1. INTRODUCTION

The $La_{1-x}Sr_xMnO_3$ system receives much attention due to the extremely giant magnetoresistance [1] and the structural phase transition induced by an external magnetic field [2]. The mother system, $LaMnO_3$, has four d electrons with a configuration of $d\varepsilon^3 d\gamma^1$; therefore, a Jahn–Teller distortion of the oxygen octahedron occurs within the *ab* plane of the orthorhombic lattice. The system is an antiferromagnetic insulator. With doping it with holes, it becomes a ferromagnetic metal at hole concentrations more than 0.16. A structural phase transition from the orthorhombic to the rhombohedral structure takes place at nearly the same hole concentration at which the magnetic phase transition takes place. There is no Jahn–Teller distortion in the rhombohedral structure.

In this paper, we demonstrate a close relation between the magnetic structure and the Jahn–Teller distortion by the first-principle total-energy band structure calculation in the local spin-density approximation (LSDA). For the calculation, we take the $La_{1-x}Ba_xMnO_3$ system, which is treated in the virtual crystal approximation.

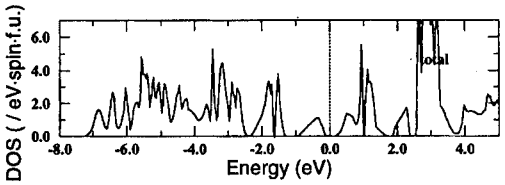


Fig. 1. The density of states of A-type antiferromagnetic $LaMnO_3$ in the orthorhombic structure with the Jahn–Teller distortion. The zero of energy is the Fermi level.

Table 1. Total energies (meV/formula-unit) of various magnetic configurations measured from the most stable configuration for $LaMnO_3$ with and without the Jahn–Teller distortion(JTD), respectively. In three types of antiferromagnetic (AF) configuration, the nearest magnetic moments are arranged in *parallel* direction within an *ab* plane for A-type AF and along the *c* axis for C-type AF, and otherwise in *antiparallel* direction.

	with JTD	without JTD
Ferro.	18 meV	0
A-type AF	0	1 meV
C-type AF	52 meV	-
G-type AF	42 meV	-

2. ELECTRONIC STRUCTURE OF $LaMnO_3$

The crystal of $LaMnO_3$ takes an orthorhombic structure distorted from an ideal cubic structure. A Mn–O distance on the ab plane is 0.29 Å longer than the other Mn–O distance [3]. The Jahn–Teller distortion splits the $d\gamma$ (e_g) level into two levels below and above the Fermi level. The density of states is shown in Fig. 1. The O $2p$ states are located below −2.4 eV; the Mn $d\varepsilon$ (t_{2g}) states from −2.3 eV to −1.3 eV; the Mn $d\gamma$ states from −0.9 eV to 1.6 eV with a 0.2 eV gap around the Fermi level. Two high peaks around 1 eV are the opposite-spin Mn $d\varepsilon$ states, and the opposite-spin $d\gamma$ states are located above 1.9 eV. The large peak around 3 eV is La $4f$ states. The Jahn–Teller splitting in $d\gamma$ states is estimated as 1.2 eV, which is not small in comparison with the octahedral crystal field splitting of 1.8 eV. If we assume a crystal structure without the Jahn–Teller distortion, we do not obtain a energy band gap at the Fermi level.

The Jahn–Teller distortion is important also to give rise to the correct A-type antiferromagnetic ground state. Table 1 shows the total energies in various magnetic structures. Although the A-type antiferromagnetic configuration is the ground state with the Jahn–Teller distortion, the ferromagnetic configuration becomes slightly lower in energy than the A-type antiferromagnetic configuration without the distortion.

Table 2. Relative total energies (meV/formula-unit) of ferromagnetic and A-type antiferromagnetic configurations for $La_{0.5}Ba_{0.5}MnO_3$ with and without the Jahn–Teller distortion(JTD), respectively.

	With JTD	Without JTD
Ferro.	7 meV	0
A-type AF	0	24 meV

3. ELECTRONIC STRUCTURE OF $La_{1-x}Ba_xMnO_3$

The crystal structure of $La_{1-x}Ba_xMnO_3$ changes from orthorhombic through rhombohedral to cubic with increasing the Ba concentration, x. However, in order to study the effect of the Jahn–Teller distortion on the magnetic structure, the same orthorhombic structures as in the case of $LaMnO_3$ are assumed for $La_{0.5}Ba_{0.5}MnO_3$. The band structure calculation has been performed in the virtual-crystal approximation; i.e. a virtual atom with a non-integer nuclear charge between 56(Ba) and 57(La) is put at the La/Ba site. As shown in Table 2, the ferromagnetic configuration is higher in energy than the A-type AF configuration with the Jahn–Teller distortion, while the ferromagnetic structure becomes lower without the Jahn–Teller distortion in agreement with the experiment.

In the ferromagnetic phase, the density of states at the Fermi level is non-zero only for majority spin; i.e. the system is half-metallic. This is a band theoretical picture for Zener's double exchange mechanism [4]. The ferromagnetic state is stabilized by a broad conduction band consisting of the dy states, which favors an undistorted structure. The crystal structure is cubic at $x > 0.35$ [5].

4. CONCLUDING REMARKS

We have demonstrated that details of the crystal structure affect the electronic structure by the first-principle band structure calculation. For $LaMnO_3$, which is a d^4 system, the Jahn–Teller distortion is very important to determine the stable A-type AF structure and the insulating nature. For $La_{0.5}Ba_{0.5}MnO_3$, the distortion prevents the system from stabilizing the the ferromagnetic state. Such an interplay of the lattice structure and the magnetic structure is very common and remarkable in perovskite transition-metal oxides.

Acknowledgments—The present work is partly supported by New Energy and Industrial Technology Development Organization (NEDO).

REFERENCES

1. Tokura Y. *et al.*, *J. Phys. Soc. Jpn* **63**, 3931 (1994).
2. Asamitsu A. *et al.*, *Nature* **373**, 407 (1995).
3. Elemans J. B. A. A., van Laar B., van der Veen K. R. and Loopstra B. O., *J. Solid State Chem.* **3**, 238 (1971).
4. Zener C., *Phys. Rev.* **82**, 403 (1951).
5. Jonker G. H., *Physica* **22**, 707 (1956).

Pergamon

J. Phys. Chem. Solids Vol. 56, No. 12, pp. 1721–1723, 1995
Copyright © 1995 Elsevier Science Ltd
Printed in Great Britain. All rights reserved
0022–3697/95 $9.50 + 0.00

0022-3697(95)00135-2

TUNNELING SPECTROSCOPY OF *d*-WAVE SUPERCONDUCTORS

S. KASHIWAYA,* Y. TANAKA,† M. KOYANAGI,* H. TAKASHIMA* and K. KAJIMURA*

* Electrotechnical Laboratory, Tsukuba, Ibaraki 305, Japan
† Niigata University, Igarashi, Niigata 950-21, Japan

Abstract—Tunneling spectroscopy of anisotropic superconductors is theoretically investigated. Contrary to the case of isotropic superconductors, the tunneling spectrum of anisotropic superconductors does not always correspond to the bulk density of states. In the case of a *d*-wave superconductor, the spectra show zero-bias conductance peaks when the *a*-axis is not normal to the surface. The physical origin of the peaks in the tunneling spectra is discussed in terms of surface bound states.

1. INTRODUCTION

The symmetry of the pair potential in high-T_c superconductors is a controversial problem, although many tunneling experiments have been made. For example, conductance spectra with flat bottoms are rarely observed. Instead, experimental data often show zero-bias conductance peaks. In this paper, we present a new tunneling theory for anisotropic superconductors by extending the theory of Blonder *et al.* [1] to include the **k**-dependence ofthe pair potential. Contrary to the conventional classical theory, the conductance spectra do not always correspond to the bulk density of states. The discrepancy originates from the formation of discrete bound states at the surface of superconductors. The relationship between surface bound states and the tunneling spectrum is discussed using a quantum condition. Our discussion is restricted to the case at 0 K.

2. TUNNELING CONDUCTANCE

We assume a two-dimensional normal–insulator–superconductor (N–I–S) junction with perfectly flat interfaces. The pair potential is assumed to have **k**-dependence $\Delta(\mathbf{k})$, where **k** is the wave-vector of the quasiparticle. The Fermi wave-number k_F and the electron mass m are assumed to be equal in all regions. The potential of the insulator is represented by delta-function with amplitude H. When quasiparticles are injected from the normal metal side with an angle β, they are transmitted to the superconductor as electron-like quasiparticles of wave-vector $\mathbf{k}_+$ and hole-like quasiparticles of wave-vector $\mathbf{k}_-$. These two types of quasiparticles feel different pair potentials,

$$\Delta(\mathbf{k}_\pm) \equiv |\Delta_\pm| \exp(i\theta_\pm). \tag{1}$$

In this situation, the normalized conductance $\sigma(eV, \beta)$ of the N–I–S junction is calculated as [2],

$$\sigma(eV, \beta) = \frac{(1+Z^2)(1+|\Gamma_+|^2) + Z^2(1-|\Gamma_+\Gamma_-|^2)}{1+Z^2 1-\Gamma_+\Gamma_- \exp i(-\theta_+ + \theta_-)|^2} \tag{2}$$

Here,

$$\Gamma_\pm = \frac{eV - \sqrt{(eV)^2 - |\Delta_\pm|^2}}{|\Delta_\pm|}$$

$$Z = \frac{mH}{\hbar^2 k_F \cos\beta},$$

with V being the bias voltage. The experimental conductance spectra $\sigma(eV)$ can be calculated by integrating the conductance with respect to the angle β using an appropriate weighting function $D(\beta)$ whose functional form depends on the geometry of the junction [3],

$$\sigma(eV) = \int_{\frac{-\pi}{2}}^{\frac{\pi}{2}} D(\beta)\sigma(eV, \beta)\mathrm{d}\beta. \tag{3}$$

Figure 1 shows the comparison of the bulk density of states with the calculated conductance spectra of a $d_{x^2-y^2}$-wave superconductor. The conductance spectrum shows a BCS-like gap structure for the *a*-axis normal to the interface, while it shows a zero-bias conductance peak for the *a*-axis tilted by $\pi/4$ from the surface normal. Both conductances are not identical to the bulk density of states. The comparison between experimental data with the calculation is given in Ref. [3].

3. SURFACE BOUND STATES

The property of conductance spectra in Fig. 1 is well understood in terms of the surface bound states. At the surface of the superconductor, the quasiparticles alter their wave-vector by specular reflections. Accordingly, the effective pair potentials felt by the quasiparticles change through the reflection. The surface corresponds to a node of the pair potential surrounded by two pair potentials $\Delta(\mathbf{k}_+)$ and $\Delta(\mathbf{k}_-)$. We call this structure a pseudo-quantum well (PQW) [4]. In

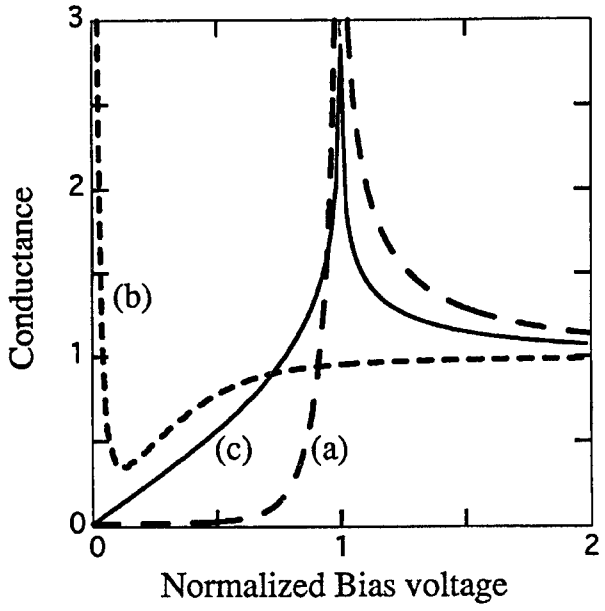


Fig. 1. Conductance spectra and density of states of $d_{x^2-y^2}$-wave superconductors. (a) Crystal a-axis being normal to the interface, (b) a-axis being tilted by $\pi/4$ from the surface normal, (c) densoty of states.

this PQW, discrete bound states are formed and they serve as a channel for the current flow just like the case of resonant tunneling process. Thus the conductance spectrum of the N–I–S junction has peak at the energy levels of the surface bound states.

To see clearly the role of the bound states, the superconductor is assumed to have two-dimensional $s + id_{xy}$-wave symmetry. The amplitude ratio of s-wave component relative to d-wave component is changed using a parameter $\alpha(1 > \alpha > -1)$,

$$\hat{\Delta}(\varphi) = \frac{\Delta_0}{\sqrt{2}}[\alpha + 2i\sqrt{1-\alpha^2}\sin(2\varphi)], \tag{4}$$

where φ is the angle between the wave-vector $\mathbf{k}_+$ and a-axis of the superconductor. For a fixed injection angle $\beta = \pi/12$, $\Delta(\mathbf{k}_+) = \hat{\Delta}(\beta)$ and $\Delta(\mathbf{k}_-) = \hat{\Delta}(\pi - \beta) = \hat{\Delta}(-\beta)$. The energy levels of the bound states in the PQW can be calculated using a quantum condition [4]. The bound states are classified into two types according to the direction of net current: p-process bound states (PBS) and n-process bound states (NBS). PBS and NBS carry the net current along opposite directions. Figure 2 shows the dependence of surface-bound-state levels on α. Only when α is an integer, the enrgy levels of PBS and NBS are degenerate. When $\alpha = 0$, the mid-gap states are formed at the Fermi Level (FL).

Figure 3 shows the conductance spectra calculated form eqn (2) for various α values. When $\alpha = 1$, the conductance spectrum has peaks at Δ_0/e [Fig. 3(a)], which reflect the degenerated bound states at $\pm\Delta_0$ at the surface [Fig. 2(a)]. With increasing α, the voltage at the peak becomes smaller [Fig. 3(b)] because of the decrease of bound states levels [Fig. 2(b)]. When $\alpha = 0$, the peak exists at the zero-bias

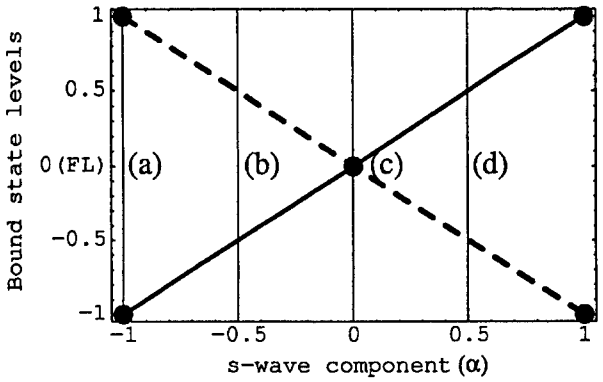


Fig. 2. Dependence of surface-bound-state an α. Solid line represents the bound states for n-process and the dotted line for p-process. Closed circles indicate the degenerated bound states. For lines (a)–(d), see Fig. 3.

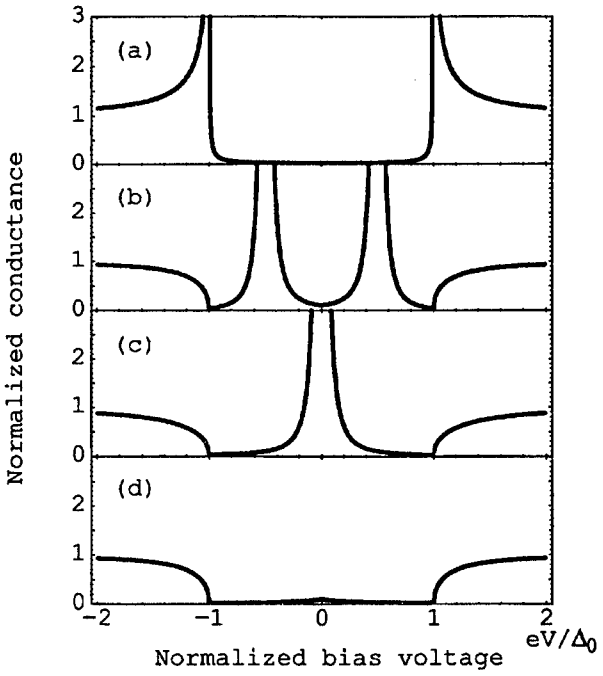


Fig. 3. Conductance spectra for $\sigma(eV, \pi/12)$ for various α: (a) $a = 1$; (b) $a = 0.5$; (c) $a = 0$; (d) $a = 0.5$. Compare the peak voltages in the spectra with the bound state levels marked by the lines (a)–(d) in Fig. 2.

level [Fig. 3(c)] reflecting the formation of mid-gap states [Fig. 2(c)]. When α is a negative value, PBS exists below FL, and NBS above FL [Fig. 2(d)]. They cannot contribute to the current flow, since the connection of the injected quasiparticles to these bound states breaks the conservation law of the group velocity. The physical meaning is that the flow direction of current in the bound states does not match the direction of injected electrons. Thus the peaks in the conductance spectra do not appear [Fig. 3(d)].

The peaks in the conductance spectra indicate the existence of both PBS above FL and NBS below FL at the

surface. PBS below FL and NBS above FL contribute to the density of states, but not to the conductance of N–I–S junctions.

4. SUMMARY

The conductance spectra of anisotropic superconductors are discussed in terms of surface bound states. The peak structures in the conductance spectra indicate the existence of surface bound states. The direction of electron flow have importance meaning for the tunneling spectra in the case of $s + id_{xy}$-wave symmetry superconductors.

REFERENCES

1. Blonder G. E., Tinkham M. and Klapwijk T. M., *Phys. Rev. B* **25**, 4515 (1982).
2. Tanaka Y. and Kashiwaya S., to be published in *Phys. Rev. Lett.* **74**, 3451 (1995).
3. Kashiwaya S., Tanaka Y., Koyanagi M., Takashima H. and Kajimura K., *Phys. Rev. B* **51**, 1350 (1995).
4. Kashiwaya S., Tanaka Y., Koyanagi M. and Kajimura K., *Jpn J. Appl. Phys.* **34**, 4555 (1995).

Pergamon

J. Phys. Chem. Solids Vol. 56, No. 12, pp. 1725–1726, 1995
Copyright © 1995 Elsevier Science Ltd
Printed in Great Britain. All rights reserved
0022-3697/95 $9.50 + 0.00

0022-3697(95)00136-0

EFFECT OF IMPURITY SCATTERING ON A $d + s$ WAVE SUPERCONDUCTOR: LOW TEMPERATURE BEHAVIOR OF PENETRATION DEPTH

HEESANG KIM and E. J. NICOL
Department of Physics, University of Guelph, Guelph, ON, N1G 2W1 Canada

Abstract—Currently there exist several experimental reports on high-T_c oxides which favor d-wave order parameter symmetry. However, several others would support an s-wave gap. Recent measurements of the penetration depth in $YBa_2Cu_3O_{7-\delta}$ single crystals show large differences in a and b directions in the basal plane, which implies that orthorhombicity due to the chains is not small. As an attempt to understand current experimental results we consider an order parameter with $d + s$ wave symmetry, which can arise naturally as a deviation from d-wave due to the presence of orthorhombicity. We provide a detailed study of the characteristics of such an order parameter in the low temperature behavior of the penetration depth in the presence of non-magnetic impurity scattering. The results are discussed in comparison with d-wave and anisotropic s-wave cases.

In recent years, there have been many theoretical and experimental efforts to identify the order parameter symmetry in high T_c oxide superconductors. In the frame work of an idealized tetragonal symmetry, two possible candidates ($d_{x^2-y^2}$ wave and extended s-wave pairing) have been highlighted the most [1]. However, recent measurements of the temperature dependent penetration depth in clean $YBa_2Cu_3O_{7-\delta}$ single crystals show large differences in a and b directions: $\lambda_a^2(T=0)/\lambda_b^2(T=0) = 2 \sim 6$, and a linear behavior with different coefficients at low tempertaures [2,3]. These results suggest that the orthorhombicity due to the chains might be important in understanding the properties of high-T_c oxides.

In this paper we consider an order parameter with $d+s$ wave symmetry [4], $\Delta(\hat{\mathbf{k}}) = \Delta(\hat{k}_x^2 - \hat{k}_y^2 + \beta)$, along with an elliptic Fermi surface, $\epsilon_F = (k_x^2/2m_x) + (k_y^2/2m_y)$. Here β is a constant s-wave component. We consider $|\beta|$ less than one, meaning that the d-wave part is still dominant over the s-wave part. This form of order parameter has characteristics that are a hybrid of both d-wave and s-wave. It has full lattice symmetry, since the system is orthorhombic, not tetragonal any longer. It has four nodes and changes its sign on the Fermi surface. It has a non-vanishing average over the Fermi surface. This order parameter exhibits interesting properties, especially in the presence of non-magnetic impurity scattering.

The calculations are handled easily with a transform $p_i \equiv k_i\sqrt{(m_x+m_y)/2m_i}$ which changes the elliptic Fermi surface into a circular one. Under the transform, $\tan\varphi = \sqrt{m_y/m_x}\tan\phi$ where φ and ϕ are the polar angles in the $\mathbf{k}$ and $\mathbf{p}$ frames respectively; $\Delta(\hat{\mathbf{p}}) = \Delta(\cos 2\phi + \alpha)$ where $\alpha \equiv \beta + (m_x - m_y)/(m_x + m_y)$.

In the pure case, the nodes on the Fermi surface lead to a linear temperature dependence of the penetration depth at low temperatures. Here we give the superfluid density tensors at low temperatures. The temperature dependence of the penetration depth, which is also a tensor, is then easily obtained using the relation $\rho^s(T) \propto \lambda^{-2}(T)$.

$$\rho_{xx}^2(T) \approx \rho_{xx}^2(T=0) - N(0)M\left(\frac{\epsilon_F}{m_x}\right)\left(\frac{T}{\Delta}\right) 8\ln 2 \frac{\cos^2\phi_0}{|\sin(2\phi_0)|} \quad (1)$$

$$\rho_{yy}^2(T) \approx \rho_{yy}^2(T=0) - N(0)M\left(\frac{\epsilon_F}{m_y}\right)\left(\frac{T}{\Delta}\right) 8\ln 2 \frac{\sin^2\phi_0}{|\sin(2\phi_0)|} \quad (2)$$

where M is the bare electron mass, and $\phi_0 \equiv \frac{1}{2}\arccos(-\alpha)$ is a position of a node in $0 < \phi < \pi/2$. The other nodes are at $\phi = \pi - \phi_0$, $\pi + \phi_0$ and $2\pi + \phi_0$. In the case with impurity scattering.

$$\rho_{xx}^s(t) \approx \rho_{xx}^s(T=0) + N(0)M(\pi T)^2\left(\frac{2\epsilon_F}{3m_x}\right)\left(\frac{T}{\Delta}\right) \times \int_0^{2\pi}\frac{d\phi}{2\pi}\cos^2(\phi)F'(w_n \to 0^+) \quad (3)$$

$$\rho_{yy}^s(t) \approx \rho_{yy}^s(T=0) + N(0)M(\pi T)^2\left(\frac{2\epsilon_F}{3m_y}\right)\left(\frac{T}{\Delta}\right) \times \int_0^{2\pi}\frac{d\phi}{2\pi}\sin^2(\phi)F'(w_n \to 0^+) \quad (4)$$

where

$$F'(w_n \to 0^+) = \frac{(\Delta(\hat{\mathbf{p}}) - \gamma_1)[2c_1\gamma_3^2 - 3(\Delta(\hat{\mathbf{p}}) - \gamma_1)\gamma_3(1+c_3) - c_1(\Delta(\hat{\mathbf{p}}) - \gamma_1)}{[\gamma_3^2 + (\Delta(\hat{\mathbf{p}}) - \gamma_1)^2]^{5/2}}$$

Here γ_1, c_1, and γ_3 are defined from the impurity self-energies at low-frequencies: $ia_3(w_n) \sim \gamma_3 + c_3 w_n$; $ia_1(w_n) \sim$

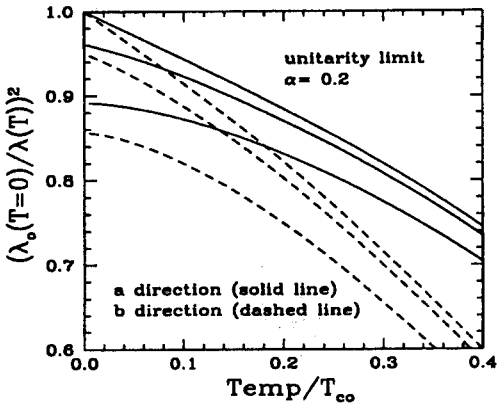


Fig. 1. The penetration depths (or the superfluid density tensor) normalized by their clean limit, zero temperature values in a (solid lines) and b (dotted lines) directions. From the top to the bottom curves, $1/2\tau T_{c0} = 0$ (pure case), 0.01 and 0.04. Here, $\alpha = 0.2$.

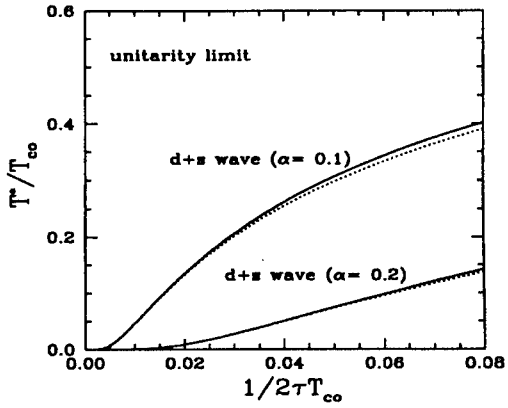


Fig. 2. The crossover temperatures T^* in a (solid lines) and b (dotted lines) directions. The top curves are for $\alpha = 0.1$, and the bottom curves are for $\alpha = 0.2$.

$\gamma_1 + c_1 w_n$ as $w_n \to 0^+$. The ia_3 renormalize the frequencies, and ia_1 renormalize the order parameter. We follow the notation in [5]. Note that non-vanishing average on the Fermi surface makes ia_1 non-zero. In the low scattering rate limit ($2\tau \ll T_c$), $\gamma_1 \sim -(\pi/2\tau)/(4\phi_0 - \pi)$ and $\gamma_3 \sim Se^{2\tau S(4\phi_0-\pi)^2/(2\pi)}$ in unitarity limit, and $\gamma_1 \sim -(4\phi_0 - \pi)/(2\tau\pi)$ and $\gamma_3 \sim Se^{-2\tau\pi S/2}$ in the Born limit. Here, $S \equiv \Delta|\sin(2\phi_0)|$. Equations (1)–(4) show that the $d + s$ wave order parameter has desirable low temperature behaviors: linear T dependence in the pure case, and T^2 dependence in the impurity case; yet different coefficients in the a and b directions. These equations give standard d wave results, when we set $\alpha = 0$, $m_x = m_y$, and $ia_1(w_n) = 0$. Figure 1 shows the peneration depth at low temperatures for various impurity scattering rates $1/2\tau$. Crossover temperatures T_{ii}^* can be defined by $\lambda(T) = \lambda(0) + bT^2/(T + T^*)$, as introduced by Hirschfeld and Goldenfeld [6]. From eqns (1)–(4), they are found to be:

$$T_{xx}^* \sim \frac{-12\ln 2\cos^2(\phi_0)}{\pi^2\Delta|\sin(2\phi_0)|\int_0^{2\pi}\frac{d\phi}{2\pi}\cos^2(\phi)F'(w_n \to 0^+)} \quad (6)$$

$$T_{yy}^* \sim \frac{-12\ln 2\sin^2(\phi_0)}{\pi^2\Delta|\sin(2\phi_0)|\int_0^{2\pi}\frac{d\phi}{2\pi}\sin^2(\phi)F'(w_n \to 0^+)} \quad (7)$$

$$(8)$$

Figure 2 shows the crossover temperature as a function of impurity scattering.

We have studied the low temperature behaviors of penetration depth in a superconductor with $d+s$ wave order parameter symmetry, concentrating on effects of non-magnetic impurity scattering. A superconductor with such an order parameter symmetry exhibits the same kind of low temperature behaviors as a d-wave order parameter in the tetragonal framework. Yet this model naturally shows anisotropy in a and b directions as well. This feature and other properties [7], not shown in this paper, appear to suggest that the $d+s$ wave order parameter may be a suitable candidate for hight-T_c oxide superconductors, such as YBCO.

Acknowledgements—We are grateful to P. Muzikar and J. Carbotte for enlightening discussions. This work is supported by the Natural Sciences and Engineering Council of Canada (NSERC).

REFERENCES

1. Scalapino D., *Phys. Rep.* **250**, 330 (1995).
2. Basov D. N. *et al.*, *Phys. Rev. Lett.* **74**, 598 (1995).
3. Zhang K. *et al.*, *Phys. Rev. Lett.* **73**, 2484 (1994).
4. Recently this form of order parameter was considered also by O'Donovan C. *et al.* (unpublished), and by Pokrovsky V. L. (unpublished).
5. Choi C. and Muzikar P., *Phys. Rev. B* 39, 11296 (1969).
6. Hirschfeld P. and Goldenfeld N., *Phys. Rev. B* **48**, 4219 (1993).
7. Kim H. and Nicol E. J., (unpublished).

Pergamon

J. Phys. Chem. Solids Vol. 56, No. 12, pp. 1727–1728, 1995
Copyright © 1995 Elsevier Science Ltd
Printed in Great Britain. All rights reserved
0022–3697/95 $9.50 + 0.00

0022–3697(95)00137-9

WEAK ELECTRON–PHONON INTERACTION AND STRONG PHONON FEATURES IN *a–b*-PLANE OPTICAL CONDUCTIVITY OF HIGH-T_c SUPERCONDUCTORS

VLADIMIR N. KOSTUR
Center for Superconductivity Research, Department of Physics, University of Maryland, College Park, MD 20742, U.S.A.

BOŽIDAR MITROVIĆ
Department of Physics, Brock University, St. Catharines, Ontario L2S 3A1, Canada

Abstract—It is shown that a correlation between the positions of the *c*-axis longitudinal optic (LO_c) phonons and "notch"-like structures in the $a-b$ plane conductivity of high-T_c superconductors results from phonon-mediated interaction between electrons in different layers.

Keywords: Optical properties (D), superconductors (A), phonons (D).

The correlation between the positions of the *c*-axis longitudinal optic (LO_c) phonons and "notch"-like absorption structures in the *a–b*- plane conductivity $\sigma_{ab}(\mathbf{q}^0, \omega)$ was found by Reedyk and Timusk [1] for most of the high-T_c copper-oxide superconductors. It was shown that such antiresonant features are not present in infrared measurements if the wave vector of light $\mathbf{q}^0$ is perpendicular to the *c*-axis. Here we propose a simple microscopic mechanism for this effect. We consider a contribution $\delta\sigma$ to the conductivity arising from the coupling of the charge carriers in different layers via the exchange of one LO_c-phonon. For the electron-LO_c phonon Hamiltonian of the form

$$H_{e-LO_c} = \sum_{l\mathbf{k}\sigma} c^{\dagger}_{l\mathbf{k}\sigma} c_{l\mathbf{k}\sigma} \sum_{q_z} g^{(l)}_{\mathbf{k}}(q_z) \left[b_{q_z} + b^{\dagger}_{-q_z} \right], \qquad (1)$$

where l labels the layers stacked along z-direction (parallel to the *c*-axis), $\mathbf{k}$ is the momentum in the *a–b*-plane and σ is the spin index, one gets $\delta\sigma = i\delta\Pi/\omega$ with

$$\delta\Pi(q_z^0, \omega) = \sum_{ll'} \delta\Pi_{ll'}(\omega)\, e^{iq_z^0(z_l - z_{l'})} \qquad (2)$$

where $\delta\Pi_{ll'}(\omega)$ is the contribution from the diagram with one-phonon line which connects two particle-hole polarization bubbles.

$$\delta\Pi_{ll'}(\omega) = \frac{\Pi_l(\omega)\Pi_{l'}(\omega)}{N(0)} D(\Omega_{ph}, \omega)$$

$$\times \sum_{q_z, \mathbf{k}, \mathbf{k}'} e v_x(\mathbf{k}) g^{(l)}_{\mathbf{k}}(q_z) g^{(l')}_{\mathbf{k}'}(q_z)^* e v_x(\mathbf{k}') \qquad (3)$$

Π is the electron polarization for a single layer, D is the LO_c-phonon propagator, $v_x(\mathbf{k})$ is the electron velocity coming from the current vertex when electric field is parallel to *a*-axis. Sums over $\mathbf{k}, \mathbf{k}'$ are restricted to the Fermi surface (FS). The factors under the sum in eqn (3) are written in the same order as they appear in the diagram. We propose an *ansatz* that the quantity

$$\lambda_{ll'}(\mathbf{k}, \mathbf{k}') = N(0) \sum_{q_z} g^{(l)}_{\mathbf{k}}(q_z) g^{(l')}_{\mathbf{k}'}(q_z)^*, \qquad (4)$$

is sharply peaked at $\mathbf{k} = \mathbf{k}'$. This means that the electrons from different layers interact appreciably via the exchange of the LO_c-phonon only when their momenta are nearly equal. With this *ansatz* one finds *non-zero* contribution at $q_z^0 \neq 0$

$$\delta\sigma_1(\omega) = -\frac{\lambda_{ph}(q_z^0)\omega_p^2}{4\pi\omega} Im\left[\Pi(\omega)^2 D(\Omega_{ph}, \omega)\right]. \qquad (5)$$

Here ω_p is the plasma frequency and

$$\lambda_{ph}(q_z^0) = \sum_{\mathbf{k}, k' \in FS} v_x(\mathbf{k}) v_x(\mathbf{k}')$$

$$\times \sum_{ll'} e^{iq_z^0(z_l - z_{l'})} \lambda_{ll'}(\mathbf{k}, \mathbf{k}') / \sum_{\mathbf{k} \in FS} v_x(\mathbf{k})^2. \qquad (6)$$

In the case when $\mathbf{q}^0$ is perpendicular to the *c*-axis $\lambda_{ph}(q_z^0 = 0) = 0$, because the electron–phonon matrix element of the LO_c-phonon is proportional to $\mathbf{e}_{LO_c} \cdot \nabla \propto \partial/\partial z_l$, and it vanishes after summation over l. The propagator $D(\Omega_{ph}, \omega)$ for optical phonon can be modeled by a Lorentzian of half-width γ_{ph}. One finds $\delta\sigma$ to be negative if $|Im\tilde{\Pi}(\omega)| > Re\tilde{\Pi}(\omega)$, which is realised if the in-plane electron scattering rate near the position of the LO_c-phonon satisfies $1/\tau > \Omega_{ph}$. Moreover, the relative depth of the "notch", $\delta\sigma/\sigma$, is found to be proportional to $\lambda_{ph}(q_z^0)\Omega_{ph}/\gamma_{ph}$. The experimental values of Ω_{ph}/γ_{ph} for LO_c-phonons are in the range 10-200 [2]. Thus, even for $\lambda_{ph}(q_z^0) \simeq 0.01$ the effect can be large.

Acknowledgements—VK was supported by NASA Grant No. NAG3-1395, and BM by NSERC Canada

REFERENCES

1. Reedyk M. and Timusk T., *Phys. Rev. Lett.* **69**, 2705 (1992); Reedyk M., Timusk T. and Basov D., *ibid.* **71**, 2677 (1993).
2. Thomsen C., in *Light Scattering in Solids VI* (Edited by M. Cardona and M. Güntherodt), p. 285. Springer, Heidelberg, (1991).

Pergamon

J. Phys. Chem. Solids Vol. 56, No. 12, pp. 1729–1731, 1995
1995 Elsevier Science Ltd
Printed in Great Britain
0022-3697/95 $9.50 + 0.00

0022-3697(95)00270-7

CORRELATION ENERGY HIERARCHY IN TWO DIMENSIONAL HUBBARD MODEL

SHOUDAN LIANG
Department of Physics, 104 Davey Laboratory, The Pennsylvania State University, University Park, PA 16802, U.S.A.

Abstract—Numerical renormalization group has not been successfully applied to the two dimensional Hubbard model due to apparent lack of a energy-scale hierarchy in the hamiltonian. We show that with a suitable choice for the single-particle orbitals, the interaction energy can exhibit a hierarchy of energy scales. We argued that the new variables give the right low energy physics.

Electron-electron correlations are crucial in understanding normal as well as superconducting properties of high T_c cuprates[1]. Beyond perturbation theory, the only reliable ways of dealing with strong correlations are numerical methods. However, numerical methods currently available cannot be extended to large enough system sizes and low enough temperatures to study low energy physics such as transport and superconductivity. The so called 'minus sign' problem prevents quantum Monte Carlo from reaching low temperatures. In exact diagonalization method, the dimension of the Hilbert space grows exponentially with the number of electrons making it impossible to do calculation on larger clusters.

One effective method of handling many degrees of freedom is numerical renormalization group(NRG) in which the size of the Hilbert space is systematically reduced in such a way that the low energy spectrum is not much affected. The method has been successfully applied[2] to Kondo problem. The hamiltonian of this problem has a clear separation of energy scales which makes it safe[3] to prune Hilbert space. With a hierarchy of energies, the strongest interacting parts of the hamiltonian is diagonalized first. After high energy states are discarded, the next strongest interacting degree of freedom is added. Because the energy-scale hierarchy, the discarded states are always at the highest energy and will not affect much the low energy spectrum.

The trouble with applying NRG to the lattice model we are interested in is that there is no apparent separation of energy scales. For example, in the real space renormalization group, the most efficient procedure of truncating states is by adding one site at a time. The interaction between the block and the added site is the hopping integral t or the exchange interaction J which remain fixed. This lack of energy scale is reason why the real space renormalization group performs poorly for lattice models[4]. By keeping the density matrix eigenstates, White[5] has recently developed a method that is very accurate for one-dimensional systems with short range interaction. However,

it is difficult to apply this method to higher dimensional system[6].

The purpose of this note is to demonstrate by an explicit construction that with suitable transformation of single particle variables, it is possible to bring out a hierarchy of energy scales for a many-body hamiltonian. We believe our construction works for a large class of models but here we focus on Hubbard model in two dimensions. In the momentum space, the Hubbard U-term is written as: $\frac{U}{N}\sum_{\mathbf{k},\mathbf{k}',\mathbf{q}} c^\dagger_{\mathbf{k}\uparrow} c^\dagger_{\mathbf{k}'\downarrow} c_{\mathbf{k}'+\mathbf{q}\downarrow} c_{\mathbf{k}-\mathbf{q}\uparrow}$ where $c^\dagger_{\mathbf{k}\sigma}$ creates an electron with momentum $\mathbf{k}$ and spin σ. We first divide the momentum states into shells labeled by $s = \pm1, \pm2, \ldots$ according to their energies $\frac{|\epsilon(\mathbf{k})-\epsilon_F|}{\epsilon_F} < \delta$ for $|s| = 1$ and $\delta\Lambda^{|s|-1} < \frac{|\epsilon(\mathbf{k})-\epsilon_F|}{\epsilon_F} < \delta\Lambda^{|s|}$ for $|s| > 1$. The positive(negative) integers label the shells with $\epsilon(\mathbf{k})$ above(below) the Fermi energy ϵ_F. Parameter δ specifies the width of the first shell and $\Lambda > 1$ controls the width of higher shells. Next, within each shell, we make a list of all the states and rank them according to the angle $\theta_j = \tan^{-1}\frac{k_{jx}}{k_{jy}}$. We then introduce the new variables by Fourier transformation $f_{sm\sigma} = \frac{1}{\sqrt{N_s}}\sum_j e^{\frac{2\pi i m}{N_s} j} c_{\mathbf{k}_j\sigma}$, where N_s is the total number of variables $c_{\mathbf{k}_j}$ in the shell s. The Hubbard repulsion interaction can now be written in terms of $f_{sm\sigma}$:

$$\frac{U}{N}\sum_{s_1,m_1}\sum_{s_2,m_2}\sum_{s_3,m_3}\sum_{s_4,m_4} C(s_1m_1;s_2m_2;s_3m_3;s_4m_4) \times f^\dagger_{s_1m_1\uparrow} f^\dagger_{s_2m_2\downarrow} f_{s_3m_3\downarrow} f_{s_4m_4\uparrow} \quad (1)$$

$$C(\{s_i,m_i\}) = \frac{1}{\sqrt{N_{s_1}N_{s_2}N_{s_3}N_{s_4}}}\sum_{j_1j_2j_3j_4} e^{2\pi i\left(\frac{m_1j_1}{N_{s_1}}+\frac{m_2j_2}{N_{s_2}}-\frac{m_3j_3}{N_{s_3}}-\frac{m_4j_4}{N_{s_4}}\right)} \quad (2)$$

The sum in the last equation is constrained by the conservation law $\mathbf{k}_{j_1} + \mathbf{k}_{j_2} = \mathbf{k}_{j_3} + \mathbf{k}_{j_4}$. When m_i are not all the same, the scattering is effectively zero because the destructive interference[7]. The scattering terms are largest when all $m_i = 0$ where all the terms add in phase and the sums over all momenta are only limited by the conservation law. For the remaining terms with $m_i = m$, the scattering terms decay exponentially with m. Fig.1 shows the result of a calculation of $\frac{C(s_i,m_i=m)}{C(s_i,m_i=0)}$ (labeled "scattering" in the figure) for a 30×30 lattice with 6 momentum shells. Clearly, the interaction strength decays exponentially with m.

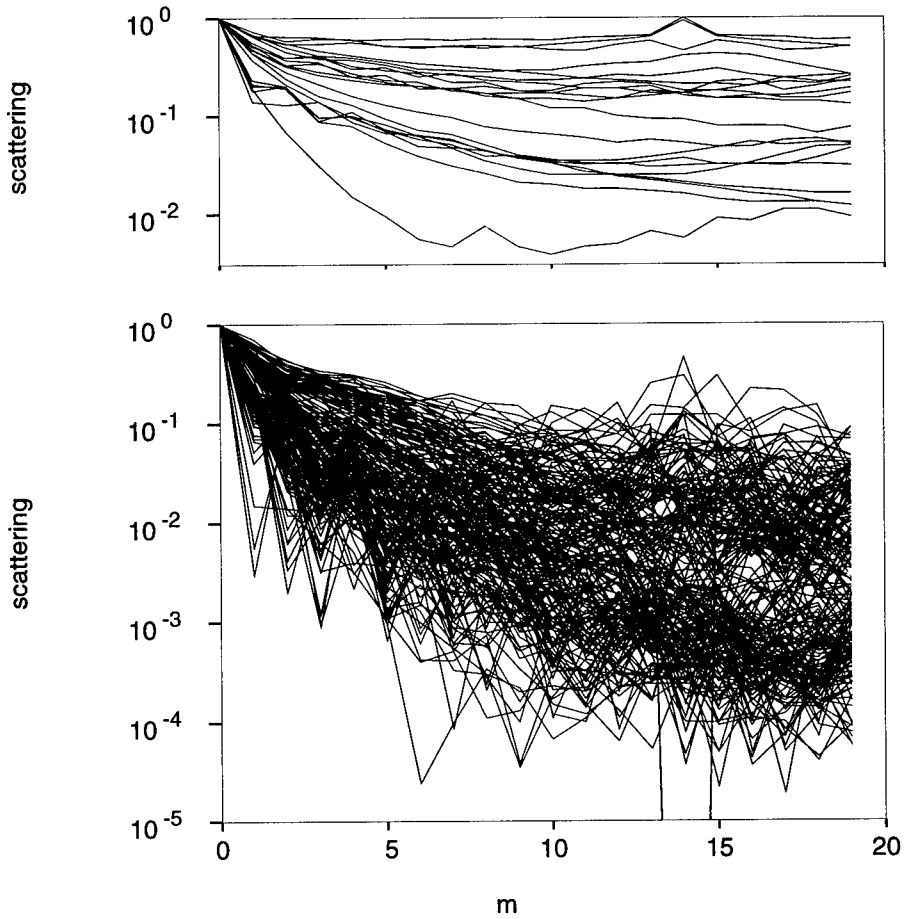


Fig. 1. The coefficient $\frac{C(s_i,m_i=m)}{C(s_i,m_i=0)}$ of Eq(2) (labeled "scattering" in the figure) for a 30×30 lattice with 6 momentum shells with $\epsilon_F = -1.3t$ and separation energies between shells at $|\epsilon - \epsilon_F| = 0.25t, t$. Each curve represents one of 6^4 configurations of (s_1, s_2, s_3, s_4). Only the terms with $m < 20$ are shown. The upper panel, which shows a slower decay, is for terms of the form $n_{sm\uparrow}n_{s'm\downarrow}$(with $n_{sm\sigma} = f^\dagger_{sm\sigma}f_{sm\sigma}$) that involve only the density and therefore no scattering(they contribute to diagonal energy only). The lower panel is for all the rest.

Unlike the Hubbard model in **k**-space, which creates particle-hole pairs with equal weight, the Hubbard interaction written in f's has a hierarchy of energy scales and is therefore a better basis for renormalization group calculation. We can for example keep $f_{sm\sigma}$ for only $m < M$. Since the scattering is the strongest in the small m channels, getting rid of $f_{sm\sigma}$ at large m have small effects on the ground state.

We now argue that the new variables have the right features. If the Hubbard U is treated by perturbation theory in the **k**-space and one asks which states are more important. Then certainly the states with particle-hole excitations near the Fermi surface will have larger weight than the states with particles and holes deeply inside or outside of Fermi surface. However, because Pauli exclusion principle, these low energy particle-hole excitations near the fermi surface have vanishingly small phase space. There are great many more particle-hole pairs away from the Fermi surface, their combined effect could be large. In the new f-variable, s-waves are most strongly interacting. The s-wave variable is increasingly smaller fraction of total number of available degree of freedoms for shell away from the Fermi surface. This fraction is adjusted by Λ. Intuitively, since we expect the momentum distribution $n(\mathbf{k})$ to change rapidly only near the Fermi surface(where therefore more variables are needed). Away from the Fermi surface, a small number of variables will be sufficient. In our method, we retain a relatively few variables away from the Fermi surface and more near the Fermi surface.

In conclusion, we have demonstrated that with suitable choice of the single-particle orbitals, the interaction energy exhibit a hierarchy of energy scales. The new orbitals are suitable starting point for numerical renormalization group calculations.

Acknowledgement—It is a pleasure to acknowledge informative

and stimulating discussions with Dr. H. Pang. The work was supported in part by the Office of Naval Research Grant No. N00014-92-J-1340 and by the National Science Foundation Grand No. DMR-9403201 as well as by the Center for Academic Computing at Pennsylvania State University.

REFERENCES

1. Anderson P.W., *Science* **256** (1992) 1526.
2. Wilson K.G., *Rev. Mod. Phys.* 47, 773 (1975).
3. Wilson K.G., in *Nobel Symposia-Medicine and Natural Sciences* (Academic Press, New York) **24** 68 (1974).
4. Hirsh J.E., *Phys. Rev. B* **22** (1980) 5259.
5. White S.R., *Phys. Rev. Lett.* **69** (1992) 2863, *Phys. Rev. B* **48** (1993) 10345.
6. Liang S. and Pang H., *Phys. Rev. B* **49** (1994) 9214.
7. The off-diagonal terms in m_i are exactly zero when the density of the **k**-states within each shell as a function of the angular variable θ_j is constant. On a finite lattice, the density fluctuate around a constant so the off-diagonal terms will not be exactly zero, but will be very small.

Pergamon

J. Phys. Chem. Solids Vol. 56, No. 12, pp. 1733–1734, 1995
Copyright © 1995 Elsevier Science Ltd
Printed in Great Britain. All rights reserved
0022-3697/95 $9.50 + 0.00

0022-3697(95)00180-8

π JUNCTIONS IN s-WAVE SUPERCONDUCTORS: BI-LAYER EFFECTS

D. Z. LIU, J. MALY and K. LEVIN
James Franck Institute, University of Chicago, Chicago, IL 60637, U.S.A.

Abstract—We study the order parameter symmetry in bi-layer cuprates such as YBaCuO, where interesting π phase shifts have been observed in Josephson junctions. While π phase shifts are known to occur in d-states, this behavior can also be associated with (orthorhombic) s-symmetry when the two sub-band gaps have opposite phase. We show that π phase shifts are general consequences of repulsive interactions, independent of whether a magnetic mechanism is operative.

The observation of π phase shifts in a corner Josephson junction experiment in YBCO [1] is one of the most important experimental results to emerge from the cuprate literature in recent years. This measurement has been widely interpreted as support for a d-symmetry of the order parameter, as well as for a magnetic mechanism for superconductivity. In this paper we show that both of these inferences may be inappropriate.

The gap equation for bi-layer systems has been studied earlier in the context of a magnetic mechanism for superconductivity [2,3]. There it was observed that the d-symmetric state of the single layer problem, is transformed to a pair of in-phase d states on each of the two sub-bands, and that these compete with a pair of out-of-phase s-states. Here we take the problem to a greater level of generality, establishing that this situation persists for a wide class of repulsive interactions, which are unrelated to the antiferromagnetic spin fluctuation picture. Alternate classes of the order parameter symmetry are also generated. These correspond to in-phase s-states and out-of-phase d-states [4].

In the presence of both intra- and inter-layer interactions ($V_\parallel$ and $V_\perp$), the weak coupling BCS gap equation becomes a set of coupled equations for the gaps on each of the sub-bands (Δ_+, Δ_-). Following the usual procedure [5], the gap equations become

$$\Delta_+ \pm \Delta_- = -\sum_{\mathbf{q}'} \frac{V_{\parallel,\perp}\Delta_+}{2E_+} \tanh\left(\frac{E_+}{2T}\right) \mp \sum_{\mathbf{q}'} \frac{V_{\parallel,\perp}\Delta_-}{2E_-} \tanh\left(\frac{E_-}{2T}\right), \quad (1)$$

where the superconducting quasi-particle energies are $E_\pm = \sqrt{\epsilon_\pm^2 + \Delta_\pm^2}$, where

$$\epsilon_\pm = -2t[\cos(q_x a) + \cos(q_y b)] + 4t' \cos(q_x a)\cos(q_y b) \pm t_\perp - E_F. \quad (2)$$

In this model $t_\perp$ is the matrix element for hopping between layers; t and t' refer to the first and second nearest neighbor in-plane hopping which may contain orthorhombic effects.

In the case of a magnetic pairing mechanism, the two interactions are related to components of the dynamical spin susceptibility [6,7]. Because the in-plane magnetism is not independent of inter-plane effects any proper treatment of spin fluctuation induced superconductivity should incorporate both components. Here we generalize the spin-fluctuation pairing models ($\lambda_A > 0, \lambda_B < 0, \mathbf{Q} = (\pi, \pi)$) to consider

$$V_{\parallel,\perp} = \frac{\lambda_A, \lambda_B}{[1 - J_o(\cos(k_x \pm Q_x) + \cos(k_y \pm Q_y))]^2} \quad (3)$$

and assume that the overall signs are unconstrained and the $\mathbf{k} = \mathbf{q} - \mathbf{q}'$ peaks occur at arbitrary wave-vector($\mathbf{Q}$)(summing over all signs). Furthermore, we vary the width of the peak structure by changing J_o and therefore incorporate the limit of rather structureless interactions, as in the phonon case.

The typical gap functions for the magnetic case which consists of repulsive intra-layer ($\lambda_A > 0$) and attractive inter-layer ($\lambda_B < 0$) interactions are shown in Fig. 1(a). The figure on the left (right) in the box corresponds to intra-layer (inter-layer) dominated behavior. For general parameterizations we find that d-symmetry is associated with repulsive and s-symmetry with attractive interactions. In phase gap behavior occurs when the intra-layer interaction is the larger; out of phase behavior arises in the opposite case [4]. It is important to note from Fig. 1(a) and that the out of phase s-wave states will exhibit π phase shifts in a corner SQUID experiment [1]. While not a general feature of all solutions, its presence requires (a modest amount of) orthorhombicity. The observation of π phase shifts in bi-layer cuprates is thus not as strong a constraint on the order parameter symmetry as in one layer materials. All orthorhombic states which exhibit these π phase shifts will also show finite c-axis tunneling in untwinned crystals [8].

In Fig. 1(b) we present the gap symmetry for our generalized pairing potential peaked at an arbitrary wavevector $\mathbf{Q}$ in the intra-layer dominated regime. It is clear that $d_{x^2-y^2}$ is rather stable for $\mathbf{Q}$ in a wide range around (π, π) demonstrating that the d-wave states may have more general origin beyond the antiferromagnetic spin exchange models.

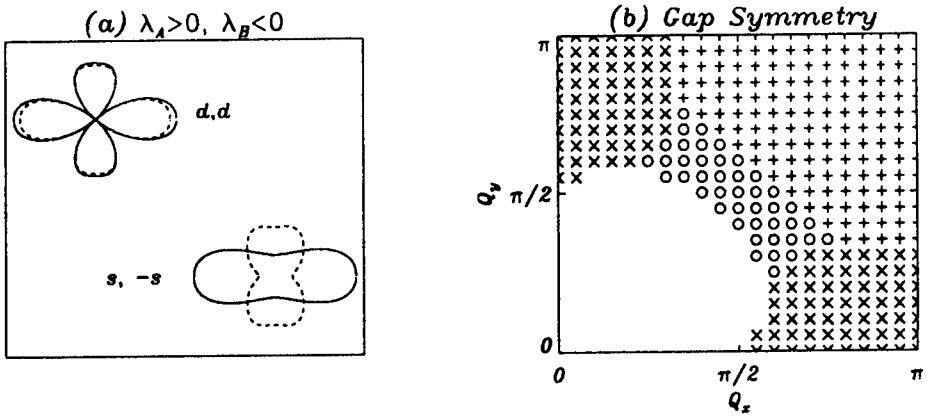


Fig. 1. (a) Superconducting gap for interactions peaked at the antiferromagnetic wave vector, at $\mathbf{Q} = \mathbf{q} - \mathbf{q}' = (\pi, \pi)$; (b) Gap symmetry for generalized pairing potential peaked at $\mathbf{Q}$. (+) represents $d_{x^2-y^2}$, (×) represents d_{xy}, and (○) represents s_{xy} (an extended s-wave).

In summary, by solving the gap equation for bi-layer models with general repulsive interactions, we find that d-symmetry states arise quite generally and are not uniquely associated with wave-vector structure along the antiferromagnetic direction. Moreover, we have established that π phase shift behavior, which is often cited as the strongest evidence for d-wave pairing can also be associated with (orthorhombic) s-symmetry when the two sub-band gaps have opposite phase. This state has some advantages over d-states in large part because of the relatively small sensitivity of T_c to non-magnetic impurities. An important conclusion from our analysis is that there are always competing states in bi-layer systems, and that the order parameter symmetry would be expected to vary from cuprate to cuprate as well as within a given cuprate class at different hole concentrations. One can conclude that the Josephson junction data, in particular, provide strong evidence for superconductivity mediated by some form of repulsive interaction. On the other hand, these collected observations (in bi-layer cuprates) weaken the often cited support for theories of spin fluctuation mediated superconductivity.

Acknowledgements—We acknowledge useful conversations with A. Leggett and P. Wiegmann, and correspondence with V. Emery. This work was supported by the NSF-DMR 91-20000 through the Science and Technology Center.

REFERENCES

1. Wollman D. A. *et al*, *Phys. Rev. Lett.* **71**, 2134 (1993); Kirtley J. R. *et al*, preprint; Mathai A. *et al*, preprint; Brawner D. A. and Ott H. R., *Phys. Rev. B* **50**, 6530 (1994).
2. Liechtenstein A. I., Mazin I. I. and Andersen O. K., preprint.
3. Bulut N., Scalapino D. J. and Scalettar R. T., *Phys. Rev. B* **45**, 5577 (1992).
4. Liu D. Z., Levin K. and Maly J., to be published in *Phys. Rev. B*, April 1995.
5. We do not include any effects of inter-band pairing, which we find are unphysical because they introduce additional transition temperatures.
6. Si Q., Zha Y., Levin K. and Lu J. P., *Phys. Rev. B* **47**, 9055 (1993).
7. Zha Y., Si Q. and Levin K., *Physica C* **212**, 413 (1993).
8. Sun A. G. *et al*, *Phys. Rev. Lett.* **70**, 3999 (1993).

Pergamon

J. Phys. Chem. Solids Vol. 56, No. 12, pp. 1735–1736, 1995
Copyright © 1995 Elsevier Science Ltd
Printed in Great Britain. All rights reserved
0022-3697/95 $9.50 + 0.00

0022-3697(95)00182-4

PHOTOEMISSION: LOW ENERGY AND HIGH ENERGY SCALES

K. MATHO

Centre de Recherches sur les Très Basses Températures, associé à l'Université Joseph Fourier, C.N.R.S., BP 166, 38042 Grenoble-Cédex 9, France

Abstract—The electron removal spectrum and momentum distribution of a many-body system are calculated, combining low energy FL phenomenology and high energy Padé approximants. The influence of non-FL power laws at low energy is also studied.

1. INTRODUCTION

In the ongoing efforts to interprete low energy ARPES signals of strongly correlated materials [1] via the electron removal spectrum of a many-body system, a k-independent self-energy $\Sigma(\omega)$ has so far been employed.

Considerable success in modeling the lineshapes and dispersions is somewhat attenuated by our uncertainty about the nature of the background, which is anomalously strong in the cuprates [2]. Since the background is dispersionless, it may be possible to explain it by $\Sigma(\omega)$.

On surfaces of constant band structure eigenvalue ϵ_k, the Green function is given by:

$$G(k, \omega) = (\omega - \Sigma(\omega) - \epsilon_k)^{-1} = (G(k_F, \omega)^{-1} - \epsilon_k)^{-1}. \quad (1)$$

It is sufficient to model $G(k_F, \omega)$. Assuming a decomposition into a singular part and a background, $G(k_F, \omega) = G_s(\omega) + G_b(\omega)$, the signal away from $k = k_F$ is nevertheless not additive. As shown [3], the lineshape is profoundly influenced by an interference term.

Fermi liquid (FL) models are obtained with $G_s(\omega) = Q^*/\omega$, a simple pole of residue Q^*. The background is then defined as the regular part of the corresponding Laurent expansion of $G(k_F, \omega)$. The quasiparticles (QP) have weight $Z(k_F) = Q^*$, dispersion $\epsilon_k^* = Q^*\epsilon_k$ and damping $\Gamma_k = Q^*\epsilon_k^2 \Im G_b(0) = \epsilon_k^{*2}/\Delta^*$. This defines the energy scale Δ^*, beyond which the QP are overdamped.

In discussions with J. Allen and his collaborators [2], two objectives for possible extensions of this phenomenology have been envisaged:

(i) define a singular part that allows for non-FL power laws [4],

(ii) obtain a physical picture of the background, its weight and structure beyond Δ^*, possibly in relation to microscopic models.

A brief description of progress on these two points is given here.

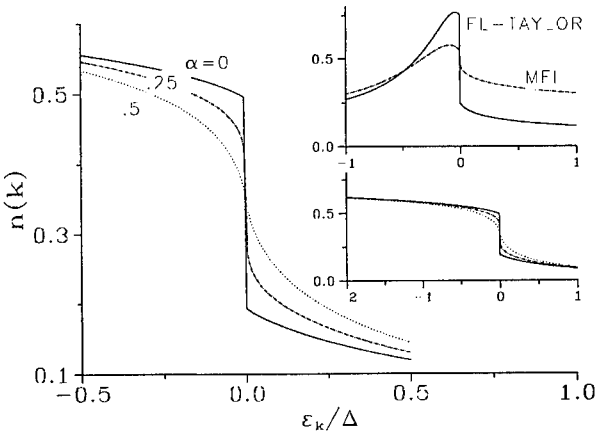


Fig. 1. Momentum distribution as function of bandstructure eigenvalue ϵ_k. The energy scale is $\Delta^{-1} = \Im G_b(0)$. Inserts: same scales; see discussion section. The influence of non-FL exponents α is shown for $Q^* = 0.3$.

2. LOW ENERGY POWER LAW

To model power law behavior [4], we define a self-energy function:

$$\Sigma_s(\omega) = \frac{\omega}{2}\left(1 - \exp\left(\frac{\alpha \ln\left(-(\Delta^*/\omega)^2\right)}{2\,(1 + (\omega/\Delta^*)^2)}\right)\right) \quad (2)$$

with $0 \le \alpha < 1$ and Δ^*, the previous energy scale of the FL. The singular part of $G(k_F, \omega)$ is $G_s(\omega) = Q^*/(\omega - \Sigma_s(\omega))$, with Q^* the previous weight, which loses the meaning of a residue, as soon as $\alpha \neq 0$.

Details leading to this particular "Ansatz" and other possible choices will be discussed elsewhere [5]. Essential requirements are: $\Im\Sigma_s(\omega) \to 0$ for large ω, and the correct analytical properties along the cuts $\Re\omega > 0$ and $\Re\omega < 0$, with $\omega = 0$ as branching point. In the limit $\alpha \ll 1$ (misprinted in [3] as $\alpha \to 1$), eqn (2) reduces to a MFL model [6].

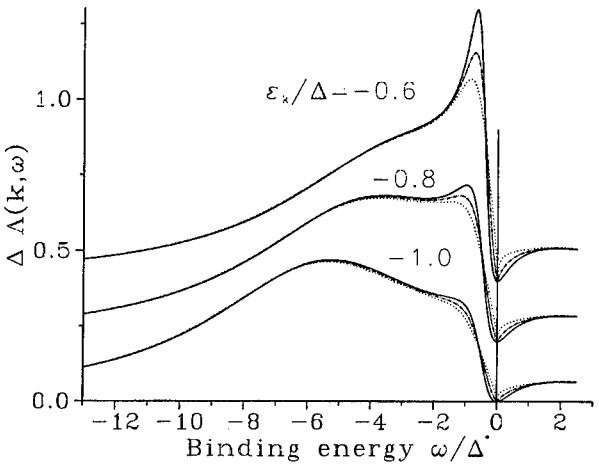


Fig. 2. Momentum resolved spectra for a particle hole symmetric $\Sigma(\omega)$. It is shown, how a QP resonance just emerges from the background, for the given bandstructure input ϵ_k. Scales $\Delta^{-1} = \Im G_b(0)$, $\Delta^* = Q^*\Delta$, $Q^* = 1/6$. Influence of α: Values as in Fig. 1

3. HIGH ENERGY SUMRULES

The high energy behavior can be obtained to a desired accuracy by terminating the continued fraction expansion

$$G(k_F, \omega) = 1/\left(\omega - \omega_1 - S_2^2/(\omega - \omega_3 - S_4^2/\ldots)\right) \quad (3)$$

at sufficiently high level, giving rise to a Padé approximant. Each real coefficient with index n in the expansion involves moments of the spectral function $A(k_F, \omega)$ up to order n. In practice, this becomes tedious beyond the level $n = 3$ [7].

We have used the levels $n = 1$ and $n = 3$, introducing also a phenomenological imaginary part $\Im\omega_n \neq 0$ to take into account the energy independent damping of the background excitations.

The low energy singular part is incorporated by introducing one more phenomenological stage, consisting of complex energies S_{n+1} and ω_{n+2}. These are uniquely determined by the conditions: (i) $\Sigma(0) = 0$; (ii) the singularity has real, positive weight $0 < Q^* < 1$.

A non-FL power law is incorporated by replacing ω by $\Omega = \omega - \Sigma_s(\omega)$, but only in the last stage, if all moments to order n are to be conserved.

The influence of the power law exponent α on the momentum distribution $n(k)$ is shown in Fig. 1, and on the k-resolved spectrum in Fig. 2.

4. DISCUSSION

Figure 1 shows $n(k)$ for a hole doped Hubbard model ($X = 0.3$), assuming $Q^* = X$. Self-consistency is obtained on the Padé level $n = 3$ [5], with input $\Im\omega_3 = 2t$, $U = 40t$ and a $d = 2$ (tight binding) square lattice. A softened step of amplitude Q^* is the characteristic of the non-FL power laws.

The lower insert shows the same result on an expanded scale, stressing the characteristic asymmetry of doped Hubbard models with large U. The correct sign of the dynamical weight transfer [8] is obtained, irrespective of the low energy power law.

The upper insert shows, that previously used self-energies FL-TAYLOR [2] and MFL [2,6] cause the total spectral weight to decay with ϵ_k. This feature, traced to $\Im\Sigma(\omega)$ growing without limitation at large ω, suppresses the background. A proper limitation of $\Im\Sigma(\omega)$ is generated by the Padé approximants.

Figure 2 shows spectra for a particle hole symmetric $\Sigma(\omega)$ with $Q^* = 1/6$ and background generated on the Padé level $n = 1$.

The case $\alpha = 0$ was used for linefits in $TiTe_2$ [1,9]. The chosen values for the bandstructure input correspond to a QP resonance just emerging, for $|\epsilon_k^*|/\Delta^* = |\epsilon_k|/\Delta \leq 1$. The influence of α is still weak. The non-FL power law influences the lineshapes and dispersions more strongly in the regime $|\epsilon_k|/\Delta \ll 1$, not shown here.

Similar spectra for the doped Hubbard model will be discussed elsewhere [5].

REFERENCES

1. Allen J. W. *et al.* this conference, 1995.
2. Liu L.-Z. *et al.*, *J. Phys. Chem. Sol.* **52**, 1473 (1991).
3. Matho K., *Physica B* **199,200**, 382 (1994).
4. Anderson P. W., *Phys. Rev. B* **42**, 2624 (1990).
5. Matho K., to be published.
6. Varma C. M. *et al.*, *Phys. Rev. Lett.* **63**, 1996 (1989).
7. Nolting W. and Borgiel W., *Phys. Rev.* **39**, 6962 (1989).
8. Meinders M. B. J. *et al.*, *Phys. Rev. B* **48**, 3916 (1993).
9. Harm S. *et al.*, *J. Electron Spectroscopy* **68**, 111 (1994).

Pergamon

J. Phys. Chem. Solids Vol. 56, No. 12, pp. 1737–1738, 1995
Copyright © 1995 Elsevier Science Ltd
Printed in Great Britain. All rights reserved
0022-3697/95 $9.50 + 0.00

0022-3697(95)0041-7

NONMAGNETIC IMPURITIES IN HIGH-Tc CUPRATES

NAOTO NAGAOSA* and TAI-KAI NG†

* Department of Applied Physics, University of Tokyo, Tokyo 113, Japan
† Department of Physics, HKUST, Clear Water Bay Road, Kowloon, Hong Kong

Abstract—Recent experiments of the effects of nonmagnetic impurities on the magnetic and transport properties are interpreted in terms of RVB theory with spin-charge separation. A nonmagnetic impurity induces spin 1/2 in the spin gap phase. The residual resistivity shows the classical value of Boltzmann transport theory for the holons not for the electrons in a sharp contrast with the prediction of Fermi liquid theory.

Keywords: RVB, high-Tc cuprates, impurity

The response to the impurities is an important subject in the study of strongly correlated systems, including high-Tc cuprates. Especially the effects of the nonmagnetic impurities, i.e., Zn, replacing Cu in the conducting planes show the following anomalous features in the underdoped region [1–8].

(1) The formation of the magnetic moments due to Zn has been revealed by magnetic susceptibility [1,8], NMR [2–5], μSR [6] and EPR [7], whose number is roughly proportional to the Zn concentration and an almost full moment appears in the underdoped region , i.e., $0.8\mu_B$ in $La_{1.85}Sr_{0.15}Cu_{1-z}Zn_zO_4$ [8] and $0.86\mu_B$ in $YBa_2(Cu_{1-z}Zn_z)_3O_{6.64}$ [5] per Zn ion. The magnitude of the induced local moments is strongly dependent on the hole concentration x and becomes smaller or even vanishes as x increases [5,8].

(2) The residual resistivity can be described in terms of the classical expression in terms of the Boltzmann transport theory [8], i.e.,

$$\rho_{res} = 4(\hbar/e^2)(n_{imp}/n)\sin^2\delta_0 \qquad (1)$$

which is independent of the effective mass of the carriers and is determined only by the phase shift δ_0, the impurity concentration n_{imp} and the carrier density n. It has been found that Zn acts as a strong scatterer at unitary limit, i.e., $\delta_0 = \pi/2$. The interesting thing is that the carrier number n is the hole concentration x in the underdoped region, and rather rapidly crosses over to the electron number $1 - x$ in the overdoped region.

In this paper we give an interpretation of these two aspects in a unified way from the standpoint of the RVB theories.

In the slave boson fromalism, the spin is represented by fermions (spinons) while the holons are bosons. In the underdoped region above Tc, the mean field theory predicts the so called spin gap state where the spinon pairing occurs while the holons are not condensed [9]. Although the total system is not superconducting, the spinon system is superconducting and the transport properties are determined by the holon according to Ioffe–Larkin law [9]. Therefore the residual resistivity ρ_{res} is that of the holon, and determined by the holon concentration x. Actually the criterion for the validity of Boltzmann expression eqn (1) is that the sheet conductance is much larger than the quantum conductance e^2/h, which is satisfied for the Zn concentration we are now interested in. Therefore it is reasonable that the holons which are not superconductive or localized give the observed resistivity.

However it may appear difficult to explain the localized moment because the kinetic energy of the spinon is larger than that of holons and more robust against localization. Also the Ioffe–Larkin law tells that the spinon resistivity will dominate if the states near the Fermi energy are localized and spinon system is insulating. Actually these two dilemma can be simultaneously resolved by the spinon pairing with d-wave symmetry. In the case of d-wave pair, the density of states for the quasi-particle is reduced near the Fermi energy as $D(E) \propto |E - E_F|$, which favors the localization. This is compared with the boson density of states which is constant even near the bottom of the band in two-dimensions.

This problem has been already analyzed by Lee in the context of localized states in d-wave superconductos. The strong scatterer considered in this paper corresponds to his model II [10]. In this model the self-energy $\Sigma(\omega)$ is determined self-consistently by $\Sigma(\omega) = -\Gamma/g_0(\omega)$, where $\Gamma = n_{imp}/(\pi\rho_0)$, $g_0(\omega) = 4/(\pi\rho_0)\sum_k G(k,\omega)$. ($n_{imp}$ is the density of the nonmagnetic impurities per area, and ρ_0 is the density of states in the normal state in the absence of the d-wave pairing.) The imaginary part γ_0 of the self-energy near the Fermi level is obtained by solving $\gamma_0 = -\frac{\Gamma}{g_0(\gamma_0)}$. In the scaling theory of localization, the localization length l_{loc}

is estimated to be $l_{loc} \sim l \exp(k_F l)$ with l being the elastic mean free path. l is estimated from the classical conductance and hence the imaginary part of the self-energy $\gamma(\omega)$, which behaves as $\gamma_\omega \cong \gamma_0$ for $|\omega| < \gamma_0$ while $\gamma(\omega) \cong \gamma_0^2/\omega$ for $|\omega| > \gamma_0$. Therefore it can be considered that the states within the region $|\omega| < \gamma_0$ are strongly localized. The density of these strongly localized states n_{loc} per area is estimated as the density of states for this energy region $-\pi\rho_0 g_0(\gamma_0)$ times the energy interval γ_0, and we obtain $n_{loc} \cong -\pi\gamma_0\rho_0 g_0(\gamma_0) = \pi\rho_0\Gamma = n_{imp}$. Now we have shown that the number of strongly localized states roughly coincides with the number of nonmagnetic impurities. When the repulsive interaction between the fermions are again taken into account, it is expected that these localized states near the fermi level are singly occupied and give rise to the Curie moments proportional to the impurity density. When the states of the quasi particle not the spinon itself are localized, the spinon system still remains superconducting and its resistivity is zero. Hence the total resistivity is still determined by the holons, and the conclusion on the resistivity above remains unchanged.

Let us now turn to the slave-fermion theory. In the spin gap phase, it has been shown that the low-energy dynamics of the spin system can be described by an effective Lagrangian of charged $S = 1/2$ bosons (spinons) coupled to U(1) gauge field [11],

$$L_{eff} = |(\partial_\mu - iA_\mu)Z|^2 + m^2|Z|^2 + \frac{1}{e^2}F_{\mu\nu}^2 + 2SA_0 e_{ij} n_{ij}^I, \quad (2)$$

where $Z^\dagger = (Z_\uparrow^*, Z_\downarrow^*)$ is a two component $S = 1/2$ spinor field carrying unit gauge charge, $F_{\mu\nu} = \partial_\mu A_\nu - \partial_\nu A_\mu$ is the usual U(1) gauge field, and A_0 is the scalar potential in the Coulomb gauge. Moreover, it can be shown that $e^2 \sim m^2$ in 1D and $e^2 \sim m$ in 2D. It is important to distinguish between the "uniform" and "staggered" gauge fields in the slave-fermion approach. The "uniform" gauge symmetry is broken because of the existence of non-zero order parameter, whereas the "staggered" gauge symmetry remains unbroken. The low energy dynamics of the system is dominated by the "staggered" gauge field, described by the effective Lagrangian eqn (2) [11]. For this reason $e_{ij} = +(-)1$ for impurities living on $A(B)$ sublattices.

In 2D the electrostatic potential $V(r) \sim e^2 \ln(r/\xi)$ ($\xi \sim m^{-1}$ is the coherence length) is induced by the nonmagnetic impurity. Hence $2S$ bosons or local moment of magnitude S is expected to be confined around an non-magnetic impurity giving rise to Curie–Weiss behaviour in spin-susceptibility.

For finite concentration of impurities the discussion has to be more careful. Notice that a finite amount of energy $\sim m$ is needed to nucleate one boson. Thus for finite concentration of impurities δ, the total energy of the system has to be considered to see whether it is energetically favourable to bind bosons to impurities. The electrostatic energy gained by nucleating bosons to screen the impurities is of order $(2Se)^2\delta(\ln(l/\xi) - \ln(l_o/\xi))$ where $l \sim \delta^{-1/2}$ is the average distance between non-magnetic impurities and $l_o \sim \xi$ is the typical "size" of a spinon. Thus the total energy required to nucleate bosons to screen the impurities is of order $2S\delta(m - 2Se^2\ln(l/\xi))$. Notice that in 2D $e^2 \sim m$. Thus for $S = 1/2$ the two terms are of comparable magnitude when $l \sim \xi$, implying that local moments are formed only when the concentration of non-magnetic impurities is small, and will be quenched when density of impurities is large enough, in general agreement with experimental observation.

In the doped case the spinless fermion represests a holon which is coupled with the gauge field. In the spin-gap phase, the spinons are "superconducting" with respect to the *uniform* gauge field. Thus the physically observable resistivity is determined by that of the holons which describe a spinless fermi gas with density of holes δ, giving rise naturally to ρ_{res} of form discussed in the introduction.

In summary the anomalous features in the effects of nonmagnetic impurities in high-Tc cuprates can be consistently explained in terms of RVB theories although the statistics of spinons and holons can not be uniquely dictated [12].

Acknowledgements—One of the authors (N. Nagaosa) acknowledges Professors S. Uchida, Y. Kitaoka, H. Takagi and Dr M. Sigrist for fruitful discussions. This work is supported by Grant-in-Aid for Scientific Research No. 05044037, No. 04240103, and No. 04231105 from the Ministry of Education, Science, and Culture of Japan.

REFERENCES

1. Xiao G., Cieplak M. Z., Xiao J. Q. and Chien C. L., *Phys. Rev. B* **35**, * * * page nos (year). * * *
2. Alloul H. *et al.*, *Phys. Rev. Lett.* **67**, 3140 (1991).
3. Zheng G. *et al.*, *J. Phys. Soc. Jpn* **62**, 2591 (1993).
4. Ishida K. *et al.*, *J. Phys. Soc. Jpn* **62**, 2803 (1993).
5. Mahajan A. V., Alloul H., Collins G. and Marucco J. F., *Phys. Rev. Lett.* **72**, 3100 (1994).
6. Mendels P. *et al.*, *Phys. Rev. B* **49**, 10035 (1994).
7. Finkelstein A. M., Kataev V. E., Kukovitskii E. F. and Teitel'baum G. B., *Physica C* **168**, 370 (1990).
8. Uchida S., unpublished.
9. Lee P. A. and Nagaosa N., *Phys. Rev. B* **46**, 5621 (1992).
10. Lee P. A., *Phys. Rev. Lett.* **71**, 1887 (1993).
11. Read N. and Sachdev S., *Phys. Rev. Lett.* **62**, 1694 (1989).
12. Nagaosa N. and Ng T. K., *Phys. Rev. B* **51**, 15588 (1995).

Pergamon

J. Phys. Chem. Solids Vol. 56, No. 12, pp. 1739–1740, 1995
Copyright © 1995 Elsevier Science Ltd
Printed in Great Britain. All rights reserved
0022–3697/95 $9.50 + 0.00

0022–3697(95)00212-X

SUPERCONDUCTIVE PHONON ANOMALIES IN HIGH-T_c CUPRATES

B. NORMAND, H. KOHNO and H. FUKUYAMA
Dept. of Physics, University of Tokyo, 7-3-1 Hongo, Bunkyo-ku, Tokyo 113, Japan

Abstract—We consider the effects of spin–phonon coupling within the slave-boson mean-field treatment of the extended t–J model. With no additional assumptions the theory gives a semi-quantitative account of the frequency and linewidth anomalies of certain phonon modes in $YBa_2Cu_3O_7$ at the superconducting transition. It contains also a good correspondence with observed spin-gap behaviour and isotope effect measurements.

Anomalies have been observed in both normal and superconducting states of high-T_c materials, not only in transport and magnetic properties but also in the frequency and linewidth of phonons around the superconducting transition. Many other studies provide evidence of a link between lattice anomalies and superconductivity, and we seek a possible unified basis for all of these low-lying excitations.

We consider the spin-phonon coupling arising within the extended t–J model, a theory shown [1,2] at the mean-field level to give a good account of many features of the spin excitations in both LSCO- and YBCO-type high-T_c systems; the transport properties may be described by treating fluctuations about this solution by a gauge-field formalism [3]. The Hamiltonian is

$$H = -\sum_{ij} t_{ij} a_{is}^{\dagger} a_{js} + \sum_{\langle ij \rangle} J_{ij} \mathbf{S}_i . \mathbf{S}_j, \qquad (1)$$

where the transfer integrals t_{ij} and superexchange interaction J_{ij} have been taken as a constant in previous treatments. However, in the presence of buckling of the CuO_2 layer, by which is meant that the oxygen atoms O(2) and O(3) lie out of the plane of the Cu atoms, as in YBCO, t_{ij} and J_{ij} have contributions linear in the magnitude of the oxygen displacement along the c-axis, u_i^{α}, given by $t_{i,i+\alpha} = t[1 - \lambda_t(u_{ij}^{\alpha}/a)]$, where a is the lattice constant, and similarly for J with coupling λ_J. The coupling constants may be estimated microscopically [4], and are found to be large, $\lambda_J = 2\lambda_t = 5.6$. While the degree of buckling is small, $u_0/a \ll 1$, its inclusion is crucial in providing an interaction which is strong and linear. Both terms in H (1) then contribute to a coupling of the phonon coordinate u_i^{α} to the spin degrees of freedom.

The effect of the coupling on phonon dynamical properties is calculated from the frequency shift and linewidth broadening due to the lowest-order spinon correction to the phonon self-energy Π_{sp}. We examine primarily the 340 cm^{-1} B_{1g} mode observed in $YBa_2Cu_3O_7$, which is an out-of-phase, c-axis oscillation of only the planar oxygen atoms. This mode has attracted experimental interest because it shows the largest effects at the superconducting transition,

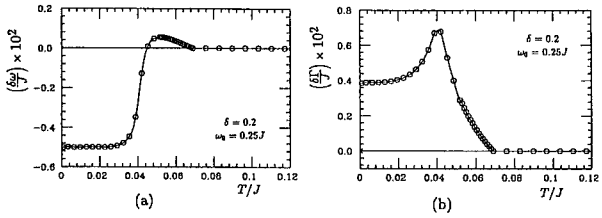


Fig. 1. Frequency shift (a) and linewidth (b) corrections of B_{1g} phonon mode as a function of temperature, for bare phonon frequency $\omega_0 = 0.25J$.

and there are available detailed Raman [5] ($q = 0$) and inelastic neutron scattering [6,7] (all q) results.

Second-order perturbation theory in terms of λ results in a frequency shift $\delta\omega = \mathrm{Re}\,\Pi_{sp}$ for $|\mathrm{Re}\,\Pi_{sp}| \ll \omega_0$, which is given at $q = 0$ by

$$\delta\omega = c\,(\lambda_J J)^2 \frac{4}{N} \sum_k B_k \frac{1}{\omega^2 - (2E_k)^2} \frac{\tanh\left(\frac{E_k}{2T}\right)}{E_k}, \qquad (2)$$

where $c = \left(\frac{3}{4a}\right)^2 \langle \delta u^2 \rangle = 1.18 \times 10^{-4}$, $\langle \delta u^2 \rangle = \frac{\hbar}{2M\omega_0} = (0.055\text{Å})^2$, with $\omega_0 = 340$ cm^{-1} the phonon frequency of interest and M the mass of the O atom, $E_k = [\xi_k^2 + \Delta_k^2]^{1/2}$ is the spinon dispersion and B_k is a form factor which depends on temperature, through the mean-field parameters [1], and on both mode and gap symmetry. Details of this calculation are given in Ref. [4].

The T-dependence of $\delta\omega$ is shown in Fig. 1(a) for $q = 0$ and frequency $\omega_0/J = 0.25$, close to that of the $340cm^{-1}$ B_{1g} mode. When the mode frequency is close to a characteristic value given by $\mathrm{Max}[2\Delta_k(T = 0)]$, the shift in frequency occurs at a temperature somewhat below T_c . This corresponds well to the observed form [5,8], where the full frequency shift develops over a range of T below the onset. By contrast, when the mode frequency is considerably less than this value, we find a sharp change near T_c , in good agreement with measurements performed on the 193 cm^{-1} B_{2u} mode [7]. The superconductivity-induced correction to the linewidth Γ is computed similarly from $\mathrm{Im}\,\Pi_{sp}$ [Fig. 1(b)].

Comparison with the experimental result [5] for the B_{1g} mode again shows a good agreement in sign and magnitude ($\delta\omega \simeq \delta\Gamma \simeq 0.01\omega_0$).

The strong anomaly in the 340 cm^{-1} mode is consistent only with predominantly $d_{x^2-y^2}$-wave singlet pairing for the gap Δ_k, while the effect is negligibly small for extended-s gap symmetry. The anomalies will be suppressed in the E-symmetric Raman-active modes, where O displacements are parallel to the plane and so have a very small effect on t and J, as also observed. However, we caution against applying the model to infrared-active modes, as it does not contain the charge fluctuations in the CuO_2 plane which can be expected to accompany these.

The phase diagram of the mean-field t–J model [1] shows a distinction between high- and low-doping regimes, since spin singlet formation and superconductivity do not coincide in the latter. This is consistent with the observation in NMR studies of different characteristic temperature scales, interpreted as a spin gap, only in the low-doping region. In the current model, phonon anomalies are connected to spin singlet formation, and the same scenario is envisaged; this picture is corroborated by recent, highly accurate Raman studies of underdoped YBCO compounds [8], which indeed show the anomalous features developing at temperatures well above T_c .

Finally, while the mechanism of superconductivity in this model is purely electronic, a spin-phonon coupling affords the possibility of an isotope effect. This may be estimated by considering the $O(\Delta^2)$ contributions of the lowest-order phonon-spinon term in the Ginzburg-Landau free energy, computed at the transition temperature. Near optimal doping, this leads to a small ($\sim$ 1%) enhancement in T_c , on which the oxygen isotope effect is approximately -0.1K. This result is in reasonable agreement with a recent experimental determination by Zech *et al.* [9], who also discovered that the primary contributions came from phonon modes of the in-plane O atoms, as predicted by the present model.

In summary, we have proposed a theory of spin–phonon coupling which accounts well for the anomalies observed in some phonon modes in typical high-T_c cuprates of the YBCO class, and gives also qualitative agreement with modes in other classes, with observed spin-gap behaviour and with isotope effect measurements. We believe that this model is a useful step in constructing a coherent theory of the spin, transport and lattice properties in high-T_c superconductors.

REFERENCES

1. Tanamoto T., Kohno H. and Fukuyama H., *J. Phys. Soc. Jpn* **62**, 717 (1993).
2. Tanamoto T., Kohno H. and Fukuyama H., *J. Phys. Soc. Jpn* **63**, 2741 (1994).
3. Lee P. A. and Nagaosa N., *Phys. Rev. B* **46**, 5621 (1992).
4. Normand B., Kohno H. and Fukuyama H., *Phys. Rev. B*, to appear.
5. Altendorf E. *et al.*, *Phys. Rev. B* **47**, 8140 (1993).
6. Pyka N. *et al.*, *Phys. Rev. Lett.* **70**, 1457 (1993).
7. Harashina H. *et al.*, *J. Phys. Soc. Jpn* **64**, 1462 (1995).
8. Käll M. *et al.*, *Physica C* **225**, 317 (1994).
9. Zech D. *et al.*, *Nature* **371**, 681 (1994).

Pergamon

J. Phys. Chem. Solids Vol. 56, No. 12, p. 1741, 1995
Copyright © 1995 Elsevier Science Ltd
Printed in Great Britain. All rights reserved
0022-3697/95 $9.50 + 0.00

0022-3697(95)00213-8

HOLE POCKETS, SHADOW BANDS AND SPIN BAGS IN THE DOPED t–J MODEL

Y. OHTA * and R. EDER †

* Department of Applied Physics, Nagoya University, Nagoya 464-01, Japan
† Laboratory of Applied and Solid State Physics, University of Groningen, Nijenborgh 4, 9747 AG Groningen, The Netherlands

Abstract—The spin-bag liquid scenario derived from numerical studies of the two-dimensional t-J model is presented for describing anomalous low-energy electronic states of cuprate high-temperature superconducting materials.

A detailed exact-diagonalization study is made for the doping dependence of the single-particle spectral function $A(\mathbf{k}, \omega)$ and momentum distribution function $n(\mathbf{k})$ of the two-dimensional t-J model as a representative model for doped Mott insulators including cuprate superconductors. The results for $A(\mathbf{k}, \omega)$ show that the rigid-band behavior is realized in the small-cluster t-J model [1,2]: upon doping, the uppermost states of the quasiparticle band observed at half filling cross the Fermi level and reappear as the lowermost states of the inverse photoemission spectrum, while the photoemission side of the band remains essentially unaffected. We next discuss problems in directly determining the Fermi surface from $n(\mathbf{k})$ and study a situation where they are largely avoided; we then find clear signatures of a Fermi surface which takes the form of small hole pockets [3]. The identical scaling with t/J of the quasiparticle weight Z_h and difference in $n(\mathbf{k})$ between neighboring $\mathbf{k}$-points suggests the existence of such a Fermi surface in the physical regime of parameters [3]. In a last step we construct spin-bag operators which describe holes dressed by the antiferromagnetic spin fluctuations and find that the elementary electronic excitations of the system can be described well in terms of weakly-interacting spin-1/2 Fermionic quasiparticles corresponding to the doped holes [4]. We make a comparison with other numerical calculations and recent angle-resolved photoemission experiment and argue that, adopting this rather conventional Fermi-liquid scenario with non-Luttinger Fermi surface, one would explain many quasiparticle-relating properties of doped cuprates in a very simple and natural way [2–5].

The dynamical spin correlation function (SCF) and density correlation function (DCF) are also studied [6–8]. We find [7] that for hole densities $\rho_h > 0.3$ the ground state of the model represents a fairly conventional Fermi liquid with a particle-hole like spin and density excitation spectrum. We show [6, 8] however that they differ drastically for the strong-correlation regime at $\rho_h \leq 0.25$: the DCF has a Boson-like dependence on the hole density and the hopping integral t as its characteristic energy scale, whereas the doping dependence of SCF is consistent with Fermions and it has the exchange constant J as energy scale. While the remarkably systematic scaling of the correlation functions suggests the existence of a simple 'effective theory' for the excitation spectrum, the particle-hole picture thus is clearly insufficient. We then show that the familiar spin-bag picture provides a promising framework for such an effective theory: the strong dressing of the hole with spin fluctuations and the resulting complex internal structure of the spin-bag-type quasiparticles lead to a qualitatively new type of excitations, namely the excitation of internal degrees of freedom of the quasiparticles. Spin and density operator differ markedly in their ability to excite the various degrees of freedom of the spin bag liquid, hence their very different spectra. It seems obvious that the existence of such new types of excitations, as well as the apparently very different response of the spin-bag liquid to 'spin-like' and 'charge-like' perturbations may lead to experimentally observable anomalies in high-temperature superconductors.

Acknowledgements—We would like to thank Professor S. Maekawa for valuable discussions. R. E. acknowledges financial support by the Japan Society for Promotion of Science.

REFERENCES

1. Eder R. and Ohta Y., *Phys. Rev. Lett.* **72**, 2816 (1994).
2. Eder R., Ohta Y. and Shimozato T., *Phys. Rev. B* **50**, 3350 (1994).
3. Eder R. and Ohta Y., *Phys. Rev. B*, **51**, 6041 (1995). (also: cond-mat #9407097).
4. Eder R. and Ohta Y., *Phys. Rev. B* **50**, 10043 (1994).
5. Ohta Y. and Eder R., *Proc. 17th Taniguchi Symposium "Spectroscopy of Mott Insulators and Correlated Metals"* (Edited by A. Fujimori and Y. Tokura). Solid-State Science Series, Springer-Verlag, 1995); also: cond-mat #9411010.
6. Eder R. and Ohta Y., *Phys. Rev. B*, in press (1995); also: cond-mat #9408057.
7. Eder R. and Ohta Y., *Phys. Rev. B* **51**, 11683 (1995).
8. Eder R., Ohta Y. and Maekawa S., *Phys. Rev. Lett.* **74**, 5124 (1995).

Pergamon

J. Phys. Chem. Solids Vol. 56, No. 12, pp. 1743–1744, 1995
Copyright © 1995 Elsevier Science Ltd
Printed in Great Britain. All rights reserved
0022–3697/95 $9.50 + 0.00

0022–3697(95)00100-X

EVIDENCE FOR $d_{x^2-y^2}$ SYMMETRY OF SUPERCONDUCTING ORDER PARAMETER IN YBCO FROM NEUTRON SCATTERING DATA

F. ONUFRIEVA
Laboratoire Léon Brillouin, CEA-CNRS CE Saclay, 91191 Gif-sur-Yvette cedex, France

Abstract—It is shown that the experimental results on inelastic neutron scattering for $YBa_2Cu_3O_{7-\nu}$ rule out a possibility of extended s-wave symmetry of superconducting pairing being, on the contrary, in a good agreement with the $d_{x^2-y^2}$ symmetry.

Recent discussions of mechanism of high-$T_c$superconductivity in cuprates have concentrated on symmetry of superconducting order parameter (OP). Almost all experiments favour a superconductivity of d-wave or extended s-wave symmetry. It is extremely difficult, however, to distinguish between the latter two: in both cases the electronic spectrum is characterized by nodes in **q**-space and therefore both give power-law dependences of density of states, a power-law low-temperature variation of thermodynamical functions, of NMR relaxation rates, etc. Moreover, in both cases the sign of the OP changes on Fermi surface when the latter has the shape observed experimentally for bilayer cuprates [1,2]. Due to the latter reason, very recent Josephson junction experiments [3,4], in which a change of the sign of superconducting (SC) OP have been discovered, also rule out all possibilities except the two mentioned.

It is shown in this paper that a measuring of dynamic spin susceptibility allows one to distinguish between the two types of symmetry rather easily and that the recent inelastic neutron scattering (INS) data for $YBa_2Cu_3O_{7-\nu}$ ($\nu \approx 0$) [5–7] rule out the extended s-wave symmetry being, on the contrary, in a good agreement with the $d_{x^2-y^2}$ symmetry.

Analysis based on the theory [8] in which the dynamic spin susceptibility is given by Larkin equation, $\chi(\mathbf{k}, \omega) = \Sigma(\mathbf{k}, \omega)/(1 + J_k\Sigma(\mathbf{k}, \omega))$, with two contributions to the irreducible part, $\Sigma(\mathbf{k}, \omega)$. The first one, a "localized" contribution, arises from the subsystem of localized on Cu spins and is sensitive to the symmetry of short-range (SR) AF correlations. The second one, an itinerant contribution, arises from the subsystem of propagating carrier quasiparticles, has a BCS structure and is sensitive to the shape of Fermi surface (FS) and to the symmetry of SC OP. This theory has allowed us to understand many exotic features observed experimentally for $YBa_2Cu_3O_{7-\nu}$in the underdoped regime.

For the overdoped regime ($\nu \approx 0$) the situation is much simpler. The dynamic "localized" contribution related to SR AF correlations becomes negligible. The static "localized" term, $S = \delta(\omega)C(T)/T$, describing a response of noninteracting spins, remains but has no influence on the spin dynamics. In fact, for this regime theory, developed in a strong-coupling limit[9] and in a weak-coupling limit [10], give almost the same expression for the spin susceptibility: the "RPA" expression with BCS structure of "zero susceptibility" $\Sigma(\mathbf{k}, \omega)$. The explicit form of the latter depends on the shape of FS and on the symmetry of SC order parameter.

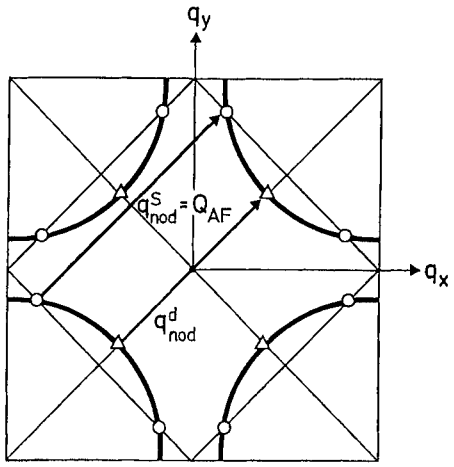


Fig. 1. Schematic plot of Fermi surface for $YBa_2Cu_3O_7$ in the metallic state. The points shown as triangles correspond to nodes in the case of d-wave symmetry, $\Delta^d_q = \Delta_0(\cos q_x - \cos q_y)$, and those shown as circles to these of extended s-wave one, $\Delta^S_q = \Delta_0(\cos q_x + \cos q_y)$. Nodal wavevectors, $\mathbf{k}_{nod}$, for which $\mathrm{Im}\chi$ is a gapless function are shown as well for both symmetries.

The features of crucial importance, which allow the two symmetries to be distinguished, are demonstrated in Fig.1 where I plot schematically a FS of the shape typical for bilayer-cuprates and show the nodes for each type of symmetry. Being, roughly speaking, two-particle density of states, $\mathrm{Im}\Sigma(\mathbf{k}, \omega)$ exhibits a low-energy gap (resulting from the SC gap in one-particle spectrum), for all wavevectors except "nodal" wavevectors, $\mathbf{k}_{nod}$, which join two nodes. For the case of (1,1) direction corresponding to measurements in [5–7], these wavevectors, $\mathbf{k}^S_{nod}$ and $\mathbf{k}^d_{nod}$, are shown in Fig. 1. The crucial point is that *for the extended s-wave symmetry*

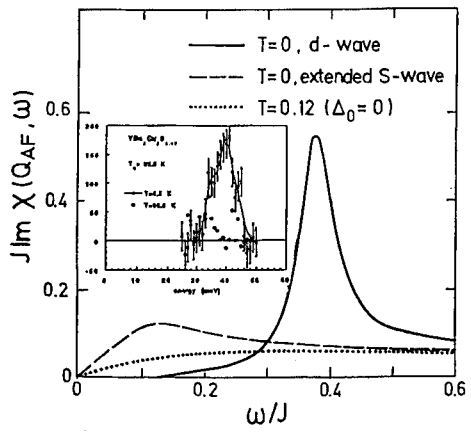


Fig. 2. Imaginary part of spin susceptibility for two considered symmetries of SC gap for T below and above T_c. In the insert the INS data from [5] are shown. When calculating we use parameters: $t/J = 1.8$, $t'/t = -0.45$, $\Delta_0/J = 0.1$.

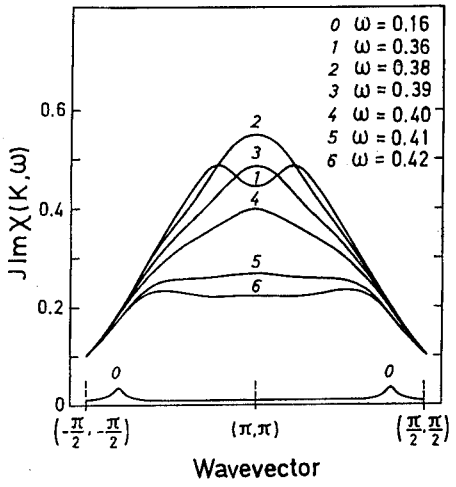


Fig. 3. Momentum dependence of Imχ(**k**, ω) for different energies.

and given shape of FS this *nodal wavevector coincides with* $\mathbf{Q}_{AF}$, $\mathbf{k}^S_{nod} = Q_{AF}$. It means that Im($\mathbf{Q}_{AF}$, ω) is a gapless function whose shape does not depend on the value of the superconducting gap. On the contrary, for the d-wave symmetry, ImΣ(**k**, ω) exhibits a largest gap just for $\mathbf{k} = \mathbf{Q}_{AF}$. (Its value is given by $\Delta^d(\mathbf{Q}_{AF}) = 2\Delta_0\sqrt{|\mu/t'|}$ where Δ_0 is an amplitude of SC gap, μ is a chemical potential, t' is a hopping between next nearest neighbours.) In addition there is a sharp peak in ImΣ($\mathbf{Q}_{AF}$, ω) in the case of d-wave symmetry. These features result in deadly different behaviour of Imχ($\mathbf{Q}_{AF}$, ω) for these two cases, see Fig. 2. The main features in the superconducting state are the resonance peak and the gap for the case of d-wave symmetry and the gapless smooth shape for the case of extended s-wave one. A second important feature is the strong difference in the shape and intensity below and above $T_c$in the case of d-wave symmetry and almost unchanged shape in the case of extended s-wave symmetry. I would like to emphasize that the peculiarities concerning the s-wave case do not depend on values of parameters used in the calculations.

The above discussed dynamic spin susceptibility is a quantity directly measured by INS. Recent INS experiments for $YBa_2Cu_3O_{7-\nu}$ ($\nu \approx 0$) have discovered that the imaginary part of the spin susceptibility is peaked at $\mathbf{Q}_{AF}$ and that Imχ($\mathbf{Q}_{AF}$, ω) as a function of ω below $T_c$has a single-peak structure and exhibits a gap [5,6] or pseudogap [7]. Both the peak and the gap disappear above T_c, Imχ($\mathbf{Q}_{AF}$, ω) becomes a smooth function of ω with intensity eight to ten times weaker than at low temperature. (The data from [5] are shown in the insert of Fig. 2.) All these features are absolutely inconsistent with the extended s-wave symmetry. (I would like to emphasize again that the normal-metal structure of Imχ($\mathbf{Q}_{AF}$, ω) in the superconducting state in the case of latter symmetry is the effect which is related only to interplay of the shape of FS and of the symmetry of SC gap but not on details of calculations.) On the contrary, in the case of d-wave symmetry the theoretical results are in a good agreement with INS data. It concerns the following points: (i) the existence of the gap (or pseudogap) and of the resonance peak below T_c, (ii) the disappearance of both above T_c(iii) negligibly small intensity above T_c, (iv) the **k**-dependence of Imχ peaked at $\mathbf{Q}_{AF}$ for ω close to resonance peak, see Fig. 3. The only difference is that for lowest energies the theoretical Imχ is peaked at $\mathbf{k} = \mathbf{k}^d_{nod}$, that is not observed experimentally. However, the intensity at these energies is so small that it hardly can be detectable by INS.

Summarizing, the d-wave symmetry of the superconducting order parameter is strongly supported by INS data for YBCO. What is more remarkable, the extended s-wave symmetry can be ruled out, being absolutely inconsistent with the results of neutron scattering. Since only these two candidates remain after precise recent measurements of Josephson junctions, one can conclude that the symmetry of the superconducting order parameter in the overdoped YBCO is $d_{x^2-y^2}$. One can also extend this statement to the whole doping range corresponding to the heavily doped regime in YBCO because of the existence of the gap and of the resonance peak in Imχ(**k**, ω) observed by INS below T_c[11]. The situation for the weakly-doped regime is not so clear, for the gap observed experimentally is small and the resonance peak is less pronounced.

REFERENCES

1. Liu R. *et al.*, *Phys. Rev. B* **46**, 11056 (1992).
2. King D. M. *et al.*, *Phys. Rev. Lett.* **73**, 3298 (1994).
3. Kirtley J. R. *et al.*, *Nature* **373**, 225 (1995).
4. Wollman D. A. *et al.*, *Phys. Rev. Lett.* **74**, 797 (1995)
5. Bourges P. *et al.*, *Phys. Rev. B* to be published (1995).
6. Hung Fai Fong *et al.*, *Phys. Rev. Lett.* **75**, 316 (1995).
7. Mook H. A. *et al.*, *Phys. Rev. Lett.* **70**, 3490 (1993).
8. Onufrieva F. and Rossat-Mignod J., *Phys. Rev. B* **52**, 7572 (1995).
9. Si Q. *et al.*, *Phys. Rev. B* **47**, 9055 (1993).
10. Bulut N. and Scalapino D. J., *Phys. Rev. B* **47**, 3419 (1993).
11. Rossat-Mignod J. *et al.*, *Physica C* **185–189**, 86 (1991).

Pergamon

J. Phys. Chem. Solids Vol. 56, No. 12, pp. 1745–1746, 1995
Copyright © 1995 Elsevier Science Ltd
Printed in Great Britain. All rights reserved
0022-3697/95 $9.50 + 0.00

0022-3697(95)00239-1

ISOTOPE EFFECT IN SPIN FLUCTUATION MODELS

C.-H. PAO and H.-B. SCHÜTTLER
Center for Simulational Physics, Department of Physics, University of Georgia, Athens, GA 30602, U.S.A.

Abstract—We have studied the *d*-wave superconducting transition temperature T_c and the isotope effect in the spin fluctuation models. We found that the isotope exponent α is at least one order order of magnitude smaller than typical observed values in the cuprates with models coupling to *harmonic* phonon degrees of freedom and reasonable limits on coupling strength and phonon spectra. Models with coupling to non-linear tunneling modes in a strongly *anharmonic* multi-well lattice potential and realistic coupling strengths have effectively larger isotopic mass dependences and *may* therefore account for the observed magnitudes of α.

Experimental evidence currently suggests that cuprates superconductors exhibit a $d_{x^2-y^2}$ pairing state, supporting antiferromagnetic (AF) spin fluctuation exchange models. However, away from "optimal" doping, the cuprates also exhibit a noticeable isotope effect [1], which reflects the electrons' coupling to the lattice degrees of freedom.

Based on recently proposed AF spin fluctuations models [2,3], we show here that the observed *order of magnitude* of the isotope exponent $\alpha \equiv -\mathrm{d}\log(T_c)/\mathrm{d}\log(M)$ does imply a large electron–phonon (EP) coupling parameter λ. For reasonable coupling strength to harmonic phonons, α is an order of magnitude less than the observed values. However, EP coupling to local large-amplitude lattice tunneling excitations in an anharmonic multiple-well lattice potential provides possible explanation to the experimental data.

Assuming a single electron tight binding band structure model with 1st and 2nd neighbor hopping t (= 250meV) and t' (= -0.45t), we solve the full **k**– and ω–dependent Migdal–Eliashberg equations. The effective electron–electron interaction potential V_{eff} includes a spin-fluctuation potential V_s, given by the phenomenological model proposed by Monthoux and Pines (MP) [3], and a phonon contribution $V_p(\mathbf{q}, i\nu_m) = -U_p\Omega_q^2/(\nu_m^2 + \Omega_q^2)$, assuming a single electron phonon branch with an energy dispersion Ω_q. $U_p/8t$ provides an estimate for the dimensionless Eliashberg parameter λ.

In Fig. 1, we show results for the d–wave superconducting transition temperature and its isotope exponent as a function of U_p for coupling to Einstein phonons with $\Omega_q \equiv \Omega_0$ = constant and assumed isotopic mass dependence $\Omega_0 \propto M^{-1/2}$. Unless otherwise stated in Fig. 1 we have used Ω_0 = 50 meV and the T–independent spin fluctuation parameters from Table II of Ref. [3] with spin fluctuation coupling constant g_s = 640 meV and electron concentration n = 0.75. The d–wave transition temperatures are significantly suppressed by the EP coupling U_p but the isotope exponent remains small even for unphysically large U_p. Because structural stability considerations and experimental resistivity data in the doped system limit U_p less than 1 eV [4], the isotope exponent is limited to $|\alpha| \leq 0.1$ in the harmonic phonon model.

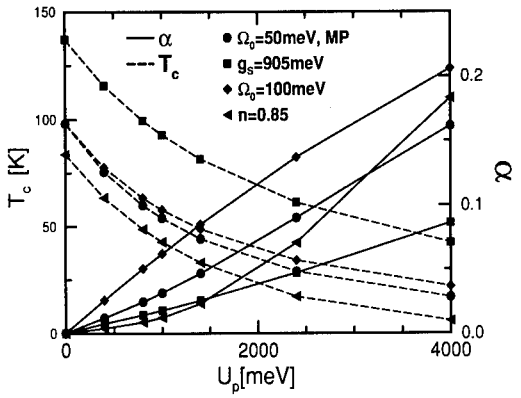


Fig. 1. d–wave transition temperature and isotope exponents in the MP model [3], vs. U_p for coupling to Einstein phonons.

Figure 2 shows α plotted vs. T_c both for the MP model and for Hubbard model, treated in the fluctuation exchange approximations, with T_c varied by increasing the EP coupling strength. In the Hubbard calculation we are thus explicitly taking into account the renormalizations of the spin fluctuations due to the presence of the phonons [2]. Again we find α limited to $|\alpha| < 0.1$ for coupling to harmonic phonons with $U_p < 1$ eV. This is much smaller than typical experimental values $|\alpha| \sim 1$, illustrated by the data for (Y,Pr)$Ba_2Cu_3O_7$, at non–optimal doping, but consistent with a general McMillan–type analysis [4].

Figure 2 also shows α vs. T_c for the exchange of strongly anharmonic lattice tunneling excitations in a system of local anharmonic double–well oscillators, with T_c varied by changing the EP coupling strength. The isotope exponent is much larger here since the effective λ is strongly enhanced and varies exponentially with the isotope mass. Thus, for a given T_c, this model leads to a larger α than the harmonic

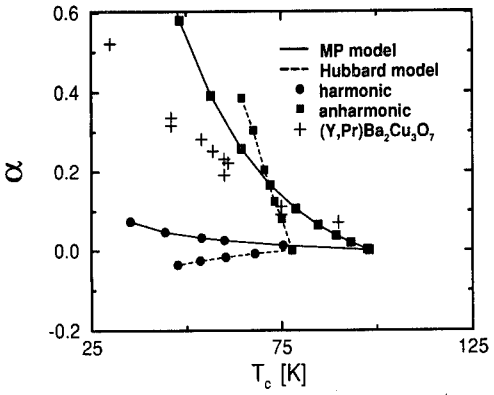


Fig. 2. Isotope exponents vs. d-wave T_c in the Hubbard model [2] with U/t=6, $n \sim 0.86$, $t' = 0$, and in the MP model for coupling to *harmonic* phonon (Ω_0 = 50meV and $0 \leq U_p \leq 2$eV), and *anharmonic* tunneling excitation (see text). Plus symbols show the O-isotope data from Ref. [1].

phonon models. In contrast to harmonic models, large values of α can be obtained here without substantial increase of the quasi-particle damping and transport relaxation rate because the isotopic mass dependence of T_c arises primarily from the quasi-particle mass enhancement λ and *not* via the quasi-particle damping (pair breaking).

In conclusion we have studied the isotope effect of the d-wave superconductors in AF spin fluctuation models. The large observed isotope exponent ($\alpha \sim 1$) might be explained by the EP coupling to anharmonic lattice tunneling excitation but not by coupling to harmonic phonons.

Acknowledgements—This work was supported by the National Science Foundation (Grant DMR-8913878 and DMR-9215123), by the University of Georgia Office of the Vice President for Research, and by computing resources from UCNS, University of Georgia, and NCSA, University of Illinois.

REFERENCES

1. Frank J. P. *et al.*, *Physica B* **194–196**, 2087 (1994).
2. Bickers N. E. *et al.*, *Phys. Rev. Lett.* **62**, 961 (1989); Pao C.-H. and Bickers N. E., *Phys. Rev. B* **49**, 1586 (1994).
3. Monthoux P. and Pines D., *Phys. Rev. B* **49**, 4261 (1994).
4. Schüttler H.-B. and Pao C.-H. (preprint 1994).

Pergamon

J. Phys. Chem. Solids Vol. 56, No. 12, pp. 1747–1748, 1995
Copyright © 1995 Elsevier Science Ltd
Printed in Great Britain. All rights reserved
0022-3697/95 $9.50 + 0.00

0022-3697(95)00184-0

MAGNETIC FRUSTRATION AND SPIN-CHARGE SEPARATION IN 2D STRONGLY CORRELATED ELECTRON SYSTEMS

W. O. PUTIKKA

National High Magnetic Field Laboratory, Florida State University, Tallahassee, FL 32306-4005, U.S.A.

Abstract—I propose that the ground state of the 2D t-J model near half-filling with $J/t \sim 1/3$ has both ferromagnetic and antiferromagnetic fluctuations leading to a magnetically frustrated ground state. I further argue that the frustrated state is spin-charge separated to account for the observed behavior of the equal time spin and charge correlation functions.

Attempts to understand high T_c superconductors have centered around the 2D copper oxide planes found in these materials. One would like to know which features of the planes in the normal state are essential to achieving high T_c's. Considerable effort has gone into understanding strongly correlated electrons on a square lattice [1]. In particular, the single band 2D Hubbard and t-J models near half-filling have been studied intensively. The data discussed in this paper are from high temperature expansions [2–4] for the 2D t-J model, concentrating on the optimal doping range $n \approx 0.80-0.85$ and $J/t \sim 1/3$. I consider a scenario for the planes in which strong correlations, two-dimensionality and the bipartite nature of the square lattice all play important roles.

For models with repulsive interactions ($U > 0$) the most likely instabilities are magnetic. It is well established [5] that the 2D Hubbard model at half-filling and $T = 0$ is an ordered antiferromagnet (AF) with ordering wavevector $\boldsymbol{Q} = (\pi, \pi)$. Away from half-filling AF order disappears rapidly for the Hubbard or t-J model and is no longer present [2] for $n \lesssim 0.95$, $J/t \sim 1/3$. For the uniform susceptibility $\chi_0(T, n)$ with similar model parameters and $T < J$ different behavior is observed. Initially upon doping $\chi_0(T<J, n)$ increases, going through a maximum [2] at $n \approx 0.80-0.85$. This maximum is larger for smaller J/t, but remains at the same density. The size of the maximum is determined by the proximity to a ferromagnetic (FM) region [3] at smaller J/t which has its greatest extent in J/t for $n \approx 0.80-0.85$. The FM region for $J/t > 0$ is not fully polarized and most likely is part of a second order transition from the fully polarized state at $J/t < 0$ to a paramagnet at larger J/t. Having a preferred density for FM behavior is due to two effects which act to suppress FM fluctuations. Near half-filling for $J/t > 0$ AF fluctuations are favored, while at low densities the strong correlation effects which produce magnetic behavior are reduced (Kanamori paramagnetism [6]).

The equal time correlation functions [2] for the 2D t-J model provide further information on the spin and charge degrees of freedom for $n \approx 0.80-0.85$. The spin correlation function $S(\boldsymbol{q})$ (charge correlation function $N(\boldsymbol{q})$) has $2\boldsymbol{k}_F$ ($2\boldsymbol{k}_F^{SF}$) as a characteristic wavevector, where $\boldsymbol{k}_F$ ($\boldsymbol{k}_F^{SF}$) is the Fermi wavevector for the non-interacting tight binding (spinless fermion) model on a square lattice. In 2D $\boldsymbol{k}_F$ and $\boldsymbol{k}_F^{SF}$ are *incommensurate* and related by a doubling of the number of occupied $\boldsymbol{k}$-states in the Brillouin zone.

The AF and FM correlation lengths ξ can be calculated from the real part of the spin susceptibility at $\omega = 0$, $\chi(\boldsymbol{q})$ by

$$\chi(\boldsymbol{q}) = \chi(\boldsymbol{Q})\left[1 - K_{AF}\left((q_x - \pi)^2 + (q_y - \pi)^2\right) + \cdots\right], \quad (1)$$

where $\boldsymbol{Q} = (\pi, \pi)$ and if $K_{AF} > 0$ we have $K_{AF} = \xi_{AF}^2$. For the FM case K_{FM} and ξ_{FM} are defined by a similar expansion around $\boldsymbol{q} = (0, 0)$. Near half-filling we expect $\xi_{AF}/a \gg 1$ where a is the lattice spacing, with $K_{FM} < 0$. This behavior is shown as curves a and b in Fig. 1. However, upon further doping to $n = 0.80$ a different picture emerges. Now ξ_{AF} is *small*, $\xi_{AF}/a \sim 0.3$ and

K_{FM}, while still negative, is closer to being positive at low T, shown as curves c and d in Fig. 1. Keeping $n = 0.80$

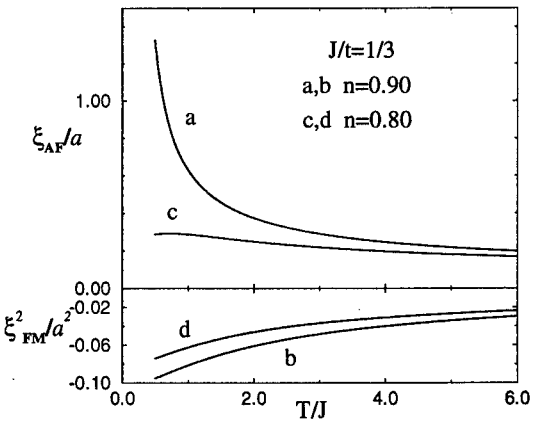


Fig. 1.

there is a crossover in the low T behavior of K_{AF} and K_{FM} for $J/t \lesssim 0.2$. Now at low T, ξ_{FM} exists as a well defined correlation length, while ξ_{AF} does not exist as shown in Fig. 2.

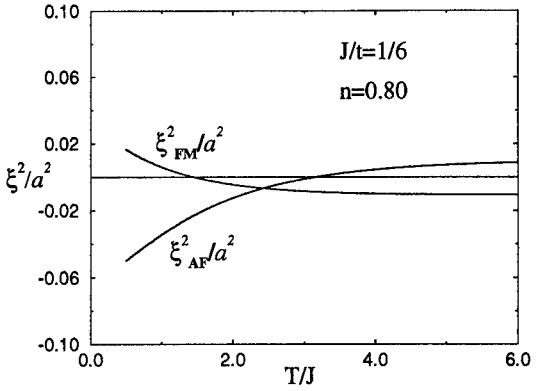


Fig. 2.

This suggests that there is a region around $n \approx 0.80$, $J/t \sim 1/3$ where the magnitude of $\chi(q)$ is enhanced, but $\chi(q)$ is also rather flat as a function of q.

The above observations for the 2D t-J model suggest that for $n \approx 0.80$, $J/t \sim 1/3$ both AF and FM fluctuations are important, leading to a magnetically frustrated [7] ground state. Further, the characteristic wavevectors observed for $S(q)$ and $N(q)$ in the same parameter region [2] suggest that the frustrated magnetic state leads to distinct 2D momentum distributions for the spin and charge degrees of freedom. This is a form of spin-charge separation unique to 2D. Another way to view the frustrated state is as resulting from competition between tendencies towards long range AF and FM order with an ordered state at $T = 0$ prevented by an exact degeneracy between the two types of fluctuations. The exact degeneracy is plausible in 2D for Heisenberg spins, which by the Mermin-Wagner theorem [8] have $T_c = T_N = 0$. This is not true in higher dimensions where in general $T_c \neq T_N$ and the ground state is likely to be the ordered state with the highest transition temperature. Only by extreme fine tuning of parameters in the model is equality likely in higher dimensions.

With the point of view expressed here the analogy of 2D to 1D strongly correlated models is indirect, resting on the idea of (different) degenerate, competing instabilities. In 1D there are competing nesting instabilities which must be treated on an equal footing to find the correct ground state, resulting in the Tomonaga–Luttinger liquid with separate spin and charge excitations [9]. In 2D the competing instabilities are AF and FM, but now if $\chi(q)$ diverges as $T \to 0$ for a fixed q there is long range order. Thus one distinguishing feature for a spin-charge separated state in 2D should be an enhanced, relatively flat $\chi(q)$ over the Brillouin zone. The nature of the competing instabilities in 2D also restricts the possible spin-charge separated state to densities near half-filling, unlike 1D where the nesting instabilities exist for all densities. The phenomenology of spin-charge separation [10] is likely common to 1D and 2D strongly correlated systems (at least for a limited range of parameters in 2D) though the underlying mechanisms are distinct.

In conclusion, I have discussed the properties of the 2D t-J model (or large U Hubbard model) for $n \approx 0.80-0.85$ and $J/t \sim 1/3$. I propose that the 2D t-J model for this parameter range is magnetically frustrated between exactly degenerate, competing AF and FM instabilities, leading to a spin-charge separated ground state distinct to 2D. This state requires the distinguishing features of the copper oxide planes: a single band, strong, repulsive correlations, two dimensionality, doping near half-filling and a bipartite lattice. The behavior of FM in the 2D t-J model also offers an explanation for the optimal doping range $n \approx 0.80-0.85$ observed in all high T_c superconductors.

Acknowledgements—This work was supported by the National High Magnetic Field Laboratory at Florida State University and by NSF Grant No. DMR-9222682.

REFERENCES

1. K. S. Bedell, *et al.*, eds., *High Temperature Superconductivity* (Addison-Wesley, Redwood City, CA, 1990); K. S. Bedell, *et al.*, eds., *Strongly Correlated Electronic Materials* (Addison-Wesley, Reading, MA, 1994).
2. R. R. P. Singh and R. L. Glenister, *Phys. Rev.* **B46** (1992) 11871; W. O. Putikka, *et al.*, *Phys. Rev. Lett.* **73** (1994) 170.
3. W. O. Putikka, *et al.*, *Phys. Rev. Lett.* **69** (1992) 2288.
4. A. Sokol, *et al.*, *Phys. Rev. Lett.* **72** (1994) 1549.
5. E. Manousakis, *Rev. Mod. Phys.* **63** (1991) 1.
6. J. Kanamori, *Prog. Theor. Phys.* **30** (1963) 276.
7. T. M. Rice in Ref. 1, *Strongly Correlated Electronic Materials*, 494.
8. N. D. Mermin and H. Wagner, *Phys. Rev. Lett.* **22** (1966) 1133.
9. J. Solyom, *Adv. Phys.* **28** (1979) 201.
10. P. W. Anderson, *Phys. Rev. Lett.* **64** (1990) 1839.

Pergamon

J. Phys. Chem. Solids Vol. 56, No. 12, p. 1749, 1995
Copyright © 1995 Elsevier Science Ltd
Printed in Great Britain. All rights reserved
0022-3697/95 $9.50 + 0.00

0022-3697(95)00185-9

SPONTANEOUS GENERATION OF *s*-WAVE COMPONENT IN A PURELY *d*-WAVE SUPERCONDUCTOR

YONG REN, J. H. XU and C. S. TING
Texas Center for Superconductivity, University of Houston, Houston, Texas 77204, U.S.A.

Abstract—We have derived microscopically the Ginzburg–Landau equations in a superconductor with $d_{x^2-y^2}$ symmetry. We have found that *s*-wave order parameter is spontaneously generated in a purely *d*-wave superconductor whenever *d*-wave order parameter is inhomogeneous. Examples presented are the structure of a single vortex and superconductor boundary. We have also obtained the time dependent Ginzburg–Laudau equations for such a superconductor.

We have derived microscopically the Ginzburg–Landau equations for a *d*-wave superconductor from Gor'kov equations [1]. We assume a two-dimensional Fermi surface and make the following ansatz for the interaction and order parameter:

$$V(\mathbf{k}-\mathbf{k}') = -V_s + V_d(\hat{k}_x^2 - \hat{k}_y^2)(\hat{k}_x'^2 - \hat{k}_y'^2),\ V_s, V_d > 0 \quad (1)$$

$$\Delta^*(\mathbf{R},\mathbf{k}) = s^*(\mathbf{R}) + d^*(\mathbf{R})(\hat{k}_x^2 - \hat{k}_y^2). \quad (2)$$

We obtain, in terms of free energy functional [2]

$$f = 2\alpha_s|s|^2 - \ln(T_c/T)|d|^2 + \frac{4}{3}|s|^4 + \frac{1}{2}|d|^4 + \frac{8}{3}|s|^2|d|^2 + \frac{4}{3}(s^{*2}d^2 + d^{*2}s^2) + 2|\Pi s^*|^2 + |\Pi d^*|^2 + \left(\Pi_x^* s \Pi_x d^* - \Pi_y^* s \Pi_y d^* + \text{H.c.}\right). \quad (3)$$

$$\frac{\delta f}{\delta s} = 0, \qquad \frac{\delta f}{\delta d} = 0 \quad (4)$$

where $\alpha_s = 2(1 + 2V_s/V_d)/N(0)V_d$ and $\Pi = -i\nabla - 2eA$. We have also made the equation dimensionless by defining $\xi_0 = \sqrt{\alpha}v_F/2$, $\Delta_0 = \sqrt{4/3\alpha}$ where $\alpha = 7\zeta(3)/8(\pi T_c)^2$.

The superconducting state described by the above equation is purely *d*-wave in the bulk with a single transition temperature. What is remarkable about our result is that we are able to show *s*-wave component exists even with a repulsive V_s. The physics is very different from the earlier works on mixed $s + d$ state where the interaction is attractive in both *s* and *d* channels and thus two different transition transition temperatures exist [3], which is unlikely to be relevant to high T_c superconductors.

The existence of the mixed gradient term implies that whenever *d*-wave order parameter varies in space, *s*-wave component will be spontaneously generated. One important example is the structure of a single vortex, previously calculated only numerically [4]. Our Ginzburg–Landau equations can be readily solved either analytically for the asymptotic behaviors or numerically for the whole space behavior. The most interesting feature is the opposite winding *s*-wave component induced near the center [5]. Far away from the core, *s* component decays as $1/r^2$ and has significant contributions from both -1 and $+3$ windings that combine to give the profile a shape of four-leafed clover. The local magnetic field also possesses four-fold symmetry which in principle could be measured directly by scanning SQUIDS.

Our Ginzburg–Landau equations can also be used to study the proximity effect at the surface of a *d*-wave superconductor. We found that a small *s*-wave component is induced near the surface. The total order parameter near surface is a real combination of *s*- and *d*-wave components and their relative sign is given by the sign of $-\cos(2\theta)$, where θ is the angle between the normal direction of the surface and *x* axis. Such a mixture of *s* and *d* could explain the gap anisotropy observed in experiments [3].

We have also obtained the time dependent Ginzburg–Landau equations for a *d*-wave superconductor,

$$-\gamma(\dot{s}^* - 2ie\Phi s^*) = \frac{\delta f}{\delta s}, \quad -\frac{\gamma}{2}(\dot{d}^* - 2ie\Phi d^*) = \frac{\delta f}{\delta d} \quad (5)$$

$$\nabla \times \nabla \times \mathbf{A} = \mathbf{J}_n + \mathbf{J}_s, \quad (6)$$

$$\mathbf{J}_n = \sigma^n \mathbf{E} + \sigma_H^n \mathbf{E} \times \mathbf{n},\ \mathbf{J}_s = -\frac{\delta f}{\delta \mathbf{A}},\ \mathbf{E} = -\nabla\Phi - \partial_t A, \quad (7)$$

and the equations to determine the longitudinal conductivity and Hall conductivity. The detailed solution will be given elsewhere.

REFERENCES

1. Gor'kov L. P., *Zh. Exp. Theor. Fiz.* **36**, 1918 (1959); *Soviet Phys. JETP* **9**, 1364 (1960).
2. Ren Y., Xu J. H. and Ting C. S., *Phys. Rev. Lett.* **74**, 3680 (1995).
3. Joynt R., *Phys. Rev. B* **41**, 4271 (1990). Betouras J. and Joynt R., preprint (1995).
4. Soininen P. I., Kallin C. and Berlinsky A. J., *Phys. Rev. B* **50**, 13883 (1994).
5. Volovik G. E., *JETP Lett.* **58**, 469 (1993).

Pergamon

J. Phys. Chem. Solids Vol. 56, No. 12, pp. 1751–1752, 1995
Copyright © 1995 Elsevier Science Ltd
Printed in Great Britain. All rights reserved
0022-3697/95 $9.50 + 0.00

0022-3697(95)00194-8

ARE SURFACE EFFECTS TO BE INCLUDED IN THE STUDY OF THE ELECTRONIC STRUCTURE OF HIGH TEMPERATURE SUPERCONDUCTORS?

C. O. RODRIGUEZ,* RUBEN WEHT,† MARIANA WEISSMANN† and N. E. CHRISTENSEN‡

* IFLYSIB, Grupo Fisica del Solido, C.C. 565, La Plata (1900), Argentina
† Div. Fisica del Solido, CNEA, Avda Libertador 8250, (1429) Buenos Aires, Argentina
‡ Institute of Physics and Astronomy, Aarhus University, DK-8000 Aarhus C, Denmark

Abstract—A first principles determination of surface effects on the electronic structure of Bi2201 is presented. We show that these effects will modify the Local Density Approximation (LDA) answer to the electronic structure of Bi2201 and thus should be considered if a comparison is made to surface sensitive experimental findings.

One of the most relevant issues in the study of high temperature superconductors is the understanding of their electronic structure at and near the Fermi edge. The great improvements in energy resolution and detection efficiency of Angular Resolved Photoemission Spectroscopy (ARPES) provides us with an scenario with many interesting features in the electronic structure. Some of these have been explained and even predicted by band theory (e.g. large Fermi surfaces) but at present many elements of the data seem not to be well described within this approach. It has recently been put forward in the interpretation of ARPES results that one must go beyond one-electron theory for a complete description of the electronic structure of these materials by use of many body approaches [1].

Nevertheless one should recall that the samples used in the experiments are not the perfect crystals which are assumed in the first principles bandlike theoretical studies and that ARPES is a surface sensitive technique. The observed distribution curves are then related to electrons confined to the outermost cell of the crystal but the experimental results are generally interpreted in terms of bulk transitions or bulk band structures.

It is then important to assess which are the modifications introduced to the LDA band structure by the complexities of real crystals: non-stoichiometry, inconmensurate superstructures or surface terminations.

Here, we concentrate on the effects introduced in the electronic structure by the surface of the crystal. We have specifically studied Bi2201. To this end we have carried out a first principles determination of surface effects on the electronic structure within the LDA. Several basal plane surface terminations are possible, but the most probable candidate (for which we carried out our study) is the Bi–O surface obtained by splitting the crystal through the Bi–O double layer. It is this surface which is known to cleave most readily.

We have used the Full Potential Linear Muffin Tin Orbital (FP-LMTO) method[2] and all details of the calculation are the same as in our previous study of the bulk electronic bands of Bi2201 and of non-stoichiometric effects [3]. Part of the results have previously been presented elsewhere [4].

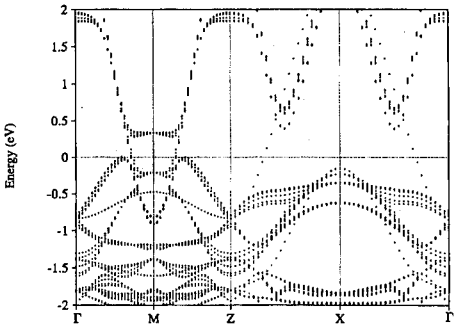


Fig. 1. Calculated PBBS for bulk Bi2201 in the high-symmetry directions of the surface BZ.

Bi2212 and to a lesser extent Bi2201 have inconmensurate superstructures. Torardi et al [5] have proposed an approximate structure that can be viewed as a distorted $\sqrt{2}\times\sqrt{2}$ version of a still simpler prototype bct phase with one Bi2201 formula unit per primitive cell. To eliminate all complications derived from structural modifications and concentrate only on surface related effects we have used the atomic positions of the stoichiometric idealized bct structure based on the work of Torrance *et al.* [6]. To simulate the surface three bulk unit cells and one cell of empty spheres were stacked along the c-axis and a three dimensional calculation ("superlattice") performed. This slab is sufficiently large so as to reproduce bulk like character in the inner cell and the size of the empty region is large enough so as to decouple the interaction of the two surfaces.

The projected bulk band structure (PBBS) of Bi2201 is shown in Fig. 1 along symmetry lines of the surface BZ. At $\overline{M}$ the c-axis dispersion is less than 0.05 eV. Near E_F, bands of two different character appear: an antibonding Cu d (x2-y2)-O(1) p(x,y) band from the CuO2 planes which have an extended character around $\overline{M}$ and bands with Bi–O(2)

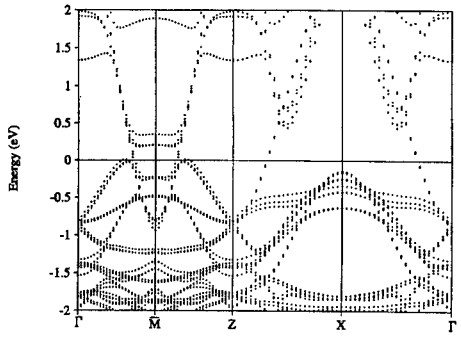


Fig. 2. Calculated band structure for (3+1) cell. Same high-symmetry directions as in Fig. 1.

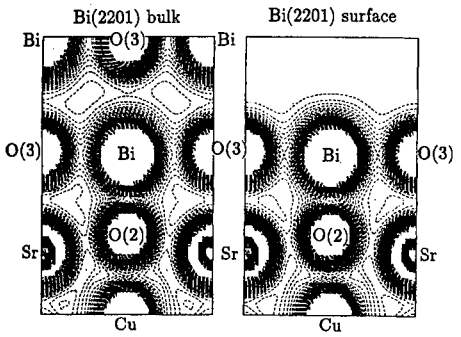


Fig. 3. Charge density contour plots of bulk Bi2201 and (3+1) cell near the surface (the Bi–O plane).

character. These latter dip below E_F near $\overline{M}$ and are antibonding combinations of Bi p(x,y)-O(2) p (x,y). In Fig. 2 the band structure corresponding to the (3+1) cell is shown. The most striking feature brought by the introduction of the surface is the splitting of the flat part of the antibonding copper–oxygen band near $\overline{M}$ above E_F . For the states close to E_F and which fall in a broad gap of the PBBS the character comes from the outer Cu–O planes. On the other hand the flat band 0.2 eV. higher is mainly bulk like coming from the central cell. The exact position of the Fermi level is somewhat undetermined since it depends critically on differerent factors not taken into account in our calculation: our simplified bct cell representation of the crystal structure, occupation of Bi on the Sr sites observed by X-ray studies [3] or apical oxygen vacancies. Because of all this it is difficult to say if the flat band will be occupied or empty. In Fig 3 the ab-initio determined electronic charge density (including valence and semicore electrons) for the bulk crystal of Bi2201 and that for the crystal with a surface is shown. Charge density contours ranging from 0 to 0.2 electrons/(au)^3 are shown for the plane that cuts Cu,Sr, apical oxygen, Bi and the oxygen of Bi–O plane. We should point out that although the changes of the charge readjustment are small they go deep all the way through a whole cell ($\approx$ 10 Å).

We conclude that termination effects will need to be included in an LDA assessment of the electronic structure of Bi2201 to make a direct comparison with ARPES findings. We have not included in our surface calculation the inconmensurate superstructure nor other complexities of real crystals but beleive that surface effects will also affect the calculated band structure in those cases too. In our (3+1) cell the surface introduced states in a gap of the PBBS with dispersion characteristics similar to those predicted experimentally.

REFERENCES

1. Shen Z. -X., Spicer W. E., King D. M., Dessau D. S. and Wells B. O., *Science* **267**, 343 (1995) and references therein.
2. Methfessel M., *Phys. Rev. B* **38**, 1537 (1988).
3. Weht R. *et al.*, in *Proc. Int. Conf. Materials and Mechanisms of Superconductivity*, Grenoble, *Physica C* **235–240**, 2109 (1994) .
4. Rodriguez C. O., Weht R., Weissmann Mariana and Christensen N. E., in *Proc. Workshop on High Temperature Superconductivity*, Miami, to be published in *J. Superconductivity*.
5. Torardi *et al.*, *Physica C* **176**, 347 (1991).
6. Torrance J. B. *et al.*, *Solid State Commun.* **66**, 703 (1988).

Pergamon

J. Phys. Chem. Solids Vol. 56, No. 12, pp. 1753–1754, 1995
Copyright © 1995 Elsevier Science Ltd
Printed in Great Britain. All rights reserved
0022–3697/95 $9.50 + 0.00

0022-3697(95)00186-7

CONFINEMENT IN THE THREE-DIMENSIONAL ANISOTROPIC t–J MODEL: A MEAN-FIELD STUDY

SANJOY K. SARKER

Department of Physics and Astronomy, The University of Alabama, Tuscaloosa, AL 35487, U.S.A.

Abstract—We consider the anisotropic t–J model with the c-axis parameters t_c and J_c different from their in-plane counterparts, t and J. Within the slave-fermion mean-field approximation it is shown that the spiral state exhibits charge-confinement in the intermediate δ regime. In the confined state the hopping amplitude $< c^{\dagger}_{i\sigma} c_{j\sigma} >= 0$ along the c direction so that c-axis resitivity is infinite at $T = 0$.

The normal-state resistivity of the cuprate superconductors is metallic in the ab plane but is characteristic of an insulator along the c direction, leading to the possibility of the remarkable phenomenon of confinement [1,2]. By continuity, such a behavior is not expected to occur in a Fermi liquid. In addition, confinement is at the heart of the proposed pair-tunneling mechanism which is in essence a deconfining process [3]. Theoretical treatments so far have been focused on a collection of weakly coupled Hubbard chains [2]. In this paper we study confinement in a collection of Hubbard planes, more specifically in the anisotropic t–J model described by the Hamiltonian

$$H = -\sum_{ij} t_{ij} c^{\dagger}_{i\sigma} c_{j\sigma} + \frac{1}{2}\sum_{ij} J_{ij}[S_i \cdot S_j - n_i n_j]. \qquad (1)$$

Here the in-plane hopping parameter $t_{ab} \equiv t$ and the exchange interaction $J_{ab} \equiv J$ are in general different t_c and J_c, the corresponding quantities along the c axis. Not all the parameters are free since the t–J model is thought to be derived from an underlying Hubbard model ($J_{ij} = 4t^2_{ij}/U$) so that $J_c/J = (t_c/t)^2$. There are therefore three independent parameters: t/J, $\xi \equiv t_c/t$ and the hole density δ.

Confinement is presumably intimately connected with spin–charge separation. While model (1) is not exactly solvable, in two dimensions a number of approximate ground states have been proposed that exhibit spin–charge separation. Here we study the spiral states in the Schwinger-boson slave-fermion representation: $c_{i\sigma} = h^{\dagger}_i b_{i\sigma}$, where $h^{\dagger}$ creats a fermionic hole and $b_{i\sigma}$ destroys a bosonic spin [4]. We will impose the constraint $h^{\dagger}_i h_i + \sum_{\sigma} b^{\dagger}_{i\sigma} b_{i\sigma} = 1$ on the average. A mean-field decomposition leads to following Hamiltonians:

$$H_h = 2\sum_{ij} t_{ij} B_{ij} h^{\dagger}_i h_j \qquad (2)$$

$$H_b = \sum_{ij\sigma} t_{ij} D_{ij} b^{\dagger}_{i\sigma} b_{j\sigma} - \sum_{ij\sigma} J_{ij} A_{ij} \sigma b_{i\sigma} b_{j-\sigma}. \qquad (3)$$

Here $D_{ij} =< h^{\dagger}_i h_j >$ is the average hopping amplitude. This is associated with ferromagnetic backflow $B_{ij} =< b^{\dagger}_{i\sigma} b_{j\sigma} >$.

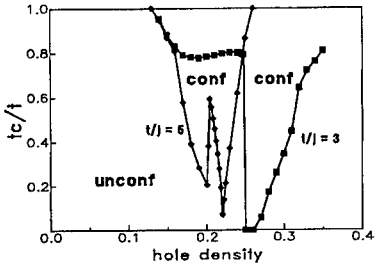


Fig. 1. Phase diagram in the δ-t_c/t plane for two $t/J = 3$ (squares) and $t/J = 5$ (diamonds). In each case, the confined state ($D_c = 0$) has a lower energy in the V-shaped region. The transition is first order.

And $A_{ij} = \frac{1}{2} < (b_{i\uparrow} b_{j\downarrow} - b_{i\downarrow} b_{j\uparrow}) >$ represents the antiferromagnetic correlations associated with the exchange term. We have shown that in two dimensions this competition gives rise to [4,5] an incommensurate spiral metallic state that evolves continuously from the Neel state at $\delta = 0$ to a ferromagnetic state at large $t\delta/J$. The spiral state is favored over double spiral and canted states and is stabilized against phase separation and domain walls by Coulomb repulsion [5,6].

In the present problem the in-plane amplitudes (D_{ab}, B_{ab} and A_{ab}) are in general different from those along the c directions (D_c, B_c and A_c). We have solved the mean-field equations numerically for various values of t_{ab}/J_{ab}, $\xi = t_c/t_{ab}$ and δ. One self-consistent solution is found to be the usual spiral metallic state which evolves continuously out of the Neel state. For this state all the mean-field amplitudes including D_c and B_c are nonzero and hence there is no confinement. In addition, the state with $D_c = 0$ (and hence $B_c = 0$) is also a self-consistent solution. This is clearly a direct consequence of spin–charge separation. Charge can propagate in the ab plane in this case ($D_{ab} \neq 0$). Hence D_c can be thought of as the order-parameter for deconfining transitions.

While spin–charge separation can lead to confinement, it does not guarantee that such a state is favored energetically.

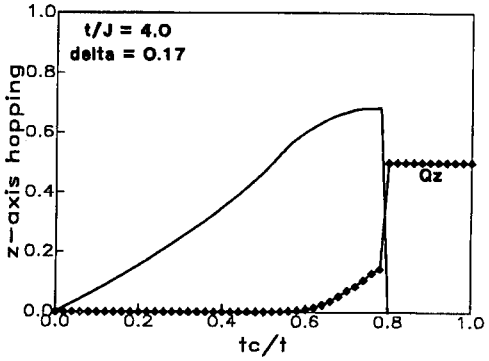


Fig. 2. The hole-hopping amplitude $D_c/(-\delta)$ and the ordering wavevector along the c-direction Qz $\equiv \frac{Q_c}{2\pi}$ (diamonds) vs t_c/t. Note that Q_c is essentially zero (ferromagnetic) in the unconfined phase. Close to the transition it aquires a spiral character, and at the transition jumps to π corresponding to antiferromagnetic correlations in the confined phase.

The ground-state energy is given by

$$E_G = 8tD_{ab}B_{ab} - 4JR_{ab} + 4t_cD_cB_c - 2J_cR_c, \qquad (4)$$

where $R_{ij} = A_{ij}^2 - B_{ij}^2/2 + (1-\delta)^2/8$. In general D and B have opposite signs and $R > 0$. For physically interesting values of $t - J$, we find that the unconfined phase has a lower energy both at small and large δ. But, as shown in Fig. 1, for intermediate δ there is a region in the δ-t_c/t plane where the *confined* state is favored. Interestingly, for fixed t/J and δ, the mean-field state is unconfined at small t_c/t, and with increasing t_c/t there is a first-order transition to a confined state. This is because as t_c decreases, $J_c \propto t_c^2$ decreases more rapidly. This favors ferromagnetic alignment and deconfinement. These results are summarized in Fig. 2.

For δ not too large the hole hopping amplitude D in the isotropic 3D case is given by $D_3(\delta) \approx -\delta + \frac{(6\pi^2)^{2/3}}{10}\delta^{5/3}$. In two dimensions, $D_2(\delta) \approx -\delta + \pi\delta^2/2$. Hence, the hopping energy *per bond* can be lower in two dimensions. When t_c and δ are not too small, the system can gain maximum exchange energy in the c direction and maximum kinetic energy in the ab plane by having $B_c = D_c = 0$.

To summarize, we have shown that spiral state in the anisotropic t–J model exhibits charge confinement. For a more realistic treatment one needs to include fluctuations that destroy long-range magnetic order and reconstruct the Luttinger-Fermi surface, as shown previously for the 2D model [7]. Such fluctuations are likely to bring the region of satbility of the confined state to smaller values of δ and t_c/t. Nonetheless, there are some interesting consequences of confinement in our simple theory. (1) In the confined state the magnetic correlations along the c direction is peaked at $Q_c = \pi$, while the correlations in the ab plane remains incommensurate. (2) The c-axis resistivity is strictly infinite at $T = 0$, since $|c_{i\sigma}^{\dagger}c_{j\sigma}| = -D_{ij}B_{ij} = 0$. However, at finite T or frequency there will be an incoherent contribution to the conductivity. Such a contribution will be activated if there is a spin gap.

REFERENCES

1. Anderson P. W., preprint.
2. Clarke D. G., Strong S. P. and Anderson P. W., *Phys. Rev. Lett.* **72**, 3218 (1994).
3. Chakravarty S., Sudbo A., Anderson P. W. and Strong S. P., *Science* **261**, 337 (1993).
4. Jayaprakash C., Krishnamurthy H. R. and Sarker S. K., *Phys. Rev. B* **40**, 2610 (1989).
5. Sarker S. K., *Phys. Rev. B* **46**, 8617 (1992).
6. Hu F. M., Sarker S. K. and Jayaprakash C., *Phys. Rev. B* **50**, 17901 (1994).
7. Sarker S. K., *Phys. Rev. B* **46**, 8617 (1992).

Pergamon

J. Phys. Chem. Solids Vol. 56, No. 12, pp. 1755–1757, 1995
Copyright © 1995 Elsevier Science Ltd
Printed in Great Britain. All rights reserved
0022-3697/95 $9.50 + 0.00

0022-3697(95)00165-4

PHASE STABILITY AND MAGNETIC PROPERTY OF $LaCo_{1-x}Ni_xO_3$

H. SAWADA, N. HAMADA and K. TERAKURA
Joint Research Center for Atom Technology (JRCAT),
c/o NAIR, 1-1-4 Higashi, Tsukuba, Ibaraki 305, Japan

Abstract—Phase stability and magnetic properties of perovskite $LaCo_{1-x}Ni_xO_3$are studied by the full-potential linearized augmented-plane-wave method. For $LaCoO_3$and $LaNiO_3$a non-magnetic state is obtained. A ferromagnetic state is stabilized in a composition range $0.25 \leq x \leq 0.7$. These calculated results agree well with experimental results qualitatively. The mechanism of stabilizing the ferromagnetic state is also presented.

Keywords: Band structure calculation, magnetic phase stability,$LaCo_{1-x}Ni_xO_3$

In some composition range of $LaCo_{1-x}Ni_xO_3$ magnetic ordering occurs despite the non-magnetic character of $LaCoO_3$ and $LaNiO_3$. Asai *et al.* [1] reported that $LaCo_{1-x}Ni_xO_3$ is a ferromagnet with a spin glass like character, while Vasanthacharya *et al.* [2] suggested a ferrimagnetic ordering from the temperature dependence of the susceptibility. In either case, a mechanism of stabilizing the magnetic ordering is not sufficiently clear. For the purpose of clarifying the mechanism of stabilizing the magnetic ordering, the phase stability between magnetic and non-magnetic states and the magnetic properties are studied for$LaCo_{1-x}Ni_xO_3$ by using the all-electron full-potential linearized augmented-plane-wave (FLAPW) method in the local spin-density approximation (LSDA). We assume that $LaCo_{1-x}Ni_xO_3$ has ferromagnetic ordering, although there are many possible magnetic orderings.

At first we study the phase stability and the magnetic properties of the parent compound $LaCoO_3$. $LaCo_{1-x}Ni_xO_3$ has a rhombohedral perovskite structure. The calculated lattice constant of $LaCoO_3$ is in good agreement with the experiment [3,4] within 1% error. This calculation shows that the non-magnetic state is more stable than the ferromagnetic state at the equilibrium lattice constant. The energy difference between these states is 9 meV (100 K) per formula unit, and it is interesting to note a good correspondence between this energy difference and the transition temperature from low spin state to high spin state [5]. Since the ferromagnetic state becomes more stable by a volume expansion, thermal expansion of the volume may be one of the origins of the temperature induced paramagnetism observed experimentally. In fact lattice constants of $LaCoO_3$ expand by about 0.7% from 4 K to room temperature [4]. For $LaNiO_3$ the calculated lattice constant is also in good agreement with the experiment [6]. In this study the system turns out to be a non-magnetic metal; ferromagnetic state is not obtained. It is consistent with the Pauli-like susceptibility in experiment [7,8].

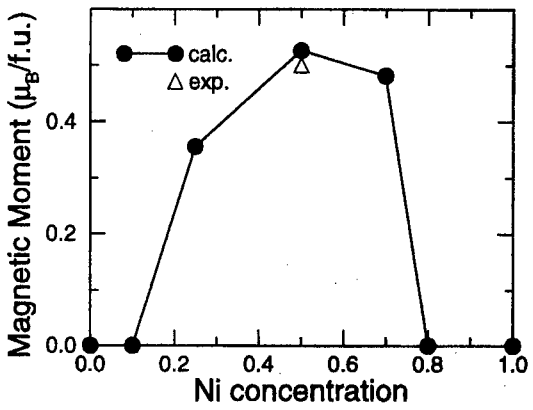


Fig. 1. The calculated magnetic moment per formula unit as a function of the Ni concentration for $LaCo_{1-x}Ni_xO_3$.

$LaCo_{1-x}Ni_xO_3$ (x = 0.1, 0.25, 0.5, 0.7, 0.8) are treated by the virtual crystal approximation. The ferromagnetic states are obtained for x = 0.25, 0.5 and 0.7. The ferromagnetic state is more stable than the non-magnetic state by about 20 meV for x = 0.25 and 0.5, while for x = 0.7 the energy difference between these states is only 2 meV. A composition dependence of the magnetic moment per formula unit is shown in Fig 1. Magnetic moments slightly increase with x for $x < 0.5$, and decrease for $x > 0.5$.

To elucidate the mechanism of stabilizing the ferromagnetic state, we compare the densities of states (DOS) between the non-magnetic state of x = 0 (Fig. 2) and the ferromagnetic state of x = 0.5 (Fig. 3). The reason why the non-magnetic state is stabilized for x = 0 is that the Fermi level is located at a dip of the DOS. This dip is due to the energy separation between Co $d\varepsilon$ and $d\gamma$ states. If the rigid band is assumed for $x > 0$, increase of the number of electrons of virtual atom moves the Fermi energy to the higher energy. For x = 0.25 and 0.5, the Fermi level is located near the spike just above the dip separating the $d\varepsilon$ and $d\gamma$ states;

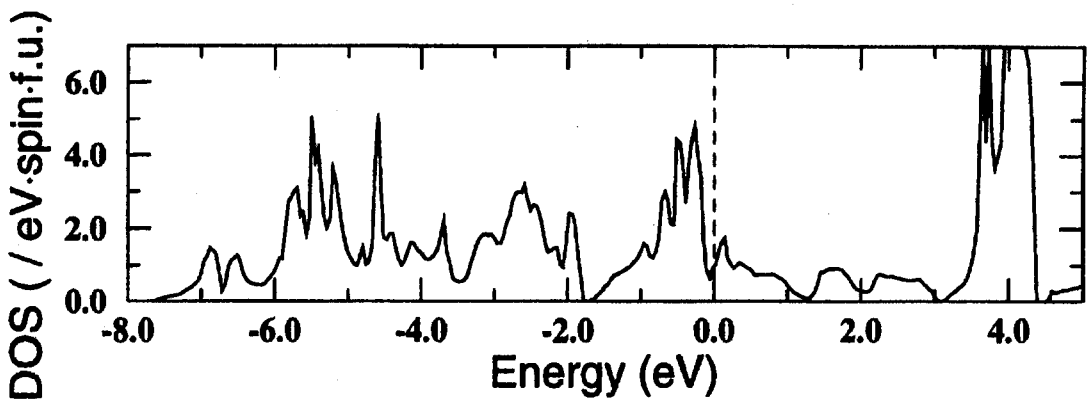


Fig. 2. Total density of states of non-magnetic $LaCoO_3$.

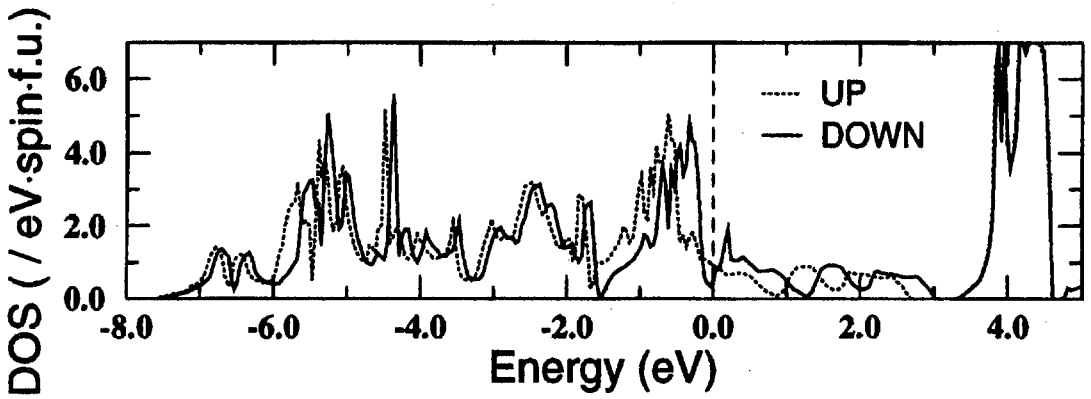


Fig. 3. Total density of states of ferromagnetic $LaCo_{0.5}Ni_{0.5}O_3$.

therefore the non-magnetic state of $x = 0.25$ and 0.5 becomes unstable to the ferromagnetic state due to the stoner condition [9,10]. For the ferromagnetic state of $x = 0.5$ the Fermi level is located at the dip of the down-spin DOS; the ferromagnetic state is stabilized. For $x = 0.7$ the Fermi level is forced to be located at higher energy than the dip of the down-spin DOS. It makes the magnetic moment smaller than that of $x = 0.5$, and the ferromagnetic state less stable.

The lattice constant is chosen to be $a = 10.1$ a.u. and $c = 24.26$ a.u. for the hexagonal unit cell which is close to the calculated equilibrium lattice constant of $LaCoO_3$ and $LaNiO_3$. The lattice constant dependence is examined only for $x = 0.5$, and there is no significant change in the DOS. We have used an extreme model for the mixed crystal; i.e. Ni and Co atoms are replaced with one species of virtual atoms. However, since the dip of DOS discussed above comes from the octahedral crystal field splitting of d states, it is very common and independent of the atomic species. Therefore, even in the real mixed compound, both Co and Ni may adjust the number of their electrons so that Co and Ni may have a common local DOS for down-spin electrons with a well defined dip at the Fermi level. Alloying effects in the up-spin electron states will not modify the present calculation either because the up-spin DOS is fairly smooth at the Fermi level. We would like to point out that the situation is quite similar to that in Fe based Fe–Co alloys [11,12].

In summary, the phase stability and magnetic properties of $LaCo_{1-x}Ni_xO_3$ are discussed. The ferromagnetic state is stabilized in the composition range $0.25 \leq x \leq 0.7$, and the magnetic moment of Co and Ni increases with x for $x < 0.5$, and decreases for $x > 0.5$. The ferromagnetic state is stabilized so that the Fermi level is fixed at a dip of minority-spin DOS which comes from the octahedral crystal field splitting.

Acknowledgments— The present work is partly supported by New Energy and Industrial Technology Development Organization (NEDO).

REFERENCES

1. Asai K., Sekizawa H., Mizushima K. and Iida S., *J. Phys. Soc. Jpn* **43**, 1093 (1977).
2. Vasanthacharya N. Y., Ganguly P. and Rao C. N. R., *J. Solid State Chem.* **53**, 140 (1984).

3. Bhide V. G., Rajoria D. S., Rao C. N. R., Rama Rao G. and Jadhao V. G., *Phys. Rev. B* **12**, 2832 (1975).
4. Thornton G., Tofield B. C. and Hewat A. W., *J. Solid State Chem.* **61**, 301 (1986).
5. Asai K., Yokokura O., Nishimori N., Chou H., Tranquada J. M., Shirane H., Higuchi S., Okajima Y. and Korn K., *Phys. Rev. B* **50**, 3025 (1994).
6. García-Munõz J. L., Rodríguez-Carvajal J., Lacorre P. and Torrance J. B., *Phys. Rev. B* **46**, 4414 (1992).
7. Sreedhar K., Honig J. M., Darwin M., McElfresh M., Shand P. M., Xu J., Crooker B. C. and Spalek J., *Phys. Rev. B* **46**, 6382 (1992).
8. Xu X. Q., Peng J. L., Li Z. Y., Ju H. L. and Greene R. L., *Phys. Rev. B* **48**, 1112 (1993).
9. Janak J. F. and Williams A. R., *Phys. Rev. B* **14**, 4199 (1976).
10. Poulsen U. K., Kollar J. and Andersen O. K., *J. Phys. F* **6**, L241 (1976).
11. Hasegawa H. and Kanamori J., *J. Phys. Soc. Jpn* **33**, 1607 (1972).
12. Hamada N., *J. Phys. Soc. Jpn* **46**, 1759 (1979).

Pergamon

J. Phys. Chem. Solids Vol. 56, No. 12, pp. 1759–1760, 1995
Copyright © 1995 Elsevier Science Ltd
Printed in Great Britain. All rights reserved
0022–3697/95 $9.50 + 0.00

0022–3697(95)00188-3

INTERPRETATION OF ELECTRONIC RAMAN AND ANGLE RESOLVED PHOTOEMISSION SPECTRA OF $Bi_2Sr_2CaCu_2O_8$

JIRO TANAKA,* MASAAKI SHIMIZU †,[1] and KOJI KAMIYA ‡

* Department of Materials Science, Faculty of Science, Kanagawa University, Hiratsuka 259-12, Japan
† Department of Chemistry, Nagoya University, Chikusa, Nagoya 464-01, Japan
‡ Department of Materials Science, Chiba University, Inage, Chiba 263, Japan

Abstract—The electronic Raman spectra of $Bi_2Sr_2CaCu_2O_8$ are measured at 35 K.The polaron model of carrier is presented and the results of Raman and angle resolved photoemission spectra are explained in reasonable way.

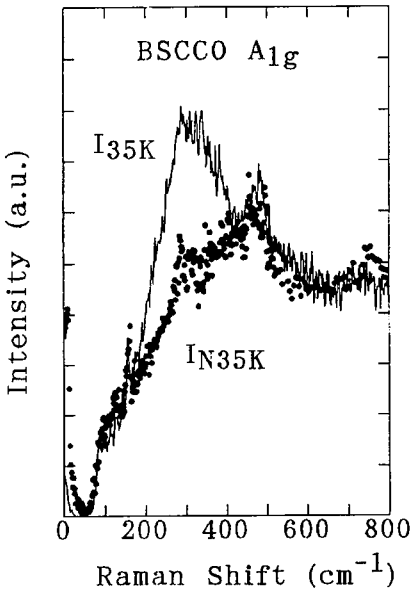


Fig. 1. Electronic Raman spectra of Bi2212 measured for (x, x) and (x, y) polarizations at 35 K. I_N(35 K) are obtained by extrapolation of 100 K (normal state) spectra with correction of temperature factors.

1. INTRODUCTION

Symmetry properties of carriers in $Bi_2Sr_2CaCu_2O_8$ (Bi2212) have been studied by Raman spectra [1], however, little attention has been paid for to significance. We have measured Raman spectra of single crystals of Bi2212 for a wide temperature range. A polaron model of Bi2212 is presented and the Raman and angle resolved photoemission spectra (ARPES) [2–5] are interpted on this model.

[1] Present address, Fuji Xerox Co., Minamiashigara, Kanagawa 250, Japan

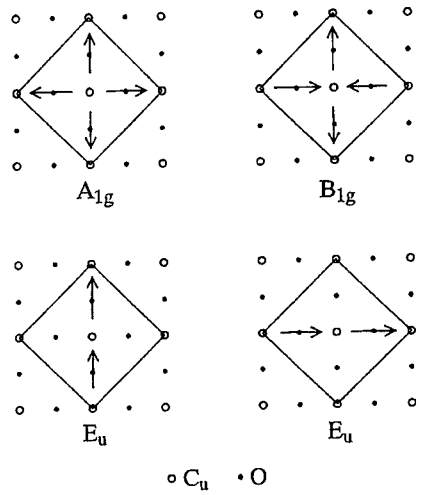


Fig. 2. Polarization modes of CuO_4^{6-} cluster HOMO.

2. RAMAN SPECTRA

Electronic Raman spectra of Bi2212 were measured by (x, y) and (x, x) polarization to select B_{1g} and A_{1g} + B_{2g} modes. (Fig. 1) In the superconducting (SC) state at 35 K, new peaks were found at 400 and 300 cm^{-1} for the B_{1g} and A_{1g} modes, respectively, and the SC gap was found only for the B_{1g}. The peak positions were different from 2Δ values.

3. POLARON STATES

The HOMO and next HOMOs (NHOMO) of CuO_4^{6-} ion are composed of O2pπ orbitals [6]. By doping, the holes are produced in the HOMO or NHOMOs, and the electronic transitions between these levels are allowed. In the crystal, these levels might be mixed by the configuration interaction, and the HOMO levels might be dressed with the electronic polarization. We call this state a polaron of Bi2212. Four

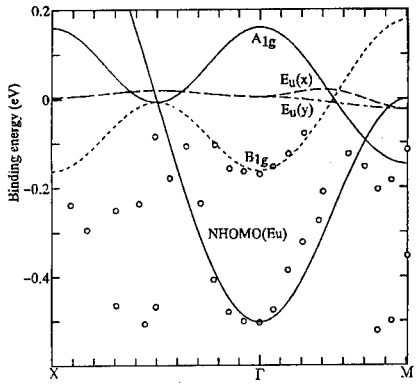


Fig. 3. Energy levels of polaron bands of HOMO and NHOMO bands.

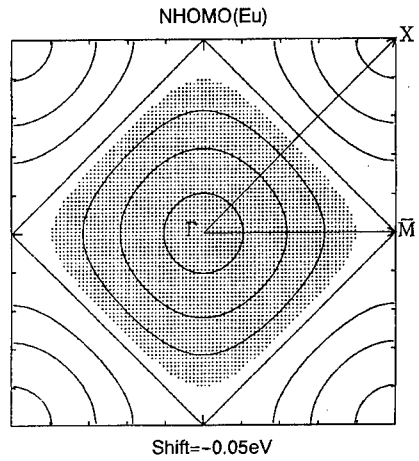


Fig. 4. Energy contour for the A_{1g} and B_{1g} and NHOMO bands. The occupied levels by setting E_F = -0.05 eV are hatched.

polaron modes, A_{1g}, B_{1g} and two E_u, are assumed to have small dipole moments as shown in Fig. 2. The energy band structure are calculated (Fig. 3) by the screened dipole interaction. For the NHOMO levels, the tight binding energy bands are calculated by taking the nearest neighbor interaction of a half cell including a CuO_2 unit. Actually, the NHOMO is degenerate, accordingly these levels below the FS are almost filled.

4. INTERPRETATION OF RAMAN AND ARPE SPECTRA

By the use of Fig. 3 and the energy contour of Fig. 4, the Raman bands at SC states are explained by the fact that the 400 cm^{-1} peak in the B_{1g} mode appears at M and the 300 cm^{-1} peak in the A_{1g} mode is found at the mid-point of Γ-M where both the A_{1g} and B_{1g} levels exist.

ARPES of Bi2212 are well correlated to the contour map (Fig. 4), where the Fermi level is set at -0.05 eV of calculated binding energy. Two FS were found around Γ [2], the inner one is due to the B_{1g} polaron band and the broad one is due to the NHOMO band. Another FS was found around X(Y) [3–5]; it may be the degenerate NHOMO band or the B_{1g} polaron band. In fact, the flat band is noticed at M in the ARPES, and this region is assigned to the A_{1g} polaron band, which is centered at M. The presence of large flat band at M is exactly coincident with the population of the A_{1g} band.

5. PAIR FORMING INTERACTION

The electronic transition between the A_{1g} polaron band to the unoccupied NHOMO band is electronically allowed. The exciton interaction is largest at M since these two levels are almost degenerate at M. The pair formation is most effective in this region. The anisotropy of gap in the Γ-M-X plane may be estimated by the exciton type dipole interaction, and it indicates that Δ is $d_{x'^2-y'^2}$ type. The polaron model of exciton interaction is consistent with a *d*-wave symmetry of the gap. The formation or population of the A_{1g} polaron band is much less in Bi2201 and NCCO, which show lower T_c, accordingly it may be correlated to the origin of high $T_c$mechanism.

REFERENCES

1. Staufer T. *et al.*, *Phys. Rev. Lett.* **68**, 1069 (1992).
2. Takahashi T. *et al.*, *Phys. Rev. B* **39**, 6636 (1989).
3. King D. M. *et al.*, *Phys. Rev. Lett.* **73**, 3298 (1994).
4. Dessau D. S. *et al.*, *Phys. Rev. Lett.*, **71**, 2781 (1993).
5. Shen Z.-X. *et al.*, *Phys. Rev. Lett.* **70**, 1553 (1993).
6. Tanaka J. *et al.*, *Physica C* **161**, 451 (1989).

Pergamon

J. Phys. Chem. Solids Vol. 56, No. 12, pp. 1761–1762, 1995
Copyright © 1995 Elsevier Science Ltd
Printed in Great Britain. All rights reserved
0022-3697/95 $9.50 + 0.00

0022-3697(95)00229-4

JOSEPHSON EFFECT IN $d_{x^2-y^2}$-WAVE SUPERCONDUCTORS

YUKIO TANAKA * and SATOSHI KASHIWAYA †

* Department of Physics, Niigata University, Ikarashi, Niigata 950-21, Japan
† Electrotechnical Laboratory, Tsukuba, Ibaraki 305, Japan

Abstract—Basic properties of the Jospephson effect in an s-wave superconductor/ Insulator/ $d_{x^2-y^2}$-wave superconductor ($s/I/d$) junction and a $d_{x^2-y^2}$-wave superconductor/ Insulator/$d_{x^2-y^2}$-wave superconductor ($d/I/d$) junction are clarified for various crystal orientations. In both junctions, the phase difference φ dependence of the supercurrent does not always exhibit the usual sinusoidal behaviour. In general the minimum Free energy occurs neither at $\varphi = 0$ or $\varphi = \pi$. Zero-energy bound states of quasiparticles which are formed at zero energy can induce anomalous temperature dependence of maximum supercurrent in some $d/I/d$ junctions.

1. INTRODUCTION

The Josephson effect involving high T_c superconductors is one of the interesting problems of the field, since several theories and experiments suggest d-wave symmetry for the pair potentials of high-T_c superconductors. We have previously investigated the Josephson effect between s-wave and $d_{x^2-y^2}$-wave superconductors for various crystal orientations [1]. At that stage, we extended the one-dimensional theory of s-wave superconductors phenomenologically. Afterwards it was revealed that zero-energy states are formed at the interface when the angle between the crystal axis of a $d_{x^2-y^2}$-wave superconductor and the normal to the interface becomes finite, where an electron-like quasiparticle and a hole-like quasiparticle feels the different sign of the pair potentials of each other [2–4]. These zero energy states produce zero energy peaks in the conductance of Normal metal/Insulator/$d_{x^2-y^2}$-wave superconductor junction which are often observed in the tunneling experiments of high-T_c superconductors [5]. It is necessary to extend our previous theory of the Josephson effect [1] for general cases, where an electron like quasiparticle and a hole like quasiparticle do not feel the same pair potentials. We express insulator as a step function barrier model whose height and thickness are given by U and d. We introduce two parameters λ_0 and λ_F, which can be expressed as $\lambda_0 = \sqrt{2mU/\hbar^2}$, and $\lambda_F = k_F/\lambda_0$, where k_F is the Fermi momentum in the superconductor. In the following, the critical temperatures of the s-wave and d-wave superconductors are chosen as T_s = 0.7 meV, and T_d = 5.7 meV, respectively.

2. JOSEPHSON EFFECT IN $s/I/d$ JUNCTIONS

In our previous paper, the phase difference φ dependence of the Josephson current $I(\varphi)$ in s-wave-superconductor/ Insulator /$d_{x^2-y^2}$-wave superconductor junction was predicted to be $\sin(2\varphi)$, when the junction is formed along the c axis.

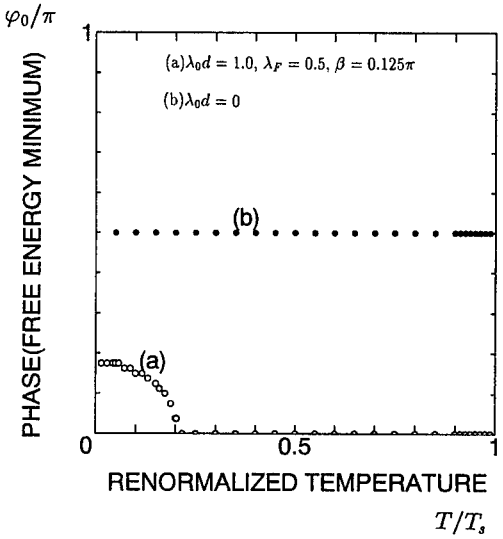


Fig. 1. Temperature dependence of φ_0 for (a)$\lambda_0 d = 1.0$, $\lambda_F = 0.5$, $\beta = 0.125\pi$ and (b)$\lambda_0 d = 0$. In the case of (b), $I(\varphi)$ and φ_0 are independent of β and λ_F.

The important fact is that the Free energy does not have a minimum at $\varphi = 0$. These features also can be seen in ab-plane contact case. We have calculated $I(\varphi)$ in ab-plane junction for various temperatures T and various β, which expresses the angle between the crystal axis of the d-wave superconductor and the normal to the interface. Both β and λ_0 become finite and zero energy states(ZES) appear at the interface of the d-wave superconductor, which are absent in the c axis oriented junction. In general, the angle φ_0 which minimizes the Free energy depends on temperature as shown in Fig. 1. For $\lambda_0 d = 0$ and $\beta = 0.25\pi$, φ_0 becomes 0.5π independent of temperature.

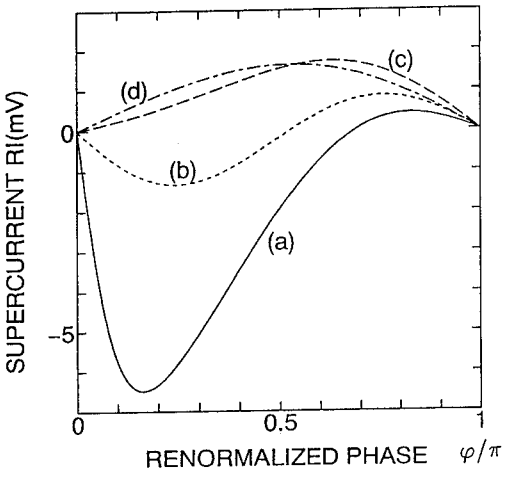


Fig. 2. $RI(\varphi)$ is plotted as a function of φ for various temperature with $\lambda_0 d = 1.0$ and$\lambda_F = 0.5$. (a)$T/T_d = 0.04$,(b)$T/T_d = 0.16$,(c)$T/T_d = 0.32$ and (d)$T/T_d = 0.64$.

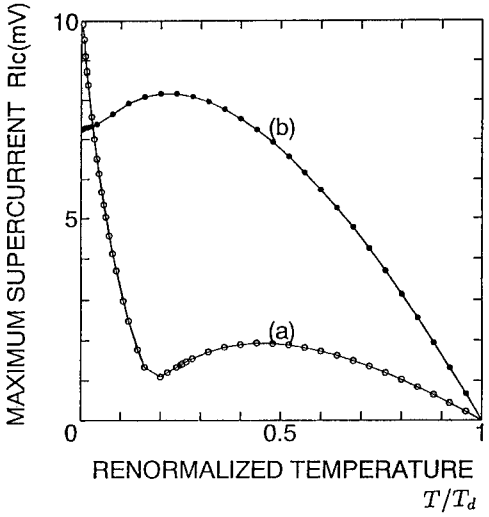


Fig. 3. Maximum supercurrent is plotted as a function of T with $\lambda_0 d = 1.0$ and $\lambda_F = 0.5$.(a) $\alpha = -\beta = 0.10\pi$ and (b) $\alpha = -\beta = 0.05\pi$.

3. JOSEPHSON EFFECT IN $d/I/d$ JUNCTIONS

In this section $I(\varphi)$ is calculated for d-wave superconductor / Insulator / d-wave superconductor($d/I/d$) junction where α (β) expresses the the angle between the crystal axis of left(right) handed superconductor and the normal to the interface of left handed superconductor. Recently Sigrist and Rice [6] proposed very simple formula which expresses the α and β dependence of the maximum supercurrent. In the light of our results, their theory ignores the bound states formed at the interface, and only the quasiparticle injected perpendicularly to the interface is considered. Their theory only can be applied for d-wave superconductor / normal metal / d-wave superconductor junctions, where the width of normal metal is sufficiently thick and where the Fermi momenta in the superconductor and the normal metal are almost the same. In the case when the ZES exist, a wide variety of $I(\varphi)$ curves are expected. Typical anomalous examples are plotted in Fig. 2. At low temperatures, the derivatives of $I(\varphi)$ at$\varphi = 0$ can become negative, while near the critical temperature the usual sinusoidal dependences are obtained. The maximum supercurrent also shows an anomalous temperature dependence. It is significantly different from the usual result for s-wave superconductors. In such cases, φ_0 strongly depends on temperature. In the case of Fig. 3(a), φ_0 becomes 0 for $0.3T_d < T < T_d$. It increases with decreasing T for $T < 0.3T_d$ and finally it becomes 0.7π for $T = 0$.

4. CONCLUSIONS

In this paper, the basic properties of the Josephson effect including d-wave superconductors were studied. Both in $s/I/d$ and $d/I/d$ junctions, the phase φ dependences of $I(\varphi)$ does not always exhibit the usual sinusoidal behaviour. The free energies of these junction are not always minima at $\varphi = 0$.[7] In some cases, the presence of ZES induce an anomalous temperature dependence of the maximum supercurrent in $d/I/d$ junction.

REFERENCES

1. Tanaka Y., *Phys. Rev. Lett.* **72**, 3871 (1994).
2. Hu C. R., *Phys. Rev. Lett.* **72**, 1526 (1994).
3. Matusmoto M. and Shiba H., *J. Phys. Soc. Jpn*,**64** 1703 (1995).
4. Kashiwaya S., Tanaka Y., Koyanagi M., Takashima H. and Kajimura K., *Phys. Rev. B* **51** 1350 (1995).
5. Tanaka Y. and Kashiwaya S., *Phys. Rev. Lett.* **74** 3451 (1995).
6. Sigrist M. and Rice T. M., *J. Phys. Soc. Jpn* **61**, 4283 (1992).
7. Yip S., *Phys Rev. B* **52**, 3087 (1995).

Pergamon

J. Phys. Chem. Solids Vol. 56, No. 12, pp. 1763–1765, 1995
1995 Elsevier Science Ltd
Printed in Great Britain
0022–3697/95 $9.50 + 0.00

0022–3697(95)00230-8

A GAPLESS TIME-REVERSAL SYMMETRY VIOLATING SUPERCONDUCTOR *

A. M. TIKOFSKY
Institute for Theoretical Physics, U.C.-Santa Barbara, Santa Barbara, CA 93106, U.S.A.

D. B. BAILEY
Department of Physics, Stanford University, Stanford, CA 94305, U.S.A.

Abstract—We consider a layered superconductor with a complex order parameter whose phase switches sign from one layer to the next. This system is shown to exhibit gapless superconductivity for sufficiently large interlayer pairing or interlayer hopping. In addition, this description is consistent with experiments finding signals of time reversal symmetry breaking in high-temperature superconductors only at the surface and not in the sample bulk.

It has been proposed that the many-particle ground state of the high temperature superconductors breaks time-reversal symmetry $\mathcal{T}$ [1,2]. As yet, no clear experimental signatures of $\mathcal{T}$-violation in the superconducting bulk have been found [3,4]. Studies of $\mathcal{T}$-violating ground states for model magnetic Hamiltonians predict a $d_{x^2-y^2} + i\epsilon d_{xy}$ order parameter [5]. This order parameter does not vanish anywhere on the Fermi surface and therefore appears to be ruled out by experimental studies of high-temperature superconductors which indicate the presence of isolated nodes on the fermi surface [6–8]. A different set of experiments finds signs of a nodeless $\mathcal{T}$-violating order parameter at the surface of the sample. Evidence of a superconducting gap has been found at isolated point on the sample surface in STM studies [9]. A gap feature of approximately 5 meV is always observed in c-axis tunneling between YBCO and a conventional superconductor [6]. Anomalous distributions of magnetic flux have been observed at crystal grain boundaries in $YBa_2Cu_3O_7$ [10]. This experiment is interpreted as evidence for $\mathcal{T}$-violation [11].

We study the properties of a complex order parameter with a two layer unit cell. The phase of the order parameter changes sign from layer to layer. We show that interlayer pairing and tunneling render this superconductor gapless at isolated nodes. Our calculation only describes bulk properties because it relies on the symmetries of the unit cell. Because these symmetries need not be satisfied at sample boundaries, our model is consistent not only with gapless superconductivity in the bulk but also with $\mathcal{T}$-violating gapped superconductivity at the boundaries.

Let us now investigate the behavior of multilayer $\mathcal{T}$-violating superconductivity. Studies of coupled $\mathcal{T}$-violating systems have found that it is energetically favorable for the sign of the $\mathcal{T}$-violation to be opposite in the two systems [12]. We therefore choose the order parameter to be $\Delta_{\mathbf{k}}$ in the first layer and $\Delta_{\mathbf{k}}^*$ in the second layer. We also assume an in-plane spectrum for the non-interacting electrons of $\epsilon_{\mathbf{k}}$, a hopping matrix element between layers of $t_{\perp\mathbf{k}}$, and a bilayer order parameter of $\Delta_{\perp\mathbf{k}}$. The standard approach is to define quasiparticle creation and annihilation operators $a^\dagger_{\mathbf{k}\sigma i}$ ($i = 1, 2$ for the first and second planes respectively, $\sigma = \uparrow, \downarrow$) [13]. The Hamiltonian is then

$$\begin{aligned}\mathcal{H} &= \sum_{\mathbf{k}\sigma i} \epsilon_{\mathbf{k}} a^\dagger_{\mathbf{k}\sigma i} a_{\mathbf{k}\sigma i} \\ &+ \sum_{\mathbf{k}\sigma} \left[t_{\perp\mathbf{k}} a^\dagger_{\mathbf{k}\sigma 1} a_{\mathbf{k}\sigma 2} + t^*_{\perp\mathbf{k}} a^\dagger_{\mathbf{k}\sigma 2} a_{\mathbf{k}\sigma 1} \right] \\ &- \sum_{\mathbf{k}} \Big[\Delta_{\perp\mathbf{k}} (a^\dagger_{\mathbf{k}\uparrow 1} a^\dagger_{-\mathbf{k}\downarrow 2} + a_{-\mathbf{k}\downarrow 2} a_{\mathbf{k}\uparrow 1}) + \text{c.c} \\ &\quad + \Delta_{\mathbf{k}} (a^\dagger_{\mathbf{k}\uparrow 1} a^\dagger_{-\mathbf{k}\downarrow 1} + a_{-\mathbf{k}\downarrow 2} a_{\mathbf{k}\uparrow 2}) + \text{c.c} \Big]. \end{aligned} \quad (1)$$

We define $\xi_{\mathbf{k}} = \epsilon_{\mathbf{k}} - \mu = -2t(\cos k_x + \cos k_y) - \mu$, $\Delta_{\mathbf{k}} = \Delta_0(\cos k_x - \cos k_y + i\epsilon \sin k_x \sin k_y)$, and take both $\Delta_{\perp\mathbf{k}}$ and $t_{\perp\mathbf{k}}$ to be real. Writing $\Delta_{\mathbf{k}} = \Delta_{R\mathbf{k}} + i\Delta_{I\mathbf{k}}$, we find that $\mathcal{H}$ has energy eigenvalues $E_\pm(\mathbf{k})$ that satisfy

$$\begin{aligned} E^2_\pm(\mathbf{k}) &= \xi^2_{\mathbf{k}} + |\Delta_{\mathbf{k}}|^2 + \Delta^2_{\perp\mathbf{k}} + t^2_{\perp\mathbf{k}} \\ &\pm 2\sqrt{(\xi_{\mathbf{k}} t_{\perp\mathbf{k}} + \Delta_{\perp\mathbf{k}}\Delta_{R\mathbf{k}})^2 + \Delta^2_{I\mathbf{k}}(t^2_{\perp\mathbf{k}} + \Delta^2_{\perp\mathbf{k}})}. \end{aligned} \quad (2)$$

The spectrum for $E_-(\mathbf{k})$ vanishes when

$$\xi_{\mathbf{k}} = t_{\perp\mathbf{k}} \alpha_{\mathbf{k}}, \qquad \Delta_{R\mathbf{k}} = \Delta_{\perp\mathbf{k}} \alpha_{\mathbf{k}}, \quad (3)$$

and

$$\alpha^2_{\mathbf{k}} = 1 - \frac{\Delta^2_{I\mathbf{k}}}{t^2_{\perp\mathbf{k}} + \Delta^2_{\perp\mathbf{k}}}, \quad (4)$$

which is consistent with experiments that find a bulk order parameter with a d-wave like node [6–8,14,15]. If the phase of the order parameter were the same in neighboring planes, the corresponding energy eigenvalue would be nodeless except for a special value of $\Delta_{\perp\mathbf{k}}$.

* Expanded version of a poster presented at the Stanford Conference on Spectroscopies in Novel Superconductors (Stanford, March 1995)

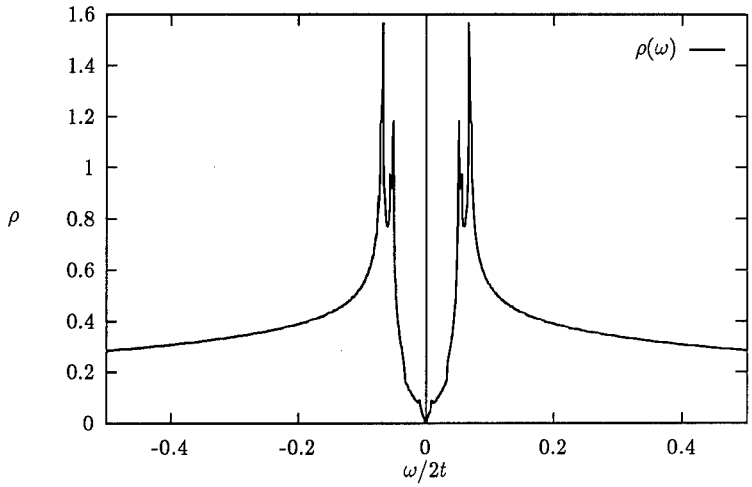


Fig. 1. Density of states $\rho(\omega)$ plotted vs $\omega/2t$ for $t = 0.5$ eV, $t_\perp = 20$ meV, $\Delta_0 = 30$ meV, $\Delta_\perp = 8$ meV, $\epsilon = 0.4$, and $\mu = 0$.

The node in the quasiparticle spectrum is apparent in the single particle density of states shown in Fig. 1. The side peaks are expected from the splitting of the bands by $t_{\perp\mathbf{k}}$.

In order to have a nodeless order parameter, we must be able to satisfy eqn (3)–(4). The constraint that $\alpha_\mathbf{k}$ be real requires

$$t_{\perp\mathbf{k}}^2 + \Delta_{\perp\mathbf{k}}^2 \geq \Delta_{I\mathbf{k}}^2 . \tag{5}$$

This intuitive result tells us that the combined effect of interlayer pairing and interlayer tunneling has to be sufficiently large in order to overcome the gap due to the imaginary component of the order parameter. The existence of a solution to eqn (3) also requires that $\Delta_\perp/\Delta_0$ be sufficiently small.

The zeros of eqn (2) need not lie on the 45° ($k_x = \pm k_y$) nodal line of the pure $d_{x^2-y^2}$ order parameter. To first order in $t_\perp/t$ and $\Delta_\perp/\Delta_o$ and in the $t >> \epsilon\Delta_o$ limit, the nodal wavevector $\mathbf{k}$ is shifted from the 45° nodal line to an angle $\pi/4 + \frac{\alpha_\mathbf{k}\Delta_{\perp\mathbf{k}}}{\pi\Delta_o}$. There are two nodes because $\alpha_\mathbf{k}$ may be either positive or negative. These effects (node splitting and angular shift of 10°) have been observed in angular resolved photoemission studies of $Bi_2Sr_2CaCu_2O_8$ [16]. A similar analysis of the momentum shifts for the case of a purely real order parameter [17,18] corresponds to taking $\alpha_\mathbf{k} = \pm 1$. Therefore, the bulk photoemission experiments cannot distinguish qualitatively between a purely real and an alternating complex order parameter.

It is expected that a $\mathcal{T}$-violating layer will couple to an electron or neutron spin as if it induced a local magnetic field. A neutron with momentum $q = (0, 0, \pi/d)$ where d is the distance between planes, will couple to the chirality oscillation. The size of this feature depends on the coupling strength which has not been accurately calculated. In addition, muon spin rotation experiments, which probe the local magnetic field, fail to find an effective magnetic field larger than that due to the Cu nuclei [4].

A rapidly oscillating complex order parameter will generate large Josephson screening currents. These currents should be heavily damped when the spectrum is gapless. If the spectrum has a gap then these currents may be observable and would be a measure of the amount of $\mathcal{T}$-reversal violation. Our complex order parameter may also explain other Josephson tunneling experiments [19–22].

The $\mathcal{T}$-violating component of the alternating order parameter should have a transition temperature $T^* < T_c$ where T_c is the bulk transition temperature. The experimental results that we attribute to $\mathcal{T}$-violation are expected to disappear for temperatures above T^*. In fact, recent experiments in oxygenated samples of YBCO have found a second transition at 30K in T_2 measurements [23].

Acknowledgements—We have benefited from useful conversations with M. Beasley, R. B. Laughlin, D. Scalapino, S. C. Zhang, N. Nagaosa and M. Sigrist. This work has been supported in part by NSF grants PHY89-04035 (A.M.T.) and DMR-9120361-002 (D.B.B.), and the NSF MRL program through the Center for Materials Researh at Stanford University. D. B. Bailey gratefully acknowledges the support of an NSF fellowship.

REFERENCES

1. Laughlin R. B., *Science* **235**, 525 (1988); Kalmeyer V. and Laughlin R. B., *Phys. Rev. B* **39**, 11879 (1989).
2. Dai Q., Levy J. L., Fetter A. L., Hanna C. B. and Laughlin R. B., *Phys. Rev. B* **46**, 5642 (1992), and references therein; Tikofsky A. M., Laughlin R. B. and Zou Z., *Phys. Rev. Lett.* **69**, 3670 (1992); Tikofsky A. M. and Laughlin R. B., *Phys. Rev. B* **50**, 10165 (1994).
3. Spielman S. *et al.*, *Phys. Rev. Lett.* **64**, 123 (1990); *ibid.*, *Phys. Rev. B* **45**, 3149 (1992); Lawrence T. W., Szöke A. and Laughlin R. B., *Phys. Rev. Lett.* **69**, 1439 (1992).
4. Kiefl R. E. *et al.*, *Phys. Rev. Lett.* **64**, 2082 (1990); Nishida N. and Miyatake H., *Hyperfine Interact.* **63**, 183 (1990).
5. Laughlin R. B., *Physica C* **234**, 280 (1995); Rokhsar D. S., *Phys. Rev. Lett.* **70**, 493 (1993).
6. Valles J. M., *et al.*, *Phys. Rev. B* **44**, 11986 (1991).

7. Hardy W. N., Bonn D. A., Morgan D. C., Liang R. and Zhang K., *Phys. Rev. Lett.* **70**, 3999 (1993).
8. Moler K., *et al.*, *Phys. Rev. Lett.* **73**, 2744 (1994).
9. Hasegawa T., *et al.*, *J. Phys. Chem. Solids* **54**, 1351 (1993).
10. Kirtley J. R., Chaudhari P., Ketchen M., Khare N., Lin S-Y. and Shaw T., IBM Yorktown Hts, preprint.
11. Sigrist M., Bailey D. and Laughlin R. B., to appear in *Phys. Rev. Lett.*, cond-mat/9407087.
12. Rojo A. G. and Canright G. S., *Phys. Rev. Lett.* **66**, 949 (1991); Rojo A. G. and Leggett A. J., *Phys. Rev. Lett.* **67**, 3614 (1991).
13. Abrikosov A. A., *Physica C* **182**, 191 (1991); Abrikosov A. A. and Klemm R. A., *Physica C* **191**, 224 (1992); Atkinson W. A. and Carbotte J. P., preprint, supr-con/9411003.
14. Wollman D. A. *et al.*, *Phys. Rev. Lett.* **71**, 2134 (1993).
15. Tsuei C. C. *et al.*, *Phys. Rev. Lett.* **73**, 593 (1994).
16. Ding H. *et al.*, Argonne preprint.
17. Kuboki K. and Lee P. A., preprint, cond-mat/9501030.
18. Ubbens M. and Lee P. A., *Phys. Rev. B* **50**, 438 (1994).
19. Bailey D. B. and Tikofsky A. M., in preparation.
20. Chaudhari P. and Lin S.-Y., *Phys. Rev. Lett.* **72**, 1048 (1994).
21. Sun A. G., *et al.*, *Phys. Rev. Lett.* **72**, 2267 (1994).
22. Beasley M. R., Lew D. and Laughlin R. B., *Phys. Rev. B.* **49**, 12330 (1994).
23. Itoh Y. *et al.*, *J. Phys. Soc. Jpn* **63**, 1455 (1994).

Pergamon

J. Phys. Chem. Solids Vol. 56, No. 12, pp. 1767–1768, 1995
Copyright © 1995 Elsevier Science Ltd
Printed in Great Britain. All rights reserved
0022-3697/95 $9.50 + 0.00

0022-3697(95)00190-5

ENERGY SPECTRUM OF QUASIPARTICLES FOR VARIOUS PAIRING STATES IN 2-D EXTENDED HUBBARD MODEL

YASUNARI USHIJIMA, YUKIO TANAKA
Department of Physics, Niigata University, Ikarashi, Niigata 950-21, Japan

HIROKI TSUCHIURA
Department of Applied Physics Osaka University, Suita Osaka 565, Japan

Abstract—The energy spectrum of superconducting state of extended Hubbard model is investigated for various pairing states based on the selfconsistent calculation. Density of states of quasiparticle (DOS) for various pairing states strongly depend on the shape of the Fermi surface. We have found there exists a qualitative difference between the DOS of $s + d$-wave state and those of $s + id$-wave state.

1. INTRODUCTION

The determination of symmetries of pair potentials is one of the hottest issues in physics of high $T_c$superconductors. Several theories and experiments support the arguments s-wave symmetry, however the controversy over whether symmetry is s-wave or d-wave is not settled yet [1–3]. At this stage we have a fundamental question— whether s-wave and d-wave pairing coexist or not? This problem is also important apart from the high-$T_c$physics. For this reasons, in this paper, we will investigate the 2-D extended Hubbard model which describes the anisotropic pairings in the simplest form in the narrow band systems. Although the phase diagram of this Hamiltonian in the one-dimensional case is determined recently by the exact diagonalization, the detailed feature of the 2-D system is not known. We will therefore investigate this model within the mean field approximation (MFA) level by the selfconsistent numerical calculations and obtain the density of states (DOS) of quasiparticles. The relevance of the shape of the Fermi surface and DOS will be discussed in detail.

2. FORMULATION

The Hamiltonian, H, of the 2-D extended Hubbard model is given as,

$$H = \sum_{ij\sigma}(t_{ij} - \mu\delta_{ij})c^{\dagger}_{i\sigma}c_{j\sigma} + U\sum_{i} n_{i\uparrow}n_{i\downarrow} - \frac{W}{2}\sum_{<ij>\sigma\sigma'} n_{i\sigma}n_{j\sigma'},\ n_{i\sigma} = c^{\dagger}_{i\sigma}c_{i\sigma}, \quad (1)$$

with on-site repulsive interaction U and inter-site attractive interaction W ($U, W > 0$). We consider this model on a 2-D square lattice with N sites. In eqn (1), $c^{\dagger}_{i\sigma}$, μ, and t_{ij} are the creation operator for spin $\sigma = \uparrow$ at site i, chemical potential, and transfer integral, respectively. Within the MFA, extensive investigations have been done by Micnas *et al.* [4]. In their calculations, the renormalization of the band width that originates from Fock term is not fully taken into account. Furthermore the coexistence of s-wave and d-wave pairing, and DOS still remains to be studied. In our previous paper [5], Free energy at zero temperature is obtained by determining the chemical potential, the renormalization factor of the band width, and pair potentials. We have found that under the coexistence of the s or d-wave pairing, $s + id$-wave pairing state becomes most stable. In this paper, we have extended our previous theory to finite temperature and have also obtained the energy spectrum of the quasi particles. The density of states of the quasiparticle (DOS) is obtained for various pairing states. In the light of our recent investigations of tunnel spectroscopy, DOS is expected to be observed in the tunneling conductance of normal metal/insulator/superconductor junction in z direction, where 2-D square lattice is in the xy plane [6,7].

3. RESULTS

We have determined the Free energy of s, d, $s+d$, $s+id$-wave pairing states, whose pair potentials $\Delta(k)$ can be expressed as $r_0 + r_s\gamma_k$, $r_d\eta_k$, $r_0 + r_s\gamma_k + r_d\eta_k$ and $r_0 + r_s\gamma_k + ir_d\eta_k$ respectively, with $\eta_k = 2(\cos k_x - \cos k_y)$, and $\gamma_k = 2(\cos k_x + \cos k_y)$. Within our numerical calculations, the $s + id$-wave state becomes the most stable. In the following, we paid special attention to the next nearest neighbor hopping effect, i.e. Fermi surface effect. The dispersion of quasiparticle for $U = W = 0$ can be expressed as

$$\varepsilon_k = -2t(\cos k_x + \cos k_y) - 4t' \cos k_x \cos k_y. \quad (2)$$

As discussed in our previous paper, the coexistence of s and d wave pairings can not occur for zero t'. Coexistence can

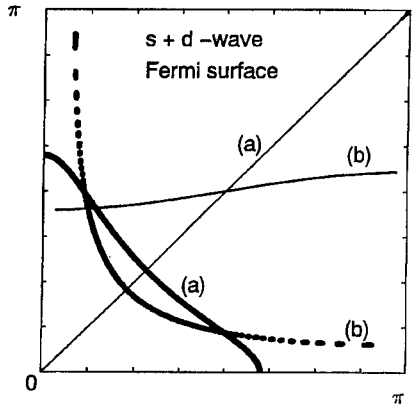


Fig. 1. Schematic illustraion of the Fermi surface and the ZL for $s + d$-wave pairing. Bold line expresses the renormalized Fermi surface. Thin line expresses the ZL. (a)$t' = -0.35t$, (b)$t' = -0.45t$.

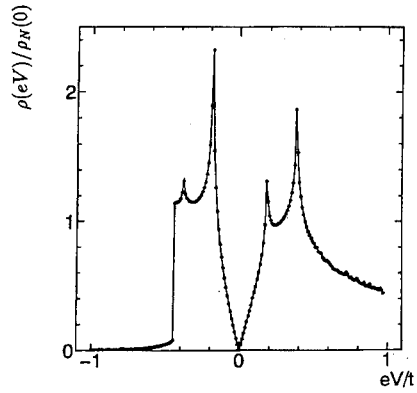


Fig. 2. $\rho(eV)$ is plotted for $s + d$-wave pairing with $t' = -0.35t$, $W = t$ $U = t$ and $n = 0.4$, where $\rho_N(0)$ expresses the DOS at $eV = 0$ at normal state.

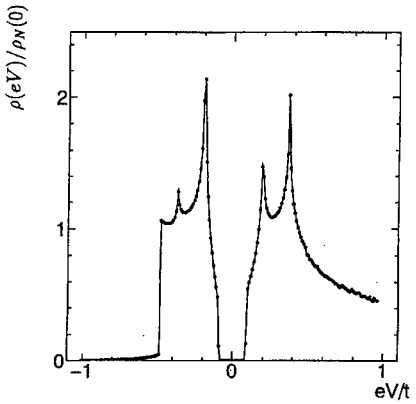


Fig. 3. Similar plots to Fig. 2 for $s + id$-wave pairing states for $t' = -0.35t$, $W = t$ $U = t$ and $n = 0.4$.

be expected for hole doped region ($n > 1$) with positive t'/t, and electron doped region ($n < 1$) with negative t'/t. In the following, let us discuss the tunneling conductance [8]

$$\frac{dI}{dV} = \frac{const}{k_B T} \int_{-\infty}^{\infty} dE \rho(E) sech^2\left(\frac{E - eV}{2k_B T}\right) \tag{3}$$

which expresses DOS of quasiparticle $\rho(eV)$ at sufficiently low temperature. In the case of s-wave pairing, the quantity U strongly destroys superconductivity. When the line, which expresses the zero of $\Delta(k)$, ZL, i.e. $\Delta(k) = 0$, intersects the Fermi surface, V shaped energy gap structure is obtained in $\rho(eV)$ (for exeample $W = 1.0t, U = 0, t' = -0.45t$). On the other hand, in the case when ZL does not intersect the Fermi surface, a U shaped energy gap structure (for example $W = 1.0t, U = 0, t' = -0.35t$) is obtained. In the case of d-wave pairing state, the pair potential is independent of U within the mean field approximation. For any U, ZL becomes a straight line from (0,0) to (π,π) in the first Brillouin zone, and a V shaped structure is obtained for $|t'| < 0.5t$. For $|t'| > 0.6t$ with $W = 1.0t$, a U shaped structure is obtained. However in such a case, the superconducting state is unable as compared with non-ordered state. Within our results, the d-wave pairing state always has a V shaped structure of DOS. The shape of Fermi surface and ZL of the pair potentials for various t' are plotted in Fig. 1 for $s + d$-wave pairing state. In every case, since ZL intersects the Fermi surface, we can expect V shaped structure of DOS as shown in Fig. 2. In the case of $s + id$-wave pairing state, ZL becomes a point, and pair potential does not vanish on the Fermi surface. In such a case, a U shaped structure like Fig. 3 is expected.

4. CONCLUSIONS

We have developed a numerical method to obtain the Free energy of the extended Hubbard model in the superconducting state determining the chemical potential, renormalization factor of the band width and pair potentials at finite temperature. It has been believed that the shape of the energy gap in DOS becomes U-shaped in the s-wave state and V-shaped in the d-wave state in the free electron model. Here we have found that the above facts do not always hold in general and the shape of DOS strongly depends on the band structure. It is revealed that DOS of $s + d$-wave state is substantially different from the DOS of $s + id$-wave state.

REFERENCES

1. Wollman D. A., Harlingen D. J. V., Lee W. C., Ginsberg D. M. G. and Legett A. J., *Phys. Rev. Lett.* **71** 2134 (1993).
2. Hasegawa T. and Kitazawa K., *J. Phys. Chem. Sol.* **54** 1351 (1993).
3. Tanaka Y. *Phys. Rev. Lett.* **72**, 3871 (1994).
4. Micnas R., Ranninger J. and Robaszkiewicz S., *Rev. Mod. Phys.* **62** 113 (1990).
5. Tsuchiura H., Tanaka Y. and Ushijima Y., to be published in *J. Phys. Soc. Jpn.*
6. Tanaka Y. and Kashiwaya S., *Phys. Rev. Lett.* **74**, 3451 (1995).
7. Kashiwaya S., Tanaka Y., Koyanagi M. and Kajimura K., *Phys. Rev. B* **51** 1350 (1995).
8. Sato O., Tanaka Y. and Hasegawa A., *J. Phys. Soc. Jpn* **61**, 2640 (1992).

Pergamon

J. Phys. Chem. Solids Vol. 56, No. 12, pp. 1769–1771, 1995
Copyright © 1995 Elsevier Science Ltd
Printed in Great Britain. All rights reserved
0022–3697/95 $9.50 + 0.00

0022-3697(95)00168-9

DESTRUCTION OF THE FERMI LIQUID BY SPIN FLUCTUATIONS IN TWO DIMENSIONS

Y. M. VILK and A. -M. S. TREMBLAY
Département de Physique and Centre de Recherche en Physique du Solide,
Université de Sherbrooke, Sherbrooke, Québec, Canada J1K 2R1

Abstract—It is shown that it is possible to quantitatively explain quantum Monte-Carlo results for the Green's function of the two-dimensional Hubbard model in the weak to intermediate coupling regime. The analytic approach includes vertex corrections in a paramagnon-like self-energy. All parameters are determined self-consistently. This approach clearly shows that in two dimensions Fermi-liquid quasiparticles disappear in the paramagnetic state when the antiferromagnetic correlation length becomes larger than the electronic thermal de Broglie wavelength.

Keywords: Hubbard model, spectral weight, spin fluctuations, vertex corrections, paramagnons, photoemission.

INTRODUCTION

We introduce a simple approach to the Hubbard model which includes vertex corrections, and achieves, for both two-particle and single-particle properties, better quantitative agreement with Monte-Carlo simulations than previous theories [1][2][3]. Our analytical approach allows us to unambiguously interpret the Monte-Carlo data and to show that in two dimensions spin fluctuations destroy the Fermi liquid in the paramagnetic state when the antiferromagnetic correlation length becomes larger than the thermal de Broglie wavelength of electrons. This corresponds to the disappearance of the quasiparticle peak and the appearance of a pseudogap, an issue that has been controversial mostly due to finite-size effects in Monte-Carlo [4].

We consider the one-band Hubbard model on the square lattice with unit lattice spacing, on-site repulsion U and nearest-neighbor hopping t. We work in units where the lattice spacing is unity, $k_B = 1$, $\hbar = 1$ and $t = 1$. The theory has a simple structure that we now explain physically.

The calculation proceeds in two steps: we first obtain spin and charge susceptibilities, then we inject them in the self-energy calculation. In the calculation of susceptibilities, spin and charge susceptibilities χ_{sp}, χ_{ch} are given by RPA-like forms but with two different effective interactions U_{sp} and U_{ch} which are then determined self-consistently, as described in Ref. [5]. This procedure reproduces both Kanamori–Brueckner screening as well as the effect of Mermin–Wagner thermal fluctuations, giving a phase transition only at zero-temperature in two-dimensions [5]. There is however a crossover temperature T_X below which the magnetic correlation length ξ grows exponentially. Quantitative agreement with Monte-Carlo simulations is obtained [5] for all fillings and temperatures in the weak to intermediate coupling regime $U < 8$.

We now turn to the discussion of the single-particle properties. In order, to be consistent with the two-particle correlation functions, the self-energy $\Sigma_\sigma(k)$ must satisfy the sum rule

$$\lim_{\tau\to 0^-} \frac{1}{\beta N} \sum_k \Sigma_\sigma(k)\, G_\sigma(k)\, e^{-ik_n\tau} = U\langle n_\uparrow n_\downarrow\rangle, \qquad (1)$$

which follows from the definition of $\Sigma_\sigma(k)$. Here, we encounter the same key quantity $\langle n_\uparrow n_\downarrow\rangle$ that appears in the sum rule for the susceptibilities. We find the following expression for $\Sigma_\sigma(k)$

$$\Sigma_\sigma(k) = Un_{-\sigma} + \frac{U}{4}\frac{T}{N} \times \sum_q \left[U_{sp}\chi_{sp}(q) + U_{ch}\chi_{ch}(q)\right] G^0_\sigma(k+q), \qquad (2)$$

which satisfies Eqn (1) with G_σ replaced by G^0_σ on the left-hand side. This self-energy expression (2) is physically appealing since, as expected from general skeleton diagrams, one of the vertices is the bare one U, while the other vertex is dressed and given by U_{sp} or U_{ch} depending on the type of fluctuation being exchanged. Equation (2) already gives good agreement with Monte-Carlo data but the accuracy can be improved even further by requiring that the consistency condition (1) be satisfied with G_σ instead of G^0_σ. To do so we replace U_{sp} and U_{ch} on the right-hand side of (2) by αU_{sp} and αU_{ch} with α determined self-consistently by Eqn (1). For $U < 4$, we have $\alpha < 1.15$. This concludes the description of the structure of our theory.

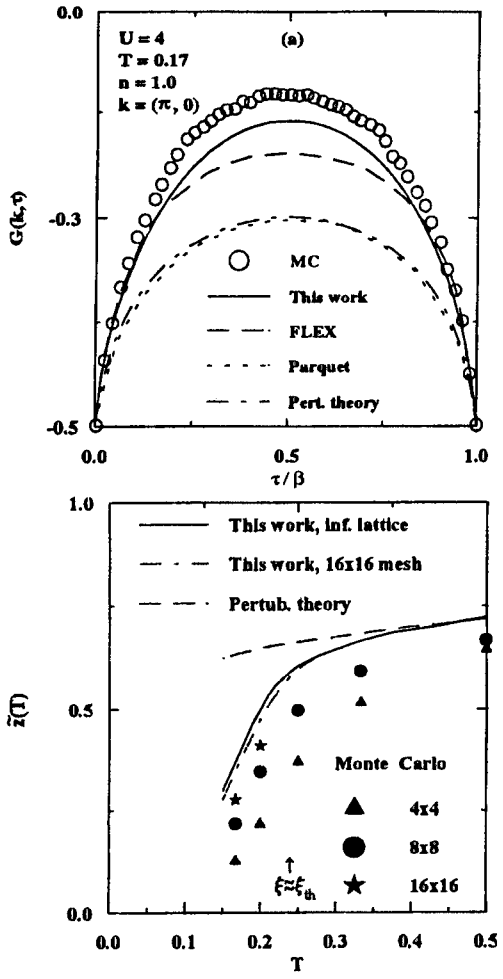


Fig. 1. (a) Comparison of our results for $G(\mathbf{k}, \tau)$ with Monte-Carlo data, FLEX, parquet, and second-order pertubation theory, all on 8×8 mesh. Monte-Carlo data and results for FLEX and parquet are from Ref. [3] $n = 1$, $T = 0.17$. (b) Temperature dependence of the generalized renormalization factor $\tilde{z}$ defined in Eqn (3). Lines are results of our calculations for infinite lattice and 16×16 mesh. Symbols are Monte-Carlo data from Ref. [3]

COMPARISONS WITH OTHER THEORIES AND WITH QUANTUM MONTE-CARLO DATA

Figure 1(a) shows $G(\mathbf{k}_F, \tau)$ for $\mathbf{k}_F = (\pi, 0)$ in a regime where the antiferromagnetic correlation length is growing exponentially. Our theory shows better agreement with Monte-Carlo than previous approaches.

Our most dramatic numerical results addressing the issue of the Fermi liquid are shown in Fig. 1(b) where we plot

$$\tilde{z}(T) = -2G(\mathbf{k}_F, \beta/2) = \int \frac{d\omega}{2\pi} \frac{A(\mathbf{k}_F, \omega)}{\cosh(\beta\omega/2)}. \qquad (3)$$

This quantity $\tilde{z}(T)$ is an average of the single-particle spectral weight $A(\mathbf{k}_F, \omega)$ within $T \equiv 1/\beta$ around the Fermi level ($\omega = 0$) and it is a generalization of the usual zero-temperature quasiparticle renormalization factor $z \equiv 1/(1 - \partial\Sigma/\partial\omega)$. For non-interacting particles $\tilde{z}(T)$ is unity. For a normal Fermi liquid it becomes equal to a constant less than unity as the temperature decreases. The quantity $\tilde{z}(T)$ gives an estimate of $A(\mathbf{k}_F, \omega)$ around the Fermi surface even when the Fermi liquid does not exist.

One can clearly see from Fig. 1(b) that while second-order perturbation theory exhibits typical Fermi-liquid behavior for $\tilde{z}(T)$, both Monte-Carlo data and a numerical evaluation of our expression for the self-energy lead to a rapid fall-off of $\tilde{z}(T)$ below T_X (for $U = 4$, $T_X \approx 0.2$ [5]). The physical origin of this effect is that the quasi-particles of the *two-dimensional* paramagnetic state become overdamped when the energy scale associated with the proximity to antiferromagnetism $\delta U \equiv U_{mf,c} - U_{sp}$ ($U_{mf,c} \equiv 2/\chi_0(\mathbf{Q}, 0)$) becomes exponentially small.

PSEUDOGAP

While size effects and statistical errors make continuation of the Monte-Carlo data to real frequencies particularly difficult, in our approach we can make this continuation analytically to show that the above effect corresponds to a pseudogap.

Since the spin susceptibility $\chi_{sp}(\mathbf{q}, 0)$ below T_X is almost singular at the antiferromagnetic wave vector $\mathbf{Q} = (\pi, \pi)$, the main contribution to Σ in Eqn (2) comes from $iq_n = 0$ and wave vectors $(\mathbf{q} - \mathbf{Q})^2 \leq \xi^{-2}$ near $\mathbf{Q}$. Approximating $\chi_{sp}(\mathbf{q}, 0)$ in by its asymptotic form $\chi_{sp}(\mathbf{q}, 0) \approx 2\left[U_{sp}\xi_0^2(\xi^{-2} + (\mathbf{q} - \mathbf{Q})^2)\right]^{-1}$ where $\xi_0^2 \equiv \frac{-1}{2\chi_0(Q)} \frac{\partial^2\chi_0(Q)}{\partial q_x^2}$ and $\xi \equiv \xi_0(U_{sp}/\delta U)^{1/2} \sim \exp\left(\pi\tilde{\sigma}^2\xi_0^2\frac{U_{sp}}{T}\right)$, the integrals over $\mathbf{q}$ can be done to obtain the low-frequency asymptotic results

$$\Sigma^R(\mathbf{k}_F, \omega) = \frac{U}{2} + \frac{UT}{8\pi\xi_0^2\sqrt{\omega^2 + v_F^2\xi^{-2}}} \times \left[\ln\left|\frac{\omega + \sqrt{\omega^2 + v_F^2\xi^{-2}}}{\omega - \sqrt{\omega^2 + v_F^2\xi^{-2}}}\right| - i\pi\right] \qquad (4)$$

Exactly at the Fermi surface ($\omega = 0$) the imaginary part of the self-energy for $\xi > \xi_{th}$ increases exponentially when the temperature decreases, $\Sigma''(\mathbf{k}_F, 0) \sim U\xi/(\xi_{th}\xi_0^2) \sim \exp(\pi\tilde{\sigma}^2\xi_0^2U_{sp}/T)$, ($\xi_{th} \equiv v_F/\pi T$). This corresponds to a pseudogap: instead of a quasiparticle peak, the spectral weight has a minimum at the Fermi level and two symmetrically located maxima away from it. Clearly this is not a Fermi liquid, yet the symmetry of the system remains unbroken at any finite T. By contrast * with $3D$, in $2D$ this effect exists in a wide temperature range $T < T_X$. These conclusions persist slightly away from half-filling. In particular, we do not find a quasiparticle peak in the pseudogap close to half-filling when $\xi \gg \xi_{th}$. This is different from the results inferred from a phenomenological zero-temperature

* In the isotropic $3D$ case $\Sigma''(\mathbf{k}_F, \omega) \sim (\ln\xi)/\xi_{th}$ and hence the pseudogap exists only in a very narrow temperature range.

calculation[6] ($\xi_{th} = \infty$) which physically corresponds to $1 \ll \xi \ll \xi_{th}$.

In photoemission experiments on real quasi two-dimensional materials we predict a rapid decrease of the spectral weight and density of states at the Fermi level in a wide temperature range, from T_X to the Néel temperature T_N ($T_X - T_N \sim 10^2$ K).

REFERENCES

1. Bickers N. E. and Scalapino D. J., *Annal. Phys.* **193**, 206 (1989).
2. Bickers N. E., *Int. J. ModPhys. B* **5**, 253 (1991).
3. Bickers N. E. and White S. R., *Phys. Rev. B* **43**, 8044 (1991).
4. White S. R., *Phys. Rev. B* **46**, 5679 (1992); Vekić M. and White S. R., *Phys. Rev. B* **46**, 5679 (1992).
5. Vilk Y. M., Liang Chen and Tremblay A. -M. S., *Phys. Rev. B* **49**, 13,267 (1994).
6. Kampf A. P. and Schrieffer J. R., *Phys. Rev. B* **41**, 6399 (1990); *Phys. Rev. B* **42**, 7967 (1990).

Pergamon

J. Phys. Chem. Solids Vol. 56, No. 12, pp. 1773–1774, 1995
Copyright © 1995 Elsevier Science Ltd
Printed in Great Britain. All rights reserved
0022–3697/95 $9.50 + 0.00

0022–3697(95)00217-0

GIANT JOSEPHSON CURRENT THROUGH A SINGLE BOUND STATE IN A SUPERCONDUCTING TUNNEL JUNCTION

G. WENDIN * and V. S. SHUMEIKO *,†

* Department of Applied Physics, Chalmers University of Technology and Göteborg University, S-41296 Göteborg, Sweden
† B. Verkin Institute for Low temperature Physics and Engineering,47 Lenin Ave., 310164 Kharkov, Ukraine

Abstract—We study the microscopic structure of the Josephson current in a one-mode tunnel junction with a wide quasiclassical tunnel barrier. In such a junction each Andreev bound state carries a current of magnitude proportional to the *amplitude* of the normal electron transmission through the junction. The currents of all bound states nearly cancel each other in equilibrium, yielding the conventional Josephson current. The giant current of a single bound level can be observed under nonequilibrium conditions.

The mechanism for Josephson current transport in weak links and tunnel junctions is a very well studied problem. A modern scenario [1–3] describes SIS-tunneling in terms of current-induced Andreev-like superconducting bound states which provide transmission of supercurrent through the tunnel barrier. However, there are still some surprises to be found. We shall demonstrate that in Josephson tunnel junctions with wide quasiclassical tunnel barriers, the usual pair of Andreev bound states becomes split into four levels, each bound state—now representing coupled *surface Andreev states*—carrying a giant Josephson current proportional to *the square root of the junction transparency*, $\sqrt{D}$ rather than D. These currents do not appear under equilibrium conditions: they nearly cancel each other and yield a relatively small residual current. This residual current together with a contribution from the continuum constitute the Josephson current measured in experiments. The net current of a single bound state can be observed only under *nonequilibrium* conditions.

We consider for the sake of clarity a single mode quantum constriction with a rectangular potential barrier of length L and height V. The structure is described by the 1D Bogoliubov–de Gennes equation [4]. Matching wave functions by means of a transfer matrix formalism [5] we find the transmission amplitudes $t^{N,A}$ of incoming quasiparticles which are scattered into the normal (N) and Andreev (A) channels.

The bound levels are determined by the poles of these transmission amplitudes. The general solution for the bound levels is:

$$E^2 = \Delta^2 \cos^2\left(\frac{|\beta| \pm |\alpha|}{2}\right), \quad (|\beta| \pm \alpha > 0) \tag{1}$$

with

$$\cos\alpha = \sqrt{R_+R_-} + \sqrt{D_+D_-}\cos\phi \tag{2}$$

$$\sin\beta = \sqrt{D_+D_-}\,\mathrm{Im}(a_+a_-^*). \tag{3}$$

$D_\pm$ is the transmission coefficient of normal electrons with energy $\pm E$:

$$D_\pm = 1 - R_\pm = |a_\pm|^{-2},$$

$$a_\pm = \cosh\kappa_\pm L - \frac{i}{2}\left(\frac{\kappa_\pm}{k} - \frac{k}{\kappa_\pm}\right)\sinh\kappa_\pm L, \tag{4}$$

$$k = \sqrt{2m\tilde{\mu}}, \quad \kappa_\pm = \sqrt{2m(V - (\tilde{\mu} \pm E))}.$$

where $k = \sqrt{2m\tilde{\mu}}$, and $\kappa_\pm = \sqrt{2m(V - (\tilde{\mu} \pm E))}$. The effect of electron–hole dephasing within the superconducting electrodes may be omitted in eqn (4); however, "dephasing" inside the barrier ($\kappa_+ \neq \kappa_-$) is crucial.

The quantity β in eqns (1) and (3) describes the effect of dephasing of electron and hole wave functions and is proportional to the difference of damping rates of electrons (κ_+) and holes (κ_-) inside the barrier, $\delta\kappa = \kappa_+ - \kappa_-$:

$$\beta \approx \sin\beta \approx -\frac{2k\delta\kappa}{k^2 + \kappa^2}\tanh(2\kappa L) \ll 1. \tag{5}$$

In the limit of low transparency of the junction, for values of the phase difference ϕ not too close to zero ($|\phi| \gg |\delta\kappa|L$), the solution to eqn (1) can be written as,

$$E^2 = \Delta^2\left[1 - \left(\frac{|\beta|}{2} \pm \sqrt{D}\sin\frac{\phi}{2}\right)^2\right], \tag{6}$$

where $|\beta|/2 \pm \sqrt{D}|\sin(\phi/2)| > 0$. The solution generally consists of two pairs of bands $E(\phi)$ lying inside the superconducting gap, $|E| < \Delta$. All branches of the bound state spectrum are fully developed if

$$|\beta|/2 > \sqrt{D}, \quad \text{or} \quad \kappa L > \ln\left|\frac{\kappa}{\delta\kappa}\right|. \tag{7}$$

In such a *"long"* SIS junction the bound levels are characterized by two independent parameters: contact transparency D and dephasing factor β. From a physical point of view, the bound states in a long SIS junction result from hybridization of degenerate superconducting surface states

situated at well separated single superconductor–insulator (SI) boundaries; the energies of these surface states follow directly from eqn (6) in the limit $D = 0$: $E^2 = \Delta^2(1 - \beta^2/4)$. These Andreev-like surface states are formed by superposition of electron-like and hole-like quasiparticle states with different signs of electron momentum, similarly to the superconducting bound states in SN sandwiches [6]. They extend inside the superconductor on the characteristic length $l \sim v_F/\sqrt{\Delta^2 - E^2}$ and inside the insulator on the characteristic length $l \sim 1/\kappa$. The splitting of the surface levels, proportional to $\sqrt{D}$ due to (bonding and antibonding) coupling through a barrier of a finite width, is analogous to the splitting of normal electron bound levels in a double well potential.

When the dephasing effect is neglected, $\beta = 0$, one pair of the bound state bands disappears into the continuum, and the remaining solution of eqn (6) corresponds to the Andreev bound states found earlier [1–3]. A finite value of $\beta \neq 0$ causes a second pair of bands to be "pulled down" from the continuum; however, as long as the inequality $|\beta|/2 \ll \sqrt{D}$ holds, the approximation of the single pair of bound bands is still valid. This inequality is always met for short quantum barriers $\kappa L \ll 1$ (δ-function barriers). However, it is also met for short quasiclassical barriers in the range $1 \ll \kappa L \ll \ln|(\kappa/\delta\kappa)|$, where the effective boundary condition of the Andreev approximation, Refs [2,8–10], therefore is applicable. These two regions could be referred to as "short" SIS junctions.

The most striking feature of long SIS junctions is their potential ability to carry a giant tunnel current due to the current carrying properties of the bound states. Using the formula $I_j = 2e(dE_j/d\phi)$ [7] for calculating the quantum mechanical current of the jth bound state we get from eqn (6):

$$I_{1,2} = \mp\frac{e\Delta}{2}(D\sin\phi + |\beta|\sqrt{D}\cos\frac{\phi}{2})$$
$$I_{3,4} = \mp\frac{e\Delta}{2}(D\sin\phi - |\beta|\sqrt{D}\cos\frac{\phi}{2}) \qquad (8)$$

(j=1,2 correspond to the upper sign in eqn (6), j=3, 4 correspond to the lower sign). In the limit of $\beta \gg \sqrt{D}$ the current of each bound state is proportional to the transmission amplitude of the tunnel barrier and exceeds the Ambegaokar–Baratoff critical current [11] by a factor of $\beta/\sqrt{D}$; it also possesses an unusual $\cos(\phi/2)$ phase dependence, different from the conventional Josephson relation $I = I_c\sin\phi$. In equilibrium, these large currents, having opposite signs, cancel each other and result in a residual current equal to twice the Josephson tunnel current:

$$I_b = \sum_j I_j n_F(E_j) = 2I_c\sin\phi. \qquad (9)$$

Half of this current is compensated for by the contribution from the continuum.The total current thus finally coincides with the result of the conventional tunnel model [11].

The present calculation shows that the Josephson current in long SIS junctions possesses nontrivial intrinsic structure which uncovers the resonance character of Cooper pair tunneling. It is commonly accepted after Josephson [12] that the transparency of a tunnel barrier for Cooper pair tunneling is proportional, due to coherence effects, to the probability of single-particle tunneling. It follows from the present calculation that the true probability of Cooper pair tunneling exceeds this value: being proportional to the amplitude of single-particle tunneling it resembles coherent tunneling ofa Schrödinger particle in a periodic potential barrier structure.

Superconducting bound levels correspond to different quantum states of the system; therefore, experimental observation of the current of a single level is fundamentally allowed. One possibility is to inject excess quasiparticles into one of the bound levels by means of tunnel coupling to an additional normal electrode (see e.g. [13]), provided that the level splitting is sufficiently large in comparison with the level width. One might expect to observe the effect—giant Josephson current—in gate controlled S-2DEG-S devices with extremely low tunnel barriers. Another possibility would be to consider high T_c breakjunctions with rather large values of Δ/μ; however, strong coupling effects might lead to undesired smearing of the Andreev level structure. One way to enhance the possibility to observe the effect would be to introduce a normal region at the SI interface—SNI—in order to increase interlevel distance and to pull the levels away from the gap edges.

Acknowledgements—We gratefully acknowledge discussion with A. Slutskin and R. Shekhter. One of the authors (GW) acknowledges computational assistance by A. Berntsson during the initial stages of this work. This work has been supported by the Swedish Natural Science Research Council (NFR), and by the NUTEK/NFR Interdisciplinary Consortium on Superconducting Materials.

REFERENCES

1. Furusaki A. and Tsukada M., *Phys. Rev. B* **43**, 10164 (1991).
2. Shumeiko V. S., Wendin G. and Bratus' E. N., *Phys. Rev. B* **48**, 13129 (1993).
3. Kuplevakhskii S. V. and Fal'ko I. I., *Sov. J. Low Temp. Phys.* **17**, 501 (1991).
4. de Gennes P. G., *Superconductivity of Metals and Alloys*. Addison-Wesley, New York (1989).
5. Hurd M. and Wendin G., *Phys. Rev. B* **49**, 15258 (1994); **51**, 3754 (1995).
6. de Gennes P. G. and Saint-James D., *Phys. Lett.* **4**, 151 (1963).
7. Anderson P. W., in *The Many Body Problem*, Vol. 2, Academic, New York (1964)
8. Svidzinsky A. V. and Slusarev V. A., *Phys. Lett. A* **27**, 22 (1968).
9. Zaitsev A. V., *Sov. Phys. JETP* **59**, 1015 (1984).
10. Kuprianov M. Yu. and Lukichev V. F., *Sov. Phys. JETP* **67**, 1163 (1988).
11. Ambegaokar V. and Baratoff A., *Phys. Rev. Lett.* **10**, 468 (1963).
12. Josephson B. D., *Phys. Lett.* **1**, 251 (1962).
13. Heslinga D. R. and Klapwijk T. M., *Phys. Rev. B* **47**, 5157 (1993).

Pergamon

J. Phys. Chem. Solids Vol. 56, No. 12, p. 1775, 1995
Copyright © 1995 Elsevier Science Ltd
Printed in Great Britain. All rights reserved
0022-3697/95 $9.50 + 0.00

0022-3697(95)00169-7

SPIN–CHARGE SEPARATION IN THE t–J MODEL

Z. Y. WENG, D. N. SHENG and C. S. TING
Texas Center for Superconductivity, University of Houston, Houston, Texas 77204, U.S.A.

Abstract—Spin–charge separation is found in the t–J model. Such a state reproduces various 1D correlations at a strong-coupling fixed-point. A long-range AF order is recovered at 2D half-filling, while a spin–charge deconfinement is obtained at finite doping. In the 2D spin–charge separation regime, residual spin–charge coupling leads to anomalous normal-state magnetic and transport properties.

Marshall sign [1] is a key characteristic for the ground-state wavefunction of the Heisenberg Hamiltonian: the relative phase between spin configurations $\uparrow\downarrow$ and $\downarrow\uparrow$ is always (-1) in order to minimize the transverse spin energy $J/2(S^+S^- + S^-S^+)$. Doped holes would generally mess up such a Marshall sign in the spin background and cause frustration in the system. The crucial question is whether one can find a proper representation to totally or partially eliminate such a phase (sign) problem. An exact spin–charge representation is obtained, under which the sign problem can be completely eliminated in 1D such that $< m|H_J|n > \leq 0$ and $< m|H_t|n > \leq 0$ and the ground state $|\psi> = \sum_n c_n|n>$ has a real positive wavefunction c_n. In this case, a mean-field treatment of c_n will become reasonable. In 2D, the phase-frustration cannot be totally gauged away. But the short-range phase frustration can be transformed into long-range topological effect in the new representation.

In this new representation, H_{t-J} in operator formalism is expressed as follows:

$$H_J = -\frac{J}{2}\sum_{<ij>\sigma\sigma'}\left(e^{i\sigma A^h_{ij}}\right) b^+_{i\sigma}b_{j\sigma}\left(e^{i\sigma' A^h_{ji}}\right) b^+_{j\sigma'}b_{i\sigma'} + \frac{J}{2}\sum_{<ij>}(1-n^h_i)n^h_j, \tag{1}$$

$$H_t = -t\sum_{<ij>}\left(e^{iA^f_{ij}}\right) h^+_i h_j \left(e^{i\sigma A^h_{ji}}\right) b^+_{j\sigma}b_{i\sigma}. \tag{2}$$

Electron operator $c_{i\sigma}$ in the new representation is given as

$$c_{i\sigma} = h^+_i b_{i\sigma}\left[e^{-\frac{i}{2}\sum_{l\neq i}\theta_i(l)\left(\sigma n^h_l - \sum_\alpha \alpha n^h_{l\alpha}+1\right)}(-\sigma)^i\right], \tag{3}$$

in terms of bosonic spinon and holon operators $b_{i\sigma}$ and h_i, with $\theta_i(l) = \mathrm{Im}\ln(z_i - z_l)$.

1D case. $A^h_{ij} = A^f_{ij} = 0$: no phase frustration in Eqns (1) and (2). Spin and charge degrees of freedom can be decoupled in Eqns (1) and (2) by mean-field approximation. All the important physical information appears in decomposition (3) as "phase-shift". One recovers the correct Luttinger liquid behaviors: $n_k \sim n_{k_f} - C|k-k_f|^{1/8}\mathrm{sgn}(k-k_f)$ near $k \sim k_f$ and $n_k \sim n_{3k_f} - C'|k-3k_f|^{9/8}\mathrm{sgn}(k-3k_f)$ near $3k_f$, etc.

2D case. A^h_{ij} and A^f_{ij} as topological phases can no longer be gauged away, and one has

$$\sum_C A^h_{ij} = \pi\sum_{l\in C} n^h_l, \tag{4}$$

$$\sum_C A^f_{ij} = \pi\sum_{l\in C}\left[\sum_\sigma \sigma n^b_{l\sigma} - 1\right], \tag{5}$$

for an arbitrary closed path C. At half-filling, $A^h_{ij} = 0$, and H_J in Eqn (1) can be treated by mean-field approximation which is equivalent to the mean-field treatment in Schwinger boson representation. At finite doping, the corresponding mean-field Hamiltonians which leave A^h_{ij} and A^f_{ij} intact are given [2] by $H_{eff} = H_s + H_h$, where

$$H_s = -J_s\sum_{<ij>\sigma}\left(e^{i\sigma A^h_{ij}}\right) b^+_{i\sigma}b_{j\sigma} + h.c., \tag{6}$$

$$H_h = -t_h\sum_{<ij>}\left(e^{iA^f_{ij}}\right) h^+_i h_j + h.c. \tag{7}$$

Beyond the mean-field level, the transverse gauge fluctuation is *gapped* ($\sim \delta J_s$) at finite doping so that a real spin–charge separation is present and the saddle-point properties are well defined. Here A^h_{ij} describes fictitious π-flux quanta attached to holons which are seen only by *spinons*. A^f_{ij} represents π-flux quanta bound to spinons (in addition to a π-lattice-flux) which can be only seen by *holons*. So new types of scattering are present, and it is due to these unconventional forces that magnetic and transport anomalies [2] are produced, consistent with those found in the high-T_c cuprates. In the present scheme, a large Fermi-surface satisfying the Luttinger theorem in 2D can be determined via the nonlocal phase in Eqn (3). When spinons are condensed, a pseudo spin-gap behavior is exhibited in the spin dynamics. When both holon and spinon are condensed, a pairing order parameter can be found in terms of Eqn (3), with a d-wave symmetry decided by the nonlocal phase.

REFERENCES

1. Marshall W., *Proc. Roy. Soc. (London) A* **232**, 48 (1955).
2. Weng Z. Y., Sheng D. N. and Ting C. S., *Mod. Phys. Lett. B* **8**, 1353 (1994); Weng Z. Y. *et al.*, *Phys. Rev. B* **52** (1995).

Pergamon

J. Phys. Chem. Solids Vol. 56, No. 12, pp. 1777–1778, 1995
Copyright © 1995 Elsevier Science Ltd
Printed in Great Britain. All rights reserved
0022–3697/95 $9.50 + 0.00

0022-3697(95)00192-1

ON THE INTERPRETATION OF NEUTRON SCATTERING IN SUPERCONDUCTING $YBa_2Cu_3O_7$

VICTOR M. YAKOVENKO † and I. I. MAZIN *

* Geophysical Laboratory, Carnegie Institution, 5251 Broad Branch Road, NW, Washington, DC 20015, U.S.A.
† Department of Physics and Center for Superconductivity, University of Maryland, College Park, MD 20742-4111, U.S.A.

Abstract—We suggest two possible interpretations of a neutron scattering peak emerging in the superconducting state of $YBa_2Cu_3O_7$ found experimentally by Fong *et al.*. One involves the spin-flip excitation of electrons from an occupied van Hove singularity to the empty states above the superconducting gap. Another relies on the excitation of a triplet electron–hole collective mode with the energy slightly below the superconducting gap and involves antiferromagnetic Cu–Cu exchange interaction. Both scenarios require a sign variation of the superconducting order parameter and are consistent with an *s*-wave state with opposite signs of the gap in the bonding and antibonding electron bands of the Cu_2O_4 bilayers. The second scenario is also compatible with the $d_{x^2-y^2}$ symmetry.

Keywords: A. superconductors, C. neutron scattering, D. Fermi surface, D. superconductivity.

Fong *et al.* [1] observed a sharp magnetic neutron scattering peak at the energy $\omega = 41$ meV and a 2D wave vector equivalent to $\mathbf{Q} = (\pi/a, \pi/b)$ (a and b being the lattice spacings of a CuO_2 plane) in $YBa_2Cu_3O_7$. This peak has the following remarkable features: (a) It appears only below the superconducting transition temperature; (b) It is localized in both energy and wave vector; (c) The intensity is proportional to $\sin^2(q_z d/2)$, where q_z is the wave vector perpendicular to the CuO_2 planes, and d is the distance between the planes in the bilayer.

Neutron scattering cross section is proportional to the imaginary part of the electron magnetic susceptibility $\chi(\mathbf{q}, \omega)$. In the framework of BCS theory, at zero temperature, it is given by the following formula:

$$\chi_0(\mathbf{q}, \omega) = \frac{1}{2}\sum_{\mathbf{k}}\left(1 - \frac{\xi_{\mathbf{k}+\mathbf{q}}\xi_{\mathbf{k}} + \Delta_{\mathbf{k}+\mathbf{q}}\Delta_{\mathbf{k}}}{E_{\mathbf{k}+\mathbf{q}}E_{\mathbf{k}}}\right) \times \left(\frac{1}{\omega - E_{\mathbf{k}+\mathbf{q}} - E_{\mathbf{k}} + i\Gamma} - \frac{1}{\omega + E_{\mathbf{k}+\mathbf{q}} + E_{\mathbf{k}} + i\Gamma}\right). \quad (1)$$

Here, $E_{\mathbf{k}} = \sqrt{\xi_{\mathbf{k}}^2 + \Delta_{\mathbf{k}}^2}$ is the quasiparticle dispersion law in the superconducting state, and Γ is a damping. Note that the coherence factor does not vanish at small energies $\xi \ll \Delta$ only when $\Delta_{\mathbf{k}}\Delta_{\mathbf{k}+\mathbf{q}} < 0$.

In Fig. 1, we show $\mathrm{Im}\chi_0(\mathbf{Q}, \omega)$ and $\mathrm{Re}\chi_0(\mathbf{Q}, \omega)$ calculated from eqn (1) using $\Gamma = 2$ meV and the $d_{x^2-y^2}$ gap computed in [2] for the following dispersion law: $\xi_{\mathbf{k}} = -2t(\cos(k_x a) + \cos(k_y a)) - 4t' \cos(k_x a)\cos(k_y a) - \mu$, where $t = 250$ meV, $t'/t = -0.45$, $\mu = -370$ meV. The corresponding Fermi surface is shown in the inset to Fig. 1. We see that $\mathrm{Im}\chi_0(\omega)$ has a step and $\mathrm{Re}\chi_0(\omega)$ has a peak at the threshold of energy absorption 2Δ equal to 36 meV. In addition, $\mathrm{Im}\chi_0(\omega)$ has a peak at about 100 meV. This peak is related to the normal-state van Hove singularity which is located $\xi_{vH} = 80$ meV below the Fermi energy. The peak in $\mathrm{Im}\chi_0(\omega)$ in the superconducting state occurs at the energy $\omega \approx \xi_{vH} + \Delta$ due to transitions between the occupied states located near the van Hove singularity and empty quasiparticle states above the gap. The logarithmic divergence in $\mathrm{Im}\chi_0(\omega)$ is absent in the normal state and appears only when the superconducting gap opens. This agrees with the experimental feature (a). Although the divergence formally exists for any vector $\mathbf{q}$, its weight, determined by the coherence and other non-singular factors in (1), decreases as $\mathbf{q}$ deviates from $\mathbf{Q}$. More precisely, the maximum of the weight is achieved at four vectors $\mathbf{q} = (\pi/a(1 \pm \delta), \pi/b)$ and $(\pi/a, \pi/b(1 \pm \delta))$, $\delta \approx 0.1$, located around $\mathbf{Q}$. With the assumption that they have not been resolved in experiment [1], this property may simulate feature (b). If ξ_{vH} is taken closer to the Fermi level, this "van Hove scenario" is a possible interpretation of the experiment.

If we take into account an exchange interaction between Cu spins, $J(\mathbf{q}) = J_{\|}[\cos(q_x a) + \cos(q_y b)]$, the spin susceptibility is renormalized in an RPA manner:

$$\chi(\mathbf{q}, \omega) = \chi_0(\mathbf{q}, \omega)/[1 + J(\mathbf{q})\chi_0(\mathbf{q}, \omega)]. \quad (2)$$

Since the *real* part of $\chi_0(\mathbf{q}, \omega)$ diverges as $\omega \to 2\Delta$, as discussed above, the renormalized susceptibility $\chi(\mathbf{q}, \omega)$ (2) has a pole at ω close to 2Δ with singularities in both real and imaginary parts of χ. Physically, the pole in $\chi(\mathbf{q}, \omega)$ describes a triplet electron–hole collective mode (an "antiparamagnon" or a "triplet exciton") with the energy slightly below 2Δ. In this picture, the singularity in $\mathrm{Im}\chi(\mathbf{q}, \omega)$ appears due to the excitation of this collective mode.

The exciton, generally speaking, should exist for any $\mathbf{q}$, in

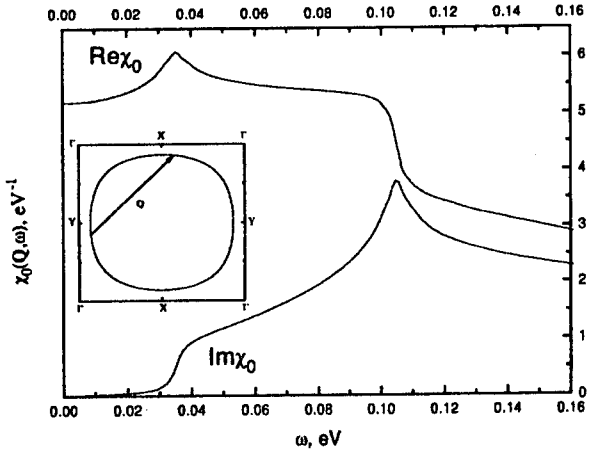


Fig. 1. The imaginary and real parts of $\chi_0(\mathbf{Q}, \omega)$ [eqn (1)], plotted as functions of ω. Inset: The Fermi surface.

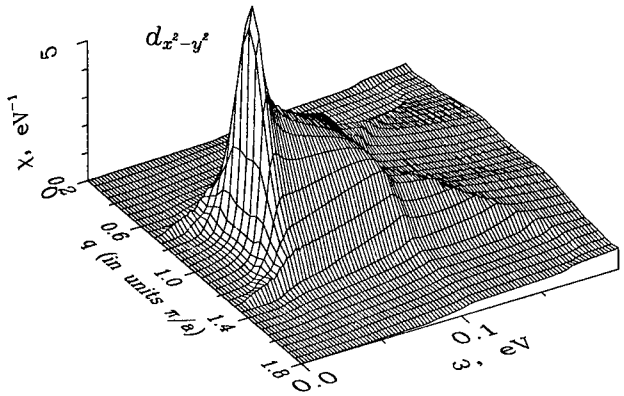


Fig. 2. The imaginary part of $\chi(q_x, q_y, \omega)$, plotted as a function of $q = q_x = q_y$ and ω for the $d_{x^2-y^2}$ order parameter.

contradiction with feature (b). However, because of the finite Γ, the position of the pole in eqn (2) shifts to the complex plane, which means that the excitons acquire a finite lifetime. For reasonable values of Γ, a pronounced peak in $\mathrm{Im}\chi(\mathbf{q}, \omega)$ exists only for $\mathbf{q}$ close to $\mathbf{Q}$ (where $J(\mathbf{q})$ is the strongest). Thus, in this "exciton scenario", the position of the neutron peak in $\mathbf{q}$-space is set by $J(\mathbf{q})$ and in ω by $\mathrm{Re}\chi_0(\mathbf{q}, \omega)$. In Fig. 2, we show $\mathrm{Im}\chi(\mathbf{q}, \omega)$ calculated according to eqn (2) for the same $d_{x^2-y^2}$ model as in Fig. 1 with $J_\parallel = 300$ meV. A single peak in $\mathrm{Im}\chi(\mathbf{q}, \omega)$, localized both in $\mathbf{q}$ and ω, is observed. This picture seems to be compatible with Fig. 4 of [1].

In the case of a bilayer system, eqn (2) is modified as follows:

$$\chi(\mathbf{q}, q_z, \omega) = \frac{\cos^2(q_z d/2)\chi_0^{(+)}}{1 + J^{(+)}\chi_0^{(+)}} + \frac{\sin^2(q_z d/2)\chi_0^{(-)}}{1 + J^{(-)}\chi_0^{(-)}}, \quad (3)$$

$$\chi_0^{(+/-)}(\mathbf{q}, \omega) = \chi_0^{(aa/ab)}(\mathbf{q}, \omega) + \chi_0^{(bb/ba)}(\mathbf{q}, \omega),$$

$$J^{(\pm)}(\mathbf{q}) = J(\mathbf{q}) \pm J_\perp. \quad (4)$$

Here, $J_\perp > 0$ is the amplitude of the antiferromagnetic interaction between Cu spins on different layers. The indices b and a of χ_0 refer to bonding and antibonding electron bands of the bilayer. The susceptibilities $\chi_0^{(ij)}$, where i and j take values a or b, are given by eqn (1), where the variables with the indices $\mathbf{k}$ and $\mathbf{k}+\mathbf{q}$ should refer to bands i and j, respectively.

According to eqn (3), experimental feature (c) suggests that only transitions between bonding and antibonding electron bands are allowed. Such behavior can be readily explained if the superconducting state in $YBa_2Cu_3O_7$ has s-wave symmetry with opposite signs of the gap in the bonding and antibonding bands [2]. In this state, intraband transitions are forbidden because the condition $\Delta_{\mathbf{k}}\Delta_{\mathbf{k}+\mathbf{q}} < 0$ is satisfied only for different bands. All of the preceding discussion about the "exciton" and the "van Hove" scenarios applies to this state.

If superconductivity in a bilayer compound is of the $d_{x^2-y^2}$ type, feature (c) can be explained if the amplitude $J_\perp$ in eqn (4) has such a value that the exciton resonance takes place in the second term of eqn (3), but not in the first term. On the other hand, the "Van Hove" scenario is difficult to reconcile with the $d_{x^2-y^2}$ pairing *and* feature (c).

More detailed presentation of the reported results can be found in Ref. [3].

Acknowledgements—The work of V.M.Y. was supported in part by NSF under grant DMR-9417451 and by A. P. Sloan Foundation.

REFERENCES

1. Hung Fai Fong *et al.*, *Phys. Rev. Lett.*, **75**, 316 (1995).
2. Liechtenstein A. I., Mazin I. I. and Andersen O. K., *Phys. Rev. Lett.*, **74**, 2303 (1995), e-print cond-mat/9501118.
3. Mazin I. I. and Yakovenko V. M., *Phys. Rev. Lett.*, **75** in press (1995), e-print cond-mat/9502025.

Pergamon

J. Phys. Chem. Solids Vol. 56, No. 12, pp. 1779–1780, 1995
Copyright © 1995 Elsevier Science Ltd
Printed in Great Britain. All rights reserved
0022–3697/95 $9.50 + 0.00

0022-3697(95)00111-5

EFFECTS OF LONG-RANGE INTERACTION IN ONE-DIMENSIONAL ELECTRON SYSTEMS

S. YUNOKI and S. MAEKAWA
Department of Applied Physics, Nagoya University, Nagoya 464-01, Japan

Abstract—Effects of long-range Coulomb interaction in one-dimensional electron systems are studied. With use of a quantum Monte Carlo method, we find that the zero-frequency wave-number dependent charge-susceptibility around quarter-filling clearly exhibits both $2k_F$ and $4k_F$ singularities, k_F being the Fermi wave-number, in contrast with the extended-Hubbard model with on-site and nearest-neighbor interactions. The results are in accord with the X-ray diffuse scattering experiments in $(NMP)_x(phen)_{1-x}(TCNQ)$. The power-law exponent α in the spectral function $\rho(\omega) \sim |\omega|^\alpha$ and the single-particle excitation spectrum $A(k, \omega)$ are calculated in the exact diagonalization method and compared with the observed value of α in the high-resolution photoemission experiments.

In the low-dimensional electron systems, the charge screening is less complete and the long-range Coulomb interaction is considered to play an important role [1,2]. Several experiments in quasi-one-dimensional (1D) conductors indicate the importance of the long-range Coulomb interaction between electrons: the X-ray diffuse scattering experiments in $(NMP)_x(phen)_{1-x}(TCNQ)$ by Epstein *et al.* [3] have shown the crossover of the electronic instability from $2k_F$ to $4k_F$ on the same TCNQ chains with decreasing x and the coexistence of both $2k_F$ and $4k_F$ instabilities for $0.57 \leq x \leq 2/3$, k_F being the Fermi wave-number. The crossover may be interpreted intuitively as that from Peierls instability to Wigner crystallization. In order to verify this scenario, it is necessary to show which model exhibits both instabilities at the same time. However, in the model with long-range interaction in the limit of vanishing hopping matrix only the $4k_F$ singularity exists [1,2], whereas in the extended Hubbard model with nearest-neighbor interaction the lack of a parameter region in which structure of both $2k_F$ and $4k_F$ coexists was concluded [4]. The recent high-resolution photoemission experiments in quasi-1D metals such as $(TMTSF)_2PF_6$ and $BaVS_3$ [5,6] revealed that the spectral function $\rho(\omega)$ shows the power-law behavior $|\omega|^\alpha$, instead of the Fermi edge in the Fermi-liquid, and the exponent α is much larger than that in the Hubbard model, indicating the importance of the long-range interaction. On the theoretical side, the wave-number dependent single-particle excitation spectrum $A(k, \omega)$ has not been understood so clearly [7,8].

The purpose of this paper is to investigate effects of the long-range Coulomb interaction on the zero-frequency wave-number-dependent charge-susceptibility $N(q)$ in 1D electron systems in the quantum Monte Carlo (QMC) method and to examine the relation among the power-law exponent α, the range of interaction and the single-particle excitation spectrum $A(k, \omega)$ in the numerically exact diagonalization (ED) method.

The system we will study is defined by the Hamiltonian

$$H = -t \sum_{i,\sigma} \left(c_{i\sigma}^\dagger c_{i+1\sigma} + h.c. \right) + U \sum_i n_{i\uparrow} n_{i\downarrow} + \sum_{j=1}^{5} V_j \sum_i n_i n_{i+j}, \tag{1}$$

where the notations are the conventional ones. First, let us calculate $N(q)$ in the QMC method with the world-line algorithm [9]. The simulations, which are carried out on the periodic ring of up to 60 sites at $t/T = 24$ (T being temperature) and (around) quarter-filling with $U/t = 4$ and 10, have clearly shown both the $2k_F$ and $4k_F$ singularities when the interaction is longer than that between nearest-neighbors. The results are in accord with the X-ray diffuse scattering observation in $(NMP)_x(phen)_{1-x}(TCNQ)$ and are in contrast with those in the extended-Hubbard model with on-site and nearest-neighbor interactions [4].

Second, the value of α is analyzed for the model of eqn (1) with $U \to \infty$, V_1 and V_2 in the ED method. We use the standard Lanczos method in the ring with up to 16 sites. To calculate α, the relations which hold generally in the Tomonaga–Luttinger liquid are used [10]. We have obtained that at quarter-filling the value of α cannot exceed the maximum one in the extended-Hubbard model, 9/16 [11], due to the instability of metallic phase. But, away from quarter-filling, the value of α can be larger than one, even in the extended-Hubbard model [12]. It is not possible to ascribe the large value of α observed in $(TMTSF)_2PF_6$, which is about 1.25 [5], to the electronic origin if this material is exactly at 3/4-filling. On the other hand, for $BaVS_3$ which is expected to be near half-filling, the observed value of about 0.8 [6] may be explained by the long-range interaction.

Finally, $A(k, \omega)$ is calculated in the ED method with the Lanczos algorithm and the continued-fraction expansion. The results are shown in Fig. 1(a) and (b) where we have 6 electrons on the periodic ring of 12 sites with $U/t = 4$

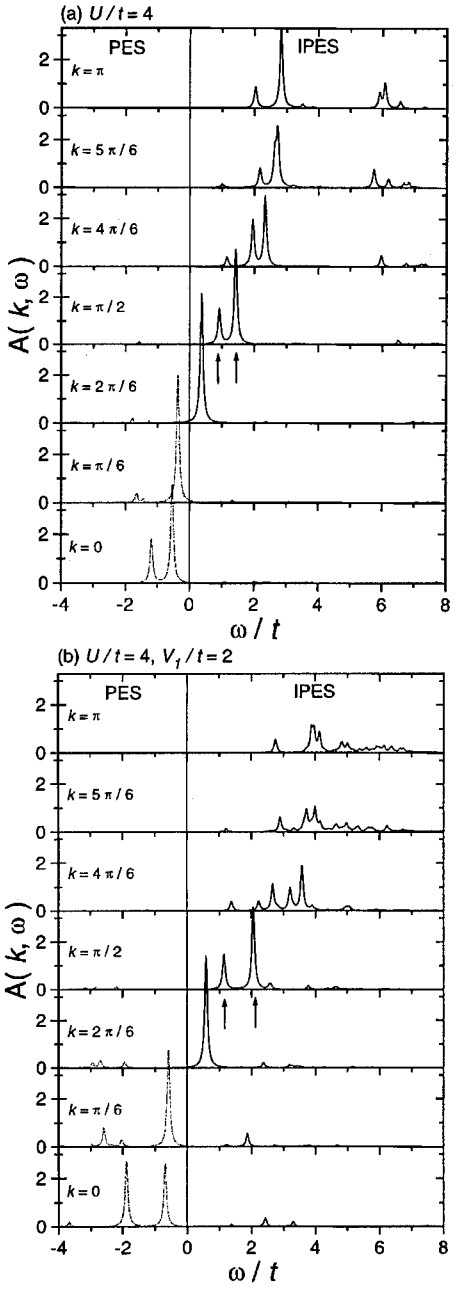


Fig. 1. Single-particle excitation spectrum $A(k, \omega)$ at quarter-filling obtained for the periodic ring of 12 sites with (a) $U/t = 4$ and (b) $U/t = 4$ and $V_1/t = 2$. Here, PES and IPES mean photoemission and inverse photoemission spectra, respectively.

[case(a)] and $U/t = 4$ and $V_1/t = 2$ [case(b)], respectively. In case (a), the value of α is 0.03 and in case (b) it is 0.18. As seen in Fig. 1, the system with large α leads to the larger weight of inverse photoemission spectrum (IPES) at the wave-numbers less than $k_F = \pi/4$. At $k = \pi/2$, two large peaks (denoted by arrows in the figure) show the singularities similar to those in the Luttinger model, where IPES shows the characteristic behavior as $A(q, \omega \simeq v_s q) \sim \theta(\omega - v_s q)(\omega - v_s q)^{\alpha-1/2}$ and $A(q, \omega \simeq v_c q) \sim |\omega - v_c q|^{(\alpha-1)/2}$ with v_s (v_c) being the spin (charge) velocity and $q = k - k_F$ [7,8]. We also note that the distance between these peaks is wider in the case (b) than (a). This is because the difference between v_s and v_c is larger in (b) than (a).

To summarize, the effects of the long-range interaction in 1D electron systems were studied. By using the QMC method, both the $2k_F$ and $4k_F$ singularities in the charge susceptibility were clearly observed as the interaction between electrons was long-ranged. We calculated the correlation exponent α for the systems with $U \to \infty$ and the single-particle excitation spectrum $A(k, \omega)$ in the ED method. The detailed results and the analyses will be given in separate publications.

Acknowledgements— We would like to thank Y. Ohta for providing computational codes of the ED method and T. Tohyama for useful discussions. This work was supported by a Grant-in Aid for scientific Research on Priority Area from Ministry of Education, Science, and Cluster of Japan.

REFERENCES

1. Kondo J. and Yamaji K., *J. Phys. Soc. Japan* **43**, 424 (1977).
2. Hubbard J., *Phys. Rev. B* **17**, 494 (1978).
3. Epstein A. J., Miller J. S., Pouget J. P. and Comès R, *Phys. Rev. Lett.* **47**, 741 (1981); Pouget J. P., Comès R., Epstein A. J. and Miller J. S., *Mol. Cryst. Liq. Cryst.* **85**, 203 (1982).
4. Hirsch J. E. and Scalapino D. J., *Phys. Rev. Lett.* **50**, 1168 (1983); *Phys. Rev. B* **27**, 7169 (1983); *ibid.* **29**, 5554 (1984).
5. Dardel B., Malterre M., Grioni M., Weibel P., Baer Y., Voit J. and Jèrôme D., *Europhys. Lett.* **24**, 687 (1993).
6. Nakamura M., Sekiyama A., Namatame H., Fujimori A., Yoshihara H., T. Ohtani, A. Misu, and M. Takano, *Phys. Rev. B* **49**, 16191 (1994).
7. Meden V. and Schönhammer K., *Phys. Rev. B* **46**, 15753 (1992).
8. Voit J., *Phys. Rev. B* **47**, 6740 (1993); *J. Phys. Chem.* **5**, 8305 (1993); preprint.
9. Hirsch J. E., Sugar R. L., Scalapino D. J. and Blankenbecler R., *Phys. Rev. B* **26**, 5033 (1982).
10. Schulz H. J., *Phys. Rev. Lett.* **64**, 2831 (1990); *Int. J. Mod. Phys. B* **5**, 57 (1991).
11. Luther A. and Peschel I., *Phys. Rev. B* **12**, 3908 (1975).
12. Haldane D. M., *Phys. Rev. Lett.* **45**, 1358 (1980).

Pergamon

J. Phys. Chem. Solids Vol. 56, No. 12, p. 1781, 1995
Copyright © 1995 Elsevier Science Ltd
Printed in Great Britain. All rights reserved
0022-3697/95 $9.50 + 0.00

0022-3697(95)00170-0

SPIN PSEUDOGAP AND *c*-AXIS TRANSPORT

YUYAO ZHA, S. L. COOPER and DAVID PINES

Department of Physics and Science and Technology Center for Superconductivity, University of Illinois at Urbana-Champaign, Urbana, IL 61801, U.S.A.

Abstract—We present a simple phenomenological model of the *c*-axis resistivity in the layered cuprates, which accounts for the major features and systematics of experiments on the *c*-axis resistivity, ρ_c, for $La_{2-x}Sr_xCuO_4$, $YBa_2Cu_3O_{6+x}$ and $Bi_2Sr_2CaCu_2O_8$. We associate the low temperature semiconductor-like upturn in the *c*-axis resistivity with the suppression of the planar density of states measured in the Knight shift experiments.

Recent *c*-axis optical measurements [1] show that the semiconductor-like resistivity "upturn" in underdoped $YBa_2Cu_3O_{6+x}$ is actually associated with a uniform suppression of the optical conductivity below $\sim 300cm^{-1}$, and the low frequency *c*-axis conductivity scales with the Knight shift, which has a pseudogap behavior. Since the Knight shift is proportional to the in-plane density of states: $K_s \propto N(0)$, a phenomenological expression for this contribution to *c*-axis transport can be written as:

$$\sigma_c^{(1)} = N(0)\frac{e^2d^2}{\hbar^2}t_\perp^2\tau_c \qquad (1)$$

where d is the interlayer spacing, N(0) is the in-plane density of states, and $t_\perp$ is the interlayer coupling. Here τ_c corresponds to the electron scattering in the "barrier" layer between CuO_2 "cells" (i.e. layers, bilayers, trilayers, etc.), which is temperature independent. On the other hand, *c*-axis transport measurements of $La_{2-x}Sr_xCuO_4$ and $Bi_2Sr_2CaCu_2O_8$ yield $\rho_c \propto \rho_{ab}$ at high temperatures [2,3], suggesting that in-plane scattering or fluctuations may dominate *c*-axis transport in this regime. This contribution to *c*-axis transport can be written [4],

$$\sigma_c^{(2)} = N(0)\frac{e^2d^2}{\hbar^2}t_1^2\tau_{ab} \qquad (2)$$

where τ_{ab} can be derived from the planar conductivity $\sigma_{ab} = \omega_{p\|}^2\tau_{ab}/4\pi$, and the temperature-independent quantity, t_1, measures the effectiveness of planar fluctuation processes to *c*-axis transport. Because eqns (1) and (2) describe independent physical processes, it seems natural to consider the corresponding tunneling and/or scattering mechanisms as additive in the resistivity. We are thus led to propose the following expression for ρ_c,

$$\rho_c = \frac{\hbar^2}{N(0)e^2d^2}\left(\frac{1}{t_1^2\tau_{ab}} + \frac{1}{t_\perp^2\tau_c}\right) \qquad (3)$$

in the limit that one mechanism or the other is dominant, it yields the corresponding conductivity given in eqns (1) and (2).

Using eqn (3), we may analyze the existing *c*-axis resistivity data of $La_{2-x}Sr_xCuO_4$ [2], $YBa_2Cu_3O_{6+x}$ [5] and $Bi_2Sr_2CaCu_2O_8$ [6], since we can obtain $N(0)$, d, τ_{ab}, and $t_\perp$ from different magnetic and transport experiments [8], we are left with a two-parameter fit for each cuprate. Details of these fits are given in Ref. [8], in which we find eqn (3) accounts well for the ρ_c data of the above three types of cuprates at various doping concentrations, and the results for $t_\perp$ and $1/\tau_c$ are consistent with optical and Raman experiments [7].

In conclusion, we have presented a model for *c*-axis resistivity of high T_c cuprates, in which the *c*-axis resistivity consists of contributions from the in-plane dephasing process and the *c*-axis "barrier" scatterings. As a result, we predict that whenever the spin pseudogap appears in the planar density of states, it will also show up in the *c*-axis resistivity as a "semiconductor-like" low temperature upturn.

Acknowledgements—Supported by NSF-DMR-91-20000 through the Science and Technology Center for Superconductivity.

REFERENCES

1. Homes C. C. *et al.*, *Phys. Rev. Lett.* **71**, 1645 (1993); Basov D. N. *et al.*, *Phys. Rev. B* **50**, 3511 (1994).
2. Nakamura Y. and Uchida S., *Phys. Rev. B* **47**, 8369 (1993).
3. Hou X. H. *et al.*, *Phys. Rev. B* **50**, 496 (1994).
4. Leggett A. J., *Braz. J. Phys.* **22**, 129 (1992).
5. Takenaka K., Mizuhashi K., Takagi H. and Uchida S., *Phys. Rev. B* **50**, 6534 (1994).
6. Martin S. *et al.*, *Appl. Phys. Lett.* **54**, 72 (1989); Forro L., Ilakovac V. and Keszei B., *Phys. Rev. B* **41**, 9551 (1990); Xiang X. D. *et al.*, *Phys. Rev. Lett.* **68**, 530 (1992); Yan Y. F., Hrris J. M. and Ong N. P., unpublished.
7. Cooper S. L. and Gray K. E., *Physical Properties of High Temperature Superconductors IV* (Edited by D. M. Ginsberg). World Scientific, Singapore (1994).
8. Zha Y., Cooper S. L. and Pines D., preprint.

QUANTUM INTERFERENCE AND TUNNELING

Pergamon

J. Phys. Chem. Solids Vol. 56, No. 12, pp. 1783–1786, 1995
Copyright © 1995 Elsevier Science Ltd
Printed in Great Britain. All rights reserved
0022-3697/95 $9.50 + 0.00

0022-3697(95)00164-6

EXPERIMENTAL EVALUATION OF THE ORDER PARAMETER SYMMETRY OF SUPERCONDUCTORS

H. R. OTT and D. A. BRAWNER
Laboratorium für Festkörperphysik, ETH – Hönggerberg, 8093 Zürich, Switzerland

Abstract—We briefly review how the order parameter symmetry of unconventional superconductors may be probed experimentally. Examples of such attempts for both heavy-electron and cuprate superconductors are discussed. Many independent results indicate that the gap of these superconductors has nodes in the form of lines or points on the Fermi surface.

1. INTRODUCTION

For common metals and alloys the occurrence of a superconducting ground state is the natural consequence of the interaction between itinerant charge carriers and lattice deformations, leading to a pairing of the charge carriers and a concomitant gap in the excitation spectrum. This is all very well described by the theory of Bardeen *et al.* [1] (BCS) where the simplest form of pairing is between charge carriers with opposite momentum and spin, triggered by a k-independent interaction potential. The resulting order parameter related with the phase transition is of s-wave symmetry and the associated energy gap is non-zero for all directions in k space. More generally, the interaction potential will depend on k and the energy gap may be anisotropic but is tied to the symmetry of the Fermi surface.

Superconductivity that occurs under, conventionally viewed, unfavourable conditions, is often suspected to be of unconventional nature. Apart from the phenomenon of superfluidity in ^{3}He [2], this possibility was first seriously considered for heavy-electron superconductors [3] but also put forward soon after the discovery of superconductivity in cuprates at unexpected high temperatures [4]. In both cases the preceding normal state reveals anomalous features which indicate that the responsible mechanisms for superconductivity are most likely not based on simple electron–phonon couplings. Alternative mechanisms may also lead to superconducting states with unconventional characteristics of pairing and order parameter symmetries. As a consequence, also the symmetry of the gap in the electronic excitation spectrum is more complicated and gap nodes of different varieties may form.

It is particularly this unusual k-dependence of the gap structure which offers experimental access to identifying unconventional superconducting states. The form of the gap in the excitation spectrum has a decisive influence on the temperature dependence of any physical quantity that depends on electronic excitations out of the ground state. This is particularly true for temperatures much below T_c, usually close to $T = 0$ K. For overall non-zero gaps, as in common superconductors, all electronically dominated physical properties are expected to decrease exponentially for $T << T_c$. This is not so, if gap nodes are developing as points or lines of zeroes on the Fermi surface. In these cases the electronic density of states is not zero up to the gap energy $E = \Delta$ but varies as power laws of E for small energies. As a consequence, the temperature variation of physical properties due to electronic excitations at temperatures well below T_c is given by power laws of T which, under favourable circumstances, may well be distinguished from the conventional exponential behaviour. The exponents of these power laws depend on the manifold of the gap nodes which are, of course, again related to the symmetry of the order parameter. This type of experiments has mainly been used in studies of heavy electron superconductors and some instructive examples are presented in Section 2.

More recently, another approach of directly probing the symmetry of the order parameter has been pursued. The basic idea, first introduced by Geshkenbein and Larkin [5], is to probe the phase coherence of superconducting loops, specially tailored by employing combinations of the superconductor under investigation and conventional superconducting materials. Various experimental realizations of this idea, which is expected to be of value in special cases of order-parameter symmetries, have been used to probe the superconducting state of high-T_c cuprate superconductors, as we shall demonstrate in Section 3.

2. CHARACTERISTICS OF HEAVY-ELECTRON SUPERCONDUCTORS

The normal state properties of these materials are characterized by strongly enhanced electronic specific heats and magnetic susceptibilities at low temperatures [6] and the critical temperatures T_c are of the order of 1 K or less. This means, of course, that measurements probing the electronic excitation spectrum in the limit of $T << T_c$ have to be made well below 1 K. On the other hand, most physical properties of these materials are completely dominated by exci-

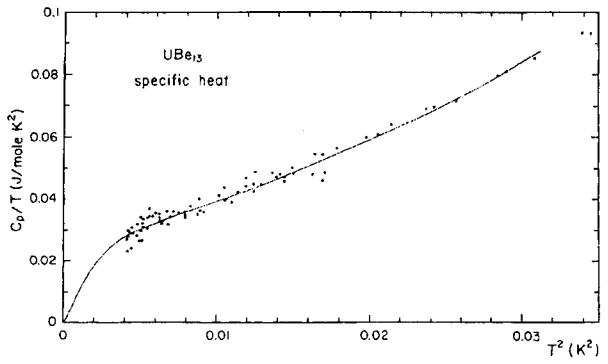


Fig. 1. C_p/T vs T^2 for UBe_{13} and $T << T_c$. The solid line is a fit as explained in the text (see also Ref. [7]).

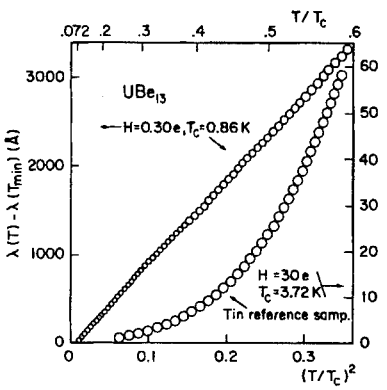


Fig. 2. Incremental magnetic field penetration depth of superconducting UBe_{13}. Also shown are data for a Sn reference sample.

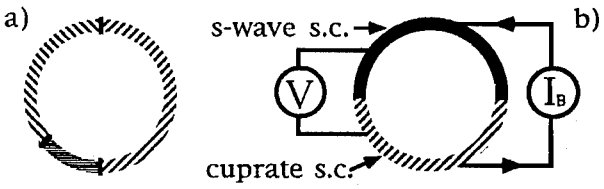


Fig. 3. Schematic diagram of loop arrangements for probing the phase coherence

well below 1 K. On the other hand, most physical properties of these materials are completely dominated by excitations of heavy-mass electrons, leading to large enhancements of the quantities under investigation. Lattice effects, which are a real problem in studying the electronic properties of cuprates, may usually be neglected. Below we discuss two examples where the difference between the experimental observation and expectations based on calculations using the basic form of the BCS theory is particularly obvious.

The quantity where the interpretation of the measured data should be least complicated is the specific heat. It is simply related to the energy dependence of the density of states and no matrix elements describing the excitation process need to be considered. The BCS solution for the electronic specific heat below T_c is of the form $C_s^{el} = a\exp(-bT_c/T)$, vanishing exponentially as T approaches 0 K. In Fig. 1 we show the result of specific-heat measurements on UBe_{13} [7], well below $T_c = 0.85$ K, plotted in the form C_p/T vs T^2. Note that the lattice contribution is orders of magnitude smaller in this temperature range and can be neglected. It may be seen that the temperature dependence is far from being exponential. The solid line is a fit resulting from a calculation [7] assuming a superconducting state with points of nodes, a so-called axial state. The calculation also takes into account effects that may strongly influence such states in the form of resonant impurity scattering [8]. Fit parameters are the maximum amplitude of the gap Δ_o, the density of scatterers and the scattering phase shift. Regardless of details, the deviation from simple BCS behaviour is rather clear.

As a second example we choose the temperature variation of the London penetration depth $\lambda_L(T)$. This quantity is intimately related with the superconducting condensate, i.e. its density n_s, via $\lambda_L = (m^*c^2/4\pi n_s e^2)^{1/2}$. Again, the temperature dependence of λ is determined by the gap symmetry and possible nodes are responsible for power law behaviour also in this case. In Fig. 2 we show the results of experiments probing the change $\Delta\lambda$ of the penetration depth. Details of the experiments and their analysis are given in Ref. [9]. What is essential here is the direct comparison of $\lambda_L(T)$, measured with the same technique on UBe_{13} and Sn, the latter serving for setting the standard behaviour of a conventional superconductor. The data are plotted in the same reduced temperature range and the difference in the overall behaviour provides convincing support for claiming different gap symmetries in the two cases. More elaborate conclusions, of course, need a more detailed discussion which is not attempted here.

3. ORDER PARAMETER SYMMETRY OF CUPRATE SUPERCONDUCTORS

Various theoretical model calculations and interpretations of experimental data have indicated a non-s-wave type order parameter for cuprate superconductors [10]. In most cases, a d-wave symmetry was predicted or claimed to be the most likely possibility, others favoured a so called extended s-wave configuration [11].

For direct experimental tests of these proposals, attempts must be made to obtain information on the variation of the sign of the order parameter amplitude in k-space. The idea for possible solutions of the problem was mentioned at the end of the introduction. A special configuration of experiments that could, in principle, verify the d-wave character of cuprate superconductors was subsequently put forward by Sigrist and Rice [12]. Their idea may be generalized by noting that a contact between superconductors with opposite signs of the order parameter amplitude generates a so called π junction [13], implying that the phase of the order parameter discontinuously changes by π. A schematic

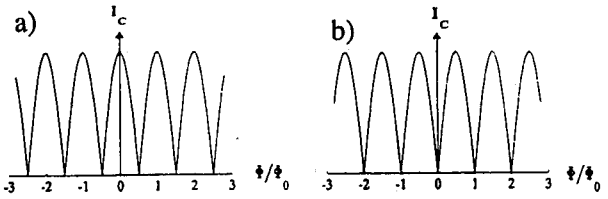


Fig. 4. (a) Critical current $I_c(\phi)$ of a loop with an even number of π junctions. (b) Critical current $I_c(\phi)$ of a loop with an odd number of π junctions.

picture of an experimental configuration is depicted in Fig. 3(a). The stability criterion for loops containing either an even (including zero) or odd number of π junctions is significantly different. In the first case the amount of possibly trapped flux is an integer number of flux quanta $\phi_o = h/2e$ and the second case requires $\phi = (n + \frac{1}{2})\phi_o$. The chosen loop may be a SQUID configuration where one or two of the contacts may be expected to be a π junction [see Fig. 3(b)]. The critical current I_c of a SQUID varies periodically with the magnetic flux inside the loop. The location of the I_c maxima or minima depends critically on the phase coherence around the superconducting loop. If the SQUID contains none or two π junctions, the $I_c(\phi)$ pattern is expected as shown in Fig. 4(a). The pattern of $I_c(\phi)$ for a SQUID with one of the contacts being a π junction is shifted by π, as shown in Fig. 4(b).

The first experimental realization of this type of SQUID measurements was accomplished by Wollman and coworkers [14], who studied the critical current behaviour of SQUIDs fabricated from single-crystalline $YBa_2Cu_3O_{6.9}$ (YBCO) and Pb. In their approach, the Pb part was in the form of thin films, making contact either around the corner of a YBCO crystal to the a and b direction of the crystal lattice or with both junctions located on the same edge of the crystal, both facing the same crystalline direction. Considering the crystal structure of YBCO, favourable for a $d_{x^2-y^2}$ symmetry of the order parameter, the first configuration is likely to contain one junction acting as a π junction. In the second case, either none or two π junctions may be expected. The modulation of $I_c(\phi)$ was monitored via measuring the dynamical resistance of the SQUIDs and the tendency of a π shift of $I_c(\phi)$ for loops around the corner of the crystals, in comparison with $I_c(\phi)$ for edge SQUIDs was recognized. The result was interpreted as being an indication of the d-wave symmetry of the superconducting order parameter of $YBa_2Cu_3O_{6.9}$. .

In another approach, Brawner and Ott [15] tried to compare the performance of a hybrid SQUID fabricated from single-crystalline YBCO and Nb, expected to contain one π junction, with that of two adjacent SQUIDs made out of Nb alone and expected to behave in the usual manner. Details of the experimental setup are given in reference [15]. A comparison of $I_c(\phi)$ for the two configurations, again accomplished by measurements of the dynamical resistances, indicates quite clearly a considerable shift in phase for $I_c(\phi)$ between the two types of SQUIDs. The observed relative phase shift is 160 ± 20 degrees, including the anticipated result for the superconducting state of YBCO revealing an order parameter with pure d-wave symmetry. It also allows for more complicated solutions for the order parameter wave function, where phase shifts other than π may occur.

The maxima of I_c for $\phi = n\phi_o$ imply that a closed superconducting loop may trap flux quantities given by an integer number of flux quanta, i.e. the situation with no trapped flux is also possible. A closed loop with an odd number of π junctions, as mentioned above, will help trap flux of values $\phi = (n + \frac{1}{2})\phi_o$ and therefore a spontaneous moment corresponding to an I_c maximum is always generated. This idea was tested in experiments of Tsuei and coworkers [16] and Kirtley and coworkers [17]. Small, ring shaped films of YBCO were deposited on suitably tailored $SrTiO_3$ substrates. These substrates were composed of differently oriented crystals, mended in a way that would allow the preparation of different rings deposited on the substrates with an even (including zero) or odd number of π junctions. The amount of trapped flux in these rings was monitored with a scanning micro-SQUID probe. Again, it was found that loops with an odd number of π junctions behaved differently from those with an even number or none at all, in the sense that they trap flux values close to $\phi = (n + \frac{1}{2})\phi_o$ instead of $\phi = n\phi_o$, as in the latter cases. This result is, as indicated, equivalent to those obtained with the SQUID experiments.

With these experiments of different style and some others [18, 19], there is increasing evidence that the order parameter of $YBa_2Cu_3O_{6.9}$, a standard representative of high-T_c cuprate superconductors, is not of the common s-wave variety. This result inevitably implies that nodes in the energy gap of the electronic excitation spectrum also should influence the temperature dependencies of thermal and transport properties of this material [20]. It should not be concealed that a few experiments of the above mentioned type or similar in character gave contradictory results [21, 22]. These discrepancies must be resolved. It also remains to be seen whether similar experiments with other cuprate materials give analogous results. A first attempt in this direction, namely SQUID experiments with oxygen depleted YBCO ($T_c = 60$ K), confirms the phase shift observations obtained with fully oxygenated YBCO [23].

4. CONCLUDING REMARKS

Of course, the order parameter symmetry still gives no real clue for an unequivocal identification of the mechanism of superconductivity neither in heavy-electron nor cuprate superconductors. It is still necessary to combine available information on properties both in the normal and the superconducting state and to try to establish a reasonable picture describing the experimental facts consistently.

REFERENCES

1. Bardeen J., Cooper L. N. and Schrieffer J. R., *Phys. Rev.* **108**, 1175 (1957).
2. See, for example, Leggett A. J., *Rev. Mod. Phys.* **47**, 331 (1975).
3. Anderson P. W., *Phys. Rev. B* **30**, 1540 (1984).
4. Anderson P. W., *Science* **235**, 1196 (1987).
5. Geshkenbein V. B. and Larkin A. I., *Pis'ma Zh. Eksp. Teor. Fiz.* **43**, 306 (1986); *JETP Lett.* **43**, (1986) 395.
6. Ott H. R., *J. Low Temp. Phys.* **95**, 95 (1994).
7. Ott H. R., Felder E., Bruder C. and Rice T. M., *Europhys. Lett.* **3**, 1123 (1987).
8. Ueda K. and Rice T. M., *Phys. Rev. B* **31**, 7114 (1985).
9. Gross F. *et al.*, *Z. Phys. B* **64**, 175 (1986).
10. Scalapino D. J., *Phys. Rep.* **250**, 331 (1995); and references therein.
11. Chakravarty S., SudbøA., Anderson P. W. and Strong S., *Science* **261**, 337 (1993).
12. Sigrist M. and Rice T. M., *J. Phys. Soc. Jpn* **61**, 4283 (1992).
13. Bulaevskii L. N., Kuzii V. V. and Sobyanin A. A., *Pis'ma Eksp. Teor. Fiz.* **25**, 314 (1977); *JETP Lett.* **25**, 290 (1977).
14. Wollman D. A., van Harlingen D. J., Lee W. C., Ginsberg D. M. and Leggett A. J., *Phys. Rev. Lett.* **71**, 2134 (1993).
15. Brawner D. A. and Ott H. R., *Phys. Rev. B* **50**, 6530 (1994).
16. Tsuei C. C. *et al.* , *Phys. Rev. Lett.* **73**, 593 (1994).
17. Kirtley J. R. *et al.*, *Nature* **373**, 225 (1995).
18. Iguchi I. and Wen Z., *Phys. Rev. B* **49**, 12388 (1994).
19. Mathai A., Gim Y., Black R. C., Amer A. and Wellstood F. C., preprint.
20. See, for example, Hardy W. N., Bonn D. A., Morgan D. C., Liang R., Yhang K., *Phys. Rev. Lett.* **70**, 3999 (1993).
21. Chaudhari P. and Lin S. Y., *Phys. Rev. Lett.* **72**, 1084 (1994).
22. Sun A. G., Gajewski D. A., Maple M. B. and Dynes R. C., *Phys. Rev. Lett.* **72**, 2267 (1994).
23. Brawner D. A. and Ott H. R., unpublished results.

Pergamon

J. Phys. Chem. Solids Vol. 56, No. 12, pp. 1787–1795, 1995
1995 Elsevier Science Ltd
Printed in Great Britain
0022-3697/95 $9.50 + 0.00

0022-3697(95)00263-4

FLUX QUANTIZATION IN TRICRYSTAL CUPRATE RINGS — A NEW PROBE OF PAIRING SYMMETRY

C. C. TSUEI, J. R. KIRTLEY, M. RUPP, J. Z. SUN, LOCK-SEE YU-JAHNES, C. C. CHI,[1] A. GUPTA and M. B. KETCHEN

IBM Research Division, Thomas J. Watson Research Center, Yorktown Heights, NY 10598, U.S.A.

Abstract—Based on macroscopic quantum coherence effects, flux quantization and pair tunneling, a tricrystal experiment has been designed and carried out to study the microscopic phase of the pair wavefunction in high T_c cuprate superconductors. Using a high-resolution scanning SQUID microscope, we have made the first direct observation of spontaneously generated half integer flux quanta in controlled-orientation tricrystal rings. By varying the grain misorientation and the grain boundary angles in the tricrystal, we have proved that the order parameter in YBCO has nodes and lobes consistent with d-wave, but not with the g-wave pairing symmetry. The results of this work demonstrate that the half-integer flux quantum effect in superconducting systems containing multi-grains with deliberately designed grain orientation can be used as a general technique for probing the pairing symmetry.

1. INTRODUCTION

An unambiguous determination of the symmetry of the pair wavefunction in cuprates is important to understanding the mechanism of high-temperature superconductivity in this class of novel superconductors [1–4]. In this brief article, we will describe a technique of probing pairing symmetry in cuprate superconductors using the recently observed, half-integer flux quantum effect in tricrystal cuprate rings[5].

A pair wavefunction, $\Psi(r, R)$, can be written in a factorizable form as follows:

$$\Psi(r, R) = \phi(r)\psi(R) \tag{1}$$

where $\phi(r)$ describes the internal structure of the Cooper pairs and $| r |$ is the distance between the paired electrons, $\psi(R)$ defines the centers of mass motion of the pairs with respect to a fixed point in space at a distance of $| R |$. It is well known that the function $\phi(r)$ contains the microscopic phase information of the pair state, while $\psi(R)$ is related to the macroscopic phenomena of superconductivity. Experimental manifestations of effects arising from $\psi(R)$ are well-established and abundant. Examples include: Josephson effects, the Meissner effect, flux quantization...etc. On the other hand, it has been very difficult to measure the microscopic part of the pair wavefunction. In terms of the BCS formalism, the wavevector k-space counterpart of $\phi(r)$, $\phi(k)$ (where $\phi(r) = \sum \phi(k)e^{ik\cdot r}$) is directly related to the order parameter, the k-dependent energy gap $\Delta(k)$, ($\phi(k) = \Delta(k)/E(k)$, where $E(k)$ is the quasiparticle energy in the superconducting state, $E(k) = \sqrt{\epsilon^2(k) + \Delta^2(k)}$, $\epsilon(k)$ is the one-electron energy). Since $\phi(r)$ and $\Delta(k)$ transform the same way under the symmetry group operation of the crystal lattice, the symmetry of the gap reflects that of the pair wavefunction. A systematic study of the pair tunneling across the tunnel barrier of the Josephson junction should, in principle, reveal the pairing symmetry of the superconductors that the junction electrodes are made of. In practice, such measurements are invariably plagued by issues associated with sample (junction) quality, junction geometry, trapped flux...etc. As a consequence, the results of such experiments are highly controversial. Spectroscopic techniques such as the high-resolution ARPES can measure the magnitude of the gap parameter, $| \Delta(k) |$, over the Brillouin zone but not its sign [6]. Inferences about the gap-parameter symmetry from measurements on the anomalous dependencies of properties such as the penetration depth, NMR...etc. are not very conclusive due to the indirect nature of the experiments [4]. In view of the experimental issues mentioned above, we have designed a new experiment for obtaining microscopic phase information from $\phi(r)$ in the pair wavefunction $\Psi(r, R)$ by making use of two macroscopic quantum phenomena, flux quantization and the Josephson pair tunneling — both are quantum coherent effects arising from the $\psi(R)$ part of the pair wavefunction.

2. THE TRICYRSTAL EXPERIMENT

2.1. *Theoretical Consideration*

Before the design of the tricrystal experiment is presented, let us consider the following: a) the symmetry of the order parameter in cuprate superconductors and, b) the ground state of superconducting rings containing Josephson junctions.

[1] Present address: Materials Science Center and Department of Physics, National Tsing-Hua University, Taiwan, Republic of China.

2.1.1. *The pairing symmetry in cuprate superconductors:*

The symmetry of the order parameters $\Delta(\boldsymbol{k})$ has to preserve that of the crystal lattice. In principle, one could use the group - theoretical technique to enumerate all possible pair states that correspond to the irreducible representations of the point group of the lattice. In high - T_c cuprate superconductors, superconductivity presumably originates from the quasi-2D Cu–O square (tetragonal) lattice. The effect of orthorhombic distortion in cuprates such as YBCO and Bi2212 will be considered later. With the tetragonal (4 - fold rotational) symmetry D_{4h} as the premise, one can consider the following major possible pair states:

s-wave pair state: The s-wave order parameter is always of one sign and nodeless. It corresponds to the identity irreducible representation of any point group symmetry. The s-wave pairing probably prevails in most low-T_c conventional superconductors. In the case of cuprate superconductors, it is generally believed that simple s-wave pairing is ruled out because of the strong on-site Coulomb repulsion which is a common characteristic shared by all Cu–O superconductors.

d-wave pair state: In the $d_{x^2-y^2}$ pair state, the energy gap as a function of k can be expressed as:

$$\Delta(\boldsymbol{k}) = \Delta_0(\cos k_x - \cos k_y) \tag{2}$$

where Δ_0 is a constant. In polar coordinates, the gap function varies as $\cos 2\theta$ (θ is the angle of $\boldsymbol{k}$ with respect to axis k_x) and is characterized by four lobes with opposite signs and node lines along the diagonal directions (i.e. $\Delta = 0$, for $\theta = \pi/4$ and $3\pi/4$). The d-wave pairing is favored by high - T_c mechanisms based on spin fluctuations [1,2]. D-wave electron-phonon mechanisms for high-temperature superconductivity are also proposed. [7]

generalized s-wave pairing: The gap function of the so-called extended s-wave pair state [8] has, in its simplest form, eight nodes on the Fermi surface and it varies as:

$$\Delta(\boldsymbol{k}) = \Delta_0(\cos k_x + \cos k_y) \tag{3}$$

or as $\cos 4\theta$ in polar coordinates. This kind of pair state has been suggested as the electronic mechanisms for superconductivity in heavy-fermion systems and more recently in cuprates.

anisotropic s-wave pairing: In this pair state, the order parameter, $\Delta(\boldsymbol{k})$ is nodeless but may vary its magnitude to have lobes of the same sign. For example, $\Delta(\boldsymbol{k})$ can assume the following functional form:

$$\Delta(\boldsymbol{k}) = \Delta_0((\cos k_x + \cos k_y)^2 + 1) \tag{4}$$

A recent APRES study on Bi2212 single crystals by Ding et al.[9] provides supporting evidence for anisotropic s-wave pairing[10].

2.1.2. *The ground state of a superconducting ring containing Josephson junctions*

The ground state of a superconducting ring is determined by the number of the so-called π-junctions [11–14] in the ring. A π-junction is a Josephson junction with a negative supercurrent, an effect first predicted in 1979, due to a phase shift of π at the junction interface. A junction with a positive Josephson current is called 0-junction. The usual expression for supercurrent of a Josephson junction between superconductors i and j can be written as follows:

$$I_s^{ij} = | I_c^{ij} | \sin(\delta\phi_{ij} + \phi_J) \tag{5}$$

where $\delta\phi_{ij}$ is the phase difference across the junction interface and

$$\phi_J = \begin{cases} 0 \\ \pi \end{cases} \quad \text{if} \quad I_c \begin{cases} > 0 \\ < 0 \end{cases} \tag{6}$$

Various mechanisms have been proposed as the origin of the π-junction. Of particular interest is the possibility that a π-junction can be made between two unconventional superconductors such as heavy-fermion systems(12) and d-wave cuprates(14) in which the gap function has lobes and nodes. In the following, the ground state of a superconducting ring interrupted by N π-junctions will be considered from the viewpoints of flux quantization and free energy:

Flux quantization As a consequence of the singlevalueness of the pair wavefunction, the fluxoid in a superconducting ring, containing Josephson junctions or not, is always quantized as an integral multiple of the flux quantum, $n\Phi_0$ (n is an integer $\Phi_0 = \frac{h}{2e} = 2.07 \times 10^{-7}\text{Gcm}^2$). In the case of a superconducting ring with N π-junctions, it is shown that the flux quantization can be described as follows [5]:

$$\Phi = n\Phi_0 \ , \ n = 0, 1, 2, \ldots \quad \text{if } N \text{ is an even number} \tag{7}$$

$$\Phi = (n + \tfrac{1}{2})\Phi_0 \ , \ n = 0, 1, 2, \ldots \quad \text{if } N \text{ is an odd number, and } | I_c | L \gg \phi_0, \text{ where L is the self-inductance of the ring.} \tag{8}$$

From Eq. (7) and (8), the ground state of the ring containing N π-junctions corresponds to zero flux quantum state if $N = 0, 2, \ldots$ and to a half-integer flux quantum state if $N = 1, 3, \ldots$

Free energy Based on free energy considerations, Sigrist and Rice[14], and others [12] showed that the ground state of a ring with one π-junction results in a spontaneously generated supercurrent, $I_s = \frac{1}{2}\Phi_0/L$. The free energy of such a ring can be expressed as a function of the circulating current I in the ring and the externally applied flux Φ_a:

$$U(I, \Phi_a) = \tfrac{1}{2}LI^2 - \left(\frac{\Phi_0 I_c}{2\pi}\right)\cos\left(\frac{2\pi(\Phi_a + LI)}{\Phi_0} + \phi_J\right) \tag{9}$$

In the case of a π-ring (i.e. $\phi_J = \pi$), minimization of U and the condition of $\Phi_a = 0$ lead to a doubly - degenerated

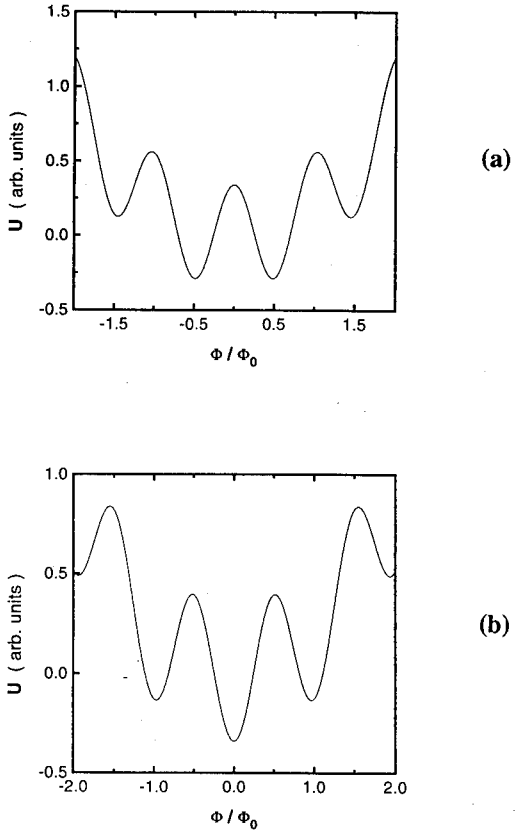


Fig. 1. Free energy of a superconducting ring with (a) one π - junction, or (b) one 0-junction as a function of the amount of flux $\Phi = LI$ in the ring, (where L = 100pH, is the self-inductance of the ring and I is the circulating current).

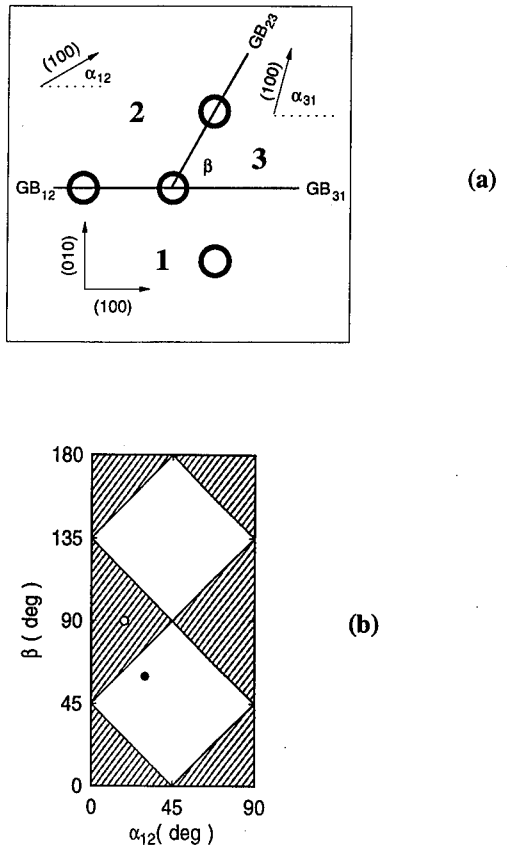


Fig. 2. (a) A schematic illustrates the general geometrical configuration of a tricrystal. (b) Based on the clean limit of Sigrist and Rice for d-wave pairing symmetry, a plot shows regions of the tricrystal design parameters corresponding to integer (shaded) and half-integer (open) flux quantization. The solid and open circles show the design parameters for the π-ring and 0-ring tricrystal samples used in the present work respectively.

ground state with a spontaneous magnetization of $I_sL = \pm\frac{1}{2}\Phi_0$ threading through the ring (Fig. 1a), provided that $I_cL \gg \Phi_0$, a condition that assures that the cost of magnetic energy due to the circulating current I_s is well-compensated by the gain in Josephson energy. When this condition is relaxed, the minimum of the free energy U deviates from its asymptotical value of $\frac{1}{2}\Phi_0$ as $| I_c |$ of the junction decreases. In sharp contrast, a ring with one 0-junction exhibits the conventional integer flux quantization and its ground state corresponds to a zero flux quantum state of the ring (Fig. 1b).

The extension of the above treatment to the more general case of a ring containing any odd number of π-junctions is not straight forward. Sigrist and Rice [14] suggested that such a system should exhibit half-integer flux quantization $\Phi = (n+\frac{1}{2})\Phi_0$ and with a spontaneous magnetization of half flux quantum in the ground state. This is definitely consistent with the conclusion drawn from the flux quantization consideration discussed earlier. [5]

2.2. *The Design of the Experiment*

It is clear from the previous discussions that, to detect an unconventional (non s-wave) pairing symmetry in cuprates, one needs to make cuprate rings containing an odd number (at least one) of π-junctions. And the relative orientation of the junction electrodes can be varied systematically from ring to ring. The presence or absence of the half-integer flux quantum effect in such rings can be used then as a probe of pairing symmetry. For this purpose, a tricrystal (100) $SrTiO_3$substrate was designed for depositing epitaxial cuprate films and for making a ring centered at the tricrystal meeting point, which is interrupted by the grain boundaries three times. As defined in Fig. 2a, the misorientation angles α_{12}, α_{31} and the angle between the grain boundary planes (β) are chosen to ensure that the sign of the supercurrent in the 3-junction ring is negative as required by a certain pair state. For example, the Sigrist-Rice formula can be used for testing d-wave pairing symmetry:

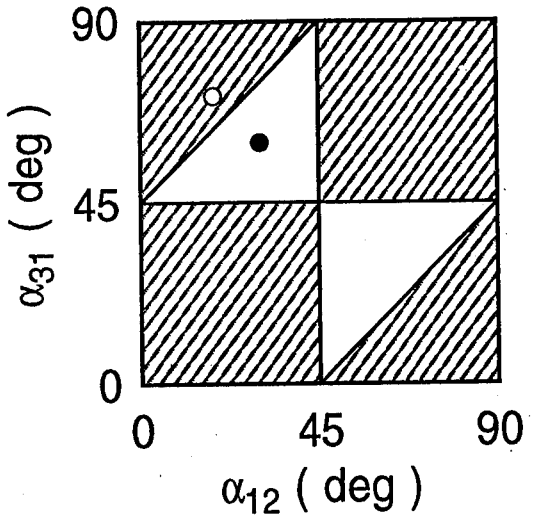


Fig. 3. The same as Fig. 2(b) except for the case of maximum disorder at the junction interface.

$$I_s^{ij} = (A^{ij} \cos 2\theta_i cos2\theta_j) \sin(\delta\phi_{ij}) \tag{10}$$

where θ_i and θ_j are angles of the crystallographic axes (100) in the grains i and j with respect to the junction interface GB_{ij}. The product of the signs of the critical currents of the grain boundary junctions in the ring determines whether it will be a 0-ring (positive sign) with conventional integer flux quantization, or a π-ring (negative sign) with half integer flux quantization. If one assumes that $\alpha_{12} = \frac{\pi}{2} - \alpha_{31}$ for simplicity, the sign of the supercurrent in a 3-junction ring enclosing the tricrystal meeting point based on Eq. (10) is given by the sign of $\cos 2(\alpha_{12} + \beta) \cos 2(\alpha_{12} - \beta)$. In Fig. 2b the design parameters (α_{12}, β) corresponding to the π-ring designs are plotted as open areas while those for the 0-ring configuration are shown in the shaded areas. The geometrical configuration for a tricrystal (100) $SrTiO_3$ substrate is schematically shown in Fig. 2a. The design parameters ($\alpha_{12} = 30°$, $\alpha_{31} = 60°$, $\beta = 60°$) for a tricrystal experiment to test the d-wave pairing symmetry are indicated by a solid dot in Fig. 2b.

To ensure that this tricrystal design is indeed a valid test of d-wave pairing symmetry, the following aspects of the experiment are also considered:

2.2.1. *The effect of disorder at the junction interface:*

The magnitude and the sign of the pair tunneling current across a Josephson weak link (such as a grain boundary junction) between two unconventional (non s-wave) superconductors i and j are determined by the product of the projections of the k-dependent pair wavefunctions onto the normal to the junction interface ($\hat{n}_i$ and $\hat{n}_j$) . [14]

$$I_s^{ij} \propto (\phi_k^i \cdot \hat{n}_i)(\phi_k^j \cdot \hat{n}_j) \tag{11}$$

As a consequence, the presence of any disorder at the grain boundary can significantly alter the outcome of the tricrystal ring experiment. Unfortunately, the Sigrist-Rice formula, on which the design of the tricrystal substrate is based, implicitly assumes that the junction interface is smooth and without any disorder. Experimentally, it is well-established that grain boundaries in high-T_c cuprates are inhomogeneous and meandering, very much depending on the film growth conditions [15]. Furthermore, impurities, strain, oxygen deficiency...etc, at the boundaries all represent significant deviations from the Sigrist-Rice clean limit. To model these disorder effects, a maximum disorder formula for I_s^{ij} is derived[5] by allowing a distribution of angular deviations at the junction interface and by recognizing the fact that, due to the four-fold symmetry of a square lattice, the maximum angle of deviation is $\pi/4$:

$$I_s^{ij} = I_c^{ij} \cos 2(\theta_i + \theta_j) \sin \delta\phi_{ij} \tag{12}$$

The corresponding design parameter regions for the d-wave 0- and π-ring configurations in the dirty limit are presented in Fig. 3. The design parameters of the tricrystal substrate used in this work, represented by the solid circle in the figure, are well-within the bounds of the π-ring geometry.

In short, the tricrystal ring design for d-wave pairing symmetry should exhibit spontaneous magnetization of $\frac{1}{2}\Phi_0$ in its ground state, regardless of whether the junction interface is in the clean or dirty limit.

2.2.2. *The twinning effect*

Due to the in-plane anisotropy in the CuO_2 planes, twinning is known to exist in high-T_c cuprate superconductors such as the Bi2212 and YBCO systems. The fact that twinning does not contribute significantly to the current-carrying capability in these superconductors suggests that twinning boundaries do not act as Josephson weak links nor as strong flux pinning centers. Therefore, twinning should not play an important role in the tricrystal ring experiment. However, the presence of twins does result in sign switch of the lobes in the gap functions from one twin domain to the next. Such twinning effect on the sign of the 3-junction ring experiment can be calculated in a straightforward manner. Based on the Sigrist-Rice and the maximum disorder formula Eq. (10) and (12), one can calculate the effect of twinning on the sign of the supercurrent in the tricrystal ring made from the epitaxial film deposited on the $SrTiO_3$ substrate shown in Fig. 2a. The result of the calculations for all eight possible twinning configurations is that the Josephson current of at least one or all three grain boundary junctions in the ring will be negative. In other words, the π-ring behavior based on this tricrystal design will not be affected by twinning.

2.2.3. *The IV-characteristics of the grain-boundary junctions*

The theoretical considerations presented in the last two sections reasonably assure us that the tricrystal ring design

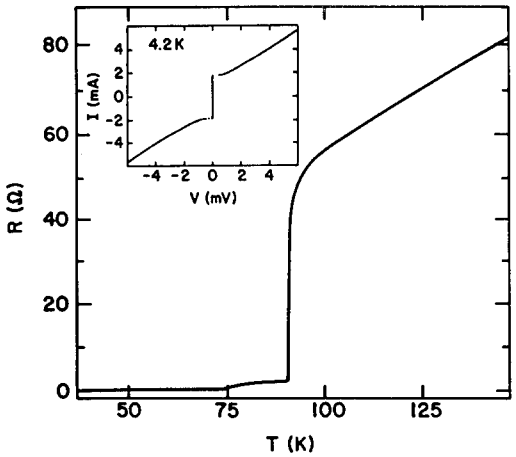


Fig. 4. The electrical resistance as a function of temperature, R(T), for one of the grain boundary junctions in the d-wave tricrystal experiment. The corresponding IV-curve at 4.2K is shown in the inset.

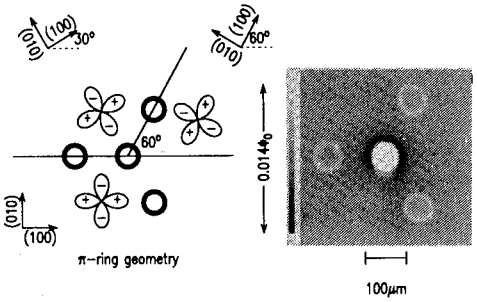


Fig. 5. A schematic of the tricrystal geometry designed to test the d-wave pairing symmetry (left). The four YBCO rings are patterned using a standard photolithographic process. The inner diameter, width and the center-to-center distance are 48 μm, 10 μm and 150 μm respectively. Scanning SQUID microscope image of the YBCO rings at 4.2K, cooled in nominal zero magnetic field (right).

is basically sound as a viable test for d-wave pairing symmetry. However, it is also important to check the actual IV-characteristics of the grain-boundary junctions in the ring to ensure that (1) the IV-characteristic of each grain-boundary junction in the ring is consistent with the Josephson weak link behavior, (2) the magnitude of I_c is large enough that the condition of $I_cL \gg \Phi_0$ is satisfied for a well-defined measurement of the half-integer flux quantization. For this purpose, bicrystal strips were cut from the tricrystal substrate and were placed next to the remaining central piece of the tricrystal substrate for cuprate film deposition. The grain boundary junction made in these bicrystal side strips should be a close approximation to those in the rings. As shown in Fig 4, the electrical resistance as a function of temperature, R(T), for one of such junctions shows a small shoulder below the sharp drop at $T_c = 90.7K$ – a feature typical of a grain boundary weak link. The IV curve at $4.2K$ shown in the inset displays a typical resistively shunted Josephson junction characteristic. The critical current I_c as measured from the IV-curve is $1.8mA$ ($J_c = 1.5 \times 10^5 A/cm^2$) which yields a I_cL product of about $100\Phi_0$ ($L = 100pH$). The condition for observing $\frac{1}{2}\Phi_0$ spontaneous magnetization is thus well-satisfied. Of interest to note, the misorientation angles of the tricrystal substrate used in this study, are designed to have identical critical currents across the three grain boundaries. Experimental values of I_c^{ij} for the three test junctions indicate indeed an agreement within 20%.

3. Scanning SQUID Microscope Measurements and Results

To measure directly the magnetic flux threading through the superconducting rings deposited on the tricrystal substrate, a high-resolution scanning SQUID microscope was used. Its design and operation has been described elsewhere[16]. The microscope basically consists of a mechanical scanning mechanism and an integrated miniature SQUID magnetometer. The SQUID, made of one-micron $Nb - AlO_x - Nb$ junctions, and an octagonal pick-up loop ($10\mu m$ across with $1.2\mu m$ linewidth) structure are integrated on a silicon substrate with a sharpened tip which is in direct contact with the sample during the scan. The pick up loop is located $10\mu m$ from the tip and the SQUID chip is about 20° inclined with the sample plane. The ratio of mutual inductance between loop and ring to the self-inductance of the ring is about 0.02, indicating that there is very small SQUID flux coupling into the ring. The SQUID, operated in flux locked mode, has a flux sensitivity of $2 \times 10^{-6}\Phi_0/\sqrt{Hz}$. Fig 5b shows the scanning SQUID microscope image of four epitaxial YBCO rings on a tricrystal substrate with a d-wave configuration as shown Fig. 5a. Data were taken at 4.2K and in nearly zero external field. It is clear that only the tri-junction ring has flux threading through it, while the two two-junction and zero-junction rings contain no flux at all. These rings are visible because of the mutual inductance coupling between the scanned part of the superconducting ring and the SQUID pick up loop. To determine quantitatively the amount of flux enclosed by the center ring, we have used three different techniques for the calibration of the microscope.

3.1. *Single flux quantum imaging*

One can quantitatively analyze the shape and magnitude of the SQUID image of one of the superconducting vortices trapped in a superconductor. Basically the single flux quantum is used as a point source to image the shape of the pick up coil and its lead structure. A best fit to the SQUID sensor output yield a precise calibration of the microscope.

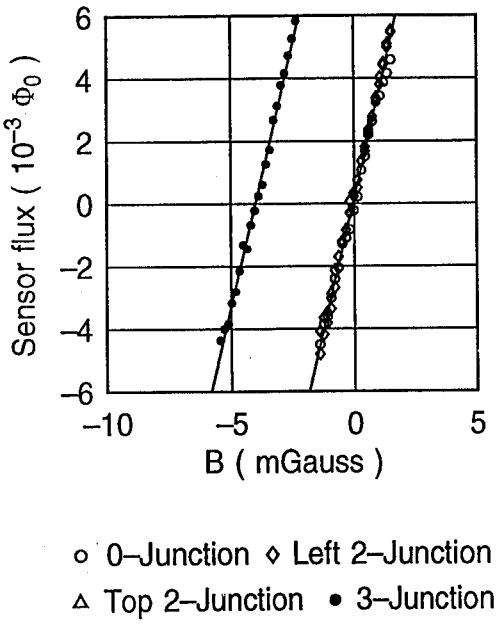


Fig. 6. Difference in sensor flux for the sensor positioned at the center of the ring vs outside the ring, for all of the rings, for the d-wave tricrystal geometry shown in Fig. 5. Measurements of the zero intercepts of the lines gives a value of $0.505 \pm 0.02\Phi_0$ flux enclosed in the π-ring while the other rings have $0.00 \pm 0.01\Phi_0$.

3.2. *Magnetic "oil drop" experiment*

One can park the pick up loop of the microscope in the center of the ring and measure the SQUID output as a function of magnetic field. A staircase pattern in the SQUID output vs. field curve is always observed if the external field is not too high. In a small intermediate field range, the step heights and widths reach their minimum values, suggesting that single flux quanta are admitted. Such smallest units can be used for calibration. Of course, there is always the possibility that the smallest step may correspond to the entering of two flux quanta instead of one. Such uncertainty can be removed by comparing the experimental values with those based on detailed but straight forward calculations of the self inductances of the rings and the mutual inductances between the rings and the pick up loop [5]. For the case of a 3-junction $YBa_2Cu_3O_{7-\delta}$ ring, the minimum step heights derived from the experiments are $\Delta\Phi_s = 0.0237\Phi_0$, in excellent agreement with the calculated value of $\Delta\Phi_s = M(0)\phi_0/L = (0.024 \pm 0.003)\phi_0$.

3.3. *Magnetic field "titration technique"*

In response to the change of the externally applied magnetic field, a screening current is generated in a superconducting ring. The amount of flux threading through the $YBa_2Cu_3O_{7-\delta}$ rings can be determined by running the scanning SQUID microscope line scans through the centers of the rings while varying the external field until the SQUID sensor signal inside the ring is exactly nullified by the screening-current induced field [5] (see Fig. 6). The flux originally enclosed in the ring is just this field times and effective area of the ring. With the effective area estimated to be $2642 \pm 80\mu m^2$, the 3-junction ring in Fig. 5b has $0.505 \pm 0.02\Phi_0$ more flux threading through it than the 0-junction, or 2-junction rings (see Fig. 5b). Furthermore, from the data shown in Fig. 5b, one can see that the difference in flux between any of the other rings on the same substrate is $| \delta\Phi | < 0.01\Phi_0$

It should be mentioned that among the three techniques just described, the magnetic field titration technique is probably most direct, accurate and reliable, although these three methods of calibrating the scanning SQUID microscope agree within 10%.

To make definitive measurements on the ground state of the rings, the tricrystal sample was cooled to 4.2K in nominal zero field. From the results of 12 separate cooldowns, the flux quantization behavior of these rings can be summarized as follows:

3-junction ring: $\Phi = \pm(n + \frac{1}{2})\Phi_0$

2-, 0-junction rings: $\Phi = \pm n\Phi_0$

where the integers $n = 0, 1, 2, 3...$

From these results, one can conclude that spontaneous magnetization of one half magnetic flux quantum, $\pm\frac{1}{2}\Phi_0$ has been observed directly only in the 3-junction ring, but not in the 2- and 0-junction rings.

In addition, there are several aspects of our experiment that are worthwhile to mention:

- Our recent experiments [17] with tricrystal YBCO disks, blanket films, rather than rings, clearly demonstrate that the half-integer quantum effect is independent of the sample's macroscopic geometry.
- Our d-wave tricrystal experiments with YBCO samples in the forms of rings, disks and blanket films show that the half-integer flux quantum effect is observed in all the cooldowns. No exception has been encountered. This remarkable thermal stability at 4.2K is probably a consequence of the deep potential well associated with the doubly-degenerated ($\pm\frac{1}{2}\Phi_0$) ground state of a π-shift configuration. From Eq. 9, the depth of the potential well is equal to $I_c\Phi_0/\pi$. A critical current of $1\mu A$ corresponds a well depth of 47K in thermal energy. The values of I_c for the tricrystal samples studied in this work are in the range of 10^{-4} to $10^{-3}A$. The observed stability is, of course, not too surprising because it reflects the stability of the ground state. It is however a powerful testimony to the fact that our tricrystal experiment is not sensitive to experimental complications such as trapped flux, thermal fluctuations ... etc.
- Trapped vortices do not constitute a problem in our experiments because they can be spotted easily by us-

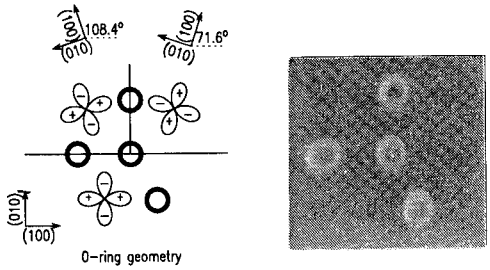


Fig. 7. A schematic of the tricrystal geometry (left) designed to test symmetry-independent mechanisms for the observed half-integer flux quantum effect. Also shown is the scanning SQUID microscope image of the four YBCO rings in this configuration at 4.2K, cooled in nominal zero magnetic field (right).

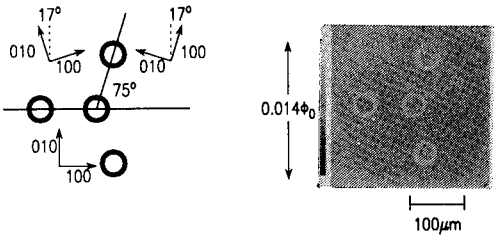


Fig. 8. A schematic of the tricrystal geometry (left) designed to test the g-wave pairing symmetry. Also shown is the scanning SQUID microscope image of the four YBCO rings in this configuration at 4.2K, cooled in nominal zero magnetic field (right).

ing our scanning SQUID microscope.

- The fact that the ratio of the mutual inductance between the SQUID's pick up loop and the ring to the self-inductance of the ring is only 0.02 suggests very little interaction between the SQUID sensor and the sample. Therefore, our experiment represents a truly non-invasive ground state measurement.

4. FLUX QUANTIZATION AND PAIRING SYMMETRY

4.1. *Origin of the half-integer flux quantum effect:*

From the experimental results described so far, it is clear that half-integer flux quantum effect in the tricrystal configuration has been directly observed. The origin of this effect, however, remains to be elucidated. The following possibilities will be considered:

4.1.1. *d-wave pairing*

This is, of course, a natural explanation for the observed effect, because the tricrystal experiment was designed based on the d-wave pairing symmetry (Eq. 1.). An order parameter with d-wave symmetry is indeed consistent with recent SQUID experiments [18–20] for testing pairing symmetry and with many other supporting evidence [4] such as the penetration depth, NMR,...etc.

4.1.2. *Symmetry-independent mechanisms*

Several symmetry independent mechanisms have also been suggested to explain the observed π-junction effect. For example, spin-flip scattering by magnetic impurities at the tunnel barrier [11] (e.g. grain boundary), or indirect tunneling via a localized state (the electronic correlation effects) can also produce a π-phase-shift across the tunnel junction [13]. Since these anodal mechanisms are expected to be insensitive to any specific geometry of the tricrystal, a new tricrystal has been designed, based on the clean limit and maximum disorder formula (the tricrystal design parameters are denoted in Fig. 2b and Fig. 3 as open circles), so that half integer flux quantum effect will be observed only if the symmetry independent mechanisms are in operation. The failure to observe this effect in this particular tricrystal configuration (see Fig. 7) has convincingly ruled out any symmetry-insensitive mechanisms including the two possibilities mentioned above.

4.1.3. *g-wave pairing:*

The tricrystal experiment based on the design shown in Fig. 5a can not rule out even parity states with a gap parameter varying as $\Delta(k) = \Delta_0(\cos k_x + \cos k_y) \propto \cos 4\theta$ (termed as g-wave – the simplest form of the generalized s-wave pair state [8]). To remove such ambiguity, we have designed a new tricrystal experiment (see the left of Fig. 8) which would exhibit a π-shift in the 3-junction ring only if the superconducting state is of g-wave symmetry (i.e. 8 nodes instead of the 4 nodes as in the d-wave case). As shown in the right of Fig. 8, the absence of the half-integer flux quantum effect in the 3-junction ring has eliminated the g-wave pairing in YBCO. This experiment has been repeated three times, by using three such g-wave tricrystal substrates. The junction quality of these experiments was examined carefully to assure that the negative results do represent a valid test of the g-wave pairing symmetry. It is of interest to point out that the g-wave tricrystal experiment can also be used to rule out any symmetry-unrelated mechanisms for the observed half-flux quantum effect.

4.1.4. *Pair state with time reversal symmetry breaking*

Certain theories of superconductivity for high-T_c cuprates and heavy-fermion systems call for time reversal symmetry breaking in the superconducting ground state. There have been numerous suggestions for testing such exotic pair state [20,21]. Our tricrystal experiment can serve as a definitive probe for violation in time-reversal symmetry in cuprate superconductors such as $YBa_2Cu_3O_{7-\delta}$. For this purpose, one can use the phase-sensitive measurements of the order parameter in three different ways:

- the magnitude of the phase-shift:

  A time reversal breaking order parameter of pair states

such as s + id will preserve the 4-fold rotation symmetry but will alter the spontaneous magnetization condition away from exactly $\frac{1}{2}\Phi_0$ by roughly the fractional portion that is s-wave, even if the condition of $LI_c \gg \Phi_0$ is satisfied. From our measured values of the flux threading through the 3-junction rings ($0.490 \pm 0.015\Phi_0$) and the 0- and 2-junction rings ($0.00 \pm 0.01\Phi_0$), we can conclude that the s-wave component of an assumed s + id symmetry is less than 3% in YBCO. A recent SQUID experiment by Mathai et al. [20] also suggests time reversal invariant symmetry in YBCO.

- degeneracy of the $\pm\frac{1}{2}\Phi_0$ ground state:
  A less-than-π phase shift at the nominal π-junction will remove the degeneracy of the $\pm\frac{1}{2}\Phi_0$ ground state. In principle, if the tricrystal experiment can be performed in stable, near zero magnetic field condition, the relative abundance of the observed $+\frac{1}{2}\Phi_0$ vs. $-\frac{1}{2}\Phi_0$ states can give information on the amount of s-wave in the s + id state. Based on our limited statistics, the population of the $\pm\frac{1}{2}\Phi_0$ states is roughly equal, suggesting very little, if any, time reversal symmetry breaking.
- temperature dependence of the $\frac{1}{2}\Phi_0$ spontaneous magnetization:
  A violation of the time reversal symmetry can lead to a second phase transition below T_c [21]. In principle, one can find out the exact temperature at which the time reversal symmetry is broken by monitoring the magnitude of spontaneous magnetization as a function of temperature from low temperature (say 4.2K) all the way to T_c. Our recent success in tricrystal experiments with disks and blanket films [17] has made such measurements using a Hall probe or other magnetic field sensors feasible, because the half-integer vortices in the non-ring tricrystal samples are concentrated within a dimension of the Josephson penetration depth (~ a few microns squared).

4.2. *Complications associated with* $YBa_2Cu_3O_{7-\delta}$

So far, our tricrystal experiments are limited to $YBa_2Cu_3O_{7-\delta}$. The structure of $YBa_2Cu_3O_{7-\delta}$is characterized by two special features: an orthorhombic crystal structure (i.e. in the CuO_2 planes, directions a and b are not equivalent), and a unit cell with two CuO_2 layers. Both of these two structural characteristics complicate the determination of pairing symmetry in this material.

4.2.1. *The orthorhombic effect*

The orthorhombicity of the YBCO structure has been experimentally established as about 2%. Electronic anisotropy in the CuO_2 planes is, however, much larger. For example, anisotropy in the in-plane resistivity is about 2: $\rho_a/\rho_b \sim 2$; the London penetration depth [22]: $\lambda_a/\lambda_b \sim 2$. Whether anisotropy in these electrical properties means equally strong orthorhombic effect in pairing remains to be established experimentally. From the viewpoint of crystal point group symmetry, orthorhombic structure with its 2-fold rotation symmetry is, of course, consistent with a s + d pairing symmetry. A simple calculation of the sign of the supercurrent for the tricrystal configurations studied in the present work indicates that the node line ($\Delta = 0$) for the assumed s + d pair state is at most 14°. away from the pure d wave node line ($\theta = 45°$). A more systematic tricrystal study can place more stringent limits on the s + d pair state.

4.2.2. *The bi-layer effects:*

By taking advantage of the existence of two CuO_2 planes in the YBCO structure, several bi-layer models [23] claim that the pairing symmetry is basically s-wave but have opposite sign in each layer. The experimentally observed π-junction behavior can be interpreted as a result of orthorhombic s-symmetry instead of being a strong evidence for d-wave pairing. Other possible effects on the pairing symmetry in YBCO are also proposed [24].

The resolution of these issues can be best settled by a d-wave tricrystal experiment with a tetragonal single-layer cuprate system such as Tl2201. Such work is in progress.

5. SUMMARY AND CONCLUSIONS

In summary, we have designed and carried out a tricrystal experiment using macroscopic quantum effects, flux quantization and pair tunneling to probe the microscopic internal structure of the pair wavefunction in high-T_c cuprate superconductors. Using a scanning SQUID microscope, we have made the first direct observation of half flux quantum qround state in controlled-orientation tricrystal YBCO rings with three grain boundary junctions. By varying the grain boundary and misorientation angles, we have proved that the energy gap order parameter in YBCO has nodes and lobes consistent with d-wave, but not with g-wave pairing symmetry. We have also ruled out any symmetry-independent mechanisms for the half-integer flux quantum effect. The results of the present work demonstrate that the presence or absence of the half-integer flux quantum effect in superconducting systems containing multiple-grains with deliberately designed orientation can be used for probing the phase of the pair wavefunction. Future work includes tricrystal experiments with tetragonal single-layer cuprate system Tl2201, and other cuprate superconductors such as Hg1212, Bi2212, NdCeCuO systems ... etc. Of course, heavy-fermion superconductors are also of great interest to study with our technique using the half-integer flux quantum effect.

REFERENCES

1. Scalapino D. J., *Phys. Report* **250**, 329 (1995); Bickers N. E., Scalapino D. J. and White S. R., *Phys. Rev. Lett.* **62**, 961

(1989).
2. Pines D., *Physica C* **235–240**, 113 (1994); Monthaux P., Balatsky A. V. and Pines D., *Phys. Rev. B* **46**, 14803 (1992).
3. Beasley M. R., *Proc.* 1994 *Appl. Superconductivity Conf.*, to be published.
4. Annett J. F., Goldenfeld N. and Renn S. R., The pairing state of $YBa_2Cu_3O_{7-\delta}$ in *Physical Properties of High Temperature Superconductors*, Vol. II (Edited by Donald M. Ginsberg), pp. 573–685. World Scientific, Singapore (1990). Also the brief review by B. G. Levi in *Physics Today* May, 17, (1993) and the references therein; also the letters in *ibid.* February (1994)
5. Tsuei C. C. *et al.*, *Phys. Rev. Lett.* **73**, 592 (1994); Kirtley J. R. *et al.*, *Nature* **373**, 225 (1995).
6. Shen Z. X. *et al.*, *Phys. Rev. Lett.* **70**, 1553 (1993).
7. Jinsuk Song and Annett J. F., *Phys. Rev. B* **51**, 3840 (1995).
8. Littlewood P. B. and Varma C. M., *Phys. Rev. Lett.* **63**, 2602 (1989).
9. Ding H. *et al.*, *Phys. Rev. Lett.* **74**, 2784 (1995).
10. Abrikosov A. A., *Physica C*, **244**, 243 (1995).
11. Bulaevski L. N., Kuzii V. V. and Sobyanin A. A., *JEPT Lett.* **25**, 290 (1977).
12. Gershkenbein V. B., Larkin A. I. and Barone A., *Phys. Rev. B* **36**, 235 (1987).
13. Spivak B. I. and Kivelson S., *Phys. Rev. B* **43**, 3740 (1991).
14. Sigrist M. and Rice T. M., *J. Phys. Soc. Jpn* **61**, 4283 (1992).
15. Moeckly B. H., Lathrop D. K. and Buhrmann R. A., *Phys. Rev. B* **47**, 400 (1993). Early E. A., Steiner R. L. and Clark A. F., *Phys. Rev. B* **50**, 9409 (1994)
16. Kirtley J. R., Ketchen M. B., Stawiasz K. G., Sun J. Z., Gallagher W. J., Blanton S. H. and Wind S. J., *Appl. Phys. Lett.* **66**, 1138 (1995).
17. To be published.
18. Wollman D. A., van Harlingen D. J., Lee W. C., Ginsberg D. M. and Leggett A. J., *Phys. Rev. Lett.* **71**, 2134 (1993). Wollman D. A., van Herlingen D. J., Giapintzakis J. and Ginsberg D. M., *Phys. Rev. Lett.* **74**, 797 (1995).
19. Brawner D. A. and Ott H. R., *Phys. Rev. B***50**, 6530 (1994).
20. Mathai A., Gim Y., Black R. C., Amar A. and Wellstood F. C., *Phys. Rev. Lett.* **74**, 4523 (1995).
21. Beasley A. M., Lew D. and Laughlin R. B., *Phys. Rev. B* **49**, 12330 (1994).
22. Basov D. N. *et al.*, *Phys. Rev. Lett.* **74**, 598 (1995).
23. for example, Liu D. Z., Levin K. and Maly J. (preprint) and also in *Phys. Rev. B* **51**, 8680 (1995).
24. Kuboki K. and Lee P. A., preprint.

Pergamon

J. Phys. Chem. Solids Vol. 56, No. 12, pp. 1797–1799, 1995
Copyright © 1995 Elsevier Science Ltd
Printed in Great Britain. All rights reserved
0022-3697/95 $9.50 + 0.00

0022-3697(95)00110-7

TUNNELING IN Pb–YBCO JUNCTIONS: DETERMINING THE SYMMETRY OF THE PAIRING STATE

D. A. WOLLMAN, D. J. VAN HARLINGEN, J. GIAPINTZAKIS and D. M. GINSBERG
Department of Physics and Materials Research Laboratory, University of Illinois at Urbana-Champaign, 1110 West Green Street, Urbana, IL 61801, U.S.A.

Abstract—We report on our efforts to understand the origin of supercurrent observed in *c*-axis tunnel junctions on YBCO [Sun A. G. *et al.*, *Phys. Rev. Lett.* **72**, 2267 (1994).] by studying the phase coherence of *a*-axis/*c*-axis and *b*-axis/*c*-axis Pb–YBCO SQUIDs and Josephson junctions. We also discuss the quasiparticle tunneling spectra measured in *c*-axis Pb–YBCO junctions which should give information about the pairing mechanism responsible for high temperature superconductivity.

Much theoretical and experimental evidence suggests that the high temperature cuprate superconductors have an unconventional pairing state with an anisotropic order parameter. Phase-sensitive measurements have played an important role in determining the symmetry of the order parameter, providing a clear distinction between leading candidate states. Our initial interferometry experiments, using bimetallic corner dc SQUIDs and Josephson junctions in which we found evidence for a sign change of the order parameter in YBCO between orthogonal directions [2,3], have been corroborated by several subsequent experiments [4–7]. However, a small number of Josephson tunneling experiments [1,8] seem to contradict the d-wave model. In particular, the observation of supercurrent in *c*-axis Pb–YBCO junctions with excellent Fraunhofer diffraction patterns [1] is often cited as evidence against a simple d-wave model.

We propose an extension of our SQUID experiments designed to understand the origin of the *c*-axis supercurrent. As shown in Fig. 1, the strategy is to construct dc SQUIDs or corner junctions by connecting Josephson junctions on the *c*-axis and the *a* or *b* axes of YBCO crystals with a thin film of the conventional superconductor Pb. Through the phase coherence of these *a*-axis/*c*-axis and *b*-axis/*c*-axis SQUIDs and Josephson junctions, we hope to measure the intrinsic phase shifts of supercurrent in YBCO between the *a* and *c* directions (δ_{ac}) and the *b* and *c* directions (δ_{bc}), and compare them to the phase shift of π that we have found between the *a* and *b* directions (δ_{ab}) [2,3].

Since it is generally believed that YBCO has a cylindrical Fermi surface and thus no density of states in the *c* direction, it is likely that the tunneling process must involve some component of transverse momentum. We assume that tunneling samples the in-plane order parameter according to this small transverse momentum. In a simple d-wave model, the angular average of equal magnitude positive and negative order parameter lobes is zero. Thus, to first order, no supercurrent would be expected in a *c*-axis junction between an s-wave and d-wave superconductor.

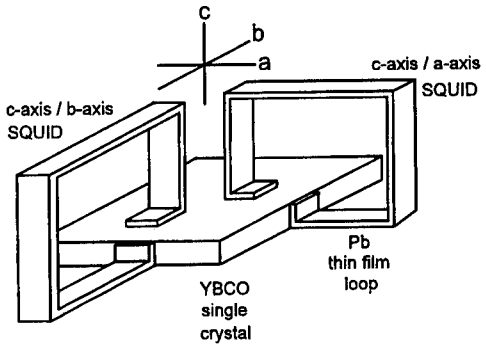


Fig. 1. Proposed SQUID experiments designed to understand the origin of supercurrent in c-axis Pb-YBCO junctions.

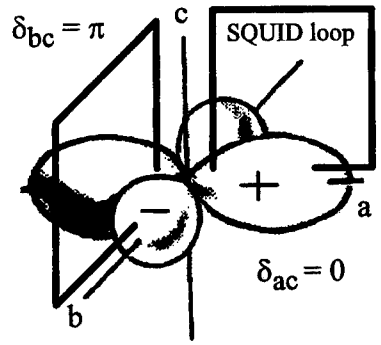


Fig. 2. a-axis / c-axis and b-axis / c-axis SQUIDS for orthorhombic distortion scenario.

There are several possible explanations for supercurrent in *c*-axis Pb–YBCO junctions. The order parameter could have a component that intrinsically allows s-wave coupling. One example is a d-wave order parameter with an imaginary s-wave component. Here, the angular average is nonzero due to the s-wave component, but the complex phase between the s and d components will be seen in the *c*-axis SQUIDs. For simplicity, we assume the positive lobes of

the $d_{x^2-y^2}$ order parameter lie along the a-axis, and define intrinsic phase shifts with respect to the c-axis supercurrent. For a d + is order parameter with equal amounts of d and s, an a-axis/c-axis SQUID would have a phase shift of $\delta_{ac} = \frac{\pi}{4}$, compared to a phase shift of $\delta_{bc} = -\frac{\pi}{4}$ for b-axis/c-axis SQUIDs. For a non-equal mixture of d and s, such as d + is, the phase shifts are $\delta_{ac} = \arctan(\frac{1}{\varepsilon})$ and $\delta_{bc} = -\arctan(\frac{1}{\varepsilon})$.

Another possibility is that the c-axis supercurrent is simply a result of the orthorhombicity of YBCO, which breaks the in-plane symmetry of the order parameter. One pair of order parameter lobes, for example the positive lobes oriented along the a-axis, can be larger in magnitude than the negative lobes, causing a non-zero angular average. This can occur in a d + s (or d + ϵs) order parameter where the nodes are shifted away from 45 degrees. In this scenario, shown in Fig. 2, an a-axis/c-axis SQUID would sample the same sign of the order parameter and would have no intrinsic phase shift, $\delta_{ac} = 0$. A b-axis/c-axis SQUID, on the other hand, would have an intrinsic phase shift $\delta_{bc} = \pi$. This explanation seems to fit certain aspects of the data in that the I_cR_n product of twinned crystals and films is substantially reduced compared to junctions on untwinned crystals [9].

Another possibility is tunneling preferentially into the a and b faces exposed by the etch which is needed to prepare a fresh c-axis surface. We find that the standard 1% (by volume) Br_2 in methanol etch is anisotropic, creating rectangular etch pits with aspect ratios of 2–3 in untwinned regions of YBCO single crystals. These etch pits are always elongated along the b-axis so that more a-face edges are exposed. This would result in the same respective phase shifts for c-axis SQUIDs as mentioned directly above. This argument is plausible but not probable, since the San Diego group obtains layer by layer etching of the c-axis YBCO surface as characterized with a STM, with no difference in the amount of a and b faces exposed [9].

Finally, it is possible to have both an intrinsic imaginary s-wave component of the order parameter and orthorhombic symmetry-breaking. This is equivalent to an order parameter symmetry of d + $\epsilon e^{i\phi}$s, where the angle ϕ is dependent on the relative magnitude of the orthorhombic distortion compared to the intrinsic imaginary s component. In this case, the phase shifts δ_{ac} and δ_{bc} would in general be different in magnitude and sign.

From an experimental standpoint, the necessary first step to making SQUIDs and measuring δ_{ac} and δ_{bc} is to obtain c-axis supercurrent. We start with excellent YBCO crystals that have been extensively characterized. A junction is prepared by etching a twinned YBCO crystal in the standard 1% Br_2 in methanol (or ethanol) solution for 5–15 min, exposing a fresh c-axis YBCO surface with shallow etch pits roughly 10 μm × 10 μm in lateral size. The YBCO crystal is set in polyamide and the junction areas are defined using a flexible shadow mask. A diffusion barrier [1] of 10–20 Å of Ag is thermally evaporated followed by 8000 Å of Pb. The samples are then mounted in a variable temperature cryogenic insert and quickly cooled to 100 K. The measurements are taken in a mu-metal shielded cryostat in a rf shielded room down to 2 K. Our junction sizes are roughly 200 μm × 200 μm, with normal state resistances, R_n, ranging from 10–1000 Ω but generally 20–250 Ω. To date, we have not been able to reproduce the c-axis junction supercurrent observed by the San Diego group. Although we have tried to duplicate their procedure [10], we do not get as low normal state resistances as they report (0.1 Ω–1 Ω). Thus we speculate that we are limited by thermodynamic noise rounding, or that the I_cR_n product falls with increased R_n.

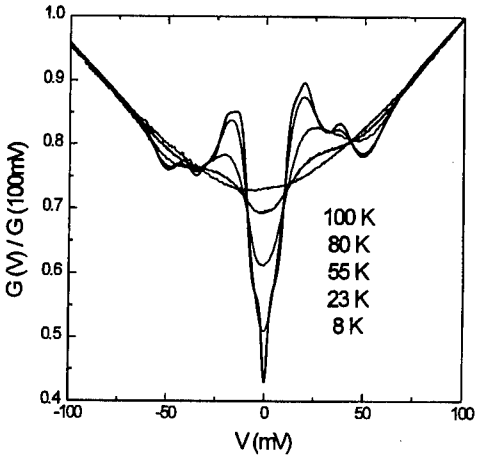


Fig. 3. Conductance vs voltage for a Pb-YBCO c-axis tunnel junction.

On the other hand, the junctions show good quasiparticle tunneling characteristics. Tunneling is important because it should provide information about the microscopic interactions responsible for pairing in high temperature superconductivity. The conductance as a function of voltage for a typical junction is shown in Fig. 3 for several temperatures. Following previous work [11] the conductance is normalized to the conductance at 100 mV, although the dynamic resistance at 100 mV for this junction only changed from 100 Ω to 95 Ω between 105 K and 8 K. The voltage polarity refers to the YBCO electrode. Below the Pb critical temperature, a Pb superconducting gap appears along with weak structure due to Pb phonons at 6 and 10 mV. The tunneling characteristics include very reproducible structure as shown in Fig. 4 for four junctions measured at a temperature of 2 K. The normal state resistances of these junctions ranged from 50 Ω to 250 Ω. In Fig. 5 the asymmetry of positive and negative voltages is shown for two junctions, with most features symmetric in voltage except for the peaks at roughly 38 mV and −42 mV. The junctions had leakage currents of 1% to 2% at 2 K, as seen in the current–voltage characteristic in Fig. 6.

In summary, we have presented experiments designed to understand the origin of supercurrent observed in c-axis tunnel junctions on YBCO [1] by studying the phase coherence of a-axis/c-axis and b-axis/c-axis Pb–YBCO SQUIDs

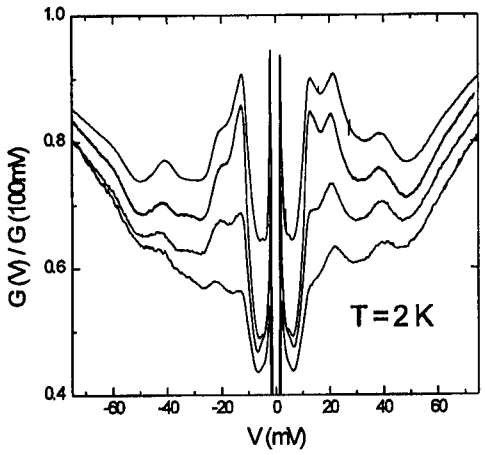


Fig. 4. Conductance vs voltage for four 4 Pb-YBCO c-axis junctions at 2K.

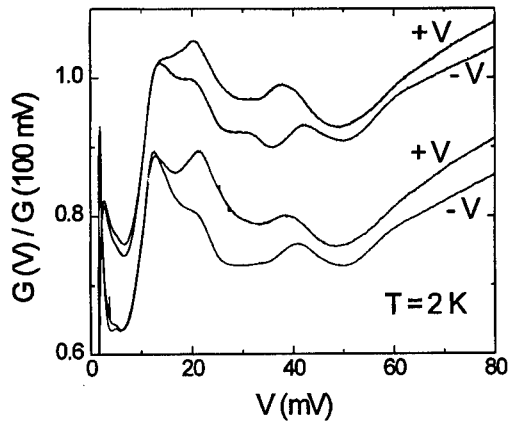


Fig. 5. Conductance vs voltage asymmetry for two Pb-YBCO c-axis tunnel junctions, with voltage polarity as indicated. The top set of curves has been shifted vertically by 0.15 for clarity.

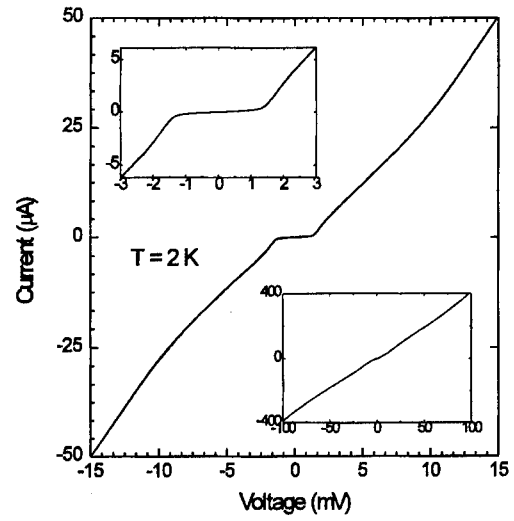


Fig. 6. Current vs voltage showing low leakage at 2K.

and Josephson junctions. We have attempted to obtain *c*-axis supercurrent, as yet without success, although we do find good tunneling characteristics in Pb–YBCO *c*-axis junctions.

Acknowlegements—We would like to acknowledge fruitful discussions with I. Kosztin, Mark Covington and Laura Greene. This work was supported by the NSF Science and Technology Center for Superconductivity under Grant No. NSF DMR 91-20000. We also acknowledge extensive use of the facilities of the MRL Microfabrication Laboratory.

REFERENCES

1. Sun A. G., *et al.*, *Phys. Rev. Lett.* **72**, 2267 (1994).
2. Wollman D. A., Van Harlingen D. J., Giapintzakis J. and Ginsberg D. M., *Phys. Rev. Lett.* **74**, 797–800 (1995).
3. Wollman D. A., Van Harlingen D. J., Lee W. C., Ginsberg D. M. and Leggett A. J., *Phys. Rev. Lett.* **71**, 2134–2137 (1993).
4. Tsuei C. C., *et al.*, *Phys. Rev. Lett.* **73**, 593 (1994).
5. Brawner D. A. and Ott H. R., *Phys. Rev. B* **50**, 6530 (1994).
6. Mathai A., *et al.*, *Phys. Rev. Lett.***74**, 4523 (1995).
7. Iguchi I. and Wen Z., *Phys. Rev. B* **49**, 12388 (1994).
8. Chaudari P. and Lin S. -Y., *Phys. Rev. Lett.* **72**, 1084 (1994).
9. Dynes R. C., *et al.*, these proceedings.
10. Sun A. G., private communication.
11. Gurvitch M., *et al.*, *Phys. Rev. Lett.* **63**, 1008 (1989); Valles J. M., *et al.*, *Phys. Rev. B* **44**, 11986 (1991).

Pergamon

J. Phys. Chem. Solids Vol. 56, No. 12, pp. 1801–1802, 1995
Copyright © 1995 Elsevier Science Ltd
Printed in Great Britain. All rights reserved
0022-3697/95 $9.50 + 0.00

0022-3697(95)00159-X

TUNNELING OBSERVATION OF PHONON CONTRIBUTION TO THE PAIRING INTERACTION IN OXIDE SUPERCONDUCTORS

R. AOKI, H. MURAKAMI, T. KITA
Department of Electrical Engineering, Faculty of Engineering, Osaka University, 565 Suita, Japan

M. SHIRAI
Department of Material Physics, Faculty of Engineering Science, Osaka University, 560 Toyonaka, Japan

V. M. SVISTUNOV, A. I. DYACHENKO and D. N. AFANASSYEV
Donetsk Physico-Technical Institute, Academy of Science, 340114, Donetsk, Ukraine

Abstract—Tunneling conductance spectra were observed by point contact junction of SIN on single crystals of BSCCO (2212). Outside of the definite gap structure edge, significant fine structures were observed almost reproducibly ranging to 0.2 eV. The conductance derivative peaks both in positive and negative bias range were found in well one by one correspondence with the phonon spectrum peaks reported by Renker *et al.* [1]. Most of the peak modes were attributed to the optical phonons due to the oxygen oscillations in and around the $[CuO_2]_n$ net-plane. Numerical computation in terms of the Eliashberg gap equation was carried out, and the electron–phonon coupling intensity function $\alpha^2F(\omega)$ was elucidated and it turns out that the breathing mode relating to the polaronic valence fluctuations are predominant as compared with the B_{1g} mode regarding the spin correlations.

Keywords: Tunneling spectroscopy, $Bi_2Sr_2CaCu_2O_y$, Cooper pairing, Optical phonon, Eliashberg gap equation

1. INTRODUCTION

The high Tc superconductivity mechanism still remains unclear, especially how the strong Cooper pairing is achieved, and by what kind of mediator, however, its signature should appear in the quasiparticle tunneling spectrum.

2. EXPERIMENT

NIS junction was prepared on cleaved surface of BSCCO (2212) single crystal by SiO_x thin layer deposition during plasma oxidation and Au tip contact press with fine regulation, so as the junction resistance is several kΩ. This point contact junction provided us with a more reproducible observation of the fine structure spectrum than the vacuum gap STS, because of sufficient tunneling probability current and less probelm from mechanical vibrations .

3. RESULT

The observed conductance $\sigma = dI/dV$ spectrum is shown in Fig. 1, and one finds good fitting of the in-gap structure by the BCS curve with the broadening parameter Γ [2].Beyond the gap edge, step-like fine deviations from the smooth curve is recognized. This fine steps brings peak structures in $d\sigma/dV$ curve (see Fig. 1); negative peaks in positive bias range and vice versa [2]. In terms of the Eliashberg gap equation, this antisymmetric character in peak structure is considered as evidence of spectrum reflection of the quasiparticle that mediates the Cooper pairing. Similar kinds of the fine structure was also observed at the junction of a break-off tip of the BSCCO crystal contacted with Al plate covered with Al_xO_y barrier [2].

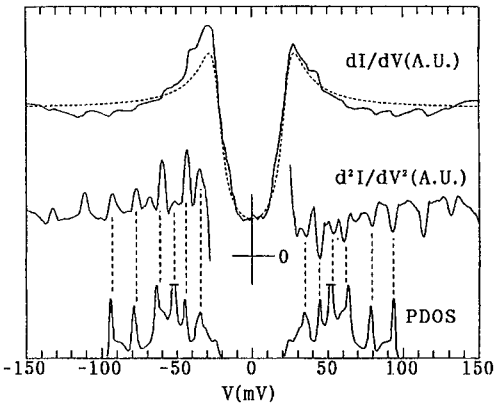


Fig. 1. Tunneling dI/dV and d^2I/dV^2 spectrum for BSCCO(2212). The dotted curve shows the BCS fit with 2Δ=47 meV and Γ=6.1 meV. For comparison calculated PDOS is cited from Ref. [1].

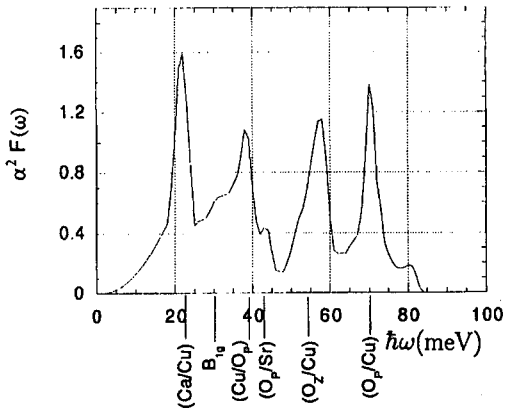


Fig. 2. Numerically computed electron–phonon coupling $\alpha^2 F(\omega)$ function from the dI/dV data of $eV \leq \Delta + \hbar\omega_D$, while the ordinate scale is rather sensitive to the computational conditions. Corresponding phonon mode is denoted under the energy scale.

4. ANALYSIS AND CALCULATION

As a likely Cooper pair mediator, optical phonons can be taken into consideration, since the oxides show strong optical and polarizable activities. For the BSCCO crystal structure, Renker *et al.* [1] calculated phonon mode oscillations in terms of a Born–von Karman model, and their neutron scattering experiment realized its peak structures in generalized phonon density of states (PDOS). Their calculated PDOS spectrum is cited in Fig.1 and we find here well peak to peak correspondence with the observed $d^2I/dV^2 - V$ curve. Similar kinds of correspondence with the phonon spectrum have also been reported by other investigators [3]. From these facts it turns out that phonons contribute substantially to the high Tc oxide superconductivity. In order to investigate which kinds of th ephonon mode are significantly effective on the high Tc Cooper pairing, the electron–phonon coupling function $\alpha^2 F(\omega)$ was numerically computed in terms of the Eliashberg equation [4] and a result is presented in Fig. 2. Here the corresponding phonon mode to each peak is assigned by the Renker's calculation [1] and other informations by optical spectroscopies. They are denoted under the energy scale of Fig. 2; e.g. (O_P/Cu) and (O_Z/Cu) mean the optical phonons due to O(in-plane)–Cu and O(apical)–Cu bond stretching oscillations and (Cu/O_P) is the acoustic mode. B_{1g} is a well known transverse motion of the O_P in the Cu–O_P–Cu zigzag bonding.

5. DISCUSSION

From this correspondence, it turns out that most of the intensity peaks in $\alpha^2 F(\omega)$ come from optical phonon modes due to oxygen oscillations in and around the $[CuO_2]_n$ net-plane, wherein the superconducting electronic state takes place. Accordingly, the oxygen ion oscillation has a significant role in high Tc superconductivity, either working alone or coworking with other kinds of particles. In the case of the phonon assisted quasiparticle mediation, the phonon mode is restricted for each specific quasiparticle; for instance the spin correlation is enhanced by the B_{1g} mode, (32 meV) and the charge fluctuation is induced by the breathing mode (72 meV).In Fig. 2, we find a distinct peak of $\alpha^2 F(\omega)$ at 72 meV, but only slight evidence of a peak at 32 meV. This fact suggests that the breathing mode oscillation is more effective to the high T_C superconductivity as compared with the B_{1g} mode.

REFERENCES

1. Renker B., Gompf D., Ewert D., Adelmann P., Schmidt H., Gering E. and Mutka H., *Z. Physik B* **77**, 65 (1989)
2. Aoki R., Murakami H. and Kita T., *Physica C* **225**, 1 (1994); *ibid.* **235–240**, 1891 (1994)
3. Gonnelli R. S. *et al. Physica C* **235–240**, 1861 (1994), Vedeneev S. I. *et al. ibid* 1851; Miyakawa *et al. J. Phys. Soc. Jpn* **62**, 2445 (1993)
4. vistunov V. M., Belogolovskii M. A. and Khachaturov A. I., *Physics Uspekhi* **36** (2), 65 (1993)

Pergamon

J. Phys. Chem. Solids Vol. 56, No. 12, pp. 1803–1804, 1995
Copyright © 1995 Elsevier Science Ltd
Printed in Great Britain. All rights reserved
0022–3697/95 $9.50 + 0.00

0022-3697(95)00162-X

A STUDY OF THE CuO CHAINS IN $YBa_2Cu_3O_{7-x}$ BY SCANNING TUNNELING MICROSCOPY AND SPECTROSCOPY

H. L. EDWARDS, D. J. DERRO, A. L. BARR, J. T. MARKERT and A. L. de LOZANNE
Department of Physics, University of Texas at Austin, Austin, TX 78712-1081, U.S.A.

Abstract—We review the topographic and spectroscopic results we have obtained on cold-cleaved $YBa_2Cu_3O_{7-x}$ single crystals using a low temperature scanning tunneling microscope. The most important feature is the observation of CuO chains on the surface which show modulations with a periodicity of about three times the unit cell.

The metallic CuO_2 planes are widely believed to contain the superconducting condensate in the copper-oxide high-temperature superconductors. One compound, $YBa_2Cu_3O_{7-x}$ (YBCO), has an additional crystallographic feature which gives rise to a partially-filled (and hence potentially metallic) band: the CuO chains. This one-dimensional feature of YBCO is of interest for two reasons. First, the CuO chains' electronic structure may serve to obscure or modify the traditional signatures of superconductivity in the CuO_2 planes. Second, the CuO chains' electronic structure may be interesting in its own right. For instance, far-infrared spectroscopy has recently detected a superfluid response in the CuO chains which indicates superconductivity [1]—a startling result, since the CuO_2 planes are though to be the sole possessors of superconductivity.

We have studied the CuO chains of YBCO for several years using scanning tunneling microscopy (STM) and spectroscopy (STS) [2–4].

In this paper, we briefly review this line of research to set the perspective for our more recent work, which we are preparing for publication [5].

To study YBCO by STM, it is necessary to prepare a pristine sample. The only way to do this is to cleave YBCO at 20 K. Warming over 40–50 K destroys the surface, possibly due to the loss of the weakly bound CuO-chain oxygen ions on or near the surface. We have perfected a method of cleaving single crystals of YBCO along *a–b* planes. As a verification that they must be cold-cleaved, we have tried repeatedly to achieve STM on crystals cleaved at 60–80 K; we have never obtained CuO-chain images (see below) on these "hot-cleaved" crystals.

Once a crystal is cleaved, we have several days over which to observe its structure: the vacuum inside our helium-temperature cryostat is very good; at the very least there are no water vapor or reactive air components. We observe several types of topography on such a cold-cleaved crystal. Most importantly, we see images with chain-like features separated by the *a*-direction lattice constant; these must be attributed to the CuO chains, the only one-dimensional feature in YBCO [2] The image shown in Fig. 1, which is not previously published, shows these CuO chains and some of the features discussed in this paper. We also see regions with a square lattice of atomic corrugations, sometimes littered with disordered islands; these may be BaO or CuO_2 planes with Cu clusters [3]. The cleaved surface often has many steps. From the step-height distribution, we garner support for our assignment of the chain-like features to the CuO chain layer [2].

These sharp CuO-chain images all display several interesting topographic features. Sometimes (usually dependent upon the tip quality), we observe atomic corrugations along the CuO chains: one atom per unit cell [3]. The CuO chains should have two, and it is unclear whether it is Cu or O which is shown by these images.

Another feature of the CuO chain images is a several-unit-cell-wavelength electronic modulation of the CuO chains. These modulations reverse phase under bias reversal, indicating that they are electronic rather than topographic [3]. This property and the relation their wavelength bears to the Fermi wave vector k_F are consistent with a charge-density wave state in the CuO chains [4] Unfortunately, these properties do not provide a smoking gun, since they may occur for a broad class of spatial features of the Fermi-level electrons.

Yet another feature of the CuO chain images is the occasional depression along the CuO chains. These depressions are several nm in length, and the electronic modulations discussed above are enhanced in the depressions. Because the spatial density of these depressions closely matches that expected from oxygen vacancies in the CuO chains, we assign these features to oxygen vacancies. The reversed-bias behavior of the electronic modulations near these depressions is more complicated than away [3], indicating some type of dispersion or other local behavior.

We have also taken $I(V)$ curves which display a 20–30 meV gap (giving $2\Delta/kT_c$ = 6–8) [2]. These curves were obtained on a freshly cleaved sample and the current showed

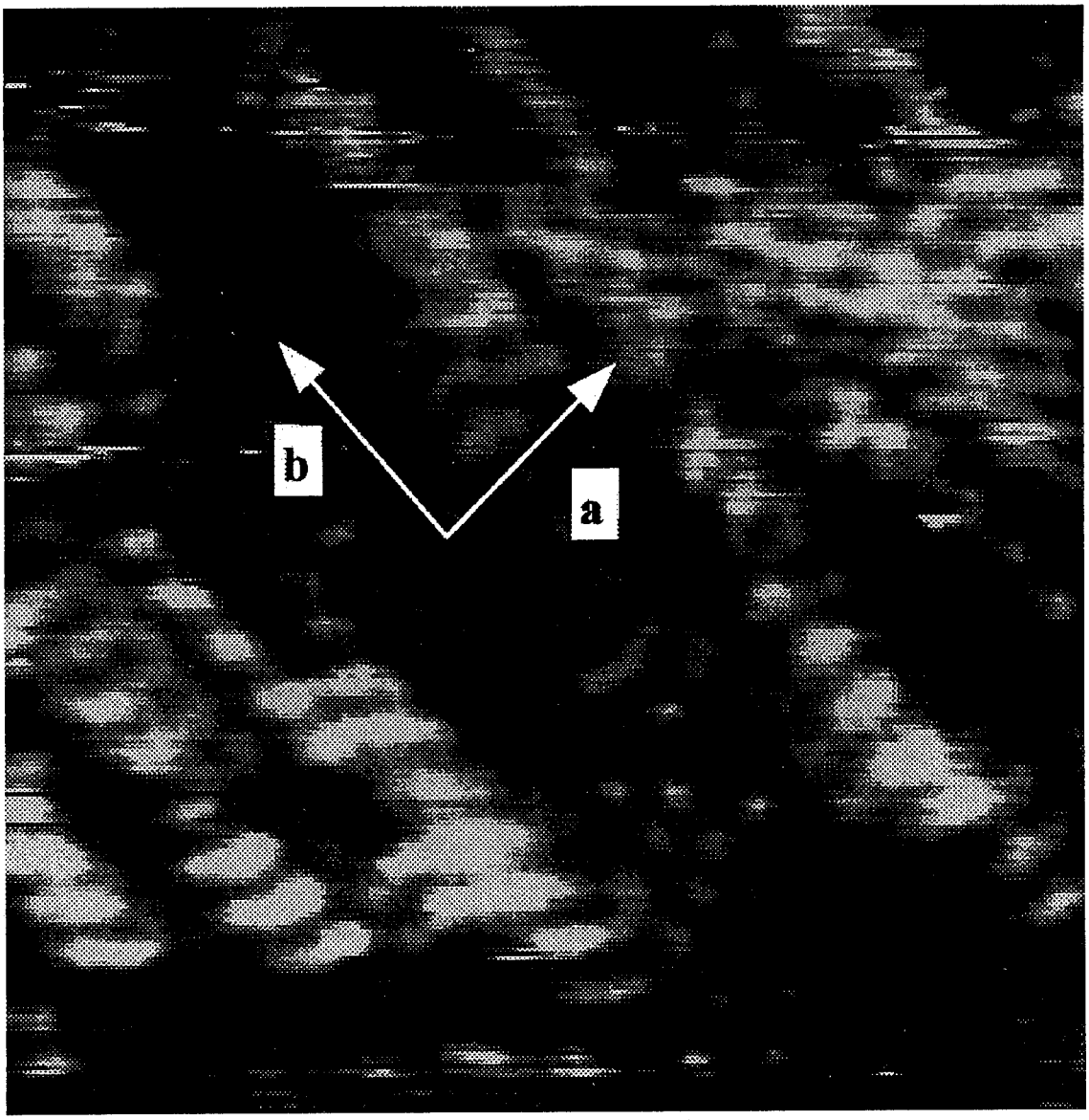


Fig. 1. STM image taken at 24 K on a surface of freshly cleaved YBCO. The bumps are the modulations discussed in the text, while the dark depressions are thought to be due to oxygen vacancies.

an exponential dependence on tip–sample distance with a work function of 1 eV, indicating vacuum tunneling [2].

Most recently, we have used current-imaging tunneling spectroscopy (CITS), a type of STS, to study the $I(V)$ behavior of YBCO as a function of position. Our new data indicate that there is an energy gap far from the depressions which is filled in near the depressions [5]. This data is exciting, but we have not yet explained it uniquely. Possible candidates include a dynamic CDW with strong local pinning and proximity-induced superconductivity in the CuO chains with local pair-breaking at the oxygen vacancies. This data may explain the lack of consistency in $I(V)$ data for YBCO in the literature. Tunneling in different places results in different $I(V)$ curves.

REFERENCES

1. Basov D. N. *et al.*, *Phys. Rev. Lett.* **74**, 599 (1995).
2. Edwards H. L., Markert J. T. and de Lozanne A. L., *Phys. Rev. Lett.* **69**, 2967 (1992).
3. Edwards H. L., Markert J. T. and de Lozanne A. L., *J. Vac. Sci. Technol. B* **12**, 1886 (1994).
4. Edwards H. L., Barr A. L., Markert J. T. and de Lozanne A. L., *Phys. Rev. Lett.* **73**, 1154 (1994).
5. Edwards H. L., Derro D. J., Barr A. L., Markert J. T. and de Lozanne A. L., manuscript in preparation.

Pergamon

J. Phys. Chem. Solids Vol. 56, No. 12, pp. 1805–1806, 1995
1995 Elsevier Science Ltd
Printed in Great Britain
0022–3697/95 $9.50 + 0.00

0022–3697(95)00105-0

USE OF CUPRATE TRICRYSTAL MICROBRIDGES AS PROBES OF SUPERCONDUCTING PAIRING STATE SYMMETRY

J. H. MILLER Jr., Q. Y. YING, Z. G. ZOU, J. H. XU, M. F. DAVIS and N. Q. FAN
Texas Center for Superconductivity at the University of Houston, 4800 Calhoun Road, Houston, TX 77204-5932, U.S.A.

Abstract—We have carried out field-modulated critical current measurements of nominally pure, doped, and ion-irradiation YBCO tricrystal microbridges in order to probe superconducting pairing state symmetry. Our results in the short junction limit are consistent with a real combination of large d-wave and small s-wave components of the order parameter.

Keywords: Superconductors, oxides, superconductivity.

1. INTRODUCTION

A determination of the pairing state symmetries of high-T_c superconductors is one of the paramount problems of condensed matter physics. Most experiments that directly probe the pairing state symmetry of YBCO using Josephson devices are consistent with $d_{x^2-y^2}$-symmetric pairing, with little or no imaginary s-wave component. However, some experiments are consistent with the existence of an s-wave component, suggesting that a real mixture of large d-wave and small s-wave components cannot be ruled out.

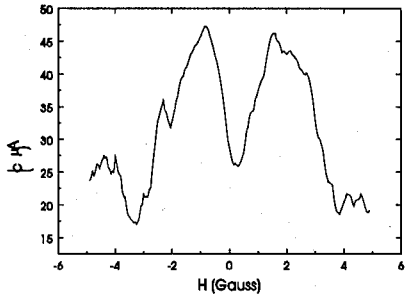


Fig. 1. Frustrated tricrystal microbridge, in which the narrow region is 3 μm wide and the misorientation angles are 30°.

2. EXPERIMENT

Our method of probing superconducting pairing state symmetry [1] is to measure the field-modulated critical current of a cuprate thin film microbridge on a $SrTiO_3$ tricrystal substrate, as illustrated in Fig. 1. The critical current is limited by the two shortest of the three grain boundaries crossing the microbridge. This device is analogous to an s–d corner junction, since one of the two short boundaries acts as a π-junction, while the other acts as a 0-junction, if the pairing symmetry is $d_{x^2-y^2}$. Our measurements provide more information than just the phase shift, and are capable of detecting either a complex or a real mixture of s- and d-wave components of the order parameter.

Two central peaks, of approximately equal height, are observed in the field modulated critical currents of frustrated nominally pure YBCO tricrystal junctions operating in the short junction limit, as shown in Fig. 2. These results are consistent with predominantly $d_{x^2-y^2}$ pairing symmetry with little or no imaginary s-wave component. However, the critical current is nonvanishing at zero field, consistent with the existence of a real mixture of large d-wave and small s-wave components. A pairing state with such $d + \alpha s$ symmetry is equivalent to a distorted (orthorhombic) $d_{x^2-y^2}$ symmetric order parameter, which exhibits a sign change but has different magnitudes along the two principal symmetry directions. This behavior is consistent with the substantial anisotropy in the London penetration lengths along the a- and the b-directions. We observe only a single central peak in the field-modulated critical current of an unfrustrated tricrystal device, thus allowing us to rule out artifacts unrelated to pairing state symmetry, such as spin-flip scattering across the boundaries or corner demagnetization effects.

A single peak is observed in the field-modulated critical currents of *frustrated* tricrystal junctions operating in the *long* junction limit. Theoretical calculations [2], in which a superconducting "$0 - \pi$ junction" is modeled as a Sine-Gordon system with a π-discontinuity in the Josephson coupling energy, show that the behaviors of s- and d-wave superconductors are indistinguishable in the long junction limit.

Experiments on cuprate superconducting tricrystal microbridges with a wide range of critical temperatures, including doped and ion-irradiated YBCO, have also been carried out. The behaviour of a 10% Pr-doped YBCO tricrystal device has been found to be essentially the same as nominally pure YBCO tricrystal devices. The field-modulated critical current behavior appears to approach that expected

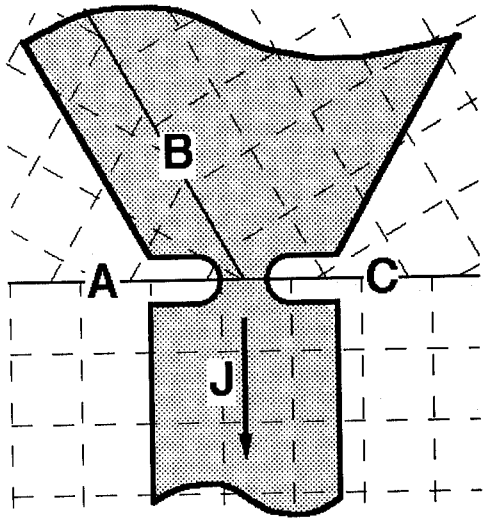


Fig. 2. Field-modulated critical current of a frustrated YBCO tricrystal microbridge operating in the short junction limit at T=8 K.

for an ideal d-wave superconductor as the T_c is suppressed in YBCO tricrystal devices irradiated with α-particles. In particular, the ratio $T_c(H = 0)/I_c(\max)$ of the zero field minimum to the maximum critical current exhibits an overall decrease with increasing ion irradiation. Some of this behavior might be attributed to the fact that the tricrystal junction becomes further into the short junction limit as the T_c and J_c are reduced. In addition, the magnitude of any real s-wave component of the order parameter might be reduced due to reduced orthorhomicity as the number of defects induced by irradiation increases. However, this apparent overall decrease in s-wave component with decreasing T_c is not monotonic, and we observe an apparent *increase* in the ratio Δ_s/Δ_d (with decreasing T_c) in the range 55 K $< T_c <$ 65 K, which corresponds to the temperature range of the "60 K plateau" often observed in oxygen-depleted YBCO samples. We do not, as of yet, have a satisfactory explanation for this behavior.

Acknowledgements—This research was supported by the State of Texas through the Texas Center for Superconductivity and the Advanced Research Program, and by the Robert A. Welch Foundation.

REFERENCES

1. Miller Jr. J. H., Ying Q. Y., Zou Z. G., Fan N. Q., Xu J. H., Davis M. F. and Wolfe J. C., *Phys. Rev. Lett.* **74**, 2347 (1995).
2. Xu J. H., Miller Jr. J. H. and Ting C. S., *Phys. Rev. B* (in press).

Pergamon

J. Phys. Chem. Solids Vol. 56, No. 12, pp. 1807–1808, 1995
Copyright © 1995 Elsevier Science Ltd
Printed in Great Britain. All rights reserved
0022–3697/95 $9.50 + 0.00

0022-3697(95)00236-7

LT-STM/STS OBSERVATION ON DIFFERENT ATOMIC LAYERS OF BSCCO (2212)

H. MURAKAMI and R. AOKI
Osaka University, Department of Electrical Engineering, Suita, Osaka 565, Japan

Abstract—To investigate the intrinsic superconducting electronic state originating in the CuO_2 layer, tunneling spectra were observed on several cleaved surfaces of BSCCO single crystal by using LT-STM/STS. As a result, it was confirmed that two substantially different types of superconducting gap structures were observable on the cleaved surface. One is a definite gap structure with a low conductance level near E_F, and was reproducibly observed at some special surface area not covered with a BiO atomic layer. Another is a gapless-like one usually observed on a BiO surface when the STM tip approaches near enough to the surface.

Keywords: Tunneling, LT-STM/STS, gap structure, BSCCO, BiO defect area

INTRODUCTION

Tunneling is an effective method to probe the details of the quasiparticle density of states near E_F of high-T_C superconductors (HTS). Particularly, the micro-spot observation by using a low temperature scanning tunneling microscope and spectroscope (LT-STM/STS) is the most useful for HTS because of HTS's unique layer structure composed of different atomic layers with different electronic states.

We carried out tunneling observations on the fresh cleaved surfaces of $Bi_2Sr_2CaCu_2O_{8+X}$ (BSCCO) single crystal by means of a specially designed LT-STM/STS, and could succeed in observation of more intrinsic gap structures at some specific area not covered with a BiO atomic layer.

EXPERIMENT

LT-STM/STS observations were carried out on the clean surfaces of a well grown BSCCO crystal rod (T_C=81K) under ultra high vacuum (UHV) conditions at T~5K. The clean surfaces were prepared by cleavage under different conditions as follows: [i]*in situ* cleavage under UHV at low temperature (below 12K), [ii]cleavage under UHV at room temperature just before observation and [iii] cleavage in air just before introducing the specimen into the LT-STM/STS apparatus.

RESULTS AND DISCUSSION

Fig.1 shows typical STS spectrum patterns observed on the cleaved surfaces. Through LT-STM observations it was confirmed that most parts of the cleaved surface showed BiO atomic layer with characteristic modulation structure along the crystal b-axis. The STS spectra observed on the BiO surfaces showed semiconducting gap structures with E_g ~0.1 eV commonly to the cleaved surface prepared by [i], [ii] and [iii] method, as shown in spectra-A.

However, when the probe tip was made close enough to the BiO surface, superconducting gap structure appeared on the tunneling spectrum as shown in spectra-B probably owing to the contribution of the tunneling probability from under-layered CuO_2 plane. Spectra-B shows the V-letter shape feature just predicted by d-wave superconductivity, a feature of which has been also reported by many investigators [1]. Hence, they considered the tunneling results as evidence of the d-wave superconductor. However,it must be noted that most of these gapless-like spectra have been observed at BiO surface, then the tunneling process to the [CuO_2] superconducting layer takes place through the non-superconducting BiO (and SrO) surface layer. Therefore, we must take into account various extrinsic effects, e.g., indirect tunneling through the BiO localized states and the band edge bending of these semiconducting layers.

Here, more direct tunneling process to the CuO_2 superconducting electronic state was ascribed as follows. We attempted to look for a specific area not covered with BiO (and SrO) layer. Although the detection of those areas is occational, we have succeeded in the detection by LT-STM and in the observation of tunneling spectra at the area as shown in spectra-C. Here, Spectra-C1 and C2 were observed on different cleaved surfaces as follows; C1 at the cleaved surface prepared by the cleavage method of [ii] and C2 by the method of[iii], respectively. Nevertheless, we could reproducibly observe almost similar gap structure all over each defect area.

As for the spectrum characteristic, spectra-C show substantially different characteristics from that of spectra-B inside the gap region, i.e., substantially low conductance level forming a certain flat region near the zero-bias point. Furthermore, it is interesting that the dotted lines extrapolated along both inner gap walls never intersect the zero con-

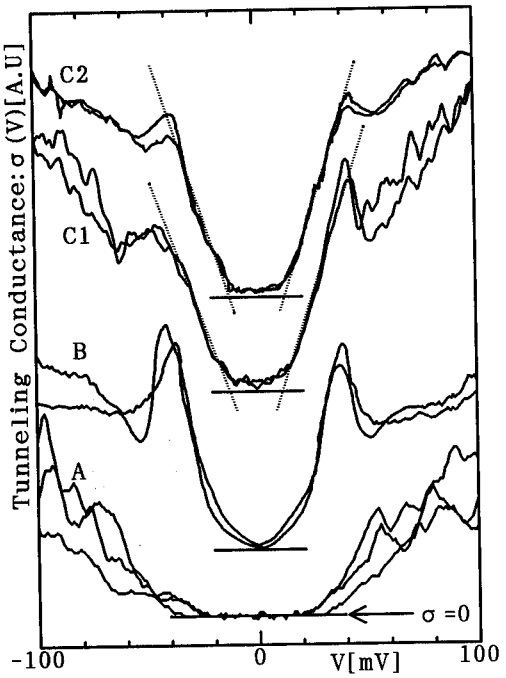


Fig. 1. Typical spectrum patterns observed on the cleaved surface of BSCCO

thermore, it is interesting that the dotted lines extrapolated along both inner gap walls never intersect the zero conductance level at the zero-bias point, as shown here. These spectrum characteristics wouldn't be explained simply by using the d-wave theory, and rather indicate a considerably anisotropic but finite superconducting gap state. However, it is also fact that there are commonly low conductance level of about 5% at the gap bottom regions. It may possibly be explained by a little poor superconducting characteristic of the CuO_2 layer exposed to the specimen surface, because the oxygen decomposition of the unprotected CuO_2 surface might easily occur under UHV condition at room temperature.

On the other hand, we couldn't observe any atomic images on the defect areas by LT-STM observation, while the periodic atomic images could be observed on the BiO area right near the defect area. This result may indicate that the defect surface corresponds to some metallic or disordered surface different from such a semiconducting surface as the BiO surface. These experimental details were mentioned elsewhere [2,3].

SUMMARY

Tunneling spectrum observations were carried out on several cleaved surfaces of BSCCO single crystal by using LT-STM/STS.

The gap spectrum which more directly reflects the CuO_2 superconducting electronic state could reproducibly be observed all over some specific area not covered with a BiO layer. These more intrinsic spectra show substantially different characteristics from the gapless-like one usually observed on BiO layers, and show a definite gap region of low conductance level. As for the gapless-like one, we consider that it appears for some extrinsic reasons, e.g., due to the tunneling process through the semiconducting BiO (and SrO) layer.

Acknowledgements—The authors are much indebted to Dr I. Shigaki for supplying $Bi_2Sr_2CaCu_2O_{8+X}$ single crystals.

REFERENCES

1. Oda M., Manabe C. and Ido M., *Physica C* **235–240**,797(1994)
2. Murakami H. and Aoki R.,*J. Phys. Soc. Jpn* **64**, 1287 (1995)
3. Murakami H., Ohbuchi S., Hiramatsu S. and Aoki R., *Advances in Superconductivity* **VI**, 93 (1994)

Pergamon

J. Phys. Chem. Solids Vol. 56, No. 12, p. 1809, 1995
1995 Elsevier Science Ltd
Printed in Great Britain
0022–3697/95 $9.50 + 0.00

0022–3697(95)00191-3

ELECTRON TUNNELING SPECTROSCOPY NEAR THE MAGNETIC FIELD TUNED SUPERCONDUCTOR TO INSULATOR TRANSITION [1]

J. M. VALLES, Jr, SHIH-YING HSU and J. A. CHERVENAK
Department of Physics, Brown University, Providence, RI 02912, U.S.A.

Abstract—We present measurements of the tunneling density of states of ultrathin $Pb_{0.9}Bi_{0.1}$ films in magnetic field that strongly suggest a field tuned superconductor to insulator transition driven by the suppression of the superconducting order parameter amplitude.

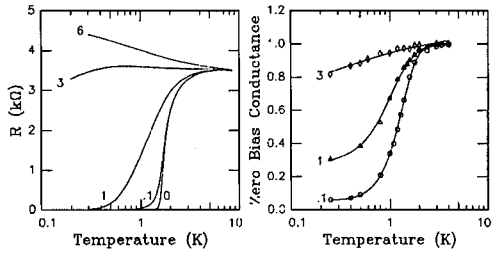


Fig. 1. Temperature dependence of the sheet resistance, $R(T)$, and ZBC normalized to the normal state in the perpendicular magnetic fields indicated in units of Tesla.

A number of groups have shown that magnetic fields can induce a superconductor to insulator transition (SIT) in homogeneous thin film superconductors with normal state sheet resistances, $R_N \sim h/4e^2$ [1]. A magnetic field, H, can weaken the superconducting state and drive a SIT by inducing mobile vortices that cause phase fluctuations [1] and by causing pairbreaking that enhances amplitude fluctuations [2]. Quasiparticle tunneling experiments are sensitive to the amplitude of the superconducting order parameter and therefore, can probe the latter effect. We have performed tunneling measurements in magnetic field on ultrathin, homogeneous $Pb_{0.9}Bi_{0.1}$ films that indicate that the order parameter amplitude is substantially reduced near its field tuned SIT and hence, likely to fluctuate.

An example of a magnetic field tuned SIT (H perpendicular to the film plane), that is similar to that observed in many systems [1], is given in the figure. The resistive transitions, $R(T)$, of a 5 Å thick $Pb_{0.9}Bi_{0.1}$ film doped with a slight amount of Au (0.4 Å) that was quench condensed onto two monolayers of quench condensed Ge [2] are shown. In zero field, the resistive transition width ($0.9R_N$–$0.1R_N$) is large, $\simeq$1.2 K, compared to the transition midpoint T_{c0} =1.78 K, in agreement with expectations for a film with such a high R_N [2]. The transition widths increase significantly with increasing field. At a well defined field, $H^c \simeq 3$ T, $R(T)$ becomes nearly temperature independent from well above T_{c0} to a factor of 9 below. At higher fields, $R(T)$ exhibits only insulating behavior, i.e. $dR/dT < 0$.

Accompanying the transport data are measurements of the normalized zero voltage bias conductance (ZBC) as a function of temperature of an SIN tunnel junction on the same film. An oxidized Al cross strip underneath the Ge served as the normal counterelectrode. This junction fabrication technique yields high quality, low leakage tunnel junctions [3]. The ZBC measures the density of states within $\pm 1.75 k_B$ T of the Fermi energy relative to the normal state density of states. In a BCS superconductor, the temperature dependence of the ZBC changes discontinuously when the energy gap opens. As shown in the figure, the ZBC of the tunnel junction at 0.1 T drops in the vicinity of T_{c0}. The drop is more gradual in this thin film than in a bulk superconductor probably because of the strong fluctuation effects alluded to above. Stronger magnetic fields make the drop more gradual. At H^c, the ZBC decreases by less than 20% from T_{c0} to T/T_{c0} <0.15.

The tunneling data show that the quasiparticle density of states near E_F (within 0.45 K) is approximately 80% of its normal state value at $H = H^c$ and T/T_{c0} =0.15. This result implies that only a small fraction of the electrons that form pairs in zero field form pairs at H^c. Consequently, we suggest that applied magnetic fields drive the SIT in homogeneous $Pb_{0.9}Bi_{0.1}$ films by reducing the density of Cooper pairs below a critical value necessary for the formation of the superconducting state.

REFERENCES

1. for a review, see Hebard A. F. in *Strongly Correlated Electronic Materials: The Los Alamos Symposium*. Addison Wesley, Reading MA (1993).
2. Hsu S. Y., Chervenak J. A. and Valles J. M., Jr., *Phys. Rev. Lett.* **75** 132 (1995).
3. Dynes R. C. *et al.*, *Phys. Rev. Lett.* **57**, 2195 (1986).

[1] Supported by ONR N00014-93-1-0275 and NSF DMR-9296192.

OPTICAL AND RAMAN SPECTROSCOPIES

Pergamon

J. Phys. Chem. Solids Vol. 56, No. 12, pp. 1811–1814, 1995
Copyright © 1995 Elsevier Science Ltd
Printed in Great Britain. All rights reserved
0022-3697/95 $9.50 + 0.00

0022-3697(95)00261-8

OPTICAL STUDY OF HIGH-T_c SUPERCONDUCTORS AND RELATED OXIDES

H. EISAKI and S. UCHIDA
Department of Applied Physics, The University of Tokyo, Bunkyo-ku, Tokyo 113, Japan

Abstract—Optical reflectivity measurements have been carried out on the two- and one-dimensional Cu and Ni oxides, $La_{2-x}Sr_xCuO_4$, $La_{2-x}Sr_xNiO_4$ and $Y_{2-x}Ca_xBaNiO_5$ with focus on the doping-induced changes. In the parent compounds, the optical spectra are dominated by the excitations from the O2p valence band to the upper Hubbard band. Upon doping holes, the transfer of the spectral weight into the low-energy excitations is commonly seen in these systems. However, the profile of the transferred spectral weight shows remarkable material dependence and anisotropy. We discuss the orbital character and the charge dynamics of the holes doped into these quantum spin fluids based on the experimental results.

1. INTRODUCTION

It is well known that the high-temperature (T_c) superconductivity takes place by introducing charge carriers into two-dimensional CuO_2 planes. The parent compounds, such as La_2CuO_4 and $YBa_2Cu_3O_6$, are charge transfer (CT) insulators, characterized by the O2p to $Cu3d_{x^2-y^2}$ excitation gap with a threshold at 1.5-2.0eV [1]. By doping charge carriers, the spectral intensity of the CT excitation is transferred to lower energies below ~1.0eV, indicating that the rearrangement of the electronic states within CuO_2 planes occurs by carrier doping [2]. Within CuO_2 planes, the doped carriers are highly itinerant. On the other hand, out-of-plane conduction is severely suppressed [3], suggesting that the electronic structure of the high-T_c copper oxides is two-dimensional.

'Two-dimensionality' and 'carrier doping' might be the two key words to understand the electronic structure of these copper oxides. Besides the high-T_c copper oxides, there exist many low-dimensional transition metal (TM) oxides which satisfy above conditions. For example, one dimensional NiO chain system, Y_2BaNiO_5, is another candidate for such study. Recently it has been made clear that the system has a finite gap for spin excitations [5], consistent with the Haldane's conjecture that integer-valued spin chains would exhibit a gap in the spin-wave excitation spectrum [6]. The most interesting fact is that hole carriers can be doped in this system by substituting Y^{3+} with Ca^{2+} [7]. This is the first case that a Haldane system is successfully doped with carriers.

In order to study the electronic structure of such anisotropic systems, the optical spectroscopy is a powerful tool since it provides information on charge dynamics over the wide energy scale along each direction. In this paper, we present the optical reflectivity of the following systems, $La_{2-x}Sr_xCuO_4$ (2D,S=1/2), $La_{2-x}Sr_xNiO_4$ (2D, S=1) and $Y_{2-x}Ca_xBaNiO_5$
(1D, S=1). Based on the experimental results, we discuss the charge dynamics of the holes doped into these quantum spin liquids.

2. TWO-DIMENSIONAL SYSTEMS – $La_{2-x}Sr_xCuO_4$ AND $La_{2-x}Sr_xNiO_4$

$La_{2-x}Sr_xCuO_4$ and $La_{2-x}Sr_xNiO_4$ systems can be regarded as the typical two-dimensional S=1/2 and S=1 system, respectively. In both systems, the parent compounds are charge transfer insulators. With doping holes, they become metallic with $x = 0.05$ for $La_{2-x}Sr_xCuO_4$ and $x = 1.0$ for $La_{2-x}Sr_xNiO_4$.

The in- and out-of-plane optical conductivity for both systems calculated from the optical reflectivity using the Kramers-Kronig transformation are shown in Fig.1. The optical spectra of the parent compounds are characterized by the O2p-TM3d CT excitations. In La_2CuO_4, the CT excitation is seen in the in-plane spectrum at about 2eV. In La_2NiO_4, the CT gap is seen at 4-5eV in both polarizations reflecting different electron configuration : $d_{x^2-y^2}$ hole for Cu^{2+} and $d_{x^2-y^2}d_{3z^2-r^2}$ holes for Ni^{2+}. By doping holes, the in-plane CT spectral weight becomes weakened and the spectral weight in low energy region increases typically below mid-IR energy region. This directly indicates that the rearrangement of the electronic states ranging up to several eV takes place by hole doping. Similar transfer of the of the spectral weight has also been observed by x-ray absorption (XAS) spectroscopy in both systems [4]. In $La_{2-x}Sr_xCuO_4$, the doping induced spectral weight is composed of a Drude peak centered at $\omega = 0$ and a mid-IR band. On the other hand, in $La_{2-x}Sr_xNiO_4$, the peaks of the mid-IR band do not shift to lower energies and a Drude peak does not appear although the mid-IR band extends down to almost zero frequency.

There exist distinct differences between in- and out-of-plane spectra for both systems. The most apparent difference is that the transferred spectral weight below ~0.5eV is almost missing in the out-of-plane spectra of cuprates. It should be noted that the rearrangement of the electronic

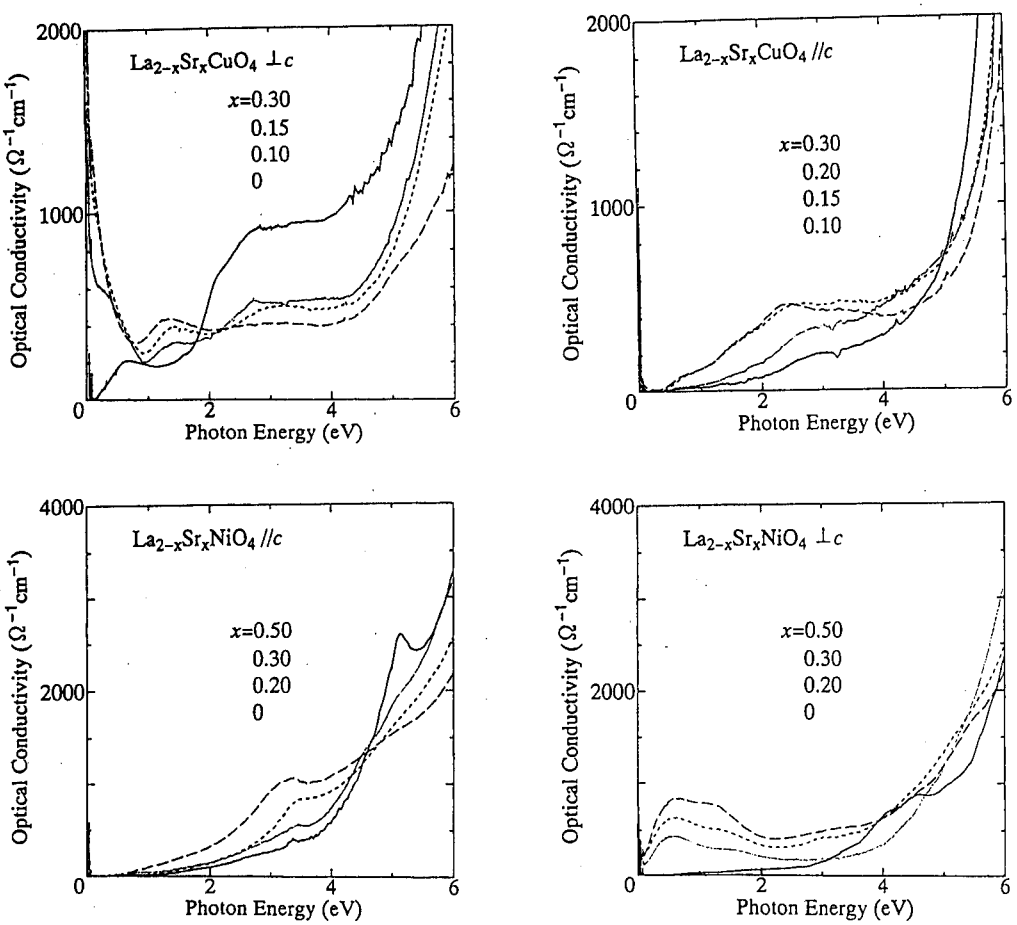


Fig. 1. In- and out-of-plane optical conductivity spectra of $La_{2-x}Sr_xCuO_4$ and $La_{2-x}Sr_xNiO_4$.

states is occurring also in this direction. This is clear in the optical spectra of nickelate. The CT spectral weight is transferred to lower energy region with an isosbestic point at 4.7eV, indicating that the low-energy conductivity is induced by the shift of the spectral weight from the high-energy part. In $La_{2-x}Sr_xCuO_4$, the low-energy spectral weight is transferred from the high energy region above 4eV, probably from $Cu3d_{3z^2-r^2}$ states hybridized with Cu4s or 4p states. The out-of-plane spectral weight seems pinned at $\sim$ 2.5eV in cuprate and at $\sim$ 3.0eV in nickelate, respectively.

For quantitative discussion, the effective electron number $N^*_{eff}(\omega)$ defined by the formula $N^*_{eff}(\omega) = \frac{2m_0V}{\pi e^2}\int_0^\omega \sigma(\omega')d\omega'$ is estimated at representative energies in Fig. 2. As regards the in-plane optical spectra, what is distinct in the cuprates is a very rapid transfer rate at initial dopings and a subsequent saturation seen already at $x \sim 0.15$. This originates from a rapid development of a Drude band owing to distinctively high itinerancy of the doped carriers in the CuO_2 plane. In contrast, the mid-IR absorption spectral weight increases almost linearly in $La_{2-x}Sr_xNiO_4$.

In the out-of-plane spectra, the low-energy optical spectral weight is considerably suppressed by one order of magnitude compared with the in-plane ones. The spectral weight induced by hole doping spreads out up to 4 or 5eV. This is clear from the fact that the integration should be done up to such high-energies in order to fulfill the sum rule.

In $La_{2-x}Sr_xCuO_4$, the transferred spectral weight below 3eV is the same order as the amount of doped holes x from the earlier stage of doping. However, the Drude part, reflecting the coherent motion of the carriers, is only seen in the overdoped region $x > 0.2$. This suggests that there exists a mechanism which suppresses the out-of-plane itinerant motion of the carriers in low doping region.

3. ONE DIMENSIONAL S=1 SYSTEM – $Y_{2-x}Ca_xBaNiO_5$

The charge transfer insulator, Y_2BaNiO_5, containing Ni^{2+} chains, has been attracting much attention since it is the first one-dimensional S=1 system which can be doped with hole carriers. It has a finite gap in the magnon spectrum, consistent with Haldane's conjecture. By substituting Y^{3+} by Ca^{2+}, holes are doped into the system. From the viewpoint of magnetism, the doped holes behave as

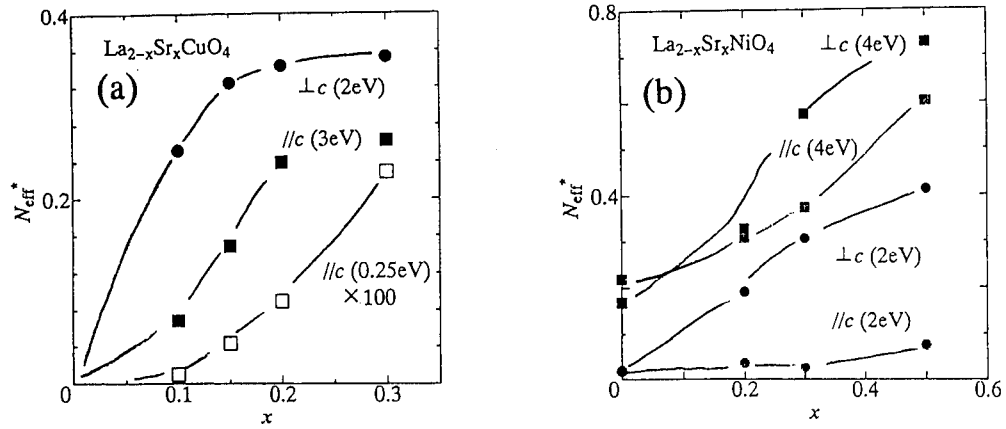


Fig. 2. Integrated spectral weight of in-plane and out-of-plane electronic contribution plotted against x in $La_{2-x}Sr_xCuO_4$ (a) and $La_{2-x}Sr_xNiO_4$ (b).

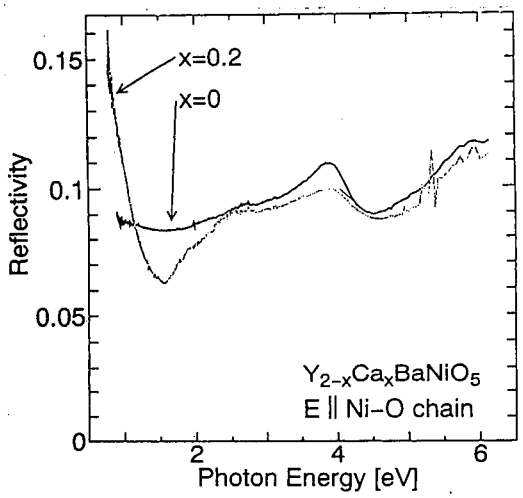


Fig. 3. Optical reflectivity spectra of $Y_{2-x}Ca_xBaNiO_5$.

S=1/2 local spins, inducing other two S=1/2 spins at the edge of the broken Haldane chains. The dc conductivity increases with hole doping although it is still of the activation type. In Fig. 3, we show the reflectivity spectra of the $Y_{2-x}Ca_xBaNiO_5$ for x = 0 and 0.2 with the light polarization along NiO chains. In the parent compound, the spectrum is characterized by a prominent reflectivity peak at 4eV, as in La_2NiO_4. This peak corresponds to the CT excitation from the O2p valence to the Ni3d upper Hubbard band. Upon doping, the CT excitation peak weakens and a reflectivity edge appears at 1.5eV. This behavior is similar to that observed in $La_{2-x}Sr_xNiO_4$. As shown in Fig.3 (b), the reflectivity edge appears only in the light polarization along NiO chains, indicating the doped holes are confined in the NiO chain direction.

As far as the optical reflectivity is concerned, the change in the electronic state in $Y_{2-x}Ca_xBaNiO_5$ is analogous to those in two-dimensional Cu and Ni oxides. It would be interesting to test whether the system becomes metallic with further doping as in the case of the two-dimensional Cu and Ni oxides.

4. DISCUSSION

The spectral weight transfer induced by carrier doping is a general feature of doped CT insulators, suggesting that the doping redistributes the states which form an upper and lower Hubbard band in a parent insulator. O2p and TM 3d states initially separated by a CT energy gap are redistributed to form a new band of states in the CT gap region. Along the conducting path, the formation of the new band can be easily detected as an appearance of the reflectivity edge at around 1eV. The typical energy scale of the new band is ~1eV. Similar spectral change also takes place in the direction across the conducting path although it is less dramatic. This is because the doping-induced states are distributed centering at high energies, typically 3eV in case of nickelate. In $La_{2-x}Sr_xCuO_4$, the induced spectral weight cannot contribute to the coherent motions and the Drude peak appears only when the material is overdoped. In the in-plane spectrum the mid-IR spectral weight rapidly softens and merges into the Drude peak at ω=0, suggesting its essentially two-dimensional electronic structure.

5. CONCLUSIONS

The effect of carrier doping on the low-dimensional CT insulators,
$La_{2-x}Sr_xCuO_4$, $La_{2-x}Sr_xNiO_4$ and $Y_{2-x}Ca_xBaNiO_5$, is commonly characterized by the spectral weight transfer

from CT excitation to lower energies. The transferred spectral feature shows strong polarization dependence reflecting their anisotropic electronic structure.

Acknowledgements— The authors would like to thank H. Takagi and K. Tamasaku for collaboration in the experiments.

REFERENCES

1. Tokura Y. *et al.*, *Phys. Rev. B* **41**, 11657 (1990).
2. Uchida S. *et al.*, *Phys. Rev. B* **43**, 7942 (1991).
3. Tamasaku K. *et al.*, *Phys. Rev. Lett.* **72**, 3088 (1994).
4. Pellegrin E. *et al.*, *Phys. Rev. B* **47**, 3354 (1993).
5. Cheong S.-W. *et al.*, *Bull. Am. Phys. Soc.* **37**, 116 (1992); Darriet J. and Regnault L. P., *Solid State Commun.* **86**, 409 (1993).
6. Haldane E. M. F., *Phys. Rev. Lett.* **50**, 1153 (1983).
7. DiTusa J. F. *et al.*, *Phys. Rev. Lett.* **73**, 1857 (1994); Takagi H. *et al.*, preprint

Pergamon

J. Phys. Chem. Solids Vol. 56, No. 12, pp. 1815–1819, 1995
1995 Elsevier Science Ltd
Printed in Great Britain
0022-3697/95 $9.50 + 0.00

0022-3697(95)00237-5

RE-EXAMINING THE VORTEX STATE OF CUPRATE SUPERCONDUCTORS WITH GAP ANISOTROPY *

BETH PARKS,* J. ORENSTEIN,* RICHARD MALLOZZI,* D. T. NEMETH,* FRANK LUDWIG,* JOHN CLARKE,* PAUL MERCHANT,† D. J. LEW,‡ I. BOZOVOC§ and J. N. ECKSTEIN§

* Materials Sciences Division, Lawrence Berkeley Laboratory, and Department of Physics, University of California, Berkeley, California 94720, U.S.A.

† Hewlett-Packard Laboratories, 3500 Deer Creek Road, Palo Alto, California 94304, U.S.A.

‡ Department of Applied Physics, Stanford University, Stanford, CA 94305, U.S.A.

§ Edward L. Ginzton Research Center, Varian Associates, Palo Alto, CA 94304-1025, U.S.A.

Abstract—We consider the effect of gap nodes on the electrodynamic response of superconductors in the vortex state. We show that for a gap with line nodes it is not possible to ignore the effect of field-induced pairbreaking on the electrodynamic response. We describe measurements of both the diagonal and the Hall components of the resistivity which support this conclusion.

1. INTRODUCTION

The high-frequency electrodynamics of cuprate superconductors in zero magnetic field has provided important information about the superconducting state [1]. By measuring the real and imaginary parts of the response, it is possible to determine both the fraction of carriers that has condensed and the scattering rate of the thermally-excited quasiparticles. The linear dependence of the condensate fraction on temperature that is measured is consistent with a linear density of states and *d*-wave superconductivity.

The change in the electrodynamics in an applied magnetic field could provide additional information about the superconducting state and is important in developing microwave technology based on the cuprates. However, such effects have been much less well explored, both theoretically and experimentally. The physics is complex because an additional component, the vortex, is added to the two-fluid system of superfluid and quasiparticles. In addition, time-reversal symmetry is broken so that a complete measurement of the response involves two complex parameters, such as σ_{xx} and σ_{xy} or σ_+ and σ_-, rather than one.

In spite of the challenges, there is growing interest in vortex state electrodynamics over a broad range of frequencies. Recent measurements extend from the few GHz regime to the near-infrared (approximately 10 THz) [2–8]. Our group has reported direct measurements of the complex response tensor in the frequency range from 100 to 500 GHz [8]. In the process of analyzing our results, we have found evidence that some time-honored assumptions regarding vortex state dynamics may need re-examination when applied to cuprate superconductors. The purpose of this paper is to describe some of this evidence and to discuss a new picture which may provide a better framework for understanding electrodynamics of cuprates in a magnetic field.

2. VORTEX DYNAMICS—THE CONVENTIONAL APPROACH

The response functions in the vortex state reflect the combined effects of vortices, superfluid, and quasiparticles. To find its contribution to the resistivity, the vortex is traditionally modeled as a composite object subject to viscous, pinning, and Magnus forces. This approach is valid if the energy of the probe is small compared to the intravortex excitation energy. In an *s*-wave superconductor there is a well-defined gap for internal excitation of the vortex, which can be approximated using the uncertainty principle: $E_{gap} \sim \hbar^2/2m^*\xi^2 \sim \Delta^2/E_F$, where ξ is the coherence length, Δ is the superconducting gap, and E_F is the Fermi level. Since the cuprate superconductors have a very short coherence length, the corresponding frequency would be quite high, $\sim$ 1 THz. However, the internal excitation spectrum is not necessarily the same with *d*-wave pairing. Since there is no gap for quasiparticle excitations even with $B = 0$, we might expect to find the vortex state gapless as well. This reasoning suggests that above zero frequency the partitioning of the response into super, normal, and vortex contributions may be suspect.

Most previous experimenters have assumed in their analyses that this partitioning is valid, and, moreover, that all changes in the resistivity when a field is applied can be attributed to vortices. Within this conventional approach, measurement of the real and imaginary parts of the magnetoresistance leads directly to values for the vortex viscosity η and the pinning force constant κ.

The conventional model makes the following additional assumptions: (1) Vortex motion generates an electric field

* Expanded version of a talk presented at the Spectroscopies of Novel Superconductors Conference (Stanford, CA, March 1995).

but carries no current. This assumption leads to a three-component electrodynamics in which the vortex *resistivity* is added to that of the super and normal fluids. This is in contrast to the two-fluid model, where the assumption of parallel current-carrying channels leads to the addition of *conductivities*. (2) Vortices form a rigid, massless lattice whose dynamics can be described by a restoring force κ, a viscous damping coefficient η, and a Magnus parameter α [9]. Balancing forces in equilibrium yields the equation of motion

$$\eta \mathbf{v}_L + (\kappa/i\omega)\mathbf{v}_L = (n_s \pi \hbar \mathbf{v}_s - \alpha \mathbf{v}_L) \times \hat{\mathbf{z}}. \quad (1)$$

Eq. 1 yields the vortex velocity $\mathbf{v}_L$ arising in response to the superfluid velocity $\mathbf{v}_s$, with $\mathbf{J}_s = n_s e \mathbf{v}_s$. $\hat{\mathbf{z}}$ is the direction of the magnetic field. This vortex motion generates an electric field $\mathbf{B} \times \mathbf{v}_L = \mathbf{E}_v \equiv \rho_v \mathbf{J}_s$, which yields a vortex resistivity tensor

$$\rho_v^{xx} = iX_v \frac{1 + i\omega/\Gamma}{(1 + i\omega/\Gamma)^2 - (\alpha\omega/\kappa)^2}$$
$$\rho_v^{xy} = X_v \frac{\alpha\omega/\kappa}{(1 + i\omega/\Gamma)^2 - (\alpha\omega/\kappa)^2} \quad (2)$$

where $X_v = \omega\phi_0 B/\kappa$ has dimensions of resistivity and $\phi_0 = h/2e$ is the flux quantum. The characteristic frequency $\Gamma = \kappa/\eta$ separates the response into two frequency regimes. In the experimentally-observed limit where $\rho_{xy}/\rho_{xx} \ll 1$, the high-frequency response is purely dissipative, $\rho_{xx} = \phi_0 B/\eta$ [10]. The low-frequency response is purely inductive, $\rho_{xx} = i\phi_0 B\omega/\kappa$.

When $\rho_{xy} \ll \rho_{xx}$, the real and imaginary parts of ρ lead directly to the values for κ and η plotted in Fig. 1. These results were collected from several experiments that, taken together, measure the electrodynamic response of $YBa_2Cu_3O_x$ in a range from 2–500 GHz. These phase-sensitive techniques, which distinguish the real and imaginary parts of the response, were converted using the above model to values for the vortex viscosity and pinning force constant.

The results for both κ and η are problematic. The top graph, which shows κ vs. T for different frequencies, shows remarkable agreement between measurements using different samples and frequency regimes. One might expect that pinning, an extrinsic parameter, would depend strongly on the quality of the sample. However, despite the fact that the samples for which values are plotted include single crystals, epitaxial *c*-axis films, and mixed *a* and *c*-axis films, the values of κ obtained are quite close, within a factor of two at low temperatures. In contrast to the uniformity of the measured values of κ, the values of η vary widely and are roughly inversely-proportional to the measurement frequency. This variation is equivalent to the observation that these experiments all find that the characteristic vortex relaxation frequency, $\Gamma = \kappa/\eta$, is within or near the measurement frequency range. This behavior may be due to a scattering rate that is strongly dependent on frequency, as is discussed in the following section.

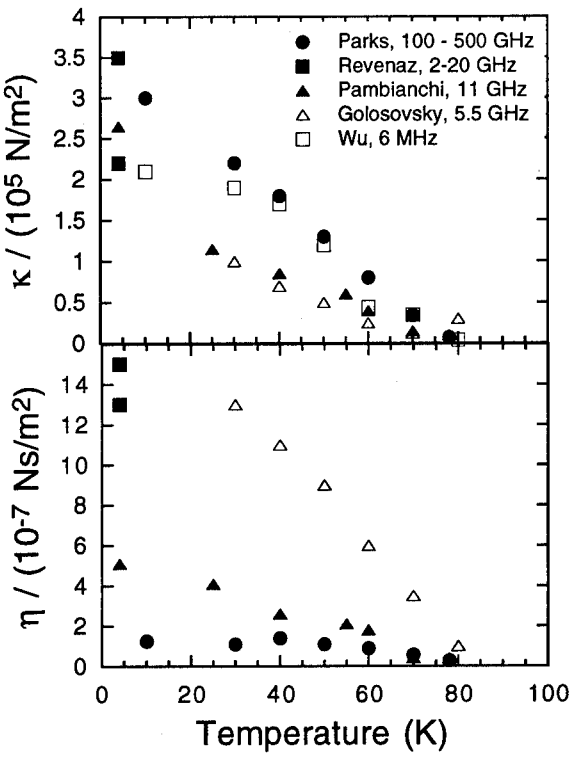


Fig. 1. Values of κ and η inferred using phase sensitive techniques. [4–8].

3. TWO FLUID MODEL

The model described above assumes that the application of a magnetic field leaves the superconducting condensate basically unchanged. The entire change in the resistivity of the sample is attributed to the harmonic motion of the vortex lattice. We consider now an alternative model in which the entire change in the response is attributed to the depletion of superfluid condensate. This depletion would cause an increase in the superfluid inductance, since $\rho_s = im^*\omega/n_s e^2$. It would also cause a corresponding increase in the finite frequency dissipative response.

3.1. *S-Wave Pairing*

Traditionally, the depletion of the superfluid condensate in a magnetic field $B \ll B_{c2}$ is not considered in the analysis of the magnetoresistance. This is because in a superconductor with an isotropic gap, this depletion is small. In the two-fluid model, the fractional superfluid depletion, $\Delta n_s(B)/n_s(0)$, is equal to the fractional density of states at the Fermi level, $N_F(B)/N_F$, where N_F is the normal state density. This fractional density of states is proportional to the ratio of the area occupied by vortex cores to the total area of the sample, so $N_F(B)/N_F = \xi^2/R^2 = B/B_{c2}$, where R is the distance between vortices. Because of the short coherence length of the cuprate superconductors, this effect would be very small for laboratory-scale fields. Since a

large change in the inductance is observed, it is commonly assumed in the literature that the change in the superconductor's resistivity when a magnetic field is applied is entirely due to the motion of vortices. However, for a gap with nodes, the inductance change due to pairbreaking could be much larger.

3.2. *D-Wave Pairing*

If the gap has nodes, then the circulating current around each vortex will break more Cooper pairs. Yip and Sauls [11] showed that at zero temperature the fractional change $\Delta n_s/n_s \cong |v_s|/v_c$, where v_s is the local superfluid velocity, $v_c = \Delta_0/mv_F$ and Δ_0 is the maximum value of the gap. Volovik [12] showed that this leads to a density of states at the Fermi level of order $N_F(B/B_{c2})^{1/2}$ in the vortex state.

3.3. *Dirty D-Wave Pairing*

This singular turn on at $B = 0$ would only be observed in a perfectly clean sample. Disorder complicates the field dependence of the density of states. In a dirty sample, the $B^{1/2}$ behavior would be observed above a crossover field B^*, defined such that $\Delta_0(B^*/B_{c2})^{1/2}$ exceeds an energy E^* characterizing the transition from intrinsic to impurity dominated excitations. Below B^*, pairbreaking should be linear in B with magnitude $\Delta n_s/n_s \sim B/B^*$. (This is analogous to the penetration depth of $YBa_2Cu_3O_x$ crystals in which the linear temperature dependence is only observed above a crossover temperature such that $kT^* > E^*$ [13].) This relationship between the field-dependence of the response and the characteristic energy scales allows the use of a magnetic field as a spectroscopic tool to measure the density of states.

4. EXPERIMENTAL EVIDENCE FOR THE TWO FLUID MODEL

The magnitude of the observed $\Delta\rho(B)$ is consistent with pairbreaking playing a significant part. In a clean d-wave superconductor, pairbreaking leads to a change in resistance $\Delta\rho(B)/\rho(0) \sim \xi/R \sim 0.1$ for a field of 6T. In the dirty limit, the size of $\Delta\rho(B)/\rho(0)$ could be larger, depending on the parameter B^*. In Fig. 2 we plot the resistivity at 10 K in both zero field and 6 T. The magnitude of $\Delta Im[\rho(B)]/Im[\rho(0)] \sim 0.4$, showing that pairbreaking could contribute significantly to the magnetoresistance.

We are in the early stages of mapping the field dependence of the magnetoresistance. We show preliminary measurements on $Bi_2Sr_2CaCu_2O_x$ and $YBa_2Cu_3O_x$. In Fig. 3 we plot the magnitude of the resistivity at 200 GHz as a function of field up to 7 T. The resistivity of $YBa_2Cu_3O_x$ is linear in B up to 7 T. $Bi_2Sr_2CaCu_2O_x$ displays sublinear behavior which could be explained by a crossover to clean d-wave behavior.

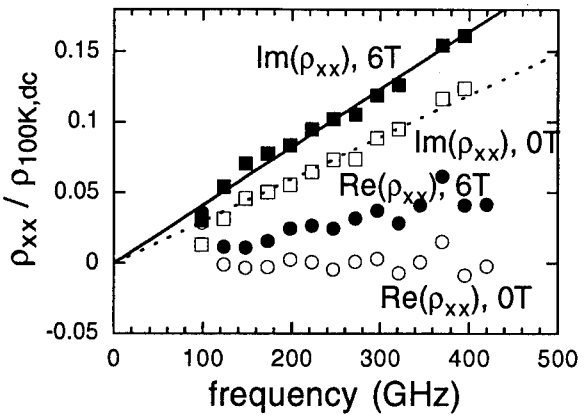


Fig. 2. Diagonal component of the resistivity at 10 K plotted versus frequency for a 70 nm $YBa_2Cu_3O_x$ film on a CeO_2 on sapphire substrate with $T_c = 85$ K. Sample preparation is described in [14].

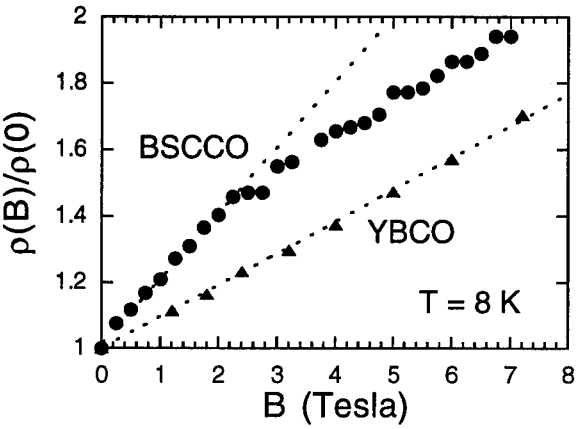


Fig. 3. The magnitude of the resistivity plotted versus field for a 40 nm $YBa_2Cu_3O_x$ film and a $Bi_2Sr_2CaCu_2O_x$ film. Both data sets are taken at temperature 10 K and frequency 200 GHz. The sample preparations are described in [15] and [16].

We can also reinterpret the results shown in Fig. 1 in terms of the two-fluid model. When we do so, we arrive at an appealing explanation of the surprising results for the values of the pinning force constant and the viscosity. As a consequence of the finite density of states at E_F, the fractional reduction in the superfluid density, $\Delta n_s(B)/n_s(0)$, will be far greater than for an s-wave superconductor. The reduction in n_s corresponds to an increase in the inductivity, which mimics the effect of pinned vortex motion (see Eq. 2). The apparent uniformity of κ in Fig. 1 may be due to the fact that the inductivity increase with B reflects pairbreaking, rather than vortex pinning.

The results for η also have a natural interpretation in terms of the two-fluid model. The increase in the normal component, corresponding to the decrease in n_s, leads to increased dissipation (σ_1) above zero frequency. Since in the vortex model with a negligible Hall effect $\eta = \phi_0 B\sigma_1$ (see Eq. 2), any frequency dependence of the dissipation is reflected in η. This frequency dependence need not take

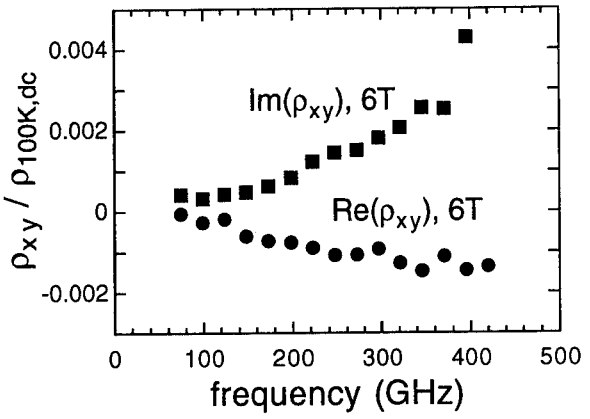


Fig. 4. Off-diagonal component of the resistivity at 10 K plotted versus frequency for the 70 nm sample on sapphire described in Fig. 2.

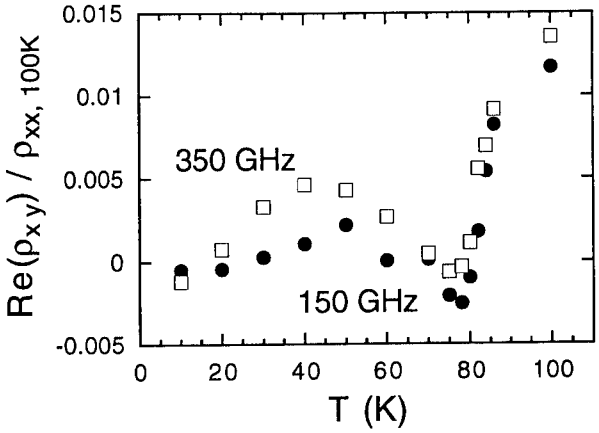


Fig. 5. Real part of the Hall resistivity at 6 T plotted versus temperature at 150 GHz and 350 GHz for the 70 nm film on sapphire.

a Lorentzian form, since either a frequency dependence of the scattering rate or the density of states would lead to a non-Lorentzian form for $\sigma_1(\omega)$.

5. HALL EFFECT

Understanding the off-diagonal, or Hall, dynamics in the vortex state of the cuprates also appears to require re-examination of the conventional vortex model. In the model described in Section 2, the Hall response is traced to the Magnus force, parameterized by α. Several recent papers have concluded that, at least at $T = 0$, $\alpha = n_s h/2$ [17]. This value, combined with the values of κ from Fig. 1, predicts $\rho_{xy}/\Delta\rho_{xx}$ on the order of unity over our frequency range. This is clearly inconsistent with the data, as is shown by a comparison of Fig. 2 with Fig. 4, in which $\rho_{xy}/\Delta\rho_{xx} \sim 0.01$. This discrepancy in magnitude can be accounted for if the actual value of κ is much larger than that plotted in Fig. 1. This would be the case if the true value of κ was masked by the effect of superfluid depletion in the presence of a magnetic field, as we have argued in the previous section.

Even if the small magnitude of ρ_{xy} at low T is explained, the temperature dependence and sign of ρ_{xy} remain mysterious. Fig. 5 shows $Re\rho_{xy}$ at two frequencies, 150 and 350 GHz, as a function of T below 100 K. The temperature dependence is quite complex: the sign changes at three temperatures, twice near T_c and again near 20 K. In a previous paper [18] we have associated the peak in ρ_{xy} near 40 K with the cyclotron motion of thermal equilibrium quasiparticles. However, this effect cannot account for the Hall effect just below T_c and for $T < 20$ K. The data seem to suggest that, for some reason, the vortex Hall effect is opposite in sign to the quasiparticle Hall effect [19]. The vortex Hall effect would dominate at temperatures for which the quasiparticle Hall effect was small: at high temperatures where the quasiparticle scattering rate is high and at low temperatures where the number of thermally-excited quasiparticles is small.

Acknowledgements—This work was supported by NSF Grant No. FD92-04394. Instrumentation funding was provided by the Director, Office of Basic Energy Sciences, Department of Energy under Contract No. DE-AC03-76SF00098, the University of California, Berkeley, and the AT&T Foundation.

REFERENCES

1. D. A. Bonn, Ruixing Liang, T. M. Riseman, D. J. Baar, D. C. Morgan, Kuan Zhang, P. Dosanjh, T. L. Duty, A. MacFarlane, G. D. Morris, J. H. Brewer, and W. N. Hardy, Phys. Rev. B **47**, 11314 (1993). W. N. Hardy, D. A. Bonn, D. C. Morgan, Ruixing Liang, and Kuan Zhang, Phys. Rev. Lett. **70**, 3999 (1993).
2. K. Karraï, E. J. Choi, F. Dunmore, S. Liu, H. D. Drew, Qi Li, D. B. Fenner, Y. D. Zhu, and Fu-Chun Zhang, Phys. Rev. Lett. **69**, 152 (1992), K. Karraï, E. Choi, F. Dunmore, S. Liu, X. Ying, Qi Li, T. Venkatesan, and H. D. Drew, Phys. Rev. Lett. **69**, 355 (1992).
3. Y. Matsuda, N. P. Ong, Y. F. Yan, J. M. Harris, and J. B. Peterson, Phys. Rev. B **49**, 4380 (1994).
4. S. Revenaz, D. E. Oates, D. Labbe-Lavigne, G. Dresselhaus, and M. S. Dresselhaus, Phys. Rev. B **50**, 1178 (1994).
5. M. S. Pambianchi, D. H. Wu, L. Ganapathi, and S. M. Anlage, IEEE Trans. Applied Superconductivity **3**, 2774 (1993).
6. M. Golosovsky, M. Tsindlekht, H. Chayet, and D. Davidov, Phys. Rev. B **50**, 470 (1994).
7. D. H. Wu and S. Sridhar, Phys. Rev. Lett. **65**, 2074 (1990).
8. Beth Parks, S. Spielman, J. Orenstein, D. T. Nemeth, Frank Ludwig, John Clarke, Paul Merchant, and D. J. Lew, Phys. Rev. Lett. **74**, 3265 (1995).
9. V.M. Vinokur, V. B. Geshkenbein, M. V. Feigel'man, and G. Blatter, Phys. Rev. Lett. **71**, 1242 (1993); W. F. Vinen and A. C. Warren, Proc. Phys. Soc. bf 91, 399 (1967); as pointed out by E.-J. Choi, H.-T.S. Lihn, H. D. Drew, and T. C. Hsu, Phys. Rev. B **49**, 13271 (1994), Eq. 2 is the low frequency limit of the equation derived by T. C. Hsu, Physica C **213**, 305 (1993).
10. J. I. Gittleman and B. Rosenblum, Phys. Rev. Lett. **16**, 734 (1966), J. Appl. Phys., **39**, 2617 (1968).
11. S.K. Yip and J. A. Sauls, Phys. Rev. Lett. **69**, 2264 (1992).
12. G.E. Volovik, JETP Lett., **58**, 469 (1993).
13. P. J. Hirschfeld, W. O. Putikka, and D. J. Scalapino, Phys. Rev. Lett., **71**, 3705 (1993), Phys. Rev. B **50**, 10250 (1994).

14. P. Merchant, R. D. Jacowitz, K. Tibbs, R. C. Taber, and S. S. Laderman, Appl. Phys. Lett. **60**, 763 (1992).
15. C. B. Eom, J. Z. Sun, B. M. Lairson, S. K. Streiffer, A. F. Marshall, K. Yamamoto, S. M. Anlage, J. C. Bravman, T. H. Geballe, S. S. Laderman, R. C. Taber, and R. D. Jacowitz, Physica (Amsterdam) **171C**, 354 (1990).
16. J. N. Eckstein, I. Bozovic, and G. F. Virshup, MRS Bulletin **XIX** (9), 27 (1994).
17. P. Ao and D. J. Thouless, Phys. Rev. Lett. **70**, 2158 (1993); D. M. Gaitonde and T. V. Ramakrishnan, Physica (Amsterdam) **235-240C**, 1:245 (1994). F. Gaitan, J Phys. Cond. Mat. **7**, L165 (1995).
18. S. Spielman, Beth Parks, J. Orenstein, D. T. Nemeth, Frank Ludwig, John Clarke, Paul Merchant, and D. J. Lew, Phys. Rev. Lett. **73**, 1537 (1994).
19. J. M. Harris, Y. F.Yan, O. K. C. Tsui, Y. Matsuda, and N. P. Ong, Phys. Rev. Lett. **73**, 1711 (1994).

Pergamon

J. Phys. Chem. Solids Vol. 56, No. 12, pp. 1821–1823, 1995
Copyright © 1995 Elsevier Science Ltd
Printed in Great Britain. All rights reserved
0022-3697/95 $9.50 + 0.00

0022-3697(95)00189-1

THE STRANGE INTERPLANE CONDUCTIVITY OF HTSC

T. TIMUSK and D. N. BASOV
Department of Physics and Astronomy, McMaster University, Hamilton, Ont. Canada L8S 4M1

C. C. HOMES
Department of Physics, Simon Fraser University, Burnaby, BC Canada V5A 1S6

Abstract—We review recent results on the anomalous c-axis optical conductivity of several high temperature superconductors, both double layer and single layer materials. We find that the double layer materials are characterized by a narrow pseudogap in the normal state that is also responsible for the temperature dependence of the transport. In the single layer material the pseudogap is much broader and less well defined. In the superconducting state, in both double and single layer materials, there is a transfer of spectral weight from very high frequencies to the condensate delta function at zero frequency.

1. INTRODUCTION

The interplane conductivity of the high temperature superconductors is peculiar [1]. The fully doped materials exhibit a metallic temperature dependence but with a high residual resistivity which does not result from impurity scattering, since samples from the same source show no sign of defect scattering when the resistivity is measured in the ab-plane [2,3]. Furthermore the frequency dependence of the conductivity of the fully doped samples is Drude-like with a very high scattering rate, high enough to correspond to a mean free path of less than a lattice spacing [4]. This lack of coherent conductivity can be understood in terms of the magnetism of the copper oxygen planes. There is no cell-to-cell coherence in the c- direction [5] and to transfer a hole from one unit cell to another, in that direction, it is necessary to rearrange the local magnetic structure. Thus each cell looks like a defect.

In this brief review we describe the results of recent work on the c-axis conductivity of some two-layer materials, underdoped $YBa_2Cu_3O_{6.70}$ [6,8] and $YBa_2Cu_4O_8$ [7] the double chain material that is naturally underdoped. We also show recent results on $La_{2-x}Sr_xCuO_4$ [9], a single layer material, also slightly underdoped.

2. EXPERIMENTAL RESULTS

Figure 1 shows the optical conductivity in the c-direction of an underdoped $YBa_2Cu_3O_{6.70}$. A series of strong phonon lines dominate the spectrum. As the temperature is lowered there is reduction in the conductivity at low frequency but the high frequency conductivity is temperature independent. The phonon structure in the oxygen mode region undergoes major changes as a function of temperature. There is a transfer of spectral weight from the bridging oxygen modes a

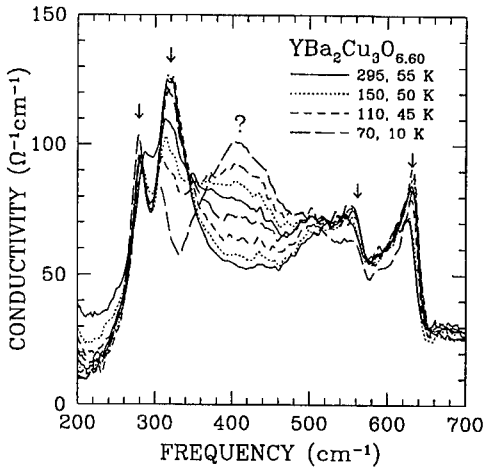


Fig. 1. The temperature dependence of the c-axis optical conductivity of $YBa_2Cu_3O_{6.6}$. The superconducting transition is at 58 K. A massive rearrangement of spectral weight occurs as the temperature is lowered: a feature at ≈ 400 cm^{-1} grows, and the correspondingly there is a loss of spectral weight of all the sharp phonon bands marked with arrows except the lowest one corresponding to chain buckling modes — there is no anomalous behavior near T_c.

570 and 610 cm^{-1} to a broad band centered at 400 cm^{-1}. The plane buckling mode at 310 cm^{-1} also loses spectral weight but the chain mode at 285 cm^{-1} is temperature independent.

In Fig. 2 the phonons and the broad line at 400 cm^{-1} have been removed from the spectrum. The resulting spectrum is dominated by a gap-like feature in the 200–300 cm^{-1} range. The feature deepens as the temperature is lowered towards 70 K, just above T_c. The bottom of this pseudogap is flat and the conductivity extrapolated to zero frequency (plotted in the inset) is in excellent agreement with d.c. transport measurements [10]. It is clear that the so-called semiconducting behavior of the c-axis resistivity in the underdoped materials is due to this pseudogap and that the conductiv-

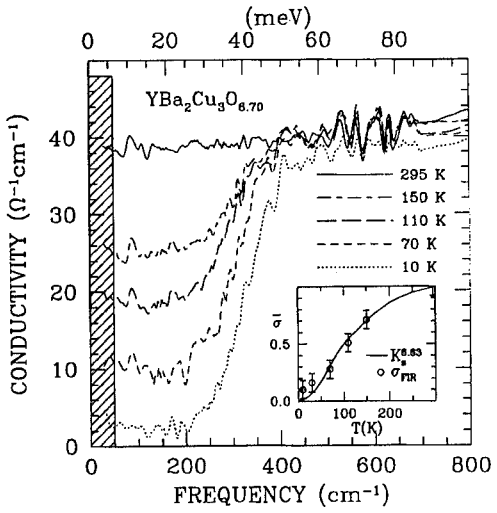


Fig. 2. The optical conductivity of $YBa_2Cu_3O_{6.70}$ (T_c=63 K) along the c-axis at 295, 150, 110, 70 and 10 K. Five strong phonons, and a feature at $\approx$ 400 cm^{-1} (believed to be due to phonons) have been removed. A gaplike feature develops in the conductivity near room temperature deepening as the temperature is lowered. In the superconducting state a further depression of conductivity takes place but over a much larger frequency range. The shaded rectangle shows the spectral weight under the superconducting condensate. Inset: The low frequency optical conductivity, normalized at room temperature, as a function of temperature shown as circles with error bars. The normalized NMR Knight shift is also shown.

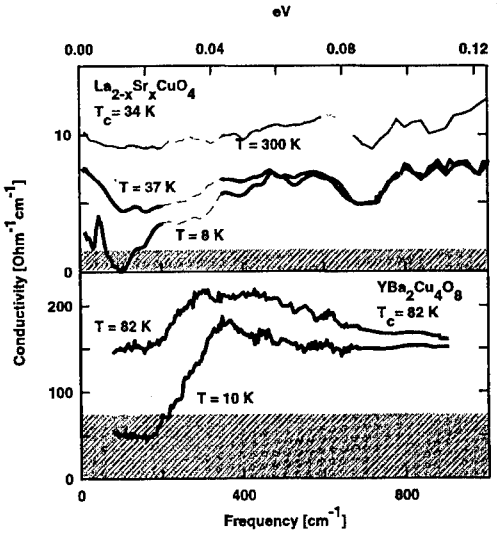


Fig. 3. The c-axis conductivity of the single-layered $La_{2-x}Sr_xCuO_4$ (top panel) and of the double-layered $YBa_2Cu_4O_8$ (bottom panel) at different temperatures. Phonon peaks have been subtracted for clarity. The dashed fragments of the spectra in the top panel show the frequency range where the subtraction of phonons has considerable uncertainty. Dashed areas in both panels correspond to area under the superconducting condensate determined from the imaginary part of the conductivity.

ity at high frequency, above 400 cm^{-1}, is temperature and frequency independent. The spectral weight missing from the pseudogap region must go to much higher frequencies, outside of our range of accurate measurements.

By evaluating the imaginary part of the conductivity it is possible to calculate the area under the superconducting delta function peak, shown as the dashed box in Fig. 1. It can be seen that this area corresponds approximately to the area missing between the 70 K curve and the 10 K curve, but this area extends beyond the normal state pseudogap.

Figure 3, lower panel, shows frequency dependent c-axis conductivity for the double chain material $YBa_2Cu_4O_8$ [7]. The normal state conductivity for this material is of the same order of magnitude as the fully doped $YBa_2Cu_3O_{6.95}$ [6] and the frequency dependence has a Drude-like component with a scattering rate of approximately 400 cm^{-1}, superimposed on an incoherent background. Despite this, almost metallic, behaviour the material is underdoped and shows a clear pseudogap as the temperature is lowered. The 82 K curve shows the pseudogap clearly. In the superconducting state, at 10 K, the pseudogap has deepened but the most striking development is the high density superconducting condensate, shown as the shaded area at the bottom of the diagram. It is clear that the spectral weight for the condensate is coming from a frequency range of the order of 1000 cm^{-1}.

The top panel of Fig. 3 shows the c-axis conductivity of $La_{2-x}Sr_xCuO_4$ [9]. Here the overall room temperature conductivity is lower and the temperature dependence is quite different from the two-layer materials. There is approximately a factor of two reduction in the conductivity to low temperatures but the pseudogap, if present, is an order of magnitude larger than in the two layer materials. We have been able to isolate the destination of the spectral weight by careful measurements on very large samples. We find that the conductivity is reduced up to 5000 cm^{-1} but increased between 5000 cm^{-1} and 8000 cm^{-1} (1 eV) and the sum rule is obeyed, at all temperatures, if the conductivity is integrated up to 1 eV.

In $La_{2-x}Sr_xCuO_4$, too there is a further reduction in the conductivity when the superconductivity develops and again the spectral weight of the condensate, shown as the gray area in the top panes of the figure, comes from a much larger region than $3.5kT_c$ = 83 cm^{-1}.

3. DISCUSSION

The pseudogap observed in the underdoped two-layer cuprates has several unusual properties. First, the missing spectral weight does not reappear near the gap frequency as it does in the case of an spin density wave gap [13] or as a low frequency collective mode as seen in the superconducting transition. The second unusual effect is the lack of temperature dependence of the gap frequency. This gap with a value of only 2Δ = 200 K persists to nearly room temperature with out closing up or broadening much. Most importantly, it is a *pseudogap* in the sense that even at lowest temperatures there is no region of zero conductivity, the conductivity remaining finite at all frequencies and temper-

atures.

The relationship between superconductivity and the pseudogap is subtle. It seems, more from the higher resolution Knight shift measurements [11] than the optical conductivity, that the depth of the pseudogap, has an inflection point at the superconducting T_c as if the pseudogap ceased to develop below this temperature [12]. It seems that the process of transfer of spectral weight is arrested at T_c.

Another possibility is that the pseudogap is associated with lattice vibrations in some way. Thus for example, in parallel with the gap in the electronic conductivity, much of the spectral weight of oxygen phonons corresponding to plane buckling and apical c-axis motion is shifted to a new broad mode at 400 cm^{-1} [14].

Acknowledgements—We thank P. W. Anderson, J. C. Carbotte. V. J. Emery, C. Kallin, T. E. Mason, D. Pines, M. L. Rice, D. B. Tanner and M. B. Walker for valuable discussions and above all B. Dabrowski, R. Liang and H. A. Mook for excellent crystals. T. T. would like to acknowledge the hospitality of the University of Toronto during the spring term of 1995.

REFERENCES

1. Cooper S. L. and Gray K. E., Anisotropy and interlayer coupling in the high T_c cuprates, in *Physical Properties of High Temperature Superconductors IV* (D. M. Ginsberg, ed.), p.61. World Scientific, Singapore (1994).
2. Friedmann T. A., Rabin M. W., Giapintzakis J., Rice J. P. and Ginsberg D. M., *Phys. Rev. B* **42**, 6217 (1990).
3. Bonn D. A., Ruixing Linang, Dosanjh P. and Hardy W. N., *Phys. Rev. Lett.* **68**, 2390 (1992).
4. Bozovic I., Kirillov D., Kapitulnik A., Char K., Hahn M. R., Beasley M. R., Geballe T. H., Kim Y. H. and Heeger A. J., *Phys. Rev. Lett.* **59**, 2219 (1987).
5. Tranquada J. M., Gehring P. M., Shirane G., Shamoto S. and Sato M., *Phys. Rev. B* **46**, 5561 (1992).
6. Homes C. C., Timusk T., Liang R., Bonn D. A. and Hardy W. N., *Phys. Rev. Lett.* **71**, 1645 (1993); Homes C. C., Timusk T., Liang R., Bonn D. A. and Hardy W. N., unpublished.
7. Basov D. N., Timusk T., Dabrowski B. and Jorgenson J. D., *Phys. Rev. B* **50**, 3511 (1994).
8. Homes C. C., Timusk T., Liang R., Bonn D. A. and Hardy W. N., unpublished.
9. Basov D. N., Mook H. A., Dabrowski B. and Timusk T., unpublished.
10. Iye Y., Sakakibara T., Goto T., Miura N., Takeya H. and Takei H., *Physica C* **153–155**, 26 (1988).
11. Takigawa M., Reyes A. P., Hammel P. C., Thompson J. D., Heffner R. H., Fisk Z. and Ott K. C., *Phys. Rev. B* **43**, 247 (1991).
12. We are grateful to D. Pines for pointing out this possibility to us.
13. Bonn D. A., Garrett J. D. and Timusk T., *Phys. Rev. Lett.* **61**, 1305 (1988).
14. Homes C. C., Timusk T., Liang R., Bonn D. A. and Hardy W. N., unpublished.

Pergamon

J. Phys. Chem. Solids Vol. 56, No. 12, pp. 1825–1828, 1995
Copyright © 1995 Elsevier Science Ltd
Printed in Great Britain. All rights reserved
0022–3697/95 $9.50 + 0.00

0022–3697(95)00240-5

IN-PLANE AND OUT-OF-PLANE CHARGE DYNAMICS OF HIGH-T_c CUPRATES

D. VAN DER MAREL and JAE H. KIM

Laboratory of Solid State Physics, Materials Science Center, University of Groningen, Nijenborgh 4, 9747 AG Groningen, The Netherlands

Abstract—We propose a theoretical expression for the k- and ω-dependent dielectric function of a stack of two-dimensional layers coupled along the direction perpendicular to the layers, and discuss some of its properties. We argue that the plasma frequencies at $k = 0$ should correspond to those which are experimentally obtained from optical measurements on *e.g.* $La_{1-x}Sr_xCuO_4$ via the f-sum rule analysis, regardless of the fact that such systems are strongly correlated. We discuss some of the ramifications due to strong anisotropy of the charge transport in these systems, and the lack of coherence for the transport in the direction perpendicular to the layers.

In theoretical discussions of the high-T_c cuprate superconductors it is usually emphasized, that there exists a strong anisotropy in the electrodynamical properties between the in-plane and out-of-plane directions. Usually this anisotropy is regarded as resulting from a large mass anisotropy of the charge carriers, so that effectively $m_c \gg m_{ab}$ where m_c and m_{ab} are the in-plane and out-of-plane effective masses. Ideally one prefers to use a model dielectric function where these superconductors are treated as a stack of layers which are completely decoupled in the c direction, which amounts to taking $m_c \to \infty$. Such models are indicated as layered electron gas (LEG) models. An important consequence $m_c \to \infty$ is, that the plasmon dispersion in the long-wavelength limit ($kd \ll 1$ where k is the wavevector and d is the interlayer spacing) is given by $\omega(k)/\omega_{ab} \approx k_{ab}/\sqrt{k_{ab}^2 + k_c^2}$. For a given finite value of k_c this is an acoustical dispersion as a function of k_{ab}. If we write the dispersion in the form $\omega(k)/\omega_{ab} \approx \sin\theta$, where θ is the angle between $\boldsymbol{k}$ and the c axis, it becomes clear, that $\boldsymbol{k} \to 0$ is a singular point in the dispersion, with $\omega_c = 0$ for $\boldsymbol{k} \parallel \boldsymbol{c}$, whereas for $\boldsymbol{k} \perp \boldsymbol{c}$ the plasma frequency is $\omega_{ab} = (4\pi ne^2/m_{ab})^{1/2}$.

Indeed it is known from optical measurements on cuprates, that with the electric field oriented along the planes a plasmon is observed at around 1 eV [1–3] whereas above T_c there is no zero crossing of $\mathrm{Re}\epsilon_c$ associated with a free-carrier plasmon (only optical phonons are observed)[4–7]. In Fig. 1 we demonstrate this by plotting the energy loss function ($-\mathrm{Im}1/\epsilon$) for both directions as obtained from our optical experiments. However, the actual situation is more complicated in two respects:

(1) In the normal state the absence of the plasmon along the c direction can *not* be attributed to having $m_c \to \infty$, but is rather due to overdamping. This can be seen in the following way: With finite damping $\epsilon = \epsilon_\infty - \omega_p^2/\omega(\omega + iy)$ is the (optical) dielectric function at $k \approx 0$, so that for $4\omega_p^2 < \epsilon_\infty y^2$ the zero crossings are along the *imaginary* frequency axis, *i.e.* for $2i\omega = y \pm \{y^2 - 4\omega_p^2/\epsilon_\infty\}^{1/2}$. On the other hand, one can use the f-sum rule

$$\int_0^x \omega \mathrm{Im}\epsilon(\omega) d\omega = \frac{\pi}{2}\omega_p^2 \qquad (1)$$

to obtain ω_c from the optical data by integrating the imaginary part of the dielectric function upto a suitably chosen cutoff frequency x below the onset of interband transitions (in practice such a clean separation is not always possible). In Fig. 1(c) we display ω_p as obtained from Eq. (1) as a function of cutoff frequency x along the horizontal axis. The step at 200 cm^{-1} in the c-axis data, as well as a somewhat broader step at 150 cm^{-1} in the ab-plane data are phononic contributions. After correction for these phonon-contributions we find that the ratio of *electronic* plasma frequencies ω_{ab}/ω_c drops from 10 to 4 as a function of increasing cutoff frequency. The ratios with (solid line) and without (dashed curve) correction for the phonon contributions are displayed in Fig. 1(d).

From LDA band structure calculations we obtained $\omega_{ab}/\omega_c = 5$, in good agreement with the experimental sum-rule analysis. By fitting the optical data to a Drude model, we obtained for the optical scattering-rate that $\tau_{ab}/\tau_c > 50$, which is consistent with the DC conductivity ratio.

(2) In the superconducting state there is a *partial* recovery of a plasmon in the c direction, essentially because there exists a finite probability for pair-hopping in the superconducting state. This is equivalent to having a small but finite critical current perpendicular to the layers, which has a finite penetration depth associated with it. Using again sum rule arguments, we expect that the penetration depth is now given by the dirty limit formula $2\pi\lambda_c = c(3E_g\sigma_c(0)/h)^{-1/2}$, which is determined by the 'missing area' in the optical conductivity. The zero crossing of $\mathrm{Re}\epsilon$ occurs now at frequencies below the superconducting gap, and corresponds to a collective mode of the superconducting condensate at a frequency $\tilde{\omega}_\phi^2 = c^2/\lambda_c^2\epsilon_\infty$. The ratio between this frequency and the undamped normal-state plasmon in the ab direc-

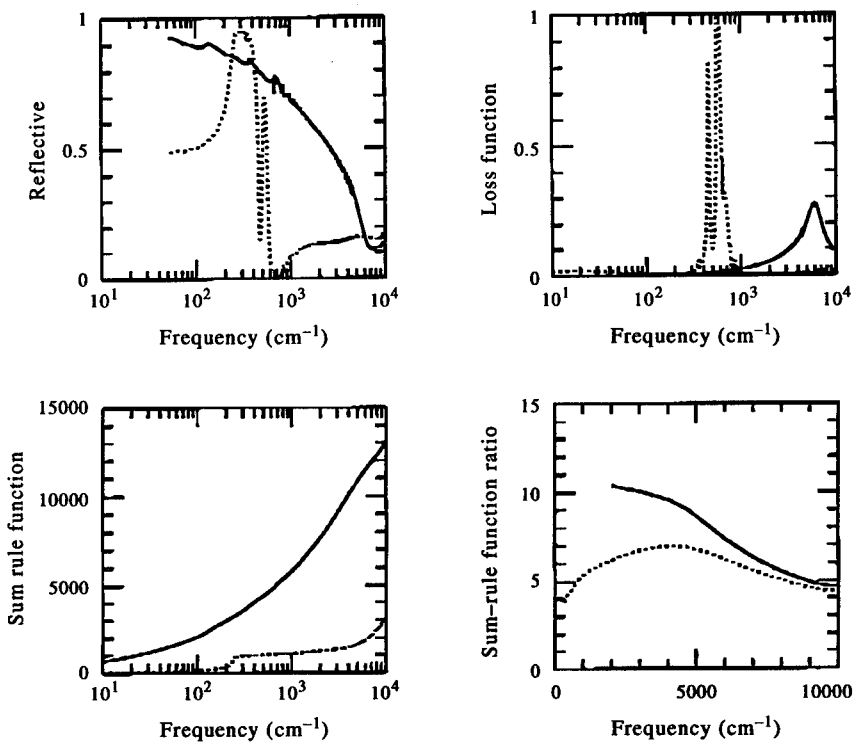


Fig. 1. Spectral functions of $La_{1.9}Sr_{0.1}CuO_4$ at room temperature for *ab* plane (solid curves except (d)) and *c* axis (dotted curves except (d)). In (d) we display $\omega_{ab}/\omega(c)$ obtained from Eq. (1) with (solid) and without (dotted) correction for the phonon-contributions.

tion is

$$\frac{\tilde{\omega}_\phi}{\omega_{ab}} = \left[\frac{\epsilon_{ab\infty} m_{ab} \arctan(2.3E_g/h\gamma)}{\epsilon_{c\infty} m_c \pi/2}\right]^{1/2}. \qquad (2)$$

The left side of the expression is $50/12000 = 0.009$, whereas the righthand side becomes 0.011, assuming that $E_g = 3.5k_BT_c$ and using the other parameters as discussed above. Hence if we take into account that $m_c/m_{ab} < 40$ and that $\tau_{ab}/\tau_c > 50$, we obtain a consistent description of the anisotropies in $\sigma(0)$, the penetration depth, the screened plasma frequency, and the bare plasma frequency obtained from the *f*-sum rule.

From the above discussion, we may conclude that the LEG model for the anisotropic dielectric properties of the high-T_c cuprates is not realistic. The major flaw is the fact that taking $m_c \to \infty$ is a gross oversimplification. The second problem arises due to the strong damping terms. Microscopically the anisotropic damping is quite interesting, and has been predicted as a result of spin-charge separation [8,9]. To derive the full k- and ω-dependent dielectric function including the damping effects is a very difficult theoretical problem. The presence of strong anisotropy makes the solution of this problem already quite formidable even if the only source of scattering is (elastic) impurity scattering, which becomes more difficult if the damping has a many-body origin. In this paper we present a formula for the k- and ω- dependent dielectric function without taking into account damping. Although there is no hope that such an expression for ϵ gives a complete description of the optical properties or electron-energy loss function of high-T_c cuprates, the expressions are nevertheless quite relevant in the discussion of the optical sum rule. Even though the optical spectral shape will be very different from that of the undamped and unrenormalized plasma poles discussed above, the imaginary part of the dielectric function should still obey Eq. (1).

Let us extend the layered electron gas model [10,11], by including a finite hopping between the planes. The electrons are confined to a stack of 2D sheets a distance l_c apart, coupled by a finite interlayer hopping parameter t. The dispersion relation close to the Fermi-level is

$$E_k = E_F + v_F\hbar(k_\parallel - k_F) + 2t\cos(k_\perp l_c) \qquad (3)$$

We indicate such systems as a coupled layered electron gas (CLEG). The plasmon-dispersion was derived for such a model by Grecu[12] using perturbation theory. The bare polarization propagator for $k_BT \to 0$ and $q \to 0$ can be expressed as an integral over the Fermi surface

$$\Pi^0(\boldsymbol{q},\omega) = 2\frac{\Omega_u}{8\pi^3}\int_{S_F}\frac{\boldsymbol{q}\cdot d\boldsymbol{s}}{\hbar\omega - \hbar\boldsymbol{q}\cdot\boldsymbol{v}(s)} \quad (4)$$

Using straightforward mathematical manipulations, the full expression for the k and ω dependent polarizability can be easily obtained. To simplify the expression we introduce the effective velocity perpendicular to the layers $v_c \equiv 2\hbar^{-1}tl_c$. In calculating Π^0 we use the fact that the angular averages of terms of the type $\cos\theta\sin^{2n+1}\theta$ are all zero, so that we obtain

$$\Pi^0(\boldsymbol{q},\omega) = 2\frac{k_F\Omega_u}{4\pi^3\hbar v_F l_c}\int_0^{2\pi}d\theta\int_0^{2\pi}d\phi\frac{v_F q_\parallel\cos\phi - v_c q_\perp\sin\theta}{\omega - (v_F q_\parallel\cos\phi - v_c q_\perp\sin\theta)} \quad (5)$$

In reciprocal space the expression for the Coulomb interaction between electrons confined to an infinite stack of δ-layers is $v_q = 4\pi e^2 S|\boldsymbol{q}|^{-2}$

where S is the form-factor of the single electron wavefunctions. For δ-layers this is $S(ql_c) = S(x) = \frac{1}{2}x_\parallel^{-1}|x|^2\sinh(x_\parallel)/\{\cosh(x_\parallel) - \cos(x_\perp)\}$.

The dielectric function as obtained from the random phase approximation is $\epsilon = 1 - v_q\Pi^0$. In the limit $\boldsymbol{q}\to 0$ we obtain the plasma frequencies $\omega_{p\parallel} = e(2k_F v_F)^{1/2}(\hbar l_c)^{-1/2}$ and $\omega_{p\perp} = 2et(2k_F l_c)^{1/2}\hbar^{-3/2}v_F^{-1/2}$ for the directions of propagation parallel and perpendicular to the planes. In the case of LEG the dielectric function is

$$\epsilon(\boldsymbol{q},\omega) = 1 - 2S\left[\frac{\omega_p}{|\boldsymbol{q}|v_F}\right]^2\left(\left(1 - \frac{q_\parallel^2 v_F^2}{\omega^2}\right)^{-1/2} - 1\right) \quad (6)$$

On the other hand, from LDA band structure calculations we obtained, that for doped La_2CuO_4 the ratio $\omega_{p\perp}/\omega_{p\parallel} \approx 0.2$, from which we conclude that the full plasmon-dispersion formula should be used. The CLEG dielectric function using the RPA approximation is

$$\epsilon(\omega,\boldsymbol{q}) = 1 - \left[\frac{q_\parallel}{|\boldsymbol{q}|}\right]^2\frac{S\omega_{p\parallel}^2 p^0\left(\frac{v_F q_\parallel}{\omega},\frac{v_c q_\perp}{\omega}\right)}{\omega(\omega + i0^+)} - \left[\frac{q_\perp}{|\boldsymbol{q}|}\right]^2\frac{S\omega_{p\perp}^2 p^0\left(\frac{v_c q_\perp}{\omega},\frac{v_F q_\parallel}{\omega}\right)}{\omega(\omega + i0^+)} \quad (7)$$

where p^0 is the function

$$p^0(a,b) \equiv \frac{2}{\pi a}\int_0^\pi\{(1 - a\cos\phi)^2 - b^2\}^{-1/2}\cos\phi d\phi \quad (8)$$

Let us first consider the plasma dispersion. In Fig. 2 we display this dispersion for the LEG and the CLEG models. The dispersion of the upper branch calculated with these parameters is in agreement with electron energy loss experiments of high-T_c cuprates[13,14]. The c-axis plasma frequency is the lower bound of a continuum of plasmon states. In the limit $\boldsymbol{q}\to 0$ both $S(ql_c)\to 1$ and $p^0\to 1$, and the optical conductivity for $\boldsymbol{E}$ parallel and perpendicular to the planes becomes $\sigma_{jj} = \omega_{pj}^2/4\pi(\gamma_j - i\omega)$.

Let us first point out that the above formula for ϵ contains two nontrivial terms. In the small-$\boldsymbol{q}$ limit (where the distinction between longitudinal and the transverse dielectric functions disappears), the first term describes the dielectric function for fields parallel to the planes, whereas the second one enters the description for electric fields perpendicular to the planes. Although we have not been able to give a microscopic justification hereof, the experimental results [4,5,15,1] indicate that the many-body effects affect these two terms in a very different way: in the cuprates there is a strong anisotropy (of the order of hundred), both in ω_{pj}^2 *and* in the scattering rate γ_j. In fact, the c-axis conductivity turns out to be practically frequency-*in*dependent, whereas the in-plane conductivity has a relatively small (but frequency dependent) scattering rate. These phenomena cannot be explained from weak elastic or inelastic scattering of fermionic charge carriers [16,17], but rather require charge carriers with a renormalization factor Z which is very small or zero. Anderson and coworkers address all these issues within a single framework of carrier confinement to the planes due to the formation of a 2D Luttinger liquid, with a de-confinement due to the onset of superconductivity [8,9].

As we discussed above, the effect of finite scattering is a quite formidable theoretical problem yet to be solved. However, from inspection of Eq. (7), and Fig. 2, we see that the first term determines the dispersion of the plasma frequency with $q_\parallel$, whereas the dispersion with $q_\perp$ due to the second term is relatively small. A simple, and somewhat crude 'shortcut', which is only valid for the collective-mode part of the dielectric function (*i.e.* for frequencies outside the particle hole continuum), is to replace each of the two terms with a q-dependent plasma pole, each of which has a different damping term. This suggests that we can make the following approximation in the normal state

$$\epsilon(\omega,\boldsymbol{q}) = 1 - \frac{q_\parallel^2}{|\boldsymbol{q}|^2}\frac{\omega_p(q_\parallel)^2}{\omega[\omega + i\Gamma_s(\boldsymbol{q},\omega)]} + \frac{q_\perp^2}{|\boldsymbol{q}|^2}\frac{4\pi i\sigma_s(\omega)}{\omega}. \quad (9)$$

This approximation is consistent with our experimental results at k=0. The modifications of this function in the superconducting state are quite small, and require a very thorough analysis, as in *e.g.* [18,19]. This dispersion and the corresponding loss functions could be measured with *e.g.* electron energy loss spectroscopy or with inelastic X-ray scattering.

CONCLUSIONS

From an analysis based on the f-sum rule we showed, that the experimental values for the anisotropy in plasma frequency along and perpendicular to the planes is between 4 and 10. We conclude that the absence of a c-axis plasmon in the normal state of high-T_c cuprate superconductors results from a non-Drude smearing of the optical conduc-

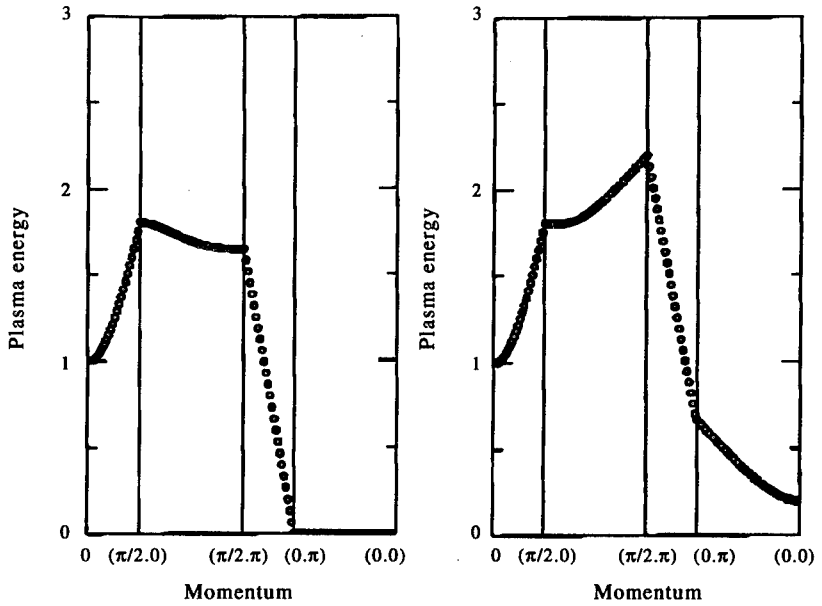


Fig. 2. Plasmon dispersion of a layered electron gas (left) and that of a coupled layered electron gas with $\omega_\perp/\omega_\parallel = 0.2$. The reciprocal-space coordinates are indicated as $[q_\parallel l_c, q_\perp l_c]$ at a number of points. For the Fermi velocity we assumed $v_F/l_c\omega_\parallel = 1$.

tivity perpendicular to the CuO_2 planes over a very wide energy range. This assignment alleviates the discrepancy by two orders of magnitude existing in the literature, between the plasma frequency obtained from optical experiments and that from the single-electron interlayer-hopping matrix element. We present an analytical expression for the k and ω dependent dielectric function for an electron gas, with a Fermi surface in the shape of a corrugated cylinder. We propose a phenomenological extension of this expression, to take into account the incoherent nature of the charge transport in the c direction.

Acknowledgments— We gratefully acknowledge Ir. H. S. Somal for his assistance with the experiments, and V.H.M. Duijn, N.T. Hien and A.A. Menovsky for providing single crystals. This investigation was supported by the Netherlands Foundation for Fundamental Research on Matter (FOM) with financial aid from the Nederlandse Organisatie voor Wetenschappelijk Onderzoek (NWO).

REFERENCES

1. Kim J. H., Bozovic I., Harris Jr. J. S., Lee W. Y., Eom C. -B., Geballe T. H. and Hellman E. S., *Physica C* **185–189**, 1019 (1991).
2. van der Marel D., van Elp J., Sawatzky G. and Heitmann D., *Phys. Rev. B* **37**, 5136 (1988).
3. Tajima S., Gu G. D., Miyamoto S., Odagawa A. and Koshizuka N., *Phys. Rev. B* **48**, 16164 (1993).
4. Jae Kim, Feenstra B. J., Somal H. S., Lee Wen Y., Gerrits A. M., Wittlin A. and van der Marel D., *Phys. Rev. B* **49**, 13065 (1994).
5. Kim Jae H., Somal H. S., van der Marel D., Gerrits A. M., Wittlin A., Duijn V. H. M., Hien N. T. and Menovsky A. A., *Physica C* **247**, 297 (1995).
6. Tamasaku K., Nakamura Y. and Uchida S., *Phys. Rev. Lett.* **69**, 1455 (1992).
7. Schützman J., Tajima S., Miyamoto S. and Tanaka S., *Phys. Rev. Lett.* **73**, 174 (1994).
8. Clarke D. G., Strong S. P. and Anderson P. W., *Phys. Rev. Lett.* **72**, 3218 (1994).
9. Chakravarty S. and Anderson P. W., *Phys. Rev. Lett.* **72**, 3859 (1994).
10. Fetter A., *Ann. Phys.* **88**,1 (1974).
11. Morawitz H., Bozovic I., Kresin V. Z., Rietveld G. and van der Marel D., *Z. Phys. B* **90**, 277(1993).
12. Grecu D., *Phys. Rev. B* **8**, 1958 (1973).
13. Nuecker N., Romberg H., Nakai S., Scheerer B., Fink J., Yan Y. F. and Zhao Z. X., *Phys. Rev. B* 39, 12379 (1989).
14. Nuecker N., Eckern U., Fink J. and Mueller P., *Phys. Rev. B* **44**, 7155 (1991).
15. van der Marel D., Bauer M., Brandt E. H., Habermeier H. -U., Heitmann D., König W. and Wittlin A., *Phys. Rev. B* **43**, 8606 (1991).
16. Rojo A. G. and Levin K., *Phys. Rev. B* **48, 16861** (1993).
17. Graf M. J., Rainer D. and Sauls J. A., *Phys. Rev. B* **47**, 12098 (1993).
18. van der Marel D., *Phys. Rev. B* **51**, 1147 (1995).
19. Zha Y., Levine K. and Liu D. Z., *Phys. Rev. B* **51**, 6602 (1995).

Pergamon

J. Phys. Chem. Solids Vol. 56, No. 12, pp. 1829–1830, 1995
Copyright © 1995 Elsevier Science Ltd
Printed in Great Britain. All rights reserved
0022-3697/95 $9.50 + 0.00

0022-3697(95)00103-4

OXYGEN DIFFUSION IN LASER HEATED $YBa_2Cu_3O_7$ FILMS

A. BOCK, R. KÜRSTEN and U. MERKT
Institut für Angewandte Physik und Zentrum für Mikrostrukturforschung,
Universität Hamburg, Jungiusstraße 11, D-20355 Hamburg, Germany

Abstract—Phonons of laser-deposited $YBa_2Cu_3O_7$ ($YBCO_7$) films on MgO(100) are investigated in a calibrated Raman set-up as a function of the power density of the argon-ion laser. While four A_g modes are visible for low power densities additional modes appear when the power density is increased. These are the defect-induced modes at 230 cm^{-1} and 585 cm^{-1}, normally assigned to infrared active phonons of $YBCO_{7-\delta}$, and Raman active modes of the oxygen-reduced tetragonal phase $YBCO_6$. At still higher power densities the phonons of the tetragonal phase dominate the spectra. We compare spot temperatures deduced from Stokes and anti-Stokes Raman spectra with those calculated from the solution of the heat equation. By varying the cryostat temperature and the ambient pressure we investigate the oxygen out-diffusion mechanism.

Keywords: Raman spectroscopy, oxygen diffusion, laser heating.

1. INTRODUCTION

Raman spectroscopy has proven to be a proper method for the determination of various $YBCO_{6+x}$ film properties, e.g., the chain-oxygen content x, possible impurity phases, and the epitaxial quality [1,2]. However, it has been demonstrated that the experimental conditions, in particular the power density, have to be chosen with care in order to avoid a damage of the sample during the measurement [3]. The heating, induced by the absorbed laser light, can lead to a depletion of the chain-oxygen content, as the chain oxygen O(1) has the highest mobility at a given temperature [4]. With the oxygen loss at the chain site the electrical properties of the sample deteriorate as the critical temperature decreases. Here we present investigations of the damage threshold of the power density when a $YBCO_7$ film is heated with the 514 nm line of an argon-ion laser at different ambient temperatures and pressures. In these Raman experiments the laser serves the dual role of heating and investigating the sample simultaneously.

2. EXPERIMENTAL

The samples are mounted on the cold finger of a helium cryostat whose temperature T_0 is measured by a silicon diode. The cryostat can be evacuated to residual pressures p_0 of 10^{-6} mbar. Calibrated and straylight-corrected Raman spectra are taken in quasi-backscattering geometry. Details of the set-up, the calibration, and the straylight correction are given elsewhere [3]. The radii of the laser focus on the sample are determined to be $r_h = (6 \pm 1)\ \mu m$ and $r_v = (11 \pm 1)\ \mu m$ in the horizontal and vertical directions, respectively. Given the laser power P on the sample the maximum power density P_L inside the Gaussian spot is $P_L = P/(\pi r_h r_v)$, which we will call the "power density" in the following. We investigate a c-axis oriented $YBCO_7$ film on MgO(100) prepared by laser deposition [5]. The film has a thickness of 240 nm, a critical temperature $T_{c0} = 85.2$ K, and a critical current density $j_c(77K) = 4 \times 10^6$ Acm^{-2}. Using procedures described elsewhere [3] we determined the thermal boundary resistance at the film-substrate interface to be $R_{bd} = (0.5 \pm 0.1) \times 10^{-3}$ Kcm^2W^{-1}.

3. RESULTS AND DISCUSSION

In Fig. 1, we present spectra from a Stokes/anti-Stokes series which were taken for increasing power densities. At the lowest power density we observe four A_g phonons of $YBCO_7$, i.e., the Ba mode at 117 cm^{-1}, the Cu(2) mode at 151 cm^{-1}, the B_{1g} mode at 339 cm^{-1}, and the apex oxygen O(4) mode at 502 cm^{-1}, which gives $x = 1$ [1]. From an analysis of the polarized and depolarized spectra at the lowest power density we determine the c-axis oriented fraction of the film $\delta = 87 \pm 5$ % and the in-plane orientation of this fraction $Q_c = 93 \pm 5$ % [2]. In order to obtain these informations the spectra have been fitted using Fano profiles for the Ba and the B_{1g} mode, Lorentz profiles for the Cu(2) and O(4) mode, and an almost constant background. When the power density is increased to values above 96 $kWcm^{-2}$ new modes begin to develop at 230 cm^{-1} and 585 cm^{-1}. Up to a power density of 150 $kWcm^{-2}$ the intensity of these new modes grows continuously. At still higher power densities the intensity of these modes starts to decrease until they almost vanish at the highest power density of 290 $kWcm^{-2}$. In addition to the above findings, we observe with increasing power density that the Cu(2) mode shifts to lower frequen-

cies, the B_{1g} rises in intensity, the Ba and the O(4) mode diminish, and another mode appears at 450 cm^{-1}. The additional modes were fitted using a Fano profile for the 230 cm^{-1} mode and Lorentz profiles for the 450 cm^{-1} and the 585 cm^{-1} mode. To improve the fit we have included a broad Lorentzian at 280 cm^{-1}. The modes at 230, 280, and 585 cm^{-1} are infrared active modes of $YBCO_{7-\delta}$ dominated by vibrations of Cu(1), O(1), and O(4), respectively [6,7]. They become Raman active due to disorder in the occupancy of the chain-oxygen site. Thus, the appearance of these modes indicates the onset of oxygen out diffusion. The mode at 450 cm^{-1} is a Raman active plane-oxygen mode of $YBCO_6$. The remaining Raman active phonons of $YBCO_6$ expected in the applied polarization geometry are the Cu(2) mode at 140 cm^{-1} and the B_{1g} mode at 340 cm^{-1} [8]. Both are clearly visible at the highest power density. Comparison of Stokes and anti-Stokes intensities allows to determine the maximum spot temperature T_{max}, which is located in the center of the Gaussian laser spot at the film surface [3]. The thus determined temperatures agree well with the temperatures calculated from the solution of the heat equation as can be seen in the inset of Fig. 1.

Above the damage threshold at $P_{damage} = (96 \pm 5)$ $kWcm^{-2}$, i.e., at $T_{max} = (500 \pm 10)$ K the observed changes of the intensities reflect the decrease of the chain-oxygen content [8]. We have carried out damage measurements at various ambient pressures p_0 and temperatures T_0 on the same film. The thresholds and concomitant spot temperatures T_{max} are depicted in Fig. 2. The temperature dependence of the threshold indicates that the oxygen out-diffusion starts at $T_{max} = (490 \pm 10)$ K, independent of the power density. Therefore, we role out a solely photo-activated diffusion. Within the experimental errors, we observe merely a weak dependence of the threshold on the ambient pressure. Also, the amount of out-diffused oxygen at the maximum power density (not shown here) depends only slightly on the pressure. These observations are in contrast to the p-T phase diagram of $YBCO_{6+x}$ [9]. According to this diagram a pronounced pressure dependence would be expected, and $YBCO_7$ would expected to be stable even for our highest power density in an ambient pressure of 1 bar. Hence, we conclude that the reaction of oxygen out-diffusion is of mixed type containing thermal-activated and photo-activated processes.

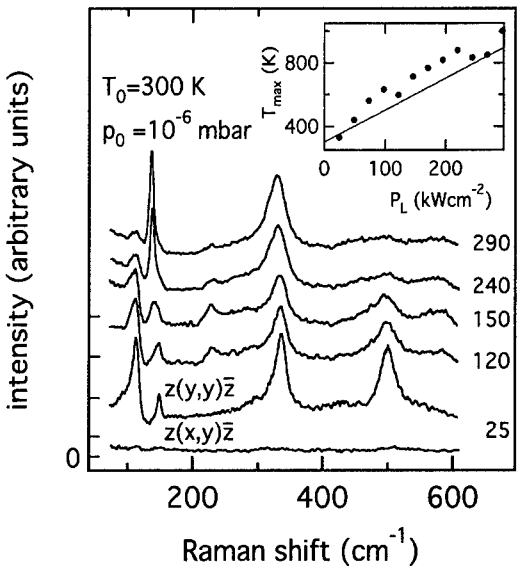


Fig. 1. Stokes Raman spectra in polarized $(z(y,y)\bar{z})$ and depolarized $(z(x,y)\bar{z})$ geometry for different power densities P_L. The spectra are offset as indicated, their intensities are normalized with respect to the power density. The inset shows spot temperatures T_{max} versus power density. Dots represent experimental Stokes/anti-Stokes temperatures, the solid line has been calculated as described in Ref. [3].

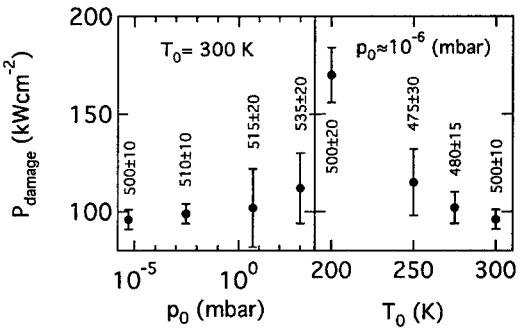


Fig. 2. Damage thresholds versus ambient pressure and cryostat temperature. The corresponding spot temperatures T_{max} in K are indicated.

Acknowledgement—This paper was supported by BMFT, contract number 13N5807A

REFERENCES

1. Feile R., *Physica C* **159**, 1 (1989).
2. Dieckmann N. *et al.*, *Physica C*, **245**, 2112 (1995).
3. Bock A., *Phys. Rev. B*, **51**, 15506 (1995).
4. Conder K. *et al.*, *Physica C* **210**, 282 (1993).
5. Schilling M. *et al.*, *Thin Solid Films* **235**, 202 (1993).
6. Wake D. R. *et al.*, *Phys. Rev. Lett.* **67**, 3728 (1991).
7. Thomsen C. *et al.*, *Phys. Rev. B* **45**, 8154 (1992).
8. Burns G. *et al.*, *Physica C* **181**, 37 (1991).
9. Somekh R. E. *et al.*, *Physics and Materials Science of High Temperature Superconductors II*, edited by R. Kossowsky *et al.* (Kluver Academic Publishers, Netherlands, 1992).

Pergamon

J. Phys. Chem. Solids Vol. 56, No. 12, pp. 1831–1832, 1995
Copyright © 1995 Elsevier Science Ltd
Printed in Great Britain. All rights reserved
0022-3697/95 $9.50 + 0.00

0022-3697(95)00208-1

MODULATION MEASUREMENTS OF $YBa_2Cu_3O_{7-\delta}$ OPTICAL REFLECTIVITY USING A THERMAL WAVE TECHNIQUE

G. S. KINO, I. M. FISHMAN, X. D. WU and W. R. STUDENMUND
Ginzton Laboratory, Stanford University, Stanford, CA 94305-4085, U.S.A.

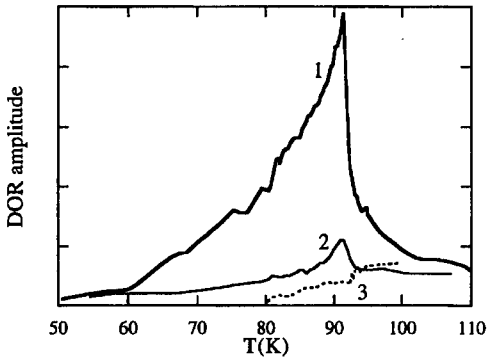


Fig. 1. Measured DOR signals for different quality twinned $YBa_2Cu_3O_{7-x}$ crystals, with a critical temperature T_c = 92.5 K (curves 1 and 2) and induction coil response (curve 3).

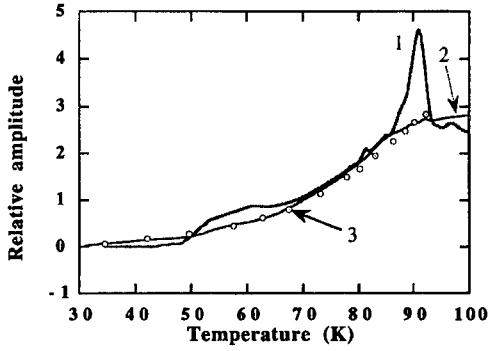


Fig. 2. The DOR signal for a sample with a critical temperature T_c = 92.5 K (curve 1), curve 2 is a normalized plot of $1/D$ for the same sample, and curve 3 is the function $1 - \lambda^2(0)/\lambda^2(T)$ representing density of the normal component below T_c [7].

We have measured the differential optical reflectivity (DOR) of $YBa_2Cu_3O_{7-d}$ single crystals in the temperature range 20–300 K using a photothermal technique [1–3] in which the sample temperature is varied periodically by an incident modulated argon laser beam with a wavelength of 546 nm. The periodic change in temperature at the source is ~ 2 K. The AC component of optical reflectivity, the DOR, is measured with a second diode laser beam, of wavelength of 780 nm, spaced 10 micrometers from the pump, where the periodic temperature variation is ~ 0.2 K peak. In the visible range, the optical constants of high-T_c superconducting materials do not show any noticeable temperature dependence [4]. However, this differential technique emphasizes the small effects caused by the superconducting transition close to T_c and is far more sensitive to these effects. We attribute our experimental results to the opening of the superconducting gap and the temperature dependence of electron scattering time.

The YBCO samples used in this study were twinned, with critical temperatures in the range 60–93 K. No anisotropy in the unmodulated and modulated parts of the reflected signal was observed which implies that the real domain size must have been less than the diameter of the focused probe beam. In Fig. 1, the DOR responses are shown for two different twinned YBCO crystals with a critical temperature of $T_c \approx 92.5$ K (curves 1 and 2). Samples of lower quality (judging by their optical image) and thin *c*-oriented films gave a far weaker peak in amplitude (curve 2). The observed signal demonstrates distinctive structure in the vicinity of the critical temperature, as determined from a comparison with the induction coil response (curve 3).

The observed signal can be considered as a sum of two contributions. One DOR term is a background which varies slowly with temperature. The other gives rise to a sharp asymmetric peak, with a temperature width of about 15 K below T_c and a relatively small precursor in the temperature range ~5 K above T_c. The superconducting transition occurs near the onset of this peak, close to the inflection point of the DOR signal. With a sample with a lower transition temperature, all significant features are repeated in the lower temperature range.

We have used a simple two-fluid Drude model to obtain some insight into the magnitude of the power reflection coefficient, R [5]. This approach yields the result:

$$\frac{dR}{dT} = K\left[(1-f)\frac{d(\delta\Gamma)}{dT} - \delta\Gamma\frac{df}{dT}\right] \qquad (1)$$

where f is the fraction of electron density related to the superconducting condensate ($f = 0$ at $T \geq T_c$), K is a temperature-independent constant, Γ_n and Γ_s are effective collision frequencies for the normal and superconducting states, their difference, $\delta\Gamma = \Gamma_n - \Gamma_s$ is assumed to be small compared to either Γ_n or Γ_s, and that the optical frequency $\omega \gg \Gamma_n$ or Γ_s.

Equation (1) provides a qualitative description of the experimental results. Above T_c, the DOR signals 1 and 2 of Fig. 1 show a weak temperature dependence of the electron scattering rate $d(\delta\Gamma)/dT$. Below T_c, the $d(\delta\Gamma)/dT$ term is multiplied by the fractional density of the normal component $(1 - f)$. This quantity can be determined inde-

pendently from our thermal diffusion measurements on the same sample using the same technique. The phase change between source and probe of the thermal wave excited by the modulated laser is $\phi = x\sqrt{\Omega/2D}$, where Ω is the modulation frequency, x the distance between the exciting and probe beams, and D is the diffusion coefficient. We assume that, below T_c, the scattering rate of phonons by electrons, and hence $1/D$, is proportional to the normal electron density. Microwave penetration depth measurements also give a measure of the fractional density of normal electrons. Normalized estimates of $(1 - f)$ taken from penetration depth (curve 3) and diffusion measurements (curve 2) are plotted along with our amplitude measurements in Fig. 2. It will be seen that the results tend to agree with the simple Drude model hypothesis for the background signal variation, provided that we assume that the electron collision rate does not vary much with temperature.

The peak DOR component has a rather complicated structure. Beyond a smooth signal slowly decreasing at low temperatures and disappearing below $\sim$ 60 K, there is a distinctive "precursor" $\sim$ 5 K above T_c and a sharp peak in the similar temperature range below T_c. It can be shown from general Landau-Ginzburg considerations that there should be a jump in the value of dR/dT at $T = T_c$[6]. This mean field theory cannot explain the large precursor above T_c and the sharp peak just below T_c. It is tempting to attribute these features close to T_c as being due to shortcomings of the mean field approach and explain them as manifestation of critical fluctuations. However, the fluctuation contribution to the normal component should be more or less symmetrical on both sides of T_c. The contribution of the superconducting component is essential for samples with large peaks and should look like a derivative of this symmetric peak, a conclusion very different from the experimental results. At the same time, the shape of the df/dT component is self-consistent with the smooth background shape. Below T_c, the higher quality sample shows a larger peak which may be explained by assuming different values of $\delta\Gamma$ for different samples.

Our main conclusion is that this technique is a new and powerful tool for investigation of high-T_c materials. We found for both the normal and superconducting component, that their DOR responses are not properly described by the mean field (BCS) theory.

Acknowledgements—This work was supported by the Department of Energy under Contract No. DE-FG03- 90ER14157. We thank T. Timusk for his suggestion that we use a two-fluid model, and A. Abrikosov, A. Varlamov and A. Buzdin for discussions, at an early stage of this work, of the optical response theory for a superconductor.

REFERENCES

1. Fanton J. T., Mitzi D. B., Kapitulnik A., Khuri-Yakub B. T. and Kino G. S., *Appl. Phys. Lett.* **55**(6), 598 (1989).
2. Fishman I. M., Kino G. S., *Phys. Rev. Lett.* **72**, 588 (1994).
3. Fishman I. M., Kino G. S. and Wu X. D., *Phys. Rev. B* **50**, 7192 (1994)
4. Cooper S. L., Reznik D., Kotz A., Karlow M. A., Liu R., Klein M. V., Lee W. C., Giapintzakis J., Ginsberg D. M., Veal B. W. and Paulikas A. P., *Phys. Rev. B* **47**, 8233 (1993).
5. Timusk T. and Tanner D. B., in *Physical Properties of High Temperature Superconductors I* (Edited by D.M. Ginsberg), p. 339S. World Scientific, Singapore (1989); Inderhees J., Salamon M. B., Goldenfeld N., Rice J. P., Pazol B. G., Ginsberg D. M., Liu J. Z. and Crabtree G. W., *Phys. Rev. Lett.* **60**, 1178 (1988).
6. Abrikosov A. A. and Gor'kov L. P., *JETP* **35**, 1558 (1958); **36**, 319 (1959).
7. Inderhees S. J., Salamon M. B., Goldenfeld N., Rice J. P., Pazol B. G., Ginsberg D. M., Liu J. Z. and Crabtree G. W., *Phys. Rev. Lett.* **60**, 1178 (1988).

Pergamon

J. Phys. Chem. Solids Vol. 56, No. 12, p. 1833, 1995
Copyright © 1995 Elsevier Science Ltd
Printed in Great Britain. All rights reserved
0022-3697/95 $9.50 + 0.00

0022-3697(95)00179-4

SUBSTITUTION OF Pr FOR Y IN $YBa_2Cu_4O_8$ AND $YBa_2Cu_{3.5}O_{7.5-\delta}$ SUPERCONDUCTORS: PHONON MODES AND CHARGE TRANSFER EFFECTS

A. P. LITVINCHUK,* M. KÄLL,* L. BÖRJESSON,† P. BERASTEGUI,‡ and L. -G. JOHANSSON‡

* Department of Physics, Chalmers University of Technology, S-41296 Göteborg, Sweden
† Department of Physics, The Royal Institute of Technology, S-10044 Stockholm, Sweden
‡ Department of Inorganic Chemistry, Chalmers University of Technology, S-41296 Göteborg, Sweden

Abstract—We report on a Raman scattering study of $(Y_xPr_{1-x})_2Ba_4Cu_{6+n}O_{14+n-\delta}$ (n = 1, 2) superconductors with $0 \le x \le 1$ in the temperature range 10–300 K. The observed changes of the phonon frequencies, including the double chain modes, with Pr-content x in general follow from the variations of the bond distances. The apex-oxygen mode is, however, found to exhibit stronger variation with x in single (n = 0) then in double-chain (n = 1, 2) materials, which may indicate charge redistribution effects between chains and planes.

The superconducting transition temperature T_c of $(Y_xPr_{1-x})_2Ba_4Cu_{6+n}O_{14+n-\delta}$ materials with n = 1 and 2 decreases with increasing of Pr-content. This dependence is, however, weaker and superconductivity persists up to $x \approx 0.8$ for n = 2 and $x \approx 0.65$ for n = 1 in comparison to $x \approx 0.55$ for n = 0. The origin of the T_c suppression is still a matter of debate. In order to obtain additional information which may be relevant to an understanding of the T_c suppression we have investigated the variation of the phonon parameters with x and n.

Among the most important experimental results we list the following:

(i) similar to the single-chain material (n = 0), the out-of-plane out-of-phase B_{1g} oxygen mode of the double-chain (n = 1, 2) superconductors is found to exhibit two-mode behavior and for intermediate x both "Y-like" and "Pr-like"phonons are observed in the Raman spectra;

(ii) in contrast to the single-chain $(Y_{1-x}Pr_x)Ba_2Cu_3O_{7-\delta}$ superconductors, we found much slower increase of the apical oxygen vibrational frequency ($\omega \approx 507$ cm^{-1} for x=0) with Pr-content x (Fig. 1) for n = 2 material despite a similar variation of the relevant bond lengths. This could be an indication of a charge transfer between the chains and planes which may be responsible for the difference in behavior of T_c vs x for these materials;

(iii) for $(Y_xPr_{1-x})_2Ba_4Cu_7O_{15-\delta}$, which can be viewed as a sequence of $(Y_{1-x}Pr_x)Ba_2Cu_3O_{7-\delta}$ and $(Y_{1-x}Pr_x)Ba_2Cu_4O_8$ units along the z-axis, we clearly identified two apical-oxygen modes corresponding to the constituent building blocks (Fig. 1); their behavior upon Pr-substitution is very similar to those of the "pure" $YBa_2Cu_3O_{7-\delta}$ and $YBa_2Cu_4O_8$;

(iv) several phonons in non-superconducting $PrBa_2Cu_4O_8$ display asymetries which are similar to those observed for the corresponding modes in superconducting $YBa_2Cu_4O_8$. This is an indication of a negligible variation of the electronic states to which the Raman-active phonons couple.

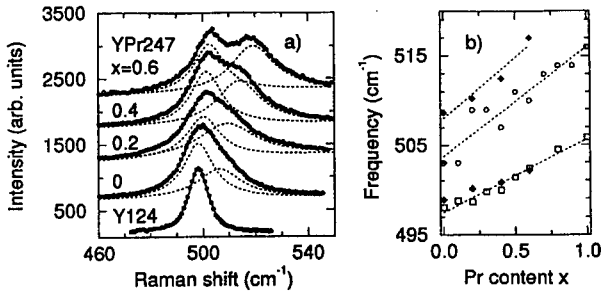


Fig. 1. (a)Raman scattering spectra of $YBa_2Cu_4O_8$ (the lowest curve) and $(Y_xPr_{1-x})_2Ba_4Cu_7O_{15-\delta}$ with x=0, 0.2, 0.4 and 0.6 in the range of apex oxygen vibrations at T=20 K. Points are the experimental data; solid curves—fits of the spectra to Lorentzian lineshapes which are shown by dotted lines. Note the increasing splitting between the two apex-oxygen lines in $(Y_xPr_{1-x})_2Ba_4Cu_7O_{15-\delta}$ with x; (b) phonon frequencies vs Pr content x for $(Y_xPr_{1-x})Ba_2Cu_3O_{7-\delta}$ (circles, T=300 K, after Ref. [1]), $(Y_xPr_{1-x})Ba_2Cu_4O_8$ (squares) and $(Y_xPr_{1-x})_2Ba_4Cu_7O_{15-\delta}$ (diamonds).

REFERENCE

1. Radousky H. B. *et al.*, *Phys. Rev. B* **39**, 12383 (1989).

Pergamon

J. Phys. Chem. Solids Vol. 56, No. 12, p. 1835, 1995
Copyright © 1995 Elsevier Science Ltd
Printed in Great Britain. All rights reserved
0022-3697/95 $9.50 + 0.00

0022-3697(95)00183-2

INFLUENCE OF Zn-DOPING ON THE ELECTRONIC RAMAN SCATTERING OF $YBa_2Cu_3O_{7-\delta}$

A. MATIC,* M. KÄLL,† L. BÖRJESSON,* and Y. ELTSEV*

* Department of Physics, The Royal Institute of Technology, S-100 44 Stockholm, Sweden
† Department of Physics, Chalmers University of Technology, S-412 96 Göteborg, Sweden

Abstract—We present temperature dependent Raman measurements on single crystal $YBa_2(Cu_{1-x}Zn_x)_3O_{7-\delta}$ with x = 0, 1.5%, and 3.5%. The superconductivity induced redistribution of the electronic background in the B_{1g} symmetry scattering configuration was found to disappear already for the smallest Zn concentration. In contrast, for A_{1g} symmetry the redistribution is observed for all samples even though the magnitude decreases with increasing doping. The peak position in A_{1g} symmetry decreases with increasing Zn doping and scales approximately with T_c, indicating a superconducting gap energy of $2\Delta/k_BT_c \approx 5.0$.

High-T_c superconductors exhibit an almost frequency independent Raman scattering background that is thought to be of electronic origin. The low frequency part of the background redistributes below T_c into a broad hump, which is thought to be related to the increase in the density of electronic states just above the gap energy [1]. The frequency of the hump is symmetry dependent indicating a symmetry dependent anisotropic gap. In this contribution we report on a Raman scattering investigation of the effects of partial Zn substitution for Cu on the redistribution of the electronic Raman scattering in $YBa_2Cu_3O_{7-\delta}$ (Y123). Zn is known to enter preferentially into the CuO_2 planes. The decrease of T_c with Zn doping is very rapid compared to most other substitutions in Y123. The reason for this effect is unclear, but recently several authors have suggested that the main effect of Zn is to disturb the spin system in the CuO_2 planes. Three single crystals were investigated; one pure Y123 crystal and two in which 1.5% and 3.5% of the Cu atoms were substituted by Zn. The T_c of the samples were 93 K, 86 K and 68 K, respectively. Polarized Raman measurements were performed in *ab*-plane scattering geometries which correspond to B_{1g} and A_{1g} symmetry. In Fig. 1 we show the difference between spectra recorded at 20 K and spectra recorded just above T_c for the different crystals.

The background redistribution below T_c was highly affected by the Zn substitution. In the B_{1g} symmetry the effects disappear almost completely already for the 86 K sample [see Fig. 1(b)]. We note that the effect observed in the B_{1g} symmetry is highly dependent on the annealing conditions. In samples annealed under conditions which gave rise to stronger disorder induced Raman scattering, the hump was considerably more pronounced and could also be observed for the Zn doped crystals. In contrast, in the A_{1g} symmetry the redistribution effect is observed in all the investigated crystals even for well annealed samples [see Fig. 1(a)]. As seen in the figure, the hump is clearly visible also for the 68 K sample, although the magnitude of the redistribution effect decreases with increasing Zn doping. However, the hump moves to lower frequencies, indicating a decreasing gap energy in A_{1g} symmetry. In the inset of Fig. 1(a) we show the hump frequency as a function of T_c. The frequency follows roughly a linear dependence with a slope corresponding to $2\Delta/k_BT_c \approx 5.0 \pm 0.3$. In contrast, the B_{1g} redistribution show no such scaling. One may speculate that at least part of the B_{1g} hump is induced by disorder in the CuO-chains.

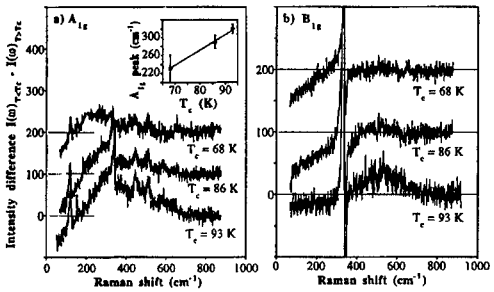


Fig. 1. (a) Difference spectra taken in the A_{1g} symmetry for $YBa_2(Cu_{1-x}Zn_x)_3O_{7-\delta}$ with various x. Inset shows the variation of the hump frequency as a function of the T_c of the samples. (b) Difference spectra taken in the B_{1g} symmetry for various x.

REFERENCE

1. Cooper S. L. *et al. Phys. Rev. B* **38**, 11934 (1988).

Pergamon

J. Phys. Chem. Solids Vol. 56, No. 12, pp. 1837–1838, 1995
Copyright © 1995 Elsevier Science Ltd
Printed in Great Britain. All rights reserved
0022-3697/95 $9.50 + 0.00

0022-3697(95)00238-3

COMPARISON OF CHAIN (Co) AND PLANE (Zn) DOPANTS ON CHARGE TRANSPORT IN $YBa_2Cu_3O_{7-\delta}$

KATHLEEN M. PAGET and THOMAS R. LEMBERGER
Department of Physics, The Ohio State University, Columbus, OH 43210, U.S.A.

STEVE R. FOLTYN and XINDI WU
Los Alamos National Laboratory, Los Alamos, New Mexico 87545, U.S.A.

Abstract—We report the penetration depth, λ, and infrared reflectance of a $YBa_2(Cu_{0.97}Co_{0.03})_3O_{7-\delta}$ film from 35 cm^{-1} to 600 cm^{-1} and from 10 K to 300 K. Co is a chain dopant in contrast to previous work on Zn which is a plane dopant. The effects of the chain dopants and the plane dopants are similar in the normal state. For example, the reflectance of the 3% Co sample is very similar to 4% Zn sample at 100 K and 300 K. However, in the superconducting state, 3% Co has a high reflectance similar to pure $YBa_2Cu_3O_{7-\delta}$ while 4% Zn has a gapless reflectance. The penetration depth of the Co doped sample is close to that of pure $YBa_2Cu_3O_{7-\delta}$ while that of the Zn doped film is a factor of five larger.

1. INTRODUCTION

The purpose of this study is to compare the effects of plane and chain doping on $YBa_2Cu_3O_{7-\delta}$. It is expected and found that the plane dopants have a larger effect on the superconducting properties than the chain dopants.

2. SAMPLES

The sampled films are 300 nm thick, made by laser ablation on $SrTiO_3$ substrates. The samples are about 1.5 cm in radius. They are highly oriented with the *c*-axis perpendicular to the substrate. Cobalt substitutes exclusively for the chain coppers while Zn substitutes preferentially for the plane coppers in $YBa_2Cu_3O_{7-\delta}$ [1]. T_c= 72 K for the 3% Co film and T_c= 43 K for the 4% Zn doped film.

3. REFLECTANCE SPECTRA

Figure 1 shows a comparison of the infrared reflectances of a 3% Co doped and 4% Zn doped $YBa_2Cu_3O_{7-\delta}$ film measured at 10 K, 100 K , and 300 K. The strong features in the spectra at 86 cm^{-1}, 176 cm^{-1}, and 550 cm^{-1} are from phonons in the substrate. The infrared reflectance spectra of the 3% Co doped sample and the 4% Zn doped sample are nearly indistinguishable at 300 K. This implies that the normal state properties such as the Drude scattering rate and plasma frequency averaged over the *a–b* plane of our twinned films are the same for the plane and chain doped samples. At 100 K the 3% Co and 4% Zn reflectance spectra are both higher than at 300 K and still similar to each other.

In the superconducting state, the spectra of the 3% Co and 4% Zn doped samples are quite different. The reflectance of the 4% Zn sample is higher at 10 K than at 100 K but it is not close to unity so the sample is 'gapless' [2]. Kim *et al.* have fit the 10 K reflectance with a mid-infrared band and a Drude conductivity which has no missing area [2]. They get a better fit by using a modified Drude conductivity with missing area corresponding to the measured penetration depth. In contrast, the 3% Co sample has a much higher reflectance at 10 K than at 100 K. In fact

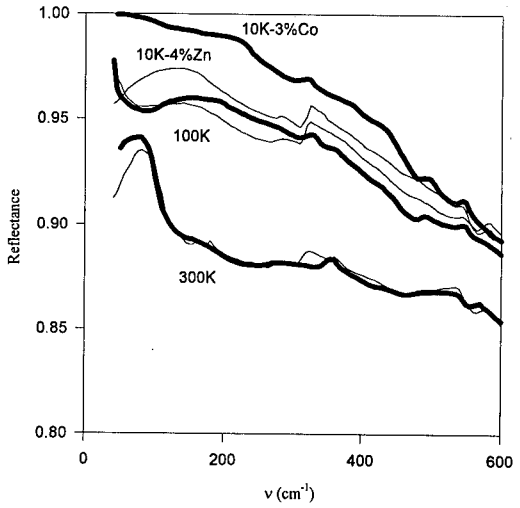


Fig. 1. Reflectance of $YBa_2(Cu_{0.97}Co_{0.03})_3O_{7-\delta}$ and $YBa_2(Cu_{0.96}Zn_{0.04})_3O_{7-\delta}$ films at 10, 100 and 300 K. The thick lines are the Co doped sample and the thinner lines are the Zn doped sample. Note that the 300 K reflectances for the Co and Zn doped samples are the same while their 10 K reflectances are very different. The 10 K reflectance for the Co goes to unity, but the 10 K Zn reflectance stays low. The data have been smoothed digitally for clarity.

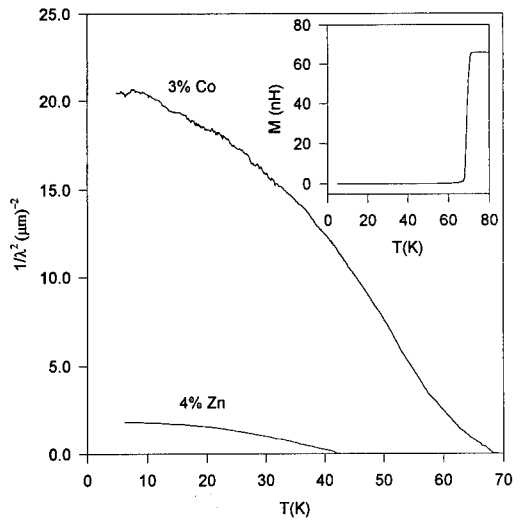


Fig. 2. $1/\lambda^2(T)$ for a $YBa_2(Cu_{0.97}Co_{0.03})_3O_{7-\delta}$ and a $YBa_2(Cu_{0.96}Zn_{0.04})_3O_{7-\delta}$ film. Note that $1/\lambda^2$ for the 3% Co doped film is much higher than $1/\lambda^2$ for the 4% Zn doped film. For comparison, pure films have $1/\lambda^2 = 40\ \mu m^{-2}$. The inset shows the mutual inductance as a function of temperature for the Co doped sample.

it goes to unity at low frequency, within experimental error. The higher reflectance is consistent with the smaller penetration depth of the 3% Co film compared to that of the 4% Zn film. The 10 K spectrum of the 3% Co doped sample is qualitatively similar to that of pure $YBa_2Cu_3O_{7-\delta}$ [3,4]. At low frequencies, both pure and Co doped $YBa_2Cu_3O_{7-\delta}$ have a reflectance of nearly unity. The reflectances decrease with increasing frequency and have a shoulder which occurs near 230 cm^{-1} in the Co spectrum. Although the normal state properties of the two samples are the same, the superconducting properties of the plane doped sample are more greatly suppressed than those of the chain doped sample.

3. PENETRATION DEPTH

The magnetic penetration depth, $\lambda(T)$, was measured by the two coil method [5,6]. Two coils are placed on opposite sides of the film and the mutual inductance is measured as a function of temperature. The penetration depth is determined from the mutual inductance with no fitting parameters [7]. The sharpness of the transition in the mutual inductance, shown in the inset to Fig. 2, indicates that the Co is distributed evenly throughout the sample, since T_c is very sensitive to Co doping near the 3% doping level [8]. At 2% Co T_c= 91.5 K [8] but for 3% Co T_c= 72 K so a spread in concentration of Co between 2.5 and 3%, for example, would lead to a 10–20 K transition width.

Figure 2 is a comparison of the temperature dependence of $1/\lambda^2$ for the 3% Co and 4% Zn doped samples. The penetration depth at 4 K for the 3% Co film is 210 nm ± 15 nm which is about 40% larger than that of pure $YBa_2Cu_3O_{7-\delta}$ films, where λ(4 K)=150–170 nm. The penetration depth, λ(4K)=750 nm ± 80 nm, for the 4% Zn doped sample is much larger than pure or Co doped $YBa_2Cu_3O_{7-\delta}$. The superfluid density, which is proportional to $1/\lambda^2$, is only decreased by a factor of 2 between the pure film and the 3% Co doped film while it is decreased by a factor of 25 between the pure film and the 4% Zn film.

4. CONCLUSIONS

In the chain doped sample the superconducting properties are not greatly altered from the pure sample, while the plane doped sample the superconducting properties are altered. 3% Co doped $YBa_2Cu_3O_{7-\delta}$ has a penetration depth and an infrared reflectance at 10 K similar to pure $YBa_2Cu_3O_{7-\delta}$. 4% Zn doped $YBa_2Cu_3O_{7-\delta}$ has a much larger penetration depth than pure $YBa_2Cu_3O_{7-\delta}$ and a 'gapless' reflectance spectra.

REFERENCES

1. Hriljac J. A., Moodenbaugh A. R. and Youwen Xu, *Physica C* **219**, 315 (1994).
2. Kim J.-T., Lemberger T. R. *et al.*, *Phys. Rev. B* **49**, 15970 (1994).
3. Kamaras K., Herr S. L., Porter C. D. *et al.*, *Phys. Rev. Lett.* **64**, 84 (1990).
4. Orenstein J., Thomas G. A., Millis A. J. *et al.*, *Phys. Rev. B* **42**, 6342 (1990).
5. Jeaneret B., Gavilano J. L., Racine G. A. *et al.*, *Appl. Phys. Lett.* **55**, 2336 (1989).
6. Fiory A. T. and Hebard A. F., *Appl. Phys. Lett.* **52**, 2165 (1988).
7. Ulm E., Kim J.-T., Lemberger T. R. *et al.*, *Phys Rev. B* **51**, 9193 (1995).
8. Neiman R. L., Giapintzakis J., Ginsberg D. M. and Mochel J. M., to be published.

Pergamon

J. Phys. Chem. Solids Vol. 56, No. 12, pp. 1839–1840, 1995
Copyright © 1995 Elsevier Science Ltd
Printed in Great Britain. All rights reserved
0022-3697/95 $9.50 + 0.00

0022-3697(95)00214-6

DOPING DEPENDENCE OF THE OPTICAL *c*-AXIS CONDUCTIVITY IN $YBa_2Cu_3O_y$

J. SCHÜTZMANN,* S. TAJIMA,* S. MIYAMOTO*,† and S. TANAKA*

* Superconductivity Research Laboratory, International Superconductivity Technology Center, Shinonome 1-10-13, Koto-ku, Tokyo 135, Japan

† Department of Physics, Tokai University, Kitakaname 1117, Hiratsuka 259-11, Japan

Abstract—We report on the infrared *c*-axis reflectivity of overdoped, optimally doped and underdoped $YBa_2Cu_3O_y$ crystals. For overdoped crystals the *c*-axis conductivity exhibits a metallic temperature and frequency dependence, whereas in the optimally doped regime a crossover from metallic to semiconducting-like behavior occurs. The semiconducting-like dc conductivity is related with a suppression of the optical conductivity below a certain frequency which decreases from 700 cm^{-1} in the heavily underdoped regime to 500 cm^{-1} in the optimally doped one. An additional absorption threshold is observed in the far-infrared conductivity in the optimally and underdoped regime, whose onset frequency (at $\approx$ 230 cm^{-1}) is almost independent on the oxygen content. For low doping, anomalous spectral growth around 400 cm^{-1} occurs, which seems to be associated with a transfer of the oscillator strength of the planar oxygen bending mode to this new excitation.

The anisotropy ratio ρ_c/ρ_{ab} of $YBa_2Cu_3O_y$ increases strongly with decreasing doping, indicating that a change in the hole concentration cannot only account for the change in the transport properties. This also manifests in the crossover of the *c*-axis resistivity from a metallic to a semiconducting behavior at a specific temperature T^* that decreases with doping [1]. From infrared measurements, it was suggested that the semiconducting-like T-dependence is associated with a suppression of the conductivity below a pseudogap at $\approx$ 230 cm^{-1} that is possibly related with a gap in the spin density of states [2].

Single crystals of $YBa_2Cu_3O_y$ with *c*-axis dimension up to 8 mm were grown by a pulling technique. After cutting several pieces, they were annealed under different conditions, described elsewhere [3], to obtain an overdoped crystal with oxygen content $y \approx 6.9$and$T_c \approx 89$ K, optimally doped (6.8, 91 K) and underdoped (6.5, 45 K). Infrared reflectivity measurements were performed with light polarized parallel to the *c*-axis of the crystals ($E \parallel c$) between 300 K and 10 K. The infrared conductivity σ_1 was calculated via a Kramers–Kronig analysis of the reflectivity data. In the overdoped state σ_1 increases with reducing temperature and shows a metallic decrease with frequency at 100 K indicating coherent charge transport (Fig. 1). At $T \ll T_c$, σ_1 is suppressed due to the opening of a superconducting gap but increases again at low frequencies. It can be attributed to residual normal carriers in the overdoped state [4]. For the optimally doped crystal only a weak temperature dependence is observed in the normal state and a clear suppression below T_c. σ_1 of the underdoped crystal is characterized by a gradual suppression at low frequencies and an increase of spectral weight around 400 cm^{-1} accompanied by a drastical decrease of the oscillator strength of the in-plane oxygen bending mode at 320 cm^{-1}. This transfer of spectral weight might indicate that 400 cm^{-1}-absorption is of phononic origin. After subtracting phononic contributions (fitted by Lorentzian and Fano lineshapes) in σ_1 for

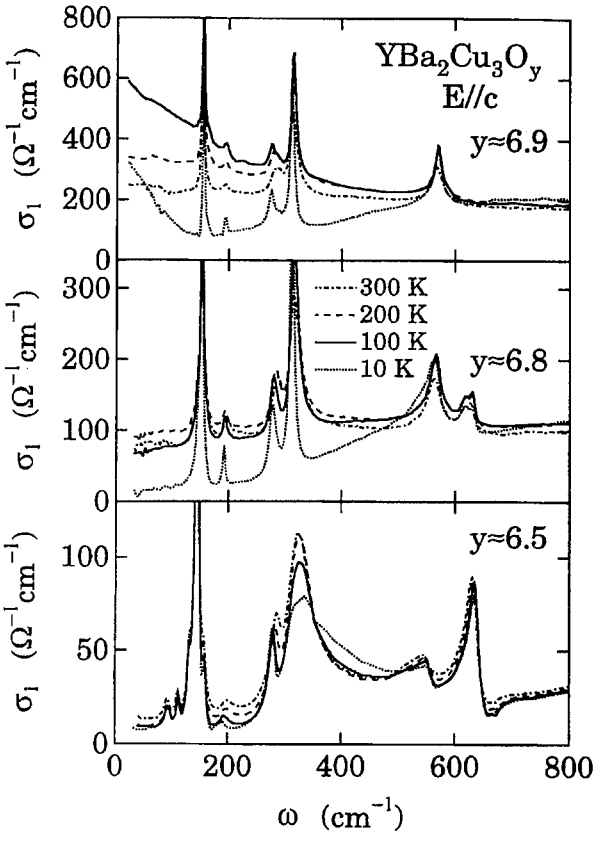


Fig. 1. Doping dependence of the infrared *c*-axis conductivity of $YBa_2Cu_3O_y$.

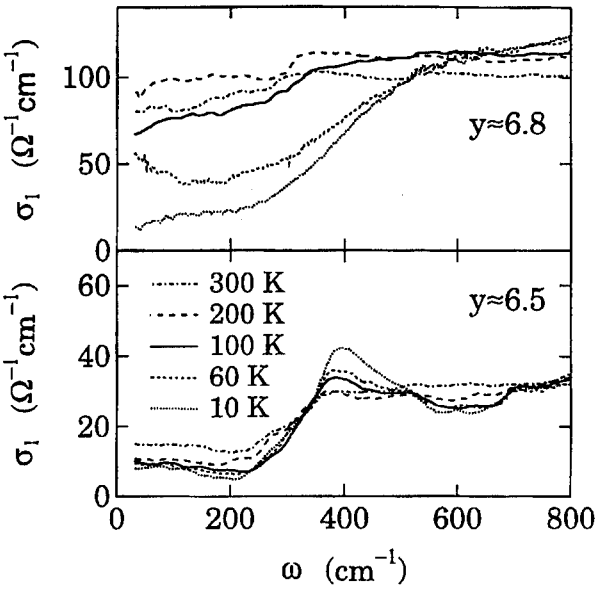


Fig. 2. Infrared conductivity after subtracting phononic contributions.

the crystal with $y \approx 6.8$ and 6.5, but without removing the 400 cm^{-1} peak, the remaining conductivity is displayed in Fig. 2. The absorption edge in σ_1 around 230 cm^{-1} for $y \approx 6.8$ seems to be superimposed on a weakly frequency dependent background that first increases with reducing temperature and decreases for $T < 230$ K and $\omega < 500$ cm^{-1}. In the case of the underdoped crystal, the anomalous growth of spectral weight at 400 cm^{-1} makes it difficult to extract up to which frequency the semiconducting-like temperature dependence extends. However at frequencies between 500 and 700 cm^{-1} σ_1 reveals the same T-dependence as below 230 cm^{-1}. Therefore, although the strong 400 cm^{-1}-anomaly hides the T-dependence of the electronic part in σ_1, the semiconducting-like behavior seems to extend in the infrared conductivity up to 700 cm^{-1}. The absorption threshold seems to be common for double layer systems as $YBa_2Cu_3O_y$ and $YBa_2Cu_4O_8$ [5], but it is not observed in the single layer compounds such as $La_{2-x}Sr_xCuO_4$. Therefore, it may indicate an onset of interband transition between two plane bands which are separated by twice the interlayer hopping integral [6]. T^* and the onset temperature of the suppression in σ_1 as well as its frequency can be explained within a doping dependent spin gap that is suggestive from NMR data. The 400 cm^{-1} anomaly could be associated with changes in the spin system causing a weak structural distortion.

In summary, we observed for overdoped crystals a clear metallic behavior of the infrared c-axis conductivity. In the optimally and underdoped regime a doping independent threshold (230 cm^{-1}) in σ_1 is observed and may be attributed to interband transition between two plane bands. The characteristic energy responsible for the semiconducting-like behavior of the dc conductivity lies above 500 cm^{-1}.

Acknowledgements—This work was partially supported by NEDO.

REFERENCES

1. Takenaka K. *et al.*, *Phys. Rev. B* **50**, 6534 (1994).
2. Homes C. C. *et al.*, *Phys. Rev. Lett.* **71**, 1645 (1993).
3. Miyamoto S. *et al.*, in *Advances in Superconductivity* (Edited by T. Fujita and Y. Shiohara). Springer Verlag, Tokyo (1995), to be published.
4. Schützmann J. *et al.*, *Phys. Rev. Lett.* **73**, 174 (1994). Schützmann J. *et al.*, *Solid State Commun.* **94**, 293 (1995).
5. Basov D. N. *et al.*, *Phys. Rev. B* **50**, 3511 (1994).
6. Gartstein Yu. N., Rice M. J. and van der Marel D., *Phys. Rev. B* **49**, 6360 (1994).

Pergamon

J. Phys. Chem. Solids Vol. 56, No. 12, pp. 1841–1842, 1995
Copyright © 1995 Elsevier Science Ltd
Printed in Great Britain. All rights reserved
0022-3697/95 $9.50 + 0.00

0022-3697(95)00187-5

STUDY OF k-DEPENDENT ELECTRONIC PROPERTIES IN CUPRATE SUPERCONDUCTORS USING RAMAN SPECTROSCOPY

B. STADLOBER, G. KRUG, R. NEMETSCHEK, M. OPEL, R. HACKL, D. EINZEL, C. SCHUSTER
Walther–Meissner–Institut für Tieftemperaturforschung, D–85748 Garching

T. P. DEVEREAUX
Department of Physics, University of California, Davis, CA 95616, U.S.A.

L. FORRÓ
Départment de Physique, École Polytechnique Fédérale de Lausanne, CH–1015 Lausanne

J. L. COBB and J. T. MARKERT
The University of Texas at Austin, TX 78712–1081, U.S.A

J. J. NEUMEIER
MTL-10, Los Alamos National Laboratory, Los Alamos, NM 87545, U.S.A.

By simply rotating the polarizations of the incident and scattered light different parts of the Fermi surface can be probed by Raman spectroscopy. Therefore **k**-dependent information about electronic properties such as the quasiparticle scattering time $\tau_{\mathbf{k}}$ and the superconducting energy gap $\Delta_{\mathbf{k}}$ is obtained.

In all cuprate superconductors the Raman spectra consist of several phonon lines superimposed on a broad continuum, the interpretation of which is still controversial. Due to the fact that in all cuprate families the symmetry selection rules for the frequency and temperature dependence of the continuum are solely determined by the orientations of the Cu–O bonds we conclude that this background has its origin in inelastic light scattering from excitations in the CuO_2 planes. Further we believe that at least in the low energy range the contribution from carrier fluctuations is dominant. Therefore we use the fluctuation–dissipation theorem which relates the Raman cross section with the imaginary part of the response function $\chi(\omega, T)$ to extract electronic properties from the Raman data.

In the normal state for the B_{1g} and B_{2g} symmetries the dynamics of the carriers is reflected in the Raman response according to

$$\chi''(\omega, T) = -N_F \left\langle \frac{\omega \Gamma_k(\omega, T)}{\omega^2 + \Gamma_k^2(\omega, T)} \gamma_k^2 \right\rangle_{FS} \qquad (1)$$

where $\langle \ldots \rangle$ denotes an average over the Fermi surface (FS). Here N_F means the carrier DOS at the Fermi level and $\gamma_k = \hat{e}_i \{\partial^2 \epsilon_k / \partial k_i \partial k_j\} \hat{e}_j$ is the Raman vertex including the polarization vectors of the incoming ($\hat{e}_j$) and scattered ($\hat{e}_i$) light and the bandstructure ϵ_k. In order to mimic the nearly constant high energy part of the spectra a ω and T-dependent scattering rate

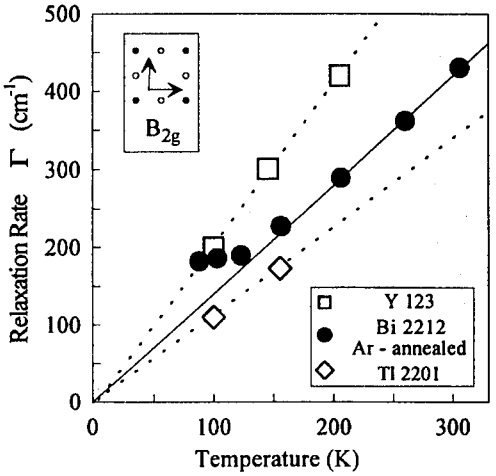


Fig. 1. Relaxation rate $\Gamma_{B_{2g}}(0, T)$ as deduced from the fits to the Raman spectra of several cuprate families.

$$\Gamma_k(\omega, T) = \sqrt{(\alpha\omega)^2 + \Gamma_k^2(0, T)} \qquad (2)$$

was introduced as specified within the microscopic nested Fermi liquid model [1]. From eqn (1) it follows that in the low-frequency limit the Raman response is inversely proportional to the static carrier relaxation rate $\Gamma_k(0, T)$. Putting all this together the fits to the electronic part of the spectra reveal the static scattering rate to be strongly symmetry dependent. In detail, it turns out that for B_{2g} symmetry the static relaxation rate $\Gamma_{B_{2g}}(0, T)$ increases linearly in temperature for all compounds and, with the exception of Bi 2201, extrapolates to zero in the low-T limit. As shown in Fig. 1 $\Gamma_{B_{2g}}(0, T)$ as obtained from Raman scattering is in almost quantitative agreement with the results from longitudinal transport measurements. In contrast, for B_{1g} scattering geometry the static relaxation rate

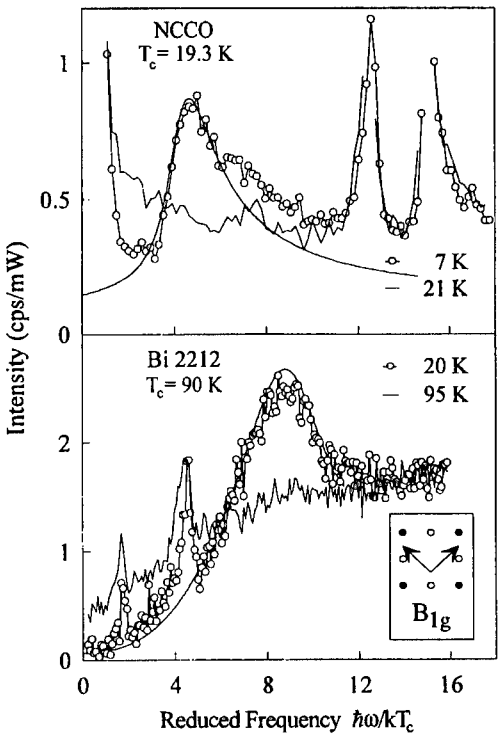


Fig. 2. Comparision of the pair breaking features in NCCO and Bi2212 for B_{1g}–symmetry. The smooth curves are fits to the data using $\Delta_\phi = \Delta_0 \cos 2\phi$ for Bi2212 and $2\Delta_\phi = (\Delta_{max} + \Delta_{min}) - (\Delta_{max} - \Delta_{min}) \cos 4\phi$ for NCCO.

$\Gamma_{B_{1g}}(0, T)$ is almost constant in optimally doped as grown single crystals. In post–annealed Bi2212 $\Gamma_{B_{1g}}(0, T)$ becomes slightly T-dependent. For the single layer Bi2201 crystal the transport measurement revealed a considerable residual resistivity at $T = 0$, a fact also appearing in the relaxation rates extracted from the Raman spectra (inset of Fig. 3).

Below T_c the spectral weight is redistributed in that the spectrum piles up close to a characteristic energy ($\hbar\omega_p$) which can be interpreted as a breaking of Cooper pairs (Fig. 2). In the $Nd_{1.84}Ce_{0.16}CuO_4$ crystal the response shows a threshold-like behavior with a sharp rise right below $\hbar\omega_p$ similar to what was observed in classical superconductors like Nb_3Sn. In contrast, in the other cuprate families, the intensity starts to increase continuously from zero energy exhibiting characteristic low–frequency power laws for the different symmetries.

Another fingerprint in the Raman spectra of p-type high-T_c materials is the large (30%) difference in the positions of the pair-breaking peaks for different polarizations. Again, this contrasts with the situation in NCCO where the gap anisotropy is similar to that in Nb_3Sn and does not exceed 15%. Finally the maximum gap values $\hbar\omega_p$ for the hole doped cuprates lie in the range 8–9 kT_c in contrast to 5 kTc for the NCCO crystal (see Fig. 2). Although in Bi2201 the T_c is considerably reduced compared to the double-layer

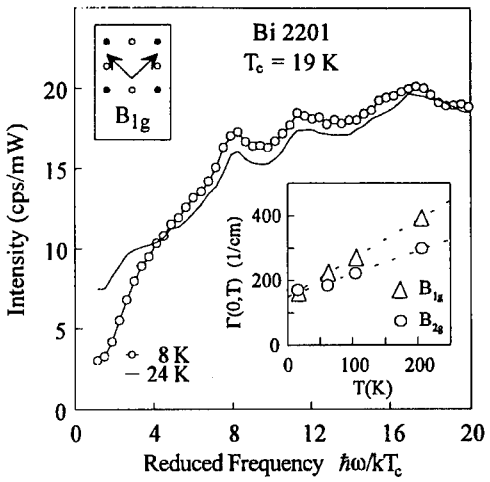


Fig. 3. Raman spectra of Bi2201 at temperatures well below and right above T_c. The inset shows the Raman results for the static relaxation rates in B_{1g} as well as B_{2g} symmetry.

compound the peak maximum for B_{1g} symmetry again lies around 8 kT_c (Fig. 3). Consequently, we believe that the peak values are rather related to the mechanism of high-T_c superconductivity than to the individual T_c. The small peak height in Bi2201 comes from the large carrier relaxation rate $\Gamma \cong 3.5\Delta_0$(see inset in Fig. 3) [2]. All these features can quantitatively be accounted for within a theoretical model described elsewhere [3] by assuming $d_{x^2-y^2}$ symmetry for the order parameter in the high–T_c cuprates and anisotropic s-wave symmetry for the gap in NCCO (see Fig. 2). This suggests that NCCO is comparable with the weakly anisotropic phonon-coupled BCS superconductor Nb_3Sn [4].

REFERENCES

1. Virosztek A. *et al.*, *Phys. Rev. B* **45**, 347 (1992)
2. Devereaux T. P., unpublished.
3. Einzel D. and Devereaux T. P., to be published in *Phys. Rev. B.*
4. Hackl R. *et al.*, *Physica C* **162**, 431 (1989).

Pergamon

J. Phys. Chem. Solids Vol. 56, No. 12, pp. 1843–1844, 1995
Copyright © 1995 Elsevier Science Ltd
Printed in Great Britain. All rights reserved
0022–3697/95 $9.50 + 0.00

0022-3697(95)00144-1

SYMMETRY OF DIFFERENTIAL OPTICAL RESPONSES OF NORMAL AND SUPERCONDUCTING PHASES IN SINGLE-CRYSTAL YBCO

W. R. STUDENMUND, I. M. FISHMAN, G. S. KINO
Edward L. Ginzton Laboratory, Stanford CA 94305 - 4085, U.S.A.

J. GIAPINTZAKIS
Department of Physics and Materials Research Laboratory, University of Illinois, 110 West Green Street, Urbana, IL 61801, U.S.A.

Abstract—We measured differential optical reflectivity (DOR) of YBCO single domains. DOR measurements reject the temperature independent bulk reflectivity and reveal dR/dT. These measurements detect the superconducting transition, and reveal specific anisotropy associated with high-T_c superconductivity.

We describe measurements of differential optical reflectivity (DOR) of untwinned single crystal $YBa_2Cu_3O_{7-d}$ (YBCO) crystals obtained by a photothermal technique. DOR measurements reject temperature-independent electron transitions and are sensitive to YBCO's optical anisotropy. To measure the angular DOR dependence, the polarization vector of the probe beam is changed at the sample surface. The superconducting transition is determined from the change in susceptibility associated with exciting and detecting coils located just below the sample. Details of the experimental technique are described elsewhere [1–3] and summarized in [4]. Some of our findings are confirmed by microwave penetration depth measurements [5]. However, certain features of the DOR response, such as the presence of a narrow peak ~ 1 K wide at T_c, for the probe light polarized along the a axis, are unique and have no analog in earlier experiments using traditional methods.

The samples investigated in this study were untwined YBCO crystals with critical temperature of 92.5 K, 91.2 K and 89.5 K. All samples had comparatively large untwinned areas of approximately $50 \times 200 \mu m$. All measurements were conducted in the $a - -b$ plane.

Over most of the temperature range, the DOR data (Fig. 1) showed angular anisotropy of the same form as in the standard reflectivity measurements, with strong temperature dependence. The single domain data consist of a continuous smooth "background" in the entire temperature range 20–300 K, and a sharp peak in the vicinity of T_c. The maximum observed signals are about 10^{-4} of the average reflected intensity of the probebeam. The critical temperature is identified as the DOR signal inflection point, and the signal maximum is shifted below T_c by approximately 0.3 K(see inset in Fig. 1). This sharp peak observed in the vicinity of T_c, varies radically in shape with the angle of polarization. For the probe beam polarized along the b axis (curve b in Fig. 1), the signal has a significant precursor in the range $\sim$ 5 K above T_c and a low temperature tail below T_c. For the probe polarized along the a axis (curve a in Fig. 1), a very narrow peak is observed, approximately 1 K wide, just below T_c, which varies in shape and width from sample to sample. Both the small temperature width and variation from sample to sample of the a response are new and puzzling effects.

Figure 2 shows a comparison of the a axis response, $1/D$ (which we take as proportional to the normal electron density [4]), and the normal electron density obtained from microwave experiments [5] as $1 - \lambda^2(0)/\lambda^2(T)$. The striking overlap of these three curves encourages our association of the three quantities and motivates our theoretical treatment.

To qualitatively understand some of our results, we use a two-component Drude model in which the dielectric constant ϵ is of the form

$$\epsilon = 1 - \frac{(1-f)\omega_p^2}{\omega^2 + i\omega\Gamma_n} - \frac{f\omega_p^2}{\omega^2 + i\omega\Gamma_s}$$

where ω_p, Γ_n and Γ_s are the plasma frequency and electron collision rates for the normal and superconducting phases, respectively. This formula treats the holes in YBCO as a free electron gas. Superconductivity alters the electron damping by slightly reducing Γ_s. This model is admittedly crude, but it provides a starting-point for understanding the DOR signal.

Within this model, the DOR response dR/dT is

$$\frac{dR}{dT} = \frac{2R_0\Gamma_n}{\omega^2 - \omega_p^2}\left[(1-f)\frac{d(\delta\Gamma)}{dT} - \frac{df}{dT}\delta\Gamma\right]$$

where $\delta\Gamma = (\Gamma_n - \Gamma_s) << \Gamma_n$ or Γ_s, $|\omega - \omega_p| >> \Gamma_n$ or Γ_s, R_0 is the reflection coefficient for an unmodulated probe beam, and it is assumed that $|d\Gamma_s/dT| << |d(\delta\Gamma)/dT|$.

This equation shows that the DOR signal consists of two components which are proportional to the rates of change of $\delta\Gamma$ and the fraction of superconducting phase f with temperature, respectively. Above T_c ($f = 0$), the observed signal is proportional to the temperature derivative of the collision frequency $d(\delta\Gamma)/dT$ in the normal state. It will

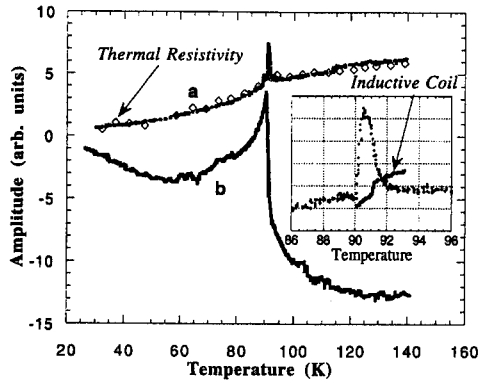


Fig. 1. Temperature dependence of *a* and *b* axis DOR, thermal resistivity. Inset shows *a* axis DOR response and Inductive coil response

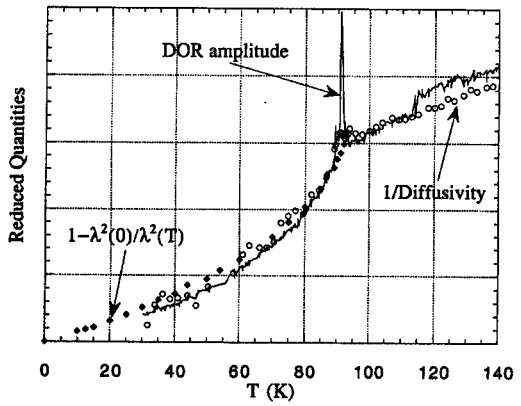


Fig. 2. Plot of DOR signal, 1/Diffusivity, and normal carrier density as a function of temperature

component decreases with temperature as $(1 - f)$, or the density of the normal component as discussed above. The second DOR component is proportional to df/dT, which can be identified as a superconducting component response.

The *b* axis DOR approximately fits this model. At low temperatures (below ~ 50 K), it has the shape of n_{normal}, consistent with $d(\delta\Gamma)/dT \sim$ constant. As the temperature rises, the second response appears, as qualitatively predicted by the df/dT term.

The *a* axis DOR does not fit this model; its shape fits exclusively the $(1 - f)$ term. However, the df/dT term cannot explain the sharp spike seen in all the samples at T_c.

This sharp spike is also not explainable within Landau–Ginzberg theory [6]. A second-order phase transition should show a step discontinuity in the derivative, followed by a gradual decline as the temperature drops. The *b* axis DOR, the twinned sample DOR [4], and, for instance, the specific heat approximately fit this description.

We suggest that this behavior can be explained as the result of interference of transmission amplitudes within the optical reflectivity matrix elements. In the case of YBCO, this interaction could arise from a difference in the response of the plains and chains. It would be interesting to investigate whether the observed effects exist in YBCO only with its specific chain–plane configuration, or are inherent to all high-$T_c$materials.

In summary, we have presented DOR measurements from single-crystal YBCO samples. These measurements give an optical indication of the superconducting transition, and reflect a significant anisotropy; much more anisotropy than is typically associated with high-T_c superconductivity. We also present a rough theoretical explanation of the observed signals which interprets some of the noted features.

Acknowledgements—The authors are indebted to S. Doniach for stimulating theoretical insight, and to D. M. Ginsberg, W. N. Hardy and M. Beasley for useful discussions. This work was supported by the Department of Energy under Contract No. DOE DE-FGO3-90ER14157 (I.F., G.K., and W.S), by an NSF Fellowship (W.S.) and by NSF Grant DMR 91-20000 through the Science and Technology Center for Superconductivity (J.G.)

Note added in press

Recent work by Holcomb *et al.* [7] may be compared with this work. Our technique measures changes in R and T a factor of 10–100 times smaller than in [7], and is sensitive to polarization. On the other hand, the Thermal Difference Spectrometer has the advantage that it can be used over a wide range of optical wavelengths. A more detailed comparison of the two techniques must wait until they are both used to examine similar material systems.

REFERENCES

1. Fishman I. M., Kino G. S., *Phys. Rev. Lett.* **72**, 588 (1994); Fishman I. M., Kino G. S. and Wu X. D., *Phys. Rev. B* **50**, 7192 (1994)
2. Fanton J. T., Mitzi D. B., Kapitulnik A., Khuri-Yakub B. T. and Kino G. S., *Appl. Phys. Lett.* **55**(6), 598 (1989)
3. Fishman I. M., Kino G. S., Wu X. D. and Studenmund W. R., *Phys. Rev. Lett.* , submitted (1993)
4. Kino G. S., Fishman I. M., Studenmund W. R., *Proceedings of this conference*
5. Hardy W. N., Bonn D. A., Morgan D. C., Ruixing Liang, and Kuan Zhang, *Phys. Rev. Lett.* **70**, 2134 (1993)
6. Ascroft N. W. and Mermin N. D., *Solid State Physics*, pp. 747–749. Saunders College (1976).
7. Holcomb M. J., Collman J. P. and Little W. A., *Phys. Rev. Lett.* **73**, 2360–3 (1994)

PHOTOEMISSION EXPERIMENTS

Pergamon

J. Phys. Chem. Solids Vol. 56, No. 12, pp. 1845–1847, 1995
Copyright © 1995 Elsevier Science Ltd
Printed in Great Britain. All rights reserved
0022–3697/95 $9.50 + 0.00

0022–3697(95)00223-5

COMPLETE FERMI SURFACE MAPPING OF Bi-CUPRATES

P. AEBI,* J. OSTERWALDER,† P. SCHWALLER,† H. BERGER,‡ C. BEELI§ and L. SCHLAPBACH*

* Institut de Physique, Université de Fribourg, CH-1700 Fribourg, Switzerland
† Physik-Institut, Universität Zürich-Irchel, CH-8057 Zürich, Switzerland
‡ Institut de Physique Appliquée, EPFL, CH-1015 Lausanne, Switzerland
§ Centre Interdépartemental de Microscopie Electronique, EPFL, CH-1015 Lausanne, Switzerland

Abstract—We review recent angle-scanned photoemission experiments on $Bi_2Sr_2CaCu_2O_{8+x}$. The Fermi surface has been mapped completely revealing previously unobserved "shadow bands" interpreted as due to antiferromagnetic correlations. Since $Bi_2Sr_2CaCu_2O_{8+x}$ exhibits a relatively complicated incommensurate lattice modulation new measurements on a Pb-doped, unmodulated Bi-cuprate are presented for comparison.

Keywords: Angle-scanned photoemission, Fermi surface mapping, High-temperature superconductor

1. INTRODUCTION

A new mode of angle-resolved photoemission has recently been applied to map the Fermi surface (FS) of $Bi_2Sr_2CaCu_2O_{8+x}$ (Bi2212) completely [1]. The validity of this method has been proven by the mapping of sections through the bulk FS of Cu [2]. While the traditional procedure for measuring FS transitions relies critically on photoemission line shapes near the Fermi level, this new approach takes the absolute photoemission intensity at the Fermi level directly as indicator for the FS transition. The present method probes instead of the conventional band structure $E(\mathbf{k})$ its inverse function $\mathbf{k}(E)$, therefore being complementary to the traditional approach. Using motorized sequential angle scanning data acquisition [3], a full FS mapping typically consists of 6000 intensity measurements uniformly distributed over the full first and part of the second two-dimensional Brillouin zones of the compound under investigation. This high sampling density of the parallel component of the wave vector ($\mathbf{k}_{||}$) does not miss any direct transitions crossing the Fermi level (E_F). As a matter of fact, this method revealed previously unobserved features, so called "shadow bands" (SB), on the FS of Bi2212 [1]. Since Bi2212 has a relatively complicated incommensurate lattice modulation, measurements on a Pb-doped, unmodulated crystal are presented for comparison.

2. RESULTS AND DISCUSSION

Figure 1(a) shows the Bi2212 $\mathbf{k}_{||}$ mapping of the intensity of He I excited photoelectrons collected within an energy window of about 30 meV centered at E_F. [1] High intensities result at $\mathbf{k}_{||}$ locations where transitions move through E_F. These locations present themselves as relatively fine, well defined lines. A sketch of the measurement is shown in Fig. 1(b). For a truly two-dimensional system the high symmetry points Γ and Z would be equivalent. Points X and Y correspond to $(\pi/a, \pi/a)$ with respect to the Cu–O planes and are not equivalent because of a slightly different lattice constant of the a and b axis (the b axis going along Γ Y) and because of the lattice modulation along the b axis. Transmission electron microscopy and low energy electron diffraction are characteristic for an incommensurate "5x1" superstructure along the crystal b axis (not shown). We observe different features in Fig. 1(a). First, there is a strong set of lines drawn as strong solid lines in Fig. 1(b). No pronounced nesting is observed among these lines. [1] Second, there is a weaker set of lines corresponding to SB, appearing as dashed lines in Fig. 1(b). The third feature, plotted as pieces of fine solid lines, occurs near the Γ and Z points with a banana-like shape.

If we take a copy of the stronger set of lines centered at Γ and center it at X or Y, it covers the weaker set of lines. The weaker set thus seems to behave around Y or X just as the main set of lines around Γ . This behavior is further confirmed by the dispersion observed in constant energy maps for different binding energies, where the strong lines close in towards Γ and the weaker lines towards X or Y [1,4].

X and Y points acting like Γ points, in a simplified picture, corresponds to a reduction of the Brillouin zone and in real space to a larger unit cell. This is the case if the Cu lattice is occupied with antiferromagnetically (AF) correlated spins. The fine lines observed on the FS also coincide with SB predicted for AF correlated metals by Kampf and Schrieffer [5] and are compatible with the result of an analysis of this model by Haas, Moreo and Dagotto [6] using Monte Carlo and exact diagonalisation techniques.

However, also a reconstruction of the atomic structure with the same change of the unit cell is expected to have the same consequences on the FS. Note that our experiment does not specifically detect the magnetism and there-

fore cannot distinguish between the two effects. Truly magnetic measurements are necessary or experiments on compounds with well known structures without modulation related complications.

The banana-like features near Γ and Z have been identified in Ref. [4] as due to the incommensurate "5x1" lattice modulation along the crystal b axis. This can be understood as follows: Changing the periodicity in real space will influence the repeat period of features in reciprocal space accordingly. The modulation therefore induces replicas of the FS displaced corresponding to the new periodicity. Then, the banana-like features can be understood as the appearance of such replicas of the main FS. [4]

We have carried out FS mapping experiments on lead-doped samples with a Pb to Bi ratio of 0.42:1.73 and a T_c of 83K. [7] These crystals are modulation-free and the idea was to obtain a structurally simplified situation and through this clarity on the influence of the modulation on the SB. Figure 1(c) displays the FS mapping on such a crystal. Clearly, the shadow bands are still present whereas the modulation related banana-like features do not appear. Transmission electron microscopy and low energy electron diffraction measurements (not shown) on these Pb doped samples show no indication of modulation related superlattice spots. However, faint diffraction spots occur corresponding to a larger real space layer unit cell with a lattice constant of about 5.4 Å. Such a layer unit cell is identical to the one assumed in the model of AF correlations. Thus, the Pb doping provides the intended elimination of the modulation but it also introduces a larger layer unit cell than the primitive, Cu–O plane related one with a lattice constant of about 3.8 Å. Therefore, there are also arguments for a structural origin of SB in these crystals and the situation is not clear-cut. If all layers in the crystal have the larger unit cell, main bands and SB on the FS should exhibit almost identical intensities. This is clearly not the case. More structural information is needed to determine the atomic arrangement in this Pb-doped unmodulated high T_c superconductor. While there is evidence for a larger layer unit cell somewhere in the three-dimensional unit cell AF spin correlations remain a probable origin of the SB.

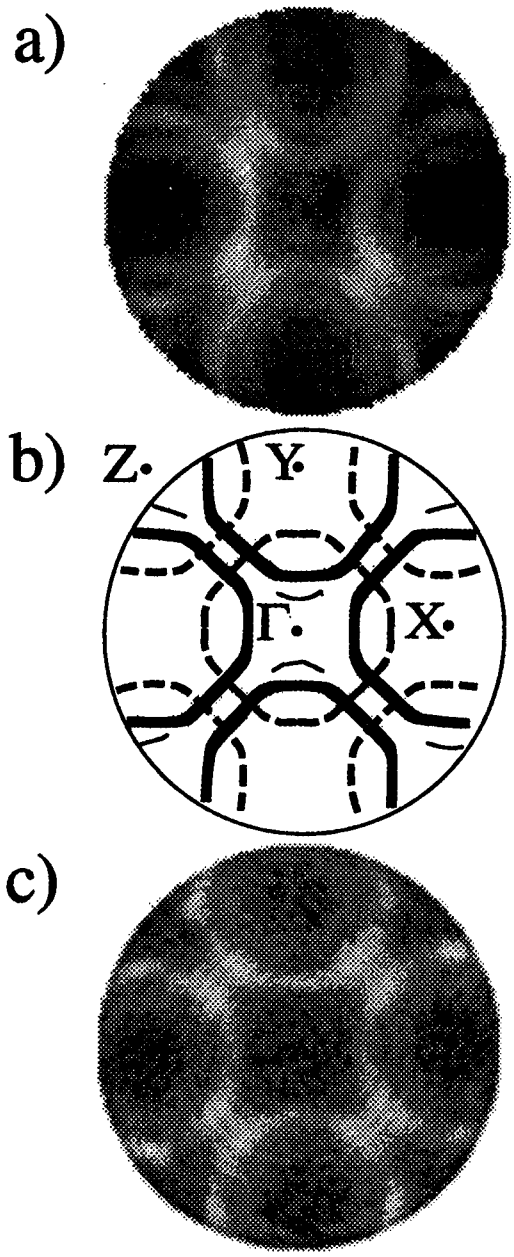


Fig. 1. (a) Bi2212 $\mathbf{k}_{||}$ mapping of the HeI (21.2 eV) excited photoelectrons collected within an energy window of about 30 meV centered at E_F. A logarithmic intensity scale is used to enhance weaker features. (b) Outline of (a) indicating high symmetry points and different sets of lines. (c) Same as (a) but for a modulation-free lead-doped sample (see text).

3. CONCLUSIONS

Essential findings of our angle-scanned photoemission experiments [1] are: (i) no pronounced nesting is observed, (ii) the observation of a weak superstructure on the FS which coincides with SB predicted by Kampf and Schrieffer [5] based on the presence of AF spin fluctuations in the metallic state, and (iii) the identification of a second superstructure on the FS as due to the incommensurate lattice modulation present in the Bi-cuprates [4].

Measurements on Pb-doped, modulation free crystals also exhibit the SB. These crystals, however, exhibit weak diffraction spots corresponding to a layer unit cell identical to the one for a model with AF correlated spins. While this does not rule out AF correlations in the Cu–O planes it does not clarify the situation. More structural information is required, truly magnetic measurements and/or FS maps on samples not presenting structural difficulties.

Acknowledgements— We wish to thank R. Fasel, R. Agostino, T.

Kreutz and G. Margaritondo for stimulating discussions, D. Zech for the T_c measurements and P. Buerri and G. Trolliet for the chemical analysis. Skillful technical assistance was provided by E. Mooser, O. Raetzo, F. Bourqui and H. Tschopp. This work has been supported by the Swiss National Foundation and the NFP30.

REFERENCES

1. Aebi P., Osterwalder J., Schwaller P., Schlapbach L., Shimoda M., Mochiku T. and Kadowaki K., *Phys. Rev. Lett.* 72, 2757 (1994); Comment by Chakravarty S., *Phys. Rev. Lett.* 74, 1885 (1995); Reply by P. Aebi, J. Osterwalder, P. Schwaller, L. Schlapbach, M. Shimoda, T. Mochiku, K. Kadowaki, *Phys. Rev. Lett.* 74, 1886 (1995).
2. Aebi P., Osterwalder J., Fasel R., Naumovioć D. and Schlapbach L., *Surf. Sci.* 307–309, 917 (1994).
3. Osterwalder J., Greber T., Stuck A. and Schlapbach L., *Phys. Rev. B* 44, 13764 (1991); Naumovioć D., Stuck A., Greber T., Osterwalder J. and Schlapbach L., *Phys. Rev. B* 47, 7462 (1993).
4. Osterwalder J., Aebi P.,Schwaller P., Schlapbach L., Shimoda M., Mochiku T. and Kadowaki K., *Appl. Phys. A* 60, 247 (1995).
5. Kampf A.P. and Schrieffer J.R., *Phys. Rev. B* 42, 7967 (1990); *Phys. Rev. B* 41, 6399 (1990).
6. Haas S., Moreo A. and Dagotto E., *Phys. Rev. Lett.* **74**, 4281 (1995).
7. Schwaller P., Aebi P., Beeli C., Osterwalder J., Berger H., Fasel R., Kreutz T.J. and Schlapbach L., in preparation.

Pergamon

J. Phys. Chem. Solids Vol. 56, No. 12, pp. 1849–1853, 1995
Copyright © 1995 Elsevier Science Ltd
Printed in Great Britain. All rights reserved
0022-3697/95 $9.50 + 0.00

0022-3697(95)00258-8

FERMI LIQUIDS AND NON-FERMI LIQUIDS—THE VIEW FROM PHOTOEMISSION

J. W. ALLEN,* G.-H. GWEON,* R. CLAESSEN† and K. MATHO‡

* Randall Laboratory, University of Michigan, Ann Arbor, MI 48109-1120, U.S.A.
† Universität des Saarlandes, Fachrichtung 10.2-Experimentalphysik, D-66041, Saarbrücken, Germany
‡ Centre de Recherches sur les Tres Basses Temperatures,C.N.R.S., BP 166, 38042 Grenoble-Cedex 9, France

Abstract—This paper presents an improved Fermi liquid lineshape analysis of the ARPES spectra of 1T-$TiTe_2$, and a brief overview of recent efforts to identify Luttinger liquid type behavior in photoemission spectra of quasi one-dimensional materials such as $K_{0.3}MoO_3$.

1. INTRODUCTION

A currently exciting topic in condensed matter physics is the possibility [1] that its fundamental paradigm for describing electrons in solids, the Fermi liquid (FL) theory [2], may fail. As developed in the spectral analysis of Luttinger [3], the spectral weight $\rho(\mathbf{k}, \omega)$ of the $\mathbf{k}$-resolved single particle Green's function $G(\mathbf{k}, \omega)$ [4] has definite characteristics for a FL. With careful attention to certain important technical difficulties [5], which are minimized in quasi low dimensional materials, angle-resolved photoemission spectroscopy (ARPES) can be used to measure $\rho(\mathbf{k}, \omega)$ below the Fermi energy E_F and thus ARPES is in principle a very direct experimental probe for Fermi liquid behavior, or its absence. The slowly falling tails of the ARPES lineshapes of the quasi two dimensional superconducting cuprates, which are much too large to be ascribed to inelastic electron scattering [6,7], have been proposed to signal a deviation from FL behavior, from the viewpoints of the marginal Fermi liquid phenomenology [8] and the Luttinger liquid (LL) [9]. These aspects of ARPES lineshapes have received only limited study in the past, posing a clear challenge to ARPES workers to develop further evidence and understanding. This paper focuses on the differences between the FL and the LL, as viewed by ARPES.

2. FERMI LIQUID CASE: $TiTe_2$

$TiTe_2$ is a layered compound which is a semimetal due to a small energetic overlap of a set of nominally Te p bands and one orbitally non-degenerate Ti 3d band. Its transport properties give no indication of any behavior lying outside of the FL framework [10]. In previous work with our collaborators [11], we have measured at low temperature and with high resolution the ARPES spectra of the Ti 3d band as it crosses E_F along a direction in $\mathbf{k}$-space where there are no other bands to produce interfering or overlapping spectral structures. The spectra are essentially free of inelastic backgrounds, consistent with the arguments of [6] and [7]. Ref. [11] also reported an analysis aimed at establishing the near $\mathbf{k}_F$ spectra as a standard showing FL behavior. This section explores an improved analysis which considerably elucidates the original aim.

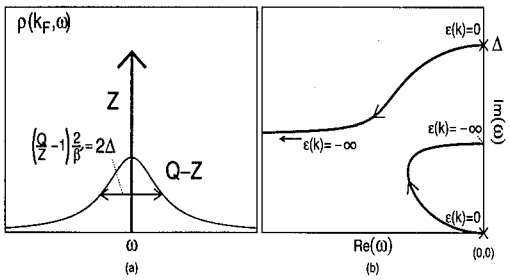


Fig. 1. (a) Spectral function for the Green's function of eq. (2). (b) The trajectories of the two poles derived from eq. (2) and $\mathbf{k}$-independent Σ, shown here for $Q/Z = 2.1$. The X's show the poles for $\mathbf{k}=\mathbf{k}_F$.

The previous analysis used the simplest FL ansatz, in which $\rho(\mathbf{k}, \omega)$ is calculated as $(1/\pi)\mathrm{Im}G(\mathbf{k}, \omega)$ where $G(\mathbf{k}, \omega)=(\omega - \epsilon_{\mathbf{k}} - \Sigma)^{-1}$ and the self energy Σ has the $\mathbf{k}$-independent FL Taylor's series form $\Sigma_T = \alpha\omega + i\beta\omega^2$. For $\mathbf{k} = \mathbf{k}_F$ (i.e. $\epsilon_{\mathbf{k}} = 0$) $G_T(\mathbf{k}, \omega)$ has a simple two pole structure, with real residues:

$$G_T(\mathbf{k}_F, \omega) = \frac{Z}{\omega - i0^+} - \frac{Z}{\omega + i/\beta'} \qquad (1)$$

Here $Z = 1/(1 - \alpha)$ and $\beta' = Z\beta$. $\rho_T(\mathbf{k}_F, \omega)$ is as shown in Fig. 1(a), with the parameters Q and Δ (defined below) set to $2Z$ and $1/\beta'$, respectively. One sees the FL property as described by Luttinger, of a perfectly sharp quasiparticle peak with weight Z. There is also a Lorentzian incoherent spectrum of weight Z and width $2/\beta'$ centered on E_F. This ansatz was found [11] to describe the spectra for $\mathbf{k}$ near $\mathbf{k}_F$ very well, using a fixed value of $\beta' = 40\mathrm{eV}^{-1}$ and varying only $\epsilon_{\mathbf{k}}$. The experimental energy and angular resolutions

were treated, respectively, by convolution with a resolution function and by an appropriate sum over $\mathbf{k}$, requiring iterative fitting to self-consistency. [12] An important point is that the shape of the spectra approaching E_F is determined entirely by the experimental resolutions, so that β' is determined by the high binding energy tail arising from the incoherent part. For $\mathbf{k}$ far from $\mathbf{k}_F$ the theoretical lineshapes were found to differ from the data qualitatively.

A great conceptual shortcoming of this ansatz is that, due to truncating Σ, $G_T(\mathbf{k}, \omega)$ has a pole in the lower half plane, and is causal only for $\omega < 1/\beta'$, which is less than the range over which the data were fit. An associated problem is that the total weight of the spectrum is not 1, but $2Z$, which could even exceed 1. Further, the total weight is not constant, but decreases as $\mathbf{k}$ departs from $\mathbf{k}_F$. The simplest causal, normalized $G(\mathbf{k}, \omega)$ consistent with the FL idea can be generated [13] by starting with a $\rho(\mathbf{k}, \omega)$ for $\mathbf{k} = \mathbf{k}_F$ that is identical to $\rho_T(\mathbf{k}_F, \omega)$ except that the Lorentzian has a generalized width Δ and its weight is set to $Q - Z$ rather than Z, as in Fig. 1(a). Thus the weight of $\rho(\mathbf{k}, \omega)$ is normalized to Q, which can be set to 1 or less than 1, depending on whether or not the experimental spectrum being analyzed is thought to contain all the spectral weight. Using a well-known causal back-transform connecting $\rho(\mathbf{k}, \omega)$ and $G(\mathbf{k}, \omega)$ [4], one then calculates the corresponding causal $G(\mathbf{k}_F, \omega)$ and finds again a simple two-pole function with causal poles and real residues.

$$\frac{G(\mathbf{k}_F, \omega)}{Q} = \frac{Z}{Q}\frac{1}{\omega - i0^+} + (1 - \frac{Z}{Q})\frac{1}{\omega - i\Delta} \qquad (2)$$

$\Sigma(\omega)$ for $\mathbf{k}=\mathbf{k}_F$ can then be extracted from $G(\mathbf{k}_F, \omega)$ and, again assuming Σ to be $\mathbf{k}$-independent near the Fermi surface, used to calculate $G(\mathbf{k}, \omega)$ and $\rho(\mathbf{k}, \omega)$ for $\mathbf{k}$ different from $\mathbf{k}_F$. As discussed further below, this Σ differs greatly from Σ_T for large ω. For small ω it retains the Σ_T-form with $Z = 1/(1-\alpha)$ and $\beta' = Z\beta = (Q/Z-1)/\Delta$. More fundamentally, if the incoherent Lorentzian spectrum of Fig. 1(a) is generalized further to $\rho_{inc}(\mathbf{k}_F, \omega) = (Q - Z)g(\omega)$, where $g(\omega)$ is a function of integrated weight 1, one can show that $\beta' = Z\beta = (\pi/Z)\rho_{inc}(\mathbf{k}_F, 0) = (Q/Z - 1)\pi g(0)$. This makes precise the extent to which FL behavior can be shown by this analysis for $TiTe_2$. For the Lorentzian case, which is shown below to fit the spectral tails in $TiTe_2$, $g(0) = 1/(\pi\Delta)$. Determining Δ and Z/Q from the tails yields thereby an estimate for $g(0)$ and β'. But note that if $g(\omega)$ continues from the fitted energy range to any finite value at $\omega = 0$, FL behavior obtains.

For $\mathbf{k}$ near $\mathbf{k}_F$ it is not surprising that $\rho(\mathbf{k}, \omega)$ produces an excellent least squares fit of the $\mathbf{k}_F$ spectrum with values similar to the ones found previously [11] for $\rho_T(\mathbf{k}, \omega)$, $Q/Z = 2.1$ and $\beta' = 17$ eV^{-1}. This fit is shown for the $\theta = 14.75°$ spectrum in Fig. 2, identified [11] as having $\mathbf{k}_F$ nearly centered in the k-resolution window because it shows the minimum width and the nearest approach to E_F. In marked contrast to the spectra of high T_C cuprates, the lineshape tail falls quadratically. Keeping these parameters

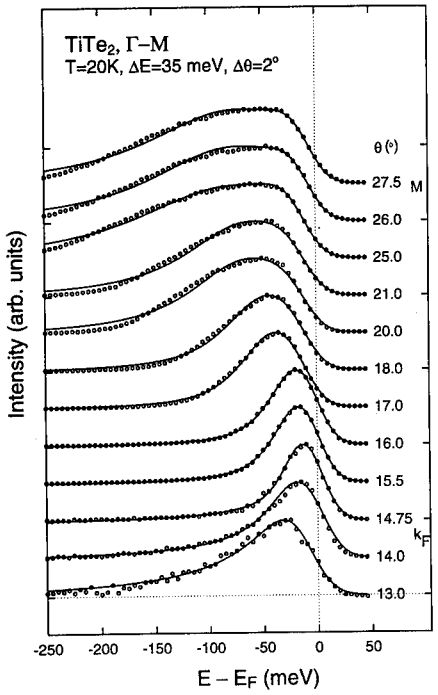


Fig. 2. Fits of Ti 3d derived conduction band of $TiTe_2$, as described in the text. The spectra are normalized to the same maximum height.

fixed and allowing only $\epsilon_{\mathbf{k}}$ to vary, one finds very poor fits of the structured experimental lineshapes for $\mathbf{k}$ far from $\mathbf{k}_F$. However, if one also allows the parameters β' (or Δ) and Q/Z to vary with $\mathbf{k}$, one can achieve excellent least squares fits of all the spectra, as shown in Fig. 2, without making any other change in the ansatz. Note that with the unknown total weight Q factored out, $G(\mathbf{k}, \omega)/Q = 1/((G(\mathbf{k}_F, \omega)/Q)^{-1} - Q\epsilon_{\mathbf{k}})$, and the appropriate parameters are Z/Q, Δ, and $Q\epsilon_{\mathbf{k}}$. With few anomalies, the parameters vary smoothly with $\mathbf{k}$, as shown in Table 1. The surprising and non-intuitive result that this ansatz can produce the structured lineshapes for $\mathbf{k}$ far from $\mathbf{k}_F$ has been reported previously [14], but without further elucidation.

The origin of the structured lineshapes is the following. As $\epsilon_{\mathbf{k}}$ changes from 0 the poles of $G(\mathbf{k}, \omega)$ shift in the complex ω-plane as shown in Fig. 1(b), with the interesting behavior that the pole evolving from the quasiparticle pole at $\mathbf{k}_F$ bends backward to remain close to the Im(ω) axis. Because in addition the residues become complex, there is interference between the contributions to $\rho(\mathbf{k}, \omega)$ from each pole, the details depending mostly on Q/Z. For Q/Z roughly in the range of that for the fit for the $\mathbf{k}_F$ spectrum, one finds that as $|\epsilon_{\mathbf{k}}|$ increases from zero the movement of the poles and the effect of interference in the weights conspire so that there is a single peak moving away from E_F and broadening, much as we found [11] for $\rho_T(\mathbf{k}, \omega)$. However, for larger Q/Z one finds a sharing of weight

$\theta(°)$	k_F-k ($Å^{-1}$)	Z/Q	Δ (meV)	$Q\epsilon_k$ (meV)
13.0	0.06	0.48	34	37
14.0	0.02	0.48	20	25
14.75	0.00	0.48	62	-18
15.5	-0.03	0.28	27	-21
16.0	-0.05	0.40	33	-25
17.0	-0.08	0.35	40	-47
18.0	-0.12	0.27	47	-55
20.0	-0.19	0.23	68	-76
21.0	-0.22	0.22	72	-78
25.0	-0.36	0.19	107	-102
26.0	-0.39	0.15	93	-90
27.5	-0.44	0.14	96	-91

Table 1. Fit parameters (Z/Q, Δ, $Q\epsilon_k$) for Fig. 2.

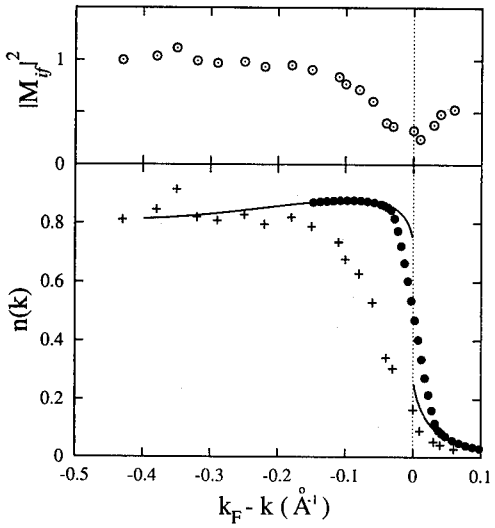


Fig. 3. n_k obtained from the fits of Fig. 2, assuming $Q = 1$ for all **k**. The fit parameters were modeled with polynomials to obtain a continuous function. The filled circles show the effect of our finite angular resolution. The pluses show the (scaled) areas from ARPES. Shown in the upper panel is the area (crosses) divided by n_k (filled circles), i.e., the matrix element if $Q = 1$ for all **k**.

between the two poles so as to produce a two-structure lineshape having considerable weight near E_F even for **k** far from $\mathbf{k}_F$, just as occurs in the data. Varying β' tunes the separation of the two structures to produce a good fit. Thus these structured lineshapes are latent in this ansatz and the additional **k**-dependence of the parameters, introduced in the fitting, acts only to tune to the desired weight-sharing regime and to adjust the energy scale.

Having obtained good fits for a properly normalized $G(\mathbf{k}, \omega)$, one can then calculate a relative occupation number Qn_k, where n_k is [4] the integral of $\rho(\mathbf{k}, \omega)$ for ω less than E_F. In this connection, note that the spectra fitted include ones for which **k** is outside the Fermi surface but where there is nonetheless weight below E_F as discussed in [11]. The solid line in the bottom panel of Fig. 3 shows the

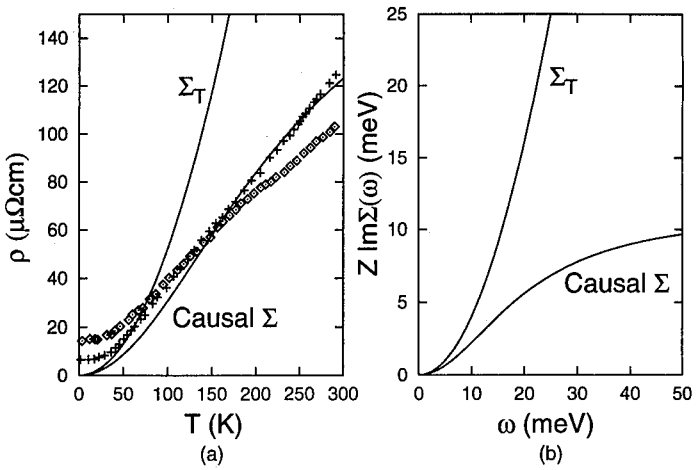


Fig. 4. (a) The resistivities calculated (solid lines) for $TiTe_2$ with Σ_T in [10] and with the causal Σ, compared to experiment (data points) [15], as explained in the text. (b) $Z\mathrm{Im}\Sigma(\omega)$ for the Σ_T fit in [11] and for the causal Green's function fit based on Eq. (2).

resulting Qn_k, plotted for $Q = 1$. The filled circles show the effect of our finite **k**-resolution for directly measuring n_k and the pluses show the actual measured areas of the spectra. The difference reveals the fact that the data fitting requires also an overall scale factor which, in this ansatz, must be attributed to a **k**-dependence of the photoemission cross-section, if **k**-independent Q is assumed. The modest and smooth variation of this factor, shown on a relative scale in the upper panel, is reasonable based on general experience except perhaps for the tendency to a minimum at $\mathbf{k}_F$. Note that the **k** at which the ARPES area has decreased by 1/2 is definitely not $\mathbf{k}_F$, in contrast to the assumption which is used increasingly in $\mathbf{k}_F$ determinations for high T_c materials.

In principle an energy dependence of ImΣ implies a temperature (T) dependence of the dc resistivity ρ(T). For the case $\mathrm{Im}\Sigma = \beta\omega^2$, FL arguments lead to $\rho = (1/ne^2)(m^*/\tau)$ with $m^* = m/Z$ and $(1/\tau) = 2Z\ \mathrm{Im}\Sigma = 2\beta Z[\omega^2 + (\pi k_B T)^2]$. Then one has $\rho(\mathrm{T}) = 2(m/ne^2)(\pi k_B)^2\beta T^2$. The authors of [10] have calculated ρ(T) for $TiTe_2$, assuming our Σ_T [11] applies to the entire Fermi surface, computing from an LDA bandstructure the average Fermi velocity which gives n/m, and taking for β our experimental β'. They compared their result with experimental data [15] and found a large disagreement at high T, a result reproduced in Fig. 4(a). Fig. 4(b) shows the large difference at large ω between the purely ω^2-dependence of $\mathrm{Im}\Sigma_T$ from [11] and that of the causal Σ obtained above. Fig. 4(a) also shows the ρ(T) obtained if the causal Σ is used in place of Σ_T, again taking $\beta = \beta'$ for a consistent comparison, and if one is willing to speculate that the ω-dependence of ImΣ can be a guide to the T dependence of $\rho(T)$ even away from the ω^2 regime. The causal Σ essentially eliminates the large disagreement with experiment

implied by Σ_T. However, the numerical agreement should not be taken too seriously because a detailed treatment should account for the probably different lifetimes on the Te p and Ti d parts of the Fermi surface, as well as for the considerable difference between β and β'.

3. LUTTINGER LIQUID CASE

The Luttinger liquid generalization [16] of the Tomonaga Luttinger (TL) model [17] of a one dimensional (1-d) interacting electron gas provides the theoretical paradigm of non-Fermi liquid behavior for a lattice. Anderson has proposed [1,9] that this Luttinger liquid behavior extends also to quasi 2-d systems, e.g. the high T_c cuprates. The form of $\rho(\mathbf{k}, \omega)$ for the LL [18,19] differs greatly from that of the FL because the LL excitation spectrum has no quasiparticles and there are only uncoupled collective excitations of the spin and charge density, sometimes called spinons and holons, respectively. The addition or removal of an electron of momentum $\mathbf{k}$ results entirely in holon-spinon pair generation. The kinematics of this process lead in general to $\rho(\mathbf{k}, \omega)$ having two peaks with energies which reflect the holon and spinon dispersions, and the dynamics produce lineshapes which are edge singularities with power law decay to high energy. For $\mathbf{k}$ away from $\mathbf{k}_F$ there is no weight between E_F and the lowest energy singularity, and in consequence the $\mathbf{k}$-integrated single particle spectrum goes to zero at E_F as a power law with a non-universal exponent, commonly denoted α (different from the α of the preceding section) [18,19], even though the system is metallic. Although the vanishing weight at E_F is not observed, or not resolved, in the $\mathbf{k}$-integrated spectra of the high T_c cuprates, Anderson [9,20] has proposed that the slowly falling tails and certain other features of their ARPES lineshapes are manifestations of LL dynamics and kinematics, respectively.

Several quasi-1-d compounds such as $K_{0.3}MoO_3$[21], $Li_{0.9}Mo_6O_{17}$ [22], Ta_2Se_8I [21,23], and $(TMTSF)_2PF_6$ [24] do indeed show vanishing single particle weight at E_F, as measured by photoelectron spectroscopy (PES). For only one of these materials, the organic $(TMTSF)_2PF_6$, is there independent evidence [25] of Luttinger liquid behavior. For the others, which are inorganic, the situation is complicated by the fact that they show charge density wave (CDW) transitions which signal the presence of $\mathbf{q}=2\mathbf{k}_F$ electron-phonon interactions. As is carefully discussed in [21] various mechanisms deriving from electron-phonon interactions, such as polaron formation [26] or a CDW pseudogap [27], may also result in low spectral weight at E_F. Thus it is difficult to infer Luttinger liquid behavior from the $\mathbf{k}$-integrated PES spectrum alone, but ARPES spectra could be decisive. ARPES spectra to date, e.g. of $K_{0.3}MoO_3$[28,29], $Li_{0.9}Mo_6O_{17}$ [22], Ta_2Se_8I [23], have not shown features which could be identified with holon or spinon dispersion.

We point out here a simple and potentially useful relation between the α of the $\mathbf{k}$-integrated spectrum and the magnitude of the holon dispersion. This relation is an important part of arguments to identify holon dispersion in ARPES spectra of $K_{0.3}MoO_3$. [30] For the TL model with a repulsive spin-independent interaction, algebraic manipulation of relations in [18] or [19] shows that the holon Fermi velocity v_{Fc} is ξv_F where v_F is the underlying one-electron Fermi velocity and $\alpha = (1/4)[\xi + \xi^{-1} - 2]$. The spinon Fermi velocity is just v_F. Analyzing the near E_F $\mathbf{k}$-integrated spectrum of $K_{0.3}MoO_3$ [21], one finds power law behavior with $\alpha=0.9\pm0.1$ extending to about 200 meV. This value of α is considerably larger than would occur for a short ranged interaction such as one has in the Hubbard model [31], but it is consistent with the even larger value (1.25) found experimentally for $(TMTSF)_2PF_6$ from nuclear magnetic resonance [25] and PES data [24]. There are strong theoretical indications [32] that large α values can result from long range Coulomb interactions. For this value of α one finds that $\xi=5.4$. As reported and discussed in detail in [30], new ARPES spectra for $K_{0.3}MoO_3$, obtained with our collaborators, show a feature with nearly this anomalously large dispersion, relative to predictions [33] from band theory. In this connection, it is notable that Voit [34] has discussed other evidence for spin-charge separation in $K_{0.3}MoO_3$.

Acknowledgements—We gratefully acknowledge essential discussions with our collaborators [11,30], and with V. Meden, K. Schönhammer, J. Voit, and M. Whangbo. Work at U-M was supported by the U.S. Dept. of Energy (DoE) under contract DE-FG02-90ER45416 and by the U.S. National Science Foundation (NSF) grant DMR-91-08015. The U-M Rackham Graduate School supported a visit of G.-H.G. to Uni-Saarlandes through its Program to Promote International Partnerships.

REFERENCES

1. Anderson P. W., *Phys. Rev. Lett.* **64**, 1839 (1990); *Phys. Rev. Lett.* **65**, 2306 (1990).
2. Landau L. D., *Sov. Phys. JETP* **30**, 1058 (1956); **32**, 59 (1957).
3. Luttinger J. M., *Phys. Rev.* **119**, 1153 (1960).
4. See, e.g., Negele J. W. and Orland H., *Quantum Many Particle Systems*. Addison-Wesley, Menlo Park (1988).
5. Smith N. V., Thiry P. and Petroff Y., *Phys. Rev. B* **47**, 15476 (1993).
6. Sawatzky G. A. in *High Temperature Superconductivity* (Edited by K. S. Bedell, D. Coffey, D. E. Meltzer, D. Pines and J. R. Schrieffer), p. 297. Addison-Wesley, Redwood City (1990).
7. Liu L.-Z., Anderson R. O. and Allen J. W., *J. Phys. Chem. Solids* **52**, 1473 (1991).
8. Varma C. M., Littlewood P. B., Schmitt-Rink S., Abrahams E. and Ruckenstein A. E., *Phys. Rev. Lett.* **63**, 1996 (1989).
9. Anderson P. W. in *High Temperature Superconductivity* (Edited by K. S. Bedell, D. Coffey, D. E. Meltzer, D. Pines and J. R. Schrieffer), p. 3. Addison-Wesley, Redwood City (1990).
10. Allen P. and Chetty N., *Phys. Rev. B* **50**, 14855 (1994).
11. Claessen R., Anderson R. O., Allen J. W., Olson C. G., Janowitz C., Ellis W. P., Harm S., Kalning M., Manzke R. and Skibowski M., *Phys. Rev. Lett.* **69**, 808 (1992).
12. The perpendicular dispersion of the $\mathbf{k}_F$ peak has been measured to be $\leq$ 0.1eVÅ. Following the discussion of [5], we then estimate that the photohole width arising from the photoelectron lifetime is $\leq$ 10 meV. This and other results of

a detailed study of the entire valence band ARPES spectrum will be published in the near future [Claessen *et al*].
13. Matho K., *Physica B* **199-200**, 382 (1994); and this conference.
14. Harm S., Dürig R., Manzke R., Skibowski M., Claessen R. and Allen J. W., *J. Electron Spectrosc.* **68**, 111 (1993).
15. Koike K., Okamura M., Nakanomyo T. and Fukase T., *J. Phys. Soc. Jpn* **52**, 597 (1983); de Boer D. K. G., van Bruggen C. F., Bus G. W., Coehoorn C., Haas C., Sawatzky G. A., Myron H. W., Norman D. and Padmore H., *Phys. Rev. B* **29**, 6797 (1984).
16. Haldane F. D. M., *J. Phys. C* **14**, 2585 (1981).
17. Luttinger J. M., *J. Math. Phys.* **4**, 1154 (1963); Mattis D. C. and Lieb E. H., *J. Math. Phys.* **6**, 304 (1965); Luther A. and Peschel I., *Phys. Rev. B* **90**, 2911 (1974).
18. Meden V. and Schönhammer K., *Phys. Rev. B* **46**, 15753 (1992); Schönhammer K. and Meden V., *Phys. Rev. B* **47**, 16205 (1993).
19. Voit J., *Phys. Rev. B* **47**, 6740 (1993)
20. Anderson P. W., *Physica B* **199,200**, 8 (1994).
21. Dardel B., Malterre D., Grioni M., Weibel P., Baer Y. and Lévy F., *Phys. Rev. Lett.* **67**, 3144 (1991).
22. Smith K. E., Breuer K., Greenblatt M. and McCarroll W., *Phys. Rev. Lett.* **70**, 3772 (1993).
23. Hwu Y., Alméras P., Marsi M., Berger H., Lévy F., Grioni M., Malterre D. and Margaritondo G., *Phys. Rev. B* **46**, 13624 (1992).
24. Dardel B., Malterre D., Grioni M., Weibel P., Baer Y., Voit J. and Jérôme D., *Europhys. Lett.* **24**, 687 (1993).
25. Bourbonnais C., Creuzet F., Jérôme D., Bechgaard K. and Moradpour A., *J. Phys. (Paris) Lett.* **45**, L-755 (1984); Wzietek P., Creuzet F., Bourbonnais C., Jérôme D., Bechgaard K. and Batail P., *J. Phys. (Paris) I* **3**, 171 (1993).
26. Sawatzky G. A., *Nature* **342**, 480 (1989).
27. Rice M. J. and Strassler S., *Solid State Commun.* **13**, 1389 (1973); Lee P. A., Rice T. M. and Anderson P. W., *Phys. Rev. Lett.* **31**, 462 (1973).
28. Veuillen J. Y., Cinti R. C. and Al Khoury Nemeh E., *Europhys. Lett.* **3**, 355 (1987).
29. Breuer K., Smith K. E., Greenblatt M. and McCarroll W., *J. Vac. Sci. Tech. A* **12**, 2196 (1994).
30. Gweon G.-H., Claessen R., Allen J. W., Ellis W. P., Reinert F., Benning P. J., Zhang Y. X., Matsuura A., Olson C. G. and Schneemeyer L. F., to be published.
31. Schulz H. J., *Phys. Rev. Lett.* **64**, 2831 (1990).
32. Kopietz P., Meden V. and Schönhammer K., *Phys. Rev. Lett.* **74**, 2997 (1995).
33. Whangbo M. H. and Schneemeyer L. F., *Inorg. Chem.* **25**, 2424 (1986).
34. Voit J., *J. Phys. (Cond. Matt.)* **5**, 8305 (1993); and private communication.

Pergamon

J. Phys. Chem. Solids Vol. 56, No. 12, pp. 1855–1862, 1995
1995 Elsevier Science Ltd
Printed in Great Britain
0022–3697/95 $9.50 + 0.00

0022-3697(95)00292-8

ANGLE-RESOLVED PHOTO-INTENSITIES IN HIGH-T_cs: SURFACE STATES, CuO_2 PLANE BANDS, LINESHAPES, AND RELATED ISSUES

A. BANSIL *, M. LINDROOS *,†

* Physics Department, Northeastern University, Boston, Massachusetts 02115, U.S.A.
† Physics Department, Tampere University of Technology, Tampere, Finland

Abstract—We have carried out first-principles angle-resolved photo-intensity computations in a number of high-T_c compounds. This article provides an overview of some of the results of current interest in connection with the relevant photoemission data. Specific issues discussed are: (i) surface states in $Nd_{2-x}Ce_xCuO_4$, (ii) extended van Hove singularity in $YBa_2Cu_4O_8$ at the Y-point, (iii) signature of CuO_2 plane bands in the cuprates, and (iv) constant initial state photoemission spectra.

Keywords: A: High-T_c superconductors, C: *ab initio* calculations, photoelectron spectroscopy, D: Fermi surface, surface properties

1. INTRODUCTION

Angle-resolved photoemission spectroscopy (ARPES) is continuing to make important contributions towards understanding the electronic structure of the normal as well as the superconduting state of the high-T_cs.[1–4] Progress in answering a number of crucial questions has been possible by analyzing lineshapes, polarization and energy dependences, and other spectral details, even if in some cases near the limits of energy and momentum resolution of the current ARPES setups. Given the complexity of the spectra, especially when we are dealing with systems as complicated as the high-T_cs, it is obvious that theoretical modelling of the ARPES spectra will greatly aid in the interpretation of the data.

So motivated, we are pursuing theoretically the investigation of ARPES spectral intensities in the high-T_cs.[5–7] For this purpose we have generalized the one step model of photoemission[8,9] to treat arbitrarily complex lattices.[5,7,10] In this approach, the emission process is properly treated as a quantum mechanical event involving an interaction between the external radiation field and the electron gas in a semi-infinite solid. In particular, the computations include lifetimes of the initial and final states, use the full crystal wave functions, and take into account multiple scattering effects in the presence of the surface. By and large, the results presented in this article implicitly invoke the local density approximation (LDA), although simulations to assess correlation effects have been carried out in a few instances. We emphasize however that our first-principles methodology allows incorporation of correlation effects relatively straightforwardly, especially if the self-energy correction to the crystal potential is assumed to be only energy (rather than energy and/or k) dependent. It is important of course to consider effects of correlations beyond the LDA on the spectra since the undoped parent compounds are predicted by the LDA to be metallic in most high T_cs contrary to the physically observed insulating phases.

The applications of the theory considered in this article concern some issues of current interest to the high-T_c community. The specific topics are: (i) Surface states (SSs) in $Nd_{2-x}Ce_xCuO_4$ (NCCO). Our computations[7] predict the presence of SSs on the (001)-surface of NCCO, and suggest clearly for the first time that a rich variety of SSs can exist in complex systems with implications for various physical properties. (ii) The van Hove singularity in $YBa_2Cu_4O_8$(Y124). Direct comparisons between the measured and computed ARPES spectra[6] show that Y124 possesses an *extended* van Hove singularity at the Y-symmetry point arising from CuO_2 planes. Such a singularity in the density of states could provide a simple mechanism for the occurrence of high T_cs in the cuprates. (iii) Signature of CuO_2 plane bands. We argue that the ARPES data in $YBa_2Cu_3O_7$ (Y123) and Y124 is most sensibly interpreted as containing the signature of *two* rather than *one* CuO_2 plane bands.[5] The characteristic polarization dependence of the plane band signal is delineated. (iv) Constant initial state (CIS) spectra. ARPES data in this form have recently drawn attention with the work of Ref. 11. We present the first calculation of a high quality CIS spectrum from Cu(111) as a step towards understanding the nature and promise of the CIS spectroscopy more generally.

Within the limitations of space, this article gives a brief overview of some of the relevant results concerning issues outlined in the preceding paragraph. Much of this work has been or will be presented in greater detail elsewhere.[5–7]

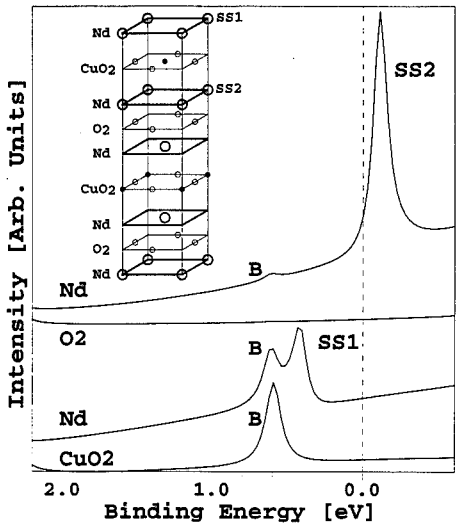


Fig. 1. A set of theoretical ARPES spectra from the Nd-compound for four different terminations of the (001)-surface. The inset shows the schematic arrangement of layers in the lattice. SS1 and SS2 denote two different surface states, and B a bulk peak related to CuO_2 plane bands. The spectra are for $h\nu$=17 eV, for an emission angle of 16° along the $\Gamma - X$ line. The dashed vertical line marks the Fermi energy in NCCO for 15% Ce doping. The spectra have *not* been folded with the Fermi function.[After Ref. 7].

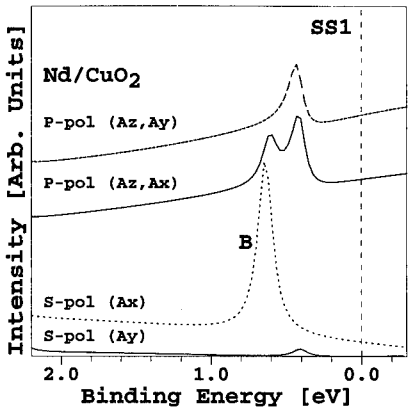


Fig. 2. The polarization dependence of the surface state SS1 of Fig. 1, see caption to Fig. 1 for notation and other relevant details. Non-zero components of the vector potential **A** are indicated on each curve; s-polarized light corresponds to $A_z = 0$, p-polarized light to $A_z \neq 0$. A_x is parallel to the ΓY symmetry direction.[After Ref. 7].

2. SURFACE STATES IN $Nd_{2-x}Ce_xCuO_4$

A few words concerning the significance of SSs in connection with the ARPES data are appropriate first. The possible presence of SSs in the vicinity of the Fermi energy (E_F) would complicate the mapping of bulk bands and Fermi surfaces since the SSs generally disperse much like the bulk states as a function of $k_\parallel$. Also, the SSs would influence lineshapes, making it more difficult to deduce the size and symmetry of the order parameter from the ARPES data. Finally, we note that SSs may induce higher T_cs in the surface layer and cause tunneling measurements to be sensitive to the specifics of the experimental geometry in various methods.[12]

Figure 1 shows a typical set of calculated ARPES spectra from the (001)-surface of NCCO where all four unique ideal terminations for the body centered tetragonal NCCO lattice are considered. Since the spectra have not been folded with the Fermi function, only the peaks below E_F would be observable in an ARPES measurement, the peaks above E_F are relevant for an inverse ARPES experiment. SS1 and SS2 are surface state peaks while B is a bulk feature which arises from the CuO_2 planes. SS1 and SS2 possess the character of Shockley type surface states[13], i.e. these states are the result of changed boundary conditions which allow new states localized in the surface region to come into existence when the bulk crystal is terminated. The nature of the topmost layer is then obviously important, and in NCCO only the Nd-terminated surfaces appear to admit SSs, the order of layers in the case of SS2 and SS1 being $Nd/O_2/Nd/CuO_2$ and $Nd/CuO_2/Nd/O_2$ respectively (see inset). For the $k_\parallel$ value of Fig. 1, SS2 and SS1 lie above and below E_F respectively. However, these states possess considerable dispersion, so that at other $k_\parallel$ values both states can lie either above or below E_F.

We emphasize that although the computations of Fig. 1 employ the LDA-based band theory framework, our main conclusion, namely, the existence of SSs in NCCO, is quite robust. In this connection, we have simulated the effect of correlations by adding *ad hoc* self-energy corrections to the Cu and O–muffin–tin potentials which shifted the Cu–O complex of bands by as much as 1 eV, but yielded only minor shifts (less than 0.1 eV) on SS positions.[7] In order to simulate the effect of surface relaxation, the relative position of the topmost layer was varied with respect to the second layer by as much as 10% of the interlayer spacing, but the resulting shifts in SS positions were found to be less than a few tenths of an eV. Note also that the present SSs, being of the Shockley type, are generally expected to be insensitive to the nature of the crystal potential in the surface region in contrast to the Tamm- or dangling-bond type surface states[14]. These considerations indicate that despite uncertainties in the absolute computed positions of the SSs, our prediction of their existence in NCCO is fairly insensitive to the limitations inherent in our approach. Incidently, similar computations in YBCO do not yield any Shockley-type SSs.

Figure 2 delineates the polarization dependence of SS1; the results for SS2 are similar and are not shown in the interest of brevity. SS1 is seen to be excited mainly by p-polarized light, consistent with the expectation that SSs generally couple with A_z; further, SS1 is insensitive to the component of

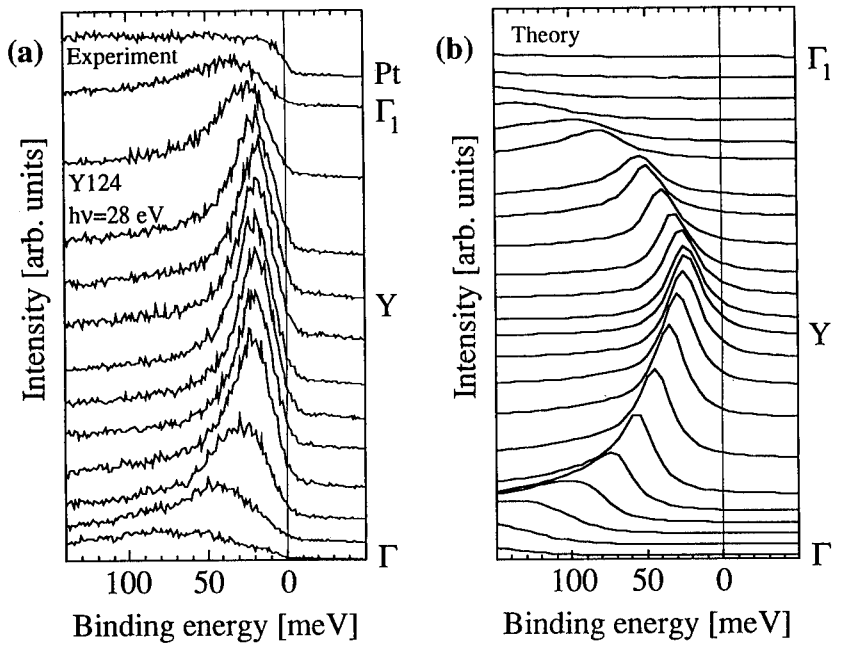


Fig. 3. Comparison of experimental(a) and theoretical(b) ARPES spectra in Y124 in the vicinity of the E_F for $k_\parallel$-values around the Y-point as one moves towards the Γ or Γ_1 points. The extended van Hove feature at the minimum binding energy of about 19 meV at Y is seen dispersing away from the E_F. Photons are polarized along the b-axis of the crystal.[After Ref. 6].

A in the x–y plane, compare the two uppermost curves. Fig. 2 also shows that the bulk feature B possesses a substantial intensity only when the incident photon has a non-zero A_x component, indicating that B is not excited by either A_y or A_z; we will return to the polarization dependence of B in Section 4 below.

It is important to understand the behavior of SS1 and SS2 as a function of the energy and polarization of the incident photon, as well as the dispersion (with $\mathbf{k}_\parallel$) of the associated surface state bands. These characteristics can be useful in identifying signatures of these states in the ARPES data. We have remarked on the polarization dependence in the preceding paragraph, other aspects are considered in Ref. 7 where it is also shown that although the existing ARPES data[15–17] is consistent with the presence of a surface state in NCCO, further ARPES and inverse ARPES measurements will be valuable in this connection. In particular, the experimental feature denoted by A in Ref. 17 may reasonably be interpreted as the surface state SS1 instead of a Kondo-type renormalized heavy electron band.

3. AN EXTENDED VAN HOVE SINGULARITY IN Y124 AT THE Y-POINT

In considering Y124, we note that this compound is closely related to the more familiar Y123. Y124 contains two parallel Cu-O chains per unit cell compared to one chain in Y123, otherwise the crystal as well as the electronic structures of the two materials are quite similar.[18] The crystals of Y124 are, however, naturally untwinned and more stable than Y123, making Y124 an attractive system from an experimental viewpoint.

We discuss the nature of the van Hove singularity in Y124 with reference to Figs. 3 and 4 which compare theoretical and experimental ARPES spectra around the Y-symmetry point along two perpendicular directions, Y to Γ, and Y to S, respectively. For orientation, Γ–X–S–Y is the basal plane of the Brillouin zone, S denotes the zone corner, and ΓY is parallel to the Cu–O chains. A small range of binding energies (~150 meV) are considered in order to highlight the intense narrow feature located about 19 meV below E_F in the experimental spectra which is our main concern. The characteristic shapes of the computed and measured peaks are seen to be similar in Figs. 3 and 4. The peak possesses a high intensity around the Y-point and rapidly broadens as it disperses below E_F in Fig. 3, and above E_F in Fig. 4. The theoretical dispersion is however greater than the experiment which is particularly evident in Fig. 3. This 'flattening' of the bands in the real material is due presumably to the electron correlation effects approximated in the present LDA based computations.

The peak in the theoretical spectra of Figs. 3(b) and 4(b) arises from a bulk CuO_2 plane band. The comparisons of Figs. 3 and 4 indicate that the associated band is nearly flat as one moves from Y towards either Γ or Γ_1 (the Γ-point in the second Brillouin zone), but that the band is roughly parabolic in the perpendicular YS direction. These

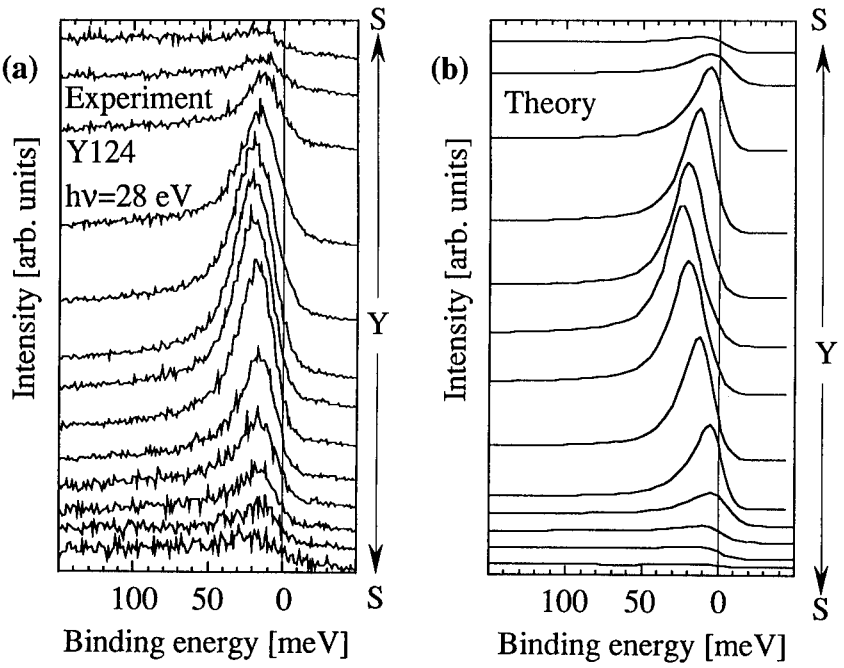


Fig. 4. Same as Fig. 3, except that here the $k_{\|}$-values are varied from Y towards the S point in a direction perpendicular to that of Fig. 3, showing the spectral feature dispersing towards the Fermi energy.[After Ref. 6].

results thus establish the existence of an *extended* van Hove singularity in Y124 at Y with a binding energy of about 19 meV. Such an extended saddle point would render the band structure quasi-1D, making it possible to explain the occurrence of T_cs of ~100K even in a weak coupling BCS scheme.[6,19,20] We emphasize that although the LDA band structure could lead to a bifurcated saddle point[21], the LDA by itself does not appear to be able to yield an extended saddle point; however, the LDA bands could presumably be renormalized and 'flattened' by various mechanisms[22].

4. SIGNATURE OF CuO_2 PLANE BANDS IN THE CUPRATES

We comment first on whether the ARPES data from Y123 and Bi2212 indicates the presence of *two* CuO_2 plane bands or of only *one* related emission peak. This question is significant because some theoretical models of the correlated electron gas[23] suggest that the electrons in the cuprates become localized along the c-axis and that the interlayer coupling between the planes is strictly zero. If so, the ARPES data from the two CuO_2 planes should show a single photoemission peak. In sharp contrast, the conventional band theory picture involves a finite interlayer coupling and an associated splitting of the bands.

Insofar as Bi2212 is concerned, we are not in a position to delineate anything quantitative since we have not performed photo-intensity computations on this compound. However, the splitting between the two plane bands predicted by the band theory in Bi2212 is quite small, and may actually be even smaller in the real material, making its observation difficult via ARPES. Further, we should keep in mind that given the intrinsic broadening of lines, and various experimental constraints (finite analyzer solid angle, difficulties of orienting samples, etc.), ARPES may not be able to resolve two very closely placed peaks even with improvements in energy resolution.

The situation in YBCO is more favorable because the splitting predicted by the band theory between the two CuO_2 plane bands[18] is greater than in Bi2212 reflecting the more 3D-nature of YBCO. In particular, only one of the two plane bands was involved in our consideration of the van Hove singularity in Y124 in the preceding section. In Y123, detailed comparisons between the computed and measured photo-intensities[5] along the Γ-S line show a good overall level of accord. Some of these results are reproduced in Fig. 5. The experimental feature B, Fig. 5(a), is interpreted as a combination of the signal due to the two plane bands b and b' in Fig. 5(b). With these results in mind, we conclude that the ARPES data from YBCO is most sensibly interpreted as containing the signature of two rather than one CuO_2 plane bands.

The theoretical polarization dependence of the intensity of the plane bands b or b' in Y123 is seen from Fig. 6 to be in remarkable agreement with the measurements. The characteristic signal depicted in Fig. 6 deserves further comment since it may help identify the presence of CuO_2 plane bands in the ARPES data more generally. The fact that the intensity is small, nearly zero, for light polarized along the ΓS

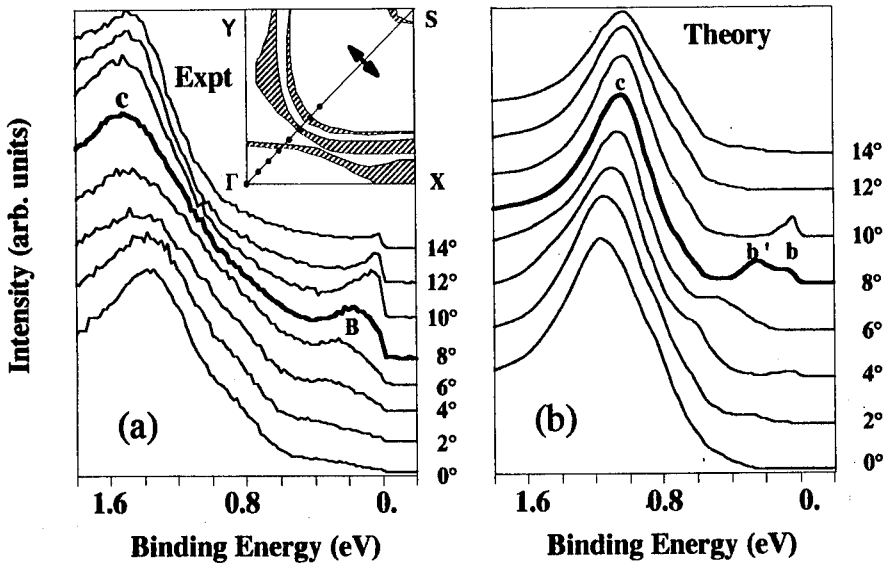


Fig. 5. Theoretical and experimental ARPES spectra from Y123 (001)-surface for incident light polarized perpendicular to the ΓS direction. The inset shows the Fermi surface of Y123 projected on to the Γ–X–S–Y plane; the solid dots in the inset give the $k_{\|}$-values for various spectra (the polar angles of detector also indicated on the spectra). The thick curves highlight the case where the CuO_2 plane bands lie just below E_F.[After Ref. 5].

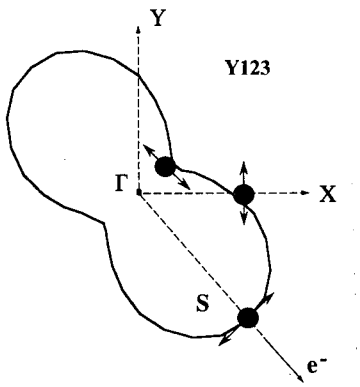


Fig. 6. Comparison of computed (solid curve) and measured (filled circles, polarization direction shown by double arrows) intensity of the CuO_2 plane band feature in Y123 as a function of the azimuthal angle of polarization of the incident light, keeping the value of $k_{\|}$ fixed along the ΓS direction. Theoretical intensity shown is for either of the plane bands b or b' of Fig. 5.[After Ref. 5].

line can be argued on the basis of selection rules obeyed by the relevant matrix element assuming perfect tetragonal symmetry. By carrying out computations for various terminations of the (001)-surface of Y123, Ref. 5 shows that the shape of the theoretical polarization curve of Fig. 6 is quite insensitive to the relative placement of the CuO_2 layer in relation to the surface, see Fig. 6 of Ref. 5. [The intensity of the emission of course decreases as the CuO_2 layer lies deeper.] This result is consistent with the notion that the electronic states in question are more or less two-dimensional in nature so that these states do not undergo a substantial modification when the bulk crystal is terminated to create a surface. Finally, Fig. 7 shows the calculated polarization dependence of the CuO_2 plane band feature B of Figs. 1 and 2 for NCCO. The similarity of Figs. 6 and 7 is striking. These considerations indicate that the shape of Figs. 6 and 7 is a highly robust spectral signature of photoemission from CuO_2 plane bands in the cuprates. A similar polarization dependence should be obeyed by emission from the CuO_2 planes in Bi2212; the present situation with regard to the ARPES data[24–26] is unclear and should be investigated further.

5. CONSTANT INITIAL STATE ARPES SPECTRA

A constant initial state (CIS) type of an ARPES measurement has recently been reported in Ref. 11 to investigate the Fermiology of high-T_cs. The idea is to arrange the geometrical parameters of the experiment in such a way that photoemission from the vicinity of E_F is measured over a fairly dense grid of $\mathbf{k}_{\|}$-values in the x–y plane. It is then argued that rapid variations in the observed intensity can be used to track quasi-particle excitations dispersing across the Fermi energy as a function of $\mathbf{k}_{\|}$. However, photoemission is a complex process which involves energy and k (crystal momentum) conservation in the presence of finite lifetimes of initial and final states, and the matrix element for emission can be influenced strongly by the final state

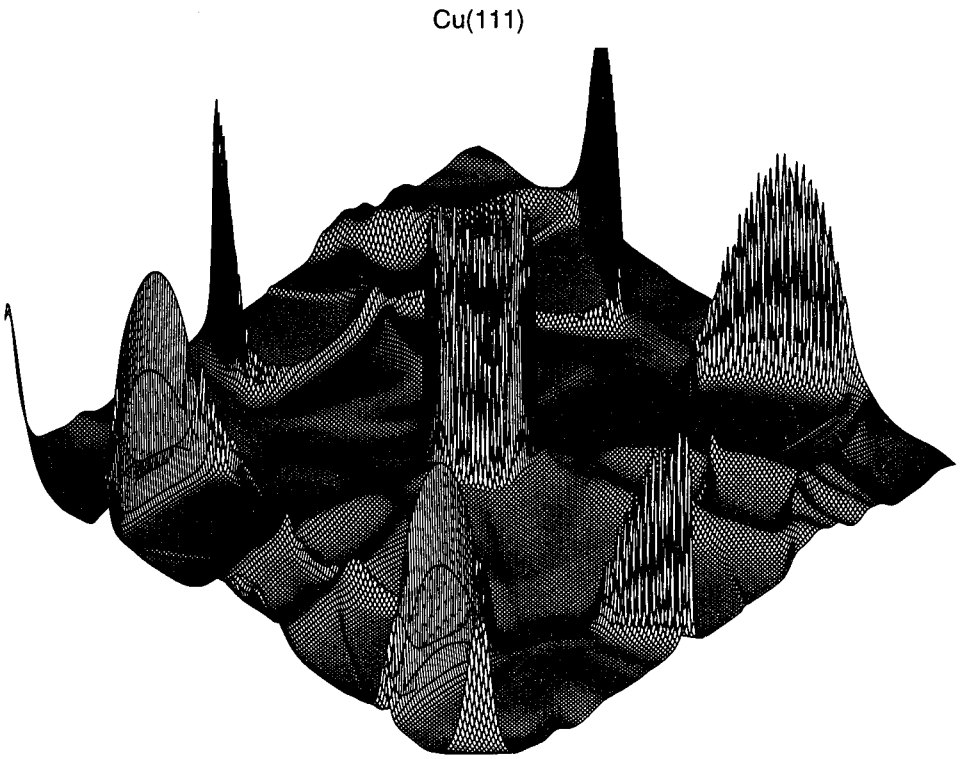


Fig. 8. The constant initial state spectrum from Cu(111). The intensity of emission from states at E_F is shown for 21 eV unpolarized photons.

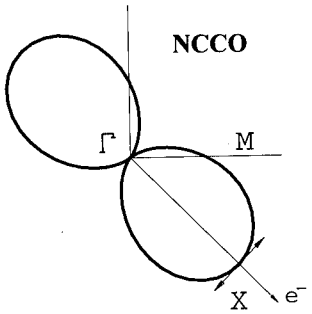


Fig. 7. Same as Fig. 6, except this figure refers to the (001)-surface of $Nd_{2-x}Ce_xCuO_4$. Only theoretical results are shown since the corresponding experimental data is not available.

wavefunction; the situation is often complicated further by effects of experimental resolution and statistics. For these reasons, it is important to establish clearly the relationship between structures in the CIS spectra and the underlying Fermi surface. As a first step towards exploring this issue, we mention a few preliminary results in Cu(111) here; further details will be presented elsewhere.

Fig. 8 shows the computed CIS photo-intensity for 21 eV photons from Cu(111) when the initial state lies at the E_F. The calculations were carried out for three different polarizations of the incident light on a fairly dense 160×160 grid of $\mathbf{k}_\parallel$ values in the (111)-plane in order to ensure that various spectral features are reproduced properly. Here, the results for unpolarized light (obtained by averaging the spectra for different polarizations) are shown since these are most relevant for the experimental setup of Ref. 11. Fig. 9 gives a gray scale representation of the surface plot of Fig. 8. The spectrum of Figs. 8 and 9 is seen to contain a strikingly rich level of structure. The dark circular ring at the center of Fig. 9 is due to the well known surface state at $\bar{\Gamma}$ in Cu(111). The imprint of the 'dog's bone' Fermi surface orbit[27] is also seen clearly around the Brillouin zone edges (hexagon drawn in solid lines in Fig. 9). Beyond these, the origin of various spectral features and their relationship to Fermi surface is unclear and requires further investigation. Our preliminary work does however suggest that density of states effects play an important role in this regard.

Additional computations (not shown) indicate that the CIS spectra from low index faces of Cu are quite strongly dependent on the energy and polarization of the incident light. The CIS spectrum in a layered material will likely

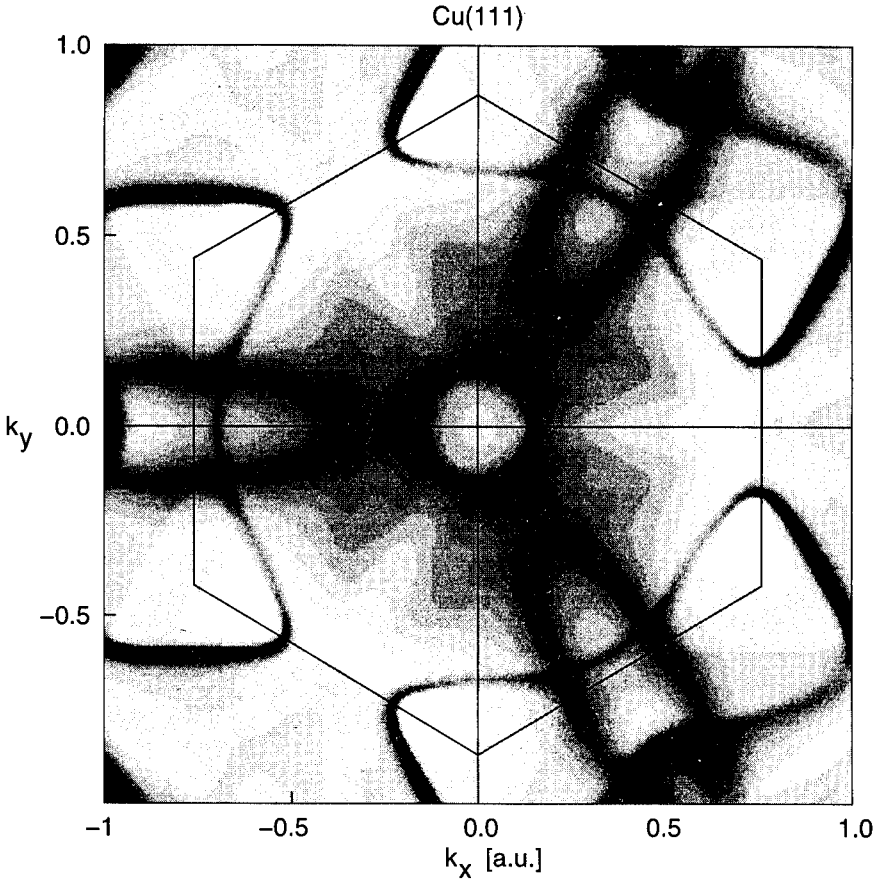


Fig. 9. A gray scale rendition of the surface plot of Fig. 8. Highs are shown dark.

be simpler than that of a 3D-metal such as Cu in some aspects, even though there will likely be other complicating factors. The projection of the Fermi surface involved in the 3D-case is probably more complicated than in a 2D-system because the bands in the latter case will possess relatively little dispersion perpedicular to the layers. On the other hand, the small size of the Brillouin zone along the c-axis, and the final state effects may produce complicated spectral features in the 2D-case. Nevertheless Figs. 8 and 9 suggest that with a proper analysis the CIS spectra could potentially reveal interesting details about the electronic structure which may be difficult to obtain otherwise.

In summary, we have briefly discussed several applications of first principles photo-intensity computations which offer insight into the nature of electronic states and the ARPES data from the cuprates. Comparisons between theory and experiment along these lines should help assess the limits of validity of the conventional LDA based picture in describing the electronic states in the high-T_cs.

Acknowledgements—This work is supported by the US Department of Energy under contract W-31-109-ENG-38, including a subcontract to Northeastern University, the Academy of Finland, and has benefited from travel grants from the NSF and NATO, and the allocation of supercomputer time at NERSC and the Pittsburgh Supercomputer Centers.

REFERENCES

1. See this conference proceedings, and previous proceedings in this series of conferences, Refs. 2–4.
2. Spectroscopies in Novel Superconductors, edited by F. M. Mueller, A. Bansil, and A. J. Arko, *J. Phys. Chem. Solids* **54**, No. 10(1993).
3. Electronic Structure and Fermiology of High−T_c Superconductors, edited by Takahashi T. , Bansil A. and Katayama H.–Yoshida *J. Phys. Chem. Solids* **53**, No 12(1992).
4. Fermiology of High T_c Superconductors, edited by A.Bansil *et al. J. Phys. Chem. Solids* **52**, No 11/12(1991).
5. Bansil A. *et al., J. Phys. Chem. Solids* **54**, 1185(1993); Lindroos M. *et al., Physica* **C212**, 347(1993).
6. Gofron K. *et al., Phys. Rev. Lett.* **73**, 3302(1994).
7. Lindroos M. and Bansil A. , *Phys. Rev. Lett.* **75**, 1182 (1995).
8. Pendry J. B. , *Surface Science* **57**, 679(1976); Hopkinson J.F.L., Pendry J. B. and Titterington D.J., *Computer Phys. Commun.* **19**, 69(1981).
9. Pendry J. B., *Low Energy Electron Diffraction*. Academic Press, New York, 1974.
10. Bansil A. , Kaprzyk S. and Tobola J., *MRS Proc.* **253**, 505(1992); Bansil A. and Kaprzyk S., *Phys. Rev.* **B43**,

10335(1991); Kaprzyk S. and Bansil A. , *Phys. Rev.* **B42**, 7358(1990).
11. Aebi P. *et al.*, *Phys. Rev. Lett.* **72**, 2757(1994).
12. Liu S. H. and Klemm R. A., *Phys. Rev. Lett.* **73**, 1019(1994), and references therein.
13. See, e.g., A. Zangwill: Physics at Surfaces, Cambridge University Press, 1988; Lindroos M. *et al.*, *Phys. Rev.* **B33**, 6798(1986).
14. See, e.g., D. P. Woodruff and T. A. Dechar: Modern Techniques of Surface Science, Cambridge University Press, 1986.
15. Anderson R. O. *et al.*, *Phys. Rev. Lett.* **70**, 3163(1993).
16. King D. M. *et al.*, *Phys. Rev. Lett.* **70**, 3159(1993).
17. Sakisaka Y. *et al.*, *Phys. Rev* **B42**, 4189(1990).
18. Yu J. and Freeman A. J., *J. Phys. Chem. Solids* **52**, 1351(1991); Pickett W. E., Cohen R. E. and Krakauer H. , *Phys. Rev.* **B42**, 8764(1990); Andersen O. K. *et al.*, *Physica* **185C**, 147(1991); Yu J., Park K. T. and Freeman A. J., *Physica* **172C**, 467(1991).
19. Abrikosov A. A., Campuzano J. C. and Gofron K., *Physica* **214C**, 73(1993).
20. King D. M., Shen Z. X. and Greene R. L., *Phys. Rev.* Lett. **73**, 3298(1994).
21. Andersen O. K., Jepsen O. and Liechtenstein A. I. , *Phys. Rev.* **B49**, 4145(1994).
22. See e.g., contributions by Markiewicz R. M. and by E. Dagatto *et al.* in this volume; Alexandrov S. S. , Bratkovsky A. M., and N. F. Mott, *Phys. Rev. Letters* **74**, 2840(1995).
23. See, Anderson P. W., this proceedings; *ibid.*, *J. Phys. Chem. Solids* **52**, 1313(1991).
24. Ding H. , Campuzano J. C. and Jennings G. , *Phys. Rev. Letters* **74**, 2784(95).
25. Dessau D. S., Shen Z. X. and King D. M., *Phys. Rev. Lett.* 71, 2781(93).
26. Ma J. , Quitman C. and Onellion M., *Phys. Rev.* **B51**, 3832(95).
27. Aebi P. *et al. Surface Sci.* 307–309, 917(1994).

Pergamon

J. Phys. Chem. Solids Vol. 56, No. 12, pp. 1863–1864, 1995
1995 Elsevier Science Ltd
Printed in Great Britain
0022-3697/95 $9.50 + 0.00

0022-3697(95)00224-3

ARPES STUDIES IN THE NORMAL AND SUPERCONDUCTING STATE OF $Bi_2Sr_2CaCu_2O_8$

J. C. CAMPUZANO, H. DING, A. BELLMAN
Department of Physics, University of Illinois at Chicago, Chicago IL 60607 Materials Science Division, Argonne National Laboratory, Argonne, IL 60439, U.S.A.

M.R. NORMAN, M. RANDERIA, and G. JENNINGS
Materials Science Division, Argonne National Laboratory, Argonne, IL 60439, U.S.A.

T. YOKOYA, T. TAKAHASHI and H. KATAYAMA-YOSHIDA
Tohoku University, Sendai, Japan

T. MOCHIKU and K. KADOWAKI
National Research Institute for Metals, Sengen, Tsukuba, Ibaraki 305, Japan

High resolution ARPES measurements were carried out on Bi2212 samples [T_c=87 K]. Most of the results have either appeared in print or will appear soon; here we briefly summarize the various points together with the relevent references.

Due to the low cross sections in Bi2212, we set the energy resolution in this experiment to a FWHM=18.8 meV, equivalent to a gaussian of σ= 8 meV, and the angular resolution was ±1°, equivalent to 1/22nd of the Brillouin zone edge, or 1/32nd of the zone diagonal. Normal state spectra [1,2] show only one peak corresponding to the CuO_2 planar band; no resolvable bi-layer splitting is seen above T_c. All other spectral features can be attributed to umklapp bands corresponding to a superlattice with $Q = (0.21, 0.21)\pi$ which has been independently seen in structural studies. We also find some evidence for "shadow bands" which are (π, π) fold-backs of the main bands; details will be presented elsewhere [2].

The main CuO_2 Fermi surface corresponds to a doping of 0.17 holes per *Cu* atom. While the Fermi surfaces and the dispersion of the peak positions appear to be like that in band theory, the spectra themselves are anomalously broad in the normal state.

With decreasing T the spectra sharpen up enormously [3]. We have carried out careful studies of the lineshape, and by studying sum rules, came to the conclusion that our ARPES data can be interpreted simply in terms of the one-particle spectral function $A(\boldsymbol{k}, \omega)$. Thus the intensity can be expressed as $I(\boldsymbol{k}, \omega) = I_0(\boldsymbol{k}) f(\omega) A(\boldsymbol{k}, \omega)$ where $f(\omega)$ is the Fermi function and I_0 includes all the matrix element effects. Even though the lineshape changes a lot with temperature, the integrated intensity at $\boldsymbol{k}_F$ does not. We note that the sharpening up of the spectra below T_c is not due to a pile-up of states below the gap, as previously interpreted in the photoemission literature, since ARPES measures the spectral function, and not the density of states. The sharpening of the spectra is due instead to a dramatic increase of the quasiparticle lifetime in the superconducting state, as observed in optical experiments. As the lifetime increases, $\Sigma''(\boldsymbol{k}, \omega)$ decreases, decreasing the width of the spectrum. Using the sum rule $\int_{-\infty}^{+\infty} f(\omega) A(\boldsymbol{k}, \omega) = n(\boldsymbol{k})$ where $n(\boldsymbol{k})$ is the momentum distribution, together with the fact that $n(\boldsymbol{k}_F)$ is independent of temperature, we find that the peak intensity must increase. We note in passing that the energy-integrated ARPES intensity can be used to experimentally measure the momentum distribution $n(\boldsymbol{k})$ [3].

We now turn to the extraction of the momentum dependence of the gap $|\Delta(\boldsymbol{k})|$. Since the intrinsic linewidth deep in the superconducting state is much smaller than the energy resolution, we can make *BCS* spectral function fits to the leading edge of the Energy Distribution Curves (EDC's) to extract $|\Delta(\boldsymbol{k})|$ at T=13 K; see ref. [1]. We find that the excitation gap is strongly $\boldsymbol{k}$-dependent, being largest near the $\bar{M} = (\pi, 0)$ point and much smaller at the Fermi surface crossing along the $(0, 0) \rightarrow (\pi, \pi)$ direction, as seen in earlier work. Unlike the earlier work, we find a highly non-trivial momentum dependence of the gap in the vicinity of the diagonal direction, where *d*-wave would have predicted a simple node.

We find limited evidence for a non-zero gap along the diagonal direction in the Y quadrant. However in the X quadrant the gap is quite sizable along the diagonal, 7 ± 2 meV, and vanishes 10° on either side of it.

A simple *d*-wave gap of the form $\Delta(\boldsymbol{k}) = \Delta_0(\cos(k_x a) - \cos(k_y a))$ is ruled out. Various possible interpretations are discussed in detail in ref. [4]. The simplest interpretation is in terms of an anisotropic *s*-wave gap which has two nodes per quadrant. Potential complications arising from the superlattice are pointed out in [1] and discussed in detail in [4] which can apply to data in the X quadrant.

In conclusion, we have shown that ARPES is a very useful probe of quasi-2D materials where one can study spectral functions, their $\boldsymbol{k}$- dispersion, the effect of the

many-body physics on the line shapes, the momentum distribution, and the detailed $\boldsymbol{k}$-variation of the superconducting gap.

Acknowledgement—Work supported by DOE contract W-31-109-ENG-38 and NSF grant DMR 8914120. The Synchrotron Radiation Center is supported by NSF Grant DMR-9212658.

REFERENCES

1. Ding H., Campuzano J.C., Bellman A.F., Yokoya T., Norman M.R., Randeria M., Takahashi T., Katayama-Yoshida H., Mochiku T., Kadowaki K. and Jennings G., *Phys. Rev. Letters* **74**, 2784 (1995).
2. Ding H. *et al.*, (unpublished).
3. Randeria M., Ding H., Campuzano J.C., Bellman A., Jennings G., Yokoya T., Takahashi T., Katayama-Yoshida H., Mochiku T. and Kadowaki K., (preprint).
4. Norman M.R., Randeria M., Campuzano J.C. and Ding H., *Phys. Rev.* **B**, (to appear).

Pergamon

J. Phys. Chem. Solids Vol. 56, No. 12, pp. 1865–1869, 1995
1995 Elsevier Science Ltd
Printed in Great Britain
0022-3697/95 $9.50 + 0.00

0022-3697(95)00262-6

ELECTRONIC STRUCTURE EVOLUTION FROM MOTT INSULATOR TO SUPERCONDUCTOR—AN ANGLE-RESOLVED PHOTOEMISSION INVESTIGATION

D. M. KING, D. S. DESSAU, A. G. LOESER and Z.-X. SHEN [1]

Solid State Laboratory and Applied Physics Department, Stanford University, Stanford, CA 94305, U.S.A. and Stanford Synchrotron Research Laboratory, Stanford, CA 94309, U.S.A.

B. O. WELLS

Physics Department, Massachusetts Institute of Technology, Cambridge, MA 02139, U.S.A.

Abstract—A critical analysis of new and earlier experimental data from the cuprate superconductors, in light of recent advances in many-body theory, shows that effects previously thought to be explained by band theory alone (such as the large Fermi surface) may also be accounted for by an idealized many-body approach. In addition, there are many elements of the data which can be better described using many-body approaches. Therefore, it appears that a comprehensive many-body description is needed to understand the electronic structure of the cuprate superconductors in the normal state. Angle-resolved photoemission has also revealed a large gap anisotropy, fueling the current debate on the symmetry of the pairing state.

Most angle-resolved photoemission studies on high-temperature superconductors have focused on the metallic phases. With recent work on undoped compounds, we now have the opportunity to investigate the evolution of the electronic structure as doping transforms an antiferromagnetic insulator into a high-temperature superconductor. Strong correlation effects, derived from the large Coulomb interactions, clearly play an important role in the insulating phase. As the Mott insulators are doped and the antiferromagnetic order is suppressed, the question becomes whether we can start using one-electron band theory, which has proven very successful in the past, or whether we continue to need many-body theories, which are very difficult to solve. In this paper, we compare some of our earlier results from metallic samples with more recent data from insulating materials to investigate whether a comprehensive description of the electronic structure is available. We also discuss the current status of our experimental investigation of the superconducting gap anisotropy.

Early on it was thought that a possible test of the applicability of one-electron theory and many-body theory was to measure the size and shape of the Fermi surface (FS). Several many-body theoretical calculations predicted that the Fermi surface would form small pockets centered at $(\pi/2, \pi/2)$ for small doping [Fig. 1(a)], in contrast to one-electron predictions of a large Fermi surface centered at (π, π) [Fig. 1(b)]. Angle-resolved photoemission (ARPES) experiments have succeeded in mapping out the Fermi surface of highly doped superconductors and discovered that the measured FS does agree very well with one-electron LDA calculations despite the fact that band theory fails for undoped samples. Recently however, additional ARPES data and advances in many-body theory now show that effects previously thought explainable by band-theory alone (such as the large Fermi surface) may also be accounted for by a many-body approach. In addition, there are many elements of the data that can be better described using many-body approaches. It appears that one must include antiferromagnetic interactions and strong correlation effects in order to understand the electronic structure of the cuprate superconductors in the normal state.

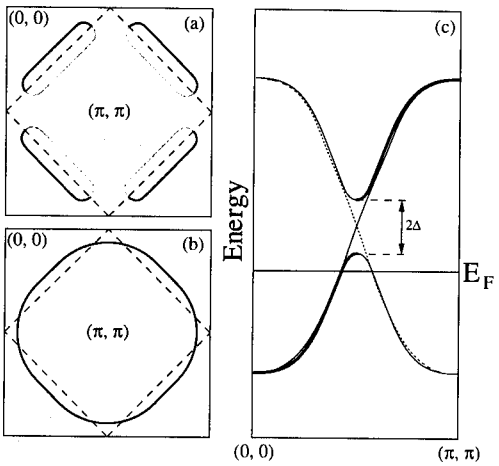
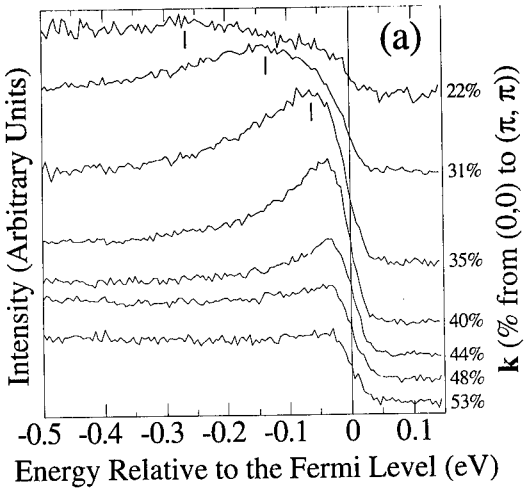


Fig. 1. (a) Model picture of the Fermi surface of a lightly hole doped Mott insulator. (b) The Fermi surface of hole doped cuprate as expected from band theory. (c) SDW analogy of the insulating gap formation. The bands corresponding to the original band, before electron-electron correlations are turned on, have stronger oscillator strength (thick lines).

Angle-resolved photoemission data from highly doped samples reveals a large Fermi surface centered at (π, π) [1–7], which agrees well with one-electron LDA cal-

[1] Author to whom all correspondence should be addressed



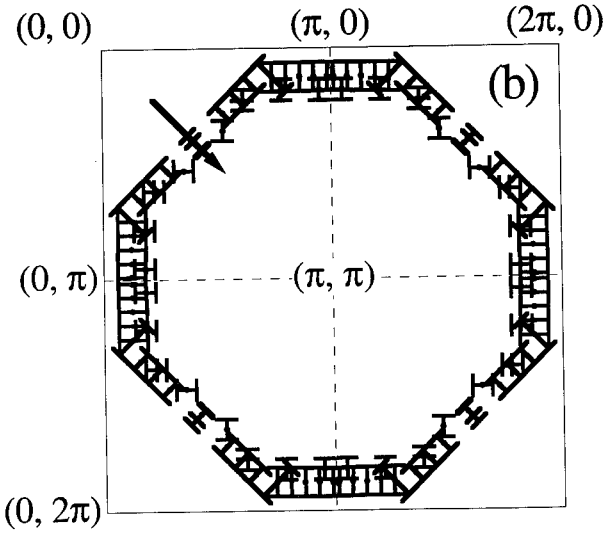


Fig. 2. (a) ARPES data from $Bi_2(Sr_{0.97}Pr_{0.03})_2Cu0_{6+\delta}$ showing the peak dispersion along the (0, 0) to (π, π) direction in the Brillouin zone. (b) Measured Fermi surface of $Bi_2(Sr_{0.97}Pr_{0.03})_2Cu0_{6+\delta}$. The points with error bars indicate **k**-space locations where the peak is observed crossing the Fermi energy. The arrow shows the **k**-space locations of the data displayed in panel (a).

culations [8–12]. In Fig. 2, we present the results from $Bi_2(Sr_{0.97}Pr_{0.03})_2Cu0_{6+\delta}$ (Bi2201) by King *et al.* [5]. Bi2201 is one of the simpler compounds, containing only one CuO_2 plane per unit cell and is hole doped (p-type). Along the (0, 0) to (π, π) direction, presented in Fig. 2(a), we clearly see a peak emerge from the background, sharpen up, and disperse towards the Fermi energy. By the time we are 40% from (0, 0) to (π, π), the Fermi energy is more than halfway up the leading edge of the feature and by 44%, the peak has lost the majority of its intensity, indicating a Fermi crossing between 40% and 44%. The locations where this dispersive band crosses E_F determine the experimental FS. The measured crossing points are plotted in Fig. 2(b). The data, all from the first quadrant, has been reflected about the high symmetry directions to reveal the large FS centered at (π, π). Similarly, large Fermi surfaces which agree with LDA calculations are observed in metallic $Nd_{2-x}Ce_xCuO_{4+\delta}$ [2,3], $YBa_2Cu_3O_{6.9}$ [6], $YBa_2Cu_3O_7$ [7], and $Bi_2Sr_2CaCu_2O_8$ [4].

If one only considers the Fermi surface data from metallic samples, it is tempting to believe that we should model the electronic structure of these superconductors using a one-electron band picture [11]. This scenario severs the relationship between the metals and insulators and attributes the separation to either a phase transition [13] or the creation of band-like states near E_F with doping [14]. There are, however, several reasons to question the use of the delocalized approach to describe the metallic copper oxides. First, photoemission satellite structures are present near the Cu core levels and near the valence band, indicative of a large U in the metallic samples . Second, the band picture predicts a large Fermi surface which should correspond to a high carrier density which varies with doping like 1-x. This contradicts the results of transport measurements in the low doping regime which reveal a carrier density proportional to x, instead of 1-x [15,16]. In addition, although $Nd_{2-x}Ce_xCuO_{4+\delta}$ appears to have a hole like Fermi surface, it is found experimentally to have n-type carriers [2,3]. Third, the experimentally observed band near E_F is always much narrower than predicted by LDA calculations everywhere in **k**-space. It is difficult to tell just how much narrower the experimental dispersion is since the peak becomes hard to distinguish at larger binding energies and the top of the band is always unoccupied in a metal and therefore cannot be measured by photoemission. Estimates for the ratio of the LDA calculated dispersion to the experimental data vary from a factor of two for some measurements along (0, 0) to (π, π), [1,17] to a factor of five near the saddle point at (π, 0) [18,19].

To further differentiate the localized and itinerant approaches, it is instructive to study undoped samples where we know band theory breaks down. The recent work by Wells et al. [20] measured the dispersion of the single photohole in the copper oxide insulator $Sr_2CuO_2Cl_2$. $Sr_2CuO_2Cl_2$ is closely related to the high-T_c superconductors (see contribution by Wells in this volume). The study of this insulator not only gives information on the phenomenology of the doping process but also provides a test of the localized models in the insulating state where the models are best defined. In Fig. 3 we plot the E versus **k** relationship of the lowest binding energy peak from the $Sr_2CuO_2Cl_2$data. The measured data was only collected in the first quadrant and has been replicated in the other quadrants using the symmetry operations available in the tetragonal system. The total measured dispersion of this peak, or bandwidth, is around 2J which agrees very well with the predictions of the t-J model [21–23]. Since the band reaches its maximum, or lowest binding energy, at ($\pm\pi/2$, $\pm\pi/2$), one would ex-

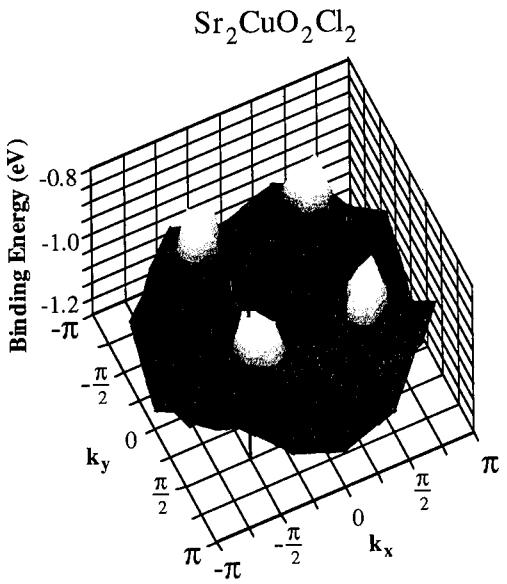


Fig. 3. The E versus **k** relationship of the experimental data from $Sr_2CuO_2Cl_2$.

pect small Fermi surface pockets centered at $(\pm\pi/2, \pm\pi/2)$ for very small doping levels and a carrier density proportional to doping. This is consistent with the transport data [15,16] and optical data [24].

The key question is how the Fermi surface evolves from the small pockets centered at $(\pm\pi/2, \pm\pi/2)$ for small doping levels to a large LDA Fermi surface centered at (π, π) for very high doping levels. Since most of our angle-resolved photoemission data are from the p-type compounds, we will focus our discussion on the p-type case [25,26]. There are two critical aspects of the data which must be explained to understand the evolution in the electronic structure as a function of doping: the decrease in oscillator strength observed in the insulator for **k** greater than $(\pi/2,\pi/2)$ and the development of the electronic structure at $(\pi, 0)$.

Although it is not clear whether many-body theory should give small Fermi surface pockets as shown in Fig. 1a, the decrease in oscillator strength observed in the insulator for **k** greater than $(\pi/2,\pi/2)$ may make part of the Fermi surface hard to observe by photoemission. We can describe this intensity change in the language of the spin-density wave (SDW) model, illustrated in Fig. 1c, although the weak coupling SDW model is not rigorous here. The folded back "shadow band" results from the antiferromagnetic order (dashed line) and will have much less oscillator strength and spectral intensity than the original band (solid line). Therefore, between the mixture of the two bands in the SDW state, one can see part of the band better than the others (dark solid line). This oscillator strength effect is preserved in the intermediate coupling regime [27], and complicates the study of the cross-over from Fig. 1a to Fig. 1b. If there are small Fermi surface pockets, centered at $(\pm p/2, \pm p/2)$ in the lightly doped material as shown in Fig. 1a, then because of the oscillator strength effect only the side of the small Fermi surface, corresponding to the original band (dark line in Fig. 1a), will be clearly seen in a photoemission experiment. If one does not sample **k**-space thoroughly, it is very difficult to distinguish Fig. 1a from Fig. 1b. This may account for the puzzling experimental data by Liu et al. from $YBa_2Cu_3O_x$ which shows that the band crossing behavior along (0, 0) to (π, π) is basically the same as x varies from 6.9 to 6.4 [17]. Therefore, the oscillator strength and "shadow Fermi surface" issues are important for a comprehensive understanding of the photoemission data and provide a heuristic understanding of the subtleties in the evolution of the Fermi surface data as a function of doping. This also suggests that the electronic structure in the metallic phase may be affected by the short range antiferromagnetic spin fluctuations even though they may be very difficult to detect. Aebi et al. recently reported that they have observed these effects in angle-resolved photoemission data from Bi2212 at room temperature [28] although the interpretation of the data is still controversial [29] (see also contributions by P. Aebi et al. and Schrieffer and Kampf in this volume). More experiments are underway to further investigate this issue.

Another key difference between the insulating and metallic data is the development of the electronic structure at $(\pi, 0)$. For insulating $Sr_2CuO_2Cl_2$, from $(\pi, 0)$ to $(0, \pi)$ the band shows considerable dispersion with the peak much higher in energy near $(\pi/2, \pi/2)$ than near $(\pi, 0)$. This behavior is very different from that observed in all the p-type metals, where we find an extended flat band saddle-point near E_F at $(\pi, 0)$, as well as the theoretical models such as the t-J model and Hubbard model, where the band near $(\pi/2, \pi/2)$ has similar energy as the band near $(\pi, 0)$. This indicates that the flat bands near E_F develop with doping.

Since we are using different materials to compare the electronic structure of the CuO_2 plane at different doping levels, it is difficult to rule out other effects which might complicate the comparison. However, recent doping studies of $Bi_2Sr_2CaCu_2O_{8+\delta}$(Bi2212) provide additional evidence which supports the conclusion that a comprehensive many-body description is needed to understand the electronic structure. In Fig. 4, we present high resolution ARPES measurements performed on two Bi2212 samples with different oxygen doping levels, one near optimal doping (T_c=85K) and one underdoped (T_c=67K). In panels 4a. and 4b., we find that the FS crossing is still present along the (0, 0) to (π, π) direction as the Bi2212 sample goes from near optimal doping to underdoping. In contrast, along the $(\pi, 0)$ to (π, π) direction, displayed in panels 4c and 4d, the intensity of the peak near the Fermi energy is significantly reduced, and it no longer reaches the Fermi level.

In Fig. 5, we compare the experimental E versus **k** relationship from insulating $Sr_2CuO_2Cl_2$, optimally doped Bi2212 (T_c=85 K), and underdoped Bi2212 (T_c=67 K) along the three high symmetry directions. Along the (0, 0) to (π, π) direction, we see that the behavior for all the samples is

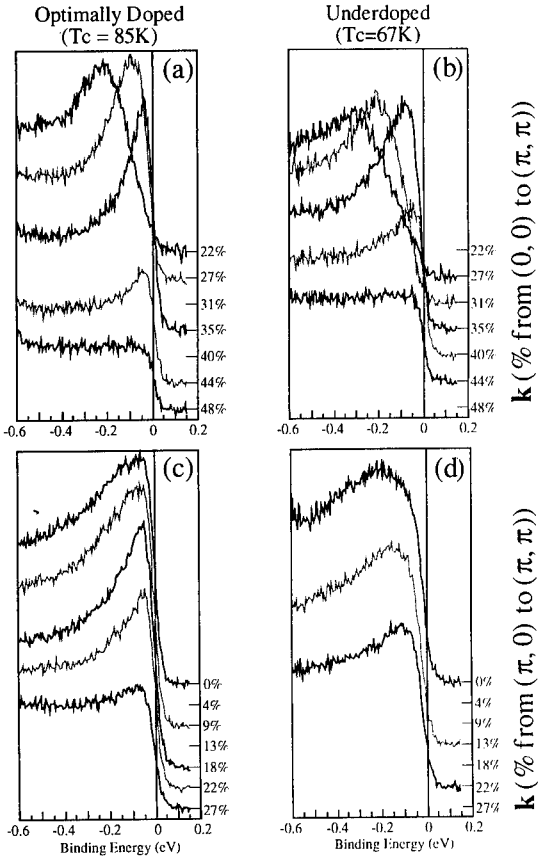


Fig. 4. APRES data from $Bi_2Sr_2CaCu_2O_{8+\delta}$(a) optimally doped (Tc=85 K) along the (0, 0) to (π, π) direction, (b) underdoped (Tc=67 K) along the (0, 0) to (π, π) direction, (c) optimally doped along the (π, 0) to (π, π) direction, and (d) underdoped along the (π, 0) to (π, π) direction.

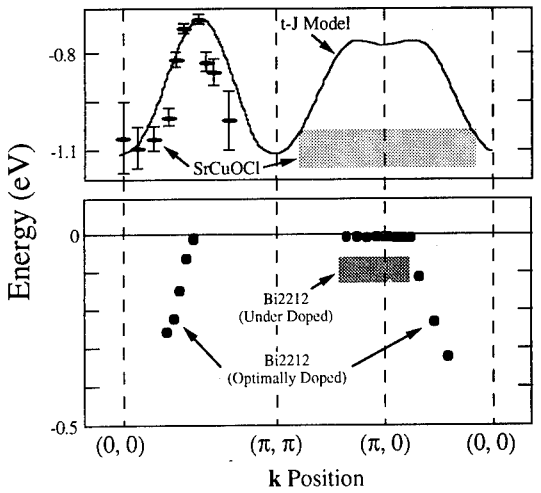


Fig. 5. The E versus **k** relationship of the experimental data from $Sr_2CuO_2Cl_2$, optimally doped $Bi_2Sr_2CaCu_2O_{8+\delta}$, and under doped $Bi_2Sr_2CaCu_2O_{8+\delta}$plotted against a calculated dispersion for the t-J model (21). Note that the band along the (0, 0) to (π, π) direction in the underdoped sample is very similar to the optimally doped case and has been omitted from the figure for clarity.

very similar except that the antiferromagnetic shadow band is only clearly visible in the insulating data. It would be difficult to detect a shift in the location of the Fermi crossing with small changes in doping since the band is very steep along this direction. Along the (π, 0) to (π, π) direction, the results from the three samples are very different. Near (π, 0), the optimally doped Bi2212 sample exhibits a flat band very close to E_F while insulating $Sr_2CuO_2Cl_2$ does not exhibit a band near E_F at all. For the underdoped Bi2212 sample, we see that the band lies farther below E_F at (π, 0) than for the optimally doped sample. This trend supports the belief that the flat band at (π, 0) grows with hole doping. Since we lose the Fermi crossing along the (π, 0) to (π, π) direction for the underdoped Bi2212 sample, it appears that the FS evolves from the large hole pocket centered at (π, π) (Fig. 1b) to the smaller hole pockets centered at (π/2, π/2) (Fig. 1a) as the hole doping is reduced, even though we can not positively identify the shadow FS because of complications arising from the background and superstructure.

We have also performed extensive angle-resolved photoemission experiments to measure the superconducting gap as function of crystal momentum. We found that the superconducting gap of Bi2212 is highly anisotropic. The gap is very small or zero along the (π, π) direction , and the gap is large at the Fermi crossings near the (π, 0) direction [30,31]. This anisotropic behavior is qualitatively consistent with either a d_x2-$_y2$ pairing state or an anisotropic s-wave theory (see contributions by Pines, Scalapino, Rice, Lee, and Anderson in this volume). The gap anisotropy has been confirmed by other groups [32,33].

More recently, Ding et al. [34] have reported new results from Bi2212 in which they claim to see a finite gap along the (π, π) direction with nodes at either side. They interpreted their data as evidence against the d_x2-$_y2$ pairing state. It is a very difficult task to quantify the gap when it is less than 5 meV since it is pushing the limits of the photoemission experiment in terms of energy and momentum resolution, sample quality (superstructure modulation, for example), and the understanding of the photoemission lineshape (normal, superconducting, and background). Our data, taken with comparable energy and momentum resolution, does not exhibit a bump in the gap along the (π, π) direction, as reported by Ding et al. We believe that all the data reported so far can be reconciled with the the d_x2-$_y2$ state, given the error bars and the fact that we do not fully understand the effects of the superstructure and the photoemission lineshape.

Recent ARPES data from insulating $Sr_2CuO_2Cl_2$ and doping dependent studies of metallic Bi2212 suggest that

shadow bands and the evolution of the band at $(\pi, 0)$ may play an important role in understanding the evolution of the Fermi surface as a function of doping. This, in addition to several problems identified using a delocalized approach to describe the metallic cuprates, suggests that a comprehensive many-body description is needed to understand the cuprate superconductors in the normal state. Some recent theoretical studies have been able to account for many aspects of our experimental results. R.B. Laughlin (see contribution this volume) has found that the dispersion of the near Fermi energy feature in insulating $Sr_2CuO_2Cl_2$agrees very well with predicted spinon dispersion. Xiao-Gang Wen and Patrick Lee [35], using slave-boson theory for the t-J model at finite doping, suggest that the evolution of the small Fermi pockets at low doping to a large Fermi surface at high doping concentrations is a natural outcome of the highly correlated many-body models.

Acknowledgements—The data presented here was obtained from the Stanford Synchrotron Radiation Laboratory (SSRL) which is operated by the DOE Office of Basic Energy Sciences, Division of Chemical Sciences. The Office's Division of Materials Science has provided support for this research. The Stanford work was also supported by NSF grant DMR-9311566 and the Sloan foundation. Beamline 5 of SSRL was built with DARPA, ONR, AFOSR, AOR, DOE and NSF support. We would like to acknowledge our colleagues, D.M. Marshall, A. Matsuura, C.H. Park, W.E. Spicer, A. Kapitulnik, M. Greven, M. Kastner, and R.J. Birgeneau for many successful collaborations which contributed to this work. We are grateful to R.B. Laughlin, Xiao-Gang Wen, and Patrick Lee for providing early access to their work.

REFERENCES

1. Olsen C. G. *et al.*, *Phys. Rev. B* **42**, 381 (1990).
2. King D. M., Shen Z.-X., Dessau D. S., Wells B. O., Spicer W. E., Arko A. J., Marshall D. S., Ratner E. R., Peng J. L., Li Z. Y. and Greene R. L., *Phys. Rev. Lett.* **70**, 3159 (1993).
3. Anderson R. O., Claessen R., Allen J. W., Olson C. G., Janowitz C., Liu L. Z., Park J.-H., Maple M. B., Dalichaouch Y., de Andrade M. C., *Phys. Rev. Lett.* **70**, 3163 (1993).
4. Dessau D. S. *et al.*, *Phys. Rev. Lett.* **71**, 2781 (1993).
5. King D. M. *et al.*, *Phys. Rev. Lett.* **73**, 3298 (1994).
6. Liu R. *et al.*, *Phys. Rev. B* **46**, 11056 (1992).
7. Campuzano J. C. *et al.*, *Phys. Rev. Lett.* **64**, 2308 (1990).
8. Massida S. *et al.*, *Physica C* **152**, 251 (1988).
9. Massidda S., Hamada N., Jaejun Yu, Freeman A. J., *Physica C* **157**, 571 (1989).
10. Novikov D. L. and Freeman A. J., *Physica C* **212**, 233 (1993).
11. Pickett W. E., Krakauer H., Cohen R. E. and Singh D. J., *Science* **255**, 46 (1992), and references therein.
12. Mazin I. I. *et al.*, *Phys. Rev. B* **45**, 5103 (1992).
13. Liu R., Veal B. W., Paulikas A. P., Downey J. W., Shi H., Olson C. G., Gu C., Arko A. J. and Joyce J., *Phys. Rev. B* **45**, 5615 (1992); *Phys. Rev. B* **46**, 11056 (1992).
14. Takahashi T., Matsuyama H., Katayama-Yoshida H., Okabe Y., Hosoya S., Seki K., Fujimoto H., Sata M., Inokuchi H., *Nature* **334**, 691 (1988); Takahashi T. in "Strong Correlation and Superconductivity" (Edited by H. Fukuyama, S. Maekawa, and A. P. Malozemoff), p. 311. Springer-Verlag, Berlin (1989).
15. See overview articles in *Physics Today* **44**(6) (1991).
16. Ong N. P., Wang Z. Z., Clayhold J., Tarascon J. M., Greene L. H. and McKinnon W. R., *Phys. Rev. B* **35**, 8807 (1987); Ong N. P., in *Phys. Prop. of the High Temperature Superconductors*, **2** (Edited by D. M. Ginsberg). World Scientific, Singapore (1990).
17. Liu R., Veal B. W., Paulikas A. P., Downey J. W., Shi H., Olson C. G., Gu C., Arko A. J. and Joyce J., *Phys. Rev. B* **45**, 5615 (1992); *Phys. Rev. B* **46**, 11056 (1992).
18. Dessau D. S., Shen Z.-X., King D. M., Marshall D. S., Lombardo L. W., Dickinson P. H., DiCarlo J., Park C.-H., Loeser A. G., Kapitulnik A. and Spicer W. E., *Phys. Rev. Lett.* **71**, 2781 (1993).
19. Gofron K. *et al.*, *Phys. Rev. Lett.* **73**, 3302 (1994).
20. Wells B. O., Shen Z.-X., Matsuura A., King D. M., Kastner M., Jepsen O., Greven M. and Birgeneau R. J., *Phys. Rev. Lett.* **74**, 964 (1995).
21. Liu Z. and Manousakis E., *Phys. Rev. B* **45**, 2425 (1992).
22. Dagotto E. *et al.*, *Phys. Rev. Lett.* **74**, 310 (1995).
23. Hanke W., see contribution this volume.
24. Uchida S. *et al.*, *Physica B* **186-188**, 975 (1993).
25. Shen Z.-X., Spicer W. E., King D. M., Dessau D. S. and Wells B. O., *Science* **267**, 343 (1995).
26. Shen Z.-X. and Dessau D. S., *Physics Reports* **253**, 1 (1995).
27. Bulut N., Scalapino D. J. and White S. R., *Phys. Rev. Lett.* **73**, 748 (1994).
28. Aebi P. *et al.*, *Phys. Rev. Lett.* **72**, 2757 (1994).
29. Chakravarty S., *Comment in Phys. Rev. Lett.* **74**, 1885 (1995).
30. Wells B. O. *et al.*, *Phys. Rev. B* **46**, 11830 (1992).
31. Shen Z.-X. *et al.*, *Phys. Rev. Lett.* **70**, 1553 (1993).
32. Yokoya T. *et al.*, *Solid State Commun.* **87**, 553 (1993).
33. Ding H. *et al.*, *Phys. Rev. B* **50**, 1333 (1994).
34. Ding H. *et al.*, *Phys. Rev. Lett.* **74**, 2784 (1995).
35. Xiao-Gang Wen and Lee P., preprint.

Pergamon

J. Phys. Chem. Solids Vol. 56, No. 12, pp. 1871–1874, 1995
Copyright © 1995 Elsevier Science Ltd
Printed in Great Britain. All rights reserved
0022-3697/95 $9.50 + 0.00

0022-3697(95)00216-2

BAND MAPPING OF THE MODEL INSULATOR $Sr_2CuO_2Cl_2$—DISPERSION OF A SINGLE HOLE IN AN ANTIFERROMAGNETIC BACKGROUND

B. O. WELLS,* Z.-X. SHEN,† A. MATSUURA,† D. M. KING,† M. A. KASTNER,* M. GREVEN* and R. J. BIRGENEAU*

* Department of Physics, Massachusetts Institute of Technology, Cambridge, MA 02139, U.S.A.
† Department of Applied Physics, Stanford University, Stanford, CA 94305, U.S.A.

Abstract—We report angle resolved photoemission measurements on $Sr_2CuO_2Cl_2$, an insulating layered copper oxide. We map the energy–momentum dispersion of the highest energy band. We find that the width of this band is consistent with calculations based on variations of the Hubbard model. The dispersion in some directions and the position of the valence band maximum at $(\frac{\pi}{2}, \frac{\pi}{2})$ match predictions of the $t-J$ model. However the overall shape of the band differs from these predictions. A comparison of our data with spectra previously reported on metallic samples leads to surprising new suggestions for the phenomenology of doping.

During the past several years there has been an extensive effort to understand the properties of the layered copper oxides. When undoped, with one hole per copper site, these materials are antiferromagnetic Mott insulators. When doped with sufficient carriers they are superconductors with very high transition temperatures. Most theories for the copper oxides are related to the Hubbard model for strongly correlated electrons. Such a correlated model is best understood for the insulating phase. The effect of adding carriers to such a model is unclear and the subject of much research. Even in the well defined undoped case it is unclear which models give an accurate description of the real materials.

Most of the PES experiments to-date have been on the metals and there has been little work on the undoped compounds [1]. We have recently reported angle resolved photoemission results on $Sr_2CuO_2Cl_2$, a carrier free layered copper oxide [2]. In this work we recap the results presented in [2], extend the comparison between the insulating and metallic copper oxides, and add to our discussion. Photoemission in $Sr_2CuO_2Cl_2$ measures the dispersion of a single hole in an antiferromagnetic background, and thus is a test of correlated models for the electronic structure of the copper oxides. We find a band width of about $2J$, as predicted by numerical calculations for the $t-J$ and single-band Hubbard models. However, the shape of this band is not well described by these calculations. We know of several recent efforts which attempt to address the differences between the current calculations for the simple correlated models and the results of our previous publication [3]. In addition, this band in $Sr_2CuO_2Cl_2$ is in many respects similar to the band that crosses E_F in the metallic copper oxides, but there is a large difference between the insulators and the metals in the states near $(\pi,0)$, the region of the van Hove singularity in the metals. The change in these states between the insulating and metallic phases of the copper oxides remains largely unaddressed theoretically.

Single crystals of $Sr_2CuO_2Cl_2$ were grown following the procedure used by Miller *et al.* [4] $Sr_2CuO_2Cl_2$ has the K_2NiF_4 structure with CuO_2 layers separated by double layers of SrCl. The material is tetragonal down to at least 10 K. Crystals grown by the identical method have a Néel temperature of 256.5 ± 1.5 K as determined by neutron scattering. Neutron scattering studies have shown that at the temperature of our experiment, 350 K, the magnetic correlation length is about 250 Å [5]. Two magnon Raman scattering measurements of Tokura *et al.* imply a nearest neighbor exchange $J = 125 \pm 6$ meV [5,6]. Doping $Sr_2CuO_2Cl_2$ with carriers has been difficult, giving us confidence that we are really studying undoped material. However, there has been a recent report of the synthesis of a closely analogous compound, $Sr_2CuO_2F_{2+\delta}$, which for large enough δ is a superconductor with $T_c = 46$ K [7].

Our experiment was performed at the undulator beam line 5 at the Stanford Synchrotron Radiation Laboratory. The spectra shown here were taken with an overall system energy resolution of 75 meV and angular resolution of the emitted electrons of $\pm 1°$, or $\pm\frac{1}{20}\pi$ in k_x and k_y. In this paper we use the notation of the two dimensional Brillouin zone for the square-planar copper oxygen sheet with a lattice parameter equal to one which has corners at $(\pm\pi, \pm\pi)$. We deduced the peak position for each spectrum using a simple fit to a Lorentzian plus a background and convolved with the experimental resolution function. The data were taken at 350 K because at this temperature the conductivity was high enough to insure that there was no charging of the sample.

The valence band spectrum of $Sr_2CuO_2Cl_2$ is very similar to the spectra for the metallic copper oxides [8,9]. Figure 1 shows the full valence band of both $Sr_2CuO_2Cl_2$ and $Bi_2Sr_2CaCu_2O_{8+\delta}$, a material for which excellent photoe-

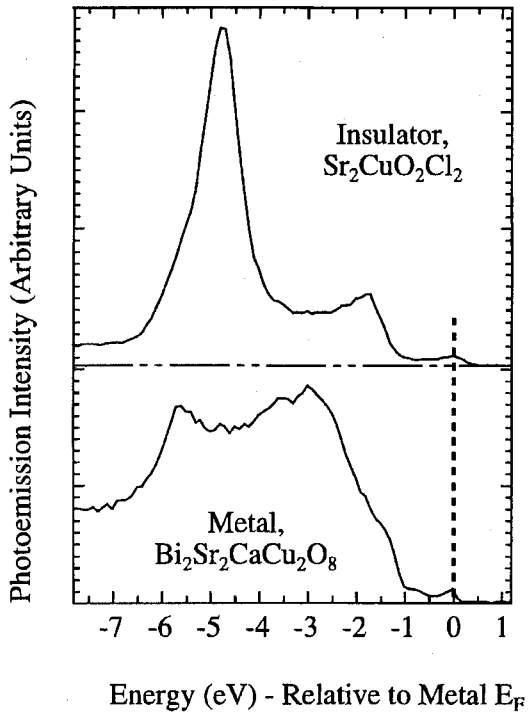


Fig. 1. Photoemission spectra taken near $(\frac{\pi}{2}, \frac{\pi}{2})$ of the entire valence band of both insulating $Sr_2CuO_2Cl_2$ and metallic $Bi_2Sr_2CaCu_2O_{8+\delta}$. The spectra are aligned so that the peaks at highest energy match and the energy scale for $Bi_2Sr_2CaCu_2O_{8+\delta}$ is used.

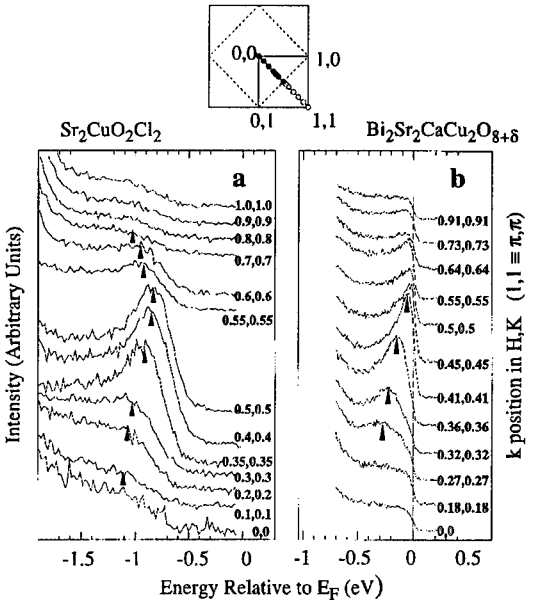


Fig. 2. PES data showing the peak dispersion along the (0,0) to (π, π) direction for insulating $Sr_2CuO_2Cl_2$ (a) and for metallic $Bi_2Sr_2CaCu_2O_{8+\delta}$ (b). The figure is labeled with (1,1) = (π, π). The circles in the legend indicate the positions where the data were taken in the insulator.

mission data are available. The spectrum for each is approximately seven electron volts wide with several intense peaks and a foot with small intensity extending over the highest electron volt of the valence band. There are no obvious new states near E_F in $Bi_2Sr_2CaCu_2O_{8+\delta}$ created by doping, in contradiction to some early work [10]. Using the more intense peaks as a rough reference energy indicates that the Fermi level for the metal has shifted into the energy region that corresponds to the top of the valence band in the insulator. As we will point out below, this does not imply a simple rigid band shift with doping. Also, the available data for the electron doped copper oxides indicate that the Fermi level for the electron-doped metal does not shift into the conduction band of the insulator [11]. All of the rest of the spectra presented in this paper show only this foot region.

Figure 2(a) shows a set of scans taken at different **k** positions along the direction from the zone center (0,0) to the antiferromagnetic superlattice position (π, π). As **k** is increased, a peak appears and shifts towards higher energies as k approaches $(\frac{\pi}{2}, \frac{\pi}{2})$. At larger **k** values there is a sudden drop in the intensity of the peak and it appears to move back to lower energies. The $(\frac{\pi}{2}, \frac{\pi}{2})$ point is the global valence band maximum (VBM). The closest that the peak approaches to the Fermi energy is approximately -0.8 eV. We measure a total dispersion of 280 ± 60 meV. For parallel cuts, the peak intensity always drops at **k** locations forming a line connecting $(\pi,0)$ and $(0,\pi)$.

Figure 2(b) shows similar data along the same direction in the square lattice Brillouin zone for the metallic copper oxide $Bi_2Sr_2CaCu_2O_{8+\delta}$ from Dessau *et al.* [9] The peaks in the metal are sharper and disappear after crossing the Fermi level near $(0.45\pi, 0.45\pi)$. The spectra are quite similar indicating that the states detected in the metal and insulator can be considered to represent fundamentally the same band, although it is altered by doping as shown below. For comparison, the measured dispersion in $Bi_2Sr_2CaCu_2O_{8+\delta}$ is 270 ± 30 meV over a **k** range from $(0.27\pi, 0.27\pi)$ to $(0.45\pi, 0.45\pi)$. Over the same **k** region we see dispersion of 240 ± 30 meV in $Sr_2CuO_2Cl_2$, which is the same within the errors.

The peak intensity drops across a line connecting $(\pi,0)$ to $(0,\pi)$, the boundary of the antiferromagnetic Brillouin zone. The weak part of the band results from a folding of the zone due to antiferromagnetic order. This drop in spectral weight is analogous to that expected for a weak coupling spin density wave model [12,13] and is also evident in calculations of the spectral weight function for models with intermediate to strong coupling strengths [13]. These states with little spectral weight are often described as ghost bands in the literature. For strong coupling we expect that the original and folded sections of the band would have nearly equal weight while for truly weak coupling we would expect a larger band width. Thus the variation in spectral weight in conjunction with the narrow observed band width could indicate that $Sr_2CuO_2Cl_2$ is in an intermediate coupling regime.

Figure 3(a) shows the peak dispersion along a line from

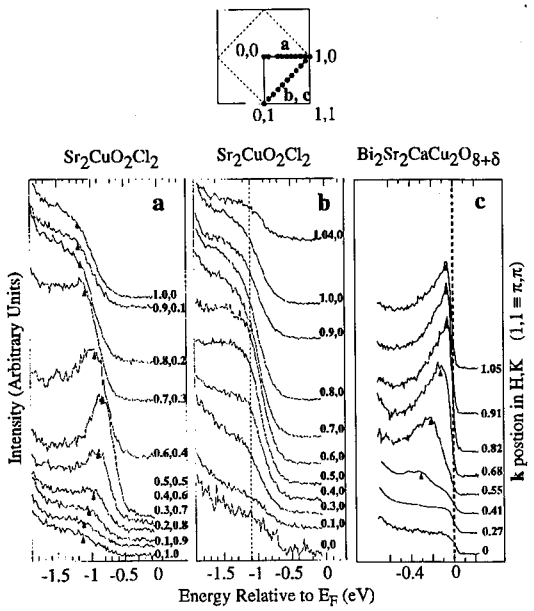


Fig. 3. PES data for $Sr_2CuO_2Cl_2$ in parts (a) and (b). The spectra in (a) are along along a line connecting $(0,\pi)$–$(\frac{\pi}{2}, \frac{\pi}{2})$–$(\pi,0)$, perpendicular to the data in figure 2a. Parts (b) and (c) compare data along the (0,0) to $(\pi,0)$ direction in $Sr_2CuO_2Cl_2$ and $Bi_2Sr_2CaCu_2O_{8+\delta}$.

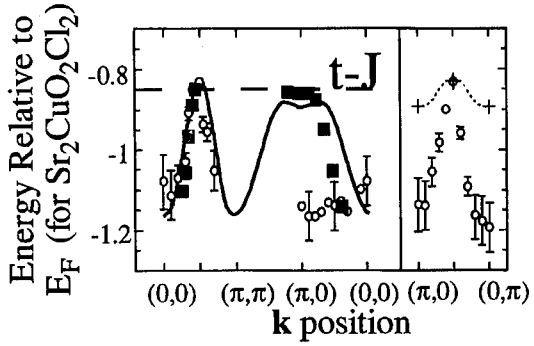


Fig. 4. A comparison of the experimentally determined E vs $\mathbf{k}$ relations of $Sr_2CuO_2Cl_2$ (open circles) and $Bi_2Sr_2CaCu_2O_{8+\delta}$ (solid squares) with a calculation for the $t--J$ model. Error bars for $Sr_2CuO_2Cl_2$ are shown when larger than the symbol size except for the region from (0,0) to $(\pi,0)$ where for clarity only some representative error bars are shown. The far right panel shows the direction along the antiferromagnetic zone edge from $(0,\pi)$ to $(\pi,0)$. Here only the points marked by a + are calculated in reference 17 and the dotted line is our interpolation between these points.

$(0,\pi)$,through $(\frac{\pi}{2}, \frac{\pi}{2})$, to $(\pi,0)$. This is perpendicular to the direction of the data in Fig. 2. From a global maximum at $(\frac{\pi}{2}, \frac{\pi}{2})$, the peak in $Sr_2CuO_2Cl_2$ disperses to lower energies in an isotropic manner. Figure 3(b) and (c) shows the band dispersion from (0,0) to $(\pi,0)$ in $Sr_2CuO_2Cl_2$ and in $Bi_2Sr_2CaCu_2O_{8+\delta}$, respectively. The data for $Bi_2Sr_2CaCu_2O_{8+\delta}$ are from Dessau *et al.* [9]. Clearly, the two materials do not behave in a similar manner in this region of the Brillouin zone. While in $Bi_2Sr_2CaCu_2O_{8+\delta}$ a peak disperses to near E_F and remains near E_F for a wide range of $\mathbf{k}$, no peak dispersion is seen in $Sr_2CuO_2Cl_2$, although there is some variation in spectral weight.

All of the hole doped compounds that have been studied with photoemission show a band at E_F over a wide region of $\mathbf{k}$-space near $(\pi,0)$. This has been described as an extended saddle point and there has been speculation that it is important to the physics of the superconductors [9,14]. Most of the weight in the density of states near E_F in the metallic copper oxides comes from this region of $\mathbf{k}$-space and this is the region where the largest superconducting gaps have been found in $Bi_2Sr_2CaCu_2O_{8+\delta}$. There are no states near the top of the band in $Sr_2CuO_2Cl_2$ at $(\pi,0)$. The states forming the extended saddle point must move up in energy as a result of doping.

In Fig. 4 the experimentally determined E vs $\mathbf{k}$ relations for both insulating $Sr_2CuO_2Cl_2$ and metallic $Bi_2Sr_2CaCu_2O_{8+\delta}$ are compared with that found for a numerical solution of one hole in a t–J model. [15] We discuss the insulator data first. For the region from (0,0) to (π,π) the t–J model provides a good description of the experimental results. However, near $(\pi,0)$ the calculation does not describe the data and we see much greater dispersion from $(\pi,0)$ to $(0,\pi)$ than the calculation predicts. The band width (W) determined by fitting the peaks over the entire region from (0,0) to $(\frac{\pi}{2}, \frac{\pi}{2})$ is 280 ± 60 meV. This corresponds to $W/J = 2.2 \pm 0.5$. The t–J model calculation that gives the curve in Fig. 4 predicts the quasiparticle bandwidth to be about $2J$ for a wide range of t/J [15]. There are other t–J model calculations that give a comparable band width [16,17]. Calculations on small clusters of the Hubbard model with intermediate U show a similarly narrow quasiparticle band width [13]. However, the disagreement near $(\pi,0)$ is still present. One-electron calculations predict a much broader band with a total occupied band width of about 1 eV at half filling, and a total band width of about 3.25 eV [18].

The comparison between the $Bi_2Sr_2CaCu_2O_{8+\delta}$ data and the t–J model calculation has been made with an energy offset in the data to fit the calculation. This is equivalent to assuming that doping holes into a t–J model produces a rigid band filling of the undoped states. For regions in the first magnetic Brillouin zone, the agreement is remarkably good. In the second magnetic zone no dispersing peaks are detected in $Bi_2Sr_2CaCu_2O_{8+\delta}$, but in analogy to the insulator we might expect to have only weak, ghost bands here. It is difficult to understand this apparent agreement between the calculation and the $Bi_2Sr_2CaCu_2O_{8+\delta}$ experiment. The t–J model is only truly defined for a single hole dispersing in an otherwise half-filled band. However, in this undoped regime the calculation does not describe the data well, as discussed above.

There are other photoemission results which appear to be consistent with ours. Liu *et al.* reported PES data on insulating, but not carrier free, $YBa_2Cu_3O_{6.35}$ [1]. They saw a strong shoulder that appeared to disperse along the (0,0) to (π,π) direction, reach a maximum at E_F near $(\frac{\pi}{2}, \frac{\pi}{2})$,

and then disappear. Although no well-defined peak was detected, the $YBa_2Cu_3O_{6.35}$ data are consistent with our results. This supports our belief that $Sr_2CuO_2Cl_2$ reveals universal behavior of planar copper oxide insulators

Aebi *et al.* have recently reported a mapping of the Fermi surface in $Bi_2Sr_2CaCu_2O_{8+\delta}$ using PES in a mode that scans across **k** space at a fixed energy [19]. They found a Fermi surface defined by peaks with large spectral weight close to that expected from the LDA calculation in addition to a Fermi surface defined by peaks with small spectral weight. The Fermi surface from the weak peaks could be derived from the strong, LDA-like Fermi surface by adding a translation of (π,π). The Fermi surface they reported is adumbrated in this work. The shifted Fermi surface defined by the weak peaks in $Bi_2Sr_2CaCu_2O_{8+\delta}$ corresponds to the regions where we found a weak band in $Sr_2CuO_2Cl_2$.

In summary, we have measured the **k** dependent single particle excitation spectra of the highest energy band in the model insulating copper oxide $Sr_2CuO_2Cl_2$. Analysis of this band indicates that a Hubbard based model may be a proper starting point to describe these materials. However, results from a single band t–J model or a single band Hubbard model do not describe the correct band shape. There is a strong variation in spectral weight as a function of **k** which reflects the antiferromagnetic order. In addition, states near $(\pi,0)$ appear to undergo large changes in energy as a function of doping. Clearly additional experimental and theoretical work is necessary to explore further the issues raised in this paper.

Acknowledgements—We would like to acknowledge helpful conversations with P. W. Anderson, V. Emery, E. Dagotto, R. B. Laughlin, P. A. Lee and D. J. Scalapino. We thank D. S. Dessau for help with the experimental set up and P. Blakeslee for assistance in characterizing the crystals. SSRL is operated by the DOE Office of Basic Energy Science, Division of Chemical Sciences. The work at Stanford was supported by DOE Division of Materials Science, NSF grant DMR9357057, and the Stanford Center for Materials Research. The work at M.I.T. was supported by NSF grants number DMR90-22933 and DMR93-15715.

REFERENCES

1. In reference 10 angle integrated data on La_2CuO_4 were reported. There is a previous angle integrated study of $Sr_2CuO_2Cl_2$; Fujimori A. *et al.*, *Phys. Rev. B* **40**, 7303 (1989). $YBa_2Cu_3O_{6.35}$ is insulating but not completely carrier free. An angle resolved study of this material is reported by Liu R. *et al.*, *Phys. Rev. B* **46**, 11056 (1992).
2. Wells B. O. *et al.*, *Phys. Rev. Lett.* **74**, 964 (1995).
3. private communications with Andersen O. K., Bulut N., Dagotto E., Gooding R. J., Laughlin R. and Reiter G.; see also the papers from Andersen O. K., Dagotto E. and Laughlin R. in these proceedings.
4. Miller L. L. *et al.*, *Phys. Rev. B* **41**, 1921 (1990).
5. Greven M. *et al.*, *Phys. Rev. Lett.* **72**, 1096 (1994); *Z. Phys. B* **96**, 465 (1995).
6. Tokura Y. *et al.*, *Phys. Rev. B* **41**, 11657 (1990).
7. Al-Mamouri M. *et al.*, *Nature* **369**, 382 (1994).
8. Olson C. G. *et al.*, *Phys. Rev. B* **42**, 381 (1990); Campuzano J. C. *et al.*, *Phys. Rev. Lett.* **64**, 2308 (1990).
9. Dessau D. S. *et al.*, *Phys. Rev. Lett.* **71**, 2781 (1993); Gofron K. *et al.*, *J. Phys. Chem. Solids* (1993).
10. Allen J. W. *et al.*, *Phys. Rev. Lett.* **64**, 595 (1990).
11. Anderson R. O. *et al.*, *Phys. Rev. Lett.* **70**, 3163 (1993).
12. Anderson P. W., private communication.
13. Bulut N., Scalapino D. J. and White S. R., *Phys. Rev. B* **50**, 7215 (1994).
14. King D. *et al.*, *Phys. Rev. Lett.* **73**, 3298 (1994).
15. Liu Z. and Manousakis E., *Phys. Rev. B*, **45**, 2425 (1992).
16. Dagotto E., *Rev. Mod. Phys.* **66**, 763 (1994).
17. Dagotto E. *et al.*, *Phys. Rev. B* **46**, 3183 (1992).
18. Jepsen O. supplied us with an unpublished LDA band calculation for $Sr_2CuO_2Cl_2$. For a review of band calculations for the high T_c materials see Pickett W. E., *Rev. Mod. Phys.* **61**, 433 (1989).
19. Aebi P. *et al.*, *Phys. Rev. Lett.* **72**, 2758 (1994).

Pergamon

J. Phys. Chem. Solids Vol. 56, No. 12, pp. 1875–1876, 1995
Copyright © 1995 Elsevier Science Ltd
Printed in Great Britain. All rights reserved
0022–3697/95 $9.50 + 0.00

0022–3697(95)00176-X

SPECTRAL WEIGHT TRANSFER AND MASS RENORMALIZATION IN LnNi$_2$B$_2$C (Ln = Y, La)

A. FUJIMORI, K. KOBAYASHI, T. MIZOKAWA, K. MAMIYA, A. SEKIYAMA
Department of Physics, University of Tokyo, Bunkyo-ku, Tokyo 113, Japan

H. TAKAGI
Institute for Solid State Physics, University of Tokyo, Roppongi, Tokyo 106, Japan

H. EISAKI, S. UCHIDA
Department of Applied Physics, University of Tokyo, Bunkyo-ku, Tokyo 113, Japan

R. J. CAVA, J. J. KRAJEWSKI, W. F. PECK, Jr
AT & T Bell Laboratories, Murry Hill, New Jersey 07974, U.S.A.

Abstract—We have studied the electronic structure of rare-earth Ni boro-carbides by high-resolution photoemission. The spectra of superconducting YNi$_2$B$_2$C and non-superconducting LaNi$_2$B$_2$C are remarkably similar in spite of large differences predicted by band-structure calculations. The disappearance of the peak in the density of states at the Fermi level is attributed to spectral weight transfer towards higher energies concomitant with the conduction-band mass renormalization.

The discovery of superconductors LnNi$_2$B$_2$C (Ln = rare earth) [1] has provided us with new opportunities to investigate problems pertinent to high-T_c cuprates as well as to conventional superconductors. Previous photoemission studies on YNi$_2$B$_2$C [2] have shown a multi-electron satellite in the valence-band spectra, indicating that the on-site Coulomb interaction at the Ni site is strong, $U \sim 4$ eV . Further, a narrow peak in th density of states (DOS) arising from flat energy bands near the Fermi level (E_F) predicted by band-structure calculations [3] is absent in the photoemission spectra [2]. In this work, we have made a comparative study of superconducting YNi$_2$B$_2$C and non-superconducting LaNi$_2$B$_2$C in order to gain further insight into the electronic states in these materials.

Figure 1 shows the valence-band photoemission spectra of both materials taken with a resolution of ~ 40 meV. In the figure the spectra are compared with the DOS given by the band-structure calculations [3,4] taking into accout photoionization cross sections, instrumental resolution and thermal and life-time broadening. The calculated DOS shows a sharp peak at (Ln = Y) or slightly below (Ln = La) E_F whereas the measured spectra show an ordinary Fermi edge without additional structures near it. The temperature dependence of the near-E_F spectra (20 K < T < 300 K) is simply described by that of the Fermi-Dirac distribution function. In going from Ln = Y to Ln = La, the Ni 3d band centered at ~1.5 eV is slightly (~ 0.1 eV) shifted towards higher binding energy whereas the calculated DOS shows a large shift of ~ 0.4 eV in the opposite direction. These results indicate that the electronic structure of the Ni boro-carbides are influenced by those effects which are not included in the band-structure calculations such as electron–phonon interaction and electron–electron correlation.

We point out that a similar discrepancy between band theory and experiment exists for A15-type superconductors: The spectra of Nb$_3$Al show a simple Fermi edge [5] while band-structure calculation shows a sharp DOS peak at E_F [6]. Meanwhile, angle-resolved photoemission of V$_3$Si has revealed flat bands just below E_F, in agreement with the band-structure calculation [7]. This indicates that the disappearance of the DOS peak is not due to the disappearance of the flat bands themselves but to a transfer of spectral weight from the flat bands to away from E_F. In high-T_c cuprates, too, the existence of flat bands near E_F has been demonstrated by angle-resolved photoemission [8] but no peak has been found in the angle-integrated photoemission spectra. The disappearance of a DOS peak in the photoemission spectra has also been pointed out for Ba$_{1-x}$K$_x$BiO$_3$ [9].

According to Fermi-liquid theory, the suppression of photoemission intensity at E_F compared to the calculated DOS is given by a factor m_k/m_b, where m_k is the k-mass, which is derived from the momentum dependence of the self-energy [10,10], and m_b is the bare band mass; spectral weight transfer from the coherent quasi-particle excitations near E_F to incoherent excitations away from E_F results in the reduction of the coherent spectral weight by a factor m_ω/m_b, where m_ω is the ω-mass [10,10]. Since our results show $m_k \sim (0.3 - 0.5)m_b$ for the Ni boro-carbides and the thermal mass $m^* \equiv m_k m_\omega/m_b$ is enhanced by a factor of ~2 compared to m_b [11], we obtain $m_\omega \sim 5m_b$, meaning

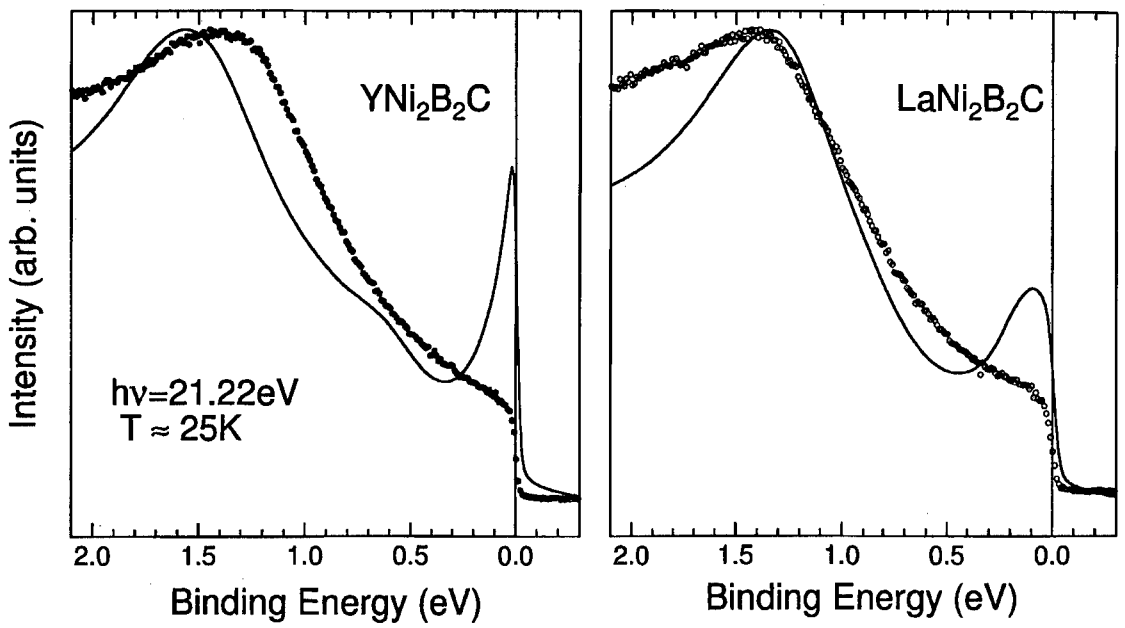


Fig. 1. Photoemission spectra of YNi_2B_2C and $LaNi_2B_2C$ (dots) compared with the DOS given by the band-structure calculations (solid curve) of Mattheiss *et al.* [3,4].

that ~ 80% of the spectral weight is transferred from the coherent part to the incoherent part of the spectral function. The energy scale of the spectral weight transfer is large, at least ≈ 0.5 eV. Therefore, it may be difficult to explain this as due to electron–phonon interaction or spin fluctuations and electron–electron interaction may have to be involved in the microscopic origin of the spectral weight transfer. This problem remains to be clarified in future studies.

Acknowledgements—We would like to thank L. F. Mattheiss for providing the results of the band-structure calculations and S. Shin for useful discussions. This work is supported by a Grant-in-Aid for Scientific Research from the Ministry of Education, Science and Culture of Japan and by the New Energy and Industrial Technology Development Organization (NEDO).

REFERENCES

1. Cava R. J. *et al.*, *Nature* **367**, 252 (1994).
2. Fujimori A. *et al.*, *Phys. Rev. B* **50**, 9660 (1994); Golden M. S. *et al.*, *Europhys. Lett.* **28**, 369 (1994).
3. Mattheiss L. F., *Phys. Rev. B* **49**, 1327 (1994).
4. Mattheiss L. F., Siegrist T. and Cava R. J., *Solid State Commun.* **91**, 587 (1994).
5. Grioni M. *et al.*, *Phys. Rev. B* **43**, 1216 (1991).
6. Mattheiss L. F. and Weber W., *Phys. Rev. B* **19**, 1734 (1979).
7. Aono M., Himpsel F. J. and Eastman D. E., *Solid State Commun.* **39**, 225 (1981).
8. Dessau D. S. *et al.*, *Phys. Rev. Lett.* **71**, 2781 (1993).
9. Namatame H. *et al.*, *Phys. Rev. B* **50**, 13674 (1994).
10. Inoue I. H. *et al.*, *Phys. Rev. Lett.* **74**, 2539 (1995).
11. Takagi H., unpublished.

Pergamon

J. Phys. Chem. Solids Vol. 56, No. 12, pp. 1877–1878, 1995
Copyright © 1995 Elsevier Science Ltd
Printed in Great Britain. All rights reserved
0022-3697/95 $9.50 + 0.00

0022-3697(95)00096-8

SUPERCONDUCTING GAP OBSERVATION BY HIGH-RESOLUTION PHOTOELECTRON YIELD SPECTROSCOPY

S. GONDA * M. KAWASAKI, *,† S. OHASHI, * Y. KOTAKA, ‡ K. KISHIO ‡ and H. KOINUMA *

* Research Laboratory of Engineering Materials, Tokyo Institute of Technology, Japan
† PRESTO-JRDC, Nagatsuta 4259, Midori-ku, Yokohama 226, Japan
‡ Faculty of Engineering, University of Tokyo, Hongo, Bukyo-ku, Tokyo 113, Japan

Abstract—We designed and constructed a cryogenic photoelectron yield spectroscopy having high resolution (≈ 10 meV) and wide dynamic range (≈ 10^7). The yield spectra taken for $Bi_2Sr_2CaCuO_y$ (BSCCO)single crystals at 10 K showed a dip structure in the vicinity of the Fermi level. The measured data could be well fitted with a curve simulated from the BCS function with a gap value of 20 meV.

For elucidating the electronic structure and the pairing mechanism in high T_c superconductors, extensive studies using photoemission spectroscopy have been carried out[1–3]. Conventional pho toelectron spectroscopic tools such as XPS and UPS, however, suffer from poor energy resolutions and low signal to noise ratios. These problems make it difficult to judge by XPS and UPS whether *s*- or *d*-wave symmetry resides in the superconducting wave function. Thus, we are tempted to develop an alternative technique for pho toemission spectroscopy. Photoelectron yield spectroscopy (PYS), where the yield of photoemission caused by the irradiation on monochromated UV light is measured as a function of photon energy, was proved to have such a high signal to noise ratio 10^{10} [4] and a high resolution as $\Delta E <$ 100meV [5] for the analyses of metals and semiconductors. By designing and constructing a cryogenic PYS with higher resolution [6], we have investigated the possibility of observing superconducting gaps (≈ 20 meV) in high-T_c superconductors.

UV light ($3.5 < h\nu < 6.2$ eV) from a Xe lamp was monochromated by a double pass monochromator (f=25 cm) and irradiated on a sample surface set on the cryostage in the UHV chamber. All the photoelectrons regardless of the kinetic energy, emitted from the sample, were detected by a channeltron placed just above the sample surface. Scanning the light from the longer wavelength side gave the spectrum corresponding to the integrated occupation of density of states which have energies as deep as the photonenergy from the vacuum level.

First we show the spectra taken for (111) surface of Ag film deposited *in situ* on an as-cleaved graphite substrate in order to evaluate the energy resolution of our system. Fig. 1(a) shows PYS of the Ag film measured at an emission angle normal to the surface (0°) at temperatures of 280, 80, and 10 K. From the Fowler plot ($Y^{1/2}$ vs $h\nu$) for these data, the work function of Ag (111) surface is evaluated to be 4.23 eV, which agrees well with the value (4.25 eV) in literature [7]. The sharp threshold of photoemission at E_F indicates the metallic nature of electronic structure and sharp Fermi cut-off. It is noteworthy that the tail of PYS for the photon energies $h\nu < E_F$ diminishes rapidly as the temperature decreases. Since the tail corresponds to the population of electrons excited above E_F by the thermal energy, the integration of Fermi–Dirac distribution function at each temperature should fit to the observed data. Indeed, the experimental data were well fitted with the curves calculated by assuming the resolution of our system to be 10 meV. This resolution, the highest among the values ever reported, was achieved primarily by the high UV-light source.

A single crystal of BSCCO (4 × 4 × 0.5mm, T_c(zero) =84 K) grown by a floating zone method was cleaved in high vacuum (2×10^{-11} Torr) along the *ab*-plane just prior to the PYS measurement. Fig. 1(b) shows PYS of BSCCO measured by irradiating the monochromated UV-light to the surface with an incident angle of 25° and by collecting electrons emitting at an angle of 20° along (110) (Cu–O bond) direction. Spectra at 280 K and 80 K showed a clear cut-off at E_F (4.40 eV below the vacuum level) and could be well fitted with the curves calculated as described above, suggesting a clear appearance of Fermi surface. At 10 K, considerable deviation from the calculated curve was observed at 30 meV below the E_F and the spectrum merged again to the calculated curve above the E_F. Such dip structure in the photoelectron yield just below the E_F was reproducibly observed and to verify by the presence of a gap in the density of states, presumably superconducting gap. Assuming the BCS superconducting mechanism, the PYS curve was calculated by integrating the BCS function, and by taking into account the equipment resolution of 10 meV for a temperature of 10 K and gap values of 5, 10, 15, and 20 meV. As indicated in Fig. 1(b), the curve calculated for Δ=20 meV reproduced well beginning of dip structure. The considerable amount of residual states observed in the gap may originate from adsorped impurities on the surface during the measurement.

In summary, we have demonstrated that the cryogenic

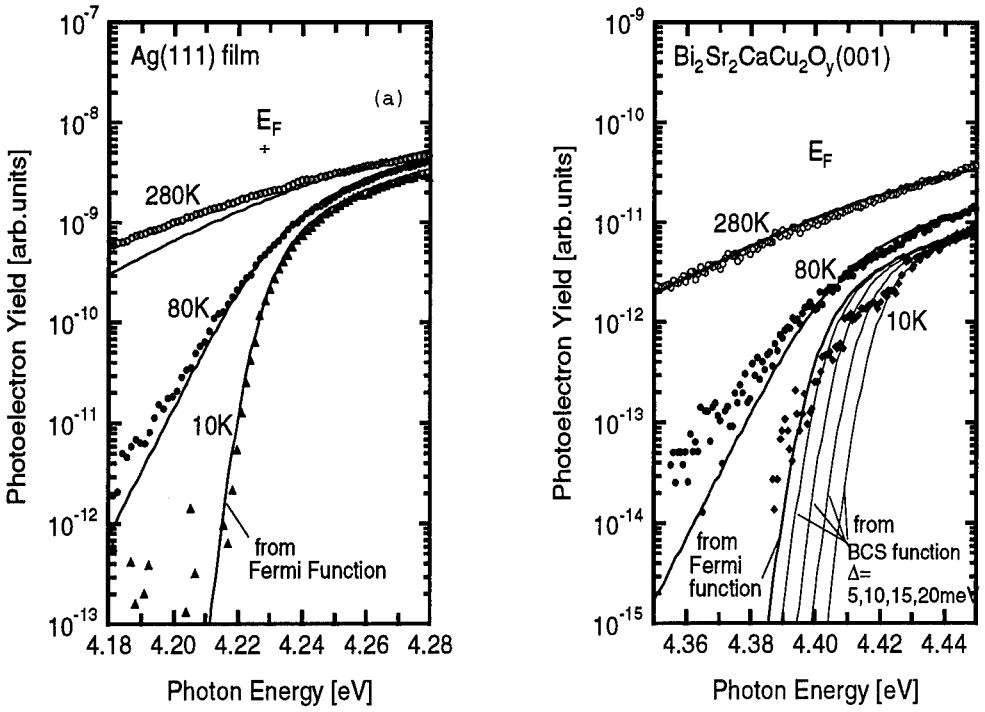


Fig. 1. Photoelectron yield spectra of (a) Ag film and (b) cleaved $Bi_2Sr_2CaCu_2Oy$ single crystal measured at 280 K, 80 K, and 10 K. The Fermi level is marked by the vertical tick. The dashed curves are simulation based on the Fermi distribution function. The solid curves in (b) are simulation from the BCS function at 10 K with gap values of 5, 10, 15 and 20 meV.

PYS is capable of probing the electronic structure close to E_F with a high resolution (10 meV) and a wide dynamic range (10^7). We observed a dip structure in PYS of BSCCO and assigned it to the superconducting gap of 20 meV.

Acknowledgements—This work was partly supported by a Grant-in-Aid for Scientific Research from the Ministry of Education and Iketani Science and Technology Foundation.

REFERENCES

1. Imer J. M. *et al., Phys. Rev. Lett.* **62**, 336 (1989).
2. Olson C. G. *et al., Science* **245**, 731 (1989).
3. Dessau C. G. *et al., Phys. Rev. Lett.* **66**, 2160 (1991).
4. Winer K. and Ley L., *Amorphous Silicon and Related Materials*, ed. H. Frtzche (World Scientific, 1989), p. 365.
5. Schäfer J. *et al., Rev. Sci. Instrum.* **64**, 653 (1993).
6. Gonda S. *et al., Mater. Res. Soc. Symp. Proc.* **349** (4–8 April, 1994, San Francisco), p. 325.
7. Valette G., *Electoanal. Chem.* **139**, 285 (1982).

Pergamon

J. Phys. Chem. Solids Vol. 56, No. 12, pp. 1879–1880, 1995
Copyright © 1995 Elsevier Science Ltd
Printed in Great Britain. All rights reserved
0022–3697/95 $9.50 + 0.00

0022-3697(95)00142-5

THE 1 eV PEAK: A CONSISTENT FEATURE OF THE CUPRATE SUPERCONDUCTORS

C. G. OLSON * J. G. TOBIN † G. D. WADDILL ‡ D. W. LYNCH * J. Z. LIU §

* Ames Laboratory and Dept. of Physics and Astronomy, Iowa State University, Ames, IA, U.S.A.
† Lawrence Livermore National Laboratory
‡ University of Missouri-Rolla
§ University of California-Davis

Abstract—We report data supporting the view that the sometimes controversial 1 eV peak in the angle-resolved photoemission spectrum of $YBa_2Cu_3O_{6.9}$ is, in fact, representative of cuprate superconductors. Detailed spectra for $YBa_2Cu_3O_{6.9}$ show that the peak is composed of a family of initial states of both even and odd symmetry.

The "1 eV peak" in $YBa_2Cu_3O_{6.9}$ photoemission spectra continues to be a topic of discussion because of its possible origin as a surface state. The termination dependent layer calculations of Bansil *et al* [1] predict surface states that might explain why angle-resolved photoemission does not see the superconducting gap in YBCO. The surface state model of Liu and Klemm [2] addresses the question of the measured gap isotropy/anisotropy in $Bi_2Sr_2CaCu_2O_8$. We have previously concluded that the 1 eV structure was inherent to the bulk, and arose from well defined dispersive states at the top of the parent insulator valence band [3]. These conclusions were driven by the observation that the structure(s) were pervasive throughout the zone, that they were durable with time and nonreactive gas exposure, and that they persisted through a variety of surface terminations as characterized by Ba core level shifts. In this note we would like to point out that the structures are a consistent feature in the cuprate superconductors, and that the peak comes from multiple states with well defined symmetries.

Representative spectra for four materials from three of the classic cuprate superconductor systems are shown in Fig. 1. All spectra are taken at equivalent zone boundary points: X or Y for (Y,Lu)$Ba_2Cu_3O_{6.9}$, and M for $Bi_2Sr_2CaCu_2O_8$ [4] and $Nd_{1.85}Ce_{0.15}CuO_4$ [5]. Different photon energies are used because of the large matrix element effects pointed out in the next figure. Not shown, the insulator $Sr_2CuO_2Cl_2$ also has a well-defined valence band local maximum feature at the M point [6]. These similarities reinforce the view that these structures are inherent to the largely copper–oxygen bulk valence band and do not result from a specific termination layer.

These structures can be studied in detail in the YBCO materials, perhaps because of the higher crystalline quality achieved in these samples. Figure 2 shows the upper part of the valence band at the X/Y point as a function of photon energy and emission geometry. These spectra were taken on the ISU/MSU ERG-Seya beamline at Aladdin [7], where the photon polarization from the Seya is nearly 100%.

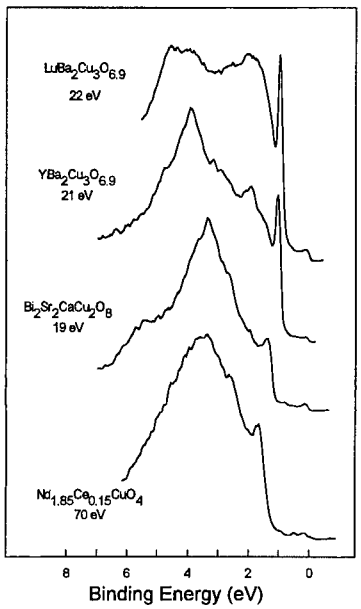


Fig. 1. Angle-resolved photoemission spectra of representative cuprate superconductors at equivalent zone boundary points.

Twinned samples were mounted with the a/b axes in the plane of polarization, and spectra were taken at equivalent zone boundary points both in (upper curves) and out (lower curves) of the plane of polarization. The spectra have been normalized to incident flux, with the 24 eV spectra shown at half scale and the 28 eV spectra magnified by a factor of two as noted. A twinned sample was used so that equivalent crystal geometries would be sampled in both directions. The effect of using twinned samples can seen in the top curve of the 17 eV spectra. From our previous study of untwinned samples, we know that the sharp Fermi level peak is the saddle point at the Y point, and the underlying strength which is also seen as a shoulder at slightly greater binding energy, is the emission from the X point [3].

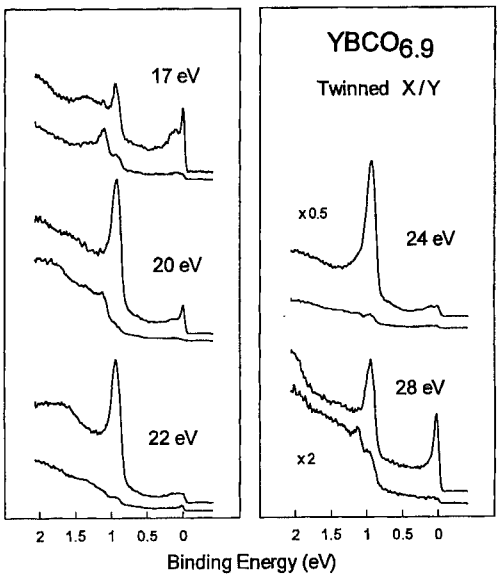


Fig. 2. Angle-resolved photoemission spectra of twinned $YBa_2Cu_3O_{6.9}$. The X/Y direction is in the plane of polarization of the light, and at each photon energy the upper curve is emission in the plane and the lower curve is emission out of the plane of polarization.

Three things are very clear. First, all structures show strong photon energy matrix element effects. This is still true at the 70 eV photon energy used for $Nd_{1.85}Ce_{0.15}CuO_4$ in Fig. 1. Second, since the two mirror plane emission geometries sample different initial state symmetries, we know that the saddle point at the Fermi level and the lowest binding energy state at 1 eV have the same symmetry even though their strengths do not track because of differing matrix elements. Third, since the out of plane emission suppresses that initial state, we can see that there is a second set of states at slightly greater binding energy. This is particularly clear at 17 and 28 eV.

This data reinforces the view [3] that the so called "1 eV peak" is in fact multiple initial states in general parts of the zone that become degenerate and sharpen at the zone boundaries. Selection rules and strongly varying matrix elements allow specific states to become dominant features of an angle resolved photoemission spectrum under specific conditions with high quality crystalline samples. The significance of Fig. 2 is in its message on the importance of a full sampling of the large parameter space of ARUPS in order to get a complete picture.

Acknowledgements—The Ames Laboratory is operated by Iowa State University for the U.S. DOE under Contract No. 7405-ENG-82. The Synchrotron Radiation Center is supported by NSF under Contract No. DMR8601349.

REFERENCES

1. Bansil A., Lindroos M., Gofron K. and Campuzano J. C., *J. Phys. Chem. Solids* **54**, 1185 (1993); and Bansil A. *et al.*, this meeting.
2. Liu S. H. and Klemm R. A., *Phys. Rev. Lett.* **73**, 1019 (1994).
3. Tobin J. G., Olson C. G. *et al.*, *Phys. Rev. B* **45**, 5563 (1991) and Olson C. G., Tobin J. G. *et al.*, *J. Phys. Chem. Solids* **52**, 1419 (1991).
4. From the data set of: Olson C. G., Liu R. *et al.*, *Solid State Commun.* **76**, 411 (1990).
5. From the data set of: Anderson R. O. *et al.*, *Phys. Rev. Lett.* **70**, 3163 (1993).
6. Schmidt M., Benning P. J., Olson C. G., Miller L. L. and Lynch D. W., preprint.
7. Olson C. G., *Nuclear Inst. Meth. in Physics Res. A* **266**, 205 (1988).

Pergamon

J. Phys. Chem. Solids Vol. 56, No. 12, pp. 1881–1882, 1995
Copyright © 1995 Elsevier Science Ltd
Printed in Great Britain. All rights reserved
0022-3697/95 $9.50 + 0.00

0022-3697(95)00108-5

OBSERVATION OF BAND DISPERSION IN YNi_2B_2C

D. M. POIRIER, C. G. OLSON, D. W. LYNCH, M. SCHMIDT,[1] B. K. CHO and P.C. CANFIELD
Ames Laboratory and Department of Physics and Astronomy, Iowa State University, Ames, IA 50011, U.S.A.

Abstract—We report the first angle resolved photoemission spectroscopy (ARPES) study of single crystals of a borocarbide superconductor. In the normal state, there is clear evidence of dispersion within the manifold of Ni 3d features between ~ 1 and 3 eV binding energy. Dispersive features were also observed within ~ 1 eV of the Fermi level (E_F) near the Γ and Z points of the bulk Brillouin zone. Resonant photoemission indicates partial Ni character for these states. An E_F crossing occurs at a k-space position that is consistent with a predicted hole pocket centered on the G_1 point of the reciprocal lattice. In the photon energy range used (17–200 eV), symmetry points in multiple Brillouin zones were consistently located assuming a free electron final state.

Keywords: YNi_2B_2C, superconductor, angle resolved photoemission.

Band structure calculations for YNi_2B_2C, and related borocarbide superconductors predict an electronic density of states (DOS) peak at the Fermi level that is about 50% Ni-derived [1–4]. However, a corresponding spectral feature was absent in angle integrated photoemission studies of scraped YNi_2B_2C polycrystals [5,6]. It was suggested that correlation effects shift spectral weight away from E_F, but the details of energy dispersion and the extent of modification from a local density approximation picture remained open questions. Here, we show significant variation in the angle resolved spectra of cleaved YNi_2B_2C single crystals and delineate a portion of the near E_F dispersion. Full experimental details will be given in a future paper.

Symmetry points in multiple Brillouin zones were located for both (110) and (100) cleaves allowing an accurate determination of the surface normal and indicating that a free electron final state dispersion and an inner potential of V_0=12.4 eV could be assumed. Figure 1 shows a series of spectra at varying photon energies taken with the detector positioned $\theta = 20°$ from the surface normal. The energy resolution was 0.2 eV and the analyzer acceptance was 2°. A pronounced peak observed at ~ 0.5 eV is attributed to a dispersing state which makes its closest approach to E_F at the Z point in this cut through the Brillouin zone. A corresponding band appears at a binding energy of 0.547 eV at Z in the calculation of ref. [1]. While this feature could be located in at least six different experimental geometries, it was not observed in normal emission from the (100) surface at the appropriate photon energy, nor for any electron momentum vector in the *ac* plane. This suggests even symmetry for the state about the *ac* plane since free electron final states in this plane would be even and transitions would then be symmetry forbidden [7].

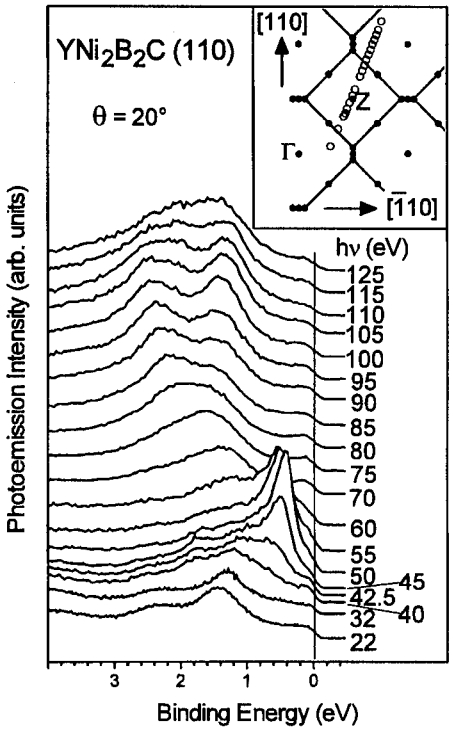


Fig. 1. ARPES spectra of the YNi_2B_2C valence band region as a function of photon energy. A distinct peak appears at a binding energy of 0.5 eV as the momentum varies through the Z point of the Brillouin zone. The momentum space path traversed by the data is shown in the inset using the periodic zone scheme. Symmetry points are indicated with solid dots, lines indicate zone boundaries, and the Fermi momentum for each spectrum is plotted with an open circle.

While Fig. 1 shows spectra in the $k_z = 0$ plane for the (110) surface, Fig. 2 shows data in the $k_z = 0.65\text{Å}^{-1}$ plane (~ 1/2 of a zone up along k_z). Here, the Γ point is encoun-

[1] Current address: Forschungszentrum Karlsruhe, INFP, Karlsrhue, Germany.

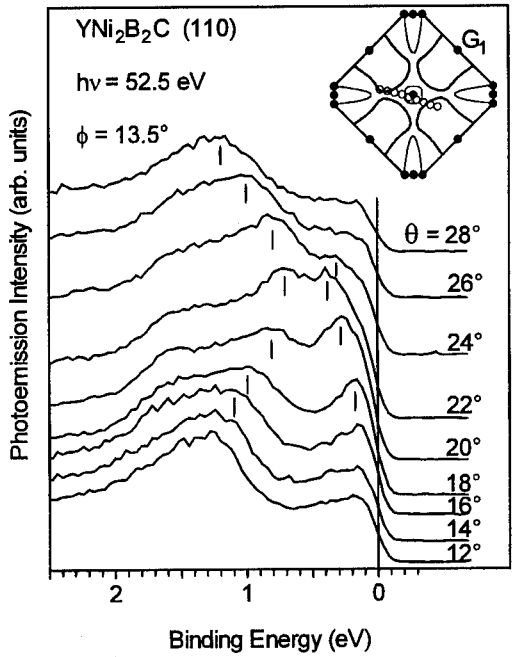


Fig. 2. ARPES spectra showing a feature with 0.4 eV binding energy near Γ dispersing to E_F. A crossing in this part of the zone corresponds with a predicted hole pocket centered on the G_1 point. Symbols are as in Fig. 1, but the calculated Fermi surfaces of ref. [1] have been added. Thin (thick) lines indicate electron (hole) surfaces.

tered at $\theta \sim 22°$ for the photon energy used. The spectra show a feature with binding energy of 0.4 eV at Γ dispersing toward the Fermi level with variations in θ. A band corresponding to the observed feature was calculated to have a binding energy of 0.535 eV at Γ. Decreases in the emission intensity at $\sim 25°$ and $\sim 15°$ suggest that the feature moves across E_F. Calculated Fermi surfaces from Ref. [1], shown in the inset of Fig. 2, predict E_F crossings very near those observed experimentally. A second feature in Fig. 2 disperses from 0.7 eV to higher binding energy away from Γ. This feature corresponds to a band calculated to intersect Γ at 0.861 eV binding energy. The experimental features are thus consistently found at lower binding energies than the calculated bands, with discrepancies of ~0.1 eV within 1 eV of E_F. The calculated and observed $E(k)$ behavior is quite similar, but a contraction of the calculated bands toward E_F would further improve the agreement. Spectral features corresponding to several bands calculated to cross E_F were not discerned. This may be the result of unfavorable photoionization matrix elements at the photon energies required to obtain the desired electron momentum vectors. In particular, a flat band calculated to lie just at E_F at Γ, which contributes largely to the calculated DOS peak was not clearly detected. New features were not observed when the projection of the polarization vector on the *c*-axis was changed from zero to 0.7 by rotating the sample 90°.

A spectral feature not accounted for in band calculations appeared 6.6 eV below the main Ni 3d manifold for photon energies above the Ni 3p absorption threshold. We attribute this peak, as in refs [5] and [6], to a final state with two 3d holes resulting when a 3d electron relaxes to fill a 3p core hole and the excess energy ejects a second 3d electron. Overlap of the $n = 3$ shell wavefunctions drives this process as well as resonant photoemission (one hole final state) of the Ni 3d valence electrons. Resonant PES was used to test the parentage of the states in the vicinity of E_F with photon energies swept through the Ni 3p edge. In agreement with ref. [5], the near E_F emission exhibited an intensity increase at the Ni 3p threshold suggesting at least partial Ni character for these states.

In conclusion, we observed dispersing electronic states near E_F in YNi_2B_2C. The states are at least partially Ni-derived. Spectral features corresponding to all predicted bands were not observed, but the observed features showed dispersion in reasonable agreement with calculation. A minor importance of electron correlation effects is suggested. Unfavorable matrix elements for remaining bands may explain the lack of a peak at E_F in angle integrated PES studies.

Acknowledgements—We gratefully acknowledge the authors of Ref. [5] for sharing their results prior to publication. The ARPES measurements were performed at the Synchrotron Radiation Center which is supported by the NSF under contract No. DMR8601349. Ames Laboratory is operated for the U.S. Department of Energy by Iowa State University under Contract No. W-7405-ENG-82.

REFERENCES

1. Lee J. I. *et al.*, *Phys. Rev. B* **50**, 4030 (1994); Min B. I., private communication.
2. Pickett W. E. and Singh D. J., *Phys. Rev. Lett.* **72**, 3702 (1994).
3. Mattheiss L. F., *Phys. Rev. B* **49**, 13279 (1994).
4. Coehoorn R., *Physica C* **228**, 331 (1994).
5. Golden M. S., *et al.*, *Europhys. Lett.* **28**, 369 (1994).
6. Fujimori A. *et al.*, *Phys. Rev. B* **50**, 9660 (1994).
7. Hermanson J., *Solid State Commun.* **22**, 9 (1977).

Pergamon

J. Phys. Chem. Solids Vol. 56, No. 12, pp. 1883–1884, 1995
Copyright © 1995 Elsevier Science Ltd
Printed in Great Britain. All rights reserved
0022-3697/95 $9.50 + 0.00

0022-3697(95)00109-3

PHOTOEMISSION SPECTROSCOPY OF $Cu_{1-x}Ba_2Ca_{n-1}Cu_nO_{2n+4-\delta}$ CERAMICS AND THIN FILMS

N. TERADA, K. TOKIWA, H. OZAWA, A. IYO, S. ISHIBASHI and H. IHARA
Electrotechnical Laboratory, 1-1-4 Umezono, Tsukuba, Ibaraki 305, Japan

Abstract—X-Ray photoemission spectroscopy has been performed on $Cu_{1-x}Ba_2Ca_{n-1}Cu_nO_{2n+4-\delta}$ ceramics and epitaxial films. A considerable oxygen loss from the vicinity of ($BaO/CuO_y/BaO$) blocking layers has been observed even on the *in situ* measured films or the ceramics just scraped in vacuum. A heat treatment under 100% O_3 beam is useful to develop their intrinsic surfaces. Binding energy of constituents of the treated samples are similar to those of Tl system superconductors.

Keywords: $Cu_{1-x}Ba_2Ca_{n-1}Cu_nO_{2n+4-\delta}$, XPS, O_3.

1. INTRODUCTION

Cu-system superconductor, $Cu_{1-x}Ba_2Ca_{n-1}Cu_nO_{2n+4-\delta}$, is characterized as a coexistence of a high superconducting critical temperature T_c of 117 K in case of n=4 and the lowest anisotropy in transport properties among high temperature superconductors (HTSC) with $T_c > 100$ K [1]. A key parameter for the latter seems to be a local structure of its "single CuO_y blocking layer" sandwiched with Ba–O planes, such as oxygen concentration in it. In their X-ray structure refinements, some ambiguities still remain, especially in oxygen-site-occupancy in the CuO_y and Ba–O planes [2]. For surfaces of most of superconducting cuprates, serious chemical degradation by air-exposure, and significant oxygen-loss in vacuum environments have been observed. From fundamental and application points of view, therefore, investigation of its surface nature and development of preparation techniques of their intrinsic surfaces are desired. In this study, X-ray photoelectron spectroscopy (XPS) has been performed on $Cu_{1-x}Ba_2Ca_{n-1}Cu_nO_{2n+4-\delta}$ (n = 3–5) ceramics and epitaxial thin films. The effect of annealing in pure O_3 beam has also been examined to develop "clean surfaces" of them.

2. RESULTS AND DISCUSSION

CO_3-free superconducting ceramics were prepared by sintering at 1150° under a pressure about 4 GPa. Thin film samples with c-axis preferred orientation were epitaxially grown by multi-target sputtering in layer-by-layer manner. Details of sample preparations were reported in our previous papers [3][4]. Absence of impurity-phase and epitaxial growth of them were confirmed by X-ray and reflection electron diffractometry. For both kinds of the samples with various number n of CuO_2 sheets in unit cell, a- and c-axis parameters agreed with reported data. Surfaces of ceramics samples were primarily cleaned by scraping in vacuum prior to spectroscopy. Film samples were characterized by *insitu* measurements. XPS has been performed at room temperature. After this measurement, in order to improve their surface nature, vacuum annealing up to 400° was applied under an incidence of 100% O_3 beam with flux $> 1 \times 10^{15} cm^{-2}\ sec^{-1}$.

Table 1. Summary of core emission spectra of $Cu_{1-x}Ba_2Ca_{n-1}Cu_nO_{2n+4-\delta}$ ceramics and thin films

	Cu $2p_{3/2}$ ($2p3d^9$) /($\underline{2p}3d^{10}\underline{L}$)	$Ba4d_{5/2}$	$Ba3d_{5/2}$	Ca 2p
As-grown films & scraped ceramics	0.25	88.8–89.0	779.0	345.6
O_3 treated	0.33	87.8–88.0	778.4	345.5
$Tl_2Ba_2CaCu_2O_8$	0.34	87.9	778.3	345.6, 344.4

All of the film samples showed, only physically absorbed CHx and O_2, of which there was little; for example, intensity of absorbed oxygen peak around binding energy of 531 eV was less than 5% of the intrinsic one. As described below, each of core emission spectra of the as-grown films was consist of almost single component. These surfaces were, therefore, fairly clean. Core emission signals of the ceramics just after the scraping were quite similar to the as-grown film, with an exception that peak-intensities of the absorbed species were stronger because of existence of grain boundaries. After the O_3 treatment, the absorbed species were close to our detection limit on the both kinds of the specimens. Therefore, the two kinds of the samples are not distinguished in discussion of core signals of other constituents.

Before the O_3 treatment, the Cu $2p_{3/2}$ core emission peak corresponding to $\underline{2p}3d^{10}\underline{L}$ (L: hole in ligand) final states was rather narrow. Relative intensity of a peak of $2p3d^9$ to $\underline{2p}3d^{10}\underline{L}$ was about 0.25, which was remarkably low in comparison with the value about 0.35 of well-oxidized HTSC [5]. For the samples both before and after the treatment, Ba 4d doublet was almost consist of single component. It means

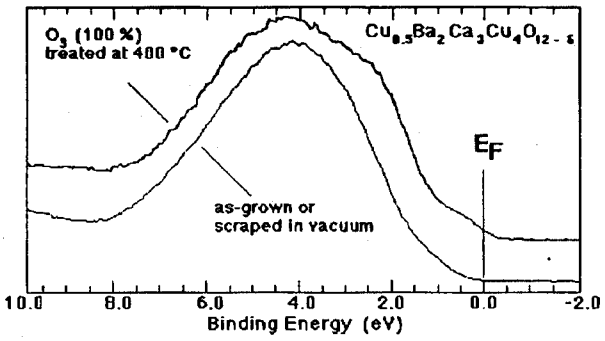


Fig. 1. Comparison of valence band spectra measured on $Cu_{1-x}Ba_2Ca_{n-1}Cu_nO_{2n+4-\delta}$ before and after the O_3 treatment.

that surface-reactions should be negligible. In as-grown or just scraped states, however, Ba $4d_{5/2}$ peak positioned at binding energy of 88.8–89.0 eV. It was much higher than that of Tl system superconductors which have structural similarities to the Cu system [6]. This value coincided with that of tetragonal phase of $YBa_2Cu_3O_{7-\delta}$ ($\delta > 0.5$) [6]. Taking it into consideration that core-binding energy of Ba in various compounds shows a negative shift with oxidation states, these result indicated that, for the vacuum-scraped or as-grown samples, there should be oxygen vacancies in the vicinity of Ba ions. In other words, as-received samples should already lose a part of oxygen from their surface region. As summarized in Table 1, the O_3 beam treatment resulted simultaneously in a decrease of binding energy of Ba $4d_{5/2}$, and of Ba $3d_{5/2}$, a rise of spectral weight of the Cu $2p_{3/2}$ $\underline{2p}3d^{10}\underline{L}$ in higher binding energy side and an increase of ratio of $(\underline{2p}3d^9)/(\underline{2p}3d^{10}\underline{L})$ in Cu $2p_{3/2}$. On the other hand, a much smaller shift was observed in Ca 2p signal. These results mean that a considerable oxygen vacancies should be present around ($BaO/CuO_y/BaO$) blocking layers, even in the samples just in vacuum-scraped and as-grown states. These vacancies have been effectively filled by the O_3 beam treatment. The binding energies of the treated specimens were close to those of Tl system superconductor, which is consistent with their structural similarity. Figure 1 shows valence band spectra of the sample of $n = 4$ before and after the treatment. In contrast to no discontinuity around Fermi level of the specimen before the treatment, the Fermi edge was clearly observed after the treatment. As a result, the shape of the spectrum of the treated samples gets similar to Tl-system.

Even for the treated samples, $\underline{2p}3d^{10}\underline{L}$ peak was much narrower than that of Bi2212 and La_2CuO_4, whereas it was rather close to CuO [5]. Taking into account the fact that Cu ions in La_2CuO_4, Bi2212 and CuO respectively have oxygen-coordination number of 6, 5 and 4, the result means that the averaged coordination number in the specimen should be fairly close to 4. Though a higher coordination numbers beyond 4.5 was assumed on a model in X-ray structure refinement, the results obtained in this study indicate that the number should be selfconsistently determined.

In conclusion, XPS have been performed on the Cu system ceramics and epitaxial films. A considerable oxygen loss from the vicinity of blocking layers was observed on the *in situ* measured or just scraped samples. The annealing under the 100% O_3 beam was useful to develop intrinsic surface nature. XPS signal of the treated samples are quite similar to those of Tl system, with an exception of a narrower Cu 2p $\underline{2p}3d^{10}\underline{L}$ peak which suggests a lower oxygen coordination number of Cu ions.

REFERENCES

1. Ihara H., Tokiwa K., Iyo A., Hirabayashi M., Terada N., Tokumoto M., Song Y. S., in *Advances in Superconductivity*, Vol. VII (in press).
2. Akimoto J., Oosawa Y., Tokiwa K., Hirabayashi M. and Ihara H., *Physica C*, (in press).
3. Tokiwa K., Kanehira T., Shiroki K., Ozawa H., Song Y. S., Iyo A., Terada N., Tokumoto M., Hirabayashi M. and Ihara H., in *Advances in Superconductivity*, Vol. VII (in press).
4. Terada N., Ishibashi S., Jo M., Hirabayashi M. and Ihara H., *J. Phys. Chem. Solid* **54**, 1207 (1993).
5. Parmigiani F., Depero L. E., Minerva T. and Torrance J. B., *J. Electron Spectrosc. Relat. Phenom.* **58**, 351 (1992).
6. Vasquez R. P. and Orson W. L., *Physica C*, **177**, 223 (1991); Vasquez R. P., *J. Electron Spectrosc. Relat. Phenom.* **66**, 241 (1994).

Pergamon

J. Phys. Chem. Solids Vol. 56, No. 12, pp. 1885–1886, 1995
Copyright © 1995 Elsevier Science Ltd
Printed in Great Britain. All rights reserved
0022–3697/95 $9.50 + 0.00

0022-3697(95)00193-X

ANGLE-RESOLVED AND RESONANT PHOTOEMISSION STUDY OF Sr_2RuO_4

T. YOKOYA,* A. CHAINANI,* T. TAKAHASHI,* H. KATAYAMA-YOSHIDA,* M. KASAI† and Y. TOKURA†,‡

*Department of Physics, Tohoku University, Sendai 980-77, Japan
†Joint Research Center for Atom Technology (JRCAT), Tsukuba, Ibaraki 305, Japan
‡Department of Applied Physics, The University of Tokyo, Tokyo 113, Japan

Abstract—Resonant and angle-resolved photoemission measurements were performed for the non-cuprate layered superconductor Sr_2RuO_4 (T_c = 0.93 K). Resonant valence band photoemission spectroscopy shows the existence of a correlation induced satellite to the main *d* band across the Ru 4*p*–4*d* threshold. Angle-resolved measurements show a surprisingly narrow band of about 50 meV width and positioned at 26 meV below the Fermi level, along the ΓX and ΓZ directions. This band, arising fom Ru 4*d*–O 2*p* antibonding states, is nearly dispersionless over a wide range of *k* points about the zone boundary along the Γ–*Z* direction (Ru–O direction), reminiscent of the extended Van-Hove singularity observed in the cuprates. The results emphasize the presence of strong correlations, substantial charge-transfer character to states at the Fermi level and the existence of a singular flat band near the Fermi-level in this low T_c layered superconductor, just like the cuprates.

Keywords: Non-cuprate layered superconductor, Sr_2RuO_4, resonant photoemission, angle-resolved photoemission, strong correlations, charge-transfer character, Van-Hove singularity

1. INTRODUCTION

Recently, it was discovered that Sr_2RuO_4, a non-cuprate Perovskite layered oxide exhibits superconductivity at 0.93K [1]. This material has the same crystal structure as La_2CuO_4(i.e. K_2NiF_4 structure) with two-dimensional RuO_2 planes instead of the CuO_2 planes. This finding has provoked much attention on how the non-cuprate layered superconductor is similar to or different from the cuprate superconductors with much higher T_cs.

A recent band structure calculation on Sr_2RuO_4 [2] predicts that the electronic states at Fermi Level (E_F) consists of Ru4$d\epsilon(xy, yz, zx)$–O2$p\pi$ anti-bonding bands in contrast to the cuprates, where Cu3$d(x^2 - y^2)$–O2$p\sigma$ anti-bonding bands cross the E_F. We study the electronic structure of single-crystal Sr_2RuO_4 using resonant and angle-resolved photoemission spectroscopy.

2. EXPERIMENTAL

Photoemission spectroscopy was performed on single-crystals prepared by the floating zone method. The resonant photoemission measurements were performed at UVSOR, IMS, Okazaki. The energy resolution was 0.3–0.5 eV (21 eV - 60 eV). The measurements were done on clean and fresh surfaces obtained by *in situ* cleaving at 120 K. The intensity is normalized to the incident photon flux and the E_F was referenced to that of a gold film deposited on the surface.

Angle-resolved photoemission measurements using HeI photons(21.22 eV) were performed in a home-built photoemission spectrometer [3]. The energy and angular resolutions were 50 meV and 2°. Samples were cleaved *in situ* and measured at 20 K in a vacuum of better than 5×10^{-11} Torr.

3. RESULTS AND DISCUSSION

Figure 1 shows resonant photoemission valence band spectra of Sr_2RuO_4. In the 21 eV spectrum, the valence band shows a feature (A) at E_F, a feature (B) at about 3 eV, and a broad peak (C) at about 6 eV binding energy. Comparison with LAPW band-structure calculations allows us to assign the feature at 6 eV binding energy to have primarily bonding O2$p\pi$ character mixed with the Ru4$d\epsilon$ states. The peak at E_F consists of anti-bonding states of Ru4$d\epsilon$ and O2$p\pi$ while non-bonding states are at about 3 eV binding energy.

The resonant photoemission spectra show a clear resonance feature across the Ru 4*p*–4*d* threshold (about 40 eV) at a binding energy of nearly 3 eV. This is surprising because XPS measurements show primarily Ru 4*d* derived states at E_F. The observation that the resonance occurs, not at the main Ru 4*d* band, but at a higher binding energy indicates the existence of a correlation induced satellite to the main *d* band. This indicates a local d^3 final state occuring at about 3 eV binding energy, while the well-screened feature at E_F corresponds to the d^4L configuration (where *L* denotes a ligand hole) implying Sr_2RuO_4 has substantial charge-transfer character in the ground state similar to the high-T_c oxides and NiO.

Since the satellite arises due to intra-site Coulomb interaction (U_{dd}) between *d* electrons, one can make a simple

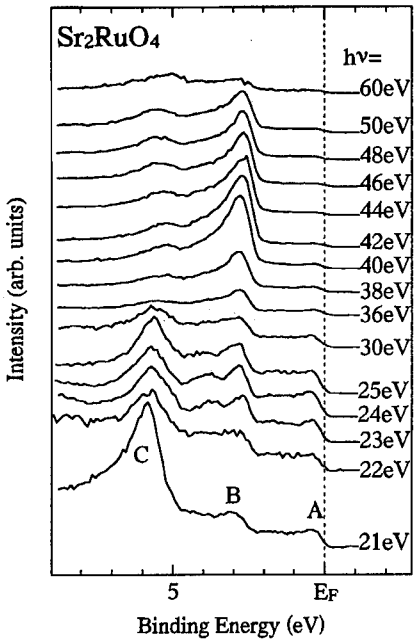


Fig. 1. Angle-resolved normal-emission spectra from Sr_2RuO_4(001) taken with photon energies between 21 and 60 eV at 120 K.

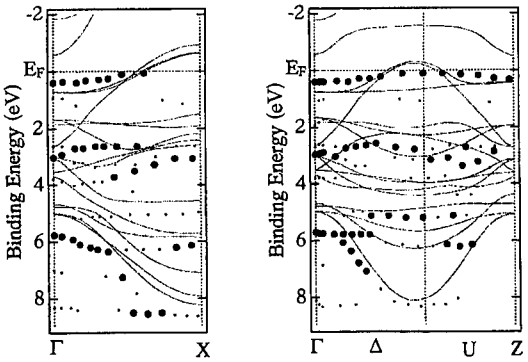


Fig. 2. Band structure of Sr_2RuO_4 determined by the present ARUPS study using the HeI(21.2 eV) resonance line. Big and small circles represent major and minor features of ARUPS spectra. A representative-band structure calculation [2] is shown as broken lines for comparison.

estimate of U_{dd} starting from the one-electron band picture. The binding energy of the valence band satellite, $E_0 = 2\epsilon_d + U_{dd}$, where ϵ_d is the binding energy of the primarily d derived states. $E_0 = 2.7$ eV and from XPS data, $\epsilon_d = 0.6$ eV, and thus, $U_{dd} \sim 1.5$ eV. From a tight binding fit to the LAPW band calculation [2], the orbital energy difference, $E(d\epsilon) - E(\mathrm{O(I)}p\pi) = 1.5$ eV, $E(d\epsilon) - E(\mathrm{O(II)}p\pi) = 0$ eV, and hopping integrals, $pd\pi(d\epsilon - \mathrm{O(I)}p\pi) = 1.5$ eV, $pd\pi(d\epsilon - \mathrm{O(II)}p\pi) = 1.0$ eV, indicating the ground state of Sr_2RuO_4 is similar to the high-T_c oxides, i.e. exhibiting on-site Coulomb interactions, strong hybridization and substantial charge-transfer character.

Figure 2 shows the band structure of Sr_2RuO_4 determined by angle-resolved photoemission (ARUPS) for two high symmetry directions of the Brillouin zone (ΓX and ΓZ direction). A LAPW band-structure calculation [2] for Sr_2RuO_4 is shown by broken lines. For bands at binding energy more than 1.5 eV, the observed bands shift to about 1.0 eV higher binding energy. The band at about 6 eV at Γ-point, due to bonding states of O2p and Ru 4d, disperses to higher binding energy and reaches up to about 8 eV binding energy for both the measured directions. Bands around 3–4 eV due to non-bonding states of O2p show similar dispersion as in the calculation. On the other hand, the band near E_F at Γ-point, which is derived from anti-bonding states of Ru 4d and O2p is closer to E_F compared to the calculation, suggestive of strong correlation effects. For the ΓX direction, this band approaches E_F and becomes very sharp, before crossing it as in the calculation. For the ΓZ direction, it also approaches E_F and becomes sharp, but does not cross it. This flat and narrow band is very similar to the Van Hove singularity reported for the cuprate superconductors [4,5].

In summary, the electronic structure of single-crystal Sr_2RuO_4, a non-cuprate layered superconductor has been studied using resonant and angle-resolved photoemission spectroscopy. The study shows the existence of a correlation induced satellite to the main Ru 4d band which exhibits a remarkable resonance across the 4p–4d threshold. Angle-resolved measurements show a surprisingly narrow band about 50 meV width, at 26 meV binding energy, along the ΓX and ΓZ directions. This band, arising fom Ru 4d–O 2p antibonding states, is nearly dispersionless over a wide range of k points along the Γ–Z direction (Ru–O direction), reminiscent of the extended Van-Hove singularity observed in the cuprates. The results indicate strong correlations, substantial charge-transfer character and the existence of a singular flat band near E_F in this low T_c layered superconductor, just like the cuprates.

Acknowledgements—This work was supported by grants from the NEDO and the Ministry of Education, Science and Culture of Japan.

REFERENCES

1. Maeno Y. *et al.*, *Nature* **372**, 532 (1994).
2. Oguchi T., *Phys. Rev. B* **51**, 1385 (1995).
3. Yokoya T. *et al.*, *Solid State Commun.* **87**, 553 (1993).
4. Dessau D. S. *et al.*, *Phys. Rev. Lett.* **71**, 2781 (1993).
5. Gofron K. *et al.*, *Phys. Rev. Lett.* **73**, 3302 (1994).

TRANSPORT AND THERMODYNAMIC PROPERTIES

Pergamon

J. Phys. Chem. Solids Vol. 56, No. 12, pp. 1887–1889, 1995
Copyright © 1995 Elsevier Science Ltd
Printed in Great Britain. All rights reserved
0022-3697/95 $9.50 + 0.00

0022-3697(95)00094-1

DOPING EFFECT ON THE PENETRATION DEPTH OF $HgBa_2CuO_{4+\delta}$

C. W. CHU, Y. Y. XUE, Y. CAO
Department of Physics and Texas Center for Superconductivity, University of Houston, Houston, TX 77204-5932, U.S.A.
and
Q. XIONG
Department of Physics, University of Arkansas, Fayetteville AR 72701, U.S.A.

Abstract—We have investigated systematically by magnetization measurements the penetration depth λ of $HgBa_2CuO_{4+\delta}$ with doping $0.1 \leq \delta \leq 0.3$, ranging from the underdoped region of $\delta < 0.22$ to the overdoped region of $\delta > 0.22$. The penetration depth was found to vary with temperature quadratically for the underdoped samples below the transition temperature (T_c) over the entire temperature region examined, while linearly for the optimally doped and overdoped samples below 0.5 T_c. The observation suggests that the temperature dependence of λ is affected by doping in a complex way and its inference to the pairing symmetry should be taken only with extreme care.

Keywords: Superconductivity, doping, pairing symmetry.

1. INTRODUCTION

It is known that the penetration depth λ of a superconductor is related to the superfluid density n_s as $\lambda^2 \propto 1/n_s$. The temperature dependence of n_s is determined by that of the superconducting energy gap Δ which depends on the superconducting pairing symmetry. According to the BCS Theory, λ of an s-wave superconductor below its superconducting transition temperature T_c is given by [1]:

$$\lambda(T) \sim \lambda(0)[1 - 2.5(\Delta_0/T)^{1/2}\exp(-\Delta_0/T)]$$

for $\Delta_0/T \gg 1$, where $\lambda(0)$ is λ at 0°and Δ_0 is the smallest Δ over the Fermi surface at 0°. The observation of the exponential T-dependence of λ is an indication of the absence of nodes or lines of nodes. For a d-wave superconductor where nodes and/or lines of nodes exist, $\Delta\lambda(T) = \lambda(T) - \lambda(0) \propto T$ at low temperatures has been predicted [2]. Experimentally, different T-dependences of $\Delta\lambda$ of high quality $YBa_2Cu_3O_7$-samples ranging from linear to quadratic and occasionally exponential, have been reported [3]. The difference usually is attributed to the unknown difference in sample quality. This appears to be consistent with the recent prediction [4] that, in a d-wave superconductor with a non-zero concentration n_i of strongly scattering impurities, $\Delta\lambda \propto T^\alpha$ where $\alpha = 2$ for $T < T^* \ll T_c$ and $\alpha = 1$ for $T^* < T \ll T_c$, where T^* is the cross-over temperature and increases with n_i. Unfortunately, most of the experiments reported were carried out on samples with T_cs close to the maximum value of $YBa_2Cu_3O_7$ and a sample with the highest T_c does not guarantee a structurally perfect sample. Therefore, we have decided to investigate systematically the effect of doping on $\Delta\lambda(T)$ of $HgBa_2CuO_{4+\delta}$. We found that $\Delta\lambda(T) \propto T^2$ below T_c for all underdoped samples, whereas $\Delta\lambda(T) \propto T$ below 0.5 T_c for the optimally doped and overdoped samples. The observations cannot be easily reconciled with predictions by impurity scattering in a d-wave superconductor.

2. OUR EXPERIMENT

The compound system examined—$HgBa_2CuO_{4+\delta}$

$HgBa_2CuO_{4+\delta}$ has displayed the largest T_c-variation by anion doping only with minimum perturbation to the structural integrity of the compound [5]. By increasing δ from 0 to 0.4, T_c can be varied parabolically from 0 K to its maximum value of 97 K at optimal doping $\delta_{op} = 0.22$ and back to 20 K. The compound is known as underdoped when $\delta < 0.22$, and overdoped when $\delta > 0.22$. We have examined six samples of $HgBa_2CuO_{4+\delta}$: three are underdoped with T_c = 40 and 88, respectively; one optimally doped with a T_c = 96.5 K and two overdoped with T_c = 20, at 45 and 87.5 K, respectively.

The experimental method used—dc magnetization measurements

The dc magnetization (M) of the samples studied were determined as a function of field (H) at different temperatures, and as a function of the temperature (T) at different fields. Relaxation effects of M of several samples were also measured at different Hs and Ts.

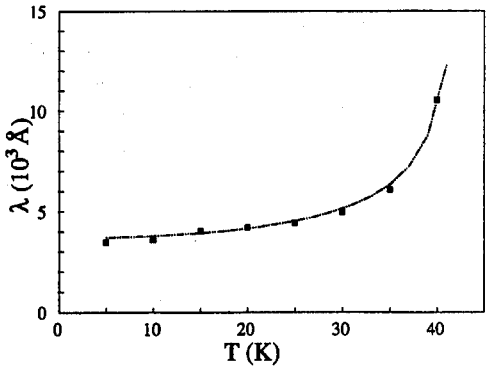


Fig. 1. The underdoped sample with $T_c = 40$ K: with $\lambda(0) \sim 3700\mathring{A}$ and $\alpha = 2$.

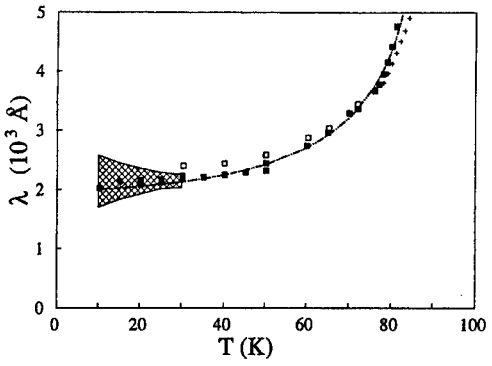


Fig. 2. The underdoped sample with $T_c = 88$ K: with $\lambda(0) \sim 1950\mathring{A}$ and $\alpha = 2$.

The data analyses adopted

λ at temperature T was obtained by analyzing the reversible $M(H)$ at different Ts, according to the following models due to:

(1) London who considered only the electromagnetic energy: $dM/d\ln H = 1/(4\pi\lambda^2)$,
(2) Hao and Clem, who added the free-energy associated with the vortex cores to London's model: $dM/d\ln H = \beta/(4\pi\lambda^2)$, with $0.75 \leq \beta \leq 0.84$,
(3) Bulaevskii *et al.* who included the fluctuation effect in the Hao and Clem model: $dM/d\ln H = \beta/(4\pi\lambda^2) - (M^*/T^*)T$, above a critical field when a field independent magnetization (M^*) exists at a temperature (T^*), and
(4) Tesanovic *et al.* who proposed a characteristic scaling behavior in the thermodynamic quantities in quasi 2D Type-II superconductors in the fluctuation region near H_{c2} : by scaling.

The $\lambda(T)$-results

Typical results of $\lambda(T)$ are shown in Figs 1–5 in order of increasing d: [■]—London model;[□]—Hao and Clem model;+—Bulaevskii *et al.* model;×—Tesanovic *et al.* model; [···]—$\lambda(0)[1 - (T/T_c)^\alpha]$; and [—··] — $\lambda(0)[1 - (T/T_c)]$.

Caveats

The deduction of $\lambda(T)$ from $M(T)$ can be complicated by the sample quality, the measuring field inhomogeneity, the flux pinning and the model used. Special steps have been adopted to address the above issues. The largest uncertainty of $\Delta\lambda(T)$ is associated with the paramagnetic background of unknown origin, shown as the shaded area in the figures.

Self-consistent check

While $M(T)$ provides meaningful information about the T-dependence of λ, the uncertainty in the absolute value of

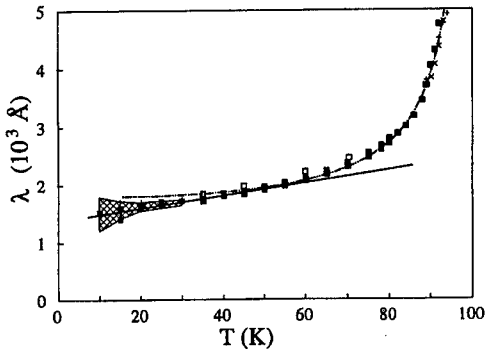


Fig. 3. The optimally doped sample with a T_c =96.5 K:[···] $\lambda(0) \sim 1800\mathring{A}$ and $\alpha = 2.8$; and [—] $\sim 1350\mathring{A}$.

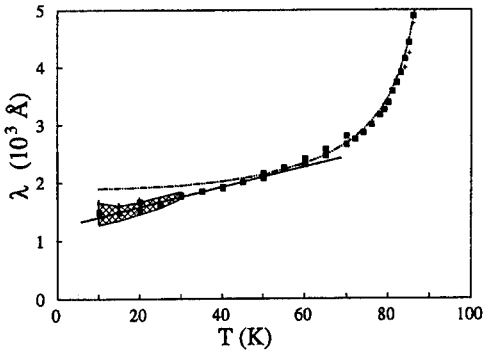


Fig. 4. The overdoped sample with $T_c = 87.5$ K:[···] $\lambda(0) \sim 1900\mathring{A}$ and $\alpha = 2.5$; and [—] $\lambda(0) \sim 1250\mathring{A}$.

λ has not been assessed. However, the variation of n_s with T_c by our best fits at low temperatures can be obtained, and can be compared with that according to the high temperature fits to $\lambda(0)[1 - (T/T_c)^\alpha]$. The results are displayed in Fig. 6. It is clear that the low temperature fits stated above lead to a meaningful n_s normalized to the total carrier density n, i.e. $n_s/n \propto 1/n\lambda^2(0)$ which varies only slightly near the maximum T_c as expected, in contrast to the n_s obtained from high temperature fits.

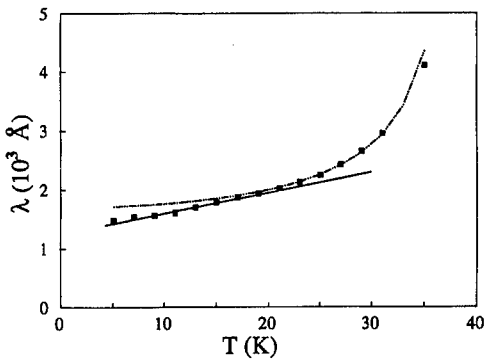


Fig. 5. The overdoped sample with $T_c = 40$ K: [–··] $\lambda(0) \sim 1660\mathring{A}$ and $\alpha = 2$; and [–··] $\lambda(0)1300\mathring{A}$.

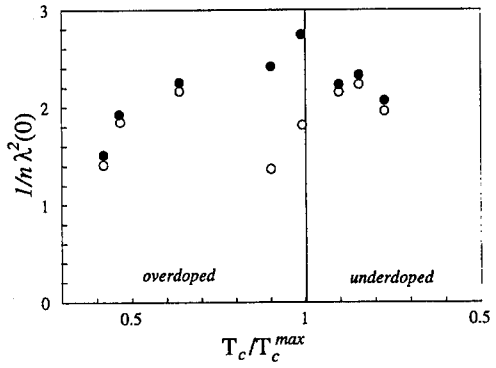


Fig. 6. $n_s \propto 1/n\lambda^2(0)$: n is total density, [•]— low temperature fits and ∘—high temperature fits.

3. CONCLUSION

We have determined $\Delta\lambda(T)$ of $HgBa_2CuO_{4+\delta}$ with a wide d-range by measuring $M(T)$. The results show that $\Delta\lambda(T) \propto T^2$ for all underdoped samples below T_c down to 5 K and $\Delta\lambda(T) \propto T$ for the optimally doped and the overdoped samples below $\approx 0.5T_c$. The results cannot reconcile with previous suggestion that the defects are responsible for the T^2-behavior of $\Delta\lambda$ as doping deviates from the optimal value where T_c is maximum. The impasse may be partially alleviated by arguing that, for $HgBa_2CuO_{4+\delta}$, larger δ may imply a more perfect structure for the samples. Unfortunately, the predicted variation of the cross-over temperature T^* with scattering defects was not born out by the above argument. It is therefore concluded that doping influences $\Delta\lambda(T)$ in a more complex way than previously envisioned and the inference of $\Delta\lambda(T)$ to the superconducting pairing symmetry should be taken with extreme caution.

Acknowledgement—This work is supported in part by NSF Grant No. DMR 91-22043, USAFOSR Grant No. F49620-93-1-0310 by BMDO, EPRI, the State of Texas through the Texas Center for Superconductivity at the University of Houston, and the T. L. L. Temple Foundation.

REFERENCES

1. Muhlschegel B., *Z. Phys.* **155**, 313 (1959).
2. Annett J. F. and Goldenfeld N. D., *J. Low Temp. Phys.* **89**, 197 (1992).
3. See, for example, Levi B. G., *Physics Today*, May 17, 1993.
4. Hirschfeld P. and Goldenfeld N., *Phys. Rev. B* **48**, 4219 (1993).
5. Xiong Q. *et al.*, *Phys. Rev. B* **50**, 10346 (1994).

Pergamon

J. Phys. Chem. Solids Vol. 56, No. 12, pp. 1891–1893, 1995
Copyright © 1995 Elsevier Science Ltd
Printed in Great Britain. All rights reserved
0022–3697/95 $9.50 + 0.00

0022-3697(95)00206-5

MATERIALS AND HIGH T_c

Z. FISK and J. L. SARRAO
National High Magnetic Field Laboratory, Florida State University, Tallahassee, Florida 32306, U.S.A.

Abstract—We discuss material aspects of high $T_c$compounds with reference to what is known about the pre-cuprate superconductors. A correlation between cuprate in-plane lattice parameter and $T_c$is pointed out.

Keywords: A. superconductors, D. crystal structure, D. phonons, D. superconductors.

In the pre-cuprate search for higher $T_c$superconductors, a number of regularities were noticed which provided a kind of loose direction towards where and where not to search for higher transition temperatures. These regularities included electron per atom ratio, particular structures and structural characteristics, electrical resistivity behavior, the interplay between magnetism and superconductivity, and the influence of instabilities, structural or otherwise. It is worth comparing what we know from these earlier studies with what we have learned about cuprates, in order to see if the latter are really that different and perhaps to provide someone with the germ of an idea for another new materials direction.

Probably the most famous regularities observed in transition metal superconductivity are the Matthias rules [1]: $T_c$is maximum near the odd integer electron per atom counts of 3, 5 and 7. For example, the highest known $T_c$for an intermetallic is 24 K, in the A15 structure material Nb_3Ge, with $e/a = 4.75$ [2]. A good explanation for these rules has never been found, but their general applicability in transition metal intermetallics appears connected with rigid band ideas. In various cluster-type and other complex compounds, making the rules work requires somewhat ad hoc modifications. Recently, Cava *et al.* reported $T_c = 23$ K in YPd_2B_2C [3]. The straight forward $e/a = 33/6 = 5.5$. This value is not near one of the special e/a values, but, for example, considering C as an interstitial not contributing any electrons, but still in the atom count, gives $e/a = 4.83$. On the other hand, perhaps this indicates that even higher T_cs may be achieved in borocarbide systems. The essential point, however, is that there appears to be an optimal electron count in a given structure in many cases, and this is clearly also the case for the high $T_c$cuprates. Perhaps the way to think about the rules is in terms of electron counts slightly less than half filling.

A second regularity is that certain structures are more favorable for superconductivity than others, for example the A15 structure [4]. An aspect of this regularity seems to be that higher symmetry is better than lower symmetry. This manifests itself in the observation that when an element or compound exists in two polymorphs, the high temperature, and in general higher symmetry, polymorph has a higher transition temperature. We see this in elemental La (6 K vs 4.8 K) and Ti (3 K vs 0.4 K) [5]. Related is that structural distortions lower T_c—the "$x = 1/8$" anomaly in $La_{2-x}Ba_xCuO_4$ being the most striking cuprate example [6].

In addition to the overall crystal structure, it is also interesting to consider structural components of particular classes of superconductors. This is brought to mind, for example, by the quasi-two dimensional nature of the cuprates, as well as by the ubiquitous presence of the CuO_2-planes. In the A15s, the 3 mutually orthogonal sets of transition metal chains seem an important aspect of their physics, and we can point to the claim that cross coupling of the chains by tetrahedrally located interstitial hydrogen is disastrous for T_c. In the molybdenum sulfide based superconductors, many different superconducting compounds have been found with various and different clusters of molybdenum sulfide based units, extending from simple polyhedral units to infinite chains [7]. Much research has also gone into layered materials, such as TaS_2 and $MoSi_2$. In TaS_2 one can intercalate organics between the S-layers. This causes $T_c$to be depressed, but does not kill it, even for 50 Å spacings. In contrast, the graphite compound CsC_8 has $T_c = 0.1$ K, while the double graphite layer CsC_{16} is not superconducting [8]. The conclusion here is that the reduced dimensionality in itself does not particularly favor superconductivity—a feature that is also observed in the cuprates' non-universal dependence of $T_c$on the number of CuO_2 layers.

There was a general expectation in the 1970s that the progression from element to binary to ternary should produce ever higher T_cs. This hope was based on the fact that elements get to 12 K (La under pressure), binaries to 24 K. It is only just recently that an intermetallic quaternary has come close to this, YPd_2B_2C at $T_c = 23$ K [3]. Surprising is the fact that the Th–Pd–B–C compound with $T_c = 21$ K occurs in an entirely different structure, related to the hexaborides [9,10]. In the meantime, however, the doped buckeyballs have gotten into the high 30s, and the 3D perovskite-type BKBO nearly as high. The conclusion to draw from these continuing developments seems to be that we do not have

a deep understanding of real materials, especially when it comes to knowing where to look for low energy phenomena such as superconductivity.

The temperature dependence of the electrical resistivity of transition metal superconductors is unusual and interesting. The high $T_c$intermetallics, such as Nb_3Sn (T_c = 18 K), show the so-called saturating behavior: little temperature dependence above room temperature, with the resistivity approaching asymptotically a saturation value of order 150 $\mu\Omega$ cm [11]. This is closely related to the Mooij criterion, that transition metal alloys with resistivities greater than approximately 120 $\mu\Omega$ cm tend to have negative temperature coefficients of resistivities [12]. This is seen in the saturating resistivity compounds, in that fairly modest disorder produces a resistivity of this order near T_c(with small effect on T_c) and an accompanying negative temperature coefficient of resistivity. Also interesting is the ease with which this disorder resistivity is introduced. Nothing like this has been found in the cuprate superconductors, and in fact the linear temperature dependence of the electrical resistivity of the cuprates and the very large values of this resistivity are the subject of continuing speculation.

An important part of low temperature superconductivity concerned the influence of magnetic impurities on T_c. The culmination of these studies was the discovery of the re-entrant and coexistent phases, such as the Chevrel and rare earth rhodium borides [13]. These materials appear to be such that the magnetism and superconductivity are associated with different sublattices in the structures, and that these sublattices are only weakly coupled. The heavy Fermion materials are different in this respect, in that the high masses arise from magnetic interactions, and the superconductivity occurs in the high mass band. The appropriate description of the superconductivity in the heavy Fermions which are both magnetically ordered and superconducting still remains a problem [14]. It is interesting that these heavy Fermions have $T_N > T_c$, unlike the great majority of the Chevrel and rhodium boride materials. The recent discovery of re-entrance in the borocarbides may shed new light on this problem [15]. In the cuprates, the relevance of magnetism to superconductivity still remains unclear. There is good evidence that there is no co-existence of magnetism and superconductivity here, but the importance of what might be called residual magnetic interactions (as might be seen in $\chi(q, \omega)$) are still very much debated. Defects in the CuO_2-planes give rise to a Curie–Weiss susceptibility, just as in heavy Fermions. This similarity points up the highly correlated nature of both classes of materials.

The final regularity on our list concerns instabilities. In particular, it is a quite general rule for the low $T_c$materials that the maximum $T_c$is found next to some kind of instability, be it structural or electronic. This is to say that it is hard to achieve the highest T_cs. What do we really mean by this? We know that we can vary the $T_c$of A15s smoothly with e/a. However, the A15ss cover a wide range of T_cs even at a given e/a: V_3Si, Nb_3Sn and Nb_3Ge do not all have the same

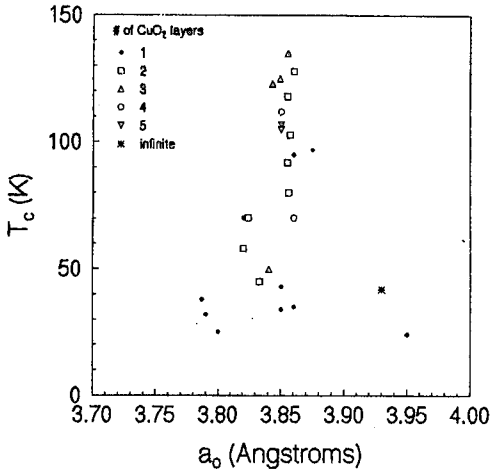


Fig. 1. In-plane lattice constant (a_o) vs superconducting critical temperature (T_c), for many of the cuprate superconductors. Different symbols denote different numbers of CuO_2 planes per conduction block.

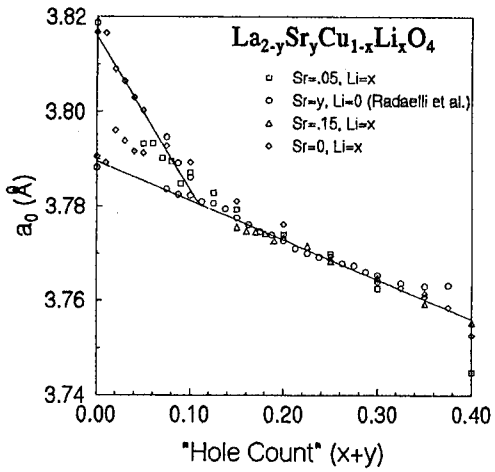


Fig. 2. In-plane lattice constant (a_o) as a function of hole count ($x+y$) for $La_{2-y}Sr_yCu_{1-x}Li_xO_4$. The lines, which are guides to the eye, show the transition from orthorhombic to tetragonal crystal symmetry as a function of hole concentration at room temperature. The data for $La_{2-y}Sr_yCuO_4$ are after [19].

T_c. And Nb_3Ge is difficult to make with T_c = 24 K. There is good reason to think that Nb_3Si would have $T_c$around 28 K if it could be made stoichiometric. But nobody has come close, and the highest $T_c$found is 9.3 K [16].

Something similar may be going on in the cuprates. It is reasonable to suppose that the Cu–O–Cu distance is relevant to T_c. A plot of $T_c$versus the tetragonal a_o parameter (appropriately scaled for the orthorhombic structures) for cuprates shows an interesting feature: only two superconductors (with more modest T_cs) exist beyond a_o = 3.88 Å (see Fig. 1). These two cases in fact are n-doped superconductors. So we can conjecture that a larger a_o parameter could give higher $T_c$in hole-doped cuprates. And we can also see in the plot the influence of layer number as a weaker

effect on T_c. A similar plot has been shown by Rao *et al.* [17], although they draw a somewhat different conclusion. The size cannot be the whole story, since pressure raises $T_c$in almost all cases, showing that something else goes on at the same time. We have also made a related observation in our work on $La_{2-y}Sr_yCu_{1-x}Li_xO_4$ (Fig. 2) in which a_o depends only on the combined hole count $(x + y)$ and not on their individual values. Since Sr and Li substitute on different sites and with different amounts of size mismatch (Li is approximately the same size as Cu while Sr is 10% bigger than La), the lattice constant must be determined by the net hole concentration in the CuO_2 plane, independent of its source [18].

The original theory of superconductivity using the phonon mechanism turned, in a sense, the superconducting materials problem around. All metals have phonons, so we should ask not why a given one is superconducting, but why not all metals are. How high a $T_c$we can find is a detail, but the one we want an answer to. The lattice instability-$T_c$relation had a clear logic to it within the phonon mechanism. Any other mechanism should be manifest in a similar way. The various correlations guiding the search for new and higher T_cs before the cuprates still remain poorly or not at all understood. But when $T_c$can be seen being limited at some kind of barrier, then we have a clear direction to move in. The 20% increase in $T_c$occasioned by Nb_3Ge came from just such reasoning, and cuprates give no obvious reason to be thought different in this respect.

Acknowledgements—We gratefully acknowledge support of this work by the Japanese New Energy and Industrial Technology Development Organization (NEDO).

REFERENCES

1. Matthias B. T., *Phys. Rev.* **97**, 75 (1955) and Matthias B. T., *Progress in Low Temperature Physics* Vol. II (Edited by C. J. Gorter), p. 138. North Holland, Amsterdam (1957).
2. Gavaler J. R., *Appl. Phys. Lett.* **23**, 480 (1973).
3. Cava R. J. *et al.*, *Nature* **367**, 148 (1994).
4. See, for instance, Testardi L. R., *Rev. Mod. Phys.* **47**, 637 (1975).
5. See, for instance, Roberts B. W., *J. Phys. Chem. Ref. Data* **5**, 581 (1976).
6. Axe J. D. *et al.*, *Phys. Rev. Lett.* **62**, 2751 (1989).
7. Chevrel R. and Sergent M., *Superconductivity in Ternary Compounds* (Edited by I. O. Fischer and M. B. Maple), p. 25. Springer-Verlag, Berlin (1982).
8. Hannay N. B. *et al.*, *Phys. Rev. Lett.* **14**, 225 (1965).
9. Sarrao J. L. *et al.*, *Physica C* **229**, 65 (1994).
10. Zandbergen H. W. *et al.*, *Phil. Mag. Lett.* **71**, 131 (1995).
11. Fisk Z. and Webb G. W., *Phys. Rev. Lett.* **36**, 1084 (1976).
12. Mooij J. H., *Phys. Status Solidi A* **17**, 521 (1973).
13. See, for instance, *Superconductivity in Ternary Compounds I & II*, (Edited by M. B. Maple and O. Fischer). Springer-Verlag, Berlin (1982).
14. See, for instance, Fisk Z. *et al.*, *Science* **239**, 33 (1988).
15. Eisaki H. *et al.*, *Phys. Rev. B* **50**, 647 (1994).
16. Testardi L. R. *et al.*, *J. Appl. Phys.* **45**, 447 (1974).
17. Rao C. N. R. and Ganguli A. K., *Physica C* **235–240**, 9 (1994).
18. Sarrao J. L. *et al.*, in preparation (1995).
19. Radaelli P. G., *Phys. Rev. B* **49**, 4163 (1994).

Pergamon

J. Phys. Chem. Solids Vol. 56, No. 12, pp. 1895–1897, 1995
Copyright © 1995 Elsevier Science Ltd
Printed in Great Britain. All rights reserved
0022-3697/95 $9.50 + 0.00

0022-3697(95)00139-5

QUASI-PARTICLE MEAN-FREE-PATH AND THERMAL HALL CONDUCTIVITY IN $YBa_2Cu_3O_7$

K. KRISHANA, J. M. HARRIS and N. P. ONG
Joseph Henry Laboratories of Physics, Princeton University, Princeton, NJ 08544, U.S.A.

Abstract—We have measured the Hall component of the thermal conductivity κ^e_{xy} in the mixed state of YBCO. κ^e_{xy} is observed to be unusually large. From its strong field dependence we deduce the quasi-particle mean free path ℓ_0. Between 90 K and 15 K, ℓ_0 increases rapidly from 80 Å to 2500 Å.

Microwave loss measurements suggest that the lifetime of quasi-particles (*qp*) in $YBa_2Cu_3O_7$(YBCO) crystals becomes very long at low temperatures (T) [1]. Is it possible to observe directly the long mean-free-path (*mfp*) implied by the lifetime? In principle, the *qp mfp* may be derived from the in-plane thermal conductivity κ_{xx}. However, κ_{xx} is comprised of electronic and phonon contributions, κ^e_{xx} and κ^{ph}, respectively, viz. $\kappa_{xx} = \kappa^e_{xx} + \kappa^{ph}$. There is, at present, disagreement [2–5] on the relative size of the two terms (in YBCO the electronic part includes contributions from the chain electrons). Cohn [3, 4] and coworkers argue that the well-known peak in κ_{xx} is primarily phononic while Yu *et al.* [2, 5] propose that it is largely caused by *qp* excitations.

We describe an experiment in which we have used the asymmetric scattering of *qp* by pinned vortices to isolate the in-plane electronic component. We find that, in YBCO, the off-diagonal (Hall) component κ^e_{xy} is very large. The mean free path ℓ_0 in zero-field may be determined from its field dependence. The Hall current allows us to distinguish the in-plane electronic excitations from phonons and the "chain" *qp* (since they do not see the asymmetric scattering). While many studies exist of the field dependence of κ_{xx} in the cuprates, the thermal Hall current (usually called the Righi–Leduc effect) does not seem to have been investigated. The experiment also provides new information on the role of quasi-particles in the flux-flow electrical Hall effect.

In our experiment the field **H** is applied normal to the *ab* plane while a longitudinal thermal current $\mathbf{J_Q}//\hat{\mathbf{x}}$ is applied in-plane, parallel to an edge of the crystal. The crystal used is twinned, with T_c = 92.4 K. Both the longitudinal and transverse thermal gradients, $-\partial_x T$ and $-\partial_y T$, respectively, were measured as H is swept from −14 to +14 Tesla. To correct for the large effect of remanence below 45 K, the measurements were repeated sweeping in the opposite direction. The thermal resistivity tensor W_{ij} was calculated from $-\partial_x T$ and $-\partial_y T$ measured in the four field sweeps. By inverting the matrix W_{ij}, we obtain κ^e_{xy} and κ_{xx}. Figure 1 displays the field dependence of κ^e_{xy} at selected temperatures.

At high temperatures, κ^e_{xy} is almost linear in H. As T decreases, negative curvature becomes increasingly apparent. The overall magnitude of κ^e_{xy} also increases rapidly. As we argue below, the negative curvature reflects the rapidly increasing *mfp* of the *qp* in zero field ℓ_0. Below 40 K, the overall magnitude of κ^e_{xy} decreases with decreasing T (this reflects the decrease in the entropy carried by each *qp*). However, the curvature in the trace of κ^e_{xy} continues to increase monotonically. The rapid shift from weak-field to strong-field behavior shown in the figure provides rather direct evidence for very long *qp* mean free paths in single-crystal YBCO.

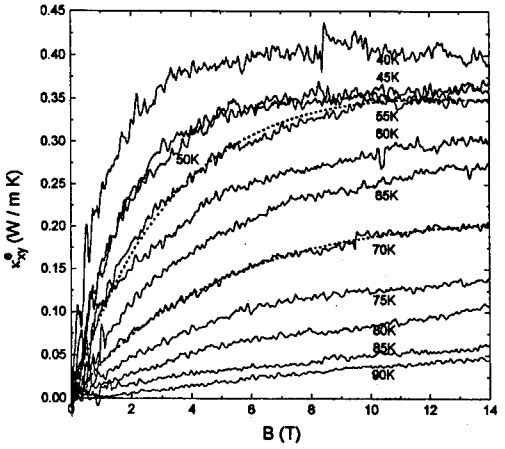


Fig. 1. The Hall thermal conductivity κ^e_{xy} measured in YBCO.

The differential cross-section $\frac{d\sigma(\theta,\phi)}{d\Omega}$ for scattering of a *qp* by a vortex line has been calculated by Cleary [6]. The transition rates are expressed by the transverse (or Hall) cross section $\sigma^{\perp}$ and the transport cross section σ^{tr}. We may treat the asymmetric scattering in a way similar to skew scattering of electrons from magnetic ions using the Boltzmann equation approach for the *qp* [7], $\mathbf{v_k}.(-\nabla T)(-\frac{\partial f^0_k}{\partial E_k}) = I_s + I_a$, where $\hbar\mathbf{v_k} = \frac{\partial E_k}{\partial \mathbf{k}}$, with $E_k = \sqrt{\epsilon_k^2 + \Delta(\mathbf{k})^2}$. Here, I_s and I_a are the collision integrals and $\Delta(\mathbf{k})$ is the gap parameter. Solving the equation by the variational approach [8], we may express the conductivities in terms of $\sigma^{\perp}$ and σ^{tr}, viz.

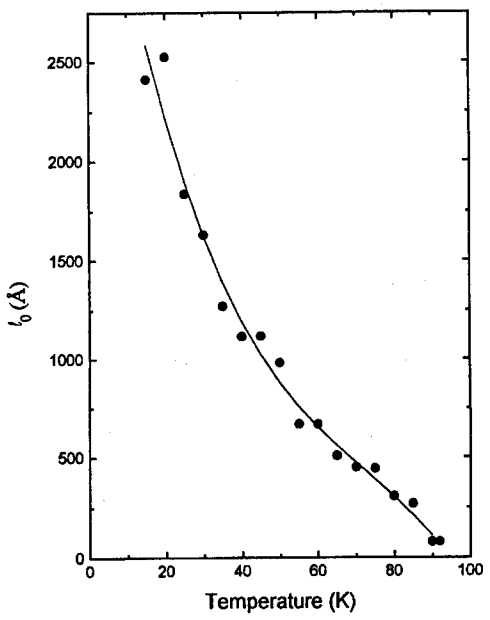


Fig. 2. The zero-field mfp ℓ_0 in YBCO derived from the curves in Fig. 1. The line is a guide to the eye.

$$\kappa^e_{xx} = \frac{4}{T}\int d\epsilon\, \epsilon^2 \left(\frac{-\partial f^0_k}{\partial E_k}\right) \frac{\ell_0}{[1 + \ell_0 \mid \mathbf{B} \mid \sigma^{tr}\phi_0^{-1}]} \quad (1)$$

$$\kappa^e_{xy} = \kappa^e_{xx} \frac{\ell_0 \sigma^{\perp} B \phi_0^{-1}}{[1 + \ell_0 \mid \mathbf{B} \mid \sigma^{tr}\phi_0^{-1}]} \quad (2)$$

with ϕ_0 the flux quantum. Here, the scattering rates are defined as an average over the Fermi Surface weighted by $\epsilon^2(-\frac{\partial f^0}{\partial E})$. We also assume that the elastic scattering process from vortices and the inelastic scattering process (that determines ℓ_0 in zero field) are additive, viz. $\ell_{tot}^{-1} = \ell_0^{-1} + \sigma^{tr} \mid \mathbf{B} \mid \phi_0^{-1}$.

In Fig. 1 the fit of κ^e_{xy} to eqn 2 is shown at two temperatures. The curvature depends only on ℓ_0 while the vertical scale depends on the product $\kappa^e_{xx}\ell_0$. The fits allow a direct determination of ℓ_0 at each temperature. The steep increase in ℓ_0 is shown in Fig. 2.

A significant result is the sharp upturn in ℓ_0 at T_c. The abrupt change in lifetime implies that the intense scattering that leads to the linear-T resistivity in the normal state is rapidly suppressed below T_c. We note that if the intense scattering above T_c were caused (mainly) by phonons we should see practically the same qp scattering rate a few K below T_c. The sharp upturn in ℓ_0 seems to provide very strong evidence against dominant phonon scattering. The mechanism responsible for the intense inelastic scattering in the normal state is strongly suppressed when superconductivity occurs. Therefore it must be electronic in origin. Our data support models in which superconductivity removes strongly fluctuating fields (such as gauge fluctuations) that exist in the normal state.

At our lowest temperature, ℓ_0 attains values near 2,500 Å (in our calibration, we adopt the value σ^{tr} = 25 Å, reported in Ref. [9]). No saturation in the growth of ℓ_0 is apparent at 15 K. The T dependence of ℓ_0^{-1} is in good agreement with the scattering rate τ^{-1} obtained by Bonn *et al.* [1] in a Zn-doped YBCO crystal. Quantitative comparison with their lifetime values implies an average velocity $v_N = 2\times10^7$ cm/s. (τ^{-1} has a rather steeper T dependence in untwinned crystals).

Equation 2 shows that it is possible to compute the zero-field value of κ^e_{xx} at each temperature from the Hall term κ^e_{xy} alone, once ℓ_0 is known. Using the data for ℓ_0 shown in Fig. 2 for this calculation, we have computed κ^e_{xx} from the weak-field value of κ^e_{xy}. We will report elsewhere a comparison of the κ^e_{xx} obtained in this way with the total κ_{xx}.

The present results also add new insight to the sign-reversal problem in the electrical Hall conductivity σ_{xy}. Recent work [9–11] shows that the total Hall current may be decomposed into a positive qp electrical Hall conductivity σ^n_{xy} and a negative vortex term σ^f_{xy}, viz. $\sigma_{xy} = \sigma^n_{xy} + \sigma^f_{xy}$.

However, there is disagreement over the meaning of σ^n_{xy}. Is it associated with normal excitations within the vortex core, or with qp excitations outside the core? The former interpretation is implicit in some recent flux-flow studies [12], whereas Harris *et al.* [9, 10] propose the second viewpoint. In the present experiment, the vortices are pinned. Thus, the complication of dealing with the chemical potential gradient caused by flux motion is not a factor. The thermal current experiment offers direct evidence that qp excitations *outside* the core carry a substantial current because of the long mfp. The values of ℓ_0 estimated from κ^e_{xy} here are in good agreement with those obtained from σ^n_{xy} [9]. This strongly suggests that both the electrical and thermal Hall experiments probe excitations outside the core. Thus, the term σ^n_{xy} is properly identified with excitations outside the core. In addition to the flux-flow Hall effect, we expect the qp current to be important in studies of the Ettinghausen, Nernst and thermopower coefficients in the mixed state, even at low T.

The thermal conductivity provides a promising probe of the superconducting state in the cuprates provided one can separate the electronic and phononic components unambiguously. Asymmetric scattering from vortices, amplified by the unusually long mfp, seems especially promising. At temperatures below 10 K, the qp may travel distances exceeding 0.5 μm between collisions in zero field. This may provide a sensitive probe of both the vortex lattice as well as the condensate itself. Close to T_c, detailed measurements of κ^e_{xy} may yield information on the growth of the gap that is difficult to obtain using other probes. Further progress relies on an improved understanding of vortex scattering with d-wave (or mixed s and d) pairing symmetry.

Acknowledgements–Research Contract N00014-90-J-1013.

REFERENCES

1. Bonn D. A., Dosanjh P., Liang R. and Hardy W. N., *Phys. Rev. Lett.* **68**, 2390 (1992); Bonn D. A. *et al.*, *Phys. Rev. B*

47, 11314 (1993).
2. Yu R. C., Salamon M. B., Jian Ping Lu and Lee W. C., *Phys. Rev. Lett.* **69**, 1431 (1992).
3. Richardson R. A., Peacor S. D., Nori F. and Uher C., *Phys. Rev. Lett.* **z67**, 3856 (1991); Peacor S. D., Cohn J. L. and Uher C., *Phys. Rev. B* **43**, 8721 (1991).
4. Cohn J. L., Kresin V. Z., Reeves M. E. and Wolf S. A., *Phys. Rev. Lett.* **71**, 1657 (1993).
5. Yu R. C., Salamon M. B. and Lu J. P., *Phys. Rev. Lett.* 71, 1658 (1993).
6. Cleary R. M., *Phys. Rev.* **175**, 587 (1968).
7. Bardeen J., Rickayzen G. and Tewordt L., *Phys. Rev.* **113**, 982 (1959).
8. Ong N. P., to be published.
9. Harris J. M., Ong N. P., Matl P., Gagnon R., Taillefer L., Kimura T. and Kitazawa K., *Phys. Rev. B*, in press.
10. Harris J. M., Yan Y. F., Tsui O. K. C., Matsuda Y. and Ong N. P., *Phys. Rev. Lett.* **73**, 1711 (1994).
11. Ginsberg D. M. and Manson J. T., *Phys. Rev. B* **51**, 515 (1995).
12. Kunchur M. N., Christen D. K., Kabunde C. E. and Phillips J. M., *Phys. Rev. Lett.* **72**, 2259 (1994).

Pergamon

J. Phys. Chem. Solids Vol. 56, No. 12, pp. 1899–1904, 1995
1995 Elsevier Science Ltd
Printed in Great Britain
0022-3697/95 $9.50 + 0.00

0022-3697(95)00163-8

SPECIFIC HEAT OF $YBa_2Cu_3O_{7-\delta}$ SINGLE CRYSTALS: IMPLICATIONS FOR THE VORTEX STRUCTURE

KATHRYN A. MOLER and AHARON KAPITULNIK
Departments of Physics and Applied Physics, Stanford, CA 94305, U.S.A.

DAVID J. BAAR [†,‡] RUIXING LIANG [†,‡] and WALTER N. HARDY [†]
[†] Department of Physics, University of British Columbia, Vancouver, BC, Canada V6T 1Z1
[‡] Quantum Innovations, Inc., P. O. Box 78512, Vancouver, BC, Canada V6T 2E7

Abstract—The anisotropy of the magnetic field dependence of the specific heat of $YBa_2Cu_3O_{7-\delta}$ can be used to identify different low-energy excitations, which include phonons, spin-$\frac{1}{2}$ particles, and electronic contributions. With a magnetic field H applied perpendicular to the copper oxide planes, we find that the specific heat includes a linear-T term proportional to $\sqrt{H}$. The nonlinear field dependence of the density of states at the Fermi level suggests that there are quasiparticle excitations throughout the entire vortex, not just in the vortex core. The $\sqrt{H}T$ term agrees quantitatively with G. Volovik's prediction for a superconductor with lines of nodes in the gap. A similar, but much smaller, effect is predicted for fields parallel to the planes, and sensitive measurements of the in-plane anisotropic magnetic field dependence of the specific heat could be used to map out the nodes.

1. INTRODUCTION

Among recent experiments supporting the possibility of lines of nodes in the gap function of some of the high-T_c materials [1], measurements on single-crystal $YBa_2Cu_3O_{7-\delta}$ (YBCO) show a linear temperature dependence of the penetration depth [2], as predicted for superconductors with lines of nodes in the clean limit [3]. The density of states $N(E)$ in such superconductors rises linearly with energy at the Fermi level in zero field, which should result in a quadratic term αT^2 in the specific heat [4]. A material with a finite $N(E_F)$, such as a normal metal or a disordered superconductor with lines of nodes [5], has a linear term γT in the zero-field specific heat, with $\gamma \propto N(E_F)$.

G. Volovik predicted that for a superconducting state with lines of nodes, the dominant contribution to the magnetic field dependence of the density of states at the Fermi level is $N(E_F, H) = \kappa N_n \sqrt{H/H_{c2}}$, where N_n is the normal-state DOS and κ is a factor of order 1 [6]. The factor κ is defined by the vortex lattice structure, by the slope of the gap near the gap node, and by possible structure in N_n. The quasiparticles which contribute to $N(E_F, H)$ are outside the vortex cores, and are close to the nodes in momentum space. By contrast, it is usually thought that in a clean s-wave superconductor the quasiparticles are confined to the vortex cores [7].

In previous papers [8,9] we reported measurements of the magnetic field dependence of the specific heat of twinned and untwinned single crystals of $YBa_2Cu_3O_{6.95}$ which were prepared identically to those showing linear temperature dependence of the penetration depth [2,10]. These crystals have a linear term $\gamma(0)T$ in the zero-field specific heat, a quadratic term αT^2 which is only a few percent of the total zero-field specific heat, and an additional field-dependent linear-T term $\gamma_\perp(H)T$ which obeys $\gamma_\perp(H)T = A\sqrt{H}T$. Two of these terms, αT^2 and $A\sqrt{H}T$, agree quantitatively with the predictions of lines of nodes.

In this paper we summarize the previous analysis, including alternative fits, and present results on the sample dependence of the zero-field linear term, $\gamma(0)T$. We also discuss the physical origin of the $\sqrt{H}$ dependence of the density of states and the prospects for observing this effect in a magnetic field applied parallel to the plane. In principle, measurements of the in-plane anisotropic magnetic field dependence of the specific heat could be used to map out the nodes.

2. TECHNIQUE

The specific heat was measured using a relaxation method described in detail elsewhere [11]. The sample was mounted on a sapphire substrate with a weak thermal link (thermal conductance κ_w) to a constant-temperature copper block. At each temperature and field, κ_w was measured by applying power $P = \kappa_w(T_{sample} - T_{block})$. A smaller temperature difference was then used to make a relaxation measurement of the thermal time constant $\tau = C\kappa_w$, where C is the total heat capacity. The precision of the measurement in the temperature range 2–10 K is ~ 0.5%. The addenda heat capacity can be as high as half of the total heat capacity, limiting the absolute accuracy in some measurements to ~ 10%. The addenda specific heat is mostly due to phonons, so that most of the systematic uncertainty effects only the Debye βT^3 term. Measurements of an empty substrate showed that the

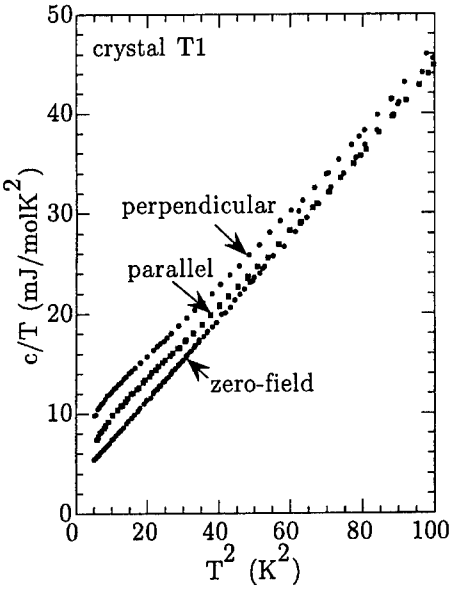


Fig. 1. Total specific heat at 0 and 8 Tesla for sample T1.

addenda heat capacity does not depend on the applied magnetic field within the precision of the data. The accuracy of the field dependence of the specific heat is better than 1%.

3. CRYSTALS

All of the samples are single crystals of $YBa_2Cu_3O_{7-\delta}$ grown by the same flux-growth technique [10] as crystals which show linear temperature dependence of the penetration depth [2]. Results have been obtained on two nominally pure, twinned single crystals (samples T1 and T2). A 0.8 mg piece was cleaved from one of the twinned crystals, sample T1, and detwinned to create sample U1. About 20% of the surface of sample U1, near two of the corners, had a high density of visible twins remaining after the detwinning process. Sample T2 was mostly detwinned to create sample U2, which had visible twin boundaries remaining. Both U1 and U2 were reoxygenated subsequent to detwinning.

4. RESULTS

Fig. 1 shows the specific heat of sample T1 in an 8 Tesla field applied either parallel or perpendicular to the copper oxide planes. The total specific heat includes the Debye phonon contribution, βT^3, which has a similar value in all three data sets; the zero-field linear term $\gamma(0)T$, which appears as a finite intercept on the c/T-axis; a magnetic contribution from spin-$\frac{1}{2}$ particles, $nc_{\text{Schottky}}(T, H)$, which appears as a low-temperature bump peaking around 3–4 K in both parallel and perpendicular fields; and a substantially increased linear term in perpendicular field, $\gamma_\perp(H)T$.

Table 1. Global Fit Parameters (mJ, mol, K, and T).

	Sample T1	Sample U1
$\gamma(0)$	3.0 ± 0.1	$2.1 + 0.1 - 0.2$
n	24 ± 1	23 ± 1
β	0.392 ± 0.001	0.380 ± 0.004
α	0.11 ± 0.02	0.10 ± 0.06
$\gamma_\perp(H)$	$0.91\sqrt{H}$	$0.88\sqrt{H}$

4.1. *Perpendicular field—global fit*

To model the perpendicular field dependence, identical analyses are performed on data from samples T1 (H = 0, 0.5, 2, 4, 6 and 8 Tesla) and U1 (H = 0, 0.5, 2, 4, 6, 8 and 10 Tesla). A global fit is used to constrain the concentration of spin-$\frac{1}{2}$ particles, n, and the phonon specific heat, βT^3, to be field-independent. Allowing for the possibility of a small quadratic term, αT^2, as predicted for lines of nodes, the zero-field specific heat is described by:

$$c(T, 0) = \gamma(0)T + \alpha T^2 + \beta T^3. \quad (1)$$

The specific heat for $H \geq 0.5$ T is described by:

$$c(T, H) = (\gamma(0) + \gamma_\perp(H))\, T + \beta T^3 + nc_{Schottky}(g\mu_B H/k_B T), \quad (2)$$

where

$$c_{\text{Schottky}}(x) = x^2 \frac{e^x}{(1 + e^x)^2}. \quad (3)$$

All data sets are fit simultaneously to eqns 1, 2, and 3 with a Landé g-factor of $g = 2$ [9]. Thus, β and n are constrained by multiple data sets, $\gamma(0)$ and α are constrained by the zero-field data, and $\gamma_\perp(H)T$ is allowed a different value at each field. The statistical confidence levels are determined by a boot strapping technique [12], in which alternative data sets are randomly chosen from the original data set and the fitting procedure is repeated. This procedure for determining the statistical error bars avoids making any assumption about the statistical error distribution of the data set.

The parameters determined from this fit are shown in Table 1, with 90% statistical confidence levels. The coefficient of the Schottky anomaly, n, indicates 0.1% spin-$\frac{1}{2}$ particles per Copper. The coefficient of the Debye term, $\beta = 0.39$ mJ/mol K^4, corresponds to a Debye temperature of 400 K. The difference in the Debye term between the two samples is within the systematic error of the Debye term of the addenda. The rms deviation of the data from the fit is 0.8% for T1 and 2.7% for U1. The higher scatter in the data for the untwinned crystal U1 results from the smaller sample size. The data and fits for both samples are shown in Fig. 2, with the phonon specific heat (βT^3) subtracted.

In the measurements on single crystals of YBCO reported here, the phonon specific heat obeys the Debye βT^3 law up to 8 K. In the zero-field data set on sample T1, for example, fits from 2 to 4 K and from 4 to 7 K give the same value of

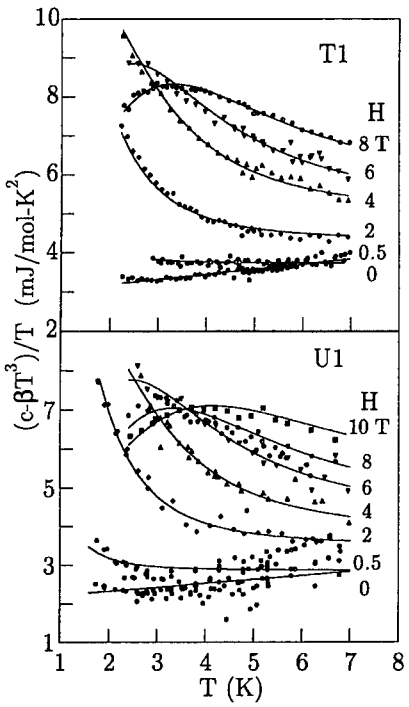


Fig. 2. Nonphonon specific heat for samples T1 and U1, with the global fit described in the text.

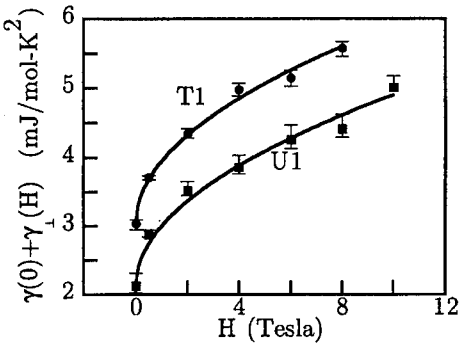


Fig. 3. Coefficient of the linear term for crystals T1 and U1, determined by the global fit described in the text.

β within statistical error, indicating that higher powers of temperature are not necessary to describe the data. Above 8 K, the deviations from βT^3 are better described by a gapped excitation such as an optical phonon mode than by a sum of T^5, T^7, and T^9 terms. In contrast, the data on many polycrystalline samples require a large T^5 term to describe the phonon specific heat even below 5 K [13]. In order to avoid the extra parameters necessary to describe the phonon specific heat above 8 K, all of the fits reported in this paper are restricted to $T \leq 7$ K.

The field-dependent linear term, $\gamma_\perp(H)T$, has a nonlinear dependence on field (Fig. 3). This nonlinear field dependence is well-described by $\gamma_\perp(H) = A\sqrt{H}$, with $A = 0.9$ mJ/mol K^{2}T$^{1/2}$ for both samples T1 and U1.

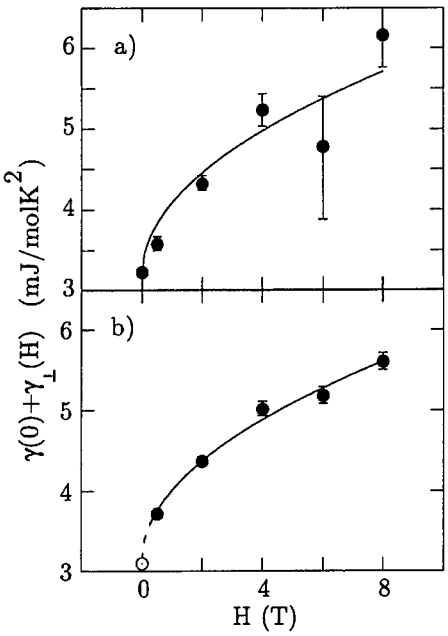


Fig. 4. Coefficient of the linear term for crystal T1, determined by (a) independent fits in which all parameters might be field-dependent, and (b) a global fit with the $H = 0$ data set excluded.

4.2. *Perpendicular field—alternative fits*

The qualitative nonlinearity of $\gamma_\perp(H)$ is robust to the assumptions used to describe the total specific heat, and is well described by $\gamma_\perp(H) = A\sqrt{H}$. To check the assumptions of the global fit and the interdependence of the αT^2 and $A\sqrt{HT}$ terms, each data set of sample T1 is fit independently to eqn (2). There are thus three parameters each for five data sets ($H = 0.5$–8 T) and two parameters for the zero-field data set (note that $c_{\text{Schottky}}(T, 0) = 0$), totaling seventeen parameters for six data sets. No zero-field quadratic term was allowed in this fit. A small quadratic term, if present, could easily be absorbed into a slightly larger cubic term, and this fit results in a $\beta(H = 0)$ which is $\sim 5\%$ higher than $\beta(H \neq 0)$. The coefficients of the linear term are shown in Fig. 4a with error bars at the statistical 90% confidence level. Fitting the coefficients of the linear term to $\gamma_\perp(H) = A\sqrt{HT}$ gives $A = 0.89$ mJ/mol K^{2}T$^{1/2}$.

In another check which avoids the zero-field data entirely, the five data sets with $H \geq 0.5$ T are globally fit to eqn (2), again keeping β and n independent of field. There are thus two global parameters, plus values of $(\gamma(0) + \gamma_\perp(H))$ in five fields (Fig. 4b). The resulting linear-T term is better described by a $\sqrt{H}$ dependence than by an H dependence, and from the fit shown in Fig. 4b, $A = 0.87$ mJ/mol K^{2}T$^{1/2}$. This fit also returns an extrapolated value of $\gamma(0) = 3.1$ mJ/mol K^2, which is in agreement with the value determined by independently fitting just the zero-field data.

Table 2. Zero-field linear term, $\gamma(0)$ (mJ/mol K^2).

Sample	$7-\delta$	Untwinned	$\gamma(0)$	$N(E_F)/N_n$
T1	6.95	no	3.1	~ 15%
U1	6.95	yes	2.1	~ 10%
U1	6.97	yes	1.9	~ 10%
T2	6.95	no	2.8	~ 15%
U2	6.95	yes	2	~ 10%

4.3. *Parallel field*

The data on sample T1 in an 8 Tesla parallel field show a linear-T term, $\gamma_{\|}(H)T$, which is increased by about 0.5 mJ/mol K^2 from $\gamma(0)$, as determined by fitting the data in Fig. 1 to eqn (2). Because of uncertainties in the Schottky anomaly and the sample alignment, the results are also consistent with no increase in the parallel-field linear term, $\gamma_{\|}(H)T$.

4.4. *Zero-field linear term*

The coefficient of the zero-field linear term, $\gamma(0)T$, in the specific heat of each of the four samples is shown in Table 2. The zero-field linear term for the two twinned samples, samples T1 and T2, is $\gamma(0) = 3$ mJ/mol K^2, while in both untwinned samples, U1 and U2, the linear term is reduced to $\gamma(0) = 2$ mJ/mol K^2. In contrast, most YBCO samples have $\gamma(0) \geq 4$ mJ/mol K^2 [13]. The coefficient of the linear term in the normal state of optimally-doped YBCO, γ_n, has been shown by other measurements to be about 20 mJ/mol K^2 [13,14]. The residual density of states $N(E_F)$ in the superconducting state is therefore about 15% of the normal-state density of states for the twinned samples and about 10% for the untwinned samples.

5. DISCUSSION

5.1. *Comparison with lines of nodes*

The quadratic term is predicted to disappear in a magnetic field, where the energy dependence of the density of states close to the nodes, $N(E, H=0) \propto |E - E_F|$, is replaced by a finite $N(E_F, H)$. The αT^2 term is comparable in magnitude to the systematic uncertainty in the addenda T^3 phonon specific heat, but is several times larger than the relatively small systematic uncertainty of the field dependence, < 1%. The global fit is thus the only possible way to identify the quadratic term in these data sets. The slight positive slope of the zero-field data set in Fig. 2 can be described either as a phonon term which is about 5% larger in zero field, which is difficult to explain, or as an αT^2 term.

From the slope of the density of states in a superconductor with lines of nodes it is possible to predict $\alpha \approx \gamma_n/T_c \approx 0.2\,\mathrm{mJ/molK^3}$ for YBCO within factors of order unity [8], in good agreement with the value $\alpha = 0.1\,\mathrm{mJ/molK^3}$ obtained from the global fits (Table 1) on samples U1 and T1.

For the field dependence of the density of states, Volovik predicts $N(E_F, H) = \kappa N_n \sqrt{H/H_{c2}}$ [6], where κ is of order 1 and is defined by the vortex lattice structure, by the slope of the gap near the gap node, and by possible structure in N_n. Taking $\gamma_n = 20\,\mathrm{mJ/molK^2}$ [13,14] and $H_{c2,\perp} = 150\,\mathrm{T}$ gives the prediction $\gamma_{\perp}(H) = A\sqrt{H}$ with $A = \kappa * 1.6\,\mathrm{mJ/molK^2T^{1/2}}$, in good agreement with the value $A = 0.9\,\mathrm{mJ/molK^2T^{1/2}}$ found for both samples U1 and T1.

Both of the above comparisons used the measured value of γ_n, the angular averaged normal state density of states. Because both the αT^2 and $A\sqrt{H}T$ terms are a consequence of the nodes, these terms should be sensitive to the normal-state density of states close to the nodes. The above comparisons may indicate that the density of states close to the nodes is smaller than the angular average of the density of states, as indicated by photoemission measurements on BSCCO [15].

These predictions do not distinguish between different types of lines of nodes, such as d-wave or extended s-wave [16]. In principle, this interpretation could also apply to a gap function with no nodes, but with a very small minimum gap, $\Delta \ll k_B T \approx 0.5\,\mathrm{meV}$. In order to produce these results, such a gap function would need to have an unusual energy dependence of the density of states similar to that associated with lines of nodes, $N(E, H=0) \propto |E - E_F|$.

A quadratic T^2 term has been known for some time in the specific heat of heavy-fermion superconductors, and has recently been reported in the specific heat of $La_{2-x}Sr_xCuO_4$ [17]. Two other recent works support the existence of a $\sqrt{H}$ term in superconductors with lines of nodes: a reanalysis of existing data on polycrystalline YBCO samples shows a nonlinear $\gamma(H)$T term which appears consistent with $\sqrt{H}$ [18], with similar but less dramatic curvature on Ca- and Sr-doped La_2CuO_4 samples, and a $\sqrt{H}$ term has also been recently reported in the low-temperature specific heat of UPt_3 [19].

5.2. *Residual density of states*

The total residual density of states $N(E_F)$ in the superconducting state, as determined from the $\gamma(0)T$ term in the specific heat, is about 15% of the normal-state density of states for the twinned samples and about 10% for the untwinned samples (Table 2). The residual density of states can also be extracted from fitting the temperature dependence of the penetration depth [2] to the d-wave model with scattering of Hirschfeld *et al.* [5]. In samples similar to the samples measured here, these fits are inconsistent with a density of states which is greater than 1% of N_n [5]. It appears difficult to reconcile the zero-field linear term $\gamma(0)T$ with the αT^2 and $A\sqrt{H}T$ terms, and with the interpretation of the temperature dependence of the penetration depth. It is possible that the zero-field linear term has a separate origin from the excitations which give rise to the quadratic term and the field dependence of the specific heat. This assumption leads to a self-consistent analysis of the specific

heat, and is given additional support by the measurements on the untwinned crystal U1, in which $\gamma(0)$ is decreased substantially but the αT^2 and $A\sqrt{H}T$ terms are unchanged within statistical error bars.

5.3. *Interpretation of the $A\sqrt{H}T$ term*

Conventional high-κ superconductors are expected to have a linear-T term in the specific heat which is proportional to the volume of normal material in the cores, $c \approx \gamma_n TH/H_{c2}$ [7,20], and such an HT term has been observed in A15 superconductors [21]. The analysis which predicts this HT term does not apply to cuprate superconductors for two reasons. First, the small coherence length of the cuprates may result in a large excitation gap for quasiparticles which are confined to the vortex cores [7,22]. Secondly, Caroli, deGennes, and Matricon [7] assumed a fully gapped superconductor in showing that the quasiparticle excitations are confined to the vortex core.

Some form of a linear-H term might be expected in the specific heat for any excitations which are confined to the vortex cores. Although there may in principle be some dependence of the core excitations on magnetic field, it is likely that for $H \ll H_{c2}$ the core excitations would be roughly independent of field. Thus, any signal resulting from these excitations would simply be proportional to the number of cores, or linear in H. The nonlinear field dependence of the observed $N(E_F, H)$ suggests excitations outside the vortex core.

The physical origin of the density of states predicted by Volovik [6] is the same as the physical origin of the depairing current in a conventional superconductor. In the presence of a supercurrent with velocity $\vec{v}_s$, the quasiparticle excitation spectrum $\xi(\vec{k})$ is shifted by an amount $\vec{k} \cdot \vec{v}_s$. Far from the vortex core in a fully gapped superconductor, this shift is not large enough to change the density of states at the Fermi level, which is given by

$$N(E_F) = \int \frac{d^3k}{(2\pi)^3} \int d^2r \delta\left(\xi(\vec{k}, \vec{r}) - \vec{k} \cdot \vec{v}_s\right). \qquad (4)$$

For a superconductor with lines of nodes, the shift is significant everywhere that the superfluid velocity is not zero. Assuming a vortex superfluid flow $v_s \propto 1/r$, the local density of states at the Fermi level also falls off as $1/r$ (Fig. 5). Integrating over an entire vortex, with the intervortex spacing $R(H)$ as the upper cutoff in the integral, gives a density of states per vortex $N(E_F, H) \propto R(H) \propto 1/\sqrt{H}$. Multiplying by the number of vortices, which is proportional to H, then gives the total density of states $N(E_F, H) \propto \sqrt{H}$.

The shift in the excitation spectrum depends on the angle between the local superfluid velocity and the nodes, giving the vortex the same symmetry as the gap (Fig. 5). Because the nodes are 90° apart, the superfluid velocity can never be perpendicular to all nodes, and there are no places where $N(E_F)$ becomes zero. Both the density of states, and in a clean system the anisotropy in the density of states, extend throughout the entire vortex.

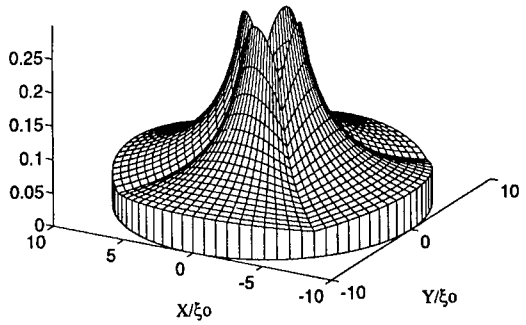


Fig. 5. Schematic of the local density of states $N(E_F)/N_n$ throughout a d-wave vortex.

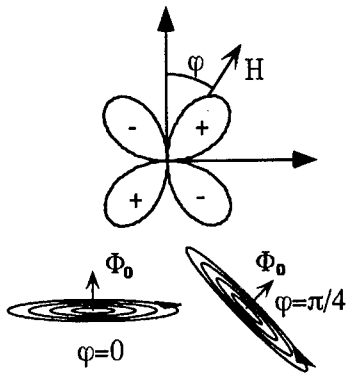


Fig. 6. The azimuthal field angle φ relative to a tetragonal d-wave order parameter, and sketch of the current flows associated with an in-plane vortex for $\varphi = 0$ and $\varphi = \pi/4$.

Parks *et al.* [23] have pointed out that their measurements of vortex dynamics in YBCO thin films are best explained by the presence of the extra quasiparticles expected for a vortex with an anisotropic gap. Recent theoretical work suggests that the structure of the vortex core in a d-wave superconductor is both interesting and complicated [6,24,25]. We have deliberately omitted the core region from Fig. 5, since we are not aware of any model for the core which suggests that our measurements are probing the core states.

5.4. *Predicted parallel field dependence*

Because $N(E_F, H)$ depends on the orientation of the current with respect to the nodes, improved measurements of the full angular dependence $\gamma_{\theta,\varphi}(H)T$ should be sensitive to the positions of the nodes. Define the orientation of the applied field $\vec{H}$ as (θ, φ), where θ is the polar angle measured with respect to the c-axis and φ is the azimuthal angle measured with respect to the (110) crystalline axes. For tetragonal $d_{x^2-y^2}$ symmetry with antinodes along the Cu–O bonds, $\varphi = 0$ corresponds to a field parallel to a node (Fig. 6). In this orientation, $(\theta = \pi/2, \varphi = 0)$, the currents in the ab-plane are flowing parallel to a single node.

The density of states at the Fermi level is $\sqrt{2}$ larger at ($\theta = \pi/2, \varphi = \pi/4$), where the currents flow parallel to the antinodes (Fig. 6): in this orientation, the density of states picks up contributions from all of the nodes. The complete in-plane angular magnetic field dependence of the density of states is given by

$$N(0, H, \theta = \pi/2, \varphi) = \frac{\kappa'}{2} (|\sin\varphi| + |\cos\varphi|) N_F \sqrt{\frac{H}{H_{c2\|}}}, \quad (5)$$

as shown by Volovik [26]. Using $\gamma_n = 20\,\mathrm{mJ/molK^2}$ and taking $H/H_{c2\|} = 0.005$ as an experimentally accessible field, the field-dependent linear term $\gamma_\|(H)$ will vary from 0.7 to 1.0 mJ/mol K^2 as a function of the azimuthal angle φ. This predicted angular dependence of the linear term in the specific heat may be within achievable experimental resolution, although preliminary measurements at 8 Tesla on a heavily twinned sample with the field parallel to the twins and at a 45 deg angle to the twins did not detect any angular variation in $\gamma_\|(H)$.

6. SUMMARY

The residual density of states at the Fermi level in the superconducting state of single-crystal $YBa_2Cu_3O_{7-\delta}$, $N(E_F, H = 0)/N_n$, is determined by the zero-field linear term $\gamma(H = 0)T$ in the specific heat. $N(E_F, H = 0)/N_n$ is qualitatively larger than would be expected from fitting the temperature dependence of the penetration depth [2] to expressions for lines of nodes with scattering [5]. In two twinned single crystals, $\gamma(H = 0)/\gamma_n \approx 0.15$, while in two untwinned single crystals, $\gamma(H = 0)/\gamma_n \approx 0.10$.

The specific heat also includes a $\gamma_\perp(H)T$ term, which obeys $\gamma_\perp(H) \approx \gamma_n\sqrt{H/H_{c2}}$ as predicted for superconductors with lines of nodes in the gap function [6]. This nonlinear field dependence of the density of states suggests quasiparticle excitations outside the vortex core, and appears to be independent of twinning, unlike the zero-field linear term. The in-plane angular magnetic field dependence of the specific heat, which is smaller than the perpendicular magnetic field dependence, is predicted to be sensitive to the locations of the nodes.

Acknowledgments— We thank M. R. Beasley, C. Varma, and especially G. Volovik for many useful discussions, and R. A. Fisher, N. E. Phillips and J. Gordon for sharing their analysis prior to publication.

REFERENCES

1. see e.g. Scalapino D., *Physics Reports* **250**, 329 (1995); Pines D. and Monthoux P., *J. Phys. Chem. Solids*, to be published, 1995.
2. Hardy W. N. *et al.*, *Phys. Rev. Lett* **70**, 3999 (1993).
3. Annett J. *et al.*, *Phys. Rev. B* **43**, 2778 (1991).
4. Prohammer M. *et al.*, *Phys. Rev. B* **47**, 15152 (1993).
5. Hirschfeld P. J. *et al.*, *Phys. Rev. B* **50**, 10250 (1994).
6. Volovik G. E. *JETP Lett.* **58**, 469 (1993).
7. Caroli, deGennes and Matricon, *Phys. Lett.* **9**, 307 (1964).
8. Moler K. A. *et al.*, *Phys. Rev. Lett.* **73**, 2744 (1994).
9. Moler K. A. *et al.*, *Proc. U-Miami Workshop*, to be published in *J. Supercond.* (1995).
10. Ruixing Liang *et al.*, *Physica C* **195**, 51 (1992).
11. Urbach J. S. *et al.*, *Phys. Rev. B* **39**, 12391 (1989).
12. Efron B., *An Introduction to the Bootstrap*. Chapman & Hall, New York (1993).
13. see e.g. Phillips N. E. *et al.*, *Prog. in Low Temp. Phys. XIII* (Edited by D. F. Brewer). Elsevier Science Publishers B. V., Amsterdam (1992); Junod A., *Physical Properties of HTSC II* (Edited by D. Ginsberg). World Scientific, Singapore (1990).
14. Loram J. W. *et al.*, *Phys. Rev. Lett.* **71**, 1740 (1993).
15. Dessau D. S. *et al.*, *Phys. Rev. Lett.* **71**, 2781 (1993).
16. Varma C. M., private communication; Littlewood P. B. *et al.*, *Phys. Rev. Lett.* **63**, 26002 (1989).
17. Momono N. *et al.*, *Physica C* **233**, 395 (1994).
18. Fisher R. A. *et al.*, unpublished.
19. Ramirez A. *et al.*, *Phys. Rev. Lett.* **74**, 1218 (1995).
20. Fetter A. L. and Hohenberg P., in *Superconductivity*, Vol. II (Edited by Parks). (1969).
21. Stewart G. R. and Brandt B. L., *Phys. Rev. B* **29**, 3908 (1984).
22. Karrai K. *et al.*, *Phys. Rev. Lett.* **69**, 152 (1992).
23. Parks B. *et al.*, *Phys. Rev. Lett.*, to be published.
24. Soininen P. I. *et al.*, *Phys. Rev. B* **50**, 13883 (1994).
25. Berlinsky A. J. *et al.*, preprint.
26. Volovik G. E., unpublished.

Pergamon

J. Phys. Chem. Solids Vol. 56, No. 12, pp. 1905–1906, 1995
Copyright © 1995 Elsevier Science Ltd
Printed in Great Britain. All rights reserved
0022–3697/95 $9.50 + 0.00

0022–3697(95)00092-5

ANOMALIES IN VORTEX STATES OF CUPRATE SUPERCONDUCTORS

C. BOEKEMA, I. M. SUAREZ-BARNES and V. A. GUBANOV
Physics Department, San Jose State University, San Jose, U.S.A.

D. W. COOKE and M. LEON
Los Alamos National Laboratory, Los Alamos, NM 87545, U.S.A.

Abstract—A maximum-entropy (ME) technique has been applied to transverse-field (TF) muon-spin relaxation (μSR) data of several cuprate superconductors [1, 2]. For the $RBa_2Cu_3O_7$ (R1237) vortex states, we have seen low-field tails and cliffs in the ME field distribution estimates for TFμSR data recorded near 5 K at 1 kOe. The sharp fall-off is *only* present when R is a magnetic ion (like Er or Gd), or occurs for Pr-doping in Y1237. The ME vortex field distributions of $Bi_2Sr_2CaCu_2O_x$ (Bi2212) and $Tl_2Ba_2Ca_2Cu_3O_x$ (Tl2223) show *no* low field tails well below T_c , which is consistent with vortex pancake formation. ME transforms for $Pb_{0.9}In_{0.1}$ (a *typical* type-II superconductor) show the expected vortex field distributions. All the (magnetic) non-BCS like anomalies seen for the cuprate vortex states suggest that perhaps the cuprate superconductors are not (typical) type-II superconductors [Alves S. *et al.*, *Phys. Rev. B* **49** 12396 (1994)].

Keywords: A. ceramics, A. superconductors, D. magnetic structure, D. muon-spin resonance, D. superconductivity.

1. INTRODUCTION

For CuO-based superconductors, the question whether the vortex field distribution is best described by a vortex lattice, a vortex glass or vortex pancakes is crucial. TFμSR, a microscopic magnetic probe technique, may provide direct answers. In our earlier communications [1], we have shown that the ME method to analyze TFμSR data is superior at identifying fine features in magnetic field distributions, such as potential van Hove singularities. Analysis by means of Fourier methods and Gaussian curve fitting of TFμSR data has been succesful at a macroscopic scale, i.e. determination of penetration depths and flux-pinning strengths.

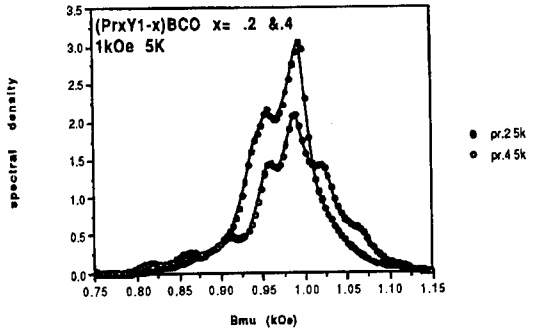


Fig. 1. ME transforms for $(Pr_xY_{1-x})1237$ (x=0.2 (∘) and 0.4 (∘) ; 5 K and 1 kOe)

2. MEμSR FOR R1237, Bi2212, Tl2223

Below, we highlight the results of the ME–Burg application [2] to TFμSR data recorded for R1237 [R = (Pr,Y), Er, Gd, Eu], Bi2212 and Tl2223. The polycrystalline cuprate samples are high quality single phase ceramics; the samples were field-cooled in a 1 or 5 kOe transverse field. The Er and Gd ions, and the Pr ions doped in Y1237, carry magnetic moments, while Eu and Y do not. Three *non*-Abrikosov features are seen for R1237 vortex field distributions: a sharp fall-off for magnetic R ions, a low-field tail (which appears to be enhanced by the R magnetism) and a small contribution from non-superconducting grain boundaries [1]. For $(Pr_xY_{1-x})237$, we have observed a fall-off for x = 0.2 and 0.4 at about 50 Oe below the applied field (see Fig. 1). The (sharp) fall-offs may be signatures of van Hove singularities; normally, these are expected only for single crystal type-II vortex states. These anomalies occur only when magnetic ions are present in our polycrystalline samples. These "magnetic" van Hove singularities, if confirmed, may be essential ingredients in any cuprate vortex model description. Further analysis for all x, especially around 0.5, is in progress.

In an *in*direct way, the low-field tail in the vortex field distribution has also been shown to exist: Gaussian curve fitting was used to analyze Triumf TFμSR data [3] recorded for a single crystal Y1237 at 5 and 15 kOe. Below about 30 K the Gaussian μ-spin relaxation rate (σ) does depend on the applied field. For type-II vortex states, σ should *not* depend on the transverse field magnitude. Gaussian curve fitting of *simulated* TFμSR data with a field distribution *including* a 300 Oe long low-field tail for applied fields of 5 and 15 kOe reproduces their artificial fit results [3]. Thus, Gaussian curve fitting, which uses only *one* average μ-spin

precession frequency is not adequate to describe completely the unusual field distribution. The low field tail does *not* show up in the vortex field distributions of Bi2212 and Tl2223 below T_c [1]. This remarkable difference is probably caused by pseudo two-dimensional vortex pancake formation in Bi2212 and Tl2223, and not in R1237, where the vortex structure is still three-dimensional.

3. MAGNETIC FRUSTRATION

The existence of the low-field tail for all R1237 vortex field distributions reveals that, in the mixed state, atomic regions exist for which the magnetic field is significantly lower than predicted by Abrikosov theory. The electrons in the superconducting layers have managed to screen the applied field for these "low-field tail" muons, probing competing, perhaps random, magnetic fields. The presence of magnetic ions appears to influence this magnetic frustration. For the largest magnetic moment (R=Er), the low-field tail at 4.5 K stretches even out to near zero field [1]. Field-induced magnetic frustration in the vortex glass state may be a possible explanation for the vortex tails in R1237. We have begun modeling frustration in vortex systems, similar to one used for spin-glass freezing [4], and we explore its connections to the two-dimensional Coulombic gas, which serves as a model for vortex behavior in pseudo two-dimensional superconductors.

REFERENCES

1. Alves S. *et al.*, *Phys. Rev. B* **49**, 12396 (1994) and *Hpf InterA* **86**, 513 (1994); Boekema C. *et al.*, *Hpf InterA* **86** 487, (1994) and *Physica C* **235–240**, 2663 (1994).
2. An extensive article on ME applications to TFμSR is in preparation; the first two references in [1] provide a comprehensive summary.
3. Kiefl R. F. *et al.*, *Hpf InterA* **86**, 537 (1994).
4. Boekema C., Suarez I. M. *et al.*, *Hpf InterA* **64**, 467 (1990).

Pergamon

J. Phys. Chem. Solids Vol. 56, No. 12, pp. 1907–1908, 1995
Copyright © 1995 Elsevier Science Ltd
Printed in Great Britain. All rights reserved
0022–3697/95 $9.50 + 0.00

0022–3697(95)00095-X

QUASIPARTICLE CONTRIBUTION TO THE MIXED-STATE THERMOPOWER IN $Tl_2Ba_2CaCu_2O_{8+\delta}$

J. A. CLAYHOLD and C. W. CHU
Texas Center for Superconductivity, University of Houston, Houston, TX 77204-5932, U.S.A

Abstract—Measurements of the thermopower and resistivity of $Tl_2Ba_2CaCu_2O_{8+\delta}$ in the vortex state indicate a significant contribution to the thermopower from normal quasiparticles below T_c .

The significance of normal-quasiparticle currents in mixed-state transport phenomena in cuprate superconductors has been underscored by recent measurements [1] and analyses [2] of the Hall effect below T_c . The Hall conductivity is comprised of two additive components, from vortices and quasiparticles respectively, which are distinguishable by their different dependences on the applied magnetic field. We provide evidence here that the same two sources, vortices and quasiparticles, can also be distinguished by their seperate contributions to the mixed-state thermoelectric power.

The vortex thermopower has a particularly simple form, sharing the same magnetic-field dependence as the mixed-state electrical resistivity. Using a simple kinetic equation for the total current, j, (which is zero in the experimental measurement):

$$j = 0 = \sigma E - P\nabla T \tag{1}$$

where E is the electric field, T is the temperature, σ is the conductivity and P is the kinetic coefficent commonly called L_{12}. We follow the notation of Caroli and Maki [3]. The thermopower S is the ratio of P to σ:

$$S = \frac{E}{\nabla T} = \frac{P}{\sigma} = P\rho \tag{2}$$

where ρ is the resistivity. As suggested by Caroli and Maki [3] and verified experimentally by Fiory and Serin [4], the quantity P is an intrinsic property of the normal-core electrons and is therefore independent of the magnetic field.

For quasiparticles, the coefficient P is of a different form, varying inversely with magnetic-field strength at high-field. P is given by a Boltzmann integral over occupied states, as in standard textbooks

$$P_{qp} = \frac{e}{T}\int \frac{\mathbf{dk}}{4\pi^3}\left(-\frac{\mathrm{d}f}{\mathrm{d}\varepsilon}\right)(\varepsilon-\mu)v^2\tau(\varepsilon), \tag{3}$$

where ε is the energy, μ is the chemical potential, and v is the velocity. The magnetic-field dependence enters through the relaxation time, τ. Recent measurements [5] have shown that vortices are the dominant scatterers of quasiparticles below T_c in magnetic fields greater than a few Tesla. It follows that both τ and P_{qp} vary inversely with the magnetic field strength: $P_{qp} \propto 1/H$.

When both vortices *and* quasiparticles are present, then the total conductivity is the sum of the conductivities of each species. Similarly the coefficients, P_{qp} and P_v are additive. The ratio of the measured thermoelectric power to the measured resistivity is given by

$$\frac{S}{\rho} = P_{qp} + P_v = \frac{\alpha}{H} + \beta, \tag{4}$$

where α and β are constants, independent of the magnetic field.

We measured the thermoelectric power and resistivity as a function of magnetic field at several temperatures in an epitaxial film [6] of $Tl_2Ba_2CaCu_2O_{8+\delta}$ with T_c = 105 K. The curves were non-hysteretic and linear in current and applied thermal gradient respectively. The magnetothermopower of the Au contact wires causes a small systematic underestimate, no more than 5 %, of the thermopower signal, at our lowest temperature. At the highest temperature, the error is less than 0.2 %. The ratio of the thermopower to the resistivity, S/ρ, is shown in Fig. 1(a).

At high field, the values of S/ρ approach constant, field-independent values, as was seen for the vortex thermopower in conventional superconductors [4]. At low field, the curves diverge, possibly indicating the presence of the α/H term from normal quasiparticles. Figure 1(b) shows the same data multiplied by the magnetic field strength to remove the divergence at H = 0. According to eqn (4), the data for HS/ρ should fall on straight lines, with the intercepts representing the quasiparticle currents.

The solid lines in Fig. 1(b) are linear least-squares fits to the data above H = 4 T. The temperature-dependences of the coefficients, α and β, are shown in Fig. 2. The coefficient β, representing the vortex contribution, increases slowly by a factor of 2 as the temperature decreases to 65 K, but the extrapolated normal-state resistivity would decrease by the same factor, indicating that nothing special is happening to the vortex thermopower as a function of temperature. In contrast, the quasiparticle term, α, increases sharply with decreasing temperature, possibly reflecting the diverging relaxation time below T_c [5].

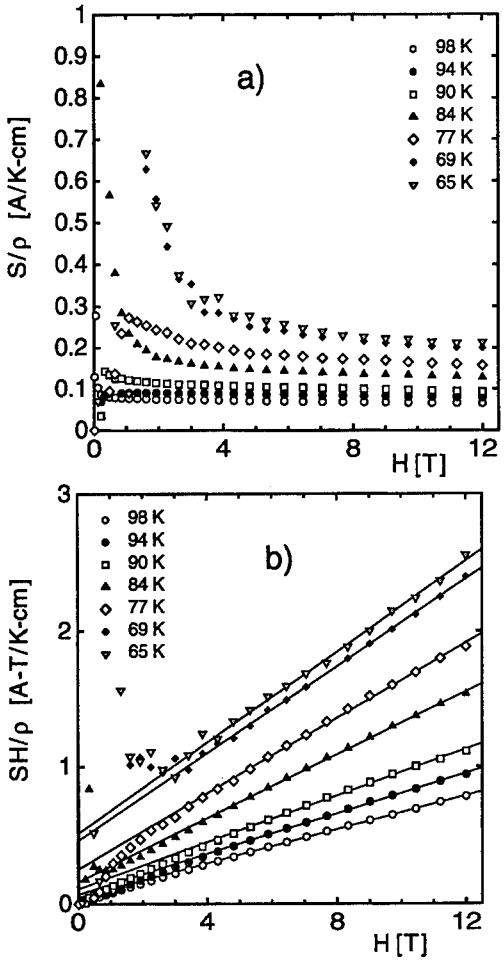


Fig. 1. (a) Ratio of the measured thermoelectric power to the measured resistivity, showing the magnetic field dependence of the coefficient, P. (b) The same data multiplied by the magnetic field strength, H, illustrating the agreement of the data with eqn (4).

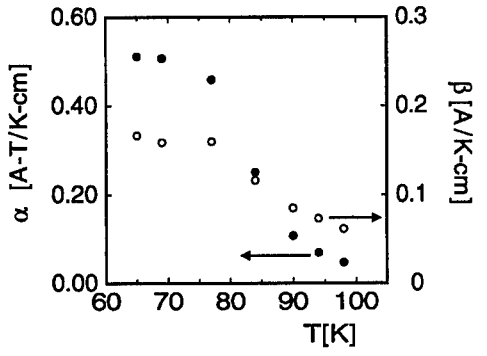


Fig. 2. T-dependence of fit parameters α and β.

F49620-93-1-0310, NSF Grant No. DMR 91-22043, ARPA Grant MDA 972-90-J-1001, the Texas Center for Superconductivity at the University of Houston, and the T. L. L. Temple Foundation.

REFERENCES

1. Harris J. M., Ong N. P. and Yan Y. F., *Phys. Rev. Lett.* **73**, 610 (1994).
2. Geshkenbein V. B. and Larkin A. I., *Phys. Rev. Lett.* **73**, 609 (1994).
3. Caroli C. and Maki K., *Phys. Rev.* **164**, 591 (1967).
4. Fiory A. T. and Serin B., *Physica* **55**, 73 (1971).
5. Krishana K., Harris J. M. and Ong N. P., these proceedings.
6. Superconductor Technologies Inc., 460 Ward Drive, Santa Barbara, CA 93111-2310, U.S.A..

Pergamon

J. Phys. Chem. Solids Vol. 56, No. 12, pp. 1909–1910, 1995
Copyright © 1995 Elsevier Science Ltd
Printed in Great Britain. All rights reserved
0022–3697/95 $9.50 + 0.00

0022-3697(95)00218-9

FIELD-INDEPENDENT MAGNETIZATION AND FLUCTUATIONS IN Hg-BASED CUPRATES

Y. Y. XUE, Y. CAO, Q. XIONG, F. CHEN and C. W. CHU[1]

Department of Physics and Texas Center for Supercoductivity at University of Houston, University of Houston, Houston, TX 77204-5932, U.S.A.

Abstract—The crossing of the magnetization M of cuprates in different fields at (M^*,T^*) has been widely interpreted as a result of 2D vortex-fluctuations. Therefore, it is expected that the M^*/T^* of $HgBa_2Ca_mCu_{m+1}O_y$ will be proportional to the 2D sheet-density $1/s$, where s is the size of the unit cell. However, our data show that the M^*/T^* is independent of both m and s in the Hg-based cuprates with $1 \leq m \leq 3$. A survey further suggests that the value of M^*/T^* is a universal constant for all studied Bi-, Tl- and Hg-based cuprates. This observation suggests that the coupling between neighboring CuO_2-blocks may have non-negligible effects on the magnetization.

It has been observed in nearly all high temperature superconductors that the reversible magnetization $M(H)$ at different $H \gg B_{cr}$ crosses at (M^*,T^*) with $T^* < T_c$, where B_{cr} is a threshold field [1–3]. $-M$ decreases with H below T^* as predicted by the London model. However, $-M$ increases with H above T^* similar to that in the fluctuation region above T_c. This field-independent magnetization was commonly interpreted in terms of 2D fluctuations of either the vortex-pancake position [2] or the overall amplitude of the order parameter [3]. Fluctuations, therefore $-M^*$, should be enhanced with the increase of the sheet-density in any purely 2D models. A theoretical expression of $-M^* = k_BT^*/(\phi_0 s)$ was deduced [2,3] with ϕ_0 and s being the flux-quantum and the size of the effective unit-cell along the c direction, respectively. These 2D models were widely used in analyzing magnetization data [4]. However, the measured $-M^*$ was always smaller than the predicted $k_BT^*/(\phi_0 s)$, and the ratio $M^*\phi_0 s/(k_BT^*)$ was taken as the superconducting volume fraction f in some works to accommodate the discrepancy.

To study the proposed $M^* - s$ correlation, we measured M^* of well-characterized and optimally-doped $HgBa_2Ca_mCu_{m+1}O_y$ with $1 \leq m \leq 3$. To estimate the change of f between the samples with different m experimentally, the normal-state carrier concentration n (deduced from the thermopower at 290 K) and the slope $\partial M/\partial lnH \propto f/\lambda_{ab}^2$ were measured for the samples with different m. The ratio $n/[\partial M/\partial \ln H]$ was used to estimate the change of f, assuming that $n\lambda_{ab}^2$ is the same for all optimally-doped samples in the Hg-family at the same reduced temperature. A variation of f at $\sim$ 20% level is experimentally detectable .

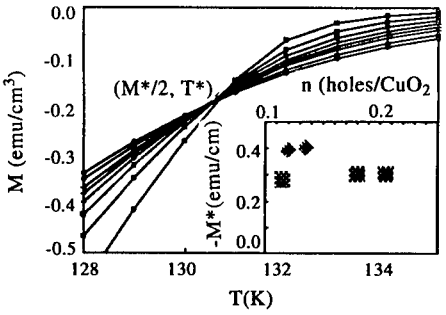


Fig. 1. M vs T at different H (0.5, 1, 1.5, 2, 3, 4 and 5 T from top to bottom below 130 K) for a Hg-1223 sample. the lines are a guide to the eye. Inset: $-M^*$ at various doping levels for ■ Hg-1201, ♦ Hg-1223.

Hg-1201 was synthesized at ambient pressure in a sealed quartz tube, Hg-1212 and Hg-1223 were synthesized under 3 GPa pressure [5]. Various annealing procedures were used to change the doping level of the samples [5]. X-ray/neutron diffraction data demonstrated that the possible impurity phases are at a few percent level for all used samples. The measured $n/(\partial M/\partial \ln H)$ are independent of m within 20% for the optimally-doped $HgBa_2Ca_mCu_{m+1}O_y$ at the same reduced temperatures. All these demonstrate that the change of f is not a significant factor here. The superconducting transition width of the samples is 1–2 K measured by the field-cooled magnetization at 5 G. The paramagnetic background was estimated from the Curie-Weiss fit above T_c and subtracted from the raw data. 2D critical-scaling fits [3] above $\sim H_{c2}/3$ were made to crosscheck the background-subtraction procedure. The measured M of our ceramic samples was converted into the magnetization of a corresponding single crystalline with $H \parallel c$ following the procedure suggested in Ref. [6]. The crossing of M is clearly

[1] Present address: Physics Department, University of Arkansas, Fayetteville, AR 72701, U.S.A.

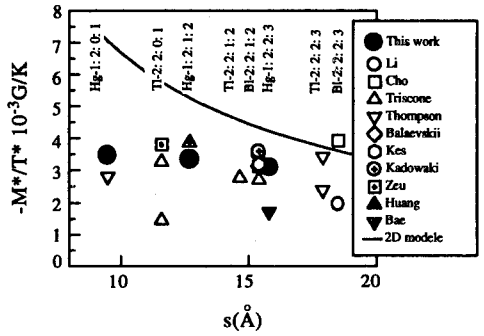


Fig. 2. $-M^*/T^*$ vs s. •: this work; other symbols: Refs [2,3,4,7];—:2D model prediction

observed in all samples above ~ 1 Tesla (Fig. 1).

On one hand, our data support the conclusion of Refs [2] and [3] that M^* is a fundamental scale in the fluctuation region. The measured M^*/T^* appears to be independent of the doping level (inset of Fig. 1), therefore is a parameter of the compound. A change of $\partial M/\partial lnH$ across a field B_{cr} was observed in a wild temperature range below T^*. The measured value of $[\partial M/\partial \ln H|_{H=0.1T} - \partial M/\partial \ln H|_{H=5T}] \times T^*/(TM^*)$ is ~ 1, demonstrating that the change $\Delta(\partial M/\partial \ln H)$ across B_{cr} is scaled with M^* as suggested in Ref. [2]. The dimensionless variables M/M^*, $(T - T^*)/(T_c - T^*)$, and $H/H_{c2}(T)$ fit into the proposed 2D-scaling function rather well above $H_{c2}/3$, as observed early in Bi-2223 [3], again demonstrating that the observed crossing is not purely accidental.

On the other hand, the measured M^*/T^* appears to be independent of both m and $1/s$, the sheet-density of 2D vortex-pancake, which is in strong contrast with the 2D vortex-fluctuation models (Fig. 2). A survey of the published magnetization data on the Bi-, Tl- and Hg-based cuprates further demonstrates that M^*/T^* has no systematic dependence of m, $1/s$, or the charge reservoir (Bi_2O_2, Tl_2O_2 or HgO) (Fig. 2). Although the lower $-M^*/T^* \sim 1 * 10^{-3}$ G/K in $YBa_2Cu_3O_y$ [8] may suggest some effects of interlayer coupling. Since a purely 2D fluctuation should depend on the sheet-density regardless detail assumptions, the observation suggest that either our understanding of the vortex-fluctuation or the interlayer coupling in cuprates need modifications.

In summary, a nearly universal $-M^*/T^* \sim 3 * 10^{-3}$ G/K was observed in $HgBa_2Ca_mCu_{m+1}O_y$ with $1 \leq m \leq 3$ which is strong contrast with the existing 2D vortex-fluctuation models.

Acknowledgements—This work is supported in part by NSF Grant No. DMR 91-22043, USAFOSR Grant No. F49620-93-1-0310 by BMDO, EPRI, the State of Texas through the Texas Center for Superconductivity at University of Houston, and the T. L. L. Temple Foundation.

REFERENCES

1. Kes P. H. *et al.*, *Phys. Rev. Lett.* **67**, 2382 (1991).
2. Bulaevskii L. N. *et al.*, *Phys. Rev. Lett.* **68**, 3773 (1992).
3. Tesanovic Z. *et al.*, *Phys. Rev. Lett.* **69**, 3563 (1992).
4. Kogan V. G. *et al.*, *Phys. Rev. Lett.* **70**, 1870 (1993); Li Q. *et al. Phys. Rev.* **B46**, 3195 (1992).
5. Xiong Q. *et al.*, *Physica C***231**, 233 (1994); He Z. H. *et al.*, *Physica C* **241**, 211 (1995).
6. Cho J. H. *et al.*, *Physica C* **212**, 419 (1993); Huang Z. J. *et al.*, *Physica C* **228**, 211 (1994).
7. Thompson J. R. *et al.*, *Phys. Rev. B* **46**, 14928 (1993); Triscone G. *et al.*, *Physica C* **224**, 263 (1994); Kadowaki K., *Physica C* **185–189**, 2249 (1991); Zuo F. *et al.*, *Phys. Rev. B* **47**, 8327 (1993); Bae M.-K. *et al.*, *Physca C* **228**, 195 (1994).
8. Welp U. *et al.*, *Phys. Rev. Lett.* **67**, 3180 (1991).

NEUTRON AND NMR EXPERIMENTS

Pergamon

J. Phys. Chem. Solids Vol. 56, No. 12, p. 1911, 1995
1995 Elsevier Science Ltd
Printed in Great Britain
0022-3697/95 $9.50 + 0.00

0022-3697(95)00131-X

MAGNETIC FLUCTUATIONS IN LAMELLAR COPPER OXIDES

G. AEPPLI
AT&T Bell Labs, Engineering Research Center, P.O. Box 900, Princeton, NJ 08540, U.S.A.

T. E. MASON
University of Toronto, Toronto, Ontario, Canada

H. A. MOOK
Oak Ridge National Laboratory, Oak Ridge, TN, U.S.A.

S. M. HAYDEN
University of Bristol, Bristol, U.K.

It has been recognized that the magnetic characteristics of the lamellar cuprates are as peculiar as their transport properties. The talk by Mook gives an account of our work on $YB_2Cu_3O_{7-\delta}$, including especially data on the "41 meV" peak which appears to dominate the magnetic response in the superconducting phase [1]. In the present talk, we describe what is by now the quite complete set of neutron scattering data on the magnetic fluctuations in $La_{2-x}(Ba,Sr)_xCuO_4$ from the insulating antiferromagnetic ($x = 0$) regime to the superconductor ($x = 0.14$). Principal results include:

1. The complete spin-wave dispersion relation for $x = 0$, which both shows the validity of an essentially classical approach to the magnetic dynamics of this $s = 1/2$ planar antiferromagnet and gives—in the most direct fashion—the value for the underlying nearest neighbor exchange constant [2].

2. Demonstration that in the metallic temperature regime for a sample near the metal–insulator boundary ($x = 0.05$), the only obvious energy scale for the magnetic fluctuations is the temperature itself [3], in accord with the marginal Fermi liquid hypothesis.

3. Discovery that at low frequencies, the commensurate magnetic fluctuations first broaden and then separate into four remarkably sharp peaks along $(0, \pi)$ and $(\pi, 0)$ as the metallic, superconducting regime is entered from the insulator. Indeed, the widths of these peaks correspond to several inter-impurity (Sr) spacings, suggesting that the impurities are effectively screened at doping levels which are also optimal for superconductivity [4,5].

4. One of the most direct demonstrations of spin pairing in any superconductor in the form of the suppression of low frequency magnetic fluctuations below the superconducting transition [5]. The unrivalled access of magnetic neutron scattering to general momentum and energy transfers has then allowed magnetic gap spectroscopy to be performed with unprecedented detail, showing—among other things—that the low frequency excitations found in the superconducting state for our $x = 0.14$ ($T_c = 35$ K) samples are not those associated with a clean d-wave state [6]. We look forward to seeing our measurements repeated on more perfect samples.

REFERENCES

1. See e.g. Mook H. A. *et al.*, *Phys. Rev . Lett.* **70**, 3490 (1993).
2. Hayden S. M. *et al.*, *Phys. Rev. Lett.* **67**, 3622 (1991); Aeppli G. *et al.*, *Phys. Rev. Lett.* **62**, 2052 (1989).
3. Hayden S. W. *et al.*, *Phys. Rev. Lett.* bf 66, 821 (1991).
4. Cheong S.-W. *et al.*, *Phys. Rev. Lett.* **67**, 1791 (1991).
5. Mason T. E. *et al.*, *Phys. Rev. Lett.* **68**, 1414 (1992).
6. Mason T. E. *et al.*, *Phys. Rev. Lett.* **71**, 919 (1993).

Pergamon

J. Phys. Chem. Solids Vol. 56, No. 12, pp. 1913–1919, 1995
Copyright © 1995 Elsevier Science Ltd
Printed in Great Britain. All rights reserved
0022–3697/95 $9.50 + 0.00

0022–3697(95)00234-0

MAGNETISM AND MAGNETIC FLUCTUATIONS IN $La_{2-x}Sr_xCuO_4$ FOR x = 0 (2D ANTIFERROMAGNET), 0.04 (3D SPIN GLASS) AND x = 0.15 (SUPERCONDUCTOR)

R. J. BIRGENEAU,* A. AHARONY,† N. R. BELK,* F. C. CHOU,* Y. ENDOH,‡ M. GREVEN,* S. HOSOYA,§ M. A. KASTNER,* C. H. LEE,‡ Y. S. LEE,* G. SHIRANE,¶ S. WAKIMOTO,‡ B. O. WELLS* and K. YAMADA ‡

* Department of Physics and Center for Materials Science and Engineering, Massachusetts Institute of Technology, Cambridge, MA, 02139, U.S.A.

† School of Physics and Astronomy, Raymond and Bevery Sackler Faculty of Exact Sciences, Tel Aviv University, Tel Aviv 69978, Israel

‡ Department of Physics, Tohoku University, Aramaki Aoba, Sendai, 980-77, Japan

§ Institute of Inorganic Synthesis, Faculty of Engineering, Yamanashi University, Miyamae-cho 7, Kofu 400, Japan

¶ Department of Physics, Brookhaven National Laboratory, Upton, NY 11973, U.S.A.

Abstract—We review recent studies of the static and dynamic magnetic fluctuations in $La_{2-x}Sr_xCuO_4$. In La_2CuO_4 (T_N = 325K) the instantaneous two-dimensional (2D) spin correlations have been studied over the temperature range $340K < T \leq 820K$. We find quantitative agreement for the correlation length over the complete temperature range with no adjustable parameters with predictions for the 2D quantum non-linear sigma model in the renormalized classical regime. We have carried out bulk magnetization measurements in $La_{1.96}Sr_{0.04}CuO_4$ which has neither antiferromagnetic long range order nor superconductivity. All of the features that characterize a canonical spin glass transition have been seen: irreversibility, remnant magnetization and scaling behavior. Finally, neutron inelastic scattering experiments have been performed on homogeneous single crystals of $La_{1.85}Sr_{0.15}CuO_4$ with T_c=37.3K (at onset), higher than any previously studied single crystals. The temperature dependence of the low energy incommensurate peak intensity at $(\pi(1 \pm \delta), \pi)$ and $(\pi, \pi(1 \pm \delta))$ exhibits a pronounced maximum near T_c. In contrast to the results reported on lower T_c crystals, the intensity for energies below 3.5 meV dramatically decreases as the temperature decreases below T_c, vanishing into the background below ~ 15K. The behavior is consistent with predictions based on a $d_{x^2-y^2}$ superconducting order parameter.

1. INTRODUCTION

As has by now been extensively discussed in the literature, the lamellar copper oxides exhibit unusually rich and interesting microscopic magnetic properties [1]. Our own efforts have concentrated on the single layer material $La_{2-x}Sr_xCuO_4$, which is arguably the simplest of the high temperature superconducting systems. We have used a variety of techniques to study these materials including especially bulk magnetization and magnetic neutron scattering measurements. This experimental work has been complemented by an extensive single crystal growth effort at each of Tohoku, Yamanashi and MIT. Our neutron scattering measurements up to 1993 have been discussed in detail by Shirane *et al.* [2]. In this paper we review some new results in $La_{2-x}Sr_2CuO_4$ which have emerged over the last two years [3–5].

We review new results in the three principal domains of the phase diagram: (a) the antiferromagnetic region [3], (b) the spin-glass region [4], (c) the superconducting region [5]. Full descriptions of each of these will appear separately elsewhere [3–5].

2. 2D ANTIFERROMAGNETIC CORRELATIONS IN La_2CuO_4

Perhaps the area which has advanced most in the high-T_c problem is that of the 2D S=1/2 Heisenberg Antiferromagnet [6]. A comprehensive theory for the 2D square lattice Heisenberg antiferromagnet has been given by Chakravarty, Halperin, and Nelson (CHN) [7]. The CHN result for the correlation length in the renormalized classical (Néel) region has been further refined by Hasenfratz and Niedermeyer (HN). They show that in the renormalized classical (RC) region the correlation length is given rigorously by

$$\xi/a = \frac{e}{8}\frac{c/a}{2\pi\rho_s}\exp(2\pi\rho_s/T)[1 - \frac{1}{2}(\frac{T}{2\pi\rho_s}) + O(\frac{T}{2\pi\rho_s})^2] \quad (1)$$

where ρ_s is the spin stiffness, and c is the spin wave velocity. The relationships between c, ρ_s and J are now accurately known for the S=1/2 nearest neighbor 2D square lattice Heisenberg antiferromagnet. Specifically, c=1.18 $\sqrt{2}$ J a and 2 $\pi\rho_s$ = 1.15 J. This then yields

$$\xi/a = 0.493e^{1.15J/T}[1 - 0.43(\frac{T}{J}) + O(\frac{T}{J})^2]. \quad (2)$$

Detailed experiments by Greven and coworkers [7] in $Sr_2CuO_2Cl_2$ show remarkably good agreement with Eq(2). First generation experiments by Keimer *et al.* [9] in

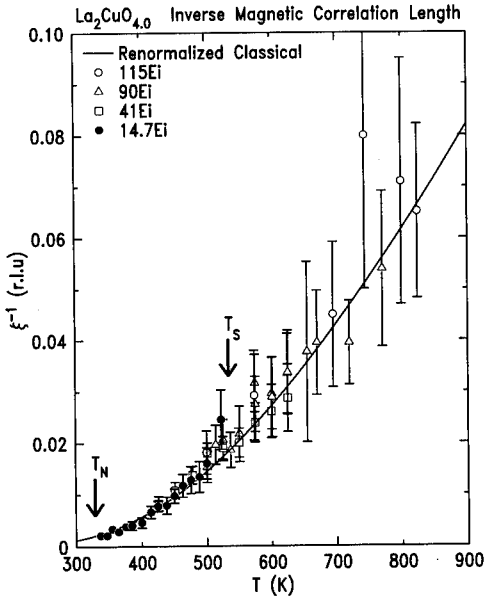


Fig. 1. Inverse magnetic correlation length in La_2CuO_4. The solid line is Eq(2) with J = 135 meV. The Néel and structural transition temperatures are indicated by arrows.

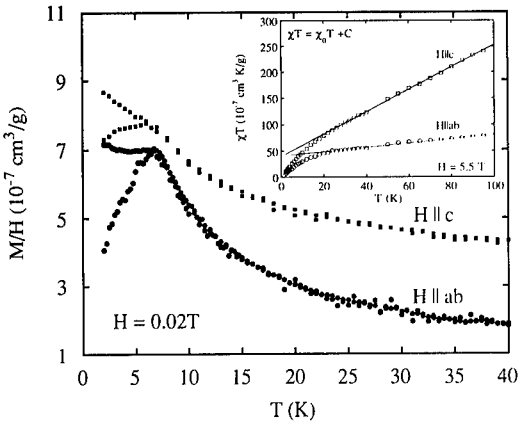


Fig. 2. Magnetization of $La_{1.96}Sr_{0.04}CuO_4$ versus temperature for a field of 0.02 T applied perpendicular (H||c) and parallel (H||ab) to the CuO_2 plane. The field-cooled (FC) data deviate from the zero-field-cooled (ZFC) data at low T indicating irreversibility. The data for H||c have been shifted by 10^{-7}cm^3/g. A plot of χT vs. T at H = 5.5 tesla (inset) demonstrates the Curie behavior. (Fig. from Ref. [4]).

La_2CuO_4 also show good agreement with Eq(2) although there does appear to be some systematic discrepancies at the limits of the error bars. More importantly, NMR measurements by Imai *et al.* [10] have suggested that for T > 600K there is a crossover from the renormalized classical behavior of Eq(1) to quantum critical behavior ($\xi \sim 1/T$) [7].

In order to elucidate this possible crossover, Birgeneau *et al.* [3] have extended the measurements of Keimer *et al.* [9] to both lower and higher temperatures. To guarantee complete integration over all important dynamical fluctuations, they have used progressively higher incoming neutron energies at higher temperatures and hence shorter correlation lengths. The results so-obtained are shown in Fig. 1. The spin wave velocity c=850 meV Å^{-1}, and hence J=135 meV, are known from inelastic neutron scattering measurements [11]. The solid line in Fig 1 is Eq(2) with J=135 meV; there is therefore no adjustable parameter. Clearly the agreement between the CHN-HN theory [7,8] for the 2D quantum non-linear sigma model and the Birgeneau *et al.* [3] data in La_2CuO_4 is excellent. There is, in addition, no evidence for the predicted crossover from renormalized classical to quantum critical behavior for T > 600K [10,12]. Based on more recent work [13] in higher spin 2D systems this excellent agreement with the low T RC prediction Eq(1) over such a wide range of length scales and to such high temperatures must be considered surprising.

3. SPIN GLASS BEHAVIOR IN $La_{1.96}Sr_{0.04}CuO_4$

Spin glass (SG) behavior at intermediate dopings in the lamellar copper oxides was first predicted by Aharony *et al.* [14]. However, although experimental evidence for slowing down of the spin fluctuations in this region has been found in neutron [9], muon spin relaxation (μSR) [15] and nuclear quadrupole resonance (NQR) [16] measurements, until very recently there had been no report of the magnetization behavior typical of canonical SGs: irreversibility and remnant magnetization below the glass transition and scaling behavior above and below it.[17] However, in a recent study in $La_{1.96}Sr_{0.04}CuO_4$, Chou *et al.* [4] have shown that this crystal has a uniform magnetization characterized by a low density of effective free spins which undergo a conventional 3D SG transition.

The zero-field cooled (ZFC) and field cooled (FC) magnetizations M at H = 0.02 T in $La_{1.96}Sr_{0.04}CuO_4$ for the field parallel (||) to and perpendicular ($\perp$) to the CuO_2 planes are plotted in Fig. 2. History dependence sets in at the irreversibility temperature, identified by the splitting of the ZFC and FC curves. This irreversibility temperature is the same for H||ab (in-plane) and H||c (out-of-plane). A peak is evident in the ZFC magnetization near 7K at low field, especially for H||ab. Such a sharp peak in the ZFC magnetization, which broadens with increasing field, is one identifying feature of a spin glass.

Before discussing other aspects of the SG behavior, it is important to appreciate that the apparent density of free spins is very small, as can be seen from the magnetization at high T. Between ~ 20K and ~ 100K the Curie form, $\chi = \chi_0 + C/T$, provides an excellent fit to the T dependence of $M = \chi H$ for fields between 0.02 and 5.5T. A fit to the Curie-

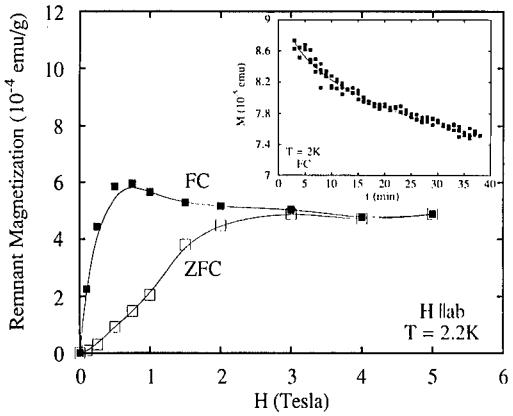


Fig. 3. The remnant magnetization of $La_{1.96}Sr_{0.04}CuO_4$ plotted versus applied magnetic field. The moment is measured one hour after setting the field to zero. The inset shows the time dependence of the moment immediately after the field is set to zero. (Fig. from Ref. [4]).

Weiss form gives a Curie-Weiss temperature $\Theta = 0$ within experimental error. The inset of Fig. 2 shows a plot of χT vs T at 5.5T illustrating that C, which has the value (4.7 ± 0.05) x 10^6 cm^3K/g, is isotropic. Using g=2 and S=1/2, this value corresponds to only 0.5% of the Cu spins or ~ 10% of the Sr atoms. Thus, the moment apparently arises from a small density of weakly interacting spins with an isotropic g tensor.

As is typical of spin glasses, [18] the magnetization for T < T_g remains after the field is turned off. Fig. 3 shows the magnetic moment measured by Chou *et al.* [4] 1 hour after setting the field to zero. For the ZFC case the field was applied for 5 minutes at 2.2K and then turned off. The behavior of this remnant magnetization is typical of canonical spin glasses such as Cu:Mn and $Eu_{1-x}Sr_xS$ [17]. As for other SG systems, the time decay of the magnetization follows the stretched exponential form, $M(t) = M_0 \exp[-\alpha t^{1-n}]$ (see inset of Fig. 3) and Chou *et al.* [4] find $1 - n = 0.32 \pm 0.07$. Theoretical predictions [19] and experiments on traditional spin glasses [20,21] give $1 - n \sim 1/3$.

The last feature that is used to identify spin glass ordering involves the nonlinear susceptibility $\chi_{nl} = \partial^3 M/\partial H^3|_{H=0}$. More generally, a spin glass is expected to show scaling behavior. Scaling theory predicts that

$$\chi - \chi_0 = \frac{C}{T}(1-q) = \frac{C}{T}[1 - |t|^{\beta} f_{\pm}(H^2/|t|^{\beta+\gamma})], \quad (3)$$

where t is the reduced temperature $t = (T-T_g)/T_g$, q is the SG order parameter and the scaling functions f_+ and f_- apply for t > 0 and t < 0, respectively [22]. This expression reduces to the Curie form at high T where q=0. Eq(3) also predicts that χ_{nl} diverges as H → 0 and T → T_g; in particular, an expansion of M for small H using Eq(3) gives coefficients of H^3 and H^5 that are predicted to follow $\chi_3 \sim |t|^{-\gamma}$ and $\chi_5 \sim |t|^{-(\beta+2\gamma)}$. For t < 0, Eq(3) predicts that $q \sim |t|^{\beta}$ for H = 0, that is, $f_-(0)$ is non-zero, while $f_+(0) = 0$.

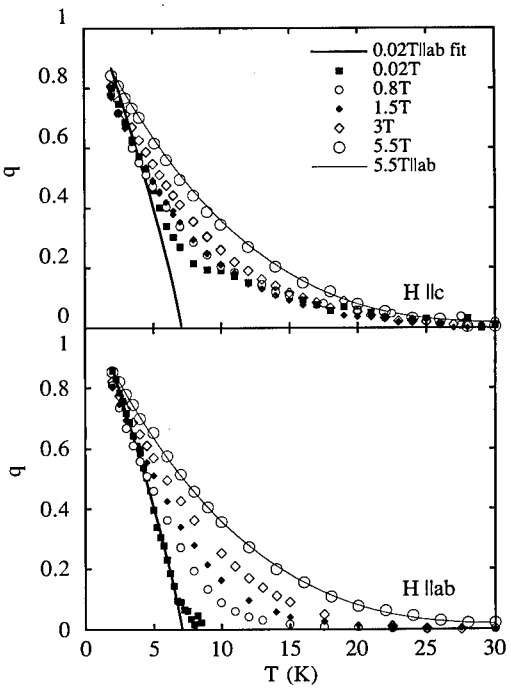


Fig. 4. The ZFC SG order parameter q(T) versus temperature in $La_{1.96}Sr_{0.04}CuO_4$ for fields applied in the two directions. The thick line is the result of a power law fit $q(T) \sim (T_g - T)^{\beta}$ to the 0.02 T data. The fit gives $T_g = 7.1 \pm 0.1$ K and $\beta = 0.85 \pm 0.12$. The thin lines are the result of a polynomial fit to the H = 5.5 T (H||ab) data.

Using the measured values of C and χ_0, Chou *et al.* [4] extract q(T) from the ZFC measurements of the χ; the results so-obtained are shown in Fig 4. For H||ab, q shows evidence for a phase transition at 7K which broadens with increasing H. For H||c, q appears to grow with decreasing T between ~20K and 7K even at H = 0.02 T. This behavior is seen in several samples prepared in different ways. Above ~ 1T, q becomes isotropic. To emphasize this, the data have been fitted to a polynomial for H||ab at 5.5T; the same curve has been plotted without adjustment with the H||c data.

To test whether Eq(3) describes the data, β and γ were determined in the following way: first, for $H^2 \ll t^{\beta+\gamma}$ and T < T_g, Eq(3) gives $q \sim |t|^{\beta}$. Fitting the data for H||ab at 0.02T to this form (heavy curve in Fig. 4) one finds β = 0.85 ± 0.12 and T_g = 7.1 ± 0.1K. Second, since q should become independent of t for $H^2 \gg |t|^{(\beta+\gamma)}$, Eq(3) predicts that $q \sim H^{2/\delta}$ where $\delta = 1 + \gamma/\beta$. This form describes the data near T_g well, and the fit gives δ = 5.9 ± 0.6, which, with β = 0.85 ± 0.12, gives γ = 4.2 ± 1.1.

Using these values, the data for all fields and temperatures are plotted in Fig. 5 using the variables $q|t|^{-\beta}$ vs $H^2|t|^{-(\beta+\gamma)}$. All of the data collapse onto two curves, that is, $f_-(x)$ for $t < 0$ and $f_+(x)$ for $t > 0$. Note that for these data the quantity $H^2|t|^{-(\beta+\gamma)}$ varies over seven decades. As noted above, the magnetization is isotropic for H > 1 T so the data collapse for H||c as well as for H||ab at high fields.

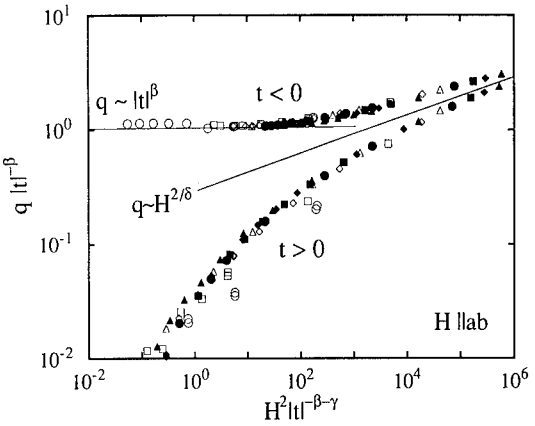


Fig. 5. Log–log plot of $q|t|^{-\beta}$ versus $H^2|t|^{-(\beta+\gamma)}$. Different symbols represent different fields: ∘ 0.1T, □ 0.5T, ◇ 1T, △ 1.5T, closed ∘ 2T, closed □ 3T, closed ◇ 4T, closed △ 5.5T. All data in the ranges 2K < T < 30K and 0.1T < H < 5.5T collapse demonstrating the scaling described by Eq(3). The data for t < 0 correspond to ZFC measurements; FC data scale similarly.

The line $q \sim H^{2/\delta}$ with $\delta = 5.9$ is drawn in the figure to illustrate the asymptotic behavior for $t \to 0$. The observation that $q|t|^{-\beta}$ approaches a constant for small $H^2|t|^{-(\beta+\gamma)}$ for $t < 0$ is consistent with the observed scaling $q \sim |t|^{\beta}$ discussed above. In the scaling plot we have used ZFC data for t < 0; essentially identical results are obtained with FC data.

It is evident, therefore, that the apparently isotropic free spins that contribute to the magnetization undergo a canonical 3D spin glass transition at 7K in $La_{1.96}Sr_{0.04}CuO_4$. However, interesting questions remain to be elucidated. Since it is known from neutron measurements [9] that there is one spin per Cu atom with an antiferromagnetic correlation length of $\sim 40\AA$, the origin of the low density of effective free spins remains to be understood. Specifically, since the majority of Cu spins are strongly antiferromagnetically coupled, it is important to determine whether the spins seen in the magnetization are the residue of the Cu spin system, for example, coming from the antiferromagnetic domain walls, or result from defects. In either case, however, the agreement with μSR and NQR measurements as well as the universality of the basic results show that the free spins measured by Chou *et al.* [4] reflect the freezing of the entire Cu spin system.

4. OBSERVATION OF A MAGNETIC GAP IN SUPERCONDUCTING $La_{1.85}Sr_{0.15}CuO_4$ (T_c = 37.3K)

As discussed in Ref. [2], the spin fluctuations in $La_{2-x}Sr_xCuO_4$ (LSCO) and $YBa_2Cu_3O_{7-\delta}$ (YBCO) are similar in many ways. There are, however, two fundamental differences in the results reported to-date. First, in superconducting LSCO the spin fluctuations are incommensurate [23,24], resulting in peaks at $\vec{Q}_\delta = [\pi(1 \pm \delta), \pi]$ and $[\pi, \pi(1 \pm \delta)]$ with $\delta \sim 1/4$, whereas in YBCO the fluctuations are essentially commensurate [25,26]. In the two-dimensional (2D) square lattice with unit lattice constant, (π, π) is the corner of the Brillouin zone. Second, in YBCO a gap in the magnetic fluctuation spectrum seems to be observed in the superconducting state [25,26] whereas in LSCO incommensurate spin fluctuations at quite low energies, $\omega \sim 1.2$ and 1.5 meV, have been found to persist down to the lowest temperatures measured [23,24]. The absence of a magnetic gap in LSCO represents a major conundrum for any model of the superconductivity in the single layer CuO_2 superconductors and indeed has led to rather diverse interpretations of the experimental results [23,24,27–29].

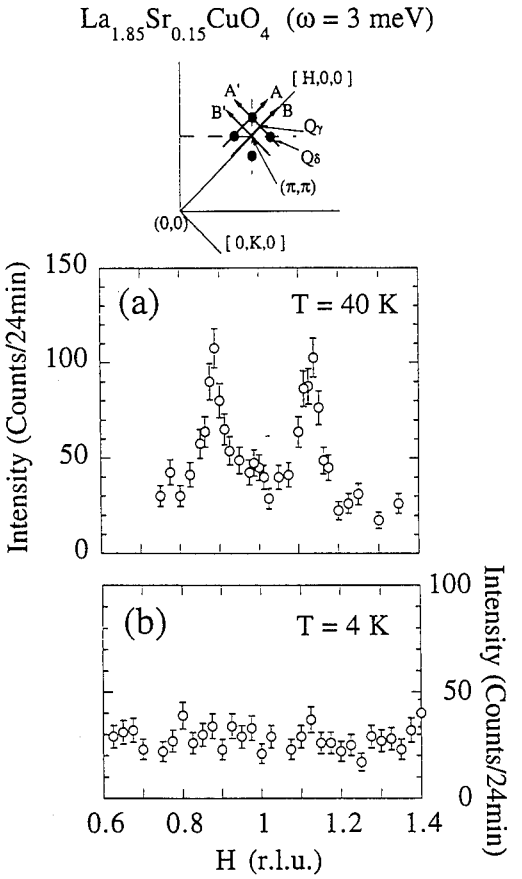


Fig. 6. Neutron inelastic scattering spectra at 3 meV for $La_{1.85}Sr_{0.15}CuO_4$ 1 at T = 40 K (> T_c) (a) and T = 4K(b) taken by scan A. The collimator sequence was $40' - 80' - S - 80' - 80'$. At the top is a schematic drawing of reciprocal space near the (π, π) position; typical scan directions are denoted by A, A′, B and B′. The closed circles denote the peak positions of the incommensurate magnetic fluctuations. In the [H H L] zone, scans A and B can be performed with tilts of the crystal around the c* axis equal to 6° and 0°, respectively. (Fig. from Ref. [5]).

Clearly, it is essential to know whether the observed absence of a magnetic gap in LSCO is intrinsic, or, as suggested

previously, arises from magnetic impurities or disorder. This question can only be properly resolved by preparing single crystals of progressively higher quality and studying the consequent evolution of the low energy spin fluctuations in the superconducting state. Recently, through a concentrated materials effort, the Tohoku group [5] has managed to grow a number of single crystals which appear to be markedly more homogeneous than the samples studied previously with neutrons [23,24]. Gratifyingly, they find that for E $\lesssim$ 3.5 meV the T-dependence of the generalized susceptibility $\chi''(\vec{Q}_\delta, \omega)$ shows a sharp peak at $\sim T_c = 37.3$K and diminishes rapidly towards zero as the temperature is lowered. Thus, the magnetic gap issue in LSCO is now resolved.

The results of Yamada *et al.* [5] may be briefly summarized. The [H K 0] zone of $La_{2-x}Sr_xCuO_4$ is illustrated at the top of Fig. 6. The magnetic scattering corresponds to four rods along (0,0,L) which intersect the (H,K,0) plane at the indicated positions. Basic in-plane scans which characterize the geometry of the 2D spin fluctuations are labelled A, B, A′ and B′. For a sample oriented in the [H 0 L] zone by tilting the sample about the (0,0,1) axis by an angle ϕ, scans with $q_x = H \cos\phi$, $q_y = H \sin\phi$ and $q_z = L$ arbitrary are possible [23]. Such tilt scans are parameterized by the variable H. Yamada *et al.* [5] have used $\phi = 6°$ which corresponds closely to scan A in Fig. 6 except for the different orientation of the instrumental resolution function. Scan B corresponds simply to a scan along (H,0,L) with the tilt $\phi = 0$ and L fixed.

Figure 6(a) and (b) shows results of 6 degree tilt scans for $\omega = 3$ meV at T = 40K, which is just above T_c, and at T = 4K. At T = 40K two sharp incommensurate peaks are observed, but at T = 4K the peaks are not visible above the background. This contrasts sharply with results reported in [23] and [24] where both groups find significant intensity at $\sim$ 3 meV down to 4K. It should be noted that the normalized integrated intensity at T = 40K for $\omega = 3$ meV is about a factor of 2 weaker than that measured in Ref. [23]. Scans with tilt $\phi = 0$ along (H,0,0) at T = 40K show no scattering above the background. This agrees with the results reported in Ref. [23], but not with those in Ref. [24], where Mason *et al.* [24] report measurable peak intensity for such zone diagonal scans. The latter may have resulted from either poorer crystal quality or poorer resolution, but clearly is not intrinsic to higher-T_c, homogeneous $La_{1.85}Sr_{0.15}CuO_4$.

Detailed temperature dependences at 2, 3 and 4.5 meV have also been measured. The results so-obtained are shown in Fig. 7. The data at 2 meV correspond to the integral of $\chi''(\vec{q}, \omega)$ with respect to $\vec{q}$ along scan A while the results at 3 and 4.5 meV are simply $\chi''(\vec{q}=\vec{Q}_\delta, \omega)$, that is the measured peak intensity (integrated over the resolution function) with the Bose factor removed. It is clear that at both 2 meV and 3 meV χ'' shows a peak at $\sim T_c = 37.3$K and diminishes to zero as T decreases toward 0 K. By contrast, at $\omega = 4.5$ meV $\chi''(\vec{q}=\vec{Q}_\delta, \omega)$ is $\sim$ constant below

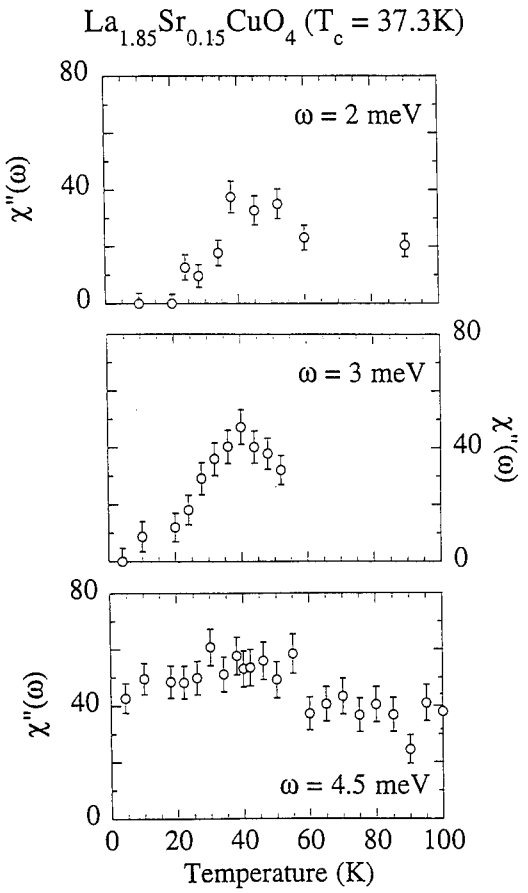


Fig. 7. Temperature evolution of $\chi''(q, \omega)$ at Q_δ with energies of 2, 3 and 4.5 meV. The data for 2 meV correspond to the 2D integral of the intensities around $\vec{Q}_\delta$. (Fig. from Ref. [5]).

T_c. This immediately implies a magnetic gap energy between 3 meV and 4.5 meV. This should be contrasted with the superconducting BCS weak coupling s-wave gap energy of $2\Delta = 3.54T_c = 11.4$ meV. We note that the temperature dependence of $\chi''(\vec{q}=\vec{Q}_\delta, \omega)$ for $\omega = 2$ meV is similar to the behavior of $1/T_1$ T measured with NMR for ^{63}Cu [27]. The latter measures $\sum_{\vec{q}} \chi''(\vec{q}, \omega)/\omega$ in the limit $\omega \to 0$.

We show in Fig. 8 the energy dependences of $\chi''(\vec{Q}_\delta, \omega)$ at T = 4 K and T = 40 K measured in two separate crystals. For T = 40 K (> T_c) $\chi''(\vec{Q}_\delta, \omega)$ varies gradually with energy possibly going to 0 as $\omega \to 0$. On the other hand at T = 4 K $\chi''(\vec{Q}_\delta, \omega)$ is non-zero above 3.5 meV but is not measurable above the background for lower energies. We conclude, therefore, that there is a superconducting magnetic gap of 3.5 ± 0.5 meV for the spin fluctuations at $\vec{q}=\vec{Q}_\delta$ in $La_{1.85}Sr_{0.15}CuO_4$ (T_c = 37.3K). This resolves the major conundrum discussed at the beginning of this section. Concomitantly, it also suggests that the low energy spin exci-

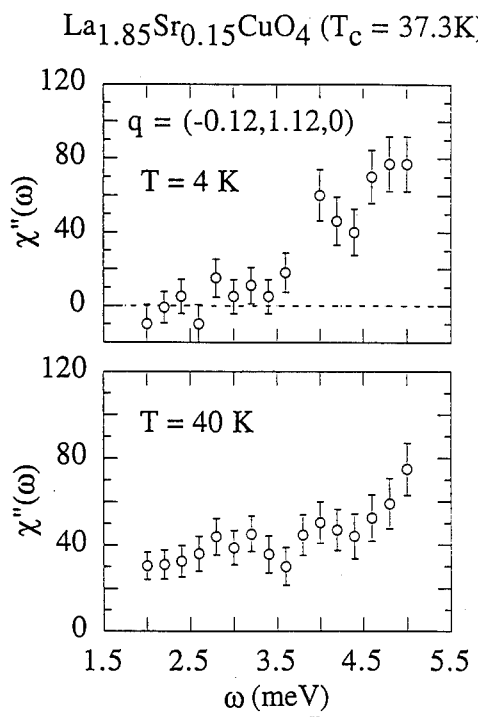


Fig. 8. The energy dependences of $\chi''(\vec{q}=Q_\delta, \omega)$ at T = 4 K and T = 40 K measured in $La_{1.85}Sr_{0.15}CuO_4$. (Fig. from Ref. [5]).

tations in the superconducting state reported in Refs [23] and [24] originated from disorder. Detailed analysis suggests that the measured gap energy is consistent with $d_{x^2-y^2}$ models [28–30] for the superconductivity provided that $2\Delta_0 \simeq 6\ KT_c$. At the same time, a highly anisotropic s-wave state cannot be ruled out. Finally, it is now important to relate the magnetic gap measured in LSCO [5] with that measured in YBCO [25,26]; in the latter case, the apparent magnetic gap depends sensitively on the oxygen concentration δ, decreasing rapidly with increasing δ.

5. CONCLUSIONS

Since the discovery of high T_c superconductivity, our approach has been to try to understand the entire phase diagram of the CuO_2 layer as a function of doping and specifically the evolution from the insulating to the superconducting state by studying single crystals. Although this has been motivated by our interest in the microscopic mechanism leading to superconductivity, each regime of the phase diagram has revealed elegant new physics, as the results reviewed here demonstrate. It is likely that this approach will continue to be fruitful.

Acknowledgements— The research at MIT was supported by the National Science Foundation under grant No. DMR93-15715 and by the MRSEC Program of the National Science Foundation under Award Number DMR94-00334. Work at Brookhaven National Laboratory was carried out under contract No. DE-AC-2-76CH00016, Division of Material Science, U.S. Department of Energy. The work at Tel-Aviv was supported by the United States-Israel Binational Science Foundation (BSF). The work at Tohoku was supported by a Grant-in-Aid for Scientific Research on Priority Areas, "Science of High T_c Superconductivity" (04240103) Ministry of Education, Science and Culture Japan and by a Grant of the Science, and Technology Agency Japan.

REFERENCES

1. Birgeneau R. J., *Am. J. Phys.* **58**, 28 (1990); Birgeneau R. J. and Shirane G., in *Physical Properties of High Temperature Superconductors I* (Edited by D. M. Ginsbeng), pp. 151–212. World Scientific, Singapore (1989).
2. Shirane G., Birgeneau R. J., Endoh Y. and Kastner M. A., *Physica B* **197**, 158 (1994).
3. Birgeneau R. J., Endoh Y., Greven M., Kastner M. A., Lee Y. S., Shirane G., Wells B. O. and Yamada K. (unpublished).
4. Chou F. C., Belk N. R., Kastner M. A., Birgeneau R. J. and Aharony A., *Phys. Rev. Lett.* **75**, 2204 (1995).
5. Yamada K., Wakimoto S., Lee C. H., Kastner M. A., Hosoya S., Greven M., Endoh Y. and Birgeneau R. J., *Phys. Rev. Lett.* **75**, 1626 (1995); for a discussion of the crystal growth technique, see Hosoya S., Lee C. H., Wakimoto S., Yamada K. and Endoh Y., *Physica C* **235–240**, 547 (1994).
6. Greven M., Birgeneau R. J., Endoh Y. and Kastner M. A., Matsuda M. and Shirane G., *Z. Phys. B* **96**, 465 (1995).
7. Chakravarty S., Halperin B. I. and Nelson D. R., *Phys. Rev. B* **39**, 2344 (1989).
8. Hasenfratz P. and Neidermayer F., *Phys. Rev. Lett. B* **268**, 231 (1991).
9. Keimer B., Belk N., Birgeneau R. J., Cassanho A., Chen C. Y., Greven M., Kastner M. A., Aharony A., Endoh Y., Erwin R. W. and Shirane G., *Phys. Rev. B* **46**, 14034 (1992).
10. Imai T., Slichter C. P., Yoshimara K., Katoh M. and Kosuge K., *Phys. Rev. Lett.* **71**, 1254 (1993).
11. Aeppli G., Hayden S. M., Mook H. A., Fisk Z., Cheong S. W., Rytz D., Remeika J. P., Espinosa G. P. and Cooper A. S., *Phys. Rev. Lett.* **62**, 2052 (1989).
12. Chubukov A. and Sachdev S., *Phys. Rev. Lett.* **71**, 169 (1993); Sokol A., Glenister R. and Singh R. R. P., *Phys. Rev. Lett.* **72**, 1549 (1994).
13. Elstner N., Sokol A., Singh R. R. P., Greven M. and Birgeneau R. J., *Phys. Rev. Lett.* **75**, 938 (1995).
14. Aharony A., Birgeneau R. J., Coniglio A., Kastner M. A. and Stanley H. E., *Phys. Rev. Lett.* **60**, 1330 (1988).
15. Budnick J. I., Chamberland B., Yange D. P., Niedermayer Ch., Golnik A., Recknagel E., Rossmanith M. and Weidinger A., *Europhys. Lett.* **5**, 651 (1988).
16. Cho J. H., Borsa F., Johnston D. C. and Torgeson D. R., *Phys. Rev. B* **46**, 3179 (1992).
17. Binder K. and Young A. P., *Rev. Mod. Phys.* **58**, 801 (1986).
18. Bouchiat H. and Monod P., *J. Mag. Mag. Mat.* **30**, 175 (1982).
19. Campbell I. A., *Phys. Rev. B* **37**, 9800 (1988).
20. Chamberlin R. V., *J. Appl. Phys.* **57**, 3377 (1985).
21. Chu D., Kenning G. G. and Orbach R., *Phys. Rev. Lett.* **72**, 3270 (1994).
22. Malozemoff A. P., Barnes S. E. and Barbara B., *Phys. Rev. Lett.* **51**, 1704 (1983).
23. Thurston T. R., Gehring P. M., Shirane G., Birgeneau R. J., Kastner M. A., Endoh Y., Matsuda M., Yamada K., Kojima H. and Tanaka I. *Phys. Rev. B* **46**, 9128 (1992); Matsuda M., Birgeneau R. J., Yamada K., Endoh Y., Thurston T. R., Kuroda K., Shirane G., Kastner M. A., Tanaka I. and Kojima H. , *Phys. Rev. B* **49**, 6958 (1994).

24. Mason T. E., Aeppli G., Hayden S. M., Ramirez A. P. and Mook H. A., *Phys. Rev. Lett.* **71**, 919 (1993).
25. Rossat-Mignod J., Regnault L. P., Bourges P., Barlet P., Vettier C. and Henry J. Y. in *Frontiers in Solid State Science: Selected Topics in Superconductivity*, pp. 265. World Scientific, Singapore (1993).
26. Sato M., Shamoto S., Kiyokura T., Kakurai K., Shirane G., Sternlieb B. J. and Tranquada J. M., *J. Phys. Soc. Jpn* **62**, 263 (1993).
27. Oshugi S., Kitaoka Y., Ishida K. and Asayama K., *J. Phys. Soc. Jpn* **60**, 2351 (1991).
28. Bulut N. and Scalapino D. J., *Phys. Rev. B* **50**, 16078 (1994); Quinlan S. M. and Scalapino D. J., *Phys. Rev. B* **51**, 497 (1995); Scalapino D. J., private communication.
29. Zha Y., Levin K. and Si Q., *Phys. Rev. B* **47**, 9124 (1993); Zha Y., Levin K., private communication; these authors estimate $4kT_c < 2\Delta < 20kT_c$.
30. Tanamato T., Kohno H. and Fukuyama H., *J. Phys. Soc. Jpn* **63**, 2739 (1994).

Pergamon

J. Phys. Chem. Solids Vol. 56, No. 12, pp. 1921–1925, 1995
Copyright © 1995 Elsevier Science Ltd
Printed in Great Britain. All rights reserved
0022-3697/95 $9.50 + 0.00

0022-3697(95)00226-X

SUPERCONDUCTIVITY AND SPIN FLUCTUATIONS IN THE ELECTRON-DOPED INFINITELY-LAYERED HIGH T_c SUPERCONDUCTOR $Sr_{0.9}La_{0.1}CuO_2$ (T_c=42 K)

TAKASHI IMAI *,[1], CHARLES P. SLICHTER *,†

* Department of Physics, Science and Technology Center for Superconductivity, The University of Illinois at Urbana-Champaign, 1110 West Green Street, Urbana, IL 61801-3080, U.S.A.

† Department of Chemistry, The University of Illinois at Urbana-Champaign ,1110 West Green Street, Urbana, IL 61801-3080, U.S.A.

JONATHON L. COBB ‡, JOHN T. MARKERT ‡

‡ Department of Physics, The University of Texas at Austin Austin, TX78712-1081, U.S.A.

Abstract—We report ^{63}Cu NMR studies on uniaxially aligned and unaligned powder samples of an electron-doped infinitely-layered high T_c cuprate superconductor $Sr_{0.9}La_{0.1}CuO_2$ (T_c= 42 K). We measured the nuclear spin-lattice relaxation rate $1/T_1$ up to 800 K. We found from the temperature dependence of $1/T_1T$ that the wave-vector-averaged spin susceptibility is highly enhanced by spin-fluctuations in the normal state, resulting in a Curie-Weiss behavior. Below T_c, we did not observe a Hebel-Slichter coherence peak of $1/T_1$, suggesting an unconventional nature of the symmetry of the superconducting order parameter. These results are quite similar to those observed for some hole-doped high T_c cuprates.

1. INTRODUCTION

The mechanism of high temperature superconductivity in doped cuprate high T_c superconductors is a very controversial issue. So far, no consensus has been reached. However various experiments have established that undoped parent compounds of high T_c cuprates are spin S=1/2 antiferromagnets. Microscopic experimental probes including NMR (Nuclear Magnetic Resonance), NQR (Nuclear Quadupole Resonance) [1], neutron scattering[2], and Raman scattering[3] revealed that one can describe the magnetic properties of the undoped parent compounds based on the two dimensional Heisenberg model reasonably well. The next crucial step toward the complete understanding of high temperature superconductivity is to figure out the nature of the carriers doped into the conducting CuO_2 planes, and the influence of mobile carriers on the electronic states of the undoped quasi 2d Heisenberg antiferromagnets. The undoped compound La_2CuO_4 is a quasi 2d Heisenberg antiferromagnet with intraplane exchange interaction J/k_B = 1520 K and bulk 3d Neel ordering temperature T_N~ 325 K [2]. Recently, after several years of painful trials and errors, the Illinois-Kyoto collaboration reported the first successful detection of $^{63,65}Cu$ NQR in the paramagnetic state of La_2CuO_4[1]. Their discovery of the NQR signal opened a way to investigate the influence of hole-doping in the entire doping range between the undoped La_2CuO_4 and the optimum hole-doped high T_c superconductor $La_{1.85}Sr_{0.15}CuO_4$ (T_c=38 K) by directly observing the nuclear resonance in the CuO_2 planes. They measured the temperature dependence of the nuclear spin-lattice relaxation rate $1/T_1$ and the Gaussian component of the spin-spin relaxation rate $1/T_{2G}$. These quantities probe the imaginary and real parts of the weighted wave-vector **q**-averaged dynamical electron spin susceptibility $\chi''(\mathbf{q}, \omega = \omega_n)$ and $\chi'(\mathbf{q}, \omega = 0)$, respectively, where ω is frequency and ω_n is the resonance frequency [4,5]. Theoretical calculations for the 2d-Heisenberg model based on dynamical scaling[6], high temperature expansion[7], and finite cluster calculations[8] reproduce the experimental data of La_2CuO_4 quite well without any adjustable parameters. The most surprising observation by Imai et al. is that $1/T_1$ levels off above 750 K at approximately the same value regardless of the doping level [1]. This finding demonstrates that at high temperatures the spin dynamics of the high T_c superconductor $La_{1.85}Sr_{0.15}CuO_4$ retains essentially the same properties of the undoped antiferromagnet La_2CuO_4. In other words, in the first order approximation, copper d-spins in the superconducting phase may be viewed as localized moments at elevated temperatures [9]. More recently Sato and coworkers also reported that the Hall coefficient levels off at elevated temperatures for $La_{2-x}Sr_xCuO_4$ ($0.04 \leqq x \leqq 0.15$) at approximately the same value [10]. This suggests that charge dynamics in the hole-doped superconducting phase may also keep the fundamental characteristic of the insulating phase at elevated temperatures. On the other hand, King et al. reported that the dispersion relations of the bands crossing or close to the Fermi surface are very different in an electron-doped high T_c superconductor $Nd_{1.85}Ce_{0.15}CuO_4$ compared with those in hole-doped materials [11]. The temperature dependence of the penetration depth below T_c in $Nd_{1.85}Ce_{0.15}CuO_4$ reported by Wu et al. is also regarded to be an evidence for

[1] Present Address: Department of Physics, Massachusetts Institute of Technology, #13-3149, Cambridge, MA 02139, U.S.A.

the isotropic s-wave pairing realized in the electron-doped system [12], in contrast with the result for a hole-doped system $YBa_2Cu_3O_{6.95}$ by Hardy et al. which clearly indicates an unconventional nature, most likely to be d-wave pairing[13]. In view of these results, a naive question is *what happens to the NMR properties if one dopes electrons instead of holes into the CuO_2 planes*? Unfortunately it is not easy to answer this question because of the following two reasons. Firstly, the physical properties of the well-known electron-doped high T_c superconductor $Nd_{1.85}Ce_{0.15}CuO_4$ are extremely sensitive to the oxygen content as may be seen in the results of Kambe et al.[14]. This makes preparation of high quality samples as well as reproducible studies very hard. Secondly, the presence of the large Nd moments masks the intrinsic physical properties of CuO_2 planes. In particular, ^{63}Cu NMR experiments on $Nd_{1.85}Ce_{0.15}CuO_4$ are almost completely dominated by the large Nd moments as demonstrated by Zheng et al.[15]. In this paper, we discuss our recent NMR results [16] for the electron-doped high T_c superconductor $Sr_{0.9}La_{0.1}CuO_2$ (T_c= 42 K) [17], and compare the results with those of hole-doped materials. This material is suited for NMR experiments because *unlike the case of $Nd_{1.85}Ce_{0.15}CuO_4$ there are no unpaired spins outside the CuO_2 planes in $Sr_{0.9}La_{0.1}CuO_2$* [18]. This enabled us to obtain information intrinsic to the electron-doped CuO_2 planes from ^{63}Cu NMR for the first time. In addition, the infinitely-layered structure of $Sr_{0.9}La_{0.1}CuO_2$ allows us to investigate the possible influence of interlayer coupling between adjacent CuO_2 planes on the physical properties of high T_c cuprates [19]. Our key finding is that the spin fluctuation and superconducting properties of $Sr_{0.9}La_{0.1}CuO_2$ probed by NMR exhibited very similar results to those of hole-doped compounds.

2. EXPERIMENTAL

Polycrystalline samples of $Sr_{0.9}La_{0.1}CuO_2$ were prepared by utilizing high pressure apparatus at Texas. Details of the preparation of the samples and their characterization are discussed elsewhere [17]. The hard pellet samples were crushed and sieved to obtain fine ceramic powder samples. A part of the fine powder was uniaxially aligned in external magnetic field of 8.3 Tesla in Stycast 1266 resin at room temperature. Since Stycast reduces the high T_c cuprate samples above approximately 500 K, NMR measurements above 400 K were carried out utilizing a powder sample with no epoxy sealed in a nitrogen gas atmosphere. After we completed the measurements of the NMR line shape and $1/T_1$ up to 600 K, we cooled down the sample to room temperature to check the reproducibility. We found that $1/T_1$ at room temperature was identical to that before the heat cycling. We repeated the same procedures after the measurements at 800 K, again confirming the reproducibility of $1/T_1$ at room temperature, though we found a weak ^{63}Cu NMR signal from small amount of copper metal reduced from the sample. All the NMR measurements were carried out at Illinois using standard home made pulsed NMR spectrometers. Superconducting magnets operating either at 8.3 Tesla or at 9.4 Tesla were utilized. NMR line shape was measured by integrating the spin echo signal point by point scanning the resonance frequency. $1/T_1$ was measured by inverting the population of nuclear magnetization with a 180 degree pulse.

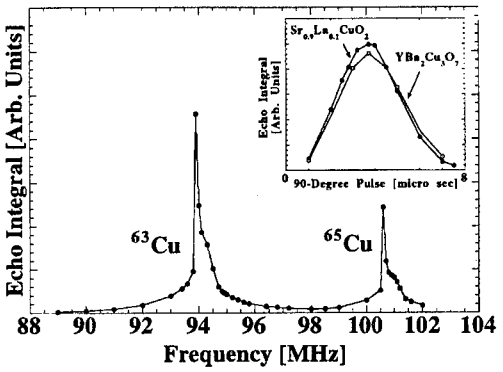


Fig. 1. ^{63}Cu and ^{65}Cu NMR spectra observed for the unaligned powder sample at 295 K in 8.3 Tesla. Inset: Echo intensity of the central peak of $Sr_{0.9}La_{0.1}CuO_2$ and $YBa_2Cu_3O_7$ observed for the aligned powder sample plotted as a function of the width in time of the pulse width.

3. RESULTS AND DISCUSSION

3.1. *Static Properties*

In Fig.1, we present the ^{63}Cu and ^{65}Cu NMR line shape of an unaligned powder sample of $Sr_{0.9}La_{0.1}CuO_2$ measured at 295 K. There is a small 'shoulder' in the broad line shape at the higher frequency side of each of the ^{63}Cu and ^{65}Cu NMR spectra, characteristic of the NMR line shape with anisotropic Knight shift with axial symmetry. In fact we confirmed that the angular dependence of the peak position of ^{63}Cu NMR in the aligned powder sample fits the theoretical curve expected for the case of an anisotropic Knight shift [20] quite well. In Fig. 2 (a) and (b), we present the ^{63}Cu NMR line shapes observed for the uniaxially aligned powder sample with the magnetic field applied parallel to the crystal c-axis and the ab-plane, respectively. One notices that there is a relatively sharp transition and broad tails for both higher and lower frequency sides. We attribute the sharp peak to the transition from nuclear spin quantum number I_z=1/2 to I_z=-1/2 (*i.e.* the central transition), and the broad tail to the transition from I_z=3/2 to 1/2 and from I_z=-3/2 to -1/2 (*i.e.* satellite transitions).

We verified the assignment by comparing the nutation curves of the spin echo signal as a function of t_w, the width in time of the RF exciting pulse for Cu metal, the I_z=1/2 to I_z=-1/2 transition of the planar Cu site of $YBa_2Cu_3O_7$, and the central peak of the aligned powder of $Sr_{0.9}La_{0.1}CuO_2$

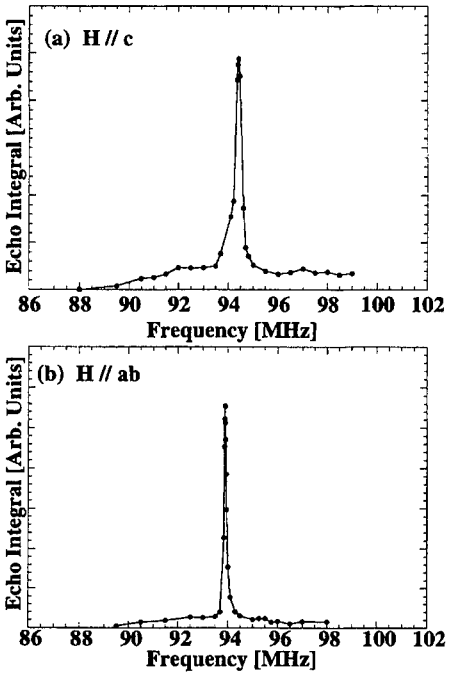


Fig. 2. ^{63}Cu NMR spectra observed at 77 K for the uniaxially aligned powder sample of $Sr_{0.9}La_{0.1}CuO_2$. The magnetic field of 8.3 Tesla is applied parallel to (a) aligned c-axis, and (b) aligned ab-plane.

under identical experimental conditions. For Cu metal, a 90 degree pulse occurs when $\gamma H_1 t_w = \pi/2$, where γ and H_1 are the nuclear gyromagnetic ratio and the strength of RF magnetic field, respectively. For the +1/2 to -1/2 transition, a 90 degree pulse occurs when $2\gamma H_1 t_w = \pi/2$ due to the matrix element effects [20]. We found that the results for $YBa_2Cu_3O_7$ and $Sr_{0.9}La_{0.1}CuO_2$ were identical, as shown in the inset to Fig.1, while t_w for $YBa_2Cu_3O_7$ and $Sr_{0.9}La_{0.1}CuO_2$ was 2 times shorter than that for Cu metal. From the separation of the satellite transitions, we estimate the nuclear quadrupole coupling ν_Q to be 4 MHz or below. In general the peak position of the NMR line for the I_z=1/2 to I_z=-1/2 transition is shifted by both the NMR Knight shift, ^{63}K, and the second or higher order effects due to the quadrupole interaction [20]. We confirmed that the relative shift of the apparent peak position is identical for both ^{63}Cu and ^{65}Cu isotopes for 8.3 and 9.4 Tesla when the magnetic field is applied parallel to the aligned c-axis. This indicates that the main principle axis of the quadrupole coupling tensor is parallel to the c-axis, and the contribution from the quadrupolar effects to the NMR shift is null in the case. By taking ν_Q =4 MHz, the contribution of the quadrupole effects to the shift for the field applied parallel to the ab-plane is 0.03% at 8.3 Tesla. By taking into account these considerations, our preliminary results on the temperature dependence of Knight shifts are as follows. $^{63}K_c$ saturates at elevated temperatures and decreases below room temperature from 0.92% at 295 K to 0.86% at T_c=42K. In contrast, $^{63}K_{ab}$ = 0.29 % is independent of temperature. These results are in remarkable

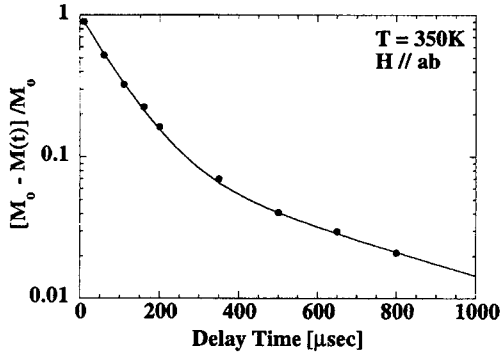


Fig. 3. Plot of the normalized intensity of echo integral M(t) at time t after inversion of the population of spins. M_o is the saturated value of the echo intensity for infinitely large t. Solid line is the fit to the solution of the rate equation.

contrast with the case of underdoped region of the hole doped systems, where $^{63}K_c$ is temperature independent and $^{63}K_{ab}$ decreases with temperature [21]. The hyperfine coupling tensor in $Sr_{0.9}La_{0.1}CuO_2$ seems to be rather different from that in $YBa_2Cu_3O_x$ and $La_{2-x}Sr_xCuO_4$.

3.2. *Spin Dynamics*

In Fig. 3 we present an example of the dependence of the echo integral M(t) on the delay time t of the echo sequence after a 180 degree inversion pulse. The result fits very well the solution of the rate equation for the I_z=1/2 to I_z=-1/2 transition of nuclear spin I=3/2, $M(t) = A - B[0.9\exp(-6t/T_1) + 0.1\exp(-t/T_1)]$, where A and B are constants, and T_1 is the spin-lattice relaxation time. The temperature dependence of the spin-lattice relaxation rate $1/T_1$ measured for an aligned powder sample under the external magnetic field 8.3 Tesla applied parallel to the crystal c-axis or ab-plane is presented in Fig.4. The anisotropy of $1/T_1$, ^{63}R, is approximately ^{63}R ~ 2.6. This is comparable to but somewhat smaller than the value observed for undoped La_2CuO_4 [1] and hole-doped $YBa_2Cu_3O_7$ [22], ^{63}R ~ 3.7, and much smaller than that for an antiferromagnet CuO, ^{63}R~8 [23]. The large value of ^{63}R in CuO is due to the absence of the transferred hyperfine interaction. Our observation suggests that the mechanism of transferred hyperfine interaction between nearest neighbor Cu sites [24] are present in electron-doped systems, too. Mild scattering of the data for $(1/T_1)_c$ caused by the broad line width and the resulting contamination by the satellite transition make it difficult to obtain the precise value and temperature dependence of ^{63}R. It appears that ^{63}R does not show any strong temperature dependence above T_c.

Above 450 K, we found that the ceramic powder sample was reduced and destroyed in stycast 1266. To avoid this, we carried out measurements of $1/T_1$ for an unaligned powder sample at the peak position of the powder spectrum at higher temperatures. We normalized the data for powder, $(1/T_1)_{powder}$, to that measured for aligned powder, $(1/T_1)_{ab}$, at 295 K by multiplying with a factor 1.4. We plotted the

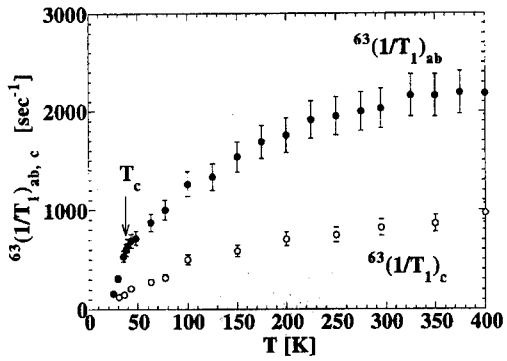


Fig. 4. Temperature dependencies of $^{63}(1/T_1)_{ab,c}$ measured for the uniaxially aligned powder sample.

data of $(1/T_1)_{ab}$ and $1.4(1/T_1)_{powder}$ together in Fig. 5. Since the normalized results showed good agreement also at 77 K, the normalization procedure should not alter any essential aspect of the data.

It is clear from Fig. 5 that the results for the electron-doped compound is semi-quantitatively similar to that of various hole-doped compounds. A high relaxation rate $1/T_1$ with negative curvature in its temperature dependence indicates that the electronic states can not be described by the canonical Fermi liquid state, and strong correlation effects have to be taken into account. As shown in Fig. 5(c), the temperature dependence of T_1T follows a Curie-Weiss law, $T_1T = c\ (T-T^*)$, where $c = 3 \times 10^{-4}$ sec and $T^* = -174$ K are constants, in the entire temperature range between $T_c = 42$ K and 800 K. As demonstrated by Moriya [4], $1/T_1$ probes the weighted **q**-average of the imaginary part of the electron spin susceptibility. Therefore our finding indicates that *the wave vector* **q** *averaged spin susceptibility in the electron doped superconductor* $Sr_{0.9}La_{0.1}CuO_2$ *satisfies a Curie-Weiss law*. The negative value of T* means that the electron spin system in the electron-doped CuO_2 planes are not approaching the Neel ordered ground state. These findings are essentially the same as those previously reported for $YBa_2Cu_3O_7$ by Barrett et al. [25] We also attempted to fit $1/T_1$ to a power law, $1/T_1 \sim T^n$ ($n \sim 1/2$), as suggested by Ren and Anderson for a Luttinger liquid system [26]. Though our data is in general accord with a power-law behavior with $n \leqq 1$, we found that the fit is not good. One unique feature of $Sr_{0.9}La_{0.1}CuO_2$ is in the strong interlayer coupling. In fact the undoped parent compound $(Ca_{0.85}Sr_{0.15})CuO_2$ has the highest Neel ordering temperature, 540K, among various cuprates [27]. Moreover Cobb and Markert found that the superconducting anisotropy is relatively small in $Sr_{0.9}La_{0.1}CuO_2$. Their observation is an evidence for strong interlayer coupling in the electron doped compound [28]. The interlayer coupling of CuO_2 bi-layers has been proposed to be responsible for the spin gap behavior in underdoped $YBa_2Cu_3O_x$ and $YBa_2Cu_4O_8$, where $1/T_1T$ shows a significant reduction above T_c [21]. Though one may anticipate that the spin gap behavior is even enhanced in the infinitely-layered compound compared with

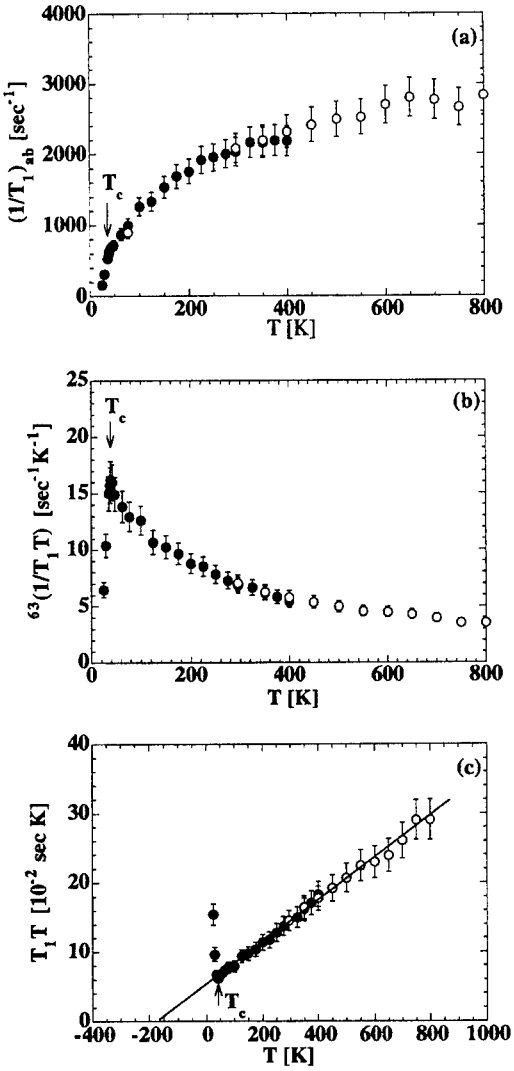


Fig. 5. (a)Temperature dependence of $^{63}(1/T_1)_{ab}$ obtained from the measurement for aligned powder sample (filled circles) and for unaligned powder sample (unfilled circles, normalized by multiplying a factor 1.43). (b) $^{63}(1/T_1T)_{ab}$. (c) $^{63}(T_1T)_{ab}$. Solid line is a fit to Curie-Weiss law, $^{63}(T_1T)_{ab} = 3\text{x}10^{-4}(T+174)$.

the bi-layer systems, we did not observe spin gap behavior in $Sr_{0.9}La_{0.1}CuO_2$. As presented in Fig. 5(b), $1/T_1T$ increases monotonically down to T_c. The interplay between the doping level, the nature of doping (hole or electron), interlayer coupling, and in-plane anisotropy [29] needs further investigation to clarify the mechanism of spin gap behavior observed in some hole-doped systems. Another important finding in our data is that $1/T_1$ exhibits monotonic and sudden decrease just below T_c. Various model calculations showed that isotropic s-wave superconducting pairing results in a Hebel-Slichter coherence peak [30] just below T_c even for the systems with strong antiferromagnetic spin fluctuations. The absence of the coherence peak in the magnetic field of 8.3 Tesla makes the s-wave scenario unlikely in the electron-doped superconductor $Sr_{0.9}La_{0.1}CuO_2$.

3.3. *Summary*

We reported our ^{63}Cu NMR measurements for an electron-doped infinitely-layered high T_c superconductor $Sr_{0.9}La_{0.1}CuO_2$. This material is unique in the sense that the doping is made by adding electrons into CuO_2 planes instead of holes, and the interlayer coupling might be strongest among various cuprates. Our experimental results indicate that the spin dynamics in the electron-doped $Sr_{0.9}La_{0.1}CuO_2$ show essentially the same temperature dependence as those in hole-doped compounds. The symmetry of the orbital pairing in the superconducting state is unlikely to be isotropic s-wave, again analogous to the case of hole-doped systems. Investigation of further details of some aspects of our experiments including NMR shifts, hyperfine coupling, and the comparison with the undoped insulating antiferromagnet $Ca_{0.85}Sr_{0.15}CuO_2$ are under way.

Acknowledgement—The work at Illinois was supported by NSF-DMR 91-20000 through the Science and Technology Center for Superconductivity, and by DOE-DEFG-02-9ER45439 through the Frederick Seitz Materials Research Laboratory. The work at Texas was supported by NSF-DMR-9158089, and by the Robert Welch Foundation under F-1191.

REFERENCES

1. T. Imai, C. P. Slichter, K .Yoshimura, and K. Kosuge, Phys. Rev. Lett. **70** (1993) 1002. T. Imai, C. P. Slichter, K .Yoshimura, M. Katoh, and K. Kosuge, Phys. Rev. Lett. **71** (1993) 1254. T. Imai, C. P. Slichter, K. Yoshimura, M. Katoh and K. Kosuge, Physica **B197**, 601 (1994).
2. K. Yamada, K. Kakurai, Y. Endoh, T. R. Thurston M. A. Kastner, R. J. Birgeneau, G. Shirane, Y. Hidaka, and T. Murakami, Phys. Rev. **B40** (1989) 4557. S. M. Hayden, G. Aeppli, H. A. Mook, S-W. Cheong, and Z. Fisk, Phys. Rev. **B42** (1990) 10220.
3. For example, see S. Sugai and Y. Hidaka, Phys. Rev. **B40** (1991)809, I. Tomeno et al., Phys. Rev. **B43**(1991)3009.
4. T. Moriya, *Prog. Theor. Phys. (Kyoto)*, **16** (1956) 33.
5. C. H .Pennington and C. P. Slichter, *Phys. Rev. Lett.* **66** (1991) 381.
6. S. Chakravarty, B. I. Halperine, and D. R. Nelson, *Phys. Rev.* **B39**, (1989) 2344. S. Chakravarty and R. Orbach,*Phys. Rev. Lett.* **64** (1990) 1254. A. Chubukov and S. Sachdev, *Phys. Rev. Lett.* **71** (1993) 169. A. Chubukov, S. Sachdev and A. Sokol,*Phys. Rev.* **B49** (1994) 9052.
7. R.P.P. Singh and M. P. Gelfand, *Phys. Rev.* **B42** (1990) 996. A. Sokol, R. L. Glenister, and R. P. P. Singh, *Phys. Rev. Lett.* **72** (1993) 1549.
8. A. Sokol, E. Gagliano, and S. Bacci, *Phys. Rev.* **B47** (1993) 14646.
9. Q. Si, J. H. Kim, J. P. Lu, and K. Levin, *Phys. Rev.* **B42**(1990) 1033.
10. T. Nishikawa, J. Takeda, and M. Satoh, *J. Phys. Soc. Jpn.* **63**(1994)1441.
11. D.M. King, Z.X. Shen, D.S. Dessau, B.O. Wells, W.E. Spicer, A.J. Arko, D.S. Marshall, J. DiCarlo, A.G. Loeser, C.H. Park, E.R. Ratner, J.L. Peng, Z.Y. Li, and R.L. Greenn, *Phys. Rev. Lett.* **70**(1993)3159.
12. D.H. Wu, J. Mao, S. N. Mao, J. L. Peng, X. X. Xi, T. Venkatesan, R. L. Greene, and S. M. Anlage, *Phys. Rev. Lett.* **70**(1992)85.
13. W. N. Hardy, D. A. Bonn, D. C. Morgan, R. Liang and K. Zhang, *Phys. Rev. Lett.* **70**(1993)3999
14. S. Kambe, H. Yasuoka, H. Takagi, S. Uchida, and Y. Tokura, *J. Phys. Soc. Jpn.*, **60** (1991) 400.
15. G. Zheng, Y. Kitaoka, Y. Oda, and K. Asayama, *J. Phys. Soc. Jpn.***58** (1989) 1910.
16. T. Imai, C. P. Slichter, K. Yoshimura, M. Katoh, K. Kosuge, J.L. Cobb and J. T. Markert, *Physica* **C235–240** (1994) 1627.
17. M. G. Smith, A. Manthiram, J. Zhou, J. B. Goodenough, and J. T. Markert, *Nature* **351** (1991) 540. J.L. Cobb, A. Morosoff, L. Stuk and J. T. Markert, *Physica* **B194–196**(1994)2247..
18. We found that the nuclear spin-lattice relaxation rate of ^{139}La is very slow in $Sr_{0.9}La_{0.1}CuO_2$. This indicates that the valence of La is three with no unpaired spin in the 5d-orbital.
19. A. J. Millis and H. Monien, *Phys. Rev. Lett.* **70** (1993) 2810. M. Ubbens and P. A. Lee, *Phys. Rev.* **B50** (1994) 438.
20. C. P. Slichter, *Principles of Magnetic Resonance*, 3rd ed. (Springer-Verlag, Heidelberg, 1990).
21. M. Taligawa, A.P. Reyes, P.C. Hammel, J. D. Thompson, R.H. Hefner, Z. Fisk and K.C. Ott, *Phys. Rev.* **B43**(1991)247.
22. C. H. Pennington, D. J. Durand, C. P. Slichter, J. P. Rice, E. D. Bukowski, and D. M. Ginsberg, *Phys. Rev.* **B39** (1988) 2902.
23. T. Imai, Thesis, The University of Tokyo, 1991.
24. F. Mila and T. M. Rice, *Physica* **C157** (1989) 561.
25. S. E. Barrett, D. J. Durand, C. H. Pennington, C. P. Slichter, T. A. Friedmann, J. P. Rice, and D. M. Ginsberg, *Phys. Rev.* **B41**(1990) 6283.
26. P. W. Anderson and Y. Ren, in *The Proceedings of Los Alamos symposium on High Temperature Superconductivity, eds. K. S. Bedell, D. Coffey, D. E. Meltzer, D. Pines and J. R. Schrieffer*, (Addison and Wesley, California, 1990).
27. A. Keren, L. P. Le, G. M. Luke, B. J. Sternlieb, W. D. Wu, Y. J. Uemura, S. Tajima, and S. Uchida, *Phys. Rev.* **B48**, 12926 (1993).
28. J. L. Cobb and J. T. Markert, *Physica* **C226** (1994) 235.
29. H.-Q. Ding, *Phys. Rev. Lett.* **68** (1992)1927.
30. L.C. Hebel and C.P.Slichter, *Phys. Rev.* **113**(1959)1504.

Pergamon

J. Phys. Chem. Solids Vol. 56, No. 12, pp. 1927–1929, 1995
1995 Elsevier Science Ltd
Printed in Great Britain
0022-3697/95 $9.50 + 0.00

0022-3697(95)00097-6

RESONANT NEUTRON SCATTERING FROM $YBa_2Cu_3O_7$

B. KEIMER *, HUNG FAI FONG *, D. REZNIK †, F. DOGAN ‡, I.A. AKSAY ‡

* Dept. of Physics, Princeton University, Princeton, NJ 08544, U.S.A.
† National Institute of Standards and Technology, Gaithersburg, MD 20899, U.S.A.
‡ Dept. of Chemical Engineering, Princeton University, Princeton, NJ 08544, U.S.A.

Abstract—We have developed a new scattering geometry for magnetic neutron scattering experiments on $YBa_2Cu_3O_7$ in which the phonon background around $\mathbf{q} \sim (\frac{\pi}{a}, \frac{\pi}{a})$, $\hbar\omega \sim 40$meV is significantly reduced. We use this new approach to study the previously detected sharp magnetic excitation at ~ 40meV in the superconducting state in detail. The excitation does not shift substantially in energy up to at least 75K ($\sim 0.8T_c$). Polarized neutron scattering experiments (horizontal minus vertical field) confirm the magnetic origin of the 40meV excitation and put stringent limits on the magnetic scattering intensity in the normal state.

Over the past seven years, numerous magnetic neutron scattering experiments on the underdoped $YBa_2Cu_3O_{6+x}$ system have been performed and have revealed a wealth of important information on the magnetic ground state and excitations [1,2]. Until recently similar experiments on the fully oxygenated compound $YBa_2Cu_3O_7$ have been more controversial [2,3], because the magnetic cross section is smaller and occurs at higher energies. Since in all neutron scattering experiments on $YBa_2Cu_3O_7$ (unpolarized as well as polarized) the background is comparable or larger than the signal, the background subtraction has to be carried out with extreme care. For unpolarized beam experiments, the background from one-phonon and multiphonon scattering is dominant. While multiphonon scattering gives a background which is featureless in energy and momentum, dispersion and dynamical structure factor effects in scattering from single optical phonons generally lead to distinct features of the scattering cross section in energy and momentum which are difficult to distinguish from magnetic excitations.

We have therefore begun to develop a detailed understanding of the phonon spectrum with emphasis on the energy range ($\hbar\omega \sim 40$meV) in which magnetic excitations had previously been reported [2,3]. Detailed lattice dynamical calculations, together with experimental studies of the temperature and momentum dependence of the scattered intensity, allowed us to separate a phonon involving predominantly c-axis motion of the in-plane oxygen from a magnetic excitation with a similar energy and dynamical structure factor [4]. Our measurements were performed at the High Flux Beam Reactor at Brookhaven at the H7, H8 and H4M triple axis spectrometers.

Figure 1 shows the scattering geometry we developed for this purpose. As first reported by Rossat-Mignod *et al.* [2], the magnetic excitation occurs at ~40meV and $\mathbf{Q} = \left(\frac{1}{2}(2i+1), \frac{1}{2}(2j+1), 1.7(2k+1)\right)$ with the momentum transfer $\mathbf{Q} = (H, K, L)$ measured in units of the reciprocal lattice vectors $\frac{2\pi}{a}$, $\frac{2\pi}{b}$ and $\frac{2\pi}{c}$, and i, j and k integer. As the point $(\frac{1}{2}, \frac{1}{2}, 1.7)$ cannot be studied because of kinematical constraints, and the magnetic form factor suppresses the magnetic intensity for $(\frac{3}{2}, \frac{3}{2}, 1.7)$, all previous neutron scattering experiments had been carried out at the point $(\frac{1}{2}, \frac{1}{2}, 5.2)$. However, we found that the phonon dynamical structure factor is peaked at this point, which makes it difficult to separate the magnetic excitation from the phonon background. For $\mathbf{Q} = (\frac{3}{2}, \frac{1}{2}, 1.7)$, on the other hand, the phonon cross section is very small and the magnetic excitation can be isolated. The phonon can be isolated by increasing the momentum transfer to $L = 14$, where the magnetic form factor suppresses the magnetic intensity almost completely, but the phonon intensity is greatly enhanced. (The phonon cross section contains a

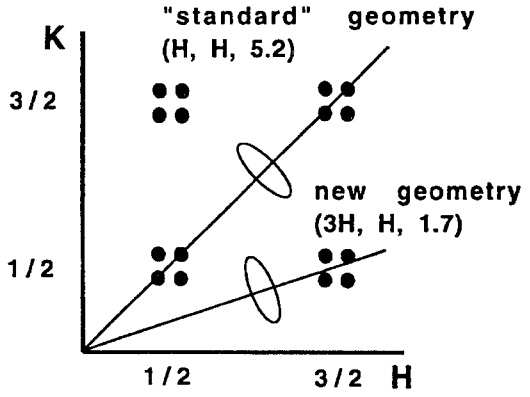


Fig. 1. Geometries used for magnetic neutron scattering experiments on $YBa_2Cu_3O_7$. The long axis of the resolution ellipsoid is perpendicular to the (horizontal) scattering plane. The four peaks shown would be expected if the scattering were peaked at $\mathbf{q} = (k_F, k_F)$ instead of $(\frac{\pi}{a}, \frac{\pi}{a})$.

term proportional to Q^2.) While the phonon experiences a momentum dependent softening below T_c [5], its *intensity* is unaffected by superconductivity. By contrast, the 40meV magnetic excitation exists in the superconducting state *only*, that is, there is no evidence in our measurements of any significant magnetic peak centered around an energy of 40meV in the normal state. We note that the same conclusion was recently reached independently by Bourges *et al.* [6] using very different (but equally valid) reasoning.

40meV thus appears to be an energy characteristic of the superconducting state. Of course, because of the significant background our data do not rule out magnetic scattering at 40meV in the normal state if it is very weak (conservatively, at least a factor of 3 weaker than in the superconducting state) or broadly distributed in energy and momentum. Polarized beam experiments (see below) put even more stringent limits on the magnetic scattering intensity in the normal state, as compared to the superconducting state. The fact that the magnetic excitation can be clearly observed at two symmetry-related positions of reciprocal space also rules out any spurious processes as the origin of the signal. Experimental artefacts such as accidental Bragg scattering generally do not have the symmetry of the reciprocal lattice. We have therefore ruled out any other explanation for the 40meV feature in the superconducting state, and even from unpolarized beam measurements alone we can conclusively identify it as a magnetic excitation.

Figure 2(a) shows a scan through the $(\frac{3}{2}, \frac{1}{2}, 1.7)$ position. As indicated in the figure, the intrinsic width of the profile is consistent with a sharp peak at $\mathbf{q}_{2D} = (k_F, k_F)$ and its Umklapp counterparts. If the scattering were indeed peaked at $\mathbf{q}_{2D} = (k_F, k_F)$, the peaks could not be resolved because of the poor vertical resolution of our triple axis spectrometer [long axis of the resolution ellipsoid shown in Fig. 1(a)]. The intrinsic momentum width of the excitation may thus indicate a Fermi surface effect, but alternative explanations have also been given [8]. All theories must explain the sinusoidal modulation of the scattering intensity as a function of the momentum transfer perpendicular to the CuO_2 layers [4].

As a crosscheck of our unpolarized beam experiments, we have performed polarized beam experiments both in the "standard" scattering zone around $(\frac{1}{2}, \frac{1}{2}, 5.2)$ and in the newly developed zone around $(\frac{3}{2}, \frac{1}{2}, 1.7)$. As in the case of unpolarized neutron scattering experiments the weakness of the signal makes an extremely careful background subtraction indispensable. In particular, it is difficult to discriminate between genuine magnetic scattering processes (Bragg scattering from monochromator and analyser; inelastic scattering from the sample) and accidental nuclear Bragg scattering (Bragg scattering from monochromator and sample; incoherent, diffuse or inelastic scattering from the analyser). Although the latter process does not involve a spin flip at the sample, limitations of the polarized beam setup nevertheless allow some such neutrons to reach the detector. We have conducted extensive checks for these spurious effects

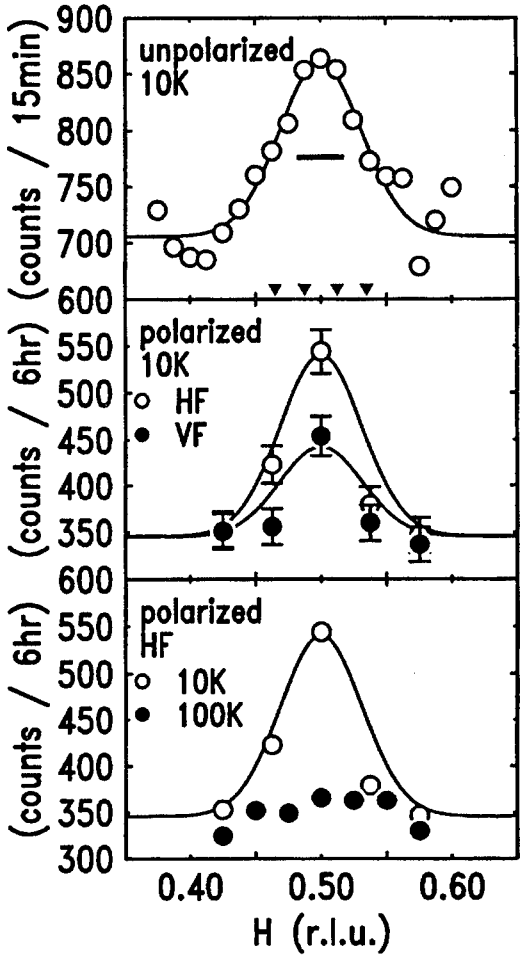


Fig. 2. (a) Scattering profiles along $(3H, H, 1.7)$ at $\hbar\omega = 41$meV. The approximate locations of the four peaks of Fig. 1 are indicated by arrows. k_F was taken from the photoemission data of Ding *et al.* [7] on $Bi_2Sr_2CaCu_2O_{8+\delta}$, which has a structure and T_c very similar to $YBa_2Cu_3O_7$. The bar indicates the momentum resolution. (b) $(3H, H, 1.7)$ scan taken with a polarized beam, with horizontal (HF) and vertical (VF) neutron guide fields at the sample. The lines are the same as in panel a), rescaled without adjustable parameters. (c) Horizontal field scans in the same geometry at 10K and 100K.

and found that in the standard geometry they dominate the signal, so that polarized beam experiments are very difficult. Spurious effects are in fact the origin of the small 41 meV "resonance" in the normal state observed in the polarized-beam experiments of Mook *et al.* [3] Fortuitously, the new scattering geometry is far less affected by this contamination, and data taken in this mode allowed us to confirm the magnetic origin of the 40meV excitation in the superconducting state unambiguously [Fig. 2(b)]. The solid line through the points is the line of panel a), rescaled to adjust for the reduced efficiency of the polarized beam equipment. This confirms that all the intensity which is peaked around $\mathbf{q}_{2D} = (\frac{\pi}{a}, \frac{\pi}{a})$ in the superconducting state arises from magnetic scattering.

For fixed neutron guide field at the sample, one measures the magnetic cross section plus an extrinsic background. The

standard way of removing the background is to measure the intensity for vertical guide field (yielding only half magnetic cross section because of polarization effects) and subtracting it from the intensity for horizontal guide field (yielding the full magnetic cross section). Figure 2(b) shows that the the 40meV excitation survives this test as well. Figure 2(c) confirms that the the magnetic cross section at 40meV in the normal state is much smaller than in the superconducting state. While on general grounds one expects some magnetic scattering at any temperature, the magnetic scattering intensity at 40meV in the normal state is indistinguishable from zero within our present errors.

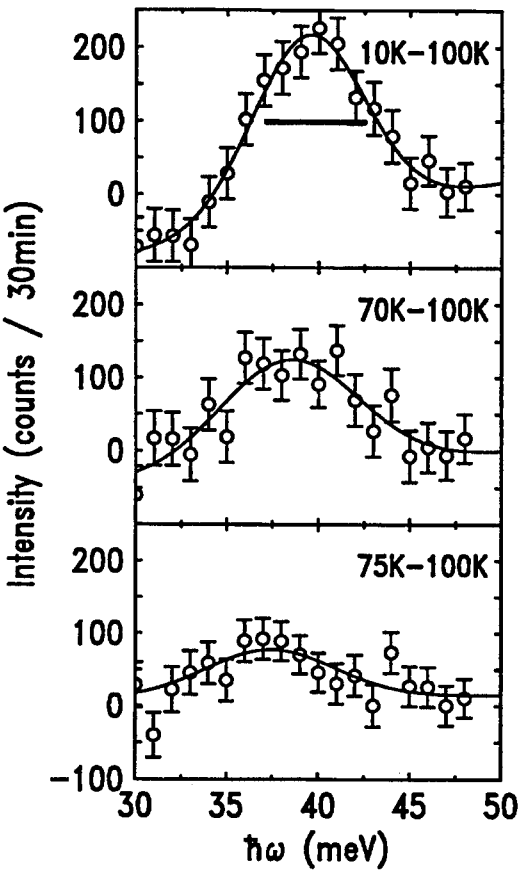


Fig. 3. Energy scans of the magnetic excitation at $\mathbf{Q} = (\frac{3}{2}, \frac{1}{2}, 1.7)$. The data were taken under different experimental conditions, and the relative intensities were normalized approximately. The bar indicates the energy resolution.

In Fig. 3 energy scans at $\mathbf{Q} = (\frac{3}{2}, \frac{1}{2}, 1.7)$ are shown. The intensity of the magnetic excitation (and concomitantly the data quality) diminishes rapidly as T_c is approached. A slight shift (~ 2 meV) of the excitation energy is suggested by the data taken at 75K ($\sim 0.8T_c$), but is within the experimental uncertainty. As there is no evidence of scattering centered around 40meV in the normal state, we may associate this energy with the spectroscopic energy gap (2Δ) in the superconducting state. If this interpretation is correct, the gap must be essentially temperature independent below $\sim 0.8T_c$. Further, the coherence factor for quasiparticle creation by magnetic neutron scattering necessitates a sign reversal of the energy gap on the Fermi surface [4]. Other interpretations in which the excitation energy is determined by weakly temperature dependent microscopic parameters have also been proposed [8].

Acknowledgements—We are very grateful to P. W. Anderson for many enlightening discussions, and to the Brookhaven neutron scattering group, in particular G. Shirane, J. D. Axe, B. J. Sternlieb and J. M. Tranquada, for their hospitality and many helpful conversations. The work at Princeton was supported by the MRSEC program of the NSF under grant DMR94-00362. The work at the HFBR at Brookhaven was supported by the US DOE under contract DE-AC02-76CH00016.

REFERENCES

1. Tranquada J. M. *et al.* , *Phys. Rev. B* **40**, 4503 (1989); *ibid.* **46**, 5561 (1992).
2. Rossat-Mignod J. *et al.* , *Physica B* **185–189**, 86 (1991); *Physica Scripta T* **45**, 74 (1992); *Physica B* **199 & 200**, 281 (1994).
3. Mook H. A. *et al.*, *Phys. Rev. Lett.* **70**, 3490 (1993).
4. Hung Fai Fong, Keimer B., Anderson P. W., Reznik D., Dogan F. and Aksay I. A., *Phys. Rev. Lett.* **75**, 316 (1995).
5. Pyka N. *et al.*, *Phys. Rev. Lett.* **70**, 1457 (1993); Reznik D. *et al.*, *Phys. Rev. Lett.* **75**, 2396 (1995).
6. Bourges P. *et al.*, preprint
7. Ding H. *et al.*, *Phys. Rev. Lett.* **74**, 2784 (1995).
8. For theoretical discussions of our experiment, see e.g., Mazin I. I. and Yakovenko V. M. (unpublished); Demler E. and Shou-Cheng Zhang (unpublished); Liu D. Z., Levin K. and Maly J. (unpublished); Onufrieva F. (unpublished); Barzykin V. and Pines D. (unpublished); Bulut N. and Scalapino D. J. (unpublished); and references therein. See also Monthoux P. and Scalapino D. J., *Phys. Rev. Lett.* **72**, 1874 (1994), and Maki K. and Won H., *ibid.* **72**, 1758 (1994).

Pergamon

J. Phys. Chem. Solids Vol. 56, No. 12, pp. 1931–1935, 1995
Copyright © 1995 Elsevier Science Ltd
Printed in Great Britain. All rights reserved
0022-3697/95 $9.50 + 0.00

0022-3697(95)00098-4

NMR STUDY IN NOVEL SUPERCONDUCTORS: HEAVY-FERMION SYSTEM AND HIGH-T_c CUPRATE

Y. KITAOKA, K. ISHIDA, G.-Q. ZHENG, H. TOU, K. MAGISHI,
S. MATSUMOTO, K. YAMAZOE, H. YAMANAKA and K. ASAYAMA
Department of Material Physics, Faculty of Engineering Science, Osaka University, Toyonaka, Osaka 560, Japan

Abstract—From the NMR and NQR studies, we show the unconventional superconducting properties in the antiferromagnetic (AF) heavy-fermion (HF), UPd_2Al_3 and high-T_c cuprate systems. In UPd_2Al_3 with T_N=14.5 K and T_c=2 K, the superconductivity is shown to be of d-wave pairing type with lines of vanishing gap on the Fermi surface. The potential scattering associated with some defects at the Al site is the cause for the T_c suppression and the appearance of the density of states (DOS) at the Fermi level. This unusual impurity effect is consistent with a d-wave scenario, because the potential scattering leads to a gap opening for an anisotropic s-wave scenario. In high-T_c cuprate which are argued to be either a d-wave or an anisotropic s-wave, the potential scatterer like Zn in the plane induces the gapless superconductivity as well, which can not be interpreted in terms of an anisotropic s-wave scenario if the order parameter does not change sign largely. It is shown from the NMR experiment at the Al site for Al-doped $La_{1.85}Sr_{0.15}CuO_4$ that local moments at near neighbor Cu sites induced around Al impurity do not play a role to suppress the T_c and to induce the DOS at all. The NMR studies in novel superconductors have provided important clues to identify their symmetry of order parameter to be d-wave.

Keywords: heavy fermion system, high-T_c cuprate, d-wave superconductivity, NMR, NQR

1. INTRODUCTION

Novel superconductors such as heavy fermions (HF) and high-T_c cuprates systems are unconventional, possessing a highly anisotropic gap function. Whereas the symmetry of the order parameter (OP) in the HF systems is established to be either p- or d-symmetry with lines of vanishing gap, the candidates for the OP in the high-T_c seem to be a $d_{x^2-y^2}$ or a highly anisotropic s-wave (ASW) type, since the formation of singlet pairing state is evidenced by the large decrease of the spin susceptibility measured by the NMR Knight shifts.

Recently, a growing list of experiments suggests to be consistent with the $d_{x^2-y^2}$ pairing state for the high-T_c [1]. Firstly, the NMR relaxation study pointed to a possibility of unconventional superconductivity in analogy with the behavior in the HF systems [2–4], whereas the subsequent experiments such as the penetration depth and the Knight shift seemed to be in agreement with an s-wave pairing. Our systematic NMR studies on Zn-doped $YBa_2Cu_3O_7$($YBCO_7$) [5] and a single crystal $Bi_2Sr_2CaCu_2O_8$(Bi2212) [6] with $T_c \simeq 86 \sim 87$ K revealed that impurities and/or some defects could actually either obscure or mimic the presence of line nodes for the $d_{x^2-y^2}$ pairing state, producing a finite density of states (DOS) at the Fermi level. Eventually, the d-wave model explained quantatively the NMR results that the nonmagnetic Zn impurities in $YBCO_7$ and some defect in Bi2212 induce the DOS in spite of the slight T_c suppression, in case that the impurity scattering is incorporated in terms of the unitarity limit [7]. Recent measurements of the low-T penetration depth in the high quality $YBCO_7$ single crystal show a linear dependence characteristic of line nodes [8], and then by controlling impurity content of Zn, the same trend as the NMR results has been found for the penetration depth results as well, demonstrating that the earlier measurements are more or less affected by impurity contributions at low-T. There are further experimental evidences from angle-resolved measurements by photoemission [9] and Ramman scattering [10] that the energy gap function is anisotropic in the momentum space. Above all measurements do not, however, probe a sign change of the OP between the a- and b-direction inherent to the $d_{x^2-y^2}$ symmetry, whereas measurements of the phase coherence such as dc SQUIDs [11] and flux quantization [12] on $YBCO_7$ have exhibited a sign change of the OP, excluding an anisotropic s-wave state [13]. When these types of experiments reach the consensus, it would be established that $YBCO_7$ has the $d_{x^2-y^2}$ symmetry. For another route to identify the symmetry of the OP in general, we note that the impurity effects can be sensitive to a sign change of the OP as argued by several authors [14–16]. The case of the $d_{x^2-y^2}$ was contrasted with an ASW gap if the phase of an s-wave OP does not change sign. So far, the appearance of magnetic moments induced by nonmagnetic impurities in the underdoped high T_c systems [17,18] make it difficult to apply the argument for the Zn-doped $YBCO_7$ and Bi2212 system in general. Recent NMR study for the Al impurity site enables us to estimate quantitatively the magnetic coupling between

trace of T_c suppression by induced moments [19]. We conclude that the impurity effect is most consistent with the d-wave pairing, but in serious discrepancy with an ASW if the sign of the OP is largely unchanged.

2. HEAVY FERMION SUPERCONDUCTIVITY

UPd_2Al_3 is an antiferromagnetic superconductor of T_c =2 K with a rather moderate mass renormalization, i.e. the T-linear coefficient of specific heat γ = 150 mJ/(mole.K^2), which coexists with an antiferromagnetically ordered state below T_N = 14.5 K [20]. The nuclear-spin-lattice relaxation rate, $^{27}(1/T_1)$ of the high-quality polycrystalline UPd_2Al_3 with the narrowest Al-NQR linewidth of 12 kHz to date was measured in zero external field by the NQR technique [21]. As shown in Fig. 1, the T-dependence of $1/T_1$ obeys the T^3-law down to 0.15 K, giving a strong evidence that the energy gap vanishes along lines on the Fermi surface. In UPd_2Al_3 with lower T_c =1.75 K and larger FWHM=20 kHz than T_c =1.98 K and FWHM=12 kHz of our sample, a T_1T=const. behavior emerges below 0.6 K as indicated by a dash line [22] in Fig. 1. Thus a slight inhomogeneity in the Al site for the lower T_c sample changes the anisotropic gap state with line nodes into the gapless state with the residual DOS at the Fermi level. Furthermore, it is noteworthy that the T_c reduction rate, $R = \frac{T_c(1.75\mathrm{K})}{T_{co}(1.98\mathrm{K})}$ = 0.88 against the fraction of residual to normal DOS, $\frac{N_{res}}{N_o} = \sqrt{\frac{(T_1T)^{-1}_{res}}{(T_1T)^{-1}_0}}$ = 0.23 is consistent with the prediction($\frac{N_{res}}{N_0}$ = 0.36 for $\frac{T_c}{T_{co}}$ = 0.88) from *the unitary scattering limit* for the anisotropic superconductivity with lines of vanishing gap as argued extensively in the literature [23]. Together with ^{27}Al spin Knight shift results which decrease to nearly zero, we have shown that the superconductivity in UPd_2Al_3 is the d-wave with lines of vanishing gap [21].

3. SYMMETRY OF THE ORDER PARAMETER IN HIGH-T_c CUPRATE

In most of the high-T_c cuprates, the relaxation behavior below T_c is almost the same [24] except for the oxygen deficient YBCO and Y124. A universal feature, namely, lack of coherence peak of $1/T_1$ and a power-law like behavior at low-T is reminiscent of the behavior in the HF systems (see Fig. 1). An anisotropic s-wave model was, however, suggested to be also applicable in explaining the above unusual relaxation behavior, but qualitatively [25]. Extensive NMR and NQR studies of the impurity effect on the superconducting state in $YBCO_7$ and Bi2212 revealed, however, that the high-T_c superconductivity is most consistent with the d-wave model with line nodes at the Fermi surface [5,6]. In particular, it was crucial evidence against the s-wave that a single crystal Bi2212, which shows no trace of magnetic impurities and possesses high T_c of 86 K, was the gapless

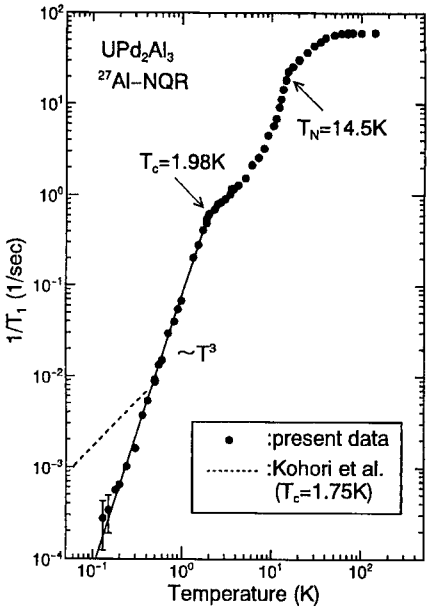


Fig. 1. T-dependence of $^{27}(1/T_1)$ in UPd_2Al_3 with T_c =1.98 K. Solid line shows T^3-dependence. Dash line indicates the T_1T=const. law for the lower T_c sample with T_c =1.75 K at low-T behavior.

superconductor with a DOS at the Fermi level. This is because such a gapless state is not possible in an anisotropic s-wave except for impurity concentrations so large as to nearly destroy the superconductivity in the case where the OP does not change sign.

Nevertheless it makes the impurity effect complicated that the nonmagnetic impurities induce magnetic moments in the CuO_2 plane in the underdoped systems such as LSCO, oxygen deficient YBCO and Y124. Induced local moments were argued to play some role in suppressing the T_c in addition to the potential scattering effect. This fact makes it hard to apply the same argument on the impurity effect in $YBCO_7$ and Bi2212 to the underdoped systems. In order to clarify to what extent the T_c is suppressed by induced moments, the ^{27}Al-NMR study has been made on Al-doped $La_{1.85}Sr_{0.15}(Cu_{0.97}Al_{0.03})O_4$ [19].

Figure 2 indicates the T-dependence of the susceptibilities for undoped and 3% Al-doped $La_{1.85}Sr_{0.15}CuO_4$. It is evident that doping Al impurity into the CuO_2 plane induces local moments. The T-dependence of the ^{27}Al NMR spectrum, which is well articulated by the electric quadrupole interaction of Al nuclei (I = 5/2), allows us to extract the T-dependence of ^{27}Al Knight shift, $^{27}K(T)$ precisely. Since $^{27}K(T)$ is proportional to the susceptibility associated with induced moments, the transferred hyperfine coupling constant, A_{hf}(Al) with induced moments at nearest neighbor Cu sites was estimated to be 16.5 kOe/μ_B. Hence, measurement of the ^{27}Al nuclear relaxation rate, $^{27}(1/T_1)$ provides a direct estimation of the magnetic relaxation rate, $1/\tau_{obs}$ of induced moments. Figure 3 shows the T-dependence of $^{27}(1/T_1)$ (open circle), which decreases moderately with in-

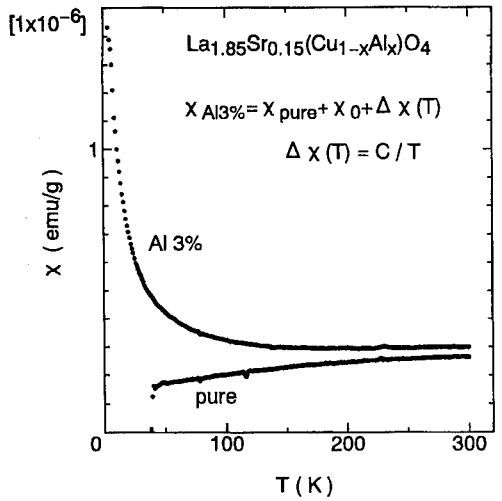


Fig. 2. T-dependence of susceptibilities for undoped and Al-3% doped $La_{1.85}Sr_{0.15}CuO_4$.

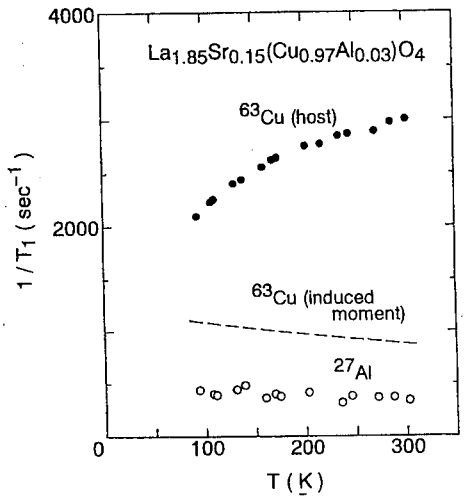


Fig. 3. T-dependence of $^{27}(1/T_1)$ for impurity Al in $La_{1.85}Sr_{0.15}(Cu_{0.97}Al_{0.03})O_4$. Solid circle indicates the T-dependence $^{63}(1/T_1)$ for the host ^{63}Cu. Dash line corresponds to the $(1/T_1)$ of ^{63}Cu dominated by induced moments in nearest neighbor Cu sites around Al impurities (see text).

creasing temperature. The magnetic relaxation rate, $1/\tau_{obs}$ of induced moments can be estimated from the relation

$$^{27}(1/T_1) = 4\gamma^2(\mathrm{Al})A_{hf}^2(\mathrm{Al})\frac{g^2S(S+1)}{3}\tau_{obs}(T)$$

with A_{hf}(Al)=16.5 kOe/μ_B and gS_{eff}=0.14, the magnitude of induced moments per one Cu site. Furthermore, by using $\tau_{obs}(T)$ and the on-site hyperfine coupling constant between the Cu nuclei and induced moments, the $^{63}(1/T_1)$ for the Cu sites with induced moments around Al impurity is indicated by dashed line in Fig. 3 together with the T_1 data (closed circle) for host Cu nuclei dominated by AF spin fluctuations. A difference is clear, showing that $1/\tau_{obs}$ of induced moments is isolated from AF spin fluctuations for

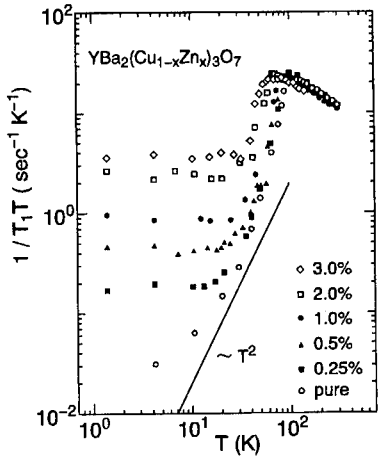


Fig. 4. T-dependences of $(1/T_1T)$ of ^{63}Cu in Zn-doped $YBa_2Cu_3O_7$.

the host, instead dominated by the exchange coupling with spin of conduction holes, $(1/\tau_{sd})$ and among induced moments $(1/\tau_{ex})$. Namely, the observed $1/\tau_{obs}$ is composed of two contributions as

$$\frac{1}{\tau_{obs}(T)} = \frac{1}{\tau_{sd}(T)} + \frac{1}{\tau_{ex}}$$

where

$$\frac{1}{\tau_{sd}} = \frac{\pi}{\hbar}J_{sd}^2N(E_F)^2k_BT$$

and τ_{ex} is independent of the temperature. Accordingly, the T-dependence of τ_{obs} enables us to extract quantatively the exchange coupling, J_{sd} to be 0.055 and to calculate the T_c reduction to be ΔT_c =0.62 K with $N(E_F)$=3.6 states/(eV, both spins) from the formula of

$$\Delta T_c = \frac{\pi^2 n_{\mathrm{imp}}N(E_F)J_{\mathrm{sd}}^2S(S+1)}{k_B}$$

according to the AG theory. A magnetic scattering rate, $\Gamma_s = 0.4\times10^{-4}$ eV is two orders of magnitude smaller than a total scattering rate, $\Gamma_{obs} = 30\times10^{-4}eV$ expected from the experiment. Apparently, the magnetic scattering mechanism of holes by induced moments is not the cause of the T_c suppression.

Next, we argue quantitatively the potential scattering effect by Zn impurity in $YBCO_7$. In order to extract the potential scattering rate, Γ_n by Zn single impurity, we have carried out a systematic measurement of $^{63}(1/T_1)$ of ^{63}Cu at low-T and zero field for $YBa_2(Cu_{1-x}Zn_x)_3O_7$ slightly doped with x = 0.0025 and 0.005. In Fig. 4 are shown the T-dependences of $^{63}(1/T_1T)$ measured by the Cu-NQR method in zero field together with the data reported previously [5].

The $^{63}T_1T$=const. law observed for x = 0.0025 and 0.005 well below T_c demonstrates directly that a DOS is induced at the Fermi level in the superconducting state. It is noteworthy that Cu nuclei away from the Zn impurity show

T_1T=const. law, namely the low-lying excitation in the superconducting state is in a gapless regime. Furthermore, we note that the relaxation behavior at low-T for the undoped $YBCO_7$ is more or less affected by inherent impurites and/or imperfections. It has, furthermore, been found that $\sqrt{^{63}(T_1T)^{-1}}$ in proportion to a DOS, N_{res} increases following a relation of $N_{res} \propto \sqrt{n_{imp}}$. A fraction $\frac{N_{res}}{N_0}$ of a DOS normalized at the value in the normal state,

$$\frac{N_{res}}{N_0} = 1.2\sqrt{\frac{\alpha}{\Delta_0}}$$

is derived as a function of the pair-breaking parameter, α defined as $\alpha = \frac{N_{imp}}{\pi N_0}$ for the case of unitarity limit for the $d_{x^2-y^2}$ pairing state [26]. Figure 5(a) indicates the impurity content (n_{imp}) dependence of N_{res}/N_0 extracted from $\sqrt{\frac{(T_1T)^{-1}_{obs}}{(T_1T)^{-1}_{c}}}$. From a fit of the data for $n_{imp} \leq 0.01$ to a theoretical calculation indicated by solid line, the potential scattering rate, $\Gamma_0 = \frac{n_{imp}}{\pi N_0 \Delta_0} = 2.34 n_{imp}$ is obtained. For instance, $\Gamma_0 = 7 \times 10^{-4}$ eV is obtained for $n_{imp} = 0.01$ with $2\Delta_0 = 8k_BT_c$, being more than one order of magnitude larger than the magnetic scattering rate,Γ_s estimated above. Furthermore, by using the experimental relation of $\Gamma_0 = 2.34 n_{imp}$ an initial slope of the T_c reduction is quantitatively evaluated to be $\frac{\Delta T_c}{T_{c0}} = 7.35 n_{imp}$ as a function of the Zn impurity content, n_{imp}. As indicated in Fig. 5(b), $\Delta T_c/T_{c0} \sim 7.35 n_{imp}$ is comparable to that obtained by Monthoux and Pines from N_0 deduced from the spin susceptibility above T_c [27]. For $YBCO_7$, we found that a small concentration Zn impurity alters significantly the low frequency spin dynamics measured by the Cu spin lattice relaxation rates at sites near the Zn impurity, namely, a substitution of Zn destroys the short range antiferromagnetic (AF) spin correlation locally [5]. On the other hand it should be noted that for magnetic Ni-doped $YBCO_7$ and a single crystal Bi2212 where some defects cause the gapless superconductivity with a DOS at the Fermi level, any changes of low frequency spin dynamics do not take place. Therefore, it seems to be natural that the larger T_c reduction than the unitarity limit is relevant to the local suppression of the AF spin correlation. Actually Monthoux and Pines pointed out that Zn is a "super unitarity" scatterer in which it does more than act as a potential scatterer and hence it must change the effective interaction responsible for superconductivity [27]. These experiments were suggested to provide a "smoking gun" for the spin-fluctuation exchange mechanism in the cuprate superconductors [28]. By assuming that Zn acts to destroy magnetic correlation over a distance of the order of the AF correlation length, ξ, a reduction in T_c comparable to that found experimentally was obtained [27]. The spin-fluctuation mediated mechanism which provides a natural explanation of the $d_{x^2-y^2}$ pairing state is the best candidate for high-T_c cuprate superconductivity [28].

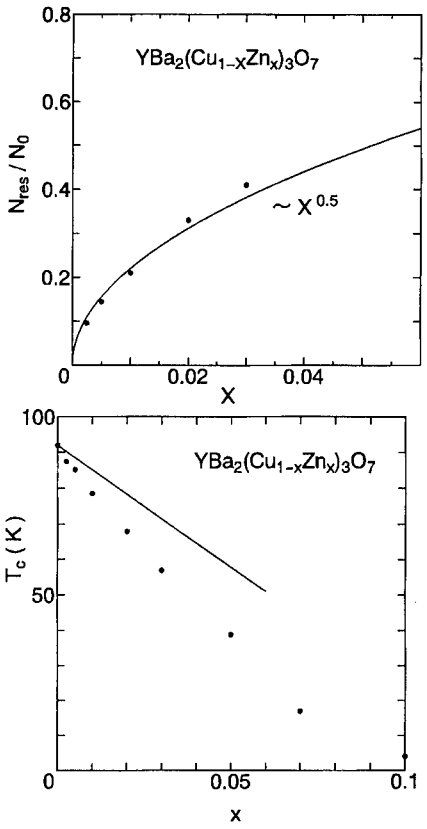


Fig. 5. (a) Impurity content, n_{imp} dependence of the fraction of a density of states at the Fermi level, N_{res}/N_0 estimated from $\sqrt{\frac{(T_1T)^{-1}_{obs}}{(T_1T)^{-1}_{c}}}$. Solid line corresponds to the calculation in case of unitarity scattering for the $d_{x^2-y^2}$ state (see text). (b) Zn concentration dependence of T_c for $YBCO_7$. Solid line corresponds to the reduction rate for the unitarity limit.

4. CONCLUSIONS

In Fig. 6 are summarized the impurity effect of the superconducting state in $YBCO_7$, Bi2212 and LSCO, the contrast between Zn- and Ni-impurity effects in LSCO is remarkable as well as in $YBCO_7$ [5]. The strong potential scattering causes the gapless superconductivity, inducing a DOS at the Fermi level, even though the T_c is not reduced so much. This unconventional impurity effect, which is common in high-T_c oxides, can not be understood in terms of an anisotropic s-wave model because it is unexpected that the OP of an anisotropic s-wave changes its sign largely in the momentum space as in the $d_{x^2-y^2}$ state [14–16]. The impurity effect can thus help to identify the symmetry of the order parameter in high-T_c oxides.

Acknowledgements—The work on UPd_2Al_3 is being done in collaboration with C. Geibel, C. Schank and F. Steglich.

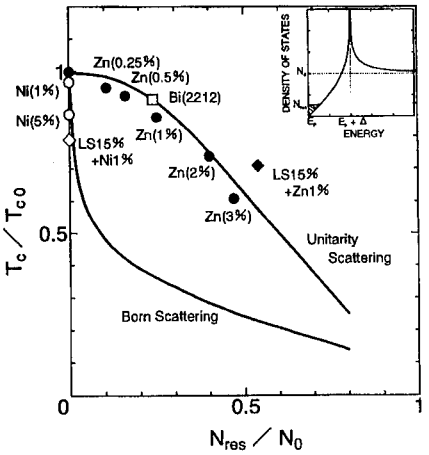


Fig. 6. Reduction rate of T_c normalized by T_{c0} = 93 K in $YBCO_7$, highest T_{c0} = 89 K reported so far in Bi2212 and T_{c0} = 38 K in LSCO. (T_c /T_{c0}) is plotted as a function of the fraction of DOS, (N_{res}/N_0) deduced from NMR measurements in Zn- and Ni-doped $YBCO_7$ [5,7], Bi2212 [6] and LSCO [19] where N_{res} and N_0 are the residual DOS in the superconducting state and the DOS in the normal state, respectively. Solid lines indicate the theoretical calculations based on the $d_{x^2-y^2}$ model with line nodes [14]. Here the impurity scattering is treated in Born (weak) and unitarity (strong) scattering limits.

REFERENCES

1. See, for example, *Physica C* **235–240** (1994), *Proc. M^2S IV*, Grenoble, France.
2. Kitaoka Y. *et al.*, *Physica C* **153–155** 83 (1988).
3. Imai T. *et al,. Phys. Soc. Jpn* **57** 2280 (1998).
4. Martindale J. A. *et al.*, *Phys. Rev. Lett.* **68** 702 (1992).
5. Ishida K. *et al.*, *Physica C* **179** 29 (1991); *ibid.*, *J. Phys. Soc. Jpn* **62** 2803 (1993).
6. Ishida K., Kitaoka Y., Asayama K., Kadowaki K. and Mochiku T., *J. Phys. Soc. Jpn* **63** 1104 (1994).
7. Kitaoka Y., Ishida K. and Asayama K., *J. Phys. Soc. Jpn* **63** 2052 (1994).
8. Hardy W. N. *et al.*, *Phys. Rev. Lett.* **70** 3999 (1993).
9. Shen Z.-X. *et al.*, *Phys. Rev. Lett.* **70** 1553 (1993).
10. Devereaux T. P. *et al.*, *Phys. Rev. Lett.* **72** 396 (1994).
11. Wollman D. A. *et al.*, *Phys. Rev. Lett.* **71** 2134 (1993).
12. Tsuei C. C. *et al.*, *Phys. Rev. Lett.* **71** 593 (1994).
13. Chakravaty S., Sudbo A., Anderson P. W. and Strong S., *Science* **261** 337 (1993).
14. Hotta T., *J. Phys. Soc. Jpn* **62** 274 (1993).
15. Borkowski L. S. and Hirschfeld P. J., *Phys. Rev. B* **49** 15404 (1994).
16. Fehrenbacher R. and Norman N. R., *Physica C* **235–240** 2407 (1994).
17. Alloul H. *et al.*, *Phys. Rev. Lett.* **67** 3140 (1991).
18. Zheng G.-q. *et al.*, *J. Phys. Soc. Jpn* **62** 2591 (1993).
19. Yamazoe K., Ishida K., Kitaoka Y. and Asayama K., in preparation.
20. Geibel C. *et al.*, *Z. Phys. B–Cond. Matter* **84** 1 (1991).
21. Kyogaku M. *et al.*, *J. Phys. Soc. Jpn* **61** 2660 (1992); Tou H. *et al.*, *J. Phys. Soc. Jpn* **63**(3) (1995).
22. Kohori Y. *et al.*, to be published in *Physica B*.
23. Schmitt-Rink S., Miyake K. and Varma C. M., *Phys. Rev. Lett.* **57** 2575 (1986); Hirschfeld P. J., Wolfle P. and Einzel D., *Phys. Rev. B* **37** 83 (1988).
24. Asayama K. *et al.*, *Physica C* **178** 281 (1991).
25. Sudbo A. *et al.*, *Phys. Rev. B* **49** 12245 (1994).
26. Hotta T., unpublished.
27. Monthoux P. and Pines D., *Phys. Rev. B* **49** 4261 (1994).
28. Moriya T., Takahashi Y. and Ueda K., *J. Phys. Soc. Jpn* **59** 2905 (1990); Ueda K., Moriya T. and Takahashi Y., *J. Phys. Chem. Solids* **53** 1515 (1992); Monthoux P. , Balatsky A. V. and Pines D., Phys. Rev. Lett. 67 (1991) 3448; Pines D., *Physica C* **185–189** 120 (1991); Monthoux P. and Pines D., *Phys. Rev. B* **47** 6069 (1993).

Pergamon

J. Phys. Chem. Solids Vol. 56, No. 12, pp. 1937–1938, 1995
Copyright © 1995 Elsevier Science Ltd
Printed in Great Britain. All rights reserved
0022-3697/95 $9.50 + 0.00

0022-3697(95)00204-9

COMPARISON OF ANTIFERROMAGNETIC FLUCTUATIONS IN ZINC-FREE AND ZINC-DOPED YBCO IN FULLY OXIDIZED SAMPLES. STUDIES BY INELASTIC NEUTRON SCATTERING

P. BOURGES,* Y. SIDIS,* L. P. REGNAULT,† B. HENNION,* R. VILLENEUVE,* G. COLLIN,* C. VETTIER,‡ J. Y. HENRY† and J. F. MARUCCO§

* Laboratoire Léon Brillouin, CEA-CNRS, CE Saclay, 91191 Gif sur Yvette, France
† CEN Grenoble, DRFMC/SPS, Magnétisme et Supraconductivité, 85 X, 38041 Grenoble cedex, France
‡ European Synchrotron Research Facility, BP 220, 38043 Grenoble cedex, France
§ Laboratoire des composés non-stoechiométriques CNRS URA 446, Batiment 415, Université Paris-Sud centre d'Orsay, 91405 Orsay, France

Abstract—Inelastic neutron scattering experiments have been carried out to investigate magnetic fluctuations on $YBa_2Cu_3O_{6+x}$ single crystals as well as on $YBa_2(Cu_{1-y}Zn_y)_3O_{6+x}$ (y = 2 %) single crystal for fully oxidized samples. Direct comparaison of the imaginary part of the magnetic susceptibility, $\chi''(Q_{AF}, \omega)$, in both systems has been made possible using the same experimental conditions at LLB, Saclay.

In cuprates which develop high-T_c superconductivity, substitution of copper atoms by zinc atoms is the one which reduces the most strongly the superconducting properties [1]. This is why, among all the impurities which affect the superconducting state, this substitution by non-magnetic atoms in CuO_2 plane has received a considerable amount of attention.

High-T_c cuprates are also known to display unusual magnetic properties. From NMR and inelastic neutron scattering (INS) experiments, antiferromagnetic (AF) fluctuations persist in the metallic and superconducting states of all samples studied. In the $YBa_2Cu_3O_{6+x}$ system, a systematic investigation of magnetic correlations has been successfully performed by INS as a function of doping and temperature [2]. Shortly, as a result of doping, antiferromagnetic fluctuations are more and more restricted over an energy range around 30–40 meV yielding an almost single excitation at 40 meV in the overdoped state ($x > 0.94$) [3–5]. Here, we report on the effect of zinc substitution on these dynamical AF correlations in the overdoped regime of YBCO. We present the imaginary part of the magnetic susceptibility at the AF wavevector, $\chi''(Q_{AF}, \omega)$, as obtained by INS experiments on two samples having the same oxygen content ($x = 0.97$) but with and without zinc impurities. Our data clearly indicate a strong modification of the magnetic response through zinc substitution. An additional contribution appears at low energy, exhibiting a maximum around $\simeq$ 9 meV, which therefore seems induced by the zinc impurities [6].

Figure 1 displays the imaginary part of the magnetic susceptibility at the antiferromagnetic wavector in the superconducting phase of zinc free and zinc-doped YBCO samples. By the determination of the c lattice parameter, both samples appear to have the same oxygen concentration. The amount of zinc is known from the T_c reduction

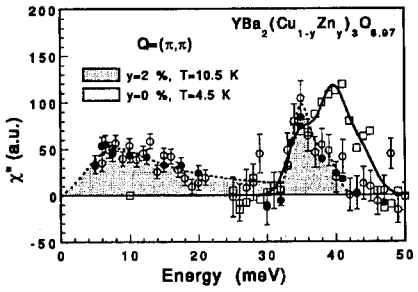


Fig. 1. Quantitative comparison of the imaginary part of the magnetic susceptibility as deduced from INS experiments, $\chi''(Q_{AF}, \omega)$ for zinc-free sample (squares) and zinc-doped sample (circles) from [6]. Details on the determination of $\chi''(Q_{AF}, \omega)$ can be found in [3] for zinc-free compound and in [6] for the zinc-substituted sample.

which is T_c=92.5 K in zinc-free sample and T_c=69 K when zinc is substituted to copper, yielding a zinc content of 2% per one copper [1]. Both INS experiments have been performed at Saclay on the same triple-axis spectrometer (2T) installed on a thermal beam. Details of experiments can be found in Refs [2,3,6]. Here, one has to stress that experimental conditions were the same for both studies, allowing a direct comparison of the magnetic intensity. Furthermore, we did measure a longitudinal acoustic phonon in order to scale the magnetic intensity of both samples. We obtained a scaling factor in agreement with the ratio of their volume. Therefore, we are able to discuss the quantitative change on $\chi''(Q_{AF}, \omega)$ due to these 2% non-magnetic zinc atoms.

All the observed magnetic fluctuations are peaked at the antiferromagnetic wavevector. In zinc-free sample, the magnetic response is restricted over a limited energy range ($\hbar\omega$ = 33–46 meV) in the superconducting state. Magnetic fluctuations are only sizeable above an energy gap, so-called spin-gap, located for $x = 0.97$ at E_G=33 meV. The most striking feature in $\chi''(Q_{AF}, \omega)$ is the resonance feature which is char-

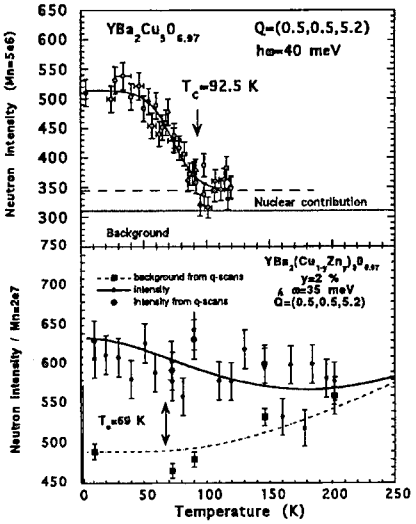


Fig. 2. (a) Temperature dependence of the neutron intensity at the resonance position ($\hbar\omega$= 40 meV) in zinc-free sample (from [3]) as compared with (b) the temperature dependence of the neutron intensity at $\hbar\omega$= 35 meV in zinc-substituted sample. Squares and dashed lines indicate the background.

gap, located for x = 0.97 at E_G=33 meV. The most striking feature in $\chi''(Q_{AF}, \omega)$ is the resonance feature which is characterized by an enhancement of intensity around 40 meV, almost energy resolution limited and associated with a reduction of the q-width. Moreover, the intensity at the resonance energy presents a strong temperature dependence in the superconducting state (Fig. 2). In the normal state, such a feature completely vanishes meaning unambiguously that it is strongly related to the superconductivity phenomenon. Above T_c, as shown in Fig. 2, there is at this energy a remaining intensity which is correlated in q-space. It has been previously mistakenly attributed to magnetic fluctuations [4], and actually, corresponds to a phonon mode [3,5].

Looking carefully at the wavevector and temperature dependences shows that $\chi''(Q_{AF}, \omega)$ is composed of two distinct contributions. In addition to the above mentioned resonance, a shoulder around 35 meV is clearly visible in $\chi''(Q_{AF}, \omega)$ response which is characterized by a q-width twice larger than the resonance q-width [3]. This second part of $\chi''(Q_{AF}, \omega)$ persists in the normal state. However, in this overdoped state, this contribution is so reduced that AF fluctuations above T_c have almost one order of magnitude smaller in intensity as compared to the resonance peak at 39 meV at low temperature [3]. Such a conclusion can be reached from the data reported in the normal state of $YBCO_7$ [5]. Additional work is on progress to ascertain this point.

In zinc-substituted sample, the second contribution remains in the magnetic response at $\hbar\omega$ = 35 meV (Fig. 1). Its temperature dependence reveals no change at the superconducting temperature (Fig. 2). This behaviour rules out the possibility of a renormalization of the resonance energy by zinc doping. In contrast, it seems more likely that the resonance is strongly reduced in magnitude but remains located at the same energy as suggested in Fig. 1. Indeed the q-width measured at $\hbar\omega$ = 38 meV is still smaller than at $\hbar\omega$ = 35 meV [6], accordingly. It is also very interesting to notice that the magnetic response displays an inflexion point around 33 meV. Our data clearly show in both samples that these is more magnetic intensity at 35 meV than at 30 meV [3,6]. In zinc-free sample, such a behaviour is characteristic of the opening of the spin-gap observed at the same energy for the same oxygen content. However, in contrast to pure-YBCO another antiferromagnetic contribution is sizeable at lower energy. This mainly points out that the system keeps a reminiscence of the spin-gap phenomenon upon zinc substitution. That may indicate that the spin-gap is strongly related to the hole doping as zinc substitution is known not to affect the hole doping in CuO_2 plane [7].

As depicted in Fig. 1, antiferromagnetic fluctuations occur at low energy in zinc-doped sample which therefore may be reliably associated with the presence of zinc impurities. This intensity is spread over a large energy range, but goes through a maximun around 9 meV. Its wavevector dependence can be accounted for by a gaussian line, Δq= 0.16 r.l.u. [6], yielding a correlation length of $\xi \simeq 7$ Å after deconvolution of the spectrometer resolution function. This low energy magnetic contribution might be linked to the appearance of finite electronic density of states at the Fermi level due to the zinc impurities [8]. Therefore, this contribution may originate from a local suppression of the superconducting gap in a range related to the above wavevector extension. Besides, the perturbation of the superconducting state has been estimated to become significant in a similar range around zinc atoms [8] for similar zinc content.

In summary, zinc-substitution induces marked modifications of the dynamical magnetic susceptibility in the superconducting state of the overdoped regime $YBCO_{6.97}$. The strong reduction of the resonance feature as well as the appearance of low energy excitations suggest the weakening of the itinerant nature of the magnetism in cuprates [9]. As both the superconducting properties and AF fluctuations are strongly affected through zinc-doping, the present work might indicate that magnetic fluctuations in cuprates is playing a major role in high-T_c superconductivity mechanism.

REFERENCES

1. Xiao C. *et al.*, *Phys. Rev. Lett.* **60** ,1446 (1988).
2. Rossat-Mignot J. *et al.*, *Physica C* **185–189** 86 (1991); Regnault L. P. *et al.*, *Physica C*, **235–240**, 59 (1994).
3. Bourges P. *et al.*, to be published in *Phys. Rev. B.*
4. Mook H. A. *et al.*, *Phys. Rev. Lett.* **70**, 3470 (1993).
5. Fong H. F. *et al.*, *Phys. Rev. Lett.* **75**, 316 (1995); Keimer B. *et al.*, this conference.
6. Sidis Y. *et al.*, preprint submitted to *Phys. Rev. B.*
7. Alloul H. *et al.*, *Phys. Rev. Lett.* **67**, 3140 (1991).
8. See e.g., Janossy A. *et al.*, *Phys. Rev. B* **50**, 3442 (1994).
9. Onufrieva F. *et al.*, *Physica C* **235–240**, 1687 (1994); *Phys. Rev. B* **52**, 7572 (1995).

Pergamon

J. Phys. Chem. Solids Vol. 56, No. 12, pp. 1939–1940, 1995
Copyright © 1995 Elsevier Science Ltd
Printed in Great Britain. All rights reserved
0022–3697/95 $9.50 + 0.00

0022–3697(95)00167-0

^{63}Cu NMR IN HEAVILY DOPED La_2CuO_4

Y.-Q. SONG,[1] A. P. REYES, X. P. TANG, W. P. HALPERIN
Department of Physics and Astronomy, Science and Technology Center for Superconductivity, Northwestern University, Evanston, IL 60208, U.S.A.

D. HINKS
Materials Science Division, Argonne National Laboratory, Argonne, IL 60439, U.S.A.

Abstract—We report ^{63}Cu NMR and NQR studies on $La_{2-x}Sr_xCuO_4$ and our results of ^{63}Cu Knight shift show a progressive variation of the temperature dependence as a function of x, for $0.10 < x < 0.3125$. These results appear to be consistent with the theoretical calculations of "$t-J$" model [Singh and Glenister, *Phys. Rev.* **B46**, 11871 (1992)].

There has been recent interest in the effects of carrier concentration on metallic antiferromagnets partly due to its perceived relevance to high temperature superconductivity [1]. The La_2CuO_4 system is ideal for such studies since the carrier concentration can be varied by doping. The effects of antiferromagnetic (AF) spin-correlations have been studied extensively by Nuclear Magnetic Resonance (NMR) and Nuclear Quadrupole Resonance (NQR) technique [2]. Previous work focuses primarily on the doping range of $x < 0.20$ and our knowledge about the higher doping materials is rather limited. This is partly due to the difficulties to prepare high quality $La_{2-x}Sr_xCuO_4$ samples for $x > 0.20$ since the compound tends to phase separate. A high temperature preparation method enables us to obtain high quality and homogeneous samples up to $x = 0.3125$ and to explore the heavily doped regime of this compound.

The measured Knight shift for two orientations is shown in Fig. 1, for x=0.2375, 0.2625 and 0.3125. For $H \parallel C$, Fig. 1A, measurements shown a temperature independent shift, $K_\parallel = 1.20 \pm 0.10\%$, for all samples with a very wide doping range, $0.10 \leq x \leq 0.3125$. A similar value of $K_\parallel$ was reported previously for $La_{2-x}Sr_xCuO_4$[3] for $x < 0.24$. This indicates strongly that the hyperfine coupling constants of copper is independent of the Sr concentration and the character of the electronic orbitals is conserved across the entire accessible phase diagram. This has been argued for the transverse components of the hyperfine coupling, from spin-lattice relaxation rate measurements [4], for $x \leq 0.15$.

Figure 1B shows $K_\perp$ at $H \perp C$, for x =0.2375, 0.2625 and 0.3125. Previous measurements on x = 0.10, 0.16,0.20 [5] are shown as lines for comparison. Marked change inthe temperature dependence of $K_\perp$ is observed at different doping levels. Data from Ref. [3] shows a similar overall variation in the temperature dependence, although their $K_\perp$ for x=0.20 and 0.24 are somewhat lower than ours at similar doping levels, likely due to sample differences. A trend in the doping-dependent $K_\perp(T)$ is very clear: at low doping, $\partial K_\perp(T)/\partial T > 0$, and as x increases, the slope of $K_\perp(T)$ decreases and crosses over to negative. A minimum slope and a maximum low temperature $K_\perp$ are reached at $x \approx 0.25$. At even higher doping, $K_\perp$ drops down and becomes temperature independent, similar to the case of a conventional metal. This type of behavior has been observed much earlier from DC magnetic susceptibility measurements [6] on $La_{2-x}Sr_xCuO_4$, although such data, in principle, may be more susceptible to contributions from impurity phases.

Our measurements of the ^{63}Cu spin-lattice relaxation rates, $1/T_1$, for x=0.3125 shows a linear temperature dependence, $1/T_1 \propto T$, below 300 K, a general result for metallic system with Fermi quasiparticles as the low energy excitations. In addition, the $1/T_1$ anisotropy of this compound is found to be 1.5–2, which is substantially lower than that for the lower doping materials [4]. This also indicates that the antiferromagnetic correlationsare not important in this high doping level at low temperatures [7].

It is interesting to consider the different doping dependence of Knight shift and $1/T_1$. As shown in Fig. 1, the low temperature $K_\perp$ increases as x is increased from low doping and reaches a maximum around x=0.2–0.25. Onthe other hand, $1/T_1$ has been observed to decrease monotonically as x is increased [4,3]. $1/T_1$ is an integral of $\chi''(q)$ over the reciprocal space while $K \propto \chi'(0)$, the real part of the uniform spin susceptibility. For $La_{2-x}Sr_xCuO_4$ and most high T_c superconductors, the main contribution to $1/T_1$ comes from χ around the zone corner due to antiferromagnetic correlations. It might be natural to consider the decrease in $1/T_1$ as a function of x to be due to the gradual suppression of antiferromagnetic correlations in this material at high doping. However, it appears necessary to study the complete spin dynamics in order to understand the behavior at long wave length, such as $\chi(0)$ [8].

[1] Present address: Department of Chemistry, University of California,Berkeley, CA 94720, U.S.A.

Theoretical studies of the "$t-J$" model [9] at various hole concentrations have reported calculations of the spin susceptibility using a high temperature expansion technique [10]. Even though such calculations become very difficult at temperatures lower than $\frac{1}{4}J$ (J, the antiferromagnetic exchange coupling), it nevertheless shows a trend in the change of the temperature dependence as a function of doping which is consistent with our experimental findings. A summary of Singh and Glenister's results [10] is the following. χ for various dopings is found to be independent of x above the temperature J/k_B, and significant doping dependence appears only at lower temperatures. For very low doping material, $\rho < 0.1$ (ρ is the hole concentration), χ decreases as temperature decreases similar to a Heisenberg antiferromagnet. When doping increases, the low temperature χ increases. At intermediate doping, χ increases as temperature decreases. At higher doping, $\rho > 0.25$, χ is found to decrease with further doping, and be much less temperature dependent. Throughout the whole doping range, the antiferromagnetic correlations, as determined by $\chi(\mathbf{Q}_{AF})$ ($\mathbf{Q}_{AF}$ is the antiferromagnetic wave vector), is found to decrease continuously as holes are doped into the system. This overall picture of the progressive change of magnetic propertiesas a function of hole doping is qualitatively consistent with our experimental results, however, it would be desirable to extend such calculations to lower temperatures for a quantitative comparison.

In summary, we have explored the entire accessible phase diagram of $La_{2-x}Sr_xCuO_4$ and studied the spin susceptibility and its temperature dependence. Study of the spin-lattice relaxation rate and Knight shift at higher temperature is currently underway to further elucidate the spin dynamics in this compound.

Acknowledgements—This work was supported by the National Science Foundation (DMR 91-20000)through the the Science and Technology Center for Superconductivity. YQS acknowledges the support from the Miller Research Fellowship from Miller Institute for Basic Research in Science.

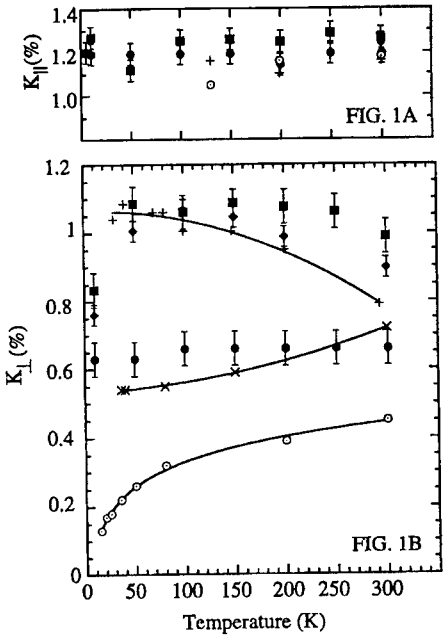


Fig. 1. ^{63}Cu Knight shift, (A) $K_{\|}$ for $H \| C$, and (B)$K_{\perp}$ for $H \perp C$, as a function of temperature for x=0.2375(filled diamonds), 0.2625 (filled squares), and 0.3125 (filled circles). Published data for x=0.10 (open circles), 0.15 (crosses) and 0.20 (pluses) are shown for comparison and the lines are guides for the eye.

REFERENCES

1. Monthoux P. and Pines D., *Phys. Rev.* **B49**, 4261 (1994); Monthoux P. and Pines D., *Phys. Rev. Lett.***69**, 961 (1992); Chubukov A. V., *Phys. Rev.* **B46**, 5588 (1992).
2. For a review, see *Physical Properties of High Temperature Superconductor II* (Edited by D. M. Ginsberg). World Scientific, Singapore (1990); *High Temperature Superconductivity Proc. The Los Alamos Symposium* (Edited by K. Bedell *et al.*). Addision-Wesley (1989).
3. Ohsugi S., *et al.*, *J. Phys. Soc. Jpn* **63**, 700 (1994).
4. Imai T., *et al.*, *Phys. Rev. Lett.***70**, 1002 (1993).
5. Song Y.-Q. *et al.*, *Phys. Rev. Lett.***70**, 3131 (1993).
6. Johnston D. C., *Phys. Rev. Lett.***62**, 957 (1989); Torrance J. B. *et al.*, *Phys. Rev.* **B40**, 8872 (1989).
7. Monien H., Pines D. and Slichter C. P., *Phys. Rev.* **B41**, 11120 (1990). In section III, they use the Mila-Rice type hyperfine coupling constant [*Physica C*, **157**, 561 (1989)] and show the effects of AF correlationson $1/T_1$ anisotropy. In the case of no AF correlations, their formula gives $1/T_1$ anisotropy of 2.5, much lower than the value of 4.0 when including AF correlations.
8. However, the observed doping dependence of the uniform spin susceptibility is inconsistent with the weak coupling calculation based on random phase approximation. See, for example, Bulut N. *et al.*, *Phys. Rev.* **B41**, 1797 (1990); Lu J. P. *et al.*, *Phys. Rev. Lett.***65**, 1445 (1990).
9. Zhang F. C. and Rice M. T., *Phys. Rev.* **B37**, 3759 (1988).
10. Singh R. R. P. and Glenister R. L., *Phys. Rev.* **B46**, 11871 (1992); Singh R. R. P. and Gelfand M. P., *Phys. Rev.* **B42**, 996 (1990).

MICROWAVE EXPERIMENTS

Pergamon

J. Phys. Chem. Solids Vol. 56, No. 12, pp. 1941–1943, 1995
Copyright © 1995 Elsevier Science Ltd
Printed in Great Britain. All rights reserved
0022-3697/95 $9.50 + 0.00

0022-3697(95)00172-7

THE MICROWAVE SURFACE IMPEDANCE OF $YBa_2Cu_3O_{7-\delta}$

D. A. BONN, S. KAMAL, KUAN ZHANG, RUIXING LIANG and W. N. HARDY
Department of Physics, University of British Columbia, Vancouver, British Columbia V6T 1Z1, Canada

Abstract—A complete set of measurements of the anisotropic penetration depth (λ_a, λ_b, λ_c) of $YBa_2Cu_3O_{7-\delta}$ indicates that the qualitative behaviour of the superfluid density is the same in both the T_c = 60 K and 93 K phases of this material. The linear behaviour of λ_a and λ_b and the relatively flat temperature dependence of λ_c at low temperatures seem to depend little on the oxygen doping of the CuO chains. The penetration depth is also largely unaffected by impurities, except for the case of Zn doping which quickly gives rise to gapless behaviour. The surface resistance is strongly affected by both Ni and Zn doping but only Zn changes the linear temperature dependence of R_s at low temperatures.

Keywords: High T_c, surface resistance, penetration depth.

1. INTRODUCTION

Microwave surface impedance studies are still providing a wealth of new information on the superconducting state of $YBa_2Cu_3O_{7-\delta}$. One of the useful features of microwave measurements as a probe of the superconducting state of high T_c superconductors is that the short coherence length is actually an advantage. A coherence length that is much smaller than the London penetration depth ($\xi \ll \lambda$) guarantees that the electrodynamics at low frequency are in the local limit in these materials. In this case the surface impedance $Z_s = R_s + iX_s$, where R_s is the surface resistance and X_s is the surface reactance, is related to the complex conductivity by the relation

$$Z_s = \left(\frac{i\mu_0\omega}{\sigma_1 - i\sigma_2}\right)^{1/2}. \quad (1)$$

In the superconducting state at low frequencies ($\omega\tau \ll 1$, where τ is the transport scattering time) the conductivity can be expressed as [1]

$$\sigma(\omega, T) = \sigma_1(\omega, T) - i\frac{1}{\mu_o\omega\lambda^2(T)}. \quad (2)$$

The real part is a measure of absorption processes, both direct electronic excitations and absorption by thermally activated quasiparticles. The imaginary part is the inductive response of the superconducting condensate. At microwave frequencies in the superconducting state $\sigma_2 \gg \sigma_1$ up to temperatures within less than 1 K of T_c. Thus almost immediately below T_c eqns (1) and (2) yield simple expressions in the local limit for the surface resistance and surface reactance:

$$R_s(T) = \frac{\mu_o^2}{2}\omega^2\lambda^3(T)\sigma_1(\omega, T) \quad (3)$$

$$X_s(T) = \mu_o\omega\lambda(T). \quad (4)$$

2. ANISOTROPIC PENETRATION DEPTH

At microwave frequencies the temperature dependence of $X_s(T) - X_s(0)$ provides a direct measure of $\Delta\lambda(T) = \lambda(T) - \lambda(0)$ which, along with far infrared measurements of $\lambda(0)$, can be used to determine the temperature dependence of the normalized superfluid fraction via $x_s(T) = \lambda^2(0)/\lambda^2(T)$. In our measurement geometry in a superconducting split-ring resonator at 1 GHz an a.c. magnetic field lying along the a (or b) axis of a plate-like crystal drives screening currents that run mainly in the b (or a) direction with a small contamination from the currents that must close the path by running down the edges in the c direction. The effective, measured penetration depth is $\Delta\lambda = a\Delta\lambda_{a,b} + c\Delta\lambda_c$, where a is the width of the crystal in the ab plane and c is the thickness [2]. Although λ_c can be quite large, it usually does not significantly affect the results in thin ($c \sim 5 - 20\mu$m) crystals. However, by cleaving a crystal into narrow needles it is possible to enhance the c axis contribution, so measurements of $\Delta\lambda$ before and after cleaving provide a means of determining $\Delta\lambda_c$. Figure 1(a) shows the results obtained by measuring $\Delta\lambda_a$ and $\Delta\lambda_b$ in a detwinned crystal of $YBa_2Cu_3O_{6.95}$ (T_c = 93 K). The crystal was subsequently cleaved into five narrow blades in order to extract $\Delta\lambda_c$. The values used for $\lambda(0)$ in the a, b and c directions were 1600, 1030 and 11,000 Å, respectively [3,4]. The superfluid fraction in the a and b directions are very similar, both displaying the linear behaviour at low temperatures that suggests the presence of nodes in the energy gap. The c axis behaviour is flatter at low temperature, with a temperature dependence that is somewhat faster than linear. When scaled by T_c the results for an oxygen-depleted crystal, $YBa_2Cu_3O_{6.60}$ (T_c = 59 K), are strikingly similar. Figure 1(b) shows the superfluid fraction in all three directions obtained with the same technique as that used for the optimally doped sample. $\lambda(0)$ values of 2000, 1500 and

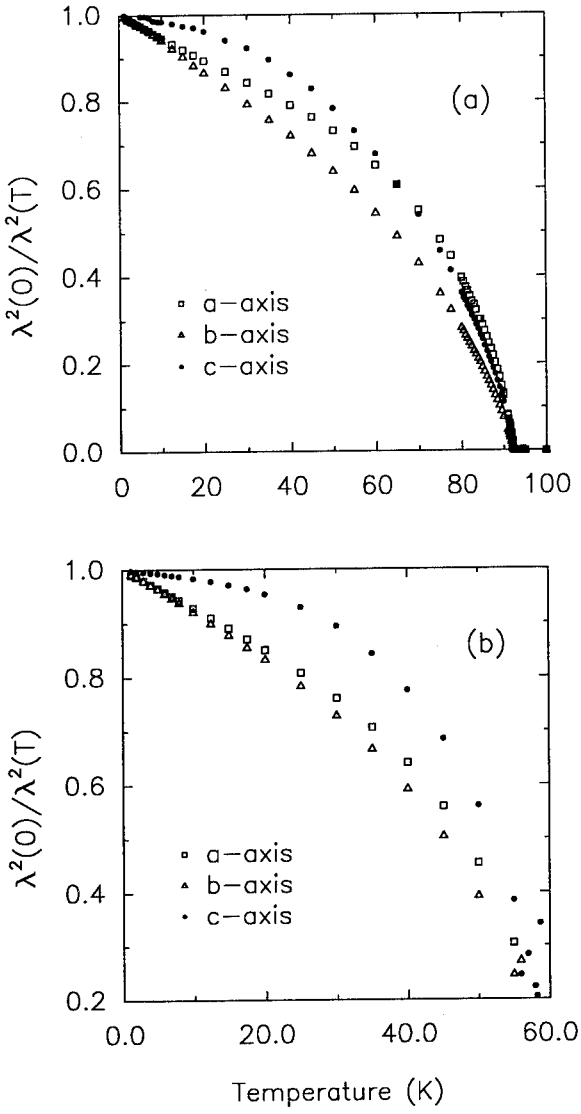


Fig. 1. The three components of the normalized superfluid density for (a) $YBa_2Cu_3O_{6.95}$ (T_c = 93.5 K) and (b) $YBa_2Cu_3O_{6.60}$ (T_c = 59 K).

65,000 Å were used for the *a*, *b* and *c* directions, respectively. The presence of the nearly linear penetration depth in both the *a* and *b* directions at both doping levels argues against the chains being a source of the low-lying states responsible for this behaviour.

3. IMPURITY STUDIES

The surface resistance of the high purity crystal shown in Fig. 2 is shaped by three competing temperature dependences [1]. The screening term $\omega^2\lambda^3(T)$ [see eqn (3)] causes the rapid drop in $R_s(T)$ below T_c as the superconducting condensate builds up. At the same time the inelastic scattering of quasiparticles collapses as the carriers condense

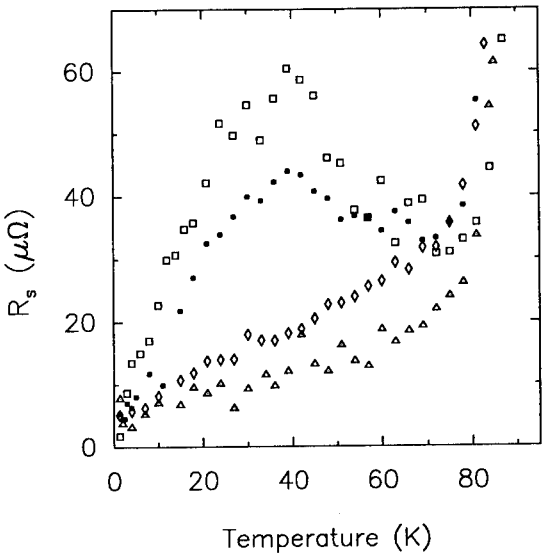


Fig. 2. At 3.7 GHz the rise in R_s below 75 K in a high purity crystal of $YBa_2Cu_3O_{6.95}$ (squares) is caused by a rapid increase in the scattering time below T_c. This rise in τ is only slightly affected by 2% Ca substitution for Y (solid circles), but is drastically suppressed by 0.75% (triangles) and 1.4% (diamonds) substitution of Ni for Cu.

[1,6], which causes σ_1 to rise rapidly below T_c, leading to the gradual rise in R_s below 75 K. Eventually τ hits a limit that is highly sensitive to impurities. In our purest crystals the surface resistance stops rising near 35 K and falls away linearly with temperature as the density of thermally excited quasiparticles decreases with temperature. The addition of impurities can strongly limit the increase in τ, completely suppressing the rise in R_s below 75 K. A wide variety of impurities can be doped into $YBa_2Cu_3O_{7-\delta}$, and many of them substitute preferentially at certain sites in the lattice. Substitution of 2% Ca on the Y site that lies between the CuO_2 planes has only a small effect on the peak in R_s. Ni impurities which mainly replace Cu in the CuO_2 planes have a more dramatic effect. Only 0.75% substitution of Ni for Cu limits the rise in the scattering time of the thermally excited quasiparticles enough to completely suppress the peak in R_s [2]. An even higher concentration of Ni increases the overall magnitude of R_s. Far infrared measurements indicate that this is due to an increase in the overall magnitude of λ for the sample with 1.4% Ni doping [5].

Although Ni impurities cause a large amount of scattering, they do not alter the linear temperature dependence of R_s at low temperatures. The only impurity that we have found to alter the low temperature behaviour is Zn, which also substitutes for Cu in the CuO_2 planes. As little as 0.31% Zn substitution suppresses the peak in R_s and causes a quadratic temperature dependence at low temperatures [7]. The striking effect of Zn impurities is also observed in the behaviour of the penetration depth at low temperatures. As shown in Fig. 3, neither Ca nor Ni substitution significantly

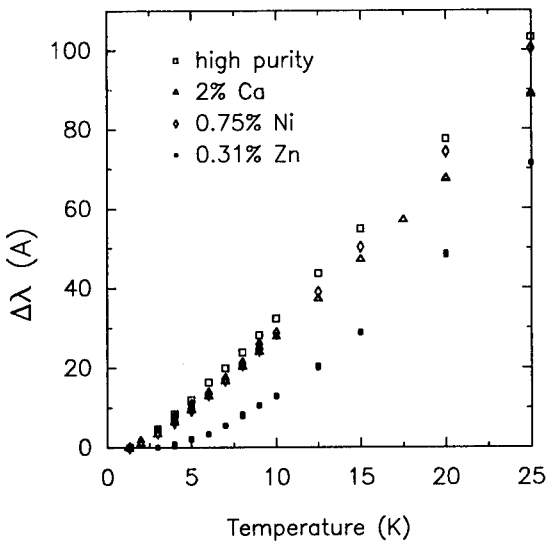


Fig. 3. The nearly linear temperature dependence of $\Delta\lambda(T) = \lambda(T) - \lambda(1.3\ \mathrm{K})$ is most strongly affected by Zn impurities which give rise to gapless, quadratic behaviour.

alters the linear temperature dependence of $\Delta\lambda(T)$ at low temperatures, but 0.31% Zn substitution completely alters the temperature dependence to quadratic behaviour [2,8].

4. CONCLUSIONS

A number of the qualitative features of the surface impedance of $YBa_2Cu_3O_{7-\delta}$ are surprisingly insensitive to anisotropy, doping level, and impurity content. The linear behaviour of the penetration depth is present for currents running both parallel and perpendicular to the CuO chains and is largely unaffected by oxygen doping level in the chains, at least for oxygen contents of 6.60 and 6.95. This robustness of the qualitative features of the *ab*-plane penetration depth, despite the large anisotropy in the magnitude of $\lambda(0)$ in the *a* and *b* directions, suggests that the low energy excitations responsible for the linear penetration depth are not associated with the CuO chains. The shape of the *c*-axis penetration depth, which is relatively flat at low temperatures, changes slightly with oxygen content, becoming somewhat flatter in the T_c = 59 K phase. This change is not very striking when compared to the six-fold increase in the magnitude of λ_c in the range of oxygen doping studied here [4].

The linear behaviour of both $\lambda(T)$ and $R_s(T)$ at low temperature is also rather insensitive to many types of impurities. The only exception to this that we have found so far is Zn substitution for Cu in the CuO_2 planes, which quickly gives rise to the quadratic temperature dependence expected for a gapless superconductor. This behaviour suggests that Zn acts as a unitary scatterer in this system [10]. The anomalous effects of Zn doping are seen microscopically in NMR measurements where Zn has been shown to cause local suppression of the spin fluctuations and gapless behaviour in the CuO_2 planes [9].

REFERENCES

1. Bonn D. A., Liang Ruixing, Riseman T. M., Baar D. J., Morgan D. C., Zhang Kuan, Dosanjh P., Duty T. L., MacFarlane A., Morris G. D., Brewer J. H., Hardy W. N., Kallin C. and Berlinsky A. J., *Phys. Rev. B* **47**, 11314 (1993).
2. Bonn D. A., Kamal S., Zhang Kuan, Liang Ruixing, Baar D. J., Klein E. and Hardy W. N., *Phys. Rev. B* **50**, 4051 (1994).
3. Basov D. N., Liang R., Bonn D. A., Hardy W. N., Dabrowski B., Quijada M., Tanner D. B., Price J. P., Ginsberg D. M. and Timusk T., *Phys. Rev. Lett.* **74**, 598 (1995).
4. Homes C. C., Timusk T., Bonn D. A., Liang Ruixing and Hardy W. N., submitted to *Physica C* (1995).
5. Homes C. C., private communication.
6. Nuss Martin C., Mankiewich P. M., O'Malley M. L., Westerwick E. H. and Littlewood Peter B., *Phys. Rev. Lett.* **66**, 3305 (1991).
7. Zhang Kuan, Bonn D. A., Kamal S., Liang Ruixing, Baar D. J., Hardy W. N., Basov D. N. and Timusk T., *Phys. Rev. Lett.* **73**, 2484 (1994).
8. Achkir D., Poirier M., Bonn D. A., Liang Ruixing and Hardy W. N., *Phys. Rev. B* **48**, 13184 (1993).
9. Kitaoka Y., Ishida K., Zheng G. -Q., Ohsugi S. and Asayama K., *J. Phys. Chem. Solids* **54**, 1385 (1993).
10. Hirschfeld Peter J. and Goldenfeld Nigel, *Phys. Rev. B* **48**, 4219 (1993).

Pergamon

J. Phys. Chem. Solids Vol. 56, No. 12, pp. 1945–1949, 1995
Copyright © 1995 Elsevier Science Ltd
Printed in Great Britain. All rights reserved
0022-3697/95 $9.50 + 0.00

0022-3697(95)00264-2

MICROWAVE SURFACE IMPEDANCE OF $Y_1Ba_2Cu_3O_{7-\delta}$ CRYSTALS: EXPERIMENT AND COMPARISON TO A *d*-WAVE MODEL

T. JACOBS and S. SRIDHAR *
Physics Department, Northeastern University, Boston, MA 02115, U.S.A.

C. T. RIECK and K. SCHARNBERG
Institut für Angewandte Physik, Universität Hamburg, Germany

T. WOLF and J. HALBRITTER
Forschungszentrum Karlsruhe Technik und Umwelt, 76021 Karlsruhe, Germany

Abstract—We present measurements of the microwave surface resistance R_s and the penetration depth λ of $Y_1Ba_2Cu_3O_{7-\delta}$ crystals. At low T, $\lambda(T)$ obeys a polynomial behavior, while R_s displays a characteristic non-monotonic T-dependence. A detailed comparison of the experimental data is made to a model of *d*-wave superconductivity which includes both elastic and inelastic scattering. While the model reproduces the general features of the experimental data, three aspects of the parameters needed are worth noting. The elastic scattering rate required to fit the data is much smaller than measured from the normal state, the scattering phase shifts have to be close to $\pi/2$ and a strong coupling value of the gap parameter $2\Delta(0)/kT_c \sim 6$ is needed. On the experimental side the uncertainties regarding the material parameters $\lambda(0)$ and $R_{s,res}(0)$ further complicate a quantitative comparison. For one sample, $R_{s,res}(0)$ agrees with the intrinsic value which results from the *d*-wave model.

Keywords: High T_c, surface resistance, penetration depth, *d*-wave theory

Microwave measurements of the surface impedance $Z_s = R_s + iX_s$ of superconductors are in principle capable of yielding a wealth of precise information regarding the superconducting state, such as the gap parameter, quasiparticle density and nature of scattering. In low T_c superconductors the BCS theory provides a remarkably accurate description of experimental data for R_s and X_s over several orders of magnitude variation, including detailed effects of impurity scattering [1].

Recently, experiments which directly explore the order parameter symmetry suggest a $d_{x^2-y^2}$ order parameter [2–4] for high T_c superconductors, although some experiments which suggest a *s*-wave order parameter also exist [5,6]. It is therefore useful to ask to what extent a *d*-wave model of superconductivity can describe the measured surface impedance of the cuprate superconductors, particularly $Y_1Ba_2Cu_3O_{7-\delta}$. Some work has been already initiated in this regard [7]. Here in this paper, we present detailed results on the microwave (10 GHz) surface impedance of $YBa_2Cu_3O_{7-\delta}$ crystals. We also compare the complete temperature dependence to numerical calculations based upon semi-microscopic models of *d*-wave and *s*-wave superconductivity, including elastic as well as inelastic scattering effects.

The measurements were carried out in a specially designed, high sensitivity Nb cavity. The method of measuring the surface impedance of superconductors at elevated temperatures using a "hot finger" cavity method was first introduced by one of the authors in reference [8], and the principle has been used in a variety of systems reported in the literature. In the present setup, the Nb cavity is maintained either at 4.2 K or below 2 K. The typical background Q_b of the cavity can be as high as 10^8. The surface resistance is measured from the temperature dependent Q using $R_s(T) = \Gamma\,[Q^{-1}(T) - Q_b^{-1}(T)]$ and the penetration depth using $\Delta\lambda(T) = \zeta\,[f(T) - f_b(T)]$. The geometric factors are determined by the cavity mode, sample location and the sample size. All measurements were done in the TE_{011} mode with the sample at the midpoint of the cavity axis, where the microwave magnetic fields have a maximum and the microwave electric fields are zero. The method enables measurement of small crystals and thin film samples.

The crystals were grown in a ZrO_2/Y crucible using highly pure Y_2O_3, $BaCO_3$ and CuO powders. Crystal growth took place while slowly cooling the melt at a rate of 0.40°C/h in the temperature range 970°C to 904°C and in an atmosphere of 100 mbar O_2. After the growth the crystals were annealed in flowing oxygen in the temperature range 600°C to 400°C during 600 h.

We start with an analysis of the normal state properties in the hope to fix some of the normal state parameters which

* Present address: Physics Department, University of Karlsruhe, Germany.

Table 1. Some sample properties: T_c is obtained by dc-measurements and agrees with the first deviation that is observed in small microwave fields as the first deviation from the normal state behavior. ΔT_c is defined as the temperature interval between 10% and 90% of $R_s(T_c)$. δ is the oxygen vacancy.

Sample	T_c	ΔT_c	R_s(4 K)	δ
A	91.0 K	1.0 K	5 $\mu\Omega$	0.06
B	91.5 K	1.5 K	150 $\mu\Omega$	0.11

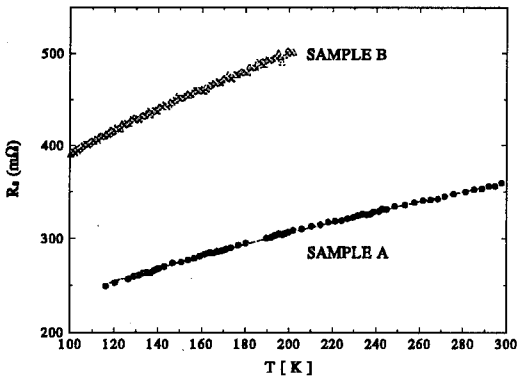


Fig. 1. Normal state surface resistance $R_s(T)$ for the $YBa_2Cu_3O_{7-\delta}$ crystals with fits to eq. (2). The fit parameters are given in table 2.

Table 2. Experimental normal state scattering parameters

Sample	ρ_0 [Ωm]	γ [Ωm/K]	Γ_{el} [sec^{-1}]	α [sec^{-1} K^{-1}]
A	$5.3\,10^{-7}$	$9.1\,10^{-9}$	$1.1\,10^{13}$	$1.9\,10^{11}$
B	$1.4\,10^{-6}$	$2.4\,10^{-8}$	$2.9\,10^{13}$	$5.0\,10^{11}$

the microwave resistivity ρ_n should be the same as the dc resistivity, which is known to be linear. If $\rho_n = \rho_0 + \gamma T$, then

$$R_n = \sqrt{\omega\mu_0(\rho_0 + \gamma T)/2} \tag{1}$$

Figure 1 shows a comparison of the experimental data between 100 K and 200 K to the above equation. The data clearly has a *sub-linear* T dependence, and the fit to eq. (1) is *extremely good*. From the fit the scattering rate Γ can be obtained as

$$\Gamma = \Gamma_{el} + \Gamma_{inel}(T) = \Gamma_{el} + \alpha T \tag{2}$$

where $\Gamma_{el} = \rho_0/(2\mu_0\lambda(0)^2)$, and $\alpha = \gamma/(2\mu_0\lambda(0)^2)$. Table 2 gives these parameters for the studied samples under the assumption $\lambda(0) = 1400$ Å.

Figure 2 displays the low temperature behavior of R_s for the two samples of $Y_1Ba_2Cu_3O_{7-\delta}$. Sample B shows a characteristic peak in R_s first reported by [9]. This is not present in sample A, whose behavior is instead closer to that of thin films [10].

It is evident that the λ vs. T data displayed in figure 4 do not show the exponential dependence $\Delta\lambda(T) \propto (T_c/T)^{1/2}\exp(-\Delta/kT)$ expected for an isotropic s-wave superconductor. Instead the data clearly have a polynomial temperature dependence with a leading linear term [11,12].

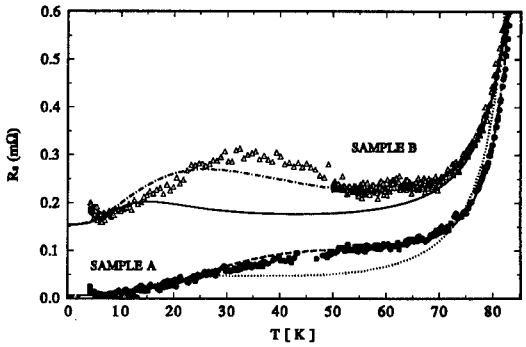


Fig. 2. Low temperature behavior of R_s for the $YBa_2Cu_3O_{1-\delta}$ samples A (•) and B (△). Theoretical results are plotted for the parameters given in table 3.

Table 3. Theoretical parameter with $f_1(t) = e^{7(t-1)} - e^{-7}$

Sample	symbol	Γ_{el} [meV]	Γ_{inel} [meV]	$2\Delta_0(0)/kT_c$
A	dashes	0.25	$10.86 f_1(t)$	6.4
	dots	0.20	$10.91 t^3$	6.0
B	dash dot	0.05	$24.15 f_1(t)$	6.4
	line	0.05	$24.15 t^3$	7.0

This, together with the nonexponential decrease of R_s at very low temperatures could be taken as indication for d-wave pairing.

An important prediction for any superconducting state with nodes in the gap is the presence of a finite residual conductivity σ_{00} due to elastic scattering [13,14]. Its value depends on the particular pair state and, if determined experimentally, could help to identify the type of pairing present. For the d-wave state

$$\Delta(T, \hat{k}_F) = \Delta_0(T)\cos(2\phi) \tag{3}$$

commonly studied for systems with cylindrical Fermi surfaces of circular cross section one has [13,14] $\sigma_{00} = ne^2/m\pi\Delta_0$ at $T = 0$ K.

This can be related to $\sigma_n(T_c)$ by $\sigma_{00}/\sigma_n(T_c) = 2\Gamma(T_c)/\pi\Delta_0$. Using the values $2\Gamma(T_c) = 33$ meV, and $2\Delta_0/kT_c = 4.3$ we get $\sigma_{00}/\sigma_n(T_c) \sim 1$. Thus the residual conductivity is comparable to the normal state conductivity at T_c, which is a surprisingly large value. Note that in BCS the conductivity $\sigma_1 \to 0$ as $T \to 0$.

The relation to R_s is obtained from the limiting result when $\sigma_2 \gg \sigma_1$, whence $R_s(T \to 0) = \omega^2\mu_0^2\lambda(0)^3\sigma_{00}/2$. This can also be written as $R_s/R_n = 0.5(\sigma_1/\sigma_n)/(\sigma_2/\sigma_n)^{3/2}$. Since the above relationship shows that $\sigma_1/\sigma_n \sim 1$, the reduction in R_s from its value at T_c is entirely due to the reduction in λ from δ_n *i.e.* to the superfluid response. The intrinsic residual surface resistance $R_{s,res}(0)$ which results from σ_{00} is much smaller than the value measured for sample B but is compatible with the low temperature data for sample A.

Detailed numerical calculations based on the microscopic models for s-wave and d-wave superconductivity [15–17] were carried out.

With suitable choices for the Eliashberg functions it is possible to fit the measured surface resistances within the framework of isotropic strong coupling theory over a wide range of temperature from T_c down to 0.4 T_c [17], highlighting the importance of inelastic scattering processes. This is consistent with earlier measurements over the same temperature range [18]. However at lower temperatures the isotropic gap should make its presence known in the form of an $\exp(-\Delta/kT)$ dependence, which is clearly not observed in either R_s or $\Delta\lambda$.

For this reason we focus in this paper on models of d-wave superconductivity, including inelastic scattering. Here we list the main ingredients of the model - details of the model are described elsewhere [17]. A weak-coupling pairing interaction was suitably chosen to give the $d_{x^2-y^2}$ order parameter $\Delta(T, \vec{k}_F)$, see eq. (3). The self-consistency equation for the order parameter was solved to give the temperature dependence of the amplitude $\Delta_0(T)$, and which is found to be very similar to that for an isotropic order parameter except that $2\Delta_0(0)/kT_c = 4.29$ rather than 3.52.

Elastic scattering is parameterized by a normal state scattering rate Γ_{el} and a phase shift δ_N, which can take any value between 0 (Born approximation) and $\pi/2$ (Unitary limit). Inelastic scattering in the superconducting state is parameterized in the form

$$\Gamma_{inel}(T) = \alpha T_c f(t) \tag{4}$$

with some function f of the reduced temperature $t = T/T_c$.

The inputs to the calculation of the surface impedance $Z_s = (2i/\sigma_s)^{1/2}$ are then Γ_{el}, δ_N, α, and $f(t)$. In order to fit the steep drop of R_s below T_c we have found it necessary to treat $2\Delta_0(0)/kT_c$ as a variable parameter.

The surface impedance is not as sensitive to the choice of model parameters as is the real part of the conductivity σ_1, which is also of some intrinsic interest. Unfortunately, the peak height of the experimentally determined $\sigma_1(T, \omega)$ depends strongly on the choice of the zero temperature penetration depth $\lambda(0)$ while the low temperature behavior of σ_1 can be changed substantially by subtracting from the measured surface resistance R_s a residual loss R_s^o [9]. The choice of R_s^o is limited by the consideration that $\sigma_1(T = 0, \omega)$ should neither be negative nor should it exceed $\sigma_1(T_c, \omega)$ by a wide margin. With these restrictions we find $R_s^o = 0.15$ mΩ for sample B while for sample A R_s^o is negligible.

The peak heights in σ_1 are reduced when larger values for $\lambda(0)$ are selected. We have chosen $\lambda(0)$ such that the experimental X_s is linear over as large a temperature range below T_c as possible. This gives $\lambda(0) = 1800$ Å and $\sigma_1^{max}(T, \omega) = 30\,[m\Omega cm]^{-1}$ for sample A and $\lambda(0) = 2000$ Å and $\sigma_1^{max}(T, \omega) = 42\,[m\Omega cm]^{-1}$ for sample B.

Experimental results for σ_1 are shown in figure 3. In the presence of purely inelastic scattering a peak in σ_1 should occur near $\omega/2\Gamma(T) = 1$. This peak is thus expected to shift to higher temperatures as the frequency is increased and to lower temperatures when the overall magnitude α

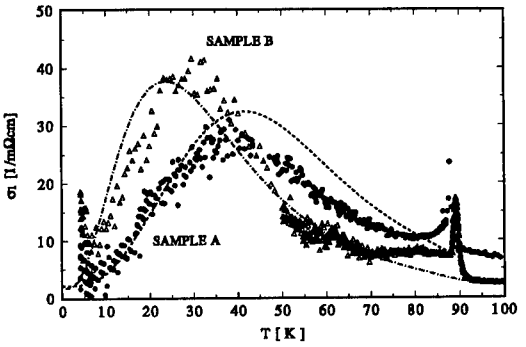


Fig. 3. Real part σ_1 of the measured conductivity and theoretical behavior (lines). The parameters are given in table 3.

(eq. (2) and (4)) of the scattering rate is increased. For $f(t) = f_1(t) = e^{7(t-1)} - e^{-7}$ which has been suggested by Bonn *et al.* [9] and which is close to the result from the Nested Fermi Liquid model [19,17], the peak in σ_1 occurs near 10 K with the peak height greatly exceeding the experimental value. This observation, taken together with the normal state data, shows that elastic scattering needs to be taken into account. When Γ_{el} given in table 2 is used as input parameter, the peak in σ_1 is greatly reduced. In the Born approximation σ_1 rises very steeply from its limiting value σ_{00} so that the peak is still located at too low a temperature. In the unitary limit a peak is barely observable. In order to reproduce the experimental results, Γ_{el} has to be chosen much smaller than the analysis of normal state data would suggest. Figure 3 contains a reasonably close fit to the σ_1 data. The fit cannot be improved by varying the phase shift δ_N. Reducing δ_N from 0.5π shifts some of the weight of the peak shown in figure 3 to the temperature at which the peak occurs in the Born approximation. At around $\delta_N = 0.35\pi$, $\sigma_1(T)$ acquires a distinct double peak structure not compatible with the data. We conclude that the phase shift must be close to the unitary limit $0.45\pi \leq \delta_N \leq 0.5\pi$.

The only way to improve the fit would be to choose different temperature dependencies for Γ_{inel} with $f(t)$ decreasing faster then $f_1(t) = e^{7(t-1)} - e^{-7}$ for sample B and more slowly for sample A. Even though the two samples differ in oxygen contents (table 1) and by a factor of four in thickness, it does not seem plausible that intrinsic scattering events in the two samples should differ significantly in their temperature dependencies. A more likely source for this discrepancy is a temperature dependence of the "residual" surface resistance $R_{s,res}(t)$ [20]. Models have been put forward to explain $R_{s,res}(T)$ by weak links and relate them to ρ_0 [21].

The theoretical surface resistance for the same model parameters as those used to calculate σ_1 is shown in figure 2. In the case of sample B the phenomenological residual resistance $R_{s,res}(0) = 0.15$ mΩ has been added. Note the intrinsic residual surface resistance in the case of sample A. To fit the data near T_c we had to increase $2\Delta_0(0)/kT_c$ to 6.4. This is substantially larger than the weak coupling value

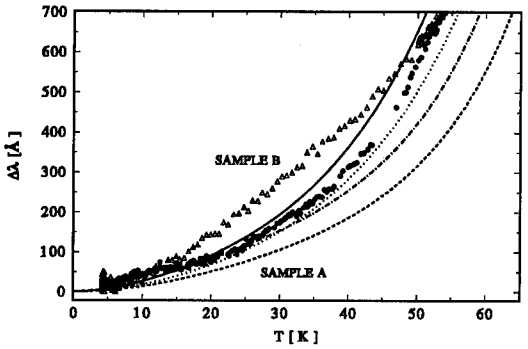


Fig. 4. Low temperature data and theory of $\lambda(T)$. Theoretical curves are obtained with the parameters of table 3.

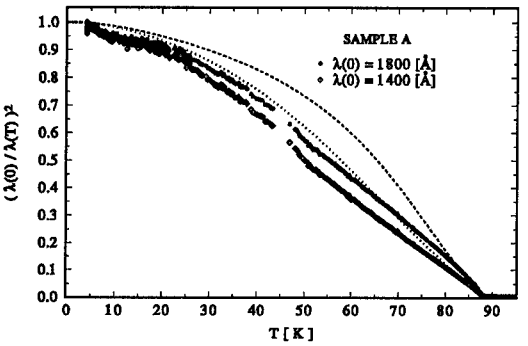


Fig. 5. Superfluid density of sample A. Dashed and doted lines are obtained with the parameters of table 3.

4.29, which has important implications for conclusions regarding fluctuations. The overall fit to the data is very good, showing the same small discrepancies already apparent in figure 3.

The case for *d*-wave pairing would be strengthened considerably if we could fit the shift in penetration depth equally well using exactly the same model. Experimental and theoretical results are compared in figure 4. Clearly, the agreement is less than satisfactory. *Note that the calculated* $\Delta\lambda$ *is by no means linear*, although a polynomial fit in a limited temperature range can certainly be found. The agreement could be much improved by choosing different temperature dependencies for Γ_{inel}. A good fit for sample A is obtained with $f_2(t) = t^3$, see figure 4. Decreasing $2\Delta_0(0)/kT_c$ substantially would also improve agreement in the case of $\Delta\lambda$ but would lead to serious discrepancies in the case of R_s.

In figure 5 the penetration depth for sample A is plotted over the whole temperature range in the form of the superfluid density $(\lambda(0)/\lambda(T))^2$. For such a plot, it is necessary to assume a value of $\lambda(0)$ and this figure shows the variation of $(\lambda(0)/\lambda(T))^2$ resulting from different choices of $\lambda(0)$. By varying $\lambda(0)$ one can actually change the sign of the curvature of $\lambda^2(T))$ near T_c. It is obvious that near T_c, since a straight line fits the data pretty well, the behavior is described quite well by a $(1 - T/T_c)^{1/2}$ dependence with $T_c = 88$ K. The exponent agrees with a mean-field behavior of the order parameter, in contrast to the 3-D XY behavior observed by ref. [22].

Our *d*-wave calculations give a positive curvature for $1/\lambda^2(T)$ near T_c, indicating a behavior which is slower than mean-field, *i.e.* $\lambda(T) \to (1 - t)^\nu$, where $\nu > 1/2$. This is possibly an artifact of the calculation because the total scattering rate (eq. (2)) at T_c is such that T_c should be substantially suppressed according to weak coupling theory. This would lead to noticeably different T_c's for the two samples. Since the T_c's are practically the same, we did not include scattering in the selfconsistency equation. Strong inelastic scattering probably has to be treated within the framework of an anisotropic strong coupling theory, which could also solve the problem of the large value for $2\Delta_0(0)/kT_c$ we had to assume.

In spite of the remaining discrepancies, some of which may be due to contributions from the c-axis conductivity which has not been included in the calculations, d-wave pairing seems to provide an adequate model for understanding features seen in $YBa_2Cu_3O_{7-\delta}$ crystals. The main features of the data appear to be reproduced, although a detailed microscopic justification of the needed parameters is not yet available. We should remark that although we have considered an explicit *d*-wave model, the essential feature is that of nodes in the gap leading to low lying quasiparticle excitations at all temperatures.

This work was supported by NSF-DMR-9223850. We thank M. Osofsky for measurements of the oxygen content of the samples, as well as the organizers of the International Symposium on HTSC in High Frequency Fields held at Cologne, where part of this collaboration was initiated.

REFERENCES

1. Sridhar S., *J. Appl. Phys.* **63**, 159 (1988).
2. Wollman D. A., Van Harlingen D. J., Lee W. C., Ginsberg D. M. and Leggett A. J., *Phys. Rev. Lett.* **71**, 2134 (1993).
3. Tsuei C. C., Kirtley J. R., Chi C. C., Yu-Jahnes L. S., Gupta A., Shaw T., Sun J. Z. and Ketchen M., *Phys. Rev. Lett.* **73**, 593 (1994).
4. Iguchi I. and Wen Z., *Phys. Rev. B* **49**, 12388 (1994).
5. Chaudhari P. and Lin S.-Y., *Phys. Rev. Lett.* **72**, 1084 (1994).
6. Sun A. G., Gajewski D., Maple M. and Dynes R. C., *Phys. Rev. Lett.* **72**, 2267 (1994).
7. Borkowski L. S. and Hirschfeld P. J., *Phys. Rev. B* **49**, 15404 (1994).
8. Sridhar S. and Kennedy W. L., *Rev. Sci. Instrum.* **59**, 531 (1988).
9. Bonn D. A., Zhang K., Liang R., Baar D. J., Morgan D. C. and Hardy W. N., *J. Supcond.* **6**, 219 (1993).
10. Klein N., Tellmann N., Wolf S. A. and Kresin V. Z., *J. Supcond.* **7**, 459 (1994).
11. Hardy W. N., Bonn D. A., Morgan D. C., Liang R. and Zhang K., *Phys. Rev. Lett.* **70**, 3999 (1993).
12. Mao J., Wu D.-H., Peng J., Greene R. L. and Anlage S. M., *Phys. Rev. B* **51**, 3316 (1995).
13. Lee P. A., *Phys. Rev. Lett.* **71**, 1887 (1993).
14. Hirschfeld P. J., Putikka W. O. and Scalapino D. J., *Phys. Rev. B* **50**, 10250 (1994).
15. Scharnberg K., *J. Low Temp. Phys.* **30**, 229 (1978).
16. Klemm R. A., Scharnberg K., Walker D. and Rieck C. T., *Z. Phys. B* **72**, 139 (1988).

17. Rieck C. T. and Scharnberg K., unpublished.
18. Sridhar S., Wu D.-H. and Kennedy W. L., *Phys. Rev. Lett.* **63**, 1873 (1989).
19. Virosztek A. and Ruvalds J., *Phys. Rev. B* **42**, 4064 (1990).
20. Wehler D., Dreibholz J., Meyer M., Müller G., Piel H. and Wolf T., *J. Alloys Comp.* **195**, 575 (1993).
21. Halbritter J., *Phys. Rev. B* **48**, 9735 (1993).
22. Kamal S., Bonn D. A., Goldenfeld N., Hirschfeld P., Liang R. and Hardy W. N., *Phys. Rev. Lett.* **73**, 1845 (1994).

POSITRON SPECTROSCOPY AND OTHER EXPERIMENTS

Pergamon

J. Phys. Chem. Solids Vol. 56, No. 12, pp. 1951–1954, 1995
Copyright © 1995 Elsevier Science Ltd
Printed in Great Britain. All rights reserved
0022-3697/95 $9.50 + 0.00

0022-3697(95)00099-2

FERMI SURFACES OF HIGH-T_c SUPERCONDUCTORS BY POSITRON 2D-ACAR

A.A. MANUEL,* A. SHUKLA,* L. HOFFMANN,* T. JARLBORG,* B. BARBIELLINI,† S. MASSIDDA,‡ W. SADOWSKI,§ E. WALKER,* A. ERB* and M. PETER*

* Département de Physique de la Matière Condensée, Université de Genève,24 quai Ansermet, CH-1211 Geneva 4, Switzerland
† Laboratory of Physics, Helsinski University of Technology, SF-02150 Espoo, Finland
‡ Dipartimento di Scienze Fisiche, Universita degli Studi di Cagliari, I-09100 Cagliari, Italy
§ Department of Physics and Mathematics, Technical University of Gdansk, ul. Majakowskiego 11/12, PL-80-952 Gdansk, Poland

Abstract—We review the work aimed at identifying the Fermi surface of high-T_c superconducting oxides using positron 2D-ACAR technique. We also present our recent observation of the *pillbox* in $YBa_2Cu_3O_{7-\delta}$ and the first identification of Fermi surface signals in $Nd_{2-x}Ce_xCuO_{4-\delta}$ obtained by 2D-ACAR.

1. INTRODUCTION

Positron 2D-ACAR (two-dimensional angular correlation of the annihilation radiation) is, with photoemission and de Haas–van Alphen, one method allowing experimental determination of the Fermi surface. 2D-ACAR measures projections $N(p_x, p_y)$ of the electronic momentum density $\rho^{2\gamma}(\mathbf{p})$ sampled by positrons:

$$N(p_x, p_y) = \int \mathrm{d}p_z \, \rho^{2\gamma}(\mathbf{p}) \qquad (1)$$

In the independent particle approximation, $\rho^{2\gamma}(\mathbf{p})$ is given by:

$$\rho^{2\gamma}(\mathbf{p}) = const \cdot \sum_j \left| \int \mathrm{d}\mathbf{r} \exp[-i\mathbf{p}\cdot\mathbf{r}]\psi_{-j}(\mathbf{r})\psi_+(\mathbf{r})\right|^2 , \qquad (2)$$

where $\psi_{-j}(\mathbf{r})$ and $\psi_+(\mathbf{r})$ are the electron and positron states. As the sum runs over occupied electronic states, $\rho^{2\gamma}(\mathbf{p})$, and consequently the measured quantity $N(p_x, p_y)$, reflect discontinuities at the Fermi surface. The observation of very fine breaks was recently possible, thanks to major developments in the data analysis [1]. Let us mention linear and non-linear filters [2] and enhancement of Fermi surface images [3] in this connection.

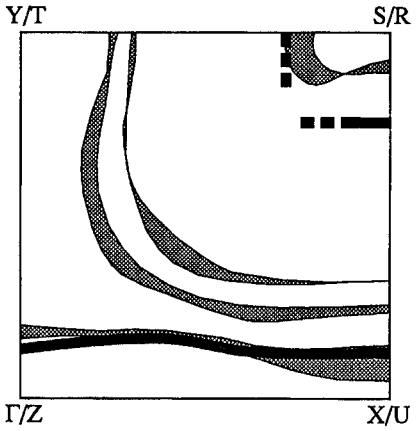


Fig. 1. Fermi surface of $YBa_2Cu_3O_{7-\delta}$ [4]. The thick lines are the 2D-ACAR results [12].

2. FERMI SURFACE STUDIES BY 2D-ACAR

2.1. $YBa_2Cu_3O_{7-\delta}$

Band structure calculations [4] predict a Fermi surface made of four principal sheets: the *ridge*, due to electronic states of the CuO chains, two *barrels* due to CuO_2 planes and a *pillbox* from the chains and apical oxygens. LDA calculations have also shown [5] that positrons are in delocalized states between the chains, such that electronic states of the CuO_2 planes are difficult to probe with 2D-ACAR in this system. The search for the Fermi surface in $YBa_2Cu_3O_{7-\delta}$ by 2D-ACAR was successful as soon as untwinned samples became available. The *ridge* was observed first by Haghighi *et al.* [6], and soon confirmed by two other independent measurements [7,8]. These early measurements have since been improved upon and a substantial amount of work has been done to precisely characterize the *ridge* [9,10]. Observed in Brillouin zones as high as the 4th [11] (in this high momentum region, the *ridge* signal, although weak, is free of wavefunction effects and thus provides extremely convincing evidence), there is nowadays a general agreement about the existence of this piece of the Fermi surface. It is worth mentioning that only 2D-ACAR measurements have allowed the determination of the *ridge* until now. In photoemission, the signals are mixed with those of the square-like *barrels* originating from the CuO_2 planes. Moreover, the cyclotron effective mass of the *ridge* electrons is so high that they are not detected by de Haas–van Alphen experiments.

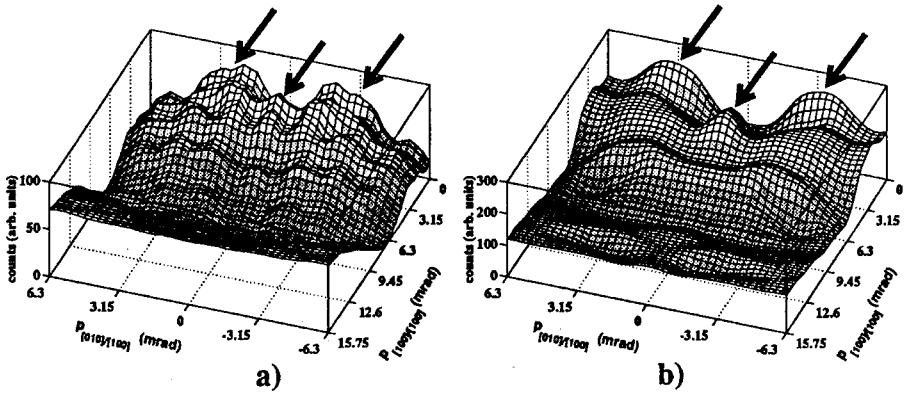


Fig. 2. 2D-ACAR of $Nd_{2-x}Ce_xCuO_{4-\delta}$ after band-pass filtering [3]. (a) Measurement, (b) calculations. The arrows show the signals induced by the Fermi surface.

Another piece of the Fermi surface predicted by band structure is the *pillbox*, centered at the S-point of the Brillouin zone. Despite previous results [7], to our point of view no clear evidence for the *pillbox* had been reported with 2D-ACAR until we recently performed measurements at high temperatures [12], as positron lifetime measurements indicate that in these conditions positrons are delocalized whereas at lower temperatures there is a substantial trapping by oxygen vacancies. Above 400 K, the *pillbox* can be clearly observed. Figure 1 shows the topology of this sheet as well as the *ridge* and band structure results.

The change of the Fermi surface with δ in $YBa_2Cu_3O_{7-\delta}$ has also been studied [10]. It has been found that the shape of the *ridge* is stable. The intensity of the related signals in the 2D-ACAR however decreases when δ increases. This suggests the existence of at least two ordered phases whose relative abundance varies with δ [13]. When the concentration of the O_7 phase decreases, the signal from the *ridge* decreases too. This model, which supposes that the second phase does not provide a Fermi surface signal, is in agreement with neutron diffraction experiments [14].

2.2. *Substitutions and alloying in* $YBa_2Cu_3O_{7-\delta}$

2D-ACAR measurements have been made when Y is substituted by rare earths [15]. We observe the *ridge* in Y-, Ho- and Dy- based metallic compounds. In the insulating compound $PrBa_2Cu_3O_{7-\delta}$, we have also identified an unambiguous signal from a *ridge*-like Fermi surface. We conclude that, microscopically, pieces of CuO chains remain conductive and that the macroscopic insulating behaviour must be explained differently. Our observation is in accord with the conclusions reached by Fehrenbacher and Rice [16] who ascribe the inhibition of the conductivity to the existence of a local 4f Pr^{IV} hybridized state which binds doped holes to Pr sites and may also act as a magnetic pair-breaker. Also, in agreement with these authors, we conclude that the dc conductivity is very sensitive to vacancies and impurities. It can be easily blocked by a small amount of disorder along the chains. Another observation we have made on $PrBa_2Cu_3O_{7-\delta}$ is the absence of the *pillbox*, in agreement with band structure calculations [17]. The difference with $YBa_2Cu_3O_{7-\delta}$ is probably related to the position of the apical oxygen which has been found to be at a reduced distance of the Cu(2) site [18].

In alloys $YBa_2(Cu_{1-x}T_x)_3O_{7-\delta}$ with T = Ni, Al and Zn, we have studied how the Fermi surface changes with the alloying process [19]. We conclude that Al atoms substitute Cu in the chains, killing the *ridge* without substantial effect on T_c. This Fermi surface is not affected by Ni or Zn substitutions, while T_c is strongly reduced. This is in agreement with the general belief that these two atoms substitute Cu on the CuO_2 planes. The correlation we have observed between T_c and the *ridge* confirms that superconductivity originates from CuO_2 planes. It is therefore important to turn now to compounds where positrons probe these CuO_2 planes.

2.3. $Nd_{2-x}Ce_xCuO_{4-\delta}$

In $Nd_{2-x}Ce_xCuO_{4-\delta}$, positrons are evenly distributed in the unit cell [20]. Therefore, 2D-ACAR is suited for the investigation of the electronic states of the CuO_2 planes. Nevertheless, previous measurements [20] performed at 10 K have not revealed any Fermi surface signature. We have recently performed new 2D-ACAR measurements at 400 K, to minimize the possible localisation of positrons at low temperatures, as found in $YBa_2Cu_3O_{7-\delta}$ [12]. Comparing the results at the two temperatures, we see that, indeed, a substantial amount of trapping occurs at low temperature. It is nevertheless difficult to affirm that data at 400 K do not contain any contributions from trapped positrons. However, the result is very encouraging. It is shown in Figure 2 together with the theoretical picture obtained using the LMTO band structure and gradient corrections for the enhancement of the electron-positron annihilation [21]. This is the first evidence obtained using 2D-ACAR for a Fermi surface in $Nd_{2-x}Ce_xCuO_{4-\delta}$.

2.4. *Other high-T_c superconducting oxides*

Howell *et al.* have performed a combined experimental and theoretical study of the effects of doping on the electronic structure of $La_{2-x}Sr_xCuO_4$ [22] . They found strong effects of the positron - electron wavefunction overlap in their data, in agreement with theoretical calculations. They also found discontinuities in the 2D-ACAR from Sr doped samples consistent with the presence of a Fermi surface. Their study of the changes in the electron momentum density with increasing Sr doping is one of the most elaborate until now. As for the Y-based compounds and $Nd_{2-x}Ce_xCuO_{4-\delta}$, the general conclusion is that experimental Fermi surfaces of $La_{2-x}Sr_xCuO_4$ agree fairly well with results of band structure calculations. The same group has recently studied the 32 K superconductor $Ba_{1-x}K_xBiO_3$ [23] and has identified a roughly cubic Fermi surface centered around Γ, in excellent agreement with that predicted by the band structure calculations.

Finally, it is worth mentioning two cases where the experimental results are yet unclear. The first is $Tl_2Ba_2CuO_6$. Although it should be a good candidate to study the Fermi surface related to the CuO_2 planes, the first 2D-ACAR results obtained [24] seem to be lacking in Fermi surface breaks. This might be related to the quality of the crystals. If so, perhaps the Fermi surface will be observable in the future with better quality crystals. We have to remember how critical the quality of the single crystals has in the study of $YBa_2Cu_3O_{7-\delta}$. Accordingly, progress in crystal quality in $Tl_2Ba_2CuO_6$ is needed before a clear statement can be made regarding the Fermi surface. The second case is $Bi_2Sr_2CaCu_2O_{8-x}$. In this compound, the momentum density suffers from an extra complication — the superlattice modulation along the b-axis of the BiO_2 layers. Subtraction techniques to get rid of these effects have been applied to 2D-ACAR [25], and lead to an electron-positron momentum distribution nevertheless consistent with the CuO_2 and BiO_2 Fermi surfaces derived from band theory. In another approach [26], Mijnarends *et al.* have shown how the incommensurate modulation can affect the way in which the 2D-ACAR reflects the Fermi surface. They observe considerable fine structure but do not interpret it in terms of a Fermi surface in the absence of momentum density calculations.

3. CONCLUSIONS

2D-ACAR positron experiments have lead to the observation of Fermi surface signatures in most of the superconducting oxides investigated until now. The recent progress is due to large improvement in the crystal quality, in development of sophisticated data analysis and the choice of suitable conditions to minimize positron trapping.

In general, the experimental findings are in agreement with LDA calculations. Some inconsistencies remain, less in the Fermi surface topologies than in the overall shape of the momentum density distribution. They can be attributed to shortcomings on the experimental side (traps, crystal quality, resolution) or the theoretical side (inadequate treatement of correlation effects for example).

In principle 2D-ACAR could provide direct measurements of the superconducting gap but there are no convincing results yet about T_c related effects. The experimental resolution should be sufficient for compounds with high T_c but currently available statistical precision is an important limitation. The forthcomming generation of intense positron beams shall be of great help to overcome this limitation.

REFERENCES

1. For a recent review: Manuel A. A., *Positron Spectroscopy of Solids* (Edited by Dupasquier A. and Mills Jr. A. P.). JOS Press, Amsterdam,p.155 (1995).
2. Hoffmann L., Shukla A., Peter M., Barbiellini B. and Manuel A. A., *Nucl. Instr. Meth. Phys. Res. A* **335**, 276 (1993).
3. O'Brien K. M., Brand M. Z., Rayner S. and West R. N., *J. Phys.: Condens. Matter* **7**, 925 (1995).
4. Yu J., Massidda S., Freeman A. J. and Koeling D. D., *Phys. Lett. A* **122**, 203 (1987).
5. von Stetten E. C., Berko S., Li X. S., Lee R. R., Brynestad J., Singh D., Krakauer H., Pickett W. E. and Cohen R. E., *Phys. Rev. Lett.* **60**, 2198 (1988).
6. Haghighi H., Kaiser J. H., Rayner S., West R. N., Liu J. Z., Shelton R., Howell R. H., Solal F., Sterne P. A. and Fluss M. J., *Phys. Rev. Lett.* **67**, 38 (1991).
7. Smedskjear L. C., Bansil A., Welp U., Fang Y. and Bailey K. G., *J. Phys. Chem. Solids* **52**, 1541 (1991).
8. Peter M., Manuel A. A., Hoffmann L. and Sadowski W., *Europhys. Lett.* **18**, 313 (1991).
9. Pankaluoto R., Bansil A., Smedskjaer L. C. and Mijnarends P. E., *Phys. Rev. B* **50**, 6408 (1994).
10. Hoffmann L., Manuel A. A., Barbiellini B., Peter M., Shukla A. and Walker E., *Acta Phys. Pol. A*, **88**, 147 (1995).
11. Adam Gh., Adam S., Barbiellini B., Hoffmann L., Manuel A. A., Peter M. and Massidda S., *Solid State Commun.* **88**, 739 (1993).
12. Shukla A., Hoffmann L., Manuel A. A., Walker E., Barbiellini B. and Peter M., *Phys. Rev. B* **51**, 6028 (1995).
13. Smedskjaer L. C., Bansil A., Welp U., Fang Y. and Bailey K. G., *Physica C* **192**, 259 (1992).
14. Mesot J., Allenspach P., Staub U., Furrer A. and Mutka H., *Phys. Rev. Lett.* **70**, 865 (1993).
15. Hoffmann L., Manuel A. A., Peter M., Walker E., Gauthier M., Shukla A., Barbiellini B., Massidda S., Adam Gh., Adam S., Hardy W. N. and Ruixing Liang *Phys. Rev. Lett.* **71**, 4047 (1993).
16. Fehrenbacher R. and Rice T. M., *Phys. Rev. Lett.* **70**, 3471 (1993).
17. Singh D. J., *Phys. Rev. B* **50** 4106 (1994).
18. Booth C. H., Bridges F., Boyce J. B., Claeson T., Zhao Z. X. and Cervantes P., *Phys. Rev. B* **49**, 3432 (1994).
19. Manuel A. A., Barbiellini B., Gauthier M., Hoffmann L., Jarlborg T., Massidda S., Peter M., Sadowski W., Shukla A. and Walker E., *J. Phys. Chem. Solids* **54**, 1223 (1993).
20. Blandin P., Massidda S., Barbiellini B., Jarlborg T., Lerch P., Manuel A. A., Hoffmann L., Gauthier M., Sadowski W., Walker E., Peter M., Jaejun Yu and Freeman A. J., *Phys. Rev. B* **46**, 390 (1992).
21. Barbiellini B., Puska M. J., Torsti T. and Nieminen R. M., *Phys. Rev. B*, **51**, 7341 (1995).
22. Howell R. H., Sterne P. A., Fluss M. J., Kaiser J. H., Kitazawa K. and Kojima H., *Phys. Rev. B* **49**, 13127 (1994).

23. Mosley W. D., Dykes J. W., Shelton R. N., Sterne P. N. and Howell R. H., *Phys. Rev. Lett.* **73**, 1271 (1994).
24. Barbiellini B., Gauthier M., Hoffmann L., Jarlborg T., Manuel A. A., Massidda S., Peter M. and Triscone G., *Physica C* **229**, 113 (1994).
25. Chan L. P., Harshman D. R., Lynn K. G., Massidda S. and Mitzi D. B., *Phys. Rev. Lett.* **67**, 1350 (1991).
26. Mijnarends P. E., Melis A. F. J., Weeber A. W., Menovsky A. A. and Kadowaki K., *Physica C* **176**, 113 (1991).

Pergamon

J. Phys. Chem. Solids Vol. 56, No. 12, pp. 1955–1956, 1995
Copyright © 1995 Elsevier Science Ltd
Printed in Great Britain. All rights reserved
0022–3697/95 $9.50 + 0.00

0022-3697(95)00104-2

POSITRON 2D–ACAR IN TTF–TCNQ

SHOJI ISHIBASHI
Electrotechnical Laboratory, 1-1-4 Umezono, Tsukuba, Ibaraki 305, Japan

ALFRED A. MANUEL and LUDGER HOFFMANN
Département de Physique de la Matière Condensée, Université de Genève,
24 quai E. Ansermet, CH-1211 Geneva 4, Switzerland

Abstract—We present the first results of a positron two-dimensional angular correlationof annihilation radiation (2D–ACAR) experiment on a typical organic conductor tetrathiofulvalinium tetracyanoquinodimethan (TTF–TCNQ). Although the observed spectrum is relatively smooth, we have succeeded inextracting the anisotropy reflecting the electronic structure of TTF–TCNQ. In order to clarify the origin of the anisotropy, we have performed theoretical simulations. Electron wave functions are expressed as TTF or TCNQ molecular orbitals obtained by self-consistent quantum chemical calculations (GAUSSIAN92) while the positron wave function is calculated by the superposed atom method. The simulated 2D–ACAR spectrum is in reasonable agreement with the experimental one. This implies that the predominant features observed can be interpreted in terms of molecular orbitals.

1. INTRODUCTION

The crystal of TTF–TCNQ (monoclinic, space group $P2_1/c$, a = 12.298 Å, b = 3.819 Å, c = 18.468 Å, β = 104.46°) consists of homologous stacks of cations (TTF) and anions (TCNQ) along the b-axis [1] and shows quasi-one-dimensional metallic conductivity along this direction above 60 K [2]. This conductivity is accomplished by charge transfer between chains of different type. In terms of molecular orbitals, 0.55 electrons are transferred from the highest occupied molecular orbital (HOMO) of TTF to the lowest unoccupied molecular orbital (LUMO) of TCNQ at room temperature [3]. Because of many interesting and exotic properties originating from the low-dimensionality [4], detailed investigation of the electronic structure is well motivated.

The positron 2D–ACAR technique is recognized as a powerful tool to measure electronic structures in momentum space [5]. In this paper, we report the first results of a positron 2D–ACAR experiment on TTF–TCNQ. We present also theoretical calculations based on molecular orbital description of the electronic structure, which we expect to be a good approximation for molecular crystals.

2. METHODS

The 2D–ACAR measurement was performed at 300 K with the spectrometer described in [6] using a single crystal (10 mm × 2 mm × 0.05 mm) with the integration axis parallel to the b axis. At this temperature the resolution has an FWHM along the two detected momentum components of about 1 mrad (1 mrad = 0.137 a.u. of momentum). About 165 × 10^6 coincidences were accumulated in an histogram with a mesh of 0.15 mrad × 0.15 mrad. The data were corrected with the angular efficiency of the spectrometer, symmetrized by the appropriate inversion operation, and the anisotropy was extracted by subtracting the cylindrical average. Finally, the anisotropy was smoothed by convolution with a square function of 1.05 mrad × 1.05 mrad.

In calculations, each molecular orbital of TTF or TCNQ is expressed as a linear combination of atomic orbitals (LCAO). In order to obtain the LCAO coefficients, we performed *ab initio* quantum chemical calculations using the GAUSSIAN92 program with the STO-3G basis set. When constructing electron wave functions with these LCAO coefficients, we used corresponding Slater orbitals (STO) for calculational simplicity.

On the other hand, we calculated the positron wave function by the superposed-neutral-atom method [7], in which no charge transfer is taken into account. The positron Schrödinger equation is replaced by a set of difference equations at three-dimensional mesh points in the real space. In the present case, the unit cell contains 61 × 21 × 91 mesh points (points on the boundary are shared with neighboring cells). The mesh spacings were ~ 0.2 Å. The positron wave function is obtained as numerical values at these mesh points.

To calculate the ACAR distribution, we first set up three-dimensional 256 × 256 × 256 grid with spacings of ~ 0.2 Å around a TTF or TCNQ molecule. Next, obtaining values of the electron wave functions ψ_{-j} (j: molecular-orbital index) and the positron wave function ψ_+, their products at the grid points (x, y, z) were calculated. By applying three-dimensional fast Fourier transformation (FFT), a partial ACAR spectrum $\rho_j^{2\gamma}$ was obtained for each molecular orbital as

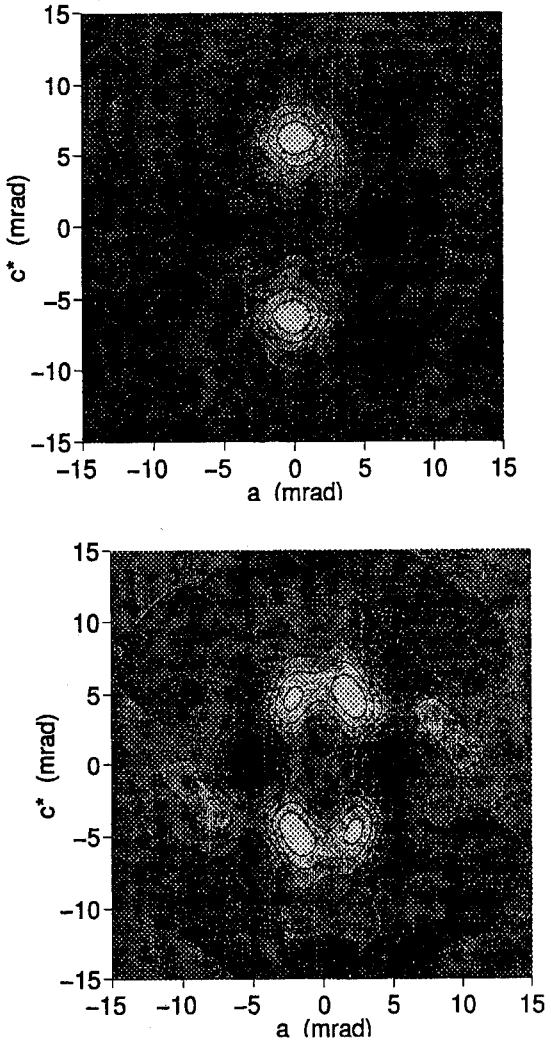


Fig. 1. Anisotropies of the positron 2D-ACAR distribution projected along the *b*-direction: (a) experiment and (b) theory. White is high and dark is low.

$$\rho_j^{2\gamma}(x', y', z') = const \cdot \left| FT\left(\psi_{-j}(x, y, z)\psi_{+}(x, y, z)\right)\right|^2, \quad (1)$$

where (x', y', z') represents each grid point in the momentum space. The 2D-ACAR spectrum $\rho_{2D}^{2\gamma}$ corresponding to the experiment was calculated by summing the partial spectra and integrating along the b axis (parallel to the y' direction in the present case) as

$$\rho_{2D}^{2\gamma}(x', z') = const \cdot \sum_{y'} \sum_{j} n_j \rho_j^{2\gamma}(x', y', z'). \quad (2)$$

26 orbitals were included for the TTF molecule while 37 for TCNQ. The occupation number n_j is 2 for all orbitals except the HOMO of TTF and the LUMO of TCNQ, where the n_j values are $2 - 0.55 = 1.45$ and 0.55, respectively. Orbital relaxations due to the charge transfer were ignored.

3. RESULTS AND DISCUSSION

Figure 1(a) shows the experimental 2D–ACAR anisotropy of TTF–TCNQ in the a–c^* plane. It is characterized by peaks and dips around ± 5 mrad in the c^* and a directions, respectively. The corresponding calculated result is shown in Fig. 1(b). Although there are additional finer structures in the calculated spectrum, the overall agreement between the two spectra is reasonable.

To discuss the anisotropic structures in some detail, we plotted anisotropies for each molecular orbital and obtained partial sums for TTF and TCNQ molecules, respectively (they are not shown here). Although it is not straightforward to assign a contribution from each orbital to the total spectrum, we can say that finer structures in the theoretical result come from molecular orbitals of TTF.

On the other hand, the experimental spectrum resembles more the partial sum for TCNQ than that for TTF. This is quite reasonable since we used superpositions of neutral atoms whereas a charge transfer of 0.55 electrons occurs. The agreement between experiment and theory is expected to improve if a self-consistent field is also used for the calculation of the positron wave function.

4. SUMMARY

We have measured for the first time positron 2D–ACAR on TTF–TCNQ. We have also made a theoretical simulation based on *ab initio* molecular orbital calculations. The agreement between experiment and theory is reasonable. This work opens a new domain of application for the positron annihilation technique: the study of electronic structures in organic crystals.

Acknowledgments—The authors are grateful to Prof. M. Peter for his continuous encouragement, and to Drs M. Tokumoto, Y. Tanaka and H. Katagiri for helpful discussions. We thank Dr A. Shukla for his careful reading of the manuscript.

REFERENCES

1. Kistenmacher T. J., Phillips T. E. and Cowan D. O., *Acta Cryst. B* **30**, 763 (1974).
2. Cohen M. J., Coleman L. B., Garito A. F. and Heeger A. J., *Phys. Rev. B* **10**, 1298 (1974).
3. Kagoshima S., Ishiguro T. and Anzai H., *J. Phys. Soc. Jpn* **41**, 2061 (1976).
4. Keller H. J. (ed.), *Chemistry and Physics of One-Dimensional Metals*. Plenum, New York (1977).
5. Manuel A. A., in *Positron Spectroscopy of Solids* (Edited by A. Dupasquier and A. P. Mills Jr). North-Holland, Amsterdam, to appear.
6. Bisson P. E., Descouts P., Dupanloup A., Manuel A. A., Perreard E., Peter M. and Sachot R., *Helv. Phys. Acta* **55**, 100 (1982).
7. Puska M. J. and Nieminen R. M., *J. Phys. F: Met. Phys.* **13**, 333 (1983).

OTHER SYSTEMS

Pergamon

J. Phys. Chem. Solids Vol. 56, No. 12, pp. 1957–1961, 1995
1995 Elsevier Science Ltd
Printed in Great Britain
0022–3697/95 $9.50 + 0.00

0022–3697(95)00259-6

ARE THERE SIMILARITIES BETWEEN THE LAYERED NICKEL BOROCARBIDE AND CUPRATE SUPERCONDUCTORS ?

G. BASKARAN
The Institute of Mathematical Sciences, Madras 600 113, India

Abstract—It is argued based on experimental results and physical arguments that the $Ni-B-C$ based layered family of superconductors RNi_2B_2C ($R = Lu, Y, Dy, Ho, Er, Tm$) and the cuprates have some fundamental features in common. We also discuss a simple modelling of the low energy electronic properties of the layered Nickel borocarbides and make certain predictions.

1. INTRODUCTION

A systematic nvestigation of the inter-metallic compounds involving Y, Ni and B by the TIFR group lead to the discovery of superconductivity in the compound $YNi_2B_3C_{0.2}$ with a $T_c \approx 13.5^oK$ by Nagarajan and collaborators [1]. This was followed by the discovery of a Y-Pd-B-C system having a T_c as large as 23^oK by Cava and collaborators [2]. A single phase compound $LuNi_2B_2C$ with a $T_c \approx 16.6^oK$ was also synthesised by Cava and collaborators [3]. Even newer systems with the Lu atom replaced by non-magnetic rare earth Y as well as magnetic rare earths Dy, Ho, Er, Tm have been synthesised. In the case of magnetic rare earths, the T_c is found to have a de Gennes scaling form [3]. Similarly, systems with Ni replaced by Pt or Pd have been synthesised and they also exhibit superconductivity [2]. When Ni is replaced by Cu or Co, superconductivity is easily destroyed [4]. It is hoped that the structurally characterised system $LuNi_2B_2C$ holds the key to understanding the mechanism of superconductivity in the multiphase compound with $T_c \approx 23^oK$. The aim of the present paper is to bring out some fundamental similarities and also differences between the layered $LuNi_2B_2C$ and the layered cuprate superconductors. We also propose a simple model to understand the low energy electrical and magnetic properties of this system.

2. CRYSTAL STRUCTURE

$LuNi_2B_2C$ can be considered as a filled variant of the tetragonal body centered $ThCr_2Si_2$ type structures [5]. That is, it contains an additional carbon atom in each lanthanide layer. There are two different layers: $(NiB)_2$ and LuC. In the $(NiB)_2$ layer, the Ni atoms form a simple square lattice with a lattice parameter of 2.45 Au. Each Ni atom is tetrahedrally co-ordinated by 4 Boron atoms. This leads to a square lattice of Ni atoms sandwitched by two square lattice layers of B atoms. The second is the LuC layer, a 2-d rock-salt structure with the carbon bridging two B atoms of the adjacent $(NiB)_2$ layers. Thus crystallographically it is a layered structure. Some important structural features are i) the short Ni-Ni distance of 2.45 Au, which is shorter than the corresponding distance of 2.5 Au in metallic Ni, ii) almost ideal tetrahedral coordination of Ni by Boron atoms, suggesting a strong sp^3-type of bonding and iii) short B-C distance of 1.47 Au, characteristic of covalent bonding. The covalent coupling between the $(NiB)_2$ layer and the LuC layer through the carbon atom is an important structural difference between the cuprates and the present Ni system. The strong 'metallic binding' along the ab-plane and covalent coupling along the c-axis is expected to provide interesting (less ?) electronic anisotropy.

3. TRANSPORT AND THERMODYNAMIC PROPERTIES

$LuNi_2B_2C$ is a good metal with a room temperature resistivity as low as 70 μOhms. It exhibits a striking linear temperature dependence in the temperature range 80 to 350 K without any indication of saturation. Owing to the absence of large single crystals, a systematic anisotropic transport measurements have not been made. Hall constant, frequency dependent conductivity, thermo electric power and some other important properties are yet to be measured.

The specific heat [6,7] has a small effective mass enhancement with a $\gamma \approx 20$ to $30mJ$. $LuNi_2B_2C$ is a type II superconductor [7] in the clean limit with a coherence length $\xi \approx 60Au$, mean free path $l \approx 700Au$, $H_{c2}(0) \approx 800Oe$, $H_{c1} \approx 50Oe$. The temperature dependence of the upper critical field $H_{c2}(T)$ is unlike the ordinary type II superonductor [8]. The ratio $\frac{\Delta}{2k_BT_c}$ is larger [7] than the weak coupling value of 3.52.

4. ELECTRONIC STRUCTURE

Our primary aim is to find the nature of orbitals that are involved in determining the low energy electrical and magnetic properties . How dominant are the Ni orbitals at the fermi level ? If they are, does it make the system a strongly correlated 2-d metals like the cuprates.

Direct information about the naturte of electronic states at the fermi level is available from photo-emission experiments. There are at least four different results available [9–12] including the first ARPES measurements presented by Poirior et. al. [12] at this meeting. All the groups find a suppression of the photo-emission peak at the fermi level, also about 30 percent band narrowing. They conclude that the states at the fermi level have 60 to 70 percent Ni d-character and that the on-site repulsion at the Nickel orbital is about 5 eV, indicating the presence of a correlated Ni band at the fermi level. Pelligrin et.al [10] also conclude that the Ni d-occupancy is close to 9, which remains stable with respect to rare earth replacement . This is close to a d-occupancy of about 9.5 that Matheiss suggest from the LDA calculations [13].

An important recent result is the ARPES data from the Ames group [12], who find a dispersing band close to the fermi level. The location of the fermi surface, within the limited scan in k-space is in agreement with the LDA calculations [15]. What is more significant is that small fermi surface pockets as predicted by LDA calculations seems to be absent in the experiments. This could be a matrix element effect. More likely, in view of strong correlation in the Ni layer, these small fermi surface pockets are in fact artificats of LDA rather than some thing real. That is, it is similar to layered BISCO materials where LDA predicts small fermi surface pockets corresponding to conudcting BiO planes with low carrier density. But in practice correlation effects remove such small fermi surfaces and as a result they are absent in photo-emission experiments.

As far as electronic structure calculations are concerned, they give us good insights provided we do not take them literally. The LDA calculations [13–17] have brought out the presence of a strong s-p hybridization. There is an s-p manifold of bands spread over about 20 eV. The individual s-p bands are however only a few eV wide. When it comes to the dispersion of bands, the dispersion along the three directions are nearly isotropic for the s-p bands. However, the bands that are close to the fermi level, which are the Nickel d-bands have less dispersion along the c-axis in comparison to the dispersion along the a-b direction. Thus, LDA calculations clearly indicate the presence of a primarily Nickel like band at the fermi level which disperses less along the c-axis. The shape of the fermi surface [15] indicates a large hole like fermi surface and small pockets of electron like fermi surface. The smaller electron like small fermi surfaces are likely to be artifacts of the neglect of electron correlations.

5. NMR AND μSR STUDIES

Magnetic resonance continues to be one of the best probes to understand the low energy spin dynamics. At least three groups [18–20] have studied NMR of B^{11} nuclei and one group [20] the in addition the Y nuclei. The results are interesting. The B^{11} NMR gives an almost temperature independent Knight shift. On the other hand, the relaxation rate $\frac{1}{T_1}$ exhibits marked departure from the Korringa law. Also the Hebel-Schlichter peak is absent.

The temperature dependence of $\frac{1}{T_1}$ for the B^{11} nuclei almost coincides with that of the Cu nuclei in $La_{2-x}Sr_xCuO_4$ except for a overall factor of 300 for $x \approx 0.13$ in the range of temperature upto about 350 Kelvin. The difference between the temperature dependence of Knight shift and $\frac{1}{T_1T}$ signifies that there exist finite wave vector low energy spin fluctuations, perhaphs very similar to that in the cuprates.

Very recently, the Ames group [21] has studied the Y NMR and found a Korringa like behaviour, which is to be contrasted with the non-Korringa behaviour of B^{11} nuclei. This difference between the NMR in B and Y nuclei is significant, particularly in the conducting state. This is reminiscent of the corresponding difference between the Cu and O nuclei in cuprates. In a conducting state, such a difference is not a simple geometric and matrix element effect - according to some recent discussions [22] it points to some fundamental property of the non-fermi liquid state at least for the case of cuprates. The result of Ames group also indicates the presence of lower carrier concentration in the vicinity of the Y site. This points out that any three dimentionality will be primarily through the Boron-Carbon-Boron bonds. The above difference between Y and B NMR as well as the presence of spin-fluctuations points towards the existence of a non-fermi liquid normal state. This statement becomes more relevant in view of a recent suggestion of Anderson [23] that in a one band situation antiferromagnetic spin fluctuations in the matallic state implies a non-fermi liquid normal state.

There also exists a μSR result from Cook et. al., [24] who claim that perhaphs Ni has a slowly fluctuation spin-$\frac{1}{2}$ magnetic moment at temperatures less than 2 K in the case of $HoNi_2B_2C$. Once confirmed this will be a significant result, which will be a good support for one band modelling to be proposed in a following section.

6. RARE EARTH MAGNETISM

There are other important experiments which distinguish $LuNi_2B_2C$ from other conventional superconductors like Hg or Al. These experiemtns are the study of co-existence of magnetism and superconductivity in the same system with rare earth replacement[3] of Lu; that is, RNi_2B_2C with $R = Sm, Tm, Er, Ho$. In these systems one sees a de Gennes scaling of the superconducting T_c. What is important is the fact that the rare earth magnetic subsystem is electronically

well isolated from the superconducting system like in the Chevrel phase and Rhodium boride cluster compounds.

Let us discuss briefly the well studied Holmium system. This has a complex phase diagram resulting from an interesdting competition between magnetism and superconductivity. What is significant is that the Holmium moments order ferromagnetically [25] along the ab plane within each Ho-C layer. Neighbouring basal plane ferromagnetic sheets of Ho are antiferromagnetically ordered along the C-axis. And the superconducting T_c is about 8.7^0 K.

If the Ho-C layer were truly involved in three dimentional conductivity, the non-zero exchange field due to the ferromagnetic order within the Ho-C layer would have drastic consequence to superconductivity as a pair breaker of the cooper pair singlets. Since a finite superconducting T_c exists, it means that a strong singlet correlation exists within each NiB layer and that the pairing correlation does not spill over strongly to the the HoC layer. Even though the mean exchange field arising from the ferromagnetically ordered Ho layers in the NiB layer vanishes by symmetry, the flucutation in the local exchange field will have drastic effect and reduce T_c much more than what is observed experimentally. Thus the NiB layer is likely to be a strongly singlet dominated system, and which is electronically well isolated from the HoC layer. This means a strong electrical anisotropy.

Another support for the strong anisotropy along the c-axis comes from our observation that the fluctuating orbital fields from the ferromagnetically ordered Ho layers, which will predominantly lie in the ab plane (with zero mean) will strongly modify the one electron as well as pair transport along the c-axis. One way by which this strongly fluctuating orbital field could be escaped is if there is no coherent one electron conduction along the c-axis in the normal state.

7. QUANTUM CHEMISTRY OF THE NiB_2 LAYERS

The nature of chemical bonds in $LuNi_2B_2C$ is more complicated in comparision to that in the cuprates in view of the fact that B is an electron defficient atom [26]. Electron deficient atoms have more number of stable valence orbitals than the number of valence electrons. They tend to have more ligancy than the number of stable valence orbitals. Boron has four (2s and 2p) valence orbitals and three electrons. The ligancy of Boron in $LuNi_2B_2C$ is 5 (four nearest Ni atoms and one C atom), which is more than the number of stable valence orbitals. This brings in fluctuating valence bonds or the related multi center bonds [26] in Boron based compounds. A good example of this phenomenon is the molecule diborane, B_2H_6. The difference between the fluctuating valence bond states and the multi-center bonds in the case of extended systems is a fundamental one [27].

We have an electronic coupling between the Ni subsystem and the BC subsystem. The Ni sub sysetem is strongly correlated. In view of the fluctuating valence band character, the B-C-B sub system can not be thought of as a band insulator with some amount of carriers present in them. This is to be contrasted with the CuO_2 planes in the cuprates where the electronic coupling involves the strongly correlated Cu subsystem and the oxygen band (no valence bond fluctuation) with holes.

It is not clear if this valence bond fluctuations bring in any fundamental difference to the low energy physics. It definitely complicates building of simple tight binding schemes. We believe that at the end valence bond fluctuations only modifies parametrically a one band tJ model that we suggest below.

We have an interesting situation in which the Ni atoms feel two strong perturbations of different symmetries. The first is the tetrahedral perturbation from the four neighbouring B atoms. The second is the square planar perturbation from the four nearest neighbour Ni atoms in the plane. The tetrahedral perturbation lifts the 5 fold degeneracy of the d level into the three fold degenerate t_{2g} at the top and the two fold degenerate e_g at the bottom. In particular, the xy, yz and zx orbitals can nicely form σ type bonding hybridisation with any sp^3 orbitals that is directed towards Ni from one of the four B atoms. When the square planar perturbation acts in addition, it lifts the degeneracy between the xy and the xz, zy states.

Ni is nominally in $3d^9$ configuration and Lu is in a charged state Lu^{3+}. NMR results, photo emission results and LDA calculations suggest a Ni configuration close to d^9. Strong covalent bonding is present in C and B atoms. The bond distance between C and B is about 1.47 A, which is in between the double bond distance and single bond distances in C-C bonds. Thus the C and B bond is fluctuating quantum mechanically. A total of 7 electrons per formula unit (3 from Lu and 4 from the two Ni atoms) has to be shared among the B-C-B atoms that links two neighbouring Ni layers.

We suggest two chemical bonding schemes: the first one is consistent with the overall symmetry of the system and a second that has a reduced symmetry and which perhaphs gains back the symmetry after the effects of quantum fluctuations of the valence bonds. In the first bonding scheme the $2p_x$ and $2p_y$ orbitals of carbon are filled. The $2s + 2p_z$ and $2s - 2p_z$ orbitals of one Carbon atom hybridize with the $2s - 2p_z$ and $2s + 2p_z$ orbitals of the two adjacent Boron atoms. The two bonding states of the above hybridization has two electrons each. Thus we have two single bonds B-C and C-B among the three atoms B-C-B, which are linear. We are left with an average of 2.5 electrons to be put in the rest of the three sp orbitals of each B atom, along with the remaining 2 electrons in each B atom and one undpaired electron in the Ni d-shell.

It is difficult to put one more electron in the Ni $3d^9$ state in view of the strong coulomb repulsion $\geq$ 5 eV. The three of the remaining sp orbitals of B and one Nickel d orbital will form a hybrid of 4 bands. And the fermi level lies in the third band. According to the existing LDA calculations as well as experiments the band at the fermi level is primarily

a Ni band. This is because there are 5.5 electrons per Ni-B complex after taking care of an electron that is involved in a covalent bond with the carbon atom. Thus the third band can be thought of as a Nickel band - an electron doped Mott insulator ($\frac{3}{4}$ filling). The carriers are analgue of the Zhang-Rice singlets relevant for the present case. The Zhang-Rice singlets are singlets between a d-electron and an electron in the sp hybrid of Boron atom. Thus we have essentially a one band situation.

The second bonding scheme is inspired by the near tetrahedral co-ordination of Ni by the B atoms. It is easily seen from the symmetry that a sp^3 orbital of B, directed towards Ni can hybridize with the xy,yz and zx orbitals. It can also hybridize with an sp^3 orbital of the 4s and 4p states of Ni and thereby promote a pair of electron from the filled Boron sp^3 orbital to he empty sp^3 orbital of Ni. From this point of view the Ni-B coupling is rather complex.

This suggests that a filled sp^3 hybrid of a B atom (directed towards a Ni atom) is strongly hybridized with the Ni orbitals. Simple counting shows that in this case all the sp^3 bonding states of C and the two B atoms will be filled and an extra of half electron per Ni atom will live either in the Ni 4s state or some other hybrid. And the B-C bonds are double bonds.

In the second scheme, the number of boron sp^3 Boron orbitals that are available for bonding is two per Ni atoms, where as the ligancy of Ni is eight. If we choose a particular pattern of Boron sp^3 and Ni hybridization, the symmetry is reduced from what is seen experimentaly. Thus the sp^3 valence bonds should quantum fluctuate there by gaining resonance energy as well as gaining back the full symmetry.

We have a spin half magnetic moment in each Nickel Cell. The d-states involved in forming this spin are the d_{xy}, d_{yz} and d_{zx} with some what stronger d_{xy} contribution. The valance bond flunctuation of the Boron-Carbon subsystem to which this spin is coupled gives this state a "non-Slater determinant" character. However, this local many body state can be thought of as a state having zero reference charge and magnetic moment half. Similarly the Zhang-Rice singlet of the above spin half state with an electron of the B sub system is a correlated local many body state. However, it has a reference charge -e and spin zero. This entiting can move in the background of the fluctuating Ni spins. This is the origin of a one band tJ model description of our system.

8. A TIGHT BINDING MODEL, CORRELATION AND ANISOTROPY

From the above discussion we can extract the following model. Given an opportunity Ni is in a nominally d^9 state. In view of the reduced symmetry around Ni, we do not expect the d-hole to have any orbital degeneracy. The relevant valence orbital is a d-orbital that has more of a d_{xy} character and contains an unpaired electron. In view of the strong electron correlation with an $U \approx 5eV$ and narrow band, this reference state is a Mott insulator. Thus, each Ni atom carries a spin half magnetic moment. However, $LuNi_2B_2C$ has about half an extra electron per Ni atom. This extra electron lives primarily in one fluctuating valence bond state involving the Boron 2s and 2p orbitals. And this forms a singlet with the unpaired Ni electron. This is analogous to the Zhang-Rice singlet of the cuprates. The strong coulomb correlation prevents charge fluctuation in the Ni subsystem except that arising from the motion of the extra electron living in the B subsystem. Thus we have essentially a single band tJ model ! It is an electron doped Mott insulator, which is a $\frac{3}{4}$ filled band or close to it. Experimental support for the above modelling is from NMR and μSR and an one band like behaviour from the ARPES results.

In a t-J model, above half filling, the local constraint changes to absence of any empty site. Thus our model is

$$\mathcal{H} = -\sum t_{ij} C^{+}_{i\sigma} C_{j\sigma} + h.c. + J \sum \mathbf{S}_i . \mathbf{S}_j$$
$$\text{with } \sum_{\sigma} n_{i\sigma} \neq 0, \qquad (1)$$

where the hopping parameter along the ab plane is $t \approx 0.2eV$ and $J \approx \frac{t^2}{2U} \approx eV$. From the LDA calculation it is clear that the $t_\perp$ is about a factor of 3 or 4 small in comparision to the inplane t. This anisiotropy ratio is similar in magnitude to the 214 cuprates. The confinement aspects of the anisotropic to J model needs to be studied in detail [30].

9. PREDICTION OF A NON-FERMI LIQUID NORMAL STATE, c-AXIS CONFINEMENT AND INTERLAYER PAIR TUNNELING

Two key issues are the nature of the c-axis anisotropy and the possible non-fermi liquid character of he NiB sheets. Unlike the cuprates, the bonding beween $(NiB)_2$ layers is primarily covalent in character. The LDA calculations do show some amount of anisotropy in the band dispersion. However, the relative insensitivity to ferrromagnetic sheet order in the HoC sheets in $HoNi_2B_2C$, as discussed earlier indicates reduced carrier density in the HoC layers. The NMR results also indicates less carrier density in the Y site for the case of YNi_2B_2C. This is what tempts us to suggest that there is c-axis confinement.

From our modelling several results follow in a rather natural fashion, which can be experiementally tested. Firstly, the normal state of the Ni plane will be a non-fermi liquid, perhaphs a tomographic Luttinger liquid [28] with spin-charge decoupling. One of the primary consequence is the possibility of amplification of the band anisotropy to a non-metallic behaviour in the normal state along the c-axis. With the transport study envisaged with larger single crystals, this prediction can be easily tested.

Other normal state anomalies, like the Hall effect, Raman scattering, tunneling conductance, frequency and tem-

perature dependence of the Drude width and other should follow perhaps with some quantitative difference from the cuprates. We have a $\frac{3}{4}$ filled band. Since it is a t-J model, the sign of the Hall constant should be -ve (electron like) as opposed to the simple band theory prediction.

The presence of spin-charge decoupling and the consequent one electron confinement implies an appreciable Wheatley-Hsu-Anderson pair tunneling [29] as a source of superconductivity. Since the scale of T_c so far has been less than 23 K, perhaps a finite fraction of pairing amplitude derives from phonon mediated attraction of the qasi particles at the fermi level, as in the case of low T_c cuprates.

It should be mentioned that the existing resistivity results show a remarkable linear behaviour above 80K but with a quadratic component at low temperatures. It is very different from the A15 and chevrel phase compounds - perhaps more closer to cuprates. But in terms of actual value of resistivity, these systems are better conductors than the cuprates. Even though one may be tempted to attribute the linear behaviour to a fermi liquid state with low Debye temperature, one has to be careful in view of the strong experimental evidence for spin flcutuations and strong correlations within the 2-d Ni layers.

10. CONCLUSIONS

In this paper we have argued that there exists a strong similarity at a fundamental level between the NiBC system and the cuprates. Based on experimental results and theoretical reasonings we have given a one band tJ model as an appropriate model for the low energy physics, which has several interesting consequences discussed in the last section. Other existing theories talk about electron-phonon interaction [30] or a mixture of electron-electron and electron phonon interactions [31] involving many bands.

An acid test of our model will be the existence of a Mott insulating state in this class of compounds. From nominal electron counting, a replacement of Lu by a divalent ion such as Ca, which has a similar ionic radius as Lu or Y should result in a Mott insulating state. Another prediction will be that a complete replacement of Ni by Co will result in a one band with quarter filling. This should behave in a similar way to the Ni system. Existing experiments do not show superconductivity in the pure Co system [30]. Within our scenerio this absence can be only explained by invoking some other factor.

Another intriguing result is the sharp reduction of Tc with the replacement of Lu by La, whose ionic radius is rather small.

What is the origin of the superconudctivity in the Y-Pd-B-C system with a T_c of 23 K ? Our guess based on our modelling is that it is either a bi-layer material in the sense of having two closely coupled Ni layers or a structure in which our one band is optimally doped rather than over doped. The fact that the replacement of Ni by Pt or Pd while modifying y, does not affect the T_c is also an intriguing experimental fact.

Acknowledgements—It is a pleasure to acknowledge discussion in the past with L.C.Gupta, H. Takagi, A. Fujimori and P.W. Anderson. And thanks to P. Ravindran for bring to my attention many of the relevant references and S. Ramakrishnan for reference 4.

REFERENCES

1. Nagarajan R. *et al.*, *Phys. Rev. Lett.* **72**, 274 (1994).
2. Cava R. J. *et al.*, *Nature* **367**, 146 (1994).
3. Cava R. J. *et al.*, *Nature* **367**, 252 (1994).
4. Bud'ko S. L. *et al.*, CBPF/CNPQ preprint 1994 ; see also Ghosh K. *et al.*, TIFR preprint (1994).
5. Siegrist T. *et al.*, *Nature* **367**, 254 (1994).
6. Kim J. S. *et al.*, *Phys. Rev. B* **50**, 3485 (1994) ; Cava R. J. *et al.* **PR 49**, 12384 (1994); Cava R. J. *et al.*, *Phys. Rev. B* **50**, 4216 (1994). Movshovich R. *et al.*, *Physica C* **227**, 381 (1994).
7. Takagi H. *et al.*, *Physica C***288**, 389 (1994).
8. Godart C. *et al.*, *Phys. Rev. B* **51**, 489 (1994).
9. Fujimori A. *et al.*, *Phys. Rev. B* **50**, 9660 (1994).
10. Pelligrin E. *et al.*, *Phys. Rev.* (1994)
11. Golden M. S. *et al.*, *Euro. Phys. Lett.* **28** 369 (1994).
12. Poirier D. M. *et al.*, *J. Phys. Chem. Solids* (1995) (Stanford Conference on Spectroscopy of Novel Superconductors, March 95).
13. Matheiss L. F., *Phys. Rev. B* **49**, 13279 (1994).
14. Pickett W. E. and Singh D. J., *Phys. Rev. Lett.* **72**, 370 (1994).
15. Lee J. I. *et al.*, *Phys. Rev. B* **50**, 4030 (1994).
16. Coahoorn R., *Physica C* **228**, 5671 (1994).
17. Ravindan P. *et al.*, Ann University preprint (1995)
18. Ikushima K. *et al.*, *J. Phys. Soc. Jpn* **63**, 2878 (1994).
19. Hanson M. E. *et al.*, *Phys. Rev. B* **51**, 674 (1995).
20. Borsa F. *et al.*, *Physica C* **235–240** (1994).
21. Borsa F. *et al.*, *Bull. Am. Phys. Soc.* **40**, 629 (1995)
22. Baskaran G. and Anderson P. W., unpublished.
23. Anderson P. W., *Bull. Am. Phys. Soc.* **40**, 234 (1995).
24. Cooke D. W. *et al.* Los Alamos preprint (LA-UR-94-1286).
25. Grigereit T. E. *et al.*, *Phys. Rev. Lett.* **72**, 2758 (1994); Goldman A. I., *Phys. Rev.* **350**, 9668 (1994) ; Sinha S. K., *Phys. Rev. B* **51**, 681 (1995).
26. Pauling L., *The Nature of Chemical Bond.* Cornell University Press (1960); Cotton F. A. and Wilkinson G., *Advanced Inorgonic Chemistry*. John Wiley and Sons, NY (1988).
27. Anderson P. W., *Phys. Rev. Lett.* **65**, 2306 (1990); **66**, 3226 (1991)
28. Baskaran G., unpublished.
29. Wheatley J. M. *et al.*, *Phys. Rev.* **37**, 5897 (1988); Chakravarty S. *et al.*, *Science* **261**, 337 (1993).
30. Matheiss *et al. Solid State Commun.* **91**, 887 (1994).
31. Hakisglu T. *et al.*, *Physica C* (1994).
32. See however Ghosh K. *et al.* of Ref.4.
33. Arjunwadkar M. *et al.*, *Phys. Rev. Lett.* **70**, 674 (93); Sarkar S. K., Alabama preprint 1995 and reference therein.

Pergamon

J. Phys. Chem. Solids Vol. 56, No. 12, pp. 1963–1968, 1995
Copyright © 1995 Elsevier Science Ltd
Printed in Great Britain. All rights reserved
0022–3697/95 $9.50 + 0.00

0022–3697(95)00271-5

RECENT ISSUES IN THE PHYSICS OF HEAVY FERMION MATERIALS

M. B. MAPLE, Y. DALICHAOUCH, M. C. DE ANDRADE, N. R. DILLEY, J. HERRMANN
Department of Physics and Institute for Pure and Applied Physical Sciences, University of California, San Diego, La Jolla, CA 92093-0319, U.S.A.

R. MOVSHOVICH
Los Alamos National Laboratory, Los Alamos, NM 87545, U.S.A.

Abstract—The basic properties of heavy fermion materials are briefly summarized. Several recent issues in the physics of heavy fermion materials are discussed, including the unconventional superconductivity of UPt_3, non Fermi liquid behavior in strongly correlated f-electron systems, and the possible observation of the Fulde-Ferrel-Larkin-Ovchinnikov spatially nonuniform superconducting state.

1. INTRODUCTION

Heavy fermion f-electron superconductors and high T_c cuprate superconductors share several striking similarities: (1) strong electron correlations; (2) anisotropic superconductivity with an energy gap that may vanish at points or lines on the Fermi surface; (3) the proximity of superconductivity and antiferromagnetism, suggesting that electron pairing may be mediated by antiferromagnetic spin fluctuations; and (4) non Fermi liquid characteristics in the normal state physical properties in certain regimes of chemical composition and temperature [1]. In this paper, we briefly summarize the basic properties of heavy fermion compounds and discuss several recent issues in the physics of these materials. These issues include the unconventional superconductivity of UPt_3, non Fermi liquid behavior in strongly correlated f-electron systems, and the possible observation of the Fulde-Ferrel-Larkin-Ovchinnikov spatially nonuniform superconducting state.

2. BASIC PROPERTIES OF HEAVY FERMION f-ELECTRON MATERIALS

The small class of heavy fermion superconductors includes one Ce compound, $CeCu_2Si_2$[2], and five U compounds, UBe_{13}[3], UPt_3[4], URu_2Si_2[5], UNi_2Al_3[6], and UPd_2Al_3[7], all listed in the order in which they were discovered. Another U superconductor with unusual properties, U_6Fe, may be related to the heavy fermion superconductors [8].

The heavy fermion compounds derive their name from the enormous linear coefficient γ of the electronic specific heat $C_e = \gamma T$, which attains values as high as ≈ 1 J/mol-K^2, from which large electron effective masses $\approx 10^2$–10^3 m_e, where m_e is the free electron mass, have been inferred. For the heavy fermion compounds $CeCu_2Si_2$ [2] and UBe_{13} [3], γ is strongly dependent on temperature below ≈ 10 K and attains a value ≈ 1 J/mol-K^2 near 1 K, indicating that these materials have a low effective degeneracy temperature T_o of the order of several K. Both compounds have a large specific heat jump ΔC at the superconducting critical temperature ($T_c \approx 0.6$ K for $CeCu_2Si_2$; $T_c \approx 0.85$ K for UBe_{13}) of $\approx \gamma(T_c)T_c$, comparable to the value expected from the BCS theory ($\Delta C = 1.43\gamma T_c$). This demonstrates that the heavy electrons that are responsible for the enormous values of γ are the same ones that are involved in the superconductivity. Many researchers believe that the narrow feature in the density of states at the Fermi level which is responsible for the low degeneracy temperature T_o in heavy fermion f-electron materials is associated with the Kondo effect; i.e., the counterpart, for a lattice of localized magnetic moments associated with f-states that are hybridized with conduction electron states, of the Abrikosov-Suhl (or Kondo) resonance for a dilute Kondo system. In a metal containing dilute concentrations of paramagnetic impurities, the Kondo temperature T_K delineates the cross-over from high temperature local moment behavior to a low temperature nonmagnetic state. In the high temperature local moment regime, the magnetic susceptibility can be described by a Curie-Weiss law with an effective magnetic moment close to the free ion value and a Curie-Weiss temperature $\theta_p \approx 3$-$4\ T_K$; the low temperature nonmagnetic state is characterized by saturation of the magnetic susceptibility to a finite value $\chi(0)$ at $T = 0$ K as $\approx 1 - (T/T_K)^2$.

Power law temperature dependences in various superconducting properties of the heavy fermion compounds have been interpreted as evidence of anisotropic superconductivity in which the energy gap $\Delta(\mathbf{k})$ vanishes at points or lines on the Fermi surface. The anisotropic superconductivity may be associated with pairing of electrons in states with finite angular momentum, mediated by antiferromagnetic spin fluctuations, rather than phonons. Several of the heavy fermion compounds exhibit the coexistence of weak antiferromagnetism (AFM) and superconductivity, with a Néel temperature $T_N > T_c$, over different

parts of the Fermi surface (UPt_3[9], URu_2Si_2[5,10,11,12], UNi_2Al_3[6,13,14], UPd_2Al_3[7,13,15]). The heavy fermion compounds UBe_{13} and UPt_3 have multiple superconducting phases that appear upon doping with another element ($U_{1-x}Th_xBe_{13}$) or the application of a magnetic field H or pressure P (UPt_3).

Another common behavior that is emerging for superconducting heavy fermion uranium compounds is that chemical substitutions tend to suppress both superconductivity and weak AFM and induce local moment AFM or ferromagnetism (FM) with moments of the order of a μ_B. In UPt_3, local moment AFM is produced by substituting Th for U [16,17] and Pd [18] or Au [19] for Pt, while in URu_2Si_2, local moment AFM appears upon substitution of Rh for Ru [20] and local moment FM occurs when Re or Tc is substituted for Ru [21], the first example of a ferromagnetic instability in a heavy electron system.

3. UNCONVENTIONAL SUPERCONDUCTIVITY OF UPt_3

In zero magnetic field, the heavy fermion superconductor UPt_3 exhibits two distinct superconducting transitions, manifested as two specific heat jumps, one at a critical temperature T_{c1} ($\approx$0.5 K) and the other at a critical temperature T_{c2}, about 50 mK below T_{c1} [22]. Specific heat measurements in magnetic fields applied perpendicular to the c-axis of a UPt_3 single crystal [23] revealed that the two superconducting transitions converge with increasing field and coalesce into a single transition above $\approx$0.5 tesla. These and other measurements such as ultrasonic attenuation have been used to construct an H – T phase diagram which has three different superconducting phases and a tetracritical point for both the cases H$\perp$ *c* and H||c [24]. The occurrence of the multiple superconducting phases in UPt_3 has been attributed to the coupling between a multicomponent superconducting order parameter and the AFM order parameter [25]. The two superconducting transitions in UPt_3 are also very sensitive to applied pressure and merge into a single transition at a pressure of $\approx$3.7 kbar, above which only a single transition is observed [26]. The two zero field phases, which we denote as A and B for the high and low temperature phases, respectively, have different superconducting characteristics; for the B-phase, point contact spectroscopy reveals a gap-like feature which is not present in the A-phase [27]. Zero field μSR measurements indicate a spontaneous internal magnetic field of $\approx$ 0.1 G in the B-phase (the lower critical field is $\approx$ 20 G) [28]. A recent investigation of the relaxation of the remanent magnetization of magnetic vortices in superconducting UPt_3 showed that there are striking differences in the low-field flux dynamics between the A- and B-phases [29]. In the low temperature B-phase, the logarithmic creep rate is practically zero, while in the high temperature A-phase, it is finite and increases rapidly as the temperature is increased towards T_{c1}. It was speculated that the reduced bulk creep rate in the B-phase may be due to the trapping of vortices on walls between domains of degenerate superconducting phases [29]. One of the experiments that provides the strongest evidence for anisotropic superconductivity in UPt_3 consists of ultrasonic attenuation measurements on single crystals in the superconducting state by Shivaram and coworkers [30]. For the propagation vector of the ultrasound wave in the basal plane of UPt_3, the ultrasonic attenuation coefficient α was found to vary as $\approx T$ for the polarization $\hat{e}||\hat{a}$ and $\approx T^3$ for $\hat{e}||\hat{c}$. In the normal state, the same dependence of α vs T was observed for both $\hat{e}||\hat{a}$ and $\hat{e}||\hat{c}$. This system has been investigated extensively and the reader is referred to several recent reviews for a more complete discussion [24,25,31].

Recently, the depression of T_c of UPt_3 by rare earth, Th, and Zr substitutions for U was investigated [32]. The results are shown in Fig. 1 where the depression of T_c, $T_{co} - T_c$, for a series of $U_{0.997}R_{0.003}Pt_3$ compounds where R = rare earth (except Pm and Lu), Th, and Zr is plotted vs (a) R ionic radius, and (b) residual resistivity ρ_o. The linear increase of the depression of T_c with increasing residual resistivity indicates that the primary pair breaking mechanism is the impurity potential scattering, rather than the exchange interaction. The scaling of T_{co} - T_c with residual resistivity is strong evidence for anisotropic superconductivity in UPt_3; the absence of a marked correlation of the depression of T_c with the de Gennes factor $(g_J\text{-}1)^2 J(J+1)$, where g_J and J are, respectively, the Landé g-factor and total angular momentum, of the rare earth ion suggests that the superconducting order parameter in the A-phase of UPt_3 has odd parity.

4. NON FERMI LIQUID GROUND STATES IN STRONGLY CORRELATED f-ELECTRON MATERIALS

During the past several years, a new class of f-electron systems which exhibit non Fermi liquid (NFL) behavior at low temperatures has been attracting a great deal of interest [33,34]. These materials are Ce and U intermetallics which, with a few possible exceptions, have been doped with a nonmagnetic element. Many of the f-electron systems exhibit the following NFL temperature dependences of the electrical resistivity ρ, specific heat C, and magnetic susceptibility χ for $T << T_o$, where T_o is a characteristic temperature [33]: $\rho(T) \approx 1 - aT/T_o$, where $a < 0$ or > 0, $C(T)/T \approx (-1/T_o)\ln(T/bT_o)$, and $\chi(T) \approx 1 - c(T/T_o)^{1/2}$. In several of the f-electron systems, the characteristic temperature T_o can be identified with the Kondo temperature T_K.

Presently, no theoretical model can account for the linear temperature dependence of $\rho(T)$, as far as we are aware. The two channel spin 1/2 Kondo model is consistent with the temperature dependence of C(T), but not $\chi(T)$, while the quadrupolar Kondo model (the electric analogue of the magnetic Kondo effect which maps onto the two channel spin 1/2 Kondo model) can account for both C(T) and

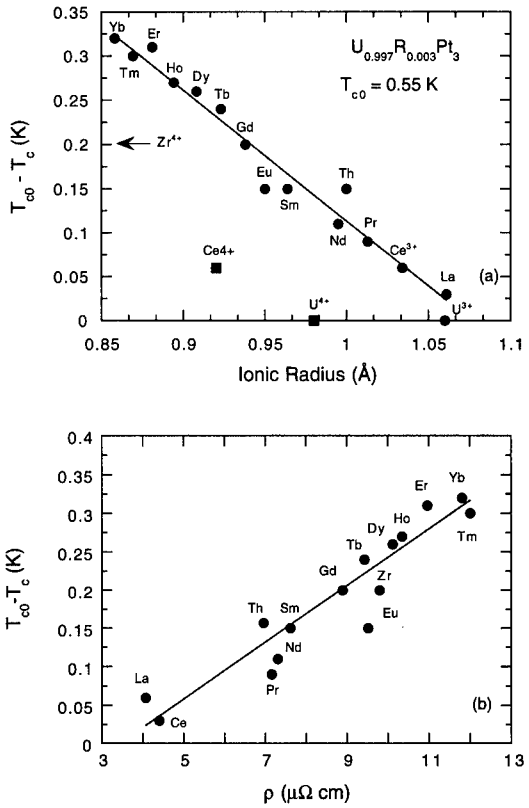


Fig. 1. (a)Depression of T_c, T_{co} - T_c, vs R ionic radius for $U_{0.997}R_{0.003}Pt_3$ compounds where R = rare earth (except Pm and Lu), Th, and Zr. T_{co} is the superconducting transition temperature of UPt_3. (b)T_{co} - T_c vs residual resistivity for the same compounds as in Fig. 15(a). After ref. [32].

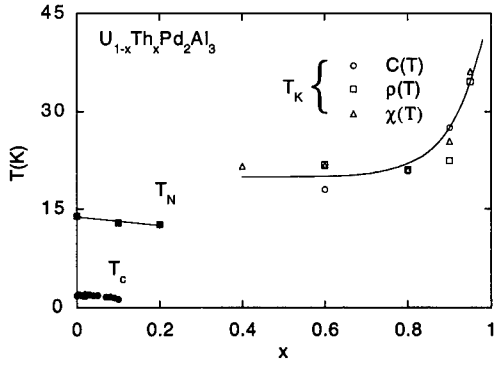


Fig. 2. Low temperature phase diagram of the $U_{1-x}Th_xPd_2Al_3$ system. As the Th concentration x is increased, the Néel temperature T_N and the superconducting critical temperature T_c decrease slightly, but the features associated with AFM and superconductivity are rapidly suppressed and eventually become undetectable. The line in the right hand side of the figure represents the estimated values of the Kondo temperature T_K. After ref. [34].

χ(T). However, the applicability of these models requires particular f-electron ground states in the presence of the crystalline electric field of the material under consideration [33,34]. In our analysis of the specific heat data for f-electron systems which exhibit NFL behavior, we have operationally applied the two channel spin 1/2 Kondo model formula for C(T) without rigorous justification.

An interesting example of NFL behavior in a strongly correlated f-electron system is found in $U_{1-x}Th_xPd_2Al_3$ in the concentration range $0.4 \lesssim x < 1$ where an unconventional Kondo effect is observed. The parent compound UPd_2Al_3 is a heavy fermion antiferromagnetic superconductor with T_N = 14.6 K and $T_c \approx 2$ K that crystallizes in the hexagonal $PrNi_2Al_3$ structure [7]. The compound UPd_2Al_3 has the highest T_c of the heavy fermion superconductors and an ordered moment of 0.85 μ_B [15], much larger than the small ordered moments ($\approx$0.02 μ_B) observed for URu_2Si_2 [12] and UPt_3 [9], two other heavy fermion compounds in which superconductivity and AFM coexist with $T_c < T_N$. The antiferromagnetic structure of UPd_2Al_3 consists of alternating ferromagnetic sheets, with the moments lying in the hexagonal basal plane [15]. The temperature dependence of the upper critical field is consistent with singlet superconductivity and the antiferromagnetic transition appears to involve the opening of a 30 meV gap over part of the Fermi surface [13], similar to that observed in URu_2Si_2 [11].

The low temperature phase diagram of the $U_{1-x}Th_xPd_2Al_3$ system, based upon measurements of ρ(T), C(T), and χ(T), is shown in Fig. 2. As the Th concentration x is increased, T_N and T_c decrease slightly, but the features associated with AFM and superconductivity are rapidly suppressed and eventually become undetectable. The line in the right hand side of the figure represents the estimated value of the Kondo temperature T_K, inferred from ρ(T), C(T), and χ(T). However, this phase diagram is incomplete near x = 1. During the course of our investigation of the $U_{1-x}Th_xPd_2Al_3$ system, we discovered that the compound $ThPd_2Al_3$ is superconducting with a T_c = 0.2 K. To our knowledge, this is the first case where an isostructural counterpart based on a rare earth or actinide element with an empty or filled f-shell (i.e., Sc, Y, La, Lu, Th) of a Ce or U heavy fermion superconductor is also superconducting. Measurements to determine the $T_c(x)$ curve for the $U_{1-x}Th_xPd_2Al_3$ system near x = 1 are currently in progress.

Electrical resistivity ρ(T) measurements on the $U_{1-x}Th_xPd_2Al_3$ system reveal Kondo like behavior in which the contribution due to scattering from the U ions increases with decreasing temperature. However, the Kondo like behavior in the range $0.4 \lesssim x < 1$ appears to be unconventional in the sense that the U contribution to ρ(T) is linear between a few K and about 20 K, similar to that of the $M_{1-x}U_xPd_3$ (M = Sc, Y) system [33,34]. At temperatures below a few K, ρ(T) levels off, indicating a cross-over from NFL to FL behavior as the temperature decreases. Within the context of a multichannel Kondo model, this would suggest that the

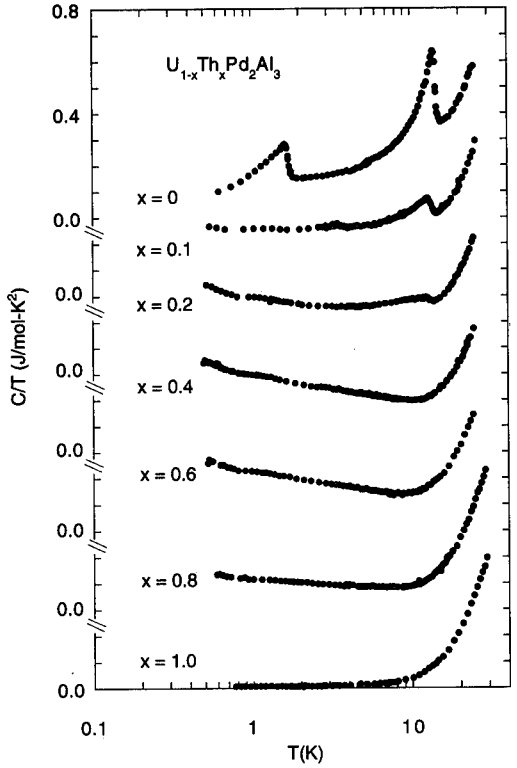


Fig. 3. Specific heat divided by temperature C/T vs T of $U_{1-x}Th_xPd_2Al_3$ for various values of x between 0 and 1. After ref. [34].

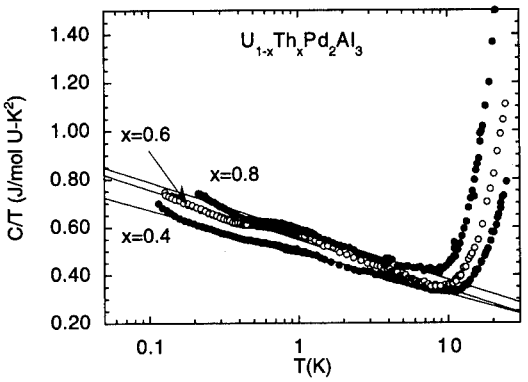


Fig. 4. Low temperature specific heat divided by temperature C/T vs log T for $U_{1-x}Th_xPd_2Al_3$ alloys with x = 0.4, 0.6, and 0.8 to temperatures as low as ≈100 mK.

degeneracy of the conduction electron channels or the localized electron spin or charge degrees of freedom has been lifted by some residual interaction, producing an evolution towards single channel behavior. In the range 4 K ≤ T ≤ 20 K, the U contribution to the resistivity can be described by the relation $\Delta\rho(T) = \Delta\rho(0)(1 - a(T/T_K)^n)$ with n ≈ 1 and a = 0.1 for T_K values consistent with those inferred from the specific heat for various values of x between 0.6 and 0.95.

Displayed in Fig. 3 are plots of C/T vs log T for the $U_{1-x}Th_xPd_2Al_3$ system with various values of x between 0 and 1. The specific heat anomalies due to AFM at T_N and superconductivity at T_c, which are evident in the data for x = 0, are rapidly suppressed with increasing x, similar to what is observed in the $U_{1-x}Th_xRu_2Si_2$ system [35]. A ln T divergence in the C/T data, emerging in the sample with x = 0.2, is fully developed for the samples with x = 0.4, 0.6 and 0.8. The results of an extension of the measurements on the samples with x = 0.4, 0.6, and 0.8 shown in Fig. 3 down to ≈100 mK are displayed in Fig. 4 as plots of C/T, per mol U-K^2, vs log T. Analysis of the specific heat data in terms of the two-channel spin 1/2 Kondo formula yields values of T_K of ≈20 K.

For values of x > 0.2, $\chi(T)$ follows a Curie-Weiss law between ≈50 K and 300 K; the effective magnetic moment μ_{eff} and Curie-Weiss temperature θ_p vary somewhat with x and have values $\mu_{eff} \approx 2.4\ \mu_B$ and $\theta_p \approx$ -40 K in the NFL regime x > 0.8. Since for Kondo systems, $|\theta_p| \approx 3$ - 4 T_K, this suggests a value $T_K \approx$ 10 K, in reasonable agreement with values of T_K obtained from the scaling of the electrical resistivity and specific heat. At lower temperatures, the $\chi(T)$ data can be described by the relation $\chi(T) = \chi(0)(1 - c(T/T_K)^{1/2})$, with values of T_K in reasonable agreement with those obtained from $\rho(T)$ and C(T) for c = 1.15.

Some of the interest in non Fermi liquid behavior in strongly correlated electron systems, particularly copper oxides and f-electron materials, is associated with the unconventional superconductivity found in these two classes of materials. In spite of the disparity in the values of T_c, which are as high as ≈133 K for the copper oxide superconductors but only ≲2 K for the f-electron heavy fermion materials, the superconducting states of both of these materials share some striking similarities — the superconducting state appears to be anisotropic, with an energy gap that may vanish at points or lines on the Fermi surface, and the superconducting electron pairing may be mediated by antiferromagnetic spin fluctuations. An understanding of the source of the NFL behavior in these systems may provide important information about the electronic structure and excitations in these systems, as well as the origin of the unconventional superconductivity.

5. POSSIBLE OBSERVATION OF THE FULDE–FERRELL–LARKIN–OVCHINNIKOV SPATIALLY NONUNIFORM SUPERCONDUCTING STATE

Thermal expansion in high magnetic fields and magnetostriction measurements on a single crystal specimen of the antiferromagnetic heavy fermion superconductor UPd_2Al_3 by Gloos et al. [36] have revealed the existence of a first order phase transition within the superconducting state distinctly below T_c and somewhat below the upper critical field curve. The authors have interpreted this as evidence for the existence of a spatially nonuniform superconducting state in the presence of a magnetic field acting on the spins pre-

dicted independently by Fulde and Ferrel [37] and Larkin and Ovchinnikov [38] (referred to as the FFLO state). In the FFLO state, the superconducting order parameter is spatially modulated with a wavevector q of order ξ_0^{-1}, the inverse of the superconducting coherence length at T = 0 K. The FFLO state occurs only at temperatures smaller than $\approx 0.55\ T_c$ for a type I superconductor, and the transition between the nonuniform state and the ordinary uniform state is first order. Norman [39] has recently derived a formula for the upper critical field for the FFLO state at all temperatures in the clean limit and found that the ratio T/T_c for a type II superconductor is less than 0.55, the value previously derived for a type I superconductor. From fits to the UPd_2Al_3 data, he concludes that this ratio should be zero or considerably less than 0.55, calling into question the FFLO interpretation of the data. Evidently, further research will be required to ascertain whether the remarkable H – T phase diagram of UPd_2Al_3 is associated with the FFLO state.

Another f-electron material that exhibits superconducting behavior in a magnetic field that is reminiscent of that of UPd_2Al_3 is $CeRu_2$. The compound $CeRu_2$ has a T_c of 6.1 K, the highest T_c of any intermetallic compound of Ce, and crystallizes in the cubic C15 structure [40]. Combined resonant photoemission and Bremsstrahlung isochromat spectroscopy spectra for $CeRu_2$ reveal a large amount of Ce 4f spectral weight in the vicinity of the Fermi level [41].

Magnetization measurements on $CeRu_2$ indicate that there are two irreversible regions, one at low fields and the other right below the upper critical field H_{c2} [42,43,44]. By plotting the magnetic field H_A at which the M(H) hysteresis loop closes at lower field and the upper critical field H_{c2} at which M(H) attains its normal state value, an H vs T phase diagram similar to that of UPd_2Al_3 is obtained, suggesting the possibility of a common origin. Shown in Fig. 5(a) is an M vs H isotherm at 2 K for $CeRu_2$, taken from our own work [45], which illustrates the irreversible feature near H_{c2} and how H_A and H_{c2} are defined. The corresponding H vs T phase diagram for $CeRu_2$ is shown in Fig. 5(b). One possible explanation for the hysteresis near H_{c2} is the so-called peak effect [46] in which the softening of the shear modulus of the flux line lattice near H_{c2} results in the spatial redistribution of flux lines so that they come into registry with pinning centers, thus increasing the pinning. Another possibility is the formation of the FFLO state between H_A and H_{c2} which could involve stronger pinning due to the spatially nonuniform character of the FFLO state. Further experiments are needed to clarify the relationship between the superconducting phenomena in a magnetic field exhibited by UPd_2Al_3 and $CeRu_2$ and to unravel the mystery of how these phenomena originate.

Acknowledgements— The support of the National Science Foundation under Grant No. DMR-94-08835 and the US Department of Energy under Grant No. DE-FG03-86ER45230 for research at UCSD are gratefully acknowledged. The research at Los Alamos was performed under the auspices of the US Department of Energy. JH acknowledges support from DAAD.

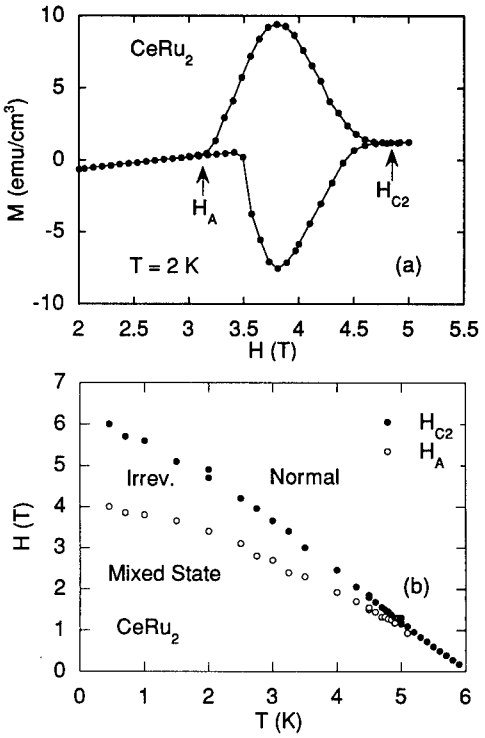


Fig. 5. (a)Magnetization M vs magnetic field H isotherms for $CeRu_2$ at several temperatures between 2 K and 4.3 K. The symbol H_A denotes the field at which the M(H) hysteresis loop closes at lower field and the upper critical field H_{c2} is defined as the field at which M(H) attains its normal state value. (b)Magnetic field H vs temperature T phase diagram for $CeRu_2$ delineating the mixed state superconducting, irreversible superconducting, and normal regions.

REFERENCES

1. D. L. Cox and M. B. Maple, *Physics Today*, February 1995, p.32.
2. F. Steglich, J. Aarts, C. D. Bredl, W. Lieke, D. Meschede, W. Franz, and H. Schafer, *Phys. Rev. Lett.***43** (1979) 1892.
3. H. R. Ott, H. Rudigier, Z. Fisk and J. L. Smith,*Phys. Rev. Lett.* **50** (1983) 1595.
4. G. R. Stewart, Z. Fisk, J. O. Willis and J. L. Smith,*Phys. Rev. Lett.***52** (1984) 679.
5. W. Schlabitz, J. Baumann, B. Pollit, U. Rauchschwalbe, H. M. Mayer, U. Ahlheim, and C. D. Bredl, *Z. Phys. B***62** (1986) 171.
6. C. Geibel, S. Thies, D. Kaczorowski, A. Mehner, A. Grauel, B. Seidel, U. Ahlheim, R. Helfrich, K. Petersen, C. D. Bredel and F. Steglich,*Z. Phys. B***83** (1991) 305.
7. C. Geibel, C. Schank, S. Thies, H. Kitazawa, C. D. Bredl, A. Böhm, M. Rau, A. Grauel, R. Caspary, R. Helfrich, U. Ahlheim, G. Weber and F. Steglich,*Z. Phys. B* **84** (1991) 1.
8. L. E. DeLong, J. G. Huber, K. N. Yang and M. B. Maple,*Phys. Rev. Lett.***51** (1983) 312.
9. G. Aeppli, E. Bucher, C. Broholm, J. K. Kjems, J. Baumann, and J. Hufnagl, *Phys. Rev. Lett.***60** (1988) 615.
10. T. T. M. Palstra, A. A. Menovsky, J. van den Berg, A. J. Dirkmaat, P. H. Kes, G. J. Nieuwenhuys and J. A. Mydosh, *Phys. Rev. Lett.* **55** (1985) 2727.
11. M. B. Maple, J. W. Chen, Y. Dalichaouch, T. Kohara, C. Rossel, M. S. Torikachvili, M. W. McElfresh and J. D. Thompson, *Phys. Rev. Lett.***56** (1986) 185.

12. C. Broholm, J. K. Kjems, W. J. L. Buyers, P. Mathews, T. T. M. Palstra, A. A. Menovsky and J. A. Mydosh, *Phys. Rev. Lett.* **58** (1987) 1467.
13. Y. Dalichaouch, M. C. de Andrade, and M. B. Maple, *Phys. Rev. B***43** (1992) 299.
14. J.-G. Lussier, A. Schröder, B. D. Gaulin, J. D. Garrett, W. J. L. Buyers, L. Rebelsky and S. M. Shapiro, *Physica B***199** (1994) 137.
15. A. Krimmel, P. Fischer, B. Roessli, H. Maletta, C. Geibel, C. Schank, A. Graul, A. Loidl and F. Steglich,*Z. Phys. B***86** (1991) 161.
16. A. P. Ramirez, B. Batlogg, E. Bucher and A. S. Cooper,*Phys. Rev. Lett.***57** (1986) 1072.
17. G. R. Stewart, A. L. Giorgi, J. O. Willis and J. O'Rourke, *Phys. Rev. B***34** (1986) 4629.
18. A. de Visser, J. C. P. Klaasse, M. van Sprang, J. J. M. Franse, A. Menovsky and T. T. M. Palstra, *J. Magn. Magn. Mater.* **54–57** (1986) 375.
19. B. Batlogg, D. J. Bishop, E. Bucher, B. Golding, A. P. Ramirez, Z. Fisk, J. L. Smith and H. R. Ott, *J. Magn. Magn. Mater.* **63–64** (1987) 441.
20. H. Amitsuka, T. Sakakibara, Y. Miyako, K. Sugiyama, A. Yamagishi and M. Date, *J. Magn. Magn. Mater.* 90 (1990) 47.
21. Y. Dalichaouch, M. B. Maple, M. S. Torikachvili and A. L. Giorgi,*Phys. Rev. B***39** (1989) 2423.
22. R. A. Fisher, S. Kim, B. F. Woodfield, N. E. Phillips, L. Taillefer, K. Hasselbach, J. Flouquet, A. L. Giorgi and J. L. Smith,*Phys. Rev. Lett.***62** (1989) 1411.
23. K. Hasselbach, L. Taillefer and J. Flouquet, *Phys. Rev. Lett.* **63** (1989) 93.
24. See, B. K. Sarma, M. Levy, S. Adenwalla and J. B. Ketterson, *Physical Acoustics XX* (1992) 107.
25. For a review, see J. A. Sauls, *J. Low Temp. Phys.***95** (1994) 153.
26. T. Trappman, H. v. Löhneysen, and L. Taillefer, Phys. Rev. B 43 (1991) 13714; H. v. Löhneysen, T. Trappman, and L. Taillefer, *J. Magn. Magn. Mater.***108** (1992) 49.
27. G. Goll, H. v. Löhneysen, I. K. Yanson and L. Taillefer, *Phys. Rev. Lett.***70** (1993) 2008.
28. G. M. Luke, A. Keren, L. P. Le, W. D. Wu, Y. J. Uemura, D. A. Bonn, L. Taillefer and J. D. Garrett, *Physica B* 186–188 (1993) 264.
29. A. Amann, P. Visani, K. Aupke, A. C. Mota, M. B. Maple, Y. Dalichaouch, P. E. Armstrong and Z. Fisk, to be published.
30. B. S. Shivaram, Y. H. Jeong, T. F. Rosenbaum and D. J. Hinks, *Phys. Rev. Lett.***56** (1986) 1078.
31. See, H. v. Löhneysen,*Physica B***197** (1994) 551.
32. Y. Dalichaouch, M. C. de Andrade, D. A. Gajewski, R. Chau, P. Visani, and M. B. Maple, to appear in *Phys. Rev. Lett.*.
33. M. B. Maple, C. L. Seaman, D. A. Gajewski, Y. Dalichaouch, V. B. Barbetta, M. C. de Andrade, H. A. Mook, H. G. Lukefahr, O. O. Bernal, and D. E. MacLaughlin, *J. Low Temp. Phys.* **95** (1994) 225.
34. M. B. Maple, M. C. de Andrade, J. Herrmann, Y. Dalichaouch, D. A. Gajewski, C. L. Seaman, R. Chau, R. Movshovich, M. C. Aronson, and R. Osborn, *J. Low Temp. Phys.* **99** (1995) 223.
35. M. A. Lopez de la Torre, P. Visani, Y. Dalichaouch, B. W. Lee, and M. B. Maple, *Physica B***179** (1992) 208.
36. K. Gloos, R. Modler, H. Schimanski, C. D. Bredl, C. Geibel, F. Steglich, A. I. Buzdin, N. Sato, and T. Komatsubara, *hys. Rev. Lett.***70** (1993) 501.
37. P. Fulde and R. A. Ferrel,*Phys. Rev.***135** (1964) A550.
38. A. I. Larkin and Y. N. Ovchinnikov, *Zh. Eksp. Teor. Fiz.***47** (1964) 1136 [Sov. Phys. JETP **20** (1965) 762].
39. M. R. Norman, *Phys. Rev. Lett.***71** (1993) 3391.
40. B. T. Matthias, H. Suhl, and E. Corenzwit, *Phys. Rev. Lett.* **1** (1958) 449.
41. J. W. Allen, S.-J. Oh, I. Lindau, M. B. Maple, J. F. Suassuna, and S. B. Hagström, *Phys. Rev. B***26** (1982) 445; J. W. Allen, S.-J. Oh, M. B. Maple, and M. S. Torikachvili, *Phys. Rev. B***28** (1983) 5347.
42. K. Yagasaki, M. Hedo, and T. Nakama, *J. Phys. Soc. Jpn.* **62** (1993) 3825.
43. A. D. Huxley, C. Paulsen, O. Laborde, J. L. Tholence, D. Sanchez, A. Junod, and R. Calemczuk, *J. Phys. Condens. Mater.***5** (1993) 7709.
44. H. Goshima, T. Suzuki, T. Fujita, M. Hedo, T. Nakama, and K. Yagasaki, International Conference on Strongly Correlated Electron Systems, '94.
45. N. R. Dilley and M. B. Maple, unpublished.
46. A. M. Campbell and J. E. Evetts, *Critical Currents in Superconductors*. Taylor & Francis Ltd. (1972).

SUMMARY

Pergamon

J. Phys. Chem. Solids Vol. 56, No. 12, pp. 1969–1971, 1995
1995 Elsevier Science Ltd
Printed in Great Britain
0022-3697/95 $9.50 + 0.00

0022-3697(95)00222-7

SPECTROSCOPIES IN NOVEL SUPERCONDUCTORS—A CONFERENCE SUMMARY

PHILIP B. ALLEN[1]
IRRMA, IN-Ecublens, CH-1015 Lausanne, Switzerland

Abstract—The author stayed awake almost all the time, awed by the responsibility of having to seem intelligent. Nevertheless, much of the work presented was beyond his grasp.

1. INTRODUCTION

The theme of this meeting was the fundamental physics of cuprate superconductors, and how various spectroscopies help to unravel their mysteries. Few of the theorists present claimed to understand these materials. Table 1 is a rough outline of the conference. Although at least 10 superconducting mechanisms were discussed, with varying degrees of Divine or empirical support, nevertheless, the mood was optimistic.

Table 1. Conference Statistics

Talks	58
Theoretical talks	24
Posters	98
Theoretical posters	39
Mechanisms	10
Smoking guns	5
Batteries of smoking guns	1
Appeals to Divine Authority	3
Requests for Divine Intervention	2 *

* 3 including this speaker

2. OLD PROBLEMS SOLVED

Two of the oldest questions now seem settled.

Nodes in the gap

Direct evidence from interference and fractional flux in loops, combined with indirect evidence of low energy electronic excitations, convinced nearly all participants that there are nodes in the gap Δ_k in the directions of k-space of a $d_{x^2-y^2}$ order parameter in $YBa_2Cu_3O_7$. Indirect evidence is available for the hole-doped bismuth, thallium and mercury compounds. However, the electron-doped Nd_2CuO_4 and the cubic non-cuprate $BaBiO_3$ may have clean gaps with no nodes. Near unanimity on this previously contentious subject is a testimony to the incisive experiments. Not all participants share the view that the positions of the nodes should be interpreted as demanding an $\ell = 2$ order parameter symmetry.

Specific heat

Experiments on $YBa_2Cu_3O_7$ by Moler *et al.* clarify this previously murky area. The new results are consistent with a gap with nodes. The $H = 0$ linear term γT seems extrinsic, and part of it disappears when samples are detwinned. This suggests that twin boundaries have bound states within the gap down to arbitrarily low energies. Perhaps this is an "intrinsic"property of a $d_{x^2-y^2}$ order parameter crossing a 90° twin boundary.

3. OLD PROBLEMS STILL DISCUSSED

Since the early months of high T_c superconductivity, certain difficult issues appeared important and probably central. Our inability to lay these problems to rest is vexing. However, progress was evident at the meeting.

How is a Mott insulator doped?

Experimentally, a "Mott insulator" is a material like NiO or La_2CuO_4 with antiferromagnetic order at low T which remains insulating even above its Neel temperature. Most Mott insulators are difficult to "dope" into the metallic state. Fortunately, La_2CuO_4 is not. Imai showed by NMR $(1/T_1)$ how magnetic fluctuations at a copper nucleus evolve as a system is doped. Interestingly, all doping dependence disappears at high enough temperature ($\geq$ 600 K). Birgeneau indicated that the evolution of magnetic behavior is different for the "n-doped" and "p-doped" materials. Theoretically, a Mott insulator is usually modelled by a Hubbard Hamiltonian with strong coupling and half filling, or by an equivalent "tJ" Hamiltonian. It is not totally obvious that these simplified Hamiltonians contain all the relevant physics of the experimental systems. Nevertheless, theory and experiment share the property that it is hard to understand what happens when a few electrons or holes are added. Kotliar's talk summarized recent advances in the

[1] On leave from Dept. of Physics, SUNY, Stony Brook, New York 11794-3800, U.S.A.

added. Kotliar's talk summarized recent advances in the theory of this subject, focusing on the effort to find an analytic approach which incorporates information from exact answers in $D = 1$ or $D = \infty$.

Is superconductivity inherent in a 2d doped Hubbard system?

In other words, can an on-site repulsive interaction alone cause superconductivity when the carrier density and crystallography are optimal? This question of principle is still not solved. Few theorists are happy to rely on the Hubbard Hamiltonian alone. Pines uses phenomenological input that goes outside the Hubbard model, while Schrieffer differs primarily in having spin fluctuations and superconductivity more spatially localized. Anderson uses strong 2d correlations but gets superconductivity from external attractive sources. Rice shows how two coupled half-filled tJ chains (experimentally realized in $SrCu_2O_3$) have an interesting magnetic state suggestive of $d_{x^2-y^2}$ superconducting pairing.

Normal state anomalies

Apart from magnetic fluctuations probed by NMR and neutron scattering, there was diminished discussion of the other "anomalies" seen in the normal state of the high T_c cuprates. It is difficult to take a global view of these anomalies, because they are sample-dependent, and change qualitatively with different degrees of doping. Other exotic metals show similar anomalies, making it unclear which aspects of the strange normal state behavior are central to superconductivity. Perhaps this old problem does not have to be solved right now.

4. NEW PUZZLES AND PROBLEMS

A good indicator of health in a field is a steady stream of new puzzles which focuses the mind on potentially soluble issues and productive directions. Many examples were discussed at this meeting, of which I mention a few.

Neutrons vs NMR

Walstedt reported that the relaxation rates $1/T_1$ and $1/T_2$ on both oxygen and copper nuclei cannot yet be reconciled with the information about spin fluctuations available from neutron scattering.

The "dip" feature

Fischer reported tunneling spectra on $Bi_2Sr_2CaCu_2O_8$ taken by an STM together with experimental proof of true vaccuum tunneling and of surface homogeneity. The $T = 0$ spectra show a very small zero bias conductance indicating very few electron states right at the Fermi energy but consistent with a gap with lines of nodes. The spectra are markedly asymmetric with bias polarity, and show a strong oscillation or "dip" in the state density below the Fermi surface, correlating with features seen earlier in photoemission (ARPES) and in "break-junction" tunnel spectroscopy. This feature possibly correlates with "flat bands" seen in photoemission.

How many sheets does the Fermi surface have?

ARPES data for $Bi_2Sr_2CaCu_2O_8$ claim sufficient resolution that it is now puzzling that only one sheet of Fermi surface is seen, where the CuO_2 bilayer structure ought to support two sheets.

Does the insulating state agree with the tJ *model?*

The magnetic state of undoped insulating cuprates agrees well with a Heisenberg Hamiltonian according to theories and experiments now several years old. Are the charged excitations of the insulators in similar agreement with the "tJ" Hamiltonian? Monte Carlo calculations are advanced enough to compare with ARPES experiments recently reported on the layered cuprate Mott insulator $Sr_2Cu_2O_2Cl_2$. Wells and Laughlin addressed this issue from experimental and theoretical perspectives, and agreed that data and theory accord well along the direction (0,0) to (π,π) but not along the direction (0,0) to $(0,\pi)$ or the direction $(0,\pi)$ to $(\pi,0)$. This may be connected with the fact that a naive hole, moving in real space from (0,0) to (a,a) does not flip antiferromagnetic spins, while one moving from (0,0) to $(0,a)$ does.

Robustness of strange superconductivity

It has always been a puzzle why high T_c is so robust; an illustration was given by Dynes on radiation-damaged samples. Bonn emphasized the robustness of the $n = 1$ exponent in the low T penetration depth $\lambda(T) - \lambda(0) \propto T^n$. In BCS theory, a d-wave superconductor becomes easily gapless, and the corresponding exponent becomes $n = 2$. Experiments show that this is surprisingly difficult to achieve.

ARPES lineshapes

A deeper understanding of ARPES spectra is needed, for example, to get intrinsic lifetime broadenings of quasiparticle states. J. W. Allen discussed his efforts to do this for a true 2D Fermi liquid, $TiTe_2$. Norman and Randeria have emphasized and checked a sum rule on the integrated intensity at the Fermi level. Bansil showed that the simplified "3 step" model which relates ARPES to single particle spectral information can differ substantially from the results of a full "1 step" calculation.

Josephson coupling of s *to* d-*wave superconductors*

The observed Josephson coupling in edge junctions between Pb and heavily twinned crystals of $YBa_2Cu_3O_7$ indicates that at twin boundaries (where x and y interchange) the $d_{x^2-y^2}$ order parameter acquires an extra phase change of π in order not to change sign. Thus the edge presents an order parameter of fixed phase and Josephson coupling is not inhibited. But c-axis Josephson junctions with Pb have been studied by Dynes, and these also have a non-zero Josephson coupling. In a perfect experiment with a perfect $d_{x^2-y^2}$ order parameter, c-axis Josephson coupling should vanish. However, the orthorhombic symmetry of $YBa_2Cu_3O_7$ causes the actual order parameter to have some s-like admixture. In a single domain sample this would permit c-axis Josephson coupling. However, in heavily twinned samples with phase changes of π, the s-component of the order parameter alternates in sign, so again no Josephson coupling should occur. One possible way out of this dilemma is if the relative phase of the order parameter in different domains is fixed by the current rather than the boundary free energy.

5. NEW PROBLEMS ALREADY SOLVED

The conference included several reports of new work where the chief issues are already resolved.

tJ *ladders*

As discussed by Rice, these systems are understood, providing a glimpse of how $D = 1$ tJ physics might spread into $D = 2$.

Vortex structure of $d_{x^2-y^2}$ *superconductors*

Kallin reported a description of the nature of an isolated Abrikosov vortex in a superconductor with a $d_{x^2-y^2}$ order parameter.

5.1. *Transverse magnetothermal effect*

Ong reported a measurement of the transverse temperature gradient when heat flows in a perpendicular magnetic field. This is the thermal analog of the Hall effect, and has two advantages over previously measured quantities. First, being a thermal rather than electrical transport property, it occurs in the superconducting as well as the normal state.

Table 2. Memorable Quotes

ZF	"Superconductivity is an epiphenomenon."
AAA	"God is lazy, and will not create a new theory if He can manage with the old one."
RCD	"The experimenters will understand—get all the computers out of the lab." *
PA	"Why only spaghetti? There's also PIZZA!" †
TMR	"*d*-wave superconductivity can be viewed as... a quantum melted striped phase." ‡
MVK	"Start from the left, rather than the right! Follow the red line, rather than the blue!" §
BOW	"Sorry about these transparencies." ¶
GA	"I'm looking forward to changing my tune when the statistics improve." ‖
TI	"So far so good!... But, there is a problem... Some theorists showed up!... Sokol and Pines... Why do you laugh? I don't get it."
PAL	"OH! We never try to put NUMBERS in!"

* Theorists have an equally valid understanding.
† Bands may be spaghetti to some, but the "shadow bands" seen in photoemission are not just for breakfast either.
‡ Most enigmatic theory award.
§ For the politically naive: left = red = Mott insulator; right = blue = band metal.
¶ Damaged by the motel air conditioner the previous night.
‖ Most honest experiment award.

Second, unlike the $H = 0$ case where heat is carried by both phonons and electrons, the magnetic effect must be caused only by charged excitations. Ong has used this to extract a carrier lifetime in the superconducting state, and in common with other measurements, it increases rapidly as temperature falls, consistent with scattering from other condensing particles, but probably inconsistent with scattering from defects or non-condensing particles like phonons. One might expect that scattering from phonons should occur at some level, but there isn't much room for it in the data.

6. SUMMARY

The organizers can be commended for a timely and stimulating meeting. Thanks to dramatic experimental progress, the field of high T_c superconductivity seems healthy. Participants were relaxed and uninhibited, as the collection of *verbatim* quotations in Table 2 illustrates.

Acknowledgements—This work was supported in part by National Science Foundation Grant No. DMR-9417755.

AFTER DINNER TALK

Pergamon

J. Phys. Chem. Solids Vol. 56, No. 12, pp. 1973–1974, 1995
Copyright © 1995 Elsevier Science Ltd
Printed in Great Britain. All rights reserved
0022-3697/95 $9.50 + 0.00

0022-3697(95)00221-9

AN AFTER DINNER TALK—A GAP THAT SHOULDN'T BE
The Stanford Conference on Spectroscopies in Novel Superconductors, 16 March 1995

THEODORE H. GEBALLE
Stanford University

In the preface to a book describing his first encounter with Richard Feynman whom he was filming for a BBC documentary, Christopher Sykes describes Feynman's Thursday morning lecture. Feynman was solving a problem and time was running out. He told the students, "There are two ways of dealing with this problem, one is complicated and messy; the other is simple and elegant. We don't have much time so I'll just do the complicated messy way" (from *No Ordinary Genius*, Christopher Sykes, W.W. Norton, NY and London, 1994).

Most of us would like to be two-thirds as effective as Feynman, so that's why I may be complicated and messy—even if I'm not short.

In keeping with the theme of this conference, I want to discuss the gap, not the one we have been discussing all day, but rather the gap that exists between the ground state of science in the U.S. and the occasionally exciting technological states it can excite.

Much of what I will say comes from a new book—*The Cultural Clash*, by Stephen Goldberg, a law professor at Georgetown University who has been on the U.S. Nuclear Regulatory Commission and teaches a seminar on law and science.

Within the scientific and the law communities individually there is coherence, but there is no overlap. Goldberg routinely asks his law class to write down spontaneously the name of the most brilliant person who ever lived. The choices always fall into the same categories—scientists, most frequently Einstein or Newton, or humanists, most frequently Shakespeare or Mozart. One thing is certain. No one ever mentions a lawyer—no Holmes, no Brandeis—and it can't be due to lack of familiarity. It's because of the different cultures. Science is cumulative. As Thomas Kuhn notes, it jumps ahead by new paradigms which are introduced by the brilliant giants and, subsequently, is expanded and refined by us ordinary mortals. Such is illustrated by Newton's *Principia* which offered a new way of thinking about heaven and earth for centuries, until it was supplanted by a new paradigm.

On the other hand, law is process-oriented. The US Supreme Court noted in a controversial case involving the anti-nausea drug Bendictin in 1993, "There are important differences between the quest for truth in the courtroom and the quest for truth in the laboratory. Scientific conclusions are subject to perpetual revision. Law, on the other, must resolve disputes finally and quickly." The communities have correspondingly different *modus operandi*. In science, priority is fundamental. This is true regardless of whether the recognition is immediate, as with Bednorz and Mueller's discovery in the cuprates, or whether the importance was appreciated only much later, as with Dennis Gabor's optical holography, or even when the rediscovery is so late that it is done by future generations (if the retrieval system is good enough) as with Mendel's laws of inherited characteristics. The laws were rediscovered decades later after Darwin's proposal that evolution proceeds via mutations, but they are still known as Mendel's Laws derived from his experiments with sweet peas.

In law, the original concept is less important than the original application. Consider the right to have control of the information of one's own genetic makeup. How does this come about? It derives from the development of laws concerning privacy. In 1928 Brandeis wrote a famous dissent calling for constitutional protection against unreasonable searches and wiretapping. This was eventually adopted by the Supreme Court which used his brief that the makers of the constitution "conferred, as against the Government, the right to be let alone—the most comprehensive of rights and the right most valued by civilized men". Even though the words come directly from Thomas Cooley, a well-known law professor and member of the Supreme Court of Michigan in the late 1880s, Brandeis is credited with introducing the "right to be let alone" because he was responsible for introducing the concept into the practice.

Basic research has flourished under the control of basic researchers not because science is free of legal control, as Goldberg notes, but because the legal system we have gives power to the scientific community. Consider the recent case of the Board of Trustees of Stanford University vs Sullivan. The NIH awarded a five-year contract for heart research with a requirement that the government contracting officer be given 45 days advance notice of intent to publish preliminary findings. If the contracting officer objected, further review was available. The government's basis was a desire to prevent the Stanford researcher from publishing "unvalidated findings" that "could create erroneous conclusions which might threaten public health or safety if acted upon". The case was decided by Judge Harold H. Greene, whom many of us remember from his tough stands in the breakup of AT&T. Judge Greene's verdict was that the government was overstepping, stressing that it would be troubling to have a non-scientist contracting officer "tell Stan-

ford University, a premiere academic institution engaged in significant scientific and medical research" what constituted "unvalidated findings".

Science has been treated well by our courts. Respect, even reverence, for science can be traced back to the age-of-enlightenment reaction to the persecution of Galileo centuries earlier. Alexander Pope wrote: "Nature and Nature's Laws laid hid in night; God said let Newton be! and all was light". The founding fathers did not suffer from C.P. Snow's art/science gap; they were well educated. Oft-cited Benjamin Franklin is of course exceptional, but he is not an exception. James Madison and Alexander Hamilton had science and math interests. Thomas Jefferson wrote to the president of Harvard in 1789, "We have spent the prime of our lives in procuring for the students at Harvard the blessing of liberty. Let them spend theirs in showing that liberty is the great parent of science and of virtue, and that a nation will be great in both always in proportion as it is free".

With technology, the tables are turned. The legal system stresses adversary-style settings and the lawyers' process dominates. Ideas that are outstanding from a scientific point of view are just one point of view. Quoting Goldberg again, "So long as our products are incubated in a setting in which scientific norms dominate, and are born into a world in which legal norms reign, smooth transitions will be the exception".

In the Bendictin case in 1993, the Supreme Court overruled a lower court and held that the Federal Rules of Evidence displaced the generally accepted reliance upon scientific community norms—thus rejecting the briefs submitted by the American Physical Society and other organizations that juries should be screened from junk science. The Supreme Court said that the judge should be a flexible gate keeper and that "evidentiary reliability will be based upon scientific validity".

The good old days are history and Vannvar Bush's "Endless Frontier" is going the way of our western frontier. The promise that the endless frontier justifies funding the "free-play of free intellects" is no longer accepted; we are learning to accept more goal-oriented research. We should recall the reply to Queen Victoria when she asked what good electricity would be now that Maxwell and Faraday finally understood it which was, "Madam, some day you'll be able to tax it". It would be a disservice to our generation and to future generations if we were to allow the pendulum to swing too far and curiosity-driven research were allowed to wither.

On the technology side of the gap, universities have a major long-range role to play because it is at the universities that the flexible gate-keeper judges, and other future leaders of society, should be exposed to some real science. They should appreciate how the technologies of today grew from the storehouse of knowledge which was obtained by previous generations (and paid for by previous budgets). Fiber optics itself is a new example, recently made much more powerful by the erbium oxide monolithic fiber amplifier. The latter was introduced in an amazingly short time because the basic research had already been done.

Goldberg goes further. He argues for a type of scientist-counselor who is part of the research establishment, but who looks ahead at the possible implications of the research. Goldberg is focused on the practical value of a scientific counselor in being able to minimize the gap early. After the technology is developed the gap is more difficult to bridge. The week's New York Times carried a story on how Monsanto is going to carry out the most expensive advertising campaign yet to overcome the gap that has arisen in connection with hormones for increasing milk production. Goldberg quotes Bob Cava as questioning whether toxic superconductors will ever be widely usable. He points to a 1986 case where a worker in a monazite ore mine who had contracted cancer might have a viable claim for damages. This ore is a source of yttrium and this might possibly turn out to be the source of a regulatory gap along with thallium and mercury. Goldberg further argues being more aware of the social considerations which might arise from a basic research effort at an early stage, the counselor might be able to change the course of the research. This, of course, has its own sets of problems, and I am not convinced that it is a good idea. In the extreme limit of dominance by science counselors, the ethic of socially acceptable progress would permeate all research. That could be a giant step back to the pre-Galileo days. But, of course, we don't have to go to the extreme, and just getting scientists to be aware of the possible scenarios their research is leading to is worthwhile.

I hope I have convinced you that it is important to think about the place science occupies in society today, and that it is important to begin with a realistic understanding of the way things are. We can no longer rely upon the "Endless Frontier" good old days, epitomized by Oppenheimer's remarks right after Hiroshima and Nagasaki: "If you are a scientist you believe it is good to find out how the world works; that it is good to find out what the realities are; that it is good to turn over to mankind at large the greatest possible power to control the world and to deal with it according to its lights and its values". Of course, in hindsight many mistakes were made by not fully informing the public of the cons as well as the pros of nuclear energy.

If we do nothing, the gap will grow. The AT&Ts and IBMs are abandoning the basic research side. The populist anti-scientists are being heard. But I am optimistic that we can be heard, too. Take the time to think about the implications of your research and make them known. This can be done in many ways, and I urge you all to pursue your own.

Science and Perspective by Gerald Holton, Harvard Press (1995) provides enlightened perspective.

You may reach Prof. Geballe by e-mail at Geballe@loki.stanford.edu if necessary.

Chemical Thermodynamics Series, Volume 2

Chemical Thermodynamics of Americium

By **R.J. Silva, G. Bidoglio, M.H. Rand, P.B. Robouch, H. Wanner** and **I. Puigdomenech**

©1995 370 pages Hardbound Price: Dfl. 375.00 (US$234.50) ISBN 0-444-82281-X

This is the second volume in a series of critical reviews of the chemical thermodynamic data of those elements of particular importance in the safety assessment modeling of high-level radioactive waste storage and disposal facilities. The objective of these reviews is to provide a set of reliable thermodynamic data that can be used to describe the behaviour of these elements under conditions relevant for radioactive waste disposal systems and the geochemical environments. The present volume is a review of experimental data reported in the literature for americium. On a few occasions, where no data existed, comparisons and estimates were made based on experimental data on analog lanthanide elements. The basic philosophy was to develop a minimum set of solid phases and solution species of americium that would fit all experimental data being reviewed.

Contents: Introduction. Background. Focus of the review. Isotopes of americium. Review procedure and results. **Standards, Conventions, and Contents of the Tables.** Symbols, terminology and nomenclature. Units and conversion factors. Standard and reference conditions. Fundamental physical constants. Uncertainty estimates. The NEA-TDB system. Presentation of the selected data. **Selected Americium Data. Selected Auxiliary Data. Discussion of Data Selection.** Elemental americium. Simple americium aqua ions. Oxygen and hydrogen compounds and complexes. Group 17 (halogen) compounds and complexes. Group 16 (chalcogen) compounds and complexes. Group 15 compounds and complexes. Group 14 compounds and complexes. Group 13 compounds. Group 9 compounds. Group 6 complexes. Group 5 complexes. Group 4 complexes. Actinide compounds and complexes. Group 2 (alkaline-earth) and group 3 compounds. Group 1 (alkali) compounds. **Reference List. Authors list. Formula List. A. Discussion of Selected References. B. Ionic Strength Corrections.** The specific ion interaction equations. Ion interaction coefficients *versus* equilibrium constants for ion pairs. Tables of ion interaction coefficients. **C. Assigned Uncertainties.** One source datum. Two or more independent source data. Several data at different ionic strengths. Procedures for data handling. **D. Corrections to the Uranium NEA-TDB Review.** Introduction. Uranium trichloride. Aqueous uranium hydroxide complexes. Uranium carbonate complexes and compounds. Uranium minerals. References to Appendix D. **List of Tables. List of Figures.**

TO ORDER

Contact your regular supplier or:

ELSEVIER SCIENCE

Customer Service Department
P.O. Box 211
1000 AE Amsterdam
The Netherlands
Tel: +31 (20) 485 3757
Fax: +31 (20) 485 3432

Customers in the USA and Canada:

ELSEVIER SCIENCE

Customer Service Department
P.O. Box 945
New York, NY 10159-0945, USA
Tel: +1 (212) 633 3650
Fax: +1 (212) 633 3680

No postage will be added to prepaid book orders. Dutch Guilder price(s) quoted applies worldwide US Dollar price(s) quoted may be subject to exchange rate fluctuations. Customers in the European Union should add the appropriate VAT rate applicable in their country to the price(s). In New York State please add applicable sales tax. All prices are subject to change without prior notice.



NORTH-HOLLAND

(AN IMPRINT OF ELSEVIER SCIENCE)

ANNOUNCING FOR PUBLICATION IN 1996

SAVE £710.00/US$1135.00—*order before* 30th June 1996

COMPREHENSIVE SUPRAMOLECULAR CHEMISTRY

11 VOLUME SET

BIBLIOGRAPHY DETAILS
Due June 1996
ISBN 0-08-0406106: 7000 pages approx
Pre-publication price: **£1990.00/US$3185.00**
(for orders placed before 30/6/96)
Post-publication price: **£2700.00/US$4320.00**
(for orders placed after 30/6/96)

Chairman of the Editorial Board
J.-M. LEHN, *France*

Executive Editors
J.L. ATWOOD, *USA*
J.E.D. DAVIES, *UK*
D.D. MACNICOL, *UK*
F. VOGTLE, *Germany*

VOLUME 1: Molecular Recognition: Receptors for Cationic Guests
VOLUME 2: Molecular Recognition: Receptors for Molecular Guests
VOLUME 3: Cyclodextrins
VOLUME 4: Supramolecular Reactivity and Transport: Bioorganic Systems
VOLUME 5: Supramolecular Reactivity and Transport: Bioinorganic Systems
VOLUME 6: Solid State Supramolecular Chemistry: Crystal Engineering
VOLUME 7: Solid State Supramolecular Chemistry: Two- and Three-Dimensional Inorganic Networks
VOLUME 8: Physical Methods in Supramolecular Chemistry
VOLUME 9: Templating, Self-Assembly and Self-Organization
VOLUME 10: Molecular Devices and Applications of Supramolecular Technology
VOLUME 11: Cumulative Index

Send for further details—use the coupon below

☐ Please send me my **FREE** *Comprehensive Supramolecular Chemistry* prospectus and fully descriptive leaflet

NAME _____

POSITION _____

ORGANIZATION _____

DEPARTMENT _____

ADDRESS _____

POST/ZIP CODE _____

COUNTRY _____

Prices and proposed publication dates are subject to change without prior notice. Sterling price(s) quoted applies worldwide, except in The Americas. US dollar price(s) quoted applies in The Americas only.

UK & all other countries:
Elsevier Science Ltd
The Boulevard, Langford Lane, Kidlington, Oxford OX5 1GB, UK
Telephone: +44 (0) 1865 843685
Fax: +44 (0) 1865 843946

The Americas:
Elsevier Science Inc
660 White Plains Road, Tarrytown, NY 10591-5153, USA
Telephone: +1-914-524-9200
Fax: +1-914-333-2444

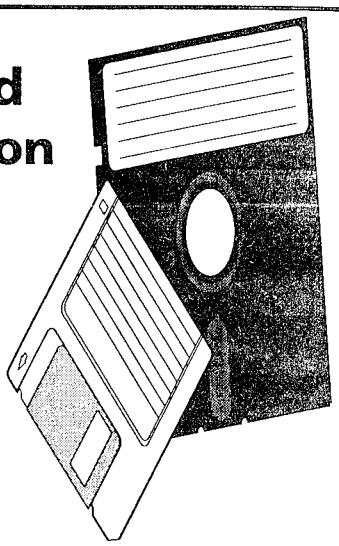


Pergamon *An imprint of Elsevier Science*

MWSA26 7/95

ELSEVIER SCIENCE

Elsevier Science Limited Encourages the Submission of Articles on Disk



Delivery of Electronic Files

Authors may now submit manuscripts on 3.5" or 5.25" disks.

Disks must be clearly marked with the following information:

Operating system
Disk format (e.g.DS/DD)
Word Processor used, including version number (users of T_EX see later)
Authors' names
Short title of article

Three printed copies of the final version of the manuscript should be submitted with the disk to the Journal Editor.
In the event of differences between disk and hard-copy, the hard-copy will be considered as the definitive version.

Preparing Electronic Text Files

When using a word processor to prepare a manuscript the following should be noted:

Page design will be handled by the Publisher. There is therefore no need to use formatting commands such as centring, justifying text, indenting etc.
Use the word processor's facilities to indicate the following text attributes: bold; underline; italic; subscript; superscript; strikeout.
Do not use the hyphenation facilities of your word processor.
When preparing tables use tabs, not spaces, to align columns.
When using symbols to denote special characters please supply a list of all codes used.

Use "hard returns" (i.e. using the enter key) only at the end of paragraphs. Use your word processor's "word-wrap" feature within paragraphs.
It is essential that the printed versions supplied are produced directly from the submitted electronic version.

$LaTeX/TeX$

Authors wishing to submit their article as a $LaTeX/TeX$ file should note the following:
Authors should use the "Article" style or the Elsevier $LaTeX$ package which is available via anonymous FTP from CTAN centres.

Host names:	CTAN directory:
ftp.dante.de	/tex-archive/macros/latex/contrib/supported/elsevier
ftp.tex.ac.uk	/tex-archive/macros/latex/contrib/supported/elsevier
ftp.shsu.edu	/tex-archive/macros/latex/contrib/supported/elsevier

(Further details on T_EX can be obtained from Martin Key)

Authors should not add their own macros.

Preparing Electronic Graphic Files

Illustrations ideally should be produced in the Macintosh environment using the following software packages:
(Please do not save images as postscript files)

Adobe Illustrator, Aldus Freehand, Cricket Graph, Macdraw, Chemdraw, Corel Draw-for PC

However we will accept any of the popular drawing programs for the Macintosh and PC.
Artwork should be drawn for finished size using a Times or Helvetica typeface at a final size of 8pt type with appropriate lineweights.
Please indicate format, operating system, program and version number of the software used. If possible also print a directory of filenames.
Scanned artwork should be saved to Tiff format for both line and half-tone and scanned at a suggested setting of 400 dpi for half-tones and 1000 dpi for linework. If it is necessary to compress the scans please indicate the software used. It is essential that a hard copy print of the scans be included.
Illustrations should be logically named and saved as individual files to 3.5" disk or a SyQuest cartridge 44mB or 88mB. If 3.5" disks are not available to you, 5.25" disks are acceptable. Please send a laser print of the artwork with the electronic file.
When submitting electronic colour images please indicate the file format and program used (including compression software). Include a 4 colour machine or cromalin proof and check that all the separations (if provided) are colour identified.

If you require any further information please contact the following:

Elsevier Science Ltd
The Boulevard
Langford Lane
Kidlington
Oxford
OX5 1GB
UK

Martin Key (Text)
Tel: 44 1865 843550
Fax: 44 1865 843905
E-mail: m.key@elsevier.co.uk

Phil Halsey (Graphics)
Tel: 44 1865 843305
Fax: 44 1865 843921
E-mail:p.halsey@elsevier.co.uk

Elsevier Science Inc
660 White Plains Road
Tarrytown
NY 10591-5153
USA

Tom Lewis Flood
(Text/Graphics)
Tel: 914 333 2535
Fax: 914 333 2626
Email:t.lewisflood@elsevier.com

Did you know that if you are a contributor to any Elsevier Science Book or Journal you are entitled to

30%

Discount on all our Books*?


Elsevier


Pergamon


North Holland


Excerpta Medica

*(except multi-volume reference works)

Contact your nearest Elsevier Science office in order to obtain a subject catalogue

Elsevier Science Ltd, The Boulevard, Langford Lane,
Kidlington, Oxford, OX5 1GB, UK
Elsevier Science Inc., 660 White Plains Road, Tarrytown, NY 10591-5153, USA

CO555/p7

Receive Regular News of Elsevier 's Publications

Elsevier Science mails information on new and existing publications regularly.
If you would like to be added to the mailing list please send us your name and full mailing address, indicating your fields of interest:

ENGINEERING
Energy Sources & Technology, Civil & Structural Engineering,
Mechanical Engineering, Electrical & Electronic Engineering,
Systems & Control Engineering, Aeronautical & Aerospace Technology,
Materials Technology, Chemical Engineering

LIFE SCIENCES & MEDICINE
Biological Sciences (including biochemistry & molecular biology), Agriculture,
Veterinary Medicine, Immunology, Cancer Research, Pharmacology, Neuroscience,
Vision Science, Clinical Medicine

PHYSICAL SCIENCES
Computer Science, Physics, Chemistry, Mathematics, Earth Science,
Environmental Science, Materials Science, Space & Planetary Sciences

SOCIAL SCIENCE & HUMANITIES
Sociology, Women's Studies, Psychology, Education,
Political Science, Geography, Economics, Management & Business, Linguistics,
Information Science, Librarianship



ELSEVIER
SCIENCE

Elsevier Science Ltd
The Boulevard, Langford Lane, Kidlington, Oxford OX5 1GB, UK

Elsevier Science Inc.
660 White Plains Road, Tarrytown, NY 10591-5153, USA

CO555/P4

• BACK ISSUES OF • THIS JOURNAL

Back issues of this and all other Elsevier Science journals are available in hard copy. New subscribers to a journal may purchase back issues of that publication in hard copy edition at 25% discount off the standard price. Elsevier Science maintains stocks of back issues and orders may be placed with confidence at your nearest Elsevier Science office. Should any issue of a volume be temporarily out of stock at the time of ordering, a high quality photoduplicated copy will be supplied at no extra charge to complete your order.

SAVE UP TO 25% BY PURCHASING COMPLETE SETS

Customers wishing to purchase complete sets can do so at a saving of 25% off the individual volume price.

MICROFORM EDITIONS

Back issues in microform of Elsevier Science research journals are also available. For further information please apply to your nearest Elsevier Science office.

BACK ISSUES PRICE LIST

Full details of the rates of back issues of all Elsevier Science journals can be found in our Back Issues Price List. Please contact your nearest Elsevier Science office for a copy.



ELSEVIER
SCIENCE

Elsevier Science Ltd, The Boulevard, Langford Lane, Kidlington, Oxford OX5 1GB, UK
Telephone: +44 01865 843699 • Fax: +44 01865 843911 • E-Mail: freesamples@elsevier.co.uk
Elsevier Science Inc., 660 White Plains Road, Tarrytown, NY 10591-5153, USA
Telephone: +1 914 524 9200 • Fax: +1 914 333 2444

CO555/p2

SEND FOR A FREE SAMPLE COPY OF ...

SOLID STATE COMMUNICATIONS

An International Journal

Editor-in-Chief: **Manuel Cardona**, *Max-Planck-Institut für Festkörperforschung, Heisenbergstrasse 1, 7000 Stuttgart 80, Germany*
Associate Editor: **Aron Pinczuk**, *AT&T Bell Laboratories, Murray Hill, NJ, USA*
Founding Editor: **Elias Burstein**, *USA*

Audience: Solid State Scientists.

AIMS AND SCOPE

Solid State Communications is an international medium for the publication of **short communications** on significant developments in condensed matter science, giving scientists immediate access to important, recently completed work. The journal publishes original experimental and theoretical research on the physical and chemical properties of solids and other condensed systems and also on their preparation. The submission of manuscripts reporting research on the basic physics of materials science and devices, as well as of state-of-the-art microstructures and nanostructures, is encouraged.
A coherent quantitative treatment emphasizing new physics is expected rather than a simple accumulation of experimental data. Consistent with these aims, the submitted manuscripts should be kept concise and short, usually not longer than four printed pages. The number of figures and tables should also be kept to a minimum. Instructions for the preparation of manuscripts appear in the first issue of each volume. *Solid State Communications* will also publish important initial results of ongoing research which should be referred to in more extensive papers being submitted elsewhere at a later date.
It is strongly recommended that authors submit their manuscripts either to a local (or nearby) Editor or to one who is an expert in their field of endeavour.

A Selection of Papers

L.F. MATTHEISS, T. SIEGRIST, R.J. CAVA, Superconductivity in the $LnNi_2B_2C$ intermetallics via boron A_{1g} phonons.
A. MOKRANI, H. DREYSSÉ, Magnetism of Rh vicinal surfaces?
N.I. ZHELUDEV, M.A. BRUMMEIL, R.T. HARLEY, A. MALINOWSKI, S.V. POPOV, D.E. ASHENFORD, B. LUNN, Giant specular inverse Faraday effect in $Cd_{0.6}Mn_{0.4}Te$.
R.R. DU, H.L. STORMER, D.C. TSUI, L.N. PFEIFFER, K.W. WEST, Shubnikov-deHaas Oscillations around v = 1/2 Landau level filling factor.
X.M. CHEN, J.J. QUINN, On the interpretation of the photoluminescence spectrum of fractional quantum hall systems.
S.P. LEWIS, M.L. COHEN, Prediction of an orthorhombic phase of germanium.
P.I. TAMBORENCA, S. DAS SARMA, Collective excitations in asymmetric parabolic quantum wells.
X.D. ZHANG, J.D. RILEY, R.C.G. LECKEY, L. LEY, Mapping the conduction band structure of GaAs along the ΓΔX direction.
D.J. LOCKWOOD, A. WANG, B. BRYSKIEWICZ, Optical absorption evidence for quantum confinement effects in porous silicon.
D. FRÖHLICH, CH. PAHLKE-LERCH, Contribution of longitudinal excitons to second harmonic generation in CuCl.
G.O SMITH, E.J. MAYER, J. KUHL, K. PLOOG (Germany), Pump-probe investigations of biexcitons in GaAs quantum wells.
H. ISHIHARA, K. CHO, A new type of nonlinear optical responses in a thin film owing to "nonlocality-induced double resonance in energy and size" of internal field.
N.F. JOHNSON, P.M. HUI, K.H. LUK, Theory of photonic band structures: a vector-wave *k* - *p* approach.

ABSTRACTED/INDEXED IN: *Cam Sci Abstr, Chem Abstr Serv, Curr Cont SCISEARCH Data, Curr Cont Sci Cit Ind, Curr Cont/Phy Chem & Earth Sci, Eng Ind, INSPEC Data, MSCI, PASCAL-CNRS Data, Research Alert, SSSA/CISA/ECA/ISMEC.*

1995: Volumes 93-96 (48 issues)
Associated Personal price: **£160.00 (US$239.00)**
Subscription price: **£1305.00 (US$1945.00)**
ISSN 0038-1098 (00230)

Pergamon

Pergamon is an imprint of Elsevier Science.
If an Associated Personal Subscription rate is available - full details accompany every sample copy requested. Sterling price quoted applies worldwide except in The Americas. US dollar price quoted applies in The Americas only.
Prices include postage and insurance. Customers resident in the EU will be charged VAT (or the equivalent) at their own country's rate, unless a VAT (or equivalent) registration number is supplied. Elsevier Science VAT registration number in the UK: GB 490 6384 25 000.

Please send me a **FREE SAMPLE COPY** of **SOLID STATE COMMUNICATIONS** (00230)

Name _____ Position _____

Organisation _____ Department _____

Address _____

_____ Post/Zip Code _____

Return to: Elsevier Science Ltd, The Boulevard, Langford Lane, Kidlington, Oxford OX5 1GB, UK
or Elsevier Science Inc., 660 White Plains Road, Tarrytown, NY 10591-5153, USA

IHA5

SEND FOR A FREE SAMPLE COPY OF ...

APPLIED SUPERCONDUCTIVITY

Editor-in-Chief: **Roger B. Poeppel**, *Argonne National Laboratory, USA*

Audience: Materials scientists, physicists, electronic and electrical engineers.

AIMS AND SCOPE
The aim of this new journal is to provide an international forum for the exchange of ideas concerning the large and small scale application of superconductivity. The focus of the journal is on any process, device, equipment, component, system, machine or structure which incorporates a superconducting element or which in some way takes advantage of or relies on the unique electrical or magnetic properties of superconductors to achieve a useful function. Examples include analog devices and SQUIDs, which are generally produced from thin superconducting films; RF cavities, which can be made from thick films and coatings; magnets, motors, generators and energy storage devices which may require long lengths of wire, tape, or multi-filament cable. Articles describing unique processing technologies aimed at achieving necessary performance characteristics are also appropriate. More specifically, the journal will contain articles on actual systems which embody various applications. These systems might include particle accelerators, magnetic levitation systems, electromagnetic launchers, fusion magnets, magnetic separation and research magnets, storage devices, imaging magnets and the facilities needed to support or augment these systems e.g. controls or cryogenics.

A Selection of Papers
P. BOEGLER *et al.* (Germany), Standardized measurements of interaction forces in autostable superconducting magnetic bearings.
W.L. HOLSTEIN (USA), Thermodynamic considerations for the vapor phase processing of Tl–Ba–Ca–Cu–O superconductors.
F. LERA *et al.* (Spain), Superconducting Ag/(Bi, Pb)–Sr–Ca–Cu–O composite wires and tapes.
I. VAN DRIESSCHE *et al.* (Belgium), Superconducting thick films based on Bi–Pb–Sr–Ca–Cu nitrate pastes, screen printed on alumina and ZrO_2 buffered alumina.
J. JOO *et al.* (USA), Role of silver addition on mechanical and superconducting properties of high-T_c superconductors.
K.C. GORETTA *et al.* (USA), Processing and properties of bulk BiSrCaCuO superconductors.
W. RAUCH *et al.* (Germany), High temperature superconducting coplanar and epitaxially grown microstrip transmission lines studied by a half-wavelength resonator technique.
N. BALCHEV (Bulgaria), Superconductivity in Cd–Ba–Ca–Cu–O system.

ABSTRACTED/INDEXED IN: *Curr Cont/Eng Tech & App Sci, Curr Cont/Phys Chem & Earth Sci, Mat Sci Cit Ind, Research Alert, Sci Cit Ind, Scisearch.*

1995: Volume 3 (12 issues) Subscription price: **£435.00 (US$649.00)**
ISSN 0964-1807 (00101)



Pergamon

Pergamon is an imprint of Elsevier Science.
If an Associated Personal Subscription rate is available full details accompany every sample copy requested. Sterling price quoted applies worldwide except in The Americas. US dollar price quoted applies in The Americas only.
Prices include postage and insurance. Customers resident in the EU will be charged VAT (or the equivalent) at their own country's rate, unless a VAT (or equivalent) registration number is supplied. Elsevier Science VAT registration number in the UK: GB 490 6384 25 000.

Please send me a **FREE SAMPLE COPY** of **APPLIED SUPERCONDUCTIVITY (00101)**

Name _____ Position _____

Organisation _____ Department _____

Address _____

_____ Post/Zip Code _____

Return to: Elsevier Science Ltd, The Boulevard, Langford Lane, Kidlington, Oxford OX5 1GB, UK
or Elsevier Science Inc., 660 White Plains Road, Tarrytown, NY 10591-5153, USA

IHA5

JOURNAL OF PHYSICS AND CHEMISTRY OF SOLIDS

NOTES FOR CONTRIBUTORS

I. GENERAL

1. Submission of a paper to the *Journal of Physics and Chemistry of Solids* will be taken to imply that it represents original research not previously published (except in the form of an abstract or preliminary report), that it is not being considered for publication elsewhere, and that if accepted it will not be published elsewhere in the same form, in any language, without the consent of the Editors. It should deal with original research work in the field of the physics and chemistry of solids.

2. Papers should be submitted to the most conveniently located editorial office.

3. Short communications may be published as "Technical Notes" and will receive somewhat more rapid handling than full length articles. Short communications requiring the maximum speed of publication should be submitted to one of the editors of *Solid State Communications*.

4. *Reprints.* A reprint form will be sent with proofs. Authors will automatically receive 25 free reprints of their article. Any additional reprints may be bought at the rate indicated on the form.

5. Authors should provide complete addresses, with fax and telephone numbers, when papers are submitted.

II. SCRIPT REQUIREMENTS

1. **Papers** submitted should be concise and written in a readily understandable style. Scripts should be typed and double spaced with good margins on one side of the paper only and submitted in duplicate to facilitate refereeing.

It will be appreciated if authors clearly indicate any special characters used. An abstract not exceeding 200 words (100 words in the case of a Technical Note or article submitted for the Software Survey Section) should be provided in the language of the paper. French and German papers should be submitted with English abstract and titles, but if this is not possible the abstract will be translated by the publishers. Normally a brief description of experimental techniques and mathematical derivations is adequate; a detailed description should be given only when these are new. References to internal reports and doctoral theses should be avoided. Authors will receive proofs for correction when their papers are first set, and **alterations must be restricted to printer's errors.** Other than these, any substantial changes may be charged to authors.

2. **Keywords** should be selected from the list provided in each issue of the *Journal*. A maximum of five should be selected. Each keyword should be accompanied by the capital letter denoting the category from which the keyword has been selected.

Example: A manuscript on electrical properties of superconducting fullerenes may have the following list of keywords:

Keywords: A. fullerenes, A. superconductors, D. electrical properties, D. superconductivity.

3. **Illustrations** should not be included in the typescript of the paper, and legends should be typed on a separate sheet. Line drawings which require redrawing should include all relevant details and clear instructions for the draughtsman. If figures are already well drawn it may be possible to reproduce them direct from the originals, or from good photo-prints if these can be provided. It is not possible to reproduce from prints with weak lines. Illustrations for reproduction should normally be about twice the final size required. The lettering should be sufficiently large and bold to permit this reduction. Photographs should only be included where they are essential and the originals should be supplied.

4. **Tables and figures** should be so constructed as to be intelligible without reference to the text. Every table and column should be provided with an explanatory heading. Units of measure must always be clearly indicated.

In the interest of economy and in order to avoid the introduction of errors, tables will be reproduced by photo-offset means directly from the author's typed manuscripts. The guidelines detailed below should be followed:
1. Page size should be 8.5 × 11 in. (or 21 × 30 cm). 2. Large or long tables should be typed on continuing sheets. 3. Table headings should be typed on separate sheets but identifying numbers should be placed on the upper righthand corner of each sheet of tabular material. 4. Original typed tables are required. It will be the author's responsibility to prepare his tables in accordance with this procedure as no facilities exist at the editorial office for retyping. The same data should not be published in both tables and figures. The following standard symbols should be used on line drawings since they are easily available to the printers: ○●+ × □■△▲◇◆▽▼.

5. **References** are indicated in the text by numbers in square brackets, and the full reference should be given in a list at the end of the paper in the following form:

1. Barnes R. G., Borsa F. and Peteson D., *J. appl. Phys.* **36,** 940 (1965).
2. Knight W. D., *Solid State Physics* (Edited by F. Seitz and D. Turnbull), Vol. 2, p. 93. Academic Press, New York (1957).

Abbreviations of journal titles should follow those given in *World List of Scientific Periodicals* (1979).

Footnotes, as distinct from literature references, should be indicated by the following symbols—†, ‡, §, ‖, ¶, commencing anew on each page; they should *not* be included in the numbered reference system.

6. Due to the international character of the journal no rigid rules concerning notation and spelling will be observed, but each paper should be consistent within itself as to symbols and units.

7. **Submission on Disk.** Authors may now submit *accepted* manuscripts on 3.5″ or 5.25″ disks according to the instructions included in this issue.

The original manuscript and diagrams will be discarded one month after publication unless the Publisher is requested to return the original material to the author.

JOURNAL OF PHYSICS AND CHEMISTRY OF SOLIDS

VOLUME 56 NUMBER 12 1995

CONTENTS

SPECIAL ISSUE

Spectroscopies in Novel Superconductors

For contents see p. vii

INDEXED/ABSTRACTED IN *Cam. Sci. Abstr., Chemical Abstracts Service, Current Contents/Engrg, Comput. & Technol., EIC Intel., Engrg. Ind. Monthly, INSPEC & PASCAL/CNRS Database, Materials Science Citation Index, SSSA/CISA/ECA/ISMEC*



Pergamon

ISSN 0022–3697
JPCSAW 56(12) 1567–1974 (1995)

Printed in Great Britain by BPC Wheatons Ltd, Exeter

